# VOLCANIC ASH AND AVIATION SAFETY:

## Proceedings of the First International Symposium on Volcanic Ash and Aviation Safety

*Symposium sponsored by*
Air Line Pilots Association
Air Transport Association of America
Federal Aviation Administration
National Oceanic and Atmospheric Administration
U.S. Geological Survey

*Symposium co-sponsored by*
Aerospace Industries Association of America
American Institute of Aeronautics and Astronautics
Flight Safety Foundation
International Association of Volcanology and Chemistry of the Earth's Interior
National Transportation Safety Board

U.S. GEOLOGICAL SURVEY BULLETIN 2047

**Cover.** Ash billows from the vent of Mount St. Helens volcano, Washington, during the catastrophic eruption that began at 8:32 a.m. Pacific Daylight Time on May 18, 1980. View is to the northeast. USGS photograph taken at about noon by Robert M. Krimmel.

# Volcanic Ash and Aviation Safety: Proceedings of the First International Symposium on Volcanic Ash and Aviation Safety

*Edited by* Thomas J. Casadevall

---

U.S. GEOLOGICAL SURVEY BULLETIN 2047

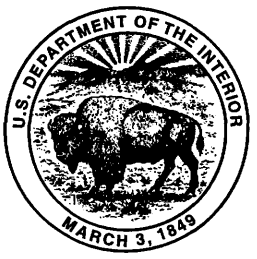


*Proceedings of the First International Symposium on Volcanic Ash and Aviation Safety held in Seattle, Washington, in July 1991*

*Symposium sponsored by*
Air Line Pilots Association
Air Transport Association of America
Federal Aviation Administration
National Oceanic and Atmospheric Administration
U.S. Geological Survey

*Symposium co-sponsored by*
Aerospace Industries Association of America
American Institute of Aeronautics and Astronautics
Flight Safety Foundation
International Association of Volcanology and Chemistry of the Earth's Interior
National Transportation Safety Board

UNITED STATES GOVERNMENT PRINTING OFFICE, WASHINGTON: 1994

# U.S. DEPARTMENT OF THE INTERIOR
## BRUCE BABBITT, Secretary

## U.S. GEOLOGICAL SURVEY
## Gordon P. Eaton, Director

For sale by U.S. Geological Survey, Map Distribution
Box 25286, MS 306, Federal Center
Denver, CO 80225



**Library of Congress Cataloging-in-Publication Data**

International Symposium on Volcanic Ash and Aviation Safety (1st : 1991 Seattle, Wash.)
Volcanic ash and aviation safety : proceedings of the First International Symposium on Volcanic Ash and Aviation Safety / edited by Thomas J. Casadevall ; symposium sponsored by Air Line Pilots Association ... [et al.], co-sponsored by Aerospace Industries Association of America ... [et al.].
p. cm.—(U.S. Geological Survey bulletin ; 2047)
"Proceedings of the First International Symposium on Volcanic Ash and Aviation Safety held in Seattle, Washington, in July 1991."
Includes bibliographical references.
Supt. of Docs. no.: I 19.3:2047
1. Volcanic ash, tuff, etc.—Congresses. 2. Aeronautics—Safety measures—Congresses. I. Casadevall, Thomas J. II. Air Line Pilots Association. III. Title. IV. Series.
QE75.B9 no. 2047
[QE461]
557.3 s—dc20
[629.13'0289] 94-17789

# FOREWORD

A Boeing 747 jumbo jet approaching the Anchorage International Airport, Alaska, on December 15, 1989, lost power to all four engines and nearly crashed as a result of flying through volcanic ash erupted from Redoubt Volcano. In separate incidents in 1982, two commercial jumbo jets en route to Australia across Indonesia suffered loss of engine thrust from ingesting volcanic ash from the erupting Galunggung Volcano, Java, and descended more than 20,000 ft before the engines could be restarted. These are not the only incidents of this kind. During the past 15 years, about 80 commercial jet aircraft have suffered damage from inadvertently flying into ash clouds that had drifted tens to hundreds of miles from erupting volcanoes.

The U.S. Geological Survey (USGS) has been involved in research on geologic hazards, such as volcanic eruptions and earthquakes, since its earliest days. With the Disaster Relief Act of 1974, the USGS was given formal responsibility "to provide technical assistance to State and local governments to ensure that timely and effective disaster warning is provided" for all geologic hazards. Addressing the threat of volcanic ash to aircraft safety, however, requires far more than the monitoring of volcanoes and warning of erupting ash clouds by the Survey. The ash must be traced and its likely trajectory must be forecast; aircraft must be alerted, and proper evasive actions must be taken by pilots. Agencies such as the National Weather Service and National Environmental Satellite Data and Information Service (both part of the National Oceanic and Atmospheric Administration), the National Aeronautics and Space Administration, and the Federal Aviation Administration are partners critical to the success of this mission. The International Civil Aviation Organization, various pilots' associations, air carriers, aircraft manufacturers, and many others are important as well.

The Redoubt encounter spurred government and university scientists, pilots, and representatives of the aviation industry to work together to reduce the hazards caused internationally by volcanic ash. As a result of the concern generated by the Redoubt eruptions and associated aircraft encounters, the First International Symposium on Volcanic Ash and Aviation Safety was held in Seattle, Washington, July 8–12, 1991. This volume contains the proceedings from that meeting.

Volcanologists and the subject of volcanic ash clouds are relatively new to discussions of aviation hazards. As a result, the various parties concerned with the hazard have had to set up new communication channels and to bridge substantial differences in organizational culture and professional language. The Seattle symposium in 1991 alerted and educated many about ash hazards to aviation. More importantly, it started a serious dialogue that resulted in a series of follow-up workshops, improvements in the detection and tracking of ash clouds, and revised warning and response procedures. These are the actions that will be needed if the hazard of ash in airways is truly to be mitigated.

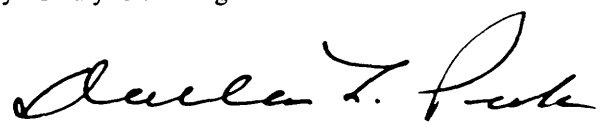

Dallas L. Peck
U.S. Geological Survey
Director, 1981–1993

# CONTENTS

## Technical Reports—Continued

### Volcanoes and Ash Clouds—Continued



### Damage and Impacts



### Communications and Procedures

## Technical Reports—Continued

### Communications and Procedures—Continued



### Meteorology and Ash-Cloud Monitoring

## Technical Reports—Continued

### Meteorology and Ash-Cloud Monitoring—Continued



### Detection and Tracking

## Technical Reports—Continued

### Detection and Tracking—Continued

# INTRODUCTION

*By* Thomas J. Casadevall

Volcanic ash from the 1989–90 eruptions of Redoubt Volcano disrupted aviation operations in south-central Alaska and damaged five jet passenger aircraft, including a new Boeing 747-400, which cost in excess of $80 million to repair (Steenblik, 1990). The Redoubt eruptions served to increase interest by the aviation community in volcanic hazards and made it clear that mitigating the hazards of volcanic ash to aviation safety would require the cooperation and efforts of volcanologists, meteorologists, air traffic managers, engine and airframe manufacturers, and pilots.

Soon after the December 1989 eruptions of Redoubt, Senator Ted Stevens of Alaska requested that Federal agencies form an interdepartmental task force to develop and coordinate both an immediate and a long-term response to the Redoubt eruptions. In March 1990, in response to this request, the U.S. Geological Survey, the Federal Aviation Administration (FAA), and the National Oceanic and Atmospheric Administration (NOAA) formed an interagency task group and began planning for an international technical symposium to review the available information about volcanic ash clouds and to assess what was being done to address the ash hazard, both domestically and internationally. This interagency group received strong support from the aviation community, and the Federal agencies were soon joined by the Air Line Pilots Association (ALPA), the Aerospace Industries Association (AIA), the Air Transport Association (ATA), the Flight Safety Foundation (FSF), and the American Institute of Aeronautics and Astronautics (AIAA). An important early result from this cooperation was the "First International Symposium on Volcanic Ash and Aviation Safety," to address the effects of volcanic activity on aviation safety in a multidisciplinary way and at a global scale. The aims of the symposium were: to bring together individuals who were interested in the volcanic ash problem but who may have been unaware of other scientists, engineers, pilots, and aviation authorities with similar interests; to encourage and define needed improvements in the detection, tracking, and warning of volcanic ash hazard so that aircraft may avoid ash clouds; and to review the effects of volcanic ash on aircraft so that pilots who encounter ash can respond appropriately. The symposium was held in Seattle, Wash., from July 8–12, 1991.

The symposium was attended by more than 200 participants from 28 countries, representing the major air carriers, airplane and engine manufacturers, pilots and aviation safety organizations, air traffic managers, meteorologists, and volcanologists. More than 100 technical presentations were made during the symposium, including a special session on the effects on aviation operations of the June 15, 1991, eruption of Mt. Pinatubo in the Philippines (Casadevall, 1991). Field trips to the Federal Aviation Administration air traffic control facility in Auburn, Wash., to the Boeing 737 assembly plant in Renton, Wash., and to the Mount St. Helens National Volcanic Monument gave participants the opportunity to view the volcanic hazard–aviation problem from several perspectives. Such broad participation demonstrated a clear need and wide support for a meeting of this type.

In the past 15 years, more than 80 jet airplanes have been damaged owing to unplanned encounters with drifting clouds of volcanic ash in air routes and at airports. Seven of these encounters caused in-flight loss of jet engine power, which nearly resulted in the crash of the airplane. The repair and replacement costs associated with airplane–ash cloud encounters are high and, to date (May 1994), have exceeded $200 million. In addition to the high economic costs of these encounters, more than 1,500 passengers aboard the seven airliners that temporarily lost engine power were put at severe risk.

The hazard is compounded by the fact that volcanic ash clouds are not detectable by the present generation of radar instrumentation carried aboard aircraft and are not likely to be detectable in the foreseeable future. Complete avoidance of volcanic ash clouds is the only procedure that guarantees flight safety, and this avoidance requires communication between the pilot and observers outside the aircraft.

Since the Seattle meeting, eruptions at Pinatubo, Sakurajima Volcano (Japan), Pacaya Volcano (Guatemala), Galeras Volcano (Colombia), Hudson and Lascar Volcanoes (Chile), Mt. Spurr (Alaska), Nyamuragira Volcano (Zaire), Sheveluch Volcano (Russia), and Manam Volcano (Papua New Guinea) have further disrupted air traffic, damaged aircraft in flight, and delayed flights and curtailed operations at a number of airports. The issue of volcanic hazards and aviation safety continues to be timely and in need of more effort

if we are to improve the margin of flight safety in the presence of volcanic ash.

## ISSUES AND NEEDS

During the symposium, discussions focused on the following technical areas: the 1989–90 Redoubt eruptions and their impacts on aviation operations, the nature of volcanoes and their ash clouds, the effects of volcanic ash on aircraft, methods and procedures of communicating the ash-cloud hazard to pilots, the role of meteorology and the use of atmospheric models to forecast cloud movement, and detection and tracking of ash clouds. This volume contains reports for 60 of the 108 technical presentations made during the symposium. The papers presented about the Redoubt eruptions have been published elsewhere (Miller and Chouet, 1994).

In addition to the technical presentations, symposium discussions identified a number of key issues and needs that participants felt must be addressed in order to mitigate the volcanic threat to aviation safety. These included:

1. Improved communications among volcano observers, meteorologists, air traffic controllers, flight dispatchers, and pilots about drifting ash clouds, including immediate notification of volcanic eruptions to pilots.
2. Improved education of pilots, flight managers, and manufacturers about the ash-cloud hazard, including specific recommendations for avoiding ash clouds.
3. Improved detection and tracking of ash-cloud movement using remote-sensing techniques and atmospheric-transport models.
4. Improved monitoring of the Earth's active volcanoes, especially in the remote Aleutian-Kamchatka-Kurile volcanic region.
5. New methods for eruption identification and ash-cloud detection.
6. Development of instruments that will enable pilots to detect ash clouds while in flight, especially useful when flying over remote, unmonitored regions of the Earth.
7. Development of better methods to remove and clean ash from airplanes and airports.
8. Determination of minimum levels of ash concentration that are capable of damaging aircraft and engines.
9. Development of a worldwide notification system and clearinghouse for information about active volcanoes, including planning charts to show the location of volcanoes relative to air routes.

## DEVELOPMENTS SINCE THE SYMPOSIUM

A number of ad hoc working groups were formed following the symposium to examine these topics and have produced significant progress on many of these technical issues. Accomplishments include:

1. A training video for pilots entitled "Volcanic Ash Avoidance," produced by the Boeing Company in cooperation with the Air Line Pilots Association and the U.S. Geological Survey (Boeing Company, 1992).
2. An international workshop on communications among volcanologists, meteorologists, air traffic managers, and pilots was held in Washington, D.C., in September 1992.
3. An FAA review on aviation safety as affected by volcanic ash (FAA, 1993a).
4. A workshop on the dynamics and characteristics of the ash clouds from the 1992 eruptions of Mt. Spurr was held in Washington, D.C., in April 1993 (FAA, 1993b).
5. An international workshop on volcanic ash and airports was held in Seattle, Wash. (Casadevall, 1993).
6. New communications links with Russians for warnings and information about Kamchatkan volcanoes, which underlie the increasingly busy air routes of the north Pacific region, were established in 1993 (Miller and Kirianov, 1993).
7. An interagency plan for volcanic ash episodes in Alaska was put into effect by the FAA, NWS, USGS, Department of Defense, and the State of Alaska in 1993 (Alaska Interagency Operating Plan, 1993).
8. A global planning chart showing the position of active volcanoes relative to air routes and air navigation aids was published (Casadevall and Thompson, 1994).

## INTERNATIONAL EFFORTS

Since 1982, the International Civil Aviation Organization (ICAO) has worked to address the volcanic threat to aviation safety worldwide (Fox, 1988, this volume). This threat came to wide public attention in 1982 when two 747 passenger jets encountered ash at night from separate eruptions of Galunggung Volcano in Indonesia. In these incidents, volcanic ash extensively damaged exterior surfaces, instruments, and engines, resulting in the loss of thrust and powerless descents of nearly 25,000 feet before the pilots of both aircraft restarted their engines and landed safely at Jakarta (Smith, 1983). The Galunggung encounters occurred for two main reasons. First, the pilots were unable to see the ash or to otherwise detect it using on-board instruments, and sec-

ond, no warnings about the activity of the volcano were contained in the aeronautical information generally available to pilots, such as notices of significant meteorological events—SIGMET's—or in notices to airmen—NOTAM's. These incidents led in 1982 to the formation of a volcanic ash warning group under leadership of the ICAO.

Eruptions and aircraft encounters with ash clouds during the past 15 years have prompted several other important international efforts to mitigate the volcanic hazard to aviation safety. Because volcanic ash clouds are carried by upper-level winds and often cross national boundaries as well as boundaries separating flight-information regions, efficient and prompt communications between regions are essential to avoiding encounters. The May 1985 encounter between a jumbo jet and an ash cloud from an eruption of Soputan Volcano in Indonesia prompted the Indonesian and Australian governments to form a bilateral volcanological/airspace liaison committee to improve communications about volcanic eruptions in the Indonesian region (Johnson and Casadevall, this volume). In North America, drifting ash clouds from the 1989–90 eruptions of Redoubt Volcano, and the 1992 eruptions of Mt. Spurr, sent ash clouds over Canada and disrupted operations in Canadian airspace. These incidents prompted establishment of closer bilateral communications between Canadian and U.S. agencies including volcanologists, meteorologists, and air traffic controllers (Hickson, this volume).

In 1988, ICAO member states adopted regulations to provide alerts to pilots about eruptive activity worldwide. These efforts included a special volcanic activity report form (VAR), which requires that pilots make a number of critical observations about the location, timing, and nature of an ash cloud. This information is communicated directly to the nearest area control center and is introduced into the communication network so that other aircraft may avoid airspace contaminated by volcanic ash (Fox, 1988, this volume).

Also in 1988, the World Organization of Volcano Observatories (WOVO), in cooperation with ICAO and with the International Association of Volcanology and Chemistry of the Earth's Interior (IAVCEI), requested WOVO member institutions to establish contacts with civil aviation authorities to improve communications between ground-based observatories and air traffic in order to minimize the volcanic hazards to aircraft. Currently, WOVO is examining ways to improve the exchange of information between observatories and agencies concerned with aviation operations, including the use of electronic mail (Riehle and Fink, 1993).

Following the 1991 Seattle symposium, ICAO addressed the volcanic threat to aviation safety at regional meetings in Bangkok (September 1992) and Mexico City (October 1992). In November 1992, changes to the international standards and recommended practices for meteorological services (ICAO, 1992) went into effect. The changes relate to the types of information about volcanic clouds that are entered into aeronautical communications networks using the SIGMET mechanism. The new regulations require that a volcanic advisory forecast be issued every 4 hours regarding the status of a volcanic cloud, with a 12-hour forecast of ash-cloud behavior.

Information for these advisories could come from many sources, but would most likely come from analysis of satellite images and from analysis of ash-cloud movement using atmospheric-transport models (Stunder and Heffter, this volume; Tanaka, this volume). For example, an important source of information for these volcanic advisories for the Southwest Asia region is the Darwin Regional/Specialized Meteorological Centre, established in 1993 by the Australian Bureau of Meteorology. The Darwin center utilizes satellite imagery to provide outlook advisory information about the occurrence and movement of ash clouds from eruptions in the Indonesian region. The center also serves as a venue for training meteorologists from the Asian region about detection and tracking of volcanic ash clouds so other countries in the region might carry out similar analysis at the local level.

To further assist ICAO member states in meeting the requirements for more detailed advisories, ICAO established a special implementation project to member states with active volcanoes as well as to those states responsible for flight information in regions adjacent to areas with active volcanoes. Through this project, an ICAO team consisting of a volcanologist and an aeronautical meteorologist visited countries in the Asia-Pacific region in 1992–93 (Casadevall and Oliveira, 1993) and the South American region in 1993–94 to advise on methods for meeting the new ICAO regulations. The new regulations should result in more rapid and clearer communications about volcanic ash clouds to the aviation community.

In addition to these bilateral efforts to improve the speed and quality of information, several countries have addressed specific volcanic threats to aviation operations by applying existing technology and by seeking to develop new methods and equipment for ash detection. For example, in 1991, scientists and aviation authorities in Japan installed specialized seismic and infrasonic detectors at Sakurajima Volcano to detect ash-producing eruptions. Results from these sensors are continuously transmitted to nearby Kagoshima Airport to provide real-time notification of explosive eruptions that threaten airport operations (Kamo and others, this volume; Onodera and Kamo, this volume). In another example, scientists in Australia are seeking ways to supplement information that is available to the pilot by developing an ash-detection sensor that can be carried onboard the aircraft to detect the presence of ash in the flight path (Barton and Prata, this volume; Prata and Barton, this volume). Such a sensor would be especially valuable for international flights over regions where volcanoes are poorly

monitored and where ground-based communications are poorly established.

## EFFORTS IN THE UNITED STATES

The United States has approximately 56 volcanoes with historical eruptive activity; 44 are located in Alaska. The U.S. Geological Survey (USGS) is the principal Federal agency with responsibility for assessing volcanic hazards and monitoring active volcanoes in the United States (Wright and Pierson, 1992). This work is carried out primarily from volcano observatories in Hawaii, Alaska, California, and Washington. For example, the Alaska Volcano Observatory monitors the activity of volcanoes in the Cook Inlet area, including Redoubt and Spurr. Continuous seismic and other monitoring of these volcanoes, day and night, in all seasons and weather conditions, enables volcanologists to detect eruption precursors as well as eruptions themselves. Early detection of eruptions and prompt communication of this information to the FAA and to the National Weather Service offices in Anchorage are an essential part of the role played by USGS scientists in mitigating the ash hazard to aircraft.

The National Oceanic and Atmospheric Administration (NOAA) and the Federal Aviation Administration (FAA) also have responsibilities for dealing with the hazard of volcanic ash clouds that affect aviation operations in the United States. Cooperation between these two agencies was formalized shortly before the December 1989 eruption of Redoubt, when a memorandum of understanding between the agencies created a volcanic hazard alert team and established procedures to respond to volcanic eruptions affecting air operations in the United States. Since 1989, these procedures have been activated for eight volcanoes in the United States (J. Lynch, NOAA-SAB, written commun., March 1993). In 1993, a letter of agreement between the USGS and NOAA attempted to speed the exchange of information that notifies the aviation community of ash-cloud hazards and formalized the de facto collaboration between these agencies that has existed since the Redoubt eruptions.

The principal tools used by NOAA for assessing volcanic activity are analysis of data from satellites (Krueger and others, this volume; Matson and others, this volume) and wind-field data, which enables the forecast of drifting ash clouds (Murray and others, this volume; Stunder and Heffter, this volume). Since 1990, the National Weather Service office in Anchorage has implemented several new techniques for detecting and tracking volcanic ash clouds from volcanoes in the Cook Inlet and Aleutian regions (Hufford, this volume). These efforts are integrated with the monitoring efforts of the Alaska Volcano Observatory and with the air-traffic-control efforts of the FAA. The FAA, through its area control centers, has the primary responsibility for communicating with pilots and for providing NOTAM's.

Following the 1989–90 eruptions of Redoubt, the 1992 eruptions of Mt. Spurr also had an important impact on aviation, affecting operations in Alaska, Canada, and the conterminous United States (Alaska Volcano Observatory, 1993). Ashfall from the August 18, 1992, eruption of Mt. Spurr deposited from 1 to 3 mm of ash in Anchorage and caused Anchorage airports to curtail operations for several days (Casadevall, 1993). The cost of airport cleanup alone in Anchorage from the August 18 ashfall was more than $650,000. The ash cloud from the September 17 eruption disrupted air traffic routing around the volcano—2 days later it disrupted air routes over western Canada and in the congested air corridors of the northeastern United States. Fortunately, there were no encounters between aircraft and the drifting Spurr ash clouds. The lack of damaging encounters following the Spurr eruptions reflects increased awareness about the hazards of ash clouds and improvements made since 1990 in the warning, detection, and tracking of volcanic clouds. These improvements are largely a direct result of the previously mentioned initiatives by Federal and international agencies to reduce the hazards from volcanic ash.

From an operational perspective, experience in the Australia-Indonesia region and in Alaska has indicated that the threat of volcanic ash can be effectively addressed at the regional or local level. For example, the 1989–90 Redoubt eruptions and the 1992 Spurr eruptions prompted Federal and State agencies in Alaska to establish a regional plan for aviation-related volcanic hazards (Alaska Interagency Operating Plan, 1993). The plan outlines the responsibilities of the agencies involved in eruption responses to meet the public's need for information to protect against volcanic ash hazards. The Redoubt and Spurr eruptions also prompted U.S. and Canadian agencies to refine bilateral operational plans for communicating about volcanic hazards (Hickson, this volume).

In addition to the efforts by international and Federal agencies, the major airplane and jet engine manufacturers have also studied the damage to aircraft from ash encounters in efforts to develop mitigation strategies, including practical steps for pilots to minimize damage should an ash cloud be entered accidentally. The manufacturer's principal trade association, the Aerospace Industries Association (AIA), formed a volcanic ash study committee in 1991 to evaluate the volcanic threat to aviation safety (AIA Propulsion Committee, this volume). The findings of this committee are reflected in a number of the reports presented in Seattle (Campbell, this volume; Dunn and Wade, this volume; Przedpelski and Casadevall, this volume).

The Air Line Pilots Association (ALPA), the Air Transport Association (ATA), and the Flight Safety Foundation (FSF), as well as the American Institute of Aeronautics and

Astronautics (AIAA) and the Aerospace Industries Association (AIA) have all taken active roles to communicate about the ash problem with their members and constituents, both nationally and internationally. ALPA and ATA were sponsors of the Seattle Symposium, along with the FAA, NOAA, and the USGS. AIA, AIAA, FSF, IAVCEI, and the National Transportation Safety Board were co-sponsors of the symposium.

## FUTURE DIRECTIONS

As we gain understanding about the nature of ash clouds and the hazard of volcanic ash to aviation operations, we constantly improve our abilities to deal with the threat (Casadevall, 1992). Multidisciplinary cooperation and communications were major factors in the success of the Seattle meeting. This cooperation created an excitement among the participants that has been kept alive at later workshops and in cooperative efforts such as the production of the Boeing training video (Boeing Company, 1992). Even though the ash–aviation safety problem is global in scope, the solutions that have worked best have often been on a local or regional scale. The optimal solutions require understanding the location and character of the nearby active volcanoes, the structure of the air routes that cross or pass by these volcanoes, and an understanding and use of all available resources to detect, track, and forecast the movement of ash clouds. At the same time, as new pilots are introduced to new routes, efforts to educate pilots must continue.

The Seattle symposium and the efforts following the symposium indicate that we have much to do to satisfactorily address concerns about the threat of volcanic ash to aviation safety. This requires application of existing technologies, such as methods that enable scientists to detect eruptions from remote, unmonitored volcanoes; early detection of ash clouds; tracking of ash clouds in real time; and development of better and faster ways to get information into the cockpit. Also, despite the recent advances in testing jet engines for their tolerances to volcanic ash (Dunn and Wade, this volume) and advances in using remote-sensing technologies to detect and track ash clouds (Schneider and Rose, this volume; Wen and Rose, 1994), it is essential that ash clouds be sampled directly as they drift from their source volcanoes (Riehle and others, 1994). Only direct sampling will allow us to obtain information with which to corroborate and validate laboratory tests and computational models. The results of the Seattle symposium should be viewed as a start of efforts to address the threat that ash clouds present to aviation safety. Volcanoes will certainly continue to erupt, and air traffic and aircraft sophistication will continue to grow. To successfully coexist with the threat of volcanic ash, we must continue to address the volcanic hazard in a responsible fashion. Open communications about these efforts are essential to successfully dealing with the volcanic hazard to aviation safety.

## ACKNOWLEDGMENTS

The success of the Seattle symposium required the energy and efforts of a large number of colleagues. The symposium was organized under the leadership of Chris Newhall of the USGS and came about through the efforts of an interagency task group that was first suggested by Senator Ted Stevens of Alaska. Principal representatives on this task group included Robert Machol of the FAA, Mike Matson of NOAA, Doug Wade of the Department of Defense, Ed Miller of the Air Line Pilots Association, and Don Trombley of the Air Transport Association. Their assistance and support in the production of this report is gratefully acknowledged. The editor of this report served on this task group as program coordinator for the symposium.

Several colleagues provided long-term encouragement for this project, including Grant Heiken (Los Alamos National Laboratory), Tom Fox (ICAO), Mike Dunn (CALSPAN), Tom Simkin (Smithsonian Institution), and Bill Rose (Michigan Technological University). A special thanks goes to Robert Wesson of the USGS, who had the earliest and clearest vision of what the Seattle symposium should be.

The cooperation of those who acted as reviewers is especially appreciated. They include: Robert Anders, Steve Brantley, Marcus Bursik, Dan Dzurisin, David Harris, Grant Heiken, Wally Johnson, Steve Lane, Steve McNutt, C. Dan Miller, Tom Murray, Tina Neal, Chris Newhall, John Power, Jim Riehle, Bill Rose, Dave Schneider, Steve Self, George Stephens, Barbara Stunder, and Bob Tilling.

Deloris Klausner of the Branch of Volcanic and Geothermal Processes (USGS, Denver) was responsible for collating all the manuscripts. Rick Scott, geologist and technical publications editor (USGS, Denver), provided editorial guidance and supervised preparation of illustrations and the final layout of the volume.

## REFERENCES CITED

Alaska Interagency Operating Plan, 1993, Alaska Interagency Operating Plan for Volcanic Ash Episodes: Anchorage, Alaska, Alaska Division of Emergency Services, Alaska Volcano Observatory, Department of Defense, Federal Aviation Administration, and National Weather Service, June 16, 1993, 18 p.

Alaska Volcano Observatory, 1993, Mt. Spurr's 1992 eruptions: Eos, Transactions, American Geophysical Union, v. 74, p. 217 and 221–222.

Boeing Company, 1992, Volcanic ash awareness: Seattle, Wash., Boeing Customer Training and Flight Operations Support, video 911202, 33 minutes.

Casadevall, T.J., ed., 1991, The First International Symposium on Volcanic Ash and Aviation Safety, Program and Abstracts: U.S. Geological Survey Circular 1065, 58 p.

Casadevall, T.J., 1992, Volcanic hazards and aviation safety—Lessons of the past decade: FAA Aviation Safety Journal, v. 2, no. 3, p. 9–17.

———1993, Volcanic ash and airports: U.S. Geological Survey Open-File Report 93-518, 53 p.

Casadevall, T.J., and Oliveira, F.A.L., 1993, Special project in the Asia/Pacific region boosts awareness of danger posed by volcanic ash: ICAO Journal, v. 48, no. 8, p. 16–18.

Casadevall, T.J., and Thompson, T.B., 1994, Volcanoes and air navigation aides—A global planning chart: U.S. Geological Survey Geophysical Investigations Map GP–1011.

Federal Aviation Administration, 1993a, Assuring aviation safety after volcanic eruptions: Washington, D.C., Office of the Associate Administrator for Aviation Safety, Special Review, 35 p.

———1993b, FAA Workshop on old volcanic ash clouds: April 22–23, 1993: Washington D.C., Office of the Chief Scientist, abstract volume, 37 p.

Fox, T., 1988, Global airways volcano watch is steadily expanding: ICAO Bulletin, April, p. 21–23.

International Civil Aviation Organization [ICAO], 1992, Meteorological service for international air navigation—International standards and recommended practices: Montreal, International Civil Aviation Organization, Annex III to the Convention for International Civil Aviation, 11th edition, 82 p.

Miller, T.P., and Chouet, B.A., eds., 1994, The 1989–1990 eruption of Redoubt Volcano, Alaska: Journal of Volcanology and Geothermal Research, v. 62.

Miller, T.P., and Kirianov,V.Y., 1993, Notification procedures for Kamchatkan volcanic eruptions: A case history of Sheveluch Volcano, April, 1993: U.S. Geological Survey Open-File Report 93-569, 9 p.

Riehle, J.R., and Fink, J.H., 1993, Some advantages of global electronic communications among volcanologists [abs.]: World Organization of Volcano Observatories workshop (Volcano observatories, surveillance of volcanoes, and prediction of eruptions), Guadeloupe, 13–17 December, 2 p.

Riehle, J.R., Rose, W.I., Schneider, D.J., Casadevall, T.J., and Langsford, J.S., 1994, Unmanned aerial sampling of a volcanic ash cloud: Eos, Transactions, American Geophysical Union, v. 75, p. 137–138.

Smith, W.S., 1983, High-altitude conk out: Natural History, v. 92, no. 11, p. 26–34.

Steenblik, J.W., 1990, Volcanic ash: A rain of terra: Air Line Pilot, June/July 1990, p. 9–15, 56.

Wen, Shiming, and Rose, W.I., 1994, Retrieval of sizes and total masses of particles in volcanic clouds using AVHRR bands 4 and 5: Journal of Geophysical Research, v. 99, p. 5421–5431.

Wright, T.L., and Pierson, T.C., 1992, Living with volcanoes: U.S. Geological Survey Circular 1073, 57 p.

# INTRODUCTORY REMARKS FOR THE FIRST INTERNATIONAL SYMPOSIUM ON VOLCANIC ASH AND AVIATION SAFETY, SEATTLE, WASHINGTON, JULY 1991

*By* Donald D. Engen, Former Administrator, Federal Aviation Admnistration

## PERSPECTIVES ON THE HAZARDS OF VOLCANIC ASH

I feel as if I have lived close to volcanoes. I was Commanding Officer of the U.S.S. Mt. Katmai—a U.S. Navy ammunitions ship—and lived on top of 28,000 tons of high explosives. The U.S. Navy has historically named ammo ships after volcanoes for some perverse reason. I was determined not to be the first Captain to go up with his ship! Twenty years ago, and even 10 years ago, no one that I knew would have even thought about organizing a symposium on volcanic ash as an air-safety issue. To those of us in aviation, volcanoes were those spectacular peaks that were reassuring landmarks en route to wherever we were going. To volcanologists, airplanes were a way to get a good view of volcanoes and a step toward getting information to provide warning to the communities near active volcanoes. I am not sure what meteorologists thought—perhaps that volcanic eruptions made for some pretty interesting clouds from time to time. Volcanic ash was not high on aviation's list of concerns, and airplanes were far from volcanologists' thoughts. To be sure, there were a few visionaries, but very few.

Then we started flying civil aircraft higher and in areas of the world where we had not flown so regularly before. Many international pilots encountered local situations in which they had little experience. Meteorologically, we found Meltemes, Mistrals, Siroccos, Willi Waws, and jet streams. Volcanoes attracted sightseers, and pilots flying near eruptions found volcanic ash to be injurious to the long life of aircraft engines and airframes. Then we found that volcanic ash clouds extended far from their source. At night or in instrument flight conditions (IFC), the ash cloud could not be seen, and we had damage incidents.

The International Civil Aviation Organization (ICAO) saw the need to address this hazard, and international networks such as the World Organization of Volcano Observatories (WOVO) were used as resources. Aviation shorthand messages to pilots, such as notices of significant meteorological events (SIGMET's) and notices to airmen (NOTAM's), were used to give wide dissemination to pilot reports (PIREP's) concerning ash clouds. The World Meteorological Organization (WMO) began using satellites for tracking ash clouds and for forecasting. The International Airways Volcano Watch was established.

We have had a number of volcanic ash encounters in the past 10 years, and we have almost lost some civil air carrier airplanes. More recently, we have had two major American military airfields shut down in the Philippines. Some say that there is a growing need for an on-the-scene knowledgeable pilot or dispatcher to provide operational information when airports are near or within a fallout area.

Today, everyone who has come to this meeting understands that we need to think about ash as an air-safety issue. To be sure, ash clouds are not an everyday issue, and they do not provide frequent hazard. But, if encountered, volcanic ash can spoil your entire day. Since Mount St. Helens awakened us in 1980, we have had 20 known encounters and three near accidents of wide-bodied jet airplanes worldwide. I will bet that Captain Moody will tell us at lunch today that his thoughts about Indonesian volcanoes changed dramatically one night in 1982. We will hear about other volcanoes as well—in Indonesia, Mexico, Japan, the former USSR, and elsewhere. These volcanoes have briefly but dangerously filled our airways with ash.

With great credit to ICAO and others, as I have said, important steps have been taken. Pilot operating handbooks have new pages, and volcanologists talk with aviation

meteorologists and air traffic control centers (ATC). But, as we saw last month near Pinatubo, the risk is not decreasing. In fact, the risk seems to be growing with the increasing numbers of long-distance night flights over remote volcanic areas. Encounters invariably cause damage and can easily be catastrophic.

Some important information is already known, but this information is not widely disseminated. Over the course of the next 3 days, we are going to hear from the world's experts about what is known about this problem. We will hear from the people who take the pulse of volcanoes, from those who have developed new methods for tracking ash from space, from those who have flown into and around ash clouds, and from those who have dealt with the damage. We will learn about the state-of-the-art warnings of impending or actual eruptions from monitored volcanoes (a relatively small subset of all volcanoes), about satellite detection of ash plumes, about subsequent movement of the resulting clouds of ash, about the most common effects of ash on airframes, instruments, and engines of airplanes, and about what pilots should do in case of an accidental encounter.

There are also many unknowns and gaps in worldwide coverage. These shortcomings will also be covered over the next 3 days. As a pilot, let me raise some questions. Suppose the volcanologists tell us that Redoubt or Pinatubo have just erupted an ash cloud. Can they tell us how high the cloud will rise? Can they tell us if it has a lot of ash or just a lot of steam? The meteorologists can tell us about winds at different altitudes. But can they tell us what altitudes actually have ash and in which direction the ash is moving? And can they revise their notices frequently as wind patterns change, as new images or data are received, and as ash progressively falls from the cloud? How will we know where the cloud is at night or if we are in instrument flight conditions? The ATC might be able to warn us that there is a hazard ahead, but can they tell us how serious it is, or how long it will remain a hazard? And can they be sure that alternative routes do not also have ash? Once ash is encountered, should we climb, descend, or reverse course? Will the ash cloud show on my radar with greater definition than moisture?

If you came to hear well-tested solutions, you are 5 years too early. If you came to be part of the solutions, you are in the right place at the right time. We are all pioneers on this subject. This is the first time that all of the world's experts have come to put their heads together, and it is the first time that so many of you who need this information have come to hear it. But, unlike some subjects, where the world really is divided into experts, beginning students, and advanced students, we need to teach each other. And to do that, we need plenty of lively discussion. Your questions are important, because nobody in this room has thought about the problem from every angle.

We have structured the meeting to encourage discussion and to make sure that we do not just talk with our own colleagues. No question will go unanswered—if we cannot handle it at the time, we will come back to it. No idea will go unrecorded—we are providing you with deposit slips for an idea bank where you can reinforce the ideas you offer in discussion. We will have poster sessions for person-to-person discussions. And, as some of you have already found, symposiums are a great place to meet the people that we will need to be talking with in the years to come.

Volcanologists seem always to talk to volcanologists, pilots to pilots, and meteorologists to meteorologists. To have communication, you must have listeners as well as talkers. There is a great need for practical communications across the disciplines represented here. There is a driving need to prevent a major aviation accident, which has not yet happened. There is a driving need for better understanding of volcanoes on the part of all of us. That is why we are here.

We are delighted to see such a diverse group. To participants from outside the United States, "Welcome!" Your participation adds meaning and knowledge to this symposium. I hope, through your participation, that other nations will join the search for knowledge. To participants from disciplines that barely knew of each other's existence, say hello to each other because the solution to your problem concerning volcanic ash may lie in your new friend's area of expertise.

VOLCANIC ASH AND AVIATION SAFETY:
Proceedings of the First International Symposium
on Volcanic Ash and Aviation Safety
U.S. GEOLOGICAL SURVEY BULLETIN 2047

# VOLCANOES AND AVIATION SAFETY IN COSTA RICA

*By* Jorge Barquero

## ABSTRACT

The active volcanoes in Costa Rica are located in Guanacaste Volcanic and Central Volcanic Ranges. Poas and Irazu Volcanoes have had several strombolian eruptions in historical times that produced large quantities of ash. Fine ash moved to the west and southwest of the volcanoes, reaching different distances and altitudes due to predominant trade-wind directions. Therefore, precautions should be taken for air traffic during future eruptions.

Costa Rica's Juan Santamaria International Airport in San Jose is located 23 km south of Poas Volcano and 42 km west of Irazu Volcano. Commercial airline routes are over or very close to the volcanoes. For example, Poas Volcano (8,884 ft high) is in the route of commercial airlines to Miami, which fly at a minimum altitude of 12,000 ft. Irazu Volcano (11,457 ft high) is in the airline route to Panama, with a minimum flying altitude of 14,000 ft.

The cooperation between pilot, air traffic controller, and volcanologists is very important. From the air, it is possible to see anomalous activity in volcanoes. For example, in 1962 a pilot called a newspaper to report the first columns of vapor issued by Irazu Volcano during the 1963–65 active period. In 1989, Poas Volcano had very strong gas emissions. At times, private and commercial airline pilots reported to air traffic controllers strong odors and the height of gas columns.

It is imperative to take into account possible ash and gas eruptions when planning air traffic and future airport sites.

## INTRODUCTION

The active volcanoes in Costa Rica are located in the Guanacaste and Central Volcanic Ranges. In recent times, Rincon de la Vieja, Arenal, Poas, Barba, Irazu, and Turrialba Volcanoes have had explosive ash-producing eruptions. Ash clouds have been carried to the west and southwest of the volcanoes because these are the directions of the prevailing winds.

The Juan Santamaria International Airport, located 20 km from the capital of San Jose and served by both national and international commercial airlines, is located in the central part of Costa Rica, to the south and west of the active volcanoes Poas and Irazu (fig. 1). As a result of the location of the airport, the air traffic routes pass over or near volcanoes that have very high eruption potential. This circumstance makes it mandatory to take precautions with air traffic during eruptions.

## DATA AND RESULTS

Poas Volcano, located 23 km, (14.4 mi) to the north of Juan Santamaria International Airport, rises to 2,708 m (8,884 ft). It has been active since 1828, and its last major active period took place between 1953 and 1955 (table 1). Ash clouds produced during this eruption were carried mainly to the west, to the southwest, and sporadically to the south.

Since 1987, Poas has ejected a gas column that sometimes reaches 2,000 m above the crater level, and its strong sulfurous odor has been reported by pilots. The minimum altitude for the airway over this volcano is 3,158 m (12,000 ft). This is the primary commercial airway to Miami, and it is used daily by planes that carry hundreds of passengers.

Irazu Volcano is located 42 km to the east of the Juan Santamaria International Airport and has an altitude of 3,443 m (11,457 ft). The commercial airway connecting Santamaria, Limon, and Panama (at a minimum altitude of 4,320 m or 14,000 ft) passes directly over Irazu Volcano; thus, there is a great deal of air traffic over this volcano daily.

In historical time, Irazu has been very active, with recorded eruptions since 1723. The last period of activity took place between the years of 1963 and 1965. Constant ash eruptions reaching heights of approximately 6,200 m (20,000 ft) were reported, and ashes were carried to the west and southwest by the prevailing winds. Deposition of this pyroclastic debris affected all of the Central Valley, in which the international airport is located. Official information concerning emergencies suffered by airplanes during this time does not exist, but there are accounts of problems during that period. The most outstanding report tells about a Pan Am DC-6 plane that flew through an ash cloud from Irazu and was forced to land in Panama in 1963. This plane had problems with its windows and engines. Ash was an effective abrasive. One precaution taken by domestic airlines and private airplane owners was to make check-ups of airplanes

more often than required. Overhauls were done more often than during normal conditions, and, in some cases, engines were replaced.

Arenal Volcano, located 73 km (45 mi) to the northwest of Juan Santamaria Airport, has an altitude of 1,630 m (5,380 ft). Planes flying to Managua, Nicaragua, follow an air route close to this volcano at a minimum altitude of 3,400 m (11,000 ft). Several airplanes carrying passengers fly this route each day. Arenal is an active volcano, and, since 1968 (23 years of activity at present), ash columns over altitudes of 3,048 m (10,000 ft) have been reported. Wind carries the pyroclastic debris toward the west and southwest, reaching different points according to the wind velocity.

Pilots have knowledge of Arenal activity and the dangers it represents, so they take precautions and report information to the airport regarding the height and direction of the ash cloud. This has helped to prevent airplane accidents on this route.

Some of the volcano-monitoring methodologies that are currently in use in Costa Rica are shown in table 2.

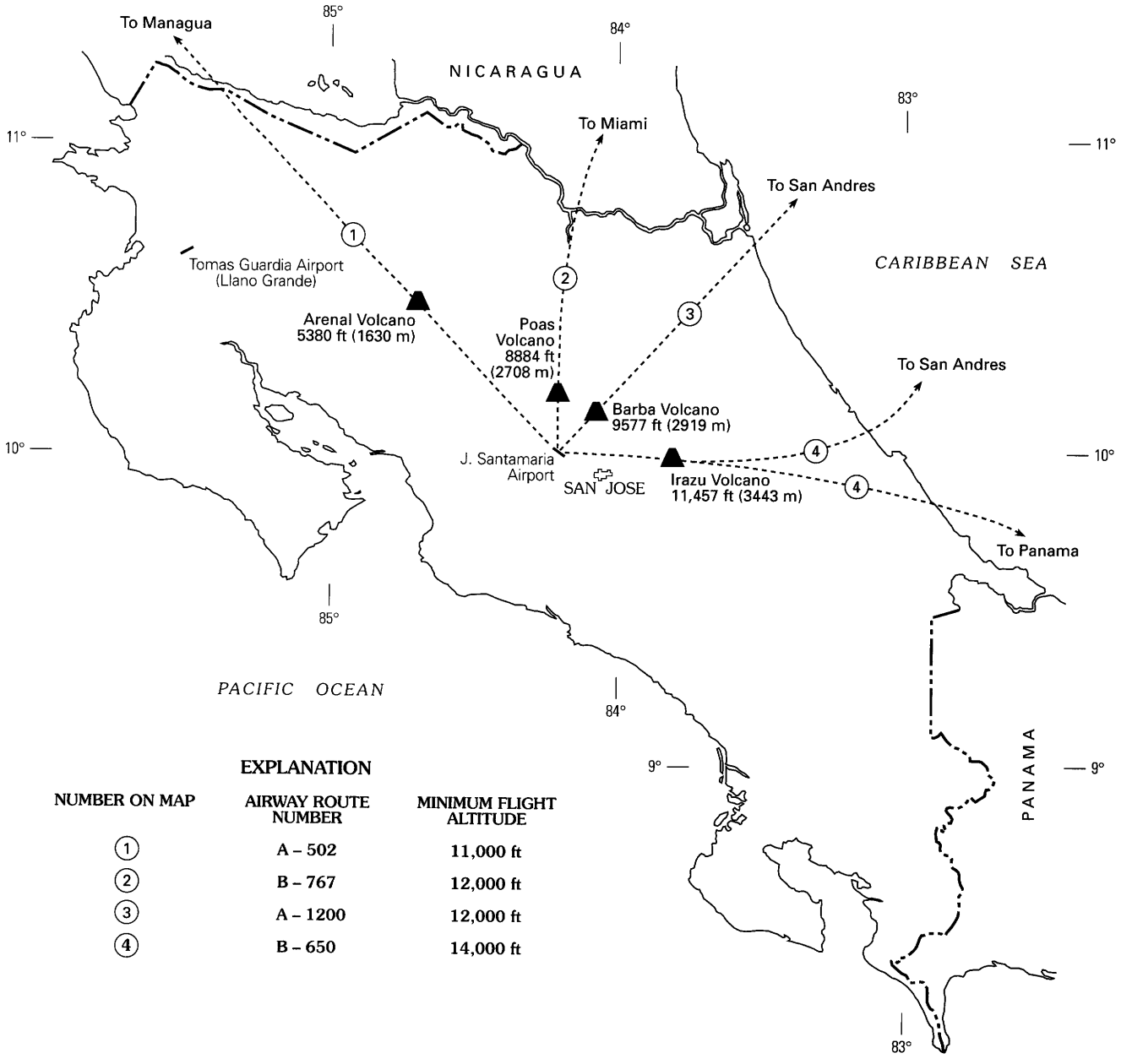


**Figure 1.** Airway routes over active volcanoes in Costa Rica.

**Table 1.** Year(s) of eruption and eruption type for some major volcanoes in Costa Rica.

| Year(s) of eruption | Eruption type |
|---|---|
| **Rincon de la Vieja Volcano** | |
| 1860 | Normal explosions. |
| 1863 | Normal explosions. |
| 1966 | Phreatic explosions. |
| 1969 | Phreatic explosions. |
| 1970 | Phreatic explosions. |
| 1983 | Phreatic explosions. |
| 1987 | Phreatic explosions. |
| 1991 | Phreatic explosions. |
| **Arenal Volcano** | |
| 1525 | Normal explosions. |
| 1968–present | Nuées ardentes, pyroclastic flows, phreatic explosions, lava flows. |
| **Poas Volcano** | |
| 1834 | Normal explosions. |
| 1838 | Normal explosions. |
| 1880 | Phreatic explosions. |
| 1907 | Phreatic explosions. |
| 1910 | Phreatic explosions. |
| 1914 | Phreatic explosions. |
| 1946 | Phreatic explosions. |
| 1952 | Phreatic explosions. |
| 1953–55 | Magmatic eruptions. |
| 1961 | Phreatic explosions. |
| 1963 | Phreatic explosions. |
| 1964 | Phreatic explosions. |
| 1972 | Phreatic explosions. |
| 1974 | Phreatic explosions. |
| 1976 | Phreatic explosions. |
| 1977 | Phreatic explosions. |
| 1978 | Phreatic explosions. |
| 1979 | Phreatic explosions. |
| 1987 | Gas eruptions. |
| 1988 | Gas eruptions. |
| 1989 | Gas eruptions. |
| 1990 | Gas eruptions. |
| 1991 | Gas eruptions. |
| 1992 | Gas eruptions. |

**Table 1.** Year(s) of eruption and eruption type for some major volcanoes in Costa Rica—Continued.

| Year(s) of eruption | Eruption type |
|---|---|
| **Irazu Volcano** | |
| 1723 | Normal explosions. |
| 1726 | Normal explosions. |
| 1821 | Normal explosions. |
| 1822 | Normal explosions. |
| 1826 | Normal explosions. |
| 1842 | Normal explosions. |
| 1844 | Normal explosions. |
| 1847 | Normal explosions. |
| 1870 | Normal explosions. |
| 1882 | Normal explosions. |
| 1917–1921 | Phreatic explosions. |
| 1924 | Normal explosions. |
| 1928 | Normal explosions. |
| 1930 | Normal explosions. |
| 1933 | Normal explosions. |
| 1939 | Normal explosions. |
| 1963–1965 | Phreatic explosions. |
| **Turrialba Volcano** | |
| 1750 | Normal explosions. |
| 1864 | Normal explosions. |
| 1866 | Normal explosions. |

## CONCLUSIONS

Several airways cross over or near Costa Rica's active volcanoes, and, therefore, air traffic is vulnerable in the event of ash eruptions. The prevailing wind direction in central Costa Rica and the location of Juan Santamaria International Airport with respect to the active volcanoes makes this airport vulnerable to ash deposition during volcanic eruptions.

**Table 2.** Volcano-monitoring methodologies in use in Costa Rica.

| |
|---|
| **Rincon de la Vieja Volcano** |
| Thermometry of crater lake; dry inclinometry; seismology. |
| **Arenal Volcano** |
| Radon emanometry; river and thermal-spring water analysis; gas traps; acid rain; ash collectors; dry inclinometry; horizontal distances network; vertical leveling lines; seismology. |
| **Poas Volcano** |
| Thermometry of fumaroles and hot-water lakes; analysis of gas condensates; river and thermal-spring water analysis; gas traps; acid rain; radon emanometry; dry inclinometry; horizontal distances network; vertical leveling lines; seismology. |
| **Irazu Volcano** |
| Thermometry of hot-water lakes; analysis of gas condensates; analysis of water samples from crater lake, rivers, and thermal springs; radon emanometry; dry inclinometry; geodetic network; vertical leveling lines; seismology. |
| **Turrialba Volcano** |
| Thermometry of fumaroles; analysis of gas condensates; gas traps; radon emanometry; dry inclinometry; seismology. |

## RECOMMENDATIONS

1. Plan, in advance, contingency or alternate airways to prevent planes from crossing over or near volcanoes that may be erupting.
2. Complete the construction of Tomas Guardia Airport as an alternate international landing site in case Juan Santamaria airport is closed.
3. Personnel of Observatorio Vulcanologico y Sismologico de Costa Rica (OVSICORI) should always be in close contact with the Office of Civil Aeronautics and should provide information on the state of activity of the volcanoes, especially when anomalous activity is present. Pilots, through the air traffic controllers, should inform OVSICORI of unusual volcanic activity as seen from the air.
4. An ad hoc group should be integrated with staff from the Office of Civil Aeronautics, pilots, and OVSICORI to draft a plan of action in case of volcanic eruptions.

VOLCANIC ASH AND AVIATION SAFETY:
Proceedings of the First International Symposium
on Volcanic Ash and Aviation Safety
U.S. GEOLOGICAL SURVEY BULLETIN 2047

# A METHOD FOR CHARACTERIZING VOLCANIC ASH FROM THE DECEMBER 15, 1989, ERUPTION OF REDOUBT VOLCANO, ALASKA

*By* Gregory K. Bayhurst, Kenneth H. Wohletz, *and* Allen S. Mason

## ABSTRACT

The development of an automated program for characterization of particles using a scanning electron microscope (SEM) with an energy dispersive X-ray detector (EDS) has greatly reduced the time required for analysis of particulate samples. The SEM system provides a digital representation of all particles scanned such that further measurement of the size, shape, and area are a product of image processing. The EDS and associated software provides information as to the particles' chemical composition. Data obtained from the SEM by this method are reduced by computer to obtain distribution graphs for size, density, shape, and mineralogy. These SEM results have been tested by comparisons with results obtained by traditional optical microscopy—the results obtained by optical microscopy support the SEM results and provide details concerning crystallinity and glass content.

This method was applied to the ash that damaged the engines from the Boeing 747-400 flight of December 15, 1989 (Brantley, 1990), which flew into the ash cloud from Redoubt Volcano. The sample was collected from the pitot-static system and had not been exposed to any engine parts that might have changed its characteristics. The sample analysis presented here demonstrates the capabilities and information obtainable from our automated SEM technique.

## INTRODUCTION

Studies of volcanic ash particles can be used to understand problems associated with volcanic ash clouds such as aircraft engine damage, visibility, atmospheric dispersion, and deposition of ash (Heiken, this volume). By using several analytical techniques, particles can be characterized in terms of size, shape, mass, mineralogy, and chemical composition. These characteristics provide detailed information necessary to understand the nature of volcanic ash clouds.

## METHODS OF STUDY

### SAMPLE PREPARATION

Loose samples, such as the ash collected from the pitot-static system, can easily be prepared by traditional thin-section techniques. This involves mixing the ash with epoxy on a microscope slide and then polishing flat to a desired thickness. Both the SEM technique and optical microscopy techniques can use the same slide.

If the sample has been collected on filters, it is necessary to remove the particles from the filter medium. For ash collected on cotton or paper filters, the filters can be ashed in a low-temperature radio-frequency oven. The ashing destroys the filter material and leaves the particles unaltered. The particles then can be mixed with epoxy and made into a thin section.

### SEM PARTICLE-ANALYSIS PROGRAM

The SEM uses a software program originally developed by L.J. Lee Group, Inc. for identification of airborne asbestos particles. It was modified to analyze volcanic ash particles. For each particle, the size, diameter, area, elemental composition and density are recorded. The location of each particle is also noted for easy return to a particular particle if detailed examination is needed.

### TREATMENT OF DATA

The data is first transferred from the SEM into a spreadsheet from which various operations are performed. These operations characterize the particles as to their mineralogy, morphology, densities, and abundances. The spreadsheet and operations are done with BBN Software Products Corporation's RS-1 software program (G. Luedemann and G. Bayhurst, unpub. data, 1989).

**Table 1.** Mineral definitions used in this report.

[Numbers in definitions column indicate weight percent]

| Mineral | Definitions |
|---|---|
| Quartz | $Si \geq 90$ |
| Calcite | $Ca \geq 90$ |
| Magnetite | $Fe + Ti \geq 90$ |
| Gypsum/anhydrite | $Ca + S \geq 90$; $Ca > 41$; $S > 29$ |
| Mica/clay | $Ca + K + Al + Si \geq 80$; $Fe > 4$; $K > 4$; $23 < Si < 80$ |
| Feldspar | $Ca + Na + K + Al + Si \geq 80$; $Fe \leq 4$; $Al + Si > 59$; $30 < Si < 80$ |
| Amphibole | $Fe + Mg + K + Ca + Al + Si \leq 80$; $Fe > 5$; $K \geq 3$; $28 > Si > 80$ |

Using the chemical analysis for each particle, the mineralogy is determined based on seven minerals or mineral classes. If the particle does not meet the criteria of the mineral definitions (table 1), it is labeled as "other." Because the SEM gives only chemical composition and not crystal structure, the glass content of the ash is not available by this method. The particles are then plotted according to the frequency of their mineral content.

The mean diameter, which is based on 16 measurements, is used to establish size frequencies. These size frequencies are calculated for both mineral type and overall bulk particles. The longest diameter measurement and the shortest measurement are ratioed without regard to mineralogy to provide an aspect ratio that gives an indication of shape. Digital image representation also allows computation of a shape factor given as the particle perimeter squared divided by the product of its area and 4 pi.

By using the results from the chemical analysis, we can determine the mass of each particle by combining densities and diameters. The densities are based on values for oxides for each element in the particle such as $SiO_2$, $Na_2O$, and CaO. The masses are used in several ways. The mass for each particle can be plotted on a log cumulative mass versus log diameter to give mass accumulation curves. The mass distribution can also be expressed as a percent total versus phi (phi = $-\log_2 \times$ (diameter in mm)) and analyzed using the sequential fragmentation/transport (SFT) model of Wohletz and others (1989).

The final function of the software is to determine various statistical values for each sample. Our statistics summary contains the mean, standard deviation, minimum, and maximum for several parameters and automatically prints out a summary sheet.

To verify our programs, we prepared chemical-composition standards by grinding well-characterized mineral standards to a fine powder. The powders were then prepared in the exact same manner as the ash particles. To verify our sizing-routine software, we used National Institute of Standards and Technology (NIST) standards for particle size. The software program that identifies minerals from chemical analysis was also tested by using these composition standards, achieving 95 percent or better correct identification.

## PETROGRAPHIC METHODS

Several hundred particles were examined and counted by standard petrographic methods on an optical microscope. This method allows us to determine not only the mineralogy of the particle but also if the particle is noncrystalline or glass. The importance of this is that the glass component of the volcanic cloud has a big influence on melting temperatures (Swanson and Beget, this volume).

# RESULTS AND DISCUSSION

The mineralogy of the ash particles determined by chemical composition was about 70 percent feldspar. The other components were quartz, magnetite, mica or clay, calcite, and amphiboles (fig. 1). An occasional particle of gypsum or anhydrite was also observed. By using fairly large ranges for defining the minerals or mineral groups, only about 10 percent of the ash was unidentified. The majority of unidentified particles appear to be mixtures of mineral phases that were probably welded on glass fragments. This result suggests that about 10 percent of the sample is composed of lithic fragments.

The optical analysis gives another perspective of the mineralogy in that the glass component can be readily identified. The results from the optical analysis showed that the particles are mostly plagioclase feldspar (46.7 percent), with many of them being fractured. The glass component was second most abundant at 28.6 percent. The following were

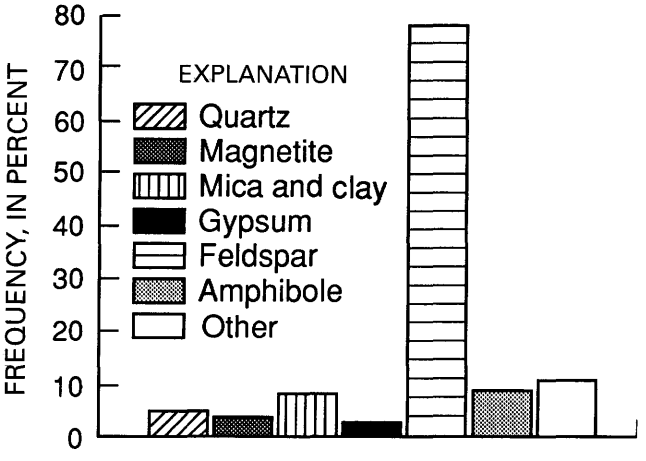


**Figure 1.** Mineralogy of ash particles from the December 15, 1989, eruption of Redoubt Volcano as determined by scanning electron microscopy.

**Table 2.** Bulk chemistry of glass from Redoubt volcanic ash from December 15, 1989, eruption.

| Species | Weight percent |
|---|---|
| $SiO_2$ | 69.9 |
| $Al_2O_3$ | 10.4 |
| FeO | 5.0 |
| MgO | 0.5 |
| CaO | 8.4 |
| $Na_2O$ | 4.3 |
| $K_2O$ | 0.1 |

minor components: pyroxene 2.8 percent, hornblendes 4.2 percent, opaque minerals 5.6 percent, altered rock 7.0 percent, and magnetite 5.2 percent. The petrographic name of this sample is a hornblende, two-pyroxene andesite.

If we assume that the glass component has nearly the same chemical composition as the crystalline minerals, then the results of the two methods are in good agreement. For example, if approximately 30 percent of the chemically defined feldspar particles are noncrystalline, then the percentage of crystalline feldspar would be approximately 49 percent.

With our method, we are able to obtain bulk-chemistry compositions by simply averaging each chemical component. For example, the average $SiO_2$ composition from our Redoubt sample was 69.9 percent. Because of the high glass content, the overall bulk chemistry (table 2) showed a higher $SiO_2$ concentration than the magma erupted during this time (Nye and others, 1990). This result is, however, consistent with other studies of Redoubt volcanic ash (Swanson and Beget, 1991).

Our sizing routine showed that, for this sample, the majority of the particles were 20 μm or less (fig. 2). The different mineral types can show slight differences in size distribution from the overall distribution, but they still show that most of the particles are smaller than 20 μm (fig. 3). The information obtained from size distributions can provide insight as to the factors controlling the type of damage done to aircraft engines. For example, if the ash encountered had a large percentage of coarse particles, then increased damage from abrasion might be observed. If the ash is fine, it will melt more rapidly and contribute to the material adhering to turbine surfaces.

Aspect ratios can be used for several purposes. The morphology of the particle can be described in this way. Aspect ratios that are close to 1 indicate that the particle is approximately equant in shape. For example, the aspect ratio of the feldspar particles (and glass) showed that about in one-third of them were equant (fig. 4). Also, the average shape factor for the sample is 1.16, which characterizes nearly equidimensional, polygonal cross sections.

The mass distribution curve gives other important information about the nature of the volcanic ash. In our Redoubt sample, even though the small particles were the most numerous, they contributed only a small amount of the mass (fig. 5). Another way of looking at mass distribution is the phi plot (fig. 6). This plot shows that over 60 weight percent of the sample occurs between 62 μm (4.0 phi) and 125 μm (3.0 phi). The overall mean diameter is 78 μm.

SFT analysis shows that the size distribution is polymodal, which is likely a consequence of the various densities and shapes in crystals, glass, and lithics that determine the mass-to-size ratio. Furthermore, SFT analysis (fig. 7) shows a mean diameter of 3.68 phi (0.078 mm) and a standard deviation of 0.79 phi (+0.57 mm, –0.033 mm) and predicts this distribution by three subpopulations: (1) crystals (mode = 0.210 mm), (2) lithic fragments (mode = 0.099 mm), and (3)

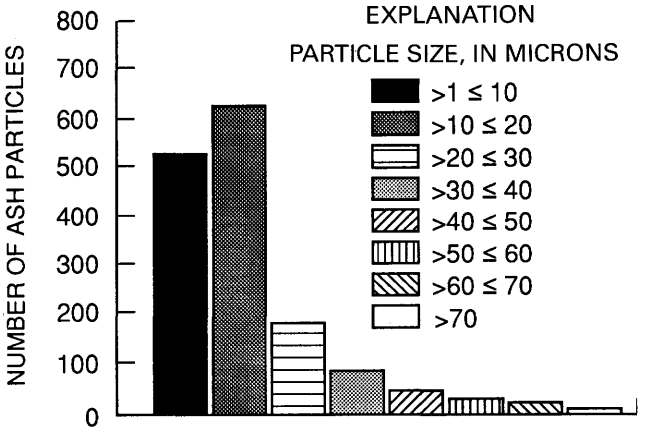


**Figure 2.** Size distribution of all minerals contained in ash from the December 15, 1989, eruption of Redoubt Volcano.

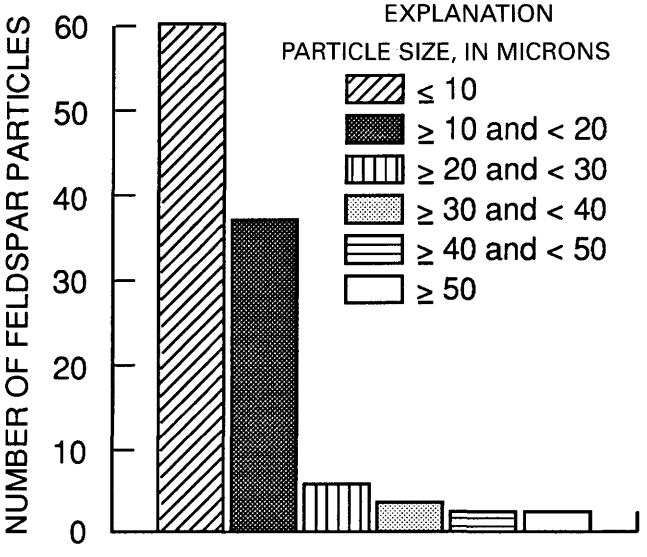


**Figure 3.** Size distribution of feldspar minerals from the December 15, 1989, eruption of Redoubt Volcano.

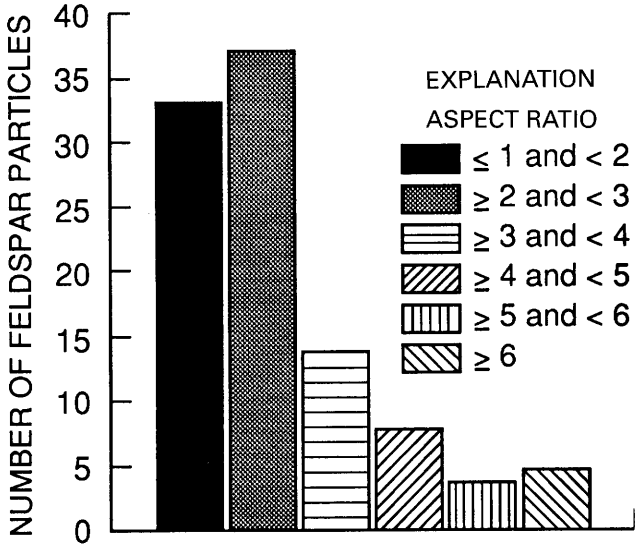


**Figure 4.** Aspect ratios of feldspar particles from the December 15, 1989, eruption of Redoubt Volcano. Aspect ratio is determined by dividing the longest diameter by the shortest diameter.

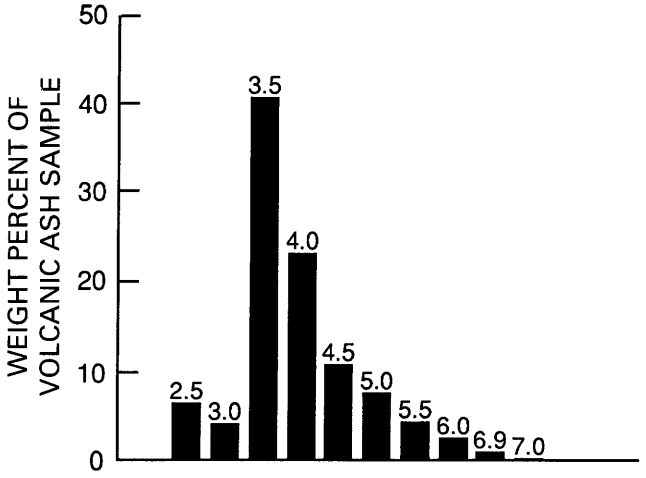


**Figure 6.** Phi size distribution plot of ash particles from the December 15, 1989, eruption of Redoubt Volcano. Phi = $-\log_2 \times$ (diameter in mm). Individual bars along *x*-axis are labeled with size in phi units.

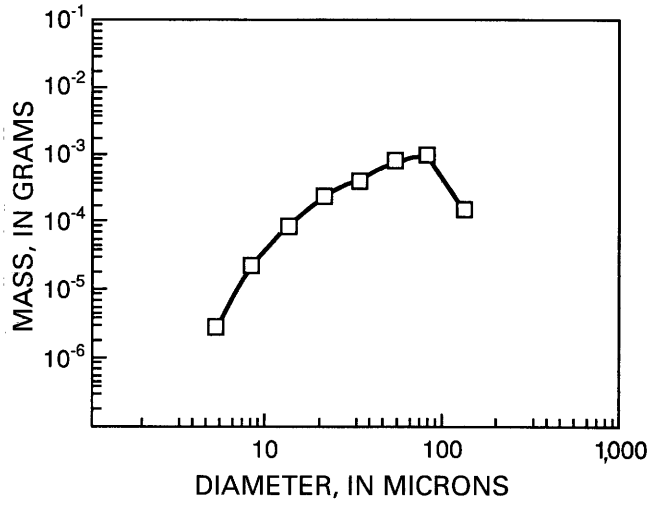


**Figure 5.** Mass distribution curve of ash particles found in ash from the December 15, 1989, eruption of Redoubt Volcano.

glass (mode = 0.041 mm). The dispersion values of these subpopulations are analogous to standard deviations for log-normal distributions. In addition, the dispersion values have physical significance: with increasing dispersion, subpopulation distributions are generally more peaked, which results from more evolved particle fragmentation and size sorting. The crystal subpopulation (1) has a dispersion value of 0.50, which reflects the tight distribution in size determined by growth kinetics. Positive dispersion values generally come about from particle aggregation or nucleation, whereas negative values arise from fragmentation and attrition. In contrast, the glass subpopulation (3) has a dispersion value of –0.51, which is a function of its fragmentation and transport history (dispersion values of –0.6 or greater are typical of fragmentation by water-magma interaction). The lithic subpopulation (2) has a dispersion value (0.15) that indicates some aggregation after its fragmentation.

The statistical summary (table 3) gives overall averages for many important parameters of the volcanic ash sample. This summary can be used to study the differences between different ashes or samples of the same ash.

**Subpopulation size characteristics analyzed by the sequential fragmentation/transport (SFT) model of Wohletz and others (1989).**

[See Wohletz and others (1989) for additional explanation]

| Subpopulation | Mode | | Dispersion | Fraction |
|---|---|---|---|---|
| | phi | mm | | |
| Crystals | 2.25 | (0.210) | 0.50 | 0.08 |
| Lithic fragments | 3.34 | (0.099) | 0.15 | 0.07 |
| Glass | 4.60 | (0.041) | –0.51 | 0.21 |

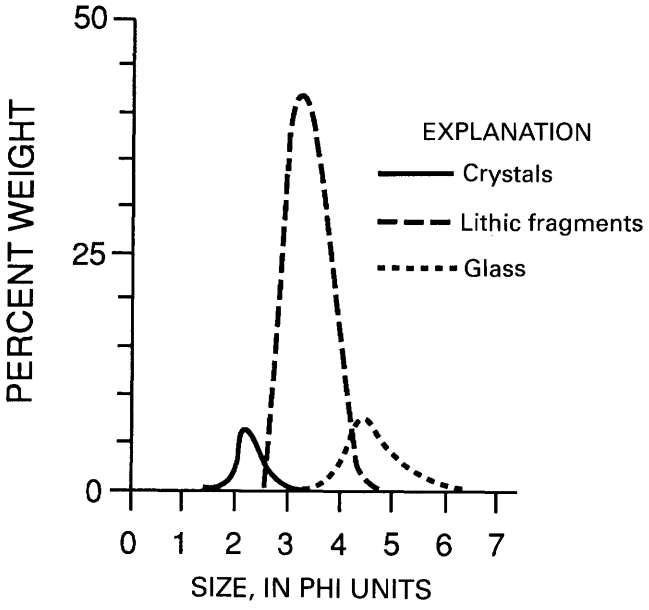


**Figure 7.** Subpopulation size characteristics of ash from the December 15, 1989, eruption of Redoubt Volcano.

## CONCLUSIONS

To understand the nature of volcanic ash clouds, we must understand the nature of the particles that make up the cloud. By combining SEM and optical petrographic techniques with powerful software analysis and theories on particle transport, we obtain detailed information on the characteristics of the particles in volcanic ash clouds. The characteristics of the ash cloud will determine where it goes, how long it will stay in the atmosphere, how much damage it will cause to an aircraft, and its effects on the environment.

**Table 3.** Statistical summary for Redoubt volcanic ash from December 15, 1989, eruption.

| | Average | Standard deviation | Maximum |
|---|---|---|---|
| Diameter (μm) | 13.3 | 12.9 | 141.0 |
| Aspect ratio | 3.5 | 3.1 | |
| Area ($\mu m^2$) | 284.0 | 889.8 | 11,989.0 |
| Density ($g/cm^3$) | 2.42 | 0.79 | 6.6 |

The volcanic ash ingested by the Boeing 747-400 that encountered the Redoubt ash cloud on December 15, 1989, has characteristics of material derived from eruption of andesitic magma by rapid release of high-pressure gases, perhaps by a hydrovolcanic mechanism. Optical microscope inspection revealed glass, blocky shards of minerals, and hydrothermally altered andesitic rock fragments. The chemical analysis derived from SEM analysis confirms the andesitic nature of the ash. Size analysis shows fragmentation characteristic of an evolved fragmentation process, such as is expected for a water-magma interaction. The shape analysis revealed dominantly low shape factors, characteristic of hydrovolcanic ash. Knowing the chemical composition and finding that a large fraction of particles have a glass structure, the melting-temperature range can be estimated.

## REFERENCES CITED

Brantley, S.R., ed., 1990, The eruption of Redoubt Volcano, Alaska, December 14, 1989–August 31, 1990: U.S. Geological Survey Circular 1061, 33 p.

Nye, C.J., Swanson, S.E., and Miller, T.P., 1990, The 1989–1990 eruption of Mt. Redoubt—Magma chemistry [abs.]: Eos, Transactions, American Geophysical Union, v. 43, p. 1705.

Wohletz, K.H., Sheridan, M., and Brown, W., 1989, Particle size distributions and the sequential fragmentation/transport theory applied to volcanic ash: Journal of Geophysical Research, v. 94, p. 15703–15721.

VOLCANIC ASH AND AVIATION SAFETY:
Proceedings of the First International Symposium
on Volcanic Ash and Aviation Safety
U.S. GEOLOGICAL SURVEY BULLETIN 2047

# THE CONCENTRATION OF ASH IN VOLCANIC PLUMES, INFERRED FROM DISPERSAL DATA

*By* Marcus I. Bursik, R.S.J. Sparks, Steven N. Carey, *and* Jennie S. Gilbert

## ABSTRACT

The mass concentration of pyroclasts of a particular grain size decreases as an exponential function of time in the body of the umbrella cloud that forms at the top of explosive volcanic-eruption plumes. Data on deposit-thickness variations and grain-size distributions of ash deposits can be used to infer particle concentrations in volcanic clouds using a simple physical model for sedimentation from umbrella clouds. The concentrations of ash in plumes that penetrate the operating heights of commercial aviation greatly exceed the concentrations that cause engine damage and failure ($> 2{,}000$ mg/m$^3$) and dangerous concentrations ($> 50$ mg/m$^3$) can persist for hundreds of kilometers downwind of the vent. However, aggregation of volcanic ash in the atmosphere can lead to much more rapid decreases in concentration.

## INTRODUCTION

Volcanic plumes spreading rapidly within the atmosphere pose a serious risk to aviation. The umbrella cloud formed at the top of a volcanic eruption column is an example of an intrusive gravity current containing suspended particles spreading within a density-stratified, less turbulent fluid (Allen, 1985; Sparks, 1986; Simpson, 1987; Self and Walker, this volume; Sparks and others, this volume). Volcanic particles remain suspended in such currents as far as hundreds of kilometers from the vent. We have developed a theory describing sedimentation from such currents and have successfully used it to evaluate the dispersal of particles from currents of contrasting scales, geometries, and source fluids (Sparks and others, 1991; Bursik and others, 1992a). We review the theory and introduce a way to reconstruct ash concentrations within a volcanic cloud from sedimentological data on tephra-fall deposits. These results can be used to infer ash concentrations that might be expected at various distances during hypothetical modern eruptions. We consider the sedimentation of individual particles from clouds with radial symmetry and infer pyroclast concentrations within the clouds. We also investigate the concentration of suspended particles within currents in which the flow has been distorted into an elongated shape by wind. Finally, we consider a generalization of the model and estimate concentrations of particles within umbrella clouds for given plume heights and initial grain-size populations.

Our approach is a valid representation of sedimentation from plumes for times and distances from the volcanic vent before the coherent gravity current thins significantly by gravity flow and sedimentation and is subsequently broken up by ambient atmospheric turbulence (Allen, 1985; Simpson, 1987). Thus, the model is certainly valid for the area near the vent and is probably valid for great distances from the vent because umbrella clouds can begin as flows several kilometers thick. Bursik and others (1992b) have shown that the dispersal of the Mount St. Helens plume is consistent with gravity-current behavior up to a distance of 600 km from the vent. After current break-up, diffusion-type models (Suzuki, 1983; Armienti and others, 1989) can be used to infer particle concentration, transport, and deposition by atmospheric advection and turbulence.

## SEDIMENTATION THEORY

For particles uniformly distributed within a fluid by turbulence, Hazen (1904) showed that the incremental number of particles deposited is proportional to the number per unit thickness of fluid times the thickness of the layer from which particles could be expected to fall. Einstein and Krone (1962) and Martin and Nokes (1988) obtained similar relationships for deposition of suspended particles in flumes and small laboratory tanks where no particles are resuspended. Applying these results to a turbulent gravity current flowing within a stratified fluid as an interflow or intrusion (Manins, 1976), we suggest that the total mass of particles, $m$, of a given size fraction being transported within a control volume moving with the fluid decreases as:

$$dm = -A\chi(0)\,v(0)\,dt \qquad (1)$$

where

$A$ is the area of the lower interface of the fluid parcel,

$\chi(0)$ is the mass concentration of particles of a given size fraction at the base of the volume,

hence, $A\chi(0)$ is the mass of particles per unit height in the volume at its base,

$v(0)$ is the terminal fall velocity of the particles at the base,

$t$ is time,

hence, $v(0)\,dt$ is the thickness of the fluid layer from which particles settle out.

If $\langle\chi\rangle$ is the mean concentration of particles averaged over the current thickness, $h$, then $A\langle\chi\rangle = m/h$, and the differential equation expressing the loss of particles from the current can be written:

$$\frac{\partial m}{\partial t} + \boldsymbol{u}\nabla m = -\frac{m}{kh(t)}v(0) \qquad (2)$$

where

$\boldsymbol{u}$ is current velocity, and

$k = \langle\chi\rangle/\chi(0)$, which is a constant if similarity is maintained.

It can be shown that, by making the proper substitutions in equation 1, equation 2 holds for concentration, $\chi$, as well as mass, $m$. Although gravity currents are inherently transient, conditions within the body of such a flow are approximately steady at a large distance from the advancing front. For steady flow, equation 2 holds not only for $m$ and $\chi$ but also for the mass of particles carried by the current through time, $M = m\pi$, where $\pi$ is any finite time. If $\pi = T$, eruption duration, then $M$ is the mass of material deposited beyond any given distance. Furthermore, for any downcurrent distance, $\xi$, equation 2 can be directly integrated, resulting in:

$$M = M_0 \exp\left\{-\int_0^x \frac{v(0)}{kh(\xi)\,u(\xi)}d\xi\right\} \qquad (3)$$

and

$$\langle\chi\rangle = \langle\chi_0\rangle \exp\left\{-\int_0^x \frac{v(0)}{kh(\xi)\,u(\xi)}d\xi\right\} \qquad (4)$$

where

$M_0$ and $\chi_0$ are boundary values.

There are two cases of volcanological interest to consider when evaluating the integral on the right hand side of equations 3 and 4. In the first case, the umbrella cloud is axisymmetric, resulting from radial spreading in a still atmosphere (fig. 1*A*). The second case arises when the cloud is modified by wind to assume an elongated shape (fig. 1*B*). We examine these two situations below, then we extend the results to a generalized geometry.

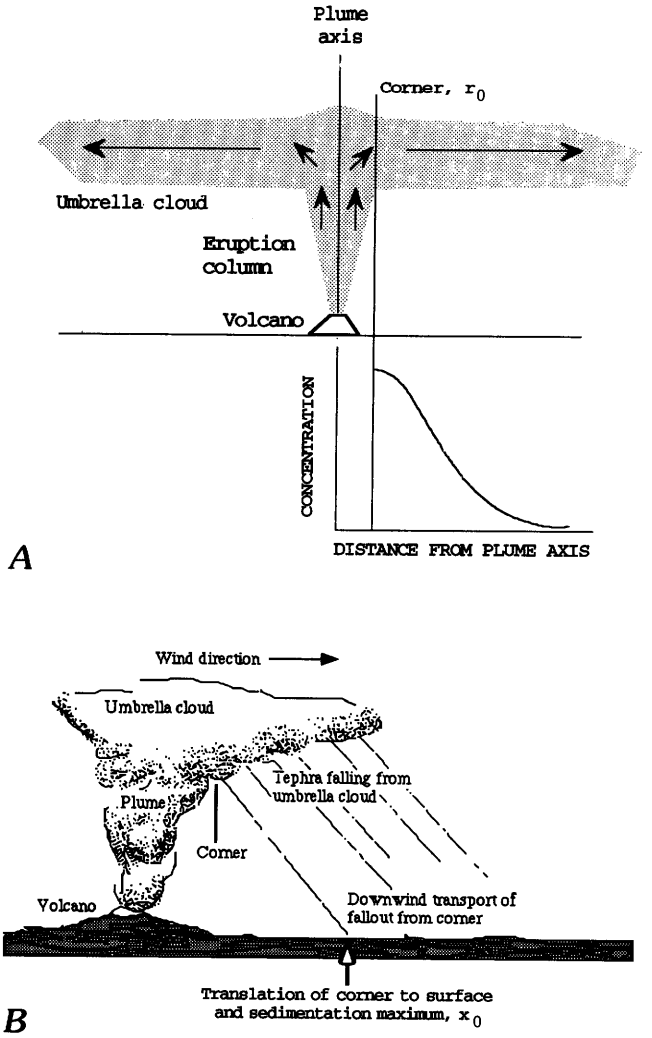


**Figure 1.** *A*, Diagram showing a physical model of the sedimentation of tephra of a particular grain size around an eruption column with no wind. The graph shows the variation of particle concentration for one grain-size fraction within the umbrella cloud. Sediment mass per unit area on the ground (unit sedimentation), $S = -dM/dr\ (1/2\pi r)$, varies in the same manner. *B*, Schematic diagram of the lateral transport of ash by wind from the corner of the column to illustrate downwind displacement of the accumulation maximum, $x_0$.

## RADIAL GEOMETRY

We first consider the case of axisymmetric (radial) flow developed at the top of a volcanic eruption plume with no wind. In the volcanic column that feeds the umbrella cloud, vertical velocities are typically 50 to over 200 m/s (Woods, 1988). Although coarse tephra falls out at the plume margins, the high velocities result in most tephra being transported to the plume top where it is swept into the umbrella current. At the height of neutral buoyancy, where the column density equals the density of the surrounding atmosphere,

the plume diverts laterally and there is a rapid decrease in vertical velocity at a well-defined corner (fig. 1*A*). With no crosswind, the flow is completely driven by gravity and assumes a near-radial symmetry. Tephra is supported by turbulence within the current as it falls out at the base into the underlying quiescent atmosphere.

Integration of the right hand side in equation 3, assuming conservation of volumetric flux, $Q$, between the ascending column and the current (thus $Q = 2\pi rhu$ and $dQ/dr = 0$) leads to the result:

$$M = M_0 e^{-\pi v (r^2 - r_0^2)/Q} \tag{5}$$

where

$r_0$ is the radial distance of the plume corner from the vent (fig. 1*A*), and

$M_0$ is the mass injected into the current during the eruption.

The mass of particles deposited in concentric rings of unit width on the ground is thus given by $-dM/dr$:

$$\frac{-dM}{dr} = \frac{2\pi v r M_0}{Q} e^{-\pi v (r^2 - r_0^2)/Q} \tag{6}$$

Sparks and others (1991) have presented laboratory experiments on sedimentation of particles from radially expanding gravity currents generated by turbulent, particle-laden plumes that show good agreement with the theory in a form analogous to equation 6.

Bursik and others (1992a) have compared the sedimentation theory to grain-size-distribution data of the Fogo A Plinian deposit on Sao Miguel in the Azores (Walker and Croasdale, 1971). Values of $M_0$ and $\pi v/Q$ were determined from field data for each grain-size class by iterative curve fitting to integrated accumulation data. The slightly elliptical geometry of the thickness contours in the Fogo deposit, caused by low winds (≅ 2 m/s) was accommodated by substituting a constant of 1.83 for $\pi$. Detailed descriptions of the deposits and analysis of the field data are presented in Bursik and others (1992a). Beyond 7 km, the field data give excellent fits to the Gaussian functions (fig. 2*A* and 2*B*) with the slopes dependent on grain size as predicted by equation 5. Tephra in the size range 500 to 2,000 μm settles through the atmosphere with a speed determined by the relationship for fall at high Reynolds number (Woods and Bursik, 1991). We therefore expect the coefficient $1.83v/Q$ to be proportional to the square root of the grain diameter. Figure 2*C* shows that the Fogo data fit this prediction well. From the data in figure 2*C*, the value of $Q$, hence the total plume height and magma discharge rate, can be estimated for the eruption. The estimated total plume height of 21 km and magma discharge rate of $1.1\times10^4$ m$^3$/s, assuming an eruption temperature of 800°C, are in reasonable agreement with an independent assessment of the plume height (27 km) and magma discharge rate ($5.3\times10^4$ m$^3$/s) based on the maximum dispersal of lithic clasts.

The above results can be used to infer particle concentrations within the Fogo A umbrella cloud. Given known masses of particles, $M$, deposited beyond a radial distance, $r$, the average concentration is given by:

$$\langle \chi \rangle = \frac{M}{QT} \tag{7}$$

where

$T$ is equal to about 12 hours (Carey and Sigurdsson, 1989).

Equation 7 can be applied to each of six grain-size fractions and the results summed to obtain the total concentration of lithics plus crystal fragments that are > 500 μm:

$$\sum_{i=1}^{6} \langle \chi \rangle_i = \frac{\sum_{i=1}^{6} M_i}{QT} \tag{8}$$

Because lithics and crystals constitute about 14 percent of the deposit mass at each locality (Walker and Croasdale, 1971), we can then estimate the average concentration of all clasts that are > 500 μm within the spreading umbrella cloud along the main (eastward) dispersal axis (fig. 2*D*). The results suggest that the cloud contained a rather concentrated suspension of these particles, with the smallest fraction becoming enriched relative to larger size fractions with distance from vent. For the Fogo A eruption, concentration dropped by an order of magnitude as the cloud spread downwind about 10 km. Note also that the concentration of pyroclasts that are > 500 μm was probably > 50 mg/m$^3$ up to 20 km from the vent. Even so, most of the ash within the cloud was probably considerably smaller than 500 μm in diameter and remained in the atmosphere for great distances from the volcano.

## VOLCANIC UMBRELLA CLOUD MODIFIED BY A CROSSFLOW

For cases in which the volcanic umbrella current has been distorted by prevailing winds, it is useful to rewrite equation 3 in the form:

$$M = M_0 \exp\left\{\int_{x_0}^{x} \frac{vw}{Q} d\xi\right\} \tag{9}$$

where

$x$ is downwind distance, and

$w$ is the maximum crosswind width to which the current has expanded due to gravity.

Equation 9 is easily integrated if $v$, $Q$, and $u$ (wind speed)

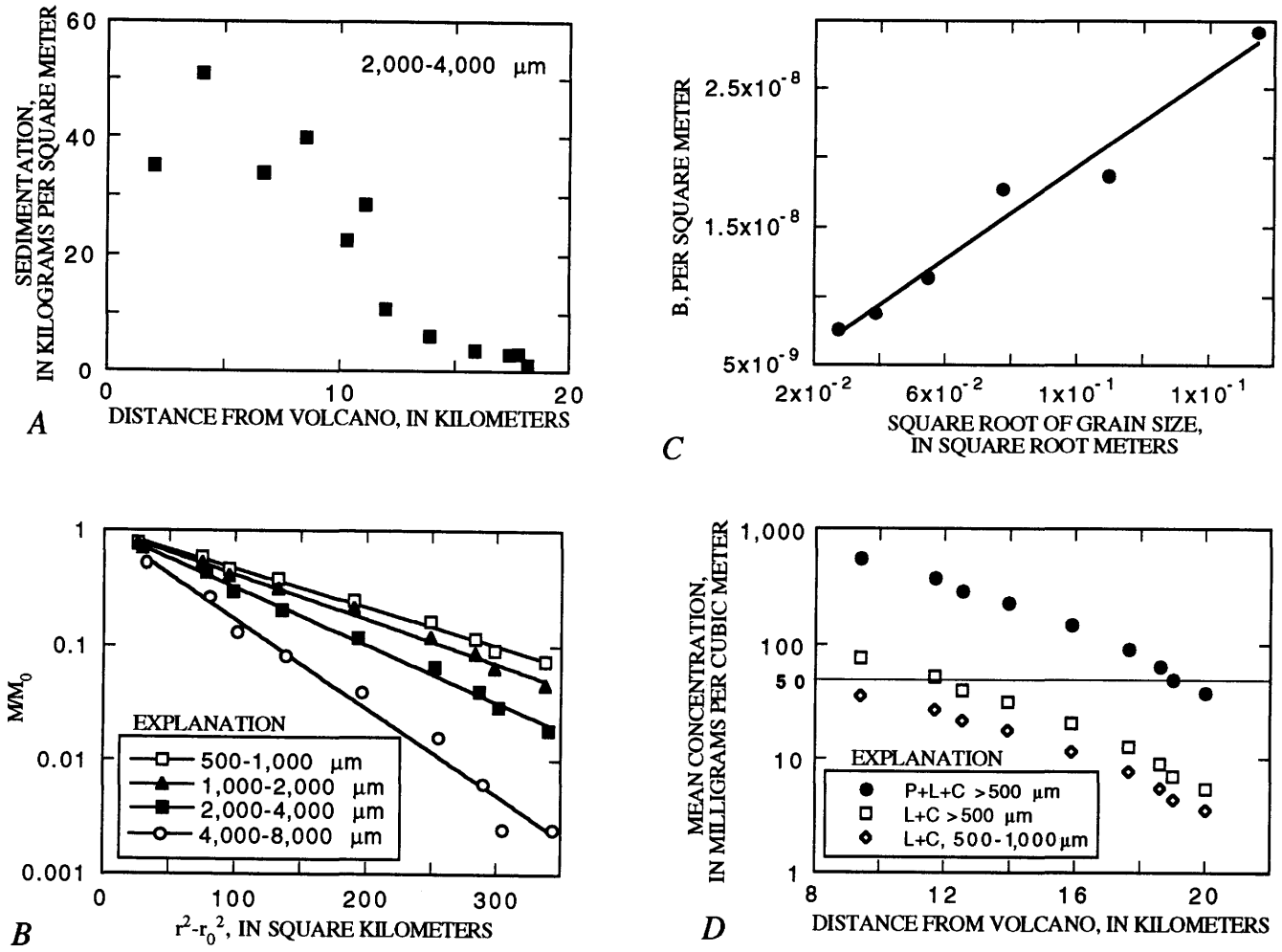


**Figure 2.** *A*, The sediment accumulation, S, of lithic clasts in the size interval 2,000–4,000 μm in the Fogo A Plinian deposit as a function of distance from vent. *B*, The natural logarithm of the ratio $M/M_0$, where $M$ is the total sedimentation beyond a given distance and $M_0$ is the boundary value, is plotted against the difference of the distance squared from the position of maximum sedimentation, $r^2 - r_0^2$. Data are shown for four different grain-size intervals, 8,000–4,000, 4,000–2,000, 2,000–1,000, and 1,000–500 μm. *C*, The Gaussian coefficient, $B = 1.83v/Q$, is plotted against the square root of grain size, showing that the data agree with the equation for settling velocity. *D*, Inferred concentration of pyroclasts in the Fogo A umbrella cloud as a function of distance from the vent along the dispersal axis. Concentrations in other directions would be somewhat lower. In this figure, $k$ (equation 2) is assumed to equal unity. P, pumice; L, lithic (rock) fragments; C, crystals.

are assumed constant, and if $dw/dt = u\ dw/dx = (g'h)^{1/2}$, where $g'$ is the reduced gravity and $h$ is current thickness, assumed constant for any $x$. Because the atmosphere is continuously stratified and the plume thins downwind, $(g'h)^{1/2}$ becomes $\lambda Nh$, where $\lambda$ is a constant of order unity that depends on flow geometry and ambient stratification (Simpson, 1987; Woods and Kienle, this volume) and $N$ is the buoyancy frequency of the atmosphere with a value of approximately 0.035 $s^{-1}$. Under these assumptions, $w$ is given by:

$$w = (2\lambda NQx)^{1/2}/u \qquad (10)$$

The solution to equation 9 is therefore:

$$M = M_0 \exp\left\{-\frac{2v}{3u}\sqrt{2\lambda N/Q}\left(x^{3/2} - x_0^{3/2}\right)\right\} \qquad (11)$$

where

$x_0$ is the distance to the maximum in mass accumulation on the ground for a particular size fraction.

The sedimentation within a unit area (unit sedimentation), $S = (-dM/dx)(1/w)$, can furthermore be shown to be equal to:

$$S = S_0 \exp\left\{-\frac{2v}{3u}\sqrt{2\lambda N/Q}\left(x^{3/2} - x_0^{3/2}\right)\right\} \qquad (12)$$

Satellite observations of the current generated by the initial blast/surge cloud of Mount St. Helens on May 18, 1980, and the subsequent Plinian tephra fall fit this model well. The blast (phase I) cloud as well as the later phase III cloud migrated downwind at a velocity of 28 m/s (Sarna-Wojcicki and others, 1981; Criswell, 1987) to distances of at least 600 km (15:15 PDT in fig. 3*A*), and the observed lateral expansion with distance agrees with equation 10, once the current attained the assumed geometry at about 10:45 PDT (fig. 3*B*). Using equation 10 and the above values for $N$ and $u$, we infer that $\lambda Q \cong 3.9\times10^9$ m$^3$/s.

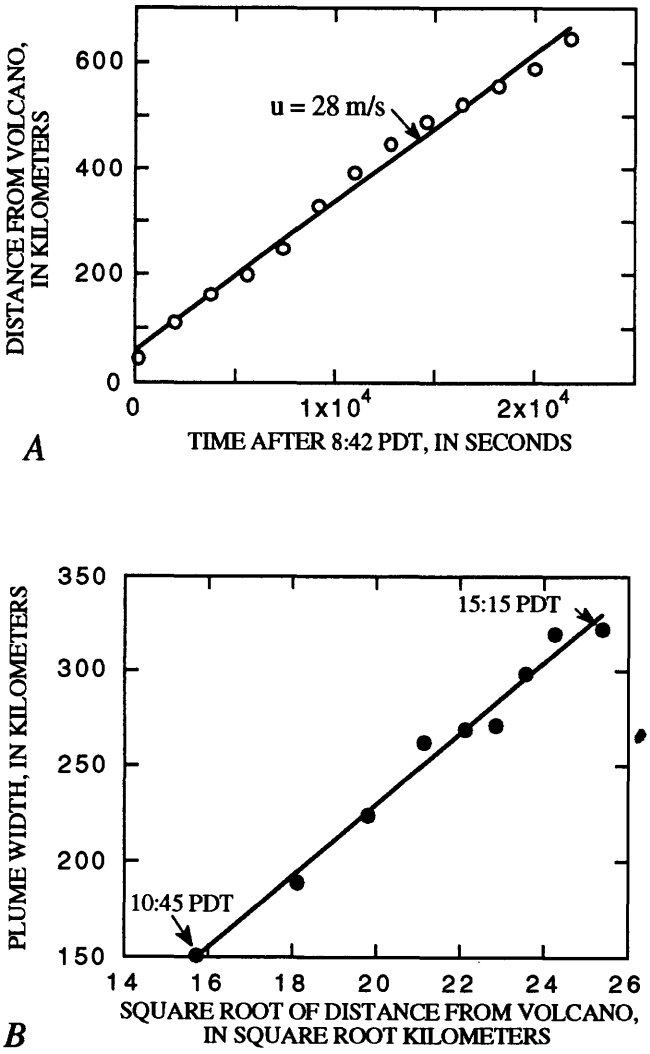


**Figure 3.** Data on the geometry and speed of the distal current generated by Mount St. Helens on May 18, 1980 (taken from Sarna-Wojcicki and others, 1981). *A*, The speed, $u$, of the eastward drift of the current front, 28 m/s, agrees well with wind speeds measured within the region of approximately 30 m/s (Sarna-Wojcicki and others, 1981; Carey and Sigurdsson, 1982; Sparks and others, 1986; Criswell, 1987). *B*, The development of plume width, $w$, with distance follows equation 10 (see text). Width was measured as the greatest north-south extent of the current at the times and maximum distances shown in *A*.

Crystal accumulation data for the 2.5-, 3-, 3.5-, and 4-$\phi$ (177-, 125-, 88-, and 63-μm) size fractions of the May 18 ash fall deposit show maxima that increase in distance from the volcano with decreasing grain size (fig. 4). Virtually all of the ash at these distances was deposited from the Plinian plume (Carey and others, 1990). These peaks probably represent the downwind translation of each sedimentation curve from the corner region between the column margin and laterally moving gravity current (fig. 5*A*). Thus, significant downwind transport occurred after the crystals fell from the base of the umbrella region. This is in contrast to the proximal data for the Fogo A ash fall deposit, where the accumulation peaks for coarser particles are displaced only negligibly one from another. Accumulation data on the downwind side of the maxima fit equation 12 well (fig. 5*B*), with a decrease in sedimentation with distance that is a function of particle settling velocity, $v$. We note that this Plinian deposit was not formed from the giant cloud generated in the initial blast but from the eruptive activity that followed it. We are therefore assuming in our analysis that the lateral spreading of the Plinian plume was similar to that of the initial mushroom cloud.

For particles in the size range 63 to 177 μm, the fall velocity, $v$, is a complex function of grain size (Bursik and others, 1992b; Armienti and others, 1989). The exponential constant in equation 12 should be proportional to the fall speeds given by Armienti and others (1989). Thus, the exponential constant in equation 12, which is proportional to $v$, should be proportional to the square root of the grain diameter. The data agree with this prediction (fig. 5*C*). The slope, $2(2\lambda N/Q)^{1/2}/3u$, has a value of $8.35\times10^{-8}$. Using wind values from Carey and others (1990), we infer that $\lambda/Q = 1.8\times10^{-10}$ s/m$^3$. Combining the values for $\lambda Q$ and $\lambda/Q$ leads to the conclusion that $\lambda \cong 0.83$, $Q = 4.7\times10^9$ m$^3$/s, and plume height above vent, $H$, ≅ 20 km, which agrees reasonably well with observed plume heights of 11–17 km observed during the Plinian phase (Harris and others, 1981) and heights of 13–16 km calculated from the dispersal of the largest clasts (Carey and others, 1990). We can examine the translation of particles below the umbrella region (fig. 5*A*) by calculating the transport using the wind intensities recorded in the area of Mount St. Helens on the morning of May 18 (Carey and Sigurdsson, 1982). The trend of the observed data crosses the predicted trends, with agreement occurring for the 177- and 125-μm fractions. Significant deviations are found to occur for grain sizes of less than 63 μm, with the predicted transport distances being much larger than the observed. This divergence is likely due to the process of particle aggregation, which resulted in the premature deposition of fine ash and the production of a secondary thickness maximum in the area of Ritzville, Wash. (Carey and Sigurdsson, 1982).

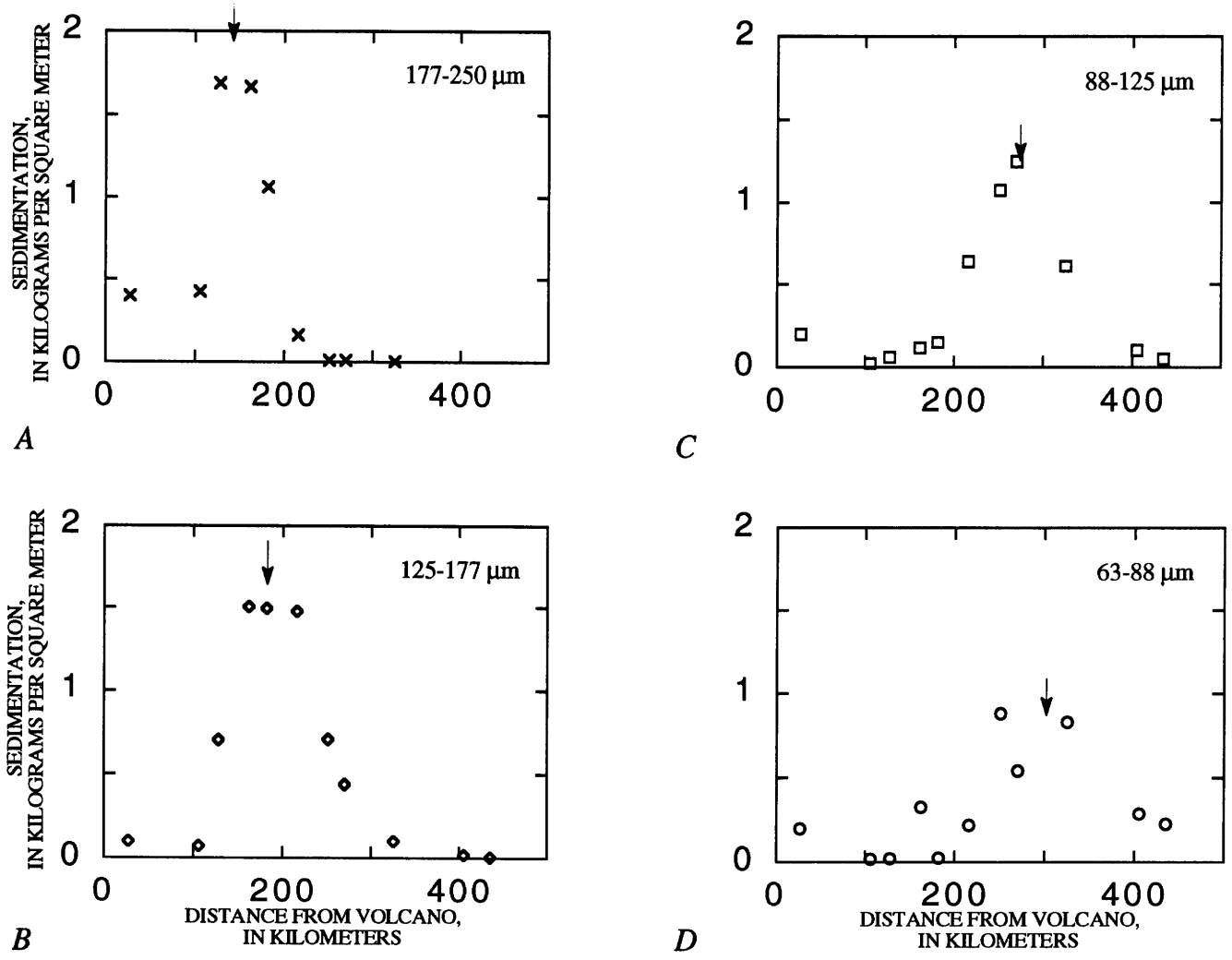


**Figure 4.** Downwind variation of felsic crystal unit sedimentation, $S$, in kg/m$^2$, with distance from the vent for the $A$, 177–250-μm size class; $B$, 125–177-μm size class; $C$, 88–125-μm size class; and $D$, 63–88-μm size class for the Mount St. Helens May 18, 1980, Plinian deposit. Accumulation maxima (peaks) from the fit of 7th-order polynomials to the data are indicated with arrows.

Concentrations within the umbrella cloud of the crystal size fractions can be calculated from:

$$\langle \chi \rangle = Sv/Tu^2 \qquad (13)$$

The May 18 eruption had a duration, $T \cong 8$ hours, hence all variables in equation 13 can be constrained with available data. Figure 5*D* is a plot of the estimated decrease of concentration of the felsic crystal fractions from 63 to 177 μm along the dispersal axis, to the east of the volcano. The concentration of these crystal fractions is rather dilute, being below the critical value of 50 mg/m$^3$. However, the crystals constitute less than about 50 percent of the total mass in each of these grain-size fractions, and most of the deposit is finer than 63 μm (Carey and Sigurdsson, 1982). As with the Fogo A cloud, the larger grain-size fractions become depleted relative to the smaller fractions with increasing distance because of their higher fall velocities. A strong wind decreases the sedimentation of pyroclasts at a given distance (equation 12). The 20 m/s wind at the base of the May 18 cloud allowed the concentration of these crystal fractions to drop by an order of magnitude only after the cloud spread downwind about 100 km, and concentration of the 63- to 177-μm crystal fractions alone was still >1 mg/m$^3$ at 100 km from vent.

## THEORETICAL PARTICLE-CONCENTRATION VARIATIONS

Reasonable agreement exists between sedimentological observations and the theoretical model of flow and sedimentation in volcanic umbrella clouds. We have shown that the sedimentological data can be used ("inverted") to infer

particle concentrations within volcanic plumes (equations 7, 8, and 13). The model can also be used in a "forward" sense to predict concentrations of particles in hypothetical plumes with distance from a volcano as a function of plume height and wind conditions. Even though a fully comprehensive model of plume dispersal by the wind has not been developed, some useful guidelines on likely concentrations can be given.

We have calculated ash concentrations as functions of distance from the vent for specific, end-member cases of plume geometry. For this purpose, we have chosen a model grain-size distribution, given in table 1, which is typical of the grain-size distributions estimated for Plinian eruptions (Woods and Bursik, 1991). We have assumed that 70 percent by weight of the ejecta are finer than 2,000 μm and have calculated the changes in concentration of each grain size with distance. The initial concentration is related to plume height as calculated by Sparks and others (this volume). Our calculations assume one particular grain-size distribution of the ejecta, but the changes in concentration are very sensitive to the initial size distribution in the plume. This point is illustrated by calculation of the residence time of particles of different diameter in a 5-km-thick layer in the atmosphere centered at 12.9 km (39,000 ft) altitude. The estimated settling velocities of different particle sizes with a density of 2,000 kg/m$^3$ at these altitudes are listed in table 1. From this information, equation 2 can be used to estimate the time taken for the concentration of each size to decrease by 1/e of the initial concentration. This time is also that for each grain size to fall a distance of 5 km under static conditions. The orders-of-magnitude changes in residence time among the

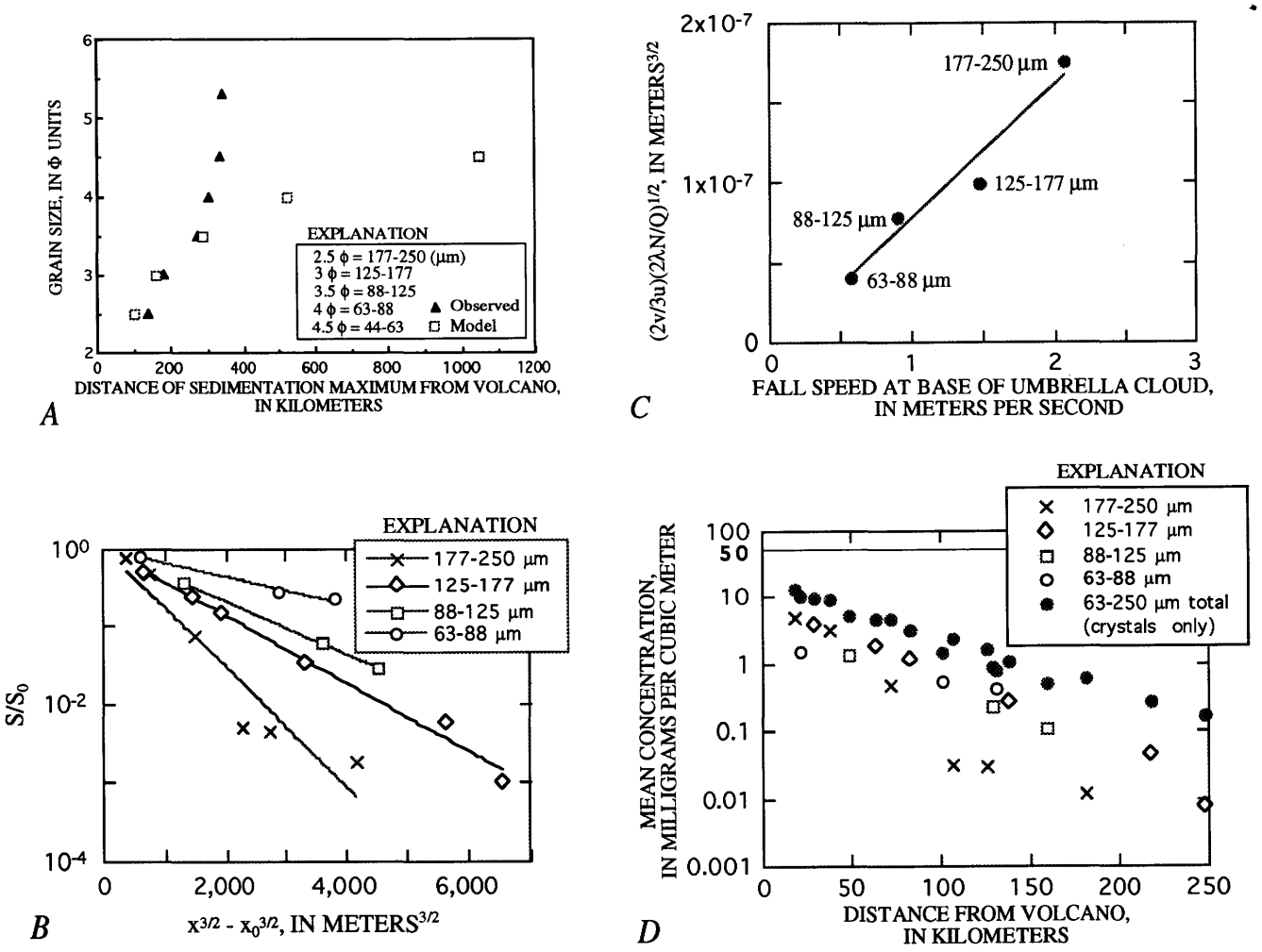


**Figure 5.** *A*, The observed positions of crystal accumulation peaks (from fig. 4) for the May 18, 1980, Mount St. Helens ash fall deposit compared to their calculated (model) positions based on their translation in the eastern Washington wind field after falling from the base of the umbrella cloud (assumed for the calculations to be at an altitude of 12 km). *B*, The decrease in normalized sediment accumulation, $S/S_0$, with distance for the Mount St. Helens fallout is consistent with a distance to the three-halves, $x^{3/2}$, dependence for the 177–250- to 63–88-μm crystal size fractions. *C*, The value of the exponent in equation 12 (see text), $2v/3u(2\lambda N/Q)^{1/2}$, is consistent with the terminal velocity for these grain-size fractions. *D*, Average crystal concentrations inferred for the Plinian umbrella cloud from data in *B* and *C*.

**Table 1.** Model grain-size distribution in weight percent for calculations of the changes of ash concentration in volcanic plumes with distance from the vent.

[The grain-size distribution assumes that 30 weight percent of the ejecta have a grain size greater than 2 mm. The estimated terminal fall velocity of each particle size with a density of 2,000 kg/m$^3$ at 12.9 km (39,000 ft) altitude is based on high-Reynolds-number settling of particles > 355 μm and on low-Reynolds-number settling of particles < 355 μm (Wilson and Huang, 1979)]

| Grain size (μm) | Weight percent | Fall speed (m/s) | Residence time |
|---|---|---|---|
| 1,400 | 9.0 | 9.0 | 9.3 min |
| 710 | 10.8 | 6.4 | 13.0 min |
| 355 | 12.4 | 3.2 | 26.0 min |
| 171 | 10.8 | 1.9 | 43.0 min |
| 90 | 9.0 | 0.64 | 2.2 h |
| 44 | 7.2 | 0.15 | 9.3 h |
| 22 | 5.4 | 0.05 | 1.1 d |
| 11 | 3.6 | 0.012 | 4.8 d |
| 5.5 | 1.8 | 0.0025 | 23.1 d |

particles typically present in plumes indicates that size distribution must have a major influence on the change of concentration with distance and time in a volcanic plume.

For dispersal in the absence of wind (equation 5), plumes that reach the stratosphere can form umbrella clouds that maintain high concentrations for substantial distances from the volcano (fig. 6*A*). For example, a 22.8-km-high plume still has a concentration of 2,000 mg/m$^3$ at 100 km, and a 9.8-km-high plume has a concentration of 50 mg/m$^3$ at 200 km distance. The sensitivity of concentration variations to total grain-size distributions is illustrated by the variations of the relative concentrations of each grain size with distance for a 22.8-km-high (75,000 ft) plume (fig. 6*B*). Large grain sizes decrease their concentration much more rapidly.

Dispersal by a constant wind blowing much faster than the gravitational spreading speed can be approximated with a cloud layer of constant thickness and width. Our calculations suggest that wind speed plays an important role in determining the concentrations of ash likely to be encountered by aircraft in dispersing plumes (fig. 7*A*). These calculations, however, do not take into consideration particle aggregation, which is likely to decrease concentrations from those predicted because of premature fallout. A number of studies (Sorem, 1981; Brazier and others, 1982; Carey and Sigurdsson, 1982; Gilbert and others, 1991) have shown that fine ash particles aggregate in the plumes and consequently fall out much more rapidly than predicted by consideration of the fall velocities of individual particles. Observations indicate that particles less than 63 μm are strongly susceptible to aggregation processes. For example, much of the sub-63-μm ash in the May 18th plume of Mount St. Helens fell out at 300 to 450 km to produce secondary thickening of the ash deposit (Carey and Sigurdsson, 1982). To illustrate the effect of aggregation on our results we have assumed that all the particles less than 63 μm in the size distribution of table 1 fall as aggregates with sizes from 90 to 1,400 μm. We assume that these aggregates are evenly distributed in each of the size intervals above 63 μm and have calculated the variation of concentration with distance in a 10 m/s wind. Figure 7*B* compares these calculations with the case of individual particle fallout and shows that ash concentration decreases much more rapidly with aggregation. These calculations indicate that much more needs to be known about aggregation processes in order to predict concentrations of ash in volcanic clouds.

The model can be generalized by calculating concentration as a function of area to which the cloud has spread. Equation 4 can be written in the form:

$$\langle \chi \rangle = \langle \chi_0 \rangle \exp\left\{-\int_0^x \frac{vp}{Q} d\xi\right\} \qquad (14)$$

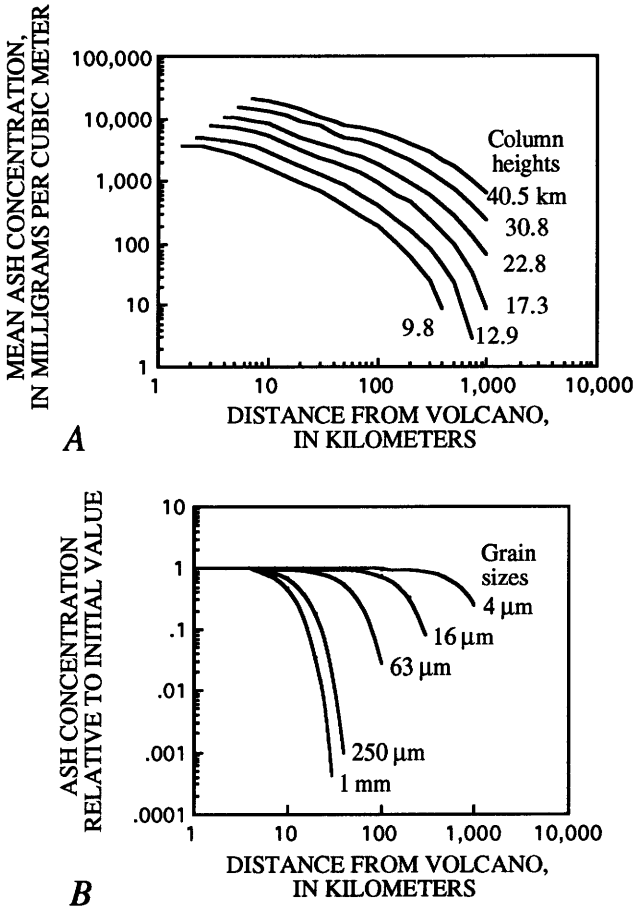


**Figure 6.** *A*, Ash concentration in an umbrella cloud (in mg/m$^3$) is plotted against distance for six different column heights and for dispersal in the absence of wind. *B*, Relative concentration of ash is plotted against distance for each grain size class for a 22.8-km-high column in the absence of wind.

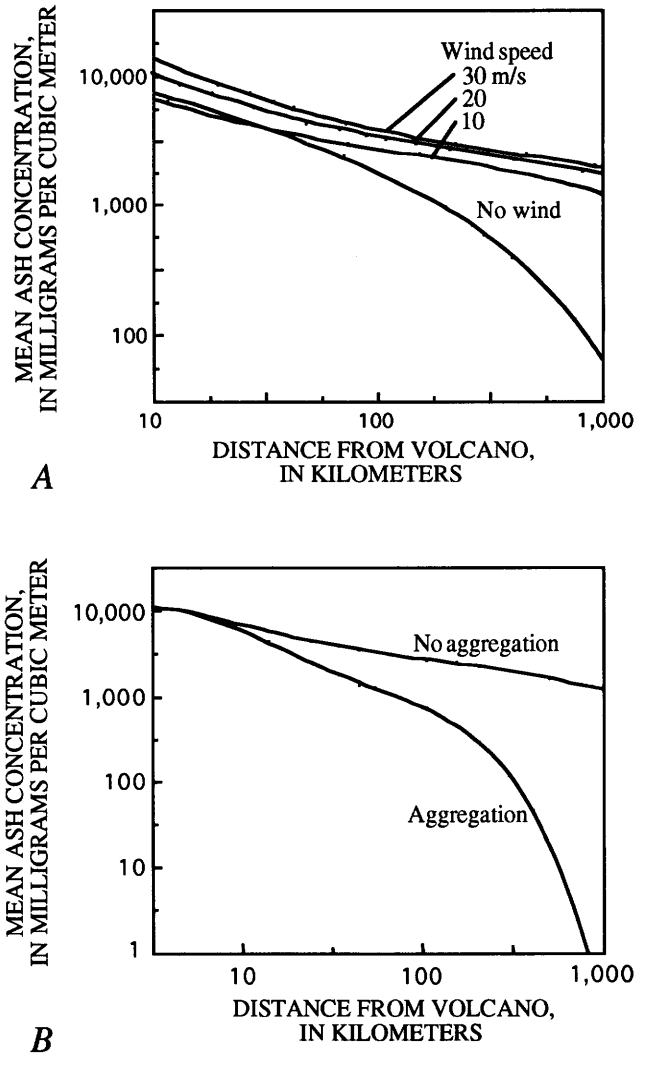


**Figure 7.** *A*, Concentration of ash (in mg/m$^3$) is plotted against distance for a 22.8-km-high column erupted in no wind and for downwind transport of a layer 5 km thick with its base at 15.9 km altitude for wind velocities of 10, 20, and 30 m/s, and for the case of no wind. *B*, Comparison of the downwind change in ash concentration between the case of individual fallout of all sizes and the case where particles less than 63 μm aggregate. Calculations are for a wind speed of 10 m/s and a 5-km-thick layer with base at 15.9 km. Details of the calculations with particle aggregation are given in text.

where

$p = Q/uh$ is the outer perimeter of a control volume defined by an isochronous surface to which material had spread by a certain time within the umbrella cloud.

Integration of (14) thus yields:

$$\langle \chi \rangle = \langle \chi_1 \rangle e^{-vA/Q} \qquad (15)$$

where

$\chi$ is measured at the perimeter of $A$, the area to which particles of a given grain size have traveled, and

$\chi_1 = \chi_0 e^{A_0 v/Q}$, the "virtual" sedimentation at $A = 0$.

If plume height, $H$, and the total grain-size distribution of material entering the umbrella cloud can be estimated, then equation 13 can be applied to predict the total concentration of particles within the cloud, $\langle \chi_T \rangle$. $\langle \chi_T \rangle$ is the sum of the concentration of particles within each of $N$ individual particle-size classes:

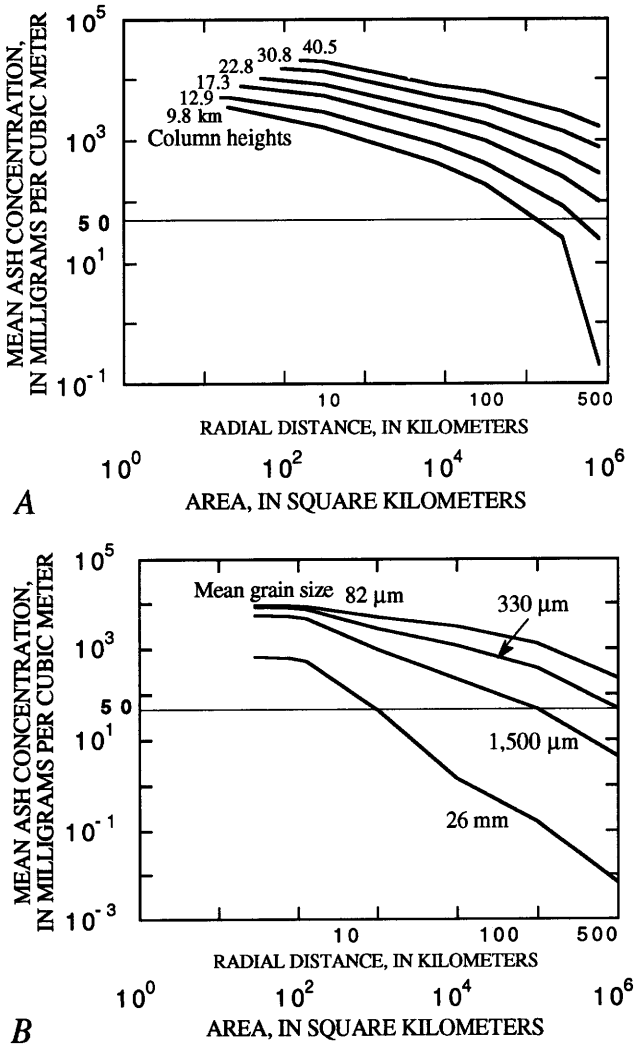


**Figure 8.** *A*, Ash concentration as a function of the area encompassed by an isochronous surface within the umbrella cloud for column heights from 10 to 40 km. The grain-size distribution is that from table 1. *B*, Concentration variation for different total grain-size distributions with means shown next to curves. The standard deviation, in $\phi$ units, for each curve was assumed to be 2.5. Distributions are for phreato-Plinian/coignimbrite (mean = 82 μm), Vulcanian (330 μm), Plinian (1,500 μm), and Strombolian (26 mm) eruptions (Woods and Bursik, 1991).

$$\langle \chi_T \rangle = \sum_{i=1}^{N} \langle \chi_{i1} \rangle e^{-v_i A/Q} \qquad (16)$$

where

$\chi_{i1}$ is the sedimentation at $A = 0$, and

$v_i$ is the terminal velocity of the $i$th particle-size class, and

$Q \cong 713H^{5.3}$ (Bursik and others, 1992a).

We have estimated concentrations with area for a range of particle-size distributions and eruption-plume heights. We have used four different particle-size distributions covering the range typical of various types of eruptions (Woods and Bursik, 1991). Figure 8*A* shows calculations for plume heights from 10 to 40 km. Even relatively small Plinian plumes, approximately 10 km high, will have dangerously high concentrations of pyroclasts over large areas ($\cong 10^6$ km$^2$). Figure 8*B* compares calculations for a 17.3-km plume with different grain-size models. As expected, plumes that contain finer grained material, such as those generated by coignimbrite or phreato-Plinian eruptions (Wilson, this volume), will retain dangerous concentrations as they spread to encompass large areas ($\cong 10^6$ km$^2$). It is much more difficult for plumes containing large particles, such as those generated by Strombolian eruptions, to persist over similar vast regions. In addition, Strombolian eruptions rarely attain the high mass eruption rates, hence column heights, of the other eruption types. Equation 16 thus gives the quantitative basis for estimation of concentration variations within volcanic umbrella clouds, including those in which wind plays an important role in tephra dispersal.

## CONCLUSIONS

The sedimentation of large, nonaggregating pyroclasts from volcanic umbrella clouds has been successfully modeled using a simple treatment. The agreement of the model with grain-size data from ash fall deposits suggests that estimates of ash concentrations within the cloud are reasonable. Using both direct estimates from sedimentological data and the predictions of a plume model, we have shown that concentrations of ash in volcanic clouds that penetrate altitudes where commercial airplanes fly can exceed (by several orders of magnitude) the concentrations known to cause severe engine damage or failure. Dangerous concentrations can potentially persist for hundreds of kilometers from the vent. However, the model is clearly sensitive to the overall size distribution of ejecta and needs to include the processes of ash aggregation due to electrostatics (Gilbert and others, 1991) and moisture within the umbrella cloud.

## ACKNOWLEDGMENTS

Research was supported by grants from the Venture Research International Unit, by NSF grant EAR 9104770, by a NERC Fellowship to J.S.G., by a NATO fellowship to M.I.B. (awarded in 1988) and by NATO collaborative research grant (CRG 910096). M.I.B. acknowledges an NRC–JPL (Caltech) research associateship, under contract to NASA.

## REFERENCES CITED

Allen, J.R.L., 1985, Principles of Physical Sedimentology: London, George Allen and Unwin, 272 p.

Armienti, P., Macedonio, G., and Pareschi, M.T., 1989, A numerical model for simulation of tephra transport and deposition: Applications to May 18, 1980, Mount St. Helens eruption: Journal of Geophysical Research., v. 93, p. 6463–6476.

Brazier, S.A., Davis, A.N., Sigurdsson, H., and Sparks, R.S.J., 1982, Fall-out and deposition of volcanic ash during the 1979 explosive eruption of the Soufriere of St. Vincent: Journal of Volcanology Geothermal Research, v. 14, p. 335–359.

Bursik, M.I., Sparks, R.S.J., Carey, S.N., and Gilbert, J.S., 1992a, Sedimentation of tephra by volcanic plumes: I. Theory and its comparison with a study of the Fogo A Plinian deposit, Sao Miguel (Azores): Bulletin of Volcanology, v. 54, p. 329–344.

Bursik, M.I., Carey, S.N., and Sparks, R.S.J., 1992b, A gravity current model for the May 18, 1980, Mount St. Helens plume: Geophysical Research Letters, v. 19, p. 1663–1666.

Carey, S.N., Gardner, J.E., and Criswell, W., 1990, Variations in column height and magma discharge during the May 18, 1980, eruption of Mount St. Helens: Journal of Volcanology Geothermal Research, v. 43, p. 99–112.

Carey, S.N., and Sigurdsson, H., 1982, Influence of particle aggregation on deposition of distal tephra from the May 18, 1980, eruption of Mount St. Helens: Journal of Geophysical Research, v. 87, p. 7061–7072.

———1989, The intensity of Plinian eruption columns: Bulletin of Volcanology, v. 51, p. 28–40.

Criswell, W., 1987, Chronology and pyroclastic stratigraphy of the May 18, 1980, eruption of Mount St. Helens: Journal of Geophysical Research, v. 92, p. 10237–10266.

Einstein, H.A., and Krone, R.B., 1962, Experiments to determine modes of cohesive sediment transport in salt water: Journal of Geophysical Research, v. 67, p. 1451–1461.

Gilbert, J.S., Lane, S.J., Sparks, R.S.J., and Koyaguchi, T., 1991, Charge measurements on particle fallout from a volcanic plume: Nature, v. 349, p. 598–600.

Harris, D.M., Rose, W.I., Jr., Roe, R., and Thompson, M.R., 1981, Radar observations of ash eruptions, *in* Lipman, P.W., and Mullineaux, D.R., eds., The 1980 Eruptions of Mount St. Helens, Washington: U.S. Geological Survey Professional Paper 1250, p. 323–334.

Hazen, A., 1904, On sedimentation: Transactions, American Society of Civil Engineering, v. 53, p. 45–88.

Manins, P.C., 1976, Intrusion into a stratified fluid: Journal of Fluid Mechanics, v. 74, p. 547–560.

Martin, D., and Nokes, R., 1988, Crystal settling in a vigorously convecting magma chamber: Nature, v. 332, p. 534–536.

Sarna-Wojcicki, A.M., Shipley, S., Waitt, R.B., Jr., Dzurisin, D., and Wood, S.H., 1981, Areal distribution, thickness, mass, volume, and grain size of airfall ash from the six major eruptions of 1980, *in* Lipman, P.W., and Mullineaux, D.R., eds., The 1980 Eruptions of Mount St. Helens, Washington: U.S. Geological Survey Professional Paper 1250, p. 577–600.

Simpson, J.E., 1987, Gravity Currents in the Environment and the Laboratory: Chichester, England, Ellis Horwood Limited, 244 p.

Sorem, R.K., 1981, Volcanic ash clusters: Tephra rafts and scavengers: Journal of Volcanology Geothermal Research, v. 23, p. 63–71.

Sparks, R.S.J., 1986, The dimensions and dynamics of volcanic eruption columns: Bulletin of Volcanology, v. 48, p. 3–15.

Sparks, R.S.J., Carey, S.N., and Sigurdsson, H., 1991, Sedimentation from gravity currents generated by turbulent plumes: Sedimentology, v. 38, p. 839–856.

Sparks, R.S.J. Moore, J.G., and Rice, C., 1986, The giant umbrella cloud from the May 18, 1980, eruption of Mount St. Helens: Journal Volcanology Geothermal Research, v. 28, p. 257–274.

Suzuki, T., 1983, A theoretical model for the dispersion of tephra, *in* Shimozuru, D., and Yokoyama, I., eds., Arc Volcanism: Physics and Tectonics: Tokyo, Terrapub, p. 95–113.

Walker, G.P.L., and Croasdale, R., 1971, Two Plinian type eruptions in the Azores: Journal of the Geological Society of London, v. 127, p. 17–55.

Wilson, L., and Huang, T.C., 1979, The influence of shape on the atmospheric settling velocity of volcanic ash particles: Earth and Planetary Science Letters, v. 44, p. 311–324.

Woods, A.W., 1988, The fluid dynamics and thermodynamics of Plinian eruption columns: Bulletin of Volcanology, v. 50, p. 169–193.

Woods, A.W., and Bursik, M.I., 1991, Particle fallout, thermal disequilibrium and volcanic plumes: Bulletin of Volcanology, v. 53, p. 559–570.

VOLCANIC ASH AND AVIATION SAFETY:
Proceedings of the First International Symposium
on Volcanic Ash and Aviation Safety
U.S. GEOLOGICAL SURVEY BULLETIN 2047

# ELECTRICAL PHENOMENA IN VOLCANIC PLUMES

*By* Jennie S. Gilbert *and* Stephen J. Lane

## ABSTRACT

Observations of lightning and St. Elmo's fire within volcanic eruption plumes suggest high degrees of charge. Measurements of electrical charge on ash particles falling from the eruption plumes of Sakurajima Volcano in Japan indicate that the particles are nearly saturated with charge. Charge-to-mass (Q/m) ratios range from $+3\times10^{-4}$ to $+6\times10^{-4}$ C $kg^{-1}$ and from $-2\times10^{-4}$ to $-5\times10^{-4}$ C $kg^{-1}$. Sequential positive and negative deviations of electric potential gradient from background of several orders of magnitude were measured during explosions that generated particles. No deflections from background were found during explosions that released only gases. During fallout of particles, negative electric potential gradients occurred, whereas positive gradients were observed during fallout of acid rain. The fluctuations of potential gradient during the generation of particle-laden plumes and the observation that falling particles carried an average negative charge, while acid raindrops carried an average positive charge, suggest a dipole arrangement of charge within plumes such that positive charges dominate at the top of the plume and negative charges dominate at the base. The charge polarity may be reversed for other volcanoes. The presence of charged liquid drops of condensed volcanic gases suggests that charge is generated mainly by fracto-emission processes during magma fragmentation within the vent, rather than by collision effects within the plume.

## INTRODUCTION

Spectacular displays of lightning are common in particle-laden volcanic plumes, indicating that locally the air ionization limit has been exceeded (Blythe and Reddish, 1979). Amongst many other examples, lightning has been observed at Vesuvius in 1872 (Palmieri, 1873), Krakatoa in 1883 (Simkin and Fiske, 1983), Vesuvius in 1906 (Perret, 1924), Stromboli in 1907 (Perret, 1924), Anak Krakatau in 1933 (Simkin and Fiske, 1983), Surtsey in 1964 (Anderson and others, 1965), Heimaey in 1973 (Brook and others, 1974), Usu in 1977 (Kikuchi and Endoh, 1982), Mount St. Helens in 1980 (Rosenbaum and Waitt, 1981), Redoubt in 1990 (Hoblitt and Murray, 1990), Hudson in 1991 (José Naranjo, University of Chile, Santiago, Chile, oral commun., 1992), and Sakurajima (present authors). Therefore, high degrees of electrical charge are present in volcanic plumes, and this electrical charge, as well as producing magnificent visual displays, may also encourage particle aggregation and thus increase the sedimentation rate of particles (Sorem, 1982; Gilbert and others, 1991). Aircraft in flight accumulate fairly large potentials (Newman and Robb, 1977) from contact with atmospheric particles, which may or may not be charged. These potentials "bleed off" in the form of a corona or point discharge, also known as St. Elmo's fire. Severe St. Elmo's fire around aircraft has been reported by pilots unfortunate enough to encounter volcanic plumes while in flight (E.H.J. Moody, British Airways, oral commun., 1991).

Our aim is to assess the magnitude of charging in volcanic plumes and to understand the origin of the charged particles. In order to do this, we present results of two series of field experiments carried out at Sakurajima Volcano in May 1990 and March–May 1991. In the first experiments, we measured the amounts of charge present on particles falling from Sakurajima's plumes, and in the second, we measured perturbations of the atmospheric electric potential gradient from the background fair-weather field during eruptions.

Sakurajima is an andesitic stratovolcano, 1,118 m high in southern Kyushu, which has had repeated flank and summit eruptions during historic times. Because Vulcanian-type summit eruptions have occurred on a daily basis since 1955, Sakurajima is the ideal "working laboratory" for volcanic-plume experiments. During May 1990, the eruptions were of a continuous style and lasted for a few days. In contrast, in March–May 1991, the eruptions were of an explosive style, accompanied by explosion earthquakes and atmospheric shock waves, and were sustained for only a few hours. During both periods, plumes reached a maximum height of 3 km above the summit and were frequently distorted by the wind so that particles were deposited asymmetrically around the vent on the surrounding countryside, including several villages, Kagoshima City, and Kagoshima International Airport. These different styles of activity complemented the type of experiment carried out each year.

# EXPERIMENTS

## I. MEASUREMENTS OF ELECTRICAL CHARGE ON FALLING PARTICLES

### PREVIOUS WORK

Hatakeyama (1958) used a collecting device in contact with an electrometer in order to measure the average charge carried by particles falling from the eruption plume of Asama, Japan, on 2 August 1941. The experiment was carried out 50 km from the vent and the average charge was found to be –1.2 esu per gram (approximately $-4\times10^{-7}$ C $kg^{-1}$).

### APPARATUS

Our experiments differed from those of Hatakeyama (1958) in that we separated positively from negatively charged particles and measured the amount of charge carried by each. Particles (> 500 μm wide) falling directly from the eruption plume were allowed to pass between two parallel copper plates mounted in a grounded case. One plate was connected to Earth, the other to a high-voltage supply (±3 kV), to yield an electric field of $1.2\times10^5$ V $m^{-1}$ between the plates that separated the positively and negatively charged particles. The charge on particles contacting the grounded plate was measured by a Keithley 614 electrometer. Leakage currents across the plastic insulators that supported the plates, or resulting from any corona discharge within the apparatus (although surfaces were rounded to minimize this effect), were only just detectable at < 0.1 pA when humidity was low. Under conditions of high humidity, leakage currents became appreciable (> 10 pA). The plates were covered with a layer of oiled aluminum foil to which particles would adhere. After each experiment, the particles were removed from the foil by reflux degreasing in isopropyl alcohol and weighed to determine the charge-to-mass (Q/m) ratio of the sample. The size distribution of the samples was determined from silicon X-ray images of particles resting on a carbon substrate using the Link Analytical Featurescan facility.

### RESULTS

Results of two experiments (figs. 1 and 2) from two different eruptions indicate substantial changes in the gradient (nC $min^{-1}$) between the shielded state of the apparatus (when no particles were collected) and the exposed state. Figure 1 shows data for an experiment carried out during fallout of dry aggregated particles. A –3-kV supply was used in order to accelerate negatively charged particles toward the grounded plate where the amount of charge carried was measured. After a stabilization period of 64 minutes, during which time the apparatus was shielded, a light ashfall was allowed to pass between the parallel plates. This resulted in an increase in gradient (nC $min^{-1}$), indicating the accumulation of negatively charged particles on the grounded plate. During the period 70 to 76 minutes into the experiment, the fall almost ceased and the nC $min^{-1}$ rate returned approximately to the background state. Between 76 and 84 minutes, light fall occurred and a steeper nC $min^{-1}$ gradient was reestablished. After 84 minutes, fall ceased and again the readings returned to the background level. The Q/m ratio for the sample collected in this experiment was $-2.7\times10^{-4}$ C $kg^{-1}$. Grain size (on a number-frequency basis) was in the range 0.9–152 μm, the mean diameter 20.7 μm, the 95th percentile 54 μm, and maximum-frequency diameter 54.5 μm. The grounded plate carried 1.5 mg and the kV plate 0.5 mg of particles. In this experiment, 93 weight percent of the sample passed between the plates and therefore carried insufficient Q/m ratio to contact the plates. No aggregated particles were observed adhering to the oiled plates. This implies either that the aggregates had insufficient Q/m ratio to be attracted to the plates or that they were fragmented by the electric field and the resulting particles were attracted to both plates.

In a different experiment (fig. 2), a +3-kV supply was used (i.e., positively charged particles were accelerated toward the grounded plate for measurement). After a stabilization period of 21 minutes, a light ashfall was allowed to pass between the plates. This resulted in an increased nC $min^{-1}$ gradient. After 68 minutes, the apparatus was shielded so that no particles could accumulate and the leakage current

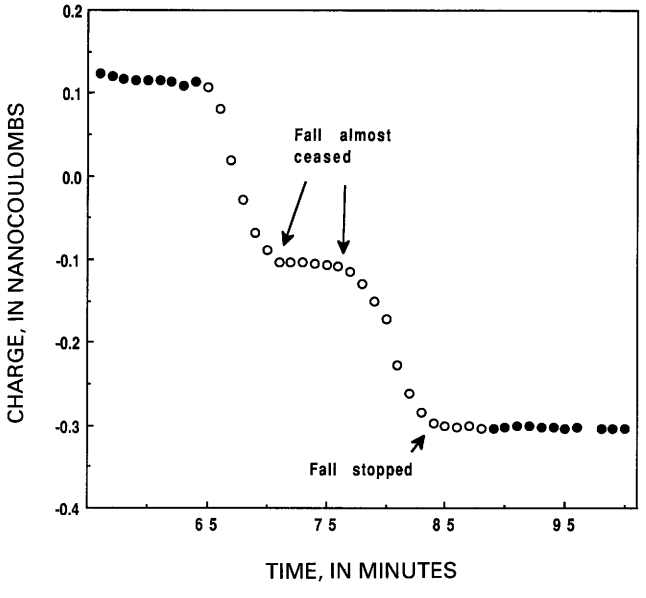


**Figure 1.** Charge (nC) versus time (minutes) for parallel plates experiment using –3-kV supply. The charge-to-mass ratio was found to be $-2.7\times10^{-4}$ C $kg^{-1}$. The period when the plates were shielded from ashfall is indicated by solid symbols; open symbols indicate the period when the plates were exposed to ashfall. Temperatures and relative humidities at the start and finish of the experiment were 25°C, 44 percent; and 23°C, 48 percent, respectively.

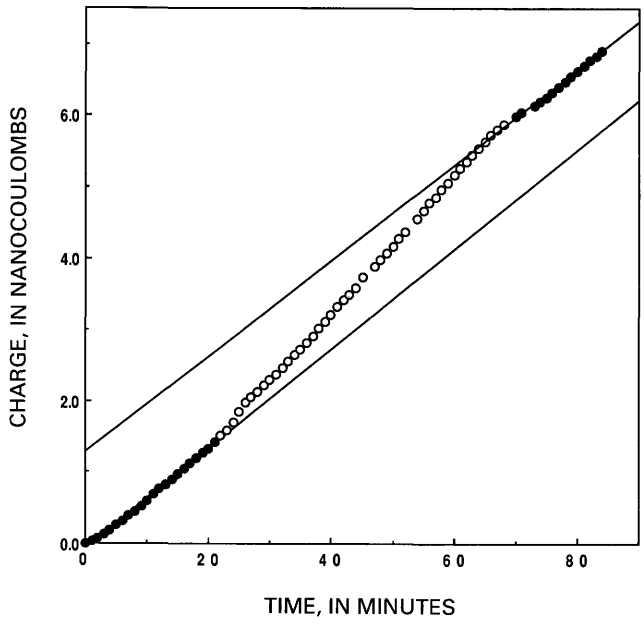


**Figure 2.** Charge (nC) versus time (minutes) for parallel plates experiment using +3-kV supply. The charge-to-mass ratio was found to be $+4.9\times10^{-4}$ C kg$^{-1}$. The period when the plates were shielded from ashfall is indicated by solid symbols; open symbols indicate the period when the plates were exposed to ashfall. Best fit straight lines for the solid symbols are shown. Temperatures and relative humidities at the start and finish of the experiment were 20°C, 66 percent; and 19°C, 74 percent, respectively.

returned approximately to the pre-collection state. The Q/m ratio for this experiment was $+4.9\times10^{-4}$ C kg$^{-1}$. Grain size (on a number-frequency basis) was in the range 1–253 μm, the mean diameter 28 μm, the 95th percentile 71 μm, and maximum-frequency diameter 49.1 μm. The grounded plate carried 2.6 mg and the kV plate 3.7 mg of particles. In this experiment, 77 weight percent of the sample passed between the plates. Again, no aggregates were observed on the plates.

### DISCUSSION

The Q/m ratios measured in this work are an average over a wide range of particle sizes (1–250 μm). Smaller particles will have a higher Q/m ratio than larger particles due to their larger surface area to volume ratios (charge resides on the surface of particles) and due to the Paschen law (Blythe and Reddish, 1979). The Q/m values used as data for figures 1 and 2 yield surface-charge densities (assuming spherical particles and maximum-frequency diameters) of $-7\times10^{-5}$ and $+9\times10^{-5}$ C m$^{-2}$, respectively. The theoretical maximum surface-charge density on a flat surface in the atmosphere is $\pm2.6\times10^{-5}$ C m$^{-2}$, above which air breakdown occurs. As particle size decreases below about 1 mm, the divergence of the electric field away from the particle surface reduces the effective spark gap of the system, allowing higher surface-charge densities to be stable in air (Blythe and Reddish, 1979). Blythe and Reddish (1979) calculated from the Paschen law that particles 50 μm in diameter may sustain surface-charge densities of approximately $1.5\times10^{-4}$ C m$^{-2}$ but that these levels are difficult to observe experimentally. They state that, for practical purposes, the maximum charge per unit mass carried by a stream of insulating particles may be calculated assuming a surface-charge density of $\pm1\times10^{-5}$ C m$^{-2}$. The particles produced during Sakurajima's eruptions thus appear to be charged almost to the air ionization limit; that is, they are nearly saturated with charge.

## II. MEASUREMENTS OF ELECTRIC POTENTIAL GRADIENT CHANGES DURING ERUPTIONS

### PREVIOUS WORK

The effect of eruption plumes, fallout of particles, and acid rain on the atmospheric electric potential gradient is not well understood. However, abundant measurements of electric-potential-gradient changes beneath and within thunderclouds suggest that most have a concentration of positive charges in their upper regions, with a lower region of negative charge and a further concentration of positive charge in a limited zone at the base of the cloud (Chalmers, 1967). This arrangement is thought to result from charge-separation processes operating at different levels within the cloud (Chalmers, 1967). Charge distributions have also been described in dust devils (Freier, 1960; Crozier, 1964), and in non-raining clouds (Whitlock and Chalmers, 1956). Electric-potential-gradient measurements made during fair weather, beneath clouds, and during rainfall and snowfall are available (Chalmers, 1967). Hatakeyama (1949) recorded a negative potential gradient during the overhead passage of the particle-laden cloud from Yake-yama Volcano in Japan. During eruptions of Aso Volcano in Japan, Hatakeyama and Uchikawa (1952) observed an eruption plume dominated by positive charge in its lower region and by negative charge in its upper region. At Surtsey, electric-potential-gradient data were collected by towing an electrometer and radioactive probe mounted on a ship beneath the particle-laden plume (Anderson and others, 1965), but the potential-gradient changes resulting from the presence of the plume were difficult to decouple from the effects of breaking sea waves on lava flows. Kikuchi and Endoh (1982), situated 5 km NE. of the vent of Usu Volcano, Japan, measured a negative field associated with the generation of a particle-laden plume on 12 August 1977. On this occasion, the plume did not pass overhead but moved to the NW. On 13–14 August, these authors measured alternating positive and negative potential gradients during particle fallout. High-speed monitoring of the atmospheric electric potential gradient during explosive eruptions at Sakurajima (Matsumoto and others, 1988) found

gradient changes of the order of 1 V $m^{-1}$ approximately one second after an explosion. These changes in gradient were correlated with shock waves. None of the above volcanic studies investigated the effect of acid rainfall on the potential gradient.

## APPARATUS

Here we report electric potential gradient measurements made: (1) as particle-laden plumes passed overhead, as well as at distance from the field meter, (2) as plumes of condensing gases passed overhead, and (3) during periods of particle fallout and acid rainfall. Measurements were made between 2 and 5 km from the vent using a stationary, tripod-mounted, grounded John Chubb electrostatic field meter (JCI 111). The height from the base of the tripod to the measuring aperture of the field meter was 1.55 m. The advantage of using the tripod was to produce a noise free amplification of the signal (measured to be a factor of 20) in order to overcome increased meter noise levels due to aperture and Earth-connection contamination. Data presented here have been corrected to ground-level potential gradients.

## RESULTS

Figure 3*A* shows data collected during an explosion at a locality 2.75 km SSE. and downwind (on axis) of the active vent. During the experiment, the weather was fine with no cloud cover and a light breeze. For the first 206 minutes of the experiment, Sakurajima erupted mainly white plumes of condensing gases, which rose approximately 300 m above the vent. Occasional particle-laden plumes of similar size were generated that produced very light ashfall. Vent noise was absent or restricted to low rumblings. At 206 minutes, a loud detonation was heard and was followed by bombs a few meters wide being thrown out of the vent, after which a dark particle-laden plume rose to a height of approximately 3 km above the vent. At this height, the plume formed a laterally spreading gravity current. At 207.5 minutes, the potential gradient had dropped to –0.4 kV $m^{-1}$ after which it started to rise rapidly. At 209 minutes, the cloud was observed to be directly overhead, and at 212 minutes, fallout of particles < 1 cm in diameter commenced. At 213 minutes, the maximum positive potential gradient of 2.5 kV $m^{-1}$ was obtained, after which the potential gradient decreased. At 219 minutes, the maximum negative potential gradient of –2.7 kV $m^{-1}$ was obtained, by which time the rate of particle fallout had slowed. By 235 minutes, the potential gradient had returned to approximately the pre-explosion background value and there was a very light fallout; the bulk of the plume had dispersed with only small emissions coming from the vent.

Data for another explosion are seen in figure 3*B*. This experiment was run at a locality 2 km SW. of the vent. At the time of the explosion, the wind direction was NNW., and therefore, the experiment was run off the dispersal axis. During the experiment, prior to the explosion, the cloud cover was 0–20 percent and there was a slight breeze. During the first 82 minutes, Sakurajima was erupting white plumes of condensing gases that rose to a maximum height of 200 m. At 82 minutes, a loud detonation was heard, at which time a dark particle-laden plume ascended to a height of 1.5 km above the vent before spreading laterally. After 84 minutes, the potential gradient had dropped from background to –1.0 kV $m^{-1}$, after which it began to rise. At 87 minutes, the potential gradient was 1.5 kV $m^{-1}$. By 88 minutes, the plume had started to disperse, leaving only a small, particle-laden plume emanating from the vent. During dispersal of the

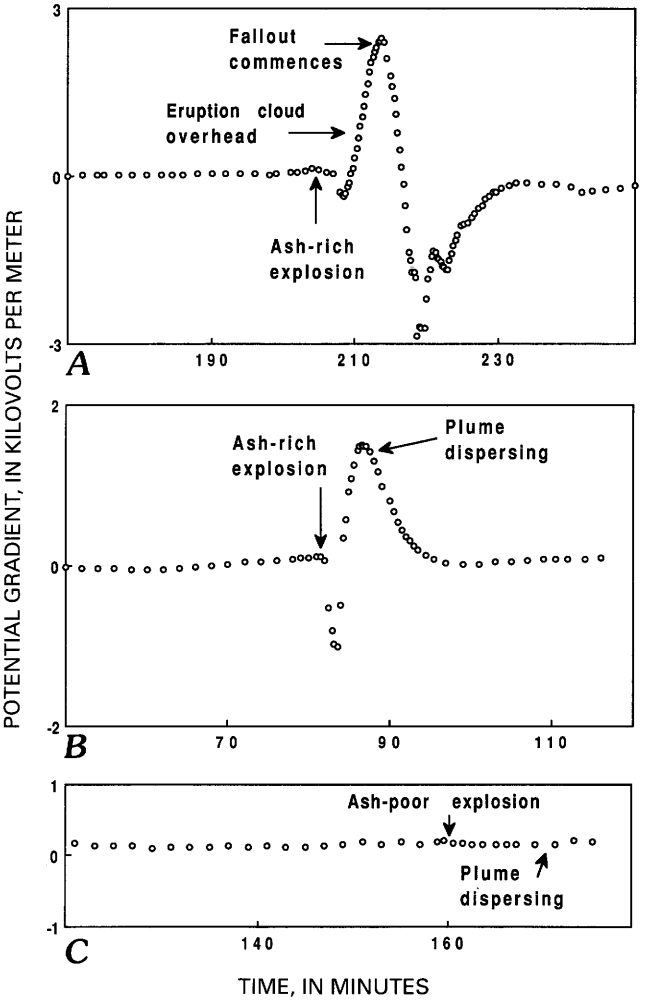


**Figure 3.** Potential gradient (kV $m^{-1}$) versus time (minutes). *A,* Explosion at 13:39 local time (local time = Greenwich mean time + 9 hours) on 3 May 1991. Temperatures and relative humidities at the start and finish of the experiment were 18°C, 45 percent; and 21°C, 39 percent, respectively. *B,* Explosion at 10:16 local time on 30 April 1991. Temperatures and relative humidities at the start and finish of the experiment were 16°C, 66 percent; and 19°C, 58 percent, respectively. *C,* Explosion at 15:44 local time on 30 April 1991. The temperature and relative humidity one-half hour into the experiment were 22°C and 54 percent, respectively.

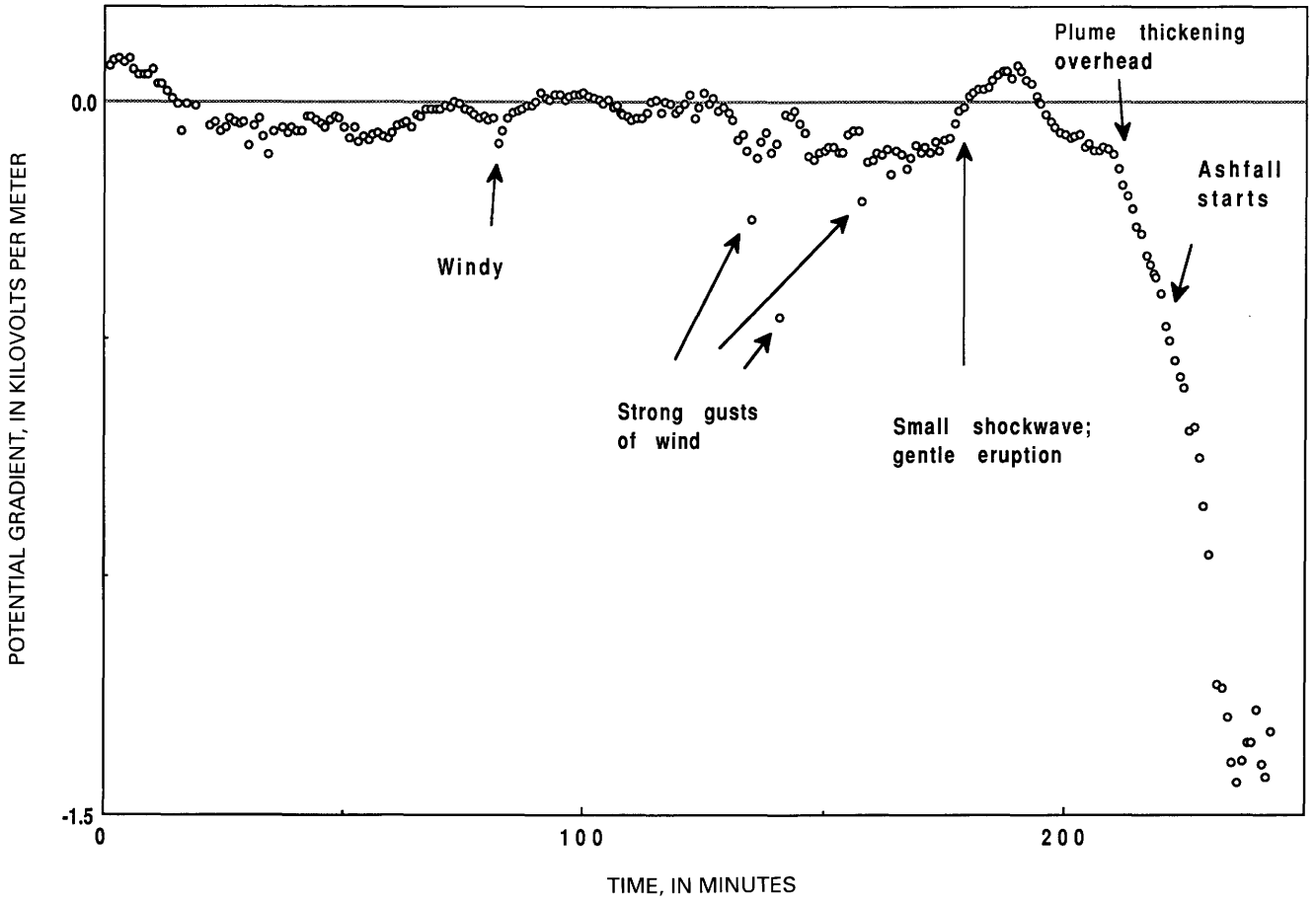


**Figure 4.** Potential gradient (kV $m^{-1}$) versus time (minutes) during ashfall on 25 March 1991. Temperatures and relative humidities at the start and 90 minutes into the experiment were 24°C, 69 percent; and 24°C, 73 percent, respectively.

plume, the electric potential gradient decayed approximately exponentially to the pre-explosion background level. No ashfall occurred at the measurement locality.

Figure 3*C* shows the effect on the potential gradient of an explosion that generated only gases. The experiment was run at a locality 2.75 km SSE. and downwind of the vent. Prior to the explosion, there was a gentle breeze and no cloud cover. During this time Sakurajima was erupting small white plumes up to 150 m high of condensing gases and low rumblings were coming from the vent. After 159 minutes, a loud detonation was heard after which a white plume rose approximately 1.5 km from the vent before spreading laterally. The generation of this plume had no observable effect on the potential gradient. By 174 minutes, the plume had dissipated. No particles fell from the plume.

Figure 4 shows the effect of ashfall on the electric potential gradient. The data were collected at a locality 3.5 km E. and downwind of the vent, at which time there was approximately 20 percent cloud cover and a breeze. During the first 180 minutes of the experiment, white plumes of condensing gases < 300 m high were erupted intermittently, at which time the volcano was either silent or rumbling. At 135, 141, and 158 minutes, strong gusts of wind gave rise to potential gradients of –0.25 kV $m^{-1}$, –0.45 kV $m^{-1}$, and –0.21 kV $m^{-1}$ respectively. After 180 minutes, a detonation was heard and a particle-laden plume ascended approximately 500 m above the vent. The plume then moved overhead. Light ashfall commenced at 219 minutes and continued until the end of the experiment. During this time, the potential gradient decreased to nearly –1.5 kV $m^{-1}$.

The effect of plume-induced acid rain on the electric potential gradient was investigated in an experiment (fig. 5) carried out a locality 2.25 km NW. and downwind of the vent. At this time, the weather was overcast with 100 percent cloud cover. Sakurajima was erupting a plume (> 300 m high), and rumblings were coming from the vent. A light fall of particles (> 2 mm in diameter) occurred for the first 30 minutes of the experiment. Between the periods 15–22 and 32–41 minutes, gentle, particle-free liquid drops fell, irritating the skin. The drops were tested with pH indicator paper and found to have a pH of < 1. The drops were generated by condensation of volcanic gases.

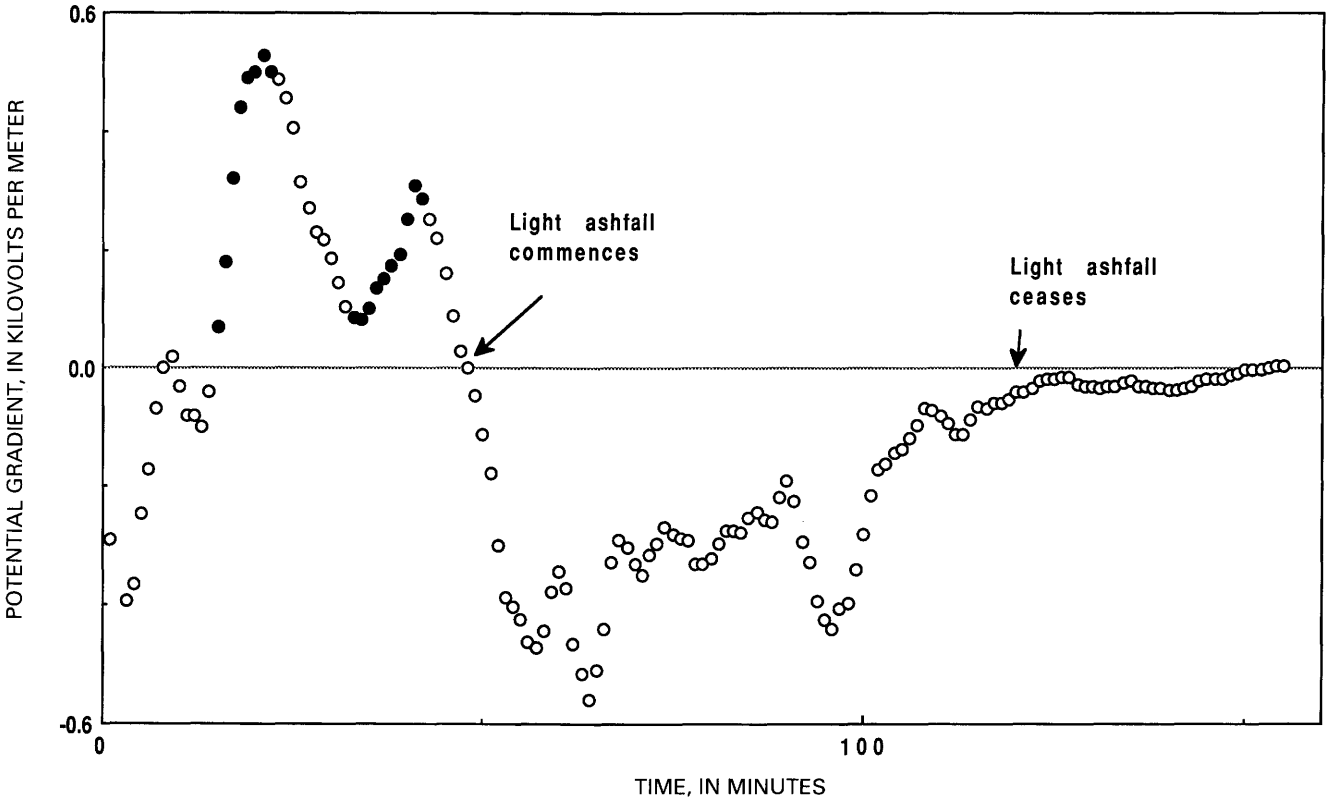


**Figure 5.** Potential gradient (kV $m^{-1}$) versus time (minutes) during plume-induced acid rainfall on 27 April 1991. At the start and finish of the experiment, temperatures and relative humidities were 16°C, 90 percent; and 19°C, 74 percent, respectively. Solid symbols indicate periods of rainfall.

## DISCUSSION

The potential gradient data are consistent with particles falling from the plume with a net average negative charge (fig. 4) and acid rainfall with an average positive charge (fig. 5). Explosions that generated no particles produced no measurable fluctuations in the potential gradient (fig. 3). Explosions that generated particles were characterized by large changes in potential gradient (figs. 3*A* and 3*B*). This implies that lava-dome rupture during explosive steam eruptions does not necessarily generate large amounts of particles or result in significant charge separation. Processes that generate considerable quantities of particles, such as degassing of magma, do result in the generation of charged particles and volcanic gases (ions).

Explosive eruptions resulting in particle generation exhibit sequences of potential gradient reversals (figs. 3*A* and 3*B*). These reversals may be explained in this case by assigning an average negative charge to particles and positive charge to the erupted gases, which condense to yield positively charged liquid drops. Figure 6 shows one series of possible explanations for the potential gradient reversals.

In the early stages of the eruption (fig. 6*A*), positively charged gases separate from the particles at the top of the column due to settling of ash particles. Particle aggregation would enhance this process by increasing the rate of fallout from the top of the cloud. Separation causes the initial negative-potential-gradient pulse seen in both on-axis (fig. 3*A*) and off-axis (fig. 3*B*) situations. This is due to the negatively charged (on average) base of the column being closer to the field meter than the positively charged (on average) top of the column. A laterally spreading gravity current develops (fig. 6*B*) and higher wind speeds accelerate the gases ahead of the particles at high altitudes and give rise to the positive potential gradient in the on-axis data (fig. 3*A*). Gases escaping from the side of the plume generate a positive potential gradient in the off-axis data (fig. 3*B*).

In the final stages of the eruption (fig. 6*C*), the plume recedes from the off-axis field meter generating the near-exponential decay in potential gradient (fig. 3*C*). As the plume moves over the on-axis field meter, negatively charged particle-laden regions of the plume dominate the potential gradient and the near-exponential decay as the plume retreats is punctuated by periods of ashfall (fig. 3*A*).

Hatakeyama and Uchikawa (1952) proposed a dipole model to explain their observations but assigned charge of one sign to large particles and charge of the other sign to small particles. We see no physical justification for particle size to control charge polarity of insulating particles because

charge transfer on contact is driven by differences in surface work function. This function depends on surface composition of particles, which may be different from their bulk composition. Previous workers (Hatakeyama and Uchikawa, 1952; Hatakeyama, 1958) have suggested that charging of particles occurs within the plume due to grain-grain collisions. This mechanism does not adequately explain the generation of charged gaseous species that condense to form charged liquid drops. We propose that charge is generated by fracto-emission (Donaldson and others, 1988) processes during vesiculation and fragmentation of magma within the vent, where particle generation is taking place. These processes yield both ionized volcanic gas and charged particles. The generation rates of charged material within a convecting low-density plume must be significantly lower than within the fragmentation zone. The polarity of the charges generated may depend on the volcano or eruption studied and may be a function of magma chemistry (Hatakeyama and Uchikawa, 1952; Anderson and others, 1965).

We calculate to a first approximation that, in order to generate a potential gradient of 2.5 kV $m^{-1}$ (fig. 3*A*), a minimum excess charge concentration in the gas cloud of approximately $10^{10}$ elementary charges per cubic meter (e $m^{-3}$) is required if a gas/particle separation distance of 10 m is assumed. Similarly, Anderson and others (1965) calculated an excess charge of $2\times10^{10}$ e $m^{-3}$ for the eruption cloud of Surtsey. Assuming the same excess charge concentration for the particle-laden cloud, a value of surface-charge density of $10^{-5}$ C $m^{-2}$ (Gilbert and others, 1991) and 25-μm-diameter particles, calculations give an excess charged-particle concentration of $10^5$ $m^{-3}$. This yields an excess mass loading of $10^{-6}$ kg $m^{-3}$ of charged particles. Hatakeyama (1958) found an overall (positive plus negative) charge-to-mass (Q/m) ratio for falling particles of $-4\times10^{-7}$ C $kg^{-1}$, and Gilbert and others (1991) found an absolute (positive or negative) Q/m ratio for falling particles of $-2\times10^{-4}$ to $-5\times10^{-4}$ C $kg^{-1}$. This implies that the excess charge is carried by approximately 0.1 percent of the particles. Therefore, the total mass loading of the Sakurajima plumes may be of the order of $10^{-3}$ kg $m^{-3}$. Assuming that the erupted material contains 2 weight percent gas and the horizontal cross-sectional-area ratio of the top of the column to the vent is $10^4$, a mass loading of $5\times10^{-3}$ kg $m^{-3}$ is calculated. The Mount St. Helens initial eruption cloud of 18 May 1980 was calculated to support a total of $8.5\times10^{-3}$ kg $m^{-3}$ of fine particles (Harris and others, 1981). This indicates that only a small difference in the generation rates of positively and negatively charged particles and gaseous ions is required to produce the observed electric potential gradient fluctuations.

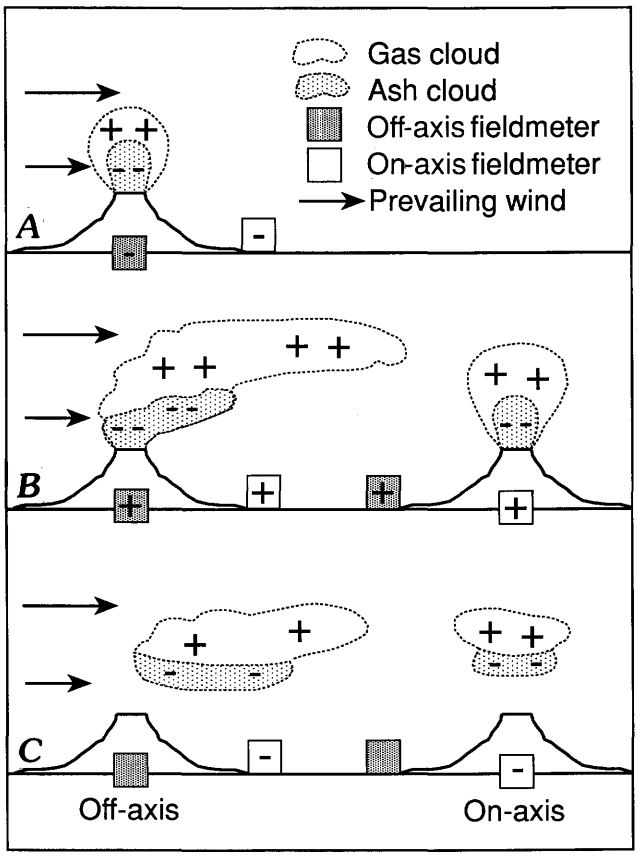


**Figure 6.** Schematic representation of the growth and dissipation of an eruption plume to explain changes in potential gradient measured at ground level. See text for explanation.

## RECOMMENDATIONS FOR AIRCRAFT SAFETY

We have shown that particles falling from volcanic plumes may be highly charged and that the presence of a particle-laden plume (in contrast to a plume of condensing gases) may significantly alter the fair-weather potential gradient. In order to detect the presence of erupted material, we suggest that aircraft in flight should monitor: (1) potential gradient changes (certain patterns may be distinctive to particle-laden plumes), (2) particulate and ion concentrations by means of current flowing from corona-discharge bars (high currents may indicate the presence of either charged or uncharged particles), and (3) atmospheric $SO_2$/HCl concentrations (high concentrations may indicate the presence of a plume).

The effects of volcanic particles on jet engines are well known (Campbell, 1991). However, particles may also effect other aircraft systems. The development of "fly-by-wire" aircraft may mean that safety becomes dependent on the functions of static-sensitive semiconductor devices. Because charged particles may be ingested into the cooling systems of aircraft electronics, therefore, the development of closed cooling systems would be desirable.

## ACKNOWLEDGMENTS

We thank Professor K. Kamo and staff of the Sakurajima Volcanological Observatory for assistance during field work and R.S.J. Sparks for comments. J.S.G. acknowledges support by the NERC and BP Venture Research for research funds and the Royal Society for expenses to attend the First International Symposium on Volcanic Ash and Aviation Safety. J.S.G. and S.J.L. thank the Royal Society for field and apparatus expenses. S.J.L. thanks the U.S. Geological Survey for providing support to attend the First International Symposium on Volcanic Ash and Aviation Safety. Link Analytical Ltd. made available the Featurescan package.

## REFERENCES CITED

Anderson, R., Bjornsson, S., Blanchard, D.C., Gathman, S., Hughes, J., Jonasson, S., Moore, C. B., Survilas, H.J., and Vonnegut, B., 1965, Electricity in volcanic clouds: Science, v. 148, p. 1179–1189.

Blythe, A.R., and Reddish, W., 1979, Charges on powders and bulking effects: Institute of Physics Conferences Series, v. 48, p. 107–124.

Brook, M., Moore, C.B., and Sigurgeirsson, T., 1974, Lightning in volcanic clouds: Journal of Geophysical Research, v. 79, p. 472–475.

Campbell, E.E., 1991, 747-400 airplane damage survey following a volcanic ash encounter [abs.], *in* Casadevall, T.J., ed., First International Symposium on Volcanic Ash and Aviation Safety: U. S. Geological Survey Circular 1065, p.14.

Chalmers, J.A., 1967, Atmospheric Electricity: London, Pergamon Press, 515 p.

Crozier, W.D., 1964, The electric field of a New Mexico dust devil: Journal of Geophysical Research, v. 69, p. 5427–5429.

Donaldson, E.E., Dickinson, J.T., and Bhattacharya, S.K., 1988, Production and properties of ejecta released by fracture of materials: Journal of Adhesion, v. 25, p. 281–302.

Freier, G.D., 1960, The electric field of a large dust devil [abs.]: Journal of Geophysical Research, v. 65, p. 3504.

Gilbert, J.S., Lane, S.J., Sparks, R.S.J., and Koyaguchi, T., 1991, Charge measurements on particle fallout from a volcanic plume: Nature, v. 349, p. 598–600.

Harris, D.M., Rose, W.I., Roe, R., and Thompson, M.R., 1981, Radar observations of ash eruptions, *in* Lipman, P.W., and Mullineaux, D.R., eds., The 1980 Eruptions of Mount St. Helens, Washington: U.S. Geological Survey Professional Paper 1250, p. 323–333.

Hatakeyama, H., 1949, On the disturbance of the atmospheric potential gradient caused by the smoke cloud of the volcano Yake-yama: Journal of Meteorological Society of Japan, v. 27, p. 372–376.

———1958, On the disturbance of the atmospheric electric field caused by the smoke cloud of the volcano Asama-yama: Meteorological Geophysics v. 8, p. 302–316.

Hatakeyama, H., and Uchikawa, K., 1952, On the disturbance of the atmospheric potential gradient caused by the eruption smoke of the volcano Aso: Meteorological Geophysics, v. 2, p. 85–89.

Hoblitt, R.P., and Murray, T.L., 1990, Lightning detection and location as a remote eruption monitor at Redoubt volcano, Alaska [abs.]: Eos, Transactions, American Geophysical Union, v. 71, p. 1701.

Kikuchi, K., and Endoh, T., 1982, Atmospheric electrical properties of volcanic ash particles in the eruption of Mt. Usu volcano, 1977: Journal of the Meteorological Society of Japan, v. 60, p. 548–561.

Newman, M.M., and Robb, J.D., 1977, Protection for aircraft, *in* Golde, R.H., ed., Lightning: New York, Academic Press, p. 659–696.

Matsumoto, S., Ueki, S., and Nishi, K., 1988, A study of the processes of explosive eruptions of Sakurajima by means of observations of electric field in the atmosphere, Earth's current, and ground motion: Sakurajima Volcano Observatory Report [in Japanese], p. 117–126.

Palmieri, L., 1873, The Eruption of Vesuvius in 1872: London, Asher & Co., 148 p.

Perret, F.A., 1924, The Vesuvius eruption of 1906: Carnegie Institution of Washington Publication 339, 151 p.

Rosenbaum, J.G., and Waitt, R.B., Jr., 1981, Summary of eyewitness accounts of the May 18 eruption, *in* Lipman, P.W., and Mullineaux, D.R., eds., The 1980 Eruptions of Mount St. Helens, Washington: U.S. Geological Survey Professional Paper 1250, p. 53–67.

Simkin, T., and Fiske, R.S., 1983, Krakatau 1883, The Volcanic Eruption and its Effects: Washington, D.C., Smithsonian Institution Press, 464 p.

Sorem, R.K., 1982, Volcanic ash clusters: Tephra rafts and scavengers: Journal of Volcanology and Geothermal Research, v. 13, p. 63–71.

Whitlock, W.S., and Chalmers, J.A., 1956, Short period variations in the atmospheric electric potential gradient: Quarterly Journal of the Royal Meteorological Society, v. 82, p. 325–326.

VOLCANIC ASH AND AVIATION SAFETY:
Proceedings of the First International Symposium
on Volcanic Ash and Aviation Safety
U.S. GEOLOGICAL SURVEY BULLETIN 2047

# VOLCANIC ASH: WHAT IT IS AND HOW IT FORMS

*By* Grant Heiken

## ABSTRACT

There are three basic eruption processes that produce volcanic ash: (1) decompression of rising magma, gas-bubble growth, and fragmentation of the foamy magma in the volcanic vent (magmatic), (2) explosive mixing of magma with ground or surface water (hydrovolcanic), and (3) fragmentation of country rock during rapid expansion of steam and (or) hot water (phreatic). Variations in eruption style and the characteristics of volcanic ashes produced during explosive eruptions depend on many factors, including magmatic temperature, gas content, viscosity and crystal content of the magma before eruption, the ratio of magma to ground or surface water, and physical properties of the rock enclosing the vent.

Volcanic ash is composed of rock and mineral fragments and glass shards; in many eruptions, there are also acid droplets coating ash-grain surfaces. The shard shapes and sizes depend upon the shape and size of gas bubbles present within the magma immediately before eruption and fragmentation of the magma. Particle sizes range from meters for large blocks expelled near the volcanic vent to nanometers for fine ash and aerosol droplets within well-dispersed eruption plumes.

## INTRODUCTION

What is volcanic ash? The question has been asked repeatedly since the time of Aristotle. Early scientists were able to do some remarkable studies of volcanic ashes and the eruptions that produced them, but they were limited by scale. It has only been during the last few decades that we have had the laboratory equipment to characterize the broad spectrum of volcanic ash types, down to a scale of tenths of micrometers. Only in the last 20 years have we had the ability to go beyond sampling ash deposits on the ground to sampling with aircraft and balloons to collect in situ samples from eruption plumes at elevations up to 20 km. This paper will review the major volcanic ash types and the broad spectrum of explosive eruption types that have produced them.

## ASH FROM A RECENT ERUPTION THAT AFFECTED AIR TRAFFIC—AUGUSTINE VOLCANO, ALASKA

The 1986 eruption of Augustine Volcano in Alaska sent eruption plumes to the east and south from the volcano and had considerable impact on airline traffic in the Anchorage area. Ash samples were collected at Anchorage International Airport, located 280 km NE. of the volcano. The airport was showered with light dustings of ash for 9 days after the eruption began (Rose and others, 1988). Median grain size of the ash at Anchorage was around 30 μm (fig. 1) and consisted of glass shards broken from the foaming, rising magma; glassy lava fragments from the older lava dome; and mineral fragments (fig. 2). As is the case for most moderate-size eruptions like this one, the glass shards were coated with acid condensates and very fine dust, which consists of even finer grained ash (fig. 3); this bonding may occur because of static charge (Carey and Sigurdsson, 1982; Sorem, 1982; Gilbert and others, 1991). These ashes are typical of the hundreds of active or dormant stratovolcanoes along the Pacific Rim. However, volcanic ashes are very diverse in their origins and compositions, and this introduction provides only a general view of explosive eruption processes and their products, which we have grouped under the category "volcanic ash."

The physical properties of volcanic ashes depend mostly on their relative proportions of glass, mineral fragments, and rock fragments. Also important to the physical properties are chemical compositions of these components and their grain size. Fine-grained glassy volcanic ash is used commercially as an abrasive, but there are few quantitative data available on the abrasive qualities of ash. The hardness of components of a volcanic ash (based on the Moh's scale used by mineralogists: talc has a hardness of 1; diamond has a hardness of 10) can be approximated with silica-rich glass (hardness = 5.5) and minerals ranging in hardness from 2 for some clays to 7 for quartz. Melting temperatures for volcanic glass and the rheology of the molten material are covered in this volume in a paper by Swanson and Beget.

## EXPLOSIVE FRAGMENTATION OF SILICIC MAGMAS

Observations of fragmentation processes within explosive eruptions are limited. We can get reasonably close to only the smallest, and generally the most silica-poor and least explosive, eruptions of magma (molten rock). These eruption types are, however, of minimal interest for aviation safety because they are small. Numerical models of magma fragmentation and the formation of volcanic ash are, at best, first approximations—at least until we find a way to place instruments within the throat of a volcano that will survive full eruption.

### MAGMATIC ERUPTIONS

Eruption explosivity is related mostly to overpressures within magma caused by gases coming out of solution as the magma nears the Earth's surface and encounters atmospheric pressure (fig. 4). Verhoogen (1951), in an analysis of gas-bubble nucleation, growth, and rise within magmas, concluded that volcanic ash formed when expanding bubbles within rising magma coalesced. That is most likely correct for lava fountains of low-viscosity magmas but not for the formation of pumice and volcanic ash from magmas with more silica-rich compositions such as those of Redoubt and Pinatubo Volcanoes. Pumice, which is a silicate foam composed of glass, gas bubbles, and minerals, would not exist if all bubbles in the magma had coalesced and disintegrated as Verhoogen had proposed. Alfred Rittmann (1936), a pioneer

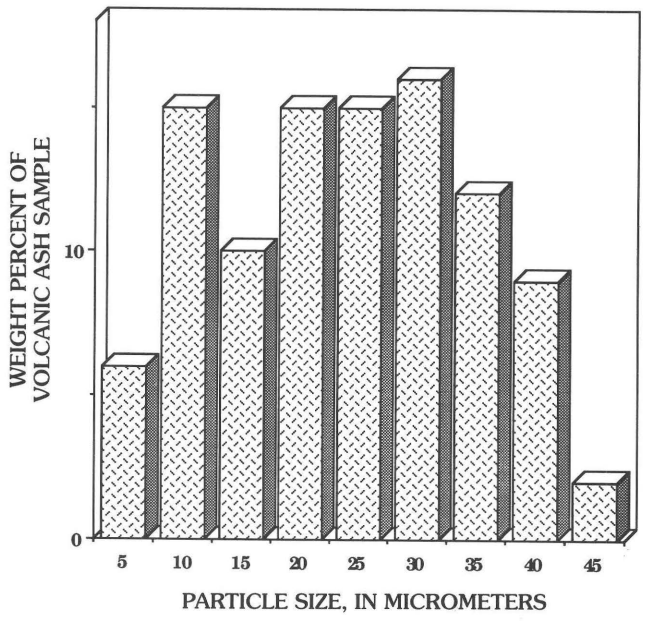


**Figure 1.** Grain size of volcanic ash from the April 2, 1986, eruption of Augustine Volcano (Alaska). This ashfall sample was collected at the Anchorage International Airport, 280 km NE. of the volcano. Eruption plumes from this eruption commonly reached altitudes of 3 to 4 km, with occasional ash columns reaching 12 km (Rose and others, 1988). Grain sizes were measured with a Horiba particle-size analyzer.

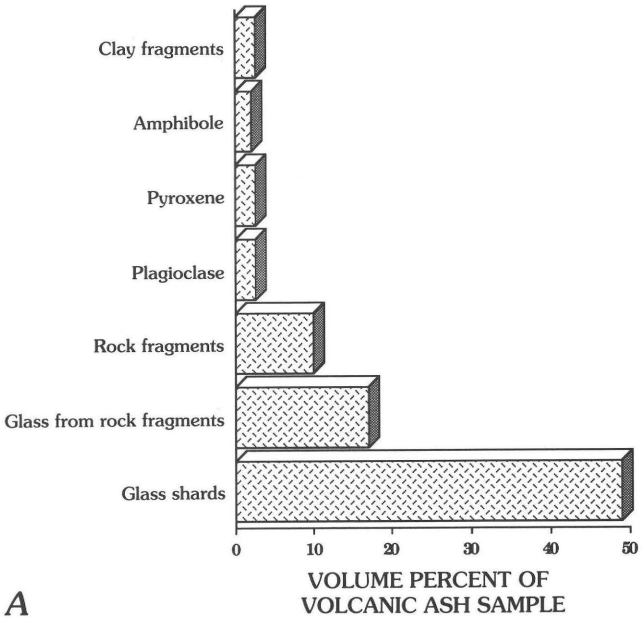


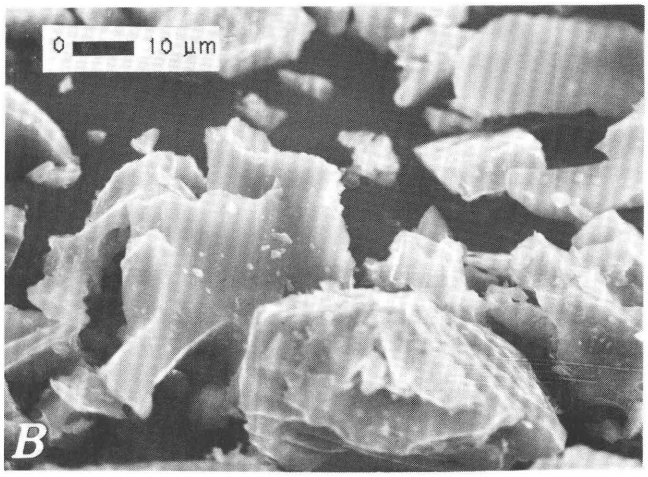


**Figure 2.** Particle types within the ashfall collected at Anchorage Airport, March 28, 1986, from the eruption of Augustine Volcano. *A*, Grain count, showing percentage of particle types within this ash. The most common particle type from this eruption was glass shards, explosively broken from a foaming magma rising in the volcano. Other particles include individual minerals from the magma, bits of a lava that occupied the volcano's throat before eruption, and fragments from the claystone underlying the volcano. *B*, Scanning electron photomicrograph that shows mostly equant, curved glass shards that were broken from a quickly chilled magma foam. The curved surfaces are remnants of bubble walls.

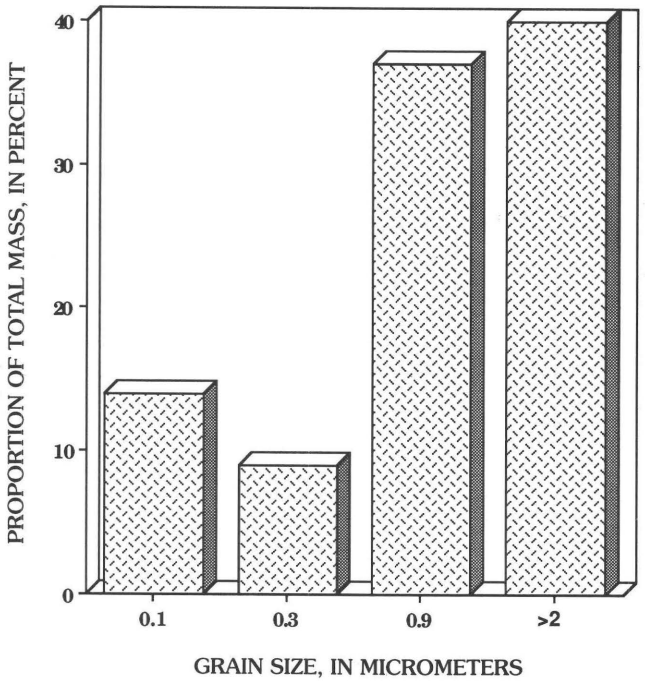


**Figure 3.** Grain size of volcanic ash from the eruption plume from the 1986 eruption of Augustine Volcano that was sampled 10 km downwind from the volcano by aircraft between major eruption phases. Even within plumes emanating from the volcano during relatively "quiet" phases, there are numerous particles, albeit small ones, as compared with ash produced during the larger eruptions (e.g., compare with fig. 1). The sample was collected with a quartz crystal microcascade sampler by Ray Chuan (Brunswick Corporation).

in volcanology, proposed that gases in the magma come out of solution as magma rises through conduits to shallow depths. After the magma reaches the Earth's surface and an eruption begins, the highly viscous foam is disrupted by decompression before bubble coalescence can occur. This theory has been supported by shock-tube analogies (Bennett, 1974), and computer experiments by several research groups in the United States and England (e.g., Wohletz and others, 1984).

The distinctive shapes and physical properties of pumice are controlled by the history of gas-bubble growth, the presence or absence of phenocrysts as nucleation points (phenocrysts are those mineral grains that crystallized within the magma before eruption), and the type of fragmentation of the magma foam during eruption. There may be as many size and shape distributions of gas bubbles within pumice as there are volcanic eruptions, but most are interpreted as having grown either continuously during shallow magma rise and eruption (i.e., one generation) or discontinuously—before and during eruption (i.e., two generations). A hypothetical example (fig. 4; adapted from Heiken and Wohletz, 1991) of how pumice and ash form during an explosive eruption of silica-rich magma, based on the characteristics of gas bubbles within pumice and volcanic ash particles, follows:

The example is a silica-rich magma (70 weight percent $SiO_2$), which contains 2 to 3 weight percent $H_2O$. Bubble growth may begin at depths of 1 to 3 km below the Earth's surface, where gas pressure exceeds lithostatic pressure (i.e., the pressure produced by the mass of rock overlying the magma body). If $CO_2$ gas is present, it may exsolve and form gas bubbles at even greater depths (Holloway, 1976). If the magma contains abundant crystals (i.e., phenocrysts), nucleation and bubble growth on mineral surfaces may produce pumice fragments containing bubble clusters. Gas bubbles clustered around phenocrysts or other inclusions may coalesce and form large cavities within the magma foam.

As rising magma approaches the Earth's surface and lithostatic pressure due to the weight of the overlying rock decreases, uniform bubble growth may create a foam consisting of evenly spaced bubbles (with the exception of larger bubble clusters around phenocrysts). Expansion of these bubbles and surface tension of thinning bubble walls may increase the bulk viscosity of the magma considerably and give it a finite yield strength, making it more brittle. The higher viscosity prevents any significant buoyant bubble rise.

If bubble growth occurs at shallow depths, near the vent, the pumice pyroclasts may contain nearly spherical vesicles. In this situation, there is no time before fragmentation for vesicles to be elongated by flow into tube-like shapes. The glassy ash particles produced in this type of eruption consist of arcuate, blocky shards.

After a vent or conduit is opened to the surface, the magma flow rate increases greatly. If this flow rate exceeds that of the rising bubbles, the gas bubbles are sheared by flow into long tubes or pita-bread-like shapes.

The more-or-less brittle mass of magma foam is disrupted by a large pressure differential at the magma/atmosphere interface. A shock wave moves ahead of the pumice and ash out of the vent, while an expansion wave propagates down into the inflated magma and allows its rapid decompression (Wohletz and others, 1984). The nearly solid foam is broken into particles at a fragmentation surface in the conduit, and the particles are accelerated out of the vent. The explosive eruption process for silica-rich magmas is likely driven by this pressure differential and only partly by bubbles coalescing and breaking.

Large magnitude explosive eruptions, with eruption columns reaching heights of as much as 50 km, are called Plinian eruptions, after the A.D. 79 eruption of Mt. Vesuvius in Italy described by the Roman, Pliny the Younger. These eruptions eject large pumice particles, which can be up to decimeters long and fall out within tens of kilometers of the vent. However, smaller ash particles produced by these extremely energetic eruptions, or those carried along with pyroclastic flows, can be found far from their source. Some

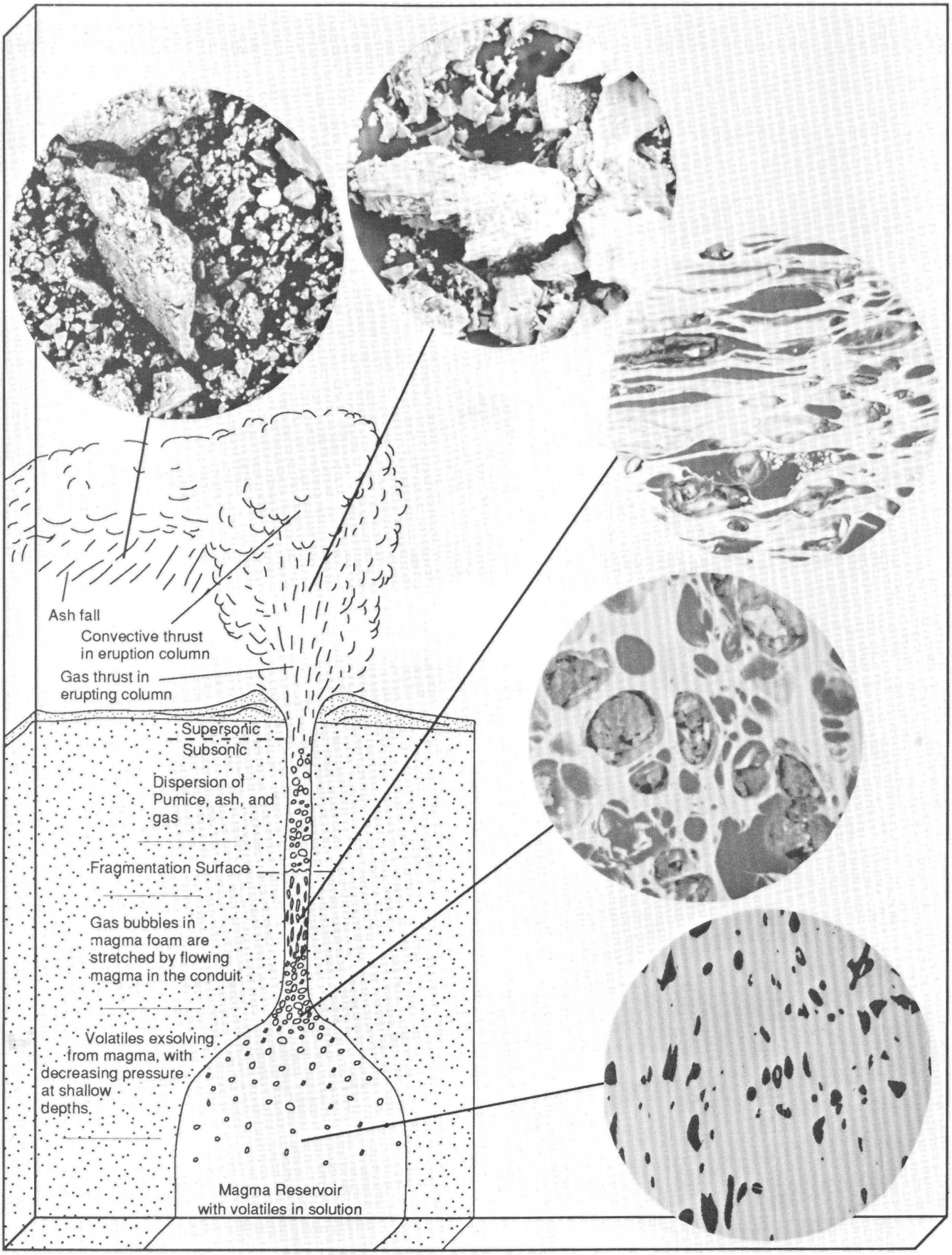
Ash fall
Convective thrust in eruption column
Gas thrust in erupting column
Supersonic
Subsonic
Dispersion of Pumice, ash, and gas
Fragmentation Surface
Gas bubbles in magma foam are stretched by flowing magma in the conduit
Volatiles exsolving from magma, with decreasing pressure at shallow depths
Magma Reservoir with volatiles in solution

**Figure 4** (facing page). Schematic diagram of processes leading to the formation of volcanic ash within explosive volcanic eruptions. This diagram is based nearly entirely on inference and some experimental studies of the processes of gas exsolution and explosive decompression of a rising magma with a composition similar to that found in the eruptions of Augustine Volcano. Scanning electron photomicrographs shown in the circles are about 300 μm in diameter. As magma rises to a depth where the pressure of gas in solution exceeds that of the overlying rock, some of that gas comes out of solution as small bubbles. As the pressure is lowered, those bubbles continue to grow. After the eruption begins, movement of the magma foam in the conduit may stretch the bubbles into elongate, tapered tubes. A fragmentation surface between the pressurized magma foam and the ambient atmosphere tears the brittle foam apart and accelerates the pieces out of the conduit in the eruption column. The particles are carried into eruption clouds and eventually fall to the ground, their final position depending on the height of the eruption column, the strength of winds, and particle size and density. (The samples used here to demonstrate the appearance of volcanic ashes within the eruption column are from coarse ash fallout deposits—in situ samples from eruption columns have never been collected.)

fine-grained ash deposits are made up mostly of the lighter glass shards, separated from denser mineral and rock grains by either gravitational segregation within the eruption plume or by the buoyant rise of gases from the eruption clouds.

Glass shards are pieces of bubble walls broken from the magma foam rising in the volcanic vent. The shard shapes depend on bubble shapes and sizes within the magma foam and the eruption processes responsible for the fragmentation. Shards exhibit a wide range of appearances, ranging from slightly curved, thin glass plates broken from large, thin-walled spherical gas bubbles, to hollow needles broken from pumiceous melts containing vesicles stretched by flow (Heiken and Wohletz, 1985). The example shown in figure 5 is a glass shard collected over central Wyoming at an altitude of 18 km, 72 hours after the May 18, 1980, eruption of Mount St. Helens.

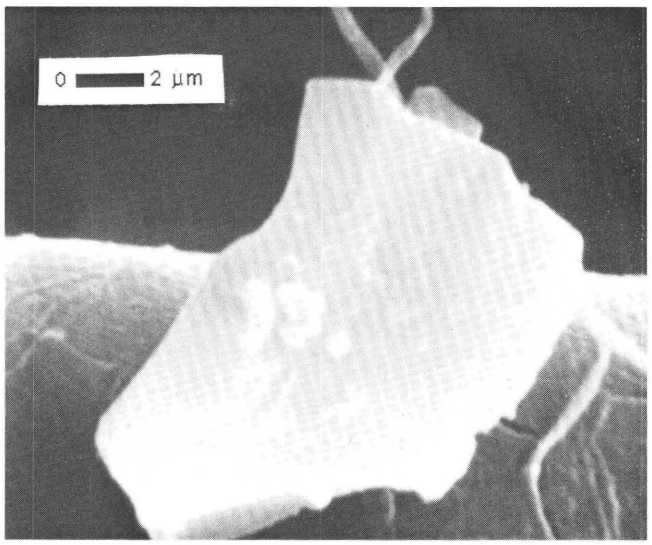


**Figure 5.** Ash from the May 18, 1980, eruption of Mount St. Helens, Washington. The 7-μm-long glass shard shown here is from a sample collected by high-altitude aircraft at an altitude of 18.3 km (60,000 ft) over south-central Wyoming on May 21, 1980. This shard is from a sample with a median particle size of 1.5 μm.

## HYDROVOLCANIC ERUPTIONS

Hydrovolcanic eruptions occur when molten rock comes into contact with ground water or the surface water in lakes, marshes, and littoral areas. Formation and collapse of steam films at the water/molten rock interface causes deformation and fragmentation of the melt and explosive expansion of high-pressure steam. The rapid superheating of water results in eruptions that are more efficient at fragmenting and dispersing volcanic ash than those eruptions that are driven only by bubble growth and decompression. Eruptions can be driven by gas-bubble growth and magmatic overpressures, as well as by magma/water interactions. Hydrovolcanic eruptions produce very fine grained volcanic ash, made up mostly of bits broken from glass bubble walls. Hydrovolcanic ashes may have median grain sizes as low as 40 μm, and we now recognize that the very fine grained components (<10 μm) of such eruptions stay in stratospheric suspensions long enough to be carried thousands of kilometers (Self and Sparks, 1978; Wilson, this volume).

# SMALL-VOLUME EXPLOSIVE ERUPTIONS

The examples given so far are from the most explosive types of volcanic eruptions, which erupt silica- and gas-rich magmas (table 1). However, the majority of the Earth's subaerial volcanoes erupt mostly basaltic lava flows and relatively small volumes of volcanic ash and coarser ejecta (Basalt is a silica-poor—< 52 weight percent $SiO_2$—and iron-rich magma type that comprises most of the Earth's volcanic rocks). Eruptions of basalt typically have only a very small explosive component.

## LAVA FOUNTAINS (HAWAIIAN ERUPTIONS)

Low-viscosity (< $10^3$ poise) basaltic magmas erupt as lava fountains and as lava flows. These eruptions are seen safely every year by thousands of tourists in Hawaii. The lava fountains range from a few meters to over 1 km in

**Table 1.** Explosive eruption types and their products.

[Approx., approximate; ang., angular; frags., fragments; med., medium]

| Height of eruption column (km) | Approx. area affected by ash fallout ($km^2$) | Ash composition (percent) | | | Types of glass particles in ash | Potential hazard to avaiation | Examples |
|---|---|---|---|---|---|---|---|
| | | Glass shards and pumice | Mineral grains | Rock fragments | | | |
| **Plinian eruptions** | | | | | | | |
| 10–40 | Hundreds to tens of thousands | ≅60–100 | ≅0–35 | 0–30 | cm- to μm-size ang. shards and pumice | High; over large regions | 1 |
| **Plinian-hydrovolcanic eruptions** | | | | | | | |
| 20–50 | Tens of thousands to hundreds of thousands | ≅60–100 | ≅0–35 | ≅0–40 | mm- to μm-size ang. shards and rare pumice | High; over large regions | 2 |
| **Vulcanian eruptions** | | | | | | | |
| 0.3–3.0[3] | Tens to hundreds | ≅10–30 | ≅10–30 | ≅70–90 | mm-size ang. frags. and rare droplets | High locally; med. regionally | 4 |
| **Strombolian eruptions** | | | | | | | |
| 0.1–2.0[5] | 0.5–5.0 | ≅60–80 | ≅1–5 | ≅20–40 | cm- to mm-size ang., blocky frags. | Low | 6 |
| **Hawaiian eruptions** | | | | | | | |
| < 0.1–0.5 | < 0.05–0.05 | ≅60–80 | ≅1–5 | ≅20–40 | cm- to mm-size droplets and bombs | Low | 7 |
| **Surtseyan (hydrovolcanic) eruptions** | | | | | | | |
| 0.3–2 | 1.0–200 | ≅70–100 | ≅0–10 | ≅5–30 | mm- to μm-size ang., blocky frags. | Med. locally | 8 |

[1] Krakatau, Indonesia, 1883; Pinatubo, Philippines, 1991; Mount St. Helens, USA, 1980.
[2] Taupo, New Zealand, approx. 150 A.D.
[3] Rarely to more than 10 km.
[4] Fuego, Guatemala, 1966; Ngauruhoe, New Zealand, 1974.
[5] Rarely to more than 3 or 4 km.
[6] Stromboli, Italy, (to the present day); Cerro Negro, Nicaragua, 1968.
[7] Kilauea volcano, Hawaii, (most of the time).
[8] Surtsey, Iceland, 1963; Taal, Philippines, 1977.

height and deposit welded spatter (bombs and ash) as a circular or oval apron around a central vent or as ridges parallel to a fissure vent. Sprays of low-viscosity basaltic liquid that form the fountains are driven by expansion of magmatic gases. Particles from lava fountains range in size from bombs 1 m or more across to spheres a few micrometers in diameter. Coarser ejecta are deposited within a few hundred meters of the vent and finer ash, including filamentous Pele's hair, is swept downwind and deposited as ashfall. Nearly all fountaining is accompanied by lava flows.

## STROMBOLIAN ERUPTIONS AND CINDER CONES

Explosive bursts of solidified and partly solidified bombs, blocks, and ash moving in ballistic trajectories are known as Strombolian activity, named after Stromboli, a volcano in the Aeolian Islands, Italy. Strombolian eruptions consist of weak to violent ejection of partly fluid blobs. Nearly all of the ejecta falls ballistically around the vent, building a "cinder" or "scoria" cone (McGetchin and others, 1974). Activity at cinder cones can switch rapidly between lava fountaining, Strombolian bursts, and Vulcanian eruptions. Volcanic ashes from Strombolian deposits range from irregular, smooth-skinned, bubbly droplets of glass to blocky, crystalline rock fragments with few gas bubbles. This spectrum of textural types is represented in all size categories, from large bombs several meters in diameter to scoria and fine ash.

## VULCANIAN ERUPTIONS

Among the smaller eruption types, Vulcanian eruptions are those characterized by intermittent explosions that deposit ash composed of mostly older solidified lava

particles (MacDonald 1972; Self and others, 1979). These eruptions are most likely caused by overpressures developed within blocked vents. The eruption mechanism is not clear but most likely consists of alternating magmatic and hydrovolcanic processes. Sometimes the eruption will shift between Vulcanian and Strombolian, controlled by either a blocked or open vent. Vulcanian eruptions are associated with some cinder cones, craters in stratovolcanoes, and lava domes. Vulcanian eruptions can produce eruption clouds that generally rise several kilometers, and occasionally to tens of kilometers, above the vent. These eruptions can also erupt small pyroclastic flows (table 1). Because the original material is rich in water vapor, steam may condense between ash grains and pyroclastic flows are turned into mudflows along the lower flanks of a volcano. At Ngauruhoe Volcano in New Zealand, the cannon-like explosions and subsequent ash falls and pyroclastic flows are believed to have been caused by pulverization of a lava plug in the conduit by a combination of magma degassing and vaporization of ground water (Nairn and Self, 1978).

### PHREATIC ERUPTIONS

Perturbations of a geothermal system by injection of new magma at depth, changes in ground-water level, or tectonic activity may cause explosive steam eruptions without the eruption of any magma. This type of activity, known as a phreatic eruption, is possible at many types of volcanoes and even in geothermal areas with no volcanic activity. Steam eruptions may occur with no subsequent activity, as was the case for Soufrière de Guadeloupe in 1976–77 (Heiken and Wohletz, 1985), or they may precede significant magmatic eruptions, such as those that occurred at Mount St. Helens, 1980, and Pinatubo, 1991. The eruptions consist of intermittent or continuous explosive steam bursts and can form large craters. Ejecta from steam eruptions are made up of hydrothermally altered or weathered rock fragments and mud.

## CONCLUSIONS

There are three basic mechanisms of fragmentation in volcanic eruptions: (1) the decompression of rising magma, gas-bubble growth, and subsequent fragmentation as it leaves the conduit, (2) the explosive mixing of magma with ground or surface water, and (3) fragmentation of country rock by rapid expansion of steam and superheated hot water. The variations of eruption style and the characteristics of volcanic ash produced in explosive eruptions depend on factors such as the temperature, volatile content, viscosity and phenocryst content of magmas, the ratio of magma to ground or surface water, and physical properties of rock enclosing the vent. The variations of physical and chemical properties of these ashes are as complex as the volcanoes that produced them.

## ACKNOWLEDGMENTS

This review was supported by the Los Alamos National Laboratory's Institutional Supporting Research Program and under the auspices of the U.S. Department of Energy. A long collaboration with Kenneth Wohletz has made this work possible.

## REFERENCES CITED

Bennett, F.D., 1974, On volcanic ash formation: American Journal of Science, v. 274, p. 648–661.

Carey, S.N., and Sigurdsson, H., 1982, Influence of particle aggregation on deposition of distal tephra from the May 18, 1980, eruption of Mount St. Helens volcano: Journal of Geophysical Research, v. 87, p. 7061–7072.

Gilbert, J.S., Lane, S.J., Sparks, R.S.J., and Koyaguchi, T., 1991, Charge measurements on particle fallout from a volcanic plume: Nature, v. 349, p. 598–600.

Heiken, G., and Wohletz, K., 1985, Volcanic Ash: Berkeley, University of California Press, 246 p.

———1991, Fragmentation processes in explosive volcanic eruptions, *in* Fisher, R.V., and Smith, G., eds., Sedimentation in Volcanic Setting: Society of Economic Mineralogists and Paleontologists Special Publication 45, p. 19–26.

Holloway, J.R., 1976, Fluids in the evolution of granitic magmas: Consequences of finite $CO_2$ solubility: Geological Society of America Bulletin, v. 87, p. 1513–1518.

MacDonald, G.A., 1972, Volcanoes: Englewood Cliffs, New Jersey, Prentice-Hall, 510 p.

McGetchin, T.R., Settle, M., and Chouet, B.A., 1974, Cinder cone growth modeled after Northeast Crater, Mount Etna, Sicily: Journal of Geophysical Research, v. 79, p. 3257–3272.

Nairn, I.A., and Self, S., 1978, Explosive eruptions and pyroclastic avalanches from Ngauruhoe in February, 1975: Journal of Volcanology and Geothermal Research, v. 3, p. 39–60.

Rittmann, A., 1936, Vulkane und ihre Tätigkeit: Stuttgart, Ferdinand Enke Verlag, 188 p.

Rose, W. I., Heiken, G., Wohletz, K., Eppler, D., Barr, S., Miller, T., Chuan, R., and Symonds, R., 1988, Direct rate measurements of eruption plumes at Augustine Volcano: A problem of scaling and uncontrolled variables: Journal of Geophysical Research, v. 93, p. 4485–4499.

Self, S., and Sparks, R.S.J., 1978, Characteristics of widespread pyroclastic deposits formed by the interaction of silicic magma and water: Bulletin Volcanologique, v. 41, p. 196–212.

Self, S., Wilson, L., and Nairn, I.A., 1979, Vulcanian eruption mechanisms: Nature, v. 277, p. 440–443.

Sorem, R.K., 1982, Volcanic ash clusters: Tephra rafts and scavengers: Journal of Volcanology and Geothermal Research, v. 13, p. 63–71.

Verhoogen, J., 1951, Mechanisms of ash formation: American Journal of Science, v. 249, p. 729–739.

Wohletz, K.H., McGetchin, T.R., Sandford, M.T., III, and Jones, E.M., 1984, Hydrodynamic aspects of caldera-forming eruptions: Numerical models: Journal of Geophysical Research, v. 89, p. 8269–8286.

VOLCANIC ASH AND AVIATION SAFETY:
Proceedings of the First International Symposium
on Volcanic Ash and Aviation Safety
U.S. GEOLOGICAL SURVEY BULLETIN 2047

# VOLCANISM IN THE CANADIAN CORDILLERA: CANADA'S HAZARD RESPONSE PREPAREDNESS

*By* Catherine J. Hickson

## ABSTRACT

British Columbia and the Yukon are geologically dynamic regions, encompassing subduction zones, rifting, and thermal anomalies (hot spots). Approximately 100 volcanic vents are arranged in five broad belts and in other more widely scattered regions. Holocene eruptions have occurred in four of the belts. The most recent documented event, a small basaltic eruption, occurred about 200 years ago in northwestern British Columbia. The most recent large explosive eruption occurred about 1.2 thousand years ago when a vent near the Alaska-Yukon border expelled about 30 $km^3$ of pyroclastic material, covering 300,000 $km^2$ of the Yukon under a blanket of ash. In southwestern British Columbia, a Plinian eruption from Mount Meager stratovolcano, occurred about 2.4 thousand years ago. This eruption spread ash across southern British Columbia into Alberta.

In Canada, an integrated response plan to deal with volcanic hazards is now in place and involves all levels of government. Four key agencies operate jointly to ensure timely and appropriate response to a volcanic eruption, including the safe passage of air traffic. Response procedures are being coordinated between the United States and Canada to ensure safety and minimize disruption among residents and aviators.

## INTRODUCTION

Canada is not generally thought of as a "volcanic" country, but there have been several large Holocene eruptions (about 10,000 years ago) in British Columbia and the Yukon that, if repeated today, would cause severe disruption of people, resource extraction, and transportation (Hickson, 1992a, 1992b). This paper summarizes what is known of Holocene volcanism in Canada, reviews concepts of volcanic hazards and risk, and comments on Canada's preparedness to deal with volcanic hazards.

Western Canada is part of the "Pacific Ring of Fire"—a continuous line of subduction zones and transform faults that encircle the Pacific Ocean. This dynamic environment has produced five broad belts of volcanoes plus other isolated and tectonically less well defined volcanic regions (fig. 1). The Garibaldi and Wrangell volcanic belts owe their origin to subduction; the Stikine volcanic belt to crustal extension, and the Anahim volcanic belt to a mantle plume or "hot spot." Deep faults and crustal dynamics in other regions formed volcanic fields such as Wells Gray–Clearwater and other isolated cones, or cone fields, in British Columbia and the Yukon.

## HOLOCENE ERUPTION HISTORY OF WESTERN CANADA

### WRANGELL VOLCANIC BELT

The volcanoes in the Wrangell belt extend from southwestern Yukon into Alaska (fig. 1 and 2). Built over a span of 25 m.y., these volcanoes are related to subduction of the Pacific plate beneath North America off the coast of Alaska (Skulski and Francis, 1986; Skulski and others, 1988; Stephens and others, 1984) and comprise the eastern end of the historically active Aleutian arc (fig. 1). The Wrangell belt is oldest in the eastern (Yukon) portion of the Aleutian arc and becomes progressively younger westward into Alaska (Richter and others, 1990). Magma compositions span basalt to rhyolite, but andesitic lavas dominate. The most voluminous eruptive activity appears to have ended 200,000 years ago as the tectonic regime at the margin progressively changed from dominantly subduction to strike-slip movement (Richter and others, 1990). The most significant Holocene eruptions produced the "White River" ash from Mount Churchill (McGimsey and others, 1990), located in Alaska just west of the Canadian border (fig. 3). Based on radiocarbon dating, two eruptions occurred at 1,800 and 1,200 years B.P. These eruptions ejected an estimated 30 $km^3$ of material and covered 300,000 $km^2$ of the Yukon with a blanket of ash (fig. 3) (Lerbekmo and Campbell, 1969).

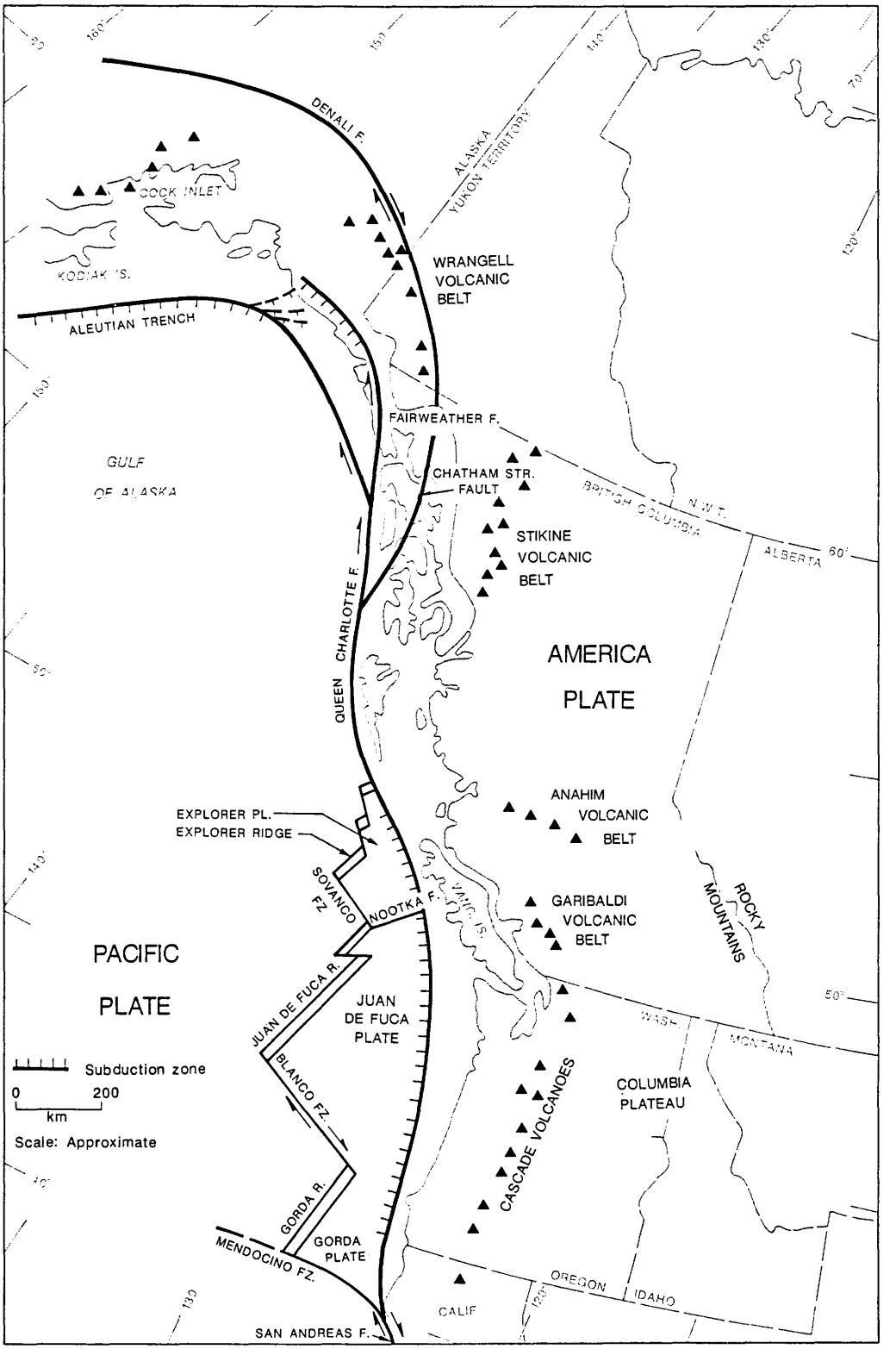


**Figure 1.** Major tectonic elements of western North America. Double lines mark the Explorer, Juan de Fuca, and Gorda ridges (R), which are active spreading centers. Subduction (zones marked by hatchured lines) occurs northward from the Mendocino fracture zone (FZ) to the northern tip of the Explorer plate and along the northern segment of the Fairweather fault (F) and Aleutian trench. Some of the more prominent Holocene volcanic vents are shown as triangles. Small arrows mark the sense of motion along major transform faults.

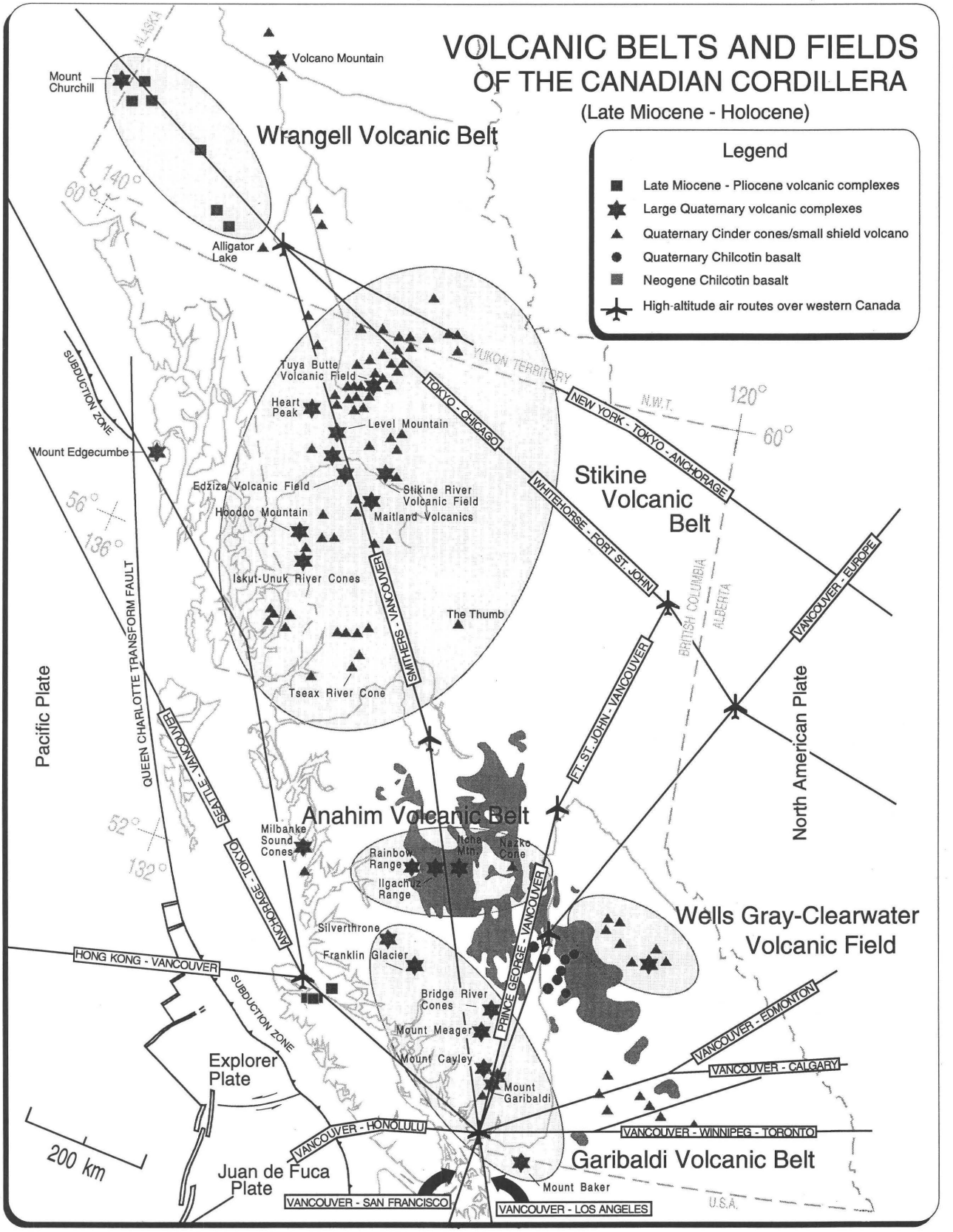


**Figure 2.** Quaternary volcanic elements that make up the Canadian Cordillera are shown overlain by major national and international air routes.

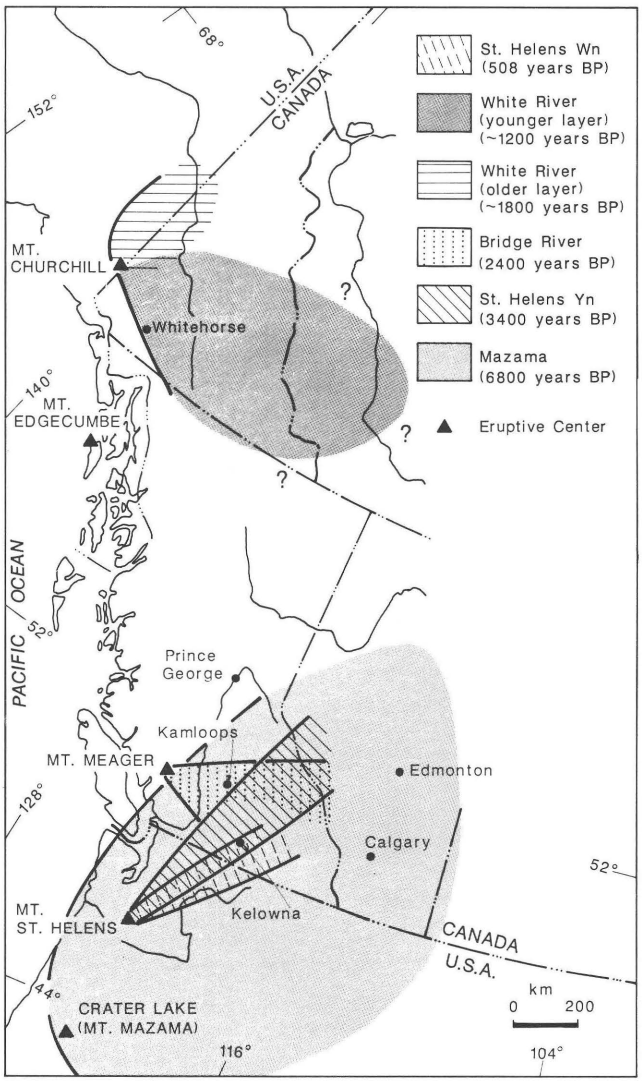


**Figure 3.** Presently known distribution of major Holocene tephras in the Canadian Cordillera, with the exception of historic eruptions. Dates are approximate radiocarbon years before present, and only selected eruptive centers are shown.

## STIKINE VOLCANIC BELT

The Stikine volcanic belt, consisting of over 50 Quaternary volcanic centers, extends northward from the Skeena River to the British Columbia–Yukon border (figs. 1 and 2). This belt lies east of the transition from transform faulting to subduction along the North American–Pacific plate margin (fig. 1) and is related to crustal extension (Souther, 1992). Eruption of alkaline basalt to rhyolite magmas has produced stratovolcanoes, shield volcanoes, and small cinder cones. Detailed mapping exists of the two largest volcanic complexes in the belt, Mount Edziza (Souther, 1990, 1992) and Level Mountain (Hamilton, 1981). Holocene eruptions in the belt are confined to small basaltic cone-building events. The Tseax River Cone (fig. 2), at the southern end of the belt, erupted about 200 years ago (Sutherland-Brown, 1969) and is Canada's youngest known volcanic eruption. Northward migration of the junction between the three tectonic plates (the Pacific, North American, and Explorer plates) during the last 25 m.y. diminished extensional stresses in the region, likely reducing the possibility of future felsic (peralkaline rhyolite and dacite) eruptions. Small basaltic cone-building events are still a possibility, and the impact of such an eruption on downstream habitation or installations must not be overlooked (Souther, 1981).

## ANAHIM VOLCANIC BELT

The Anahim volcanic belt extends across central British Columbia from the coast to the Fraser River (figs. 1 and 2). Volcanism becomes progressively younger from west (more than 12 Ma) to east (less than 7,000 years old), supporting the hypothesis that these volcanoes owe their origin to a mantle hot spot (Hickson, 1986; Souther, 1986). The belt consists of large alkalic shield volcanoes and small basaltic cinder cones. Volcanism appears to have ceased in the western parts of the belts, but if the hypothesis is correct, future volcanism can be expected in the vicinity of Nazko Cone and east of it. Radiocarbon dating of Nazko Cone suggests that the last eruptive period was 7,200 years ago (Souther and others, 1987). Future volcanism is most likely in the form of basaltic cinder cones, but eruptions of less mafic magma, typical of the eastern portions of the belt, cannot be ruled out.

## ALERT BAY VOLCANIC BELT

The Alert Bay volcanic belt is a poorly studied group of volcanic rocks at the northern end of Vancouver Island (fig. 2), which appear to have been active in Pliocene and Pleistocene time. No Holocene eruptions are known (Armstrong and others, 1985), and volcanic activity in this belt has most likely ceased.

## GARIBALDI VOLCANIC BELT

The Garibaldi volcanic belt is the northernmost segment of the Cascade arc, a chain of major andesitic to dacitic stratovolcanoes extending northward from northern California to British Columbia (fig. 1). The arc appears to be segmented (Guffanti and Weaver, 1988; Sherrod and Smith, 1990); the central portion of the arc is the most active (Scott, 1990) and the northern end least active (Sherrod and Smith, 1990). Long repose periods, up to several thousand years, between major explosive events at the major volcanoes (Mounts Meager, Cayley, and Garibaldi), appears to typify the Canadian portion of the Cascade arc. A number of studies

address volcanism in the Garibaldi volcanic belt (Mathews, 1952, 1958; Green, 1981, 1990; Green and others, 1988; Souther, 1980; Read, 1990; Stasiuk and Russell, 1989, 1990). These studies have identified eruptive periods that are shown diagrammatically in figure 4.

Volcanoes of the Garibaldi belt have been sporadically active over a time span of several millions of years (fig. 4). The most recently documented eruption was about 2,400 years ago at Mount Meager (fig. 5). This eruption may have been close in size to that of the May 18, 1980, eruption of Mount St. Helens. Ash from this eruption can be traced eastward to western Alberta (fig. 3). Hot springs in the vicinity of Mounts Cayley and Meager suggest that magmatic heat is still present. The long history of volcanism in this region, coupled with continued subduction off the coast, suggests that volcanism has not yet ended in the Garibaldi volcanic belt.

## OTHER REGIONS

Throughout British Columbia and the Yukon, isolated monogenetic cinder cones and cone fields can be found (fig. 2). The most significant concentration of these is probably

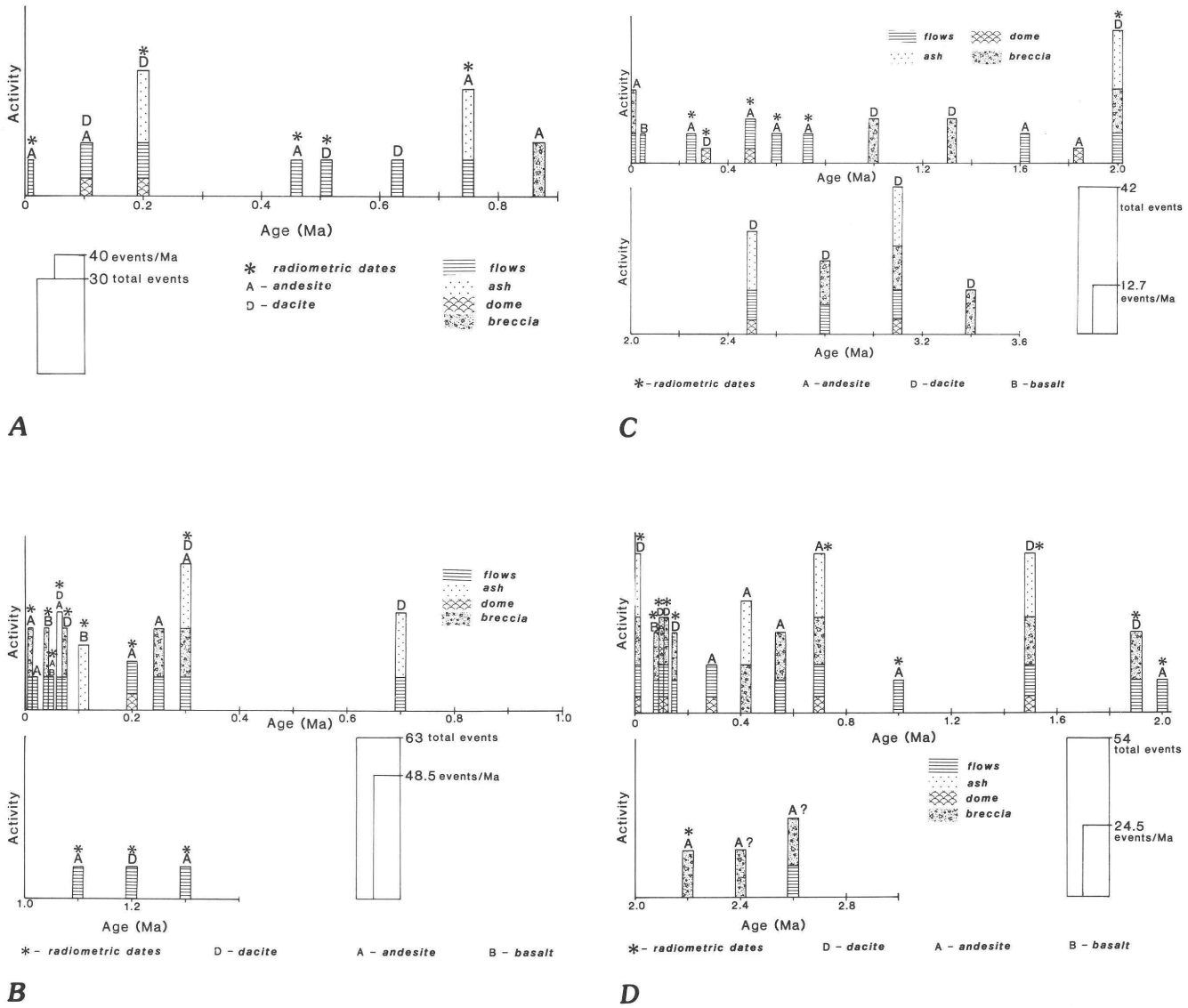


**Figure 4.** Diagrammatic representation of eruptive activity within the Garibaldi volcanic belt. Height of each histogram gives a very crude indication of the size of the eruption. *A*, Mount Garibaldi volcanic field. *B*, Garibaldi Lake volcanic field. *C*, Mount Cayley volcanic field. *D*, Mount Meager and Elaho Valley volcanic complexes. Data from Mathews (1952, 1958), Green (1981, 1990), Souther (1980), Read (1990), Stasiuk and Russell (1989, 1990).

**Figure 5.** Vent area of Mount Meager, which erupted about 2,400 years ago. Crater is open to the east (foreground) and is 1.5 km wide at the rim. The crater is outlined by steep ridges surrounding the small dome and short lava flow, which are visible in the center of the picture.

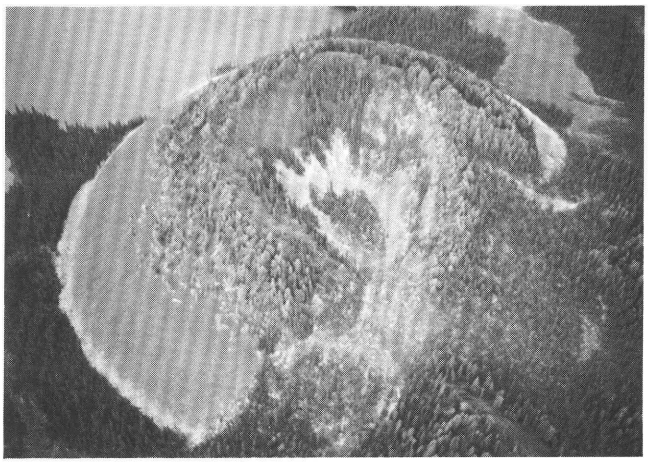

**Figure 6.** Kostal Cone, a basaltic cinder cone in Wells Gray Provincial Park, British Columbia.

the Wells Gray–Clearwater region of British Columbia (Hickson, 1986). Volcanism over several million years has produced numerous small-volume flows and cinder cones. The youngest of these, Kostal Cone (fig. 6), may be only a few hundred years old.

The scattered, isolated cones and cone fields throughout British Columbia and the Yukon, are unlikely to erupt again, but they do identify weaknesses in the crust that may preferentially channel magma to produce more small-volume basaltic eruptions in the future. An exception to this is Volcano Mountain in the Yukon, a small basaltic shield volcano and associated vents that have erupted several times in their 1- to 2-million-year history (Jackson and Stevens, 1992).

## VOLCANIC HAZARDS AND VOLCANIC RISK

Erupting volcanoes may pose a number of specific hazards such as lava flows, pyroclastic flows and surges, fallout of ash, debris flows (lahars), avalanches, seismic activity, ground deformation, tsunami, acid rain, and poisonous gases (Blong, 1984; Tilling, 1989). What hazard will occur at which volcano depends to large degree on the composition of the erupting magma (table 1). Basaltic eruptions pose a minimal hazard in comparison with explosive andesitic, dacitic, or rhyolitic eruptions.

Basaltic eruptions, though generally considered least hazardous, may have a significant impact if the eruption occurs during winter months in regions of heavy snow-pack. The eruption may trigger debris flows (lahars) or floods from rapidly melting snow. Some basaltic eruptions in Canada have been near glaciers, and subglacial volcanism has occurred in British Columbia in the past (Mathews, 1947; Hickson, 1986). This form of volcanism can produce potentially destructive water outburst floods known as jokulhlaups, and water-magma interactions can potentially produce very large phreatic or phreato-magmatic eruptions—even if the magma is basaltic.

Erupting volcanoes pose a hazard when something of value (such as human lives, property, or resources) is impacted to its detriment. Risk is usually assessed on the basis of the number of human lives that may be lost as a result of a hazardous event. Yokoyama and others (1984) devised a method for assessing risk at a volcano that takes into account past activity at the volcano, present seismicity and ground deformation, and population at risk. Using this scheme and considering our present understanding of the volcanic record in Canada, no Canadian volcano falls into the high-risk category. Canada is still relatively underpopulated, thus a volcanic eruption within Canada, with few exceptions, will probably result in few if any direct casualties, baring aviation emergencies. The legacy of any large explosive eruption in Canada will be regional disruption of aviation, loss of resources such as forests and spawning streams, and displacement of people.

In the short term, perhaps the greatest impact on Canada may be from eruptions elsewhere in western North America. Prehistoric eruptions of Mount St. Helens left thin ash layers in southern British Columbia, and the eruption of Mount Mazama deposited a blanket of ash several centimeters in thickness over southern British Columbia and much of Alberta (fig. 3). Most recently, within 24 hours of the May 18, 1980, eruption of Mount St. Helens, light ashfall in southern British Columbia, Alberta, and Saskatchewan caused concern among residents and the aviation community.

**Table 1.** General relationships between volcano types, predominant lava, eruption styles, and common eruptive characteristics.

[from Tilling, 1989, table 1.1, p. 2]

| Volcano type | Predominant lava | | Eruption style | Common eruptive characteristics |
|---|---|---|---|---|
| | Composition | Viscosity | | |
| Shield[1] | Basaltic (mafic) | Fluidal | Generally non-explosive to weakly explosive | Lava fountains, lava flows (long), lava lakes and pools. |
| | Andesitic | Less fluidal | Generally explosive, but sometimes non-explosive | Lava flows (medium), explosive ejecta, tephra falls. |
| Composite[2] | Dacitic to rhyolitic (felsic, silicic) | Viscous to very viscous, but can be non-explosive | Typically highly explosive, but can be non-explosive, especially after a large eruption | Explosive ejecta, tephra falls, pyroclastic flows and surges, lava domes. |

[1] Generally located in the interior of tectonic plates ("intraplate") and presumed to overlie "hot spots," but also may occur in other tectonic settings (e.g., Hawaii, Galapagos, Iceland, Kamchatka).

[2] Generally located along or near the boundaries of convergent tectonic plates (subduction zones); also called stratovolcanoes (e.g., Cascade-Garibaldi volcanic belt, Wrangell volcanic belt).

In Alaska, during the 1989–90 eruptions of Redoubt Volcano, tephra drifted into Canada at least twice, and in 1992, Mount Spurr erupted three times, sending ash plumes into Canadian airspace, including some parts of west-central Yukon. An eruption of Mount Baker in northern Washington State, close to one of Canada's busiest terminal areas (fig. 2), could have serious repercussions. Response procedures are being coordinated between the United States and Canada to ensure safety and minimize disruption among residents and aviators.

## VOLCANO MONITORING

In Canada at present, there is no specific program to monitor volcanoes. However, certain seismic stations in the regional seismic network, put in place to study tectonic earthquakes, are located to optimize coverage of nearby Holocene volcanoes. At present, only seismic stations in the southwestern portion of the network, covering the Garibaldi volcanic belt, are telemetered directly to the Geological Survey of Canada's (GSC) western seismic base at the Pacific Geoscience Centre (PGC) on Vancouver Island. In this part of the network, it is possible to detect and locate earthquakes of magnitude 1.0 and above. This is sufficient sensitivity to detect precursor seismic activity in the Garibaldi volcanic belt.

A program is in place to upgrade the network and to telemeter stations to PGC from other parts of western Canada. When completed, the network will allow real-time detection and location of earthquakes magnitude 3 and greater throughout western Canada. With the exception of a very large impending eruption, this will be insufficient for detection of precursor activity associated with smaller Vulcanian or Strombolian eruptions, such as those of the 1992 eruptions of Mount Spurr. It should, however, be sufficient to permit officials to confirm or deny a reported large volcanic eruption.

## PREPARING FOR AN ERUPTION

Despite infrequent natural disasters, Canadians have not ignored the fact that they live in a geologically active region in which future earthquakes and volcanic eruptions are a certainty. However, Peterson and Tilling (in press) find that countries faced with infrequent volcanic eruptions, even when that country is scientifically advanced, have extreme difficulty dealing with volcanic events. "Unrest at long-quiescent volcanoes is particularly difficult to diagnose: such unrest does not necessarily culminate in an eruption, but if an eruption does occur, it may be particularly violent. Either outcome poses difficult challenges to scientists, not only in their study of the volcano, but in their public relations." (Peterson and Tilling, in press).

Monitoring unrest at a volcano is a complex exercise that does not necessarily result in easy or straightforward answers. Figure 7 shows the communication network between the GSC and other agencies that would become involved in any volcanic emergency in Canada. Communication between the groups and emergency planning are the key to effective response to a natural disaster.

Emergency planning in British Columbia is carried out by the Provincial Emergency Program (PEP) and Emergency Preparedness Canada (EPC) (Anderson and others, 1990; Dalley, 1992; Pollard, 1992). At present, the level of preparedness for a volcanic eruption consists of a notification network set up between the government agencies involved (fig. 7) and formalized in the Interagency Volcanic Event Notification Plan (IVENP, available from the author).

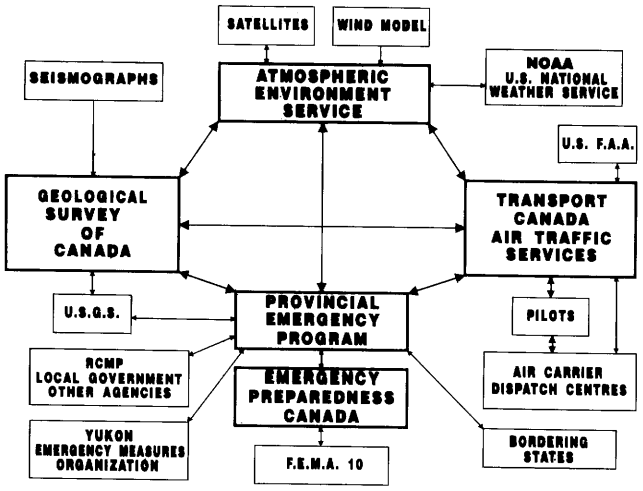


**Figure 7.** Communication pathways for notification, coordination, and response of government agencies in Canada and data-input sources, such as seismographs, satellites, and wind models. Also shown are agencies outside the formal notification network, such as local governments, which may provide an eruption alert or require information on an eruption. Also listed are agencies in neighboring American States, which may, in a similar manner, provide eruption alerts or require notification of an eruption in Canada. Abbreviations used in this figure: U.S.G.S., U.S. Geological Survey; RCMP, Royal Canadian Mounted Police; F.E.M.A., Federal Emergency Management Agency; NOAA, National Oceanic and Atmospheric Administration; F.A.A., Federal Aviation Administration.

Terms of reference for the working group include participation of the agencies in planning and simulation exercises and yearly updates to the plan.

Each agency in the plan has specific responsibility to pass information on to other involved agencies and to respond according to its individual mandate. Reports of a volcanic eruption within Canada are transmitted around the network for response and confirmation. For example, Transport Canada Aviation is responsible for transmitting, in a timely manner, information regarding an eruption to ensure the safe passage of aircraft around the affected area. The PEP will be responsible for notification of the municipality and people living in the region affected. The GSC assumes responsibility for seismic confirmation of an event (within the limitations of the current seismic network), hazard warning, monitoring and passing information on to the other involved agencies as outlined in its "statement of responsibility" in the IVENP. Presently, the "statement of responsibility" gives an optimum situation that will require resources beyond those currently available from the GSC. However, work is underway to identify sources of expertise and equipment that could be called upon to help in the case of a volcanic emergency. It will be the responsibility of the GSC Staff Volcanologist to make sure that people and equipment are identified. The IVENP, internal response plans, and interagency contacts are kept current.

## CONCLUSIONS

Western Canada has been spared volcanism on a human time frame—but has not on a geological one. Volcanic activity has occurred in the past, and we must try to look beyond the short human memory when we are dealing with geologic hazards that have recurrence intervals of longer than 50 years. Hazard zonation and planning must be an integral part of our future if we are to save lives and property. In the area of emergency planning for volcanic eruptions, we can help by increasing public awareness and putting into place well-thought-out emergency plans. Detailed geological work has begun at specific volcanoes to help quantify the risk from future eruptions, but more work is necessary. This work should be carried out before rezoning or major shifts in population occur.

## ACKNOWLEDGMENTS

M. Stasiuk compiled the data for figure 4; his help is sincerely appreciated. D. McDonald, I. Alarie, and B. Vanlier helped with preparation of the manuscript. T. Neal, T. Spurgeon, and L. Jackson provided thoughtful reviews of the manuscript.

## REFERENCES CITED

Anderson, P., Edelson, N., Hansen, B., Harding, R., Huhtala, K., and Laughy, L., 1990, Hazard management planning in British Columbia: Issues and challenges for emergency preparedness planning: University of British Columbia Centre for Human Settlements, 32 p.

Armstrong, R.L., Muller, J.E., Harakal, J.E., and Muehlenbachs, K., 1985, The Neogene Alert Bay volcanic belt of northern Vancouver Island, Canada: Descending-plate-edge volcanism in the arc-trench gap: Journal of Volcanology and Geothermal Research, v. 26, p. 75–97.

Blong, R.J., 1984, Volcanic Hazards: New York, Academic Press, 424 p.

Dalley, W.C., 1992, The role of the Provincial Emergency Program in geological hazards management and mitigation, *in* Geological Hazards in British Columbia Symposium Proceedings, Victoria, British Columbia, February 20–21, 1991: British Columbia Geological Survey Open-File Report 1992-15, p. 109–110.

Green, N.L., 1981, Geology and petrology of Quaternary volcanic rocks, Garibaldi Lake area, southwestern British Columbia: Geological Society of America Bulletin, v. 92, pt. 1, p. 697–702, pt. 2, p. 1359–1470.

———1990, Late Cenozoic volcanism in the Mount Garibaldi and Garibaldi Lake volcanic fields, Garibaldi volcanic belt, southwestern British Columbia: Geoscience Canada, v. 17, no. 3, p. 171–179.

Green, N.L., Armstrong, R.L., Harakal, J.E., Souther, J.G., and Read, P.B., 1988, Eruptive history and K-Ar geochronology of the Garibaldi volcanic belt, southwestern British Columbia: Geological Society of America Bulletin, v. 100, p. 563–579.

Guffanti, M., and Weaver, C.S., 1988, Distribution of late Cenozoic volcanic vents in the Cascade Range, volcanic arc segmentation and regional tectonic considerations: Journal of Geophysical Research, v. 93, p. 6513–6529.

Hamilton, T.S., 1981, Late Cenozoic alkaline volcanics of the Level Mountain Range, northwestern British Columbia: Edmonton, University of Alberta, unpub. Ph.D. dissertation, 265 p.

Hickson, C.J., 1986, Quaternary volcanics of the Wells Gray–Clearwater area, east central British Columbia: Vancouver, University of British Columbia, unpub. Ph.D. dissertation, 357 p.

———1992a, Volcanic hazards and volcanism in the Canadian Cordillera, *in* Geological Hazards in British Columbia Symposium Proceedings Volume, Victoria, British Columbia, 1991: British Columbia Geological Survey Open-File Report 1992-15, p. 35–56.

———1992b, Volcanic hazards in Canada: Should we worry?, *in* Geotechnique and Natural Hazards Symposium Proceedings Volume, Vancouver, British Columbia, 1992, Vancouver, British Columbia, BiTech Publishers Ltd., p. 31–40.

Jackson, L.E., and Stevens, W., 1992, A recent eruptive history of Volcano Mountain, Yukon Territory: Geological Survey of Canada Paper 92-1A, p. 33–39.

Lerbekmo, J.F., and Campbell, F.A., 1969, Distribution, composition, and source of the White River ash, Yukon Territory: Canadian Journal of Earth Science, v. 6, p. 109–116.

Mathews, H.W., 1947, "Tuyas," flat-topped volcanoes in northern British Columbia: American Journal of Science, v. 245, p. 560–570.

———1952, Mount Garibaldi, a supraglacial Pleistocene volcano in southwestern British Columbia: American Journal of Science, v. 250, p. 81–103.

———1958, Geology of the Mount Garibaldi map-area, southwestern British Columbia, Canada: Geological Society of America Bulletin, v. 69, p. 179–198.

McGimsey, R.G., Richter, D.H., DuBois, G.D., and Miller, T.P., 1990, A postulated new source for the White River ash, Alaska, *in* Geological Studies in Alaska by the U.S. Geological Survey, 1990: U.S. Geological Survey Bulletin 1999, p. 212–218.

Peterson, D.W., and Tilling, R.I., in press, Interactions between scientists, civil authorities, and the public at hazardous volcanoes, *in* McGuire, W.J., Kilburn, C.R.J., and Murray, J.B., eds., Handbook for Monitoring Active Volcanoes, University College London Press.

Pollard, D., 1992, The role of emergency preparedness Canada, *in* Geological Hazards of British Columbia Symposium Proceedings Volume, Victoria, British Columbia, February 20–21, 1991: British Columbia Geological Survey Open-File Report 1992-15, p. 115–118.

Read, P.B., 1990, Mount Meager complex, Garibaldi belt, southwestern British Columbia: Geoscience Canada, v. 17, p. 167–174.

Richter, D.H., Smith, J.G., Lanphere, M.A., Dalrymple, G.B., Reed, B.L., and Shew, N., 1990, Age and progression of volcanism, Wrangell volcanic field, Alaska: Bulletin of Volcanology, v. 53, p. 29–44.

Scott, W.E., 1990, Patterns of volcanism in the Cascade arc during the past 15,000 years: Geoscience Canada, v. 17, p. 179–187.

Sherrod, D.R. and Smith, J.G., 1990, Quaternary extrusion rates of the Cascade Range, northwestern United States and southern British Columbia: Journal of Geophysical Research, v. 95, p. 19465–19474.

Skulski, T., and Francis, D., 1986, On the geology of the Tertiary Wrangell lavas in the St. Clare Province, St. Elias Mountains, Yukon: Yukon Geology, v. 1, p. 161–170.

Skulski, T., Francis, D., and Ludden, J., 1988, Magma evolution along an obliquely convergent continental margin [abs.]: Eos, Transactions, American Geophysical Union, v. 69, p. 1476.

Souther, J.G., 1980, Geothermal reconnaissance in the central Garibaldi belt, British Columbia: Geological Survey of Canada, Paper 80-1A, p. 1–11.

———1981, Volcanic hazards in the Stikine region of northwestern British Columbia: Geological Survey of Canada, Open-File Report 770, 56 p.

———1986, The western Anahim belt, rootzone of a peralkaline magma system: Canadian Journal of Earth Science, v. 23, p. 895–908.

———1990, Mount Edziza volcanic complex, British Columbia: Geological Survey of Canada, Map 1623A, scale 1:50,000.

———1992, The late Cenozoic Mount Edziza volcanic complex, British Columbia: Geological Survey of Canada, Memoir 420, 320 p.

Souther, J.G., Clague, J.J., and Mathews, R.W., 1987, Nazko Cone, a Quaternary volcano in the eastern Anahim belt: Canadian Journal of Earth Science, v. 24, p. 2477–2485.

Stasiuk, M.V., and Russell, J.K., 1989, Petrography and chemistry of the Meager Mountain volcanic complex, southwestern British Columbia: Geological Survey of Canada Paper 89-1E, p. 189–196.

———1990, The Bridge River assemblage in the Meager Mountain volcanic complex, southwestern British Columbia: Geological Survey of Canada Paper 90-1E, p. 227–233.

Stephens, C.D., Fogleman K.A., Lahr J.C., and Page, R.A., 1984, Wrangell Benioff zone, southern Alaska: Geology, v. 12, p. 373–376.

Sutherland-Brown, A., 1969, Aiyansh lava flow British Columbia: Canadian Journal of Earth Science, v. 6, p. 1460–1468.

Tilling, R.I., ed., 1989, Short Courses in Geology: Volume 1, Volcanic Hazards: Washington D.C., American Geophysical Union, 123 p.

Yokoyama, I., Tilling, R.I., and Scarpa, I., 1984, International mobile early-warning systems(s) for volcanic eruptions and related seismic activities: Paris, UNESCO, FP/2106-82-01(2286), 102 p.

VOLCANIC ASH AND AVIATION SAFETY:
Proceedings of the First International Symposium
on Volcanic Ash and Aviation Safety
U.S. GEOLOGICAL SURVEY BULLETIN 2047

# VOLCANIC ASH IN KAMCHATKA AS A SOURCE OF POTENTIAL HAZARD TO AIR TRAFFIC

*By* Vladimir Yu. Kirianov

## ABSTRACT

The degree of hazard to air traffic from volcanic ash clouds over Kamchatka and the North Kuriles (Russian Federation) is assessed from analyses of the eruptive activity of Sheveluch, Bezymianny, Kliuchevskoi, Karymsky, Avachinsky, Gorely, Alaid, and Ebeko Volcanoes and records of wind speed and direction from the Earth's surface to 15 km. The most hazardous volcanoes are Kliuchevskoi and Alaid because they may eject tephra to altitudes of 10–15 km and their eruptions may last for several months. Ash clouds from most of the volcanoes generally move in an easterly and southeasterly direction in response to prevailing winds.

## INTRODUCTION

Since 1982, when two jumbo-jet aircraft lost engine power owing to encounters with ash clouds from eruptions of Galunggung Volcano in Indonesia, there has been a growing interest in the threat that volcanoes pose for aviation operations. In addition to the potential human costs, aircraft damaged through encounters with volcanic ash have cost in excess of $100 million to repair (Steenblik, 1990). As air transportation increases, this problem will become more acute, especially in volcanically active areas such as in Kamchatka, Eastern Russia, where 29 active and potentially active volcanoes exist and where several eruptions occur each year (fig. 1).

This study discusses explosive activity of the Kamchatkan volcanoes during the last decade in order to determine altitudes and directions of future eruption plumes and their hazards to aviation. Considered in this study are specific features of atmospheric circulation over Kamchatka; the type, frequency, and duration of eruptions; the distribution of volcanic ejecta in the atmosphere; and the altitudes and directions of eruption plumes over Kamchatka and adjoining areas.

## VOLCANIC ASH AND ATMOSPHERIC CIRCULATION

The atmospheric circulation in Kamchatka has been analyzed on the basis of data from 1961–81 and 1988 supplied by 12 meteorological and two aerological stations and from synoptic bulletins of the Kamchatkan Hydrometeorological Survey. These data indicate that the circulation regime changes drastically over Kamchatka because of the effects of both large-scale atmospheric processes and regional features. Most of the region is characterized by seasonal wind variation, particularly near the eastern coast. In the central regions, this seasonal wind variation is distorted by mountain-valley circulation.

On average, approximately 70 cyclones[1] pass through Kamchatka each year, chiefly in autumn and winter. Cyclones migrate from Japan along the Kamchatkan east coast to the Aleutian Islands or into the Bering Sea and produce strong winds. Analysis of vertical distribution of meteorological parameters (wind, temperature, moisture) demonstrates that the most pronounced variations take place in the upper troposphere near the tropopause, which in Kamchatka ranges from 8 to 11 km annually.

The distribution of volcanic ash over large distances is dependent on the character of circulation in the stratosphere. Over the northern part of the Pacific Ocean, volcanic ash is transported by wind currents from west to east, i.e., from the Kamchatka Peninsula toward the Aleutian Islands.

During an eruption, the large amounts of material ejected into the stratosphere form ash clouds in which the maximum ash concentration is at altitudes several kilometers above the tropopause. The highest altitudes of volcanic-particle concentration have been determined to be between 18

[1] Cyclone as used in this paper refers to a center or area of low pressure usually a few hundred kilometers in diameter and does not refer to the very intense, twisting storms of less than 1 km in diameter, i.e., tornadoes, as commonly used in the United States.

and 21 km. Lidar data and modeling results show that during the Fuego (Guatemala) eruption of 1974, approximately one-half of the erupted material lingered within a 15- to 22-km-wide belt at 15- to 17-km altitude. Because present-day airliners fly at altitudes not exceeding 15 km (9 km over Kamchatka), we shall consider the characteristic features of volcanic material transport up to altitudes of 15 km.

The general pattern of volcanic ash distribution shows that its transport during ejection and within the troposphere is dependent on wind speed and direction, which may vary with altitude. During the Mount St. Helens eruption on May 18, 1980, the direction of ash transport varied from northeast at 2,300 m altitude, to the east at 11,300 m altitude, and to the southeast at 26,000 m altitude (Sarna-Wojcicki and others, 1981). During the Sheveluch eruption on November 12, 1964, however, a constant wind blew from the west and northwest at all altitudes between 3,000 m and 15,000 m. Similarly, during the Avachinsky eruption on January 13, 1991, the wind blew from the northeast at all altitudes up to 11 km so that the width of the ashfall area at a distance of 25–30 km from the crater did not exceed 4 km (fig. 2). Angles of wind shear direction at all altitudes in both cases did not exceed 50°.

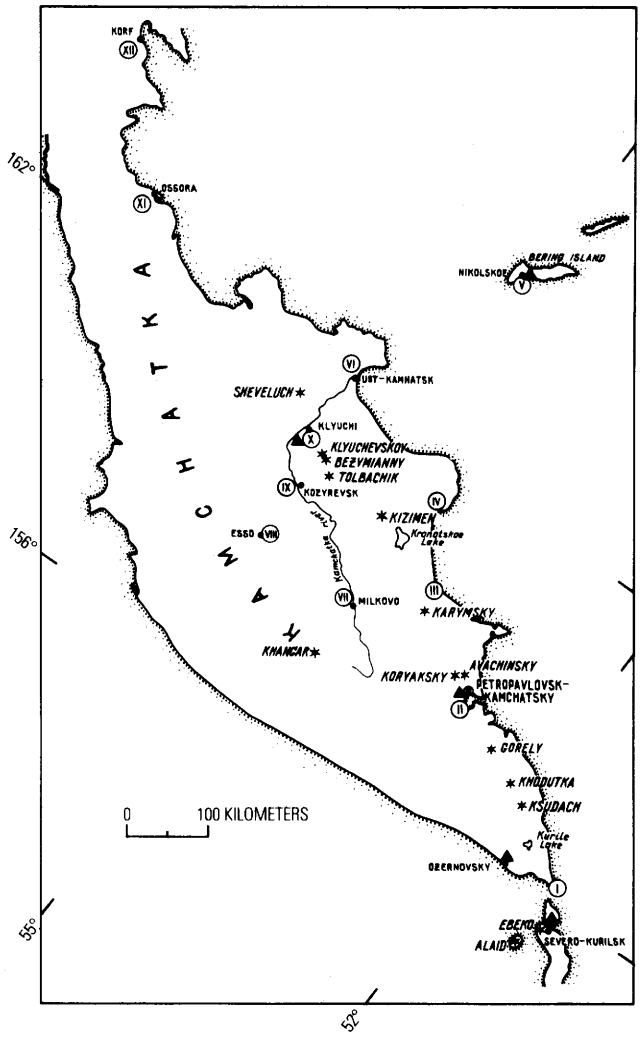


**Figure 1.** Location of volcanoes and meteorological and aerological stations in Kamchatka. Volcanoes are shown by starburst symbol; airports are shown by solid triangles; meteorological stations are shown by open circles containing roman numerals.

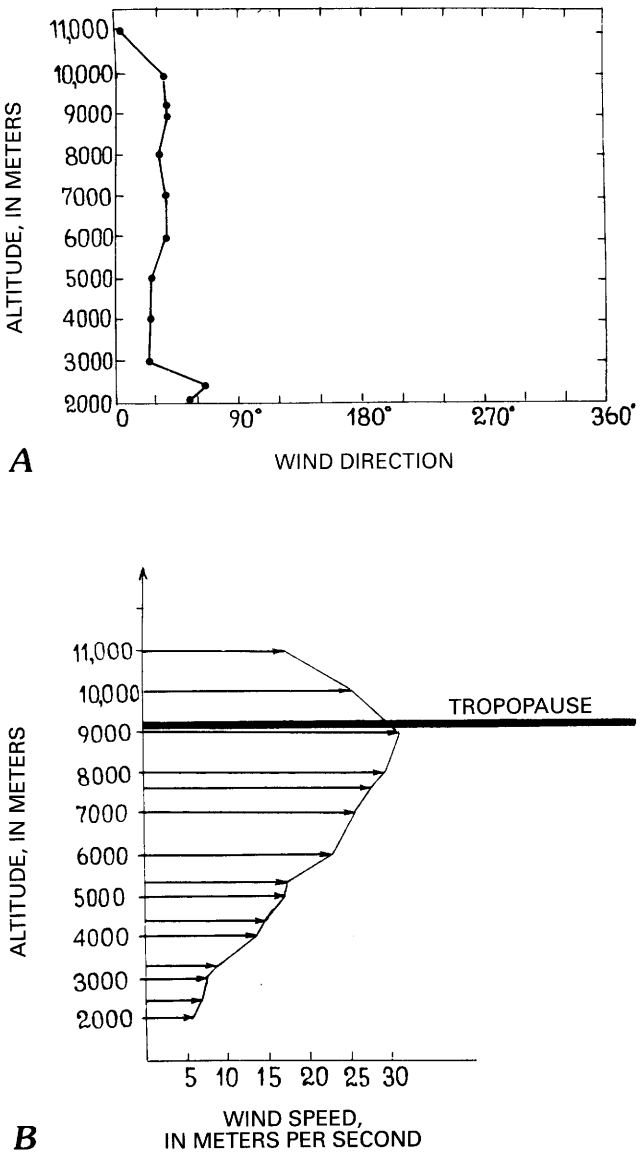


**Figure 2. The Avachinsky Volcano eruption on January 13, 1991: *A*, wind-direction profile; *B*, wind-speed profile.**

**Table 1.** Volcanoes in Kamchatka and the Kurile Islands that have erupted during the last 10 years and the possible character of their future eruptions.

[A, andesite; AB, andesitic basalt; B, basalt; comp., composition; freq., frequency. Altitude refers to the maximum altitude of the eruption cloud. Direction refers to the most likely directions that the eruption cloud may drift]

| Name of volcano | Coordinates (lat, long) | Height (m) | Date of most recent eruption | Rock comp. | Eruption freq. per year | Possible features of future eruptions | | |
|---|---|---|---|---|---|---|---|---|
| | | | | | | Altitude (km) | Duration | Direction |
| Sheveluch | 55.97°N., 161.58°E. | 3,395 | Jan. 1991 | A | 10 | 4–8 | [1] | E., SE. |
| Bezymianny | 55.97°N., 160.59°E. | 2,800 | Mar. 1990 | A | 1–2 | 5–8 | [2] | NE., E., S. |
| Kliuchevskoi | 55.06°N., 160.64°E. | 4,850 | Mar. 1990 | B | 1 | 6–10 | [3] | E., SE., S. |
| Avachinsky | 53.22°N., 159.00°E. | 2,751 | Jan. 1991 | AB, A | 1 | 4–10 | [2] | NE., SE. |
| Gorely | 52.45°N., 158.12°E. | 1,829 | 1986 | A | 1 | 3–8 | [3] | E., SE. |
| Karymsky | 54.07°N., 159.60°E. | 1,486 | 1982 | A | 1 | 2–6 | [2] | E., SE., S. |
| Alaid | 50.80°N., 155.50°E. | 2,339 | Apr.–June 1981 | B | 1 | 815 | [3] | NE., E., SE. |
| Ebeko | 50.67°N., 155.93°E. | 1,138 | 1987, 1988–90 | A | 100 | 1–2 | [1] | NE., E., SE. |

[1] A few tens of seconds to minutes.
[2] Hours to days.
[3] Days to months.

Analysis of prevalent wind directions and speeds at various altitudes over Kamchatka indicate the following:

1. Wind directions change with the seasons, which points out the monsoon character of circulation in Kamchatka.
2. The prevailing surface-wind directions at four key measurement stations in the regions of active volcanoes are: to the southeast and east at Lopatka Cape; to the northwest, southeast, and east at Petropavlovsk-Kamchatsky; to the southeast, south, and southwest at Semyachik; and to the west, east, and southeast at Klyuchi. At all these points, the winds blew to the southeast at a speed of 4.5–11.2 m/s for more than 20 percent of the year.
3. Air masses in the troposphere over Petropavlovsk-Kamchatsky between 3- to 9-km altitude flow to the east, southeast, and northeast, and the average maximum speed of the wind increases from 10.3 m/s at 3-km altitude to 23 m/s at 9-km altitude.

   In the city of Klyuchi (fig. 1), the wind at an altitude of between 3 and 9 km blows predominantly to the east, southeast, and south and the wind speed increases with increasing altitude. It is noteworthy that, during some large historic eruptions (Bezymianny in 1956 and Ksudach in 1907) and during several eruptions in the Holocene (Avachinsky, Sheveluch, and Ksudach), the ash plume drifted to the north. This is atypical because air masses here move in a northerly direction at all altitudes, on average, only about 15 days per year. Therefore, forecasting the direction of possible ashfalls in future eruptions of Kamchatkan volcanoes should be made carefully.
4. The wind direction in the stratosphere is constant, and air masses move east and southeast at speeds from 20 to 36 m/s.

## ACTIVE VOLCANOES IN KAMCHATKA

At present, the Kamchatka volcanoes most dangerous to air traffic are Sheveluch, Kliuchevskoi, Bezymianny, Avachinsky, Gorely, and Karymsky (fig. 1). The Kurile volcanoes, Alaid on Atlasov Island (the ashes of which fell on Petropavlovsk-Kamchatsky during the 1981 eruption) and the very active Ebeko on Paramushir Island, must also be considered. The characteristics of Kamchatka and Kurile eruptive activity during the last decade are discussed below and are summarized in table 1.

### SHEVELUCH

(LAT 56.78°N., LONG 161.58°E., ELEVATION 3,395 M)

The northernmost active volcano in Kamchatka, Sheveluch, is noted for formation of extrusive domes that are subsequently destroyed during great explosive eruptions with directed blasts (fig. 3). The most recent such eruption occurred on November 12, 1964 (Gorshkov and Doubik, 1965), and sent an eruption cloud to 12-km altitude as determined from a TU-104 jet airplane, which was making a scheduled flight near Sheveluch at that time.

In 1980, an andesitic extrusive dome started to grow within the crater, and gas-and-ash explosions began in 1984. These explosions are similar in style: they occurred suddenly, lasted for only a few tens of seconds, and resulted in a cauliflower-like eruption column (Zharinov and others, 1990) that reached 4- to 6-km altitude.

Recently, the frequency of eruptions increased from 4–5 per year (1984–85) up to approximately 3,340 per year beginning in 1987. The latest activity was on August 4, 1990, when the ash cloud rose to 6-km height and then drifted

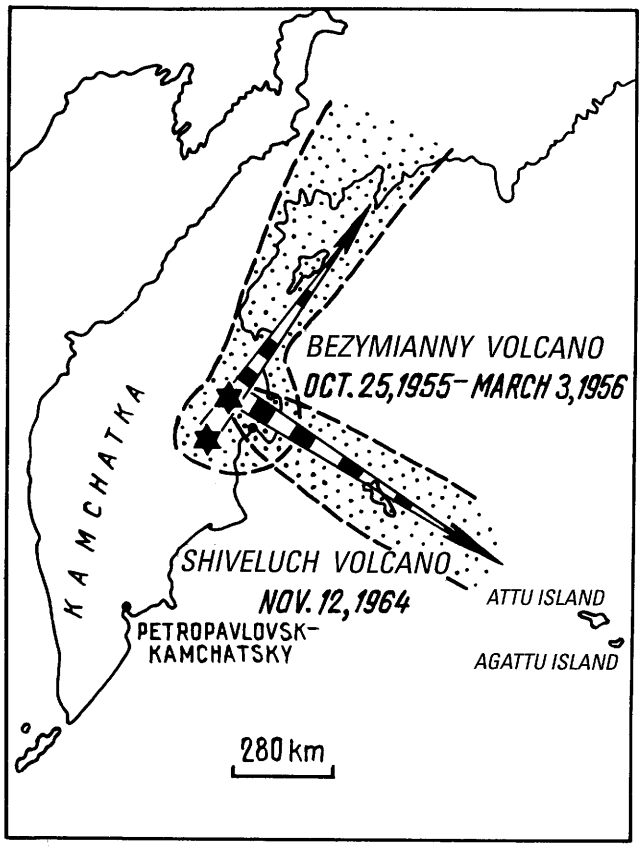


**Figure 3.** Distribution of ash for the eruptions of Bezymianny Volcano in 1955–56 and Sheveluch Volcano in 1964 (from Melekestsev, 1989).

eastward; on January 13, 1991, when the ash material was transported southward in the direction of Klyuchi; and on April 6, 1991, when the ash was transported westward.

## BEZYMIANNY

(LAT 55.97°N., LONG 160.59°E., ELEVATION 2,800 M)

Bezymianny is one of the most active volcanoes in Kamchatka. On March 30, 1956, a tremendous explosion destroyed the top of the volcano in an eruption similar to Mount St. Helens in 1980. Since then, the volcano has been in a stage of intermittent dome extrusion and eruption (Gorshkov and Bogoyavlenskaya, 1965). During the period 1981 to 1984, five eruptions of Bezymianny were recorded, the largest on October 13–14, 1984, when 0.011 $km^3$ of rock was ejected. The eruption column rose to 9-km altitude, and an ash plume drifted 40 km to the southeast (Malyshev, 1987). On June 30 and July 1, 1985, the climactic stage of one of the largest eruptions of the dome occurred at Bezymianny with the volume of material erupted placed at 0.05 $km^3$ (Alidibirov and others, 1988). From mid-December 1985 to mid-April 1986, the volcano was in a state of repose. In the remainder of 1986 and in 1987, the activity of the volcano was again high (Ivanov and others, 1984), continuing to the present. Ash ejections seldom exceed 5- to 6-km altitude, and explosive activity lasts commonly for a few hours to a few days.

## KLIUCHEVSKOI

(LAT 56.06°N., LONG 160.64°E., ELEVATION 4,850 M)

Kliuchevskoi is also one of the most active volcanoes in Eurasia, with numerous eruptions during the last decade. In April 1984, a summit eruption of the Vulcanian-Strombolian type began. During the paroxysmal activity at the summit crater, the altitude of the eruption cloud was 12 km (Fedotov and others, 1987). Because the lower boundary of the tropopause during the eruption was at 8-km altitude, this ash entered the stratosphere. The eruption ended on January 28, 1985, and the total volume of pyroclastics ejected was 0.1 $km^3$.

On December 2, 1985, a series of vigorous phreatic explosions sent a gas-and-ash column to 9.6-km altitude (Belousov, 1989). The direction of ash dispersal and the area (45×1,115 km) of the gas-ash cloud were determined by using the lidar of the Kamchatkan Hydrometeorological Survey. On December 2, 1985, the tropopause was at 7.8-km altitude, and, therefore, part of the material went into the stratosphere and the cloud started to spread horizontally. At an altitude of 9 km, a southeasterly wind with a speed of 5 m/s stretched the cloud into a plume more than 50 km long (Belousov, 1989).

Frequent explosive-effusive eruptions of the Strombolian type continued from the Kliuchevskoi summit crater during 1986–90. The maximum altitude reached by the eruption column during various stages of the eruption was 1,500–2,000 m above the crater rim. A large eruption from the summit crater lasted from January 29 to November 10, 1990. As a result, the ash fell on the Commander Islands, Sredinny Ridge, and to the north of Sheveluch Volcano. The ash cloud rose to a height of 8 km above the crater.

Other active volcanoes whose eruptions may be hazardous to aviation near Petropavlovsk-Kamchatsky are those of the Avachinsky and Zhupanovsky volcanic groups and Mutnovsky, Karymsky, Gorely, Opala, Ksudach, Alaid, and Ebeko. During the last 1,800 years, at least 17 ashfalls were related to eruptions of these volcanoes. In historic time, ashfalls were observed during the eruptions of Avachinsky Volcano in 1737, 1779, 1945 and 1991; Gorely in 1828 and 1832; Karymsky in 1963; and Alaid in 1981.

## KARYMSKY

(LAT 54.07°N., LONG 159.60°E., ELEVATION 1,486 M)

Karymsky is a small but very active andesitic stratovolcano located approximately 125 km northeast of Petropavlovsk-Kamchatsky (fig. 1). The explosive-effusive eruption that commenced in 1978 ceased in 1982. Eruptions were mainly of the Vulcanian and Vulcanian-Strombolian types. The characteristic feature of the Karymsky eruptions is the formation of a lava dome in the central part of the crater, the destruction of which is linked to large explosive eruptions of Vulcanian type that change the morphology of the crater. A series of strong Vulcanian explosions that began in August–September 1982 had ceased by October (Ivanov and others, 1984)—although a small amount of fumarolic activity occurs in the crater and near-crater part of the volcano.

The mass of pyroclastics ejected during 1980–82 was about 40 million tons. During the eruption on May 11, 1963, the ash cloud drifted over Petropavlovsk-Kamchatsky. Meteorological data obtained on May 11 in Petropavlovsk-Kamchatsky indicate that the transport of ash could take place in the troposphere at altitudes of 3 to 11 km, where a constant northerly and northeasterly wind blew at a speed of 12–18 m/s. At 12- to 15-km altitude in the stratosphere, air masses drifted in northwest and west directions.

## AVACHINSKY

(LAT 53.22°N., LONG 159.00°E., ELEVATION 2,751 M)

Avachinsky Volcano is located 27 km north of Petropavlovsk-Kamchatsky (fig. 1). On January 13, 1991, an eruption started with two explosions producing a gas-and-ash column that rose to 8- to 9-km altitude and moved southeast toward Petropavlovsk-Kamchatsky at a speed of 100 km/hr. Ash began falling at the town in less than 1 hour after the start of the eruption. The width of the ashfall was approximately 3–4 km, and the area of ashfall was 400–500 km$^2$ (I. Melekestsev, oral commun., 1991).

The eruption continued until January 24, 1991, with intense ashfalls on January 16 and 17. On January 16, the eruption cloud drifted southeast, and satellite photographs indicated it was 200 km long and 1.5–2 km wide. On January 17, the ash cloud from Avachinsky Volcano, according to satellite images, drifted northeastward. After January 13, the height of gas-ash ejections generally did not exceed 200–300 m and seldom reached 2,000 m altitude above the crater.

## GORELY

(LAT 52.45°N., LONG 158.12°E., ELEVATION 1,829 M)

Gorely Volcano, approximately 65 km south of Petropavlovsk-Kamchatsky (fig. 1), erupted in 1980–81 and 1984–85. The eruption of June 1980 to July 1981 produced eruption columns of the Vulcanian type that rose to 5 km above the crater and ejected 48 million tons of ash (Ivanov and others, 1982). The December 1984 eruption resembled the previous one: eruption clouds rose 2 km above the crater, and approximately 1 million tons of ash were ejected (Ivanov and others, 1985). During 1985, the volcano was in a stage of phreatomagmatic eruptions of different intensity, and the height of the eruption column ranged from 100 to 3,500 m above the crater. The area of ashfall was small and confined to the volcano edifice. The eruption varied from separate outbursts to a continuous emission of steam in thin jets or columns from which a cumulus cloud generally formed. The dynamics of the steam-gas jet were dependent on weather conditions (wind speed and direction and air humidity)—in clear, windless weather, the steam-gas column reached maximum altitudes. Frequently, the eruption cloud formed one or occasionally two thick steam-gas plumes 200 m high and extending 20–150 km downwind from the volcano (Ivanov and others, 1985).

During recent years, Gorely Volcano has been in a stage of minor eruption. On April 25, 1986, near the top of the

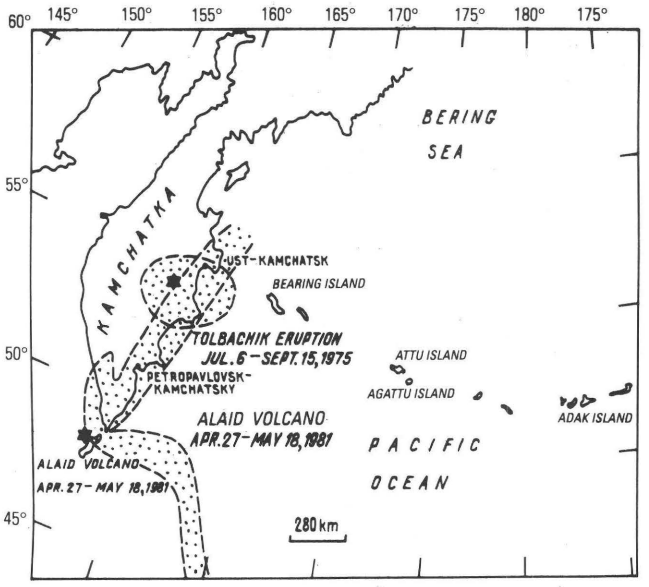


**Figure 4.** Distribution of ash for the eruptions of Alaid Volcano on April 27, 1982, and of the northern breakthrough of Tolbachik Volcano in 1975 (from Melekestsev, 1989).

active crater, a steam-gas emission of light brown color (due to entrained ash particles) was observed. Ash covered an area surrounding the crater of 300 $km^2$, and the weight of ejected ash was estimated to be 3,780 tons. Ash-and-steam clouds slowly stretched in the form of a thin plume for distances up to 100 km.

## OTHER VOLCANOES

Eruption of Alaid Volcano (lat 50.80°N., long 155.50°E.), presents substantial hazard to airliners making flights over Kamchatka. Alaid, on one of the northernmost of the Kurile Islands (fig. 1), is an almost perfect cone rising to 2,339 m high above sea level. The most recent explosive eruption from the summit crater took place between April 27 and June 5, 1981 (fig. 4), when 650 million tons of material were ejected. Satellite data indicates that ejections during the initial stage of the eruption reached 15-km altitude and an ash plume extended for more than 1,500 km (Sawada, 1983). The volume of ash that fell in Severokurilsk, within 45 km of the volcano, was 15–20 $kg/m^2$. In the western Aleutian Islands, the ash layer was 3 mm thick (Fedotov and others, 1981, 1982, 1986). On May 5 and 6, 1981, ash was detected

**Figure 5.** Eruption of Karymsky Volcano in December 1977. Photograph by N.P. Smelov.

in the atmosphere above San Francisco, Calif., at an altitude of 12–13 km.

The airport in Severokurilsk (fig. 1) can also sustain damage from nearby Ebeko Volcano (lat 50.67°N., long 155.93°E., elevation 1,138 m), whose most recent eruption began in late 1988 and continued to the summer of 1990. The frequency of gas-ash outbursts from the crater was several hundred per month, and, in some cases, the interval between eruptions was less than several minutes. Eruption material was ejected to altitudes ranging from a few hundred meters up to 1–2 km for periods up to several tens of seconds.

## CONCLUSIONS

At the time this report is being prepared (1992), international airways pass approximately 400–500 km east of Kamchatka in the region of Attu Island. (This may change shortly as new airways are planned that will directly overfly the Kamchatka Peninsula.) Volcanic hazards for airplanes arise chiefly from explosive Plinian eruptions with volcanic ash transport to the east. Eruption columns rise to 10-km altitude, and ash may be transported for hundreds of kilometers downwind from the volcano. Due to the long duration of eruptions, ash fallout near the volcano from the eruption column is possible in all directions. The most likely direction for ash transport from Kamchatkan eruptions is to the east, southeast, and south at altitudes of 6 to 10 km. Ash clouds drifting for hundreds of kilometers from the eruption center present real dangers to airplanes as well as to airports of Klyuchi, Ust-Kamchatsk, and Kozyrevsk.

Bezymianny Volcano probably causes danger to air traffic only a few days per year during periods of actual eruption. The radius of the maximum hazard reaches a few tens of kilometers from the volcano. Ash transport is likely to occur at 5- to 8-km altitude to the northeast and south. Certain dangers may arise to airliners operating to and from the airports of Klyuchi and Kozyrevsk. In its present style of activity, Bezymianny Volcano presents little danger to air traffic carried out at 9-km altitude and higher.

At Sheveluch Volcano, hazards can arise from short-term, frequent explosions at the extrusive dome with the eruption cloud reaching 8-km altitude. The comparatively small ash concentrations in the Sheveluch ash clouds suggests that the airspace at 4- to 8-km altitude within 50 km of the eruption center during a one-half-hour period beginning at the onset of the eruption is the most dangerous to airliners. Explosions usually last a few tens of seconds, and prevailing ash transport is to the east and southeast. Such eruptions of Sheveluch are of concern to local air flights operating at Klyuchi and Ust-Kamchatsk airports.

Karymsky Volcano (fig. 5) is hazardous to aviation within 100 km of the eruption center. Individual large eruptions under certain weather conditions can result in ashfall in the airports of Petropavlovsk, Elizovo, and Milkovo. Prevailing ash transport can be at 2- to 6-km altitude to the east, southeast, and south.

Future eruptions at Avachinsky Volcano can produce ash that would drift at 4- to 10-km altitude to the northeast and southeast. Eruptions may last from a few hours to a few weeks. Movement of the ash may cause certain danger to national airlines and to domestic flights, including the regions of the Petropavlovsk and Elizovo airports. At the Gorely and Mutnovsky Volcanoes, eruptions may last from a few days to several months. The probable ash transfer may take place at 3- to 8-km altitude to the east. The eruption cloud can be transported for distances from a few tens to a few hundreds of kilometers. Under certain weather conditions, the ash can cause danger to aircraft operating at the Elizovo airport.

Eruptions from Alaid Volcano are potentially hazardous to international flights along North-Pacific air routes (e.g. Anchorage–Seoul, Anchorage–Khabarovsk, etc.) as well as to domestic flights. Ash produced by Alaid may be transported many hundreds of kilometers from the volcano. The ash is likely to be transported at 8- to 15-km altitude to the northeast, east, and southeast. Large ashfalls are expected in the airports of Ozernovsky and Severokurilsk.

The eruptions at the Ebeko Volcano (Paramushir Island) can produce ash that will drift at 1- to 2-km altitude to the northeast and southeast. The greatest danger may arise to local air routes and to the airport of Severokurilsk.

## ACKNOWLEDGMENTS

I thank Drs. Thomas P. Miller (U.S. Geological Survey), I.V. Melekestsev, and O. A. Braitseva for helpful discussions of this work. I am also indebted to Loubon F. Serkova for translation of the manuscript into English.

## REFERENCES CITED

Alidibirov, M.A., Bogoyavlenskaya, G.E., Kirsanov, I.T., Firstov, P.P., Girina, O.A., Belousov, A.B., Zhdanova, E. Yu., and Malyshev, A.I., 1988, Eruption of Bezymianny Volcano in 1985: Volcanology and Seismology, no. 6, p. 3–18 [in Russian].

Belousov, A.B., 1989, Phreatic explosion from the Kliuchevskoi Volcano on December 2, 1985: Voprosy Geografii Kamchatki, no. 10, p. 108–110 [in Russian].

Fedotov, S.A., Khrenov, A.P., and Sharinov, N.A., 1987, The Kliuchevskoi Volcano, its activity during 1932–1986 and possible development: Volcanology and Seismology, v. 4, p. 3–17 [in Russian].

Fedotov, S.A., Ivanov, B.V., Avdeiko, G.P., Flerov, G.B., Andreev, V.N., Dvigalo, V.N., Doubik, Yu. M., and Chirkov, A.M., 1981, Eruption of Alaid Volcano in 1981: Volcanology and Seismology, v. 5, p. 82–87 [in Russian].

Fedotov, S.A., Ivanov, B.V., Flerov, G.B., Avdeiko, G.P., Andreev, V.N., Budnikov, V.A., Gordeev, E.I., Dvigalo, V.N., and Shirokov, V.A., 1982, Study of Alaid eruption (Kurile Islands) in 1981: Volcanology and Seismology, no. 6, p. 9–27 [in Russian].

Fedotov, S.A., Ivanov, B.V., Gushchenko, I.I., Dvigalo, V.N., Sharinov, N.A., Khrenov, A.P., and Chirkov, A.M., 1986, Volcanic activity in the Kurile-Kamchatka zone in 1980–1984: Volcanology and Seismology, no. 2, p. 3–20 [in Russian].

Gorshkov, G.S., and Bogoyavlenskaya, G.E., 1965, Bezymianny Volcano and the characteristic features of its most recent eruption in 1955–1963: Moscow, Nauka, p. 172 [in Russian].

Gorshkov, G.S., and Doubik, Yu. M., 1965, The directed blast at Sheveluch Volcano, *in* Volcanoes and Eruptions: Moscow, Nauka, p. 3–37 [in Russian].

Ivanov, B.V., Andrea, V.N., Bogoyavlenskaya, G.E., Doubik, Yu. M., Kirsanov, I.T., Rulenko, O.P., Firstov, P.P., and Chirkov, A.M., 1982, Activity of volcanoes in Kamchatka and Kurile Islands in 1981: Volcanology and Seismology, no. 4, p. 103–108 [in Russian].

Ivanov, B.V., Chirkov, A.M., Doubik, Yu. M., Khrenov, A.P., Dvigalo, V.N., Razina, A.A., Stepanov, V.V., and Chubarova, O.S., 1984, The state of activity of active volcanoes in Kamchatka and Kurile Islands in 1982: Volcanology and Seismology, no. 4, p. 104–110 [in Russian].

Ivanov, B.V., Droznin, V.A., and Vakin, E.A., 1985, The eruption of Gorely Volcano in 1985: Volcanology and Seismology, no. 4, p. 93–99 [in Russian].

Malyshev, A.I., 1987, The eruption of Bezymianny Volcano in 1981–1984: Volcanology and Seismology, no. 2, p. 89–93 [in Russian].

Melekestsev, I.V., 1989, Great volcanic ash falls in the region of Petropavlovsk-Kamchatsky: Voprosy Geografii Kamchatki, no. 10, p. 101–108 [in Russian].

Sarna-Wojcicki, A.M., Shipley, S., Waitt, R.B., Dzurisin, D. and Wood, S.H., 1981, Areal distribution of thickness, mass, volume, and grain size of air-fall ash from the six major eruptions of 1980, *in* Lipman, P.W., and Mullineaux, D.R., eds., The 1980 Eruptions of Mount St. Helens, Washington: U. S. Geological Survey Professional Paper 1250, p. 577–600.

Sawada, Y., 1983, Analysis of eruption clouds by the 1981 eruptions of Alaid and Pagan Volcanoes with GMS images: Papers in Meteorology and Geophysics, v. 34, no. 4, p. 307–324.

Steenblik, J.W., 1990, Volcanic ash—A rain of terra: Air Line Pilot, June/July, p. 9–15, 56.

Zharinov, N.A., Zhdanova, E. Yu., Belousov, A.B., Gorelchik, V.I., Belousova, M.G., Garbuzova, V.T., and Demenchuk, Yu. B., 1990, Eruptions and seismic regime of the Northern volcanic group in 1986–1987: Volcanology and Seismology, no. 3, p. 3–20 [in Russian].

VOLCANIC ASH AND AVIATION SAFETY:
Proceedings of the First International Symposium
on Volcanic Ash and Aviation Safety
U.S. GEOLOGICAL SURVEY BULLETIN 2047

# ASH CLOUDS: CHARACTERISTICS OF ERUPTION COLUMNS

*By* Stephen Self *and* George P.L. Walker

## ABSTRACT

An eruption column is the vertical or subvertical part of the ash emissions issuing from an explosive volcanic vent or from the top of a pyroclastic (ash) flow. Eruption columns range in height from low, small-scale bursts to huge convective systems that rapidly transport ash, volcanic gases, and entrained air into the stratosphere. Some eruption columns are the product of instantaneous releases of ash and gas, and their rise constitutes an isolated thermal, while others are more steady convecting systems that are fed by a nearly constant rate of release of material from the vent (maintained). Eruption columns have a lower gas-thrust region (the jet of material leaving the vent—this commonly represents less than 10 percent of the total eruption-column height) and a buoyant convective-thrust region that constitutes most of the column in large Plinian and Vulcanian eruptions but may be small in Hawaiian and Strombolian types. Above this is the umbrella region, a zone of momentum-driven rise and considerable lateral spreading from which ash fall begins as material is fed into the downwind plume. Characteristics of eruption columns vary according to the style of explosive eruption, and this paper summarizes most of the important types. Although almost all types of explosive eruption are capable of generating ash columns and plumes that are hazardous to aircraft, Vulcanian eruption columns are probably the most dangerous on a worldwide basis owing to their frequency, unpredictability, high fine-ash content, and ability to easily reach altitudes well in excess of common flight paths.

## INTRODUCTION

Volcanic ash clouds pose a considerable danger to aviation. These laterally spreading, wind-driven clouds are parts of an atmospheric dispersal system that transports pyroclastic material (ash) and gas upward from the volcanic vent and spreads them in the atmosphere. The vertical to inclined part of the dispersal system, termed the eruption column, is the major control on the heights of ash clouds. The downwind, drifting part of the system we refer to as the plume (fig. 1). We review the current understanding of eruption-column processes, discuss the range in column characteristics for different types of volcanic eruptions, and give an assessment of which eruption types may be the most hazardous to flying aircraft. Previously, Rose (1986) has reviewed volcanic clouds from the perspective of hazards to aviation. The same basic components exist in all types of explosive volcanic eruption columns, and these will be discussed first.

## COMPONENTS OF THE ERUPTION COLUMN

Our understanding of volcanic phenomena such as eruption columns comes both from observations and measurements on erupting volcanoes and from fluid-dynamic modeling of the behavior of buoyantly convecting systems, verified in some cases by analog experiments using (most often) aqueous fluids. An eruption column consists of a lowermost gas-thrust region, a convective-thrust region, and an uppermost umbrella region (Wilson, 1976; Sparks, 1986; Woods, 1988). This three-fold division applies to all columns, from those that are steady systems supplied by a maintained release of material from the vent to those that are produced by an instantaneous explosion and rise as an isolated thermal.

### GAS-THRUST REGION

At the base of the eruption column, the fragmenting eruptive mixture that has been produced in the volcanic conduit by decompression-induced expansion of volatiles in the magma (and perhaps by other mechanisms) undergoes a drop in pressure as it enters the atmosphere. The accompanying expansion of the system produces a jet at the vent mouth (the magma- or rock-air interface). The vent mouth may be deep within a crater, and not readily visible to the observer, or at the surface. The jet, which is initially denser than the ambient air, forms the gas-thrust part of the column. Air is engulfed in great quantities into this vertical or subvertical

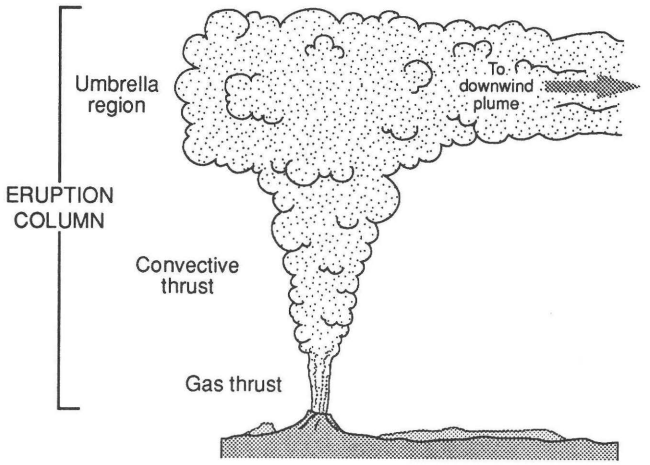


**Figure 1.** Three parts or regions of an eruption column: gas thrust, convective thrust, and umbrella.

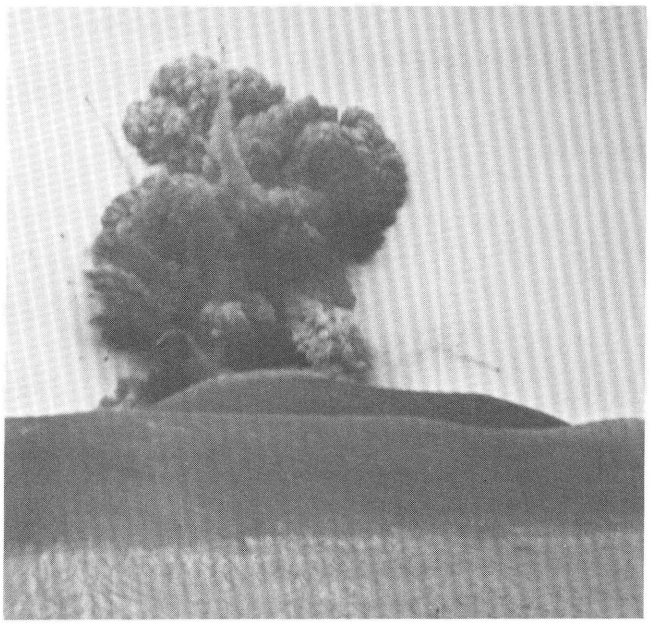

**Figure 2.** Instantaneous Vulcanian explosion from Anak Krakatau in September 1979. Note the large ballistic blocks separating from the gas-thrust region. Photograph courtesy of Michael R. Rampino.

turbulent jet (Wilson, 1976), and the structure is subjected to enormous atmospheric drag. Even in violent, high-intensity eruptions in which exit velocities approach the maximum possible for volcanic venting on Earth (about 650–700 m/s; McGetchin and Ulrich, 1973; Wilson, 1976), the gas-thrust region will not exceed about 3 km in height due to drag forces. The resulting rapid deceleration can slow the jet to speeds of a few tens of meters per second; thus, at the top of the gas-thrust region, velocities in the column may be at a minimum. In some eruption columns, the upward velocity falls below this minimum only at the top of the umbrella region, where the thermal and kinetic energy of the column is exhausted.

In many eruptions, loss of coarse material known as ballistic ejecta occurs from the gas-thrust region (fig. 2). Also, if the eruptive mixture does not entrain sufficient air to attain a bulk density less than that of the ambient atmosphere, gravitational collapse of part or all of the column will occur, forming either fire fountains or pyroclastic (ash) flows, depending on the type of eruption. This aspect will be dealt with in detail later. Although important in column dynamics, the gas-thrust zone rarely contributes more than 10 percent to the column's total height and is therefore of little concern to flying aircraft.

## CONVECTIVE-THRUST REGION

If sufficient air is entrained into the jet, the eruption column overshoots its first neutral buoyancy level and passes into the convective-thrust region where turbulent convective rise of the erupted mixture due to its heat content and lower than ambient density becomes the dominant driving force. Convective thrust exerts the greatest influence on eruption-column height, accounting for between 50–90 percent of the altitude reached, and ultimately controls the nature of the whole eruption cloud. In this region of buoyancy, the greater the heat input at the base, either as an instantaneous release or a maintained flux, the higher the column will rise (Morton and others, 1956). In basic terms, $H$, the column height, is a function of the thermal flux into the system ($Q$), such that

$$H = KQ^{1/n} \tag{17}$$

where

$n$ = 3 or 4, depending upon whether the shape of the source vent is circular or linear, respectively (Wilson and others, 1978; Woods, 1988; Stothers and others, 1986),

$K$ is a constant that varies mostly according to the density stratification of the ambient atmosphere and whether the thermal energy input is maintained or instantaneous, and

$Q$ (for a steady column from an approximately circular vent) is the heat flux given, for example, as J/s; for a linear vent or fissure, $Q$ is the heat flux per unit length of the fissure (J/s/m).

For the rise of an isolated thermal, $Q$ is the total energy in the instantaneous release (J). For steady discharge from a circular vent, $Q$ is largely determined by the amount of magma being erupted and its general properties; therefore, column height is proportional to magma flux rate, which we term intensity. Although we will not go into details here, the major constraints on column behavior are thus the mass

eruption rate and initial velocity of the fragmenting magma, the size of the vent, and the amount of volcanic gas escaping from the magma (see Sparks and others, this volume, for a more detailed treatment).

Not all convecting ash columns come directly from vents and the gas-thrust region, however. Some rise from the tops of eruptive phenomena known as pyroclastic (ash) flows, and there is a direct relationship between the magma flux at the vent feeding the pyroclastic flows, the size of the pyroclastic flows, and the height reached by ash columns rising off the flows (Woods and Wohletz, 1991). Co-ignimbrite ash columns differ from most other columns in having no gas-thrust region: rise takes place entirely by convective thrust. They also form above pyroclastic flows derived from the collapse of unstable parts of steep-sided lava domes, in which case there is no preliminary venting of material. Some of the ash columns in early 1990 from the Alaskan volcano, Redoubt, were of this type (Scott and McGimsey, in press).

Many different types of explosive eruptions occur worldwide, giving a considerable range of eruption-column characteristics such as height, width, vertical rise rates, and ash and gas contents. In the least energetic types, most of the erupted material collapses as a fire fountain at the top of the gas-thrust region, and only a small proportion of finest material, the released volcanic gases, and the engulfed and heated air rise in the convective region. Much of the magma in such eruptions is only poorly fragmented and the predominant large bombs fall out without cooling significantly, a situation of poor thermal efficiency between hot material and entrained air (Woods and Bursik, 1991). This behavior characterizes Hawaiian and Strombolian eruptions, which have the lowest columns. In the more intense eruptions, Vulcanian to Plinian, where most of the magma is highly fragmented into small pieces, almost all the erupted material passes into the convective region. The high degree of heat transfer between hot clasts and gas and the entrained air (high thermal efficiency) and the increase in column velocities above the gas-thrust region gives a strongly buoyant system. In order to maintain rise, the bulk density of the column (ash plus gas plus entrained air) must always be less than the ambient density. As the column rises, there is a complex interplay between cooling resulting from altitude in the troposphere and the cooling of the column owing to entrainment of air that is colder and denser.

Bursik and Woods (1991) recently showed that columns that undergo marked acceleration with height over some height range in the convective region are the result of particular combinations of mass eruption rate and initial velocity. They termed such columns superbuoyant as opposed to those that rise at rates similar to or only slightly above the velocity minimum. Needless to say, many eruption columns are superbuoyant and most will overshoot their upper or second neutral buoyancy level in the atmosphere, which is generally somewhere in the middle to upper troposphere. Above this point, they rise owing to momentum rather than convective lift.

There is thus a range of convective column behaviors (see also Sparks and others, this volume), from weakly rising

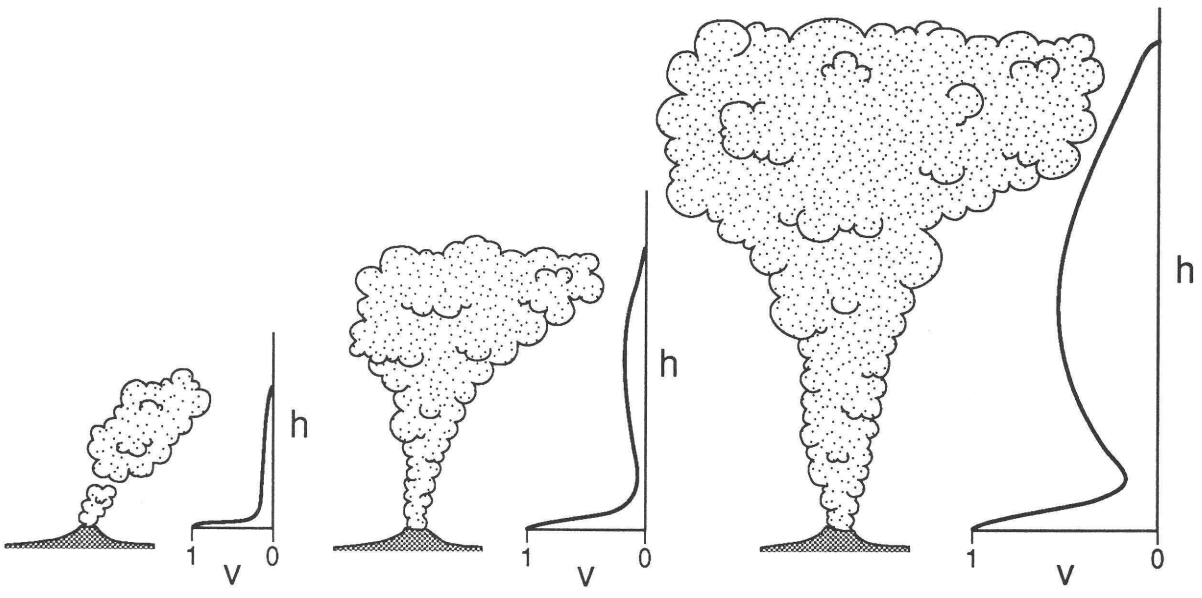


**Figure 3.** Three possible modes of behavior of eruption columns—intensity of eruption increases from left to right. Wind is from the left in each case. At side of each diagram are shown normalized velocity (v) profiles versus height (h) for these columns. Left, weak isolated thermals, which are influenced by the wind. Center, a higher intensity buoyant column, influenced by the wind only at the top. Right, a high intensity, superbuoyant column with a pronounced umbrella region.

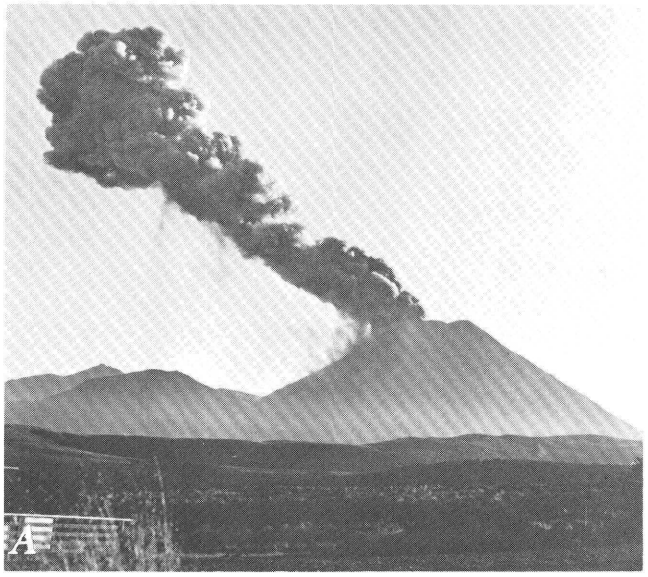


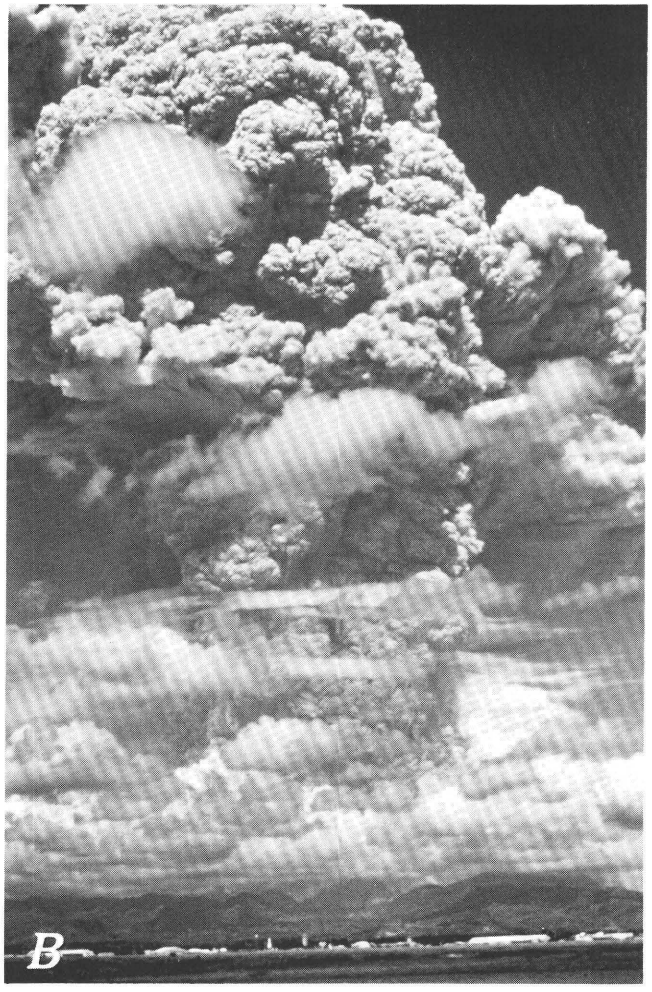


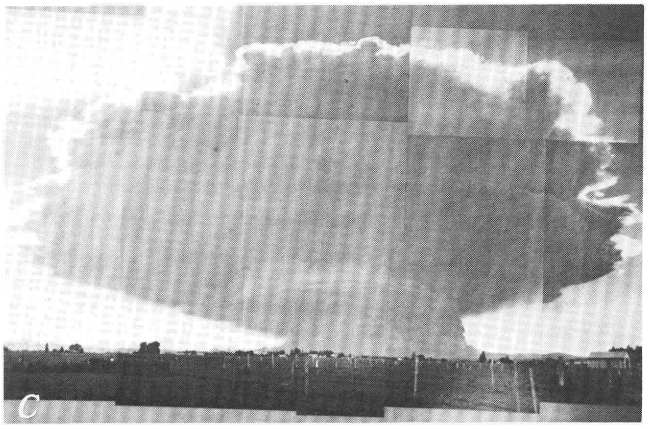


**Figure 4** (above and facing column). Examples of different types of eruption column. *A*, Instantaneously generated buoyant thermal from a Vulcanian explosion of Ngauruhoe Volcano, North Island, New Zealand, in 1975, being blown over by a wind of about the same velocity as the average column rise rate. Final elevation reached by plume top was about 12,000 ft. (Photograph courtesy of New Zealand Geological Survey.) *B*, A maintained Plinian column from Mount Pinatubo on June 12, 1991. (U.S. Geological Survey photograph courtesy of David Harlowe.) *C*, Mount St. Helens eruption column with umbrella cloud rising off blast flow at about 09:52 Pacific Daylight Time, 18 May 1980. Maximum height reached by this co-ignimbrite thermal was 85,000 ft (26 km). Photograph produced by James F. Kolberg (from Sparks and others, 1986).

ones that are easily pushed over by the wind, to those that rise to the tropopause and then stop due to the inversion in atmospheric temperature, to those that punch through the tropopause and rise considerable distances into the stratosphere (figs. 3 and 4). All convecting columns eventually slow down and stop primarily because of the density stratification of the atmosphere and the resulting fact that, at some height, they consist of material that is denser than the surrounding air.

## UMBRELLA REGION

In the upper part of the convectively rising region, velocities decrease and the slowing top of the column acts as a cap on the still rapidly rising material below. As a result, gravity forces the column to expand laterally and form the characteristic umbrella-, mushroom-, or anvil-shaped top to the convecting region (fig. 4*C*), analogous to a large cumulonimbus cloud. In the most energetic, high-intensity eruption columns, the expansion is strongly radial, and spreading may occur to distances of tens of kilometers upwind. Umbrella clouds can form in the troposphere as well as the stratosphere and may thus present a considerable hazard to aviation: flying upwind of a rising eruption column may not keep an aircraft out of the ash if a spreading umbrella cloud begins to develop.

As the material rising in an eruption column slows in the upper part of the convective-thrust or umbrella region, the largest and densest particles can be no longer supported by the upward velocity of the column and particle fall out begins (Carey and Sparks, 1986; Wilson and Walker, 1987). Spreading of the ash also takes place into the downwind plume from the umbrella region, often after the umbrella cloud has subsided from its maximum height (Bursik and others, this volume). A recent discovery, based on temperatures of the tops of eruption columns measured from the data provided by thermal infrared sensors on weather satellites, has shown that the umbrella cloud may be in marked thermal disequilibrium with the ambient and may be undercooled by up to several tens of degrees Celsius (Woods and Self, 1992). The undercooling is due in part to the extreme adiabatic expansion that occurs in the umbrella region, and the denser umbrella region therefore tends to subside until it reaches a level of neutral buoyancy, from which downwind dispersal of ash takes place.

As discussed above, eruption columns can also be subdivided into those that grow above maintained (quasi-continuous) explosive venting and those that develop above essentially instantaneous or short-lived explosions (Wilson and Self, 1980). Because the all-important heat source is not maintained in the latter, the physics governing columns from instantaneous explosions is slightly different (Morton and others, 1956). The rise height of the isolated thermal type is controlled by the total mass erupted rather than the mass flux as is the case for the maintained eruption columns (Wilson and others, 1978; Woods, 1988). A simple way of distinguishing these two modes of behavior is that, in the instantaneous type, the heat source (usually explosive magma output) cuts off before the top of the column reaches its maximum height, and the column acts as a simple thermal rising through the atmosphere. Conversely, for the maintained case, the heat source lasts longer than the time taken for the column to reach its maximum height, but it need not be steady; even a series of discrete explosions spaced seconds to minutes apart can generate a maintained column because rise times to maximum elevations are generally of the order of minutes to tens of minutes.

In an attempt to express some of these theoretical considerations as information of use to aviation, we next place the various characteristics and scales of eruption columns into a global context according to explosive eruption type and frequency of occurrence.

## FREQUENCY AND TYPES OF EXPLOSIVE ERUPTIONS

Of most importance to aviation are, (1) the height that columns can reach and then disperse their load of ash into the prevailing winds, (2) the column rise rates, (3) the content of fine ash that may be suspended or falling in the atmosphere for considerable distances or periods, and (4) the duration of the ash clouds. This information has been combined into table 1, which gives a simple breakdown into the more common eruption types, Hawaiian, Strombolian and small Vulcanian, with an average frequency of 5–10 eruptions per yr; the less frequent ones, such as sub-Plinian to small Plinian, larger Vulcanian, and phreatomagmatic eruptions, with 1–2 eruptions per yr; and the rarer types, including major Plinian and large co-ignimbrite ash-cloud-forming eruptions with, on average, less than 1–2 eruptions per decade. Although quite common, phreatomagmatic eruptions, in which magma mixes explosively with surface or subsurface water, have not been mentioned before because their eruption columns are broadly similar but less well understood than dryer, dominantly magmatic ones (Wilson, this volume). Table 1 is based on years of volcanological observation and study of erupting volcanoes and their deposits and is necessarily a summary.

Almost all types of eruption columns can inject ash to sufficient heights to be hazardous to aircraft, so even modest eruptions pose a potential danger (Simkins, this volume). The largest eruptions, with the biggest columns, although potentially the most dangerous, are also the rarest. The most common eruptions, the Hawaiian and Strombolian type, produce little fine ash and usually present no danger to aviation in general. However, their ash-producing capabilities should not be underestimated for aircraft venturing close to the eruption. For instance, the 1973 Strombolian eruption at Heimaey, Iceland, produced fine ash-laden clouds that rose to 30,000 ft during 1- to 2-day periods several times during its 3-month-long eruption.

A schematic view of the distribution of hazards to aircraft from explosive eruptions of three selected frequencies is given in figure 5. These intervals also broadly correspond to certain magnitudes (equivalent to bulk volume of magma released) and types of eruptions, as shown on table 2.

## SPECIFIC ERUPTION TYPES GROUPED BY COLUMN HEIGHT

### COLUMNS EXCEEDING 39,000 FEET (12 KM)

Such columns issue from Vulcanian and violent Strombolian (Walker, 1973) eruptions and from phreatomagmatic eruption columns that may rise above vents in shallow seas or lake water or on glacier-clad volcanoes. Many but not all result from instantaneous to intermittent explosions and, thus, behave as isolated thermals. The columns generally display normal buoyancy characteristics but can be superbuoyant; these columns seldom extend far above the tropopause. Often they are affected by the wind due to the relatively slow velocities of convection and become inclined (fig. 4*A*). Umbrella regions can develop at the tops of these columns, and during the recent 1989–90 eruption of Redoubt, several examples were

**Table 1.** Summary of characteristics of volcanic eruption columns.

[Rise velocities given are for convective-thrust region. Ash content refers to amount of material < 2 mm in diameter. See table 1 in Heiken (this volume) for further characteristics of explosive eruptions]

| |
|---|
| **Eruption type: Hawaiian/Strombolian** |
| Global frequency per year: 5–10. |
| Maximum height / width (in thousands of feet): 26–33 / 7–13. |
| Average rise rate (in feet per second): 15–35. |
| Duration (in hours); continuity: 10–1,000's; intermittent to semicontinuous. |
| Ash content: Low to moderate. |
| Other features: "Dry," volatile-bearing column; few fine particles; may be difficult to detect visually. |
| Recent examples: Kilauea, 1983–86; Pacaya, 1990; Oshima, 1986; Stromboli, continuous. |
| Potential hazard to aviation: Low. |
| **Eruption type: Surtseyan (phreatomagmatic)** |
| Global frequency per year: 1–2. |
| Maximum height / width (in thousands of feet): 26–39 / 13–20. |
| Average rise rate (in feet per second): 15–35. |
| Duration (in hours); continuity: 10–1,000's; intermittent to semicontinuous. |
| Ash content: High. |
| Other features: Wet, steam-laden columns; ash rich; much aggregation of particles. |
| Recent examples: White Island, 1976–82; Ukinrek, 1977; Surtsey, 1963–65. |
| Potential hazard to aviation: Medium locally. |
| **Eruption type: Vulcanian** |
| Global frequency per year: > 10. |
| Maximum height / width (in thousands of feet): 32–62 / 20–32. |
| Average rise rate (in feet per second): 50–260. |
| Duration (in hours); continuity: 5–100's; extremely spasmodic to semicontinuous. |
| Ash content: Moderate to high. |
| Other features: Very common; widely variable style of activity; associated with small ash flows. |
| Recent examples: Redoubt, 1989–90; Sakurajima, continuous; Fuego, 1974–79. |
| Potential hazard to aviation: High locally, moderate regionally. |
| **Eruption type: Sub-Plinian to Plinian (including phreatomagmatic)** |
| Global frequency per year: 0.1–1. |
| Maximum height / width (in thousands of feet): 39 to > 150 / 32–260. |
| Average rise rate (in feet per second): 65–233. |
| Duration (in hours); continuity: < 1 to 200; semicontinuous to continuous. |
| Ash content: Moderate to high. |
| Other features: Coarse and fine particles in high column; often short-lived but maintained. |
| Recent examples: Hekla, 1991; Mount St. Helens, 1980. |
| Potential hazard to aviation: High over large regions. |
| **Eruption type: Ash flow, co-ignimbrite ash cloud** |
| Global frequency per year: < 0.1. |
| Maximum height / width (in thousands of feet): 39 to > 130 / 262–490. |
| Average rise rate (in feet per second): 260–650. |
| Duration (in hours); continuity: a few(?) to 100(?); semicontinuous to continuous. |
| Ash content: High. |
| Other features: Very high rise rates; large magnitude; infrequent. |
| Recent examples: Small: Mount St. Helens, 1980; Pinatubo, 1991. Large: Katmai, 1912. |
| Potential hazard to aviation: High over large regions. |

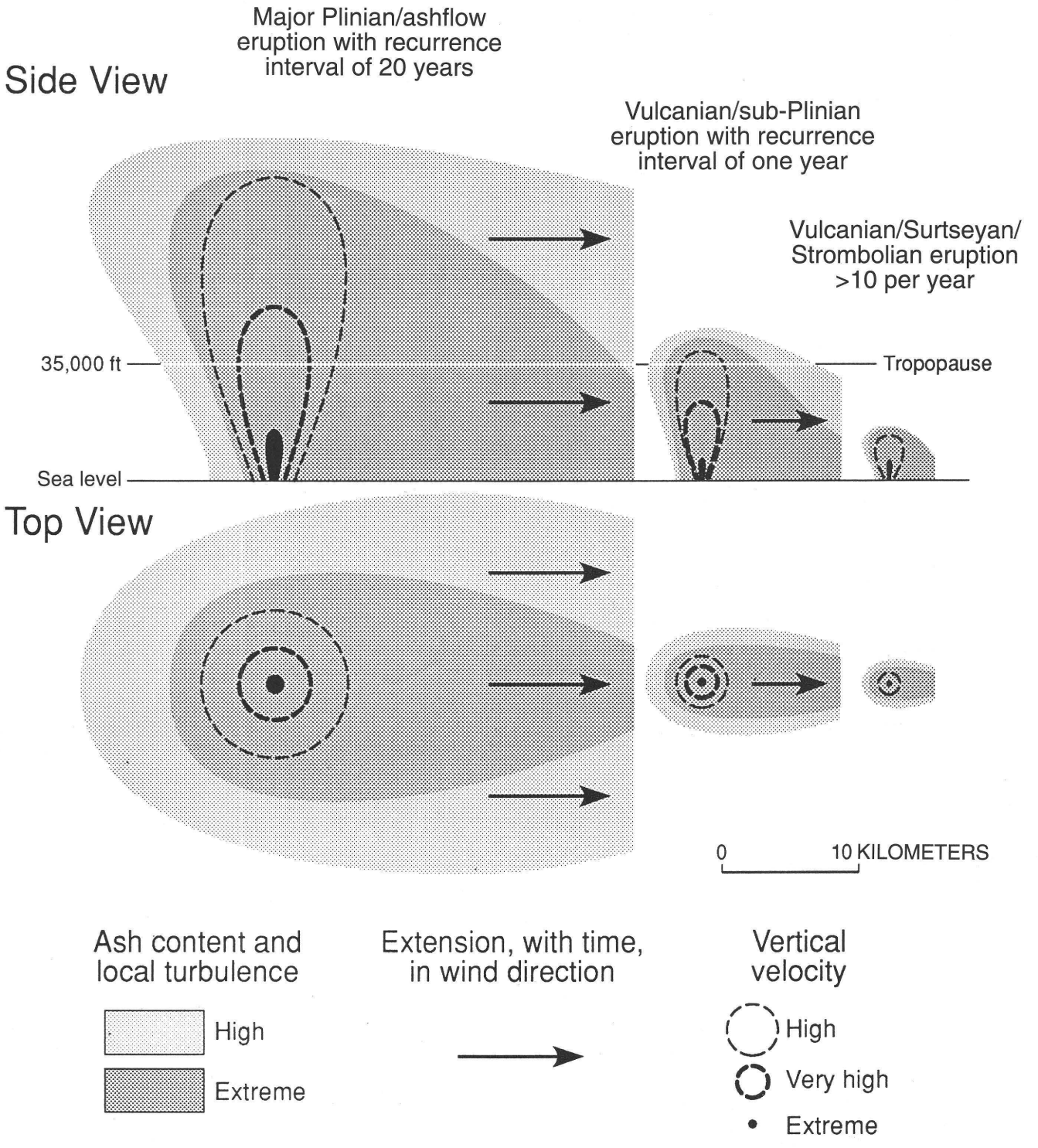


**Figure 5.** Schematic diagram showing the distribution of hazards to aircraft around explosive eruption columns of three selected frequencies. Upper diagram is sectional view; lower diagram is plan view. Vertical and horizontal scales are equal.

**Table 2.** Approximate recurrence intervals and bulk volumes of magma released for various eruption types.

| Approximate interval | Eruption type | Amount of magma ($km^3$) |
|---|---|---|
| 1 per 20 years | Major Plinian/ignimbrite | > 2–4 |
| 1 per year | Large Vulcanian or small sub-Plinian | 0.5–2 |
| 10 per year | Small Vulcanian, Strombolian, phreatomagmatic | 0.5 |

carefully monitored and observed (Woods and Kienle, in press). As mentioned above, some of these were co-ignimbrite ash clouds that rose off small pyroclastic flows and reached only 40,000 ft.

Eruptions producing these columns can be short-lived, but many last for weeks to months, during which time material is vented sporadically. They may have a single or several climactic phases when maintained columns are generated for periods of up to a few hours, as in the Redoubt case. The mechanisms of magma fragmentation, including generation of fine ash by explosive mixing with water in the phreatomagmatic examples, usually lead to a very high content of fine ash (Heiken, this volume). Because some of these eruptions last for months to years and due to their intermittent nature and the unpredictable generation of rapidly rising columns, they loom large in the list of those that have caused aircraft–ash cloud encounters, for example, Galunggung (1982–83) and Redoubt (1989–90).

## COLUMNS EXCEEDING 50,000 FEET (15 KM)

These large columns include those of maintained Vulcanian and Plinian eruptions (fig. 4*B*) and co-ignimbrite ash clouds that rise off pyroclastic flows. The columns are generally maintained, except for some co-ignimbrite ash clouds, which rise rapidly to great heights and then disperse ash into the ambient wind field. An example of the latter occurred in early stages of the May 18, 1980, Mount St. Helens eruption (fig. 4*C*), when a giant umbrella cloud rose off the whole area covered by the blast flow (a kind of pyroclastic flow) and formed a co-ignimbrite thermal that rose from a few thousand feet to 88,000 ft in about 4 minutes (Sparks and others, 1986; Woods and Self, 1992; Bursik and others, this volume). Within another 3 minutes, the umbrella cloud spread laterally to occupy an area of over 3,000 $mi^2$, including pushing some 15 mi upwind at the 60,000–70,000-ft level. The spectacular rise rate demonstrated by the Mount St. Helens example is not unusual for large Vulcanian, Plinian, and co-ignimbrite columns. Indeed, rise rates in excess of 650 ft/s (200 m/s) are estimated by models for the highest intensity columns (Woods and Wohletz, 1991).

Umbrella regions of eruption columns can cover immense areas; we have recently experienced the giant cloud from the large Plinian eruption of Mount Pinatubo on Luzon in the Philippines, which on June 15–16, 1991, attained a diameter in excess of 800 mi and an area of about 520,000 $mi^2$ (Global Volcanism Network, 1991a; S. Self, University of Hawaii, unpub. data). This cloud was the result of a combination of a Plinian eruption column reinforced by co-ignimbrite ash clouds.

In eruptions that produce very high columns, fine ash is generated in great abundance and fallout occurs from both the umbrella region and downwind plume for hundreds to thousands of miles over a period of many hours to a few days. The record of historic volcanism suggests that such high-intensity eruption columns are short-lived, usually lasting for less than a couple of days, and ash avoidance is simply a matter of waiting this period out. However, as the Pinatubo eruption has shown, pre- and post-climactic explosions, either from vents or from secondary explosive activity in freshly deposited pyroclastic flows, may produce periodic ash columns of the isolated-thermal type that attain heights of 30,000–50,000 ft. In many cases, post-climactic activity lasts for several weeks to months.

## A WORD ABOUT EXTREMES

There are several interesting and potentially dangerous aspects of eruption columns that we have not discussed. Some of these are briefly mentioned here while discussing the extremes of the spectrum of explosive eruptive phenomena. Thankfully, most of these features are rare.

Maximum column heights probably reach about 160,000 ft (50 km) above the Earth because of the combined effects of drag on the huge ash-cloud system and the steadily warming stratosphere, which limits buoyant rise. In recent historic events, the Plinian and co-ignimbrite ash columns from the Tambora 1815 eruption probably reached about 130,000 ft (40 km) altitude, as perhaps did the same types of clouds from Krakatau in 1883 (Rampino and Self, 1982; Carey and Sigurdsson, 1989). The 1956 Bezymianny eruption in Kamchatka produced a short-lived column, similar in type to the Mount St. Helens umbrella cloud described above, that is purported to have reached 148,000 ft (45 km) (Gorshkov, 1959), and the Pinatubo giant cloud reached at least 98,000 ft (30 km), although its maximum elevation is yet to be determined.

Despite the fact that the great altitudes attained by some eruption columns are well above the limits of aircraft, an important corollary of the great heights is that the fallout of

ash from such clouds will cover enormous areas. Large Plinian and co-ignimbrite umbrella ash clouds may cover more than 1 million $mi^2$; we alluded above to the half-million-$mi^2$ coverage of the Pinatubo cloud. Fallout downwind from such clouds could occur over continent- or ocean-sized areas. If clouds of these dimensions were to occur in an area of concentrated air traffic, such as over Europe from a large eruption in southern Italy or, less likely, over the continental United States from a large eruption in the Cascades, then there would be total disruption of air traffic until the cloud dispersed or was carried away from the region and fallout ceased. Moreover, because a few inches of ash can collect on the ground over the entire area encompassed by giant ash clouds, the impact on regions with many airports may be crippling.

Large Vulcanian explosions can generate strong shock waves around the eruption column (Nairn, 1976) because the initial exit velocities are supersonic (> 340 m/s at sea level). In recent eruptions, shock waves have not been propagated large distances. However, in past eruptions, most notably Krakatau 1883, shock waves, manifested as great explosions, dissipated over distances of hundreds to perhaps thousands of miles (Francis and Self, 1983). Quite how these shock waves were generated is not known, and it is also not known what damage they might cause to an aircraft because the characteristics of the shock front are unexplored.

## SUMMARY

Volcanic ash reaches altitudes where it is dangerous to aircraft by rising in eruption columns. The dominant process in the columns is thermal convection, driven by the release of heat from the erupting magma, and the most significant part of a column in terms of controlling its height is the convective-thrust region. There is a size spectrum of eruption columns, ranging from low ones above Hawaiian-type fire fountains to huge Plinian and co-ignimbrite ones that can reach well over 100,000 ft in altitude. At the upper end of many columns, ash is spread over a wide area in the umbrella region, which gradually subsides and becomes extended downwind to form the ash plume. Most eruption columns, even those from small eruptions, can reach altitudes where the ash dispersed from them will constitute a hazard to commercial and military air traffic.

This review does not consider the deleterious effects of ash encountered by flying aircraft, which is a main theme of this volume. However, one aspect that should not be overlooked is the fate of the volcanic gases that rise in the column and are dispersed with the ash plume. Some of these species, especially sulfur dioxide, form acid aerosols that have longer residence times in the atmosphere than the much denser silicate ash particles—these aerosols are essentially invisible. Aircraft that have inadvertently flown through aerosol clouds in the troposphere and lower stratosphere have sustained serious damage, particularly window crazing. Several incidents occurred in the months after the March–April 1982 El Chichón eruption in Mexico (Williams, 1989).

## RECOMMENDATIONS

It is difficult to identify the most significant type of eruption in terms of hazard to aircraft; commercial and military aviation should be concerned about ash clouds from all types of explosive eruptions. However, for several reasons, Vulcanian eruptions probably pose the most significant threat. They are common (> 10 per yr), and the eruption columns are loaded with fine ash; the eruption columns can reach up to 65,000 ft, well above flight corridors. During an eruptive episode, explosions can occur without warning and produce rapidly rising columns. Vulcanian eruptive episodes may last for weeks, months, or even years, e.g., Sakurajima in Japan. Since 1955, this volcano has been continually active in a mode of intermittent explosions, each explosion generating a simple thermal. In August 1991, an explosion at Sakurajima caused an ash-encounter incident with an aircraft (Global Volcanism Network, 1991b; Onodera and Kamo, this volume). Several examples of this type of eruption, besides Sakurajima, are already notorious in the aviation community, namely Galunggung, Redoubt, and Unzen.

## ACKNOWLEDGMENTS

We thank Andrew W. Woods and Peter W. Francis for useful discussions, Marcus I. Bursik and Thomas J. Casadevall for encouraging us to contribute to the First International Conference on Volcanic Ash and Aviation Safely and to write this article. This is School of Earth Science and Technology (SOEST) contribution number 2944.

## REFERENCES CITED

Bursik, M.I., and Woods, A.W., 1991, Buoyant, superbuoyant and collapsing eruption columns: Journal of Volcanology and Geothermal Research, v. 45, p. 347–350.

Carey, S.N., and Sigurdsson, H., 1989, The intensity of Plinian eruption columns: Bulletin of Volcanology, v. 51, p. 28–40.

Carey, S.N., and Sparks, R.S.J., 1986, Quantitative models of the fall out and dispersal of tephra from volcanic eruption columns: Bulletin of Volcanology, v. 48, p. 109–125.

Francis, P.W., and Self, S., 1983, The eruption of Krakatau: Scientist America, v. 249, p. 172–187.

Gorshkov, G.S., 1959, Gigantic eruption of the volcano Bezymianny: Bulletin of Volcanology, v. 20, p. 77–109.

Global Volcanism Network, 1991a, Bulletin of the Global Volcanism Network, Smithsonian Institution, v. 16, no. 5, p. 2–8.

———1991b, Bulletin of the Global Volcanism Network, Smithsonian Institution, v. 16, no. 7, p. 10.

McGetchin, T.R., and Ulrich, G.W., 1973, Xenoliths in maars and diatremes with inferences for Moon, Mars, and Venus: Journal of Geophysical Research, v. 78, p. 1832–1853.

Morton, B., Taylor, G.I., and Turner, J.S., 1956, Turbulent gravitational convection from maintained and instantaneous sources: Proceeding of the Royal Society, v. 225, p. 1–23.

Nairn, I.A., 1976, Atmospheric shock waves and condensation clouds from Ngauruhoe explosive eruptions: Nature, v. 259, p. 190–192.

Rampino, M.R., and Self, S., 1982, Historical eruptions of Tambora (1815), Krakatau (1883) and Agung (1963), their stratospheric aerosols, and climatic impact: Quaternary Research, v. 18, p. 127–143.

Rose, W.I., 1986, Interaction of aircraft and explosive eruption clouds: A volcanologist's perspective. American Institute of Aeronautics and Astronautics Journal, v. 25, p. 52–58.

Scott, W.E., and R.G. McGimsey, in press, Character, mass, distribution, and origin of tephra-fall deposits of the 1989–1990 eruption of Redoubt Volcano: Journal of Volcanology and Geothermal Research.

Sparks, R.S.J., 1986, The dimensions and dynamics of volcanic eruption columns: Bulletin of Volcanology, v. 48, p. 3–15.

Sparks, R.S.J., Moore, J.G., and Rice, C.J., 1986, The initial giant umbrella cloud of Mount St. Helens: Journal of Volcanology and Geothermal Research, v. 28, p. 257–274.

Stothers, R.S., Wolff, J.A., Self, S., and Rampino, M.R., 1986, Basaltic fissure eruptions, plume heights, and atmospheric aerosols: Geophysical Research Letters, v. 13, p. 725–728.

Walker, G.P.L., 1973, Explosive volcanic eruptions—A new classification scheme: Geologische Rundschau, v. 62, p. 431–446.

Williams, R., 1989, The crazy windows: American Heritage of Invention and Technology [General Motors], Winter 1989, p. 64.

Wilson, L., 1976, Explosive volcanic eruptions III—Plinian eruption columns: Geophysical Journal of the Royal Astronomical Society, v. 45, p. 543–556.

Wilson, L., and Self, S., 1980, Volcanic eruption clouds: Density, temperature, and particle content estimates from cloud motion: Journal of Geophysical Research, v. 85, p. 2567–2572.

Wilson, L., Sparks, R.S.J., Huang, T.C., and Watkins, N.D., 1978, The control of eruption column heights by eruption energetics and dynamics: Journal of Geophysical Research, v. 83, p. 1829–1836.

Wilson, L., and Walker, G.P.L., 1987, Explosive volcanic eruptions IV—Ejecta dispersal in Plinian eruptions, the control of eruption conditions and atmospheric properties: Geophysical Journal of the Royal Astronomical Society, v. 89, p. 651–679.

Woods, A.W., 1988, The fluid dynamics and thermodynamics of Plinian eruption columns: Bulletin of Volcanology, v. 50, p. 169–193.

Woods, A.W., and Bursik, M.I., 1991, Particle fallout, thermal disequilibrium and volcanic plumes: Bulletin of Volcanology, v. 53, p. 559–570.

Woods, A.W., and Kienle, J., in press, The dynamics and thermodynamics of volcanic clouds: Theory and observations from the April 15 and 21 eruptions of Redoubt Volcano, Alaska: Journal of Volcanology and Geothermal Research.

Woods, A.W., and Self, S., 1992, Thermal disequilibrium at the top of volcanic clouds and its effect on the estimation of cloud heights: Nature, v. 355, p. 628–630.

Woods, A.W., and Wohletz, K., 1991, Dimensions and dynamics of coignimbrite eruption columns: Nature, v. 350, p. 225–227.

VOLCANIC ASH AND AVIATION SAFETY:
Proceedings of the First International Symposium
on Volcanic Ash and Aviation Safety
U.S. GEOLOGICAL SURVEY BULLETIN 2047

# VOLCANOES: THEIR OCCURRENCE AND GEOGRAPHY

*By* Tom Simkin

## ABSTRACT

The explosive volcanoes that threaten air safety tend to be arranged in long, linear belts near boundaries where crustal plates are converging. These belts cover less than 0.6 percent of the Earth's surface. At least 1,300 volcanoes have erupted in the last 10,000 years and, because the lifetimes of most volcanoes are very long, they are likely to erupt again in the future. Among these 1,300 volcanoes, however, only about 60 are active in a typical year, and that activity may range from the mild pyrotechnics of Italy's Stromboli to prehistoric catastrophes that dwarf recent eruptions such as Mount St. Helens, 1980; Krakatau, 1883; or Pinatubo, 1991. Like earthquakes, the bigger eruptions happen less often than the smaller, with St.-Helens-sized events occurring perhaps once per decade and events such as Ruiz, 1985, and Redoubt, 1989, several times a year. During the years 1975–85, more than 63 eruptions penetrated the altitude range of air traffic and at least nine passed into the stratosphere where volcanic products are easily dispersed around the world.

Eruption durations are often not recorded historically, but they are known to range from minutes to thousands of years. The median duration is 7 weeks, and few eruptions last longer than 3 years. Pulses of activity mark all but the shortest eruptions, and the paroxysmal event may come at any time from the first day (as occurs in 45 percent of all eruptions) to months or even years after the start of eruption. Of particular importance for volcano hazards is the fact that unusually violent eruptions commonly occur after unusually long periods of repose. The historic record in many parts of the world is far shorter than the hundreds or thousands of quiet years that precede violent eruptions, meaning that some of our most dangerous volcanoes may be those not currently recognized as "active." Of the 16 largest explosive eruptions in the 19th and 20th centuries, all but four were the first historic eruption known from the volcano. These factors emphasize the importance of communicating reports of new eruptions. We at the Smithsonian hope for more news from "eyes in the sky" and will do our best to disseminate volcano reports as we have been doing for nearly a quarter century.

## INTRODUCTION

Anyone interested in keeping aircraft separated from erupting volcanoes needs to know where volcanoes are, what they do, and how often they do it. This paper will attempt to answer these questions, while admitting at the outset that the more fundamental questions—what is the schedule of forthcoming eruptions?—simply cannot be answered. For nearly a quarter of a century, however, our group at the Smithsonian has been gathering data on both current volcanism (McClelland and others, 1989) and earlier activity of the last 10,000 years (Simkin and others, 1981). These two allied programs offer useful background for anticipating the volcanic activity that is likely in the years ahead.

## VOLCANO GEOGRAPHY AND FORMATION

The distribution of known volcanoes is shown in figure 1. These volcanoes are on land or in sufficiently shallow water that their geologically recent eruptive activity has been recognized by humans. They are the volcanoes that pose potential threats to aviation, but the reader who is also interested in the way the Earth works should keep in mind that they make up only a small proportion of the world's true volcano population. Calculated total amounts of lava reaching the Earth's surface each year (Crisp, 1984) suggest that nearly four-fifths of this lava is erupted on the deep ocean floor, at or near the oceanic rifts where the Earth's plates are moving away from each other. Very little is known about this style of volcanism, nearly all of which passes unnoticed by humans, but it is largely non-explosive and insulated from even the lowest flying aircraft by more than 1,000 m of sea water.

About 1,300 volcanoes are shown in figure 1: roughly one-half have had historically documented eruptions (a common definition of the word "active"), and all are believed to have erupted within the last 10,000 years. Some are geographically scattered, but most are strongly concentrated in linear belts. These cover less than 1 percent of

Earth's surface but account for 94 percent of all historic eruptions. Readers familiar with the concept of plate tectonics will recognize that these volcanic belts mark the boundaries between major crustal plates. Most of the belts shown in figure 1 lie near deep oceanic trenches, where a thinner oceanic plate descends under an overriding plate. The volcanoes are roughly 100–200 km above an inclined earthquake zone that traces the downward path of the oceanic plate. This tectonic setting is important to understanding volcanoes because fluids that rise from this down-going slab induce melting in the overlying plate, thereby forming molten rock, or magma. On its path upward toward the Earth's surface, magma often stops along the way, where some of it may cool and crystallize or cause melting of surrounding rocks. This slow, complex, and varied route to the surface yields diverse, ever-changing magma compositions at different places and times. It should come as no surprise, then, that the resulting types and sizes of eruptions are complex and varied: they are therefore notoriously difficult to predict, even when warning signs are recognized.

Before reaching the surface, magma commonly forms large, irregularly shaped chambers or reservoirs only 6–8 km below the surface. Here it may reside for tens to perhaps even millions of years in apparent quiescence. During this time, however, cooling and crystallization relentlessly change the magmas to ever more explosive compositions. The remaining liquid becomes richer in volatile components such as water, carbon dioxide, and sulfur dioxide, increasing pressures within the chamber. A variety of triggers may eventually drive the magma upward toward the surface. Nearly all magmas formed in this converging-plate-margin setting are sufficiently gas rich and viscous that, within a few kilometers of the surface, the final depressurization drives the gas/liquid mixture violently upward, as a carbonated beverage leaving a quickly uncorked container. The liquid is exploded into countless fragments. These fragments, called volcanic ash, are then carried high into the atmosphere by expanding volcanic gases. This generalized description may explain why volcano repose periods can be very long, particularly on a scale of human lifetimes, and why the longer periods of apparent quiescence are often broken by unusually violent eruptions. In many parts of the world, the historic record is very short, relative to the lengths of volcanic repose periods. Thus the distinction drawn in

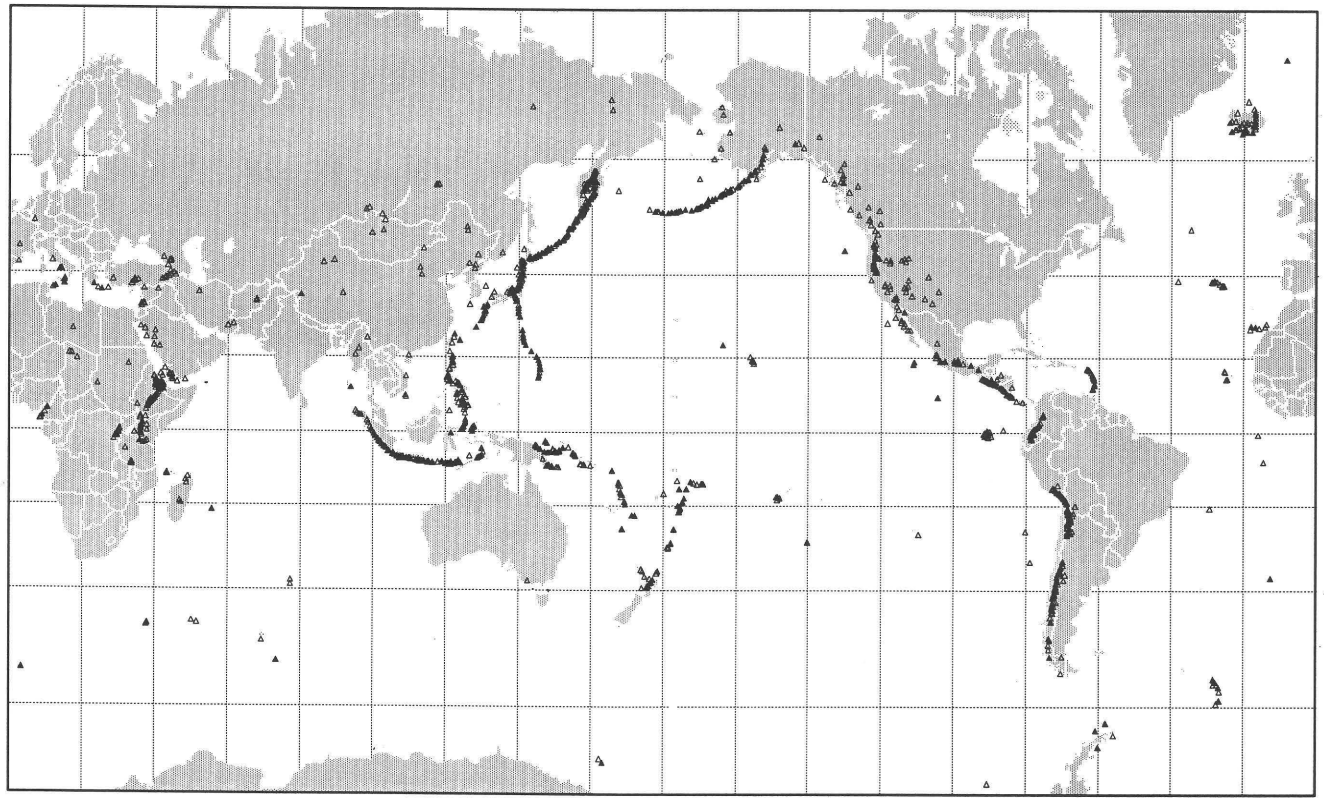

**Figure 1.** Global volcano distribution. Open triangles represent volcanoes believed to have erupted within the last 10,000 years, and filled triangles indicate those that have erupted within the 20th century. Volcanoes with uncertain status are not shown. Readers interested in more detail (plus the relationship to the world's earthquakes and physiography) are referred to the 1×1.5-m wall map, "This Dynamic Planet," available from the U.S. Geological Survey (Simkin and others, 1989), or the more detailed information in the forthcoming second edition of the Smithsonian publication, "Volcanoes of the World" (first edition is McClelland and others, 1989).

figure 1—between volcanoes that have erupted this century and those with lesser evidence for eruptions in the last 10,000 years—should not be misleading: all volcanoes must be considered potentially dangerous.

The above attempt to describe how volcanoes work has focused on those near converging plate boundaries. Volcanoes occur in other tectonic settings, and their processes differ accordingly, but these differences will not be described here because it is the converging-plate-boundary setting that poses by far the greatest volcanic threat to air safety. As mentioned above, volcanoes at diverging plate boundaries are largely on the sea floor, emerging above the oceans in only a few places like Iceland. Volcanoes in the interior of tectonic plates—the so-called "hot-spots"—make up only a small proportion of the worlds' volcano population. Those in continental interiors tend to have exceedingly long repose periods but are capable of enormous damage (an eruption of Yellowstone caldera 2 million years ago, for example, produced more than 2,500 $km^3$ of tephra, dwarfing the largest eruptions of history). Volcanoes in the interior of oceanic plates, like Hawaii, tend to erupt low-viscosity lava flows rather than explosive ash; therefore, they present a relatively low threat to aircraft.

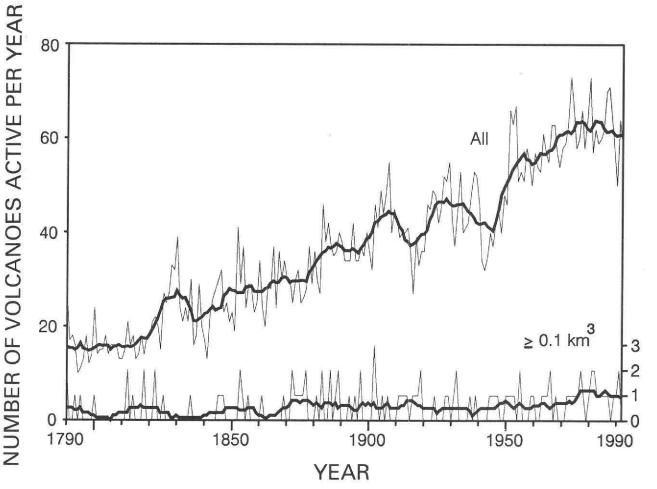


**Figure 2.** Volcanic activity since 1790. The dark line superimposed on the annual counts of active volcanoes is a 10-year running average, to show general trends. The lower plot, with expanded scale on the right, shows only larger eruptions with tephra volumes of ≥ 0.1 $km^3$ (VEI ≥ 4).

## ERUPTION FREQUENCY AND MAGNITUDE

Eruption reporting has historically depended both on human observers and on documentation in the scientific literature. We believe that the apparent increase in volcanism during the last 200 years (fig. 2) represents increased reporting—more observers, in wider geographic distribution, with better communication, and broader publication—rather than any significant change in the planet's rate of volcanism (Simkin and others, 1981). In particular, note: (1) that the number of active volcanoes has leveled off between 60 and 70 per year in the last several decades, (2) that the largest apparent drops in volcanism correspond precisely to the two world wars (when observers and publishers were otherwise preoccupied), and (3) that the apparent increase has been almost wholly in smaller eruptions, whereas the frequency of large events (product volumes ≥ 0.1 $km^3$, and less likely to be missed at a distance) has changed little in the last 120 years.

The lower plot on figure 2 raises the important point that eruption size varies, as most aspects of volcanism, over a very large range. A 1977 eruption in Iceland produced a carefully measured 26 $m^3$ of lava (a significant fraction of which has been used for scientific study), whereas the largest historic eruption, that of Indonesia's Tambora in 1815, produced over 150 billion $m^3$ (or 150 $km^3$) (Sigurdsson and Carey, 1989). Volcanology does not have an instrumentally determined magnitude scale to measure bigness, as the Richter scale that is used for earthquakes. Although global satellite monitoring allows measurement of total $SO_2$ for specific eruptions (Krueger and others, this volume), this capability has existed only since late 1978. To allow quantification through use of the historic and geologic record, the volcanic explosivity index (VEI) was developed by Newhall and Self (1982). The VEI is based primarily on volume of explosive products (called tephra, estimated or measured after the event) but also utilizes eruptive-cloud height (available for many witnessed eruptions) and more qualitative indicators as necessary. In a manner similar to the Richter scale, the VEI advances by single integers, each indicating a volume increase of roughly 10 times over the previous number. We have incorporated the VEI wherever possible with the 7,656 dated eruptions in our volcano database and find that, again like earthquakes, there are many more small ones than large (Simkin and others, 1981; McClelland and others, 1989). We estimate that, on the average, eruptions with VEI ≥ 2 (at least $10^6$ $m^3$ of tephra) take place somewhere on Earth every few weeks. Those producing $10^7$ $m^3$ of tephra (VEI ≥ 3, such as Colombia's Ruiz eruption, which generated such fatal mudflows in 1985) take place several times per year. Eruptions with VEI ≥ 5, such as Mount St. Helens, 1980 (eruptions with ≥ $10^9$ $m^3$, or 1 $km^3$, of tephra), occur perhaps once per decade, and those such as Krakatau, 1883 (VEI 6, or ≥ 10 $km^3$ of tephra), occur on the order of once per century. Eruptions of special significance to this symposium—Redoubt, 1989; Galunggung, 1982; and Pinatubo, 1991—are currently rated at VEI 3, 4, and 6, respectively. Only one known historic event, Tambora, 1815, warrants a VEI 7 (≥ 100 $km^3$ of tephra), and millennia may pass, on the average, between eruptions of this magnitude.

The Tambora eruption led to 92,000 deaths, and its globally dispersed aerosol cloud acted as a filter to reduce incoming solar radiation at the Earth's surface. Cooling of the global climate resulted, and the following summer brought June snowfalls in New England and widespread crop failures around the world. However, far larger eruptions are known from the prehistoric record and will cause enormous devastation when they occur again.

Of more immediately concern for air safety considerations is the high frequency with which ash clouds reach altitudes used by commercial aircraft. As a part of regular Smithsonian reporting of global volcanic activity, we have tried to keep track of reported cloud heights, and in compiling the first 10 years of these reports (McClelland and others, 1989) we tabulated the data shown in figure 3. During the years 1975–85, more than 63 ash clouds are known to have penetrated the 8–13-km (27,000–43,000-ft) air-traffic range. At least nine ash clouds passed through the tropopause into the stratosphere, where volcanic products are readily dispersed around the world. The fine particles that reach the upper atmosphere fall very slowly, assuring their presence as an air-traffic hazard for days after their initial eruption. Our 1975–85 average of at least six ash clouds per year to air-traffic heights, plus the volcano distribution shown in figure 1, gives some indication of the odds for encounters with commercial aircraft.

## ERUPTION DURATION

The durations of individual eruptions, as most other measures of volcanic activity discussed in this review, cover a very broad range. Some, such as the 26 $m^3$ of lava erupted from an Icelandic geothermal borehole in 1977, last only a few minutes, whereas others, such as Stromboli's long-running show north of Sicily, continue for thousands of years. However, the median duration of historical eruptions in the Smithsonian database is 7 weeks, and few eruptions last longer than 3 years. Pulses of activity mark all but the shortest eruptions, and the paroxysmal event may come at any time from the first day (as occurs in 45 percent of all

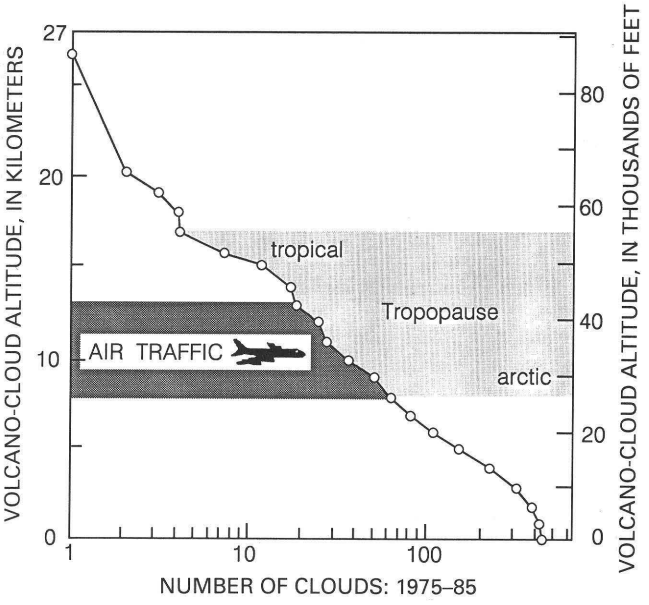


**Figure 3.** Volcano-cloud altitudes, 1975–85. Cumulative frequency of maximum cloud height for each eruption during the 10-year period. Frequency is on a logarithmic scale, with one cloud reaching 26 km, two clouds reaching at least 20 km, three clouds reaching at least 19 km, etc. Cloud heights include satellite and radar measurements, pilots' sightings, and estimates by ground observers. Some purely vapor clouds may be included in the data set, although our intent was to count only ash clouds. Multiple pulses of activity in long-running eruptions (see discussion in text under "Eruption Duration") are not counted because so many of these pulses pass unobserved—their inclusion would greatly increase the total numbers. Figure from McClelland and others (1989).

eruptions) to months or even years after the start of eruption. The dramatic event that first captured the attention of the airline community in 1982, Eric Moody's 13-minute glide over Indonesia in a powerless jumbo jet, came a full 80 days after eruptive activity began at Galunggung (although less than 2 hours after local residents saw the start of that particular eruptive pulse). The same volcano nearly brought down another aircraft 19 days later and did not end its full eruption until 9 months after it began. This eruption sequence attracted virtually no international media attention until the aircraft incidents, even though it was of a size (VEI 4) that occurs only about once a year. It had earlier caused the evacuation of 75,000 people and the deaths of 27 by mudflows. Clearly, attention must be paid by the airline community to any eruption approaching this size, and interest must continue long after its start.

## VOLCANO INFORMATION AND COMMUNICATION

The airline community can stay abreast of current volcanic activity through the Smithsonian's Global Volcanism Network (see McClelland, this volume) and may contribute information to it as well. The larger program, of which this network is a part, will also continue historical work on past eruptions and continue to provide the data necessary to place unobtrusive volcano symbols on pilots' maps. Good maps will allow volcanic belts to be recognized and individual volcanoes identified if active. All of us who set foot in airplanes are interested in improving air safety, and we will do what we can to help. In order to improve understanding of volcanoes—the fundamental element in volcano prediction—the scientific community needs more information. We hope for more volcano news from "eyes in the sky" and will do our best to disseminate volcano reports as we have been doing for nearly a quarter century. Pilots can get information to us through the reporting form designed for the purpose (Fox, this volume). This information may be sent by telephone (202-357-1511) or fax (202-357-2476).

## ACKNOWLEDGMENTS

It is a pleasure to acknowledge Lee Siebert's huge contribution to the volcano data file from which most of these data have been drawn and Roland Pool, who has both maintained the data file and constructed figures 1 and 2. The manuscript has benefited from reviews by Jim Luhr, Lindsay McClelland, Lee Siebert, Steve Brantley, and Tom Casadevall.

## REFERENCES CITED

Crisp, J.A., 1984, Rates of magma emplacement and volcanic output: Journal of Volcanology and Geophysical Research, v. 20, p. 177–211.

McClelland, L., Simkin, T., Summers, M., Nielsen, E., and Stein, T.C., 1989, Global Volcanism 1975–1985: Englewood Cliffs, N.J., Prentice Hall, and Washington, D.C., American Geophysical Union, 657 p.

Newhall, C.G., and Self, S., 1982, The volcanic explosivity index (VEI): An estimate of explosive magnitude for historical volcanism: Journal of Geophysical Research, v. 87, p. 1231–1238.

Sigurdsson, H., and Carey, S., 1989, Plinian and co-ignimbrite tephra fall from the 1815 eruption of Tambora Volcano: Bulletin of Volcanology, v. 51, p. 243–270.

Simkin, T., Siebert, L., McClelland, L., Bridge, D., Newhall, C.G., and Latter, J.H., 1981, Volcanoes of the World: A Regional Directory, Gazetteer, and Chronology of Volcanism During the Last 10,000 Years: Stroudsburg, Pa., Hutchinson Ross, 240 p.

Simkin, T., Tilling, R.I., Taggart, J.N., Jones, W.J., and Spall, Henry, 1989, This dynamic planet: Volcanoes, earthquakes, and plate tectonics: U.S. Geological Survey and Smithsonian Institution [available from the U.S. Geological Survey or the Museum of Natural History, Smithsonian Institution, Washington, D.C.].

VOLCANIC ASH AND AVIATION SAFETY:
Proceedings of the First International Symposium
on Volcanic Ash and Aviation Safety
U.S. GEOLOGICAL SURVEY BULLETIN 2047

# THE CONTROLS OF ERUPTION-COLUMN DYNAMICS ON THE INJECTION AND MASS LOADING OF ASH INTO THE ATMOSPHERE

*By* R.S.J. Sparks, Marcus I. Bursik, Steven N. Carey,
Andrew W. Woods, *and* Jennie S. Gilbert

## ABSTRACT

Eruption columns inject large masses of volcanic ash rapidly to levels in the atmosphere where commercial aircraft fly. An eruption column consists of three dynamic regions: a basal gas-thrust region, a central buoyant convective region, and an upper umbrella-cloud region where the column spreads out at its level of neutral buoyancy. The height of an eruption column is a strong function of the volumetric discharge rate of magma, which determines the flux of thermal energy into the atmosphere. Eruption columns can either be generated at a point source or can be generated from a large region due to buoyant ascent of ash from pyroclastic flows. Ascent velocities of volcanic columns are typically 50 to 200 m/s, resulting in rapid injection (on the order of a few minutes) of large concentrations of ash at heights where aircraft fly. The mass loadings of ash in the umbrella region can vary from 2,500 mg $m^{-3}$ for a 7-km-high column (23,000 ft) to over 20,000 mg $m^{-3}$ for a 40-km-high (130,000 ft) column, with a linear variation in between. These concentrations are much higher than those known to cause serious problems to aircraft and engine failure.

## INTRODUCTION

Explosive volcanic eruptions can form large plumes of tephra or ash and aerosols that penetrate to altitudes exceeding 7 km (23,000 ft), where the plumes pose hazards to aviation. The concentrations and grain-size distributions of ash particles are of particular significance to aviation safety because high ash concentrations (> 50 mg/$m^3$) have caused engine failure (Dunn and Wade, this volume). This paper provides an analysis of the factors that control the injection rate of ash into the atmosphere and the mass loading of ash that results. The paper is a companion to one by Bursik and others (this volume), which considers the dispersal and sedimentation of ash from volcanic plumes and how concentration can be inferred from sedimentological data. The general physical principles that govern the structure and dynamic behavior of eruption columns are reviewed. We will also use available models to predict the mass concentrations and mass loading rates of the atmosphere for eruptions of different intensities.

In this paper, tephra is used as a collective term for all kinds of volcanic ejecta, including common terms such as ash, pumice, scoria, lithics, crystals, rock fragments, volcanic bombs, etc. From the perspective of aviation safety, it is fine-grained tephra (volcanic ash) that is of interest.

## ERUPTION-COLUMN STRUCTURE AND DYNAMICS

### GENERAL FEATURES

A volcanic eruption column may be conveniently divided into three dynamic regimes (Self and Walker, this volume) (fig. 1). At the base of the column, mixtures of tephra and gas are discharged into the atmosphere at high velocity. Energy for the discharge is derived from decompression, liberation of gaseous phases from the magma, and vaporization of meteoric water. Velocities are typically in the range of 100 to more than 500 m/s (Wilson, 1976; Wilson and others, 1980). Explosive activity can vary from discrete explosions to continuous discharges. The lower part of the column is characterized by rapid decelerations as surrounding still air is entrained into the turbulent flow. This can be modeled as a momentum jet and has been termed the gas-thrust region (Sparks and Wilson, 1976; Sparks, 1986). In many cases, the discharge pressure at the vent is above atmospheric, and the flow rapidly expands as it adjusts to atmospheric pressure (Kieffer and Sturtevant, 1984; Woods, 1988). The flow in this region is complex, often supersonic, and remains poorly understood. However, the gas-thrust

region is only a small fraction of the total column height, and the details of the dynamic behavior in this region have little influence on ash dispersal, with the important exception of collapsing columns, which will be discussed further below.

For many eruptions, turbulent entrainment and heating of surrounding air causes the column to become buoyant. Typically, a few hundred meters to a few kilometers above the vent, buoyancy forces become dominant and the column can be regarded as a plume (Sparks, 1986; Woods, 1988). The main part of the column is thus termed the convective region (fig. 1), and the energy for ascent is a result of hot tephra heating entrained air. Two significant features of volcanic eruption columns need emphasis. First, high eruption columns derive their energy from the thermal energy of the tephra, which is at least an order of magnitude larger than the kinetic energy of the explosions. Second, the bulk density of tephra and gas emerging from the vent is always greater than the surrounding atmosphere at one bar pressure so that buoyancy is entirely a consequence of turbulent entrainment and heating of air.

Volcanic plumes eventually reach a level in the density-stratified atmosphere where they become neutrally buoyant. The momentum of the plume however causes them to ascend considerably farther—to a height, $H_t$. The cloud then subsides and spreads out as a lateral gravity flow at the height of neutral buoyancy to form the umbrella cloud (fig. 1).

## THEORETICAL MODELS

Understanding of volcanic-plume dynamics is now reasonably good and is based on the seminal work of Morton and others (1956) on plume fluid dynamics. Wilson and others (1978) and Settle (1978) showed that the theoretical analysis of plume ascent in a stratified environment could be adapted to volcanic plumes, despite their enormous scale. They proposed that the column height, $H_t$ (in meters), was directly proportional to the volumetric discharge rate of magma, $Q$ (in $m^3/s$).

$$H_t = 8.2\,(Q\rho s\Delta T)^{0.25} \qquad (18)$$

where

$\rho$ is the magma density,

$s$ the heat capacity of the magma, and

$\Delta T$ is the temperature difference between the magma and the atmosphere at vent level.

The constant of 8.2 in equation 1 is derived by taking Morton and others' (1956) theoretical results for a standard atmosphere with a temperature gradient of 6.5°C/km. Observations (fig. 2) show remarkably good agreement with equation 1 (Wilson and others, 1978; Sparks, 1986) despite the many complexities that might be expected in a volcanic plume in comparison to the simple plume analysis of

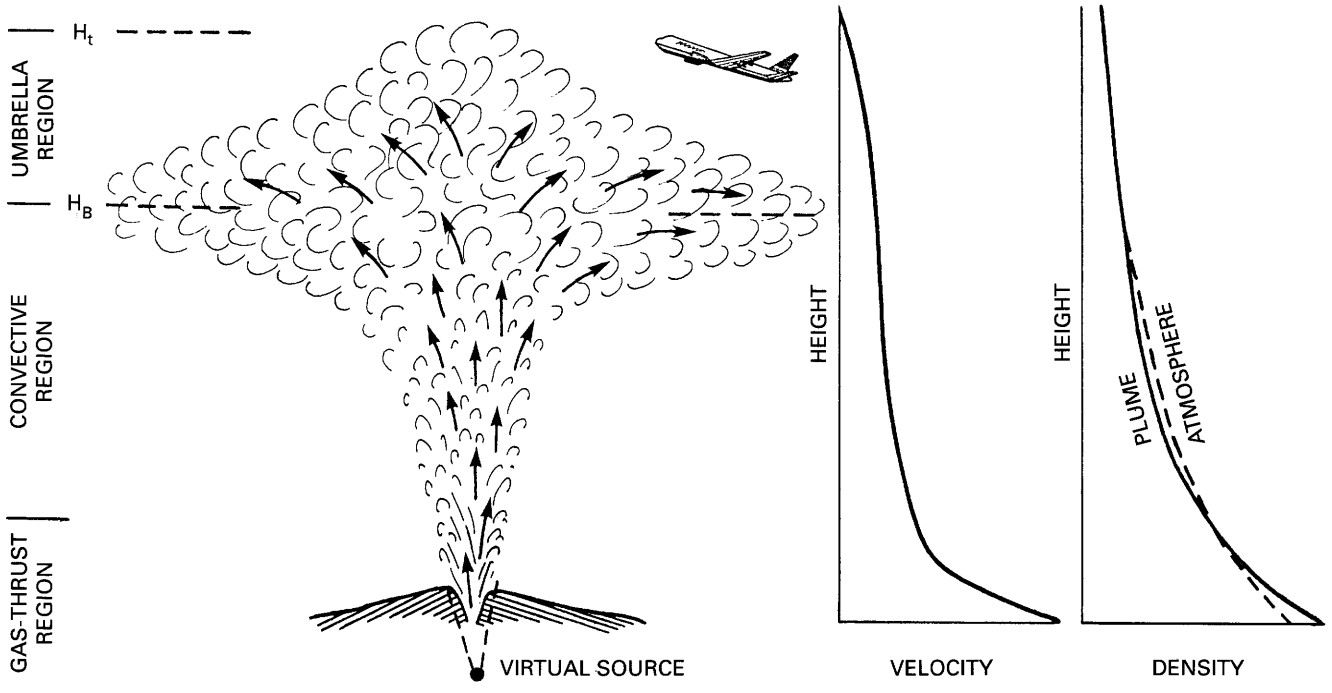


**Figure 1.** Schematic diagram of an eruption column showing three dynamic regions (after Sparks, 1986). Note the substantial overshoot of the column to height $H_t$ and spread of the umbrella cloud as a gravity current at the height of neutral buoyancy, $H_B$.

Morton and others (1956). Only eruptions with discharge rates of 500 $m^3/s$ or greater can generate plumes with heights exceeding 7.5 km (25,000 ft)—these plumes reach altitudes sufficient to pose a hazard to intercontinental flights. However, smaller plumes may pose local hazards around airports during landing and takeoff. Typically, between six and 12 eruptions a year will form columns of 7 km or more in altitude (Simkin, this volume). Most significantly, equation 1 allows a good rule of thumb for estimating the rate of mass loading of the atmosphere with volcanic ash from column-height observations.

More detailed numerical models of volcanic-plume ascent have now been published (Wilson, 1976; Sparks and Wilson, 1982; Sparks, 1986; Woods, 1988; Woods and Bursik, 1991). Woods and Bursik (1991) have presented the most comprehensive and internally consistent model of plume ascent, and the following discussion is largely based on their results. These more detailed models show that column height is dependent on many variables. Atmospheric temperature structure, grain-size distribution of the ejecta, vent dimensions, gas compositions, discharge velocity, magma temperature, exit pressure, and atmospheric moisture content can be shown to influence column height at a fixed discharge rate. However, these dependencies are rather weak, and the numerical results are sufficiently close to equation 1 for heights up to 45 km (150,000 ft) so that equation 1 forms a very useful formula for interpreting column-height observations. Indeed, the observations of heights and discharge rates from historic eruptions are simply not sufficiently accurate to be able to recognize many of the subtle effects that are apparent in the numerical results.

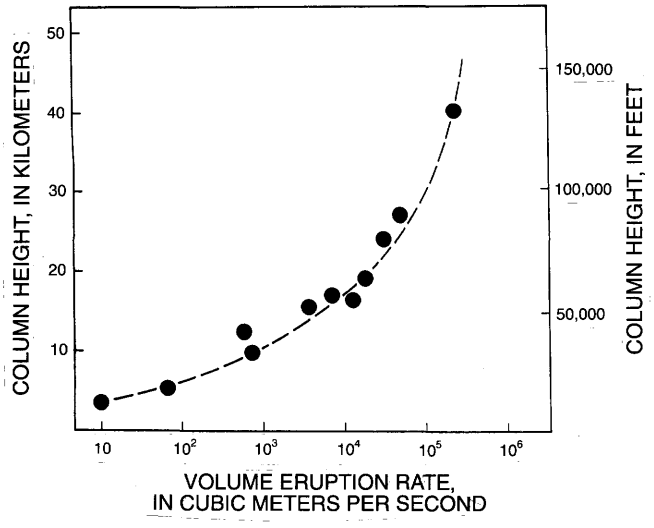


**Figure 2.** Relationship of column height to volume eruption rate for several historic eruptions (after Wilson and others, 1978; Sparks, 1986). The dashed curve represents equation 1 (see text).

Eruption columns increase in width with height due to turbulent entrainment of air. The numerical results of Woods (1988) indicate typical spreading rates ($db/dz$) of 0.2 to 0.25, where $b$ is the column radius and $z$ is the height above the vent. The spreading rate is approximately constant over most of the column height. The rather few published observations (e.g., Sparks and Wilson, 1976; Woods, 1988) show reasonable agreement with these results. Column velocities are high and are typically in the range of 50 to more than 200 m/s. Thus, eruption columns ascend to heights of 7 km or more in only a few minutes, giving little opportunity to warn aircraft at the beginning of an eruption. Broadly, ascent velocities increase with column height, reflecting the increase in intensity (i.e., discharge rate). From the point of view of tephra dispersal, the velocities in the convective region are far larger than the terminal velocities of all but the largest fragments so that almost all the tephra is transported efficiently to the top of the column. Entrainment of surrounding air creates a significant inward flow toward the column. At the plume edge, the radial inward velocities are approximately one-tenth of the ascent velocities (Turner, 1979; Sparks, 1986) so that inflow speeds of 5 to 20 m/s are typical. Only clasts exceeding several centimeters in diameter can escape from the plume margins (see Bursik and others, 1992, for a more detailed analysis).

Theoretical models (Woods, 1988) assume a steady flow and seem to provide a good description of eruptions even if they are of short duration and manifestly unsteady. Explosive eruptions of the Soufriere de St. Vincent in 1979 (Sparks and Wilson, 1982), Mount St. Helens in October 1980 and Lascar Volcano, Chile, in February 1990, consisted of several discrete explosions that merged into plumes. In the case of Lascar, three explosions occurred in less than 4 minutes. Studies of photographs and movies of these eruptions (Sparks and Wilson, 1982, and unpublished student dissertations at Bristol University) show that the motions and structure are well described by simple plume theory and the model of Woods (1988).

The umbrella cloud has an initial depth that is determined principally by the excess momentum of the plume. Theoretical analyses and experimental studies (Morton and others, 1956; Turner, 1979) suggest that the height of neutral buoyancy, $H_B$, is related to column height, $H_t$, by $H_B = 0.7\ H_t$ (fig. 1). There are little published data, but observations of plumes indicate that this is a useful approximation. Due to momentum, the cloud rises and cools and is therefore significantly denser than its surroundings, due both to lower temperature and particle content. Consequently, the umbrella cloud spreads radially as a gravity current at a level centered around the height of neutral buoyancy (Sparks and others, 1986).

## CO-IGNIMBRITE CLOUDS

An important category of eruption column is generated by a rather different mechanism. Commonly, explosive eruptions generate pyroclastic flows or nuées ardentes (glowing clouds). A pyroclastic flow is a form of gravity current that flows down the slopes of a volcano and is essentially an avalanche of tephra and gas. They can be formed by a mechanism known as column collapse (Sparks and Wilson, 1976). The explosively erupted mixture does not entrain enough air to become buoyant and forms a collapsing fountain of tephra and gas a few hundred meters to a few kilometers high, which feeds the pyroclastic flows. Flows can also be generated by lateral blast, as at Mount St. Helens on May 18, 1980 (Hoblitt and others, 1981). The deposits from pyroclastic flows are commonly termed ignimbrites by geologists, and the associated columns are term co-ignimbrite clouds.

Pyroclastic flows can generate high columns by a process known as lift-off (Sparks and others, 1986). As the flow moves away from the volcano, mixing occurs with surrounding air, and particles are deposited. The hot, dilute cloud that is generated eventually becomes buoyant and lifts off the flow. In the case of the 1980 blast flow of Mount St. Helens, a giant cloud 25 to 30 km (80,000 to 160,000 ft) high was generated over an area of 600 $km^2$ by lift-off (Sparks and others, 1986). The phenomena has been reproduced in laboratory experiments (Carey and others, 1988). Theoretical models of the process treat the co-ignimbrite cloud as a steady plume (Woods and Wohletz, 1991). Enormous amounts of fine-grained ash can be injected into the stratosphere in a very short period (a few minutes) (Sparks and Walker, 1982). The huge plume generated by Pinatubo in the Philippines on June 15, 1991, also has the features of a co-ignimbrite cloud.

## THE EFFECT OF WIND ON VOLCANIC PLUMES

There is a great deal of engineering literature on the distortion and dispersal of industrial plumes and fire plumes by wind (e.g., Briggs 1969). This literature, however, is of rather limited use with regard to the study of powerful volcanic plumes with heights sufficiently great to emplace tephra either into the stratosphere or to heights that are of concern to aviation. Relations of plume shape, height, and wind velocity are empirical and have been developed for relatively weak plumes where ascent velocities are comparable to or less than wind velocities. Even a 10-km-high column is orders of magnitude more powerful than most industrial plumes and has ascent velocities that exceed typical jet-stream velocities (> 30 m/s).

Carey and Sparks (1986) classified eruption columns into three types. First, weak plumes (typically much less than 10 km in height) are distorted by the wind, and the empirical results of industrial studies on plume shape are appropriate. Second, intermediate plumes ascend with little distortion by the wind and then mushroom into the umbrella region and spread somewhat upwind before the wind influences the dispersal of the cloud. The 1980 Mount St. Helens Plinian plume (16 to 18 km high, or approximately 55,000 ft) is a good example. Finally, very powerful plumes spread out radially in all directions as a giant gravity current in the umbrella region; the wind has very little influence in the initial stages of these eruptions. The 1980 cloud of Mount St. Helens spread to 10 km upwind (Sparks and others, 1986) and expanded to about 100-km diameter before downwind dispersal became substantial. It took only 20 minutes to expand to 100-km diameter, emphasizing the threat that a high-intensity eruption in its initial stages poses to aircraft. The 1991 Mount Pinatubo cloud is reported to have moved a remarkable 300 km upwind. Both of these examples of highly energetic plumes were co-ignimbrite clouds.

## MASS LOADING MODELS

The December 15, 1989, incident near Redoubt Volcano, Alaska, involving a Boeing 747-400, indicated that ash concentrations of 2,000 mg $m^{-3}$ were encountered (Dunn and Wade, this volume). The U.S. Military regard particle loadings of 50 mg/$m^{-3}$ or more as potentially hazardous. We have, therefore, used the dynamic models described earlier to estimate typical concentrations of ash generated in the umbrella-cloud region. In the companion paper (Bursik and others, this volume), we consider how these concentrations change as the ash is dispersed away from the volcano.

The first concern is the particle-size distribution of the ejecta. Reconstructions of the total grain-size distributions in explosive eruptions (Sparks and others, 1981; Woods and Bursik, 1991) indicate that typically 70 percent of the ejecta is less than 2 mm. Therefore, we restrict our discussion to considering the concentrations of the less-than-2-mm ash.

However, such reconstructions are limited by the poor knowledge of the proportions of very fine ash particles (< 10 μm) generated in such eruptions. Because almost all tephra is transported into the umbrella cloud, the concentrations calculated here are not sensitive to size distributions. However, the size distribution will have a strong influence on subsequent dispersal.

We have first calculated mass loadings for columns from 9.8 to 40.5 km (32,000 to 133,000 ft) and have approximated the results of Woods (1988) together with equation 1 to calculate the height of neutral buoyancy ($H_B$) and the upward flow rate at the top of the convective region (fig. 1) for an eruption temperature of 1,000°C. Figure 3 shows the calculated mass loadings as a function of column height. All columns greater than 7 km high (23,000 ft) generate mass loadings that are at least two orders of magnitude higher than the U.S. Military threshold of 50 mg $m^{-3}$, and all exceed the

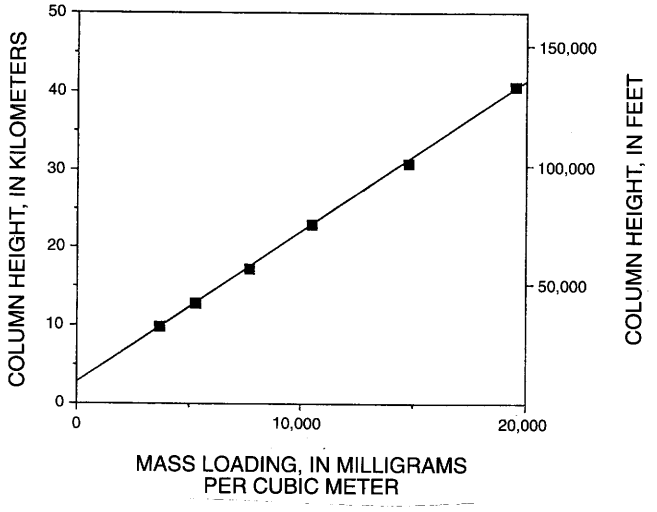


**Figure 3.** The calculated mass loadings of tephra in the umbrella region of eruption columns are plotted as a function of column height using equation 1 (see text) as an approximation.

2,000 mg $m^{-3}$ value associated with the December 15, 1989, Redoubt incident. Mass loading increases with column height because the increase in mass discharge rate has a greater influence than the decrease of atmospheric density in higher columns.

We have further examined the variation of mass loadings with temperature and eruptive style using the numerical computer code developed by Woods (1988). Calculations have been made for a steady, maintained eruption column and for release of a volcanic thermal (an instantaneous release of buoyant fluid), as might happen when a co-ignimbrite cloud lifts off at temperatures of 1,200°K, 1,000°K, and 800°K. These more detailed numerical calculations yield concentrations in general agreement with the simpler approach, but some interesting details are revealed. As eruption temperature decreases, the mass loading increases for a given column height (fig. 4*A*), showing that a wide range of loadings can occur—any ash-dispersal model should use the maximum mass loading condition to predict a worst case scenario (Harris, this volume). One other interesting feature of figure 4*A* is that the mass loading increases rapidly as column height increases for plumes that penetrate the tropopause, located at about 11 km in the present model calculations. This is because the overshoot distance above the neutral buoyancy height is reduced by the much stronger stratification above the tropopause, and, hence, the material is not as dilute when the column comes to rest.

Figure 4*B* presents similar calculations for a discrete volcanic thermal using the model of Woods and Kienle (in press). The mass loadings in volcanic thermals are similar to those in maintained plumes and vary with height in the same manner. The loadings are a little larger for a given column height and temperature because large thermals do not entrain air as efficiently as steady plumes.

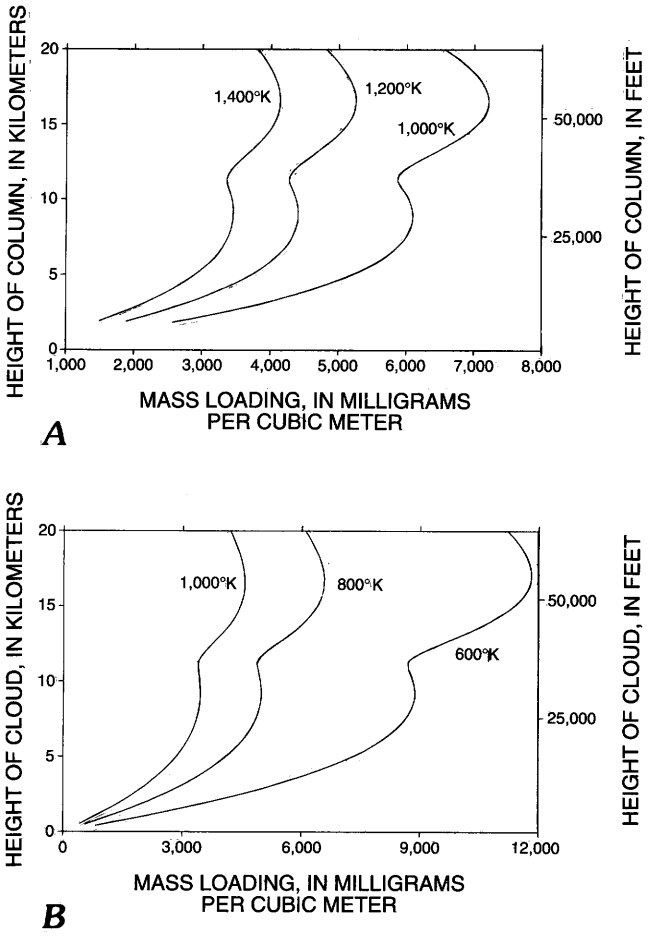


**Figure 4.** Mass loadings of tephra as a function of column height for three different eruption temperatures using the numerical model of Woods (1988) for an atmosphere with the tropopause at an altitude of 11 km. *A*, maintained eruption columns. *B*, volcanic thermals.

## CONCLUSIONS

Explosive volcanic eruptions are sufficiently powerful to inject large amounts of ash into the stratosphere. The injection height is determined by magma discharge rate and can be approximately estimated from equation 1. Explosive eruptions typically generate a large proportion of particles less than 2 mm in diameter, which are efficiently transported to the top part of the column known as the umbrella cloud. Typical mass loadings vary from 3,000 to over 20,000 mg $m^{-3}$ for columns in the height range of > 7 to 40 km (23,000 to 130,000 ft).

From the perspective of aviation safety the following points emerge:

1. The mass loadings greatly exceed the safety thresholds and values of concentration that cause engine failure. It is therefore necessary to establish how the mass concentrations change as the plume is

dispersed—this problem is addressed in the companion paper (Bursik and others, this volume).

2. Many eruptions involve fairly steady discharges of tephra over many hours or even days from point sources. Such eruptions can be monitored, and aircraft can be organized so as to avoid the plumes. However, shorter lived explosions and high-intensity eruptions can inject large masses of ash into the stratosphere in several minutes—once in the stratosphere, they can be dispersed rapidly by jet-stream winds.
3. Co-ignimbrite clouds pose a particularly difficult threat because they are generated from large areas rather than point sources and are formed very rapidly.

## ACKNOWLEDGMENTS

Research has been supported by the following organizations: Venture Research International (R.S.J.S. and J.S.G.), N.S.F. grant number EAR-8804117 (S.N.C), a NERC Fellowship (J.S.G.), and NATO collaborative grant (CRG 910096).

## REFERENCES CITED

Briggs, G.A., 1969, Plume Rise: U.S. Atomic Energy Commission, 80 p.

Bursik, M.I., Sparks, R.S.J., Gilbert, J.S., and Carey, S.N., 1992, Sedimentation of tephra by volcanic plumes: I. Theory and its comparison with a study of the Fogo A Plinian deposit, Sao Miguel (Azores): Bulletin of Volcanology, v. 54, p. 329–344.

Carey, S.N., Sigurdsson, H., and Sparks, R.S.J., 1988, Experimental studies of particle-laden plumes: Journal of Geophysical Research, v. 93, p. 15314–15328.

Carey, S.N., and Sparks, R.S.J., 1986, Quantitative models of the fallout and dispersal of tephra from volcanic eruption columns: Bulletin of Volcanology, v. 48, p. 109–125.

Hoblitt, R.P., Miller, C.D., and Vallance, J.W., 1981, Origin and stratigraphy of the deposit produced by the May 18 directed blast, *in* Lipman, P.W., and Mullineaux, D.R., eds., The 1980 Eruptions of Mount St. Helens, Washington: U.S. Geological Survey Professional Paper 1250, p. 401–420.

Kieffer, S.W., and Sturtevant, B., 1984, Laboratory studies of volcanic jets: Journal Geophysical Research, v. 98, p. 8253–8268.

Morton, B.R., Taylor, G.I., and Turner, J.S., 1956, Turbulent gravitational convection from maintained and instantaneous sources: Transaction of the Royal Society London, ser. A, v. 234, p.1–23.

Settle, M., 1978, Volcanic eruption clouds and thermal power output of explosive eruptions: Journal of Volcanology and Geothermal Research, v. 3, p. 309–324.

Sparks, R.S.J., 1986, The dimensions and dynamics of volcanic eruption columns: Bulletin of Volcanology, v. 48, p. 3–15.

Sparks, R.S.J., and Walker, G.P.L., 1982, The significance of vitric enriched air-fall ashes associated with crystal-enriched ignimbrites: Journal of Volcanology and Geothermal Research, v. 28, p. 257–274.

Sparks, R.S.J., and Wilson, L., 1976, A model for the formation of ignimbrite by gravitational column collapse: Journal of the Geological Society of London, v. 132, p. 441–451.

———1982. Explosive volcanic eruptions, V. Observations of plume rise at Soufriere St. Vincent: Geophysical Journal of the Royal Astronomical Society, v. 69, p. 551–570.

Sparks, R.S.J., Moore, J.G., and Rice, C.J., 1986, The initial giant umbrella cloud of Mount St. Helens: Journal of Volcanology and Geothermal Research, v. 28, p. 257–274.

Sparks, R.S.J., Wilson, L., and Sigurdsson, H., 1981, The pyroclastic deposits of the 1875 eruption of Askja: Royal Society of London Philosophical Transactions, ser. A, v. 299, p. 241–273.

Turner, J.S., 1979, Buoyancy Effects in Fluids: Cambridge, England, Cambridge University Press, 368 p.

Wilson, L., 1976, Explosive volcanic eruptions: III—Plinian eruption columns: Geophysical Journal of the Royal Astronautical Society, v. 45, p. 543–556.

Wilson, L., Sparks, R.S.J., and Walker, G.P.L., 1980, Explosive volcanic eruptions: IV—The control of magma properties and conduit geometry on eruption column behavior: Geophysical Journal of the Royal Astronautical Society, v. 83, p. 1829–1836.

Wilson, L., Sparks, R.S.J., Huang, T.C., and Watkins, N.D., 1978, The control of eruption column heights by eruption energetics and dynamics: Journal of Geophysical Research, v. 83, p. 1829–1836.

Woods, A.W., 1988, The thermodynamics and fluid dynamics of eruption columns: Bulletin of Volcanology, v. 50, p. 169–191.

Woods, A.W. and Bursik, M.I., 1991, Particle fallout, thermal disequilibrium and volcanic plumes: Bulletin of Volcanology, v. 53, p. 559–572.

Woods, A.W., and Kienle, J., in press, The dynamics and thermodynamics of volcanic clouds: Theory and observations from the April 15 and 21 eruptions of Redoubt Volcano, Alaska: Journal of Volcanology and Geothermal Research.

Woods, A.W., and Wohletz, K., 1991, Dimensions and dynamics of co-ignimbrite eruption columns: Nature, v. 350, p. 225–227.

VOLCANIC ASH AND AVIATION SAFETY:
Proceedings of the First International Symposium
on Volcanic Ash and Aviation Safety
U.S. GEOLOGICAL SURVEY BULLETIN 2047

# MELTING PROPERTIES OF VOLCANIC ASH

*By* Samuel E. Swanson *and* James E. Beget

## ABSTRACT

Volcanic ash from eastern Aleutian volcanoes (typical of circum-Pacific volcanoes) is composed of rhyolitic (silica-rich) glass, minerals (feldspars, pyroxene, hornblende and Fe-Ti oxides), and rock fragments. Melting temperatures of the glasses, estimated from liquidus phase relations in the system $SiO_2$–$KAlSi_3O_8$–$NaAlSi_3O_8$, ranged from 1,000°C to 1,300°C, whereas minerals begin melting at about 1,100°C.

Volcanic ash that is ingested into operating turbofan engines will partially melt (i.e., all of the glass and some of the minerals). The molten ash is then deposited on high-temperature parts of the turbine—this can result in engine shutdown.

Reduction of engine operating conditions to idle settings lowers the engine temperatures below the melting point of volcanic glass (below 1,000°C), thus preventing the melting of ingested volcanic ash. However, at idle conditions, engines still operate at temperatures in excess of the glass transition temperature (700°–860°C), and annealing of glass particles to hot parts of the turbine may still be a problem.

## INTRODUCTION

Volcanic ash is a widespread product of eruptions of volcanoes that are located around rim of the Pacific Ocean. Ash is formed by explosive fragmentation and quenching of magma (crystals + melt + gas) during an eruption. Melt in the magma is quenched to a glass when the temperature is rapidly lowered upon exposure to atmospheric conditions. The explosive character of these volcanoes is caused by the silica-rich melt, which often contains dissolved volatile components, such as $H_2O$ or $SO_2$. Crystallization of mineral phases (e.g., plagioclase, pyroxene, hornblende, Fe-Ti oxides, etc.) gradually enriches non-crystallizing components in the melt. In the case of components like silica or sodium, their concentrations in the crystallizing phases are low relative to their concentration in the melt, resulting in their overall enrichment. Bulk lava compositions from these volcanoes range from basalt to dacite (lavas generally contain from 48 to 70 weight percent $SiO_2$), and the melt fraction between mineral grains is andesitic to rhyolitic (53–78 weight percent $SiO_2$). The glassy fragments in volcanic ash are the non-crystalline part of the magma and, hence, have the lowest crystallization temperature. Conversely, the glass also has the lowest melting temperature. When volcanic ash is ingested into operating jet aircraft engines, it is the glass particles that will melt first. As aircraft engine operating temperatures are lowered in an effort to reduce the ash fusion within the engine (Campbell, this volume; Casadevall and others, 1991; Przedpelski and Casadevall, this volume), it is the melting temperature of glass particles that will determine the operating temperatures below which the ash will not melt in the engine. The purpose of this paper is to review the compositions of glasses found in volcanic ashes from typical circum-Pacific volcanoes and to estimate their melting temperatures by comparison to published phase diagrams available in the geological and engineering literature. We report here on the melting properties of the more common silica-rich glasses. Mafic (andesitic) glass, similar to that erupted in the 1992 eruption of Mt. Spurr (Alaska), is currently under study and will be the subject of a future report. Alaskan volcanoes in the eastern Aleutian arc were selected for study because of their recent activity and potential hazard to aircraft safety (Steenblik, 1990; Przedpelski and Casadevall, this volume; Kienle, this volume). Several Alaskan volcanoes in the eastern Aleutian arc (fig. 1) have produced widespread volcanic-ash deposits that have covered south-central Alaska. Ash may be produced in short-lived, large eruptions (Novarupta in 1912, Spurr in 1953 and 1992) or in a series of intermittent, small eruptions (Redoubt Volcano, 1989–90). Jet aircraft encounters with ash have been recorded from eruptions of Augustine in 1976 and Redoubt in 1989 (Steenblik, 1990; Casadevall, 1991; Kienle, this volume).

## METHODS OF STUDY

All of the glass samples used in this study were obtained from volcanic ash deposits from south-central Alaska. The White River ash and the ash from Hayes Volcano are voluminous prehistoric ashes that covered south-central Alaska (Riehle, 1985; Westgate, 1990; Beget and others, 1991). Novarupta, which erupted in 1912, is the largest historic Alaskan eruption and spread ash throughout southern Alaska (Griggs, 1922; Hildreth, 1987). Ash from Augustine Volcano, the most active volcano in the eastern

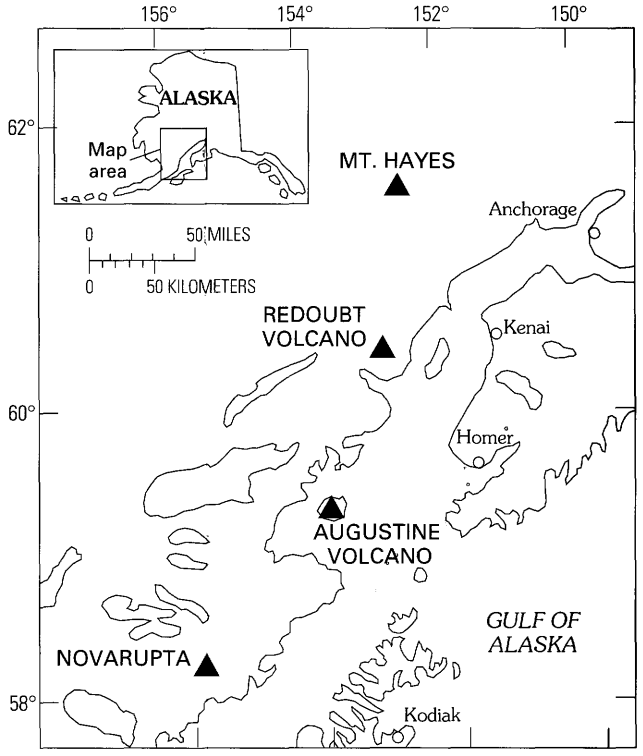


**Figure 1.** Volcanoes (solid triangles) in the eastern Aleutian volcanic arc, Alaska.

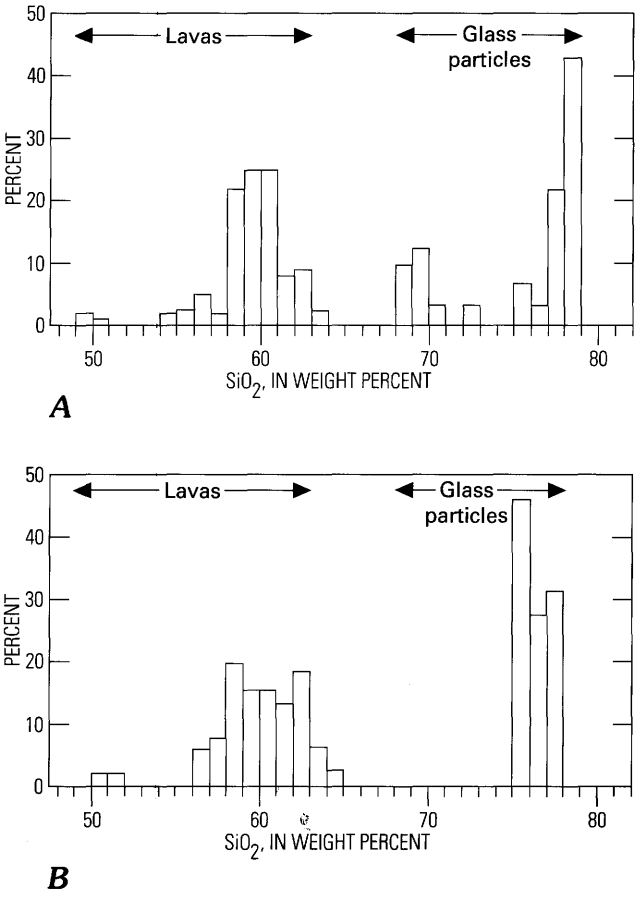


**Figure 2.** Silica contents of lavas (bulk samples) and glass particles (shards) in volcanic ashes from *A*, Redoubt and *B*, Augustine Volcanoes. The numbers of analyses of lavas and glasses from each volcano are in excess of 50 and have been normalized to 100 percent for comparison. Volcanic glass is consistently higher in silica than the whole-rock lavas. Glass analyses are from unpublished data in the authors' files (representative analyses given in table 1). Lava compositions for Augustine Volcano are from Kienle and others (1983) and Daley (1986); compositions for Redoubt Volcano are from Nye and others (in press) and Swanson and others (in press).

Aleutian arc, was collected from prehistoric deposits on Augustine Island that span approximately 2,700 years of eruptive history (Swanson and Kienle, 1986; Beget and Kienle, 1992). Ash from Redoubt Volcano is represented by samples from the 1989–90 eruption. Together, this suite of samples provides a representative collection of the ashes that is to be expected from eruptions of these Alaskan volcanoes.

## ANALYTICAL TECHNIQUES

Glass from these ash samples was analyzed with a Cameca MBX electron microprobe at Washington State University using a 15-kV electron beam and a sample current of 13.5 nA. A beam spot diameter of 8 μm was used, and the counting time was 10 seconds. The glass analyses are reported as oxides and are normalized to 100 percent. Actual totals ranged from 98 to 100 percent, depending on the degree of hydration (water in the glass.) Well-characterized natural glasses were used as standards (KCl was used for Cl measurements).

# RESULTS

When compared with lavas, glass particles (shards of quenched melt) in the volcanic ash from Alaskan volcanoes are much richer in silica as a consequence of crystallization to form phenocryst minerals before eruption. For example, lavas from Redoubt Volcano have basaltic and andesitic bulk compositions (50–64 weight percent $SiO_2$, fig. 2), whereas the glass in the volcanic ash from the 1989–90 eruption of Redoubt ranges from 69 to 78 weight percent $SiO_2$ (fig. 2). Similar relations are shown for Augustine Volcano (fig. 2), but the Augustine glasses show a more restricted range of compositions (75–78 weight percent $SiO_2$).

Representative glass compositions are shown in table 1 both as weight percent oxide and as normative minerals. The normative composition is the rock analysis recalculated to a set of standard anhydrous normative minerals. For silica-rich volcanic rocks or glasses, the abundant normative minerals are quartz (Q), albite (Ab), and orthoclase (Or), with lesser amounts of anorthite (An), corundum (C), hypersthene (Hy),

**Table 1.** Representative electron microprobe analyses of volcanic glass from ash from Alaskan volcanoes.

[Analyses are presented as weight percent of oxides and as normative minerals (see text for explanation of normative minerals). Numbers in parentheses represent units of standard deviation]

| Quantity analyzed | Redoubt Volcano (12/15/89) | | | | Augustine Volcano | | Hayes Volcano | White River ash | Novarupta | |
|---|---|---|---|---|---|---|---|---|---|---|
| **Analyses expressed as weight percent of oxides** | | | | | | | | | | |
| $SiO_2$ | 69.35 (0.45) | 71.91 (0.31) | 75.94 (0.36) | 77.81 (0.35) | 75.38 (0.36) | 76.36 (0.31) | 73.65 (0.36) | 73.77 (0.43) | 78.20 (0.37) | 76.94 (0.17) |
| $TiO_2$ | 0.51 (0.11) | 0.45 (0.03) | 0.31 (0.07) | 0.22 (0.01) | 0.39 (0.04) | 0.37 (0.06) | 0.23 (0.03) | 0.21 (0.02) | 0.18 (0.06) | 0.35 (0.07) |
| $Al_2O_3$ | 15.59 (0.54) | 14.75 (0.16) | 13.32 (0.21) | 12.40 (0.18) | 12.98 (0.10) | 12.58 (0.17) | 14.50 (0.14) | 14.54 (0.26) | 12.00 (0.15) | 12.29 (0.12) |
| $Fe_2O_3$total | 3.26 (0.31) | 2.58 (0.14) | 1.46 (0.22) | 1.22 (0.09) | 2.30 (0.15) | 2.06 (0.12) | 1.94 (0.21) | 1.71 (0.14) | 1.34 (0.15) | 1.87 (0.13) |
| MgO | 0.87 (0.17) | 0.67 (0.02) | 0.30 (0.11) | 0.23 (0.03) | 0.49 (0.05) | 0.43 (0.05) | 0.54 (0.03) | 0.36 (0.03) | 0.14 (0.05) | 0.26 (0.04) |
| CaO | 3.25 (0.29) | 2.48 (0.10) | 1.57 (0.25) | 1.16 (0.10) | 2.28 (0.27) | 2.04 (0.16) | 2.23 (0.10) | 1.85 (0.11) | 0.85 (0.19) | 1.27 (0.09) |
| $Na_2O$ | 4.37 (0.18) | 4.21 (0.08) | 3.92 (0.21) | 3.71 (0.12) | 3.95 (0.13) | 3.89 (0.09) | 3.93 (0.08) | 4.16 (0.13) | 4.07 (0.13) | 3.98 (0.13) |
| $K_2O$ | 2.54 (0.12) | 2.79 (0.11) | 3.04 (0.14) | 3.14 (0.17) | 2.00 (0.27) | 1.98 (0.08) | 2.62 (0.11) | 3.07 (0.10) | 3.03 (0.10) | 2.85 (0.08) |
| Cl | 0.17 (0.08) | 0.16 (0.02 | 0.15 (0.04) | 0.13 (0.06) | 0.24 (0.11) | 0.29 (0.07) | 0.36 (0.03) | 0.33 (0.03) | 0.19 (0.03) | 0.19 (0.03) |
| n[1] | 11 | 7 | 5 | 7 | 18 | 16 | 15 | 15 | 18 | 10 |
| **Analyses recast as normative minerals** | | | | | | | | | | |
| Q | 26.04 | 30.43 | 37.69 | 41.38 | 39.13 | 41.14 | 35.18 | 33.32 | 40.90 | 39.77 |
| Or | 15.01 | 16.49 | 17.97 | 18.56 | 11.82 | 11.70 | 15.48 | 18.14 | 17.91 | 16.84 |
| Ab | 36.98 | 35.62 | 33.17 | 31.39 | 33.42 | 32.92 | 33.25 | 35.20 | 34.44 | 33.68 |
| An | 15.70 | 12.30 | 7.7 | 5.75 | 11.31 | 10.12 | 11.06 | 9.18 | 4.22 | 6.30 |
| C | 0.00 | 0.30 | 0.73 | 0.79 | 0.17 | 0.33 | 1.14 | 1.01 | 0.48 | 0.35 |
| Hy | 2.17 | 1.67 | 0.75 | 0.57 | 1.22 | 1.07 | 1.34 | 0.90 | 0.35 | 0.65 |
| Hm | 3.26 | 2.58 | 1.46 | 1.22 | 2.30 | 2.06 | 1.94 | 1.71 | 1.34 | 1.87 |
| Tn | 0.30 | 0.00 | 0.00 | 0.00 | 0.00 | 0.00 | 0.00 | 0.00 | 0.00 | 0.00 |
| Ru | 0.39 | 0.45 | 0.31 | 0.22 | 0.39 | 0.37 | 0.23 | 0.21 | 0.18 | 0.35 |

[1] Number of points per analysis, n.

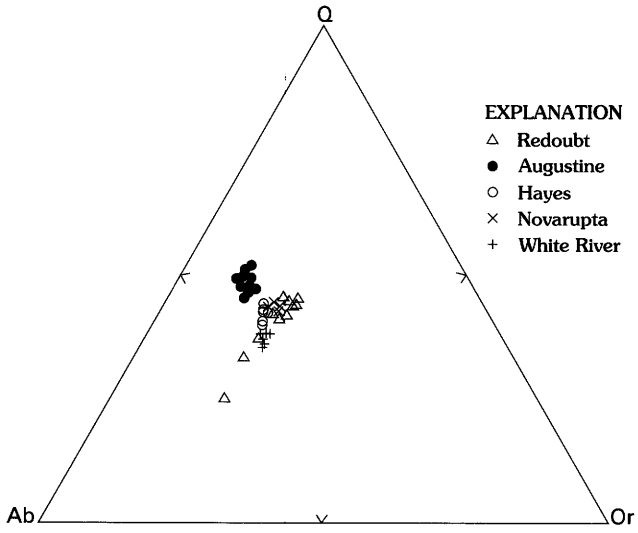


**Figure 3.** Normative compositions (in terms of albite, Ab; orthoclase, Or; and quartz, Q—see text for explanation) of glasses from the White River ash, the 1912 eruption of Novarupta, and eruptions of Mt. Hayes and Augustine and Redoubt Volcanoes. The Redoubt data are for glasses from the 1989–90 eruption. White River, Augustine, and Hayes data are from prehistoric ashes. Mt. Hayes data are from Beget and others (1991); other data are from the authors' unpublished files.

hematite (Hm), sphene (Tn), and rutile (Ru). The recalculation of the oxide components into normative minerals facilitates comparison of glass compositions to experimental laboratory results on melting temperatures of rocks.

Glass compositions displayed on triangular variation diagrams, with normative components as the variables, cluster into fields for each suite of glasses (fig. 3). Glasses from single, short-lived eruptions (e.g., White River ash and Novarupta) cluster in small fields, whereas glasses from multiple eruptions (Augustine and Hayes) define slightly larger fields. The 1989–90 Redoubt glasses form a range of compositions related to the mixing of two different magmas (with different compositions of melt quenched to glass) in the early (December 1989) stages of the eruption (Swanson and others, in press).

## MELTING RELATIONS OF GLASSES

Liquidus phase relations (temperatures required to completely melt a solid) at a pressure of 1 bar in the system $SiO_2$ (quartz, Q)–$KAlSi_3O_8$ (orthoclase, Or)–$NaAlSi_3O_8$ (albite, Ab) are shown in figure 4. This system is well known to geologists as the "granite system" because of its use in describing the melting and crystallization behavior of granitic rocks. The triangular composition diagram is divided into primary phase fields by boundary curves. Isotherms (lighter solid lines that represent constant temperature) describe the melting temperatures for any solid that contains the normative minerals quartz, orthoclase, and albite (fig. 4). The boundary curve between the primary phase fields of the $SiO_2$ polymorphs cristobalite (Cr) and tridymite (Tr), and alkali feldspar (Af) has a temperature minimum (m, fig. 4) at 960°C. For any combination of these three normative minerals (quartz-orthoclase-albite), melting at 1 bar will initially start at 960°C, and the composition of the first melt will correspond to m (fig. 4). The incongruent melting of K-feldspar (Or) at low pressure is represented by the boundary curve between alkali feldspar (Af) and leucite (Lc) phase fields (fig. 4). The small (10–20 bar) pressure increase within operating turbofan engines does little to change the 1 bar melting relations of figure 4.

In addition to the albite (Ab), orthoclase (Or), and quartz (Q) components, the volcanic glasses contain appreciable normative anorthite (An) (table 1). Addition of the anorthite component raises the melting temperatures relative to the anorthite-free albite-orthoclase-quartz compositions; however, the magnitude of this effect is difficult to predict, especially for this system without water. Experiments done on ingestion of dust containing appreciable anorthite component along with albite, orthoclase, and quartz into operating jet engines find that ash begins to melt at temperatures of about 1,000°C (Kim and others, 1992). These results are in good agreement with the predictions from figure 4, where

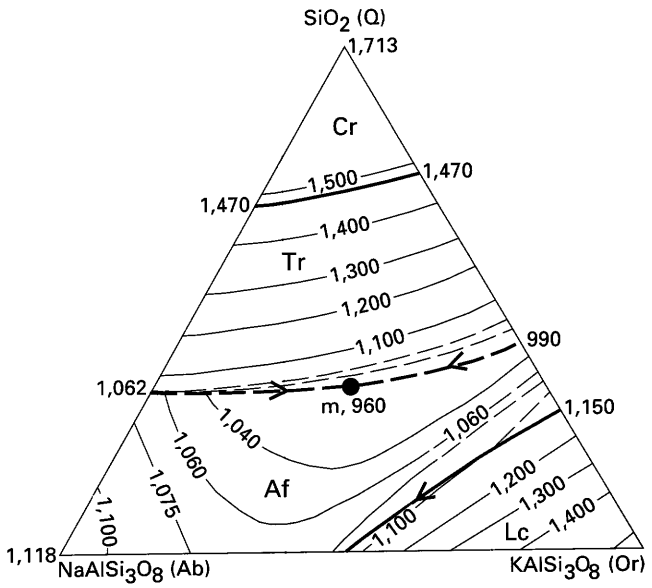


**Figure 4.** Liquidus phase diagram for the system Ab-Or-Q at one bar pressure, modified from Schairer (1950). Heavy lines are boundary curves with arrows indicating the direction to lower temperature. Primary phase fields are shown for cristobalite (Cr), tridymite (Tr), alkali feldspar (Af), and leucite (Lc). Symbol, m, indicates temperature minimum on boundary curve between cristobalite/tridymite and alkali feldspar. See text for further explanation.

the beginning of melting for anorthite-free compositions occurs at 960°C. Thus, the effect of anorthite on melting relations seems small and is probably on the order of less than 50°C. Melting of any volcanic glass that contains normative quartz, orthoclase, and albite can be modeled in the system albite-orthoclase-quartz, as illustrated for the glasses in this study on figure 5. Augustine glasses plot between the 1,200°C and 1,300°C isotherms; the glasses from the Hayes Volcano and Novarupta plot between the 1,100°C and 1,200°C isotherms; and White River glasses plot near the 1,100°C isotherm (fig. 5).

The large field of Redoubt glass compositions (fig. 5) is caused by variation in composition of glass shards erupted during December 1989 (table 1) and gives a melting range of 1,000°–1,200°C. These glasses (with the higher silica contents—77 to 78 weight percent $SiO_2$) were erupted from December 1989 to April 1990; they melt at temperatures of 1,100°C to 1,200°C. Lower silica glasses (68 to 73 weight percent $SiO_2$) were only erupted during December 1989 and melt at lower temperatures: 1,000°C to 1,100°C.

Maximum-cruise operating temperatures of high performance turbofan engines currently used on long-range commercial aircraft (747-400, DC-10, etc.) are on the order of 1,400°C (E.E. Campbell, Boeing Co., oral commun., 1991; Kim and others, 1992). Most of the compositions in the system albite-orthoclase-quartz are above liquidus temperatures at 1,400°C (fig. 4)—this includes all the volcanic glasses modeled in this study (fig. 5). Indeed, some of the minerals found in the volcanic ash (e.g., sodic plagioclase) will also melt at 1,400°C. Ingestion of volcanic ash by turbofan engines effectively grinds the ash to fine particles (≅ 7 μm; Casadevall and others, 1991) and, in the process, erodes the tips of the compressor airfoils (Przedpelski and Casadevall, this volume). This combination of small ash particle size and the high operating temperatures of the engine ensures that much of the volcanic ash will melt upon ingestion into an operating engine and be deposited on the turbine (specifically on the high-pressure nozzle guide vanes).

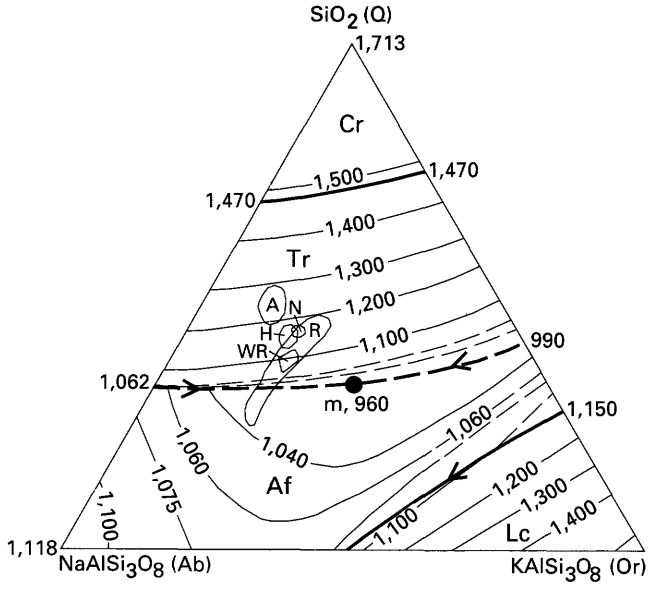


**Figure 5.** Composition fields of volcanic glasses (fig. 3) on liquidus Ab-Or-Q phase diagram at 1 bar pressure showing isotherms that define melting temperatures for various glasses. A, Augustine; N, Novarupta; H, Hayes; WR, White River; R, Redoubt.

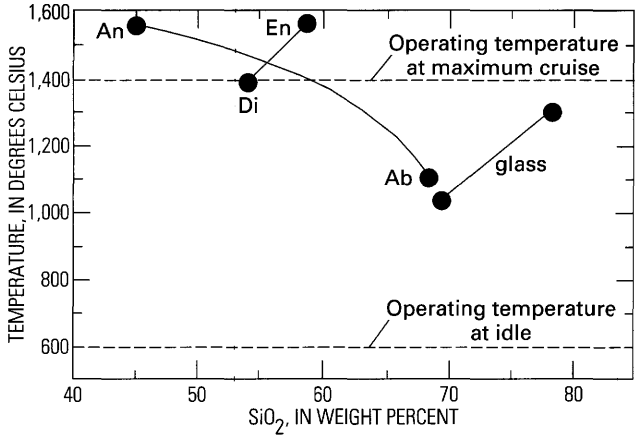


**Figure 6.** Melting relations of plagioclase (An-Ab), pyroxene (Di-En), and volcanic glasses (from fig. 5) at 1 bar pressure. Dashed lines represent the approximate operating temperatures of typical high-performance turbofan engines at idle and maximum-cruise conditions.

A reduction of engine thrust to idle has been recommended if a jet aircraft encounters volcanic ash in the air (Campbell, this volume; Przedpelski and Casadevall, this volume). Turbofan engines operating at idle run at about 600°C, considerably below the melting temperatures of all volcanic glass (fig. 6). Cooling of turbofan engines from normal operating temperatures (1,400°C) to idle temperatures is almost instantaneous. Volcanic ash will not melt when ingested into the engines at idle conditions (600°C). In addition, the rapid cooling from operating conditions to idle thrust setting induces a thermal shock related to the differential thermal expansion of the molten glass and the engine-metal substrate that can remove much of the previously melted glass that was deposited in the engine.

## CONCLUSIONS

Ingestion of volcanic ash by high performance turbofan engines at operating conditions melts glass shards and some of the minerals that make up the ash (fig. 6). Volcanic glass compositions can show wide variations and still be melted upon ingestion into the engine because of high engine operating temperatures. Operating temperatures must be lowered below the lowest melting temperature (≅ 1,000°C for glass, fig. 6) to prevent melting of ingested volcanic ash. Reduction of engine operating conditions to idle settings (≅ 600°C) will prevent melting of ingested volcanic ash.

## RECOMMENDATIONS

Industry recommendations involving aircraft encounters with airborne volcanic ash (Lloyd, 1990; Campbell, this volume; Przedpelski and Casadevall, this volume; AIA, 1991) emphasize the need to exit the ash as quickly as possible and to reduce engine thrust to idle. Reduction of engine operating temperatures will prevent the melting of volcanic ash (including glass) ingested into the engines. Dynamic experiments done on ingestion of dust into operating engines (e.g., Kim and others, 1992; Dunn and Wade, this volume) should be done with volcanic ash (including an abundance of glass) at engine-idle temperatures. The question to be answered is whether glass particles can anneal and flow as a supercooled liquid above the glass transformation temperature (*Tg*), the temperature between lower temperature glass and higher temperature supercooled liquid (Carmichael and others, 1974). For most silicate glasses, *Tg* is about 0.66 of the melting temperature (Carmichael and others, 1974). Volcanic glasses in this study thus have glass transformation temperatures of about 700°–860°C. Will these volcanic glasses anneal at engine-idle conditions and adhere to the hotter parts of the engine? Probably not. The glass transformation temperatures are close to the idle operating temperatures ($\cong$ 600°C), and the transit time of the ash through the engine is short. M.G. Dunn does not believe that glass annealing will occur (CALSPAN, oral commun., 1991) and does not find an adhesion of ash below 1,000°C in his experiments (Kim and others, 1992; Dunn and Wade, this volume). However, such ash-ingestion experiments should be tried at engine-idle conditions with a volcanic ash rich in volcanic glass.

## ACKNOWLEDGMENTS

Funding for this study was provided by the Alaska Volcano Observatory. Samples of Redoubt Volcano tephra were supplied by Robert G. McGimsey of the U.S. Geological Survey. Tephra glass analyses were done at Washington State University with the able assistance of Scott Cornelius and Diane Johnson. Discussions with Michael G. Dunn of CALSPAN and preprints of his papers on dynamic experiments with dust and jet engines provided a much needed "reality check" on some of the conclusions presented in this paper. Several industry people, including Ernie Campbell of Boeing Commercial Airplanes, Zygmunt Przedpelski of General Electric Aircraft Engines, and Peter Kingston of Rolls Royce Inc., provided useful copies of graphic materials.

## REFERENCES CITED

AIA, 1991, AIA recommendations aimed at increased safety and reduced disruption of aircraft operations in regions with volcanic activity: Washington, D.C., Aerospace Industries Association of America, 7 p.

Beget, J.E., and Kienle, J., 1992, Cyclic formation of debris avalanches at Mount St. Augustine Volcano: Nature, v. 356, p. 701–704.

Beget, J.E., Reger, R.D., Pinney, D., Gillispie, T., and Campbell, K., 1991, Correlation of the Holocene Jarvis Creek, Tangle Lakes, Cantwell, and Hayes tephras in southcentral Alaska: Quaternary Research, v. 35, p. 74–189.

Carmichael, I.S.E., Turner, F.J., and Verhoogen, J., 1974, Igneous Petrology: New York, McGraw-Hill, 739 p.

Casadevall, T.J., ed., 1991, First International Symposium on Volcanic Ash and Aviation Safety: U. S. Geological Survey Circular 1065, 58 p.

Casadevall, T.J., Meeker, G.P., and Przedpelski, Z.J., 1991, Volcanic ash ingested by jet engines [abs.], *in* Casadevall, T.J., ed., First International Symposium on Volcanic Ash and Aviation Safety: U.S. Geological Survey Circular 1065, p. 15.

Daley, E.E., 1986, Petrology, geochemistry, and the evolution of magmas from Augustine Volcano, Alaska: Fairbanks, Alaska, University of Alaska Fairbanks, unpub. M.S. thesis, 106 p.

Griggs, R.F., 1922, The Valley of Ten Thousand Smokes: Washington, D.C., National Geographic Society, 340 p.

Hildreth, W., 1987, New perspectives on the eruption of 1912 in the Valley of Ten Thousand Smokes, Katmai National Park, Alaska: Bulletin of Volcanology, v. 47, p. 680–697.

Kienle, J., Swanson, S.E., and Pulpan, H., 1983, Magmatism and subduction in the eastern Aleutian arc, *in* Shimozuru, D., and Yokoyama, I., eds., Arc Volcanism: Physics and Tectonics: Boston, D. Reidel, p. 191–224.

Kim, J., Dunn, M.G., Baran, A.J., Wade, D.P., and Tremba, E. L., 1992, Deposition of volcanic materials in the hot sections of two gas turbine engines, *in* 1992 ASME International Gas Turbine Conference, Cologne, Germany, 1–4 June 1992, 31 p.

Lloyd, A.T., 1990, Vulcan's blast: Boeing Airliner, April–June 1990, p. 15–21.

Nye, C.J., Swanson, S.E., and Miller, T.P., in press, Geochemistry of the 1989–1990 eruption of Redoubt Volcano: Part I. Evidence from major and trace element chemistry: Journal of Volcanology and Geothermal Research.

Riehle, J.R., 1985, A reconnaissance of the major tephra deposits in the upper Cook Inlet region, Alaska: Journal of Volcanology and Geothermal Research, v. 26, p 37–74.

Schairer, J.F., 1950, The alkali feldspar join in the system $NaAlSiO_4$–$KAlSiO_4$–$SiO_2$: Journal of Geology, v. 58, p. 512–517.

Steenblik, J.W., 1990, Volcanic ash, a rain of terra: Air Line Pilot, June/July p. 9–15, 56.

Swanson, S.E., and Kienle, J., 1986, The 1986 eruption of Mt. St. Augustine, field test of a hazard model: Journal of Geophysical Research, v. 93, p. 4500–4520.

Swanson, S.E., Nye, C.J., Miller, T.P., and Avery, V.F., in press, Geochemistry of the 1989–1990 eruption of Redoubt Volcano: Part II. Evidence from mineral and glass chemistry: Journal of Volcanology and Geothermal Research.

Westgate, J.A., 1990, White River ash, *in* Wood C.A., and Kienle, J., eds., Volcanoes of North America: New York, Cambridge University Press, p. 92.

VOLCANIC ASH AND AVIATION SAFETY:
Proceedings of the First International Symposium
on Volcanic Ash and Aviation Safety
U.S. GEOLOGICAL SURVEY BULLETIN 2047

# ASH-FALL DEPOSITS FROM LARGE-SCALE PHREATOMAGMATIC VOLCANISM: LIMITATIONS OF AVAILABLE ERUPTION-COLUMN MODELS

*By* Colin J.N. Wilson

## ABSTRACT

Existing models for volcanic eruption plumes are successful in predicting sizes and growth rates, and the dispersal characteristics of the resulting fall deposits given an estimate of the magma-output rate. These models work well for "dry" eruptions, where the gases involved were originally dissolved in magma. The models predict that, in "wet" activity where abundant external water mixes with the magma during eruption and flashes to steam, the eruption plume should be lower and the resulting fall deposits less widely dispersed for a given magma-output rate. However, parts of the fall deposits from the very large, wet, 22,500-year-old Oruanui eruption (New Zealand) show the opposite behavior and represent the most powerfully dispersed fall deposits yet documented. These data imply that available eruption-column models, developed for dry eruptions, break down at some stage in wet eruptions, but the relative proportions of magma to water and the magma volumes and output rates at which this breakdown occurs are unknown. Thus, predictions of the sizes and growth rates of large, wet eruption plumes and evaluation of the threats they pose to aviation are not possible at present.

## INTRODUCTION

Several theoretical models are now available for understanding the dynamics of volcanic eruption columns. They are valuable tools for quantifying the sizes, growth rates of, and particle concentrations in observed and prehistoric ash plumes, given simple field data or estimates of starting conditions. As such, these models have great potential for real-time monitoring of eruption plumes and evaluating the risks posed to aircraft (Macedonio and others, this volume).

To date, these models have been developed from and mostly applied to observed and prehistoric volcanic eruptions that were essentially dry; that is, the only gases involved were those originally dissolved in the magma (typically $\leq 6$ weight percent). However, many cases are known where mixing of the hot magma with an abundant supply of external water (e.g., lakes, rivers, glacier ice, seawater, ground water) occurred during the eruption (e.g., Fisher and Schmincke, 1984; Heiken, this volume). In such phreatomagmatic or wet activity, the magma is chilled and fragmented while the water flashes to steam with accompanying explosions. No large-scale examples of this activity have been quantitatively observed, but deposits from such eruptions are common in the geological records of many volcanoes.

Large, wet eruptions present severe problems for the aviation industry. The eruptions may produce prodigious amounts of finely divided material, and the dynamics of and settling of ash from the resulting eruption plumes are poorly understood. This paper uses data from one of the largest known, prehistoric, wet eruptions, the 22,500-year-old ($^{14}C$ years) Oruanui eruption in New Zealand, to show that, at this extreme of scale, (1) such eruptions can cause extremely wide dispersal of ash, (2) available eruption-column models cannot be applied to this style of activity, and (3) other factors need to be taken into account before a model for large, wet eruption plumes can be developed and a quantitative assessment made of hazards to aviation.

## MODELS FOR ERUPTION COLUMNS

Available models (e.g., Wilson, 1976; Wilson and others, 1978; Sparks, 1986; Woods, 1988) assume that the erupted mixture of pyroclasts (magma fragments) and gas is ejected from the vent as a dense, highly turbulent jet containing a range of particle sizes from sub-micron dust to meter-scale blocks. This jet mixes with the atmosphere; heat is transferred from the hot ash particles to cold air; large, dense blocks detach from the jet; and the jet decelerates rapidly through work against gravity and friction with the atmosphere. The jet always starts out denser than the atmosphere, but, thereafter, two modes of behavior are possible and can sometimes occur simultaneously. If the jet can mix with and heat enough cold air, it can expand to become a buoyant thermal plume and form a high eruption column (e.g., Self and Walker, this volume; Sparks and others, this volume). The column will rise to the level in the atmosphere where it is

neutrally buoyant and then spread laterally to form an "umbrella cloud" (Sparks, 1986). Particles released from the column or umbrella cloud fall back to the land surface to produce pyroclastic fall deposits. On the other hand, if the eruption rate of material is too large, or the jet does not mix effectively with enough air to reduce its density, then once its upward momentum has been lost, the jet will not be buoyant and will collapse back on itself to generate a ground-hugging current of pyroclastic debris. As this current moves, it will deposit material to form pyroclastic flow (dense current) or surge (dilute current) deposits.

For buoyant thermal plumes, the final heights reached are considered to be proportional to the thermal flux; that is, the height reached by the eruption column is, in essence, proportional to the magma-eruption rate because it is the thermal energy in the pyroclasts (magma fragments) that drives the column. Models are available (e.g., Carey and Sparks, 1986; Wilson and Walker, 1987; Pyle, 1989; Bursik and others, 1992) that relate the grain-size characteristics of fall deposits to the height of their parental eruption column and the inferred thermal (i.e., magma) discharge rate. Such models are extremely valuable because they allow us to invert field data from the geological record to reconstruct the dynamics of prehistoric eruptions. These models are also potentially valuable tools for atmospheric modelers and the aviation industry to give plausible estimates of how rapidly and high an eruption column will rise, how rapidly it will expand laterally, and what the ash concentration in a plume will be given some simple information or estimates of starting conditions.

However, these models make the key assumption that all the thermal energy is present as sensible heat, the transfer of which causes the temperature of the material to change. In many volcanic eruptions, both observed (such as Surtsey—Thorarinsson and others, 1964—and Taal—Moore and others, 1966) and prehistoric, this assumption is clearly questionable because there is evidence for the interaction between magma and an abundant external supply of water around and below the vent area. In such wet eruptions, part of the sensible heat from the magma is used to heat and boil water, reducing the temperature of the erupted jet and storing energy as latent heat that is taken up or released during a phase change at constant temperature. In existing eruption-column models, a reduction in temperature is predicted to reduce the height of any buoyant thermal plume, and the resulting fall deposits should thus be less widely dispersed than those of a dry plume with the same magma-output rate. The extreme limit of wet plume behavior is a conventional water-vapor cloud system. Although the total thermal budget of conventional cloud systems may be enormous, they are unable to penetrate the tropopause, except by minor overshooting. In contrast, dry volcanic eruption plumes may penetrate the tropopause and reach heights of 30–50 km. New studies (Glaze and others, 1991) have suggested that latent heat release from condensing water in the air ingested into and carried up with the plume may boost the heights reached by small tropospheric plumes. However, the amount of latent heat thus made available is limited by the amount of water available in the atmosphere, and, in eruptions such as that considered here, this amount of latent heat will be dwarfed by the thermal effects of large-scale interaction between the plume and surface water. In this paper, I use data from parts of the fall deposit generated during the very large, wet Oruanui eruption, New Zealand (Self and Sparks, 1978; Self, 1983; Wilson, 1991) to show that models developed for dry eruption plumes break down when applied to large, wet eruptions.

## THE ORUANUI ERUPTION

The Oruanui eruption occurred 22,500 years ago ($^{14}C$ years) at Taupo Volcano in the central North Island of New Zealand. It produced (fig. 1) a widespread and voluminous ($\geq$ 500-km$^3$ bulk volume) fall deposit from a buoyant thermal plume before, during, and after pyroclastic flow activity that generated a 300-km$^3$ (bulk volume) pumiceous flow deposit (ignimbrite) (Wilson, 1991; C.J.N. Wilson, unpub. data). The ignimbrite is nowhere welded (a process in which particles in the deposit are hot enough ($\geq$ 570°C) to stick together—comparable to sintering processes in powder metallurgy), even where the ignimbrite is > 200 m thick. This evidence, together with estimates of emplacement temperatures from paleomagnetic techniques (E.A. McClelland, Cambridge University, and C.J.N. Wilson, unpub. data) and my observations of the limited amount of charring of vegetation overrun by the pyroclastic flows, imply that none of the flows were emplaced at temperatures of more than 300°–400°C. The cooling from the magma temperature of about 800°C (Dunbar and others, 1989) is inferred to have been caused by mixing of the eruption plume with water from a proto-Lake Taupo (Self and Sparks, 1978; Self, 1983). If equilibrium between the water and fragmented magma is assumed, and the whole of the eruption jet shared the maximum 300°–400°C temperature range, then at least 100–150 km$^3$ of water was evaporated during the eruption. The Oruanui fall deposit is generally fine grained and contains evidence that much of it was flushed out of the atmosphere by water as mud, rain, or hail. Both the fall deposits and ignimbrite indicate that the wet Oruanui eruption column was distinctly cooler (because of magma-water interaction) than the typical dry eruption columns that have been modeled and, hence, should have been lower and, by implication, weaker.

### ORUANUI FALL DEPOSIT: BEDS A AND B

The Oruanui fall deposit contains several layers or beds that are distinctive and can be correlated for distances of tens to hundreds of kilometers. Two of them, informally labeled beds A and B (fig. 2), are particularly widespread and are

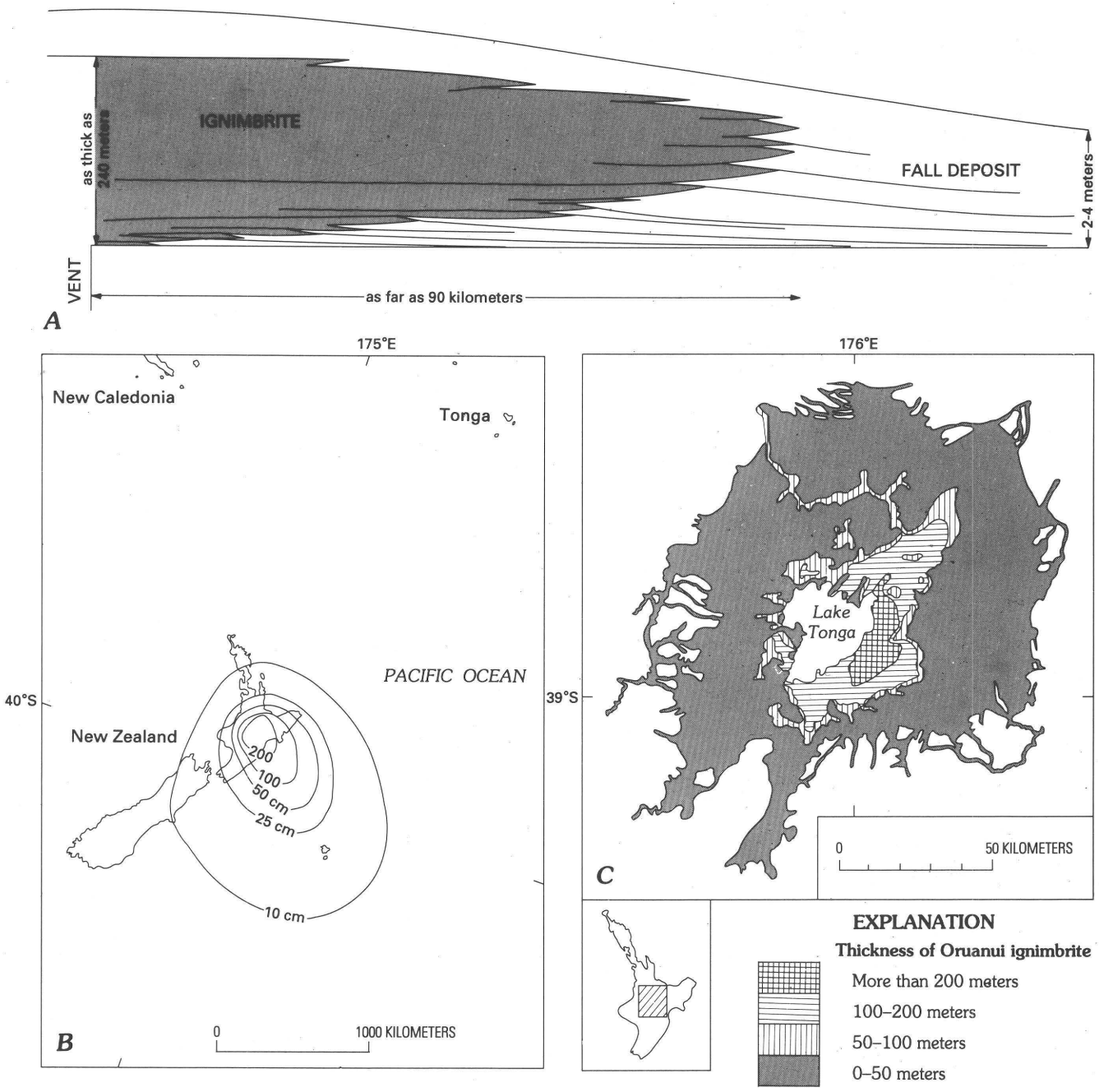


**Figure 1.** *A*, Schematic diagram showing the stratigraphic relationships of the fall deposit and ignimbrite generated during the Oruanui eruption. *B*, Map of isopachs (contours of thickness) of the Oruanui fall deposit. The thickness values represent those inferred to have been present immediately after the eruption; most of the deposit has since been removed by erosion. The source vent is now concealed beneath Lake Taupo, which infills the collapse caldera left behind after this eruption. *C*, Map showing the area covered by and thicknesses of the Oruanui ignimbrite.

considered here. Although most of the Oruanui fall deposits were clearly emplaced as wet, poorly sorted material flushed out of the plume by rain and (or) hail and are thus typical of the wet eruptive style, parts of beds A and B are moderately to well sorted, lack evidence for wet deposition, and more resemble typical dry-eruption fall deposits. However, observations on, and inferred emplacement temperatures for, ignimbrite coeval with beds A and B show that the plume was cool and water rich during emplacement of these beds. Maps (fig. 3) show the contours of thickness (isopachs) for the two beds and the variations in length of the five largest pumice fragments found in each bed (isopleths). Integration of the thickness data using the method of Pyle (1989) yields bulk-volume estimates of 8 $km^3$ for bed A and 14 $km^3$ for bed B.

## ERUPTION-COLUMN MODELS AND ORUANUI BEDS A AND B

Eruption-column models use the changes in thickness and grain size of fall deposits away from the vent as a measure of the power of the eruption and wind regime. Two models are used here, both of which use the eruption-column model of Sparks (1986) to produce theoretical relationships between dispersal patterns of pyroclasts and eruption-column height. The model of Pyle (1989) uses the overall dispersal characteristics of the deposit to infer the eruption-column height and classify the deposit. This model neglects the effects of wind but leads to reasonable estimates of column height for observed and prehistoric eruptions, even when strong winds were present. The model of Carey and Sparks (1986) uses the dispersal patterns of coarse pumice or dense, rock clasts to estimate eruption-column heights and wind speeds. In addition, the Oruanui beds are compared with the widely used eruption classification for fall deposits originally developed by Walker (1973).

In the Pyle (1989) model (fig. 4), both beds A and B plot well beyond the inferred extreme for normal, dry, fall deposits, and column-height estimates cannot be made. The rates of thinning of beds A and B are extremely low but so also are the rates at which they become finer, and their overall $b_c/b_t$ ratios (see fig. 4 for definition of parameters) are thus similar to typical dry-eruption fall deposits. Using the Carey and Sparks (1986) model (fig. 5), the Oruanui beds give high but superficially plausible values for column height and wind strength, although the column heights are significantly different from those implied by Pyle's (1989) model. However, despite the broad resemblance of beds A and B to many dry fall deposits, these figures are not reliable because of the known low temperature of the eruption plume; Carey and Sparks (1986) specifically warn against using their model for wet eruption deposits. In Walker's (1973) classification (fig. 6), both Oruanui beds show evidence for extremely powerful eruption plumes, with A and B having dispersal indices at least an order of magnitude larger than those documented for most dry-eruption fall deposits, which have been inferred by other models to have been emplaced from plumes 30–50 km high.

## DISCUSSION AND CONCLUSIONS

It is clear that there are contradictions involved in trying to model the eruption plumes of Oruanui beds A and B. Existing theory suggests that the loss of sensible heat in the plume through magma-water interaction would have reduced the eruption-column height and, hence, the power with which the clasts were dispersed. On the other hand, beds A and B plot well beyond any documented dry-eruption fall deposits in the Pyle (1989) and Walker (1973) classifications, which use dispersive power as an ordinate (figs. 4, 6). Thus, estimates of column height and wind speed made with the Carey and Sparks (1986) model (fig. 5) are almost certainly invalid, despite the often similar appearance of beds A and B to conventional, dry, fall deposits.

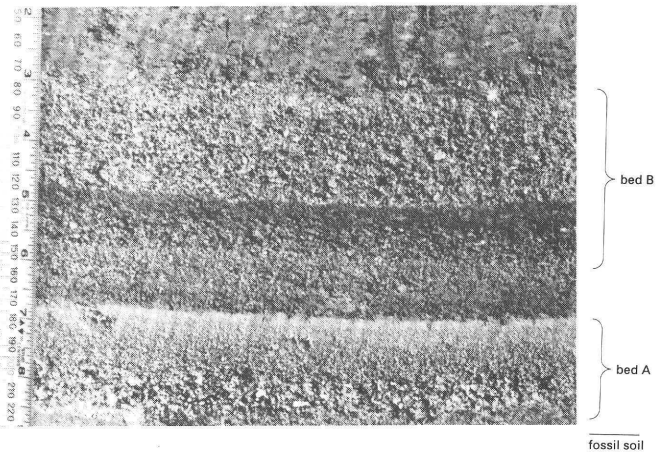


**Figure 2.** Photograph of basal parts of the Oruanui fall deposit, showing beds A and B. The darker coloration near the base of bed B is due to a higher content of fine ash material. Locality is near Taihape township (grid reference U21/710782), 90 km south of vent. Scale in inches and millimeters.

The theories behind models for dry eruption columns are soundly based. The resulting models are successful when applied to observed events (e.g., Mount St. Helens) and give plausible and realistic estimates of column parameters (height, discharge rate) for prehistoric, dry eruptions, based on measurements from fall deposits. These models have also been used to predict the thicknesses and areas covered by fall deposits from hypothetical future eruptions (e.g., Macedonio and others, 1990). However, the presence of significant magma-water interaction in an eruption makes application of these models suspect (and completely invalid at the extremes of eruptive size and violence shown by the Oruanui event).

The powerful dispersal of the Oruanui fall beds implies that if wet eruption plumes are lower in height (because of latent-heat effects), then either plume expansion rates are correspondingly more rapid or there is some as yet undiscovered mechanism (e.g., organized cellular convection) in the eruption plume that causes pyroclasts to be carried farther from the vent before deposition occurs. In either case, no model exists to predict the growth rates and nature of such an eruption cloud.

No information is yet available to show at what scale of magma-output rate and (or) amount of magma-water interaction the breakdown occurs of dry eruption-column models. In the 1,800-year-old Taupo eruption (Wilson and Walker, 1985), two wet fall deposits were generated between episodes of more voluminous dry fall activity (Walker, 1981). The two wet deposits are found in significant amounts farther upwind than the dry deposits, implying that wet eruption plumes of even moderate size (bulk volumes of the two deposits are 1.9 and 1.1 $km^3$) may start to behave in a significantly different way from dry plumes. The formulation of a model for wet eruption plumes and relating it to existing ideas about the behavior of

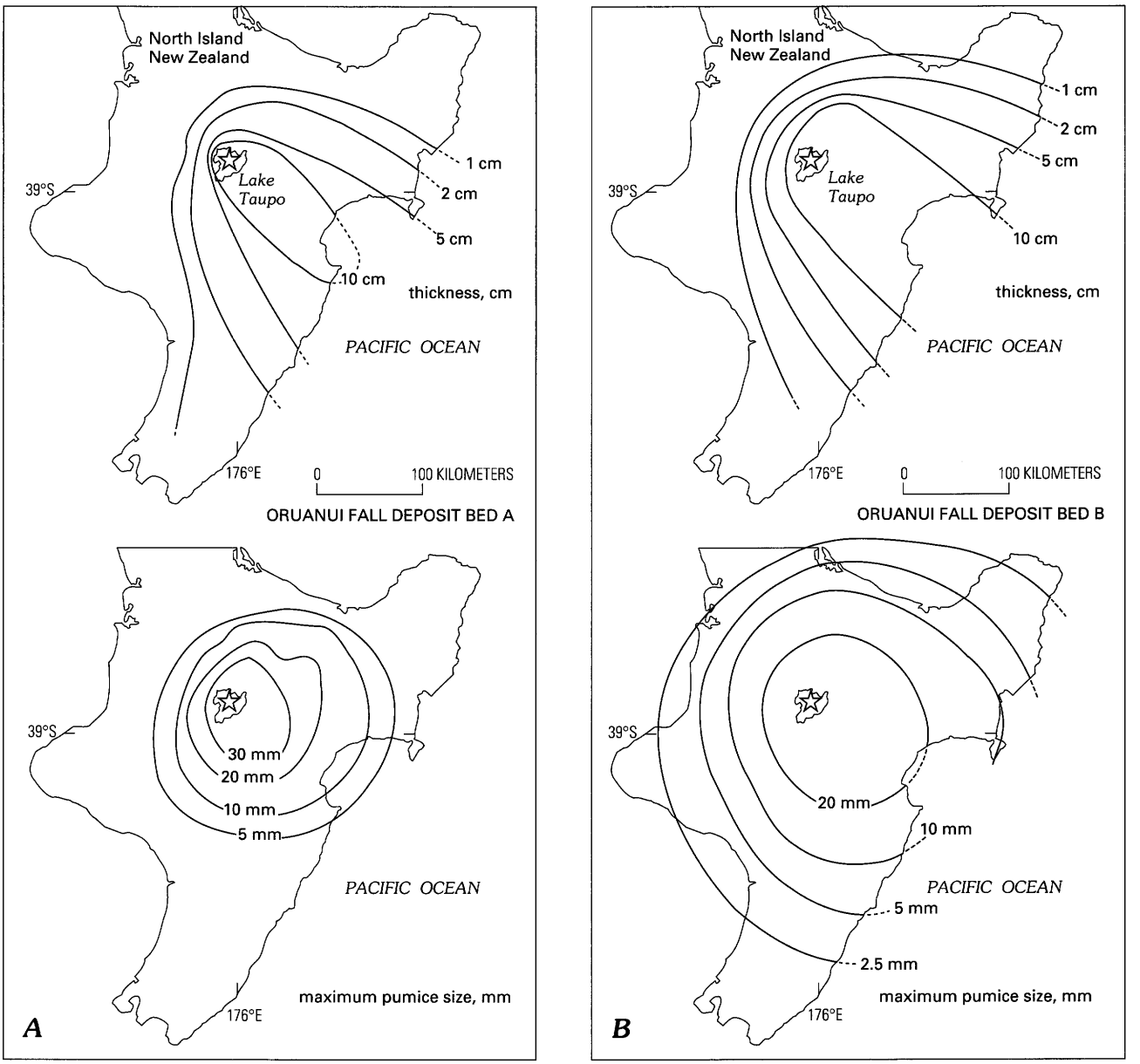


**Figure 3.** Isopach and isopleth (contours of equal grain size) maps of *A*, Oruanui fall deposit bed A and *B*, Oruanui fall deposit bed B. Maps show variations in thickness (top) and maximum pumice sizes (bottom). Maximum pumice sizes represent the average length of the five largest pumice clasts found at each locality.

dry plumes is thus an important goal, both for understanding plume dynamics as well as for predicting the nature of the hazards they pose and the rapidity with which they develop.

Four features of wet eruption plumes are particularly relevant to aviation safety: (1) Wet eruptions generate higher proportions of fine ash particles than dry eruptions, and smaller particles may thus stay aloft for longer times and persist to greater distances from the volcano than predicted by available models; (2) in large, wet eruptions such as the Oruanui, the radial expansion rate of the plume (as indicated by the extremely widespread dispersal of pyroclasts) may be significantly more rapid than predictable from dry-plume models, or the plume may incorporate organized cellular convection, which would present additional hazards to aircraft; (3) there is abundant evidence from rain- and hail-flushed beds in the Oruanui fall deposits for significant amounts of ash transport in the troposphere, and, thus, any aircraft encountering a large, wet plume may not be able to escape into ash-free air merely by diving; (4) the amounts of water inferred to be present in a large, wet plume may cause additional problems to aircraft, such as adhesion of moist to wet ash on the aircraft skin. Any schemes to identify eruption plumes and minimize the risks to aviation traffic therefore need to take account of our current lack of understanding of wet eruption plumes.

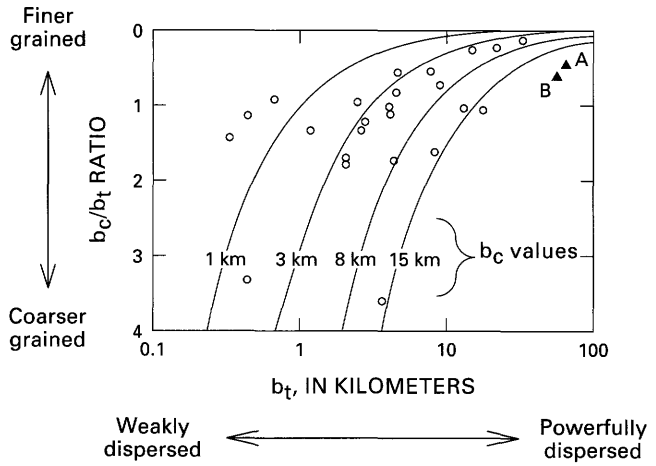


**Figure 4.** Oruanui fall beds A and B (solid triangles) plotted on the classification diagram of Pyle (1989). Parameters $b_t$ and $b_c$ are the average distances over which the deposit thickness and maximum clast sizes decrease by a factor of one-half, respectively—this is analogous to the half-life in radioactive decay. Pyle suggested that the value of $b_c$ = 15 km (corresponding to an eruption-plume height of about 55 km) represented a likely maximum for dry-eruption fall deposits. Open circles are data points from a selection of dry fall deposits.

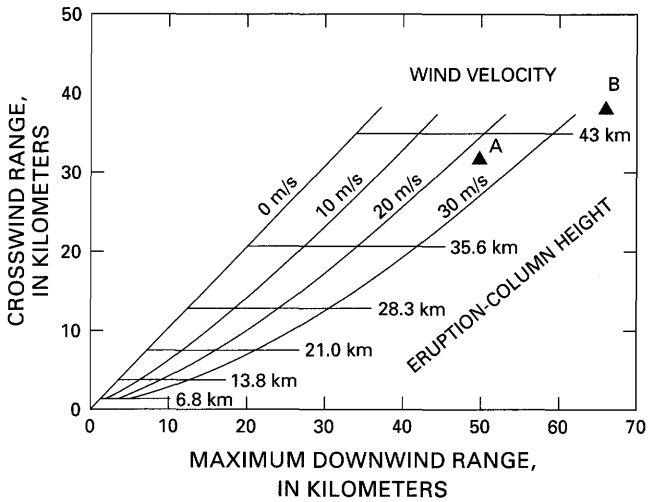


**Figure 5.** Plot of downwind range versus crosswind range of pumice clasts (approximately 40 mm in diameter) in Oruanui beds A and B (solid triangles) superimposed on the relevant model of Carey and Sparks (1986, fig. 16a). In their model, the difference between the two ranges yields a unique value of column height and average wind velocity for dry-eruption fall deposits.

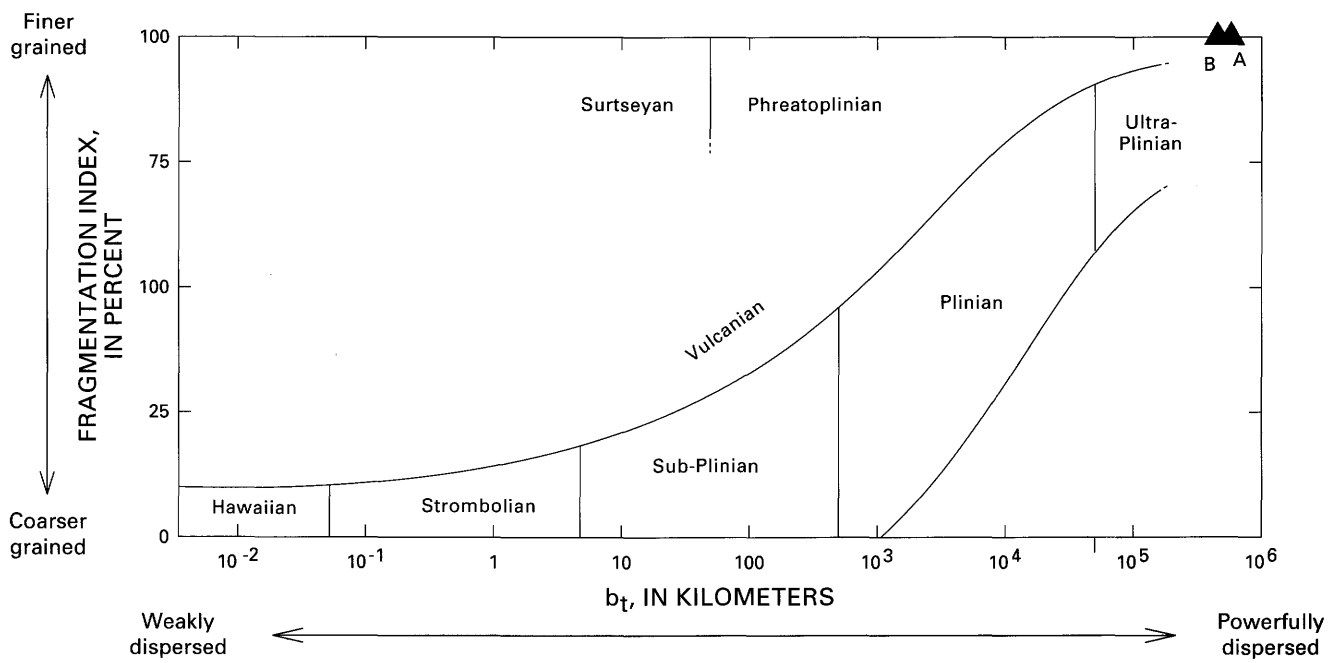


**Figure 6.** Oruanui fall beds A and B (solid triangles) plotted on the "F-D diagram" introduced by Walker (1973) and subsequently modified. This version is from Fisher and Schmincke (1984). The fragmentation index is the weight percent of the deposit finer than 1 mm along the dispersal axis where it is crossed by the 0.1 $T_{max}$ isopach ($T_{max}$ is the maximum thickness, obtained by extrapolation). The dispersal index is the area covered by 0.01 $T_{max}$ or more of material. Fields for various eruptive styles are shown. The deposits of most powerful, dry eruptions plot in the Plinian field.

## ACKNOWLEDGMENTS

This work is supported by the Royal Society of London. I thank R.S.J. Sparks for services rendered and B.F. Houghton, D.M. Pyle, and S. Self for reviews.

## REFERENCES CITED

Bursik, M.I., Sparks, R.S.J., Gilbert, J.S., and Carey, S.N., 1992, Sedimentation of tephra by volcanic plumes: 1. Theory and its comparison with a study of the Fogo A Plinian deposit, Sao Miguel (Azores): Bulletin of Volcanology, v. 54, p. 329–344.

Carey, S.N., and Sparks, R.S.J., 1986, Quantitative models of the fallout and dispersal of tephra from volcanic eruption columns: Bulletin of Volcanology, v. 48, p. 109–125.

Dunbar, N.W., Kyle, P.R., and Wilson, C.J.N., 1989, Evidence for limited zonation in silicic magma systems, Taupo Volcanic Zone, New Zealand: Geology, v. 17, p. 234–236.

Fisher, R.V., and Schmincke, H.-U., 1984, Pyroclastic Rocks: Berlin, Springer Verlag, 472 p.

Glaze, L.S., Wilson, L., and Baloga, S.M., 1991, Theoretical eruption column heights: The effects of latent heat and particle fallout [abs.]: Transactions, American Geophysical Union (Eos), Supplement, 1991 Fall Meeting Abstracts, p. 568.

Macedonio, G., Pareschi, M.T., and Santacroce, R., 1990, Renewal of explosive activity at Vesuvius: Models for the expected tephra fallout: Journal of Volcanology and Geothermal Research, v. 40, p. 327–342.

Moore, J.G., Nakamura, K., and Alcaraz, A., 1966, The 1965 eruption of Taal Volcano: Science, v. 155, p. 955–960.

Pyle, D.M., 1989, The thickness, volume and grain size of tephra fall deposits: Bulletin of Volcanology, v. 51, p. 1–15.

Self, S., 1983, Large-scale phreatomagmatic silicic volcanism, a case study from New Zealand: Journal of Volcanology and Geothermal Research, v. 17, p. 433–469.

Self, S., and Sparks, R.S.J., 1978, Characteristics of widespread pyroclastic deposits formed by the interaction of silicic magma and water: Bulletin Volcanologique, v. 41, p. 196–212.

Sparks, R.S.J., 1986, The dimensions and dynamics of volcanic eruption columns: Bulletin of Volcanology, v. 48, p. 3–15.

Thorarinsson, S., Einarsson, T., Sigvaldason, G.E., and Eliasson, G., 1964, The submarine eruption off the Vestman Islands, 1963–64: Bulletin Volcanologique, v. 27, p. 435–446.

Walker, G.P.L., 1973, Explosive volcanic eruptions: A new classification scheme: Geologische Rundschau, v. 62, p. 431–446.

———1981, Characteristics of two phreatoplinian ashes and their waterflushed origin: Journal of Volcanology and Geothermal Research, v. 9, p. 395–407.

Wilson, C.J.N., 1991, Ignimbrite morphology and the effects of erosion: A New Zealand case study: Bulletin of Volcanology, v. 53, p. 635–644.

Wilson, C.J.N., and Walker, G.P.L., 1985, The Taupo eruption, New Zealand: I. General aspects: Royal Society of London Philosophical Transactions, v. A314, p. 199–228.

Wilson, L., 1976, Explosive volcanic eruptions—III. Plinian eruption columns: Geophysical Journal of the Royal Astronomical Society, v. 45, p. 543–556.

Wilson, L., Sparks, R.S.J., Huang, T.C., and Watkins, N.D., 1978, The control of eruption column heights by eruption energetics and dynamics: Journal of Geophysical Research, v. 83, p. 1829–1836.

Wilson, L., and Walker, G.P.L., 1987, Explosive volcanic eruptions—VI. Ejecta dispersal in Plinian eruptions: The control of eruption conditions and atmospheric properties: Geophysical Journal of the Royal Astronomical Society, v. 89, p. 651–679.

Woods, A.W., 1988, The fluid dynamics and thermodynamics of eruption columns: Bulletin of Volcanology, v. 50, p. 169–193.

VOLCANIC ASH AND AVIATION SAFETY:
Proceedings of the First International Symposium
on Volcanic Ash and Aviation Safety
U.S. GEOLOGICAL SURVEY BULLETIN 2047

# THE INJECTION OF VOLCANIC ASH INTO THE ATMOSPHERE

*By* Andrew W. Woods *and* Juergen Kienle

## ABSTRACT

In this paper, we present some physical models that can describe the ascent of volcanic ash into the atmosphere during a volcanic eruption. We consider both sustained volcanic eruption columns and discrete volcanic thermal clouds. To test the modeling approach, we compare our predictions of the ascent rate of a model cloud with some observations of the ascent of the ash cloud during the April 15, 1990, eruption of Redoubt Volcano, Alaska. We also consider the radial spreading of ash as a gravity current following emplacement by the column and compare our theory with the observations from the April 21, 1990, eruption of Redoubt, Alaska. Both styles of eruption behavior are hazardous for aircraft.

## INTRODUCTION

There is a range of styles of explosive volcanic eruption that can produce large convecting ash clouds and thereby inject ash high into the atmosphere. Ash can rise high into the atmosphere if the hot, erupted material can mix with and heat up a sufficient mass of air so that the bulk density of the mixture decreases below the ambient (Self and Walker, this volume). The typical ascent time of this ash to its maximum height is on the order of a few minutes; if this time is longer than the time over which the material is erupted and becomes buoyant, then the cloud will rise as a discrete volcanic thermal cloud (Wilson and others, 1978; Woods and Kienle, in press). Such volcanic thermal clouds formed, for example, during the April 15 and 21, 1990, eruptions of the Redoubt Volcano, Alaska. Figure 1 is a photograph of the April 21 eruption cloud, which ascended about 12 km into the atmosphere. The main eruption cloud has reached its maximum height and has begun to spread laterally into the atmosphere. A relatively small, vertical column may be seen below this main cloud. This column contains material rising from the ground after the ascent of the main cloud—this material is less energetic than that in the main thermal cloud. In the photograph, a small secondary lateral intrusion has begun to develop from this column.

In a more sustained eruption, lasting several hours, material is continually erupted from the vent. In this case, a maintained eruption column, injecting ash high into the atmosphere, will form if the hot ash can entrain and heat a sufficient quantity of air so that the bulk density of the mixture falls below that of the ambient. Two different mechanisms of buoyancy generation are possible, and, during the course of an eruption, the style of eruption may change from one to the other: (1) If the erupted material is ejected upward from the vent very rapidly, the dense jet may entrain sufficient air to become buoyant before its upward momentum is exhausted; in this case, the material continues rising upward, driven by its own buoyancy thereby forming a classical Plinian eruption column (Sparks, 1986; Woods, 1988) such as the A.D. 79 eruption of Mt. Vesuvius, Italy. (2) If the erupted material is ejected from the vent with smaller momentum, that material will collapse back and spread out along the ground as an ash flow in a similar manner to the motion of water in a fountain. However, the material in the spreading ash flow may become buoyant through entrainment and mixing with air and sedimentation of large particles as it propagates along the ground. It will then rise off the ground to form a maintained eruption column, in this case called a co-ignimbrite eruption column (Sparks and Walker, 1977; Woods and Wohletz, 1991). Historical examples of eruptions, which include phases in which co-ignimbrite eruption columns developed, include the massive 1815 eruption of Tambora, Indonesia, and the 1912 eruption of Katmai, Alaska. Co-ignimbrite eruption columns tend to form during massive eruptions (Woods and Wohletz, 1991).

Both discrete and maintained eruption clouds can inject vast quantities of ash into the atmosphere—they thereby pose a serious safety problem for aircraft. However, sustained eruption columns are perhaps more hazardous for aircraft because they may persist for hours and can therefore inject very large quantities of ash, which spreads over a very wide area in the atmosphere. In order to evaluate the dangers of an eruption for aircraft, it is important to know the extent of the region in which the mass loading of ash in the air is at hazardous concentrations. When ash has been carried upward to its maximum height by the eruption column, it

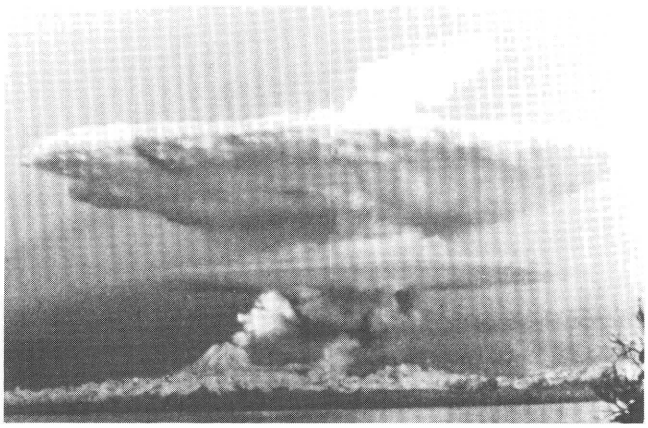

**Figure 1.** Photograph of the volcanic eruption cloud formed during the April 21, 1990, eruption of Redoubt Volcano, Alaska, seen from the Kenai Peninsula, east of the volcano. The main cloud ascended about 12 km, and the secondary intrusion ascended to an altitude of about 6 km. Photograph by Mark and Audrey Hodges.

spreads out laterally under gravity above its neutral buoyancy height and is carried by the wind to form a large, laterally spreading ash plume (fig. 2). The maximum ash concentration in this ash plume occurs at the top of the eruption column (before it is diluted through mixing with the ambient as it travels downwind).

In the following section, we describe the Plinian eruption-column model of Woods (1988) and the model of a volcanic thermal cloud of Woods and Kienle (in press). In order to test the modeling approach, we compare the predicted rate of ascent of a volcanic thermal, using the model of Woods and Kienle (in press), with the observed ascent of the thermal cloud during the April 15, 1990, eruption of the Redoubt Volcano, Alaska. We also investigate the radial spreading of the ash as a gravity current after it is emplaced into the atmosphere by the eruption; we compare a simple model with observations of the spreading umbrella cloud following the April 21, 1990, eruption of Redoubt Volcano. Details of the mass loading in eruption columns and the downwind dispersal of ash are given in other articles in this volume (Sparks and others, this volume; Bursik and others, this volume; Self and Walker, this volume).

## MODELING THE DYNAMICS OF ERUPTION CLOUDS

Although the initial momentum of the material erupted from the vent accounts for the first few kilometers of the ascent, it is the generation of buoyancy that enables the material to ascend tens of kilometers (Woods, 1988). This buoyancy is generated through the entrainment of vast quantities of ambient air, which is heated and expands, ultimately lowering the density of the column below that of the surrounding air. Once buoyant, the material rises through the atmosphere until reaching the height at which its density equals the ambient again, called the neutral buoyancy height. At this point, the inertia of the material causes the material to continue rising some distance until the material comes to rest. It then collapses downward toward the neutral buoyancy height and spreads out laterally. In this overshoot region, the density of the cloud exceeds that of the surroundings, and the cloud may actually become tens of degrees colder than the environment (Woods and Self, 1992). This undercooling of the eruption cloud causes difficulties in the interpretation of thermal satellite images of the top of eruption columns; in particular, it is very difficult to estimate the height of the cloud top using the observed cloud-top temperature and radiosonde measurements of the environmental temperature as a function of altitude (Woods and Self, 1992).

In the past 10–15 years, a number of models have been developed to describe the motion of maintained volcanic eruption columns. These are summarized and reviewed in the paper by Woods (1988), in which a dynamically consistent model is presented. This steady-state model is based upon the conservation of mass, momentum, and enthalpy, assuming that the column entrains ambient air at a rate proportional to the vertical velocity of the column at any height, following Morton and others (1956). The model incorporates a number of simplifications, which are good approximations in many explosive volcanic eruptions. These include the assumptions that (1) the material in the eruption column behaves as a single-phase, perfect gas, (2) there is little interphase mass or momentum transfer, (3) the system is in thermodynamic equilibrium, and (4) all of the solid material is fine-grained ash and therefore ascends to the top of the column.

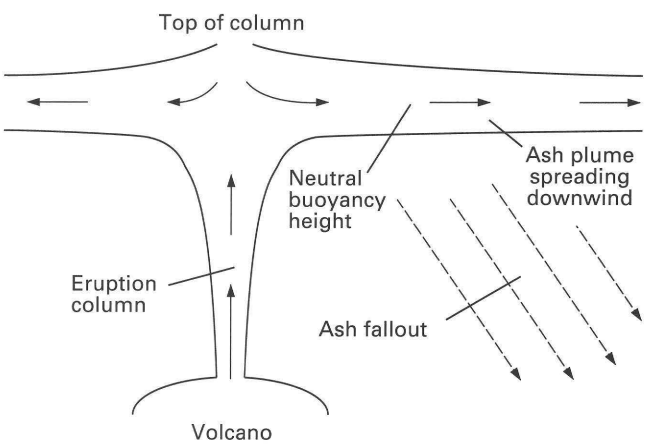


**Figure 2.** Schematic diagram of eruption column, spreading umbrella cloud, and downwind ash plume. Figure shows location of neutral buoyancy height.

In figure 3, we present a graph, calculated using this model, showing how the total height of rise of the column and the neutral buoyancy height of the column vary with the mass eruption rate for three different initial temperatures. In this graph, it may be seen that the rate of increase of column height decreases once it passes through the tropopause. This is because the temperature begins to increase with height in the stratosphere, causing the atmosphere to become much more stratified. It may also be seen that, because hotter columns generate more buoyancy, they tend to rise higher. Further details of the model are described in Woods (1988).

Woods and Bursik (1991) have extended this model to include the effects of fallout of the larger solid clasts below the top of the column. They showed that, if many of the clasts do fall out (as occurs in eruptions of larger mean grain size), then the eruption column becomes progressively smaller. This is because more of the thermal energy is removed by these solids, and, ultimately, the material in the column has insufficient thermal energy to become buoyant and a collapsed fountain forms. Woods and Wohletz (1991) have shown that the ascent of a co-ignimbrite eruption column rising off a hot ash flow (Sparks and Walker, 1977) may also be described using this model. In this case, the material being supplied to the column originates from a large area; initially it has little upward momentum and is only just buoyant relative to the surrounding ambient atmosphere. However, after entraining more air, the material rapidly expands and becomes buoyant and, as a consequence, accelerates upward. Woods and Wohletz (1991) calculated that the ascent height of these co-ignimbrite columns was much less than that of Plinian columns because, typically, only about one-third of the erupted ash and solid material is elutriated from the ash flow into the rising cloud. This reduces the source of thermal energy, which results in ascent of the cloud.

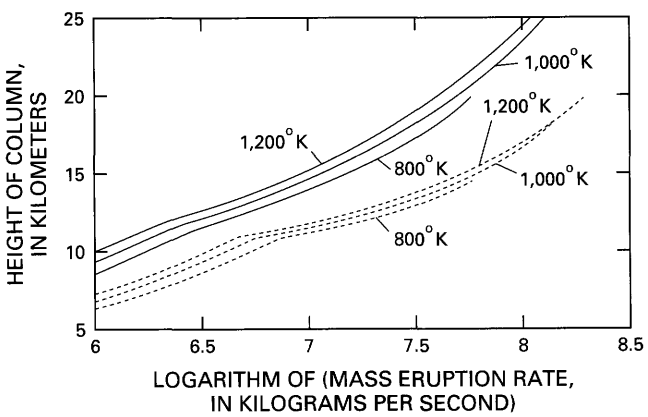


**Figure 3.** Calculations of neutral buoyancy height (dashed lines) and total column height (solid lines) as a function of erupted mass flux. Curves are given for three eruption temperatures (800°K, 1,000°K, 1,200°K). Calculations are based on the model of Woods (1988) using the standard atmosphere model described therein for which the tropopause is located at 11 km.

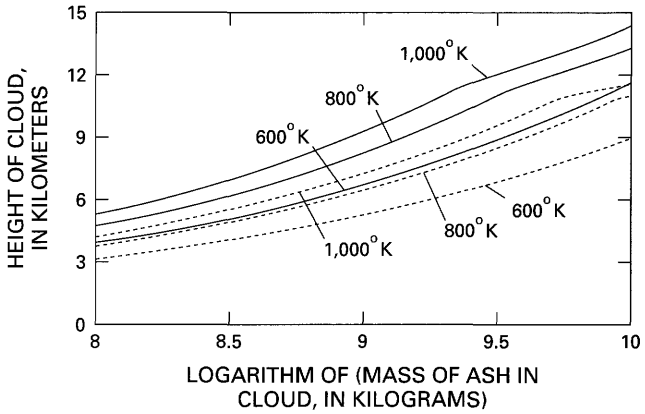


**Figure 4.** Calculations of neutral buoyancy height (dashed lines) and total cloud height (solid lines) as a function of erupted mass. Curves are given for three eruption temperatures (600°K, 800°K, 1,000°K). Calculations are based on the model of Woods and Kienle (in press) using the standard atmosphere as described in figure 3.

Using a similar approach, Woods and Kienle (in press) have presented a model of the ascent of discrete volcanic clouds. In this model, the discrete cloud is assumed to ascend as a sphere that entrains ambient air and therefore increases in radius as it ascends. The model calculates the altitude and radius of the cloud as well as the average density, temperature, and velocity in the cloud as functions of time. An important difference between the motion of a maintained, steady eruption column and a discrete volcanic thermal cloud is that, as a volcanic thermal rises, there is an additional drag exerted upon the cloud as a result of the air that must be displaced by the rising cloud. This is usually referred to as the virtual mass (Batchelor, 1967) and is incorporated in the model of Woods and Kienle (in press).

In figure 4, we present calculations using this model of the ascent height and neutral buoyancy height of a volcanic thermal cloud, such as that developed following the eruption Redoubt Volcano (fig. 1). We present calculations for three different initial temperatures as a function of the initial mass of the thermal cloud. The results are qualitatively similar to those in figure 3, which describe maintained eruption columns.

## TESTING ERUPTION-CLOUD MODELS

Relatively few detailed observations of volcanic eruptions, recording the ascent height of the cloud as a function of time or the velocity in a maintained eruption column as a

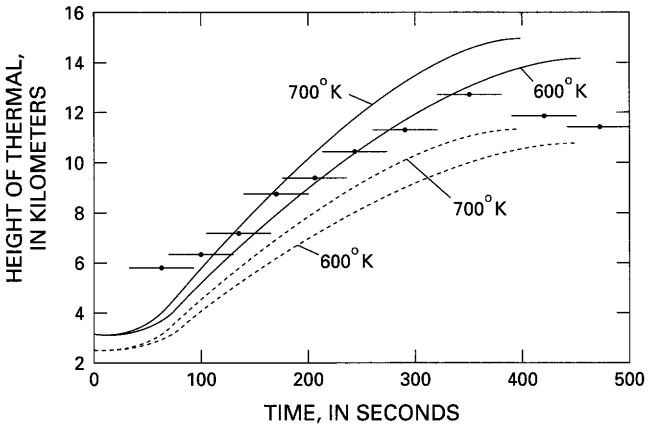


**Figure 5.** Comparison of observed ascent of the April 15, 1990, Redoubt eruption cloud with the model predictions of the total cloud height (solid lines) and the height of the center of the cloud (dashed lines). Calculations are shown for two initial, model cloud temperatures (600°K and 700°K), which represent bounds on the initial temperature of the cloud (Woods and Kienle, in press). The data were collected by analysis of video recordings of the cloud ascent. Horizontal lines through data points represent error bars.

function of height, have been published; such observations are necessary to test the accuracy of the modeling approach. Sparks and Wilson (1982) tracked several plume fronts rising from the crater of Soufriere St. Vincent and compared this with a model of a starting plume, and Sparks (1986) reported some satellite observations of the ascent of the lateral blast cloud of Mount St. Helens, May 18, 1980, and compared these with the theory of Morton and others (1956). More recently, Woods and Kienle (in press) have reported on some slow-scan video-camera recordings of the rise of the April 15, 1990, eruption cloud of Redoubt Volcano and compared this with a new model of a volcanic thermal.

During the April 15, 1990, eruption of Redoubt Volcano, a hot ash flow was produced from the explosion of a volcanic dome. This ash flow traveled along the ground for 3–4 km, following a natural ice canyon carved in a glacier. As the flow entrained and heated ambient air, the upper part of the flow became buoyant and rose into the atmosphere, forming a large, convecting volcanic thermal cloud. In figure 5, we present a graph showing the observed height of the cloud as a function of time as deduced from the slow-scan video recording. Post-eruption studies of the far-field air-fall (Scott and McGimsey, in press) and near-field flow deposits (C.A. Neal, oral commun., 1991) give estimates for the total mass of material erupted from the volcano during this eruption as approximately $2.5 \times 10^9$ kg. Using this data and the conservation of enthalpy in the flow (Sparks, 1986), we estimate that the temperature of the elutriated cloud was 600°K–700°K, assuming that it was just buoyant on ascent. This data provides the initial conditions for our model of the ascent of the thermal cloud and, in figure 5, we also present model ascent curves for clouds rising off the flow with temperatures of 600°K and 700°K. In these calculations, we have used meteorological radiosonde data from three stations near Redoubt Volcano taken at about the time of the eruption. It may be seen that the model is able to reproduce most of the features of the buoyant ascent very satisfactorily, especially the time scale of the ascent and the height of rise of the cloud. This gives us confidence in the accuracy, at least in terms of the order of magnitude, of the predictions of these models. Further details of this comparison and the field data are given in Woods and Kienle (in press).

In addition to field observations, some recent controlled laboratory experiments have been able to test aspects of these models (Woods and Caulfield, 1992). There are mixtures of methanol and ethylene glycol (MEG) with density less than that of water that, upon mixing with water, become more dense than water. Therefore, with sufficient initial momentum, a downward-propagating, but light, jet of MEG can entrain and mix with ambient water to become dense and thereby continue propagating downward (in an analogous fashion to a Plinian eruption column) (Woods and Caulfield, 1992). However, a relatively light jet of MEG, with sufficient initial downward momentum, comes to rest before it can mix with sufficient water to become dense; in this case, a collapsed fountain forms and the MEG mixture rises back up around the source. Woods and Caulfield (1992) developed a simple theoretical model of their laboratory experiments based on the same conservation laws as used in the eruption-column model of Woods (1988). The conditions under which experimental column collapse occurs were successfully compared with the model predictions; this further confirms the validity of the underlying physics in the models.

## SPREADING UMBRELLA CLOUDS

We now describe the initial spreading of the umbrella cloud once it is emplaced into the atmosphere by the eruption column—the subsequent dispersal and fallout of ash has been described by Bursik and others (1992; this volume). Following injection into the atmosphere by the eruption column, the first stage of ash dispersal consists of the radial gravitational spreading of the cloud toward its neutral buoyancy height. This is the dominant mechanism causing lateral spreading of the ash cloud during the first few minutes after the ash is injected into the atmosphere. However, when the rate of spreading decreases below typical velocities associated with the ambient wind field and ambient turbulence, this gravitational spreading may become of secondary importance in comparison to the wind as an ash-dispersal mechanism. During the May 18, 1980, eruption of Mount St. Helens, the ash plume spread out under gravity from a radius of about 20 km to nearly 50 km in about 10 minutes (Sparks, 1986, fig. 5), whereas the April 21, 1990,

eruption cloud at Redoubt Volcano spread out from a radius of about 6 km to over 15 km in about 10 minutes under gravity before being carried downwind. Woods and Kienle (in press) have described a simple model of the gravitational spreading of an ash cloud following Simpson (1987). In the model, the radial inertia of the cloud balances the gravitational force, which results from the vertical displacement of the air by the cloud. Woods and Kienle (in press) predict that an instantaneously emplaced cloud spreads radially at a rate proportional to $(\text{time})^{1/3}$, and an umbrella cloud continually supplied from below spreads at a rate proportional to $(\text{time})^{2/3}$ until the dispersal becomes dominated by wind. As can be seen in figure 6, this model compares favorably with direct observations from the spreading of the April 21, 1990, eruption cloud of Redoubt Volcano, which was emplaced nearly instantaneously.

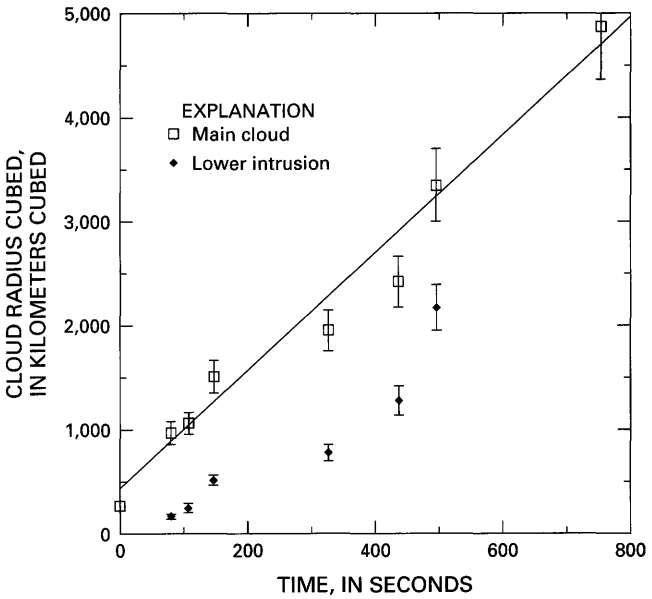


**Figure 6.** Comparison of observed spread of umbrella cloud that formed following the April 21, 1990, eruption of Redoubt Volcano and a simple model of a radially spreading gravity current, after Woods and Kienle (in press). The graph shows the rate of spread of the main cloud as well as the lower secondary intrusion, which can be seen in figure 1. The data were obtained from analysis of photographs by Mark and Audrey Hodges. Vertical lines through data points indicate error bars.

## CONCLUSIONS

We have described models of both instantaneous and maintained eruption columns. These models are based upon the conservation of mass, momentum, and enthalpy. We have compared our model of a thermal cloud with the observations of the Redoubt Volcano eruption of April 1990. We have also discussed simple models of the radial spreading of the umbrella cloud and have shown that the simple model compares favorably with observations from the April 21, 1990, eruption of Redoubt Volcano. The models have shown that even relatively small eruption clouds can ascend up to tens of kilometers into the atmosphere, causing a serious hazard for aircraft, which typically fly in the troposphere below about 11 km. Once the ash cloud has reached its neutral buoyancy height, the ash may then spread several hundred or even thousands of kilometers before settling from the atmosphere. A particularly important result of the modeling is that the upper surface of an eruption column may actually become tens of degrees colder than the surrounding environment, owing to the inertial overshoot of the erupted mixture above the neutral buoyancy height. This can lead to difficulties in interpreting the height of eruption clouds from thermal satellite images (Woods and Self, 1992). In a companion paper in this volume (Sparks and others, this volume), the models described herein have been used to calculate the ash loading at the top of eruption columns.

## REFERENCES CITED

Armienti, P., Macedonio, G., and Pareschi, M.T., 1988, A numerical model for simulation of tephra transport and deposition: Applications to May 18, 1980 Mount St. Helens eruption: Journal of Geophysical Research, v. 93, p. 6463–6476.

Batchelor, G.K., 1967, An Introduction to Fluid Dynamics: Cambridge, Cambridge University Press, 615 p.

Bursik, M.I., Sparks, R.S.J., Gilbert, J., and Carey, S., 1992, Dispersal of tephra by volcanic plumes: A study of the Fogo A eruption, Sao Miguel (Azores): Bulletin of Volcanology, v. 54, p. 329–344.

Morton, B., Taylor, G. I., and Turner, J. S., 1956, Turbulent gravitational convection from maintained and instantaneous source: Proceedings of the Royal Society, Series A, v. 234, p. 1–23.

Scott, W.E., and McGimsey, R.G., in press, Character, mass, distribution, and origin of tephra-fall deposits of the 1989–1990 eruption of Redoubt Volcano, Alaska: Journal of Volcanology and Geothermal Research.

Simpson, J., 1987, Gravity Currents in the Environment and the Laboratory: Chichester, Ellis Horwood, 244 p.

Sparks, R.S.J., 1986, The dimensions and dynamics of volcanic eruption columns: Bulletin of Volcanology, v. 48, p. 1–16.

Sparks, R.S.J., and Walker, G.P.L., 1977, The significance of vitric-rich airfall deposits: Journal of Volcanology and Geothermal Research, v. 2, p. 329–341.

Sparks, R.S.J., and Wilson, L., 1982, Explosive volcanic eruptions,V—Observations of plume dynamics during the 1979 Soufriere eruption, St. Vincent: Geophysical Journal of the Royal Astronomical Society, v. 69, p. 551–570.

Wilson, L., Sparks, R.S.J., Huang, T.C., and Watkins, N.D., 1978, The control of eruption column heights by eruption energetics and dynamics: Journal of Geophysical Research, v. 83, p. 1829–1836.

Woods, A.W., 1988, The fluid dynamics and thermodynamics of eruption columns: Bulletin of Volcanology, v. 50, p. 169–191.

Woods, A.W., and Bursik, M.I., 1991, Particle fallout, thermal disequilibrium and volcanic plumes: Bulletin of Volcanology, v. 53, p. 559–570.

Woods, A.W., and Caulfield, C.P., 1992, An experimental investigation of explosive volcanic eruptions: Journal of Geophysical Research, v. 97, p. 6699–6712.

Woods, A.W., and Kienle, J., in press, The dynamics and thermodynamics of volcanic clouds: Theory and observations from the April 15 and April 21, 1990 eruptions of Redoubt Volcano, Alaska: Journal of Volcanology and Geothermal Research.

Woods, A.W., and Self, S., 1992, Thermal disequilibrium at the top of volcanic clouds and its effect on estimates of the column height: Nature, v. 355, p. 628–630.

Woods, A.W., and Wohletz, K., 1991, The dimensions and dynamics of coignimbrite eruption columns: Nature, v. 350, p. 225–227.

VOLCANIC ASH AND AVIATION SAFETY:
Proceedings of the First International Symposium
on Volcanic Ash and Aviation Safety
U.S. GEOLOGICAL SURVEY BULLETIN 2047

# INFLUENCE OF VOLCANIC ASH CLOUDS ON GAS TURBINE ENGINES

*By* Michael G. Dunn *and* Douglas P. Wade

## ABSTRACT

Results are reported for a technology program designed to determine the behavior of gas turbine engines when operating in volcanic ash clouds. The response of several different engines, among them the Pratt and Whitney JT3D turbofan and the Pratt and Whitney J57 turbojet, has been determined.

The damage that an engine will experience depends upon the particular engine, the thrust setting at which the engine is operating when it encounters the dust cloud, the constituents of the cloud, and the respective melting temperatures of the various constituents. In addition, the rate at which events will occur depends upon the particle density (or concentration) of the ash cloud.

An important part of the research effort at Calspan Advanced Technology Center has been to identify which engine parameters available to the flight crew can provide an early warning of impending engine problems. Having determined that one is operating in a potentially dangerous environment, it is then important to determine how to safely operate a damaged engine.

## INTRODUCTION

The reality of the danger of the volcanic eruption clouds to commercial aircraft operation has been dramatically illustrated since 1980. During the past several years, the airframe and engine companies have become involved in trying to understand the nature of the problems associated with aircraft interactions with volcanic ash clouds. Campbell (1991) described four 747 aircraft encounters with volcanic ash clouds, beginning with the June 1982 encounter of a British Airways 747-200 aircraft over West Java, Indonesia, and concluding with the December 1989 encounter between a 747-400 aircraft with the Redoubt Volcano ash cloud near Anchorage, Alaska. The Boeing 747 is not the only aircraft that has experienced difficulty when operating in volcanic ash clouds (Campbell, 1991). The adverse influence of volcanic ash has been observed to occur in most modern power plants, such as the Rolls Royce RB211, the Pratt and Whitney JT9D, and the General Electric CF6. Measurement programs designed to ascertain the response of gas turbine engines when operated in dust-laden environments are needed to recommend operational procedures under those conditions. The dust of interest here is volcanic ash composed of rock and mineral particles that become airborne as a result of an explosive volcanic eruption.

Gas turbine engines are routinely tested for the effect of ingestion of solid particles according to the procedures of Military Specification MIL-E-5007D, commonly known as the "Arizona road-dust test." During the last several years the material used in this test was changed from a mixed silicate mineralogy to crushed quartz. Encounters with volcanic ash clouds are much different than those experienced with MIL-E-5007D. Specifically, these differences involve the chemical and mineralogical composition, particle-size distribution, and particle concentration in the cloud.

A research program in the area of gas turbine propulsion, ongoing at Calspan Advanced Technology Center in Buffalo, N.Y., utilizes a unique facility and experimental technique that exposes operating gas turbine engines to an adverse environment similar to that associated with a volcanic ash cloud without endangering either an airplane or a flight crew. The response of several different engines, including the Pratt and Whitney JT3D turbofan and the Pratt and Whitney J57 turbojet, to typical volcanic ash clouds has been investigated.

The behavior of individual components that make up a volcanic ash cloud are studied separately using an Allison T56 combustor canister, a row of T56 high-pressure-turbine inlet nozzle guide vanes (NGV's), a dust-injection system, and an external air compression source. Data obtained using this device provide guidance to the researcher prior to full-scale engine measurements. A reasonable estimate of the behavior of a particular ash and the threshold temperature at which some components of the material in this ash might melt and deposit on the NGV's can be determined with this test system.

The damage modes that an engine will experience depend upon the particular engine, the thrust setting at which the engine is operating when the dust cloud is encountered, the constituents of the cloud, and the respective melting

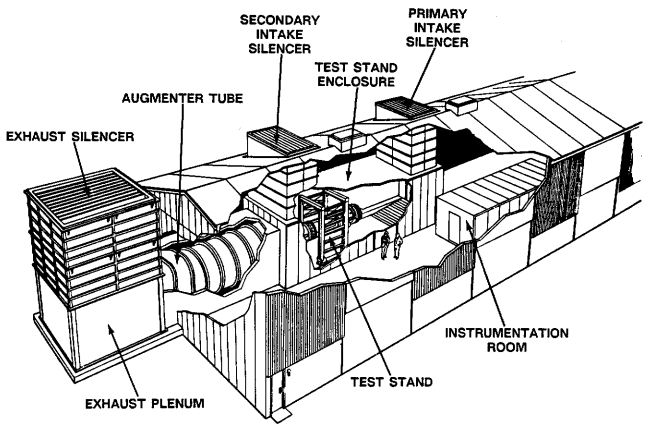


**Figure 1.** Large-engine research cell includes the engine test stand, operating equipment, and instrumentation. Major features of the experimental apparatus are a noise-suppression system and a dust-injection system. The noise-suppression system used for these measurements is an air-cooled unit consisting of a primary intake silencer, a secondary intake silencer, an engine test stand enclosure, and a silencer system made up of an augmenter tube, an exhaust plenum, and an exhaust silencer.

temperature of the cloud constituents. In addition, the rate at which events will occur depends upon the particle density (or concentration) of the cloud.

Several different mechanisms may be responsible for altering engine performance during or after exposure to a volcanic ash cloud, and the potential of each mechanism should be recognized. The volcanic-ash-cloud encounter may be manifested in one or more of the following ways: (a) deposition of material on hot-section components, (b) erosion of compressor blades and rotor-path components, (c) partial or complete blocking of fuel nozzles, (d) partial or total blockage of cooling passages, (e) oil system or bleed air supply contamination, (f) fogging of the windscreen and landing lights, (g) contamination of the electronics because of dust ingested through the environmental control system (ECS), (h) erosion of antenna surfaces, and (i) plugging of the pitot-static system. Most of these phenomena have been experienced in the ash cloud encounters reported by Smith (1983) and Chambers (1985). Compressor erosion causes a loss of surge margin even if deposition does not occur (Tabakoff and Hussein, 1971a, 1971b; Hussein and Tabakoff, 1973; Grant and Tabakoff, 1975; and Tabakoff and Bahan, 1981).

The work described in this paper shows how the ash cloud could be recognized if natural light or cloud conditions preclude direct visual observation, the type of engine damage expected from ash-cloud encounters, which of the engine diagnostics provide an indication of engine degradation, and how one manipulates the controls to generate significant thrust after engines have been severely damaged. Early results of this research were reported by Dunn and others (1987a, 1987b) and Batcho and others (1987).

# EXPERIMENTAL APPARATUS

This type of research requires a unique facility that allows detailed measurements of propulsion-system tolerance for a full-scale engine under controlled laboratory conditions. The large-engine research facility at Calspan is located within a large building, thus permitting tests unhampered by weather. The test setup includes the engine test stand, operating equipment, and instrumentation (fig. 1).

Two major features of the experimental apparatus are a noise-suppression system and a dust-injection system. The noise-suppression system used for these measurements is an air-cooled unit consisting of a primary intake silencer, a secondary intake silencer, an engine test stand enclosure, and an exhaust-silencer system made up of an augmenter tube, an exhaust plenum, and an exhaust silencer (fig. 1).

The dust-injection system (DIS) is an important part of the test apparatus and was designed to accurately regulate the dust environment. The dust-injection system must provide a controlled range of particle sizes and concentrations, all evenly dispersed in the incoming air. The DIS, shown schematically in figure 2, consists of a dust tube, dust-injection nozzles, weigh-belt feeder and dust reservoir, and a bellmouth. The weigh-belt feeder includes process-monitoring instrumentation to allow precise control of dust being fed to the test engine. The dust is delivered to the injection nozzles by compressed air. A more detailed description of the experimental apparatus is given in Dunn and others (1987b).

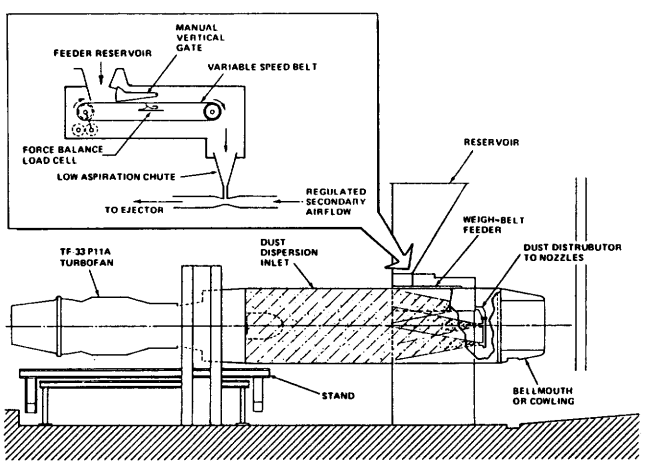


**Figure 2.** Schematic diagram of dust-injection system (DIS). The DIS is designed to accurately regulate the dust environment and must provide a controlled range of particle sizes and concentrations, all evenly dispersed in the incoming air. The DIS consists of a dust tube, dust-injection nozzles, weigh-belt feeder and dust reservoir, and a bellmouth. The weigh-belt feeder includes process-monitoring instrumentation to allow precise control of dust being fed to the test engine. The dust is delivered to the injection nozzles by compressed air. From Dunn and others (1987b).

## CLOUD PREPARATION AND ANALYSIS

The engines discussed here were all operated in air laden with particulate material from a mixture of two types of soils (sand and clay), two types of volcanic ash, and small amounts of a clay additive. The sandy soil is composed of decomposed granite obtained from the northwestern Santa Monica Mountains (Hollywood Hills area). The clayey soil is weathered material from Corona, Calif. Two different volcanic ashes have been used: 1980 Mount St. Helens ash from near Portland, Oreg., and Twin Mountain basaltic scoria from Twin Mountain quarry near Des Moines, N. Mex.

An analysis of the scoria (Dunn and others, 1987a) shows it to be approximately 85 percent basaltic glass, with the remaining 15 percent of the material being plagioclase and pyroxene. Figure 3*A* is a scanning electron photomicrograph of the scoria, and fig. 3*B* shows the elemental composition spectrum of the black scoria. Figures 4*A* and *B* are a photomicrograph and an elemental composition spectrum, respectively, for Mount St. Helens ash.

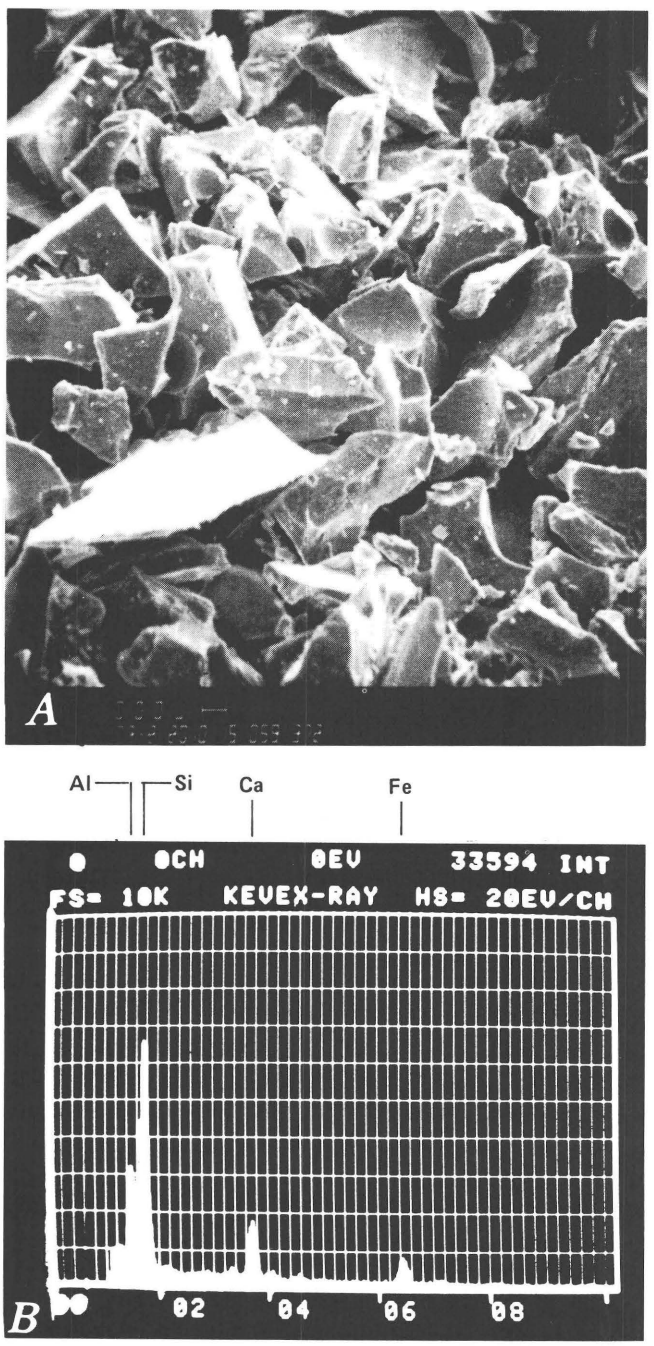


**Figure 3.** *A*, Scanning electron photomicrograph of black scoria sample. *B*, Composition spectrum of black scoria sample.

## TEST PROCEDURES AND TEARDOWN OBSERVATIONS

### TEST PROCEDURES

During the course of the engine-testing program, many different engines have been utilized. The detailed test procedure differs depending upon the engine. Prior to exposing the engine to a dusty environment, a set of baseline measurements is obtained at many different power lever angle (PLA) settings. All of the available engine parameters are recorded, including the exhaust-gas temperature (EGT), fuel flow rate, inlet total pressure ($P_{T2}$), fan-exit total pressure ($P_{T2.5}$), engine pressure ratio (EPR), interstage pressure, high-compressor static-discharge pressure ($P_{S3}$), engine thrust, burner static pressure ($P_B$), core speed ($N_2$), and fan speed ($N_1$). During this baseline measurement series, the engine also undergoes several 6-second periods of accelerations and decelerations.

### OBSERVATIONS DURING TESTING

Common to all engines tested, we find that, immediately upon introduction of the dust, a striking glow is observed at the fan face. The glow is the well-known phenomenon St. Elmo's glow (or fire) that results from a discharge of electrostatic charge that has built up because of dust particles striking the moving metallic surfaces. St. Elmo's glow was observed by the British Airways crew during their encounter with the Galunggung volcanic ash cloud (Smith, 1983).

Figure 5 shows the dust tube, the dust-injection nozzles, and the fan face glow. Figure 6 is a photograph of the fan face. The first-fan-stage rotor fence and the first-stage inlet guide vane are not obscured by the glow because the momentum exchange between these surfaces and the dust particles is too low to cause charge accumulation. The second-stage inlet guide vane appears as a shadow in the illumination field of the first and second rotors. Three silhouettes appearing on figure 6 are the

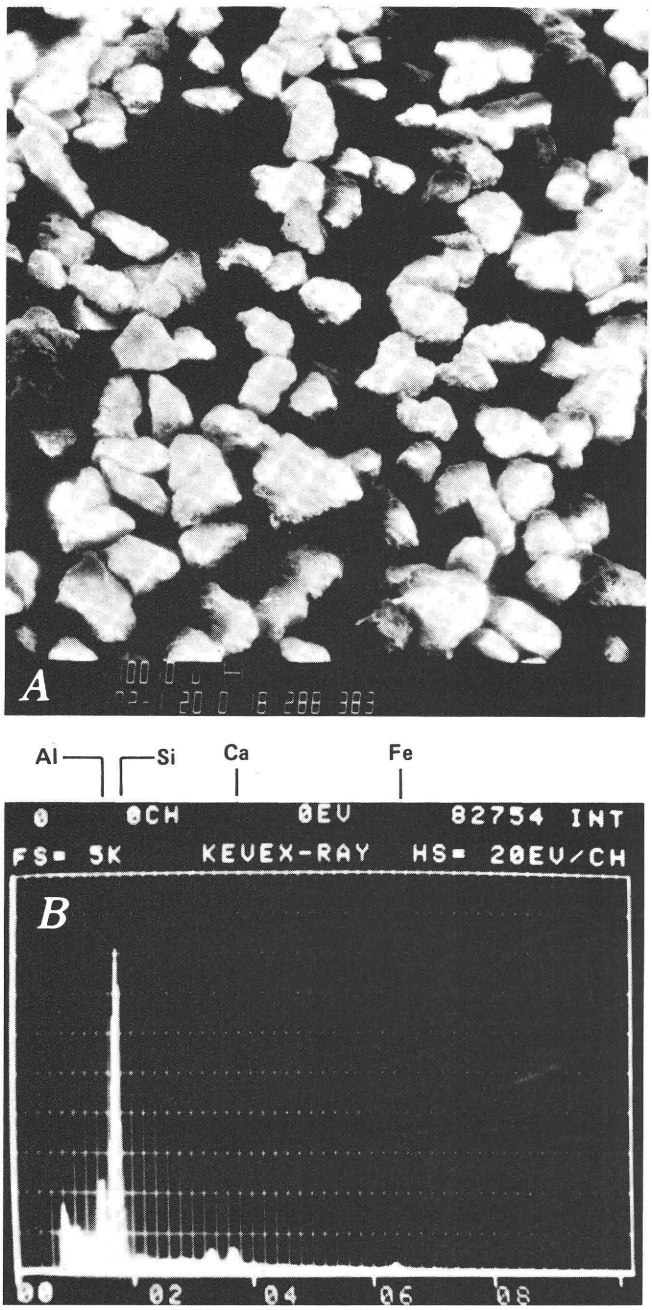


**Figure 4.** *A*, Scanning electron photomicrograph of Mount St. Helens ash. *B*, Composition spectrum of Mount St. Helens ash sample.

result of the dust-injection nozzles. The location of these nozzles can be more clearly seen on figure 5. A very bright ring of light appears at the first and second rotor tip/shroud regions. The illumination in this region may be brighter for several reasons; these include: (a) higher dust-particle concentrations caused by centrifuging, (b) greater optical depth and unobstructed view of the illumination, and (c) scintillation at the rotor tip. Also visible in this photograph is the bullet nose and a total-pressure probe.

It has also been observed that a few of the engine-readout parameters respond very quickly to the presence of a dust cloud. For example, the burner static pressure ($P_B$) and the high compressor static discharge pressure ($P_{S3}$) respond in almost identical fashion (fig. 7). The pressure increase can be very rapid. Also included on figure 7 are the fuel-flow rate and the fan total-pressure ratio, both of which are influenced by the dust cloud. The rate of pressure increase is a strong function of the power lever angle (PLA) setting and the dust cloud concentration. Figure 8 illustrates that the turbine inlet temperature (FTIT) also responds rapidly when a dust cloud is encountered, but again this response is a strong function of the PLA setting and the dust cloud concentration. The engine pressure ratio (EPR) and core speed ($N_2$) are also shown on figure 8. Changes in the core speed ($N_2$) and the fan speed ($N_1$) are indirect indicators of the material deposition or erosion as detected through the response of the control system.

## ENGINE TEARDOWN RESULTS

All of the engines tested in this program were disassembled for inspection when they could no longer be operated safely. Both in-flight experience and laboratory experience have demonstrated that if one continues to operate at high thrust levels in a volcanic ash cloud, then it is likely that the engine will surge and flame out (Przedpelski and Casadevall, this volume). As noted earlier, the three dominant factors of immediate concern to pilots are material deposition occurring on the high-pressure-turbine nozzle guide vanes (NGV's), erosion of the fan and compressor blades, and deposition of carbon-like material on the fuel nozzles. Fogging of the windscreen and landing lights, contamination of the environmental control system (ECS), and contamination of the oil supply may also become a problem.

The build-up of material on the nozzle guide vanes causes the very rapid increase in burner static pressure and in compressor discharge static pressure shown in figure 7. At high altitude, this pressure increase can lead to surge and engine flame-out. Figure 9 shows a portion of the nozzle guide vane row taken from an engine that was subjected to a dust mixture containing black scoria. This figure illustrates the heavy deposits on the leading edge and on the pressure surface. Figure 10 shows these deposits and illustrates that the cooling holes near the tip endwall are blocked, whereas those near the hub endwall are still open.

It has been observed that the remelted deposits are relatively brittle. The thermal properties of the deposited material are very different from those of the metal airfoils. One of the reasons that it has been possible to restart engines that have shut down at altitude after encountering a volcanic ash cloud is probably that some of the deposited material can be blown off the surface by ram air after the engine cools down. Evidence of partial material removal from the vanes can be seen on figure 9.

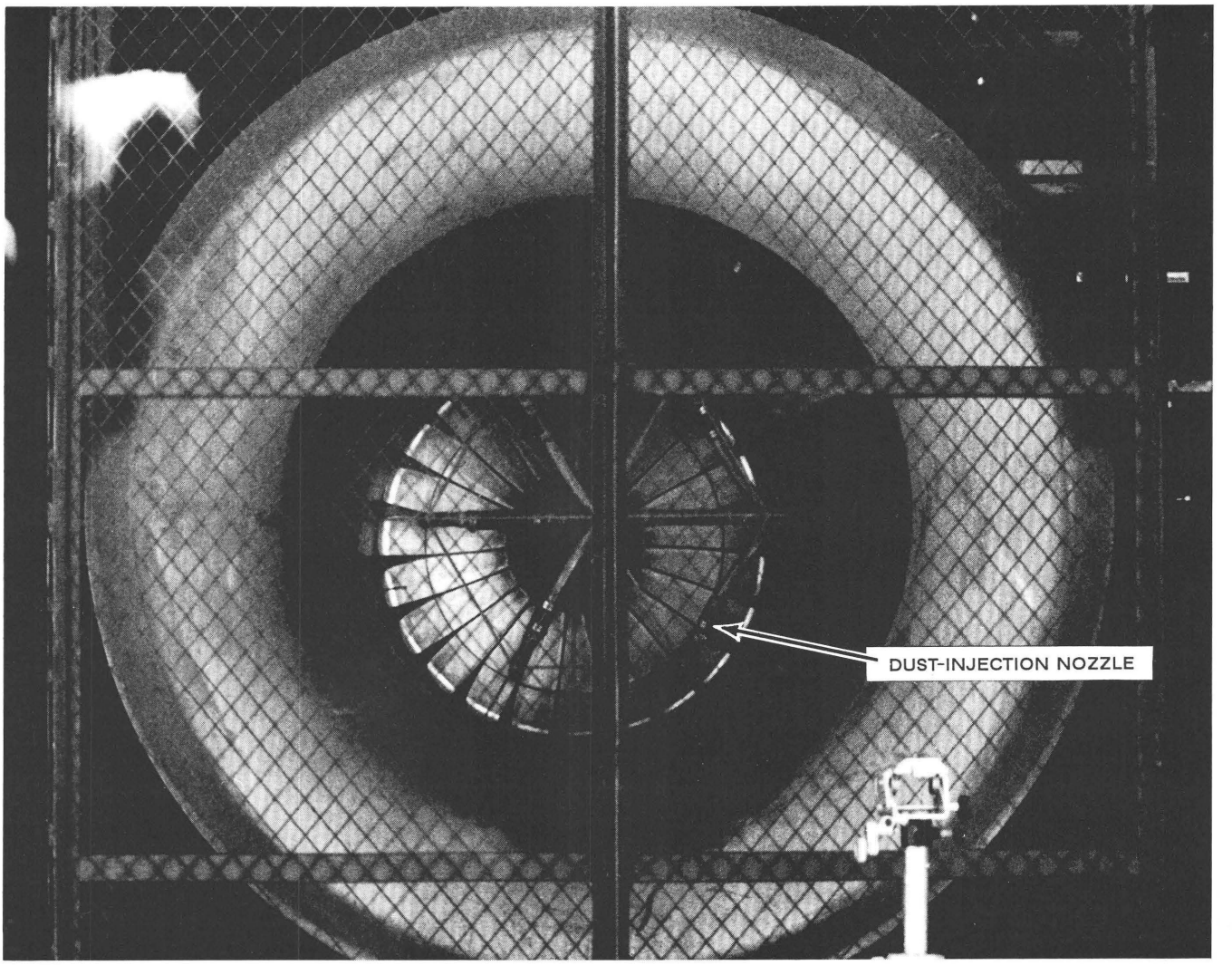


**Figure 5.** Photograph of St. Elmo's glow at fan face. Figure shows the dust tube, the dust-injection nozzles, and the fan-face glow. The first-fan-stage rotor fence and the first-stage inlet guide vane are not obscured by the glow (see text). The second-stage inlet guide vane appears as a shadow in the illumination field of the first and second rotors.

Figure 11 shows several of the fuel nozzles from the same engine mentioned above. The material on these nozzles is basically carbon (T. Casadevall, written commun., 1991). The center hole of the nozzle, from which the fuel is sprayed, was open and was found to be capable of passing fuel at the design flow rate. However, the swirl vanes were plugged, thus inhibiting atomization of the fuel. Because of this plugging, it is extremely difficult (if not impossible) to restart an engine that has been damaged in this way since this material cannot be blown off by ram air.

In addition to the difficulties caused in the hot section of the engine as a result of exposure to the volcanic ash cloud, the compressor can also sustain severe damage. Tip erosion is illustrated in figure 12. Throughout the compressor, tip-region erosion occurred on almost every stage. Figure 13 shows an example of the ninth-stage compressor blade row taken from the engine discussed in connection with figures 9–12. The trailing edge of the airfoil in the tip region became so thin that the material folded away from the pressure surface. Compressor wear is an irreversible process, and once the engine has operated in a volcanic ash cloud for any significant time period, the blades must be replaced.

As illustrated by the 747 aircraft experiences described in Smith (1983) and Campbell (1991), the volcanic ash cloud material makes its way through the environmental control system (ECS) and into the cabin. Laboratory experiments (Dunn and others, 1987b) were performed to ascertain the relative amount of dust material that is passed by the ECS. Dust particles may erode the duct-wall material (fig. 14). The absolute level of contamination of the bleed air at any inlet dust concentration is defined as the fraction of the input

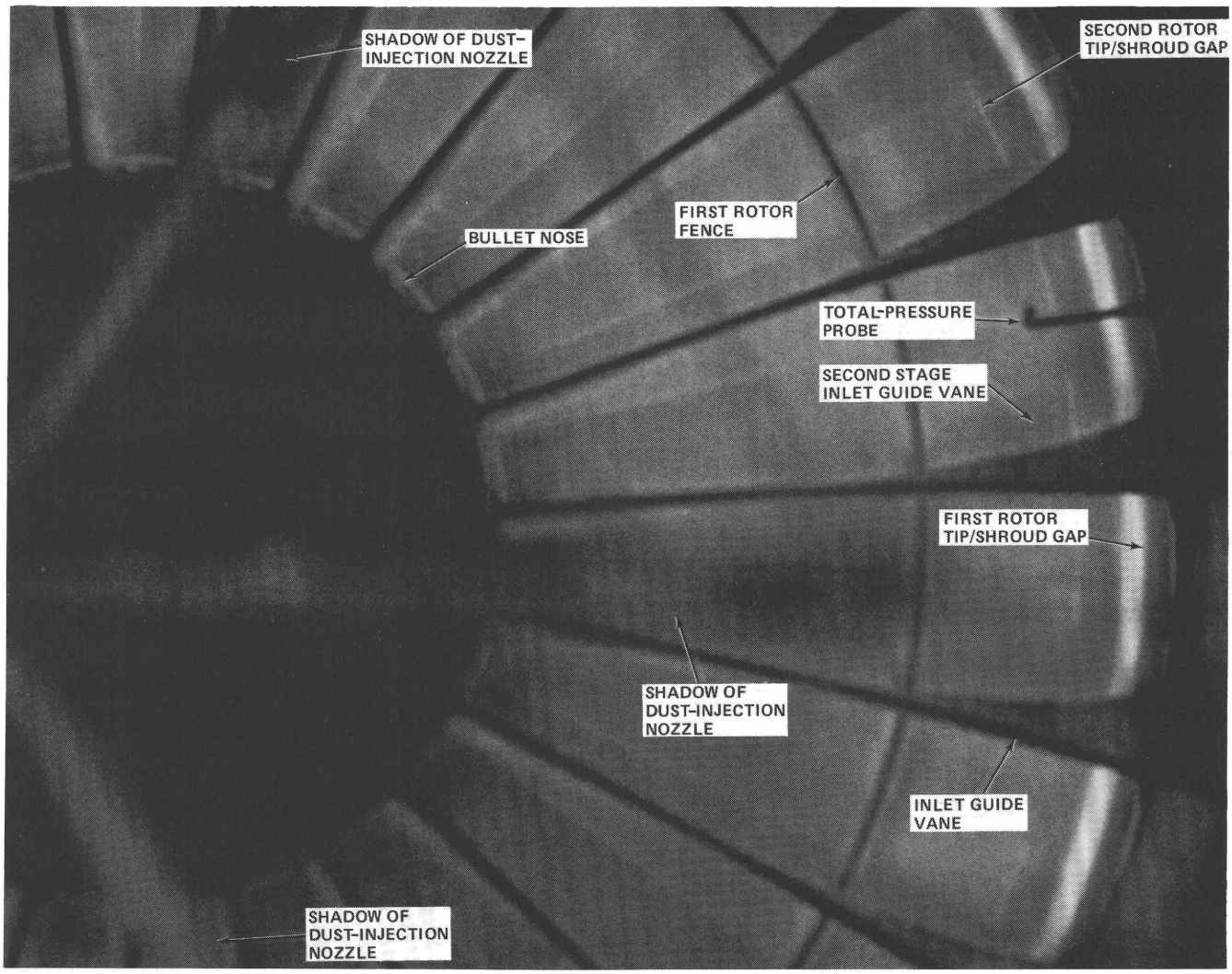


**Figure 6.** Photograph of St. Elmo's glow at fan face. Three silhouettes are the dust-injection nozzles. The location of these nozzles can be more clearly seen on figure 5. A bright ring of light appears at the first and second rotor tip/shroud regions.

dust that appears in the bleed. In the three cases sampled, this fraction was approximately constant, with an average value of 2.2 parts per thousand. The efficiency of the particle-collection process at the bleed can be obtained from this contamination level and the estimated air-mass flow in the bleed manifold. In our case, the latter is 0.5 percent of the total mass flow into the engine. This results in a 45 percent particle-collection efficiency in the ECS bleed.

The collection efficiency depends primarily on the geometry of the engine near the ECS bleed and the local air velocity. The engine geometry is fixed, and the contribution of changes in the local air velocity to the collection efficiency with moderate changes in thrust setting is expected to be small. Thus, the collection efficiency is relatively independent of thrust setting, and its measured level can be used to estimate the absolute level of contamination for the bleed air at power settings other than cruise. For example, at a high-thrust condition, an increase in ECS airflow of about 50 percent would produce an absolute level of contamination for the bleed air equal to 3.4 parts per thousand.

## CONCLUSIONS

As a result of information obtained during the course of tests utilizing many different gas turbine engines, the following conclusions can be drawn:

1. The presence of St. Elmo's glow at the engine face is indicative of dust in the environment.
2. The manner in which the engine will behave in a dust environment is dependent upon the dust concentration, the dust constituents, the operating turbine-inlet temperature of the engine, and the engine control system.
3. The turbine inlet temperature required to cause material deposition on the hot-section components is

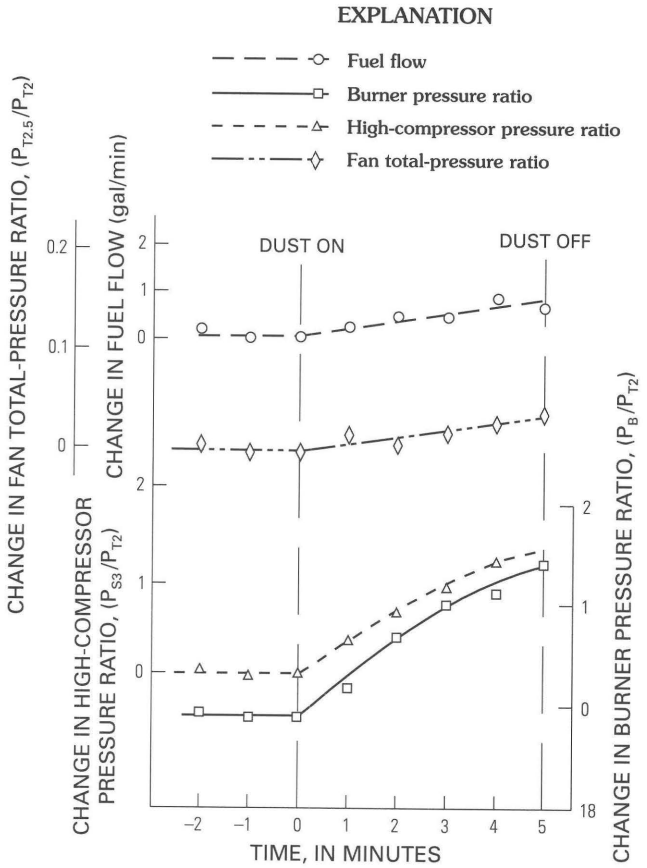


**Figure 7.** Time history of engine parameters during dust experiments. $P_{T2}$, inlet total pressure; $P_{T2.5}$, fan-exit total pressure; $P_{S3}$, high-compressor static-discharge pressure; $P_B$, burner static pressure.

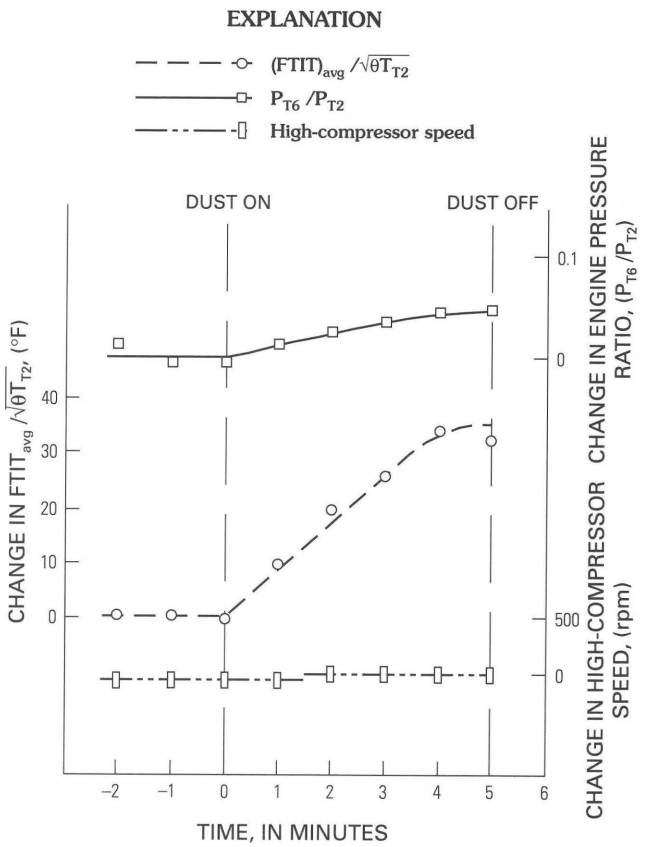


**Figure 8.** Time history of engine parameters during dust experiments. $FTIT_{avg}$, average turbine inlet temperature; θ, ratio of total temperature to National Aeronautic and Space Administration (NASA) standard sea-level temperature of 58.7°F; $T_{T2}$, turbine temperature; $P_{T2}$, inlet total pressure; $P_{T6}$, total pressure.

approximately 2,000°F (1,094°C). Many older engines, which operate at lower temperature, will not experience deposition but will experience compression system erosion. The newer engines will experience both deposition and erosion unless the thrust level is reduced in order to lower the turbine inlet temperature.

4. It must be emphasized that engine operation time in a dust-laden environment is limited. If entrance into the cloud is unavoidable, then the air crew is advised to reduce thrust, exit the cloud, and carefully monitor engine diagnostics (especially the EPR, EGT, fuel flow, core speed, and fan speed). This combination of parameters will help determine the degree of engine damage and how the control system is handling the problem. The reader is referred to the report of the Aerospace Industries Association (AIA) committee on volcanic ash for recommendations on how to operate a commercial aircraft if the air crew should unexpectedly find itself in a volcanic ash cloud (AIA Propulsion Committee 334-1, this volume; Campbell, this volume).
5. Prolonged operation in the dust-laden environment may result in permanent engine damage. If the aircraft is operating at high altitude, the surging associated with this type of damage may cause engine flame-out. If the fuel nozzles have not become covered with carbon, then it should be possible to restart the engine at lower altitude. Some of the deposited material will have blown off during the period of time that the engine was inoperable.
6. A significant amount of material will make its way through the environmental control system and into the electronics cabinets and the cabin itself. The particle size of this material is on the order of 6 μm.

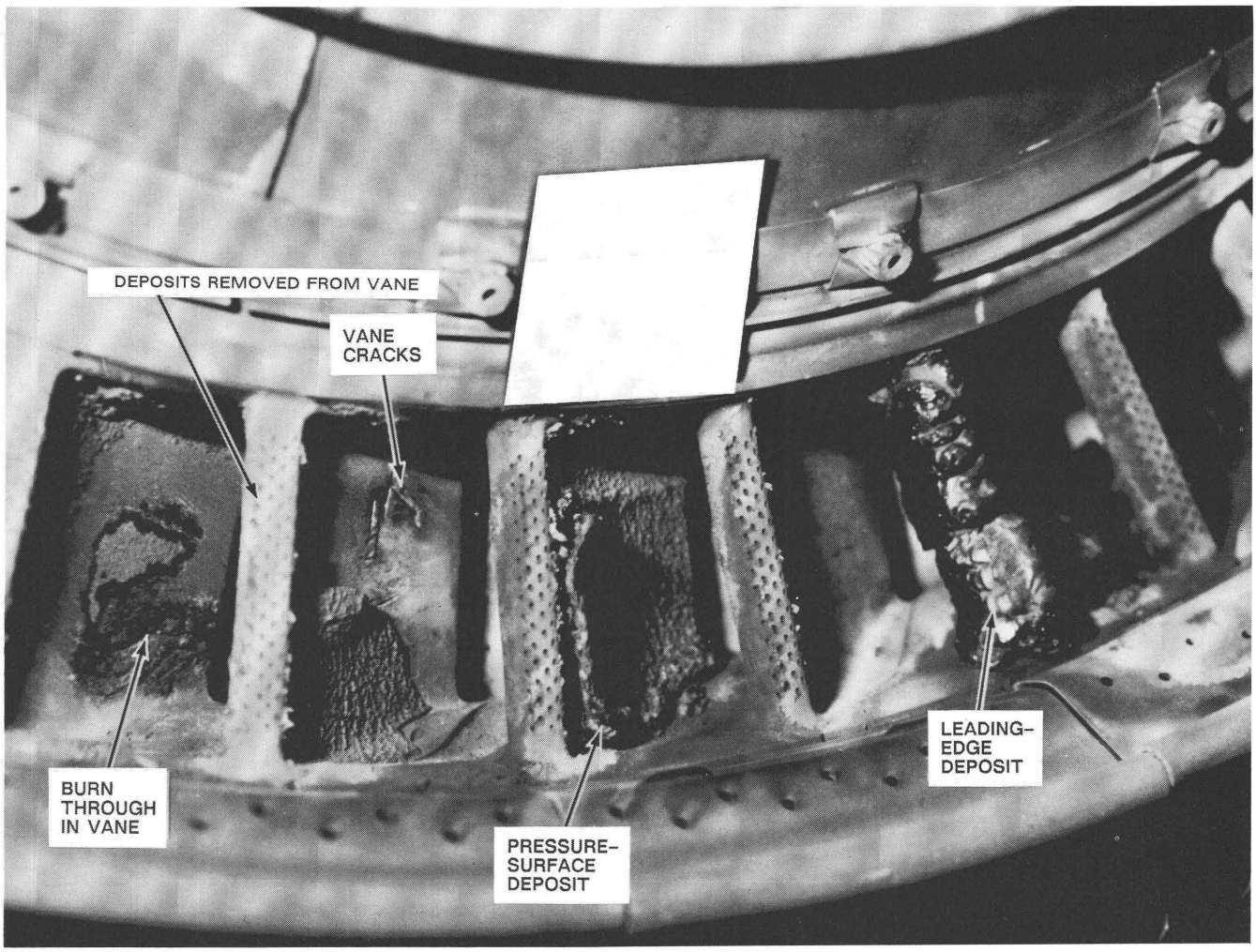


**Figure 9.** Photograph of nozzle guide vane for first-stage high-pressure turbine. Figure shows a portion of the nozzle guide vane row taken from an engine that was subjected to a dust mixture containing black scoria. This figure illustrates the heavy deposits on the leading edge and on the pressure surface.

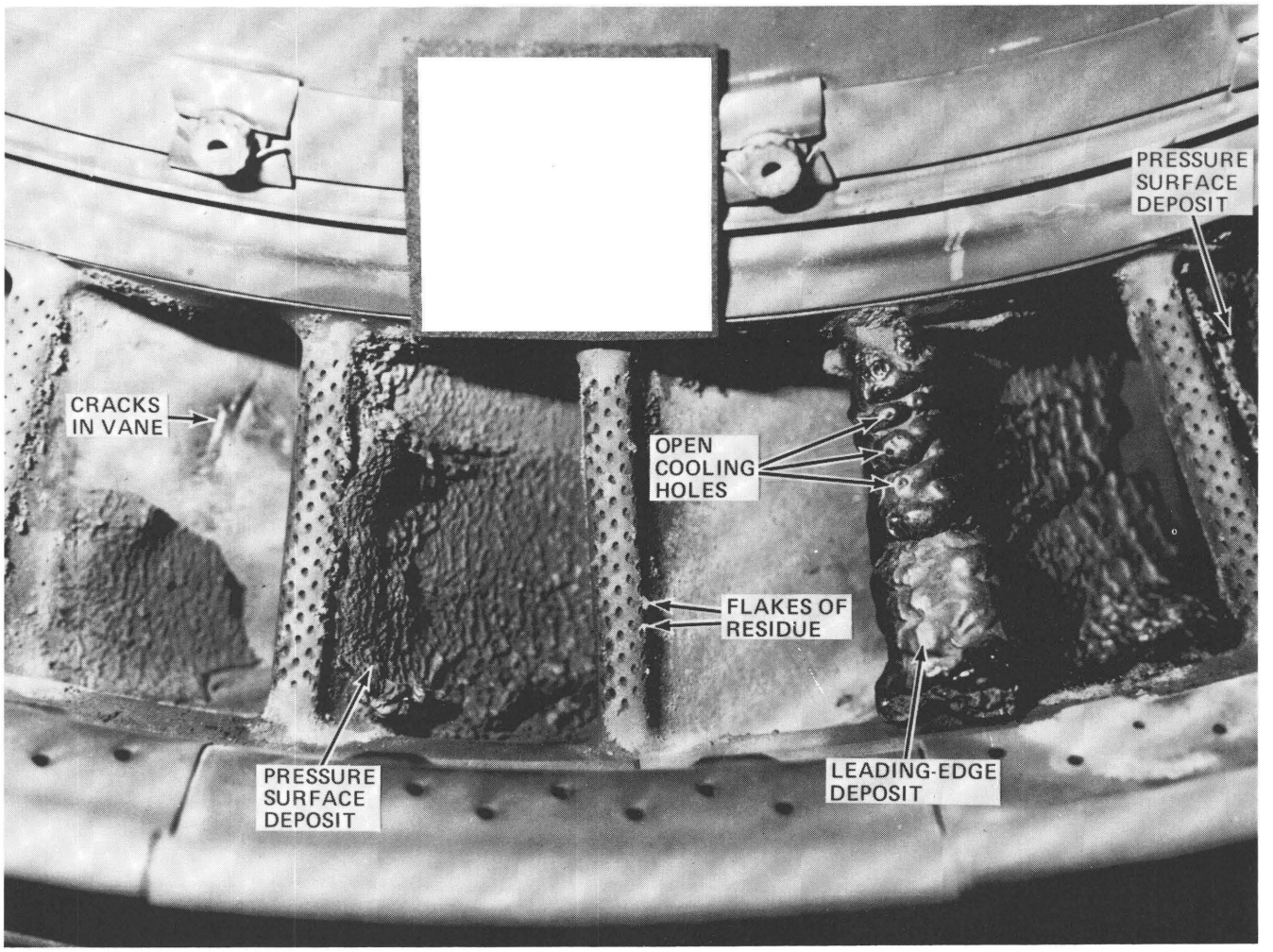


**Figure 10.** Photograph of nozzle guide vane for first-stage high-pressure turbine. Note remelted ash deposits and that the cooling holes near the tip endwall are blocked, whereas those near the hub endwall are still open. The remelted deposits are relatively brittle and some of the deposited material can be blown off the surface by ram air after the engine cools down. Evidence of partial material removal from the vanes can be seen on figure 9.

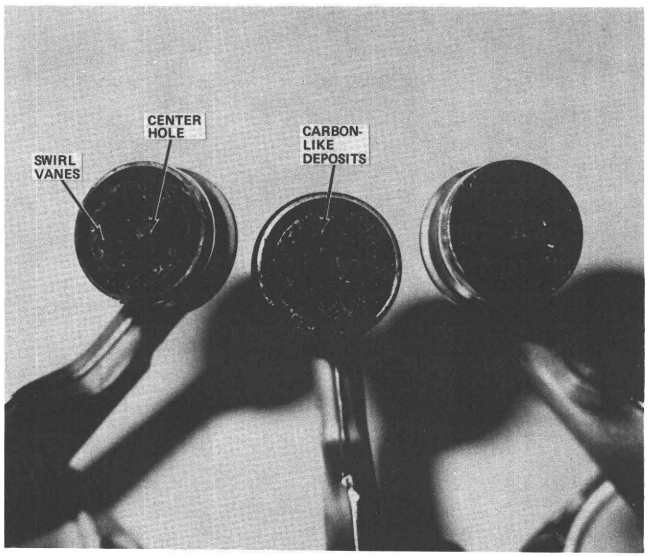


**Figure 11.** Photograph of fuel nozzles from the engine shown in figures 9 and 10. The material on these nozzles is carbon (T. Casadevall, written commun., 1991). The center hole of the nozzle, from which the fuel is sprayed, was open and capable of passing fuel at the design flow rate; however, the swirl vanes were plugged, thus inhibiting atomization of the fuel.

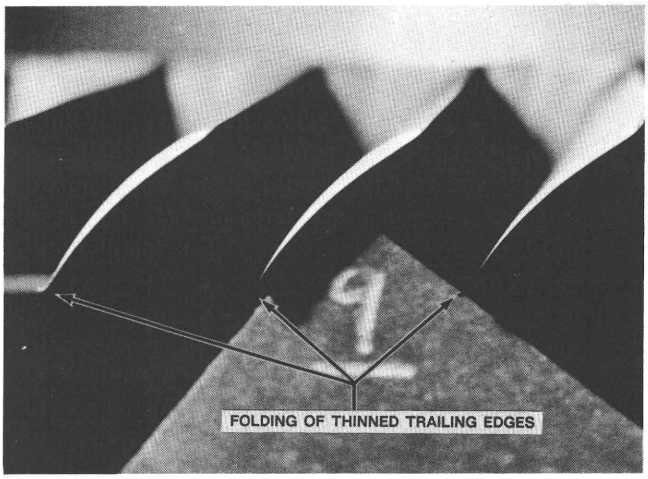


**Figure 13.** Photograph of high-pressure compressor ninth-stage rotor. Figure shows an example of the ninth-stage compressor blade row taken from the engine shown in figures 9-12. The trailing edge of the airfoil in the tip region became so thin that the material folded away from the pressure surface.

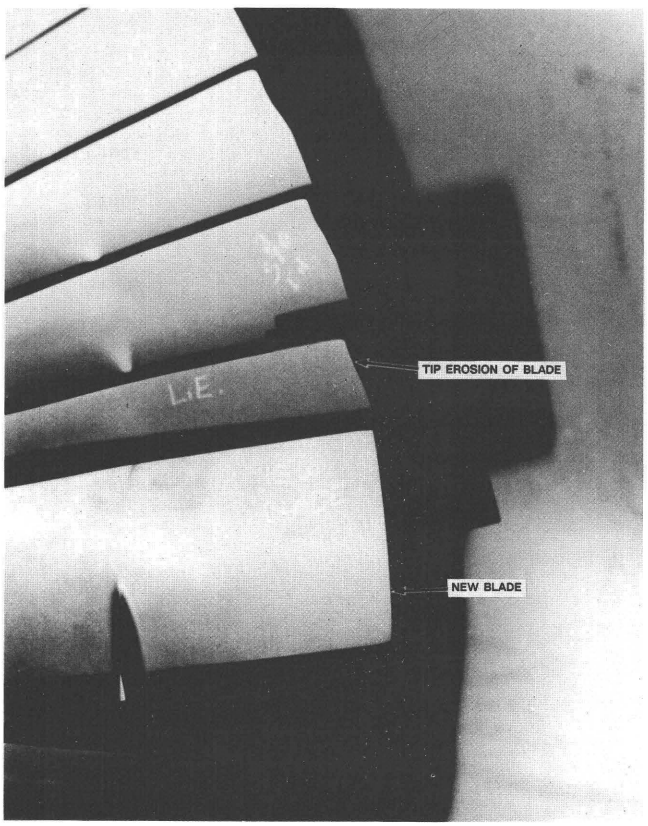


**Figure 12.** Photograph of second-stage fan showing blade tip erosion. Throughout the compressor, tip-region erosion occurred on almost every stage.

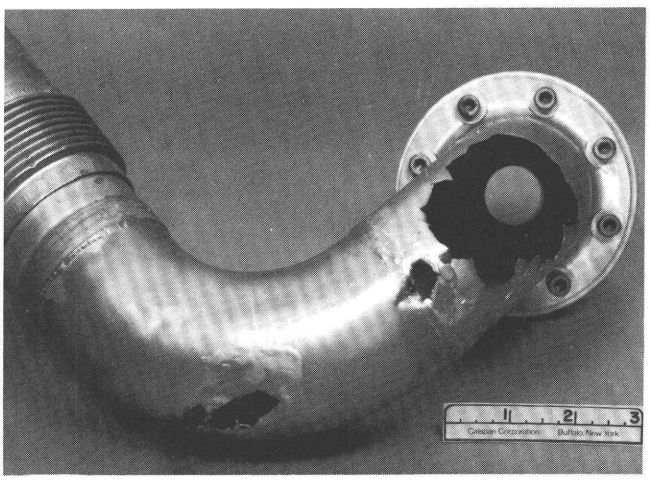


**Figure 14.** Photograph of environmental control system plumbing showing erosion of duct walls. Scale is in inches.

## REFERENCES CITED

Batcho, P.F., Moller, J.C., Padova, C., and Dunn, M.G., 1987, Interpretation of gas turbine response due to dust ingestion: ASME Journal of Engineering for Gas Turbines and Power, v. 109, p. 344-352.

Campbell, E.E., 1991, 747-400 Airplane damage survey following a volcanic ash encounter [abs.], *in* Casadevall, T.J., ed., First International Symposium on Volcanic Ash and Aviation Safety: U.S. Geological Survey Circular 1065, p. 14.

Chambers, J.C., 1985, The 1982 encounter of British Airways 747 with the Mt. Galunggung eruption cloud: Reno, Nev., AIAA 23rd Aerospace Sciences Meeting, AIAA Paper No. 85-0097, 5 p.

Dunn, M.G., Padova, C., and Adams, R.M., 1987a, Operation of gas turbine engines in dust-laden environments: Paris, France, AGARD-Advanced Technology of Aero Engine Components, May 4-8, 1987, 14 p.

Dunn, M.G., Padova, C., Moller, J.E., and Adams, R.E., 1987b, Performance deterioration of a turbofan and a turbojet engine upon exposure to a dust environment: ASME Journal of Engineering for Gas Turbines and Power, v. 109, p. 336-343.

Grant, G., and Tabakoff, W., 1975, Erosion prediction in turbomachinery resulting from environmental solid particles: Journal of Aircraft, v. 12, p. 471-478.

Hussein, M.F., and Tabakoff, W., 1973, Dynamic behavior of solid particles suspended by polluted flow in a turbine stage: Journal of Aircraft, v. 10, p. 434-440.

Smith, W. S., 1983, High-altitude conk-out: Natural History, v. 92, no. 11, p. 26-34.

Tabakoff, W., and Bahan, C., 1981, Effects of solid particles suspended in fluid flow through an axial flow compressor stage [abs.]: Bangladore, India, Fifth International Symposium on Airbreathing Engines.

Tabakoff, W., and Hussein, M.F., 1971a, Effects of suspended solid particles on the properties in cascade flow: AIAA Journal, v.9, p. 1514-1519.

Tabakoff, W., and Hussein, M.F., 1971b, Pressure distribution on blades in cascade nozzle for particulate flow: Journal of Aircraft, v. 8, p. 736-738.

VOLCANIC ASH AND AVIATION SAFETY:
Proceedings of the First International Symposium
on Volcanic Ash and Aviation Safety
U.S. GEOLOGICAL SURVEY BULLETIN 2047

# VOLCANIC ASH–AIRCRAFT INCIDENTS IN ALASKA PRIOR TO THE REDOUBT ERUPTION ON 15 DECEMBER 1989

*By* Juergen Kienle

## ABSTRACT

Commercial and military propeller-driven and jet aircraft have encountered airborne volcanic ash in the Cook Inlet region three times prior to the near crash of a Boeing 747-400 jet downwind from Redoubt Volcano on 15 December 1989. Aircraft flew into ash plumes in 1953 when Mt. Spurr erupted and in 1976 and 1986 when Augustine Volcano erupted. Damage to aircraft in all incidents was restricted to severe sandblasting, and no engine failures occurred.

## INTRODUCTION

The volcanoes of the Cook Inlet region, Alaska, make up the eastern end of the Aleutian volcanic arc. Air routes connecting Europe and North America with the Far East follow great-circle routes, which parallel much of the volcanic chain. Three volcanoes in Cook Inlet, Mt. Spurr, Redoubt Volcano, and Augustine Volcano (fig. 1), have erupted several times this century for a total of 10 eruptions between 1900 and 1992, or about once every 10 years on average. In recent decades, the eruption rate has almost doubled. Since 1950, Augustine erupted three times, Redoubt twice, and Spurr twice, totaling seven eruptions in the past 43 years or once every 6 years on average. Each eruptive cycle of the three volcanoes produced multiple explosions and associated ash plumes. Iliamna Volcano, located between Redoubt and Augustine Volcanoes (fig. 1), has not had an ash eruption in historic times, although large steam plumes have been reported frequently to the Alaska Volcano Observatory (AVO).

The Alaska Volcano Observatory gives special attention to the four Cook Inlet volcanoes, which are west and southwest of Anchorage (fig. 1). AVO operates remote, continuously recording, radio-telemetered seismic stations on all four Cook Inlet volcanoes and slow-scan television cameras, which are focused on Spurr and Redoubt. For the recent eruptions of Spurr (1992), Redoubt (1989–90), and Augustine (1986), this has allowed scientists to forecast eruptive activity and to give adequate warnings to the commercial aircraft industry and to the U.S. military, either before or at the onset of explosive, ash-producing eruptions. Because ash is mainly advected by tropospheric winds, plume-path predictions issued in recent years by AVO have been used by carriers to avoid aircraft-ash encounters (Casadevall, in press).

This paper gives a brief description of aircraft-ash incidents over Cook Inlet between 1953 and 1986, before the near-fatal encounter of a Boeing 747-400 jet with a Redoubt ash plume on 15 December 1989.

## AIRCRAFT-ASH ENCOUNTERS OVER COOK INLET, 1953–86

### MT. SPURR, 1953

On 9 July 1953, at about 17:00 local time, the Crater Peak vent on the southern flank of Mt. Spurr erupted suddenly, without much warning, sending a dark, ash-rich column to a height of 21 km (70,000 ft). Juhle and Coulter (1955) report that the ash cloud, carried by gentle westerly winds, drifted over Anchorage by noon. Heavy ash fall lasted for about 3 hours and darkened the skies so much that the city lights had to be turned on from noon until 15:00. Eventually 3 to 6 mm (1/4 inch) of fine dust settled over the city, including Anchorage Airport and Elmendorf Air Force Base, disrupting air traffic for 2 days.

By chance, the eruption was witnessed at close range by pilots of two U.S. Air Force planes on a reconnaissance mission near the volcano (Juhle and Coulter, 1955; Wilcox, 1959). The following pilots' account is quoted from an Air Force press release of 10 July 1953 (taken from Wilcox, 1959):

> At 05h 05m Lieutenant Metzner noticed a column of smoke 60 miles ahead that was about 15,000 ft high and one-eighth mile wide. As he approached the smoke it was apparent that the eruption causing it was becoming increasingly severe with the smoke growing rapidly in height. At about 25 miles distance, the volcano was recognized as the 11,070-foot high Mt. Spurr. Both planes approached the mountain at about 15,000 ft and circled the volcano at about 05h 25m. They noticed the continuing increase in the intensity and size of the column of smoke with lightning flashes through its core every 30 seconds. Smoke issued from the volcano in violent billows at

the 7,000-foot level of the mountain caused by huge subterranean explosions. Tremors on the mountainsides were visible from the aircraft and were followed by snow slides on the mountain. The smoke had by now reached the 30,000-foot level, rolling upward and assuming the shape of the atomic bomb mushroom. Clouds of smoke were every shade of gray from black at the crater to pure white at the top. By this time the width had increased to about a mile at the base and 30 miles at its widest part.

About 05h 40m Lieutenant Metzner climbed in order to estimate the height of the mushroom. The top of the stalk, or the bottom of the mushroom, was 30,000 ft and the top of the mushroom had climbed to 70,000 ft. Lightning was now flashing from top to bottom of the mushroom at three-second intervals.

At about 6h 00m volcanic ash began falling from the mushroom on all sides and finally made the entire area hazy. A clear definition of the volcano and the mushroom rapidly faded and the patrol returned to its base.

Another pilot report confirmed that ash was still being erupted vigorously 4 hours later, at 09:00. The activity declined toward noon but resumed at 15:30; other eruptions took place later that day (Wilcox, 1959). Wilcox further states that, on the next day, 10 July, the vent was only steaming, except for a strong ash-laden surge at 15:30, which rose to 6 km (20,000 ft). Juhle and Coulter were in the field at the volcano from 11 to 14 July and again on 16 July, during which time they observed steam clouds to heights of 6 km, with occasional puffs of black dust (Wilcox, 1959).

One of the two F-94 jet aircraft that were flying near Mt. Spurr on the morning of 9 July flew through the cloud and had its Plexiglas cockpit canopy frosted by the "sandblasting" action of the ash (Juhle and Coulter, 1955). The following information is summarized from a U.S. Air Force report on the Mt. Spurr eruption (U.S. Air Force, 1955):

During the peak of eruptive activity, three jet aircraft of the 66th Fighter-Interceptor Squadron were dispatched through the ash plume to bring back first-hand, eyewitness accounts of the eruption. [There is a conflict with the report of Juhle and Coulter (1955), which says that only one jet flew through the eruption cloud.] Upon return to Elmendorf AFB, all three jets had sandblasted wing leading edges, windshields, side panels, and front portions of the canopies, greatly reducing pilot visibility. Some panels later had to be replaced.

As a precaution, all aircraft of the U.S. Air Force's 5039th Air Transport Squadron in flyable condition (26 planes) were evacuated to Laird and Eielson Air Force Bases near Fairbanks. However, only four F-94 interceptors were able to engage in the evacuation; loss of power in the dusty air on take-off grounded the other interceptors. These were hangared in time, except for several large C-124 transport aircraft (Globe Trotters). Float-equipped L-28's of the 5th Liaison Squadron were moved from Anchorage to Lake Louise. Wheel-equipped Beavers were placed inside hangars. Two radar stations in the Anchorage area, one on Fire Island, were taken off the air to prevent damage to the antenna drive and generators.

Most seriously affected by the ash fall were the propeller-driven C-124 transport aircraft stored outside, which required 10 days of cleanup to remove the fine volcanic ash from the aircraft. From 9 to 13 July, tactical aircraft were unable to take to the air over Elmendorf because of dusty conditions and remobilized ash on runways and taxiways. The 10th Air Division of the Alaska Air Command lost its ability to meet its air defense mission and it passed the responsibility for fighter interception and radar control to the 11th Air Division at Laird AFB. It was only on 17 July, eight days after the eruption, that the three Elmendorf fighter-interceptor squadrons returned to normal operations. For all practical purposes, Elmendorf AFB was closed to air traffic from 9 to 17 July. The east-west runway was

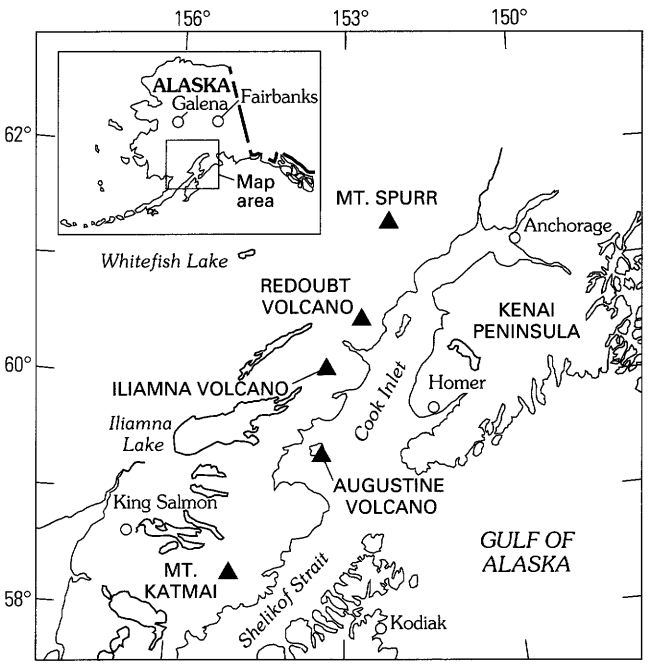


**Figure 1.** Location of volcanoes in the area of Cook Inlet (solid triangles) and places mentioned in the text. Elmendorf Air Force Base is located near Anchorage.

cleared for emergency flying only. Aircraft landed, but had to immediately cut off engines while on the runway before being towed to the hangar. The reverse procedure was used for emergency takeoffs to reduce exposure of the airplanes to the pervasive dust.

The cleanup operation produced many engineering headaches. The soft, clinging ash first had to be cleared from all aircraft surfaces, taxiways, runways and parking ramps. All moving parts, air intakes, accessory cases, filters and screens required thorough cleaning to prevent corrosion and contamination.

A truck-mounted jet engine, originally designed to remove ice from railroad tracks, proved to be the most useful tool in clearing ash from large swaths of ground; for example, within 40 hours this jet-blower cleared some 440,000 $m^2$ of pavement at the Anchorage International Airport.

There are no known records of commercial aircraft being affected by the 9 July eruption of Mt. Spurr. As became clear after encounters between volcanic ash and aircraft at Galunggung, Indonesia, in 1982, and more recently at Redoubt, propeller-driven airplanes that operate at low engine temperatures fare much better than jets in severe, dusty conditions.

## AUGUSTINE VOLCANO, 1976

Augustine Volcano, located in lower Cook Inlet (fig. 1), erupted in January 1976 after 12 years of dormancy (fig. 2). Sub-Plinian eruptions occurred from 22 to 26 January and spread ash generally northward and eastward over the Kenai Peninsula, with fine ash falling as far away as Sitka, 1,100 km (684 mi) downwind (Kienle and Shaw, 1979).

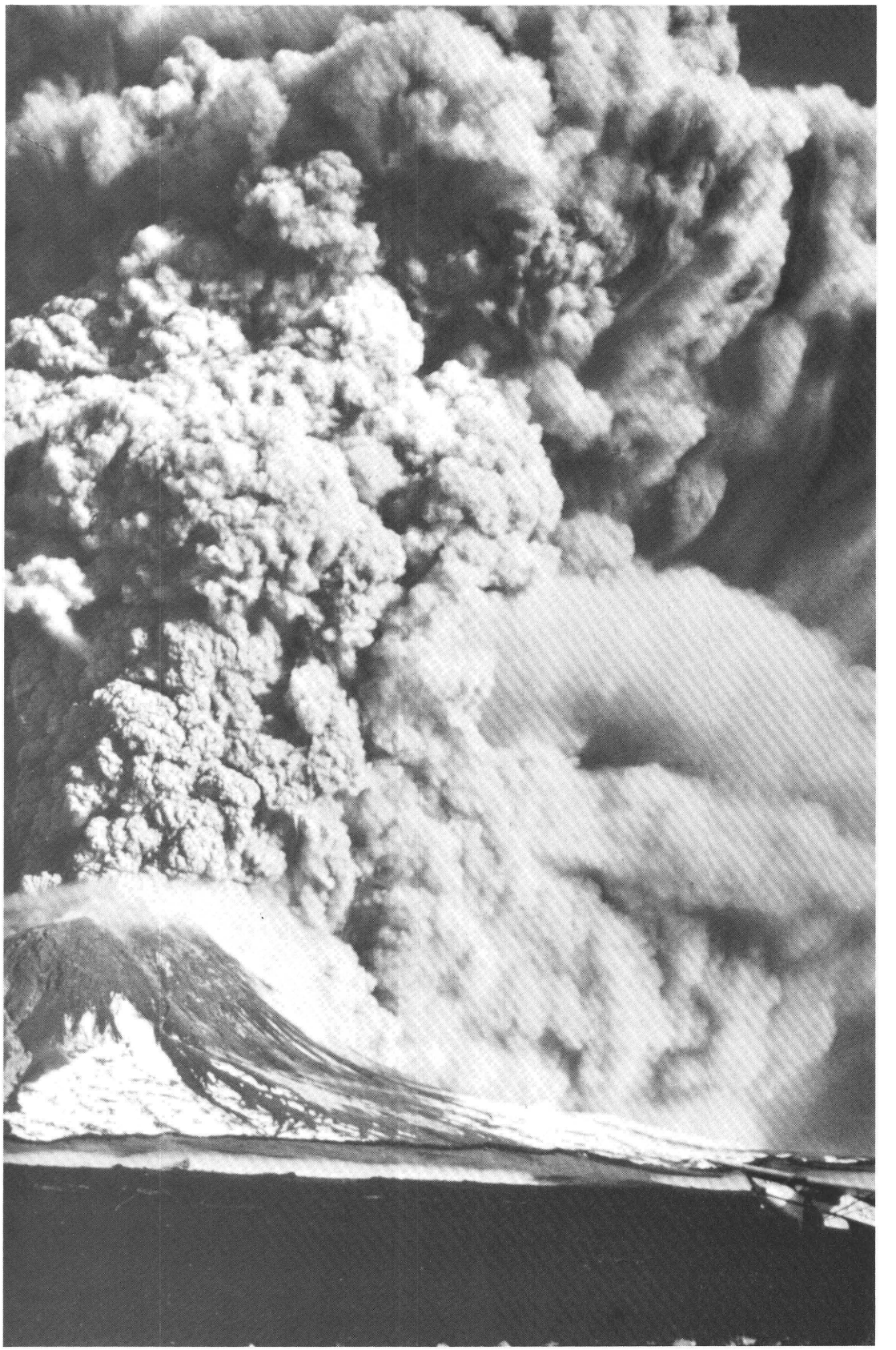

**Figure 2.** Augustine Volcano in eruption on 6 February 1976. Photograph from the west coast of Augustine Island, courtesy of Gary Gunkel.

One of the 22 January Augustine eruptions occurred in the midst of a U.S. Air Force defense exercise. Reports of greatly reduced visibility were received from pilots in two F-4E Phantom jets flying in formation through an eruption cloud. These observations were used by Kienle and Shaw (1979) to estimate the minimum mass concentration of particulate material contained in that eruption cloud. No mechanical problems or serious power loss were reported by the pilots. The following is an excerpt of a report by the two F-4E Phantom jet pilots who had taken off from Galena, Alaska, on 22 January 1976, heading south for King Salmon (from Kienle and Shaw, 1979; U. S. Air Force, 1976):

> The two jets were flying in clouds, cruising at 9 km (31,000 ft). We were still in the weather when suddenly at 14:30 AST the ordinary gray clouds slightly darkened for a moment or two, then there was instant complete darkness. There was no turbulence associated with this darkness. The two jets were flying in close formation about 10 meters apart. Had the lead plane not immediately turned on its lights, the following pilot would have lost contact; he could barely see the lead plane 10 meters away with its lights on. Upon landing in King Salmon, the canopy of the aircraft was seen to be scoured, and the paint at the wing tips was sandblasted off. Very fine, jewelers-rouge-colored material was ingested into the cockpit through the engine air intakes. The material was sticky and was found in every nook and cranny of the planes.

A second incident concerns three Japan Airline jet airplanes en route to Tokyo on the afternoon of 25 January 1976. As recounted by Mr. K. Noguchi of Japan Airlines (Kienle and Shaw, 1979):

> After cargo flight JL 672 took off from Anchorage at 16:00 AST, the DC-8 was about to reach its cruising altitude of 10 km (33,000 ft), 25 minutes after takeoff, traveling along air route J-501 when it suddenly encountered an ash cloud near Whitefish Lake (25 km southeast of Sparrevohn). Upon landing in Tokyo the scoured center windshield had to be replaced. Much ash had adhered to the plane and slight abrasion damage was found on external radio parts, landing gears and the air-conditioning system, but none of these parts needed to be replaced.

Two other passenger planes, a Boeing 747 and a DC-8, also bound for Tokyo and departing within 1 hour after flight JL 672, reported ash suddenly adhering to the planes at cruising altitude (about 10 km) near Sparrevohn, which also caused minor damage but not as extensive as that to the DC-8 flight JL 672.

Kienle and Swanson (1985), in a report on volcanic hazards for Augustine Volcano, discussed the hazard of volcanic ash to aircraft and delineated very high risk, high-risk, moderate, and low-risk hazard zones in the vicinity of Augustine Island.

## AUGUSTINE VOLCANO, 1986

Augustine erupted again in 1986, with strong eruptive activity concentrated in the period between 27 and 31 March. The sequence of events was similar to the 1976 eruption, with an initial, highly explosive vent-opening phase lasting 4 days, followed later in the year by less explosive activity associated with the extrusion of a new lava dome (Swanson and Kienle, 1988). The eruptive cycle ended in September 1986, but from April on, the eruption did not present a substantial hazard to aircraft.

During the March 1986 eruption of Augustine Volcano, airborne ash again presented a hazard to aircraft operations throughout the Cook Inlet basin and to airports in Anchorage because of predominantly southerly winds (Yount and others, 1987). The eruption was anticipated by Alaskan volcanologists (Kienle and others, 1986; Kienle, 1986), and T. Miller and M. E. Yount of the U.S. Geological Survey office in Anchorage held briefings with the Federal Aviation Administration (FAA) and the U.S. Air Force on 18 March 1986, 9 days prior to the eruption, to warn about the possibility of an eruption and the consequences to aircraft operations.

Early on the morning of 27 March 1986, just after the eruption had begun, the U.S. Air Force evacuated planes from Anchorage and kept them away until 30 March. Even though the Anchorage International Airport was never officially closed during the most explosive phase of the eruption, most commercial carriers either canceled or diverted their Anchorage flights between 27 and 29 March.

The following is a summary taken from Aviation Week and Space Technology (1986):

> From March 27 to 29, air carrier service to Anchorage was nearly at a standstill. Subsequently, the wind shifted to a northerly direction carrying the ash away from the Cook Inlet bowl, now affecting the airline traffic between Anchorage and airports at Kodiak and King Salmon. Volcanic ash generally stayed below 15,000 ft (4.5 km) but a stronger eruption on March 31 sent an ash plume up to 30,000 ft (9 km).
>
> Alaska Airlines had its worst day on 28 March, when it canceled 40 out of 68 Anchorage arrivals and departures. Twenty-seven to 29 March, the Anchorage stop of the airline's Seattle-Anchorage-Fairbanks flights, coming and going, were deleted. Western Airlines canceled all of its flights to and from Alaska 27–28 March and flew some flights on 29 March. United Airlines, Northwest Airlines and other international carriers that fly from Europe and Far East Asia over the North Pole canceled service during the worst ash conditions. United canceled 35 flights between 27 and 29 March. Local commuter airplane traffic between Anchorage and the Kenai Peninsula also was largely shut down and the Federal Aviation Agency [sic] (FAA) temporarily shut down its air-route surveillance radar at Kenai for two days. With shifting winds on 31 March 1986, ash was cleared from the air over most of the Cook Inlet basin, and normal air operations resumed.

## CONCLUSIONS

A comparison of the eruptions of these volcanoes demonstrates that, as we learn to live with the high activity level of Cook Inlet volcanoes, we improve our ability to cope with the problem of volcanic ash and aviation safety. Air traffic has increased dramatically in Alaska since the eruption of Mt. Spurr in 1953. High-bypass, turbine-powered jet aircraft have replaced larger, propeller-driven passenger planes; both factors increase the risk of danger from encountering airborne volcanic ash. On the other hand, the volcanological community in Alaska has come together since 1953. The 1953 Mt. Spurr eruption caught everyone off-guard, but we

were better prepared in 1976 and 1986 for the Augustine eruptions, having instrumented that volcano with radio-telemetered seismographs starting in 1970. In 1986, briefings with the aviation community were held by U.S. Geological Survey volcanologists 9 days prior to the onset of the eruption that paralyzed air traffic in Cook Inlet for 4 days. Significantly, there were no encounters of aircraft, either private or military, with volcanic ash during the most vigorous phase of the 1986 Augustine eruption.

The close cooperation among volcanologists of the U.S. Geological Survey, the Alaska Geological Survey, and the University of Alaska, Fairbanks, that had developed during the 1986 Augustine eruption was formalized in March 1986 with the founding of the Alaska Volcano Observatory. Since then, AVO has instrumented all four Cook Inlet volcanoes with at least four seismometers at each volcano. In addition, remotely controlled slow-scan television cameras have been installed to continuously observe Mt. Spurr and Redoubt Volcano, and we have plans to do the same for Augustine Volcano. Satellite surveillance of the volcanoes and eruptive plumes has become routine at the AVO laboratory in Fairbanks (Dean and others, this volume), and an array of lightning detectors can track electrified plumes in Cook Inlet. Radars and television cameras have been used to track rising eruption columns and their dispersal by wind.

During the two recent eruptions in Cook Inlet at Redoubt Volcano (1989–90) and at Mt. Spurr (1992), AVO went on 24-hour watches for several months. Communication with the carriers and Federal agencies involved with air traffic (Federal Aviation Administration, National Weather Service) were increased and resulted in the production of daily updates on the status of the active volcano and the forecasting of potential plume trajectories every 6 hours (or more often during active phases of ongoing eruptions) (Murray and others, this volume).

In spite of the better level of preparedness in recent years, there was a near fatal encounter of a Boeing 747-400 with an ash plume of Redoubt Volcano on 15 December 1989 (Casadevall, in press). The aviation and volcanology communities in Alaska must jointly strive to avoid any other encounters of this type.

## ACKNOWLEDGMENTS

I thank Tina Neal and one anonymous reviewer for their constructive editing of the original draft. This work was supported by the Alaskan Volcano Observatory through U.S. Geological Survey Grant 14-08-0001-0574.

## REFERENCES CITED

Aviation Week and Space Technology, 1986, Alaska air traffic disrupted by ash from volcano: v. 124, no. 14, p. 36.

Casadevall, T.J., in press, The 1989–1990 Eruption of Redoubt Volcano, Alaska: Impacts on aircraft operations: Journal of Volcanology and Geothermal Research.

Juhle, W., and Coulter, H.W., 1955, The Mt. Spurr eruption, July 9, 1953: Transactions of the American Geophysical Union, v. 36, p. 188–202.

Kienle, J., 1986, Augustine Volcano: Awake again?: Eos, Transactions of the American Geophysical Union, v. 67, p. 172–173.

Kienle, J., Davies, J.N., Miller, T.P., and Yount, M.E., 1986, The 1986 eruption of Augustine Volcano: Public safety response by Alaskan volcanologists: Eos, Transactions of the American Geophysical Union, v. 67, p. 580–582.

Kienle, J., and Shaw, G.E., 1979, Plume dynamics, thermal energy, and long distance transport of Vulcanian eruption clouds from Augustine Volcano, Alaska: Journal of Volcanology and Geothermal Resources, v. 6, p. 139–164.

Kienle, J., and Swanson, S.E., 1985, Volcanic hazards from future eruptions of Augustine Volcano, Alaska: University of Alaska Geophysical Institute, Report UAG R-275, 122 p.

Swanson, S.E., and Kienle, J., 1988, The 1986 eruption of Mt. St. Augustine: Field test of a hazard evaluation: Journal of Geophysical Research, v. 93, p. 4500–4520.

U.S. Air Force, 1955, History of the Alaskan Air Command, Part 2, natural phenomenon, Mt. Spurr eruption: Anchorage, Alaska Air Command, Elmendorf Air Force Base, p. 73–80.

———1976, History of the 21st composite wing: Anchorage, Alaska Air Command, Elmendorf Air Force Base, v. 1, 121 p.

Wilcox, R.E., 1959, Some effects of recent volcanic ash falls with especial reference to Alaska: U.S. Geological Survey Bulletin 1028–N, p. 409–476.

Yount, M.E., Miller, T.M., and Gamble, B.M., 1987, The 1986 eruption of Augustine Volcano, Alaska: Hazards and effects: U.S. Geological Survey Circular 998, p. 4–13.

VOLCANIC ASH AND AVIATION SAFETY:
Proceedings of the First International Symposium
on Volcanic Ash and Aviation Safety
U.S. GEOLOGICAL SURVEY BULLETIN 2047

# MITIGATION OF VOLCANIC ASH EFFECTS ON AIRCRAFT OPERATING AND SUPPORT SYSTEMS

*By* J.R. Labadie

## ABSTRACT

On 18 May 1980, Mount St. Helens erupted, covering 50 percent of Washington State with approximately 1 $km^3$ of ash. Government agencies, airports, utilities, and private corporations within the impacted areas were all forced to cope with ash deposits ranging in depth from 3 mm to 75 mm while maintaining essential services and carrying on normal activities. Volcanic ash is abrasive, mildly corrosive, conductive (especially when wet), and may carry a high static charge for up to 2 days. The ash is finely divided, easily entrained in the air by wind or vehicle movement, and may remain suspended for many minutes. Due to the combination of these qualities, volcanic ash is pervasive. Techniques for reducing the effects of volcanic ash are basically "low tech" and can be grouped into three broad categories: keeping the ash out, controlling what gets in, and disposing of the ash. Mitigation actions will be required on a continuous basis as long as ash is present. Effective mitigation depends on prior planning and preparation, mobilization of resources, and persistence.

## INTRODUCTION

This report addresses techniques for mitigating the effects of volcanic ash on selected categories of critical equipment. It is based on information developed and experience gained with volcanic ash fallout produced during the eruption of Mount St. Helens in the State of Washington.

On 18 May 1980, Mount St. Helens erupted, covering 50 percent of Washington with approximately 1 $km^3$ of ash. Although 19 of 39 counties in the State received some volcanic ash, five eastern counties were severely impacted. Government agencies, airports, utilities, and private corporations were all forced to cope with ash deposits ranging in depth from 3 to 75 mm while maintaining essential services and continuing normal activities. A review of the available literature (damage survey reports, newspaper and magazine articles, and Federal and State agency advisories) formed the basic groundwork for this report. In-depth interviews with equipment users, service companies, airport operators, utilities, and others impacted by the ash elicited detailed information on ash-related damage and on methods of dealing with the ash. Research for this article was originally conducted under the sponsorship of the Air Force Office of Scientific Research and the Defense Advanced Research Projects Agency (Labadie, 1983).

## EFFECTS OF VOLCANIC ASH

Volcanic ash is abrasive, mildly corrosive, and conductive (especially when wet) and may also carry a high static charge for up to 2 days after being ejected from a volcano (Heiken, this volume). The ash is easily resuspended by wind or vehicle movement and may remain suspended for many minutes. Due to the combination of these qualities, volcanic ash is pervasive. It can penetrate all but the most tightly sealed enclosures, and it can be very difficult to remove from electronic components.

Ash deposited on electronic components can cause arcing, short circuits, and intermittent failures because it is conductive. High-voltage circuits and components are especially vulnerable. Ash dampened by rain can cause arcing, flashovers, and pole fires on electrical-distribution systems. Resulting outages may hamper mitigation efforts that require electrical power.

The ash easily absorbs water and can weigh up to 1,400 $kg/m^3$; water-laden ash may collapse or damage flat roofs. Wet ash is very slippery and can cause traction problems. Dry ash, when blown into the air, reduces visibility and piles up on roads, runways, and taxiways. Ash must be physically removed and controlled after removal to prevent reentrainment.

Moving parts are subject to abrasion damage from volcanic ash. The ash is attracted to and entrained in any exposed lubricant; thus, abrasion effects will continue even after the bulk of the ash has been removed. Bearings, brakes, and transmissions will wear out very quickly. Computer disks, disk drives, and heads are very sensitive to abrasion and are easily damaged by ash. In addition, ash adhering to

painted or polished surfaces will scratch and scour the surface unless it is removed carefully.

Filters on air handling and computer systems may become clogged with ash to the point that airflow is completely stopped, leading to equipment overheating. Clogged filters may collapse and severely contaminate the internal environment. Additional filtration can reduce ash penetration, but only at the cost of reduced airflow to critical equipment. Filtration systems that incorporate centrifugal separators can handle ash much more easily.

## VOLCANIC ASH MITIGATION

Techniques for reducing the effects of volcanic ash can be grouped into three broad categories: (1) keeping the ash out, (2) controlling what gets in, and (3) disposing of the ash. These categories are more illustrative than discrete, and some mitigation techniques will apply in all three cases. Mitigation actions will be required on a continuous basis as long as ash is present. Settled ash is easily reentrained, and a 2-mm layer can be as troublesome as a 50-mm layer.

The most effective technique for reducing ash-related damage or upset to equipment is to avoid using the equipment: shut down, close up, keep inside, or seal the area until the ash can be removed. This tactic is acceptable only for short periods of time because operations must be resumed at some point. In any case, disposal techniques will not eliminate all of the ash. A residue will remain on the ground and will be blown into the air by wind, passing vehicles, and aircraft takeoffs. Thus, an accelerated and intensive program of inspection, maintenance, cleaning, and monitoring will be necessary during and after the main part of ash deposition.

Cleaning the ambient air—and keeping it clean—is the key to reducing operation and maintenance problems. Blowing ash off of a circuit board is useless if the ash is fine enough to remain suspended for several minutes. The difficulty of attempting to perform maintenance tasks in an already ash-contaminated atmosphere is obvious. "Clean-room" procedures can be used to isolate an area and keep it free of ash, but only under ideal circumstances. Some equipment—aircraft engines, for example—are too large for such treatment. Tents or tarps can be used to reduce gross contamination. However, fine particles can penetrate very small openings and seams; it is this property that makes fine particles so damaging to critical equipment.

Some mitigation procedures may cause additional problems or may actually be counterproductive, depending on the circumstances. For example, adding filtration to a computer system will reduce the amount of ash contamination, but it will also decrease the air flow. The resulting rise in temperature may change the operating characteristics of sensitive components or even cause damage. Adding a larger fan would increase the air flow, but not all computers, especially smaller units, can be easily modified. Another example is the use of moisture to control ash. Wetting carpets will increase relative humidity and help to keep the ash down; however, wet or even damp volcanic ash is conductive.

No single technique will be absolutely effective; a combination of techniques has been found to provide the best results for managing volcanic ash. Constant monitoring and reassessment of ash effects and the mitigation process will be required to achieve the most effective balance between operational requirements and the desired level of damage limitation. The following sections summarize ash mitigation techniques for selected aircraft and support systems.

### AIRCRAFT SYSTEMS

The basic mitigation tactic to protect aircraft systems is avoidance of exposure to ash. The airports and airfields surveyed after the Mount St. Helens eruption simply shut down for the duration of the ash problem or until the ash had been removed. Airlines rerouted traffic away from ash-impacted airports.

Sealing aircraft seams, ports, vents, and other openings with duct tape will keep out the bulk of the ash, especially if the aircraft is under cover. Maintaining positive pressure within aircraft components would help to keep ash out, but it is difficult, if not impossible, to pressurize an aircraft on the ground without damaging ground equipment. Techniques include:

- Blow or vacuum ash before washing; otherwise, ash tends to flow into ports, vents, or control surfaces.
- Flush or wash residue. Do not scrub or sweep.
- Wash gear, underside, air-conditioning intakes, and engines.
- Check pH of aircraft/engine surfaces for acidity.
- Neutralize acidic residue by adding petroleum-based solvent to wash water.

All of the above techniques require large amounts of time, manpower, and equipment. All have significant effects on the level and scope of continued operations. These techniques were tried under conditions of greatly reduced operating levels; however, there is some question as to their effectiveness during normal (or near-normal) operations. For example:

- Sealing an aircraft would take 4–5 hours, and removing all seals and tape would take 1–2 hours. It is very hard to seal an aircraft completely because of numerous ports, vents, seams, and joints.
- Ash buildup in or around hatch seals could cause pressurization problems.
- Fuel tank vents must be open during loading, unloading, and transfer of fuel. If vents are plugged with ash, or if sealed, the tank could collapse. A 4–5 psi vacuum is sufficient to cause collapse.

## RUNWAYS

If aircraft operations are not suspended, runways must be continually cleaned as ash is resuspended by wind, aircraft takeoff, and ground vehicle movement. There is some disagreement on the proper use of water in cleaning runways. Some sources felt that water turns the ash to sludge (or causes it to harden), whereas others found it impossible to control the ash without wetting it first. Open-graded (popcorn surface) runways are to some extent self-cleaning because the engine blast on takeoff will blow ash out of crevices. Basic techniques include:

- Wet ash with water trucks,
- Blade into windrows,
- Pick up with belt or front-end loaders,
- Haul to dump areas, and
- Sweep and flush residue.
- Sweep/vacuum ash first, then flush with water (best for ramps, etc.).
- Push ash to runway edge and plow under or cover with binder such as Coherex or liquid lignin.
- Install sprinklers along edges of runway to control resuspension of ash from aircraft engine blast or wing-tip vortices.
- Keep residue wet on taxiways and ramps.

## LANDING AIDS AND AIR TRAFFIC CONTROL

Protection of landing aids and air traffic control systems will require periodic cleaning, maintenance, and monitoring. Also, turning off unnecessary equipment will reduce exposure. Exposed light and indicator systems, radar antennas, and any equipment that requires cooling air are especially vulnerable to ash contamination and damage. Interruption of commercial power supplies will require backup generators, which are also vulnerable to ash damage. Techniques include:

- Replace antennas that have Teflon insulators. Because ash is hard to remove and will cause shorting, ceramic insulators should be used,
- Seal relay boxes and remove indicator units and light systems to prevent ash entry,
- Increase cleaning and maintenance of systems that cannot be sealed or that require cooling air,
- Vacuum or blow ash out and clean relays with contact cleaner,
- Use high-pressure water wash on exposed antenna rotor bearings and then relubricate,
- Cover exposed joints, seams, and bearings,
- Seal buildings, control access, vacuum shoes and clothes, and
- Reduce operating levels: shut down unused equipment, reduce broadband displays to a minimum, and reduce cooling and power consumption.

## GROUND SUPPORT EQUIPMENT

The consensus of those interviewed is that ground support equipment is the key to flight operations. If ground support equipment is unserviceable because of ash, aircraft cannot be launched. Unfortunately, there are more problems than solutions in the ash contamination of ground equipment.

Gas turbines, air compressors, and air conditioners operate by ingesting large volumes of air. This equipment has only coarse filtration (or none at all), and extra filtration cannot be added without impacting operation. Using air conditioners to pressurize aircraft compartments would only blow ash into the aircraft and ruin the air conditioners in the process. Techniques include:

- Constant cleaning and maintenance,
- Do not wash equipment, because water turns ash to sludge and washes it into the equipment,
- Vacuum equipment,
- Change oil and filters more often, and
- Change design to include better filtration.

## COMPUTER SYSTEMS

The most widely advised damage-prevention tactic is to shut down all computer and electronic systems until the ash has been completely removed from the area and from the equipment. Computer heads and disks, and any high-voltage circuits, are especially vulnerable to ash upset and damage. Ash on digital circuits will not cause much of a problem because of the low voltages involved. High-voltage or high-impedance circuits are very vulnerable to leakage caused by semiconductive ash. Ash that is acidic is conductive as well as corrosive. Continual cleaning and aggressive protection of computer systems should allow for continued operation in all but the heaviest ash fallout. Techniques include:

- Clean and condition surrounding air to keep ash out of equipment.
- Cotton mat filters used in clean rooms were found to be best for filtering particles, but they reduce air flow. A solution is to use larger fans to maintain required air flow. Rack-mounted equipment can be modified to add a larger fan, but smaller instruments or components with a built-in fan would require a design change to increase fan capacity.
- Use fluted filters as a compromise; this increases surface area, but reduces air flow by only about 20 percent.
- Humidifying ambient air (e.g., wetting carpets) will help to control ash reentrainment.
- Ash on equipment can be blown out with compressed air. If the air is too dry, static discharge could damage sensitive components (e.g., integrated circuits). If the air is too damp, the ash will stick. Relative humidity of 25–30 percent is best for compressed air.

- Cleaning with a pressurized mixture of water and detergent and using a hot-water rinse is quite effective; however, this process requires at least partial disassembly.
- Ash may have a high static charge and be hard to dislodge, thus requiring brushing to dislodge particles.
- Accelerate filter change; use prefilters.
- Change to absolute filters; these will keep out particles down to 1 μm and smaller.
- Keep computer power on for filtration, but do not operate, especially disk drives.
- Maintain room-within-a-room configuration, restrict access, recirculate air, and accelerate cleaning of the critical area.

### RADAR AND OPTICAL SYSTEMS

Most radar equipment in the heaviest ash-fall areas was shut down for the duration of severe ash contamination. Thus, few problems were recorded aside from cleanup and control of residual ash. The simplest mitigation tactic is to cease operations. Techniques include:

- Repair and clean high-voltage circuits.
- Wash antenna rotor bearings, relubricate, and cover exposed bearings.
- Ash on optical components should be blown away or washed with copious amounts of water. Do not wipe, brush, or rub, as this will abrade the optics.
- Take care not to wash ash into optical-instrument mounts on aircraft (e.g., sextant).
- Turn off nonessential radar equipment to reduce cooling load and power requirements.
- Transfer radar coverage to other facilities; combine sectors.
- Remove and replace camera bearings and clean gear drives.
- Protect video tape from ash because it will cause "drop-outs" and scratches.

## PLANNING FOR ASH MITIGATION

Techniques for reducing the impacts of volcanic ash are basically "low tech" and depend more on procedural approaches than on technical fixes. Also, they are quite labor and resource intensive. Normal stock of daily-use items such as filters, lubricants, spare parts, cleaning supplies, etc., may be expended much faster than they can be replaced through the normal reordering process. Prior planning is necessary to reduce the severity of ash effects. Planning actions include:

- Conduct a vulnerability analysis of equipment and facilities to determine which would be most impacted by ash, which are adequately protected, and which need long-term or expedient modification.
- Develop a priority list of facilities that must be kept in operation versus those that can be closed or shut down for the duration of ash fall.
- Ensure hazard-alert and information channels are properly maintained with the U.S. Geological Survey (USGS), Federal Emergency Management Agency (FEMA), the National Weather Service (NWS), local news media, and State and local governments.
- Establish plans and procedures for alerting and notification, reduced operations, accelerated maintenance, protection of critical facilities, and cleanup and disposal.
- Alert air traffic controllers and airport operations personnel to notify aircraft as soon as volcano "watch" and "warning" notices are received. Normal air traffic and weather radars cannot detect lower, but potentially hazardous, ash-density levels; therefore, relatively large "keep-out zones" should be established at night or during bad weather once the warning notice is issued. Personnel should also be alerted to the existence of fallout beneath the clouds and severe lightning conditions, etc.
- Stockpile spare parts for critical equipment, filters, and cleaning and disposal equipment.
- Plan for extended cleanup and maintenance activities including 24-hour operations, augmentation of the work force, and training of cleanup crews.
- Ensure that sufficient water and backup power is available to support cleanup operations, should normal supply sources fail.

Ash cleanup operations may continue for weeks or months if multiple eruptions occur. Effective mitigation of volcanic ash effects depends on prior planning and preparation, mobilization of resources, and persistence.

## REFERENCE CITED

[In addition to the cited reference, this report was based on many interviews with equipment users, service companies, airport operators, and utilities. Information pertaining to these interviews may be available from the author—see Authors' Address List section at the end of this volume.]

Labadie, J.R., 1983, Teal Granite: Mitigation of volcanic dust effects: IRT Corporation, [final report prepared for U.S. Air Force Office of Scientific Research and the Defense Advanced Research Projects Agency], 29 p.

VOLCANIC ASH AND AVIATION SAFETY:
Proceedings of the First International Symposium
on Volcanic Ash and Aviation Safety
U.S. GEOLOGICAL SURVEY BULLETIN 2047

# IMPACT OF VOLCANIC ASH FROM 15 DECEMBER 1989 REDOUBT VOLCANO ERUPTION ON GE CF6-80C2 TURBOFAN ENGINES

*By* Zygmunt J. Przedpelski *and* Thomas J. Casadevall

## ABSTRACT

The 1989–90 eruptions of Redoubt Volcano, Alaska, and the near tragedy on 15 December 1989 of KLM flight 867, a Boeing 747-400 aircraft powered by General Electric (GE) CF6-80C2 engines, underscore the threat to aircraft safety from volcanic ash clouds.

An eruption of Redoubt at 10:15 a.m. Alaska Standard Time (AST) produced an ash-rich eruption column that climbed to approximately 40,000 ft altitude. Wind speeds at high altitudes at the time were 100 knots from south-southwest. At 11:46 a.m., KLM flight 867 entered the volcanic ash cloud at approximately 25,000 ft altitude, 150 nautical miles northeast of Redoubt. Immediately the aircrew increased power and attempted to climb out of the ash cloud. Within 1 minute, the four engines decelerated below idle. The aircraft descended approximately 13,000 ft before the crew restarted the four engines and resumed flight to Anchorage. Even though there were no injuries to passengers, the damage to engines, avionics, and aircraft structure from this encounter was significant. Similar engine thrust loss and engine and aircraft damage was experienced by two Boeing 747 aircraft during 1982 volcanic eruptions of Galunggung Volcano in Indonesia.

The primary cause of engine thrust loss in these events was the accumulation of melted and resolidified ash on the stage-1-turbine nozzle guide vanes. These deposits reduced the effective flow of air through the engine causing compressor stall. Reduction of thrust level while in an ash cloud significantly reduces the rate of engine-performance degradation.

## STATEMENT OF PROBLEM

The loss of thrust on all engines during an approximately 1-minute exposure to the Redoubt volcanic ash cloud could have resulted in a major tragedy. Fortunately the alert flight crew was able to restart all engines and make a safe landing at Anchorage. The events preceding and subsequent to the cloud encounter and the engines' response and physical conditions were analyzed to identify procedures that would reduce the probability of future occurrences of similar events, which threaten flight safety. Additional discussion of the Redoubt activity and its effects on aircraft operations and airplane damage my be found in reports by Brantley (1990), Campbell (1991), Casadevall (in press), and Steenblik (1990).

## METHODS OF STUDY

The following data sources were used to reconstruct the event, to establish the specific cause(s) of thrust loss and to recommend appropriate preventive/corrective actions:

- Interviews with and statements from the flight crew of KLM flight 867.
- Tape recordings and transcripts of radio communications between air traffic controllers and KLM flight 867 and other flights in the Anchorage area prior to and during the event.
- Forecasted and recorded wind aloft data.
- Digital flight-data recorder (DFDR), aircraft condition monitoring systems (ACMS), and the non-volatile memory (NVM) of the engine full-authority digital electronic controls (FADEC).
- Event descriptions and findings from other aircraft–volcanic cloud encounters.
- CF6-80C2 engine steady-state and transient operating characteristics with normal and degraded component efficiencies.
- On-site (Anchorage) external inspection of the aircraft and all engines and borescope inspection of engines 1 and 2.
- Complete analytical disassembly and inspection of engine 1 at the KLM maintenance facility at Schiphol Airport, Amsterdam.
- General Electric experience with engines exposed to sand/dust environment in the field and during controlled factory tests.
- Analysis of samples of volcanic ash recovered from the four engines.

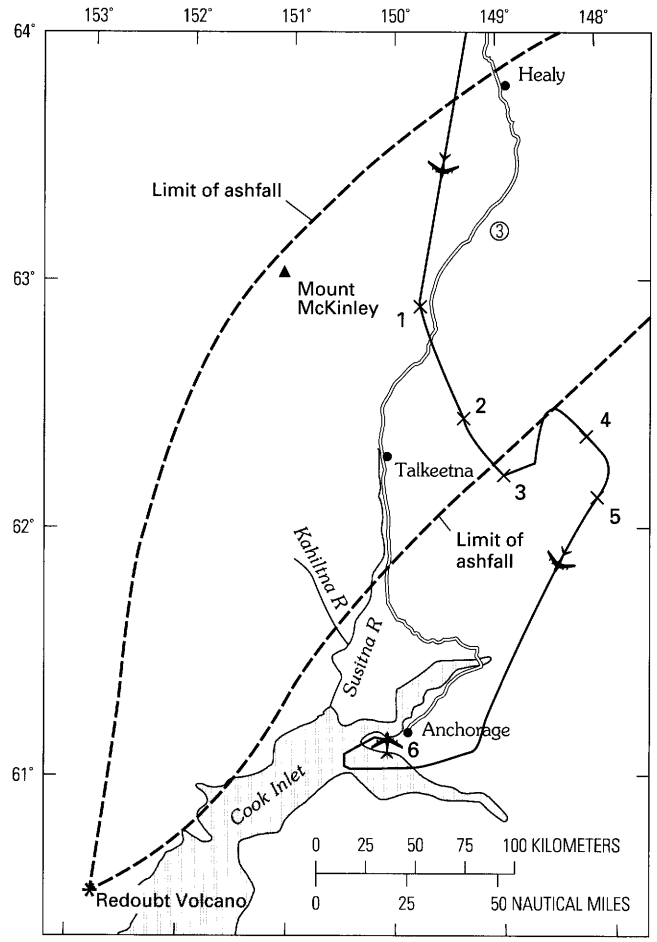


**Figure 1.** Map showing flight path of KLM 867 (heavy solid line) and limits of detectable ash fall (heavy dashed lines) from 15 December 1989 eruption of Redoubt Volcano. Numbers on map, explained below, are keyed to principal events for KLM flight 867. AST, Alaska Standard Time. 1, 11:40 AST, airplane begins descent from 35,000 ft; alters course to avoid ash cloud. 2, 11:46 AST, airplane encounters ash cloud at 25,000 ft. 3, 11:47 AST, airplane loses power on all four engines after climbing to 27,900 ft. 4, 11:52 AST, airplane engines 1 and 2 restart at 17,200 ft. 5, 11:55 AST, airplane engines 3 and 4 restart at 13,300 ft; flight is resumed to Anchorage. 6, 12:25 AST, airplane lands at Anchorage International Airport. Map modified from Casadevall (in press). Flight-route data provided by National Transportation Safety Board (1991) and FAA Flight Standard Division, Anchorage. Ash-fall data modified from Scott and McGimsey (in press).

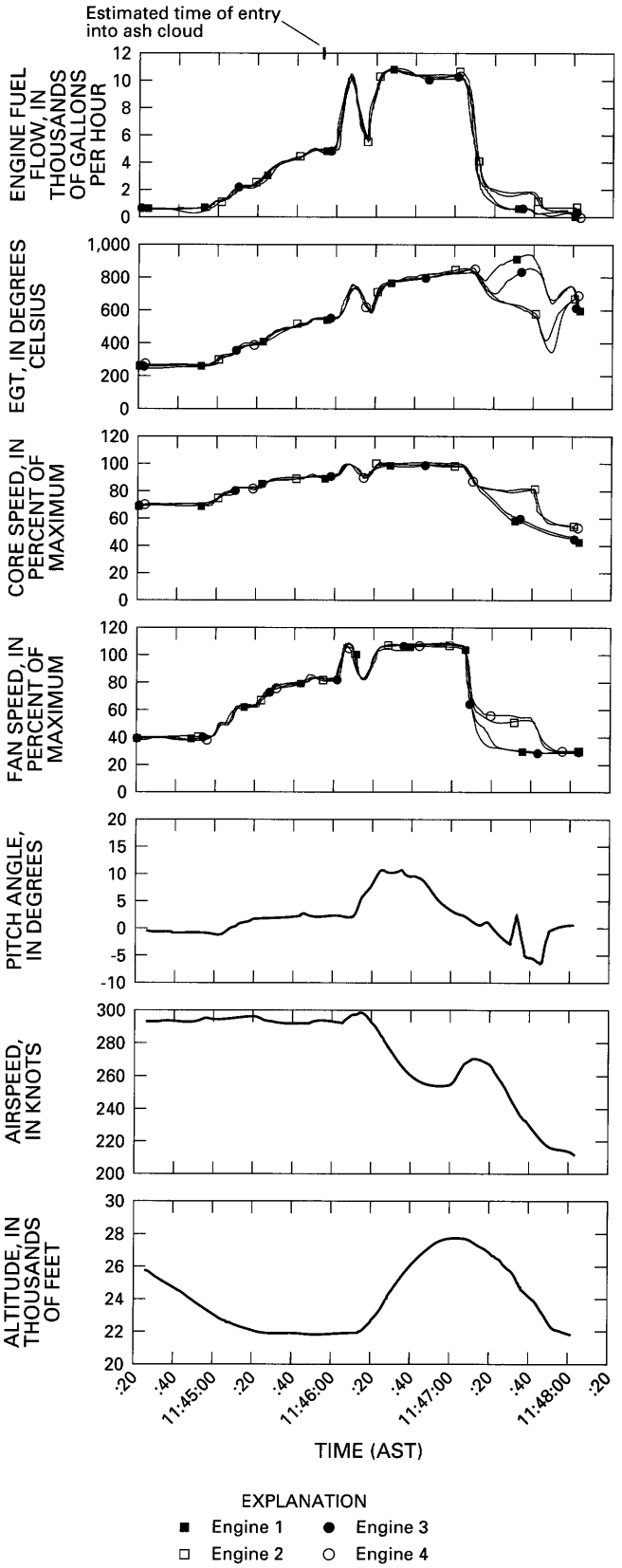


**Figure 2** (facing column). Encounter of KLM flight 867 with ash from Redoubt Volcano, 15 December 1989: engine and aircraft parameters (engine fuel flow, exhaust-gas temperature (EGT), core speed (N2), fan speed (N1), pitch angle, airspeed, and altitude) from cloud entry to shutdown. AST, Alaska Standard Time.

**Figure 3.** Dark, glassy deposits of remelted volcanic ash on leading edge of stage-1 high-pressure-turbine (HPT) nozzle guide vane (NGV).

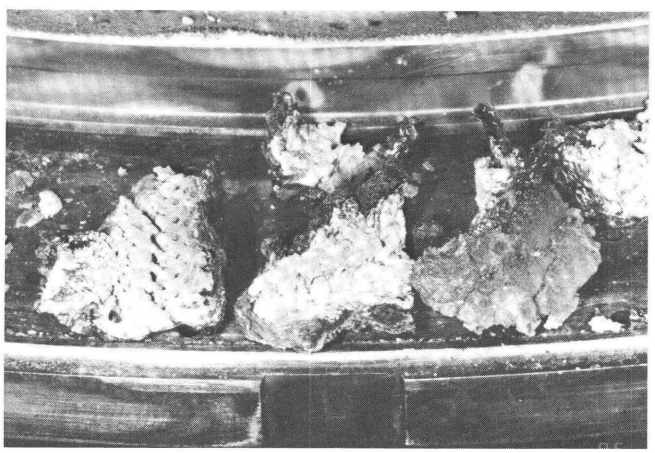

**Figure 4.** Leading-edge deposits dislodged during disassembly of stage-1 high-pressure-turbine (HPT) nozzle guide vanes (NGV's).

## RESULTS AND OBSERVATIONS

A major eruption of Redoubt Volcano occurred at 10:15 a.m. AST on 15 December 1989 and lasted for about 1 hour. This was the third large eruption from the volcano on this day (Brantley, 1990). At 11:46 a.m. AST, while leveling off at an altitude of 25,000 ft, KLM 867 entered a heavy volcanic cloud. Maximum power climb was selected and approximately 1 minute later, after climbing to approximately 27,900 ft, all engines decelerated. Engines 1 and 3 decelerated to sub-idle core rotor speed (N2), while engines 2 and 4 settled down at 80 percent N2 for approximately 20 seconds before decelerating to sub-idle N2. The time sequence of events is shown on the annotated aircraft flight path in figure 1. Aircraft and engine response during this critical period is shown in figure 2.

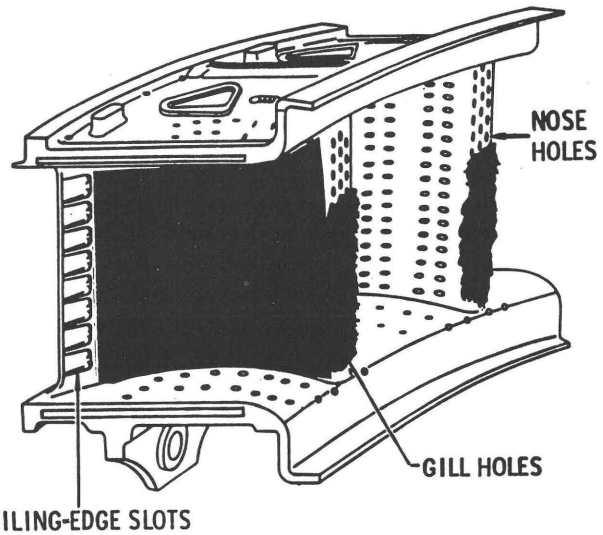


**Figure 5.** Sketch of deposits on stage-1 HPT nozzle guide vanes, based on borescope inspection of engine 1.

The location of the ash cloud (154 nautical miles from Redoubt on 217° true heading) was consistent with the forecasted and pilot-reported winds aloft and with the ash release at the beginning of the eruption cycle. Prior to the encounter, the exact location of this cloud was not known by the crew of KLM 867. Pilot reports (Pireps) and radar data available to Anchorage air traffic controllers indicated either the presence of more than one ash cloud and (or) a large dispersion of the main cloud resulting from the high velocity gradient of winds aloft as a function of altitude.

The fire warning bell and the displayed message "CARGO FIRE FWD" occurred shortly after engine deceleration and was interpreted by the Captain to be a false message. This was confirmed by inspection, which showed no evidence of compartment fire.

The engines' operation during the high-power climb was consistent with rapid reduction of the stage-1 nozzle guide vane (NGV) flow area and associated reduction in high-pressure-turbine (HPT) efficiency. Approximately one-half of the maximum deterioration was still present following the successful restarts. Visual inspection of the number 1 engine revealed thick deposits of melted and resolidified ash material on some of the stage-1 NGV's (fig. 3). These deposits were brittle at room temperature, and many pieces fell off during engine transportation and disassembly (fig. 4). The remaining deposits could be easily removed by hand. It was inferred that these deposits built up to maximum just prior to engine deceleration and gradually became dislodged during the start attempts and during subsequent engine operation. Based on borescope inspections conducted at Anchorage, approximately 40 percent of the NGV's were still covered by thick deposits after landing (fig. 5).

Engine fuel levers were moved to the "OFF" position and engine restarts were initiated immediately after the loss

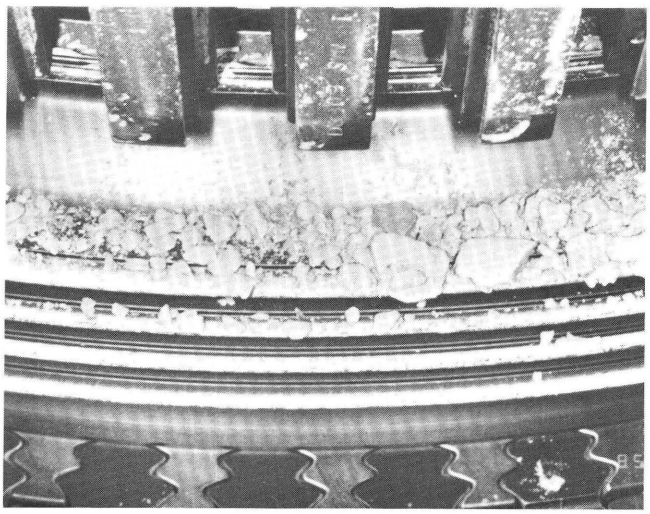

**Figure 6.** Accumulation of unmelted volcanic ash in the high-pressure-turbine rotor.

of power. Engines 1 and 2 were successfully started at an altitude of 17,200 ft (after five or six attempts). Engines 3 and 4 were successfully started at an altitude of 13,300 ft (after eight or nine attempts). "Autostart" mode was used and at least one start appeared to have been correctly terminated by the FADEC start/stall logic just before being terminated by the crew. The windmilling N2 was in excess of 30 percent, and the entire start sequence varied from approximately 30 seconds to 60 seconds during each attempt.

The engines did not overheat during deceleration or during subsequent aborted starts. The highest exhaust-gas temperature (EGT) of 930°C was recorded on engine 1 during the initial deceleration. There was no unusual thermal distress observed during disassembly of this engine.

The general condition of all hardware in engine 1 was consistent with the performance level recorded prior to landing. In addition to the remains of the heavy, stage-1 nozzle deposits, the following performance-related observations were made:

- No measurable erosion or other damage to the low-pressure system (fan, booster, and low-pressure turbine (LPT)).
- Minor compressor erosion, most pronounced in the mid and aft rotating stages.
- Stage-1 high-pressure-turbine (HPT) blade tips were "ground off" (approximately 0.060 inches of tip material was missing).
- Buildup of hard material on stage-1 HPT shrouds.
- Thin but hard deposits on stage-1 HPT blade pressure surfaces.
- Engine 1 inspection indicated that there was no significant plugging of any of the HPT cooling circuits; however, there was a heavy, fine, powdery ash buildup within the HPT rotor cavities (fig. 6).

The general physical conditions (distress and presence of ash deposit) of all four engines were very similar. The compressor-discharge-pressure ($P_{S3}$) sensing line on engine 1 was unobstructed. The $P_{S3}$ readings obtained from the ACMS system during and after the deceleration indicated that $P_{S3}$ signals to the engine electronic controls were unrestricted. The DFDR was not recording for 2 minutes 5 seconds after the initial engine deceleration when all four electrical generators dropped off line. The engine FADEC remained powered and was controlling the engines during that time and provided valuable information stored in the NVM.

# CONCLUSIONS

## SPECIFIC

Engine deceleration from high power to below idle was initiated by high-pressure-compressor (HPC) stall. The stall margin loss was caused by stage-1 HPT nozzle effective-flow-area restriction and associated HPT efficiency loss. The stage-1 HPT bucket-clearance increase was caused by local buildup of hard, resolidified ash material on the shroud surface (fig. 7), which ground off the bucket-tip material.

The stage-1 nozzle effective-flow-area restriction was caused by resolidification and buildup of melted ash particles on the leading edges and pressure surfaces of the individual NGV's. This effective-flow-area restriction was estimated to be 8 percent. This buildup also resulted in an increase in pressure loss across the nozzle and a reduction in HPT efficiency. Total HPT efficiency loss, including the stage-1 HPT blade-clearance increase was estimated to be 7 percent. High-pressure-compressor (HPC) erosion (fig. 8), caused by ingestion of ash particles, resulted in minor stall-margin decrease and compressor-efficiency loss estimated to be 1 percent.

The lowering of the temperature following manual fuel supply cut-off increased the viscosity and brittleness of the built-up material. The thermal and pressure/velocity transients associated with the fuel off/on/off cycle dislodged some of the nozzle deposits. The density of these deposits was low, and, consequently, there was no downstream airfoil

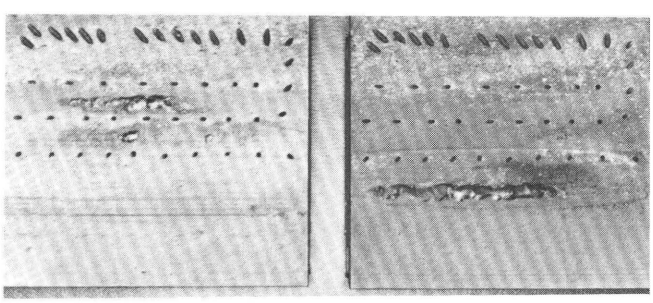

**Figure 7.** Deposits of solidified, remelted ash on stage-1 high-pressure-turbine shrouds.

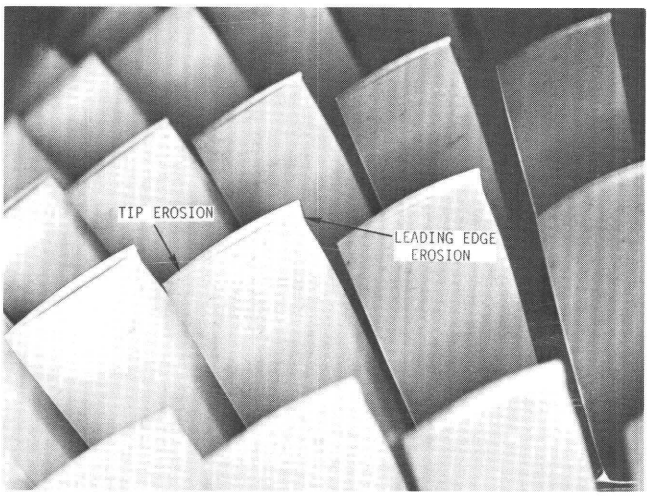


**Figure 8.** High-pressure-compressor (HPC) blades, showing erosion of leading edges and blade tips.

damage. Successful starts were achieved after a portion of these deposits were dislodged.

During the starts, "autostart" mode was used and at least one start appeared to have been correctly terminated by the FADEC start/stall logic. Most of the starts, however, were terminated by the crew overriding the autostart sequence and thus negating the adaptive automatic restart features of the control system while, in some of these cases, the engine or engines appeared to be on the way to a successful start (fig. 9). Continued engine operation, following successful restarts, dislodged additional stage-1 deposits. Permanent engine performance degradation was the result of compressor erosion and the stage-1 HPT blade-clearance increase.

The absence of any thermal damage to the engines was the result of the combination of decisive and skillful actions of the crew and the responsiveness and built-in protection in the FADEC system.

The presence of ash particles set off the fire warning bell in the cargo compartment and displayed the "CARGO FIRE FWD" message (the cargo-compartment fire detector is a smoke/particle detector—unlike the engine-compartment detector, which is activated by temperature).

The ash concentration at 25,000 ft altitude was estimated at 2 g/m$^3$, based on the rate of nozzle-deposit buildup compared to the rates measured during engine tests conducted by Calspan (Dunn and Wade, this volume).

Ash particles exiting the fan air stream ranged in size from 10 to 100 microns and most closely represent the size of particles encountered by KLM 867 in flight. The particles found within HPT passages, which were believed to be representative of the size distribution entering the combustor, were typically 6–10 microns in size. The ash contained some volcanic-glass material with a melting point of 1,200°C. This material is considered to be responsible for rapid buildup of deposits on the stage-1 NGV's; however, components of the

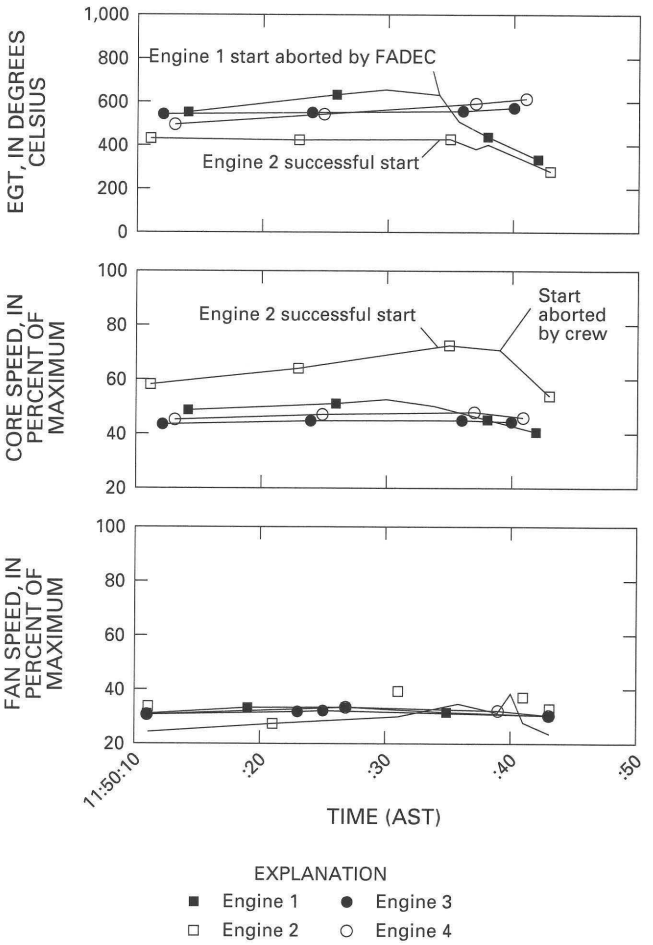


**Figure 9.** Encounter of KLM flight 867 with ash from Redoubt Volcano, 15 December 1989: engine parameters (exhaust-gas temperature (EGT), core speed (N2), and fan speed (N1)) during first recorded restart attempt. AST, Alaska Standard Time; FADEC, full- authority digital electronic controls.

ash with higher and lower melting points were also present in the NGV deposits. The unmelted particles adhered to the semi-molten layer of glassy material on stage-1 NGV's (Casadevall and others, 1991).

## GENERAL

Relatively "new" (within hours of eruption) volcanic clouds contain concentrations of ash that can cause complete loss of engine power in approximately 1 minute when the engine is operating at combustor-discharge temperatures in excess of the melting temperature of the ash. The primary mechanism of engine power loss during these high-engine-power and high-ash-concentration exposures is the buildup of melted and resolidified ash material on the stage-1 NGV's, resulting in flow-area reduction, turbine-efficiency loss, and compressor stall. Permanent damage to the engine under these conditions is limited if the engine is

not exposed to overtemperature during the stall or subsequent restart attempt(s).

Time, altitude, and airspeed permitting, the engine can be restarted by the fuel off/on/off cycles, breaking up the deposit material, which is brittle at low temperatures. FADEC with built-in start/stall/overtemperature logic in the autostart mode simplifies and speeds up the restart sequence and prevents further engine damage.

Reduction of engine power to flight idle upon inadvertent entry into a volcanic cloud will eliminate the stage-1 NGV buildup because the combustor-discharge temperature at idle is below the melting point of volcanic-ash constituents.

Operation in an ash cloud will result in compressor airfoil and flowpath erosion and eventual compressor stall. Compressor stall is an airflow discontinuity resulting in loss of thrust and internal temperature increase. The time required to reach this condition is at least an order of magnitude longer than the time to produce significant ash accumulation on the NGV's at the high-power level (assuming the same ash concentration). Compressor erosion is permanent, and engine operability and available thrust will be adversely affected. The compressor-erosion rate can be significantly reduced by decreasing the core engine rotational speed (N2).

Damage mechanisms in the longer term include the restriction of HPT cooling circuits, which may result in hot-section distress, and the contamination of the lubrication system, which may result in premature bearing distress. Another possible damage mechanism is the restriction of air-flow passages around the fuel nozzles—this leads to poor fuel atomization and the inability to start the engine.

# SAFETY RECOMMENDATIONS

## CREW ACTIONS

Entering into a volcanic ash cloud can be recognized by St. Elmo's Fire/corona discharge (night or day), dust and smell in the cockpit/cabin, and outside darkness (day time only) (Campbell, this volume). If a volcanic ash cloud is inadvertently entered, disconnect the autothrottle, reduce power to flight idle, increase compressor air bleed to maximum possible, and exit the cloud as quickly as possible. Bleed air is air extracted from the compressor for use in various aircraft systems. Increased extraction increases stall margin. There is no universal "best" procedure for exiting the cloud; however, generally a 180° turn will result in the fastest cloud exit. Avoid rapid throttle movements (up or down) to prevent a possible compressor stall (Campbell, this volume; Miller, this volume).

If power reduction to flight idle is not possible, reduce power to the lowest level consistent with other requirements and exit the cloud as quickly as possible. Monitor exhaust-gas temperature as the primary engine instrument indicating ash accumulation at the stage-1 high-pressure-turbine nozzle guide vanes. If EGT exceeds the red line or increases rapidly, the throttle should be closed and fuel levers moved to "OFF" to minimize engine thermal damage and increase the probability of successful restart.

Restarts should be initiated immediately. More than one attempt may be required to obtain a successful start. Autostart should be used (if available) because it simplifies the starting procedure and provides engine overtemperature protection. Compressor bleed should be turned on during restarts and during subsequent engine operation to maximize stall margin. Following restart, the engine performance/stall margin/EGT may improve with time, but it will not reach the pre-ash-encounter level. Rapid throttle movement and maximum-power operation should be avoided, if possible, because stall margin is decreased and some cooling-circuit plugging may be present.

## REGULATORY AGENCIES

The greatest threat to aircraft and engines is presented by "new" clouds (within hours of eruption) that contain large concentrations of ash particles. The communication network between volcanic-activity-monitoring agencies and air-traffic-control agencies should be improved so that volcanic activity of the type that can result in substantial release of ash into the atmosphere can be communicated immediately to the affected air crews. In early phases following the eruption, the cloud position should be continuously tracked at all altitudes utilizing winds aloft, pilot reports, and other available means. Appropriate air-traffic-control measures should be taken to provide aircraft-cloud separation.

The ash-particle size distribution and concentration in volcanic eruption clouds should be documented. In addition, engine and (or) combustor tests should be sponsored by the Federal Aviation Administration (FAA) to establish threshold values for "safe" levels of ash concentration and the "safe" range of combustor temperature. This information, combined with updated dispersion and theoretical fallout models (and with improved cloud tracking) can establish when an ash cloud ceases to be a flight hazard. These efforts will enhance aviation safety and reduce air traffic delays resulting from volcanic activity.

# ACKNOWLEDGMENTS

During this investigation, many GE engineers contributed to the hardware reviews and engineering analysis. The following individuals, outside the GE organization, provided background data and constructive suggestions that made this report possible: Captain K.F. van der Elst, Commander of KLM flight 867; Mr. Roy C. Daw, NTSB (National Transportation Safety Board), Anchorage Regional Office, Alaska; and Dr. Michael G. Dunn, Arvin/Calspan, Buffalo, New York. In addition, special thanks go

to the KLM maintenance personnel at Schiphol Airport who performed the disassembly and inspections of the engines involved in this event.

## REFERENCES CITED

Brantley, S.R., 1990, The eruption of Redoubt Volcano, Alaska, December 14, 1989–August 31, 1990: U.S. Geological Survey Circular 1061, 33 p.

Casadevall, T.J., in press, The 1989–1990 eruption of Redoubt Volcano, Alaska: Impacts on aircraft operations: Journal of Volcanology and Geothermal Resources.

Casadevall, T.J., Meeker, G.P., and Przedpelski, Z.J., 1991, Volcanic ash ingested by jet engines [abs.], *in* Casadevall, T.J., ed., First International Symposium on Volcanic Ash and Aviation Safety, Program and Abstracts: U.S. Geological Survey Circular 1065, p. 15.

Campbell, E.E., 1991, 747-400 airplane damage survey following a volcanic ash encounter [abs.], *in* Casadevall, T.J., ed., First International Symposium on Volcanic Ash and Aviation Safety, Program and Abstracts: U.S. Geological Survey Circular 1065, p. 14.

National Transportation Safety Board [NTSB], 1991, Aircraft Accident Report ZAN ARTCC #100, KLM 867, H/B74F December 15, 1989 2048 UTC: unpub. report, 726 p.

Scott, W.E., and McGimsey, R.G., in press, Character, mass, distribution, and origin of tephra-fall deposits of the 1989–1990 eruption of Redoubt Volcano, south-central Alaska: Journal of Volcanology and Geothermal Research.

Steenblik, J.W., 1990, Volcanic ash: A rain of terra: Air Line Pilot, June/July 1990, p. 9–15, 56.

VOLCANIC ASH AND AVIATION SAFETY:
Proceedings of the First International Symposium
on Volcanic Ash and Aviation Safety
U.S. GEOLOGICAL SURVEY BULLETIN 2047

# ECONOMIC DISRUPTIONS BY REDOUBT VOLCANO: ASSESSMENT METHODOLOGY AND ANECDOTAL EMPIRICAL EVIDENCE

*By* Bradford H. Tuck *and* Lee Huskey

## ABSTRACT

The eruptions of Redoubt Volcano in 1989–90 imposed significant economic costs on Alaska residents, airlines and other businesses serving Alaska, government agencies, and travelers going to or coming from Alaska. This paper presents a set of principles, or guidelines, for the classification and aggregation of costs and benefits associated with the eruptions. These costs include both market-measured costs and non-market-measured costs, such as waiting time.

## INTRODUCTION

This paper describes a social accounting framework designed to classify real economic costs and benefits, as well as related redistributions of economic activity associated with the eruptions of Redoubt Volcano between December 1989 and April 1990. Conceptually, we are trying to compare economic activity that would have occurred if the eruptions had not taken place with activity that actually took place. The difference between these two situations represents the net economic cost of the eruptions.

There are two major reasons for measuring these costs. The first is to provide an aggregate measure of the net economic costs associated with the Redoubt Volcano eruptions and the distribution of those costs among geographic areas. Estimates such as these are often instrumental in obtaining Federal or State government assistance (if available in a timely fashion). The second use is to provide an indication of those costs that could be avoided or lessened with the implementation of various mitigation measures. This is essential information for the evaluation of investment in mitigation measures.

## DESIGNING THE ACCOUNTS

There are several issues that have been considered in the design of the accounting framework. A review of these will help in understanding both what is and what is not being measured. Readers interested in substantially more detailed discussions of social income accounting may consult Yanovsky (1965) or Eisner (1989).

The present accounting framework is intended to reflect three measures of economic activity: real economic costs, real economic benefits, and redistributions of costs or benefits.

Costs are incurred as a result of using up factors of production, or inputs, and may be of two types: direct damage costs and mitigation costs. Direct damage costs are defined as costs resulting directly from the volcanic eruption, such as a jet engine repair, ash cleanup and removal, and "waiting time" costs of individuals. These are costs that would not have occurred except for the eruptions. Mitigation costs includes those costs associated with mitigation of the effects of present or future volcanic eruptions. These are costs intended to reduce future damages. Included in this category would be airborne radar to track ash clouds, costs of monitoring volcanic activity, and installation of special dikes to protect the Drift River oil-loading facility.

Some real economic benefits may also have resulted from the eruptions (e.g., volcanic ash used in pottery, the inevitable T-shirt, or tourist flights around the volcano). More difficult to value, but of greater potential long-run significance, might be increased knowledge related to predicting eruptions, appropriate flight procedures when encountering volcanic ash clouds, etc. However, we expect that most perceived benefits are really redistribution effects.

The third category of measurement addresses redistributions of economic activity. Distributional effects related to volcanoes are discussed in detail in Blong (1984). These redistributions occur when economic activity shifts from one geographic locale to another as a result of the eruptions. For example, a flight scheduled to land in Anchorage is diverted to Fairbanks. Fairbanks gains income that is lost in Anchorage. Redistribution also occurs when components of income are shifted from one owner to another. For example, when a damaged jet engine is replaced, there is a redistribution of economic profit from the aircraft owner (or insurer) to the firm doing the repair.

The inclusion of costs, benefits, and redistributions arising from transportation delays (and cancellations) is

another major aspect of accounting for economic costs related to the Redoubt eruptions. Consequences of travel delays, trip cancellations, and, to a lesser extent, freight and postal service delays are not directly measured by the market but are likely to be substantial.

Benefits, costs, and distributional effects depend on both the geographic area encompassed and timing. The geographic frame of reference in the present study is global, in the sense that costs, benefits, and redistributions associated with the eruptions are included regardless of where they occurred. Geographic sub-units are established to identify localized effects. The timing of costs may also provide useful information, and, where possible, we will measure costs relative to specific eruptions.

## THE BASIC RULES

Before looking at some illustrations of the application of our accounting principles, it is helpful to summarize the specific rules that we are using to measure volcano-related economic impacts.

1. Any economic action (i.e., the use of factor inputs, such as labor, capital, or purchased intermediate inputs) that occurs because of an eruption, which otherwise would not have occurred, is treated as a change from the "without eruption" state. If the action can be expected to increase the consumer's utility, or "economic well-being" compared to the non-eruption case, the change is treated as a benefit. If the action is to maintain (or attempt to maintain) a consumer's pre-eruption utility level or restore their utility level, then the change is treated as a cost. As indicated above, these costs are further divided into two categories: direct damage costs and mitigation costs.
2. Benefits or costs may be measured either by the monetary value of factor inputs used in the production process (the value added measure) or by the market price of the good or service produced but, however measured, cannot be counted twice (i.e., double counted).
3. The estimate of the net economic cost of the eruptions is the difference between measured total costs and total benefits.

## SOME EXAMPLES

We can now illustrate the use of the accounting framework with several examples. First considered is the privately owned Drift River Oil Terminal, located on the west shore of Cook Inlet at the mouth of the principal river draining the north flank of Redoubt Volcano. Oil produced from Cook Inlet platforms is transported by pipeline to the Drift River facility for storage and loading on to tankers. Debris flows from the eruptions caused flooding, threatened the physical integrity of Drift River Terminal, forced the closing of the facility, and lead to cessation of production from the Cook Inlet fields. Subsequently, the facility was repaired, levees were installed to protect the facility, and operation of the facility and production from Cook Inlet fields resumed. From a conceptual point, what costs should be charged against the eruptions?

Firstly, the cost of levees should clearly be included because the levees were a State-imposed precondition for reopening the facility. Secondly, other modifications to the facility to prevent the recurrence of adverse flooding effects would also be included. These are examples of mitigation costs. Costs of shutting down and restarting Cook Inlet production facilities should also be included and should reflect direct damage costs. State royalty income at the time of the eruptions was about $39,000 per day (Brantley, 1990). The economic cost of replacing the revenue flow (e.g., as measured by the cost of borrowing to replace the revenue flow) would also be a direct cost. The same principle would apply to the delay in producer earnings.

A second example considers the repair of damage to aircraft. A highly reported incident occurred when a Boeing 747-400 flew through an ash cloud on December 15, 1989, and lost power in all four engines. Although the engines were restarted and the plane landed safely, the aircraft required extensive repair work (Przedpelski and Casadevall, this volume). All four engines were replaced, as were portions of the electrical and avionics systems. In addition, the aircraft required a thorough cleaning to remove ash. The reported repair costs were estimated at approximately $80 million (Steenblik, 1990).

How do the account principles treat these expenditures? First, the repair and cleaning costs are a direct result of the eruption and reflect the use of resources to repair damage caused by the eruptions. Secondly, only a portion of the costs of engine and electronics replacement should be included. The portion that should be included would be equal to the cost of replacing the remaining economic life of the damaged equipment. For example, if an engine had 20 percent of its economic life remaining at the time of the incident, then replacement of that 20 percent should be charged against the eruption (i.e., a cost of the eruption), whereas the balance would be treated as new investment and not counted as a cost of the eruption.

A third illustration of our account principles relates to the treatment of a canceled or rescheduled event. The annual Anchorage "Christmas Carol" production scheduled for several performances prior to Christmas had to be postponed. The actors, actresses, and stage crew were in Anchorage, but the shipment of stage sets (to be transported by air freight) was delayed several times. Although the production did finally take place after several reschedulings, there was a significant loss in revenue.

What are the losses associated with this event? Following the principle of "resources used," the loss should be equal to the resources used in the "non-production." This

would include the opportunity cost of the actors, actresses, and stage crew (as measured by their compensation), their housing and transportation costs, the earnings that the Performing Arts Center could have obtained if used for an alternative event, the cost of promotional activity, etc. There is also an economic cost reflected in the time invested by volunteer participants.

A final example addresses the issue of waiting time. Disruption of flight schedules and outright cancellation of flights resulted in extensive, and often lengthy, delays for air travelers. In many cases, the end result was complete trip cancellation on the part of the individual traveler. There are two dimensions to these waiting-time costs with which we try to deal. The first is the temporary non-utilization of factor inputs where the foregone use cannot be recaptured in the future. For example, a business traveler stranded in Seattle on a trip from San Francisco to Anchorage (and unable to conduct business from the airport) spends a certain number of hours waiting to complete the trip. This waiting time is a cost of production and a use of the factor input, labor. As such, it can be valued at its regular rate of compensation.

The second type of waiting-time cost is associated with final consumption of air travel (i.e., consumer travel). In this case, the cost of waiting is the value of leisure time that the consumer has given up. For example, a student returning home to Anchorage for the Christmas holidays has to spend two days in the Seattle airport. These two days are days that the student does not get to spend with family (or friends already back from other schools). Typically, the value of leisure time is measured by its opportunity cost, or what the individual could have earned if they had chosen to work rather than to have taken leisure time. We follow that convention in these accounts. Thus, the cost of the student's waiting time would be equal to what the student could have been earning had that student chosen to work (instead of being a student). Discussion of the measurement and use of leisure time is more fully treated in Kendrick (1987) and Eisner (1989).

## SUMMARY

In summary, we have attempted to state a set of "rules" to guide the classification and aggregation of economic costs and benefits associated with the eruptions of Redoubt Volcano during 1989–90. Compilation of these costs and benefits provides both an indication of the overall costs to society of the eruptions and a reference against which future mitigation efforts can be evaluated.

## ADDENDUM

Since this report was prepared, we have completed the study of economic consequences of the 1989–90 Redoubt Volcano eruptions (Tuck and others, 1992). Table 1 contains a summary of the findings regarding the economic impact of the Redoubt Volcano eruptions on the aviation industry.

**Table 1.** Estimated economic impacts of the 1989–90 eruption of Redoubt Volcano on the aviation industry.[1]

["Big Four," United, Delta, Northwest, and Alaska Airlines; ?, no estimate available for economic impact for this category; Na., estimated economic impact not allocated to this category; AIA, Anchorage International Airport. All figures in U.S. dollars]

| Category | December 1989 | January 1990 | Total |
|---|---|---|---|
| Domestic passenger traffic | | | |
| "Big Four" (B4) | 837,884 | 349,138 | 1,187,022 |
| Domestic total – B4 | 433,511 | 35,673 | 469,184 |
| International passenger traffic | ? | ? | ? |
| Domestic freight | Minimal | Minimal | Minimal |
| International freight | Na. | Na. | 15,000,000 |
| AIA revenues | | | |
| Landing fees | 177,464 | 77,696 | 255,160 |
| Concessions | 508,216 | 487,339 | 995,555 |
| Fuel flowage fees | 135,060 | 205,460 | 340,520 |
| Airport support industries | | | |
| Fuel distribution | Na. | Na. | 50,000 |
| Ground crews and service | Na. | Na. | 600,000 |
| Catering | Na. | Na. | 43,500 |
| Concessions | Na. | Na. | 285,000 |
| Passenger waiting time | 1,144,800 | 689,000 | 1,833,800 |
| Estimated production losses | Na. | Na. | 21,059,741 |
| Equipment damage costs | Na. | Na. | 80,070,000 |
| Total aviation costs | | | 101,129,741 |

[1] Source of information: Tuck and others (1992).

## REFERENCES CITED

Blong, R.J., 1984, Volcanic Hazards: A Sourcebook on the Effects of Eruptions: Sydney, Academic Press, 424 p.

Brantley, S.R., ed., 1990, The eruption of Redoubt Volcano, Alaska, December 14, 1989–August 31, 1990: U.S. Geological Survey Circular 1061, 33 p.

Eisner, Robert, 1989, The Total Incomes System of Accounts: Chicago, University of Chicago Press, 416 p.

Kendrick, J.W., 1987, Happiness is personal productivity growth: Challenge, v. 30, p. 37–44.

Steenblik, J.W., 1990, Volcanic ash—A rain of terra: Airline Pilot, June/July, p. 9–15.

Tuck, B.H., Huskey, L., and Talbot, L., 1992, The economic consequences of the 1989–90 Mt. Redoubt eruptions: University of Alaska, Anchorage, Institute of Social and Economic Research, [unpub. report prepared for the U.S. Geological Survey Alaska Volcano Observatory], 39 p.

Yanovsky, M., 1965, Social Accounting Systems: Chicago, Aldine Publishing Company, 237 p.

VOLCANIC ASH AND AVIATION SAFETY:
Proceedings of the First International Symposium
on Volcanic Ash and Aviation Safety
U.S. GEOLOGICAL SURVEY BULLETIN 2047

# EFFECTS OF VOLCANIC ASH ON AIRCRAFT POWERPLANTS AND AIRFRAMES

*By* Lester M. Zinser

## ABSTRACT

This paper discusses the effects of volcanic ash on an aircraft used as a research platform to penetrate and sample volcanic eruption clouds directly over and near the vent. Scientific objectives were to acquire as pure and uncontaminated sample of the ash as possible and to determine the composition and concentration of volcanic ejecta. Over the years, aircraft have accidentally encountered volcanic clouds at different altitudes with varying effects on powerplants and airframes. However, little was known about how flying directly through a dense eruption cloud would affect aircraft performance and materials. The paper combines the results of scientific expeditions to three volcanoes in Guatemala in 1978 and 1980 and to Mount St. Helens in 1980.

## INTRODUCTION

The airplane used for this research was a Beechcraft Queen Air Model B-80 powered by two Lycoming IGSO-540 reciprocating engines. On-board research equipment and the responsible organizations were as follows:

1. Air intake/exhaust—U.S. Geological Survey (USGS),
2. Air intakes—National Center for Atmospheric Research (NCAR),
3. Quartz microbalance—California Measurements, Inc.,
4. Inertial navigation system—NCAR,
5. $H_2O$ sampler—USGS,
6. Giannini 35-mm camera—NCAR,
7. Huebert sampler—Colorado College,
8. Heidt air-sample bottles—NCAR,
9. Correlation spectrometer—Dartmouth College.

Although some equipment required special external ports extending beyond the fuselage, the scientific equipment had little to no effect on the aircraft's aerodynamic performance. The main limitation was the bulk and the weight, which reduced passenger space and fuel load and thus reduced the time spent on station. The time on station turned out to be important because volcanoes do not erupt on command. Thus, we often circled a volcano for periods up to several hours, awaiting an eruption. Logbook entries show 26 flights between the three projects with a total of 7 to 10 hours in volcanic clouds of varying density.

## METHOD OF STUDY

The first two studies (1978 and 1980) were carried out in Guatemala (Rose and others, 1980). Following the return from Guatemala in late February 1980, Mount St. Helens was showing signs of activity, and the airplane was scheduled for a trip to Portland, Oreg. For the Central America trip, logistics and obtaining permission to fly a research aircraft over three active volcanoes (Fuego, Pacaya, and Santiaguito) was the most difficult part of the program. Once the paperwork was accomplished, the procedure was to fly to the volcano of interest for the day and circle the crater until it erupted, or until fuel supply (3.5-hr maximum) warranted a return to our base at La Aurora International Airport, Guatemala City.

There were many ideas as to what triggers an eruption—high tide, low tide, sun spots, Pele was upset—however, none were correct. The best we could do in planning a flight was to pick a day and take our chances. Dr. Richard Cadle (NCAR) had some experience sampling fumes from the Hawaiian volcano, Kilauea, but none of the scientists were aware of any flights directly over a crater through an ash or vaporous emission or through low-level pyroclastic eruptions. In other words, no one knew what the maximum ash concentration in a volcanic cloud was that could be flown through without disastrous results.

## OBSERVATIONS AND RESULTS

On 10 February 1978, Fuego Volcano (3,763 m) erupted with a dense black plume (fig. 1), oxygen masks were put on and set at 100 percent oxygen; research equipment was readied; and a penetration run began. The plume was estimated to be 200-300 m above the crater when first sighted. The plume expanded rapidly as the aircraft approached and rose to an altitude between 300 and 400 m above the vent.

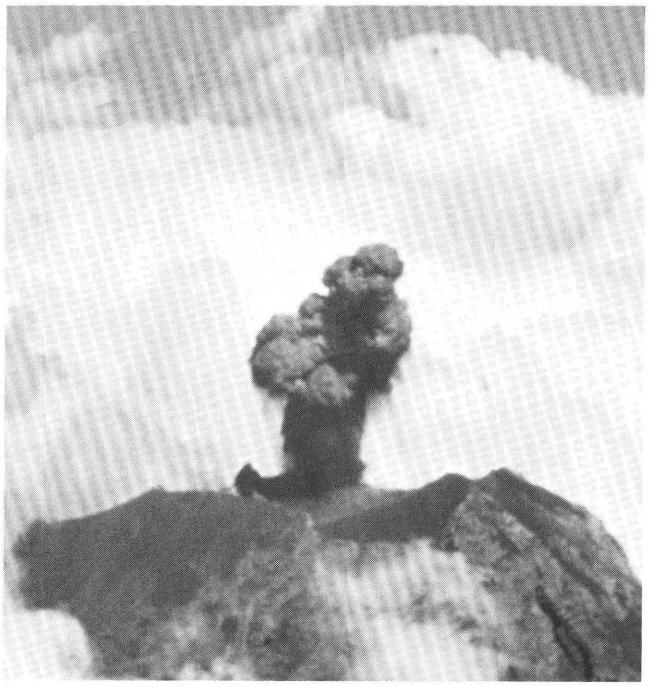

**Figure 1.** Small explosion from Fuego Volcano (3,763 m), Guatemala, produces a dark, ash-rich column that rises about 300 m above the summit, 10 February 1978.

The aircraft entered the eruption cloud about 300 m above the volcano and was traveling 70 m/s. The plume was estimated to be about 300-400 m in diameter, which gives a residence time in the plume of from 4 to 6 seconds. On a later mission, following an overnight eruption of Fuego, the plume had stagnated owing to low wind conditions and was held in place by a temperature inversion (fig. 2)—the entire 3-hour flight was flown in the ash cloud.

What happens when one penetrates a volcanic plume? In the plume shown in figure 1 we found:

1. Zero to limited visibility,
2. Heat and slight turbulence, which caused a bump with each entry into the cloud,
3. Copious quantities of ash entering the cabin through fresh air vents,
4. The fuel-air ratio was upset, engines sputtered, and manifold pressure fell off rapidly,
5. Once through the cloud, engine performance improved—everyone breathed a sigh of relief, especially the pilot.

The first flight through the Fuego plume became a standard for me, as well as for the researchers. If the eruptions looked larger and darker than the Fuego plume, direct penetration was avoided until some of the heavier material had fallen out. The plume from the Santiaguito vent at Santa Maria Volcano (3,772 m) (fig. 3) was lighter in color and less dense in appearance—I experienced no power loss while in the cloud. However, flight crews were exposed to hydrogen sulfide, and the use of 100 percent oxygen was mandatory. The plume from Pacaya Volcano (2,552 m) (fig. 4) was white, and flying through the cloud was similar to flying through a cumulus cloud. Water droplets formed on the windscreen, and there was no evidence of solid ash particles.

A total of 32 hours was flown for volcanic research in 1978—this includes an estimated 5 hours in plumes of different density. Those 5 hours were enough to etch the windshield, burn out the bearings on one generator, dull the paint, abrade and destroy the landing-light glass covers and the running lights, damage the de-ice boots, pit the leading edge of the propellers, and dull the chrome-plated prop domes. Upon return from Guatemala in 1978, substantial maintenance (including replacing the windshields) was needed to bring the Queen Air up to standard.

When we returned to Guatemala in February 1980, we were more knowledgeable about the hazards and damaging effects of volcanic ash. I devised a method to protect the forward-facing windscreen from abrasion by taping a 0.007-inch film of clear mylar to the windshield. The mylar had to be replaced after each ash flight (fig. 5).

During the 1980 program in Guatemala, we flew a total of 36 hours, including an estimated 3 hours in the plumes of Santiaguito and Pacaya. Fuego was inactive. A daily cleaning and oiling of the air-intake filters was needed. A daily inspection of all 24 spark plugs was conducted in addition to the normal pre-flight inspection, which usually required replacing the bottom-row 12 plugs because black, glassy, obsidian-like deposits completely covered the electrodes. I have not been able to determine why the top plugs stayed relatively clean.

The temperature in the cylinder at the point of ignition is near 3,000°F (1,648°C)—well above the temperature

**Figure 2.** Ash cloud and small eruption column following an overnight eruption of Fuego Volcano, February 1978. The plume had stagnated owing to low wind conditions and was held in place by a temperature inversion.

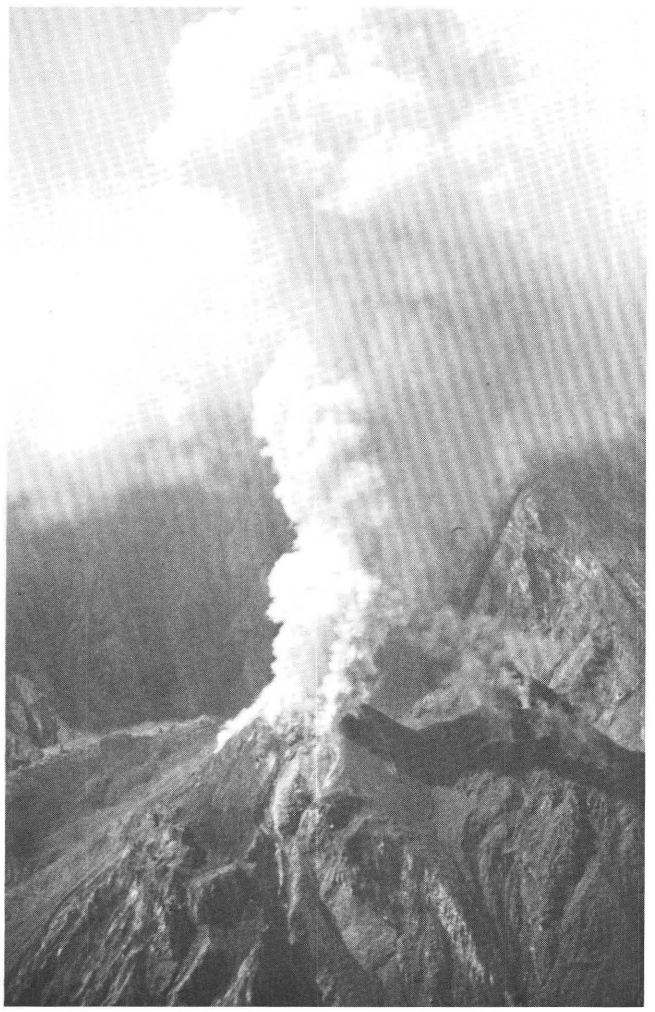

**Figure 3.** The plume from the Santiaguito vent at Santa Maria Volcano (3,772 m) was lighter in color and less dense in appearance than plumes from Fuego Volcano (figs. 1 and 2). The airplane experienced no power loss while in the cloud; however, hydrogen sulfide gas was detectable by odor.

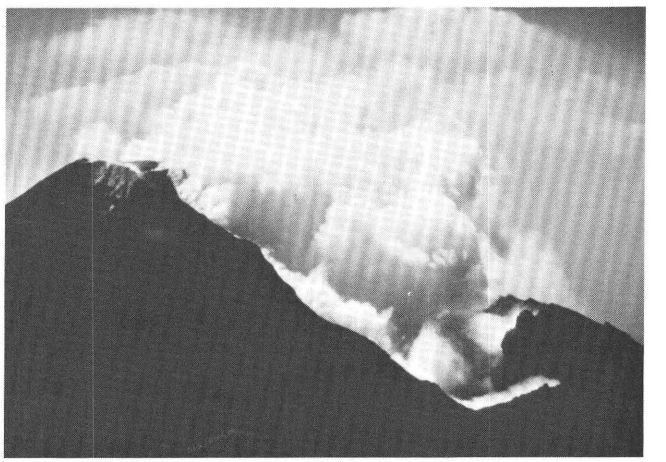

**Figure 4.** The white, water-rich plume from Pacaya Volcano (2,552 m) formed above a small lava lake. Flying through the cloud was similar to flying through a cumulus cloud. Water droplets formed on the windscreen, and there was no evidence of solid ash particles in this cloud.

**Figure 5.** To protect the forward-facing windscreen from abrasion by volcanic ash, a 0.007-inch film of clear mylar was taped to the windshield. The mylar had to be replaced after each ash flight.

needed to melt the rhyolite glass particles found in the February 1978 eruption clouds of the Guatemalan volcano, Santiaguito (Rose, 1987). Magma solidifies from 1,250°C down to 700°C (Decker and Decker, 1981), so it seems reasonable to think that both upper and lower sets of spark plugs would be exposed to the same high temperature and that both sets would keep the magma liquid and expel it along with unburned exhaust gases. However, that was not the case. Evidently, the bottom plugs cool more in the combustion cycle and allow melted ash to congeal on the electrodes.

The ejecta from the 1980 eruption of Mount St. Helens presented similar problems to those of the Central America volcanoes and added a new one: wet volcanic ash. On 7 April 1980, Mount St. Helens erupted a gray to black plume to an estimated 300 m above the vent, and, as the fallout began, a dark curtain of material fell from the plume (fig. 6). We circled and penetrated the heavy ash curtain. We were surprised. What appeared to be just an ash curtain similar to many we had flown through before was really a shower of muddy ash. The powerplants nearly stopped; the mylar-covered windscreen became opaque; and forward visibility was reduced to zero. The muddy ash shower reduced in intensity, and we made seven more trips through the cloud before returning to Portland. We landed with the aid of air-traffic-control radar.

On 10 April 1990, we returned to Jeffco Airport at Broomfield, Colo. During routine maintenance on 14 April 1990, an oil sample was analyzed with the following results (numbers in parentheses represent values before volcanic ash sampling; numbers not in parentheses represent values after volcanic ash sampling—units are in part per million): Fe: (98), 293; Ag: (0), 1; Al: (20), 119; Cr: (9), 29; Cu: (16),

**Figure 6.** On 7 April 1980, Mount. St. Helens (2,549 m) erupted a gray to black plume to an estimated 300 m above the vent, and, as the fallout began, a dark curtain of material fell from the plume. The 1980 Mount St. Helens ejecta was wet, which caused it to adhere to the exterior of the airplane.

36; Mg: (4), 18; Ni: (7), 21; Si: (39), 168; Ti: (0), 1; Mo: (0), 2. The most common elements and metallic compounds in the Lycoming IGSO-540 powerplant are: tin, aluminum, bronze, steel, and chrome. Magma contains trace amounts of the same elements (Decker and Decker, 1981).

The question is: Where did the increases in these elements come from? Was it from abrasion of the powerplant by the ingested material; was it from the volcanic ash itself; or was it a combination of factors? No doubt the high silicate count is from ingested ash. The high iron count is probably a combination of ash and engine abrasion. The origin of the silver is unknown. Some Lycoming engines used some silver in the supercharger bearings, but I could not determine if the Lycoming engines on our airplane were manufactured with silver in these bearings. Because alumina is the second most abundant part of volcanic rocks and also a very common product in aircraft engines, I would assume the high count was due to a combination of ash and abrasion. The cylinder walls were chrome plated, and silicate grinding contributed to the increase in chromium. Copper was probably ground out of the various bronze bushings in the engine. The magnesium increase appears to be mostly from ingested ash. There are probably some compounds in the engine with nickel in them—there was a large increase of nickel over the "normal" sample. Titanium probably came from the ash, and molybdenum could have been scrubbed from some engine alloy.

## CONCLUSIONS

Judging from the increase of metallic elements shown by the oil analysis, it is obvious that the ingestion of volcanic ash is detrimental to aircraft powerplants. Ash will shorten the operating life of reciprocating engines and may, under sustained, severe volcanic-ash ingestion, cause engine failure. I did not have a complete engine failure. It is my opinion that jet turbine engines, because of their higher operating temperatures and finer tolerances, are even more susceptible to complete failure than reciprocating engines. Not only is the ash damaging to the engines, but airframes and engine components can be destroyed as well. Windshields are especially vulnerable to abrasion and crazing.

## RECOMMENDATIONS

First and foremost, avoid volcanic clouds. Admittedly, avoiding volcanic clouds is difficult at best. The Air Line Pilots Association in 1990 issued a form entitled "Operation in the Vicinity of Volcanic Ash Clouds." Flight organizations who operate anywhere near areas containing active volcanoes should be in possession of these important guidelines.

Because pilots are often the first to observe volcanic activity, especially at remote volcanoes, they should report this activity using the reporting form approved by the International Civil Aviation Organization (Fox, this volume).

For scientific research of volcanoes which requires entry into an ash cloud, use an aircraft with reciprocating engines; do not use turbine engines. Protect the windscreen if at all possible. Clear mylar of 0.007-inch thickness can be taped to the windshield without affecting visibility. Check and clean the air-intake filters after every penetration. Run a frequent oil analysis. Inspect the pitot-static system for clogging by ash. Inspect spark plugs and replace

as necessary. After each flight through a volcanic plume, carry out a thorough inspection of the airplane.

## ACKNOWLEDGMENTS

Thanks are extended to Mr. Dan Fletcher, AVCO Lycoming Textron, Williamsport, Pa.; Colorado Aero Tech, Broomfield, Colo.; Mr. John Stone and the maintenance staff at National Center for Atmospheric Research; and Weststar Aviation, Grand Junction, Colo. Special thanks are due to Dr. William Rose, Michigan Technological University; Dr. Richard Cadle, National Center for Atmospheric Research, Boulder, Colo.; Dr. Richard Stoiber, Dartmouth College; and many graduate students for their valuable advice about volcanoes.

## REFERENCES CITED

Decker, R.W., and Decker B., 1981, Volcanoes: San Francisco, W.H. Freeman and Co., 110 p.

Rose, W.I., Jr., Chuan, R.L., Cadle, R.D., and Woods, D.C., 1980, Small particles in volcanic eruption clouds: American Journal of Science, v. 280, p. 671–696.

Rose, W.R., 1987, Interaction of aircraft and explosive eruption clouds: A volcanologist's perspective: American Institute for Aeronautics and Astronautics Journal, v. 25, p. 53–56.

VOLCANIC ASH AND AVIATION SAFETY:
Proceedings of the First International Symposium
on Volcanic Ash and Aviation Safety
U.S. GEOLOGICAL SURVEY BULLETIN 2047

# AIA RECOMMENDATIONS AIMED AT INCREASED SAFETY AND REDUCED DISRUPTION OF AIRCRAFT OPERATIONS IN REGIONS WITH VOLCANIC ACTIVITY

*By* AIA Propulsion Committee 334-1, Zygmunt J. Przedpelski, Chairman

## INTRODUCTION

The multiple-engine power loss on Royal Dutch Airlines (KLM) Flight 867 following an inadvertent encounter with a volcanic ash cloud from Redoubt Volcano, Alaska, on 15 December 1989 underscored the threat of volcanic eruptions to aviation. The Aerospace Industries Association of America (AIA) ad hoc propulsion committee (PC-334-1) was formed to evaluate this threat and to make appropriate recommendations to the aviation industry and responsible government agencies.

## COMMITTEE OBJECTIVES

The mission of this committee was to assess the volcanic ash threat to commercial aviation and to make recommendations to the industry and government agencies involved. The recommendations, when implemented, should accomplish the following:

- Reduce the probability of inadvertent aircraft–volcanic ash encounters of the kind that almost resulted in a tragedy in the past (KLM in 1989 and Singapore Airlines and British Airlines in 1982).
- Reduce the interruptions to normal air traffic flow in regions with volcanic activity (e.g., Anchorage, December 1989 to April 1990).

## MEMBERSHIP

Major U.S. and foreign aircraft and aircraft engine manufacturers were represented on the committee. In addition, experts in the field of volcanic activity and engine performance in dust- and ash-contaminated air were invited to join the committee. All of the individuals selected had extensive experience in aircraft and engine operations with specific expertise in volcanic-ash-environment operations, including Mount St. Helens 1980, Galunggung 1982, and Redoubt Volcano 1989–90. The committee membership is shown in table 1.

## PRESENTATIONS AND DATA ANALYSIS

The AIA committee met February 20–21, 1991, in Denver, Colo., at the Central Region headquarters of the U.S. Geological Survey. The meeting included presentations by various committee members and discussions on recommendations by the committee. The following presentations were made, reviewed, and analyzed by committee members:

- KLM Flight 867 incident including air traffic center (ATC) and crew procedures, the engine/aircraft performance, inspection findings, and conclusions.
- Mount St. Helens and Galunggung volcanic ash–aircraft encounters, with emphasis on differences and similarities to the KLM 867 incident. The specific cases analyzed in depth were:
  - Mount St. Helens: L100 (C-130) Transamerica event,
  - Galunggung: B747 British Airways event, and
  - Galunggung: B747 Singapore Airlines event.
- Results on controlled dust and volcanic-ash-ingestion engine tests conducted under contract to the U.S. Air Force by Calspan Laboratory.
- Current and proposed air-crew procedures addressing volcanic ash cloud avoidance, recognition, and recommended procedures following an inadvertent ash-cloud penetration. The recommended procedures of Airbus, Boeing, McDonnell-Douglas, Pratt and Whitney, General Electric, and Rolls Royce were reviewed. Boeing B747 procedures were used as a reference.
- Worldwide threat of volcanic eruptions with emphasis on ash-cloud-producing volcanoes and regions.
- Ash-cloud detection and tracking methods: infrared, ground and airborne radar, satellite, visual, etc.
- Braking effectiveness on wet and dry runways contaminated with ash.

## CONCLUSIONS AND LESSONS LEARNED

Modern turbine engines can sustain serious, flight-safety-threatening damage when exposed to volcanic ash for even very limited periods of time. The successful completion of military specification MIL-E 5007 (or equivalent) sand-ingestion tests by a particular engine model does not provide assurance of sustained operability in a volcanic ash cloud because concentrations of volcanic ash that are orders of magnitude higher may be present and because of the different physical and chemical nature of volcanic ash. Older generation turbine engines, which operate at a lower combustor discharge temperature, are not as susceptible to the high-pressure-turbine deposit buildup and area blockage (as is true for current production engines and future engine designs). However, all turbine engines are vulnerable to compressor erosion. The committee had no specific data on aircraft piston-engine damage caused by volcanic ash, but literature search indicates that piston engines are also damaged by exposure to volcanic ash.

Design changes to improve engine resistance to volcanic ash ingestion would, at best, result in minor improvement but at a significant increase in fuel consumption and engine weight.

Damage to aircraft systems from volcanic ash ingestion, while not primary in terms of flight-safety threat, contributes to the crew workload in an already stressful situation. The major concerns are loss of airspeed indication, reduced visibility due to windshield erosion, loss of HF (high frequency) communications and degradation of the VHF (very high frequency) communications, and possible degradation of electronic controls and instrumentation caused by ash contamination.

Volcanic-ash-ingestion events, while infrequent, are major flight-safety concerns. All members felt that a one-time spurt of activity generated by the Redoubt–KLM 867 incident is effective in reducing the probability of a volcanic-ash-caused aircraft accident in the near term. However, many of the committee members remembered similar activities following the 1980 Mount St. Helens and the 1982 Galunggung eruptions. It was agreed that institutionalized, recurring training of air crews and air traffic controllers, who may be exposed to volcanic activities, is required to achieve lasting air-safety benefits from the previously learned lessons.

Increased air crew and air traffic center (ATC) awareness of the threat posed by volcanic ash and adherence to the current operating instructions, which emphasize avoidance, recognition, and procedures to be followed in the event of inadvertent ash-cloud encounter, should reduce the probability of ash-caused aircraft accidents. Improved airborne detection means (akin to weather radar for detection of heavy precipitation) are needed. Improved ash-cloud tracking, including estimates of ash-particle density utilizing satellite and ground tracking means, is also needed to enhance safety and reduce disruptions to normal air-traffic operations in regions with volcanic activity.

**Table 1.** Membership of AIA Propulsion Committee 334-1.

[AIA, Aerospace Industries Association of America; IAE, International Aero Engines (a joint company of Rolls Royce, Pratt and Whitney, and a Japanese consortium); CFMI/SNECMA, CFM International/Société Nationale d'Étude et de Construction de Moteurs d'Aviation]

| Name | Affiliation |
|---|---|
| Michael Dunn | Calspan Laboratory |
| George P. Sallee | *Boeing Commercial Airplane Co. |
| Ernest Campbell | *Boeing Commercial Airplane Co. |
| John Lane | *McDonnell-Douglas |
| L.H. Kosowsky | *United Technology/Norden Systems |
| Al Weaver | *United Technology/Pratt & Whitney |
| William Quaile | *United Technology/Pratt & Whitney |
| Thomas Casadevall | U.S. Geological Survey |
| Craig Bolt | IAE |
| Tony Wassel | Rolls Royce |
| Michel Tremaud | Airbus |
| Yves Halin | CFMI/SNECMA |
| Zygmunt Przedpelski[1] | *GE Aircraft Engines |

* Indicates AIA member.

[1] Committee chairman.

The issue of braking effectiveness on runways covered with volcanic ash (dry and wet) was raised, and no reliable data is known to exist at this time.

In general, the existing air crew operating instructions dealing with volcanic ash environment are adequate. However, in order to facilitate transition from one aircraft model to another, these instructions should be standardized as much as possible.

An engine in-flight shut down (IFSD) is a rare event. Many airline crews never encounter one. The need to restart an engine in the air is even rarer. This, combined with the different air-start versus ground-start engine characteristics has made it unlikely that the crew will follow optimum procedures for air starts. This was demonstrated in the KLM 867 event and may have been a contributor to late and (or) unsuccessful restart attempts in other cases of engine IFSD's associated with inclement weather.

The Calspan controlled engine-test data indicates that buildup on high-pressure turbine nozzle vanes in ash environment can be avoided if combustor exit temperature can be maintained below a specified value. This suggests that, in a case where the recommended procedure of reducing power to flight idle cannot be followed (i.e., when adequate terrain clearance cannot be maintained), a higher power level that is capable of maintaining altitude can be used for a limited time period. It is estimated that the "useful"

engine life (determined by compressor erosion) is on the order of 10 times longer that the "useful" engine life when rapid buildup is occurring on high-pressure turbine (HPT) nozzle vanes. The performance/stall-margin loss caused by compressor erosion is, however, unrecoverable. It is, therefore, the committee's position that flight idle power, which eliminates nozzle buildup and greatly reduces compressor erosion, should be the recommended procedure when inadvertent ash-cloud entry is made.

The committee considered the options of shutting down some engines during inadvertent ash-cloud entry. It also considered a procedure of engine deceleration/acceleration to break loose some of the nozzle deposits, lower the compressor operating line, and regain stall margin. While these procedures may be useful under some conditions, the additional complexity these procedures force upon a crew in a very stressful situation is considered counterproductive.

## SPECIFIC RECOMMENDATIONS

All aircraft manufacturers should review the flight-manual procedures pertaining to operations in areas contaminated by volcanic ash. The Boeing 747 operating instructions can be used as a guide to achieve maximum possible standardization. Two specific items should be added to the Boeing 747 operating instructions:

1. The preferred method for exiting volcanic cloud conditions is a 180° turn.
2. APU (auxiliary power unit) start should be added to items to be accomplished in case of inadvertent volcanic cloud penetration (subject to comparison of the maximum APU combustor-discharge temperature versus the threshold for turbine-nozzle deposit buildup).

All aircraft manufacturers should provide a section in maintenance manuals that would provide the guidance for necessary maintenance and (or) inspections to be accomplished following an aircraft encounter with volcanic ash.

Aircraft manufacturers, with assistance from the engine manufacturers, should define maximum engine power levels (expressed in engine pressure ratio (EPR), fan speed (N1), and (or) exhaust-gas temperature (EGT) levels) that will minimize buildup of melted and resolidified ash on HPT nozzle guide vanes. These values should be added to flight-manual procedures and should be used only when the recommended flight idle power will not assure adequate terrain clearance.

Aircraft manufacturers should ensure that cooling air for electronic compartments is filtered to prevent ash contamination of vital electrical/electronic systems. This is most important in current and future fly-by-wire aircraft.

Aircraft manufacturers, with assistance from engine manufacturers, should consider addition of a time-delay circuit to allow an air-started engine to reach stabilized idle speed before the electrical or generator load is applied. This would facilitate engine restarts under less-than-ideal conditions.

FAA and other equivalent government agencies should require that air crews practice engine air-restart procedures in a simulator on recurring basis. Normal and deteriorated engine-start characteristics should be simulated.

FAA should support technology program efforts leading toward development of a practical airborne volcanic-ash-cloud detection device.

FAA should support efforts to improve satellite and ground tracking of volcanic ash clouds. These efforts should eventually lead to quantification of ash concentration to determine when existing clouds are or are not threatening to air traffic.

FAA and other airspace operating agencies should put in place a worldwide communication alert system to provide swift warning of the location and severity of volcanic ash clouds.

FAA should sponsor tests utilizing the B747 windshield from KLM 867. Tests should determine if spraying windshield rain repellent fluid and actuating the wipers can be used to improve visibility through an eroded windshield (the windshield is currently at the Jet Propulsion Laboratory, Pasadena, Calif.). If positive, the results should be incorporated into flight-manual procedures dealing with operation in areas contaminated with volcanic ash.

FAA should sponsor a program to quantify the coefficient of friction on runways contaminated with volcanic dust (wet and dry). The results in the form-fabricating-effectiveness advisory should be incorporated into appropriate sections of flight manuals by manufacturers of all aircraft affected.

FAA and other equivalent government agencies should require that air crews be trained and tested periodically on knowledge of inclement weather procedures, including operations in areas contaminated with volcanic ash. Similar training and testing should be conducted for ATC personnel assigned to geographic locations near known volcanic activity.

The lessons learned from aircraft–volcanic ash encounters should be communicated worldwide, utilizing all available forums (International Civil Aviation Organization (ICAO), Flight Safety Foundation, Air Transport Association and its equivalents, Federal Aviation Administration and its equivalents, Air Line Pilots Association and its equivalents).

AIA should support the effort of the ICAO volcanic warning study group. This effort, when completed, should lead to improved reporting and dissemination of worldwide volcanic activity.

VOLCANIC ASH AND AVIATION SAFETY:
Proceedings of the First International Symposium
on Volcanic Ash and Aviation Safety
U.S. GEOLOGICAL SURVEY BULLETIN 2047

# RECOMMENDED FLIGHT-CREW PROCEDURES IF VOLCANIC ASH IS ENCOUNTERED

*By* Ernest E. Campbell

## ABSTRACT

Recent major volcanic eruptions have impacted air operations and have resulted in significant airplane damage. The encounter of a 747-400 airplane with volcanic ash is reviewed to demonstrate the extent of damage that can occur in just a few minutes. In this event, all four engines flamed out in less than 1 minute. Airplane engines, surfaces, windows, electronic equipment, and the pneumatic system were severely damaged. Approximately $80 million was required to restore the airplane.

When volcanic eruptions are reported, flight crews should use all possible means to avoid the area. However, at night or during flight in clouds, the ash may not be observed visually, and airplane radar systems are not capable of detecting volcanic ash. Recognition of an ash encounter may be accomplished by observing one or more of the following: heavy static discharges, glow in engine inlets, ash appearing in the cockpit and cabin with an acrid odor, multiple engine malfunctions or flameouts, and a decrease in airspeed.

If volcanic debris is inadvertently encountered, immediately reduce thrust to idle and exit the ash as quickly as possible. Autothrottles should be turned off in order to maintain idle thrust. Turn on engine and wing anti-ice (increase air bleed) to improve engine surge margin. Monitor exhaust-gas-temperature (EGT) limits. Restart engines if required.

Monitor airspeed and pitch attitude to detect a blocked pitot system. Airplane and engine damage may or may not be apparent; therefore, a landing at the nearest suitable airport is recommended. Report all volcanic ash encounters as soon as possible.

## INTRODUCTION

The recent eruptive sequence of Redoubt Volcano and Mt. Spurr in Alaska, Mt. Unzen in Japan, and Mt. Pinatubo in the Philippines has again demonstrated the potential for a dangerous confrontation between explosive volcanic eruptions and air operations. In as much as all engines are subjected to the same adverse environment during an encounter, there is an appreciable probability of an all-engine power loss or flameout. The purpose of this paper is to discuss flight-crew procedures following an inadvertent volcanic ash encounter.

## AN ENCOUNTER OF A 747 WITH VOLCANIC ASH

Most of the recent volcanic ash encounters have occurred on 747- and DC-10-type aircraft because they are the long-range airplanes used to fly the Pacific "ring of fire" routes. The following review of a 747 encounter with volcanic ash demonstrates the extent of damage that can occur in just a few minutes. All models of modern airplanes equipped with high-bypass engines are susceptible to the same type of damage, assuming the same amount of volcanic ash is encountered.

Redoubt Volcano, near Anchorage, Alaska, experienced an eruption on December 14, 1989. On the following day, a 747-400 airplane powered by GE CF6-80C2 engines entered an ash cloud at 25,000 ft and experienced flameouts on all four engines.

During descent to 25,000 ft, the airplane entered a thin layer of altostratus clouds when it suddenly became very dark outside. The crew also saw lighted particles (St. Elmo's fire) pass over the cockpit windshields. At the same time, brownish dust with a sulfurous smell entered the cockpit. The Captain commanded the Pilot Flying to start climbing to attempt to get out of the volcanic ash. One minute into the high-power climb, all four engines flamed out. Due to the volcanic ash and dust in the cockpit, the crew donned oxygen masks.

The Pilot Flying noticed the airspeed decaying, initially at a normal rate (given the airplane's attitude), but suddenly very fast. All airspeed indications were then lost due to volcanic dust contamination in the pitot system. At the same time, there was a stall warning and the stick shaker was activated with no signs of buffeting. The Pilot Flying rather firmly put the nose of the aircraft down to avoid a stall and initiated a turn to the left in a further attempt to get out of the volcanic ash.

The crew noticed a "Cargo Fire Forward" warning and deduced that the fire warning was caused by the volcanic ash, so no further action was taken.

As the engines spooled down, the generators tripped off and all instruments were lost except for instruments powered by the batteries.

During the time the engines were inoperative, the cabin pressure remained within limits and no passenger oxygen masks deployed. The crew elected not to deploy the masks because the passenger-oxygen-mask system would have been contaminated by volcanic dust in the cabin air.

An emergency was declared when the airplane passed through approximately 17,000 ft. The crew stated that a total of seven or eight restart attempts were made before engines 1 and 2 finally restarted at approximately 17,200 ft. Initially, the crew maintained 13,000 ft with engines 1 and 2 restarted, and, after several more attempts, engines 3 and 4 were also restarted.

Volcanic ash had entered the pitot-static system; all air-data systems had become unreliable. However, the left-hand altimeter indicated correct values. Furthermore, the rudder ratio light was on, indicating contamination of this system also. Because of the rudder ratio being incorrect, the aircraft was difficult to handle, especially during the period that only engines 1 and 2 were operating. The inertial guidance ground speed was used for speed reference after having checked with air traffic control (ATC) that the indicated values were correct.

After passing abeam and east of Anchorage at 11,000 ft, the airplane was given radar vectors for a wide right-hand pattern to runway 06 and further descent to 2,000 ft. The Captain had the runway continuously in sight during the approach; however, vision through the windshields was impaired by the "sandblasting" from the volcanic ash in such a way that the Captain and First Officer were only able to look forward with their heads positioned well to the side. During the last part of the approach, an "Equipment Cooling" overheat message occurred, but the Captain elected to disregard this message because landing was imminent.

After landing, the Captain cleared the landing runway and taxied the aircraft to the assigned gate. When turning toward the gate the Captain transferred control to the Pilot in the right-hand seat, because his vision through the left-hand windshield was impaired in such a way that he could not see the gate during the last part of the docking procedure.

Inspection of the airplane revealed the following:

- All four engines suffered extensive damage and had to be replaced. Inspection of engine 1 found that, in the first stage of the high-pressure turbine, ash had melted and resolidified (or "ceramatized") on the leading edges of the nozzle vanes. The solid ash deposits extended along 75 percent or more of each leading edge with an average depth of about 1.5 mm. A preliminary hypothesis suggests that the extent of the melted and resolidified volcanic ash deposit on the high-pressure turbine nozzle vanes increased the operating-line pressure ratio of the compressors, resulting in engine surge. The repeated restart attempts resulted in partial break up of the deposit through "thermal shock." This, in combination with improved engine-surge margin at lower altitudes, resulted in a successful restart of all four engines.
- The entire pneumatic system, the air conditioning system, and the equipment cooling system were heavily contaminated by volcanic ash. A major portion of the pneumatic system was removed, cleaned, and reinstalled.
- Both the Captain's and the Copilot's windshields were "sandblasted" and had to be replaced. The leading edges of the wings, the winglets, the vertical fin, and the horizontal stabilizer were "sandblasted" and had to be replaced. Other protruding parts of the aircraft—for example, all antennas, probes, ice detectors, and angle-of-attack vanes—were damaged and had to be replaced.
- The pitot-static system was damaged and heavily contaminated. The pitot and static ports had to be removed and replaced and the system purged of all ash.
- The entire fuselage, except for the area behind the aft pressure bulkhead, had to be cleaned very carefully. This included all cockpit instrument panels; all circuit-breaker panels; passenger cabin areas; baggage compartments; and the areas above the cabin ceiling panels, including all systems present in these areas and the entire environmental control system.
- The entire electrical and avionics systems were contaminated and had been exposed to possible overheating due to loss of cooling air. All electrical and avionics units had to be replaced.
- The smoke detection system was contaminated throughout. The entire unit, including associated plumbing and ejectors, had to be replaced.
- The fuel system, the hydraulic system, and the potable-water systems had to be cleaned and checked for proper operation.
- The cabin windows, forward of the wing, were eroded and pitted and had to be replaced.
- Approximately $80 million was required to restore the airplane.

## ENGINE DAMAGE/THRUST LOSS

Of primary concern following an inadvertent encounter with a dense cloud of volcanic ash is almost immediate engine damage followed by engine surge, thrust loss, and possible flameout of all engines. During a less severe encounter, the flight crew may observe fluctuating engine parameters such as a decrease in engine speed and a slow to rapid rise in EGT and fuel flow.

The nature of volcanic ash particles is such that molten deposits accumulate rapidly upon ingestion, reducing high-pressure-turbine inlet-guide-vane area and covering turbine airfoil cooling holes. Engine power loss occurring shortly after entering volcanic ash clouds has been attributed to compressor-operating-parameter changes. The nozzle-guide-vane-throat area is radically reduced, causing the burner pressure (static) and the compressor discharge pressure (static) to increase rapidly. This event causes the engine to surge. In addition, considerable erosion occurs on compressor blades together with heavy airfoil damage.

The factors that influence the degree of erosion and that can also affect performance, particularly of the compressor blades, are: particle hardness and concentration, particle impact velocity (thrust setting) and angle, and core protection.

Volcanic ash contains materials of different compositions. Of importance to jet engine performance is the melting temperature of these materials. Glasses have a characteristic melting point of between 600°C and 800°C. Crystalline particles melt in the range of 1,100°C and 1,200°C. Thrust settings above flight idle will produce temperatures capable of melting volcanic materials. Therefore, it is extremely important to immediately retard thrust levers to idle (altitude permitting) if volcanic ash is inadvertently encountered. Reducing thrust to idle will also reduce compressor erosion damage.

In addition to engine damage or flameout, volcanic ash has a significant effect on the engine's ability to start. In severe cases, it may not be possible to restart the engines. Starting ability is enhanced by decreasing altitude and by allowing the hot section to cool. However, in the event of an all-engine flameout, an immediate restart should be attempted. Flight crews should be made aware that engine acceleration during start at altitude is very slow when compared to ground starts. Also, volcanic ash damage due to eroded compressors and deposits on fuel nozzles will further increase the engine-acceleration time during in-flight starts. Compressor bleed (engine and wing anti-ice plus all air conditioning packs) should be on during restarts and during subsequent operation to maximize engine-surge margin.

# OPERATING INSTRUCTIONS

## AVOIDANCE

Avoid flight in areas of known volcanic activity, particularly at night or in instrument meteorological conditions (IMC), when volcanic ash and dust may not be visible.

When planning a flight into an area with a reported or known potential for volcanic activity, review all notices and directives for current status of that activity.

Plan the flight to remain well clear of reported activity. If possible, stay upwind of volcanic ash and dust.

Do not rely on airborne weather radar to detect and display volcanic ash and dust. Airborne weather radar systems used on commercial airplanes are not designed to detect very small ash and dust particles.

When flying near an erupting volcano, act immediately to get as far from the ash and dust cloud as possible.

When practical, turn to a heading directly away from, and upwind from, the ash cloud.

## RECOGNITION

Volcanic ash and dust may be difficult to detect at night or during flight through clouds; however, the following conditions have been observed by flight crews:

- At night, heavy static discharges (St. Elmo's fire) around the windshield, accompanied by a bright white glow in the engine inlets.
- At night, landing lights cast sharp, distinct shadows in volcanic clouds (unlike the fuzzy, indistinct shadows that are cast against weather clouds).
- Volcanic ash and dust (haze) appearing in the cockpit and cabin. Volcanic dust collecting on top of flat surfaces.
- An acrid odor similar to electrical smoke or burnt dust. The smell of sulfur may also be present.
- Multiple engine malfunctions, such as surge, increasing exhaust-gas temperature, torching from tailpipe, and flameouts.
- Decrease in indicated airspeed.
- An increase in cabin altitude or loss of cabin pressure.

## PROCEDURES

If volcanic debris is inadvertently encountered, accomplish the following:

- Immediately reduce thrust to idle. This will lower EGT, which in turn will reduce the debris buildup on the turbine blades and hot-section components. Volcanic dust can cause rapid erosion and damage to the internal components of the engines.
- Autothrottles off (if engaged). The autothrottles should be turned off to prevent the system from increasing thrust above idle. Due to the reduced surge margins, limit the number of thrust adjustments and make changes with slow and smooth thrust-lever movements.
- Exit volcanic cloud as quickly as possible. Volcanic ash may extend for several hundred miles. The shortest distance/time out of the dust may require an immediate, descending 180° turn. Setting climb thrust and attempting to climb above the volcanic cloud is not recommended due to accelerated engine damage/flameout at high thrust settings.

- Engine and wing anti-ice on. All air conditioning packs on. Turn on engine and wing anti-ice systems and place all air conditioning packs to on to further improve engine stall margin by increasing bleed-air flow. It may be possible to stabilize one or more engines at idle thrust setting where the EGT will remain within limits. An attempt should be made to keep at least one engine operating at idle and within limits to provide electrical power and bleed air for cabin pressurization until clear of the volcanic dust.
- Start the auxiliary power unit (APU), if available. The APU can be used to power the electrical system in the event of a multiple-engine power loss. The APU may also provide a pneumatic air source for improved engine starting, depending on the airplane model.
- Oxygen mask on and 100 percent, if required. If a significant amount of volcanic dust fills the cockpit or if there is a strong smell of sulfur, don oxygen mask and select 100 percent. Manual deployment of passenger oxygen masks is not recommended if cabin pressure is normal because the passenger oxygen supply will be diluted with volcanic-dust-filled cabin air. If the cabin altitude exceeds 14,000 ft, the passenger oxygen masks will deploy automatically.
- Ignition on. Place ignition switches to "on" as appropriate for the engine model (position normally used for in-flight engine start). Cycling of fuel levers (switches) is not required. For airplanes equipped with autostart systems, the autostart selector should be in the "on" position. The autostart system was designed and certified with a "hands-off" philosophy for emergency air starts in recognition of crew workload during this type of event.
- Monitor EGT. If necessary, shut down and then restart engines to keep from exceeding EGT limits.
- If not already closed, close the outflow valves.
- Do not pull the fire switches.
- Leave fuel boost pump switches "on" and open crossfeed valves.
- Do not use fuel heat—this would be undesirable if on suction fuel feed.
- Engine restart. If an engine fails to start, try again immediately. Successful engine start may not be possible until airspeed and altitude are within the airstart envelope. Monitor EGT carefully. If a hung start occurs, the EGT will increase rapidly. If engine is just slow in accelerating, the EGT will increase slowly. Remember, engines are very slow to accelerate to idle at high altitude, especially in volcanic dust—this may be interpreted as a failure to start or as a failure of the engine to accelerate to idle or as an engine malfunction.
- Monitor airspeed and pitch attitude. If unreliable, or if a complete loss of airspeed indication occurs (volcanic ash may block the pitot system), establish the appropriate pitch attitude dictated by the operation manual for "flight with unreliable airspeed." If airspeed indicators are unreliable, or if loss of airspeed occurs simultaneously with an all-engine thrust loss, shutdown, or flameout, use the attitude indicator to establish a minus one degree pitch attitude. Inertial ground speed may be used for reference if indicated airspeed is unreliable or lost. Ground speed may also be available from approach control during landing.
- Land at the nearest suitable airport. A precautionary landing should be made at the nearest suitable airport if airplane damage or abnormal engine operation occurs due to volcanic dust penetration.

Because of the abrasive effects of volcanic dust on windshields and landing lights, visibility for approach and landing may be markedly reduced. Forward visibility may be limited to that which is available through the side windows. Should this condition occur, and if the autopilot system is operating satisfactorily, a diversion to an airport where an auto landing can be accomplished should be considered. If forward visibility is restricted, consider having the airplane towed to the parking gate.

## GROUND OPERATION AT AIRPORTS AFFECTED BY VOLCANIC ASH

- During landings, limit reverse thrust. The use of maximum reverse thrust may impair visibility and ingest dust into the engines.
- The presence of a light layer of dust that obliterates the markings on a runway could have a detrimental effect on braking. The effects of a heavy layer are unknown. Exercise caution when ash has fallen on wet surfaces because surfaces may be slippery and braking may be less effective.
- Brake wear will be accelerated; however, properly sealed bearings should not be affected.
- Avoid static operation of engines above idle power.
- Do not taxi with any engine shut down. Use all engines for taxi.
- Thrust during taxi should be limited to that which is required to sustain a slow taxi speed.
- Avoid operation in visible dust. Ash and dust should be allowed to settle prior to initiating a takeoff roll.
- Use a rolling takeoff procedure.
- Restrict ground use of the APU to engine starts.
- Avoid use of air conditioning packs on the ground if recirculation fans will maintain adequate comfort level. If air conditioning on the ground is necessary, operate at full cold setting if dust is visible and precondition at the terminal using a filtered ground cart if available. Use bleeds off for takeoff if operating procedures permit the configuration. For air conditioning pack operation, consult the operations manual.

- Do not use windshield wipers for dust removal. Wash deposits off with water and wipe residue off with a soft cloth.

## SUMMARY

Flight crews, dispatchers, and air traffic controllers must be aware of any potential volcanic activity affecting their area of operation. They must check notices and air traffic control directives for the current status of any volcanic activity. Should an inadvertent penetration of a volcanic dust cloud be made, flight crews must be aware of the potential problems and be prepared to deal with the arising flight conditions. Also, crews should be aware of the operational conditions at airfields that are contaminated with volcanic ash and dust. If at all possible, avoid penetration of a volcanic ash cloud.

## ACKNOWLEDGMENTS

I wish to acknowledge and thank the engine manufacturers (General Electric, Pratt and Whitney, and Rolls Royce) and the United States Air Force for information that they provided regarding engine operation in volcanic ash and dust.

VOLCANIC ASH AND AVIATION SAFETY:
Proceedings of the First International Symposium
on Volcanic Ash and Aviation Safety
U.S. GEOLOGICAL SURVEY BULLETIN 2047

# DEVELOPMENT OF A REAL-TIME ATC VOLCANIC ASH ADVISORY SYSTEM BASED ON THE FUTURE AVIATION WEATHER SYSTEM[1]

*By* James E. Evans

## ABSTRACT

The overall U.S. air traffic control (ATC) decision-making and communications system should incorporate volcanic ash as a type of aviation weather hazard into the planned aviation weather system, which will be deployed in the United States starting in 1996. This weather system is based on the concept of a four-dimensional (4-D) (3 spatial dimensions and time) gridded database for current and predicted hazard locations with a variety of graphics products tailored to the needs of various users. Real-time information from ground sensors, air-carrier aircraft, unmanned air vehicles, and satellites would be used to estimate the current and predicted locations of hazardous ash. To achieve this system, research is needed on defining harmful ash densities, determining an optimal approach for estimating the density and extent of ash clouds, and validating models for predictions regarding ash clouds.

## INTRODUCTION

Inadvertent ingestion of volcanic ash by jet engines has caused exstensive damage to a number of aircraft recently and could have caused fatal accidents in at least three cases. The operational system used to cope with the 1989–90 eruptions of Redoubt Volcano in Alaska utilized trajectory analysis to estimate ash locations with current textual aviation weather advisories (e.g., significant meteorological advisory (SIGMET), notices to airmen (NOTAM), or center weather advisory (CWA)) as a principal means of conveying information to pilots and controllers (Mostek, 1991; Heffter and others, 1991; Murray and others, this volume; Hufford, this volume; D'Amours, this volume). Manually generated graphics were distributed by facsimile (Criswell, 1991) to planners but not to pilots or controllers. Consequently, visual observations of ash clouds by pilots (or the lack thereof) were critical to air traffic control decision making (Criswell, 1991, Haeseker, 1991). This system had failures in assisting pilots to avoid hazardous ash-cloud encounters and has a tendency for "over warning," which negatively impacts air operations and damages the credibility of the advisory program. A major problem that may arise with operational planning based on trajectory analysis to delineate the region of hazard in a relatively short period (e.g., 24 hours) after an eruption has occurred is that the possible area of warning for an ash encounter may be enormous.

From the viewpoint of surveillance and information dissemination, the recommended system (fig. 1), treats volcanic ash as a type of spatially extended aviation weather hazard similar to in-flight icing. Real-time information from ground, aircraft, and satellite sensors would be combined with the numerical-model predictions of ash transport to provide real-time, current and predicted locations of various levels of ash concentration in the 4-D gridded database generated by the aviation gridded forecast system (AGFS). This 4-D database would be used to disseminate graphical depictions of the current and predicted ash locations by the aviation weather product generator (AWPG).

A key element of the recommended system is the determination of spatial location of damaging ash concentrations (as opposed to the current estimates of an unspecified ash concentration over very large geographical areas). A number of options are considered for achieving this capability. Particular attention is paid to the ongoing validation of ash-location and concentration estimates as the ash clouds move away from the immediate vicinity of the volcano. This paper concludes with some recommendations for the research and development program and system-deployment decisions that will be needed to achieve an operationally useful system.

Related proposals for an integrated detection and warning system have been made by Harris (this volume), D'Amours (this volume) and Stunder and Heffter (this volume). D'Amours, and Stunder and Heffter, principally treat the prediction problem without addressing how the initial ash-cloud 3-D spatial distribution will be determined. Harris suggests estimating ash-cloud parameters from the amplitude and duration of eruption-related harmonic tremor with subsequent ash-location forecasting by trajectory analysis. By contrast, we suggest the use of radars and sensors carried

[1] This work was supported by the Federal Aviation Administration.

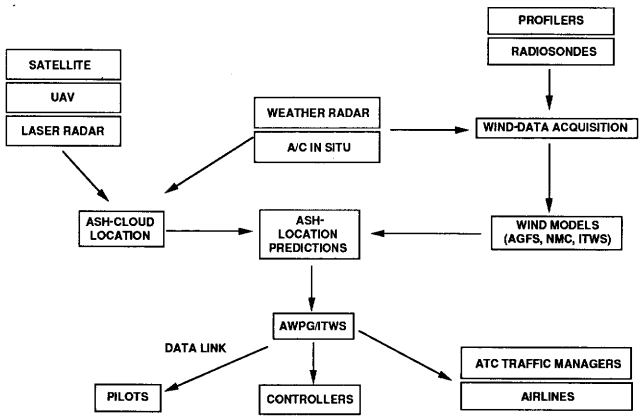


**Figure 1.** Major elements of recommended volcanic-ash-advisory system for aviation. Gridded wind forecasts are combined with ash locations measured near and downwind of volcanoes to generate 4-D, predicted locations of ash clouds. Distribution of the 4-D ash locations are accomplished by the FAA/NWS (Federal Aviation Administration/National Weather Service) weather-information systems. UAV, unmanned aircraft vehicle; A/C, aircraft; AWPG/ITWS, aviation weather product generator/integrated terminal weather system; AGFS, aviation gridded forecast system; NMC, national meteorological center; ATC, air traffic control.

by a dedicated, unmanned aircraft vehicle (UAV) to estimate the initial concentration; the use of full, 4-D, gridded models to estimate future ash locations; and the use of airborne measurements by air-carrier aircraft and dedicated UAV's to validate the estimated ash concentrations.

## THE PLANNED AVIATION WEATHER SYSTEM

The Federal Aviation Administration (FAA) and National Weather Service (NWS) are currently deploying a number of sensors useful for ash surveillance and for measuring meteorological quantities (e.g., wind and clouds) that relate to ash transport and surveillance. The next-generation weather radars (NEXRAD) being procured for en-route airspace are significantly more capable of ash detection than current NWS radars—they also provide radial-velocity estimates (Stone, this volume). NEXRAD routinely produces graphical products, such as maps of echo tops and layered reflectivities, that can be used directly by ATC planners and controllers to provide some safety information on ash clouds while they are detectable by the radar. Additionally, NEXRAD has algorithms to analyze 3-D features of storms and extract pertinent aviation variables, such as the presence of hail and tornadoes. This computation capability could be adapted to automatically estimate the spatial extent of an ash cloud as an input to subsequent prediction programs.

The knowledge of the state of the atmosphere downwind of the volcano will be greatly expanded as a result of improved wind sensors and analysis systems. National Oceanic and Atmospheric Administration's (NOAA) forecast systems laboratory has been developing the aviation gridded forecast system, which is a high-resolution, state-of-the-atmosphere estimation system that plays a key role in the recommended system. The AGFS, which will be tested in 1994 and implemented nationally in 1996, uses the current balloon atmospheric soundings (Holland and others, 1992), the aircraft communications addressing and reporting system (ACARS), and profiler data (Hassel and Hudson, 1991), as well as numerical-forecast-model results to create a high-resolution (30-km horizontal resolution, 25 vertical levels, hourly estimates based on a 6-hour analysis cycle), gridded database of meteorological variables (e.g., winds, temperature) and aviation weather impact products (e.g., cloud locations) using the mesoscale analysis and prediction system (MAPS) (Schlatter and Benjamin, this volume). Owing to computer-load constraints, the initial coverage for the AFGS will be for the continental United States. However, the computational algorithms used have been adapted for Alaska and could be implemented locally. Extension of AGFS/AWPG coverage to western Canada may also be warranted. It should be noted that the AGFS/AWPG will provide many economic benefits to aviation in that area, including better wind estimates for air routes from the United States to Japan.

Reliable real-time dissemination of ash-location information to pilots and controllers is essential. Fortunately, the distributed nature of the volcanic-ash hazard is quite analogous to many weather phenomena. A key element in the weather-information-dissemination system will be the regional and national AWPG (fig. 2), which utilizes the information from NEXRAD and gridded state-of-the-atmosphere information, such as that provided by the AGFS, to create real-time aviation terminal weather products for a variety of users and systems (Sankey and Hansen, 1993). The regional AWPG (RAWPG), associated with the various FAA enrollee centers, is a very attractive vehicle for display of the real-time and predicted ash locations to en-route controllers and various traffic management units because it also will communicate alphanumeric and graphical weather information to pilots via the data-link processor. The AWPG should be operationally available in the 1997–98 time frame. Real-time ash-location estimates would be provided both graphically and in text, to en-route air traffic controllers, flight service station specialists, and pilots to assist in tactical decision making. Since the initial AWPG graphical products would be created and distributed by commercial vendors such as Atmospheric Research Systems, Inc. (ARSI on fig. 2), airline dispatch, airport operators, and others would have ready access to the same information as FAA users.

It is also important that high resolution information be available in the terminal area of major airports that may be affected by ash clouds. Studies of aircraft routes in the vicinity of storms have shown that pilots will fly much closer to hazardous regions in conducting landing and takeoff operations than they would while en route, where they would

deviate to avoid a hazardous region. In addition, pilots are particularly concerned about the operations disruption from overly conservative hazard warnings in the terminal area. The integrated terminal weather system (ITWS) provides very high resolution, gridded analyses (2-km horizontal grid, 5-minute update), as well as dissemination of weather information for the terminal area based on information from the AWPG, Weather Forecast Office (WFO), and the FAA/National Weather Service terminal-area sensors (Evans, 1991b; Albers, 1992). The ITWS has access to a wide variety of weather sensors in and around the terminal area, such as the terminal Doppler weather radar (TDWR), and could easily be augmented to include ash-location information from other sensors, such as laser radars. The ITWS will include color displays for terminal-area traffic managers as well as graphical information for terminal radar approach control facility (TRACON) controllers. ITWS prototypes will commence long-term operationally oriented demonstrations in 1994—the ITWS will be operationally deployed in 1999 (Sankey and Hansen, 1993).

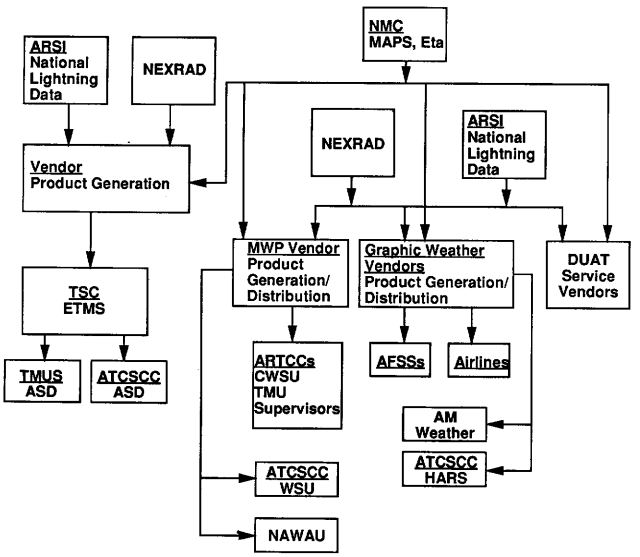


**Figure 2.** Planned aviation weather product generator system when deployed in 1996. Graphical weather products derived from 3-D, gridded database are distributed to FAA en-route and terminal facilities by the meteorological weather processor (MWP) and via aircraft situation displays (ASD) used for traffic management. Flight service stations (AFSS) and airline users will receive similar graphical products from commercial vendors. AM Weather, NOAA aviation weather program broadcast on the Public Broadcasting System; ARSI, Atmospheric Research Systems, Inc.; ARTCC, air route traffic control center; ATCSCC, air traffic control system command center; CWSU, Center Weather Service Unit; DUAT, direct-user access terminal; Eta, estimated time of arrival; ETMS, enhanced traffic management system; HARS, high-altitude routing system; MAPS, mesoscale analysis and prediction system; NAWAU, national weather advisory unit; NEXRAD, next-generation weather radar; NMC, National Meteorological Center; TMUS, traffic management units; TSC, transportation system center; WSU, weather service unit.

## OPERATIONAL REQUIREMENTS FOR AN ASH ADVISORY SYSTEM

No operational requirements have yet been formally stated by the FAA for a volcanic-ash-advisory system. The growing experience with providing operational hazardous-weather products is germane to assessing the requirements for volcanic ash surveillance. In particular, warnings of wind shear due to microbursts and gust fronts have been provided operationally to terminal controllers and supervisors at three different major airports since 1988 (Evans, 1991a). The operational analyses (Stevenson, 1991) carried out in conjunction with these and other tests and demonstrations suggest the following guidelines:

1. Air-traffic-control personnel and aircraft pilots should not be expected to interpret meteorological and ash-location data from sensors to assess the degree of hazard.
2. A sound technical basis for the hazard levels (e.g., tolerable time exposure to various ash concentrations) yielding ash alerts is essential for design of an effective advisory system.
3. Operational requirements for minimum acceptable levels for hazard detection and false-alarm probabilities must be closely related to the expected operational disruption. For example, false-alarm probabilities that were operationally acceptable in low-wind-shear environments were found to be operationally disruptive in high-traffic environments with frequent wind-shear events (Stevenson, 1991).
4. Informal systems users groups (e.g. representatives from airlines, pilot groups, airport authorities, aviation administrations, safety boards, researchers, and information providers) that periodically review the scientific knowledge, operational needs, system performance, and operational use of the products can be very useful for reaching rapid operational acceptance and utility for a new system capability such as the recommended volcanic-ash-advisory system.

A major problem in developing an effective ash-advisory system is the poor understanding of tolerable levels of ash ingestion for the engine type of concern to air carriers. Although several very useful studies have been carried out (Dunn and Wade, this volume; Przedpelski and Casadevall, this volume), there appears to be no published experimental or simulation data on damage to high-bypass engines as a function of ash concentration and exposure duration. Obtaining improved information on tolerable ash concentrations/exposure durations is essential for the development of an improved ash-advisory system.

## ASH-CLOUD-CHARACTERIZATION OPTIONS

Another essential element of the proposed system is improved initial estimates of the spatial distribution of operationally significant ash concentrations including ash type, particle size, and density in both clear air and in the presence of weather clouds. It is very important that the system have some capability to automatically accomplish this objective in the presence of clouds because many of the potentially active areas may be cloud covered during significant portions of the year.

Weather radars can provide 3-D ash-cloud characterization through rain clouds. However, three problems arise: determination that an eruption is underway, discrimination between rain and ash clouds, and estimating the pertinent parameters of an ash cloud. The initial determination of an eruption and discrimination between rain and ash clouds can be based on a variety of clues, including seismic tremors (Harris, this volume), lightning (Hoblitt, 1991), and satellite observations (Matson and others, this volume; Schneider and Rose, this volume). Initially, the determination that an eruption has occurred and delineation of ash-cloud regions (e.g., by entering bounding polygons) would be accomplished manually by Central Weather Service Unit (CWSU) meteorologists using information from sensors as well as from volcanologists. Estimation of ash-cloud parameters would then be accomplished automatically using volume-scanned radar data within the bounding polygon regions.

Estimating the distribution of ash-particle sizes and types cannot be directly accomplished with the microwave weather radars of greatest interest (Harris and Rose, 1983; Stone, this volume) or from current satellites in a time frame compatible with a real-time advisory system. Harris and Rose (1983) have discussed estimating ash-cloud parameters from radar data by using ash-fall data. It may be possible to utilize their technique for real-time estimation in situations where ash-fall measurements have been made on similar previous eruptions.

The use of a dedicated, multi-wavelength laser may also be useful in estimating particle sizes when the cloud cover permits. However, the high rate of attenuation in either ash clouds or rain clouds makes lasers an unattractive choice as a sole means of ash surveillance, particularly from ground-based locations. For example, the University of Washington measurements of Redoubt Volcano plumes showed cases where the ash in an upper layer cloud was not detected due to attenuation of the laser beam by a lower altitude, dense cloud (Hobbs and others, 1991). Similar measurements using lasers and in-situ sampling are needed for ash prediction model verification. However, suitable manned aircraft are expensive to operate and may not be available on short notice.

A UAV with instruments (payload of approximately 150–200 lb) is an attractive option for directly measuring ash concentrations and transporting lasers for ash-cloud mapping. Advances in UAV designs, autonomous guidance and worldwide availability of navigation aids and communications have made UAV's cost effective for atmospheric soundings. It appears (P. Jarvinen, Lincoln Laboratory, written commun., 1992) that the engine of a UAV can be protected from ash-particle ingestion, and impact erosion by ash particles can be kept to manageable levels. The piston-powered Amber UAV is particularly attractive at this time due to its technical characteristics (38 hours endurance at 17,000 ft altitude; operation up to altitudes of 28,000 ft—up to 40,000 ft with a turbocharger—a 70–100-lb internal payload; a 100-lb external payload) and because several U.S. Government owned Amber systems may be available. The proposed mode of operation would be to map ash-cloud extents in a vertical plane normal to the axis of the plume at some selected distance downwind of the volcano (far enough to avoid the large fragments that rapidly precipitate out of the cloud). The downwind spatial distribution of the ash cloud would be updated on a schedule dictated by the winds and the demonstrated capability of the ash-prediction models. It should be noted that there are a number of small-scale turbulence and mesoscale weather features that are not captured in the improved forecast models that will utilize the MAPS grid. Consequently, it appears necessary for the foreseeable future to have the ability to validate ash-cloud predictions downwind on an ongoing basis until ash density is no longer at hazardous levels.

It may be cost effective to instrument some air-carrier aircraft that operate in areas with many volcanoes, such as the North Pacific and Alaska regions. Data from in situ volcanic-ash-detection sensors could be reported over the ACARS link. The information from such aircraft would be used principally to provide additional confirmation of the accuracy of ash predictions and to provide a "heads up" warning to pilots of situations in which the ash densities were approaching levels that could damage the aircraft. For example, if the aircraft were to encounter much higher ash or volcanic gas concentration levels than were predicted, the ACARS could be used to identify cases where the prediction-model estimates were significantly in error. The advantage of using ACARS in this context is that the ash-prediction systems will already be accessing the ACARS data on a continuing basis in real time. Consequently, corrections to the predicted ash-cloud-concentration estimates could be generated quickly and transmitted to the aviation community.

## CONCLUSIONS AND RECOMMENDATIONS

The aviation weather system currently under development by the FAA and NWS should play a critical role in the development of a more effective, real-time, volcanic-ash-advisory system based on the generation and dissemination

of a graphical, 4-D, volcanic-ash product. A number of research and programmatic challenges exist including:

1. Quantitative assessment of ash concentrations that may be of concern for flameout of modern, high-bypass jet engines;
2. Development of an effective system for unambiguous 3-D ash-concentration measurements near and downwind of erupting volcanoes;
3. Validation of the accuracy of models that predict the spatial distribution of ash; and
4. Refinement of the human/machine interface for the system (e.g., by rapid prototype testing).

A product-users group should be established to provide feedback and suggestions as the ash-advisory system evolves. Extending the coverage of the AGFS/AWPG system to Alaska and the western portion of Canada is essential.

## ACKNOWLEDGMENTS

An unpublished review of literature on volcanic ash generation and physical properties by D.C. Johnson was of considerable assistance in developing this paper, and studies by P. Jarvinen on ash-cloud-mapping approaches formed much of the basis for the UAV recommendations. B. Carmichael of the National Center for Atmospheric Research provided figure 2.

## REFERENCES CITED

Albers, S.C., 1992, The LAPS wind analysis: Fourth workshop on operational meteorology, Whistler, B.C., Canada: American Meteorological Society, p. 186–195.

Criswell, C.F., 1991, Volcano eruption notification and aircraft avoidance [abs.], *in* Casadevall, T.J., ed., First International Symposium on Volcanic Ash and Aviation Safety: U.S. Geological Survey Circular 1065, p. 16.

Evans, J.E., 1991a, The terminal Doppler weather radar (TDWR) system at one year before deployment, *in* Third International Conference on Aviation Weather Systems, Paris, France, 1991: American Meteorological Society, p. J1–J6.

———1991b, The integrated terminal weather system (ITWS), *in* Third International Conference on Aviation Weather Systems, Paris, France, 1991: American Meteorological Society, p. 118–123.

Haeseker, E., 1991, Alaska Airlines operating procedures during the 1989–1990 Redoubt eruptions [abs.], *in* Casadevall, T.J., ed., First International Symposium on Volcanic Ash and Aviation Safety: U.S. Geological Survey Circular 1065, p. 20.

Harris, D.M., and Rose, W.I., 1983, Estimating particle sizes, concentrations, and total mass of ash in volcanic clouds using weather radar: Journal of Geophysical Research, v. 88, p. 10969–10983.

Hassel, N., and Hudson, E., 1991, Description of the wind profiles installed in Homer, Alaska [abs.], *in* Casadevall, T.J., ed., First International Symposium on Volcanic Ash and Aviation Safety: U.S. Geological Survey Circular 1065, p. 22.

Heffter, J.L., Stunder, B.J., and Rolph, G.D., 1990, Long-range forecast trajectories of volcanic ash from Redoubt Volcano eruptions: Bulletin of American Meteorological Society, v. 71, p. 1731–1738.

Hobbs, P.V., Radke, L.F., Lyons, J.H., Ferek, R.J., Coffman, D.J., and Casadevall, T.J., 1991, Airborne measurements of particle and gas emissions from the 1990 volcanic eruptions of Mount Redoubt: Journal of Geophysical Research, v. 96, p. 18735–18752.

Hoblitt, R.P., 1991, Lightning detection and location as a remote ash-cloud monitor at Redoubt Volcano, Alaska [abs.], *in* Casadevall, T.J., ed., First International Symposium on Volcanic Ash and Aviation Safety: U.S. Geological Survey Circular 1065, p. 24.

Holland, G.J., McGeer, T., and Youngren, H., 1992, Autonomous aerosondes for economic atmospheric soundings anywhere on the globe: Bulletin of American Meteorological Society, v. 73, p. 1987–1998.

Mostek, A., 1991, NOAA's response to the Mount Redoubt eruptions of December 1989 [abs.], *in* Casadevall, T.J., ed., First International Symposium on Volcanic Ash and Aviation Safety: U.S. Geological Survey Circular 1065, p. 33.

Sankey, D., and Hansen, A., 1993, FAA's work in improving aviation weather, *in* Ninth International Conference on Interactive Information and Processing Systems for Meteorology, Oceanography and Hydrology, Anaheim, CA, 1993: American Meteorological Society, p. 200–209.

Stevenson, L., 1991, Summary of findings from the PIREP-based analyses conducted during the 1988 to 1990 evaluations of TDWR-based and TDWR-LLWAS based alert services provided to landing/departing pilots: Cambridge, Mass., Volpe National Transportation Systems Center Report DOT/FAA DOT-VNTSC-FAA-91d-15, 46 p.

VOLCANIC ASH AND AVIATION SAFETY:
Proceedings of the First International Symposium
on Volcanic Ash and Aviation Safety
U.S. GEOLOGICAL SURVEY BULLETIN 2047

# WARNING SYSTEMS AND PILOT ACTIONS

*By* Peter M. Foreman

## ABSTRACT

Encounters with volcanic ash are a major threat to flight safety. Aircraft must follow flight paths that avoid ash clouds—these flight paths must be based on a knowledge of the location and probable motion of the ash clouds. There is no reliable means of detecting volcanic ash from an aircraft. Therefore, aircraft require a warning from outside.

A warning system will depend upon the cooperation of geological agencies, meteorologists, and the air traffic services. Because volcanic ash clouds are difficult to locate, eruptions should trigger activation of the aviation warning system.

Pilots require concise, self-evident messages in aeronautical language to cause them to change their flight path in a timely manner. Pilots can assist the warning system by reporting their observations. Pilots should be informed of the dangers of volcanic ash encounters, and they should be given training on recognition and mitigation.

## INTRODUCTION AND NATURE OF THE PROBLEM

The first notable encounter was the British Airways 747 near Galunggung, Indonesia, in 1982. It showed that, in such encounters, we might expect a loss of engine power, problems with airspeed indications, and extensive abrasion damage, including a loss of windshield transparency. The encounter placed the flight in great danger, and it required heroic and persistent efforts by the crew to restart the engines and bring the flight to a safe conclusion (Tootell, 1985).

During the eruption of Redoubt Volcano in Alaska on 15 December 1989, a new B747-400 on a flight from Amsterdam to Anchorage flew into the plume and lost power from all four engines. The crew were able to restart the engines and land the flight safely. The initial estimate of damage to the aircraft was $80 million, including the replacement of all four engines (Brantley, 1990).

In spite of the severity of these encounters, the persons involved were lucky. We cannot rely on luck in the future. We must implement measures to keep aircraft out of volcanic ash.

The adverse results from encounters with volcanic ash fall into six categories:

1. *Impact.*—Severe damage within several miles from the volcano.
2. *Abrasion.*—Leading edges, mechanical, and hydraulic systems.
3. *Accretion.*—Ash melts, followed by accretion on turbine nozzles: flameout.
4. *Corrosion.*—Volcanic gases combine with water vapor to form acids.
5. *Adhesion.*—Ash adheres to surfaces and clogs passages for cooling and sensing.
6. *Physiological.*—Gases and particles are noxious to aircraft occupants.

## HOW MUCH VOLCANIC ASH IS A DANGER?

It is estimated that the B747-400 encountered an ash cloud with a density of approximately 2 g/m$^3$ of air. The larger particles in that cloud were in the range of 100–400 microns. Whereas some U.S. military engines are designed to tolerate dust or sand, there is no design tolerance for dust or ash built into civil aircraft. The military specification calls for engines to be able to tolerate 0.05 g of fine sand per cubic meter of air, one-fortieth of the density encountered by the B747-400 at Redoubt. A qualified military engine in a ground-level test ran into severe difficulties and stalling at a density of 0.5 g/m$^3$ of air, or one-quarter the density encountered by the B747-400 (Dunn and Wade, this volume).

Ground tests have also revealed a previously unsuspected problem of the turbine engine: fuel-nozzle coking that occurs after prolonged exposure to ash at densities lower than those that cause accretion in the turbine. The coking problem can also lead to engine failure, and, when it does, there is no possibility of restarting the engine.

## EXTERNAL WARNING SYSTEMS

It has been asked, why do pilots not keep a sharp lookout and steer away from volcanic ash clouds? The crew of the B747-400 reported that they descended into a

smooth layer of cloud with a white top surface, which looked like a weather cloud. At night, or when flying within a prevailing meteorological cloud structure, there may be no opportunity for a pilot to detect an ash cloud before flying into it. Therefore, the safety of air transport requires an ash warning system.

Detecting and locating airborne volcanic ash is a challenge. Sometimes, visual observations are the first and best reports of a remote volcanic eruption. However, visual reports have also been responsible for large numbers of false alarms. Airborne weather radar is not useful for locating volcanic ash, and there are no airborne systems that provide reliable detection and location from a distance. Therefore, aviation needs an external warning system. If an airborne system were to become available in the future, there would be an economic debate on whether to install such equipment on board all aircraft, or whether to rely on external systems in strategic locations.

The reliability of detection of volcanic eruptions is dependent on the degree of monitoring of activity at the volcano. Real-time seismic monitoring is the fundamental method for detecting eruptions, but the seismic signals may leave ambiguities that have to be resolved before announcing an eruption. Other monitoring systems at the volcano complement the seismic information and can reduce the interval of uncertainty. These techniques include television, lightning detectors, weather radar, and infrasound. Volcanologists have a limited ability to forecast some eruptions. Short time intervals are relevant to aviation safety, and minutes of undetected eruption constitute a distinct hazard. If a few minutes of advance warning of an eruption could be provided, safety would be greatly enhanced.

## WARNING-SYSTEM CHARACTERISTICS

To ensure aviation safety, it is necessary that reports of eruptions are processed without delay into warnings to pilots and amendments to air traffic clearances. The first announcement of the start of an eruption should go to air traffic control. Initially, there is no need to try to predict where the ash is, or where it is going. It will be in an expanding, rising column over the volcano.

There are large differences between volcanic eruptions, so it is not easy to generalize. However, it is instructive to study the May 18, 1980, eruption of Mount St. Helens. Figure 1 shows the elevation and distribution of the ash in a west-to-east vertical profile of the Mount St. Helens eruption cloud. This eruption was larger than the 15 December 1989 eruption at Redoubt Volcano, Alaska, but was smaller than the 15 June 1991 eruption at Pinatubo in the Philippines.

Volcanoes are a threat to air safety from the moment that they erupt. Volcanic ash is driven into the sky by a combination of gas thrust and convection. The Mount St. Helens ash took approximately 5 minutes to reach aircraft-cruising altitudes (Rosenbaum and Waitt, 1981) at a rate of climb of approximately 5,000 ft per minute. A warning system should be capable of a 5-minute response time once an eruption has been detected. It is important that the processes of the warning system do not contribute unnecessary additional delays.

Winds play the dominant role in the distribution of volcanic ash. The agency for subsequent ash-location advisories should be the meteorological office. All reports of ash-ejecting eruptions should be sent to that office so that the computerized model of winds over the eruption site can be used, in conjunction with dispersion models, to predict

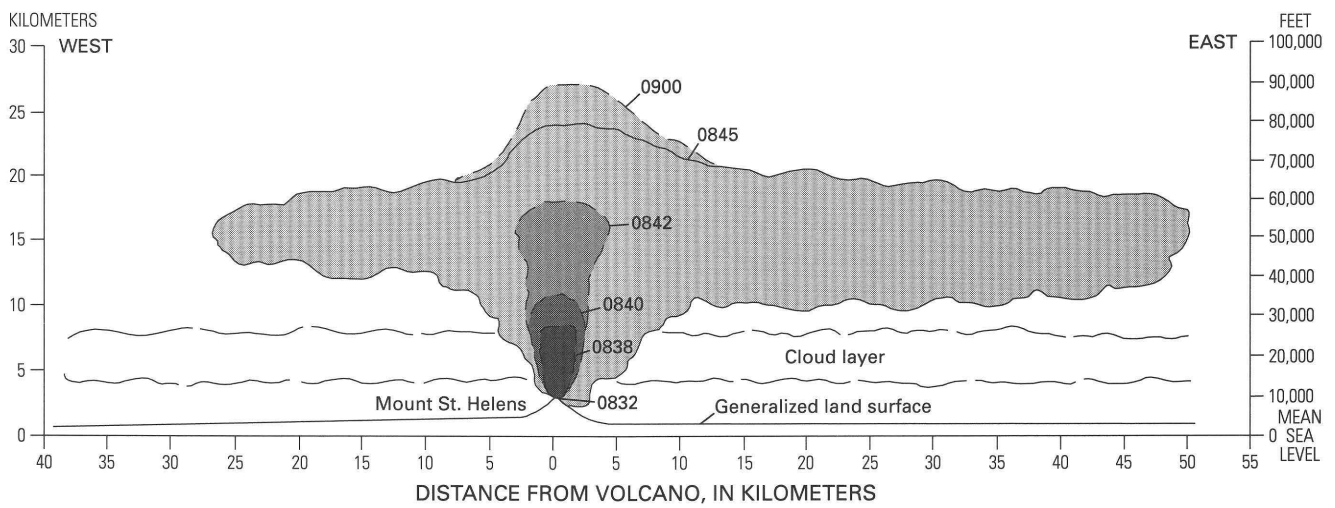


**Figure 1.** Diagrammatic east-west profile of May 18, 1980, Mount St. Helens eruption showing vertical growth and lateral expansion of plume. Times shown are Pacific Daylight Time (e.g., 0838). From Sarna-Wojcicki and others (1981, fig. 331).

ash trajectories. Figure 2 shows a synoptic plot of the May 18, 1980, eruption at Mount St. Helens.

With a knowledge of the start time of an eruption and wind velocities at different levels, an expanding envelope of "probably contaminated" airspace may be declared and updated from time to time. This information should be sent, without delay, to the appropriate air traffic control centers (ATC) to ensure that aircraft in the hazard areas are directed to safer skies. The ash-plume advisory should also be sent to airline-operations dispatch offices so that future flights are planned to avoid the ash plume.

The use of digital communications systems will permit rapid warning-response times after eruption detection. The first step to set up a fast response warning system would be establishing arrangements for intraagency exchange of digital data.

Once air traffic is safely rerouted, then other, more suitable, aircraft can probe the area to discover the nature and extent of the ash plume without necessarily having to enter the ash cloud. Satellite images and visual observations can be expected to further define the ash. Once a region has been surveyed and found to be safe for airliners, it can be reopened.

Figure 3 is a schematic diagram of a generic warning system. The prime sensor inputs are shown in rounded boxes, and the primary agencies are shown in shaded, square boxes. Primary communications links are shown by heavy lines. On the ground, these links should include digital data streams backed up by voice telephone, fax, and teletype. The ground-air link would be radio telephone and, where available, datalink. The supporting ground agencies are shown in unshaded, square boxes. These agencies protect the system by providing redundant channels for communication, shown by thin lines. The system should accept the input of visual-observation reports at any point.

Because ash on the move does not respect jurisdictional boundaries, it is vital to exchange information between countries. Links between similar agencies such as the U.S. Federal Aviation Administration and the Canadian transportation agency, Transport Canada, already exist. It is a matter of expediting the flow of information about eruptions and plume trajectories. All communication links should function in both directions.

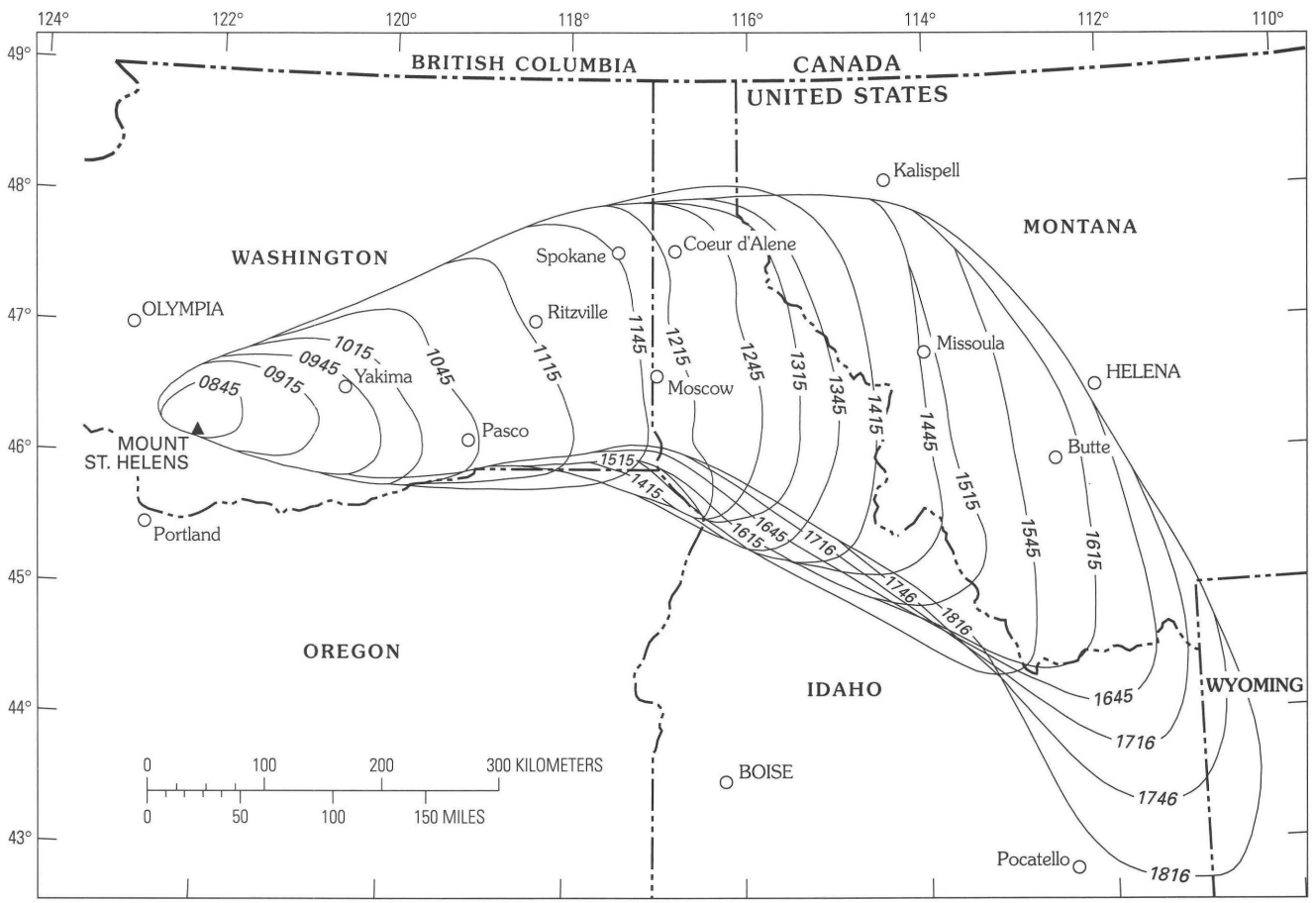


**Figure 2.** Isochron map showing maximum downwind extent of ash from airborne ash plume erupted from Mount St. Helens on May 18, 1980, and carried by the fastest moving wind layer (as observed on satellite photographs). Times shown are Pacific Daylight Time (e.g., 0845). From Sarna-Wojcicki and others (1981, fig. 332).

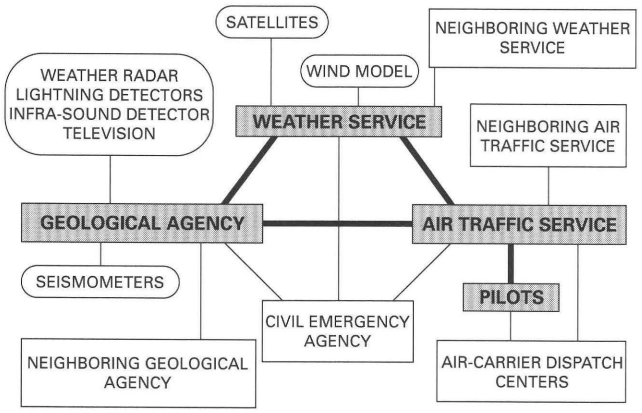


**Figure 3.** Generic warning system schematic diagram. Prime sensor inputs are shown in rounded boxes. Primary agencies are shown in shaded, square boxes. Primary communications links are shown by heavy lines. Supporting ground agencies are shown in unshaded, square boxes (these agencies provide redundant channels for communication, shown by thin lines). The system should accept the input of visual-observation reports at any point.

Ideally, volcanologists and their expert monitoring systems should be the ones to notify of an eruption. This will eliminate many false alarms. Realistically, many geological agencies do not have continuous, fast-reaction capability. When there is no expert system, the eruption report may come from aviation or civil authorities. There is great merit in the system currently operated by the Alaska Volcano Observatory, which varies the degree of alertness based on objective criteria concerning the activity at or beneath a volcano.

There may be difficulty in operating such a system in some parts of the world, but there should be little difficulty in doing so in North America, Europe, and Japan. Eruption monitoring is only required in areas of potential, explosive, volcanic eruption. However, meteorological agencies and air-traffic services should be prepared to deal with ash that has traveled downwind for considerable distances.

## THE AIR-TRAFFIC-CONTROL FUNCTION

Air traffic controllers should become more active in assisting pilots to avoid ash. It is important to appreciate the difference between avoiding thunderstorms, where the prime detection equipment is carried on board the aircraft, and volcanic ash, where primary detection and prediction is ground based.

There will be three distinct air-traffic-control scenarios. In the first, aircraft will be flying in controlled airspace and under controller surveillance. Once the air traffic controller knows where the ash plume lies, he will be in a position to issue escape advisories to all aircraft under his control and in danger of flying into the ash. Other aircraft should receive a general volcanic ash warning, giving plume location and trajectory relative to aeronautical features.

In the second scenario, the aircraft will be flying in controlled airspace under procedural control without controller surveillance. In this scenario, the controller may not be aware of precise aircraft location and will probably not be able to issue an escape advisory. However, the controller could issue a volcanic ash warning, giving plume location and trajectory relative to aeronautical features.

In the third scenario, the aircraft will be flying outside controlled airspace. There is then no air-traffic-control function, but the air traffic services for the flight-information region should issue a volcanic ash warning message, giving plume location and trajectory relative to aeronautical features.

## THE VOLCANIC-ASH-ADVISORY ESCAPE VECTOR

When aircraft are under surveillance and control by a controller who has an ash-plume location and trajectory forecast—perhaps in the form of an image on his air-traffic-display system—the controller should be able to divert conflicting air traffic away from the ash. This would be achieved by directing a message to the aircraft to cause it to turn. It would also be technically possible to use datalink to upload a plume image to an aircraft's electronic flight instrument system (EFIS).

There is a probability that more than one aircraft might need to take immediate action to avoid the plume. To ensure minimum delay, the controller should issue an escape message using phraseology similar to the following:

Pan, Pan. Pan, Pan. Pan, Pan. All stations. All stations. All stations. This is Vancouver Center. Volcanic eruption at 2143 Zulu; Vancouver VOR radial 087 DME 55. Advisory escape vectors; Air Canada 149 050; time air 1165 060; speedbird 682 300. Repeat. Advisory escape vectors; Air Canada 149 050; time air 1165 060; speedbird 682 300. Over.

There will remain a degree of uncertainty about the location and extent of an ash cloud. For this reason the escape message from ATC should be phrased as an advisory vector. It cannot override the ultimate authority of the crew to deal with any situation that threatens the safety of the aircraft. There is the possibility that, once the crew are alerted to the ash, they may be in a better position to plan their own escape route. By giving the escape vector advisory status, the crew has the option to disregard it if they see that it is not safe. However, in the absence of any other observation, they would be well advised to follow the advisory.

The advisory escape vector avoids giving a long message about the origin, location, nature, and trajectory of the ash cloud. It is in a form that pilots are used to hearing and translating quickly into a modification of the aircraft flight path. There is a minimum of cockpit data processing required to implement a vector.

## THE VOLCANIC ASH WARNING

Those aircraft not in immediate conflict with the ash cloud, or not under surveillance and (or) control, should be issued a volcanic ash warning (VAW). In a control and surveillance environment, this would follow the volcanic ash advisory escape vector transmission. The VAW should be revised from time to time as the plume develops and travels downwind. The VAW message should use aeronautical terminology and units of measurement to describe the present situation and the forecast of plume movement. It might contain phraseology similar to the following:

All stations. All stations. All stations. This is Vancouver Center. Volcanic ash warning: volcanic eruption at Mount Baker. Vancouver VOR radial 087 DME 55. Started at 2143 Zulu. Severe volcanic hazards from surface to flight level four zero zero within four zero miles. Plume spreading from flight level two zero zero to flight level four zero zero within arc zero four zero to one two zero degrees magnetic to distance one one zero miles at 2220 Zulu. Plume speed eight zero knots. Out.

After the eruption ceases, the plume will detach from the vent but will continue to remain aloft and travel downwind. The shape may be distorted by vertical wind shear and may develop two or more distinct arms; it may split into separate entities. We do not know how long it remains a hazard to aircraft, but, if we can detect it, we should avoid it.

One of the aircraft damaged in the recent Mt. Pinatubo series of eruptions met the ash 600 nautical miles west of the volcano. This ash must have been airborne for a long time. Thus, it is necessary to keep redefining the plume and passing the latest information to pilots. Simply saying that an eruption occurred several hours earlier is not much help. That information needs additional data before it can be of any use. Subsequent VAW messages should continue to describe the extent of the plume and its trajectory, in plain aeronautical language, with updates at intervals not to exceed 2 hours.

## THE ROLE OF PILOTS

Pilots are the last link in the chain of safety actions to avoid or mitigate encounters with volcanic ash. In order for pilots to be effective, it is necessary that the rest of the system meets the needs of the pilots. Pilots view the sky in terms of routes, fixes, and (or) coordinates. To cause pilots to respond rapidly to a message, it must be given to them in terms that do not require translation.

Approximately 600 of the 1,500 potentially active volcanoes are classified as active. Volcanoes are not generally marked on aeronautical route charts, and most pilots would be hard pressed to come up with the names of more than five volcanoes. Giving pilots references to volcanoes by name will not produce a rapid response. Another problem is that many of the names are unfamiliar and in foreign languages that are hard to pronounce. Even if a pilot has a chart with volcanoes on it, the spoken name may not be quickly related to the written name on the chart. There may well be ambiguity between a pilot's understanding of a spoken name and charted names. Therefore, a statement of where an eruption is occurring expressed in aeronautical terminology will be more helpful to a pilot than the name of a volcano. A bearing and distance from a navigational fix, or a latitude and longitude, will give a pilot the location.

Statements of distance should be expressed in nautical miles, rate of movement in knots, and plume heights should be given to pilots in flight levels (pressure altitude measured in hundreds of feet). References to time should always be in Coordinated Universal Time.

## PLUME AVOIDANCE

Before operating in a region of known potential volcanic activity pilots should check SIGMET's (significant meteorological information reports), NOTAM's (notices to airmen), ATC directives, and PIREP's (pilot reports) for that region. To aid in identifying regions that are potentially active at a particular time, a system based on the Alaska Volcano Observatory color codes could be useful for aviation and would draw closer attention to the situation when required. The exact definitions of the conditions indicated by the colors would need international aviation recognition and agreement before the system could be fully implemented. The conditions green and yellow might normally be supplied only to air traffic centers and air-carrier dispatch offices and, on request, to other users. Condition orange or red should give rise to a special NOTAM.

There is a need for a message priority flag on volcanic information. KLM Royal Dutch Airlines has suggested VARTAM (volcanic ash report to airmen) as a special category of volcanic NOTAM. There is a precedent for NOTAM's of this kind in the usage: SNOTAM is used in some countries for snow information. If the VARTAM idea is accepted, the International Federation of Air Line Pilots' Associations (IFALPA) would like to propose the variation SIGVAR for a significant volcanic ash report or volcanic SIGMET.

All information products mentioned above are text messages. With the aeronautical information communication systems in use today, there is a need for text messages to serve some parts of the world. However, many users and agencies have graphical capabilities. For pilots, graphic products are much easier to use and are more compelling in terms of amending flight plans for the purpose of avoidance. The standard graphic product is the significant weather chart, SIGWX. There is a new internationally recognized symbol to represent a volcanic eruption in progress on the SIGWX chart. However, volcanic ash affecting an airspace might come from a volcano off the charted area. Ash itself is not an agreed item for display on the SIGWX chart. Other graphic products that can be used to display information

about the ash-cloud envelope are trajectory and dispersion forecasts, created manually or by computer.

Armed with this information, pilots should plan to avoid known volcanic ash. In the absence of a clear understanding of the quantitative long-term effects of flight through low ash concentrations, there is no basis to justify planned flight through ash. It is best to avoid volcanic ash clouds by flying around or over them. Ash plumes contain numerous particles that settle from the cloud. Therefore, beneath the cloud there will be a rain of particles. Pilots should respond quickly and decisively to any warnings or directives received in flight.

## MITIGATION FOLLOWING AN ENCOUNTER

Emphasis must be placed on the avoidance of ash. But, if ash penetration occurs, crews should know what to do. Criteria for recognizing that one's airplane is in a volcanic ash plume, and suggested procedures for escaping from a plume, are covered in the paper by Campbell (this volume). There are procedures that are specific to certain types of aircraft, and information from the aircraft manufacturer is the best guide to the operation of individual aircraft. There are some other principles that are generic.

Several carriers have developed useful flight-simulator exercises. As with any non-normal flight condition, there is great benefit to be derived from simulated flight training. When the undesired event occurs with little warning, the simulator experience is a great help to the crew.

The type-specific procedures must take precedence, but generics are useful to know. The following recommendations are taken from a list compiled by the Aerospace Industries Association (Campbell, this volume).

## SPECIAL AIR REPORT OF VOLCANIC ACTIVITY

Pilot observations of volcanic activity are of use to others. IFALPA is a member of the ICAO (International Civil Aviation Organization) volcanic ash working group, which has produced a special air report of volcanic activity form (VAR). Pilots should make sure that VAR forms are carried on board their aircraft if they operate near any area of potential volcanic activity. The form is a guide to the reporting technique. If all the prompts on the form are answered, a detailed and useful report will result. The form should be handed in to the local meteorological office on arrival, but this may not take place for several hours. In the meantime, pilots should seek the cooperation of some air traffic controller or radio operator and report the first eight sections (Fox, 1988).

## CONCLUSIONS AND RECOMMENDATIONS

Pilots need information to alert them to the dangers of volcanic ash encounters and the procedures for avoidance. Training in procedures is vital to prepare pilots to act in a timely manner.

It would be useful to develop a full understanding of how long hazardous particles might remain aloft. Knowing when to downgrade a warning can be almost as important as issuing one.

It is recognized that upgrading our abilities to respond to the problems of volcanic ash will require additional expenditures. However, continuing to operate as we have is not only dangerous, it is also very expensive. Over the past 12 years, the air transport industry and its insurers have incurred costs running into the hundreds of millions of dollars due to encounters with ash. An effective warning system is possible with existing technologies. A system that can reduce the number of such encounters should be considered worthy of financial support.

## REFERENCES CITED

Brantley, S.R., ed., 1990, The eruption of Redoubt Volcano, Alaska, December 14, 1989–August 31, 1990: U.S. Geological Survey Circular 1061, 33 p.

Fox, T., 1988, Global airways volcano watch is steadily expanding: International Civil Aviation Organization (ICAO) Bulletin, April, p. 21–23.

Rosenbaum, J.G., and Waitt, R.B., Jr., 1981, Summary of eyewitness accounts of the May 18 eruption, *in* Lipman, P.W. and Mullineaux, D.R., eds., The 1980 Eruptions of Mount St. Helens, Washington: U.S. Geological Survey Professional Paper 1250, p. 53–67.

Sarna-Wojcicki, A.M., Shipley, S., Waitt, R.B., Jr., Dzurisin, D., and Wood, S.H., 1981, Areal distribution, thickness, mass, volume, and grain size of air-fall ash from the six major eruptions of 1980, *in* Lipman, P.W. and Mullineaux, D.R., eds., The 1980 Eruptions of Mount St. Helens, Washington: U.S. Geological Survey Professional Paper 1250, p. 577–600.

Tootell, E., 1985, All 4 engines have failed; The true and triumphant story of flight BA 009 and the Jakarta incident: Auckland, Hutchinson Group Ltd., 178 p.

VOLCANIC ASH AND AVIATION SAFETY:
Proceedings of the First International Symposium
on Volcanic Ash and Aviation Safety
U.S. GEOLOGICAL SURVEY BULLETIN 2047

# VOLCANIC ASH—THE INTERNATIONAL REGULATORY ASPECTS

*By* Tom Fox

## ABSTRACT

The incidents in Indonesian airspace in 1982 in which two jumbo-jet transport aircraft suffered engine flameout due to ingestion of volcanic ash from the Mt. Galunggung eruption prompted the International Civil Aviation Organization (ICAO) to move quickly to amend its international regulatory documents to include requirements to provide volcanic ash warnings to aircraft. In order to implement such an international warning system, it was also necessary to organize an International Airways Volcano Watch based on observations from a number of international observing networks administered by other United Nations agencies.

## INTRODUCTION

When I look back almost a decade ago and try to imagine if I would have believed it possible that, within a decade, an international symposium would be devoted entirely to the aviation hazard posed by volcanic ash, my imagination fails me. As everyone here is aware, in June 1982, the aviation community, and indeed just about everyone else, heard details of the drama involving a British Airways B747, which encountered a volcanic ash cloud from Galunggung Volcano and lost power on all four engines when flying at 37,000 ft on a flight from Kuala Lumpur, Malaysia, to Perth, Australia.

Initially, there was considerable skepticism that volcanic ash could have been the cause of the incident, and, even when this was later confirmed on examination of the affected engines and by the occurrence of a repeat performance a few weeks later when a Singapore airlines aircraft had a similar encounter, there were still those who classified the incident as a rare event.

Rare event or not, the International Civil Aviation Organization, the International Air Transport Association (IATA), and the International Federation of Air Line Pilots' Associations (IFALPA) took the warning seriously and immediately recognized the extreme hazard that a volcanic ash cloud posed for any aircraft unfortunate enough to encounter it.

## DEVELOPMENT OF INTERNATIONAL REGULATORY MATERIAL

The ICAO Air Navigation Commission moved swiftly and provided member states (i.e., countries) with interim measures to be taken when volcanic eruptions occur in flight-information regions (FIR's) for which they are responsible, pending the development of the necessary formal amendments to international regulatory documents.

The formal amendments were subsequently developed with the assistance of the volcanic ash warnings (VAW's) study group and became applicable in 1987 (Fox, 1988). The VAW study group had been created by the Air Navigation Commission to assist the Secretariat in developing amendments to international regulatory documents that provide for volcanic ash warnings. The group comprises experts in operations, aeronautical meteorology, and volcanology from three member states and five international organizations.

Presently, international regulatory provisions require that information on volcanic activity, including pre-eruption activity, and information about a volcanic eruption and the resulting ash cloud should be transmitted to aircraft operating on air routes that could be affected and, if necessary, arrangements made to activate alternative routes around the affected area. This information is required to be transmitted in the form of notices to airmen (NOTAM's) issued on the initiative of area control centers (ACC's). Information of en-route weather phenomena that may affect the safety of aircraft operations (significant meteorological advisory (SIGMET) messages) is issued by meteorological watch offices (MWO's). The provision of this information forms part of the duties of the ACC and MWO responsible, in their respective fields, for a particular flight-information region (FIR).

The fundamental question is how and from where the ACC and MWO are expected to obtain the initial information that a volcanic eruption has occurred or that a

volcanic ash cloud exists at critical flight levels near an air route.

In the final analysis, the specific means employed by a member state in discharging its responsibilities for an ACC or MWO is a matter for the member state concerned. However, it has been clear from the beginning that the volcanic ash problem is of international concern and usually of regional operational impact. Under these circumstances, ICAO, with the assistance of other international organizations, established an International Airways Volcano Watch (IAVW) in 1987 to ensure that any information available in a member state concerning volcanic activity is injected as soon as possible into the aviation system via the ACC and (or) MWO of the FIR concerned (Heiken, 1988). To achieve this, we have sought and obtained full cooperation from a number of international organizations.

## INTERNATIONAL AIRWAYS VOLCANO WATCH (IAVW)

The idea behind the IAVW was that it should be based on an observing triad comprising:

1. Observations from existing ground-based stations drawn from all known organized international observing networks, regardless of their particular specialized function,
2. Special aircraft reports, and
3. Observations from satellites (meteorological and non-meteorological, as appropriate).

## GROUND-BASED OBSERVING STATIONS

In the case of the ground-based networks, ICAO only has a direct influence on aeronautical meteorological stations, which are not normally located near active volcanoes. Nevertheless, we began with these stations by introducing provisions in the relevant international regulatory documents (i.e., ICAO Annex 3/World Meteorological Organization (WMO) technical regulations) requiring the issuance of volcanic activity reports by these stations and providing a standard format. These provisions were then used as a model when we requested the cooperation/operation of other international organizations in providing for similar reports from their observing networks.

In this regard, WMO has introduced provisions into its international regulatory documents covering the global-observing-system component of the World Weather Watch (WWW) to ensure that reports of volcanic activity are made and transmitted to the relevant ACC or MWO by synoptic, agricultural, hydrological, and climatological observing stations and by merchant ships providing routine weather reports. The World Organization of Volcano Observatories (WOVO),a commission of the International Association of Volcanology and Chemistry of the Earth's Interior (IAVCEI), has made arrangements for volcanic activity reports to be sent to the relevant ACC's and MWO's by volcano observatories strategically sited to monitor active volcanoes; the necessary telephone/telex/fax contact numbers of the ACC's/MWO's have been provided to WOVO for this purpose. Member states have also been requested to make necessary arrangements to ensure that any information on volcanic activity that may become available from other national sources, such as forestry posts, border customs/immigration/police/army posts, etc. (many of which are located in remote regions within sight of volcanoes), should also be sent to the ACC/MWO of the FIR in the member state where the event is located. It is expected that such arrangements could be made separately for each government department or, better still, as part of the member state's national disaster plan. The intended thrust of these arrangements is that all member states should be aware that if there is a volcanic eruption anywhere in their territory, aviation needs to know about it as soon as possible. The ACC concerned will then decide whether or not it is likely to be of concern to aviation and how to proceed.

## AIRBORNE OBSERVATIONS

The second leg of the observing triad is based on reports of observations of volcanic activity by pilots. This source of information is critically important because "unfortunately" a pilot is often the first to observe the eruption (or at least the resulting ash cloud). I say "unfortunately" because observation, especially at night, is generally only possible when "encountering" the ash cloud, and it is aircraft encounters with ash clouds that we wish to avoid. In order to assist the pilot in sending such reports, an ICAO special air report of volcanic activity report (VAR) form (fig. 1) was developed by the VAW study group, based upon two earlier reporting forms tested by the Air Transport Association of America and Qantas Airlines (Johnson and Casadevall, this volume).

IATA and IFALPA are making continuous efforts to ensure that airlines and pilots are aware of the special air report of volcanic activity by including such information in training documentation and in operating manuals. It will be noted that the first eight items listed in the form concern information that is needed immediately and, therefore, is to be transmitted to the air traffic service (ATS) unit by radio. An additional seven items concern information that is to be completed in written form and handed in at the next point of landing. On receipt by the ATS unit, the information is to be relayed immediately to other aircraft concerned, passed to the ACC for decision regarding the issuance of a NOTAM, and forwarded to the associated MWO for issuance of a SIGMET. Subsequent NOTAM's would include additional information, as necessary, concerning rerouting, etc.,

## MODEL VAR

| | | | | | | | | | | |
|---|---|---|---|---|---|---|---|---|---|---|
| Operator | Aircraft identification (as per Item 7 of flight plan) ..... | | Pilot-in-command ..... | | Dep. from ..... Arr. at ..... | | Date ..... Date ..... | | Time ..... UTC Time ..... UTC | |
| Addressee | | | | | | | | | | |
| | AIREP SPECIAL | | | | | | | | | |
| SECTION 1 | 1 | Aircraft identification | | | | | | | | |
| | 2 | Position | | | | | | | | |
| | 3 | Time | | | | | | | | |
| | 4 | Flight level or altitude | | | | | | | | |
| | 5 | Volcanic activity observed at | (position or bearing and distance from aircraft) | | | | | | | |
| | 6 | Air temperature | | | | | | | | |
| | 7 | Spot wind | | | | | | | | |
| | 8 | Supplementary information<br>*(Brief description of activity including vertical and lateral extent of ash cloud, horizontal movement, rate of growth, etc. as available)* | | | | | | | | |
| SECTION 2 | The following information is not for transmission by RTF | | | | | | | | | |
| | | | TICK ☑ THE APPROPRIATE BOX | | | | | | | |
| | 9 | Density of ash cloud | (a) wispy ☐ | | (b) moderate dense ☐ | | (c) very dense ☐ | | | |
| | 10 | Colour of ash cloud | (a) white ☐ | | (b) light grey ☐ | | (c) dark grey ☐ | | | |
| | | | (d) black ☐ | | | | | | | |
| | 11 | Eruption | (a) continuous ☐ | | (b) intermittent ☐ | | (c) not visible ☐ | | | |
| | 12 | Positior of activity | (a) summit ☐ | | (b) side ☐ | | (c) single ☐ | | | |
| | | | (d) multiple | | (e) not observed ☐ | | | | | |
| | 13 | Other observed features of eruption | (a) lightning ☐ | | (b) glow ☐ | | (c) large rocks ☐ | | | |
| | | | (d) ash fall out | | (e) mushrooming cloud ☐ | | (f) nil ☐ | | | |
| | 14 | Effect on aircraft | (a) communications ☐ | | (b) nav. systems ☐ | | (c) engines ☐ | | | |
| | | | (b) pitot static ☐ | | (e) windscreen ☐ | | (f) windows ☐ | | | |
| | | | (g) nil ☐ | | | | | | | |
| | 15 | Other effects | (a) turbulence ☐ | | (b) St. Elmos Fire ☐ | | (c) fumes ☐ | | | |
| | | | (d) ash deposits ☐ | | | | | | | |
| | 16 | Other information | Add any information considered useful | | | | | | | |

**Figure 1.** Volcanic ash reporting form (VAR) approved by the International Civil Aviation Organization for use by pilots. This form is carried by each pilot in their flight handbook. Items 1–8 (section 1) are to be reported immediately by the pilot to the responsible air-traffic-control center. Items 9–16 (section 2) are to be completed and filed after landing.

whereas subsequent SIGMET's would include trajectory forecasts, etc. Member states have also been requested to arrange matters so that general aviation pilots are made aware that any information they may have concerning volcanic activity is to be passed immediately to the ATS unit with which they are in contact.

## MONITORING BY SATELLITE

The third leg of the observing triad is based on monitoring volcanic eruptions and volcanic ash clouds by satellites. In this regard, ICAO has requested WMO to advise on the regional meteorological centers that could assist in monitoring volcanic ash clouds and providing trajectory forecasts. In addition, WMO is coordinating the further development of forecasting techniques needed to provide trajectory forecasts. National and regional arrangements have been made in the two regions that have been most affected by the volcanic ash problem, in Southeast Asia and in North and Central America. However, as illustrated by a number of papers in this symposium, there are a number of difficulties in the interpretation of satellite data to detect and track volcanic ash clouds. Effective satellite monitoring of all potential problem areas 24 hours per day, preferably automated, is the ideal, but it does not seem that this will be realized in the near future. Currently, work is proceeding through WMO to have the necessary WMO regulatory documents amended to introduce volcanic ash monitoring and trajectory forecasting as part of responsibility of certain regional meteorological centers that have the necessary capability. Similarly, the ICAO communications/meteorology/operations (COM/MET/OPS) divisional meeting (held in Montreal in 1990 jointly with the ninth session of the WMO Commission for Aeronautical Meteorology) recommended that volcanic ash clouds should be included on the significant weather forecasts (SIGWX) issued by regional-area forecast centers as part of the world-area forecast system (WAFS). In this regard, WMO has developed the necessary symbols for the depiction of volcanic ash clouds on WAFS SIGWX forecast charts. The IAVW is shown diagrammatically in figure 2.

## NON-REAL-TIME INFORMATION ON VOLCANIC ACTIVITY

In addition to the foregoing real-time information on volcanic activity, relevant ICAO regulatory documents also

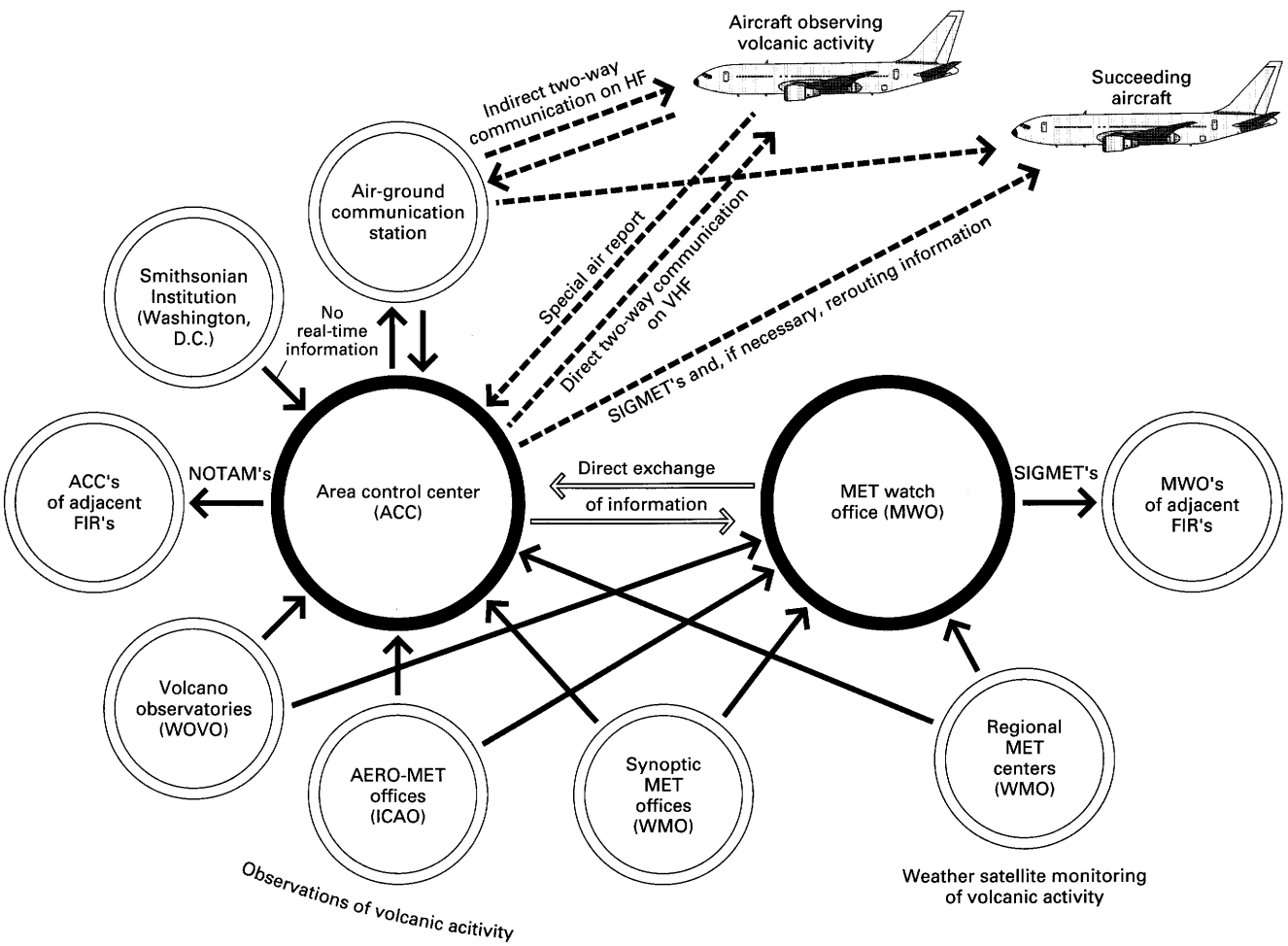


**Figure 2.** Organization of the voluntary International Airways Volcano Watch (IAVW). HF, high frequency; VHF, very high frequency; see text for other acronyms.

require that member states should include, as necessary, in their aeronautical information publications (AIP's) details concerning any volcanoes located in the flight-information region for which they are responsible. Moreover, the Smithsonian Institution has kindly agreed to routinely provide copies of their Bulletin of the Global Volcanism Network every month to ACC's/MWO's that require it (McClelland, this volume). This publication keeps ACC's/MWO's informed on the current status of active volcanoes and thereby provides important background information.

## CURRENT AND FUTURE WORK IN ICAO

The foregoing describes the international regulatory aspects of the problem as they stand today. Although there will certainly be amendments to regulatory documents to improve or add to existing procedures in the future, most effort needs to be brought to bear on the effective implementation of existing procedures. Some of the problems (such as the initial observation of an eruption by satellite or otherwise, the development of techniques to assess the content and density of the spreading volcanic ash cloud, and the associated safety margin for jet engines needed to permit the reopening of affected routes) are of a technical nature and will not be solved overnight. Other problems, however, are of a more procedural nature and should be amenable to improvement. Indeed, it is earnestly hoped that the results of the exchange of information and ideas at this symposium will help to achieve this goal.

From the international perspective, the single most important procedural problem is that of communications. The flow of information from initial observation, from whatever source, to the ACC and MWO is fraught with problems. To start, non-aviation sources generally have little or no experience in working with the aviation system, and clear channels of communication have to be developed. Necessary procedures have to be kept current because years may go by without them ever having to be activated. Such problems are to be expected, given the disparate parties involved. What is not usually expected is that a similar problem could exist in the communication of such information between the ATS unit and the pilot. In fact, however, often there is such a problem, which not only affects the provision of warnings of volcanic ash but also other hazardous phenomena, such as wind shear, clear-air turbulence, etc. The communication pressures on ATS units these days are such that it is extremely difficult for them to act as virtually the only communication interface between meteorological departments and the pilot. As air traffic continues to grow, it seems likely that major improvements will be difficult to achieve until the advent of datalink communications later in this decade. In the meantime, efforts will continue to be made to mitigate the problem and, in this regard, the need to provide information quickly in a concise, operationally relevant format will be paramount.

One example of an effort to improve communications is the color-code system developed in Alaska to indicate the status of a volcano (Brantley, 1990). A color code, based on the Alaskan code was proposed at the second meeting of the ICAO Asia/Pacific Volcanological/Airspace meeting in Bangkok in September 1992, and member states in the Asian and Pacific regions will be encouraged to use this code when reporting volcanic eruptions to ACC's and MWO's. Could this format be used worldwide, or would specific criteria need to be developed for different types of volcanoes, and, if so, how many? The views of volcanologists on these questions would be very useful because such an agreed-upon format would lend itself very well to inclusion in ICAO international regulatory documents.

In order to tackle some of the communications problems, the ICAO council, in 1992, approved a special implementation project in the Asian and Pacific regions for 1992–93 in which a two-person team (comprising an aeronautical meteorologist and a volcanologist) will visit a number of member states in the regions to advise, as necessary, on local arrangements for the routing of information on volcanic eruptions from observing stations through the ACC/MWO to the pilot.

In the immediate future, ICAO, with the assistance of the VAW study group, will finalize preparation of a handbook covering all aspects of the volcanic ash problem to serve as up-to-date guidance material for member states. Completion of the handbook was postponed until after this symposium so as to permit the inclusion of the latest experience gained during the recent volcanic eruptions at Redoubt Volcano in Alaska and Mount Pinatubo in the Philippines.

The importance of the Redoubt Volcano eruptions cannot be over emphasized because they have finally dispelled any lingering doubts about the operational hazard posed by volcanic ash; they have provided an opportunity for a detailed examination of the operational procedures; and perhaps most important, they have been the catalyst that prompted the holding of this international symposium. I am confident that, given the continued enthusiasm of the people involved in all their various fields of endeavor, the volcanic ash problem will be resolved in a satisfactory manner.

## REFERENCES CITED

Brantley, S.R., ed., 1990, The eruption of Redoubt Volcano, Alaska, December 14, 1989–August 31, 1990: U.S. Geological Survey Circular 1061, 33 p.

Fox, Tom, 1988, Global airways volcano watch is steadily expanding: ICAO Bulletin, April, p. 21–23.

Heiken, G., 1988, Volcanic ash warnings for civil aviation: A summary report on activities of the volcanic ash warnings study group of the International Civil Aviation Organization: Bulletin of Volcanology, v. 50, p. 135–136.

VOLCANIC ASH AND AVIATION SAFETY:
Proceedings of the First International Symposium
on Volcanic Ash and Aviation Safety
U.S. GEOLOGICAL SURVEY BULLETIN 2047

# SEATTLE AIR ROUTE TRAFFIC CONTROL CENTER RESPONSE TO ERUPTIONS OF MOUNT ST. HELENS

*By* Robert F. Hamley *and* Donald H. Parkinson

## ABSTRACT

Following notification of an eruption of Mount St. Helens, the Seattle air route traffic control center (ARTCC) weather service and traffic management units begin a mutual effort to determine the horizontal and vertical extent of the ash plume. Ash-cloud reports are gathered from ground and airborne observers, available imagery is used when possible, and ash-plume movement is determined using available wind data in conjunction with observations. Ash-plume area and movement must be determined as quickly and accurately as possible so that air traffic can be kept well away from the hazard.

Data sources, including satellite and radar imagery, are of extremely limited value for minor volcanic eruptions. Visual ash-cloud reports have been the primary information source on the presence of ash but are not available after dark. Credibility and completeness of reports is a major problem even during daylight hours. Considerable upper-wind data and wind forecast guidance is available but must be used with caution and considerable cross-checking. Aircraft wind reports provide an essential supplement and verification.

Based on the observed and predicted extent of the ash plume, the traffic management unit (TMU) examines the impact of the event on air traffic routes, several of which are close to Mount St. Helens. Advisories are sent to air traffic facilities and to system users that identify affected areas and suggest alternate routes.

## INTRODUCTION

When Mount St. Helens volcano erupts, the ash cloud spewed into the atmosphere can quickly create an emergency situation to the pilot who unknowingly enters it. Engines, both jet and piston, are easily damaged by volcanic ash when it is present in sufficient quantities. It is an urgent matter that pilots be made aware of the location of a volcanic ash plume.

Upon notification of an eruption, the Federal Aviation Administration (FAA) ARTCC in Seattle takes immediate action for the protection of air traffic. Under the direction of the ARTCC area manager-in-charge (AMIC), the TMU and the Center Weather Service Unit (CWSU), affiliated with the National Weather Service, become involved in a joint response effort. The problem is to determine the vertical and horizontal extent and short-term horizontal movement of the ash plume and to provide that information to pilots and the air traffic system (ATS) as quickly as possible.

The focus of this paper is on the minor eruptions of Mount St. Helens during the period 1989 through early 1991. These involved bursts of steam and unknown concentrations of ash that reached altitudes of 12,000 to 25,000 ft. The limitations confronting the response effort and the lack of knowledge regarding the actual hazard to aircraft are more acute for these smaller events than for major eruptions. The degree of uncertainty underscores the importance of treating them as legitimate hazards to air traffic even if the risks might be negligible.

## EVENT NOTIFICATION

Seattle ARTCC normally receives very early notice of an eruption of Mount St. Helens. Initial notification often comes from a pilot who is in continuous radio contact with an air traffic controller. Pilots flying under visual flight rules (VFR), and thus not required to be in radio contact with an air traffic controller, also may contact Seattle ARTCC to give notice of an observed eruption. When either the U.S. Geological Survey Cascade Volcano Observatory or U.S. Forest Service personnel in the area become aware of an eruption, Seattle ARTCC is designated as the first facility to notify (Myers and Theisen, this volume).

Seattle ARTCC is therefore in a position to provide early event notification to other agencies and to react promptly in issuing advisories to the air traffic control (ATC) system and system users. Facilities that Seattle ARTCC contacts for event notification, including those involved in advisory and forecast support, in most cases have had no prior notice of an event before being contacted by Seattle ARTCC. Notification performed by Seattle ARTCC is shown in table 1.

**Table 1.** Mount St. Helens eruption notification and forecast coordination involving Seattle air traffic control.

| Seattle center receives notification of an eruption of Mount St. Helens from: |
|---|
| • Pilot reports |
| • Cascade Volcano Observatory, U.S. Geological Survey |
| • U.S. Forest Service, Mount St. Helens office |
| **Notification given by Seattle center includes the following:** |
| • Washington and Oregon Departments of Emergency Management |
| • Cascade Volcano Observatory, U.S. Geological Survey |
| • U.S. Forest Service, Mount St. Helens and Mount Hood offices |
| • FAA regional office, northwest mountain region |
| • Air traffic control facilities (regional) |
| • National Air Traffic Control System Command Center |
| **Notification given by the center weather service meteorologist for forecast and warning coordination:** |
| • Forecast office, National Weather Service, Seattle, Wash. |
| • Synoptic analysis branch, National Meteorological Center, Camp Springs, Md. |
| • National aviation weather advisory unit, Kansas City, Mo. |

## LOCATING THE ASH PLUME

Before air traffic can be properly directed to stay clear of volcanic ash, the ash plume must be located and its height estimated as accurately as possible. Satellite and radar imagery available in the Central Weather Service Unit can be used for this purpose, and pilot reports can be solicited through center controllers.

Satellite imagery now available in the CWSU has been recently (October, 1991) upgraded. Data from the geostationary orbiting environmental satellite (GOES) is available via satellite link to a new meteorological workstation, known as the meteorologist weather processor (Hamley and Schultz, 1992).

Visible and infrared images are received each half-hour and can be viewed on a high-resolution monitor with animation capability, an unlimited degree of zoom, and the capability of infrared color enhancement. Previously, one hard-copy satellite image was received each half-hour via Harris laserfax. Radar data is derived from five air traffic control radars (FAA and military), located in Washington and Oregon, and two National Weather Service (NWS) radars.

Table 2 provides a subjective assessment of radar and satellite performance that could be expected during a major eruption. Images are viewed on the meteorologist weather processor, either individually or within a mosaic, and may also be animated. Mosaic-display capability and animation, previously unavailable, are both incorporated into the new system. Imagery now available to the CWSU is superior in many respects to that which successfully detected the ash plume following the May 18, 1980, eruption of Mount St. Helens. We therefore assume that it would yield considerable information in the event of a major eruption and large ash plume. In contrast, radar and satellite imagery provided us with little or no data during the minor eruptions of the 1989 to 1991 period, due to the small size of these events. Small plume size, low plume height, low ash content, and surrounding cloud cover all contributed to our inability to identify an ash plume in radar or satellite images. We doubt that new image-viewing and processing methods available with the meteorologist weather processor will make up for these deficiencies because the problem is insufficient image data.

**Table 2.** Imagery available in the Center Weather Service Unit through meteorologist weather processor.

[MWP, meteorologist weather processor; GOES, geostationary orbiting environmental satellite; ATC, air traffic control; NWS, National Weather Service]

**Satellite imagery**

GOES infrared and visible images available via satellite link and viewed on high-resolution monitor. Infrared color-enhancement and animation capability.

**Radar imagery**

Viewed on MWP monitors. Individual radar images or mosaic display of all; includes animation capability. Data is available from the following ATC and NWS radars:

| Site | Radar type |
|---|---|
| Portland, Oreg. | SR74C (NWS) |
| Salem, Oreg. | RSR1 (ATC) |
| Spokane, Wash. | PS67 (ATC) |
| Seattle, Wash. | RSR1 (ATC) |
| Condon, Oreg. | RSR3 (ATC) |
| Klamath Falls, Oreg. | PS67 (ATC) |
| Missoula, Mont. | WSR57 (NWS) |

**Estimated ash-plume detection capabilities and limitations of available imagery during a major eruption**

| Imagery type | Characteristics | |
|---|---|---|
| | Day | Night |
| Radar | Positive detection. Poor definition of horizontal ash distribution; no vertical discrimination. Detection limited by ground clutter and obscured by precipitation. | Same as day time. |
| Satellite images (visible light) | Detection limited by contrast with cloud cover; otherwise good during bright daylight. | No data. |
| Satellite images (infrared) | Excellent detection of ash plume extending above surrounding cloud cover. Estimation of plume height is accurate within approx. 5,000 ft. | Same as day time. |

Lack of available ash-plume data does not lessen the need to respond to a possible airborne hazard. Other resources must be used to the fullest degree, including pilot reports and observations from ground observers. These sources have provided most of the data on volcanic emissions that has been used in making decisions at Seattle ARTCC.

The meteorologist and the TMU supervisor coordinate on the need for information that can be supplied by pilots. The TMU solicits these reports through center controllers and disseminates them to both the air traffic system and the aviation community. Other visual reports may come from the Cascade Volcano Observatory, the U.S. Forest Service, or from manned weather-observing stations in the general area, depending upon the degree of daylight and the amount of cloud cover.

Sightings made by ground and airborne observers can establish the direction of movement of the plume and provide a very general description of its size, ash content, and ash fallout. Pilot reports are the best source to determine the plume altitude within narrow limits. However, none of these data, even collectively, can give us a comprehensive picture of plume area. Table 3 summarizes information provided by visual observations.

Credibility of ash reports must be questioned because they are quite often misleading. Pilots sometimes seem predisposed to observe ash around Mount St. Helens or in any area where it has been previously reported. Still, pilot reports have been our most valued, and sometimes exclusive, source of data pertaining to an ash plume.

**Table 3.** Information from visual observations about ash plumes from Mount St. Helens.

[TMU, traffic management unit]

| Information sources |
|---|
| Pilot reports |
| Pilot reports go directly to air traffic controllers and are passed on to the TMU. TMU and center weather service solicit additional reports through controllers. TMU transmits reports for distribution within the air traffic system and externally. |
| Surface observations |
| Calls are made to, or received from, Cascade Volcano Observatory (U.S.Geological Survey) and Mount St. Helens office (U.S. Forest Service). Routine, non-automated, hourly surface observations are available from: Portland, Oreg.; Toledo, Wash.; Hillsboro, Oreg.; Yakima, Wash.; Troutdale, Oreg.; The Dalles, Oreg. |
| **Information supplied** |
| Pilot reports |
| Area description of plume and plume movement. Physical description of plume, including apparent ash content. Increase or decrease in plume activity and whether plume is continuing to rise. Accurate plume-top report if aircraft is near altitude of plume top. |
| Surface observations |
| Same overall as for pilot reports except more limited, as indicated below. |
| **Limitations** |
| Pilot reports |
| Darkness, surrounding cloud cover, and flight visibility. Difficulty in describing plume area and assessing ash content. Also limited by number of aircraft in volcano area. No aircraft above about 40,000 ft; therefore, no accurate estimate of plume top is possible at altitudes significantly above 40,000 ft. |
| Surface observations |
| Darkness, surrounding cloud cover and visibility. Perspective and distance from volcano limit accurate description of real extent, movement, and physical appearance. Plume-top estimates not reliable. |

## FORECASTING SHORT-TERM PLUME MOVEMENT

Once the general area that may be subject to airborne ash has been determined, then plume drift must be considered. Because we attempt to anticipate movement in the very short term, the current drift tendency (as dictated by upper winds and seen by observers) will weigh heavily in advisory products. Ash movement through a range of altitudes must be considered because wind direction and plume travel may vary greatly through the vertical range of the plume.

Upper-air observations, including wind measurements from the surface to more than 50,000 ft, are taken twice daily (at 00 UTC and 12 UTC) by stations in the upper-air-observation network. The site at Salem, Oreg., located 85 miles southwest of Mount St. Helens, is the site closest to the volcano and it is often the most representative of wind flow over the mountain. However, this may not be the case if there is significant shear or curvature in the wind field between Salem and Mount St. Helens or in the event that wind velocity has changed since the previous observation was taken. We therefore must consider wind data observed from other sites in the region and interpolate as necessary.

Automated upper-wind forecasts (Aviation Weather Services, 1985, p. 4–18) from the National Meteorological Center in Washington, D.C., are also available to the meteorologist. These apply to numerous points in Washington and Oregon and to nine different altitude levels from 3,000 through 39,000 ft. In assessing upper winds, currency of observed data and verifying time of forecast winds must both be taken into account. A comparison of satellite photos and upper-level forecast charts can sometimes reveal a problem with the model run and its wind forecasts.

Pilot reports are another important source of upper-wind information. In the case of a minor eruption with satellite imagery unable to define an ash plume, pilot-reported upper winds are perhaps the deciding input in the determination of

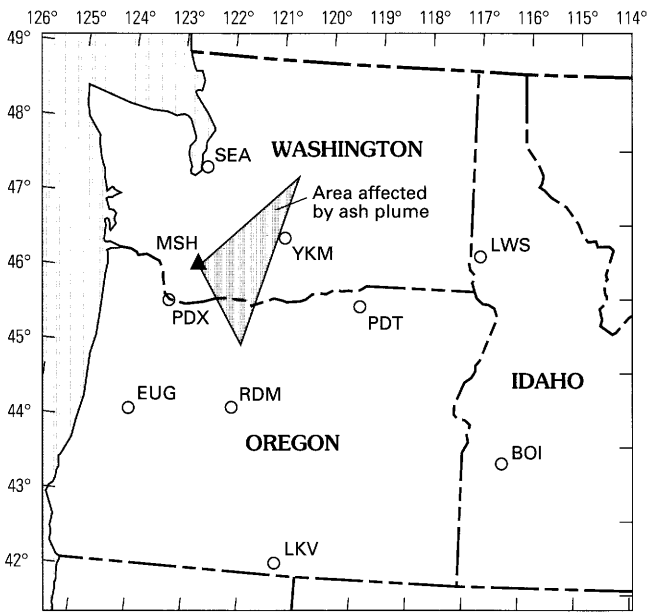


**Figure 1.** Example of plume-trajectory forecast for Mount St. Helens (MSH). Shaded triangular region shows area projected to be impacted by a hypothetical ash cloud that would be expected to move to the east of a line from Mount St. Helens to Wenatchee, Wash., and east from a line from the volcano to the area of Redmond, Oreg. (RDM). SEA, Seattle, Wash.; PDX, Portland, Oreg.; LKV, Lakeview, Oreg.; PDT, Pendleton, Oreg.; YKM, Yakima, Wash.; BOI, Boise, Idaho; EUG, Eugene, Oreg.; LWS, Lewiston, Idaho.

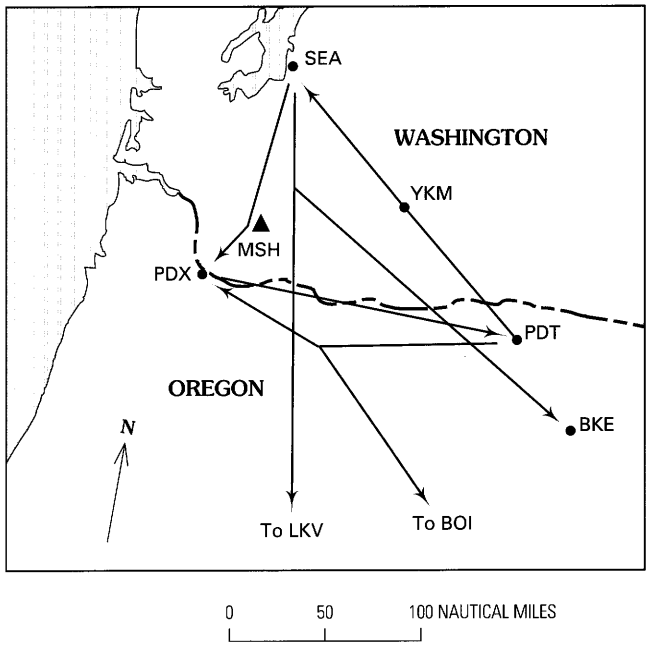


**Figure 2.** Proximity of Mount St. Helens (MSH) to major air traffic routes. SEA, Seattle, Wash.; PDX, Portland, Oreg.; BKE, Baker, Oreg.; LKV, Lakeview, Oreg.; PDT, Pendleton, Oreg.; YKM, Yakima, Wash.; BOI, Boise, Idaho.

plume movement. These can be solicited by the TMU from any aircraft, but a variety of aircraft with areal navigation systems are equipped with a digital display of wind velocity that can be communicated to the ARTCC upon request.

A plume-trajectory forecast (fig. 1), coordinated between the CWSU and the National Weather Service forecast office in Seattle, Wash., furnishes short-term input to air traffic advisories following an eruption of Mount St. Helens. This forecast depicts a triangular area intended to indicate the maximum amount of airspace into which the plume is spreading. Wind velocity and direction of plume movement are indicated for a number of levels extending from 6,000 ft to the top of the plume, if known, but not exceeding a maximum altitude of between 50,000 and 55,000 ft.

## ASSESSING POTENTIAL AIR TRAFFIC IMPACT

Although the occurrence of a volcanic event can potentially impact air traffic operations at all airports in the Pacific Northwest, the greatest impact is likely to be experienced by flights traveling to and from Seattle-Tacoma (SEA) and Portland (PDX) International Airports. Prevailing winds across the northwestern United States vary from southwesterly to northwesterly most of the time. Thus, all arrival and departure routes southeast of SEA and east of PDX are prime candidates to be affected by a volcanic eruption. These routes are shown in figure 2 and include:

1. The departure route that proceeds southeasterly from SEA. This route splits 50 nautical miles south-southeast of SEA, with one stream proceeding east-southeast to Baker, Oreg. (BKE), passing 27 nautical miles east of Mount St. Helens at its closest point. The second stream continues south-southeasterly to Lakeview, Oreg. (LKV), and passes 15 nautical miles east of the volcano. More than 140 flights are scheduled daily along these routes.
2. The arrival route that approaches SEA from the southeast, via Pendleton, Oreg. (PDT), and Yakima, Wash. (YKM). More than 80 scheduled flights daily use this route, which passes within 60 miles of the volcano at its closest point.
3. The arrival routes that approach PDX from the east, via Pendleton, Oreg. (PDT), or Boise, Idaho (BOI). This route passes just north of Mount Hood in Oregon, less than 45 miles from Mount St. Helens. Seventy to 75 flights are scheduled daily along this route.
4. The departure route from PDX to the east, which proceeds directly to PDT en route to eastern destinations. This route is flown daily by 25 to 30 scheduled flights and passes 27 miles south of the volcano.
5. The heavily traveled route for SEA departures to PDX. More than 75 scheduled flights daily use this

route, with an additional 30–50 unscheduled flights commonly using the route on a daily basis. This route passes within 6 nautical miles of the volcano and is named for the mountain (HELNS arrival).

These five routes, all of which pass within 60 nautical miles of Mount St. Helens, are utilized by more than 400 flights daily proceeding to and from SEA and PDX. Naturally, the impact of a volcanic event upon air traffic will vary according to the magnitude of the event itself, but even a fairly minor eruption, such as the one on November 5, 1990, affects these corridors, causing a major disruption of the air traffic system during the time that flight operations are restricted in the area. An event approaching the scale of the cataclysmic eruption of May 18, 1980, which produced an enormous amount of airborne volcanic ash, would impact not only the routes described above but would have a far-reaching effect on air traffic over the entire region.

## NOTIFICATION OF SYSTEM USERS

Once the scope of the volcanic ash hazard has been determined, Seattle ARTCC personnel execute a series of procedures designed to warn air traffic system users of the potential hazard and to safely and efficiently route traffic around the hazard area. Warnings and advisories are transmitted by the traffic management unit, the area manager-in-charge, and the Center Weather Service Unit (CWSU).

The CWSU meteorologist is required to issue a center weather advisory (CWA) designating the affected area and describing plume height and movement. The CWA is a meteorological advisory written in a coded format and is valid up to a maximum of 2 hours. The area affected by the plume is described in the heading of the advisory, whereas plume movement and altitude is mentioned in the text. A CWA is broadcast by all operational sectors at Seattle ARTCC. The FAA manual supplement, "Aviation Weather Services" (1985), describes the format and use of CWA's.

The following is an example of a CWA:

ZSE1 CWA 01 011400–011600. From 40SE OLM to YKM to RDM to 20N PDX to 40SE OLM. Ash plume from Mount St. Helens moving southeast above FL200 and moving east-northeast below FL200. Unknown amounts of ash to FL300.[1]

In addition to transmitting a CWA, the meteorologist will also coordinate with the National Aviation Weather Advisory Unit in Kansas City, Mo., for the possible issuance of a longer term national advisory product known as a significant meteorological advisory, or SIGMET, which can be valid up to 4 hours (Aviation Weather Services, 1985).

The AMIC is primarily responsible for ensuring that all appropriate air traffic control facilities and system users are made aware of the event. Alert messages are transmitted, either verbally or via teletype, to all ARTCC control-room personnel, the FAA northwest mountain region duty officer, the Seattle ARTCC air traffic manager and assistant manager, and all other air traffic control facilities contained within Seattle ARTCC airspace. The AMIC is also responsible for relaying a notice to airmen (NOTAM) to the appropriate FAA flight service station for immediate dissemination to pilots. For example:

Airborne hazard: Drifting volcanic ash from Mount St. Helens to a point 50 miles south of Mount St. Helens from the surface to FL300, drifting southwestward. Avoidance advised.

Such a NOTAM is transmitted by FAA flight service stations via the transcribed weather broadcast network and by ATC towers via the automatic terminal information system. The TMU supplements these broadcasts by advising the Air Traffic Control System Command Center (ATCSCC) in Washington, D.C., which, in turn, transmits advisories to all 20 ARTCC's in the contiguous United States and to all commercial air-carrier companies.

TMU is also responsible for determining alternate routes around the hazard area and for coordinating these routes with ATCSCC for transmission to air carriers and other air traffic control facilities. These advisories are updated as appropriate, depending on the scope of the event.

When conditions are severe enough to warrant restricting air traffic from a hazardous area, Seattle ARTCC has the authority to transmit a NOTAM that temporarily suspends flight operations in the affected area. This NOTAM is transmitted nationally and is regulatory in nature. An example of such a NOTAM is as follows:

Flight restrictions at Mount St. Helens effective immediately until further notice. Pursuant to FAR 91.137b, temporary flight restrictions are in effect for a 50-mile radius of Mount St. Helens and on a line from Mount St. Helens to Pendleton, Oreg., 50 miles either side, at or below 30,000 ft to provide a safe environment for aircraft operations. Seattle ARTCC is the agency in charge.

## IMPROVEMENTS IN THE RESPONSE PROCESS

### MODIFYING RESPONSE STRATEGIES

We believe that the future ability of Seattle ATC center to respond to a volcanic event can be improved by changes in response methods. One change would involve our early notification of the National Weather Service Synoptic Analysis Branch (SAB). Their use of the McIDAS III system (Soumi and others, 1983) for viewing satellite imagery has produced some plume data even during minor eruptions of Mount St. Helens. Immediate contact of the SAB may produce valuable, near real-time input to short-term air traffic advisories.

We also advocate increased awareness by ground and airborne observers of the need for accuracy and completeness of visual observations. This is especially true for pilots because we rely so heavily on their reports. Information of

[1] In air traffic control, altitudes above 18,000 ft are described in hundreds of feet. FL200 therefore represents 20,000 ft.

value to the response process includes an estimate of plume dimensions and, in the case of pilot reports, the altitude of the plume, whether it is continuing to rise, and direction of plume drift. Comments on the physical appearance of the plume, including its density and apparent ash content, would also be of value. The International Civil Aviation Organization (ICAO) format for reporting volcanic ash (Fox, this volume) would be sufficient to meet the informational needs that we have identified, and we recommend that it be used.

Recent eruptions of Mt. Spurr have demonstrated that the problems associated with forecasting ash-plume movement and routing air traffic clear of the hazard are continuing. During the most recent event (August 1992), the lack of accurate information regarding plume scope and movement resulted in aircraft being routed into areas in which airborne volcanic ash was present. These events also pointed out the need for improved communications and coordination regarding volcanic events between Canadian and U.S. agencies involved in air traffic control and aviation weather services.

## NEW TECHNOLOGY

Other improvements in the response process are inevitably linked to coming technology. The deployment of the NEXRAD (Next Generation Radar WSR-88D) national Doppler radar network will include two sites within radar range of Mount St. Helens (Seattle and Portland) and two other sites at somewhat longer range (Spokane, Wash., and Pendleton, Oreg.) but located in the direction that prevailing winds would tend to carry an ash plume (Klazura and Imy, 1992). Commissioning of these radars is scheduled during the period 1994 to 1996.

The velocity azimuth display (VAD) available with NEXRAD radars will provide the radar operator with data that can be used to interpret winds aloft, which is currently not possible with conventional radars. Winds can be interpreted using radar-return data from widespread precipitation as well as from clear air. It should be noted, however, that radar return in clear-air situations is very limited both vertically and horizontally.

We are not aware of any data on NEXRAD performance in the detection of volcanic ash. It seems plausible that NEXRAD radars would be superior to conventional radars in detecting returns from volcanic ash, given their much greater power and sensitivity. If so, they would yield considerable data on plume distribution and ash concentration in addition to data on winds that are carrying the plume.

Automated methods of tracking and characterizing an ash plume would merit consideration for the short-term period following an eruption (about 2 hours), during which Seattle center must act to protect the safety of air traffic. An example is the "atmospheric diffusion particle-in-cell" technique described by Ellis and Sullivan (1991), which was used experimentally following a minor volcanic event ("puff") of Mount St. Helens.

## SUMMARY

The efforts of the Seattle ATC center to respond to the minor eruptions of Mount St. Helens since 1989 have consistently encountered a lack of information regarding the extent and concentration of volcanic ash, or even whether a legitimate hazard exists. The response has been driven by the absolute necessity to err on the side of safety, due to the proximity of major air routes to Mount St. Helens and the known destructive effects of volcanic ash on aircraft engines.

For eruptions of small magnitude, existing satellite and radar imagery often provide little or no usable data pertinent to an ash plume. Ash-plume observations from pilots and ground observers are often limited, questionable, or unavailable due to darkness. Thus, observed and forecast upper winds often provide most of the guidance in assessing short-term plume extent and movement.

Deployment of Doppler radars is expected to bring improved ash detection as well as the capability of assessing upper winds through interpretation of radar return, but to a degree that is yet unknown.

In attempting to improve our response effort to a volcanic eruption in the region, we have proposed the following:

1. Immediate consultation with the Synoptic Analysis Branch, Washington, D.C., for plume-trajectory guidance.
2. Improvement in our coordination with Canadian air traffic and weather officials.
3. Use of the ICAO VAR (volcanic activity report) volcanic pilot report format by pilots in reporting volcanic activity (Fox, this volume).
4. Future use of short-term computer models for characterizing and forecasting ash plumes.

## REFERENCES CITED

Aviation Weather Services, 1985, A supplement to Aviation Weather AC-00-6A: Washington, D.C., U.S. Department of Transportation and U.S. Department of Commerce, 148 p.

Brown, R.A., and Wood, V.T., 1987, A guide for interpreting Doppler velocity patterns: Norman, Okla., NOAA National Severe Storms Laboratory, p. 7–21.

Ellis, J.S., and Sullivan, T.J., 1991, ADPIC calculated volcanic ash cloud transport and fallout from the 20 December 1990 Mount Saint Helens puff, *in* Casadevall, T.J., ed., First International Symposium on Volcanic Ash and Aviation Safety, U.S. Geological Survey Circular 1065, p. 18.

Hamley, R.F., and Schultz, R.F., 1992, A brief introduction to the meteorologist weather processor: Salt Lake City, National Weather Service, Western Region Technical Attachment No. 92-28, 9 p.

Klazura, G.E., and Imy, D.A., 1992, Description of initial set of analysis products available on the WSR-88D radar system: Norman, Okla., National Weather Service, Operational Support Facility, 10 p.

Soumi, V.E., Fox, R., Limaye, S.S., Smith, W.L., 1983, McIDAS III—A modern interactive data access and analysis system: Journal of Climatology and Applied Meteorology, v. 22, p. 765–778.

VOLCANIC ASH AND AVIATION SAFETY:
Proceedings of the First International Symposium
on Volcanic Ash and Aviation Safety
U.S. GEOLOGICAL SURVEY BULLETIN 2047

# AN AUTOMATED VOLCANIC ASH WARNING SYSTEM

*By* David M. Harris

## ABSTRACT

The requirements for an automated volcanic ash warning system are outlined, along with a possible system architecture and description of operation. The system would detect volcanic clouds by coexistence of anomalous electric fields and thermal infrared sources in the lower atmosphere above volcanoes. These can be measured by using ground-based electric-field mills and infrared radiometers, respectively. Antecedent, strong volcanic tremor would be used as additional evidence permitting instrumental observations to be interpreted as an eruption producing volcanic ash. Equations for estimating the cumulative mass erupted and the mass eruption rate from volcanic-tremor data, in terms of reduced displacements, are given in this paper. The equations are based on the linear relation between eruptive masses of air-fall ash and pyroclastic deposits and the integral of volcanic-tremor amplitude for six eruptions of Mount St. Helens. Mass eruption rates and eruptive masses determined from volcanic-tremor data would be used with a plume-rise model to estimate the input source parameters to an ash-transport model and forecast model. The integrated system would perform volcano monitoring, data analysis, ash-cloud forecasting, hazards evaluation, notification, and data communications. The volcano-monitoring strategy is based on coverage of volcanoes that pose the greatest risk to aviation and other interests.

## INTRODUCTION

Volcanic ash clouds pose a significant hazard to in-flight aircraft (Rose, 1987). An effective volcanic ash warning system is needed (Reddan, 1985; Foreman, this volume). This paper describes a system that might meet this need. The ideas in this paper were originally expressed in the abstract of Harris and Mitchell (1986), who proposed a system concept based on using volcanic-tremor amplitudes to determine mass eruption rates and electric-field sensors to detect ash clouds.

The purpose of this paper is to describe an automated system for detecting volcanic ash clouds, forecasting their hazards to aviation, and notifying users. This paper includes suggested functional and performance requirements for a volcanic ash warning system and outlines a possible system design. The focus of this paper is on system architecture and on methods for obtaining from volcanological observations the interpretive data required for ash-cloud detection and the quantitative data required for transport and forecast calculations.

## SYSTEM REQUIREMENTS

The design and implementation of a volcanic ash warning system must be based on detailed consideration of user requirements, eruptive phenomena, and sound engineering practices. An ad hoc approach to warning-system design and implementation is not likely to yield the best technical approach or optimum system performance. Some suggested requirements for a volcanic ash warning system are listed in table 1 (performance requirements) and table 2 (functional requirements).

## SYSTEM ARCHITECTURE

The volcanic ash warning system architecture is shown in figure 1. There are six subsystems (volcano monitoring, volcano data collection, communications, ash transport and forecasting, hazards evaluation, and notifications). Each subsystem includes a hardware layer and a software layer. Only the software layer is shown in figure 1. The system hardware (computer and communications interfaces) could be located at an existing volcano observatory or regional air route traffic control center (ARTCC). A single site could provide volcanic ash hazard warnings for volcanoes in the operations area for one or more ARTCC's. The system receives periodic status reports and data streams from data-collection subsystems at monitored volcanoes.

The monitoring strategy involves installation and maintenance of volcano data collection modules at volcanoes selected by eruption probability and risk to aviation. New sites would be added after onset of premonitory activity.

**Table 1.** Suggested performance requirements for volcanic ash warning system.

[nm, nautical miles; kft, 1,000 feet]

| Performance criteria | Suggested requirement |
|---|---|
| Detection-range limits (minimum) | |
| Mass-eruption rate | $1\times10^{6}$ to $5\times10^{9}$ kg $s^{-1}$ |
| Total mass erupted | $10^{8}$ to $10^{13}$ kg |
| Response time | |
| Initial advisory | 3 minutes after event |
| Official warning | 6 minutes after event |
| Forecast | 6 minutes after event |
| Reliability | |
| System availability | > 99 percent |
| Hazard-detection probability | > 95 percent |
| Error rate for warnings (total) | < 10 percent |
| Inappropriate warnings | < 5 percent |
| False warnings | < 5 percent |
| No warning | < 5 percent |
| Error rate for notifications | < 3 percent |
| Forecast Accuracy | |
| Ash-cloud front | 20 to 50 nm at 1 to 4 hr |
| Horizontal edge | 15 to 30 nm at 1 to 4 hr |
| Altitude (top) | 10 kft (about 3 km) |
| Ash concentrations | ± 50% of reported value |

Rapid deployment would be facilitated by a modular system architecture and use of standard data-communications hardware. Although the system coverage would not be complete, available resources would be focused on volcanoes deemed likely to erupt and (or) that are deemed to represent a high risk to aviation.

## VOLCANO DATA COLLECTION SUBSYSTEM

The purposes of the volcano data collection subsystem are to provide answers to the following questions in near real time:

1. Is an explosive eruption occurring?
2. Is an ash cloud present?
3. If an eruption occurred, how long did it last and what was the mass eruption rate as a function of time?

This is the minimum volcanological data needed by a volcanic ash hazard warning system. The monitoring methods and frequency of observation must be adequate to ensure prompt detection of an explosive volcanic eruption larger than either of two specified thresholds defined by mass eruption rate and mass erupted. Table 1 includes suggested ranges for these system-design parameters, subject to evaluation of system costs and benefits.

**Table 2.** Suggested functional requirements for volcanic ash warning system.

[ATC, air traffic controller; haz., hazard]

*Volcano data-collection subsystem*
- •Monitor volcanic tremor amplitude and frequency spectra
- •Monitor atmosphere for evidence of pyroclastic eruption
- •Monitor atmospheric electric-potential gradient

*Volcano monitoring subsystem*
- •Process messages from volcano data-collection subsystem
- •Determine whether an eruption is occurring
- •Detect explosive volcanic activity
- •Determine whether an ash cloud is present
- •Determine mass eruption rate
- •Log time, eruption rate, status, and source location

*Ash transport and forecasting subsystem*
- •Retrieve wind forecasts from database
- •Initialize plume algorithm
- •Initialize ash-transport and settling algorithm
- •Perform ash-transport and dispersion simulations
- •Generate volcanic-ash-cloud forecasts and ash-fall maps
- •Maintain atmospheric wind database
- •Generate and update plume forecast and aviation haz. maps
- •Track and report ash cloud locations

*Hazards evaluation subsystem*
- •Evaluate the ash cloud forecasts
- •Determine the type, location, and magnitude of hazards
- •Identify jet routes and aviation facilities at risk
- •Select warning messages
- •Prepare aviation hazards forecasts for release
- •Generate prioritized notification list
- •Recommend air-space closures and restrictions

*Notifications subsystem*
- •Notify users of hazards via messages and files
- •Issue warnings, route messages, and verify receipt
- •Maintain messages and distribution lists
- •Interface to ATC's and other communications systems

*Communications subsystem*
- •Communications resource management
- •Route messages
- •Acquire meteorological data from remote systems
- •Retrieve data from observatories in near real time
- •Perform notification tasks
- •Log communications activity

*Database management subsystem*
- •Maintain system and operational data

*System status monitoring requirements*
- •Perform system-level status monitoring and reporting
- •Perform subsystem status monitoring and reporting
- •Perform system calibration and testing

The volcano data collection subsystem would include a digital seismograph, an electric-field mill, a thermal radiometer, a system controller, and a radio communications interface. The digital seismograph and data-collection

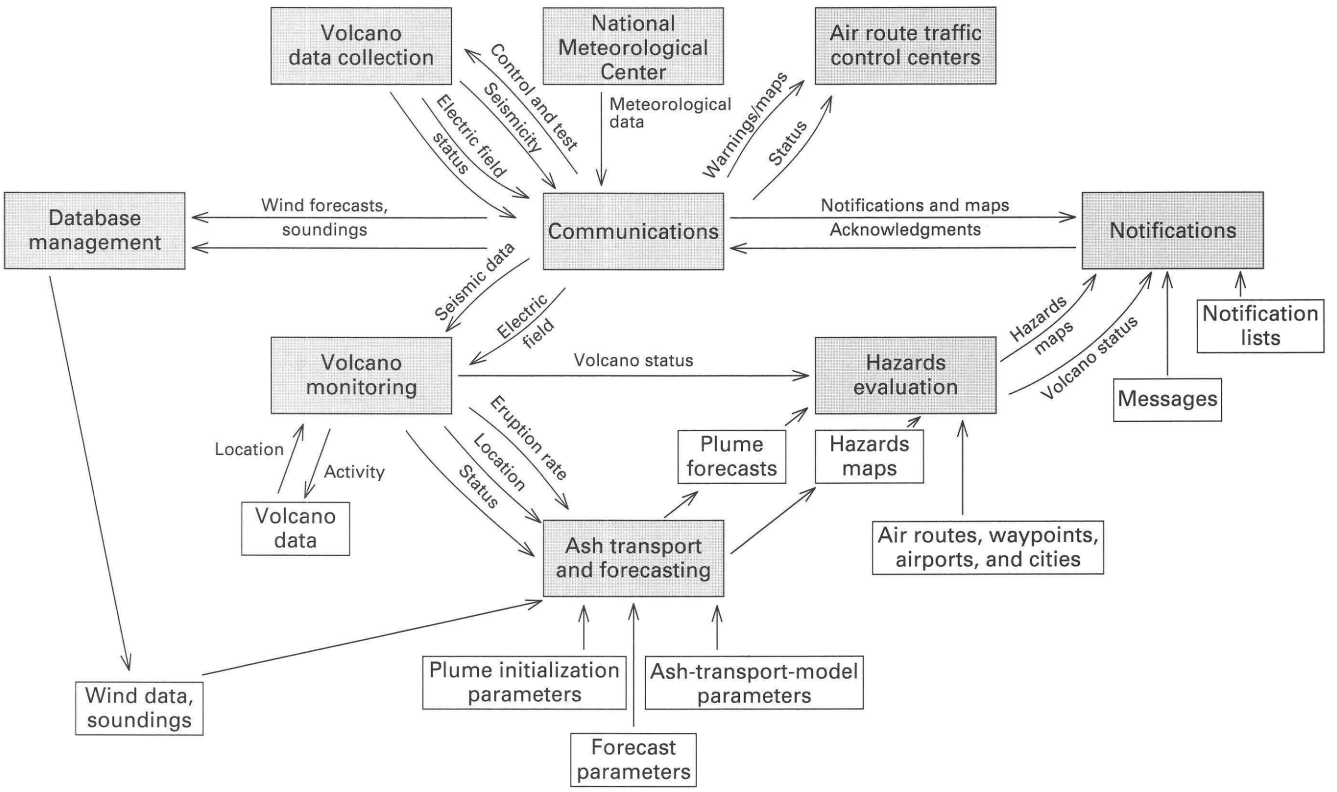


**Figure 1.** System architecture and data-flow diagram for the volcanic ash warning system (VAWS). Data flows and directions are indicated by lines. Shaded boxes represent VAWS subsystems and external systems (National Meteorological Center and air route traffic control centers); unshaded boxes represent data files. The volcano-data-collection subsystem is linked to the communications subsystem by satellite communications or some other data communications system (not shown).

system must provide the capability to record and perform spectral analysis (Nishi, 1987) of discrete seismic events and volcanic tremors in near real time (Hurst, 1985; Endo and Murray, 1991). The amplitude of volcanic tremor may be used to characterize eruption styles (McNutt, this volume; Endo and Murray, 1991) and to estimate mass eruption rates (this paper). The functional roles of the above volcano-monitoring techniques in the context of an automated volcanic ash warning system are described below.

## DETECTION OF ASH CLOUDS AND EXPLOSIVE ERUPTIONS

The capability to detect volcanic ash clouds by instrumental methods is not yet available at most volcano observatories (Brantley, 1990; WOVO, 1991). Weather radar systems can provide ash-cloud detection and tracking capabilities in areas with radar coverage, assuming the target can be correctly identified (Harris and others, 1981; Harris and Rose, 1983). Weather radar may not be practical or affordable in remote areas. Lightning-positioning and tracking systems (Lyons and others, 1985) have been used to detect cloud-to-ground lightning in ash clouds (Hoblitt and Murray, 1990; Brantley, 1990). Microbarograph arrays (Onodera and Kamo, this volume) measure acoustic waves from volcanic explosions and locate their source from atmospheric propagation times. The microbarograph array can detect onset of explosive activity under certain conditions, but its capability to detect continued eruption of ash clouds may require more evaluation.

Harris and Mitchell (1986) suggested using electric-potential-gradient sensors to detect ash clouds. Electric fields in the vicinity of ash clouds change greatly during and after ash eruptions, both near the source and in residual ash clouds (Hatakeyama, 1943, 1958; Hatakeyama and Uchikawa, 1952; Kikuchi and Endoh, 1982; Hobbs and Lyons, 1983; Gilbert and others, 1991; Gilbert and Lane, this volume). Hatakeyama's work shows that ash clouds produced by explosive eruptions can be detected by using electric-field mills to measure atmospheric electric fields and disturbances caused by electrified ash clouds. The system design described here is based on electric-field measurements, following the pioneering work of Hatakeyama and coworkers, but the particular detection technology is not important. The important matter is that the technology employed must represent the best combination of reliability, detection threshold, detection delay time, false

detection rate, and practicality, which must be determined by parallel-field evaluations of these methods.

The feasibility of using ground-based electric-field measurements to detect ash clouds has been demonstrated by Hatakeyama and coworkers (Hatakeyama, 1943, 1958; Hatakeyama and Kubo, 1943a, 1943b; Hatakeyama and Ishikawa, 1946). Ash clouds from Asama Volcano in Japan were detected about 50 km downwind from the volcano. Electric-field measurements obtained at distances of 1 to 9 km from their source indicate that the vertical potential gradients from ash clouds are initially positive (downward-directed fields), but the sign of the field typically changes with time or distance downwind from the vent (Harris, unpub. data), based on data from small eruptions of Aso (Hatakeyama and Uchikawa, 1952) and Asama (Hatakeyama, 1958). Field measurements of electric charge on falling ash (Hatakeyama, 1958; Kikuchi and Endoh, 1982; Gilbert and others, 1991) show that ash particles are electrically charged. Finally, electric fields can persist in mature ash clouds for at least several hours, as shown by Hatakeyama (1949), owing to the existence of residual charge on far-flung fine ash.

Volcanic eruption columns rise to great heights in the atmosphere only if the eruption column is hot and entrains sufficient air to develop a buoyancy force that counters the gravitational force (Morton and others, 1956; Wilson, 1976; Sparks and Wilson, 1982). Although volcanic plumes are optically thick, they provide a thermal source that should be detectable by a ground-based infrared radiometer or imaging infrared sensor such as a digital infrared camera. This provides the capability to detect an anomalous, extended infrared source generally associated only with high-temperature explosive eruptions. Thermal radiometric monitoring of the airspace immediately above volcanic vents should provide positive identification of thermal plumes and information not available from other monitoring instruments.

The volcano-monitoring system would include quantitative criteria for a logical determination of whether an ash cloud is present or absent. The criteria would be based on thermal infrared observations, atmospheric electric-field measurements, and the amplitude of antecedent volcanic tremor. The system would consider an ash cloud to be probable whenever there is evidence of thermal plumes and electrified ash clouds, based on data from thermal radiometers and electric-field mills. These sensors should provide ancillary data with the least ambiguity for identifying conditions consistent with pyroclastic eruptions whenever strong volcanic tremor is present. When such conditions are met, the mass eruption rate would be determined instrumentally from volcanic-tremor amplitude.

## DETERMINATION OF MASS ERUPTION RATE

An instrumental method for determining the mass eruption rate in near real time is an essential component of a volcanic ash warning system. Such information is needed to initialize volcanic-ash-transport and distribution models. I will show that the mass eruption rate can be determined in near real time from volcanic-tremor amplitudes.

Consider the hypothesis that volcanic-tremor amplitude is linearly proportional to the mass eruption rate during explosive eruptions. If this hypothesis is true, then the integrals of the volcanic-tremor amplitude with time must also be proportional to the integral of the eruption rate with time. The integral form of this hypothesis is satisfied for six eruptions of Mount St. Helens.

**Table 3.** Volcanic-tremor amplitude, reduced displacement integral, and mass of eruption products at Mount St. Helens, 1980.

[Tg, teragrams ($10^{12}$ g); rel., relative; disp., displacement]

| Date (1980) | Volume of pyroclastics[1] ($km^3$) | Mass of flows[2] (Tg) | Mass of air-fall deposits[3] (Tg) | Total mass of deposits[4] (Tg) | Integral of volcanic tremor amplitude[5] (rel.) | Reduced disp. integral[6] ($cm^2/s$) |
|---|---|---|---|---|---|---|
| May 18 | 0.12 | 170 | 490 | 660 | 2,880 | $1.9\times10^6$ |
| May 25 | 0.001 | 1.5 | 42 | 44 | 590 | $3.8\times10^5$ |
| June 12 | 0.01 | 15 | 45 | 60 | 463 | $3.0\times10^5$ |
| July 22 | 0.006 | 8.7 | 4.0 | 13 | 115 | $7.5\times10^4$ |
| Aug. 7 | 0.004 | 5.8 | 1.0 | 6.8 | 124 | $8.1\times10^4$ |
| Oct.16–18 | 0.001 | 1.5 | 0.7 | 2.2 | 25 | $1.6\times10^4$ |

[1] Rowley and others (1981).

[2] Calculated from volume using an in situ pyroclastic flow density of 1,450 $kg/m^3$ reported by Wilson and Head (1981).

[3] Sarna-Wojcicki and others (1981).

[4] Sum of columns 2 and 3.

[5] Calculated graphically using tremor amplitude versus time plots shown in Scandone and Malone (1985, fig. 2).

[6] This paper.

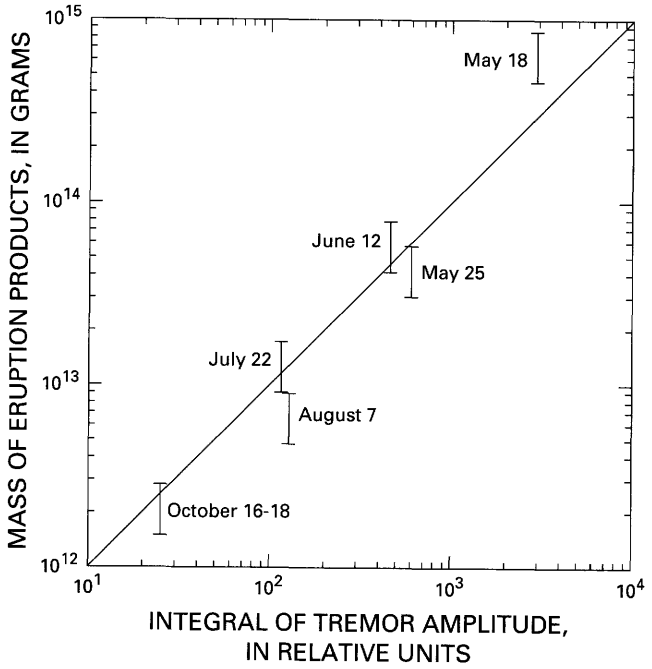


**Figure 2.** Masses of eruption products versus integral of volcanic-tremor amplitude for six eruptions of Mount St. Helens during 1980. The ordinate shows the total mass of pyroclastic flow plus air-fall ash deposit for each eruption, based on the works of Rowley and others (1981) and Sarna-Wojcicki and others (1981). The abscissa shows the integrated volcanic-tremor amplitude during each eruption, calculated from the graphs in figure 2 of Scandone and Malone (1985). The symbol sizes reflect estimated errors of ±30 percent for erupted mass and ±10 percent for the integral of tremor amplitude. The line with slope 1 shows a relation between the integral of tremor amplitude and total mass erupted.

Table 3 shows data for six explosive eruptions of Mount St. Helens. The integral of the mass eruption rate is equal to total mass erupted during the time interval. It includes the sum of air-fall ash deposits (Sarna-Wojcicki and others, 1981) and pyroclastic flow deposits (Rowley and others, 1981). The time interval is the whole eruption. The volcanic-tremor-amplitude integrals were calculated using seismic data of Scandone and Malone (1985), based on data from station SMW, located 162 km from Mount St. Helens. Figure 2 shows that the mass of eruption products and the integrated tremor amplitude are directly proportional to one another. The errors are estimated to be on the order of 30 percent or larger for eruptive masses and about 10 percent or less for the tremor amplitude. These eruptions varied in duration, peak tremor amplitudes, total amounts erupted, and in the relative masses of pyroclastic flow and air-fall ash deposits. Despite these differences, the integrals of volcanic-tremor amplitudes and eruption rates are approximately proportional to one another for these eruptions of Mount St. Helens.

If the linear relationship between tremor amplitude and mass eruption rate applies to explosive eruptions elsewhere, determination of mass eruption rates in near real time would be possible. For generality, a relationship should be based on the reduced displacement of volcanic tremor, rather than tremor amplitude. Reduced displacements of volcanic tremor (McNutt, 1992) can be calculated only indirectly from data in Scandone and Malone (1985) because they did not report absolute tremor amplitudes or seismograph magnification. The reduced displacement integrals in table 3 were calculated by scaling the peak tremor amplitudes for the Mount St. Helens eruption on the afternoon of the May 18, 1980, to peak values of reduced displacement (260 $cm^2$) reported by others (Fehler, 1983; McNutt, 1992). Using this approach, the cumulative mass erupted ($M$) at time $t$ may be determined from the integral of the reduced displacement ($R(t)$) using the relation:

$$M(t)\ (\mathrm{kg}) = \int_0^t \frac{dM}{dt} dt =$$

$$1.5 \times 10^5 \mathrm{kg\,(cm^{-2}\,s)} \int_0^t R(t)\, dt \qquad (1)$$

Similarly, the mass eruption rate is given approximately by:

$$\frac{dM}{dt}\ (\mathrm{kg\ s^{-1}}) = 1.5 \times 10^5 R\ (\mathrm{cm^2}) \qquad (2)$$

The coefficient has an uncertainty of about 50 percent. Table 3 lists the integral of the reduced displacements calculated by this method for the six eruptions.

The method described here might be used to determine mass eruption rates and eruptive masses to an accuracy of a factor of 2 for Plinian-type eruptions from a central vent, as at Mount St. Helens in 1980. The equations and predictive method described here can be tested by analyzing volcanic-tremor data and measured pyroclastic flow and air-fall ash deposits for other well-documented explosive eruptions (Wilson and Head, 1981). Much of the effort in volcano monitoring for eruption-prediction purposes involves recording and analyzing seismic data, often in near real time. During eruptions, routine seismic data analysis could include automated measurement of volcanic-tremor amplitude and reduced displacements to provide estimation of eruption rates and eruptive masses. The practicality of making tremor-amplitude measurements, including spectral analysis, in near real time has been demonstrated by Hurst (1985), Nishi (1987), and Endo and Murray (1991).

## DESCRIPTION OF OPERATION

The methods described above can be used to determine whether an ash cloud is present and the mass eruption rate in near real time. The mass eruption rate estimated from seismic data can be used along with plume-rise models (Wilson and others, 1978) and upper-atmosphere soundings to initialize ash-cloud properties (height, base, radius, particle concentration) required by an ash-transport and forecast model (Carey and Sigurdsson, 1982; Sparks and others, this volume). Some assumptions about particle-size distribution, settling speeds, and particle aggregation (Sorem, 1982) must be made. Essentially, the volcanological observations can be transformed in near real time to quantitative inputs required by ash-transport models, which may be used to generate short-range and long-range ash-cloud forecasts. The accuracy of such forecasts depends sensitively on ash-cloud initialization, atmospheric turbulence, accuracy of wind forecasts, and modeling errors. It is essential to update the wind forecast used by the transport model via incorporation of ash-cloud-tracking observations.

The volcanic ash warning system illustrated in figure 1 is based on the capability to generate meaningful ash-cloud forecasts within 1 minute after receiving volcanological data. This would be a challenging software development task, but it appears feasible. The hazards-evaluation subsystem reviews the ash-transport-model forecasts against a database of air routes, aviation facilities, and other user interests to determine notification requirements. The notifications subsystem forwards the summary information (maps, text messages, synthesized voice mail) to end users via the communications subsystem. The system should be designed to operate as an automated expert system, with provision for mandatory review of all meteorological and volcanological data, warning messages, and forecasts. The highest reliability and minimum response time for a volcanic ash warning system can be achieved only by full system integration that includes automatic transfer of operational data from volcano observatories to forecast centers and end users. The system must, however, provide the capability for a consensus review of all warnings and forecasts by a qualified volcanologist, forecast meteorologist, and air-space-operations manager.

## SUMMARY AND CONCLUSIONS

The system requirements for a possible volcanic ash warning system have been outlined. The recommended system architecture and data flows are based on use of modular subsystems, each of which performs a group of related functions. The subsystems include volcano data collection, volcano monitoring, ash transport and forecasting, hazards evaluation, notification, database management, and communications. The minimum information required from volcano observatories for source-based ash-transport and forecast models includes accurate determination of (1) whether an eruption is occurring, (2) whether ash cloud(s) were generated, and (3) the mass eruption rate as a function of time. Thermal infrared measurements and atmospheric electric-field measurements should be used to detect conditions resulting from thermal plumes and electrified ash clouds, respectively, that result from pyroclastic and explosive eruptions. Dual-sensor measurements should provide ancillary data with the least ambiguity for identifying conditions permissive of pyroclastic eruption when strong volcanic tremor is present. When such conditions are met, the mass eruption rate can be determined instrumentally from volcanic-tremor amplitude. The integral of the volcanic-tremor amplitude was proportional to the total mass of pyroclastic and air-fall ash deposits for six eruptions of Mount St. Helens in 1980. This finding is the basis for a seismic method to measure eruption rates in near real time. It is also the basis for estimating the rate and total amount of volcanic ash erupted into the atmosphere with an accuracy of a factor of 2. Representative values of cloud dimensions, heights, and particle concentrations can be estimated from plume-rise models by using the mass eruption rate. Additional data required include an assumed particle-size distribution, atmospheric sounding data, and wind data. The volcanic ash warning system described here should accept manual and automated inputs from existing volcano-monitoring systems and provide forecasts in various formats. The system should include a mandatory consensus review of all input data, forecasts, and warnings by a qualified volcanologist, forecast meteorologist, and air-space-operations manager. The system described would automate many of the operations and functions that are now performed manually. Such a system would enhance aviation safety.

## ACKNOWLEDGMENTS

I am grateful to my wife, Lorna Harris, for research support and to Advanced Control Technology of Albany, Oreg. (Mr. Jon Walker, President), for travel support. I also thank Herb J. Mitchell for early discussions of the ideas in this paper. I also extend my thanks to W.I. Rose and T.J. Casadevall for their helpful comments.

## REFERENCES CITED

Brantley, S.R., 1990, ed., The eruption of Redoubt Volcano, Alaska, December 14, 1989–August 31, 1990: U.S Geological Survey Circular 1061, 33 p.

Carey, S.N., and Sigurdsson, H.A., 1982, Transport and deposition of distal tephra from the May 18, 1980, eruption of Mount St. Helens: Journal of Geophysical Research, v. 87, p. 7061–7072.

Endo, E.T., and Murray, T.L., 1991, Real-time seismic amplitude measurement (RSAM): A volcano monitoring and prediction tool: Bulletin of Volcanology, v. 53, p. 533–545.

Fehler, M., 1983, Observations of volcanic tremor at Mount St. Helens: Journal of Geophysical Research., v. 88, p. 3476–3484.

Gilbert, J.S., Lane, S.J., Sparks, R.S.J., and Koyaguchi, T., 1991, Charge measurements on particle fallout from a volcanic plume: Nature, v. 349, p. 598–600.

Harris, D.M., and Mitchell, H.J., 1986, Automated detection of volcanic ash clouds and evaluation of hazards along jet routes [abs.]: Eos, Transactions, American Geophysical Union, v. 67, p. 397.

Harris, D.M., and Rose, W.I., 1983, Estimating particle sizes, concentrations, and total mass of ash in volcanic clouds using weather radar: Journal of Geophysical Research, v. 88, p. 10969–10983.

Harris, D.M., Rose, W.I., Roe, R., and Thompson, M.R., 1981, Radar observations of ash eruptions, *in* Lipman, P.W., and Mullineaux, D.R., eds., The 1980 Eruptions of Mount St. Helens, Washington: U.S. Geological Survey Professional Paper 1250, p. 323–333.

Hatakeyama, H., 1943, On the variation of the atmospheric potential gradient caused by the cloud of smoke of the volcano Asama, The second report: Journal of the Meteorological Society of Japan, v. 21, p. 420–426.

———1949, On the disturbance of the atmospheric potential gradient caused by the smoke cloud of the volcano Yake-yama: Journal of Geomagnetics and Geoelectricity [in English], v. 1, p. 48–51.

———1958, On the disturbance of the atmospheric electric field caused by the smoke cloud of the volcano Asama-yama: Paper Meteorological Geophysics, v. 8, p. 302–316.

Hatakeyama, H. and Kubo T., 1943a, On the variation of the atmospheric potential gradient caused by the cloud of smoke of the volcano Asama, The first report: Journal of the Meteorological Society of Japan, v. 21, p. 49–52.

———1943b, On the variation of the atmospheric potential gradient caused by the cloud of smoke of the volcano Asama, The third report: Journal of the Meteorological Society of Japan, v. 21, p. 426–428.

Hatakeyama H., and Ishikawa, T., 1946, On the variation of the atmospheric potential gradient caused by the cloud of smoke of the volcano Asama, The fourth report: Kisho-gijitsukan-yoseijo-kenkyuhokoku [in Japanese], v. 1, p. 14–18.

Hatakeyama, H. and Uchikawa, T., 1952; On the disturbance of the atmospheric potential gradient caused by the eruption smoke of the volcano Aso: Paper Meteorological Geophysics., v. 2, p. 85–89.

Hobbs, P.V., and Lyons, J.H., 1983, Electrical activity associated with the May 18, 1980, volcanic eruption of Mount St. Helens: San Diego, Calif., Final Report to IRT Corporation under P.O. 31433, 24 p.

Hoblitt, R.P. and Murray, T.L., 1990, Lightning detection and location as a remote eruption monitor at Redoubt Volcano, Alaska [abs.]: Eos, Transactions, American Geophysical. Union, v. 71, p. 1701.

Hurst, A.W., 1985, A volcanic tremor monitoring system: Journal of Volcanology and Geothermal Research, v. 26, p. 181–187.

Kikuchi, K., and Endoh, T., 1982, Atmospheric electrical properties of volcanic ash particles in the eruption of Mt. Usu volcano, 1977: Journal of the Meteorological Society of Japan, v. 60, p. 548–561.

Lyons, W.A., Bauer, K.G., Bent, R.B., and Highlands, W.H., 1985, Wide area real-time thunderstorm mapping using LPATS—The lightning position and tracking system, *in* Preprint Volume, Second International Conference on Aviation Weather System: Boston, Mass., American Meteorological Society, p. 207–214.

McNutt, S.R., 1992, Volcanic tremor, *in* Nierenberg, W.A., ed.: Encyclopedia of Earth System Science, v. 4, p. 417–425.

Morton, B.R., Taylor, G., and Turner, J.S., 1956, Turbulent gravitational convection from maintained and instantaneous plumes: Proceedings, Royal Society of London, v. A234, p. 1–23.

Nishi, K., 1987, Automatic data processing system for volcanic earthquakes and tremors: Kyoto University, Japan, Annual Report of the Disaster Prevention Research Institute, v. 30, p. 1–18.

Reddan, M., 1985, The hazards of ash clouds to civil air transport, *in* International Conference on the Aviation Weather System: Boston, Mass., American Meteorological Society, p. 146–147.

Rose, W.I., 1987, Interaction of aircraft and explosive eruption clouds: A volcanologist's perspective: American Institute of Aeronautics and Astronautics Journal, v. 25, p. 52–58.

Rowley, P., Kuntz, M.A., and Macleod, N.S., 1981, Pyroclastic-flow deposits, *in* Lipman, P.W., and Mullineaux, D.R., eds., The 1980 Eruptions of Mount St. Helens, Washington: U.S. Geological Survey Professional Paper 1250, p. 489–511.

Sarna-Wojcicki, A.M., Shipley, S., Waitt, R.B., Dzurisin, D., and Wood, S.H., 1981, Areal distribution, thickness, mass, volume, and grain size of air-fall ash from the six major eruptions of 1980, *in* Lipman, P.W., and Mullineaux, D.R., eds., The 1980 Eruptions of Mount St. Helens, Washington: U.S. Geological Survey Professional Paper 1250, p. 577–600.

Scandone, R., and Malone, S.D., 1985, Magma supply, magma discharge, and readjustment of the feeding system of St. Helens during 1980: Journal of Volcanology and Geothermal Research, v. 23, p. 239–262.

Sorem, R.K., 1982, Volcanic ash clusters: Tephra rafts and scavengers: Journal of Volcanology and Geothermal Research, v. 13, p. 63–71.

Sparks, R.S.J., and Wilson, L., 1982, Explosive volcanic eruptions—V: Observations of plume dynamics during the 1979 Soufriere eruption, St. Vincent: Geophysical Journal of the Royal Astronomical Society, v. 69, p. 551–570.

Wilson, L., 1976, Explosive volcanic eruptions—III: Plinian eruption columns: Geophysical Journal of the Royal Astronomical Society, v. 45, p. 543–556.

Wilson, L., and Head, J.W., 1981, Morphology and rheology of pyroclastic flows and their deposits, and guidelines for future observations, *in* Lipman, P.W., and Mullineaux, D.R., eds., The 1980 Eruptions of Mount St. Helens, Washington: U.S. Geological Survey Professional Paper 1250, p. 513–524.

Wilson, L., Sparks, R.S.J., Huang, T.C., and Watkins, N.D., 1978, The control of volcanic column heights by eruption energetics and dynamics: Journal of Geophysical Research, v. 83, p. 1829–1836.

WOVO (World Organization of Volcano Observatories), 1991, Directory of Volcano Observatories: Reykjavik, Iceland, WOVO/UNESCO, 99 p.

VOLCANIC ASH AND AVIATION SAFETY:
Proceedings of the First International Symposium
on Volcanic Ash and Aviation Safety
U.S. GEOLOGICAL SURVEY BULLETIN 2047

# AVIATION SAFETY AND VOLCANIC ASH CLOUDS IN THE INDONESIA-AUSTRALIA REGION

*By* R. Wally Johnson *and* Thomas J. Casadevall

## ABSTRACT

Six encounters between aircraft and volcanic ash clouds from Indonesian volcanoes took place between 1982 and 1985. These incidents reflect the high frequency of explosive eruptions during the early 1980's and an increase in the number of long-haul, international flights by jet-powered, wide-body aircraft. The ingestion of volcanic ash by jet engines, in some cases, has caused multiple engine failures. In addition, aircraft exteriors and engines are damaged by the abrasive effects of ash. The encounters raised the level of concern about the impact of volcanic eruptions on aviation in the Indonesia-Australia region and prompted joint Australian-Indonesian efforts to eliminate future encounters. The threat to aviation in the region can be mitigated through enhanced monitoring of Indonesian volcanoes, better communication between observers of eruptive activity and in-flight air crews, and more effective use of near real time satellite imagery, particularly systems that discriminate volcanic ash clouds from weather clouds. Early-warning arrangements at present are not satisfactory. Development of on-board ash detectors would represent a significant advance in an early-warning capability for aviation.

## INTRODUCTION

Indonesian volcanoes were the focus of interest and concern to the international aviation community between 1982 and 1985, when six passenger airliners, mainly wide-body Boeing 747's, encountered volcanic ash clouds produced by three volcanoes in different parts of Indonesia. There had been earlier encounters between aircraft in flight and volcanic ash in other parts of the world: Sakurajima Volcano (Japan, 1975–86), Mt. Spurr (Alaska, United States, 1953), Augustine Volcano (Alaska, 1976), and Mount St. Helens (Washington, United States, 1980). However, the June–July 1982 encounters of two 747 aircraft with ash from Galunggung Volcano in western Java, Indonesia, were especially notable because they caused multiple engine failures (Smith, 1983; Tootell, 1985). This necessitated the powerless glide of the stricken aircraft down to altitudes where the engines could be restarted in a more oxygen-rich atmosphere. The incidents generated widespread belief that two major aviation disasters had been narrowly avoided. Similar events involving multiple engine failures have taken place subsequently when aircraft encountered ash from Redoubt Volcano (Alaska, 1989) and Mt. Pinatubo (Philippines, 1991) volcanoes, and these incidents have reinforced the concern about the threat that volcanoes pose to aircraft.

Five of the six aircraft affected in Indonesia in 1982–85 were flying at night, en route to Australia. The pilots had received no early warning that they were about to fly into a volcanically hazardous area, and ash clouds were not detectable on flight-deck radar screens. Australian authorities showed particular concern about these ash encounters, especially after May 1985, when a Boeing 747 aircraft of Australia's national carrier, Qantas Airways, Ltd., flew into an ash cloud from Soputan Volcano. The purpose of this paper is to focus on the particular nature of the aircraft–ash-cloud problem in the Indonesia-Australia region, to summarize how authorities have responded to the need for improved early-warning capabilities for aviation, and to discuss methods for mitigating the threat in the future.

## AIR TRAFFIC IN INDONESIA

The frequency of air traffic in the Indonesia-Australia region has increased dramatically since the World War II. There are currently between 780 and 800 international flights into and out of Australia each week (C.G. Barnes, Australian Civil Aviation Authority, oral commun., 1991). The majority of these international flights utilize the principal air corridors of the Indonesia-Australia region, which cross volcanically active areas in a complex pattern (fig. 1).

International air traffic over Indonesia typically ends or originates in Australia or New Zealand, and many aircraft use the major international airports of Jakarta (Soekarno-Hatta International Airport) and Denpasar, Bali. Most international aircraft must cross the volcanically active part of Indonesia at night because of Australian city curfews that were established in the 1960's to minimize the noise of jet

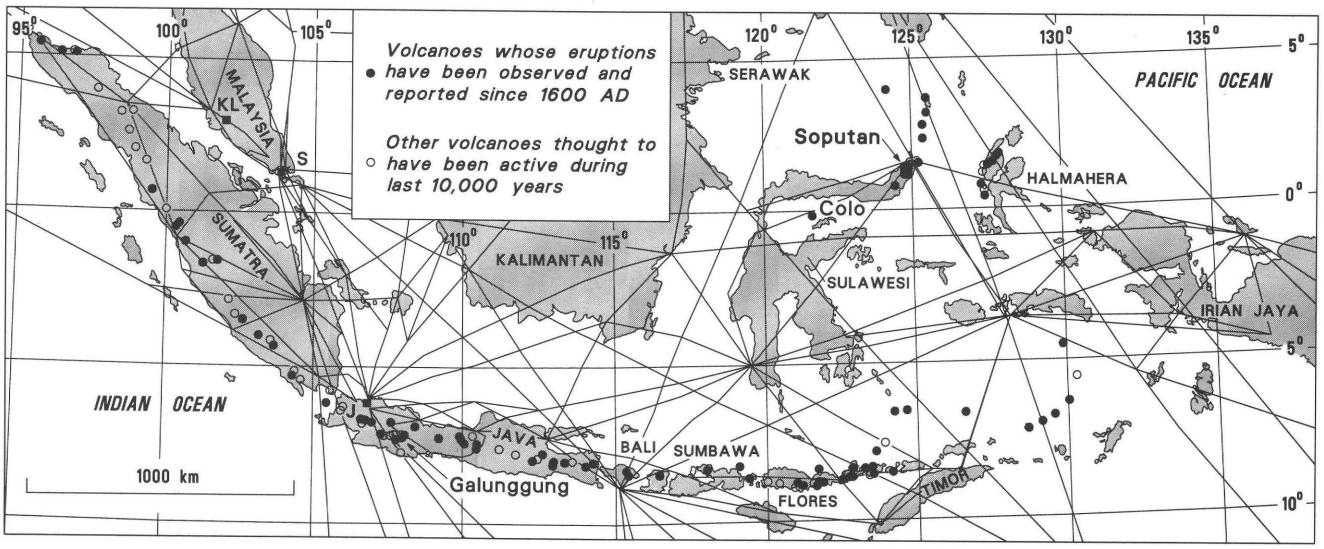


**Figure 1.** Air routes and volcanoes in Indonesia. Adapted from a chart in the Qantas route intelligence manual: "Volcanic Information, Indonesia" (ICAO, 1993). Volcano data are from Simkin and others (1981). Solid circles represent recently active volcanoes. Open circles represent other potentially active volcanoes. Solid squares represent major cities: KL, Kuala Lumpur; S, Singapore; J, Jakarta.

traffic landing and taking off at night. Aircraft are required to arrive or depart most Australian cities between 0600 and 2300 hours. Furthermore, modern jet airliners fly at high altitudes and cover long distances between refueling stops. This is in contrast to pre-jet days, before the early 1960's, when most air traffic operated during daylight hours, had frequent stops, and flew at lower altitudes. Pilots, therefore, had more opportunities to learn about and see volcanoes and to take appropriate evasive action should an eruption take place.

The 1982–85 period was exceptional in the Indonesian region for the high number of passenger jet aircraft that encountered volcanic eruption clouds and for the multiple engine failures caused by these encounters. An important point to note is that multiple engine failures appear to affect only modern, finely tuned, jet engines and that there are no reported aircraft–ash-cloud encounters in the Indonesian region involving the failure of turboprop engines in pre-jet days. The 1982–85 period of incidents, therefore, appears to coincide with the more common usage of jet engines in modern times and with the large number of eruptions in the Indonesian region during 1982–85 that produced large ash clouds that reached aircraft cruising altitudes of 10–12 km.

## AIRCRAFT–ASH-CLOUD INCIDENTS

There are six known incidents in the 1982–85 period:

1. A domestic Indonesian Douglas DC-9 of Garuda Airlines, on the Jakarta-Yogjakarta route, flew through ash from Galunggung on 5 April 1982 (Qantas Airways, Ltd., unpub. data, 1982). The aircraft required maintenance, but no abnormal engine operations were reported. Indonesian authorities issued a notice to airmen (NOTAM) on April 6, instructing that airspace within 17 km of the volcano should be avoided. However, the restricted area did not embrace the established international air routes, so the NOTAM was limited to internal Indonesian distribution.
2. A British Airways Boeing 747 (flight BA 009) cruising at 37,000 ft flew into Galunggung ash on 24 June 1982 at about 2040 hours (Jakarta time) and about 330 km south of Jakarta while en route from Kuala Lumpur to Perth, Western Australia (Smith, 1983; Tootell, 1985). St. Elmo's fire (static electricity) danced along the windscreen, and "smoke" and an acrid smell were noticed on the flight deck and in the main cabin. One engine failed within minutes, and the three others stalled shortly thereafter. The aircraft descended steeply for 13–14 minutes before the engines were restarted progressively at 13,000 ft. One engine subsequently surged and was shut down. A safe landing was made eventually at Jakarta's Halim International Airport. Aircraft damage, especially abrasion effects to leading edges and contamination of oil and air systems, was extensive, and three engines and front windshields were replaced in Jakarta before the airplane was ferried back to England. An international NOTAM was issued after the incident, and aircraft reroutings took place, but normal routing was resumed on 2 July after the NOTAM was canceled.
3. The crew of a Singapore Airlines Boeing 747 (flight SQ 24A) on the same flight path as BA 009, but 40 minutes later, on 24 June 1982, reported "smoke contamination" in the main cabin. The aircraft reached Perth without further incident where an inspection

was carried out. Small fragments of rock were found in all engine tailpipes, but no damage was noted to leading edges, and oil filters were clear.

4. A Singapore Airlines Boeing 747 (flight SQ 21A) en route between Singapore and Melbourne, ran into Galunggung ash at about 2130 hours (Jakarta time) on 13 July 1982 and suffered similarly to the BA 009 flight three weeks earlier. There were multiple engine failures and damage to airframe and powerplant systems (Singapore Airlines, 1982). A two-engine emergency landing was made at Jakarta, where all four engines had to be replaced. Aircraft rerouting recommenced.
5. A British Airways Boeing 747 flying at 10.6 km altitude between Singapore and Perth on 23 July 1983 had been rerouted north of Galunggung, but it encountered an eruption cloud from Colo Volcano (Una Una Island, Sulawesi) at 1955 hours (Jakarta time). Pilots noted a "volcanic smell, lack of visibility, and St. Elmo's Fire around the windshield" (SEAN Bulletin, 1983). The aircraft returned to Singapore for inspection, but did not sustain significant damage.
6. A Qantas Airways Boeing 747 (flight QF 28) encountered ash from Soputan Volcano, Sulawesi, at about 2400 hours (Jakarta time) on 19 May 1985 while flying from Hong Kong to Melbourne (Qantas, 1985; Bailey, 1985). The cabin filled with dust, there was St. Elmo's fire around the windshield, and the aircraft vibrated badly for several minutes, but the engines did not stall. The aircraft landed safely in Melbourne where the aircraft was withdrawn from service for five days while the engines were removed and cleaned.

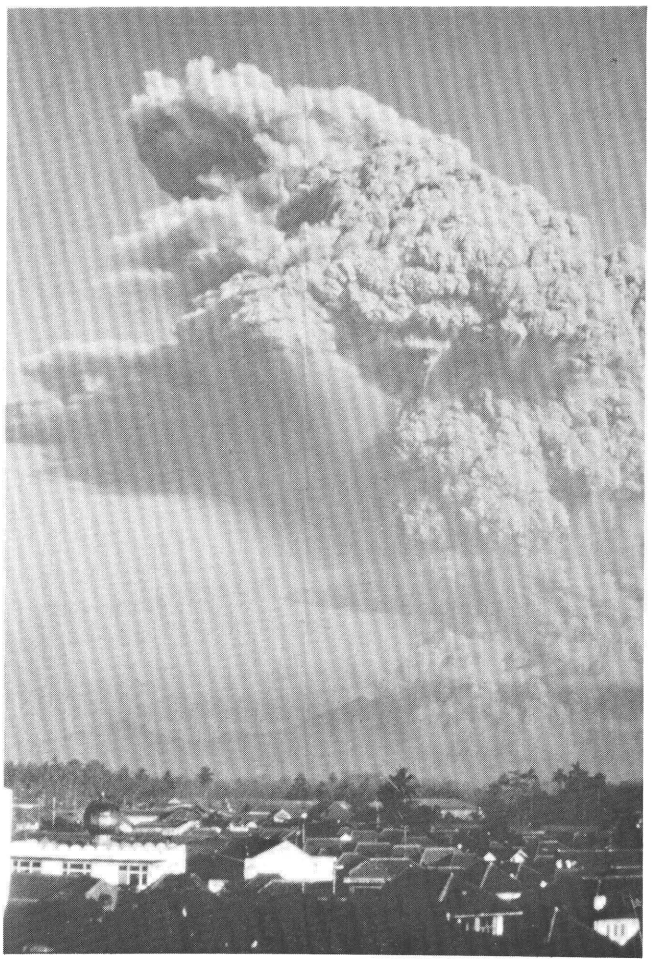

**Figure 2.** A volcanic ash column rises from Galunggung Volcano, West Java, on 16 August 1982. The city of Taskimalaya is shown in the foreground. Galunggung eruptions such as this produced ash clouds that were involved in four encounters with jet passenger aircraft during 1982. Photograph by J.P. Lockwood.

## VOLCANOES IN INDONESIA

Indonesia is only one of several countries in the southeast Asia and southwest Pacific region that have active volcanoes. Papua New Guinea, the Philippines, Solomon Islands, Vanuatu, Tonga, and New Zealand are all volcanically active, but Indonesia has more volcanoes than any of them and, indeed, more than any country in the world (Simkin and others, 1981). The Indonesian archipelago extends more than 6,000 km from the northwestern tip of Sumatra in the west to Irian Jaya in the east. It contains about 130 active volcanoes, including nearly 80 that have erupted in the past 400 years or so (fig. 1). About 50 volcanoes are monitored regularly through a network of observatories operated by the Volcanological Survey of Indonesia (VSI) (Pardyanto and others, 1986). The volcanoes are in linear belts and groups scattered along the archipelago, and their eruption clouds represent a formidable threat to aviation.

There were 35 eruptions from Indonesian volcanoes from January 1980 through September 1985—a notably high level of activity when compared to previous decades (Pardyanto and others, 1986). Twenty-seven of these eruptions required no evacuation of people and presented little threat to property, including aircraft. Major eruptions during this period that threatened life and property (and resulted in evacuations) included those of Gamalama (1980, 1983), Galunggung (1982–83), Soputan (1982, 1984–85), Colo (1983), Merapi, central Java (1984), Karengetang (1984), and Sangeang Api (1985). The largest eruptions were from Galunggung Volcano in western Java (fig. 2), which produced more than 30 large explosive eruptions between April 1982 and January 1983, including clouds that rose more than 10 km above sea level—that is, up to, or above, the cruising level of international airliners (Katili and Sudradjat, 1984a).

## VOLCANO MONITORING AND FORECASTING IN INDONESIA

Precise forecasting of volcanic eruptions is a difficult problem, but progress has been made over the last 20 years (Decker, 1986; Souther and others, 1984; Sudradjat and Tilling, 1984; Swanson and others, 1985; Banks and others, 1989). This progress has relied heavily on interpreting results from a wide range of monitoring methods, including visual observations, seismological recordings, deformation studies, temperature records, geochemical collections of gases and condensates, and geophysical methods such as magnetic and gravity recordings. However, not all of these diverse and specialized methods are necessary for the basic monitoring and forecasting of eruptions. Changes in the state of a volcano normally can be detected if the volcano is under visual and seismological observation and if the observers have an understanding of its previous eruptive activity.

Studies of volcanic earthquakes are relied on in Indonesia, as elsewhere in the world, to provide early warning of impending activity. Seismometers are the standard equipment in VSI observation posts, and visual observations and changes in seismicity are the primary methods of monitoring. Other supplementary methods include: (1) studies of ground deformation (spirit-level measurement and precise distance measurement), (2) geochemical studies of gases and condensates from fumaroles and water from crater lakes and hot springs, emission rates of sulfur-dioxide gas, and chemical analysis of eruption products (ash and lavas), (3) geophysical methods employing measurement of self-potential and geomagnetic variations (Sudradjat, 1991). In addition, satellite imagery has been used to monitor the movement of volcanic plumes (Malingreau and Kaswanda, 1986; Sudradjat, 1989).

VSI successes in its volcano-monitoring program include the 1983 Colo eruption where precursory signs of restlessness on Una Una island were detected and interpreted to indicate the likelihood of an imminent eruption (Katili and Sudradjat, 1984b). The Una Una population of 7,000 was evacuated (McClelland and others, 1989) before major eruptive activity devastated the island. However, difficulties arise where unmonitored volcanoes such as Galunggung reawaken after long periods of repose (Sudradjat and Tilling, 1984). Nevertheless, regular observations and seismological monitoring were begun following the initial activity at Galunggung in April 1982 and were used to forecast more than 20 of the eruptions that took place during the remainder of the year (Katili and Sudradjat, 1984a).

Effective eruption forecasting in Indonesia relies not only on monitoring precursory activity, but also on expedient communication of monitoring results to specialists able to interpret the data and able to evaluate probable future behavior. Indonesian volcano observatory posts are staffed typically by observers with secondary-school training. Many posts are equipped with radios for direct communication with volcanologists at VSI headquarters in Bandung, West Java. However, some observatories without radios are unable to provide timely notification of events. Old reports of activity are of limited value—delays of minutes or hours can be significant. Information at VSI headquarters then must be evaluated and interpreted before it is passed on to other agencies. VSI amended their communication system in 1986 to expedite communications with the aviation community. Observer reports of volcanic activity are still provided directly to Bandung, but observers have been authorized to contact local airports directly should they observe high-rising (higher than 1 km) eruption plumes.

Transmission of monitoring data automatically from a remote volcano directly to Bandung or other major centers may seem desirable. However, this requires development of equipment capable of operating reliably under fairly severe conditions, such as the acid and humid environments found on tropical Indonesian volcanoes. Drawbacks are that the equipment is expensive, requires specially trained personnel for maintenance, is liable to breakdown, and is susceptible to vandalism. Such expensive, "high-technology" methods, therefore, have not been a practical solution for monitoring volcanoes where government budgets are restrictive but where there is no shortage of trainable local observers. Budget restrictions also prevent monitoring being undertaken on many potentially active Indonesian volcanoes.

## VULCAN-AUS AND OTHER RESPONSES

Aviation, meteorological, and volcanological authorities in Indonesia and Australia began collaborating on ways to mitigate aircraft–ash-cloud incidents shortly after the Galunggung encounters in 1982. Collaboration was formalized in 1985 when the Volcanological/Airspace Liaison Committee–Australia/Indonesia (VULCAN) was formed. The committee consists of two working groups: the VULCAN-AUS working group is Australia based; the VULCAN-IND is Indonesia based. Each working group consists of counterpart members representing different agencies. VULCAN-AUS consists of representatives from the Australian Civil Aviation Authority (CAA), the Bureau of Meteorology (BOM), Australian Geological Survey Organization (AGSO), Qantas Airways, Ltd., and the Commonwealth Scientific and Industrial Research Organization (CSIRO). VULCAN-IND consists of representatives of the Indonesian Directorate General of Air Communications, the Bureau of Meteorology and Geophysics, and the Volcanological Survey of Indonesia, as well as representatives from the three principal Indonesian domestic carriers, Garuda, Merpati, and Bouraq.

VULCAN-AUS is an advisory and liaison group that supports the Airways Volcano Watch, part of the Australian CAA operational services section, which acts as a clearing

house for information on volcanic activity affecting Australian civil aviation. VULCAN-AUS provided major input at a special meeting organized by the International Civil Aviation Organization (ICAO) regional office in Bangkok, held in 1986, and assisted in the production of the ICAO regional handbook "Volcanic Ash and Aircraft Operation" (ICAO, 1993). Extensive discussions at the 1986 meeting led to proposed changes to the ICAO regulatory documents to take into account volcanic-ash-cloud encounters. ICAO (Montreal) in 1982 had established its Volcanic Ash Warnings (VAW) study group, of which the chairman of VULCAN-AUS is a member. The VAW study group also produced recommendations that subsequently were adopted by ICAO member states and promulgated by the ICAO Air Navigation Bureau (Fox, this volume).

VULCAN-AUS was responsible also for recommending the establishment of the volcanic ash detection and aviation safety (VADAS) study group. VADAS was set up by CSIRO in 1987 specifically to explore technological solutions (satellite and on-board detection equipment) to the aircraft–ash-cloud problem (Prata, 1990).

## SATELLITE MONITORING

The Australian Bureau of Meteorology, since 1982, has used images from the Japanese geostationary meteorological satellite (GMS), located at 35,700 km above the equator at long 140°E., in detecting volcanic eruption plumes in the western Pacific. Images from the infrared and visible channels of GMS were used by BOM meteorologists B.N. Hanstrum and A.S. Watson (Hanstrum and Watson, 1983) to determine the height of 1982 Galunggung eruption clouds and to track the clouds in conjunction with upper-wind trajectories. Sawada (1989) also reported on GMS images of Indonesian eruption plumes for the 1982–85 period.

BOM issues "volcanic ash advisories" to aviation authorities through the aeronautical fixed telecommunications network (AFTN) in Australia (fig. 3). BOM normally searches for eruption clouds on GMS images after receiving notification of a volcanic eruption from the relevant neighboring country (such as Indonesia) or from pilot reports. Eruption clouds are difficult to distinguish on GMS images when, as commonly happens in the Indonesian region, there are weather clouds on the same image. This is because both types of cloud have similar reflective properties in the visible and infrared parts of the electromagnetic spectrum. However, Australian scientists F.R. Honey and W. Carroll (Honey, this volume) proposed a concept whereby volcanic clouds could be discriminated using data from the advanced very high resolution radiometer (AVHRR) on board the polar-orbiting NOAA-7 satellite. This initial proposal was tested and developed rigorously in CSIRO by A.J. Prata (Prata, 1989a, 1989b; Prata and others, 1985). Discrimination of ash clouds from water-ice clouds is possible because

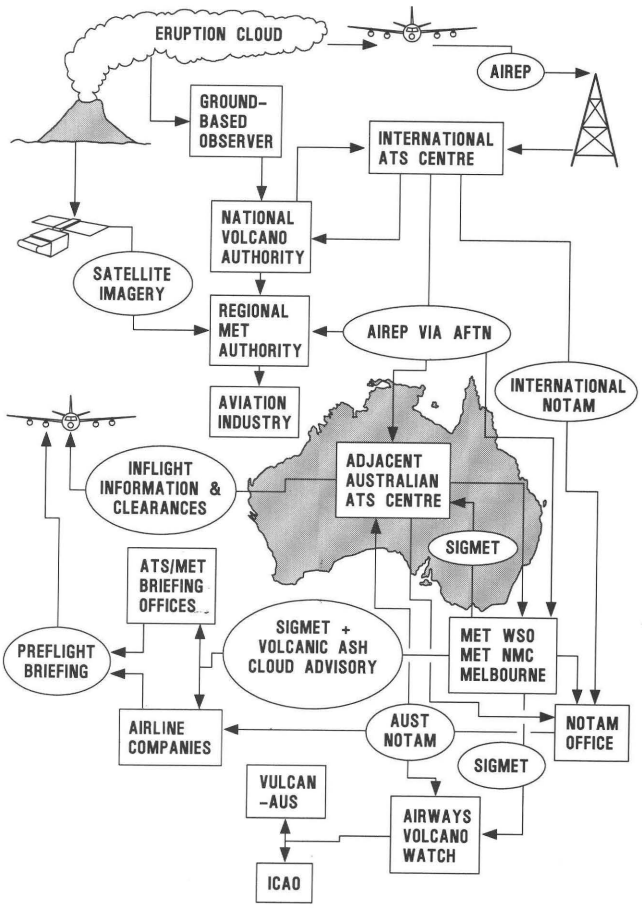


**Figure 3.** Information flow for the Australian volcanic ash warning network starts with sightings of eruption clouds in neighboring countries (for example, Indonesia) made by ground-based observers and (or) from in-flight pilot reports (AIREP's). The notifications move through the international air traffic services (ATS) center (for example, in Jakarta) and then to (1) the regional meteorological authority (for example, Jakarta), (2) an adjacent Australian ATS center (Perth, Darwin, or Sydney), (3) Australian weather services offices (WSO), and (4) the National Meteorological Centre (NMC), Melbourne, to the NOTAM (notices to airmen) office (Sydney), which is responsible for the distribution of NOTAM's. These reach pilots through preflight briefing offices and by advisories from the Australian ATS center. NMC issues SIGMET's (significant meteorological phenomena) and volcanic ash cloud advisories, which are distributed to the Australian ATS centers, briefing offices, and the NOTAM office. The Airways Volcano Watch receives both NOTAM's and SIGMET's and serves as a link to both VULCAN-AUS (see text) and the International Civil Aviation Organization (ICAO). AFTN, aeronautical fixed telecommunications network; MET, meteorology.

of the reverse absorption effect in AVHRR channels 4 and 5 (Prata and Barton, this volume).

AVHRR receiving stations are operated by BOM in Perth and Melbourne, and a third station opened in 1992 in Darwin. The Australian AVHRR receiving stations cover much of Indonesia and the Philippines, all of Papua New

Guinea, and most of the rest of the southwest Pacific (Potts and Whitby, this volume). This network of AVHRR stations is expected to enhance ash-cloud early-warning capability for aviation.

## AUSTRALIAN ASH-CLOUD WARNING SYSTEM

Warnings of the threat to aircraft from volcanic ash clouds in the Australian region are provided by means of an integrated communications network that includes volcanological, meteorological, and aviation authorities (fig. 3). There are three main features of interest in the Australian network:

1. The system relies on the provision of information on volcanic eruptions from volcanological authorities in foreign countries or from pilots flying in foreign airspace. Australia has no active volcanoes of its own (excluding Big Ben Volcano on Heard Island in the Indian Ocean) and, therefore—unlike other technologically advanced and volcanically active countries such as Japan and the United States—does not have a volcanological authority as part of its own domestic communications network.
2. Pilots receiving in-flight information about eruption clouds must hope for rapid and effective communication links between observers and ground-based authorities, but they may have to wait unacceptably long times before being notified that an eruption has taken place or is in progress. Communications may be slow or break down at some of the many links shown in figure 3.
3. Analysis of satellite images is part of the system (undertaken at the BOM National Meteorological Centre, Melbourne—MET NMC in fig. 3). Twenty-four-hour analysis of AVHRR images has been carried out since early 1993 by operational meteorologists at the Darwin receiving station.

Improvements in the communication network, therefore, are of fundamental importance to the mitigation of aircraft encounters with volcanic ash clouds in the Indonesia-Australia region. Aircraft will remain vulnerable to the effects of eruption clouds until such improvements are made.

## ON-BOARD ASH DETECTORS

The alternative to, or supplement for, an enhanced communication network is the provision of aircraft-mounted equipment that can detect ash clouds remotely ahead on the aircraft flight path. Such an instrument could employ any one of several remote-sensing techniques (Prata, 1990). The advantage of such a system is that the pilot is afforded independence from the potentially weak volcano-to-pilot communication system referred to in the previous section.

The Australian prototype of a simple, passive instrument has been constructed and tested on ash-bearing clouds emitted from Sakurajima Volcano in Japan (Prata and others, 1991; Barton and Prata, this volume; Prata and Barton, this volume). The prototype is a multi-channel radiometer that uses similar wavelengths to those of the AVHRR (see above). A unique signature for volcanic ash clouds was determined from the Sakurajima measurements: more radiation was received at 10.9 microns than at 11.8 microns, whereas the opposite effect was measured when viewing water clouds and clear skies. The instrument is expected to be capable of detecting ash clouds 100 km ahead of the aircraft, thereby providing sufficient time for pilots to take appropriate action. Further development will include a simplification of the prototype for practical use on flight decks and possible incorporation of the concept into a multifunctional sensor capable also of detecting wind shear and clear-air turbulence.

## ACKNOWLEDGMENTS

The authors gratefully acknowledge the contribution by the Australian Civil Aviation Authority, Canberra, in the production of figure 3. They also thank Subroto Motjo, Director of the Indonesian Volcanological Survey, Bandung, for reviewing an early version of the paper, and I. Barton, R. Lunt, S.D. Needham, A.J. Prata, R.I. Tilling, and R.J. Tingey for reviews of a later version of the paper. Johnson publishes with the permission of the Director, Australian Geological Survey Organization.

## REFERENCES CITED

Bailey, J., 1985, Volcanology—A first hand report!: Australian Geologist, v. 56, p. 5.

Banks, N.G., Tilling, R.I., Harlow, D.H., and Ewert, J.W., 1989, Volcano monitoring and short-term forecasts, *in* Tilling, R.I., ed., Short Course in Geology, Volume 1, Volcanic Hazards: Washington, D.C., American Geophysical Union, p. 51–80.

Decker, R.W., 1986, Forecasting volcanic eruptions: Annual Review of Earth and Planetary Sciences, v. 14, p. 267–291.

Hanstrum, B.N., and Watson, A.S., 1983, A case study of two eruptions of Mount Galunggung and an investigation of volcanic eruption cloud characteristics using remote sensing techniques: Australian Meteorological Magazine, v. 31, p. 171–177.

ICAO (International Civil Aviation Organization), 1993, Volcanic ash and aircraft operation: regional handbook: Bangkok, ICAO Asia and Pacific Office, 180 p.

Katili, J.A., and Sudradjat, A., 1984a, Galunggung: The 1982–1983 eruption: Bandung, Volcanological Survey of Indonesia, 102 p.

———1984b, The devastating 1983 eruption of Colo Volcano, Una-Una Island, central Sulawesi, Indonesia: Geologische Jharbuch, v. A75, p. 27–47.

Malingreau, J-P., and Kaswanda, O., 1986, Monitoring volcanic eruptions in Indonesia using weather satellite data: The Colo eruption of July 28, 1983: Journal of Volcanology and Geothermal Research, v. 27, p. 179–194.

McClelland, L., Simkin, T., Summers, M., Nielsen, E., and Stein, T.C., 1989, Global Volcanism 1975–1985: New Jersey, Prentice Hall, 655 p.

Pardyanto, L., Suparto, S., Suratman, Olas, and Casadevall, T., 1986, Volcanic activity in Indonesia between 1980–1985 [abs.]: Abstracts Volume, International Volcanological Congress, New Zealand, 270 p.

Prata, A.J., 1989a, Observations of volcanic ash clouds in the 10–12 micron window using AVHRR/2 data: International Journal of Remote Sensing, v. 10, p. 751–761.

———1989b, Infrared radiative transfer calculations for volcanic ash clouds: Geophysical Research Letters, v. 16, p. 1293–1296.

———1990, Volcanic ash detection and air safety: Final Report to the CSIRO Office of Space Science and Applications, Commonwealth Scientific and Industrial Research Organization, Division of Atmospheric Research, Australia, 54 p.

Prata, A.J., Wells, J.B., and Ivanac, M.W., 1985, A "satellite's eye view" of volcanoes on the Lesser Sunda Islands: Weather, v. 40, p. 245–250.

Prata, A.J., Barton, I.J., Johnson, R.W., Kamo, K., and Kingwell, J., 1991, Infrared radiometric detection of volcanic ash clouds: Nature v. 354, p. 25.

Qantas, 1985, Passage through volcanic dust, VHECC QF 028/197—19th May 1985: unpub. report to Australian Bureau of Air Safety Investigations by Qantas Flight Safety Adviser, Qantas Airways, Ltd., Sydney.

Sawada, Y., 1989, The detection capability of explosive eruptions using GMS imagery, and the behavior of dispersing eruption clouds, *in* Latter, J.H., ed., Volcanic Hazards: Assessment and Monitoring: IAVCEI Proceedings in Volcanology, v. 1, p. 233–245.

SEAN Bulletin, 1983, Una Una Volcano, Sulawesi, Indonesia: Scientific Event Alert Network Bulletin, v. 8, no. 7, p. 2–4.

Simkin, T., Siebert, L., McClelland, L., Bridge, D., Newhall, C.G., and Latter, J.H,. 1981, Volcanoes of the World: Stroudsberg, Pa., Hutchinson Ross, 233 p.

Singapore Airlines, 1982, Flight through volcanic dust cloud, SQ 21A/13.7.1982: Singapore Airlines Flight Safety Review, July/October, p. 1–4.

Smith, W.S., 1983, High-altitude conk out: Natural History, v. 92, no. 11, p. 26–34.

Souther, J.G., Tilling, R.I., and Punongbayan, R.S., 1984, Forecasting eruptions in the Circum-Pacific: Episodes, v. 7, no. 4, p. 10–18.

Sudradjat, A., 1989, Volcanic eruption monitoring using space platforms: Geologi Indonesia, v. 12, p. 437–448.

———1991, Volcanic hazard mitigation program in Indonesia: unpub. paper distributed at the IAGI/Pertamina International Conference on Volcanology and Geothermal Technology, Bandung, Indonesia, 7–8 August, Department of Mines and Energy, Jakarta.

Sudradjat, A., and Tilling, R.I., 1984, Volcanic hazards in Indonesia: The 1982–83 eruption of Galunggung: Episodes, v. 7, no. 2, p. 13–19.

Swanson, D.A., Casadevall, T.J., Dzurisin, D., Holcomb, R.T., Newhall, C.G., Malone, S.D., and Weaver, C.S., 1985, Forecasts and predictions of eruptive activity at Mount St. Helens, USA: 1975–1984: Journal of Geodynamics, v. 3, p. 397–423.

Tootell, B., 1985, All 4 Engines Have Failed; The True and Triumphant Story of Flight BA 009 and the Jakarta Incident: Auckland, Hutchinson Group, Ltd., 178 p.

VOLCANIC ASH AND AVIATION SAFETY:
Proceedings of the First International Symposium
on Volcanic Ash and Aviation Safety
U.S. GEOLOGICAL SURVEY BULLETIN 2047

# THE SMITHSONIAN'S GLOBAL VOLCANISM NETWORK: FACILITATING COMMUNICATION OF VOLCANIC-ERUPTION INFORMATION

*By* Lindsay McClelland

## ABSTRACT

The Smithsonian Institution's Global Volcanism Network (GVN, formerly SEAN, the Scientific Event Alert Network) has gathered and disseminated information about the world's volcanic activity since 1975. In its 17 years of monitoring, GVN has reported activity at nearly 300 volcanoes, including eruptions that produced the globe-circling stratospheric cloud from Mexico's El Chichón Volcano in 1982 and two of this century's largest eruptions: at Pinatubo (Philippines) and Hudson (Chile) in 1991.

Information is provided to GVN by a worldwide network of about 1,500 correspondents, scientists, government officials, airplane pilots, and others with knowledge of volcanic activity. The bulletin is sent monthly to the correspondents and is also available by subscription through the American Geophysical Union (AGU) and on electronic mail. GVN quickly notifies scientists and officials of eruptions that provide significant opportunities for research and (or) threaten life and property. News of an eruption that may affect aviation is immediately forwarded to NOAA's (National Oceanic and Atmospheric Administration) Synoptic Analysis Branch and to the Federal Aviation Administration (FAA) in Washington, D.C. Only by exchanging information among many sources—volcanologists, atmospheric scientists, satellite observers, pilots, and air traffic facilities—will fully informed decisions about the appropriate response to an eruption be possible.

## INTRODUCTION

To operate safely in the vicinity of an erupting volcano, aviation authorities and pilots must have timely, accurate information about the locations of ash clouds. Programs to provide warning to aviation personnel of eruption clouds are in place in some regions, including the United States, Japan, and Indonesia. In the United States, satellite monitoring of volcanic clouds in U.S. flight-information regions (FIR's) has been in place since 1989 via an agreement between NOAA and the FAA (Lynch, 1991). Updates of this agreement now link the observatories of the U.S. Geological Survey (USGS) with regional offices of the FAA and the National Weather Service (NWS) (Hamley and Parkinson, this volume).

Japan's Sakurajima Volcano has plagued operations at nearby Kagoshima Airport since 1955 (Katow, 1988; Onodera and Kamo, this volume), but careful planning and prompt communication from volcano-observatory personnel to aviation authorities have allowed continued air service without major mishap.

Many international flights to and from Australia pass over Indonesia, which includes more than 15 percent of the world's potentially active volcanoes (Simkin, this volume). The volcanic threat to aircraft flying in this area has been reduced through the dedicated efforts of officials from both Australia and Indonesia (Johnson and Casadevall, this volume).

Using a combination of direct visual observation and instruments, new eruptive pulses at a carefully monitored volcano should be evident within minutes (Alaska Volcano Observatory Staff, 1990; Onodera and Kamo, this volume), and news of eruptive activity can be forwarded immediately to appropriate authorities. However, only a small percentage of the world's potentially active volcanoes are rigorously monitored, and, at many of those, communications links with aviation authorities have not been established.

Volcanic cloud avoidance would be greatly aided by the development of a cockpit instrument that could reliably detect dangerous ash concentrations while they are still far from the aircraft (Honey, this volume). Work in Australia to develop an on-board sensor is encouraging (Prata and others, 1991; Barton and Prata, this volume) and may lead to a commercially available instrument. Nevertheless, before such an instrument becomes available, only a rapid, effectively targeted communications system will keep aircraft and their occupants safe in volcanically active areas.

## THE GLOBAL VOLCANISM NETWORK

The Smithsonian Institution has been communicating information about the world's volcanic activity for nearly a quarter century. Reports on current eruptions began from Cambridge, Mass., in 1968 when the Center for Short-Lived Phenomena (CSLP), with a broad-based charter to serve as a clearing house for transient natural events, sent out its first notifications by postcard. The Scientific Event Alert Network (SEAN), with its monthly bulletin, was established in 1975 with CSLP personnel brought to Washington to build closer ties with Smithsonian scientists. In recognition of SEAN's increasing focus on volcanic activity, its name was changed to the Global Volcanism Network (GVN) in 1990.

GVN is part of the larger global volcanism program that also includes an extensive database of Holocene volcanism (the last 10,000 years) and archives of volcano maps, photographs, satellite images, and other documentation. This program, in turn, is part of the Department of Mineral Sciences, which includes not only laboratory and library facilities, but also research volcanologists and major collections of volcanic products. All are housed in the Smithsonian Institution's National Museum of Natural History, on the Mall in Washington, D.C., and all constitute valuable resources for GVN personnel in tracking volcanic activity around the world.

Since 1975, activity has been reported from almost 300 volcanoes. Globe-circling stratospheric clouds were produced in 1982 by El Chichón (Mexico) and in 1991 by two of the century's largest eruptions, at Pinatubo (Philippines) and Hudson (Chile), but numerous, less dramatic eruptions with potential for regional effects on aviation occurred during the same period. Nearly 100 post-1975 eruptions had volcanic explosivity indices (VEI) of 3 or greater, indicating that they produced eruption columns that rose to at least 3 km above sea level and (or) had tephra volumes in excess of 10 million $m^3$ (Newhall and Self, 1982). Changes that might precede an eruption are also reported and can provide valuable time for short- to medium-term contingency planning.

At the heart of the global volcanism network are its 1,500 correspondents around the world, who report eruption information and, in turn, receive the monthly bulletin. Many are volcanologists who monitor a single volcano or volcanic region and can thus provide detailed information from the ground when an eruption begins. Others are atmospheric scientists, remote-sensing satellite specialists, government officials responsible for volcanic hazards, or members of the aviation community. Communication across these disciplinary and agency lines has proven valuable, yielding important new information and suggesting new and fruitful lines of inquiry. The bulletin is available by subscription through the American Geophysical Union (2000 Florida Ave. N.W., Washington, DC 20009), on electronic mail systems (OMNET, 70 Tonawanda St., Boston, MA 02124; KOSMOS/Pinet, AGU/American Institute of Physics; and Bitnet, VOLCANO Listserv, information at AIJHF@ASUCAD), and (in summary or extract form) in Bulletin of Volcanology, Eos, and Geotimes. The first 10 years of the bulletin's volcano reports were published as Global Volcanism 1975–1985 (McClelland and others, 1989), and its sequel is in preparation.

GVN quickly forwards news of any eruption that might affect aviation to NOAA's Synoptic Analysis Branch and to FAA headquarters in Washington, D.C. GVN supports their efforts by consulting local volcanologists for information about the eruption and searching Smithsonian resources for data about the volcano's geography and eruption history. In turn, GVN forwards observations from satellites and aircraft to volcanologists studying the eruption and to officials responsible for the safety of people living nearby. However, GVN has neither funding nor staff for 24-hour, 7-day operation, so responsibility for immediate monitoring and communication of volcanic hazards to aircraft must remain with other organizations.

## COMMUNICATIONS BETWEEN VOLCANO OBSERVERS AND AVIATION OFFICIALS

An eruption's effects on aviation are rarely confined to a single country. Large volcanic clouds pay no attention to national boundaries, and aircraft from dozens of nations may fly through airspace rendered hazardous by ash. Although single-nation efforts are valuable, a more effective international communications system is needed to ensure aviation safety during explosive eruptions. Unfortunately, it remains difficult for volcanologists to communicate with the aviation community. The many (16 reported) aircraft encounters with Pinatubo's recent eruption cloud suggest that news of even this dramatic, well-publicized eruption did not always reach airlines and air traffic control facilities in a timely manner. No international system yet exists through which volcanologists can directly receive the aviation system's official warnings of volcanic hazards to aircraft, such as NOTAM's (notices to airmen) and SIGMET's (significant meteorological advisories). Knowledge of these messages would help volcanologists and remote-sensing specialists evaluate the effectiveness of their communications with the aviation community during an eruption, and it would help catch errors and omissions promptly before they could lead to a disastrous aircraft-ash encounter.

When accessible, pilot reports of eruptive activity have proven very valuable in assessing the characteristics and vigor of an eruption, and a volcanic activity report form has been developed for the International Civil Aviation Organization by the International Federation of Air Line Pilots Associations and others (Fox, this volume; Miller, this volume). Eruption-cloud observations are to be immediately communicated by radio to the regional air traffic control

center, so that other pilots in the area can be promptly informed. The completed form is to be given to company officials after landing. However, communication channels are needed to forward pilot observations of eruptions to local volcanologists and, internationally, to GVN, remote-sensing specialists, other airlines, and air traffic authorities.

## COMMUNICATING SATELLITE OBSERVATIONS OF ERUPTION CLOUDS

Large explosive eruptions can often be detected by satellite and the resulting plumes tracked for long distances. Images from NOAA's polar-orbiting weather satellites were used by Matson and Robock (1984) to document the 1982 El Chichón plume for several weeks as it circled the globe. Geostationary weather satellites provide more frequent coverage, returning data as often as once every 30 minutes, although resolution is lower than for polar-orbiting satellites, spectral information is limited, and viewing angle is poor in some areas (such as at high latitudes). Analysis by Sawada (1987) of 227 eruptions within the field of view from Japan's geostationary meteorological satellite showed that only about 14 percent could be detected, but almost all eruptions were evident when their clouds rose to more than 10 km altitude. No plumes smaller than about 20 km in horizontal extent or 4 km altitude were observed.

Eruption clouds remain difficult to distinguish from weather clouds, but use of multispectral data (presently available only from polar-orbiting satellites) offers promise as a technique for detecting the silicate particles that are present in virtually all fresh volcanic plumes (Schneider and Rose, this volume). Other characteristic components of volcanic clouds, notably $SO_2$, may also aid in their remote detection. The total ozone mapping spectrometer (TOMS), now on polar-orbiting satellites, is sensitive to $SO_2$, whose presence in a cloud is a clear indication of volcanic origin (Krueger and others, this volume). Despite infrequent real-time monitoring, TOMS data have on several occasions provided the first news of eruption clouds originating from volcanoes in remote areas. TOMS tracked the main Pinatubo cloud until it extended beyond the west coast of Africa and documented the Hudson plume during its 1-week circling of the globe. By coordinating TOMS data with observations from other weather satellites, more plumes could be tracked and the number of "false alarms" significantly reduced.

Rapid communication between volcanologists and satellite observers should be established and, where it already exists, strengthened, to solicit ground confirmation of suspected plumes and to trigger satellite searches for plumes from new eruptions. Although monitoring of the entire globe could theoretically be accomplished from a single site, communication remains difficult across great distances (and many time zones)—therefore, monitoring from existing national and regional satellite-observation centers would be more effective. Most of these centers are focused on meteorology, operate on a 24-hour schedule, and are already oriented toward rapid communication of hazardous conditions. Each should establish close ties with local volcanologists, air traffic officials, and airlines in order to determine procedures to be followed in the event of a large eruption. The valuable work by NOAA's satellite specialists during recent eruptions demonstrates that existing meteorological personnel are able to search effectively for and track volcanic clouds with modest additional training.

## ANTICIPATING ERUPTIONS

The locations and recent eruptive histories of many of the world's potentially active volcanoes have been documented (Simkin and others, 1981), and others, which have not been identified, are likely to be within known volcanic belts (Simkin, this volume). The most violent eruptions typically occur from volcanoes that have been quiet for hundreds to thousands of years and can often be the first historic eruption at a site not recognized as potentially active (Simkin and Siebert, 1984), as dramatically illustrated by eruptions of El Chichón and Pinatubo. Planning for future eruptions should thus focus on entire volcanic regions, as well as on the most frequently active volcanoes within those regions.

Maps that show the relationship between volcano locations and air routes are not yet available, but they would be valuable to plan effectively for future eruptions on both a global and regional scale. Air routes downwind from active volcanic regions should be identified, and the necessary communications links between volcanologists, satellite specialists, aviation authorities, and airlines should be established. Such maps would also become powerful operational tools if current satellite data could be electronically superimposed upon them—the resulting image showing source volcano, eruption-cloud position, forecast cloud trajectories, and air routes could be transmitted to distant computer screens, both on the ground as well as in the cockpit.

Volcanic eruptions rarely occur without warning. Increased earthquake activity, swelling of the volcano, and (or) changes in gas emission generally precede an eruption by days to years. Given even minimal monitoring, one or more of these premonitory signs is usually recognized before an eruption, or they may be noticed and reported by people living near an unmonitored volcano. Although such episodes of unrest often do not culminate in an eruption (Newhall and Dzurisin, 1988), they can provide valuable time in which to prepare contingency plans, thereby reducing the risk of an ash encounter if an eruption occurs.

Detailed pre-eruption planning is essential if communications links are to work smoothly when an eruption begins,

and aviation officials should establish good working relationships with their region's volcanologists before the next large eruption. A valuable directory published by the World Organization of Volcano Observatories (Sigvaldason, 1991) describes personnel, equipment, and monitoring work at more than 40 facilities worldwide, many of which are responsible for more than one volcano.

News of possible pre-eruption activity needs wider and more rapid distribution, but money is also needed to establish at least minimal monitoring, perhaps as little as a single seismometer, at each of the world's potentially active volcanoes. The International Decade for Natural Disaster Reduction provides a logical framework for increased volcano monitoring, and the aviation community should add its considerable influence to proposals by volcanologists for improvements in monitoring capabilities.

Improved communication remains the key to avoiding disastrous aircraft encounters with eruption clouds. Effective communication must cut across international boundaries, organizational barriers, and scientific disciplines. GVN can help by catalyzing crucial communications links, providing information about monitoring efforts at individual volcanoes and volcanic regions, and continuing its primary role of supplying prompt information about current volcanic activity.

## ACKNOWLEDGMENTS

Tom Simkin deserves special thanks for editing that improved this report. This paper has also benefited from thoughtful reviews by Steve Brantley and Tom Casadevall. Captain Ed Miller of the Air Line Pilots Association has spent untold hours patiently and graciously educating me about aviation. Most importantly, the Global Volcanism Network could not function without the enthusiasm and dedication of its correspondents, who have consistently shared detailed preliminary information with their colleagues, often under the pressure of an ongoing eruption.

## REFERENCES CITED

Alaska Volcano Observatory Staff, 1990, The 1989–1990 eruption of Redoubt Volcano: Eos, Transactions, American Geophysical Union, v. 71, no. 7, p. 265, 272–275.

Katow, K., 1988, Flight operation procedure for avoiding volcanic eruption clouds, *in* Proceedings, Kagoshima International Conference on Volcanoes, p. 666–669.

Lynch, J., 1991, Mount Redoubt: Tracing volcanic ash plumes from space [abs.], *in* Casadevall, T.J., ed., First International Symposium on Volcanic Ash and Aviation Safety: U.S. Geological Survey Circular 1065, p. 30.

Matson, M., and Robock, A., 1984, Satellite detection of the 1982 El Chichón eruptions and stratospheric dust cloud: Geofísica Internacional, v. 23, p. 117–127.

McClelland, L., Simkin, T., Summers, M., Nielsen, E., and Stein, T.C., 1989, Global Volcanism 1975–1985: Englewood Cliffs, N.J., Prentice Hall, and Washington, D.C., American Geophysical Union, 657 p.

Newhall, C.G., and Dzurisin, D., 1988, Historical unrest at large calderas of the world: U.S. Geological Survey Bulletin 1855, 1108 p.

Newhall, C.G., and Self, S., 1982, The volcanic explosivity index (VEI): An estimate of explosive magnitude for historical volcanism: Journal of Geophysical Research (Oceans and Atmospheres), v. 87, p. 1231–1238.

Prata, A.J., Barton, I.J., Johnson, R.W., Kamo, K., and Kingwell, J., 1991, Hazard from volcanic ash: Nature, v. 354, p. 25.

Sawada, Yoshiro, 1987, Study on analysis of volcanic eruption cloud image data obtained by the geostationary meteorological satellite (GMS): Technical reports of the Meteorological Research Institute [Japan], no. 22, 335 p.

Sigvaldason, G., ed., 1991, Directory of volcano observatories, 1990–1991: Reykjavík, WOVO/UNESCO, 99 p.

Simkin, T., and Siebert, L., 1984, Explosive eruptions in space and time: Durations, intervals, and a comparison of the world's active belts, *in* Boyd, F.R., ed., Explosive Volcanism: Inception, Evolution, and Hazards: Washington, D.C., National Academy of Sciences Press, p. 110–121.

Simkin, T., Siebert, L., McClelland, L., Bridge, D., Newhall, C.G., and Latter, J.H., 1981, Volcanoes of the World: Stroudsburg, Pa., Hutchinson Ross, 233 p.

VOLCANIC ASH AND AVIATION SAFETY:
Proceedings of the First International Symposium
on Volcanic Ash and Aviation Safety
U.S. GEOLOGICAL SURVEY BULLETIN 2047

# VOLCANIC ASH AND AIRCRAFT OPERATIONS

*By* Edward Miller

## ABSTRACT

The aviation community has been subjected to volcanic eruption hazards on several occasions over the past decade, usually in rather dramatic fashion. Volcanic ash, injected into the stratosphere by explosive eruptions, is abrasive and will cause serious damage to aircraft engines, control surfaces, windshield and windows, and landing lights. Ash clouds are difficult and sometimes even impossible to distinguish from weather clouds.

This paper explores the ground detection, reporting, and dissemination of information critical to crew members operating in the vicinity of known volcanoes and discusses the operational needs of flight-crew members. Pilots need to be educated about the hazards of volcanic ash. Pilots need two tools for reporting and coping with volcanic ash: a copy of the ICAO volcanic activity report form (VAR) and a chart portraying air routes and locations of known volcanoes.

## INTRODUCTION

The aviation community has been dramatically introduced to volcanic eruption hazards over the past half century. Volcanic ash, a by-product of many explosive volcanic eruptions, is often injected into the upper troposphere and stratosphere and spreads laterally in the upper-level wind flow. The ash is abrasive and capable of causing serious damage to aircraft engines, control surfaces, windshields and windows, and landing lights. The dust can clog the pitot-static systems, which determine airspeed and altitude, and can damage sensors that deliver electronic data to automated systems used to fly modern aircraft. Mixed with weather-associated clouds, ash is difficult and sometimes impossible to identify.

## INTERNATIONAL EFFORTS

Since 1944, when a squadron of B-25's on the ground in Italy were destroyed by volcanic ash from Mt. Vesuvius, aircraft have been sustaining damage in varying degrees from volcanic ash. In 1982, two B747's, one British Airways the other Singapore Airlines, came very close to disaster in Indonesian airspace because of volcanic ash (Smith, 1983; Tootell, 1985). Shortly after these incidents, the air navigation commission of the International Civil Aviation Organization (ICAO) formed the volcanic ash warning (VAW) study group to deal with the threat of volcanic ash (Fox, this volume).

The study group developed procedures and guidance for dealing with volcanic activity and reporting the activity to aircraft and control centers in a timely manner. Working within the frame work of ICAO, implementation of these procedures required formal amendments to the ICAO regulatory documents. The VAW study group recommended amendments to annexes 3, 11, and 15 to document 4444 (Procedures for Air and Air Traffic Services) and document 8400 (ICAO Abbreviations and Codes)—the study group also recommended changes to the provisions for the use of notices of significant meteorological events (SIGMET's), notices to airmen (NOTAM's), and special air reports of volcanic activity (VAR's). All formal amendments require consultation with member states of ICAO, a time-consuming but necessary step. During these discussions, the air navigation commission provided interim measures for member states to use and organized an International Airways Volcano Watch, which maximizes the value of existing observing networks from several diverse fields. These networks include:

1. World Organization of Volcano Observatories (WOVO). WOVO, under the aegis of the International Association of Volcanology and Chemistry of the Earth's Interior (IAVCEI), includes volcanological observatories located in different countries and under different authorities. The member observatories form a global network that has the potential to provide volcanic activity reports in real time to air traffic control centers and world meteorological centers.
2. World Meteorological Organization (WMO). The WMO includes meteorological watch offices that receive information from meteorological, hydrological, agricultural, and climatological observing stations; merchant ships, which routinely provide meteorological reports; and meteorological satellites. Approximately 7,000 merchant ships are capable of reporting regular meteorological observations to

coastal stations. Allowing for port visits when the ship crews are not observing, the WMO estimates that about 4,000 ships actively report from all global shipping lanes. A small number of ships also make upper-air measurements. These reports are received at the World Meteorological Centre at Bracknell, England, every 24 hours.

Satellite monitoring of volcanic eruptions and volcanic ash clouds is not without problems. Geostationary weather satellites cannot track volcanic ash clouds once they mingle with weather clouds. The NASA (U.S. National Aeronautics and Space Administration) Nimbus 7 satellite, and a recently launched Soviet satellite, each have the total ozone mapping spectrometer (TOMS) on board, which is capable of detecting sulfur dioxide in the volcanic ash cloud (Krueger and others, this volume). NOAA (U.S. National Oceanic and Atmospheric Administration) satellites with the advanced very high resolution radiometer (AVHRR) are also capable of detecting a volcanic ash cloud (Schneider and Rose, this volume). Both TOMS and AVHRR methods are time consuming, and only a limited number of centers have the satellite-data receiving and processing equipment.

## RECENT EVENTS

Events of recent years have reminded us with alarming regularity that aircraft and volcanic ash do not mix well. Windshields have been rendered opaque, engines have failed, and severe damages have left air carriers with aircraft useless to them without costly repair. On December 15, 1989, a Boeing 747-400 airliner en route from Amsterdam to Anchorage encountered volcanic ash from the Redoubt Volcano in Alaska and suffered a simultaneous four-engine flameout (Przedpelski and Casadevall, this volume) and, despite state-of-the-art technology, the aircraft was rendered an expensive glider for several minutes. The crew was aware of a volcanic eruption in the vicinity of Anchorage prior to their departure from Amsterdam. At 11:27 a.m. Alaska Standard Time (AST), the flight was in the Fairbanks area and was informed of a second Redoubt eruption. The pilot requested and received a radar vector around the reported ash cloud. At 11:46 a.m., during a descent from 35,000 ft, the aircraft entered a benign-looking stratus cloud at 26,000 ft. Dust and smoke in the cockpit came to the crew's attention first. The cloud was unnaturally dark, and St. Elmo's glow shone at the windows. The crew applied full power to climb out of the ash cloud, and after about 1 minute of high power, all engines spooled down to below idle, followed by a loss of airspeed and activation of the stick shaker. The stick shaker, a stall warning device, alerted the pilot that the aircraft was approaching stall. The next alarm was a false fire warning bell and crew-alerting system message, "cargo fire forward."

The crew initiated appropriate emergency procedures, declared an emergency to the Anchorage air traffic control center, and initiated restart procedures for the engines. The aircraft departed the cloud at 20,000 ft, and, after five or six attempts, the crew successfully restarted engines 1 and 2 at an altitude of 17,200 ft, producing enough power to maintain level flight. After three additional attempts, engines 3 and 4 were also restarted. The remainder of the flight occurred without further incident, and the airplane landed safely in Anchorage.

The aircraft sustained heavy damage during its encounter with the ash cloud (Campbell, 1991). All four engines suffered damage to their compressors, combustion chambers, and turbine sections. The intake turbine blades showed excessive wear, and the combustion section had areas blocked. The ash was redeposited as a glass-like material on hot parts of the engines (Przedpelski and Casadevall, this volume). The pitot-static system was contaminated, resulting in a loss of airspeed indications. Contamination of the ventilation system caused the avionics compartment to overheat, rendering all components to be suspect of failure. The fuel system and hydraulic systems were contaminated with volcanic ash and required purging.

Even though there is no "degree" of hazard scale, pilots should know that, after loss of one or more engines due to volcanic ash and subsequent relights, they will deal with permanently damaged engines and aircraft. Further flight should be planned with that fact in mind.

## PILOT DETECTION OF VOLCANIC ASH CLOUDS

Pilots are often the first to detect a volcanic eruption, even when the volcano in question is extensively monitored. Moreover, considering the number of volcanoes not yet monitored and the potential threat to aviation, pilot reports take on new importance. Pilots must report any atmospheric hazard to flight that they observe, and volcanic ash definitely qualifies as an atmospheric hazard.

Pilots are obliged to report known atmospheric hazards along routes of flight. The ICAO-approved special air report of volcanic activity (or volcanic activity report form, VAR) was deemed necessary because of the hazardous nature of volcanic ash clouds and their unpredictability. The form was designed for the needs of pilots and volcanologists (Fox, this volume). Items numbered 1 through 8 of the VAR are to be transmitted over the air traffic control frequency to the air traffic control center. Aircraft on and monitoring the control center radio frequency will receive the information at the same time the control center does. The reported information received by the listening aircraft will aid them in discerning their degree of hazard and what response is necessary. The remainder of the form is to be filled out when duties permit and is turned in at the first point of landing.

Existing aircraft hardware is incapable of detecting volcanic ash; pilots are the only on-board system capable of

detection! Recently, the Australian Office of Space Science and Application (COSSA) has developed a prototype instrument for in-flight detection of volcanic ash—this instrument is currently being tested (Barton and Prata, this volume; Prata and Barton, this volume).

## INFORMATION AND RESPONSE

Airborne flight crews will receive radio reports of volcanic-ash-cloud information either from another flight crew or from the controlling air traffic center. Future communications linkages include printed messages received in the cockpit via datalink. The pilot's first task after receiving this information is to determine the location of the event and assess the threat to the present route of flight. A pilot observing a suspected ash cloud should report it following the format of the volcanic activity report form (VAR) (Fox, this volume, fig. 1). Section I, items 1 through 8, are all that are required to be given at or shortly after the encounter and gives other crews in the area enough information to plan a prudent course of action.

By applying the air report information to a chart that depicts volcanoes and air routes, the pilot could quickly have a graphic picture of the affected area and determine the position of the aircraft relative to the ash cloud. The pilot could plan avoidance of the ash by comparing cloud tops, aircraft performance, and other options available. Course correction, if appropriate, may be determined after looking at the information now depicted on the chart. Some questions to be asked are: Is a course correction necessary? If so, how far? What altitude is available on the other route? What will the correction cost in fuel burn? Is a new route necessary just long enough to avoid the cloud and then return to the original route, or will a whole new route be required? Is fuel sufficient to reach the planned destination after this reroute, or must an alternate destination be arranged? If the flight is short of the established point of equal time, is it necessary to return to the departure station?

The following weaknesses in accurate pilot reporting of volcanic activity are possible:

1. The initial encounter may require immediate emergency action. Filing a report by radio, and completing the report form, may initially have low priority.
2. Weather and time of day may preclude the possibility of a pilot report. A volcano may only release steam clouds whose size and color may vary due to atmospheric conditions and time of day. The steam clouds will trigger reports of an eruption that must be treated as an ash-cloud eruption. Verification of pilot reports is not always possible, and there is always a time delay, even when verification facilities are in place. This situation could be improved with pilot training that covers the hazards of volcanic ash to aircraft and aircraft systems. Understanding how and what to report when sighting volcanic activity fills that requirement.
3. Powerful eruptions that penetrate the stratosphere will form a mushroom cloud similar to an atomic explosion (Johnson and Casadevall, this volume; Self and Walker, this volume). Pilots may view the ascending column of volcanic ash and must be aware than an ash umbrella could be damaging to the aircraft.
4. Ash clouds are difficult to identify in darkness. Nighttime reporting has only been possible after entering ash clouds. Without airborne detection devices, early warning is not always possible. The following characteristics of ash encounters have been reported by flight crews:
   a. Smoke or dust in the cockpit.
   b. An acid odor similar to that of electrical smoke.
   c. Multiple engine malfunctions, such as compressor stalls, increasing operating temperatures, torching from tailpipe, and engine flameouts.
   d. St. Elmo's glow and static discharges around the windshield, accompanied by a bright orange glow in the engine inlets. Volcanic ash clouds may contain sufficient electrical charge to generate lightning (Gilbert and Lane, this volume), a recognition advantage for the pilot, particularly at night. Most pilots will avoid lightning but may not necessarily be aware that a volcanic ash cloud is in their path.

## SIGMET (SIGNIFICANT METEOROLOGICAL INFORMATION) AND PIREP (PILOT REPORT)

ICAO defines the SIGMET as "information issued by a meteorological watch office concerning the occurrence or expected occurrence of specified en-route weather phenomena that may affect the safety of aircraft operations." SIGMET's, by design, block off large areas of airspace, and volcanic ash clouds may occupy only a relatively small area of the SIGMET-noted area. With updated pilot reports, areas free of volcanic ash can be determined with more confidence.

Pilots have reported that relaying information about where the ash cloud is not, can be more important than information about where the cloud is because open areas permit aircraft to operate (Haeseker, 1991). However, such an operation requires very close monitoring, with updates as frequent as 15 minutes or less from aircraft in the operation area. Usually, this will only be possible during daylight hours—another unfortunate restriction. Considering an alternative of no operation at all, the above has valid application. Departure and arrival airports must be open and remain open, and alternate airports must be available. Aircraft must be flown in visual conditions under visual flight

rules (VFR) away from clouds, even though the pilot may be flying under instrument flight rules (IFR). Constant communication must be maintained between the aircraft and the traffic control center. The center may be receiving updates directly from a volcano-observation facility and will correlate that information with pilot reports. Base operations and airline dispatchers must also be in the information loop.

Flight regulations require that aircraft captains have the final word on whether this type of operation is safe and prudent. This plan, with the best information, may be limited by the controlling center's ability to reroute traffic. The case of limited ability may not hinge on center staff, but on terrain, volume of traffic, and limited corridors open to traffic even under normal conditions.

## CONCLUSIONS

- Although much has been done to mitigate the dangers of volcanic ash to aircraft, more is needed. There are 1,500 known volcanoes worldwide, and about 600 of these volcanoes are considered active (Simkin, this volume). An average of 55–60 volcanoes erupt each year, and about eight to ten of these eruptions produce ash clouds that reach flight altitudes.
- Considering the limited number of monitored volcanoes and the limits on satellite detection of volcanic ash clouds, we conclude that pilots must be especially attentive to the hazards of volcanic ash intruding into airspace.
- Pilots already look out for one another by reporting in-flight weather conditions such as mountain waves, clear-air turbulence, and thunderstorms that are all hazardous to flight.
- Pilots are knowledgeable about atmospheric hazards. This knowledge is acquired from actual experience and from required weather training courses for licensing purposes. Volcanic ash is a relatively new hazard, and although not many crews have experienced flight into a volcanic ash cloud, it is regrettable that the number of crews with this experience is growing.

## RECOMMENDATIONS

- Pilot training is the first priority. Pilots must understand that volcanic ash is not like sand or dust, and they must know how to recognize inadvertent entry into an ash cloud.
- Pilots must understand the recommended procedures for exiting the cloud in order to minimize damage to their aircraft (Campbell, this volume).
- A volcanic ash training video has been developed by the Boeing Company in cooperation with the Air Line Pilots' Association and the U.S. Geological Survey. This video has been distributed widely, and ICAO will provide translations into French, Russian, and Spanish.
- Presently, neither the new video nor previous volcanic ash information developed by airframe and engine manufacturers is mandated for inclusion in pilot training syllabi. Minimum requirements should be that every licensed pilot view the training video. More effective training would require the inclusion of volcanic ash hazards into ground school courses required for a pilot's license. An ideal training program would include the required ground school, the video, and a volcanic ash drill during the simulator portion of the pilot training course.
- Proper tools must be provided that will assist pilots. They must have the ICAO volcanic activity report (VAR) form. The VAR form is already in use by some airlines. In addition, commercial chart makers such as Jeppesen-Sanderson, Inc., have been encouraged to prepare charts showing volcanoes and air routes.
- Finally, airline management must be convinced that the charts, the video, and the training programs are necessary, and regulations must be rewritten to implement the change.

## REFERENCES CITED

Campbell, E.E., 1991, 747-400 airplane damage survey following a volcanic ash encounter [abs.], *in* Casadevall, T.J., ed., First International Symposium on Volcanic Ash and Aviation Safety: U.S. Geological Survey Circular 1065, p. 14.

Haeseker, E., 1991, Alaska Airlines operating procedures during the 1989–1990 Redoubt eruptions [abs.], *in* Casadevall, T.J., ed., First International Symposium on Volcanic Ash and Aviation Safety: U.S. Geological Survey Circular 1065, p. 20–21.

Smith, W.C., 1983, High-altitude conk out: Natural History, v. 92, no. 11, p. 26–34.

Tootell, B., 1985, All 4 Engines Have Failed; The True and Triumphant Story of Flight BA 009 and the Jakarta Incident: Auckland, Hutchinson Group, Ltd., 178 p.

VOLCANIC ASH AND AVIATION SAFETY:
Proceedings of the First International Symposium
on Volcanic Ash and Aviation Safety
U.S. GEOLOGICAL SURVEY BULLETIN 2047

# VOLCANIC EVENT NOTIFICATION AT MOUNT ST. HELENS

*By* Bobbie Myers *and* George J. Theisen

## ABSTRACT

During the 1980–86 eruptions of Mount St. Helens, hazards information was quickly disseminated through a U.S. Geological Survey Cascades Volcano Observatory–U.S. Forest Service notification system. Written and verbal statements issued jointly by the Cascades Volcano Observatory (CVO) and University of Washington were released to the Forest Service for telephone call-down to governmental agencies and private interests. Once the call-down was underway, public and media information tapes were updated and press releases were issued. Because most of these eruptions had recognizable precursors, a series of information statements and eruption forecasts was issued during the weeks to hours before an eruption, thus providing advance warning of volcanic activity and associated hazards.

Hundreds of small gas and ash emissions also occurred during 1980–86, most without recognizable precursors. The lack of precursors made advance warning of these events impossible; instead, information statements were issued after the larger, more visible events. The occurrence of occasional small, unpredictable, ash-producing explosions at Mount St. Helens during 1989–91, coupled with increased concern about the hazards of volcanic ash to aviation, prompted CVO to develop a seismic-alarm system that triggers on small volcanic events. This alarm system activates CVO's 24-hour telephone beeper. In addition, the Federal Aviation Administration (FAA) can also activate the CVO beeper to report possible volcanic activity. These two modifications improve CVO's response time for non-predictable, sudden-onset events and help the FAA quickly verify pilot reports of possible volcanic plumes.

## INTRODUCTION

When Mount St. Helens awoke in March 1980, there was an immediate need for the rapid dissemination of information about volcanic events and hazards. An emergency coordination center (ECC) was established at the U.S. Forest Service (USFS) facility in Vancouver, Wash. The facility was staffed 24 hours a day by USFS personnel experienced with emergency response. During critical times, the ECC was also staffed by representatives of the U.S. Geological Survey Cascades Volcano Observatory, emergency management agencies, and private companies. A communications network (fig. 1) and telephone call-down procedures were developed to facilitate rapid dissemination of information about the activity of the volcano. Information was also disseminated through public meetings, press conferences,

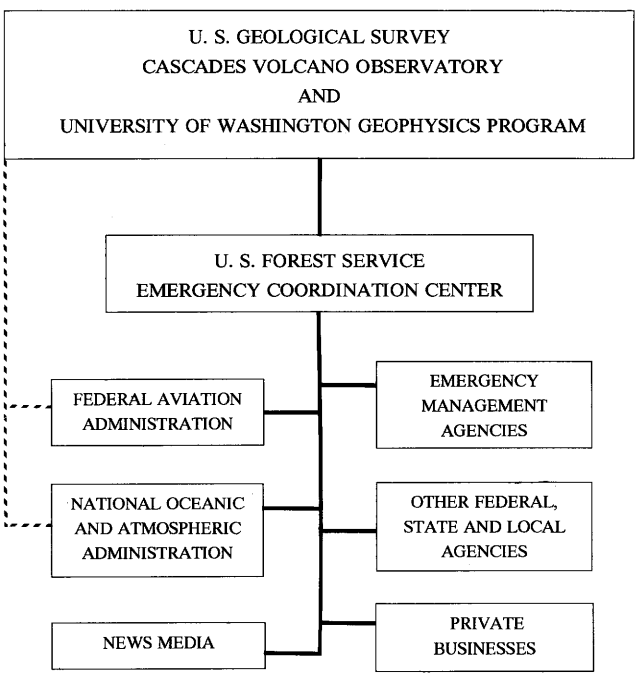


**Figure 1.** Communication and notification network for rapid dissemination of volcanic hazards information at Mount St. Helens. Statements issued jointly by the Cascades Volcano Observatory and the University of Washington are disseminated by the U.S. Forest Service emergency coordination center. Although all participants have the opportunity to communicate with each other, the main channels for distribution of formal statements and notifications are shown by heavy lines. Dashed lines represent secondary links during the early 1980's, which have become primary links in recent years.

**Table 1.** Example of statements by CVO and UW released by ECC during the March–April 1982 eruptive period of Mount St. Helens.

[CVO, Cascades Volcano Observatory; UW, University of Washington; ECC, emergency coordination center; PST, Pacific Standard Time. For most eruptions of Mount St. Helens, a series of statements predicting an eruption and providing information on eruptive activity after it began was written by CVO and UW and released by the ECC through a formal call-down procedure. These statements were based primarily on recognition of a repeated pattern of precursors. When the patterns changed, statements were necessarily less detailed. The following example represents one of the most detailed series]

| March 5, 1982 |
|---|
| 0900 PST; EXTENDED OUTLOOK ADVISORY: |
| Seismicity at Mount St. Helens increased around February 21 and has remained at a level somewhat above background since that time. Approximately 100 earthquakes that occurred during this period have been located. These earthquakes fall into two groups: (1) a "deep" group of very small earthquakes with centers at 6- to 11-km depths, and (2) a shallow group of somewhat larger (magnitude 1 or less) earthquakes located at 3–4 km up to the surface. There is a pronounced lack of seismicity at a depth of 4–6 km. |
| Although poor weather during the past week has hampered observations and monitoring on the mountain itself, measurements made last week show only slow ground deformation in the immediate vicinity of the dome and no significant increase in gas emissions. |
| **March 12, 1982** |
| 0800 PST; EXTENDED OUTLOOK ADVISORY: |
| Seismicity beneath Mount St. Helens continues at elevated levels, but individual earthquakes are of low magnitude. Earthquakes have been occurring in 1–2-day-long episodes separated by 1–2-day intervals of decreased activity. The earthquakes are occurring between the surface and a depth of about 6 miles. Rates of ground deformation in the crater area have increased during the last two weeks, and they are similar to patterns observed before previous dome-building eruptions. |
| Based on rates of deformation, an eruption is likely within the next 3 weeks. Deformation is confined to the crater areas, suggesting that renewed dome growth will occur. The current seismic patterns differ from any observed before 1980–81 eruptions, however, and raise the possibility of more hazardous variations in eruptive behavior. If there were to be any pyroclastic flows, from either an explosive eruption or collapse of the steep north face of the dome, the possibility of rapid snowmelt would be a concern. |
| **March 15, 1982** |
| 1900 PST; ADVISORY: |
| Accelerating rates of ground deformation in the crater of Mount St. Helens suggest that an eruption, most likely of the dome-building type, will probably begin within 1 to 5 days. Deep earthquakes have almost ceased, and shallow earthquakes continue at a moderate rate. A further increase in shallow seismicity is likely before the eruption starts. |

**Table 1.** Example of statements by CVO and UW released by ECC during the March–April 1982 eruptive period of Mount St. Helens—Continued.

| March 19, 1982 |
|---|
| 0900 PST; ERUPTION ALERT: |
| Seismicity at Mount St. Helens has increased significantly during the past day. This indicates that an eruption will begin soon, probably within the next 24 hours. The character of both the seismicity and deformation in the crater area indicated that the most likely type of activity is dome growth. |
| 1933 PST; ERUPTION ALERT: |
| Verbal statement that eruption had begun at 1927. (Significant increase in seismicity and pilot and radar reports of an ash plume indicated start of eruption.) |
| 2025 PST; ERUPTION UPDATE: |
| The eruption has subsided for the time being, and an ash plume is blowing to the SSE. and S. with a lesser amount to the SSW. The size of the eruption and the amount of the ash appear to be like those of the summer 1980. |
| **March 21, 1982** |
| 0900 PST; ERUPTION UPDATE: |
| There is a new lobe being added to the SE. side of the lava dome in the crater of Mount St. Helens. The new extrusion began during the night. Seismicity and tilt are now following patterns observed during other recent periods of dome growth. |
| **March 24, 1982** |
| 1730 PST; ERUPTION UPDATE: |
| Growth of the new dome lobe has slowed significantly over the past 2 days, but rates of deformation on the north side of the dome have increased over the same period. Until additional measurements are made, it would be premature to declare this eruption over. Seismometers are recording decreasing numbers of avalanches as growth of the new lobe slows. |
| **April 5, 1982** |
| 0100 PST; ERUPTION UPDATE: |
| Seismicity still continues at moderate to high levels. Fluctuations in seismicity correspond to pulses of gas and ash, the largest of which began at 1237 a.m. and rose to a maximum of about 32,000 ft. There does not appear to be much ash in the plume, but minor ashfall was reported earlier tonight at Packwood. No increases have been reported in river levels. |
| 1800 PST; ERUPTION UPDATE: |
| Seismicity is continuing at a moderate to high level. The status of the volcano remains unchanged since the previous advisory (1 a.m., 4/5/82). Some additional dome growth and (or) small-scale explosive activity is likely; larger explosive activity is less likely but cannot be ruled out. |

**Table 1.** Example of statements by CVO and UW released by ECC during the March–April 1982 eruptive period of Mount St. Helens—Continued.

| April 6, 1982 |
|---|
| 0915 PST; ERUPTION UPDATE: |
| Another new lobe is being added to the dome. This reduces the immediate likelihood of larger explosive activity, but small, intermittent gas and ash pulses may continue to occur. |
| **April 12, 1982** |
| 1515 PST; ERUPTION UPDATE: |
| Seismicity, deformation and gas emissions at Mount St. Helens have returned to low levels, indicating that the eruption that began on 3/19/82 is over. |

and briefings with governmental agencies and private businesses (Miller and others, 1981). Written "volcanic and seismic activity reports" were issued daily. These "daily updates" provided information on the status of the volcano and any significant changes or observations during the previous 24 hours.

Since 1980, this notification system has been modified in response to changes in volcanic activity, funding, and the concerns of government, business, and the public. Key changes include the capability of issuing written predictions weeks in advance of most eruptions; eliminating the need for 24-hour duty for both USFS/ECC and CVO staff except when eruptions are imminent; entering all predictions and updates into a computer "news" system for easy review by those on the call-down list; updating volcanic activity reports and information tapes weekly or monthly (rather than daily) when the volcano is quiet; and, most recently, developing a seismic alarm to alert scientists to small events that occur without precursors.

## NOTIFICATION BEFORE AND DURING EVENTS WITH PRECURSORS

Since May 18, 1980, 21 magmatic eruptions have occurred at Mount St. Helens; 5 were predominantly explosive, and 16 were predominantly non-explosive, dome-building eruptions. Several eruptions involved both explosive and dome-building activity. The last magmatic eruption was a dome-building eruption in October 1986. Scientists at CVO in Vancouver, Wash., and at the University of Washington (UW) Geophysics Program in Seattle were able to predict most of these eruptions based on evaluation and interpretation of data from an extensive monitoring network (Swanson and others, 1985). Initially, these predictions were issued as verbal statements, but, after December 1980, they were issued as written statements. Both types of statements were distributed by the USFS through the ECC.

**Table 2.** Examples of "daily updates" about Mount St. Helens issued by CVO and UW after the March 15, 1982, advisory and before the March 19, 1982, alert.

[CVO, Cascades Volcano Observatory; UW, University of Washington; PST, Pacific Standard Time]

| March 16, 1982 |
|---|
| 0800 PST: |
| Geologists and hydrologists from the Geological Survey performed on-site monitoring in and around Mount St. Helens on March 15, 1982. Measurements showed accelerated rates of ground deformation on thrusts and cracks in the crater. University of Washington–USGS reports seismicity remains at a slight increase over the weekend's activity. Shallow earthquakes continue at a moderate rate (see Mount St. Helens Advisory, 7:00 p.m., March 15, 1982). |
| **March 17, 1982** |
| 0800 PST: |
| Good weather permitted on-site monitoring in and around Mount St. Helens by geologists and hydrologists of the U.S. Geological Survey. Measurements showed continued acceleration of ground deformation localized around the lava dome. Overflights of the volcano the last two days have shown an increase in the number of incandescent areas on the dome. University of Washington–USGS reports seismicity remains at a moderate rate. |
| **March 18, 1982** |
| 0800 PST: |
| Continued good weather enabled monitoring to be carried out in the crater of Mount St. Helens for the third day in a row. Measurements performed by geologists from the U.S. Geological Survey continued to document accelerating ground deformation rates. Airborne gas monitoring around the volcano during the past several days has shown that a moderate increase in the rate of $SO_2$ emissions has occurred. The University of Washington–USGS seismic lab reports a slight increase in the level of seismicity over that of yesterday, but it still can be described as a moderate level. |

For most eruptions, a series of statements was issued (table 1), usually beginning with an "extended outlook advisory" predicting an eruption within several weeks. As the levels of precursory activity increased, the predicted eruption window was fine-tuned to days or hours, and "eruption advisories" and "eruption alerts" were issued. After an eruption began, factual statements were issued regarding the character and effects of the eruption, and, finally, a statement was issued declaring the eruption to be over. The "daily updates" and information tapes for the public and media provided additional information on a daily basis (table 2).

If the ECC and CVO, in Vancouver, and the UW seismic laboratory, in Seattle, were not already staffed on a 24-hour basis when an "eruption advisory" was issued,

24-hour duty was initiated. USFS, CVO, and UW personnel were ready to respond to rapid changes in the level of volcanic activity and to answer questions and discuss specific concerns. Because it was not always possible to determine whether there would be explosive activity during an eruption, there were regular discussions among the Federal Aviation Administration (FAA), National Oceanographic and Atmospheric Administration (NOAA), National Weather Service (NWS), USFS/ECC, and CVO personnel regarding the possibility of ash plumes and their probable trajectories. CVO and the USFS reported suspected ash-producing events to the FAA as quickly as possible, and the FAA called the ECC or CVO to confirm all pilot reports. Initially the FAA was contacted at the local Portland, Oreg., area office; however, by the mid-1980's most contact with the FAA was made directly with the regional FAA office in Auburn, Wash. (Hamley and Parkinson, this volume).

## NOTIFICATION DURING AND AFTER EVENTS WITHOUT PRECURSORS

Between 1980 and 1986, hundreds of small ash emissions also occurred. These small events were known as gas and ash emissions or explosions, and they originated from cracks and small vents on the dome and sent plumes of steam and ash 500 ft (152 m) to 22,000 ft (6,706 m) above the volcano. The more vigorous events also erupted showers of hot rock fragments from the dome, and some events generated small debris flows.

Most of these events took place without recognized precursors, which made advanced warning of these events impossible. Verbal or written statements were issued to all concerned agencies after the larger or more visible events (table 3). If an event occurred during normal working hours, the ECC and CVO updated media and public information telephone tapes and contacted the FAA, emergency management officials, and others on the call-down list shortly after the event. Because the seismic amplitude of these events was too small to trigger alarms on the UW State-wide network, scientists were often unaware (until normal working hours) of events that occurred during non-working hours. In most cases, this was not a problem because these small events were frequent enough that government officials and the public became familiar with them. However, the FAA and emergency management personnel occasionally needed to contact CVO for more information after the larger events that may

**Table 3.** Examples of statements issued by the CVO and UW after eruptive events at Mount St. Helens that occurred without precursors.

[CVO, Cascades Volcano Observatory; UW, University of Washington; PDT, Pacific Daylight Time; ECC, emergency coordination center]

| June 18, 1982 |
|---|
| 0930 PDT; DAILY UPDATES:<br>[Distributed by CVO computer "news" system]<br>University of Washington–USGS reports continued low-level seismic activity. Small gas-emission events continue to occur daily. The most recent event was at 0621 this morning, June 18. The plume rose to 12,000 ft. |
| **April 18, 1986** |
| 1200 PDT; DAILY UPDATES:<br>[Distributed by CVO computer "news" system]<br>Since yesterday's report at 1300, there have been three more gas and ash emission events. The first occurred at 1428 on the 17th and produced a plume to 14,000 ft (according to a local pilot). The second event occurred at about 1 a.m. today. Minor ashfall from this event was reported SE. of the mountain. Both of these events appeared to be slightly smaller (seismically) than the 1716 event on the 16th. The third event occurred at 1116 today and was observed by geologists working in the crater and flying in an airplane around the mountain. The event appeared to be about the same size (seismically) at Yellow Rock as the 1716 event on the 16th. Geologists reported that rock fragments were thrown on and around the dome. The ash plume rose to 14,000 ft and later drifted higher and to the southeast. The event lasted about 5 minutes seismically, with the vigorous emission lasting just under 2 minutes. |
| **April 18, 1986—Continued** |
| When crew first reached the crater this morning they reported a light dusting of tephra on the east and southeast flanks of the mountain, some tephra on the crater floor, lots of ejected material (rock fragments) on top of the dome, and lots of new snow in the crater. A pit dug in the snow revealed four, thin (dispersed) ash layers from previous events.<br>A new update will be issued on Monday unless there is significant activity over the weekend. |
| **May 6, 1986** |
| 1300 PDT; INFORMATION STATEMENT<br>[Distributed by ECC formal call-down and CVO computer "news" system]<br>More than 50 steam and ash explosions have occurred on the dome at Mount St. Helens during the last 3 weeks. Seismicity has increased from slightly elevated levels at the end of April to moderate levels today. Most monitoring equipment on the dome has been damaged by the explosion and no longer operates. One remaining tiltmeter on the dome shows gradually accelerating tilt. Other deformation measurements have been hampered by inclement weather, inaccessibility of the dome because of the explosions, and loss of many targets. Hazards from explosions are most likely to be restricted to the crater and flanks of Mount St. Helens. However, small mudflows caused by explosions in the crater may flow into the North Fork Toutle River, and areas downwind from the volcano may occasionally be dusted by small amounts of ash such as has occurred recently. |

have been visible to pilots or the public. This contact was made by calling the USFS/ECC telephone beeper number; the USFS, in turn, contacted the CVO duty scientist by telephone or through the beeper, if necessary.

During 1989–91, at least six, small, ash-producing explosions occurred at Mount St. Helens, ending a 3-year period during which no eruptive activity took place. Because none of the 1989–91 explosions had recognizable precursors, they were not predicted, and no advance warnings were issued. The first of these ash-producing explosions (December 7, 1989) occurred during normal working hours; however, the second explosion (January 6, 1990) occurred on a rainy Saturday morning, and scientists were unaware of the event until several hours later when residents of central Washington began reporting light dustings of ash on their cars. In fact, CVO was not immediately notified when ash began falling. Instead, calls from the public prompted the media to contact the Alaska Volcano Observatory (AVO) to see if the ash was from ongoing activity at Redoubt Volcano, near Anchorage. AVO verified that the ash was not from Redoubt and contacted CVO geologists.

## RECENT MODIFICATIONS TO IMPROVE CVO'S RESPONSE TIME

The delay in CVO's learning about the January 6, 1990, event, coupled with increased concerns about the hazards of volcanic ash triggered by the Boeing 747 incident in Alaska on December 15, 1989 (Brantley, 1990), prompted CVO to develop a seismic-alarm system that is activated by small, as well as large, volcanic events. CVO also made a few adjustments in the notification and call-down procedures to improve communication of hazards information during nonworking hours.

### SEISMIC ALARM SYSTEM

Because seismicity is one of the main tools used to monitor volcanoes, CVO and UW maintain a network of 18 seismic stations within 16 km of Mount St. Helens, including three stations in the crater. These stations provide a detailed record of seismic activity at Mount St. Helens, including earthquakes, tremor, rockfalls, explosions, and mudflows (Jonientz-Trisler and others, this volume). Most of these seismic events, including many of the small ash-producing explosions, are too small to record on the State-wide network at UW. However, the events cause significant local ground motions that are detected on the Mount St. Helens network by the CVO real-time seismic-amplitude monitoring system (RSAM) as peaks in the time-averaged seismic amplitude (Endo and Murray, 1991).

An RSAM-based seismic-alarm system was developed and installed for testing 2 days after the January 6, 1990, event and was fully functional by the end of February 1990.

**Table 4.** RSAM alarms that have been triggered at Mount St. Helens between March 1, 1990, and September 20, 1991.

[RSAM, real-time seismic-amplitude monitoring system]

| Type of event | Number of alarms |
|---|---|
| Explosion-like seismic events[1] | 16 |
| Rockfalls (some with dust plumes) | 22 |
| Mount St. Helens earthquakes | 1 |
| Regional earthquakes | 12 |
| Telemetry problems | 6 |

[1] Four of these events had confirmed ash plumes.

With the RSAM system, a computer program compares the amplitude of a station's average seismic signal during a 1-minute interval with empirically determined threshold values. If thresholds are exceeded during the same 1-minute interval at several (usually three) of the stations in the crater and on the volcano flanks, an RSAM alert is generated. The computer is set to automatically dial the duty scientist's 24-hour beeper and transmit a number code indicating an RSAM alert. The computer redials the beeper every time a new 1-minute RSAM alert is generated.

Many types of events, including explosions, rockfalls, earthquakes, and telemetry problems, can generate alerts (table 4). Because an alert does not indicate the nature of the event, the duty scientist must examine the seismic signature of the event recorded on the seismographs at CVO to determine the basis for the alert. Explosion signals can usually be identified by careful evaluation of the signal character (Jonientz-Trisler and others, this volume). Once an alert is received, the speed with which notification is issued will depend on the time it takes for the duty scientist to reach CVO and the scientist's skill at recognizing explosion signals (table 5).

To date, all known ash-producing explosions since March 1, 1990, have generated alerts. However, failure of any component (key seismic stations, computer, computer programs, phone system, beeper, or beeper-pager system) would prevent an alert from getting through. As a precaution, a daily test alert is sent through the system to the beeper.

### BETTER TWO-WAY COMMUNICATION

When ash-producing explosions occur during nonworking hours, the FAA needs a means of quickly contacting CVO without the cumbersome and time-consuming process of first calling the USFS beeper. Pilots often are the first to observe volcanic plumes; however, sometimes slash-burns, storm clouds, or other atmospheric phenomena are mistaken for volcanic plumes. When a pilot's report of volcanic activity is received (Fox, this volume), the FAA must quickly verify the nature of the event and identify the area affected in order to evaluate the impact on air traffic and to

**Table 5.** Example of initial CVO response to a seismic event that occurred without precursors during nighttime, November 5, 1990.

[CVO, Cascades Volcano Observatory; PST, Pacific Standard Time; RSAM, real-time seismic-amplitude monitoring system; UW, University of Washington. Note: this was the first plume-producing event in 10 months]

| Time of event (PST) | Response |
|---|---|
| 0207 | •Seismic event began. |
| 0208 | •RSAM alert transmitted to beeper. |
| 0209–0217 | •Nine more RSAM alerts are transmitted to beeper. Scientist on duty awake, dressed, and en route to CVO by fourth alert. |
| 0220–0229 | •Duty scientist arrives at CVO.<br>•Seismic signal evaluated.<br>•Scientist-in-charge notified at home—assistance requested.<br>•UW seismic analyst notified at home.<br>•FAA area manager, Seattle Center, calls with two pilot reports of plume to 30,000 ft. He gives wind direction and speed at altitude and states that plume will drift SE. Note: CVO duty scientist was dialing the FAA on one phone line when she received the FAA's call on second phone line. |
| 0230–0239 | •Forest Service duty officer notified at home—assistance requested.<br>•UW updated on situation—assistance requested. |
| 0240 | •Continued evaluation and response. |

suggest alternate routes if necessary (Hamley and Parkinson, this volume). By dialing the CVO beeper number, the FAA can now make direct contact, day or night, with the CVO duty scientist. This change provides rapid verification of pilot reports and backup notification for CVO in case the RSAM alarm system fails.

Dissemination of information through normal USFS channels may also be delayed if CVO should need to contact the USFS by beeper. To assure that the FAA and NOAA are immediately notified of any ash-producing event, they are contacted directly by CVO as soon as the signal is identified. If the USFS is delayed in responding to their beeper, CVO will initiate further call-down by notifying the Washington Department of Emergency Management and others as needed.

## CONCLUSIONS

The development of notification and call-down procedures utilized by CVO and USFS at Mount St. Helens provides a means for rapid response to both predicted and non-predicted events. Although the procedures have worked in the past, they have been regularly reviewed and updated to reflect changes in the style and frequency of eruptions and to meet the changing needs and concerns of emergency-response agencies, businesses, and the public.

## REFERENCES CITED

Brantley, S.R., ed., 1990, The eruption of Redoubt Volcano, Alaska, December 14, 1989–August 31, 1990: U.S. Geological Survey Circular 1061, 33 p.

Endo, E.T., and Murray, T.L., 1991, Real-time seismic amplitude measurement (RSAM): A volcano monitoring and prediction tool: Bulletin of Volcanology, v. 53, p. 533–545.

Miller, C.D., Mullineaux, D.R., and Crandell, D.R., 1981, Hazards assessment at Mount St. Helens, *in* Lipman, P.W., and Mullineaux, D.R., eds., The 1980 Eruptions of Mount St. Helens, Washington: U.S. Geological Survey Professional Paper 1250, p. 789–802.

Swanson, D.A., Casadevall, T.J., Dzurisin, D., Holcomb, R.T., Newhall, C.G., Malone, S.D., and Weaver, C.S., 1985, Forecasts and predictions of eruptive activity at Mount St. Helens, U.S.A.: 1975–1984: Journal of Geodynamics, v. 3, p. 397–423.

VOLCANIC ASH AND AVIATION SAFETY:
Proceedings of the First International Symposium
on Volcanic Ash and Aviation Safety
U.S. GEOLOGICAL SURVEY BULLETIN 2047

# AVIATION SAFETY MEASURES FOR ASH CLOUDS IN JAPAN AND THE SYSTEM OF JAPAN AIR LINES FOR MONITORING ERUPTIONS AT SAKURAJIMA VOLCANO

*By* Saburo Onodera *and* Kosuke Kamo

## ABSTRACT

In Japan, 21 cases of volcanic ash encounters by aircraft were reported between 1973 and 1991. More than half of these encounters were with ash clouds produced by eruptions of Sakurajima Volcano, South Kyushu. Japan Air Lines (JAL) and Sakurajima Volcanological Observatory, Kyoto University (SVO) developed the volcano watching system (VWS) to mitigate the volcanic ash hazards to aircraft in the vicinity of Sakurajima Volcano. The system functions in all weather conditions and alerts flight dispatchers at Kagoshima International Airport without delay. It has been deployed at the JAL office at Kagoshima Airport since March 1991.

Between April 1 and May 31, 1991, 159 explosive eruptions took place at Sakurajima Volcano. The VWS system was operating at the time of eruption in 56 cases—it judged 49 cases as "explosive eruptions" and 7 cases as "eruptions." The agreement ratio of the system with the observations for this term is 88 percent.

## COUNTERMEASURES TO VOLCANIC ASH HAZARDS TO AVIATION IN JAPAN

There are 83 active volcanoes and approximately 80 airports for civil aviation in Japan (fig. 1). On an average, six volcanoes erupt each year. Twenty-one cases of volcanic ash encounters by aircraft were reported between 1973 and 1991 (table 1). The records show that most of the damage was to the exterior of aircraft, including windshields—to date, no damage to engines has been reported.

The Japan Meteorological Agency (JMA) constantly watches 19 volcanoes by monitoring volcanic smoke, seismic events and tilt changes, and by field observation. JMA issues significant meteorological advisory information

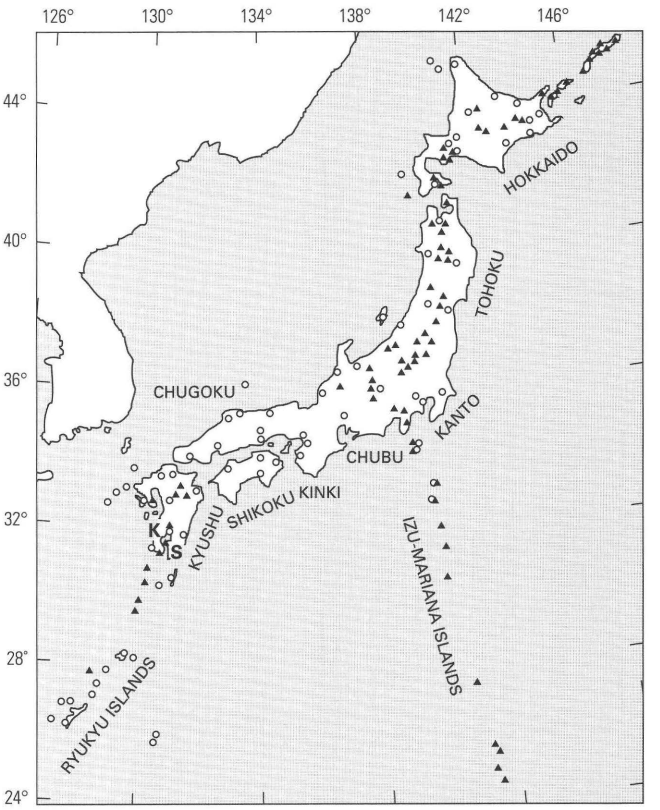


**Figure 1.** Locations of active volcanoes and airports for civil aviation in Japan. Solid triangles and open circles represent active volcanoes and civil airports, respectively. S, Sakurajima Volcano; K, Kagoshima International Airport.

(SIGMET's) concerning en-route weather phenomena that may affect the safety of aircraft operation. In the case of volcanic activity, when volcanic ash reaches an altitude of 25,000 ft above sea level, JMA issues a SIGMET and a "volcanic observation" report, which includes the name of the volcano and the time of eruption, as well as any additional information available about the activity. The eruption

**Table 1.** Effects on aircraft caused by volcanic eruptions in Japan.

| Date | Volcano | Airport | Aircraft | Effect on aircraft |
|---|---|---|---|---|
| 2/3/73 | Asama | Haneda | DC8 | Damage on windshield. |
| 4/8/75 | Sakurajima | Kagoshima | L1011 | Damage on windshield.[1] |
| 8/7/77 | Usu | Chitose | DC8 | Damage on windshield. |
| 8/7/77 | Usu | Chitose | DC8 | Damage on windshield. |
| 8/7/77 | Usu | Chitose | L1011 | Damage on windshield. |
| 8/7/77 | Sakurajima | Kagoshima | L1011 | Damage on windshield. |
| 11/19/77 | Sakurajima | Kagoshima | DC8 | Damage on windshield. |
| 12/25/77 | Sakurajima | Kagoshima | L1011 | Damage on windshield.[1] |
| 12/4/78 | Sakurajima | Kagoshima | L1011 | Damage on windshield.[1] |
| 11/18/79 | Sakurajima | Kagoshima | L1011 | Damage on windshield.[1] |
| 11/18/79 | Sakurajima | Kagoshima | L1011 | Damage on windshield.[1] |
| 12/24/79 | Sakurajima | Kagoshima | YS11 | Damage on windshield.[1] |
| 11/23/82 | Sakurajima | Kagoshima | B727 | Damage on windshield.[1] |
| 6/24/86 | Sakurajima | Kagoshima | DC9 | Damage on windshield. |
| 11/21/86 | Izu-Oshima | Narita | B747 | Spark was found on windshield. |
| 11/21/86 | Izu-Oshima | Narita | DC8 | Volcanic ash debris found on windshield. |
| 11/21/86 | Izu-Oshima | Narita | DC10 | Abrasion on leading edge flap and stabilizer. |
| 11/21/86 | Izu-Oshima | Narita | B747 | Damage on windshield. |
| 6/3/91 | Sakurajima | Miyazaki | MD80 | Some damage on fuselage.[2] |
| 6/3/91 | Unzen | Kumamoto | A300 | Encountered during climb, no damage.[2] |
| 8/5/91 | Sakurajima | Kagoshima | B737 | Damage on windshield. |

[1] Yoshitama (1984).
[2] T.J. Casadevall (written commun., 1991).

information is passed on immediately by JMA to the responsible air traffic control center (ATC) and to airline companies (fig. 2).

Airlines restrict their flights in ash-contaminated areas. Flight dispatchers prepare prediction charts of possible airspace contaminated by volcanic ash, and, on this chart, they plot the latest upper-level wind data over the volcano to predict beforehand the hazardous area for the day. The chart is referred to by pilots and dispatchers in pre-flight briefings and by dispatchers for flight advisories to pilots.

ATC provides every possible service to pilots when avoidance of ash is required. For example, ATC at Kagoshima approves any heading or altitude requests by pilots when circumstances permit and when they request them with the term "due to volcanic ash." Special contingency avoidance routes are established in the vicinity of active volcanoes (Yoshitama, 1984).

## SAKURAJIMA VOLCANO AND KAGOSHIMA AIRPORT

More than half of the incidents involving volcanic ash and aircraft in Japan were reported in the vicinity of Sakurajima Volcano, South Kyushu (table 1). The present eruptive activity at Sakurajima Volcano is from the summit crater and commenced in 1955. Explosive eruptions from the volcano are of the Vulcanian type (Self and Walker, this volume) and are accompanied by explosion earthquakes and remarkable eruptive phenomena, such as strong air-shocks, lightning, and the ejection of volcanic bombs and large amounts of ash (fig. 3). The number of the explosive eruptions between 1955 and 1991 was 6,360. On average, more than 100 explosions occurred each year, and volumes of ejected ash were estimated be 5–30 million metric tons annually (fig. 4).

Kagoshima International Airport is one of the eight busiest airports in Japan, with more than 130 takeoffs and landings per day. Operations are mostly during day time. The airport is located 25 km north of Sakurajima Volcano (fig. 5). The volcanic ash clouds ejected by the explosive eruptions have frequently reached 3,000 m above the summit crater (1,118 m). The normal operating altitude of arriving aircraft in this area is between approximately 500 m above and 800 m below the summit. Thus, around the airport, several avoidance routes have been established to prevent aircraft from encountering ash clouds (fig. 6). The route selection is mainly made by dispatchers.

The Kagoshima Local Meteorological Observatory (KLMO) of JMA, located in Kagoshima City approximately 10 km west of the crater (fig. 5), uses special procedures in reporting explosions at Sakurajima Volcano to ATC and airlines with a view to minimizing the delay in reporting. These include the use of a video camera at KLMO that produces a real-time image of the volcano that is transmitted to ATC at Kagoshima International Airport. However, because of the proximity of the airport to the volcano, even less delay in

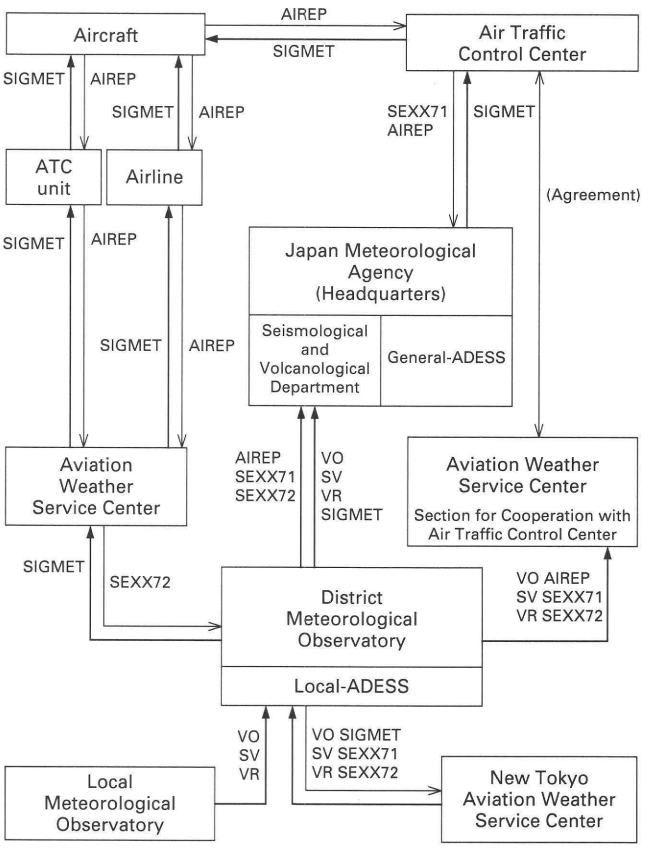


**Figure 2.** Flow of information concerning volcanic activity. ATC, air traffic control; VO, volcano observation; SV, seismic report; VR, volcano report, ADESS, automated data editing and switching system; SIGMET, information concerning en-route weather phenomena that may affect the safety of aircraft operation; AIREP, air report; SEXX71, header for message containing AIREP on volcanic activity; SEXX72, header for message containing volcanic ash information.

notification of explosions was required for promoting safe operations in darkness or under reduced visibility. This is the reason Japan Airlines and Sakurajima Volcanological Observatory have joined together to develop new countermeasures at Kagoshima International Airport for volcanic eruptions.

## VOLCANO WATCHING SYSTEM

The volcano watching system (VWS) developed jointly by JAL and SVO was designed to achieve the following objectives:

1. To detect the explosive eruptions at Sakurajima Volcano without fail in all weather conditions during both day and night, and
2. To immediately notify dispatchers at the airport when an explosive event is detected.

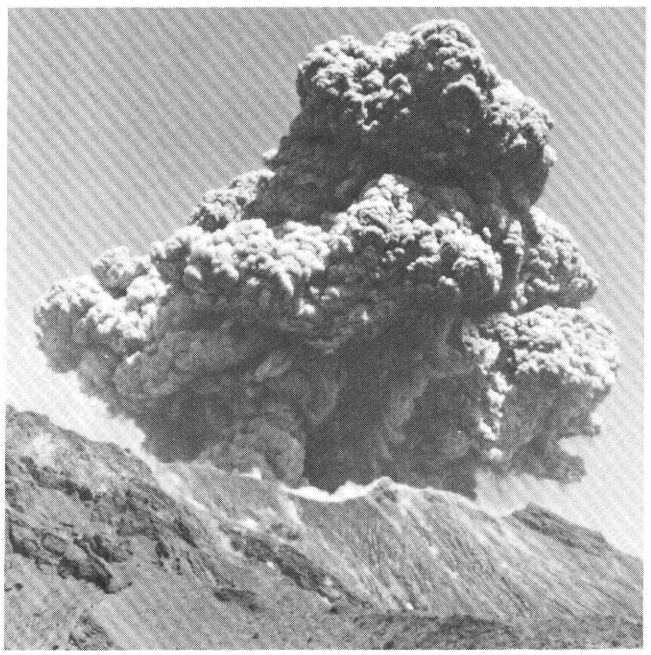

**Figure 3.** Photograph of a typical explosive eruption at Sakurajima Volcano (13:42, May 17, 1976).

Both of these objectives are essential to keep flight operations safe in the vicinity of active volcanoes.

The fundamental function of the system is to distinguish those events that are related to explosive, ash-producing eruptions from several types of volcanic earthquakes, which are not necessarily related to ash-producing eruptions. Volcanic earthquakes and tremors originated at Sakurajima Volcano are classified into five categories (Ishihara, 1988). These are A-type earthquakes, B-type earthquakes (Minakami, 1974), explosion earthquakes, C-type tremors, and D′-type tremors. An A-type earthquake is similar to a tectonic earthquake and consists predominantly of high-frequency seismic waves (> 8 Hz). B-type earthquakes are dominated by lower frequency signals, generally less than 5 Hz (McNutt, 1986). B-type earthquakes at Sakurajima Volcano are classified into BL and BH types, whose dominant frequencies are 1–3 Hz and 5–8 Hz, respectively (Iguchi, 1989). Explosion earthquakes are accompanied by remarkable eruptive phenomena, such as strong air-shocks, ejection of volcanic bombs and large amounts of ash. C-type seismic activity is a kind of volcanic tremor composed of harmonic wave trains, and D′-type seismic activity is a non-harmonic tremor.

Explosion earthquakes are accompanied by explosive eruptions, and the amplitudes of explosion earthquakes and their associated infrasonic waves are greater than those of other types of volcanic earthquakes. The maximum amplitudes of explosion earthquakes and air-shocks range from $3\times10^{-3}$ to $3\times10^{-2}$ cm/s and from 0.1 to 5 mb, respectively (Iguchi and Ishihara, 1990). The reduced displacements

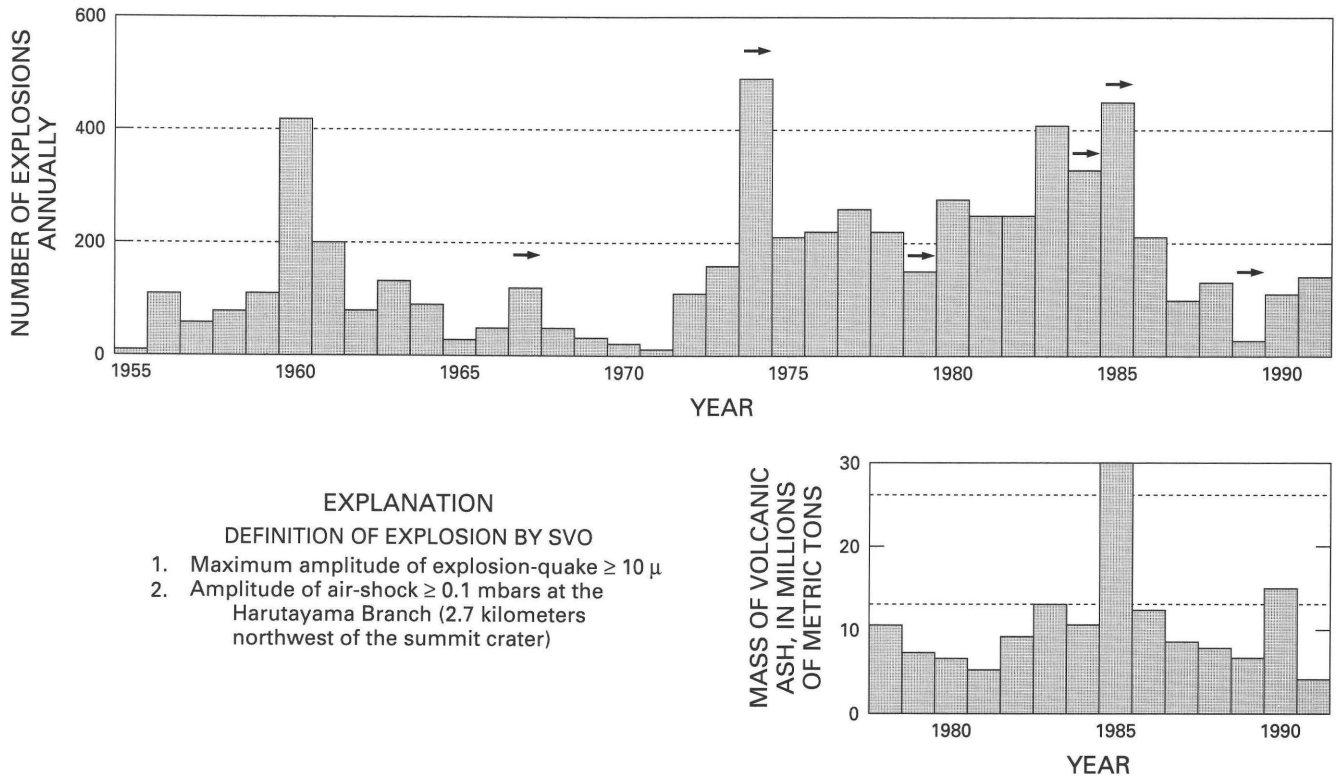


**Figure 4.** *A*, Annual numbers of explosive eruptions at Sakurajima Volcano between 1955 and 1991 (1991 represents data current as of June 1, 1991). *B*, The estimated amount of volcanic ash emitted from the summit crater of Sakurajima between 1978 and 1991 (1991 represents data current as of May 1, 1991). Arrows indicate explosions accompanied by pyroclastic flows. SVO, Sakurajima Volcanological Observatory.

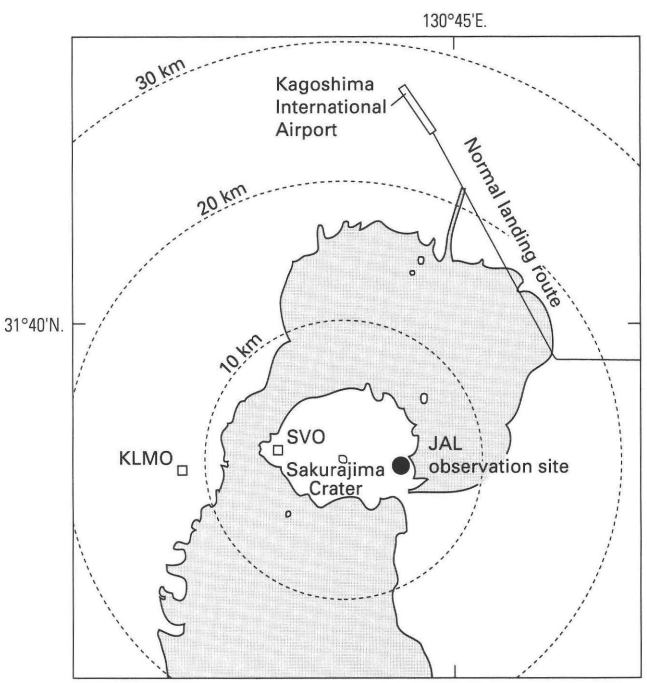


**Figure 5.** Location map of Sakurajima Volcano and Kagoshima International Airport. SVO, Sakurajima Volcanological Observatory of Kyoto University; KLMO, Kagoshima Local Meteorological Observatory of Japan Meteorological Agency; JAL observation site, Japan Air Lines observatory.

(McNutt, 1992) of explosion earthquakes are estimated to be 50–500 $cm^2$. BL-type and D′-type tremors are also associated with eruptive phenomena at the crater, and continuous emission of volcanic ash and intermittent ejection of volcanic bombs are frequently observed to accompany these earthquake types (Ishihara and Iguchi, 1990). The maximum amplitudes of earthquakes and air-shocks associated with BL-type and D′-type events are $< 7\times10^{-3}$ cm/s (reduced displacement < 60 $cm^2$) and < 0.1 mb, respectively, and are smaller than those of explosive eruptions (Iguchi and Ishihara, 1990). On the other hand, A-type and BH-type earthquakes are not accompanied by eruptive activity, and no air-shocks associated with them have been detected.

The visual observation of eruptive phenomena at the summit is strongly affected by weather conditions. However, earthquakes and air-shocks are continuously monitored by instruments. SVO defines explosive eruptions by the maximum amplitudes of explosion earthquakes and air-shocks. It is possible to distinguish an explosive eruption from the other types of volcanic events by the absolute amplitudes of earthquakes and air-shocks and by the spectra of the earthquakes. The system proposed in this paper monitors both earthquakes and air-shocks and judges whether or not explosive eruptions have occurred.

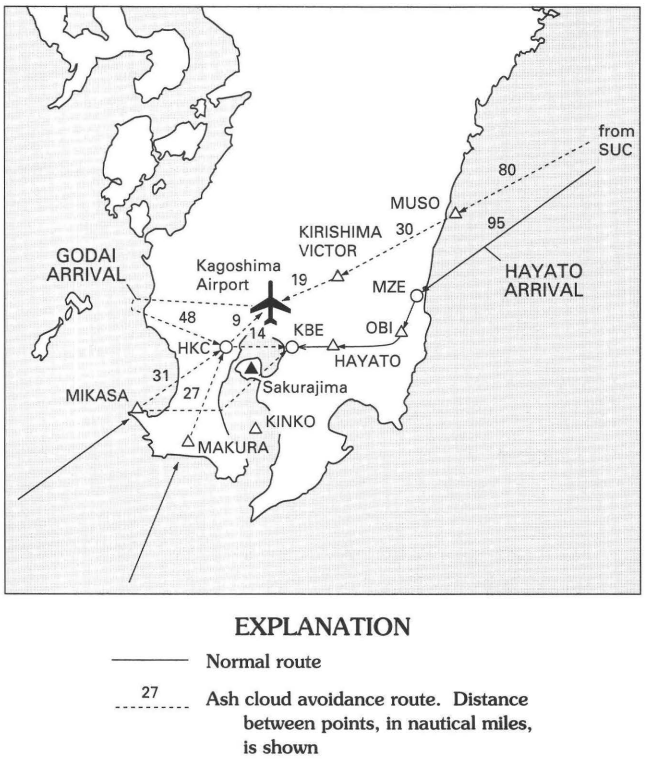


**Figure 6.** Normal and avoidance routes around Kagoshima Airport. Avoidance routes have been established to prevent aircraft from encountering ash clouds. Open triangles, waypoints; open circles, towns; solid triangle, Sakurajima Volcano.

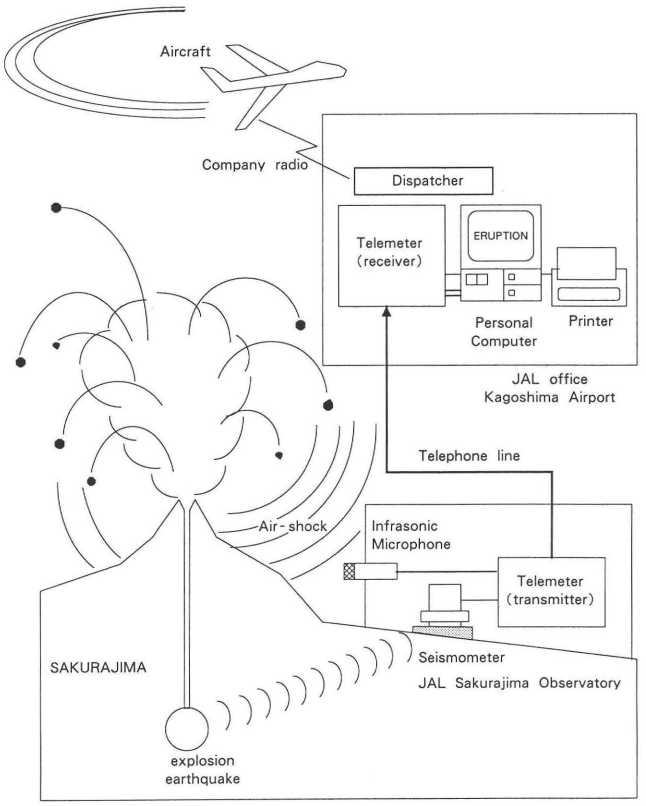


**Figure 7.** Block diagram of the overall observation system developed by JAL (Japan Air Lines) and SVO (Sakurajima Volcanological Observatory).

## HARDWARE

The overall monitoring system is shown in figure 7 and comprises an observation site at Sakurajima, 4 km east of the summit crater (figs. 5 and 8), with data processing at the JAL office at Kagoshima International Airport. At the observation site, a three-component seismometer and an infrasonic microphone are installed. The seismometer comprises up-down, north-south and east-west components and has a frequency range of 1–30 Hz and a sensitivity of 2 V/cm/s. The microphone detects infrasonic waves in the range from 0.02 to 100 Hz. Volcanic earthquakes and air-shocks generated by volcanic eruptions are observed by the seismometer and the infrasonic microphone, respectively. These signals are constantly transmitted to the airport by commercial telephone line. At the airport, these signals are transferred from the receiver of the telemetering system to a personal computer. The computer process the signals and issues alarms according to the seismic and eruptive activity. The total cost to install this system was approximately $400,000. Annual operating costs are $20,000.

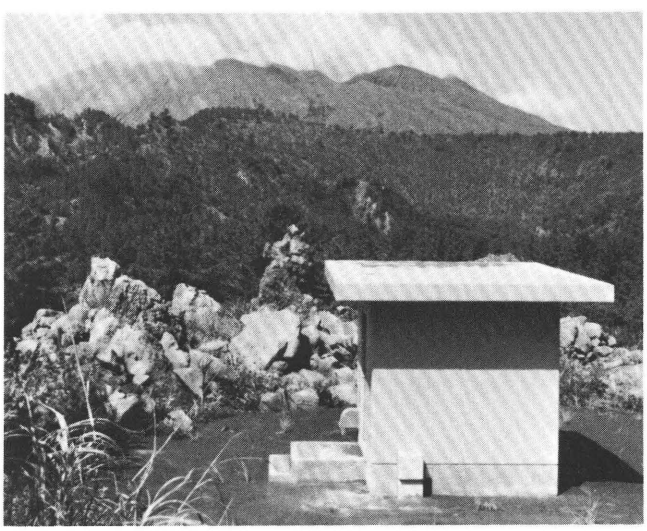

**Figure 8.** Photograph of Japan Air Lines observation site at Sakurajima Volcano.

## DATA PROCESSING

The data processing flow chart is shown in figure 9. The computer monitors amplitudes of seismic and infrasonic waves by digitizing 40 samples per second. When the

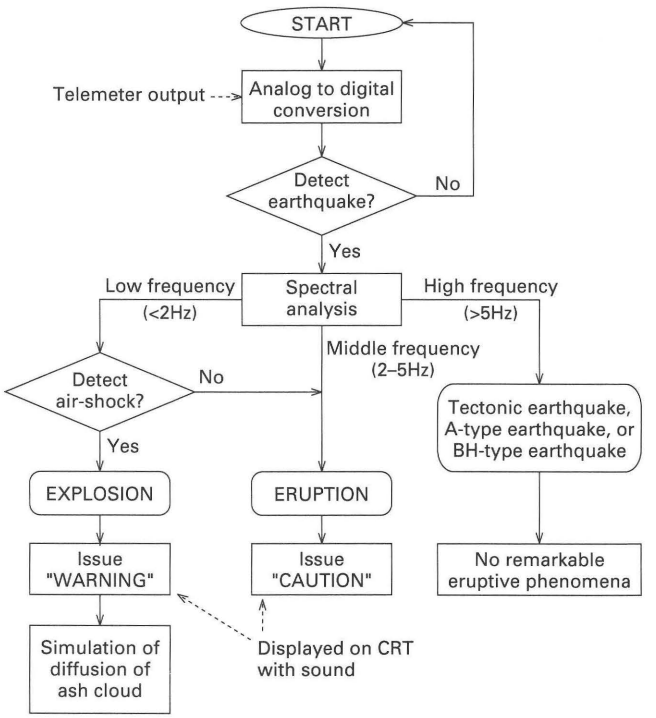


**Figure 9.** Data processing flow chart to detect volcanic explosions at Sakurajima Volcano. CRT, cathode ray tube.

amplitude of the seismic wave exceeds the preestablished threshold level ($0.1\times10^{-3}$ cm/s ), the computer judges that a seismic event has occurred. According to the levels of the infrasonic waves associated with the event and the spectra of the seismic wave, the computer categorizes the events into "explosive eruptions," "eruptions," and "non-eruptions."

"Eruptions" correspond to the generation of BL-type earthquakes or D′-type tremors and are accompanied with weak infrasonic waves and slow, sometimes continuous, low-level ejection of volcanic ash. "Non-eruptions" mean no remarkable change of eruptive activity above the crater, and they correspond to generation of A-type or BH-type earthquakes at the volcano or to tectonic earthquakes outside the area of Sakurajima Volcano.

After detection of events, the computer analyzes the spectra of the waveforms. When the dominant frequency is lower than 2 Hz and the level of infrasonic wave is beyond the level (0.13 mb), the computer judges that the seismic event was associated with an "explosive eruption" and issues a "warning", which appears on the computer monitor with blinking red color and alarm sounds. If the dominant frequency is between 2 Hz and 5 Hz, the computer judges that an "eruption" has occurred and issues an alarm "caution" with blinking yellow color. When the dominant frequency exceeds 5 Hz, the computer interprets that A-type or BH-type earthquakes or tectonic earthquakes have occurred—these are accompanied by no remarkable eruptive phenomena.

## DISPATCHER'S ACTION

The dispatcher at the JAL office at Kagoshima Airport passes the eruption information to pilots as soon as the system issues a "warning" or a "caution." Based on both the upper-level wind and visibility, which have a critical affect on the dispatcher's recommendations, the dispatcher recommends one of the following advisories to aircraft in bound to Kagoshima Airport:

1. Divert to alternate airport,
2. Hold over suitable holding position and wait for further information,
3. Select contingency or alternate arrival route and continue approach, or
4. Select normal arrival route and continue approach.

# RESULTS OF OPERATION

The system has been deployed at the JAL office at Kagoshima Airport since March 1991. A set of records of an explosion earthquake and an air-shock observed by the system is shown in figure 10. Note that the explosion earthquake has an emergent onset. The record of the infrasonic microphone shows that the air-shock arrived 10.4 s after the onset of the explosion earthquake. Ground motions excited by the air-shock were recorded in the seismograms, especially in the east-west component.

Here, we evaluate the correspondence of the judgment by the VWS system to actual explosive eruptions using the classification criteria by KLMO. As mentioned earlier, the Sakurajima Volcanological Observatory has different criteria from JMA–KLMO for recognizing explosive eruptions. SVO criteria are based on the volcanic earthquakes and infrasonic waves that can be continuously measured and does not include visual observation. The criteria of JMA–KLMO includes visual observation, as well as use of seismic recordings to distinguish explosive eruptions. For

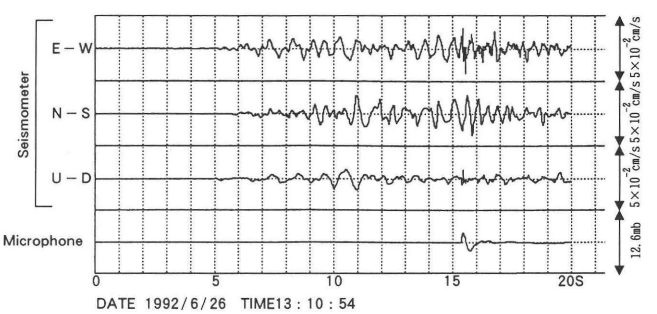


**Figure 10.** Recording of an explosion earthquake and an air-shock obtained by the system. Upper three traces represent east-west, north-south, and up-down components of seismograms, respectively. The bottom trace shows the air-shock obtained by the infrasonic microphone.

the purpose of detecting an ash-producing explosive eruption, the JMA–KLMO criteria are used here. There is generally excellent correspondence (± 10 percent) in the numbers of explosion earthquakes determined by SVO and KLMO criteria.

From April 1 to May 31, 1991, 59 explosive eruptions occurred. The system was operating at the time of the eruptions in 56 cases but not for the other 3, due to unscheduled outage of the system for maintenance. Of the 56 cases, the JAL system judged 49 cases as "explosive eruptions" and 7 as "eruptions." The agreement ratio of the system with observations by JMA for this period is 88 percent.

The seven cases, which were categorized as different types of activity by the respective definitions of the JMA and JAL systems, were recorded with a small air-shock, at or less than 0.13 mb, on both JMA and JAL equipment. On the other hand, the JAL system recorded 15 more cases of "explosive eruptions" than JMA. This is again due to the rather small explosive eruptions that are just above the threshold level that is considered to be acceptable for these types of warning systems.

The small problems we are aware of on this system are as follows:

1. During scheduled maintenance (twice a year) of this system, we do not obtain data for a couple of hours,
2. Gusty winds associated with typhoons cause nuisance warnings or false alarms, and
3. Non-explosive eruptions with small magnitudes are not always detected.

## CONCLUSIONS

The results of field testing of this system in 1991 demonstrate that this system has the capability of (1) detecting explosive eruptions of Sakurajima Volcano in all weather conditions 24 hours a day, and (2) alerting the airline dispatcher, without time delay.

The operation of the volcano watching system suggests that this is an effective countermeasure to help to reduce risks from volcanic ash in areas near airports close to active volcanoes. In the future, JAL hopes to include a program to calculate diffusion of volcanic ash based on meteorological data. The program for the simulation will be designed to automatically start when explosive eruptions are detected and followed by "caution" or "warning" signals.

## ACKNOWLEDGMENTS

The authors would like to thank Masato Iguchi and the other staff of Sakurajima Volcanological Observatory, Kyoto University, who contributed a great deal in developing the system and in preparing this paper. Thomas Casadevall and Stephen McNutt provided helpful reviews. Edward Nojiri helped us to prepare the manuscript.

## REFERENCES CITED

Iguchi, M., 1989, Distribution of the initial motions of volcanic microearthquakes (B-type) at Sakurajima Volcano [in Japanese]: Kyoto University, Annual Report, Disaster Prevention Research Institute, v. 32, p. 13–22.

Iguchi, M., and Ishihara, K., 1990, Comparison of earthquakes and air-shocks accompanied with explosive eruptions at Sakurajima and Suwanosejima Volcano [in Japanese]: Kyoto University, Annual Report, Disaster Prevention Research Institute, v. 33B-1, p. 1–12.

Ishihara, K., 1988, Geophysics, *in* A Guide Book for Sakurajima Volcano: Kagoshima International Conference on Volcanoes, p. 29–42.

Ishihara, K., and Iguchi, M., 1990, The relationship between microearthquake swarms and volcanic activity at Sakurajima [in Japanese]: Kyoto University, Annuals, Disaster Prevention Research Institute, v. 32B-1, p. 1–11.

McNutt, S.R., 1986, Observations and analysis of B-type earthquakes, explosions, and volcanic tremor at Pavlof Volcano, Alaska: Bulletin of the Seismological Society of America, v. 76, p. 153–175.

———1992, Volcanic tremor, *in* Nierenberg, W.A., ed., Encyclopedia of Earth System Science, Academic Press, v. 4, p. 417–425.

Minakami, T., 1974, Seismology and volcanoes in Japan, *in* Civetta, L., Gasparini, P., Luongo, G., and Rapolla, A., eds., Developments in Solid Earth Geophysics, Physical Volcanology: New York, Elsevier, p. 1–27.

Yoshitama, T., 1984, Improvement of the ash avoidance procedures at Sakurajima Volcano [in Japanese]: Japan Meteorological Agency, Aviation Weather Note, v. 29, p. 46–53.

VOLCANIC ASH AND AVIATION SAFETY:
Proceedings of the First International Symposium
on Volcanic Ash and Aviation Safety
U.S. GEOLOGICAL SURVEY BULLETIN 2047

# VOLCANIC ASH WARNINGS IN THE AUSTRALIAN REGION

*By* Rodney J. Potts *and* Frank Whitby

## ABSTRACT

As part of its routine operations, the Australian Bureau of Meteorology provides warnings to the aviation industry for volcanic ash clouds over the Australian region and the region to the near north. This service is provided in accordance with international procedures that have been established in recent years. The warnings define the area of the ash cloud, the cloud top, and the forecast movement of the cloud—these warnings are based on notification of a volcanic eruption, satellite imagery, and upper-level wind analyses. The high frequency of thunderstorms in the equatorial regions north of Australia often makes identification of volcanic ash clouds difficult. Multispectral infrared data in the atmospheric window region, available from National Oceanic and Atmospheric Administration polar-orbiting satellites, have been beneficial for discriminating ash clouds from water/ice clouds. The Bureau of Meteorology is currently installing an advanced very high resolution radiometer antenna in Darwin, which will give coverage over the volcanically active Indonesian region; the operational utility of AVHRR data for volcanic ash detection will be evaluated.

## INTRODUCTION

As part of its routine operations, the Australian Bureau of Meteorology (BOM) provides warnings to the aviation industry for volcanic ash clouds over the Australian region and the region to the near north. This service has been an important component of Bureau operations since its introduction in 1982 when two Boeing 747 aircraft encountered volcanic ash from Galunggung Volcano in Indonesia (Hanstrum and Watson, 1983). Both aircraft suffered engine failure and severe damage to wings and fuselage and were forced to make emergency landings at Jakarta.

Although there are no active volcanoes within Australia, there are many throughout the surrounding islands to the north (fig. 1). Most aircraft flights into and out of Australia overfly these areas, often at nighttime, and the likelihood of an encounter with a volcanic ash cloud presents a serious, albeit relatively infrequent, hazard for aircraft operations (Johnson and Casadevall, this volume). The greatest threat to aircraft arises from Plinian eruptions, which eject large amounts of finely divided rock particles (known as volcanic ash) and gases high into the atmosphere (Heiken, this volume; Self and Walker, this volume). The evolution of the ash cloud following a Plinian eruption can be divided into two stages: the eruption or nascent cloud stage immediately following the eruption and the dispersed cloud stage (Prata, 1989a; Sparks and others, this volume). During the latter stage, the ash cloud will be dispersed by prevailing winds and rock particles will settle gradually to the ground. If the ash cloud extends over a significant depth, the cloud at different levels may be spread in different directions. Although the ash may disperse and settle, a hazard for aircraft may exist for some time from sulfurous clouds, which can be carried great distances by the prevailing wind. Eventually, the ash and gases will be dispersed and diluted until there is no longer a significant hazard to aircraft.

Plinian eruptions can be observed on visible and infrared satellite imagery, and it is possible to define the horizontal and vertical extent of the resultant ash cloud (Sawada, this volume; Schneider and Rose, this volume). With consideration of the upper winds, it is further possible to determine the direction in which the cloud will be dispersed. Hanstrum and Watson (1983), Matson (1984), Prata and others (1985), and Malingreau and Kaswanda (1986) all describe cases where satellite imagery and upper-level wind data have been used for estimating the location and movement of volcanic ash clouds. The techniques described in these reports are used in the operational warning service currently provided by BOM. This paper describes this warning service and discusses the operational problems associated with the service, together with proposals for the future.

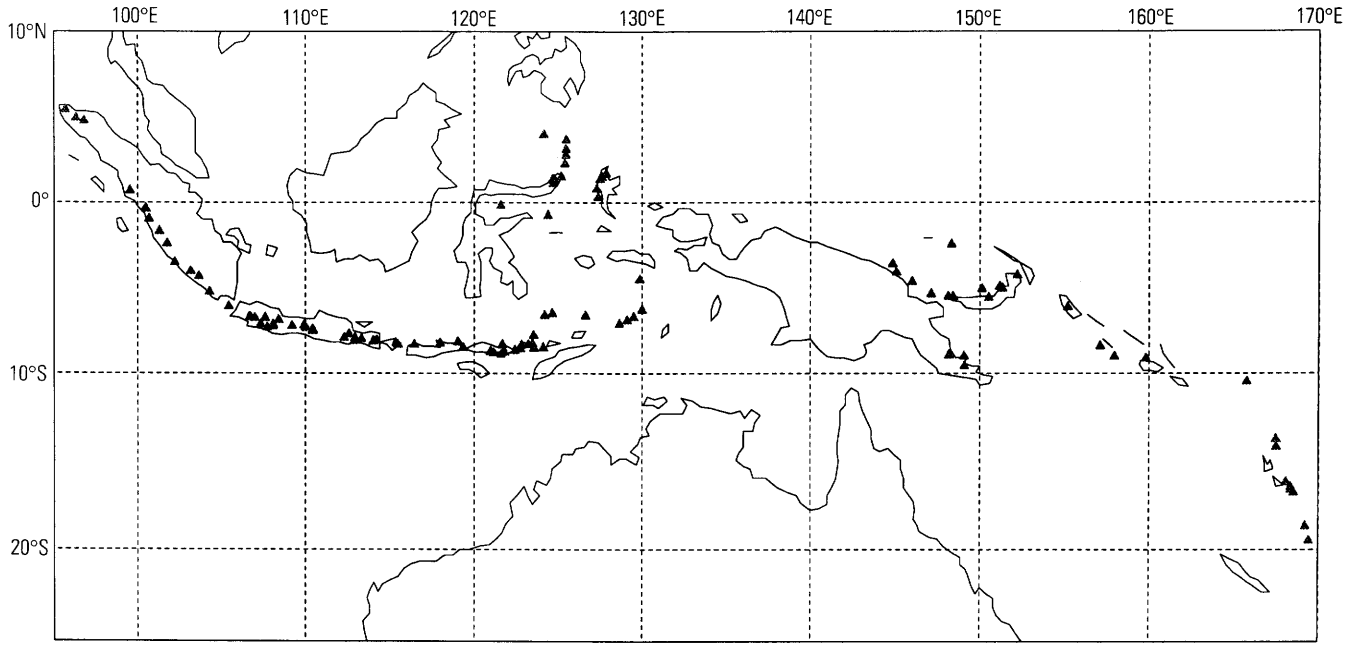


**Figure 1.** Active volcanoes in the Indonesia–Papua New Guinea region to the north of Australia. Solid triangles represent volcanoes with historical eruptive activity.

## THE VOLCANIC ASH CLOUD WARNING SYSTEM

Meteorological services for aviation are provided under guidelines established in joint consultations between the World Meteorological Organization (WMO) and the International Civil Aviation Organization (ICAO) (Fox, this volume). In accordance with international agreement, meteorological forecast and warning services are provided by the meteorological authority within the sovereign state responsible for the flight-information region (FIR). From time to time, standards and recommended practices for the provision of meteorological services for aviation are reviewed both at regional and international levels.

Warnings for hazardous weather or significant meteorological phenomena are generally provided in the form of a significant meteorological advisory (SIGMET) issued by the meteorological authority responsible for the FIR. The SIGMET is valid for a period of 4 or 6 hours and includes information on the nature of the hazardous weather, the location or area affected, and the forecast trend. Such warnings are passed rapidly to air traffic control authorities, aircraft, and meteorological offices in adjacent areas. Weather phenomena for which a SIGMET will be issued include active thunderstorms, tropical cyclones, severe turbulence, severe icing, severe mountain waves, and volcanic ash clouds. Following the aircraft incidents over Indonesia in 1982, volcanic ash clouds were included as a phenomena for which a SIGMET is to be issued.

Within the Australian, region the responsible Bureau of Meteorology (BOM) Regional Forecasting Center (RFC) will issue a SIGMET if a volcanic ash cloud enters Australian airspace. In addition to the SIGMET warning service, the Bureau of Meteorology provides a volcanic ash cloud advisory service for the Australian region and areas to the near north. This service was introduced in 1982 in cooperation with Australia's Civil Aviation Authority and representatives from the aviation industry (Johnson and Casadevall, this volume). Because the Bureau has no capability to forecast and identify volcanic eruptions, the objective of the advisory service is to confirm the presence of an ash cloud and to monitor its movement after a report of an eruption. Such reports of an eruption or the presence of an ash cloud come from nearby ground-based observers, aircraft reports, and local aviation authorities. Satellite imagery and upper-level wind analyses and forecasts are examined, and the advisory message is issued by the National Meteorological Centre (NMC).

In an effort to improve the volcanic ash cloud warning service in the Australian-Indonesian region, the Volcanological/Airspace Liaison Committee–Australia/Indonesia Australian working group (VULCAN-AUS) was established in 1985 (Johnson and Casadevall, this volume). On the Australian side, the committee comprises representatives from the Bureau of Meteorology, Civil Aviation Authority, Commonwealth Scientific and Industrial Research Organization (CSIRO), Australian Geological Survey Organization (AGSO) (formerly the Bureau of Mineral Resources), and the airlines. The objectives of this group are to develop and

improve procedures for the avoidance of volcanic ash clouds, to liaise with scientific groups, to promote research on relevant issues, and to liaise with local and international organizations and with regional governments in order to increase awareness of the dangers to aircraft from volcanic eruptions. The group has been instrumental in the development of better techniques for identifying volcanic ash clouds, improved warning procedures, and improved intragovernmental relations between Australia and Indonesia on the problem.

## OPERATIONAL PROCEDURES

A SIGMET for volcanic ash, or a volcanic ash cloud advisory that is issued by the Bureau will describe, if possible, the location, height, and forecast movement of the ash cloud and will be based on the eruption notification, hourly Japanese geostationary meteorological satellite (GMS) images and upper-wind analyses. In the Bureau of Meteorology, the amount of data and the speed with which these data can be analyzed and warnings subsequently issued have been greatly enhanced with the introduction of the Australian region man-computer interactive data access system (McIDAS) in forecast offices (LeMarshall and others, 1987). This system enables the rapid display and analysis of satellite imagery, numerical-model products, and observational data.

The potential for providing an efficient and effective service for the aviation industry can be illustrated by briefly examining events following the recent eruption of Mt. Pinatubo, Philippines, which occurred at 00:51 UTC (Coordinated Universal Time), 12 June 1991 (Potts, 1993). On subsequent days, there were further eruptions leading up to the climactic events of 15 June; however, these are not discussed here. The Bureau of Meteorology received notification of the 00:51 UTC eruption from an airline company, and immediately began issuing volcanic ash cloud advisory messages at regular intervals for the ash cloud. In the ensuing days, notification of further eruptions were received promptly from aviation authorities in the Philippines, and ash cloud advisory messages were issued that defined, where possible, the area of the ash cloud and its movement. The advisories were well received by the aviation industry.

The sky was clear over Luzon on 12 June 1991, and the 00:51 UTC eruption plume was clearly evident on GMS satellite images. Figure 2 shows a series of GMS images of the eruption from 01:30 UTC to 07:30 UTC. There were no further major ash emissions immediately following the 00:51 UTC eruption, and the ash cloud drifted to the southwest and

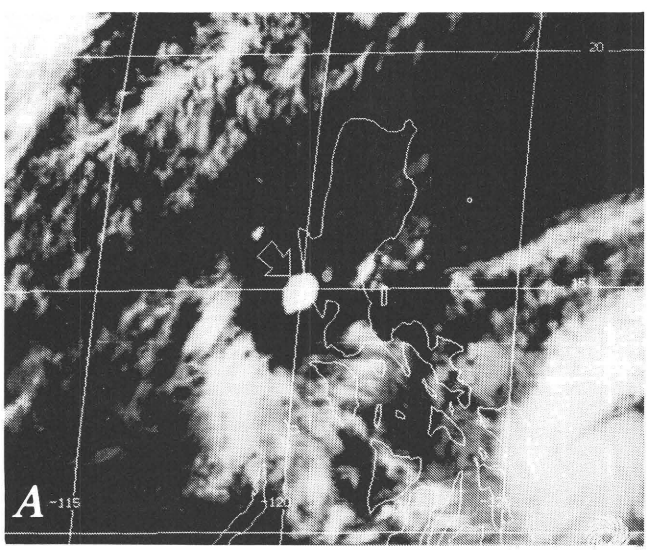


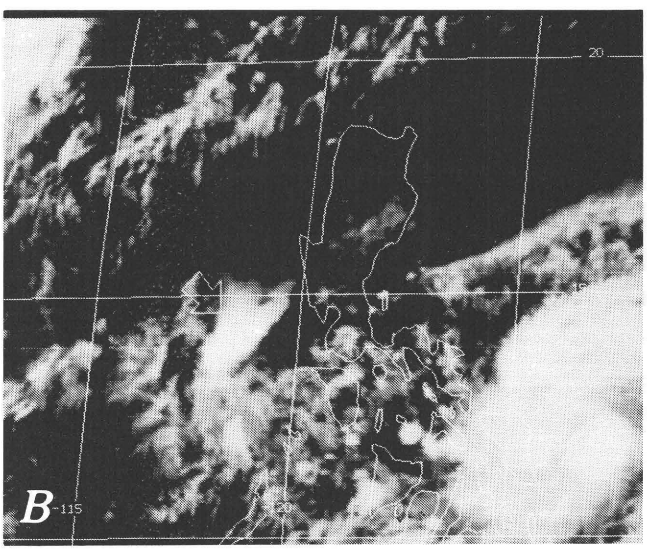


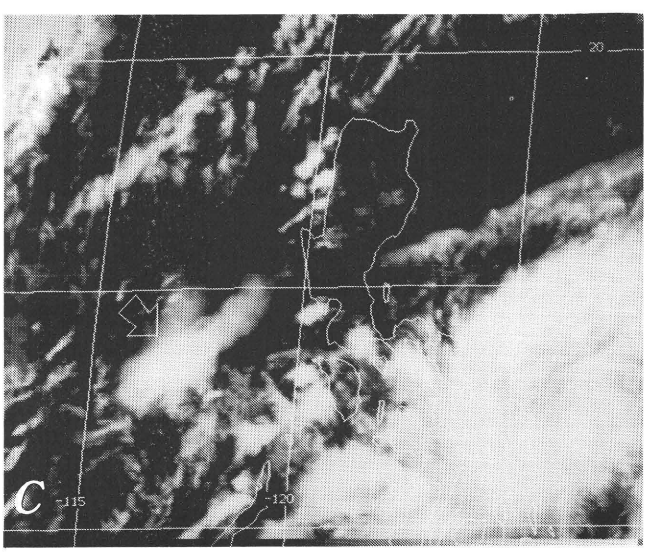


**Figure 2.** Geostationary meteorological satellite images for 12 June 1991 showing Mt. Pinatubo eruption cloud. Latitude and longitude grid at 5° intervals. Location of the ash cloud indicated by arrows. *A*, 01:30 UTC; *B*, 04:30 UTC; *C*, 07:30 UTC.

gradually dispersed, becoming elongated in a northeast-southwest direction as it moved. After 07:30 UTC, the ash cloud continued to move to the southwest, over the South China Sea and Indochina, and was visible on imagery until early the following day.

The brightness temperature of the cloud tops can be determined from infrared satellite images. Assuming the ash cloud radiates as a black body and that the temperature of the cloud quickly reaches equilibrium with the environment, the cloud height can be estimated. From the satellite-derived brightness temperature and the 00:01 UTC vertical-temperature sounding from Clark Air Base, 20 km to the east, the cloud top in figure 2 is between 130–100 hPa (15–16 km). Upper-wind analysis enable the likely trajectory of the cloud to be determined. For the period shown, the highest levels of the ash cloud moved to the southwest at approximately 15 m/s, consistent with the 00:01 UTC upper-wind analysis for 100 hPa (16 km) (fig. 3*A*). Figure 2*C* shows that the ash cloud has become elongated in a northeast-southwest direction. The ash cloud in the northeast has a top around 500 hPa (approximately 5.6 km) and moved west at approximately 6 m/s, consistent with the 00:01 UTC upper-wind analysis for 500 hPa (fig. 3*B*).

Although this example demonstrates that an effective warning service can be provided for volcanic ash clouds, there are significant technical difficulties that must be addressed if the service is to become more effective. The BOM cannot provide warnings on the likelihood of a volcano erupting. It can only detect and monitor ash clouds after emission. It is therefore essential that there is early notification of any initial or subsequent volcanic eruption by responsible authorities within the country where the eruption has occurred; it is also essential that reports from aircraft concerning the presence of volcanic ash clouds be passed to aviation authorities. Such warnings or reports must be distributed quickly on the international aviation and meteorological communications system.

Over the tropical regions north of Australia, there is a high frequency of thunderstorms, which can develop very rapidly to great heights and produce extensive areas of cloud. On present GMS satellite imagery, it is often not possible to discriminate volcanic ash clouds from water/ice clouds (Sawada, this volume). In the 6-year period, 1985–90, a total of 81 volcanic ash cloud advisories were issued by the NMC, and for 80 percent of these, it was not possible to identify a volcanic ash cloud with any confidence due to the presence of water/ice clouds. Finally, the duration for which an ash cloud remains a hazard to aircraft is not known, and further research is required on this subject.

# THE UTILIZATION OF NOAA AVHRR SATELLITE DATA

National Oceanic and Atmospheric Administration (NOAA) advanced very high resolution radiometer (AVHRR) satellite data offer some promise for the discrimination of volcanic ash clouds from water/ice clouds based on differences in the brightness temperature for a cloud measured at 10.8 μm (channel 4) and at 11.9 μm (channel 5). The difference results from variations in the wavelength dependence of emissivity for water/ice and the pyroclastic material found in volcanic ash clouds (Prata, 1989a, 1989b; Barton and Prata, this volume; Honey, this volume; Prata and Barton, this volume).

From Prata (1989b), the infrared radiance, $R_i$, measured in a narrow band centered on wavelength $\lambda_i$, for a uniform cloud layer overlying a non-reflecting surface, assuming no scattering and no angular dependence, is approximated by:

$$R_i(\lambda_i) \cong (1-\varepsilon_i)B(T_s)+\varepsilon_i B(T_c) \qquad (1)$$

where

$1-\varepsilon_i$ and $\varepsilon_i$ are the transmissivity and emissivity for the cloud at wavelength $\lambda_i$,

$B_i(T)$ is the Planck function,

$T_c$ is the cloud-top temperature, and

$T_s$ is the temperature of the surface.

The brightness temperature of the cloud is then calculated from the radiance assuming black body radiation, (i.e., $\varepsilon_i$ = 1.0). The emissivity, $\varepsilon_i$, of a cloud is dependent on the microphysical and chemical properties of the cloud, its optical depth, and the wavelength at which $\varepsilon_i$ is measured. If the cloud is optically thick ($\varepsilon_i \cong 1.0$), the brightness temperature provides a good estimate of the cloud-top temperature, whereas, for an optically thin cloud ($\varepsilon_i < 1$) overlying a relatively warm surface, the brightness temperature will be warmer than the true cloud-top temperature. Also, for a cloud of given optical depth, if $\varepsilon$ (10.8 μm) < $\varepsilon$ (11.9 μm), it follows from equation 1 that brightness temperature $T$(10.8 μm) > $T$(11.9 μm). Conversely, if $\varepsilon$ (10.8 μm) > $\varepsilon$ (11.9 μm), then $T$(10.8 μm) < $T$(11.9 μm).

In the atmospheric window region, the emissivity for water/ice clouds increases with wavelength, and, consequently, the difference, $\Delta T$, in the brightness temperature between channel 4 (10.8 μm) and channel 5 (11.9 μm), where $\Delta T = T4-T5$, is almost always positive. The temperature difference, $\Delta T$, for ash clouds is dependent on the cloud constituents, the particle-size distribution of those constituents, and the cloud temperature. Silicates and sulfur dioxide are significant constituents of an ash cloud, and, for these, emissivity decreases with wavelength. Hence, in many

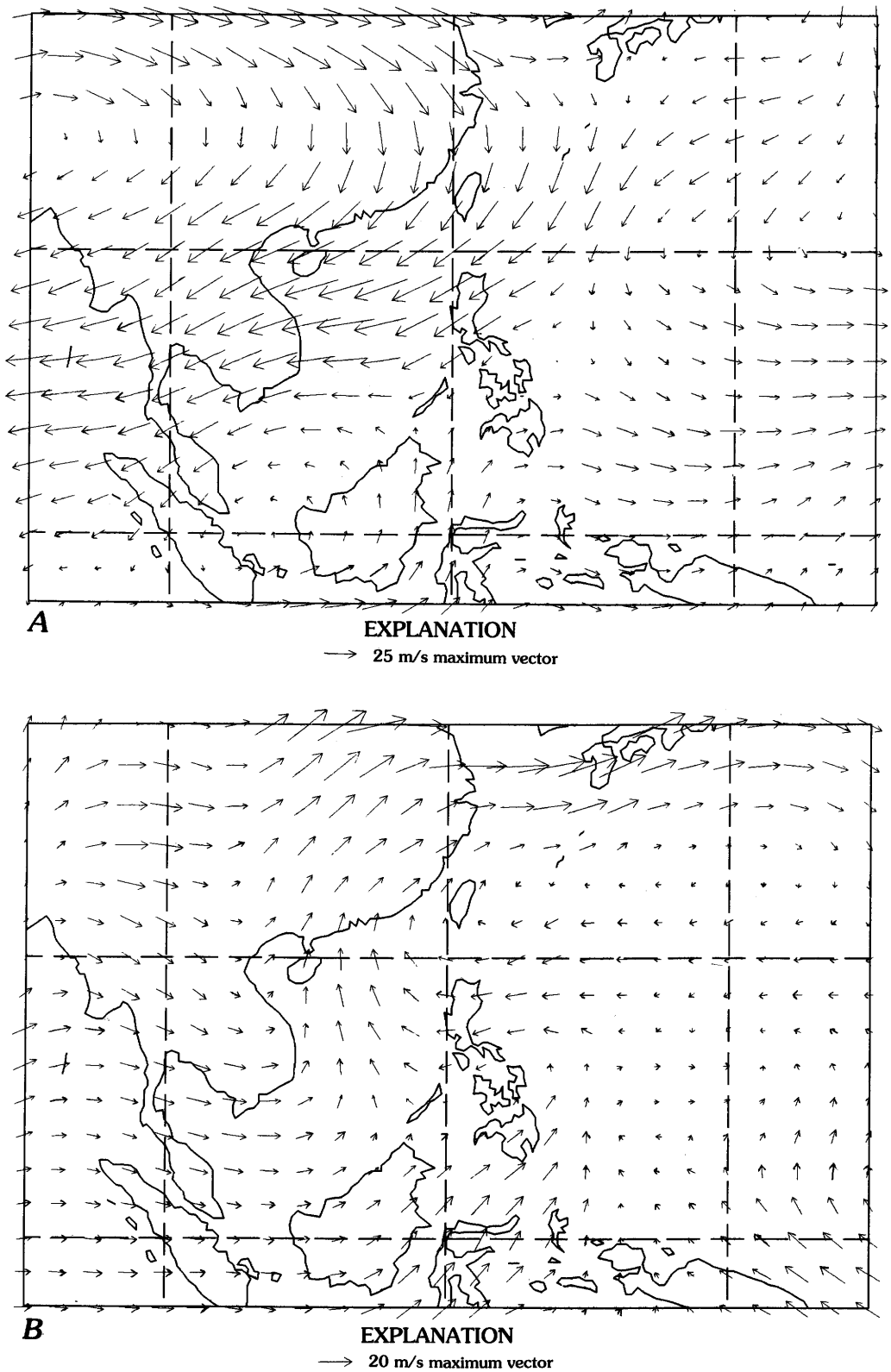


**Figure 3.** Upper-level wind analysis for 00:01 UTC, 12 June1991. *A*, 100 hPa; *B*, 500 hPa.

circumstances relevant to the volcanic ash cloud detection problem, the difference *T4–T5* will be negative, enabling the discrimination of ash clouds from water/ice clouds (Hanstrum and Watson, 1983; Prata, 1989a, 1989b). Based on the same principles, Holasek and Rose (1991) used a ratio of raw AVHRR counts for channel 4 and channel 5, rather than a difference, to discriminate volcanic ash clouds from water/ice clouds for the 1986 eruption of Augustine Volcano, Alaska.

The BOM has recently installed a satellite receiving antenna at Darwin, in northern Australia, which enables the collection of real-time AVHRR data over the Indonesian region. The area of coverage provided by the Darwin antenna is illustrated in figure 4. In the equatorial regions, the ground track of the NOAA polar-orbiting satellites and the scan width of the AVHRR sensor is such that, with two satellites, there are only four scans per day at intervals of approximately 6 hours for any given location. Although there are obvious limitations because of the time between scans, it is anticipated the AVHRR data will be a valuable complement for hourly GMS imagery. The operational utility of these data for identifying ash clouds will be evaluated in the future.

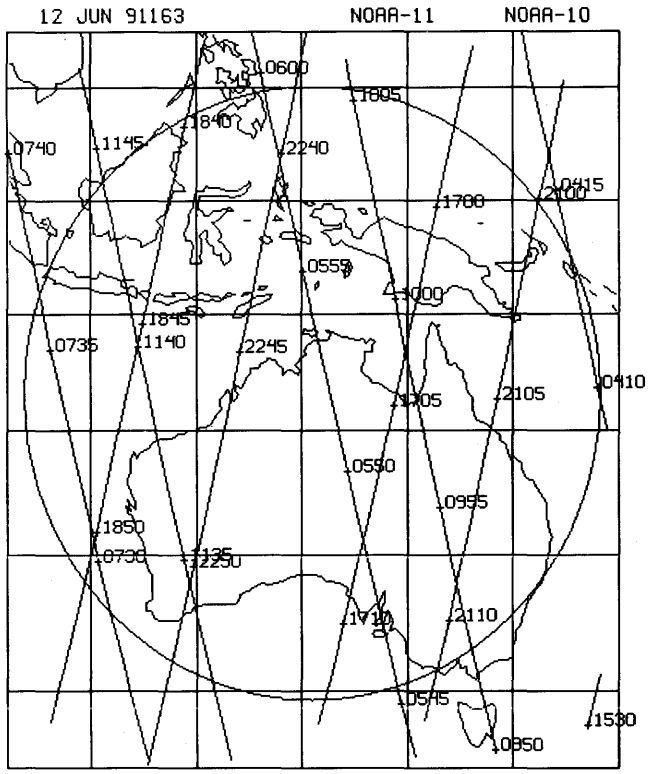


**Figure 4.** Coverage provided by Darwin NOAA satellite-data-receiving antenna. Slanted straight lines indicate satellite flight path. Satellite position indicated by time (UTC) for 12 June 1991.

## CONCLUSIONS

International standards and procedures for the provision of warnings for volcanic ash clouds have been established

(Fox, this volume), and, in accordance with these procedures, the Bureau of Meteorology provides a significant meteorological advisory (SIGMET) service for ash clouds that enter Australian airspace. In addition, the BOM provides a volcanic ash cloud advisory service for areas to the near north of Australia. These warnings describe the area of the ash cloud, the height, and the forecast movement and are based on eruption advice, hourly GMS images, and upper-level wind analyses. The possibility of providing an effective service for aviation is illustrated with a brief study of the eruption of Mt. Pinatubo at 00:51 UTC, 12 June 1991.

There are significant technical difficulties associated with the provision of warnings for volcanic ash clouds. The BOM can only detect and monitor ash clouds after eruption and confirmation of a volcanic eruption. It is therefore essential that there is early notification of any initial or subsequent volcanic eruption. Such warnings must be distributed quickly to the international aviation and meteorological communications system. Using present GMS satellite imagery, it is frequently not possible to discriminate volcanic ash clouds from water/ice clouds. AVHRR multispectral infrared satellite data does offer considerable promise in this area. The BOM has recently installed, in Darwin, a satellite receiving antenna that enables receipt of AVHRR data. These data are now available to operational meteorologists responsible for preparing advisories for volcanic ash clouds, and the benefits of the data will be evaluated in the future.

## REFERENCES CITED

Hanstrum, B.N., and Watson, A.S., 1983, A case study of two eruptions of Mt. Galunggung and an investigation of volcanic eruption cloud characteristics using remote sensing techniques: Australian Meteorological Magazine, v. 31, p. 171–177.

Holasek, R.E., and Rose, W.I., 1991, Anatomy of 1986 Augustine Volcano eruptions as recorded by multispectral image processing of digital AVHRR weather satellite data: Bulletin of Volcanology, v. 53, p. 420–435.

LeMarshall, J.F., Stirling, L.J., Davidson, R.F., and Hasset, M.J., 1987, The Australian region McIDAS: Australian Meteorological Magazine, v. 35, p. 55–64.

Malingreau, J.P., and Kaswanda, O., 1986, Monitoring volcanic eruptions in Indonesia using weather satellite data: The Colo eruption of July 28, 1983: Journal of Volcanology and Geothermal Research, v. 27, p. 179–194.

Matson, M., 1984, The 1982 El Chichón Volcano eruptions—A satellite perspective: Journal of Volcanology and Geothermal Research, v. 23, p. 1–10.

Potts, R.J., 1993, Satellite observations of Mt. Pinatubo ash clouds: Australian Meteorological Magazine, v. 42, p. 59–68.

Prata, A.J., 1989a, Observations of volcanic ash clouds in the 10–12-μm window using AVHRR/2 data: International Journal of Remote Sensing, v. 10, p. 751–761.

———1989b, Infrared radiative transfer calculations for volcanic ash clouds: Geophysical Research Letters, v. 16, p. 1293–1296.

Prata, A.J., Wells, J.B., and Ivanac, M.W., 1985, A "satellite's eye-view" of volcanoes on the Lesser Sunda Islands: Weather, v. 40, p. 245–250.

VOLCANIC ASH AND AVIATION SAFETY:
Proceedings of the First International Symposium
on Volcanic Ash and Aviation Safety
U.S. GEOLOGICAL SURVEY BULLETIN 2047

# ASH CLOUD AVIATION ADVISORIES

*By* Thomas J. Sullivan *and* James S. Ellis

## ABSTRACT

During the recent eruptions (12–22 June 1991) of the Mt. Pinatubo, Philippines, the U.S. Air Force Global Weather Central (AFGWC) requested assistance of the U.S. Department of Energy's atmospheric release advisory capability (ARAC) in creating volcanic-ash-cloud aviation advisories for the region of the Philippine Islands. Through application of its three-dimensional material transport and diffusion models using AFGWC meteorological analysis and forecast wind fields, ARAC developed extensive daily analysis and forecast advisories of ash-cloud position extending 48 hours into the future (in 12-hour increments) for a period of 5 days. The advisories consisted of "relative" ash-cloud concentrations in ten layers (surface to 5,000 ft, 5,000 to 10,000 ft, and every 10,000 ft up to 90,000 ft). The ash was represented as a log-normal size distribution of 10–200-μm-diameter solid particles. Size-dependent "ash-fall" was simulated over time as the eruption clouds dispersed. These products were distributed to the AFGWC (Offut Air Force Base, Nebraska) and Headquarters First Weather Wing (Hickam Air Force Base, Hawaii) for further distribution to U.S. Air Force weather units throughout the Pacific region, who were supporting the evacuation of U.S. personnel from the Philippines.

For the cataclysmic Pinatubo eruption of 15–16 June 1991, the complex three-dimensional atmospheric structure of the region produced dramatically divergent ash-cloud patterns. The large eruptions (> 23,000–33,000 ft high) produced ash-plume clouds with strong westward transport over the South China Sea, Southeast Asia, India, and beyond. The low-level eruptions (< 23,000–33,000 ft) and quasi-steady-state venting produced a plume that generally dispersed to the north and east throughout the support period.

## INTRODUCTION

The atmospheric release advisory capability (ARAC) is a real-time emergency response and preparedness service developed and operating at the Lawrence Livermore National Laboratory (LLNL) in Livermore, Calif., for the past 17 years. ARAC is a national resource with a suite of dispersion models to simulate the consequences of accidental releases of material into the atmosphere on local to global scales. Funded by the Departments of Energy (DOE) and Defense (DOD), the primary role of ARAC has been to provide calculations for radiological releases. Any U.S. Federal agency can request the services of ARAC through DOE as delineated in the Federal radiological emergency response plan.

This paper describes how ARAC has responded to other than radioactive material releases, summarizes its modeling system, and focuses on its response to the June 1991 eruption of Mt. Pinatubo, Luzon, the Philippines, as requested by the U.S. Air Force.

## BACKGROUND

Since the beginning of operation in 1974, ARAC has been involved in over 600 responses, primarily exercises with its supported agencies. In accordance with its charter, ARAC has been used for major domestic radiological events and some international events where the U.S. Government had interests. In addition, as table 1 indicates, ARAC has also been used for non-radiological releases within the United States. In fact, requests for assistance involving non-radiological releases have equaled those involving radioactive releases.

The current ARAC system has evolved according to the requirements and expectations of its supported agencies as well as its experience with responses (Sullivan, 1988). For example, a 1976 North Carolina train accident revealed that real-time meteorological data automatically formatted for use in dispersion models was essential to a rapid response. In 1978, the unique request by DOE to estimate the atmospheric consequences of the reentry burn-up of the Russian nuclear-powered COSMOS 954 satellite prompted the ARAC team to develop a high-altitude particle-fall model. As a result, ARAC was prepared for the subsequent COSMOS 1402 reentry in 1981. ARAC's largely manual response to the 1979 Three Mile Island accident and the 1980 Titan II missile accident showed the need for on-line U.S. topography and geography databases. The 1986 Chernobyl accident in the former Soviet Union propelled ARAC

**Table 1.** Notable ARAC responses.

[ARAC, atmospheric release advisory capability]

| Year | Location | Source | Release |
|---|---|---|---|
| 1976 | North Carolina | Train accident | Uranium hexafluoride[1] |
| 1978 | Northern Canada | COSMOS 954 reentry | Fission products |
| 1979 | Three Mile Island Harrisburg, Pa. | Nuclear power plant | Mixed fission products |
| 1980 | Damascus, Ark. | Titan II missile | Missile fuel[1] |
| 1981 | Indian Ocean | COSMOS 1402 reentry | Fission products |
| 1982 | South Carolina | Savannah River Plant | Hydrogen sulfide leak[1] |
| 1986 | Gore, Okla. | Sequoyah Fuels Plant | Uranium hexafluoride[1] |
| 1986 | Chernobyl, USSR | Nuclear power plant | Mixed fission products |
| 1988 | Miamisburg, Ohio | Mount Plant | Tritium gas release |
| 1989 | Amarillo, Tex. | Pantex Plant | Tritium gas release |
| 1991 | Persian Gulf | Nuclear facilities<br>Kuwait oil fires | Mixed fission products<br>Smoke[1] |
| 1991 | Philippines | Mt. Pinatubo | Volcanic ash[1] |
| 1991 | Northern California | Railroad car spill | Toxic gas products[1] |
| 1992 | Sosnovy Bor, Russia | Nuclear power plant | Radioactive gas |

[1] Release involved toxic chemicals.

to implement continental-to-hemispheric scale models supported by worldwide meteorological, terrain, and mapping data.

Each response has resulted in expanded capabilities. Consequently, for example, ARAC, with some adaptation to a new AFGWC wind-model data source, was ready with the necessary models and databases to simulate the daily regional-scale smoke and soot concentrations from the Kuwaiti oil fires in the Persian Gulf region from May to October 1991 (Ellis and others, 1992).

## ARAC SYSTEM

The original ARAC concept, prototype development, and initial operations from 1974 to 1982 were supported by DOE. From 1983 to 1986, the system was redesigned, and a high level of automation was implemented to support up to 100 facilities within the DOE-DOD nuclear community. Figure 1 depicts the automated flow of information during an ARAC emergency response with the current system. This simplified diagram represents only the top-level system functions of the ARAC emergency response operating system (AEROS). AEROS automatically assembles necessary information for the model-run stream once the minimum accident data have been entered using the "problem questionnaire." The questionnaire may either be completed on a computer system at one of the remote support facilities or manually entered at the ARAC center, based on information gathered.

A meteorological data interpolation code (MEDIC) initializes winds in the three-dimensional volume to be modeled. Relevant topography is applied at the lower boundary, then the calculus-of-variation code known as MATHEW (Sherman, 1978) imposes mass consistency in order to provide non-divergent flow fields for the dispersion model. The atmospheric diffusion particle-in-cell (ADPIC) model of Lange (1978) is a Lagrangian particle code that provides the dispersion physics for a wide range of substances, e.g., gases, solid particles, radioactive material, and non-radioactive material (Foster and Dickerson, 1990).

Typical model results include plots of deposition of material on the ground and instantaneous and time-integrated doses or air concentrations of particles at selected levels above the ground. Species or sources may be combined as required and contoured according to specified isopleth values. A legend is shown on each plot that describes the release, species involved, source type, units, and valid time for the contours.

After a quality assurance review by an assessment meteorologist, the plots may be transmitted to a supported site computer by modem or faxed to the emergency response manager. The time to create and deliver plots to a supported site computer can be as little as 15 to 30 minutes after receipt of incident information. For non-radiological incidents, the response time depends on the complexity of the source term, the availability of meteorological data, and the preparation of unique model-input parameters (Sullivan, 1991; Walker, 1989).

Typically, ARAC response time is equally split between computer or voice communications with the site,

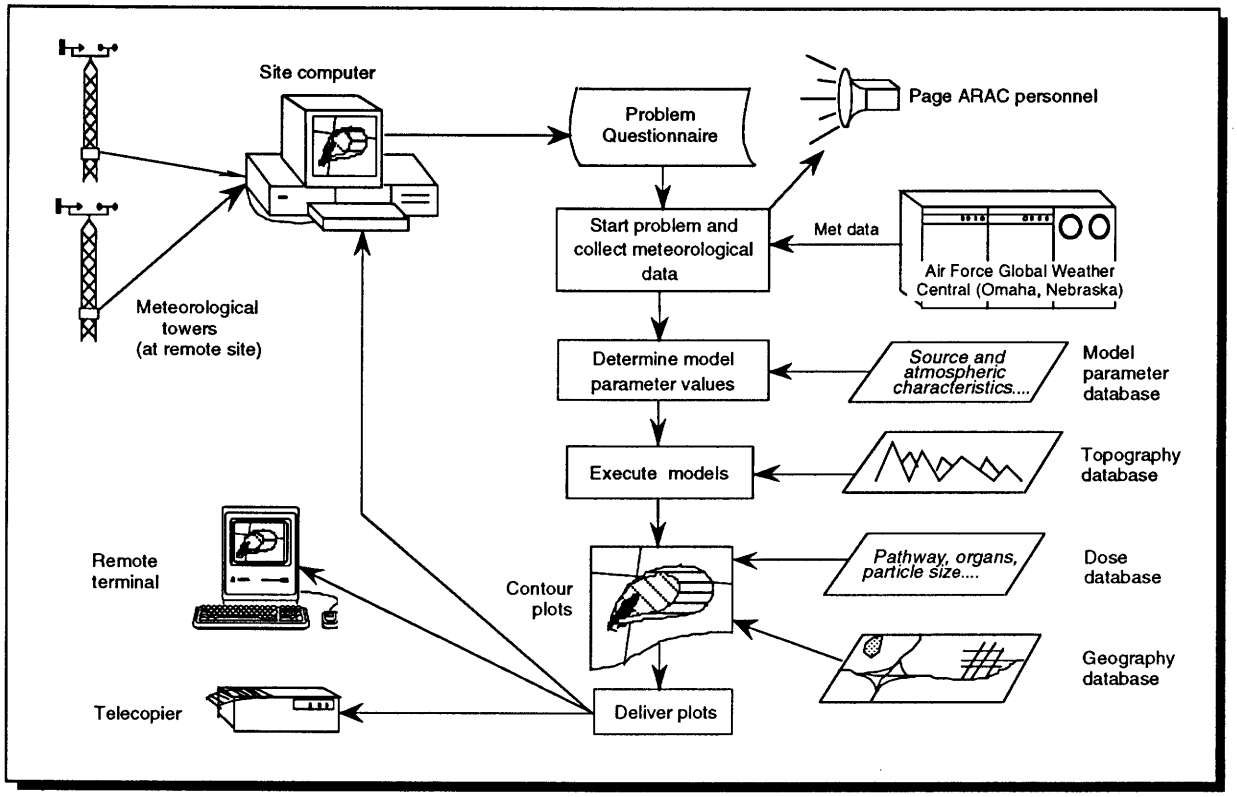


**Figure 1.** Schematic flow diagram indicating the major components of the ARAC (atmospheric release advisory capability) emergency response operating system.

automated or manual model-input preparation, model execution, and human interaction with the system. ARAC currently uses Digital Equipment Corporation (DEC) VAX 8550 computers to run the models and micro-VAX's to communicate with DEC PC350/380 support facility site computers at 1,200 baud. In 1992–93, ARAC plans to upgrade the VAX's with faster computers and to begin replacing the facility computers with Unix-based workstations communicating with ARAC at 9,600 baud.

## MODEL DATA REQUIREMENTS

To satisfy the request for the Pinatubo ash-cloud-advisory forecasts, ARAC required physical information about the events (source terms to the model), such as location, times and durations of eruptions, height, width, and diameter of the eruption cloud, and ash size and density properties. The U.S. Air Force provided the majority of this event-related information. The ash-particle information was gleaned from scientific reports about eruptions of El Chichón Volcano, Mexico, in 1982, and Mount St. Helens in 1980.

Initially, for the Pinatubo response, ARAC's "hemispheric" models, developed in response to the Chernobyl accident, were used because twice daily northern hemisphere wind-field analyses from AFGWC are routinely received and archived at ARAC. With AFGWC priority assistance, ARAC began receiving forecast-wind data for 15 standard pressure levels of the atmosphere (fig. 2) extending to 10 millibars or approximately 100,000 ft in altitude. Data to these heights were required because of the reported and estimated eruption heights of 25–30 km (80,000–100,000 ft) on 14–15 June 1991.

## ERUPTION CHARACTERIZATION FOR THE MODEL

After initial experimentation with representation of these large explosion clouds, it was decided to model the ash-cloud injections as large cylindrical volumes of several kilometers radius and vertical extent to serve as the basic geometry for release of model "marker" particles. A log-normal particle-size distribution spanning the 10–200 micron diameter range was selected; particle density was chosen as

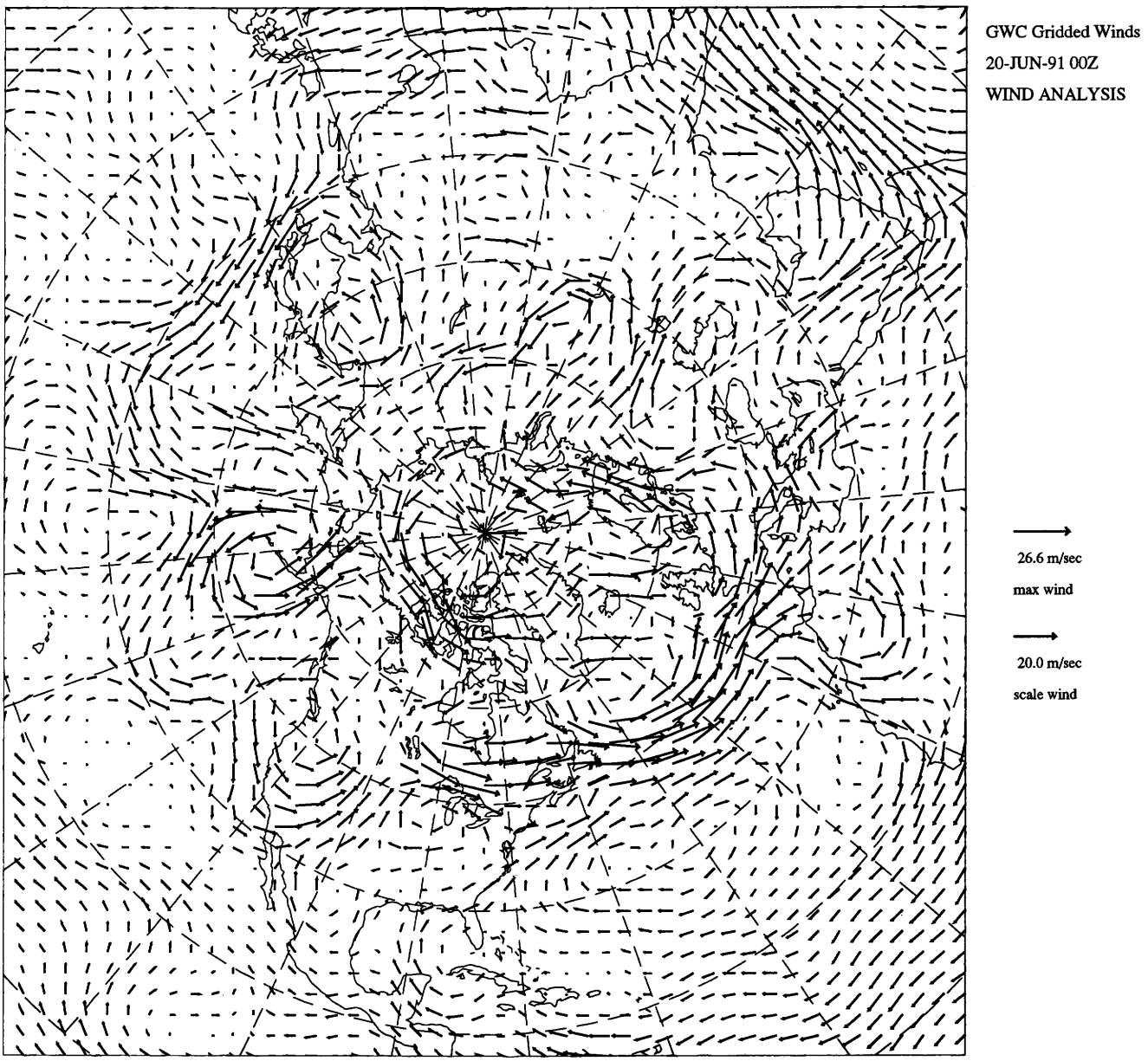


**Figure 2.** Overhead view, polar stereographic projection of the 10,000-ft level, northern hemispheric wind field for 20 June 1991, 00:00 UTC. Individual flow elements extend in the direction of the wind as indicated by arrows. Length of arrow shaft indicates relative wind speed. GWC, Global Weather Central (U.S. Air Force).

1.45 g/cm$^3$, based on a sample of ashfall from Mount St. Helens. Because several eruptions were to be modeled concurrently, a scaled (relative) release rate proportional to explosive energy estimated from the altitude of the cloud top was approximated as shown in table 2 using explosion-scale algorithms maintained at ARAC. The relative scale and chronology of the eruptions modeled are depicted in figure 3.

## RESULTS

By the conclusion of the first response day, 18 June 1991, ARAC had produced the first set of ash-cloud-advisory products (fig. 4) using the hemispheric-scale model. Plots of "relative" ambient concentrations of particles were generated for consecutive 12-hour intervals extending to 48

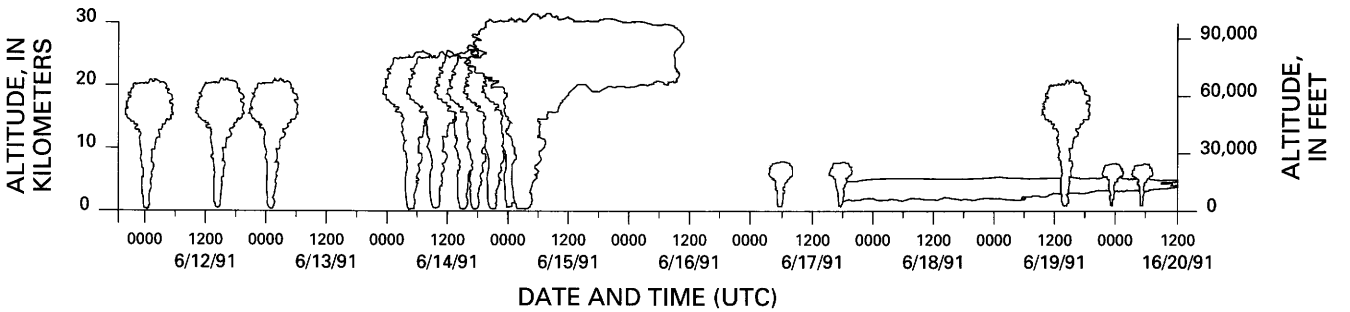


**Figure 3.** Time sequence and relative eruption heights of events included in ARAC (atmospheric release advisory capability) ash-cloud-model calculations for eruptions of Mt. Pinatubo during the period 12–20 June 1991. UTC, Coordinated Universal Time.

hours for the 10 altitude layers specified by the Air Force. In an attempt to delineate potentially hazardous areas, relative concentration divisions of "heavy/dense," "moderate," and "light/diffuse" ash were chosen by identifying the highest two orders of magnitude of relative particle concentrations, the next largest two orders of magnitude, and then the remaining concentrations, respectively. Internal to the model, a "normalized unit source" was selected due to the complete lack of actual data concerning the mass of the eruptions. A "normalized unit source" is a convenient mechanism for deriving the relative dispersed-material distribution for an assumed release or release rate, e.g., 1 g or 1 g/s. When specific measurements or estimates are determined, then the calculated distributions can be directly scaled to derive actual mass-specific concentrations. Unfortunately, the meteorological and dispersion-model domain boundary was close to the eruption site, with the consequence that these calculations were of limited utility for the areas south and southwest of Pinatubo. They did, however, cover the primary aerial evacuation route from Cebu to Guam, which remained ash-free (fig. 5).

**Table 2.** Scaled "relative" release rate, Mt. Pinatubo, 1991.

[Particle-size distribution: 10–200-μm diameter; equivalent energy released given in thousands of tons of TNT]

| Estimated cloud top (km) | Equivalent energy released | Proportional release rate |
|---|---|---|
| 30 | 6,000 | 1.0 |
| 25 | 3,000 | 0.5 |
| 19 | 500 | 0.08 |
| 7 | 7 | 0.001 |
| 4 | 4 | 0.00066 |

Shortly after transmission of the first calculations, the Air Force requested comparable advisories for a more detailed subregion of a few thousand kilometers extent centered on the Philippines. Figures 6*A* and 6*B* delineate this new model subdomain and also reveal the complex, sheared wind-flow regimes at 7,500 and 50,000 ft on 18 June 1991.

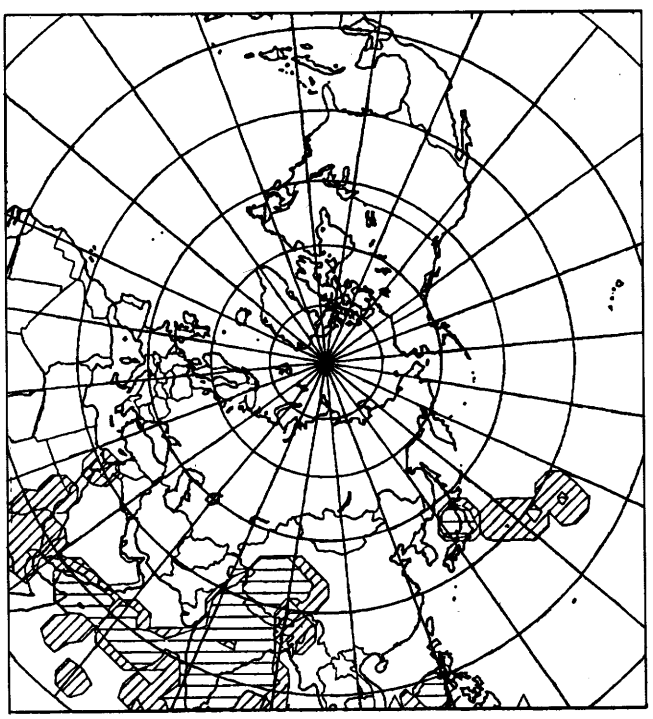

**Figure 4.** Example of the first "forecast ash cloud advisory" map prepared for the U.S. Air Force on a hemispheric scale. This plot was for the 20,000–30,000-ft altitude layer valid at 00:00 UTC, 20 June 1991. The "ash" levels are relative to the initial release as discussed in the text.

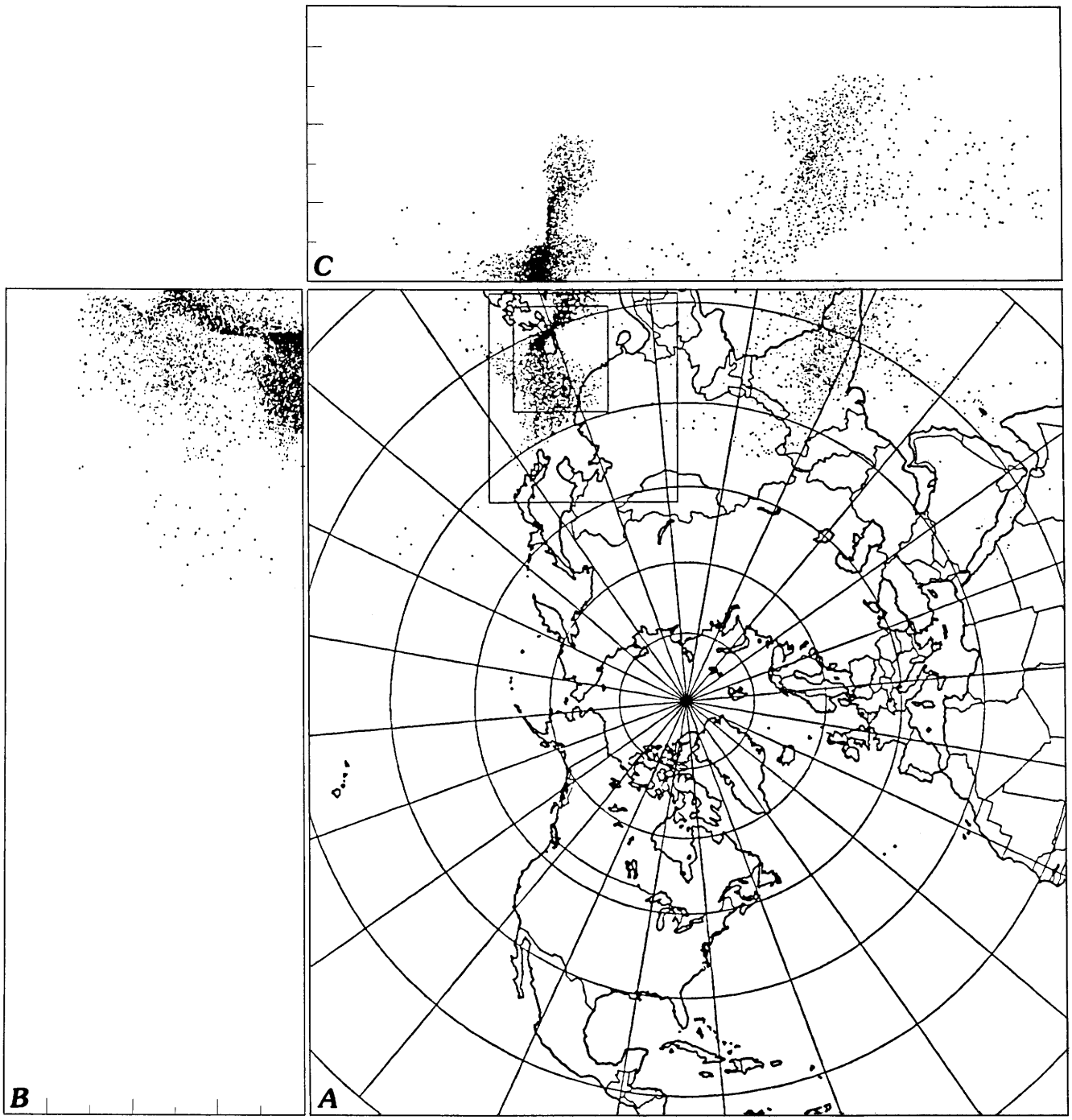


**Figure 5.** Particle-model representation of dispersing ash clouds for all eruptions of Mt. Pinatubo from 12–20 June 1991. *A*, overhead view; *B*, side view from right to left of the overhead view, looking down the axis of the plume; *C*, side view from bottom to top (or across the pole) of the overhead view—this reveals the vertical structure of the recent eruption and the dispersed debris from the cataclysmic eruption (of 15 June 1991) over India. Top of vertical scale on side views is 115,000 ft.

To prepare these calculations for the subregion, it was necessary to extract grid-point profiles from the hemispheric data grids and merge them with available regional rawinsonde data. At the time of the eruptions, this was a manual process; now it is substantially automated. Using the same "source" scaling parameters and receding eruptions, figures 7*A*, 7*B*, and 7*C* reveal the model representation of the 19 June 1991, 14:25 UTC eruption after 9 hours of dispersal

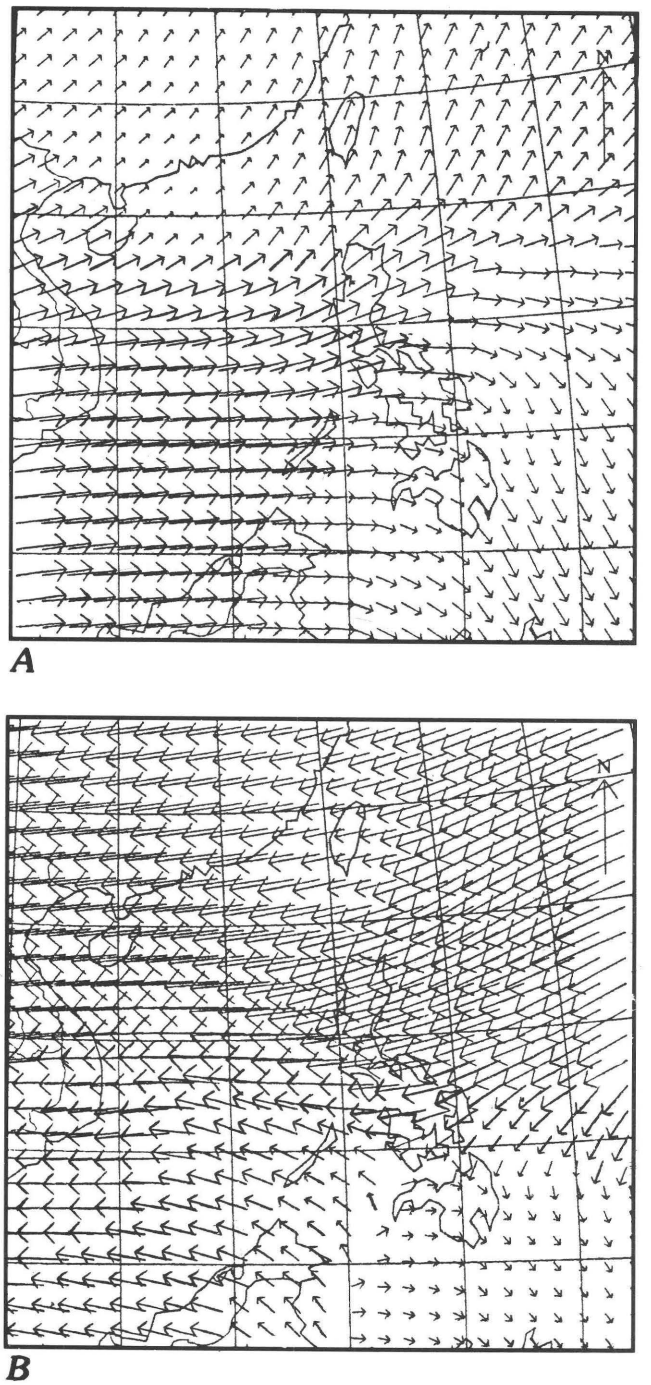


**Figure 6.** Wind-field calculations for the Philippine Island region showing details of the regional calculations for the 19 June 1991 Pinatubo eruption (during the period of U.S. military air evacuations). Individual flow elements extend in the direction of the wind as indicated by arrows. Length of arrow shaft indicates wind speed, which ranges from about 5 m/s to about 20 m/s. *A*, Lower atmosphere (≅ 7,500 ft) winds; *B*, Upper atmosphere (≅ 50,000 ft) winds.

simulation. In figure 7, the dominant plume of ash was transported west-southwest over the South China Sea by strong, high-altitude winds. A low-altitude, diffuse, meandering plume, probably related to residual venting between major eruptions, stretches north around Taiwan and wraps back around along the South China coast. Figure 8 gives an indication of this low-level plume structure on 20 June. Vertical cross-section views of the 19 June 1991 eruption plume at 00:00 UTC on 20 June show the simulated "ashfall" from the southwestward-transported upper plume (15,000–50,000 ft) and low-level plume. The resulting dispersing ash clouds are shown in figures 8*A*–8*C*, revealing the different structures of the northeast (lower level) ash stem and vent clouds and the southwest (upper level) main explosion cloud and ashfall from the above stratospheric injection. Figure 8*D* is a verifying AFGWC analysis based on defense meteorological satellite program (DMSP) visible and infrared images for 20 June at 01:34 UTC. Immediately evident is the sloped, upper cloud and particle fallout structure being driven to the southwest by the higher altitude winds, while the lower "stem" and continuous, lower level, post-eruption "venting" ash cloud is being swept northeast then northward.

For the cataclysmic eruption of 15–16 June 1991, the complex three-dimensional atmospheric structure in the region produced dramatically divergent ash-cloud patterns. The large eruptions (> 23,000–33,000 ft) produced ash-plume clouds, with strong westward transport over the South China Sea, Southeast Asia, the Bay of Bengal toward India, and beyond. It is the downwind transport, diffusion, and ash fallout of these enormous stratospheric intrusions that resulted in the numerous aircraft encounters with ash clouds (Casadevall and De Los Reyes, 1991). The low-level eruptions (< 23,000 ft) and quasi-steady-state venting produced a plume that generally dispersed to the north and east throughout the period.

## POTENTIAL IMPROVEMENTS

These results show the detailed ash-cloud structure achievable with the ARAC three-dimensional modeling system. Although the initial approach proved viable and successful, further refinement is possible. A distinct need exists to quantify eruptions consistently such that "relative" ash concentrations relate to specific aviation hazards. Research and collaboration with the volcanology community could possibly produce an "eruption mass" estimation methodology correlated to seismic detection or eruption height (Harris, this volume; McNutt, this volume). Particle sizes, density, and other relevant characteristics should be refined. Databases containing locations and characteristics of all known potentially active volcanoes should be prepared. Links to volcanologists' alerting networks should be established.

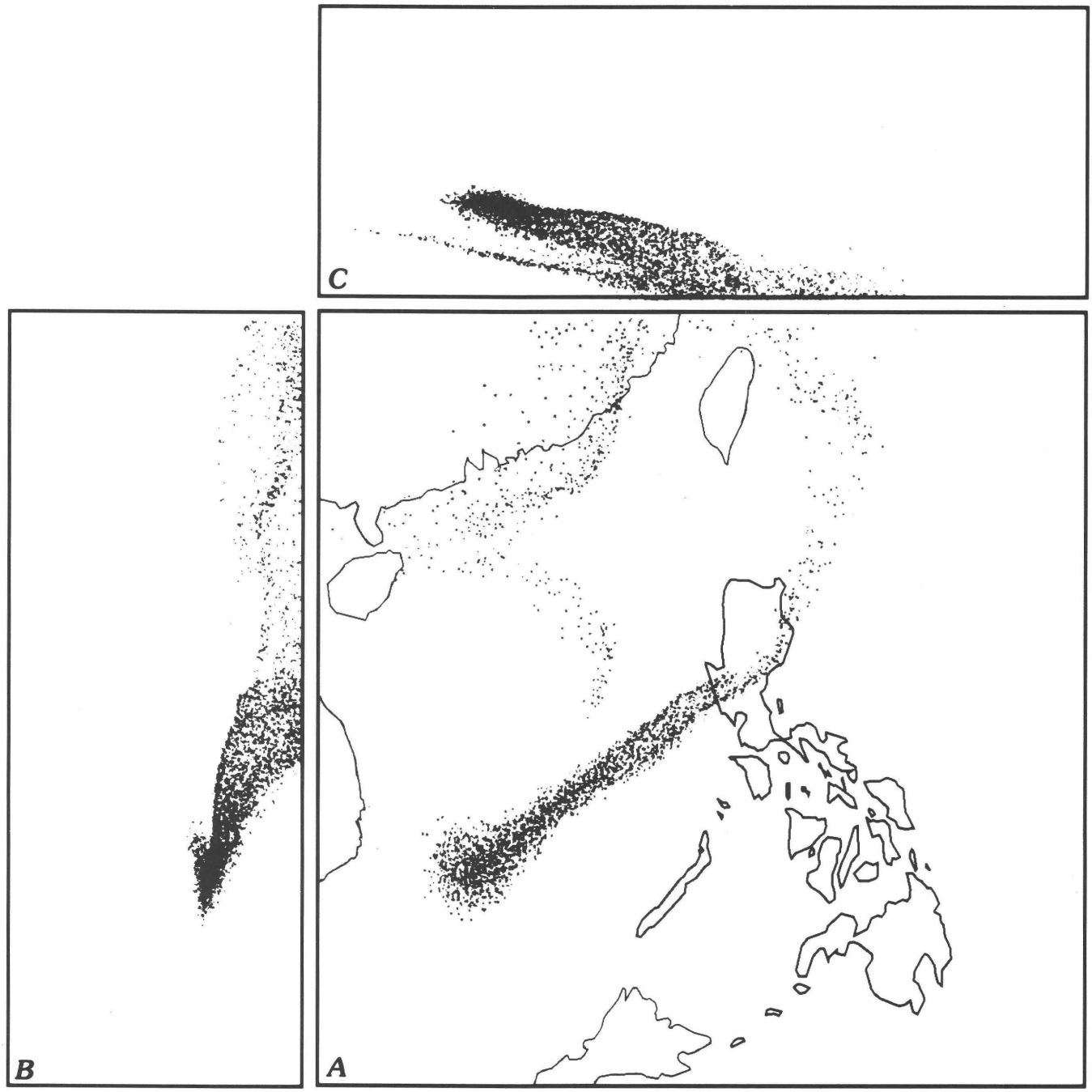


**Figure 7.** Model representation of the 19 June 1991, 14:25 UTC Pinatubo eruption after 9 hours of dispersal simulation. The dominant plume of ash was transported west-southwest over the South China Sea by the strong, high-altitude winds. A low-altitude, diffuse, meandering plume, probably related to residual venting between major eruptions, stretches north around Taiwan and wraps back around along the South China coast. *A*, Overhead "particle cloud" view for the Philippine Island region showing the regional grid calculations of the 19 June 1991 eruption; *B*, Viewed from east to west; *C*, Viewed from south to north.

## POTENTIAL VALUE TO AVIATION

A few immediate advantages of the ARAC hazard modeling system are: (1) advisory products are not limited or affected at night, (2) natural clouds do not obscure or affect the modeling technique (as, for example, detection using satellite-based techniques), (3) unaffected routes and areas unaffected by ash are apparent, (4) altitude layers can be differentiated, (5) ash-cloud dispersion is calculated with winds comparable to aircraft computerized flight plans, and (6) the

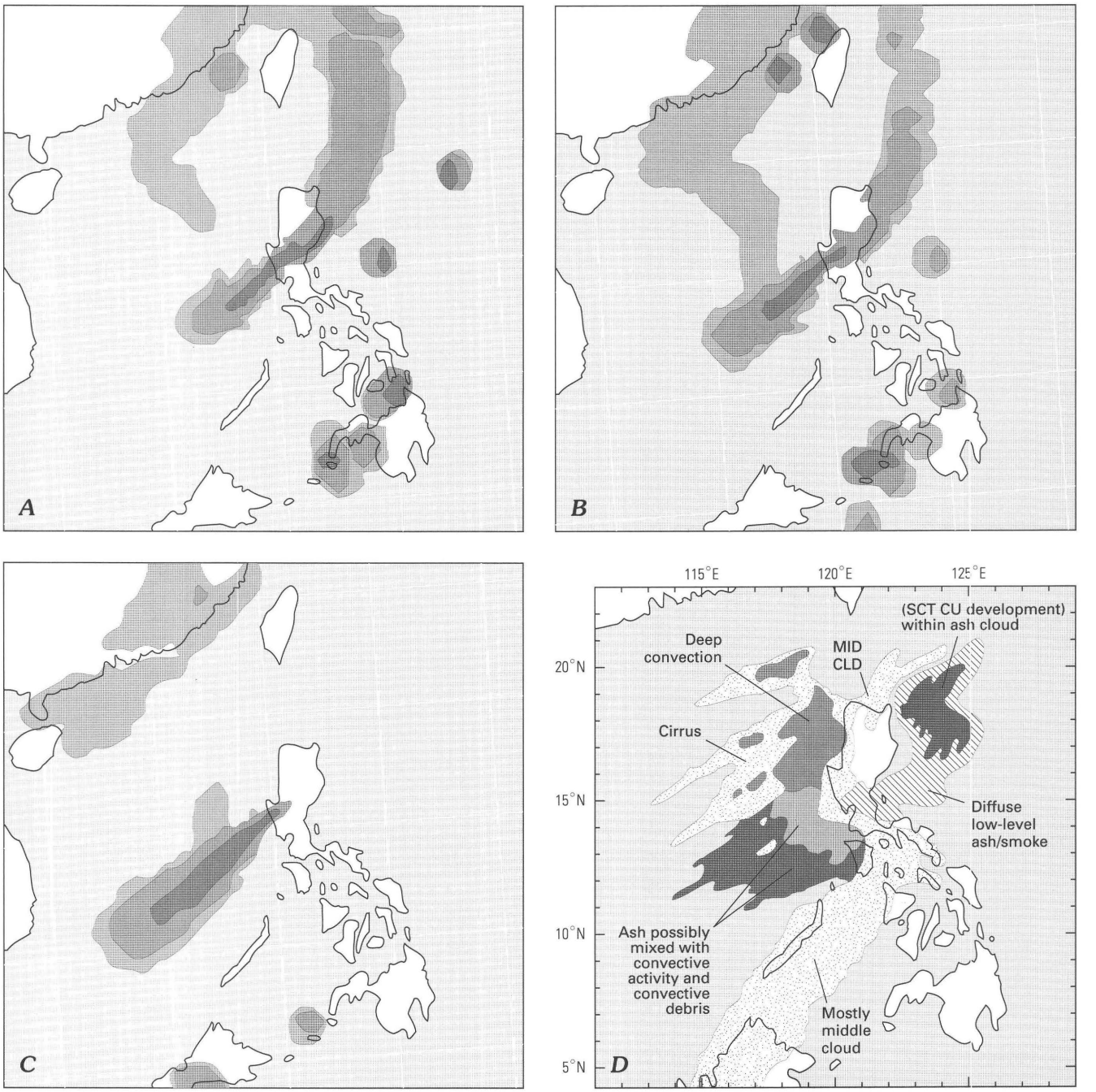


**Figure 8.** Relative ash concentration isopleths for three altitude layers show the simulated "ashfall" from the southwestward-transported upper plume (15,000–50,000 ft) and low-level plume in the Philippine Island region on 20 June 1991, following the eruption of 19 June 1991. The resulting dispersing ash clouds reveal different structures of the northeast (lower level) ash stem and vent clouds and the southwest (upper level) main-explosion cloud and ashfall from the above stratospheric injection. *A*, 5,000–10,000 ft; *B*, 10,000–20,000 ft; *C*, 20,000–30,000 ft; *D*, Air Force Global Weather Central (AFGWC) analysis based on defense meteorological satellite program (DMSP) visible and infrared images for 20 June 1991 at 01:34 UTC. Imagery shows the distribution of weather clouds and ash clouds for use as a verification of the ARAC model for the period of 20 June 1991. MID CLD, middle cloud; abbreviations in upper right portion of *D* indicate "scattered cumulus development within ash cloud."

advisories are graphic charts that are easily interpreted. Coupling of aviation operations with this type of hazard modeling provides a demonstrated, viable method to keep aircraft from unanticipated exposure to volcanic ash clouds.

Assuming there is sufficient interest from the aviation community, a protocol could be established for generation of pre-eruptive, precautionary calculations, as well as generation of advisories during and after eruption until all hazardous quantities of ash are removed from the contaminated airspace. A system for dissemination of these results would need to be determined in order that the advisories reach all potentially impacted aircraft, carriers, air traffic control, and airport authorities. With such a capability integrated into global aviation, the hazard due to flight operations in areas of volcanic eruption threat could be well defined and appropriately avoided by rerouting and rescheduling. Terminals at risk could also be avoided thus minimizing the risk of aircraft damage, as well as the risk of losses owing to grounding of airplanes—either of which could have substantial economic impacts.

## SUMMARY

Modeling the sequence of eruptions from the 1991 eruptions of Mt. Pinatubo presented ARAC with a unique challenge. Based on the results achieved, we conclude that application of this modeling methodology could provide enhanced safety for the aviation community in the event of volcanic eruptions. The modeling system improvements outlined here must be developed if ARAC is to be considered for future involvement in a volcanic-ash-cloud hazard advisory service. The U.S. Department of Energy, as manager for the ARAC program, must approve any extension of this emergency response service into this area of natural hazard mitigation before such service could be routinely provided. Technology transfer to nongovernment organizations is a possible alternative, provided a technically competent organization with strong meteorological and aviation interests assumes responsibility for generation of the advisories.

## ACKNOWLEDGMENT

This work was performed under the auspices of the U.S. Department of Energy at Lawrence Livermore National Laboratory under Contract No. W-7405-ENG-48 and by EG&G under contract number DE-AC08-NV10617.

## REFERENCES CITED

Casadevall, T.J., and De Los Reyes, 1991, Impact of the June 1991 Pinatubo eruptions on aircraft operations in the western Pacific and Southeast Asia [abs.]: Eos, Transactions, American Geophysical Union, v. 72, no. 44 [Supplement], p. 95.

Ellis, J.S., Foster, C.S., Foster, K.T., Greenly, G.G., Sullivan, T.J., Baskett, R.L., Nasstrom, J.S., and Schalk, W.W., 1992, Daily dispersion model calculations of the Kuwait oil fire smoke plume, *in* Proceedings of the 85th Annual Meeting: Pittsburgh, Pa., Air and Waste Management Association, Paper 92-76.05, 14 p.

Foster, K.T., and Dickerson, M.H., 1990, An updated summary of MATHEW/ADPIC model evaluation studies: Livermore, Calif., Lawrence Livermore National Laboratory, Report No. UCRL-JC-104134, 28 p.

Lange, R., 1978, ADPIC—A three dimensional particle-in-cell model for the dispersal of atmospheric pollutants and its comparison to regional tracer studies: Journal of Applied Meteorology, v. 17, p. 320–329.

Sherman, C.A., 1978, A mass-consistent model for wind fields over complex terrain: Journal of Applied Meteorology, v. 17, p. 312–319.

Sullivan, T.J., 1988, ARAC, evolution by accident, *in* Topical Meeting on Emergency Response Modeling, September 26–28, 1988, Charleston, S.C.: Livermore, Calif., Lawrence Livermore National Laboratory, Report No. UCRL-98033, 8 p.

———1991, ARAC, a computer-based emergency-response dose-assessment service with global application potential: Livermore, Calif., Lawrence Livermore National Laboratory, Report No. UCRL-JC-10720, 16 p.

Walker, H., 1989, Use of the 1:2,000,000 digital line graph data in emergency response, *in* Proceedings of the International Symposium on Cartography and Computing: Bethesda, Md., American Society for Photogrammetry and Remote Sensing and American Congress on Surveying and Mapping, p. 472–482.

VOLCANIC ASH AND AVIATION SAFETY:
Proceedings of the First International Symposium
on Volcanic Ash and Aviation Safety
U.S. GEOLOGICAL SURVEY BULLETIN 2047

# ALASKA VOLCANO-DEBRIS-MONITORING SYSTEM: NEW TECHNOLOGIES TO SUPPORT FORECASTING VOLCANIC-PLUME MOVEMENT

*By* Gary L. Hufford

## ABSTRACT

The eruptions of Redoubt Volcano during 1989–90 revealed a number of deficiencies in National Weather Service (NWS) operations that greatly hampered the forecaster's ability to accurately forecast and issue timely advisories on the movement of airborne volcanic debris. The forecaster lacked knowledge of (1) the physical properties of airborne volcanic debris, (2) the initial location of debris in the atmosphere, both vertically and horizontally, (3) real-time winds near and downstream of the volcano, and (4) rapid access to volcanic-debris-tracking models.

To help resolve these deficiencies, an Alaska volcano debris monitoring system has been designed, acquired, and installed at the NWS offices in Anchorage, Alaska. The system consists of a wind-profiling Doppler radar that provides hourly vertical profiles of winds near the volcano, a satellite downlink and processing system for tracking volcanic plumes using a variety of polar-orbiting satellites, a C-band radar to provide vertical and horizontal extent of the plume at and near the volcano, a new volcanic-debris-tracking model, and an upgrade to the regional computer and communications network for processing, applications, and display of the volcano debris monitoring system database.

## INTRODUCTION

Volcanic ash injected into the atmosphere from the 1989–90 Redoubt eruptions became the most common and widespread hazard (Brantley, 1990) from this series of eruptions. The ash caused significant damage to property, especially aircraft, and severely disrupted normal activities in south-central Alaska, where about 60 percent of the State's population lives.

Redoubt Volcano is one of four active volcanoes that lie along the west side of Cook Inlet (fig. 1). These four volcanoes have erupted for a combined total of seven times in the last 80 years. Some of those eruptive episodes have lasted over a 2-year period. The four volcanoes are part of an active chain that extends from upper Cook Inlet, southwest along the Alaska Peninsula, to the western Aleutians. This chain includes a total of 35 volcanoes active during the last century (Simkin and others, 1981).

During the last eruptive episode of Redoubt Volcano, the NWS found that there were a number of deficiencies in information that greatly hampered the forecaster in accurately forecasting and issuing timely advisories on the movement and concentration of volcanic debris injected into the atmosphere. The forecaster had no information on (1) ash particle size and concentration, (2) initial height or horizontal extent of the plume into the atmosphere, (3) real-time vertical profiles of the winds near and downstream of the volcano, and (4) rapid access to volcanic-ash-trajectory models.

The potential for future hazardous eruptions near Cook Inlet led Congress to support a volcano monitoring program for south-central Alaska to minimize the affects on the population and commerce. A major participant in the monitoring program is the NWS. The purpose of this paper is to describe the technologies that have been chosen by NWS for the task of ash detection, monitoring, and tracking in Alaska. The system, called the Alaska volcano debris monitoring system, consists of new remote-sensing instrumentation, development of new predictive models, and an upgrade of the NWS regional computer and communications network for processing, applications, and display of the integrated database from the monitoring system.

## REMOTE-SENSING TECHNOLOGIES

The remote sensing instrumentation in the Alaska volcano debris monitoring system consists of a Doppler wind profiler, a non-Doppler weather radar (C-band), and a polar satellite downlink, processing, and display system.

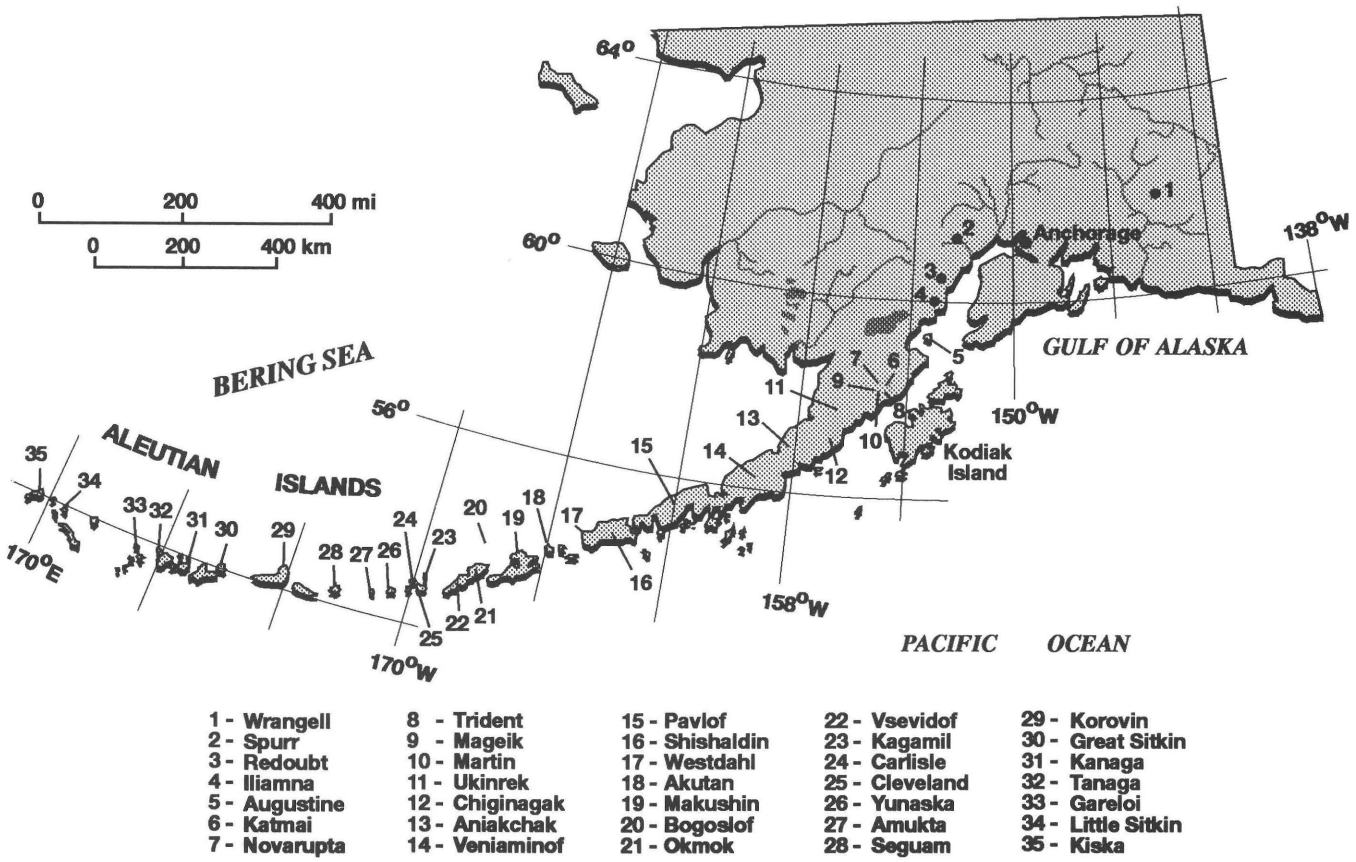


**Figure 1.** Volcanoes along Cook Inlet, Alaska, that have shown activity in the last century, including Mt. Spurr (2), Redoubt Volcano (3), Iliamna Volcano (4), and Augustine Volcano (5). Source: Alaska Volcano Observatory.

## WIND PROFILER

A wind-profiling Doppler radar observes the weak back-scatter from turbulent inhomogeneities in the atmospheric radio refractive index. The ultra high frequency (UHF) system (405 MHz) is suited for high-resolution, clear-air wind observations from 1 km to 16 km producing data every 6 minutes that is arranged into hourly, vertically averaged wind profiles (Balsley and Gage, 1982). Many studies have been made of the precision of profiler wind measurements. Thomas and Williams (1990) report that, in a comparison of profiler and rawinsonde (balloon) winds, the standard deviation was close to 3 m/s, with an inherent accuracy for the profiler of less than 1 m/s.

To support the Alaska volcano debris monitoring system, the wind profiler was installed in Homer, Alaska, about 100 km from Redoubt Volcano (fig. 2) in December 1990. The Homer site provides hourly vertical profiles of winds near the Cook Inlet volcanoes. Figure 3 shows an example of the wind measurements from the Homer profiler. Other profiler sites are proposed for Talkeetna and Middleton Island, Alaska (fig. 2). These two sites will give hourly vertical wind profiles at locations downwind from the Cook Inlet volcanoes. These sites will also provide winds along two major air-traffic corridors over south-central Alaska that have relatively poor upper-air network coverage (fig. 4).

## C-BAND RADAR (5 CENTIMETER)

Ground-based radar observations and calculations can provide significant information on estimating (1) the height of the eruptive column above the volcano, (2) the maximum vertical and horizontal dimensions of the ash cloud downwind, and (3) the location and horizontal velocity of the ash cloud. NWS radar observations of ash clouds from Mount St. Helens demonstrated that weather radar (5 cm) can yield timely information during and following volcanic eruptions (Harris and Rose, 1983). However, there are some constraints.

One- to 10-cm radars sometimes cannot discriminate between ash clouds and meteorological clouds and rain targets (Stone, this volume). Thus, on cloudy, rainy days, ash plumes may go undetected by weather radar if the radar is the only source of detection. In addition, once an ash cloud is in the dispersed stage, particle sizes may be too small to be detectable by radar. Radar must be used in conjunction with

other observational measurements to be an effective data source.

In October 1990, a 5-cm C-band radar was located in Kenai, Alaska, approximately 90 km from Redoubt (fig. 2). The radar is mounted on a modified recreational motor home and is portable. The unit can be moved rapidly to optimize observations of the other volcanoes in the Cook Inlet area. Data from the radar site is sent, in real time, by telephone to the forecaster in Anchorage for display on remote monitors.

## HIGH RESOLUTION PICTURE TRANSMISSION PROCESSING SYSTEM

NOAA/TIROS (National Oceanic and Atmospheric Administration—television and infrared observing satellite) polar-orbiting satellites have been used in some cases to detect and track ash clouds utilizing a number of instruments on the platform. Advanced very high resolution radiometer (AVHRR) visible and infrared imagery have been used to track volcanic clouds in Alaska (Holasek and Rose, 1991; Schneider and Rose, this volume) and southeast Asia (Prata and others, 1985) using standard methods to track meteorological clouds. Infrared imagery has been used to discriminate volcanic clouds from ordinary water/ice clouds utilizing two signatures in the brightness temperatures (Prata, 1989). The first signature is based on the emission characteristics of silicates in the ash cloud. Silicates have a lower emissivity at 11 μm than at 12 μm where water/ice show peak emissivity. This effect is seen as a negative temperature difference between channels 4 and 5 of the AVHRR instrument. The second signature is a lower emissivity for sulfuric acid

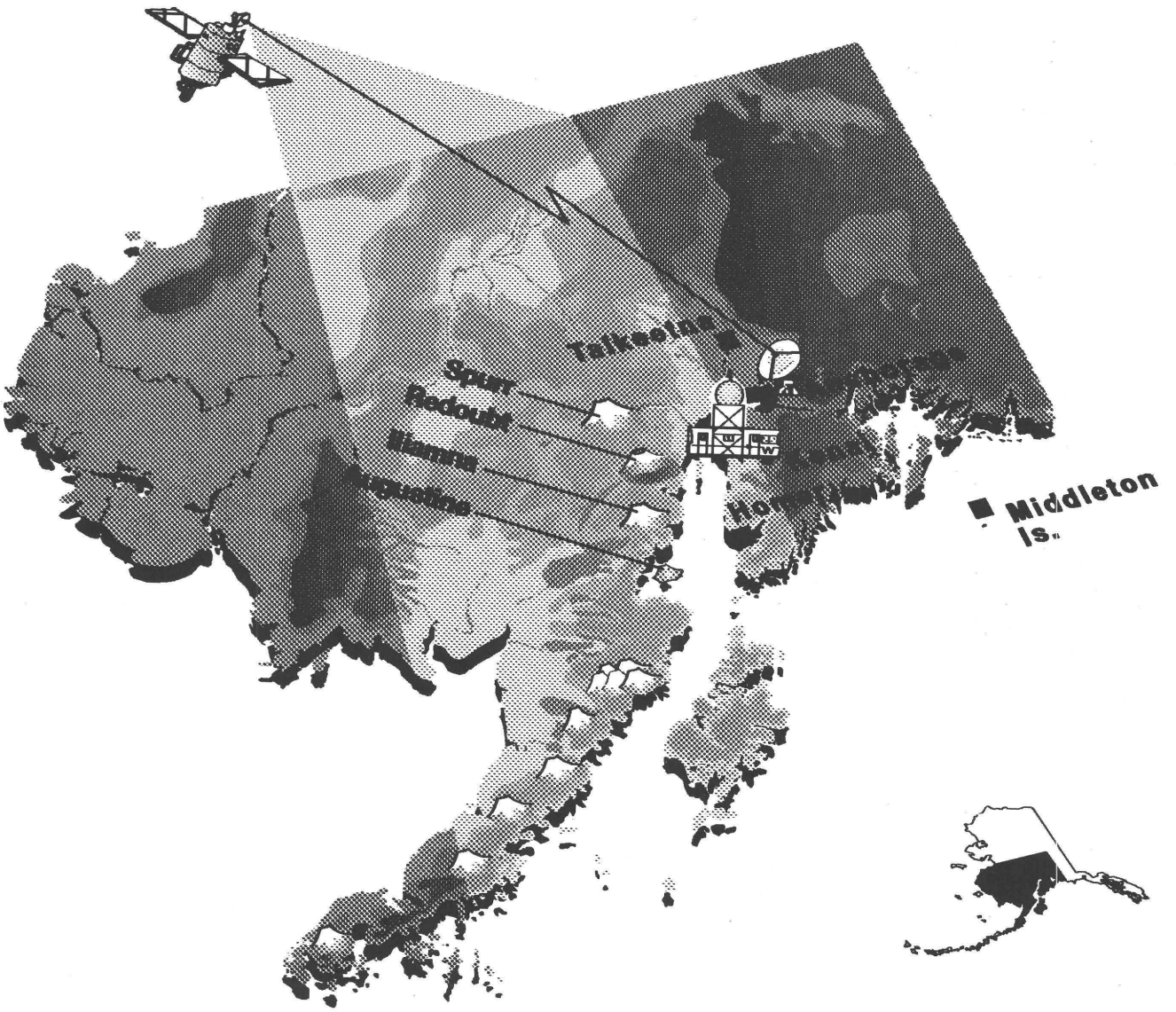


**Figure 2.** Location of remote-sensing instrumentation of the Alaska volcano debris monitoring system in relation to the four volcanoes along Cook Inlet.

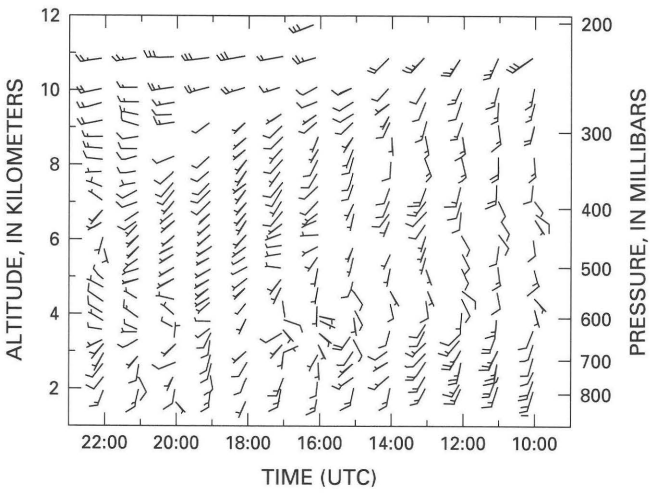


**Figure 3.** Hourly vertical profiles of wind from the Homer, Alaska, profiler for April 2, 1991. Orientation of "arrow" shaft indicates wind direction and has a precision of ±10°. "Flag" length indicates wind speed: a "half-flag" has a value of 5 knots; a "full-flag" has a value of 10 knots. UTC, Coordinated Universal Time.

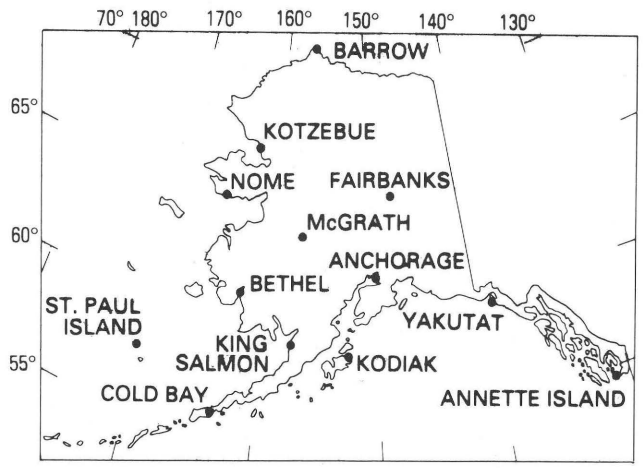


**Figure 4.** Location of the upper-air (rawinsonde balloon release) network in Alaska.

droplets or acid-coated particles (11 μm) when compared to water/ice particles (12 μm).

The high spatial resolution of the NOAA/TIROS polar-orbiting satellites (1 km), their great spectral range, and frequent coverage make these satellites a significant monitoring and tracking tool over Alaska. At low latitudes, the polar orbit limits the view of the same point to only four times per day for two satellites. Because the orbits of the satellites are near polar and sun synchronous, their orbital paths tend to converge at the poles, and, in the higher latitudes, coverage can be up to 18 passes per day from the same two polar satellites.

There are other operational instruments on-board the NOAA/TIROS polar-orbiting satellites that have potential to support the monitoring and tracking of volcanic plumes. The TIROS observational vertical sounder (TOVS) on the polar-orbiting satellites should be able to provide considerable information on volcanic clouds and conditions around them. TOVS consists of a high-resolution infrared radiation sounder (HIRS) that contains 20 infrared channels and a passive microwave sounding unit (MSU). TOVS also provides vertical profiles of temperature, moisture, and geostrophic wind down to the surface in areas of no clouds. This data can be used to estimate the maximum height and trajectory of ash clouds.

A high-resolution image-processing system (HIPS) was installed in Anchorage, Alaska, in June 1991 (fig. 2). The system includes a tracking antenna located at the international airport, an ingest/synchronization computer, a main processor, and four workstations at the three Alaska forecast offices (Anchorage, Juneau, and Fairbanks) and the Center Weather Service Unit in Anchorage. Eighteen polar-orbiting passes over Alaska can be processed to produce at least 12 satellite-image products per pass; these are distributed via the Alaska region operational communications network (ARO-NET). The HIPS system was also designed to ingest data from other polar-orbiting satellites, including those of the defense meteorological satellite program (DMSP), to increase coverage so that an image is available over any given point in Alaska every 1.5–2 hours. The aerial coverage for HIPS is within a 1,500-km radius from Anchorage.

Satellite data are displayed on workstations, and interactive software allows for complete digital manipulation of the imagery and sounding data, including animation, graphic overlay, cartographic projections, multispectral classification, windowing, and full color enhancement.

# COMPUTER, COMMUNICATIONS, DATA INTEGRATION, AND MODELS

## COMPUTER AND COMMUNICATIONS NETWORK

To insure the optimization of the NWS Alaska computers and communications to handle the large volume of data from the volcano monitoring system and the gridded data sets from various prediction models, the next-generation Alaska region operational computer and communications network (ARO-NET) was developed and made operational in October 1991 (fig. 5). Computer standards such as UNIX (OSF/1 compliance), X-Windows (Motif), and IEEE 802.3 Ethernet with TCP/IP network protocol have been selected to minimize the difficulties inherent in a heterogeneous computer environment. This allows a number of different kinds of computers to be used as workstations and coupled with an advanced wide- and local-area network

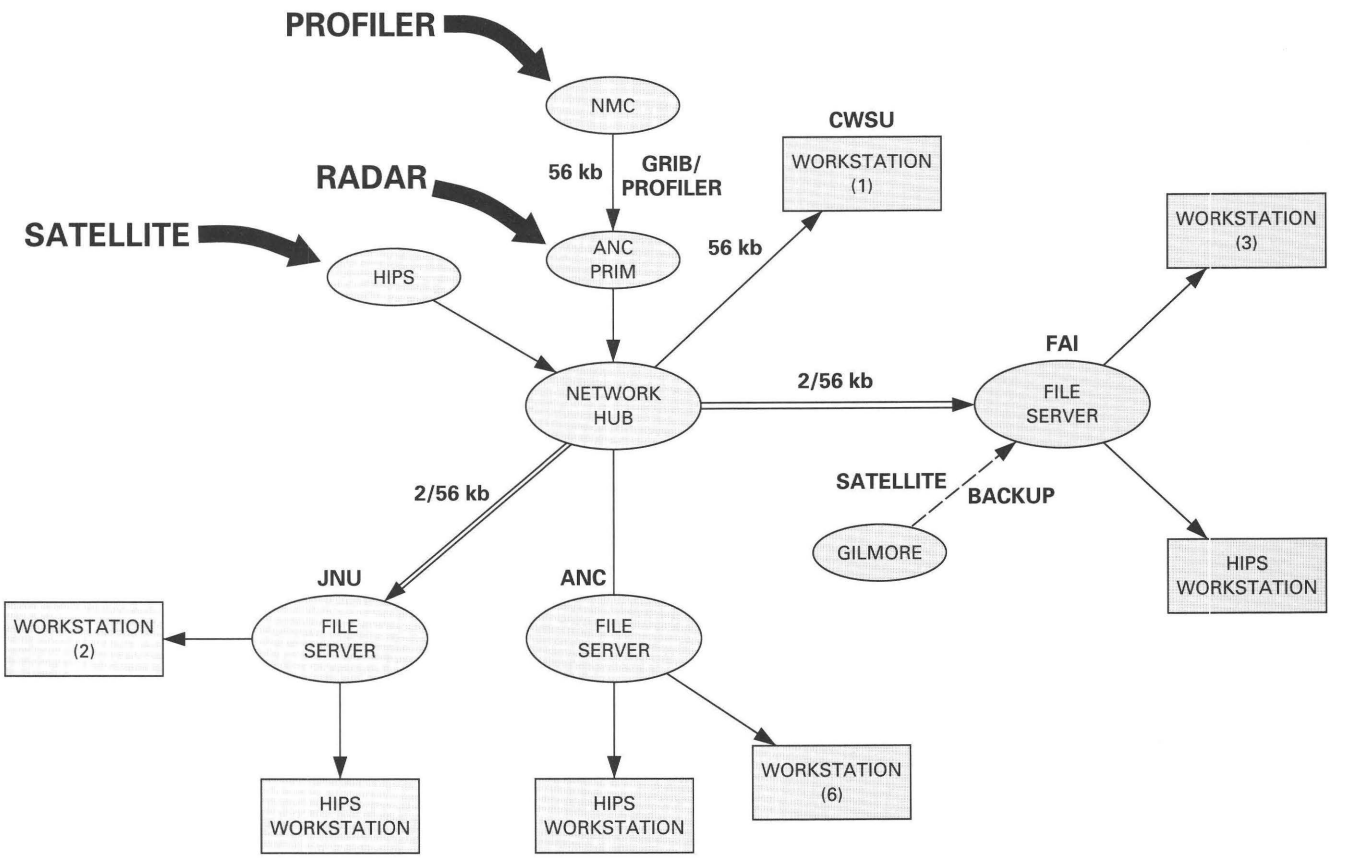


**Figure 5.** Schematic of Alaska region operational computer and communications network (ARO-NET). JNU, Juneau; FAI, Fairbanks; ANC, Anchorage; NMC, National Meteorological Center; CWSU, Central Weather Service Unit; HIPS, high-resolution image-processing system; GRIB, gridded binary format.

to integrate data from a combination of sources. New RISC (reduced instruction set chip) computers are used as application and file servers on the network, and high-speed digital communications lines (56 kb) have been incorporated to handle the increased volume of data.

## INTEGRATED DATABASE

The data from the Alaska volcano debris monitoring system, integrated with other conventional data sources in Alaska, provides the forecaster with a powerful tool to assist in producing effective and timely forecasts. Comparing the integrated database to digital predictive-model output fields and adjusting the model when necessary will provide the forecaster with capabilities never available in field offices in the past. As an example, during eruptive events, forecasters will have available forecaster-selected, multilevel winds valid at 3-hour intervals from the time of initial eruption out to 12 hours, and thereafter every 6 hours out to 72 hours. These constant-height winds will come from gridded, digital-model output and can be displayed as streamlines (wind paths). The forecaster will place observed winds from the profilers, satellites, rawinsonde balloon releases, and other observations over the streamlines. This overlay capability will assist the forecaster to initialize, verify, or adjust the predicted model winds.

## ASH DISPERSION MODEL

The air resources laboratory of NOAA is developing a four-dimensional dispersion model for airborne volcanic debris (Heffter and others, 1990; Stunder and Heffter, this volume). This model will utilize wind data from the technologies described above as well as inputs from NOAA's forecast systems laboratory mesoscale analysis and prediction system (MAPS) and National Meteorological Center (NMC) boundary-layer forecast meteorological fields. Designed to serve aviation and local forecasting, MAPS over Alaska will define the tropospheric and lower stratospheric wind fields every few hours after eruption. Over the longer term, NMC forecast winds will be utilized. In addition, satellite imagery

will provide information on the location and horizontal extent of the ash cloud. The C-band radar will supply initial vertical height and direction of the ash plume at the volcano. The dispersion model will forecast concentrations and deposition of volcanic debris for forecast periods from eruption to up to 48 hours. The model should be ready for operational use in late 1992.

## SUMMARY

The 1989–90 eruptions of Redoubt Volcano have resulted in the establishment of a volcano debris monitoring system to improve the accuracy and timeliness of NWS forecast warnings and advisories to the public during eruptions of Alaskan volcanoes. The long history of frequent eruptions from volcanoes along Cook Inlet clearly indicates that future eruptions are inevitable.

It is anticipated that improved forecast products will have their greatest impact on aviation safety in the Cook Inlet region. Because ash is not possible to detect during flight with present onboard sensors, effective and timely warnings will allow aircraft to avoid ash clouds.

These more accurate forecast products will be in both alphanumeric and graphic form. New products will include a graphical advisory, four-dimensional trajectories, and descriptive statements to the public and emergency-management agencies.

## REFERENCES CITED

Balsley, B.B., and Gage, K. S., 1982, On the use of radars for operational wind profiling: Bulletin of the American Meteorological Society, v. 63, p. 1009–1018.

Brantley, S.R., ed., 1990, The eruption of Redoubt Volcano, Alaska, December 14, 1989–August 31, 1990: U.S. Geological Survey Circular, 1061, 31 p.

Harris, D.M., and Rose, W.I., Jr., 1983, Estimating particle sizes, concentrations, and total mass of ash in volcanic clouds using weather radar: Journal of Geophysical Research, v. 88, p. 969–983.

Heffter, J.L., Stunder, B.B., and Rolph, G.D., 1990, Long-range forecast trajectories of volcanic ash from Redoubt Volcano eruptions: Bulletin American Meteorology Society, v. 71, p. 1731–1738.

Holasek, R.E., and Rose, W. I., Jr., 1991, Anatomy of 1986 Augustine Volcano eruptions as recorded by multispectral image processing of digital AVHRR weather satellite data: Bulletin Volcanology, v. 53, p. 420–435.

Prata, A.J., 1989, Observations of volcanic ash clouds in the 10–12 μm window using AVHRR/2 data: International Journal of Remote Sensing, v. 10, p. 751–761.

Prata, A.J., Wells, J.B., and Ivanac, M.W., 1985, A satellites view of volcanoes on the Lesser Sunda Islands: Weather, v. 40, p. 245–250.

Simkin, T., Siebert, L., McClelland, L., Bridge, D., Newhall, C.G., and Latter, J.H., 1981, Volcanoes of the World: Stroudsburg, Pa., Hutchinson Ross, 242 p.

Thomas, D.R., and Williams, S.R., 1990, Analysis of comparative wind profiler and radiosonde measurements, *in* Proceedings of the 10th Annual Geoscience and Remote Sensing Symposium: New York, v. 1, p. 537–540.

VOLCANIC ASH AND AVIATION SAFETY:
Proceedings of the First International Symposium
on Volcanic Ash and Aviation Safety
U.S. GEOLOGICAL SURVEY BULLETIN 2047

# A STATISTICAL APPROACH TO THE ASSESSMENT OF VOLCANIC HAZARD FOR AIR TRAFFIC: APPLICATION TO VESUVIUS, ITALY

*By* Giovanni Macedonio, P. Papale, M. Teresa Pareschi, Mauro Rosi, *and* Roberto Santacroce

## ABSTRACT

This work uses numerical models that simulate ash dispersion to quantify the hazard to aircraft flying into a volcanic plume. Mt. Vesuvius, Italy, which last erupted in 1944, was chosen as a test case by virtue of the generally good knowledge of its eruption characteristics and because it lies in an area with heavy air traffic. The airport of Napoli-Capodichino is located about 10 km from the crater.

The maximum size of an ash-producing eruption at Vesuvius was estimated on the basis of a behavior model that assumes that eruption size and explosiveness will increase with increasing repose time as a consequence of a roughly constant rate of supply of mafic magma to a shallow magma chamber. A three-dimensional model was used to simulate the transport, diffusion, and fallout of ash and to compute ash concentration in the space surrounding the volcano. The simplifying assumptions about the erupting column structure, the neglect of long-distance effects (e.g., Earth sphericity), and previous numerical simulations indicate a range of applicability of the model from 10 km to 400 km from the vent. The computed spatial distribution of ash allows an estimation of dispersed mass in a given airway and represents a method to evaluate, for an impending eruption and for an assigned wind profile, the minimum safe distance from Vesuvius. The model was used to build a three-dimensional hazard map, which represents a guide for rerouting air traffic in the area.

## INTRODUCTION

Volcanic ash clouds represent a real threat to aviation operations (Scarone, 1987). Ash clouds have caused several near disasters in the past decade: Examples include the 24 June 1982 eruption of Galunggung Volcano in Java, and the 15 December 1989 eruption of Redoubt Volcano in Alaska. In both cases, a Boeing 747 passenger airplane encountered a cloud of volcanic ash produced by an eruption that occurred several hours earlier. Ash ingestion caused all four engines to shut down, and engine restart was not possible until the aircraft descended out of the ash cloud. Both aircraft suffered extensive damage to their engines and exterior surfaces (Przedpelski and Casadevall, this volume).

Other volcanoes that have had an impact on flight operations are St. Augustine, Alaska (Kienle, this volume); Etna, Italy; Mount St. Helens, Washington; several Japanese volcanoes (Onodera and Kamo, this volume); Pinatubo, Philippines (Casadevall and De Los Reyes, 1991); and several volcanoes in Indonesia. In this report, attention is focused on Vesuvius Volcano in Italy, but the approach can be used for other case studies.

Vesuvius was chosen as a test case owing to the generally good knowledge of its eruption characteristics and because it lies in an area with heavy air traffic. The volcano erupted most recently in 1944. The airport of Napoli-Capodichino is located about 10 km from the crater and the radio beacon of the Sorrento Peninsula, an important air node, is about 25 km from the volcano (fig. 1).

## ASH DISPERSION

When a gas-pyroclast mixture erupts from a volcano to form a convective eruption column, the distribution of ash particles during fallout is controlled by the dynamics of the eruptive column itself and by the wind regime (Self and Walker, this volume; Sparks and others, this volume). The former controls the proximal distribution of particles, while the direction and speed of the wind determine distal ash distribution. To simulate the dynamics of falling particles in the air in this wind-controlled region, a continuity equation has been used for each settling velocity class, $i$ (Armienti and others, 1988; Macedonio and others, 1988):

$$\frac{\partial C_i}{\partial t} + U_x\frac{\partial C_i}{\partial x} + U_y\frac{\partial C_i}{\partial y} + \frac{\partial (Vs_i C_i)}{\partial z} =$$

$$K_x\frac{\partial^2 C_i}{\partial x^2} + K_y\frac{\partial^2 C_i}{\partial y^2} + K_z\frac{\partial^2 C_i}{\partial z^2} + S_i \qquad (1)$$

where

$C_i(x,y,z,t)$ is the concentration of the particles with settling velocity class $i$,

$U_x$ and $U_y$ are horizontal components of wind,

$Vs_i$ is the settling velocity of class $i$,

$K_x$, $K_y$, and $K_z$ are atmospheric diffusion coefficients, and

$S_i$ is the source term (the particles of settling velocity class $i$ that leave the convective column per unit time).

The above continuity equation was solved by a numerical scheme that accounts for complex wind data and mass eruption rates.

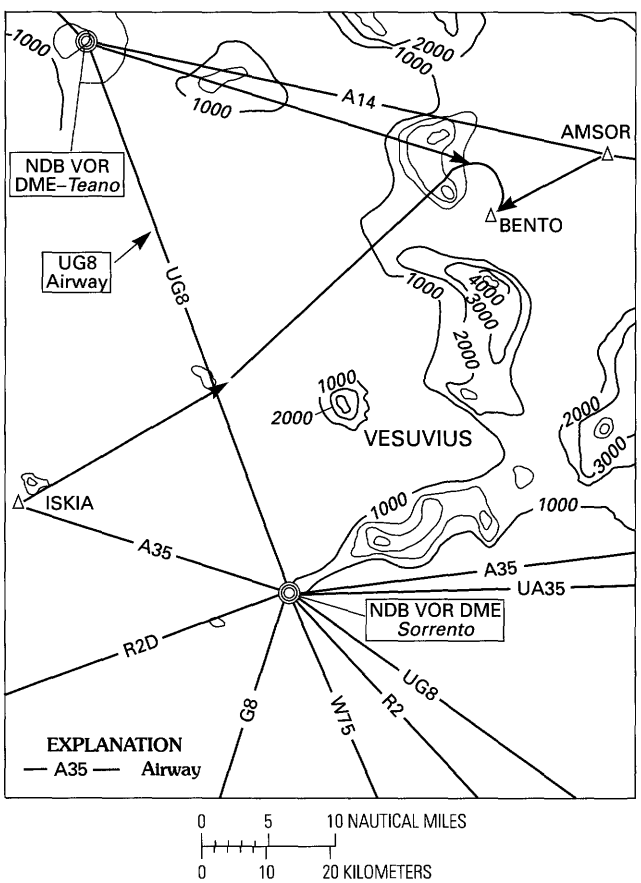


**Figure 1.** Air routes in the Vesuvius area. Terrain elevation shown by solid-line contours in 1,000-m intervals. Solid straight lines indicate airways. VOR DME, a type of airway navigational aid.

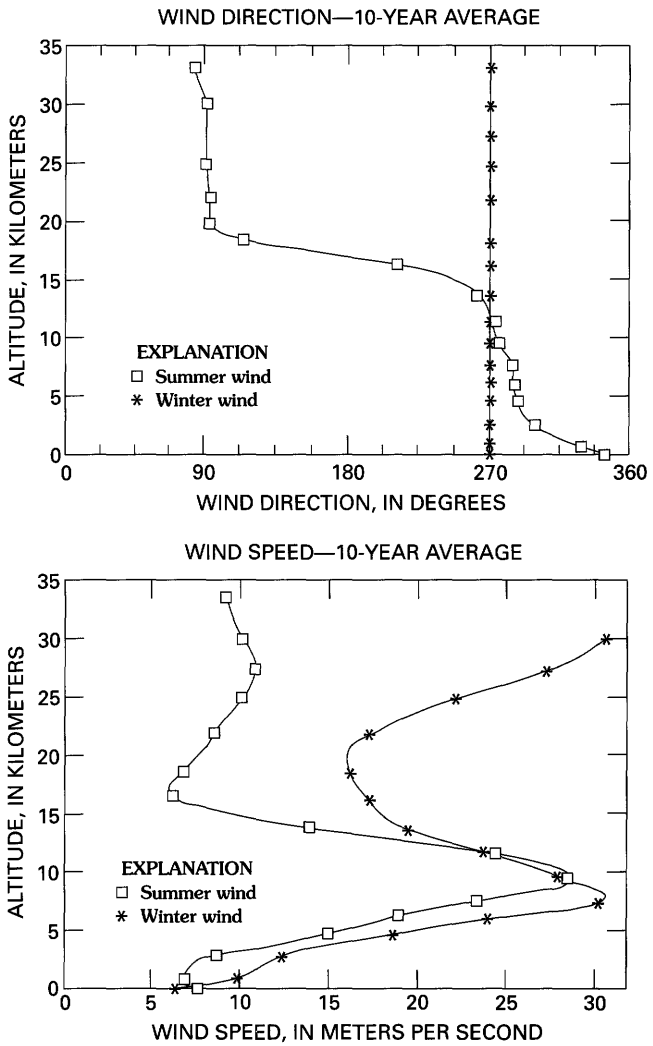


**Figure 2.** Ten-year-average mean wind directions and mean wind speeds as a function of altitude. Recorded at Brindisi, Italy, during summer and autumn-winter-spring (shown in figure as "winter wind"). After Cornell and others (1983).

For the case of Vesuvius, information concerning the wind has been derived from a record of observations by the Servizio Meteorologico dell'Aeronautica Militare Italiana over a period of 10 years at Brindisi, located 300 km east of the volcano. These data allow the recognition of two different seasonal wind profiles: a summer field and an autumn-winter-spring field (Cornell and others, 1983) (fig. 2).

The horizontal and vertical diffusion coefficients depend on the temporal and spatial scale of the phenomena. For example, if the ash particles are settling from great heights and with low velocities, turbulent eddies of increasing size have to be considered in the model, with a consequent effective increase of the diffusion coefficients. Mean values of 2,000–3,000 $m^2/s$ for horizontal diffusion coefficients are expected near Vesuvius. These values have been

empirically derived by the simulations of the 79 A.D. Vesuvius eruption (Macedonio and others, 1987, 1988).

For the model eruption treated in this report, the total eruptible mass was estimated to be $2\times10^{11}$ kg; the mass eruption rate was estimated at $9.3\times10^{6}$ kg/s for an eruption lasting 6 hours (Macedonio and others, 1990). Using the model of Wilson and Walker (1987), a column height of 13 km is calculated. The grain size of the pyroclastic particles have been assumed to be similar to that of the Plinian phase of the eruption of Vesuvius in 79 A.D., and the vertical density distribution of ash in the ascending column has been derived by the theoretical model of Suzuki (1983). The settling velocity has been derived from shape and density information of pyroclasts using the experimental data from Wilson and Huang (1979). These data have been fitted by a function $C_D = a/R + b$, which gives the aerodynamic coefficient, $C_D$, as function of the Reynolds number, R (fig. 3).

The pyroclastic material was grouped into nine classes of settling velocity, *Vs* (1 to 9 m/s). In order to reduce computational time, particles with $Vs < 1$ m/s were grouped into class 1 and those with $Vs > 9$ m/s were grouped into class 9. This assumption does not involve dramatic approximations: in fact, with regard to fast-falling particles, figure 4 shows that only about 10 weight percent of the erupted mass has a settling velocity greater than 9 m/s. With regard to the slow-falling particles, about 16 weight percent of the total mass has settling velocity lower than 1 m/s. However, due to electrostatic attraction, fine volcanic ash commonly tends to aggregate into clusters (Sorem, 1982; Gilbert and others, 1991), with typical settling velocity in the range 0.3–1.0 m/s. In addition, surface tension of condensed water that envelopes ash particles may also play a role in forming relatively large aggregates at the expense of very fine grained material. Very slow settling velocities are, therefore, scarcely represented (Carey and Sigurdsson, 1982; Armienti and others, 1988).

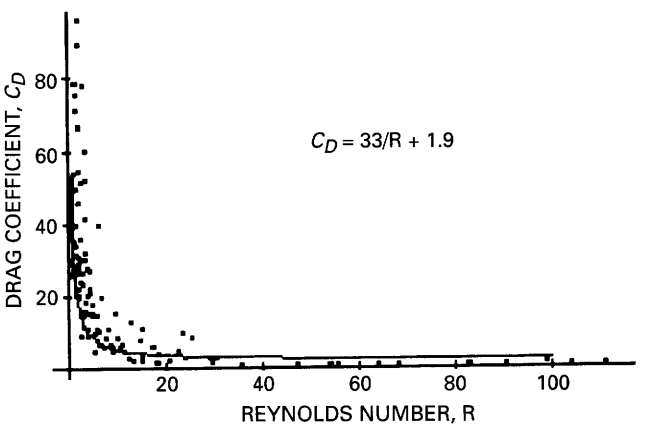


**Figure 3.** Drag coefficient ($C_D$) versus Reynolds number (R); interpolating curve shown. Data from Wilson and Huang (1979).

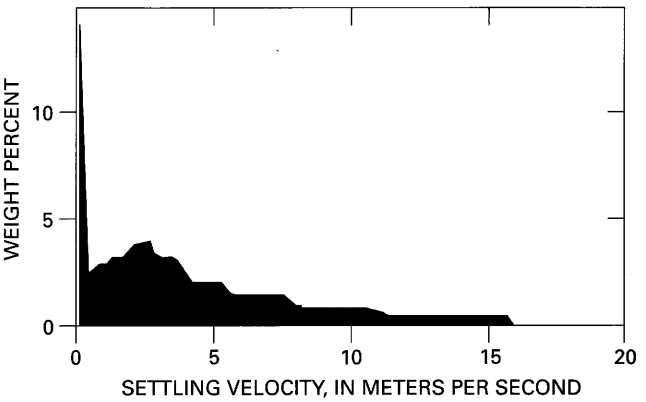


**Figure 4.** Settling velocity, *Vs*, plotted against the distribution of particles (in weight percent) for expected eruption.

## NUMERICAL RESULTS

From an analysis of the numerical solutions of equation 1, utilizing the input data described above, it results that, at a given point in space, the concentration, $C_i$, of the particles belonging to settling velocity class *i* rises from zero to a constant value in a "stabilization time," $Ts_i$, which varies from point to point. Figure 5 shows the stabilization times for the total mass (concentration integrated over the spatial domain) dispersed into the atmosphere for three classes of settling velocity. The faster the falling velocity of the particles, the quicker the stabilization time. Because the duration of the model eruption is finite (in this example 6 hours), the mass in the space decreases to zero after a certain time. The data of figure 5 refers to the summer mean wind profile (Cornell and others, 1983).

## APPLICATIONS ON AIRWAY UG8

Several simulations were performed to investigate the volcanic hazard for an aircraft traveling along the portion of airway UG8 between Sorrento and Teano. This route passes 20 km west of Vesuvius and carries heavy air traffic (fig. 1). For both dominant summer and winter winds, this route is located upwind with respect to Vesuvius. We have taken into consideration an aircraft traveling at an altitude of 11 km with a velocity of 250 m/s. At this altitude, the differences between the velocities of the mean summer and autumn-winter-spring wind profiles are small (< 10 percent, fig. 2). To evaluate the mass of ash particles that may enter the jet engines, an engine air flux of 300 kg/s/m$^2$) was assumed.

Figure 6*A* shows the concentration of ash encountered by aircraft flying northward along the UG8 airway, leaving Sorrento at different times after the beginning of

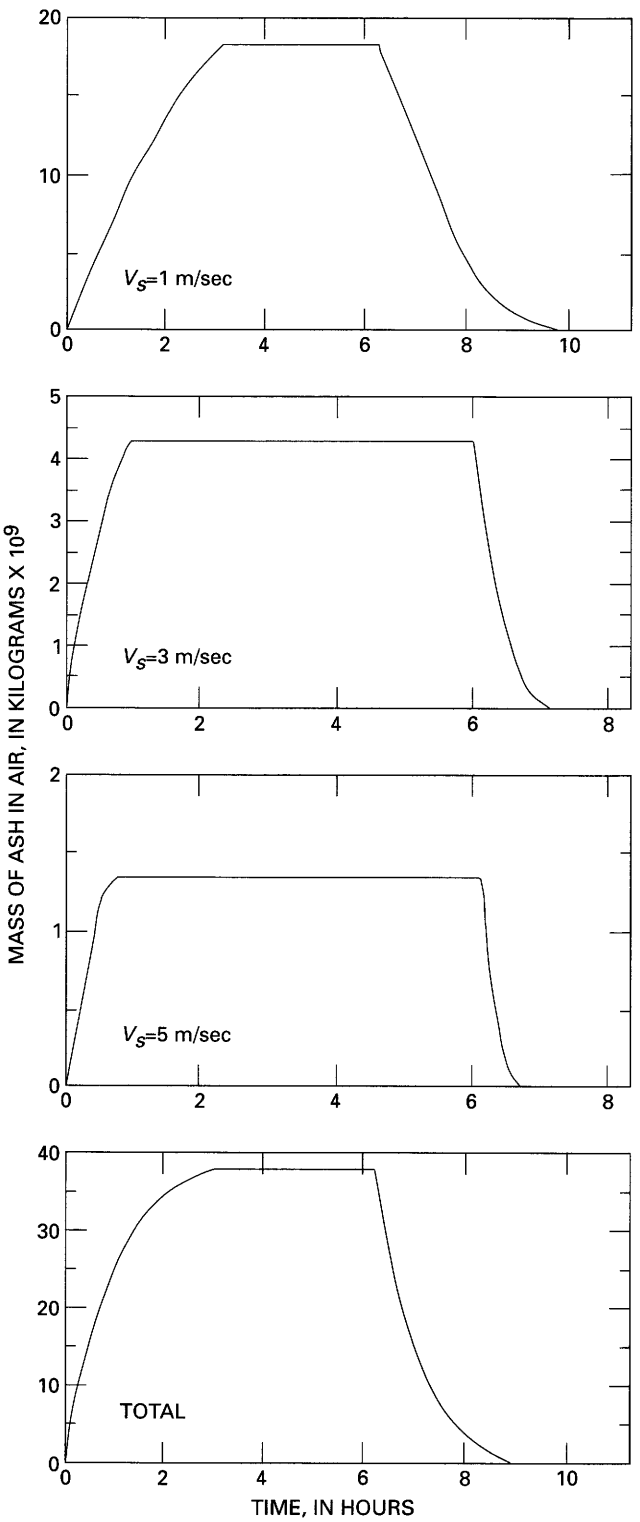


**Figure 5.** Stabilization times (horizontal axis) for the total mass (concentration integrated over the spatial domain) dispersed into the atmosphere for three classes of settling velocity (1 m/s, 3 m/s, 5 m/s). The faster the falling velocity of the particles, the quicker the stabilization time. Because the duration of the model eruption is 6 hours, the mass in the airspace decreases to zero after a certain time. The simulation was carried out using the summer mean wind profile from Cornell and others (1983).

the eruption. Figures 6*B* and 6*C* show the ash mass flux and the mass of ash entering a jet engine per unit inflow area. Figures 7*A–C* show concentration, mass flux, and collected mass (per unit inflow area of the engine) in the same conditions as in figure 6, but with a wind profile rotated 180° (here referred to as the downwind case) to account for the "maximum hazard" along the UG8 route. In the "upwind" case, a low hazard exists for the UG8 airway. In fact, after the plume concentration has reached its maximum ($T > Ts$) the maximum ash concentration along the airway is $1.5\times10^{-6}$ g/m$^3$, which results in a mass flux within the engine of about $0.5\times10^{-3}$ g/s/m$^2$; the mass collected by each engine is about 0.01 g/m$^2$. On the other hand, a very high hazard exists in the case of westward winds (the "downwind" case). For an aircraft leaving Sorrento in steady-state conditions ($T > Ts$), the mass of ash collected per meter squared is more than 30 kg for the flight time between Sorrento and Teano.

## HAZARD MAP

A hazard map for the air traffic in the Vesuvius area has been derived by using the expected eruption rate determined in previous works (Santacroce, 1983; Macedonio and others, 1990). The map was constructed by carrying out about 3,000 different simulations, one for each wind profile recorded during a period of 10 years, and then computing the probability that the spatial concentration at a given point is greater than a given threshold. To reduce computational time, vertical diffusion was neglected and only the steady-state solution of the continuity equation was considered.

Figures 8*A–C* are hazard maps for three different ash-concentration-threshold values: $10^{-5}$, $10^{-4}$, and $10^{-3}$ kg/m$^3$. These values correspond, for the portion of the UG8 route affected by dispersed ash, to masses entering an engine of the order of 0.1–1.0 kg/m$^2$ of engine inlet cross-sectional area for an aircraft flying at 250 m/s. The areas of equal probability, referring to spatial concentration higher than the given threshold, widen toward the ground as a consequence of the longer time available for dispersion processes.

## CONCLUSIONS

A diffusive-advective model was used to simulate the dispersion of a volcanic plume in the range from 10 km to 400 km from Mt. Vesuvius. The spatial concentration evaluated by the model permits estimation of the hazard from volcanic ash for aircraft flying in the area. This approach may be applied to other volcanoes, assuming that information on wind velocities, atmospheric diffusion coefficients, mass eruption rate, and particle settling velocity distribution are known. Given the size of the eruption (total erupted mass, column height, settling velocity distribution of particles,

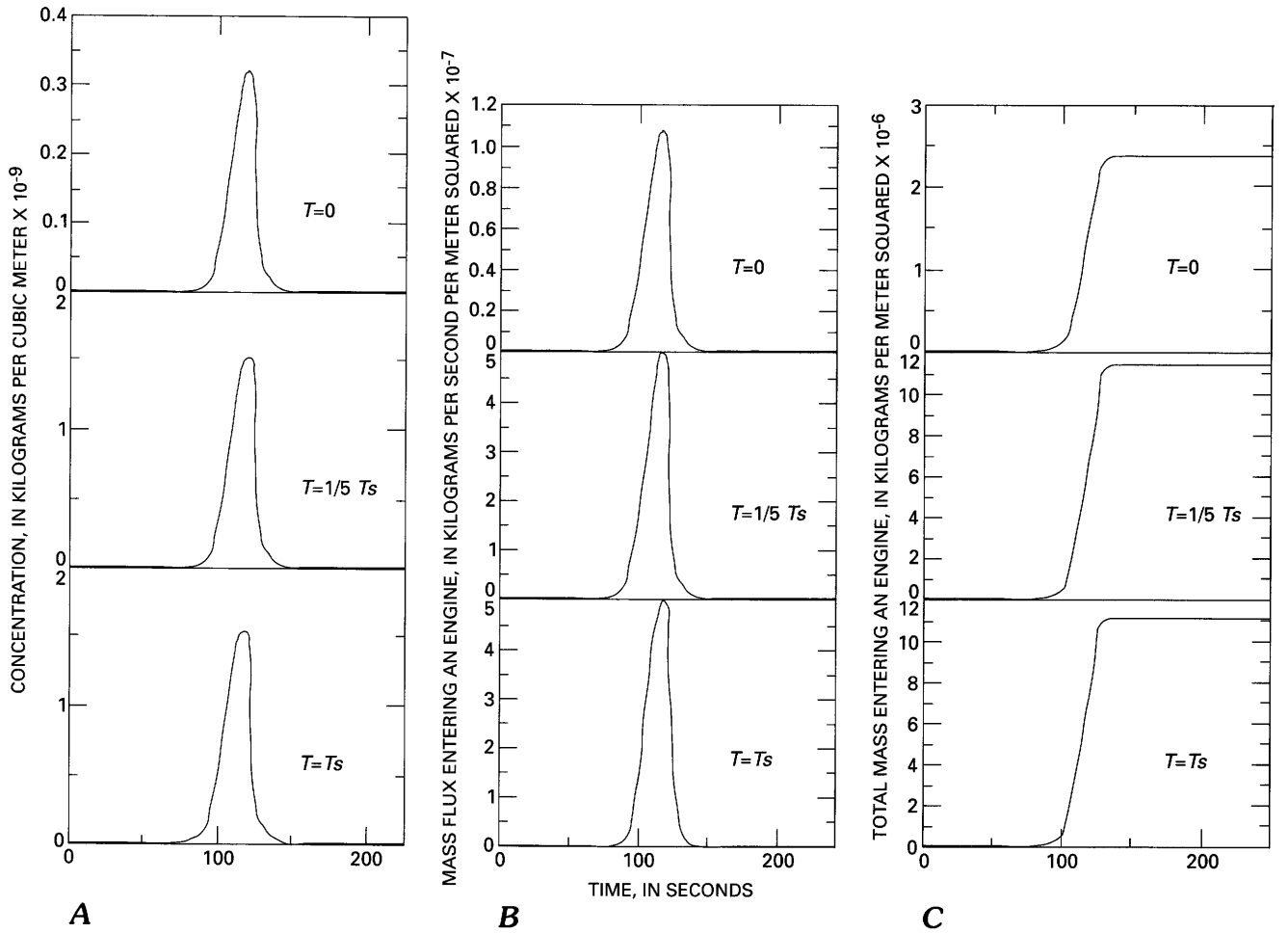


**Figure 6.** *A*, Ash concentration encountered by an aircraft flying northward along airway UG8 at an altitude of 11 km leaving Sorrento at different times, *T*, after the beginning of the eruption (upwind case). *Ts*, "stabilization time" for lower settling velocity class. Times shown are: $T = 0$ (onset of eruption), $T = 1/5Ts$, and $T = Ts$. *B*, Mass flux encountered by aircraft described in *A* (upwind case). *C*, Total mass of ash entering an engine (upwind case).

etc.) and a wind profile, the cumulative and instantaneous mass of volcanic ash can be computed for a given air-traffic route. This makes it possible to estimate the minimum safe flying distance from a volcano. Given the wind regimes in the area of interest, a hazard map can be produced and used to construct air-traffic maps in active volcanic areas.

## ACKNOWLEDGMENTS

The authors wish to thank the Aeronautica Militare for support in drawing the map of air routes in the Vesuvius area and the National Group of Volcanology (GNV) for financial support.

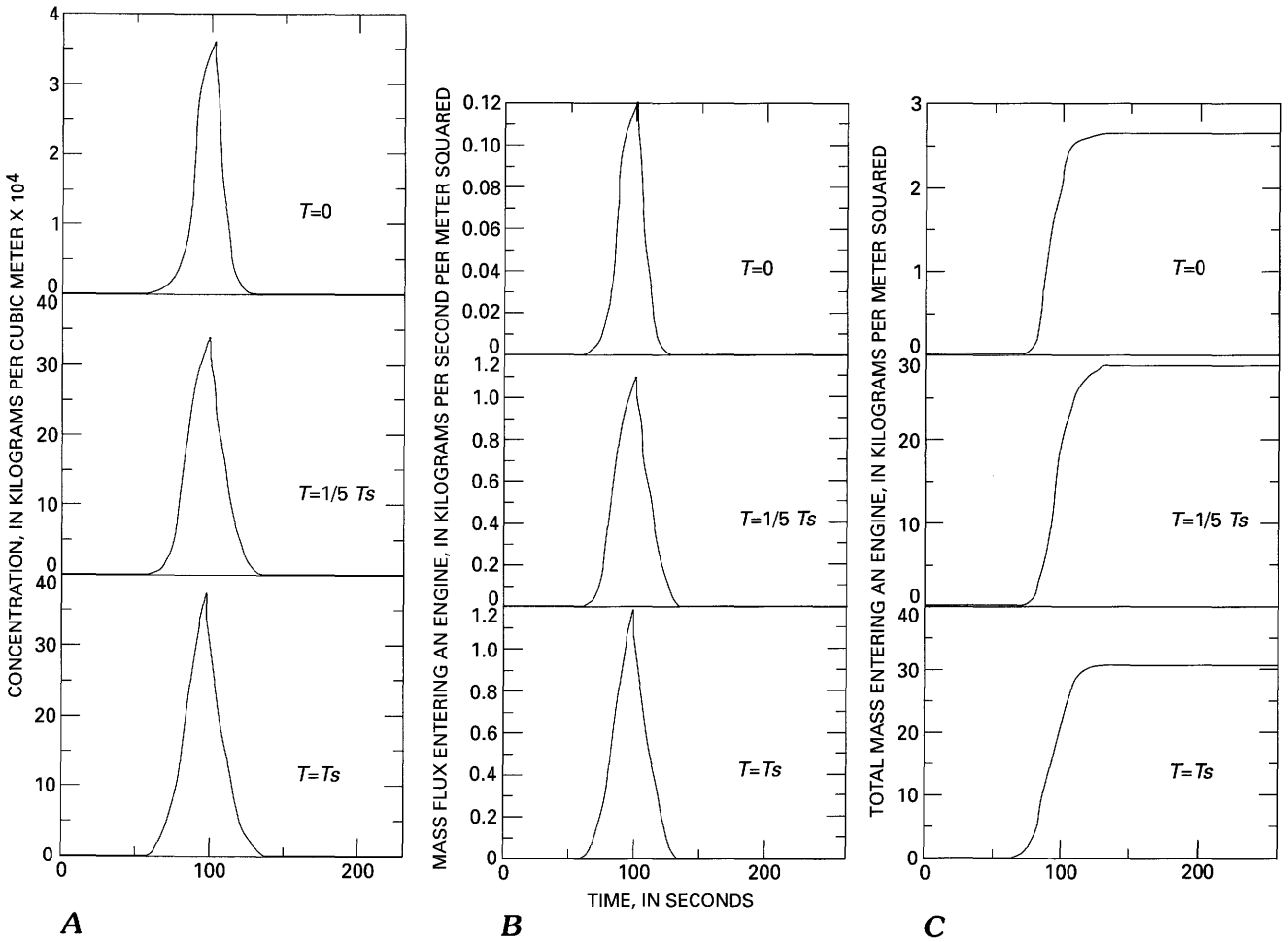


**Figure 7.** *A*, Ash concentration encountered by an aircraft flying northward along airway UG8 at an altitude of 11 km leaving Sorrento at different times, *T*, after the beginning of the eruption (wind field is rotated 180° from that shown in figure 6 to represent the maximum hazard (downwind case)). *Ts*, "stabilization time" for lower settling velocity class. Times shown are: $T = 0$ (onset of eruption), $T = 1/5Ts$, and $T = Ts$. *B*, Mass flux encountered by aircraft described in *A* (downwind case). *C*, Total mass of ash entering an engine (downwind case).

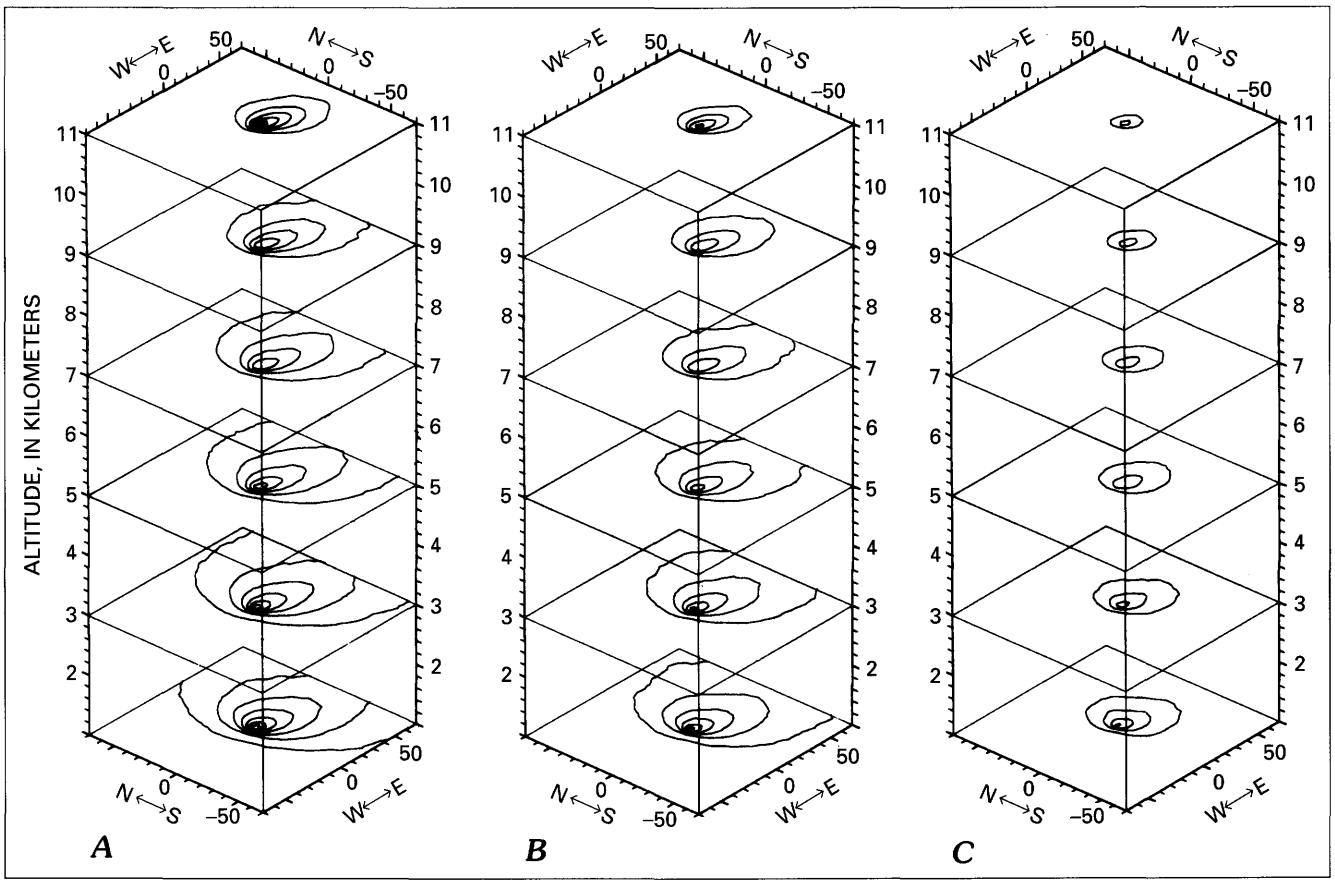


**Figure 8.** Hazard maps that show a contouring of the probability (between 0 and 100 percent) that the ash concentration at a given point be above a fixed threshold value. These maps are constructed by considering about 3,000 different simulations, one for each wind profile recorded during a period of 10 years. Results for three different threshold values are shown: *A*, $10^{-5}$ kg/m$^3$; *B*, $10^{-4}$ kg/m$^3$; *C*, $10^{-3}$ kg/m$^3$. These values result in cumulative masses of the order of 0.1–1.0 kg/m$^2$ entering an engine of a jet traveling at 250 m/s along airway UG8. The outer contour in each horizontal plane represents a probability of 10 percent. Each successive contour refers to an increase of 10 percent in the probability value. Scales on horizontal planes in kilometers.

## REFERENCES CITED

Armienti, P., Macedonio, G., and Pareschi, M.T., 1988, A numerical model for simulation of tephra transport and deposition: Applications to May 18, 1980, Mount St. Helens eruption: Journal of Geophysical Research, v. 93, no. B6, p. 6463–6476.

Carey S.N., and Sigurdsson H., 1982, Influence of particle aggregation on deposition of distal tephra from the May 18, 1980, eruption of Mount St. Helens volcano: Journal of Geophysical Research., v. 87, p. 7061–7072.

Casadevall, T.J., and De Los Reyes, P.J., 1991, Impact of June 1991 Pinatubo eruptions on aircraft operations in the western Pacific and Southeast Asia [abs.]: Eos, Transactions, American Geophysical Union, v. 72, no. 44 [Supplement], p. 95.

Cornell, W., Carey, S.N., and Sigurdsson, H., 1983, Computer simulation of transport and deposition of the Campanian Y-5 ash: Journal of Volcanology and Geothermal Research, v. 17, p. 89–109.

Gilbert, J.S., Lane, S.J., Sparks, R.S.J., and Koyaguchi T., 1991, Charge measurements on particle fallout from a volcanic plume: Nature, v. 349, p. 598–600.

Macedonio, G., Pareschi, M.T., and Santacroce, R., 1987, Valutazione e controllo di alcuni parametri fisici agenti durante la fase Pliniana dell'eruzione del Vesuvio del 79 D.C [in Italian]: Rome, Bulletin of the National Group of Volcanology, p. 445–466.

———1988, A numerical simulation of the Plinian fall phase of 79 A.D. eruption of Vesuvius: Journal of Geophysical Research., v. 93, p. 14817–14827.

———1990, Renewal of explosive activity at Vesuvius: Models for the expected tephra fallout: Journal of Volcanology and Geothermal Research, v. 40, p. 327–342.

Santacroce, R., 1983, A general model for the behavior of the Somma-Vesuvius volcanic complex: Journal of Volcanology and Geothermal Research, v. 17, p. 237–248.

Scarone, H., 1987, Volcanic ash clouds—A continuing threat to international aviation: Earthquakes and Volcanoes, v. 19, p. 65–73.

Sorem, R.K., 1982, Volcanic ash clusters: Tephra rafts and scavengers: Journal of Volcanology and Geothermal Research, v. 13, p. 63–71.

Suzuki, T., 1983, A theoretical model for dispersion of tephra, *in* Shimozuru, D., and Yokoyama, I., eds., Arc Volcanism: Physics and Tectonics: Tokyo, Terra Scientific Publishing Co., p. 93–113.

Wilson, L., and Huang, T.C., 1979, The influence of shape on the atmospheric settling velocity of volcanic ash particles: Earth Planetary Science Letters, v. 44, p. 311–324.

Wilson, L., and Walker, G.P.L., 1987, Explosive volcanic eruptions VI: Ejecta dispersal in Plinian eruptions: The control of eruption conditions and atmospheric properties: Geophysical Journal of the Royal Astronomical Society, v. 89, p. 657–679.

VOLCANIC ASH AND AVIATION SAFETY:
Proceedings of the First International Symposium
on Volcanic Ash and Aviation Safety
U.S. GEOLOGICAL SURVEY BULLETIN 2047

# USING A PERSONAL COMPUTER TO OBTAIN PREDICTED PLUME TRAJECTORIES DURING THE 1989–90 ERUPTION OF REDOUBT VOLCANO, ALASKA

*By* Thomas L. Murray, Craig I. Bauer, *and* John F. Paskievitch

## ABSTRACT

The Alaska Volcano Observatory (AVO) and the Anchorage Weather Service Forecast Office (WSFO) obtain predicted plume trajectories daily for Redoubt Volcano, Alaska. A model developed by the National Oceanic and Atmospheric Administration (NOAA) Air Resource Laboratory calculates predicted plume trajectories. The model, running on NOAA's NAS/9000 mainframe computer in Suitland, Md., uses forecast wind fields obtained from the NOAA National Meteorological Center. The model uses measured and forecast winds to predict the path of a weightless particle released at various pressure-altitudes above a specified location. The paths indicate the general direction and speed that ash from an eruption at that location will travel.

In response to the 1989–90 Redoubt eruption, we programmed an IBM-XT-style personal computer to automatically dial the NAS/9000 mainframe computer and obtain the predicted trajectories. Twice daily, after the predicted wind fields are updated, AVO and WSFO can easily collect and plot the trajectories predicted for the next 72 hours. Thus, the trajectories are immediately available in the event an eruption should occur. The predicted trajectories are plotted on a map of Alaska, showing the predicted location of the ash plume at 3-hour intervals for different altitudes between 5,000 and 53,000 ft. The plots are easily telefaxed to interested parties. The program has been modified to enable the user to obtain predicted plume trajectories for other U.S. volcanoes.

## INTRODUCTION

Volcanic ash ejected into the atmosphere can cause severe problems to airplanes and to municipal and industrial facilities, as well as to people on the ground downwind from the volcano. Knowing where ash will travel is vital to mitigating its effects. If notified in time, people in the path of the ashfall can take precautionary measures as complex as shutting down portions of a power facility or as simple as canceling a dinner date. Conversely, in areas unlikely to be affected by ashfall, industry can avoid wasting resources in preparation for ash that is not traveling in their direction. In this report, we describe a method to routinely acquire predicted wind speeds and directions (trajectories) at various pressure-altitudes and to plot and display the data in a simple, easy-to-distribute format. The predicted plume trajectories currently provide the only method that predicts, before an eruption, where ash will be blown (as opposed to tracking already-erupted ash). AVO and WSFO took advantage of this capability and informed other agencies daily as to where ash from Redoubt would go if the volcano were to erupt. In the event of an eruption, the predicted plume trajectory, having been plotted earlier, is ready for immediate use, thereby saving valuable time.

During the Redoubt eruption, plots were especially useful to the aviation industry. They were sent daily to Anchorage International Airport authorities, who then distributed them to the airlines, many of which required their flight crews to use them in flight planning (Casadevall, in press).

## DESCRIPTION OF PREDICTED PLUME TRAJECTORIES

A computer model, developed by NOAA's Air Resource Laboratory (ARL), provides predicted plume trajectories based on forecast wind fields. The wind fields are calculated twice daily by the National Weather Service (NWS) from observations taken at 00:00 and 12:00 Greenwich Mean Time (GMT) (Heffter and others, 1990). Using the latitude and longitude of the volcano and the time of the hypothetical eruption, the model predicts the locations of dimensionless, weightless particles at 3-hour increments

after they are released into the atmosphere at various pressure-altitudes above the volcano. The model ignores effects from gravity and dispersion. Unlike volcanic ash, the model's ideal particles never fall to Earth, but remain at the pressure-altitude at which they were released forever.

The model accepts times for hypothetical eruptions up to 48 hours into the future in 3-hour increments. AVO can always have the latest predicted trajectories by obtaining the predicted trajectories from the NOAA computer twice daily after the latest weather observations are processed. Owing to the time required to process weather observations and calculate the predicted wind fields, the latest predictions are typically available about 3 hours after the actual measurements, at 03:00 and 15:00 GMT (or 18:00 and 06:00 AST).

## OBTAINING PREDICTED PLUME TRAJECTORIES

Predicted plume trajectory plots were first used to predict trajectories of volcanic ash during the 1980 eruptions of Mount St. Helens, Washington (Miller and others, 1981; Smith, 1980). At that time, the technique to acquire trajectories was time consuming, requiring the full attention of a person for an hour or more (E. Brown, oral commun., 1991). As the level of activity at Mount St. Helens declined, the U.S. Geological Survey discontinued obtaining plume trajectory data.

In 1988, NOAA signed a memorandum of understanding with the Federal Aviation Administration (FAA) to provide the FAA with predicted plume trajectories (Heffter and others, 1990). During the 1989–90 eruptions of Redoubt Volcano, NOAA provided trajectory information to the FAA within 1 hour of NOAA's notification of the eruption and typically within 3 hours of the actual eruption (Heffter and others, 1990). Because an ash plume can move hundreds of kilometers during a 3-hour delay, AVO and the Anchorage WSFO felt that they needed trajectory information more quickly in order to issue timely warnings. Ideally, the trajectory information would be available before an eruption. This would allow AVO and WSFO to concentrate on the myriad other tasks involved in monitoring an eruption (data analysis, notifying interested agencies, answering media inquiries, etc.) and would avoid using personnel or phone and computer resources during an eruption to obtain the information. It would also allow AVO to include the information in daily updates sent to various public agencies and other users, including the aviation community, that could be affected by ashfall. Finally, it enabled AVO and WSFO to have the information ready for immediate distribution should an eruption occur.

In order to acquire the plume trajectories daily, even when there was little chance of an eruption, the process had to be simplified, or, as was the case with Mount St. Helens, it would fall into disuse. We were able to do this by using computer hardware and software unavailable in 1980. The necessary equipment consists of an IBM XT (or compatible) personal computer, a 1,200-baud Hayes-compatible modem, a printer, the software package PROCOMM Plus (for communication with the NOAA computer), and Geograf Utilities (for the screen and printer graphics drivers). Users initiate the program with a few keystrokes and are prompted to answer a few questions. Then the program dials the NOAA NAS/9000 computer in Suitland, Md., runs the plume trajectory program for various hypothetical eruption times and pressure-altitudes, logs the data on the XT, and finally produces plots of the paths of the predicted plume trajectories on the user's printer. The entire process takes less than 20 minutes.

## PLOTS OF PROJECTED PLUME TRAJECTORIES

Following the format of Smith (1980), trajectories at different pressure-altitudes for a single hypothetical eruption time are plotted as a map on a single 8½-by-11-inch sheet. The map shows the paths traveled by ideal particles released above the volcano at different pressure-altitudes at the hypothetical eruption time indicated on the plot (figs. 1 and 2). Symbols along the paths indicate positions of the particles at 3-hour time intervals. Stronger winds will blow the particles faster along their paths, and the symbols will be spaced correspondingly farther apart than for light winds. By plotting

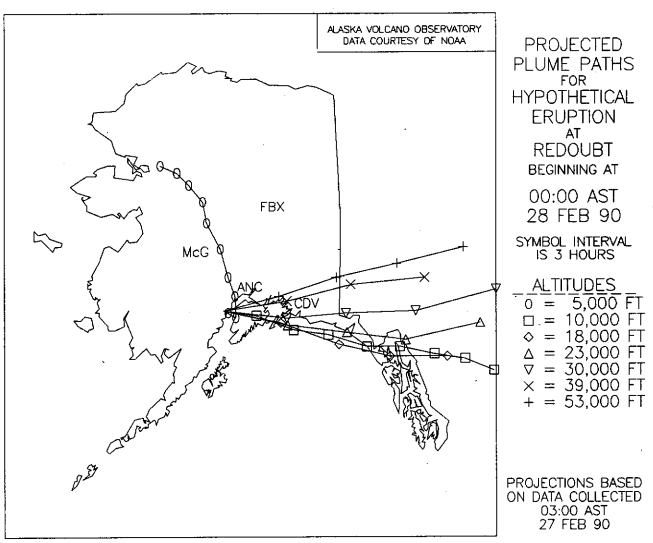


**Figure 1.** Example of predicted plume trajectories plotted over the State of Alaska for a hypothetical eruption beginning at 00:00 Alaska Standard Time (AST), February 28, 1990. Cordova (CDV), McGrath (McG), Fairbanks (FBX), and Anchorage (ANC) are approximately located. Trajectories for ideal particles released at various pressure-altitudes above Redoubt Volcano are plotted. The location of the symbols on the trajectory paths indicate the positions of the ideal particles at 3-hour intervals after eruption time.

all trajectories on a single map, the user can quickly visualize where the ash is likely to go without paging back and forth between seven plots of trajectories at individual altitudes. The data are plotted on maps of two different scales. One covers Alaska (fig. 1), and the second covers Cook Inlet and surrounding areas (fig. 2).

## USE OF PREDICTED PLUME TRAJECTORIES

Users of the projected plume trajectories must understand that the trajectories give only a general indication of where ash will travel. The accuracy of the trajectories is limited by the accuracy of the predicted winds and the model's assumption of a weightless, dimensionless particle. For instance, the plots always show a travel path extending for 24 or more hours for an ideal particle. Users need to be informed that, although they may lie in the path of the ideal particle as indicated by the plot, gravity will likely cause the actual, non-ideal ash to settle before it reaches them.

The model also does not consider the effect of dispersion of the ash as it travels along the trajectory. Users should not be fooled into thinking that they will not be affected by ash simply because they are not located directly on the line predicted by the model. Until current research (Sparks and others, this volume; Stunder and Heffter, this volume; Tanaka, this volume) is incorporated into the model, we suggest qualitatively defining the area that may be affected by ash as an arc of ±30° along the trajectory as it travels away from the volcano. This would also allow for inaccuracies in the predicted trajectory.

For small to moderate size eruptions, such as those at Redoubt, the major factor in the path's accuracy is the accuracy of the predicted winds. Rather than focusing attention on one plot at a given altitude, users should look through the suite of plots for each day to develop an idea of the stability of the weather system. Stable systems will generally have all trajectories for all altitudes, except perhaps 5,000 ft, traveling in about the same direction. The effects of the 5,000-ft trajectory are usually ignored both because the erupting vents at most volcanoes are usually above 5,000 ft in altitude and because they usually eject ash into higher altitudes where the winds are generally stronger. For stable systems, where the winds above 10,000 ft blow in the same general direction throughout the day, we feel the accuracy of the predicted winds to be quite good. Such was the case for the February 24, 1990, eruption of Redoubt (fig. 3). On days when the winds change or even reverse direction, it may be difficult to predict with any certainty where ash will travel (fig. 4). It is best to err on the side of caution during such times. Heffter and others (1990) provide a more detailed analysis of the accuracies of the trajectories.

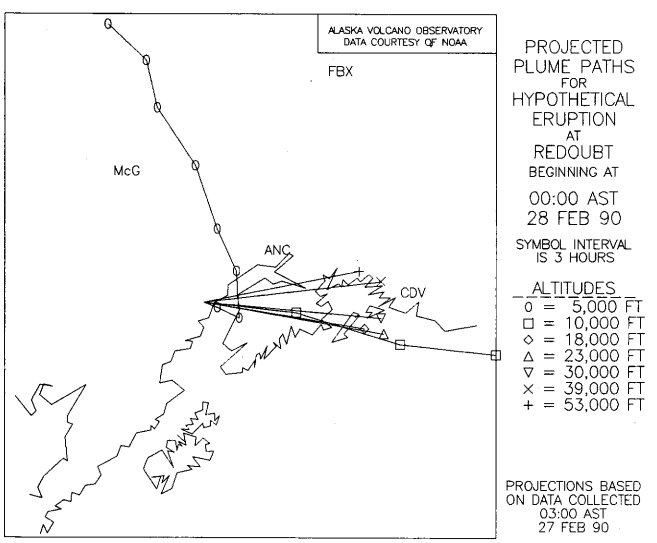


**Figure 2.** Example of predicted plume trajectories in figure 1 plotted over a map of Cook Inlet and surrounding areas for a hypothetical eruption beginning at 00:00 Alaska Standard Time (AST), February 28, 1990. Cordova (CDV), McGrath (McG), Fairbanks (FBX) and Anchorage (ANC) are approximately located.

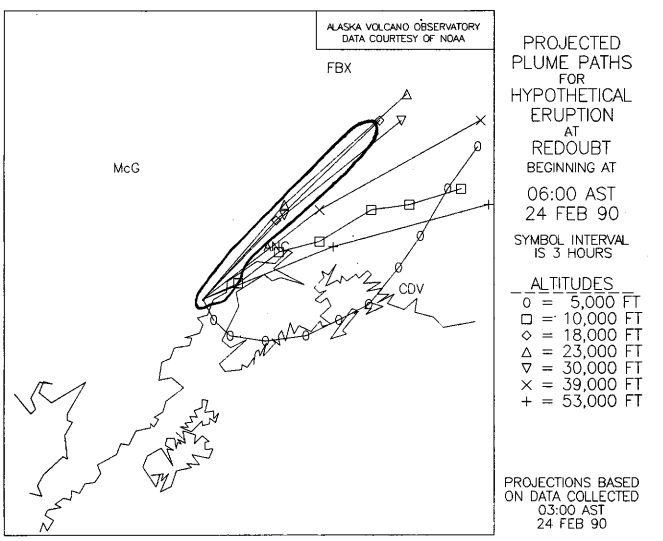


**Figure 3.** Predicted plume trajectories for the February 24, 1990, eruption of Redoubt Volcano with the actual ground deposition (heavy line) outlined (from Scott and McGimsey, in press). Because the eruption plume reached an altitude of only 28,000 ft (Brantley, 1990), the winds at 39,000 and 53,000 ft did not affect ash deposition. Note that the spacing between symbols for the winds at 18,000, 23,000, and 30,000 ft are more than twice that for winds at 5,000 and 10,000 ft—this indicates that the wind speed at higher altitudes is more than twice that at lower altitudes. For this reason, the pattern of ground deposition was influenced predominantly by the winds at 18,000, 23,000, and 30,000 ft. Cordova (CDV), McGrath (McG), Fairbanks (FBX) and Anchorage (ANC) are approximately located.

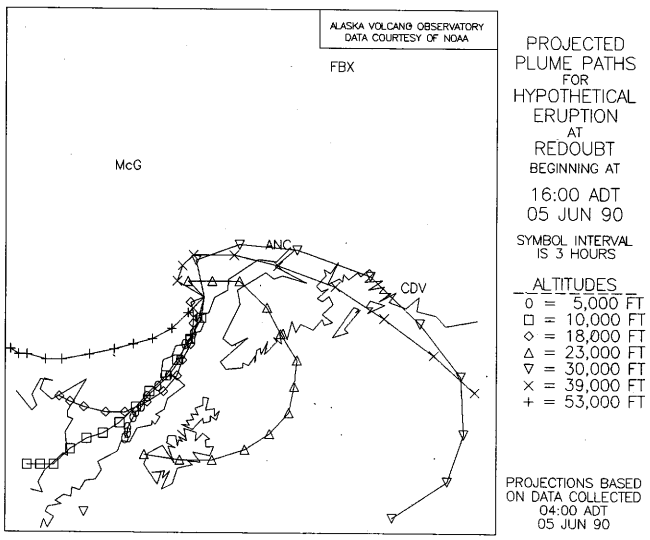


**Figure 4.** Plot showing the difficulty in determining where ash will travel when wind directions are expected to change. The 23,000- and 30,000-ft altitudes show the ash first going north and then curling to the southeast. The winds at 10,000- and 18,000-ft altitudes move the ash south as it falls through those altitudes. Note also that the spacing between symbols is significantly less than that in figure 3, indicating that the winds are much milder than on February 24, 1990. With this pattern of plume trajectories, it is not possible to say much more than the ash is likely stay in the Cook Inlet area (because of the low wind speed) and could affect any or all of the area. Cordova (CDV), McGrath (McG), Fairbanks (FBX) and Anchorage (ANC) are approximately located.

Major eruptions (such as the June 15, 1991, eruption of Mt. Pinatubo, Philippines, or those with strong horizontal wind components, such as the May 18, 1980, blast of Mount St. Helens) are special cases. They can disperse large quantities of ash in any or all directions for many kilometers before prevailing winds control the path traveled by the ash (Self and Walker, this volume).

## CONCLUSIONS

Projected plume trajectories are an important tool for mitigating hazards associated with ashfall resulting from volcanic eruptions. This is the only currently used method that predicts plume paths before an eruption. By simplifying the procedure to obtain plume-trajectory data, we enabled AVO and WSFO to obtain trajectory plots on a routine basis. AVO included the trajectory information in its daily updates that were sent to various governmental agencies and businesses (including Anchorage International Airport, where authorities distributed them to all 26 carriers located there) (Casadevall, in press). In the event of an eruption, projected plume paths were ready for immediate distribution. Thus, AVO and WSFO were able to make full use of predicted plume trajectories, both before and after eruptions.

We recommend that the ARL model be improved to include the effects of dispersion and gravity on volcanic ash. Such improvements would greatly enhance the effectiveness of plume trajectories without adding to the operational cost of acquiring them.

## REFERENCES CITED

Brantley, S.R., ed., 1990, The eruption of Redoubt Volcano, Alaska, December 14, 1989–August 31, 1990: U.S. Geological Survey Circular 1061, 33 p.

Casadevall, T.J., in press, The 1989–1990 eruption of Redoubt Volcano, Alaska: Impacts on aircraft operations: Journal of Volcanology and Geothermal Research.

Heffter, J.L., Stunder, B.J.B., and Rolph, G.D., 1990, Long-range forecast trajectories of volcanic ash from Redoubt Volcano eruptions: Bulletin American Meteorological Society, v. 71, no. 12, p. 1731–1738.

Miller, C.D., Mullineaux, D.R., and Crandell, D.R., 1981, Hazard assessments at Mount St. Helens, *in* Lipman, P.W. and Mullineaux, D.R., eds., The 1980 Eruptions of Mount St. Helens, Washington: U.S. Geological Survey Professional Paper 1250, p. 789–802.

Scott, W.E., and McGimsey, R.G., in press, Character, mass, distribution, and origin of tephra-fall deposits of the 1989–1990 eruption of Redoubt Volcano, south-central Alaska: Journal of Volcanology and Geothermal Research.

Smith, W.K., 1980, A plotting program for producing ashfall prediction maps from output of the NOAA forecast trajectory program: Application to examples from the 1980 Mount St. Helens eruptions: U.S. Geological Survey Open-File Report 80-2005, 36 p.

VOLCANIC ASH AND AVIATION SAFETY:
Proceedings of the First International Symposium
on Volcanic Ash and Aviation Safety
U.S. GEOLOGICAL SURVEY BULLETIN 2047

# VOLCANIC ERUPTIONS AND ATMOSPHERIC TEMPERATURE

*By* Reginald E. Newell *and* Zhong Xiang Wu

## ABSTRACT

Temperature changes associated with volcanic aerosol have been studied with radiosonde data since 1960 and with satellite microwave-sounding data since 1979. Radiosonde data show that temperature in the tropical lower stratosphere increased by about 5°C following eruptions of Mt. Agung in 1963 and El Chichón Volcano in 1982. The microwave data, which give a weighted response to temperature of the lower stratosphere, give a zonally averaged temperature increase of about 1.6°C in the tropics for both El Chichón and Pinatubo (which erupted in 1991). In spite of large differences in the amount of material injected into the lower stratosphere by these three volcanoes, there is little difference in the positive temperature anomalies. The possible reasons for these equilibrium anomalies are discussed. In the troposphere, temperature seems to have decreased by about 0.3°– 0.4°C after Agung, but it is difficult to be certain that there was any volcanic decrease in 1982–83 because of the concomitant occurrence of a large El Niño, which is always associated with tropospheric heating. Atmospheric temperature changes produced by volcanic activity are responsible for the largest density changes that occur in and above the tropical lower stratosphere.

On the longer time scale, there is some evidence that volcanic activity around the turn of the century caused the depression of global sea-surface temperature of approximately 0.5°C at that time.

## INTRODUCTION

Important parameters for aircraft flight are ambient air temperature and air density, which depend on the variation of temperature with altitude. Volcanic activity causes changes in atmospheric temperature patterns and therefore influences these important parameters.

Volcanic eruptions are clearly not the only factors that influence atmospheric temperature. Another major factor, which is comparable in magnitude in the lower atmosphere, is air-sea interaction, particularly as manifested by the tropical El Niño phenomenon (Philander, 1990). During El Niño, sea-surface temperatures in the eastern equatorial Pacific rise to values close to those in the west (≅ 30°C), and the entire tropical lower atmosphere responds by getting warmer. The presence of El Niño often makes it difficult to unravel the influence of volcanic activity on temperature, as will be seen below.

The exact mechanisms by which volcanic eruptions or El Niño events bring about temperature changes in the tropical atmosphere are not known. The general mechanisms controlling free-air temperature have been presented by Newell and others (1974) and fall into four broad categories: solar and infrared radiative interactions, latent heat liberation, conduction of sensible heat from the Earth's surface, and atmospheric motions. The constituents introduced into the atmosphere by volcanic activity certainly influence the first category, but the other three may also be involved. Likewise, although El Niño may involve air-sea interactions in which energy is transferred from the sea to the air (mostly as latent heat), there are also likely to be contributions from the other categories.

We review here some of the past work relating volcanic activity to atmospheric temperature and present some recent work that makes use of microwave sounding units on satellites for temperature determination that gives, for the first time, global coverage of temperature changes. Throughout, we will take cognizance of the variability of air-sea interaction.

## CHANGES IN THE TROPOSPHERE—PREVIOUS WORK

The early work on changes in surface-air temperature associated with volcanic eruptions has been summarized by Lamb (1970), who also introduced a dust veil index (DVI) as an aid to measuring the influence of volcanoes on temperature. Before 1900, the data available to evaluate the index are rather sparse—this diminishes its value then, as stressed by Bradley (1988) in his study of the DVI and other indices of volcanic activity. Lamb (1970) recognized the danger of

circular reasoning when using DVI data to compare with climate fluctuations because some of the earlier DVI estimates included temperature change values. Maximum temperature decreases of about 1°C were found after large eruptions (for example Tambora in 1815), but, as Lamb (1970) stressed, there has been much debate about the reality of the reported changes and their geographical extent. Two interesting findings by Bradley (1988) were (1) in the Northern Hemisphere, the summer and fall months experienced the greatest temperature depression, and (2) there was evidence for a small secondary peak in the negative anomalies about 1 year after the first peak response. None of the early work included factors other than volcanic activity as dependent variables.

By 1976, it was known that the influence of volcanic activity could best be brought out of the record of mean air temperature for the tropical troposphere (TTT) in the altitude region from 3 to 10 km by first removing the air temperature variability associated with El Niño. This was done using a time series of sea-surface temperature (SST) from the eastern equatorial Pacific (see Newell and Weare, 1976a, 1976b). The approximate regression equation reduced to:

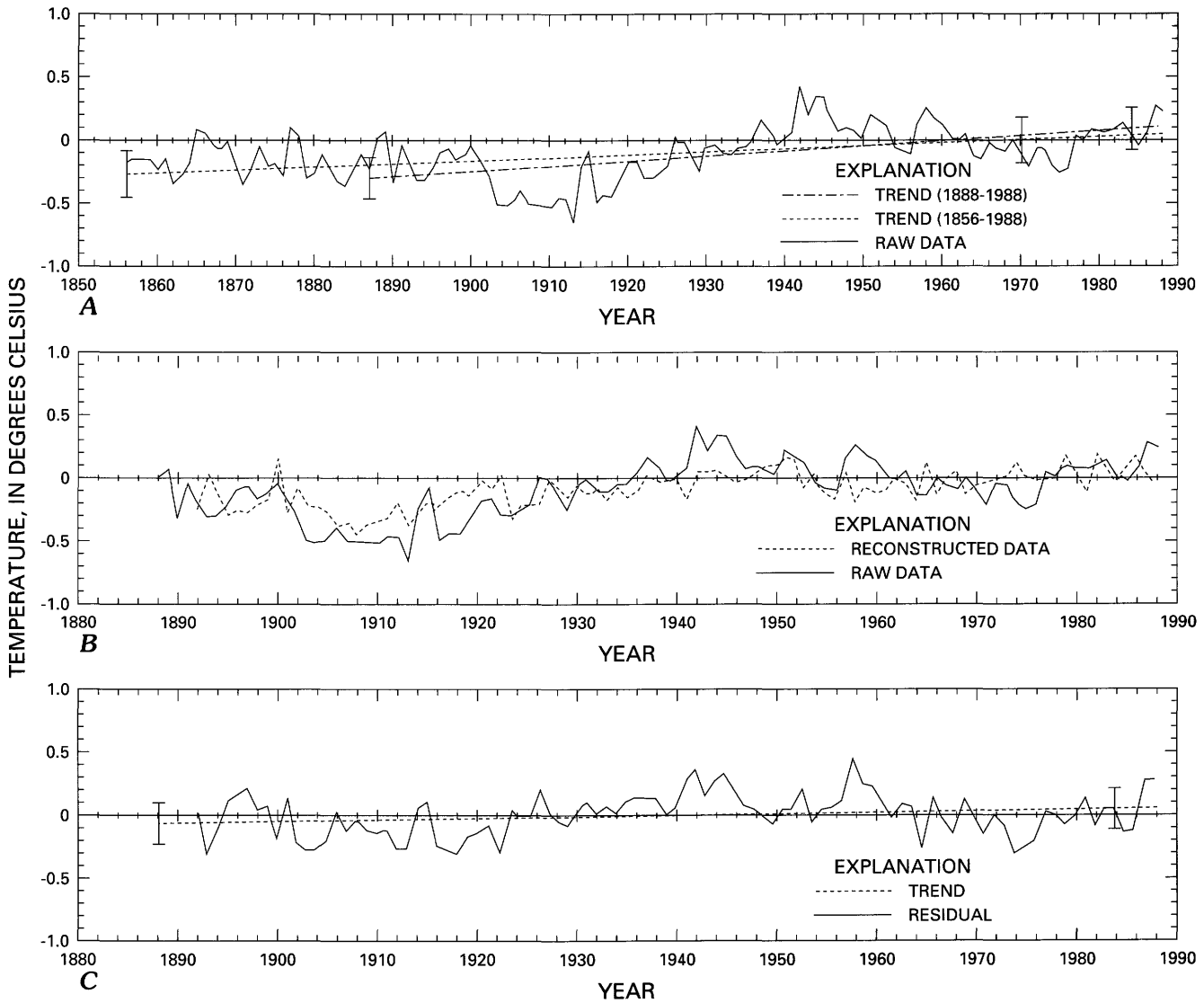


**Figure 1.** *A*, Time series (1856 to 1988) of marine air temperatures (MAT) in the Northern Hemisphere. *B*, The component of MAT (Northern Hemisphere) that is dependent on turbidity (turbidity is the first factor in a linear regression analysis); data from 1888 to 1988 is shown. *C*, MAT residuals and their trend (Northern Hemisphere) after subtraction of the turbidity component; data from 1888 to 1988 is shown. Adapted from Wu and others (1990).

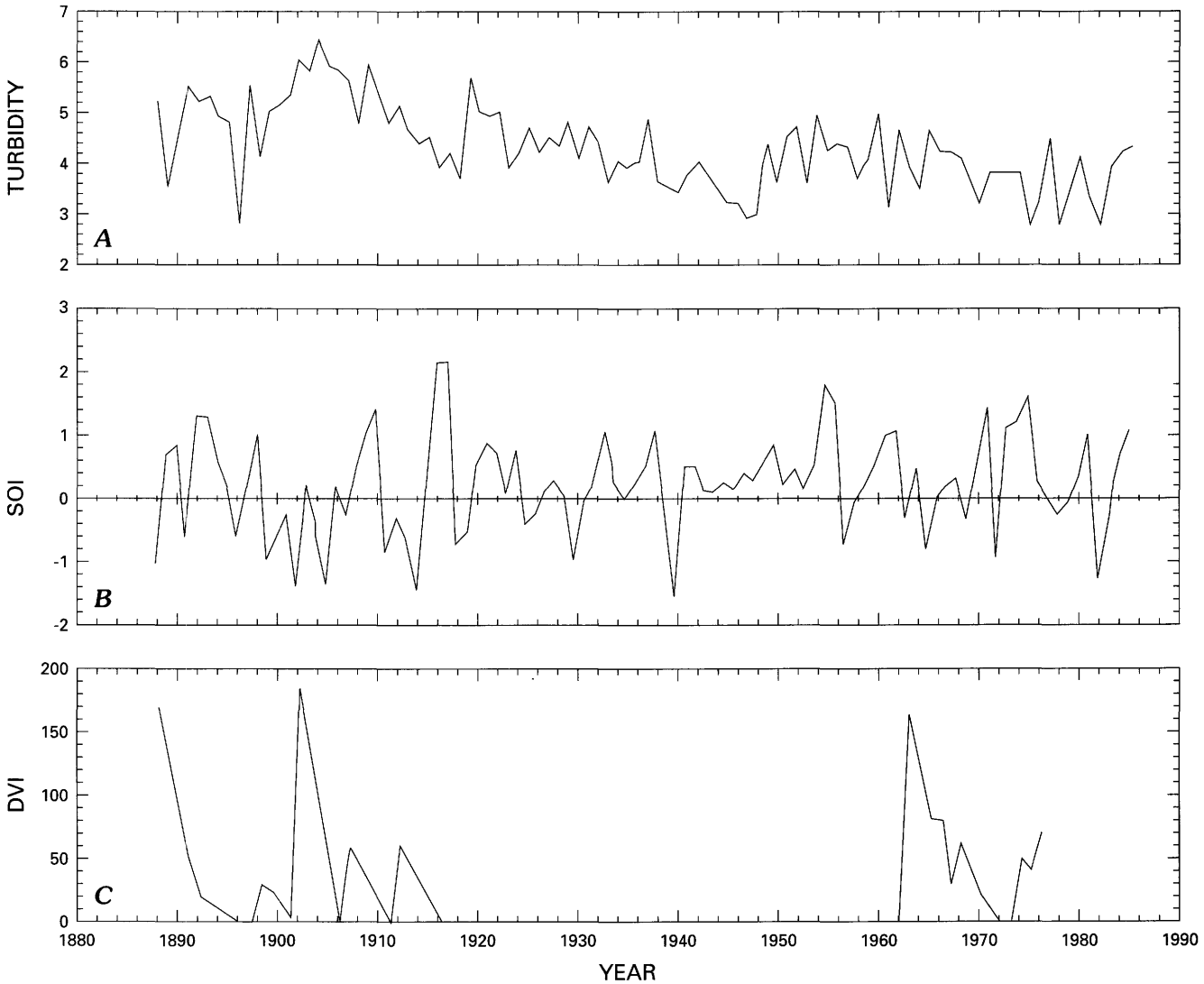


**Figure 2.** *A*, Time series of turbidity at Sonnblick, Austria (see text and Wu and others, 1990 for further explanation). *B*, The southern oscillation index (SOI), used to monitor El Niño. Obtained from an update of early work by Wright (1975). *C*, Lamb's dust veil index (DVI). See Lamb (1970). Figure adapted from Wu and others (1990).

$$\Delta TTT = 0.5\ \Delta SST + 20\ \Delta\tau_v \qquad (1)$$

where

$\tau_v$ is the atmospheric transmission measured by solar photometers at the Mauna Loa Observatory (lat. 21°N.).

For the Mt. Agung eruption of 1963, the transmission decreased by about 3 percent and ΔSST in late 1963 was about 1°C—therefore, the net effect was only about –0.1°C. But by early 1964, the SST anomaly turned negative, and the largest tropical troposphere negative anomaly of about 0.5°C then occurred. Further details may be found in papers by Newell (1984) and Newell and Hsiung (1984). A discussion of the phase lags is given by Newell and Weare (1976a, 1976b). There was a phase lag of about 6 months between the eastern Pacific SST change and the TTT change. Newell and Hsiung (1984) also applied this relationship to the El Chichón eruption of 1982, a case for which the largest phenomenon of the century up to that time occurred in each category: El Niño was associated with a rise in SST of 4°C, and the El Chichón aerosols showed atmospheric transmission to decrease by more than 13 percent. Such phenomena give rise to a net cooling of about 0.6°C when equation 1 is applied. Angell (1988) has taken the same approach in the examination of the joint effects of El Niño and volcanoes on air temperature, including the weighting of 0.5 applied to

the SST contribution—he finds that a decrease of TTT of about 0.5°C can be assigned to El Chichón (he has applied more time averaging to the data than was used in our case). An obvious flaw in this general approach is that the regression parameters cannot be applied quantitatively outside the region for which they were developed.

We have examined ships' reports of night, marine, air temperatures for the past century taken from the Global Ocean Surface Temperature Atlas (GOSTA), produced by Bottomley and others (1990), and we have related the temperature variability to three variables (Wu and others, 1990): atmospheric turbidity, solar irradiance, and the southern oscillation index (SOI), which is an index of surface pressure anomalies in the Pacific related to El Niño (Philander, 1990). Figures 1 and 2 show the time series of Northern Hemisphere air temperature, the time series of two of these variables, plus, for illustrative purposes, the DVI of Lamb (1970). Using multiple linear regression, it was shown that atmospheric turbidity explained the largest fraction of variance for Northern Hemisphere air temperatures, whereas the SOI explained the largest fraction for the tropics.

The turbidity used in these calculations was computed from sunshine records that have long been collected at many meteorological stations (Helmes, 1987). In the method used, an image of the sun produced by a glass sphere burns a trace on a card throughout the day. The Campbell-Stokes sunshine recorder was brought to its present form in 1880 (see Stokes, 1880). Stokes (1880) points out that the color selected for the card (Prussian blue) gave maximum absorption. The instrument as developed then has been used for 110 years and is therefore an excellent tool for the study of global-change effects. When volcanic eruption clouds are present, the image is only powerful enough to burn the card at a later-than-usual-time after sunrise or an earlier-than-usual time before sunset. From the sun's elevation ($\alpha$) at first or last burn, the turbidity may be obtained as follows (Jaenicke and Kasten, 1978):

Turbidity ($Tg$) is defined as:

$$Tg = \frac{1}{b_g m} \ln \frac{I_o}{I_{cs}} \qquad (2)$$

where

$b_g$ is the optical thickness of the atmosphere for Rayleigh scattering including ozone absorption and integrated over the solar spectrum,

$m$ is the relative optical air mass, which depends on solar elevation angle,

$I_o$ is the irradiance of the extraterrestrial solar constant ($\cong$1,370 W/m$^2$), and

$I_{cs}$ is the threshold value for burning to start ($\cong$ 200 W/m$^2$).

Jaenicke and Kasten (1978) show that this relation may be approximated as:

$$Tg = c_5 \alpha + c_6$$

where

$c_5 = 0.154 \ln (I_o/I_{cs})$, in deg$^{-1}$, and

$c_6 = 1.05 \ln (I_o/I_{cs})$.

The turbidity, $Tg$, so computed is a measure of the number of dust-free and dry Rayleigh atmospheres that have the same transmittance as that observed in the real dust-laden and humid atmosphere. The variation of $Tg$ is only available from a few stations before 1900. Sonnblick (lat. 47°N., long. 13°E., altitude 3,106 m), Austria, is one station that has the advantage of being above the boundary layer of the industrial plain of Central Europe. High values of $Tg$ appear after the turn of the century accompanying the three large volcanic eruptions of 1902 (Mt. Pelée, lat. 15°N., long. 61°W.; Soufriére, lat. 13°N., long. 61°W.; and Santa Maria, lat. 14°N., long. 92°W.). If the volcanic explosivity index computed by Newhall and Self (1982) was used as a criterion of activity, 1902 had the largest cumulative value in 1 year during the period from 1883 to 1981, but the volcanological record is not complete before about 1950. There are associated low values of Northern Hemisphere marine air temperature in this high-activity period—this leads to the conclusion that volcanism plays a significant role in cooling the lower atmosphere and producing this major minimum of the past 100 years. When the tropical atmosphere is considered alone (not shown), marine air temperatures show good correspondence with the SOI index, with turbidity the second most important variable. The prime physical process acting in this case is, therefore, air-sea interaction.

These relationships between SOI, turbidity, and air temperature may be of some interest for the case of the Pinatubo eruption. Based on satellite measurements of $SO_2$, Bluth and others (1992) report that Mt. Pinatubo ejected about 20 megatons (Mt) of sulfur dioxide into the stratosphere between June 10 and June 28, 1991, which is about three times the amount measured for the El Chichón eruption. McCormick and Veiga (1992), from satellite measurements of aerosol find between 20 and 30 Mt of new aerosol that were produced by the Pinatubo eruptions compared with 12 Mt from El Chichón. A substantial fraction of the new aerosol is thought to be formed from the oxidation of $SO_2$. Concomitantly, there has been a warming of the tropical Pacific by as much as about 2°C (Climate Analysis Center, 1992).

## CHANGES IN THE STRATOSPHERE—PREVIOUS WORK

Whereas the troposphere apparently cools after a large volcanic eruption, the stratosphere shows warming, probably due to the absorption of solar radiation, although infrared absorption may also be important. The tropospheric temperature increase after the eruption of Mt. Agung in March 1963

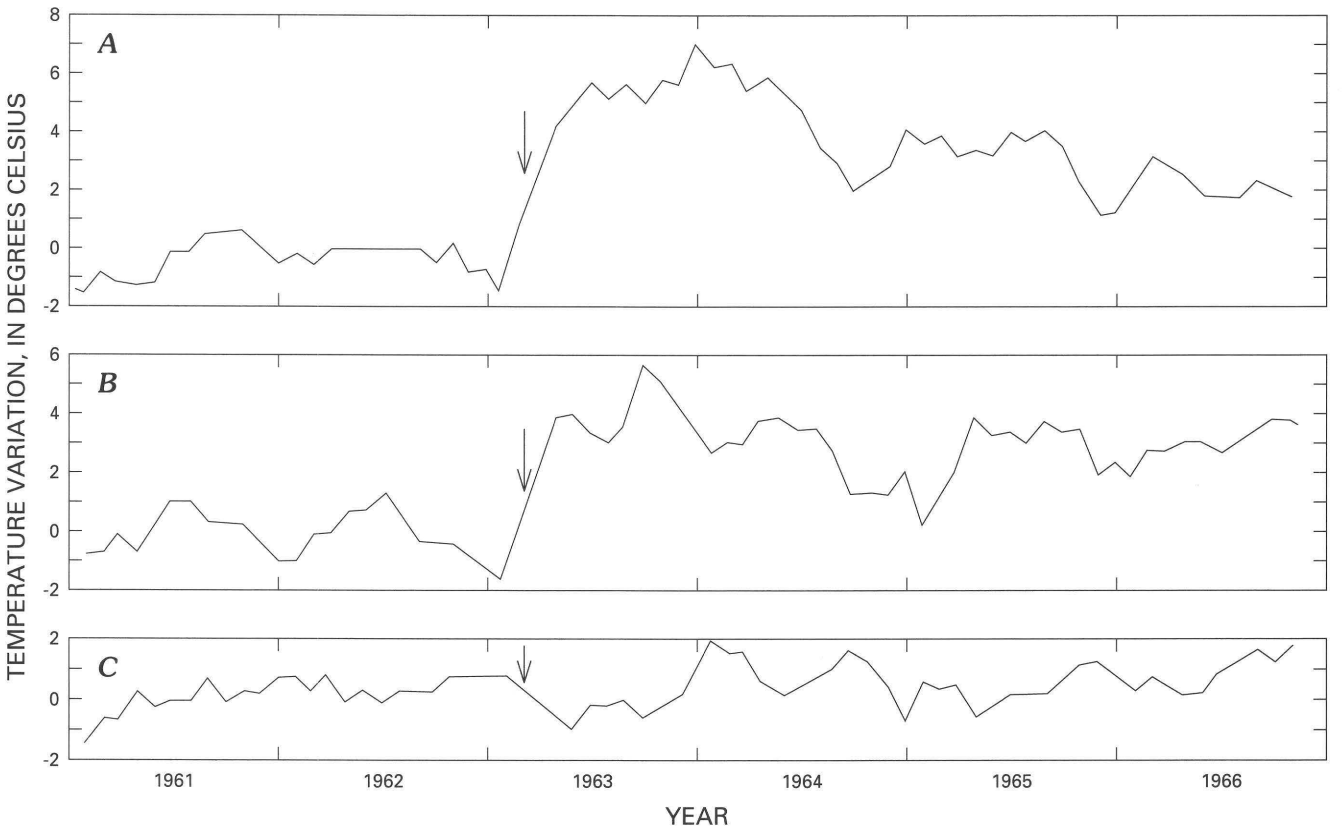


**Figure 3.** Variations in air temperature in the tropical lower stratosphere after the eruption of Mt. Agung in 1963. Arrows indicate date of eruption of Mt. Agung (March 1963). Temperature variations are shown for altitudes of: *A*, 19.5 km; *B*, 16.5 km; *C*, 9.5 km. Monthly means were calculated for 5 years before the eruption; deviations from the means were computed, and 3-month running averages were plotted. From Newell (1971). Reprinted with permission.

was the largest non-seasonal anomaly then observed by the radiosonde network (about 6°C—see fig. 3), and, although the anomaly gradually decreased during and after 1964, it persisted for several years (Newell, 1970a, 1970b, 1971). Similar increases in the temperature of the lower stratosphere occurred after the eruption of El Chichón in 1982 (Labitzke and others, 1983; Parker and Brownscombe, 1983; Selkirk and Newell, 1984; Quiroz, 1983; Newell, 1984). Somewhat surprisingly, the temperature change after El Chichón was almost the same magnitude as that after Mt. Agung in spite of the fact that the aerosol injected, or formed in situ from gas-to-particle conversion, was several times larger for El Chichón, and the transmission change illustrated in figure 4 was much larger. In fact, the change after the eruption of El Chichón was the largest in the record since 1958.

Meridional cross sections of temperature change in the lower stratosphere (Newell, 1970b) after the eruption of Mt. Agung are quite similar to those of tungsten 185 ($^{185}W$) radioactivity after Pacific nuclear tests (Newell, 1963). The $^{185}W$ originated from a single point rather like the volcanic eruptions; it was measured by high-altitude aircraft sampling. The influence of plume stabilization and the meridional spreading by atmospheric large-scale eddy diffusion may be seen in both patterns, again providing indirect evidence that it is aerosol that is controlling the temperature changes.

## MICROWAVE SOUNDING UNIT TEMPERATURE-ANOMALY DATA

The tropospheric free-air and stratospheric temperature perturbations discussed above were based on radiosonde data that have a limited geographical coverage, especially over the tropical oceans. The measurement of temperature by the detection of microwave emission from molecular oxygen using a satellite platform was proposed by Meeks and Lilley (1963) as a method to acquire global coverage; this has been implemented in a series of National Oceanic and Atmospheric Administration (NOAA) satellites since 1979

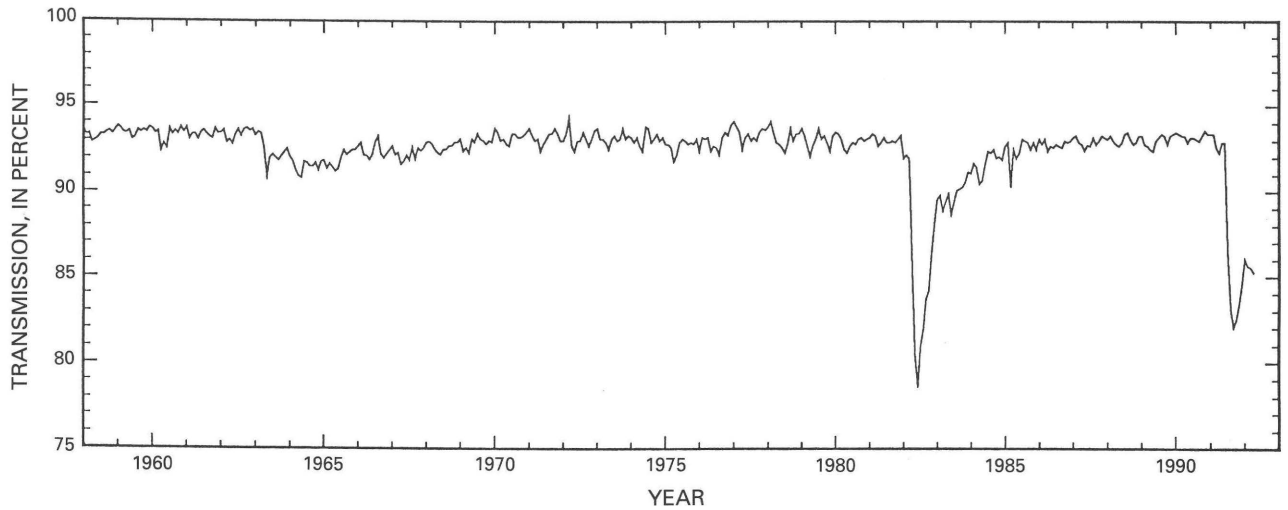


**Figure 4.** Atmospheric transmission at Mauna Loa Observatory, Hawaii (data provided by Ellsworth Dutton, NOAA/ERL climate monitoring and diagnostics laboratory, Boulder, Colo.). Major ticks represent January of indicated year.

(Spencer and Christy, 1990; Spencer and others, 1990). Microwave sounding units (MSU's) use radiometers sensitive to radiation of 50–60 GHz (0.6–0.5 cm). Examples of the weighting functions are illustrated in the two papers quoted. The 57.95-GHz channel covers the lower stratosphere; its peak response at about 100 hPa, or about 16 km, is below the maximum temperature anomalies shown in figure 3 for Mt. Agung. The 53.74-GHz tropospheric channel is centered at about 700 hPa but is also influenced by surface temperature. Time series of zonal mean values of these two channels are shown in figure 5. To provide information on the aerosol, atmospheric transmission at Mauna Loa is also included in each part of figure 5. Figure 5*C* represents tropical ocean surface temperature variations taken from GOSTA, so that the influence of oceanic changes on the temperature record may also be appreciated. All values are monthly mean anomalies calculated from the 1982–90 period means and are expressed in terms of the monthly standard deviations; 13-month running means obtained with a Gaussian filter are also shown. There is an increase in temperature in the stratosphere commencing soon after atmospheric transmittance decreases for both the El Chichón and Pinatubo eruptions. The maximum increase in both cases is about 2.4 standard deviations, or 1.6°C. The same general time sequence is evident in radiosonde data analyzed by Labitzke and McCormick (1992), but they only extended to November 1991. The magnitudes are different from the microwave results, with a maximum increase of about 4°C at a pressure level of 50 hPa (≅ 21 km). It should be emphasized, as noted above, that the maximum of the weighting function is not peaked in altitude with respect to the maximum temperature anomaly. It should also be noted from figure 3 that there are substantial changes in the anomalies with longitude, and these are smoothed out in the zonal mean values of figure 5. It is of interest that, so far, the two temperature anomalies observed by the microwave technique are roughly the same size, even though the amount of $SO_2$ gas released was about three times larger for Pinatubo than for El Chichón. The same situation occurred for radiosonde anomalies found for Mt. Agung and El Chichón. These stratospheric temperatures show some evidence of a biennial oscillation, the sequence being interrupted and perhaps changed in phase by the El Chichón eruption.

It was suggested many years ago that biennial temperature changes in the region of the lower stratosphere were reflections of a modulation of the rising motion in the tropical Hadley-cell circulation (Newell and others, 1969) and that the phase slippage, which was evident in 1963 from ozone records, was due to the eruption of Mt. Agung (Newell and others, 1974). The same explanations could apply to figure 5 and the record of the Pinatubo eruption. Dutton (1992) has shown that the Mauna Loa record of atmospheric transmission also shows evidence of a quasi-biennial oscillation, which would presumably be related to horizontal wind changes accompanying modulations of vertical motions.

Figure 5 shows that, in the troposphere, there are three major positive excursions in tropical SST and tropical free-air temperature: in early 1983, late 1987 and late 1991—all three being related to temperature changes associated with El Niño events, which show a maximum SST change in the eastern equatorial Pacific.

Maps of temperature anomalies for the lower tropical stratosphere are shown in figure 6 for September 1981 and September 1982, before and during the transmission change. In September 1981, tropical temperatures are slightly below average, whereas, in 1982, there are positive anomalies of about 1.5°C with slight maxima in the western Pacific and Atlantic, corresponding approximately to the maximum in

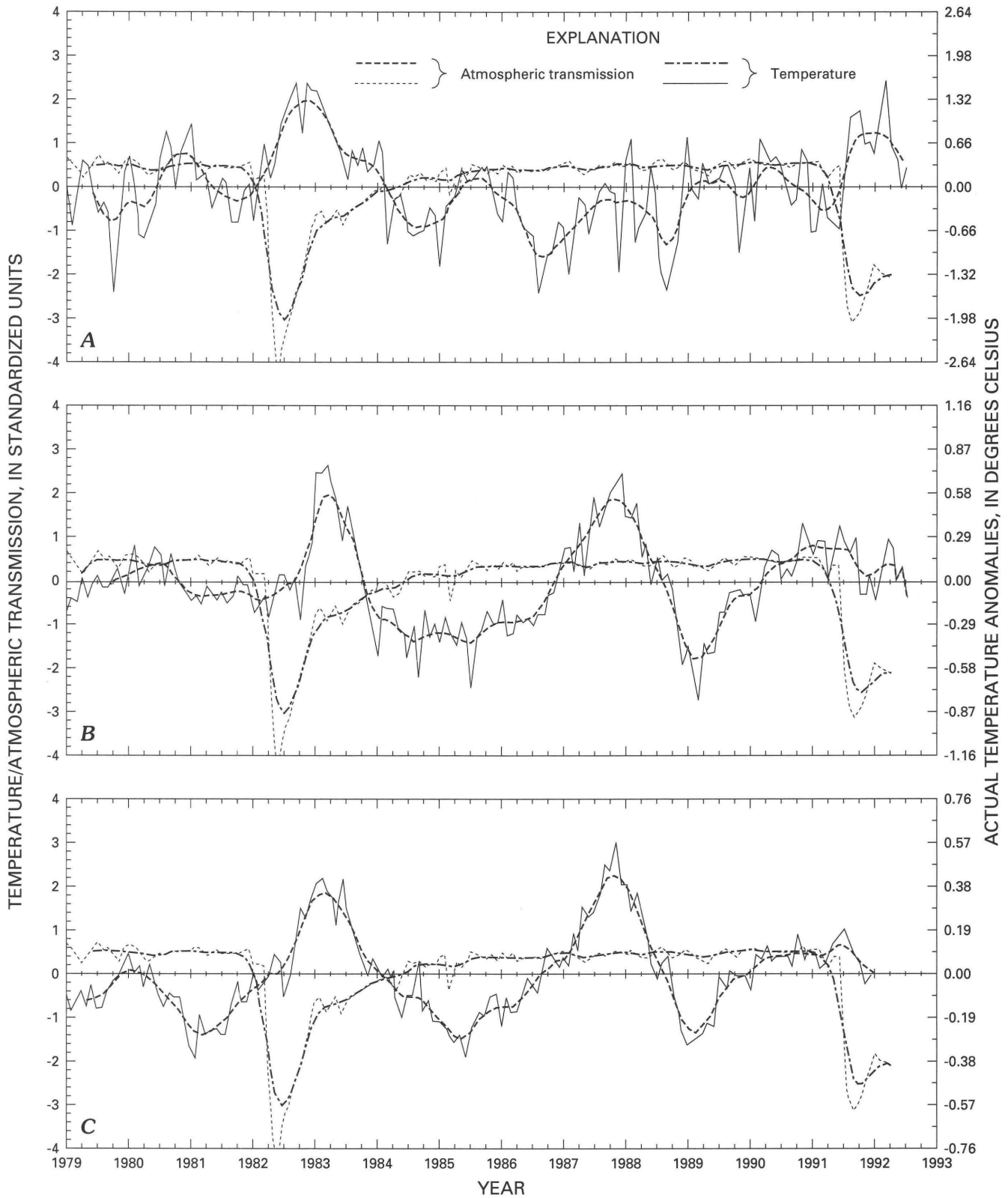


**Figure 5.** *A*, Time series of atmospheric transmission and tropical (lat. 20°S.–20°N.) lower stratospheric temperature based on microwave-sounding-unit data. Left-hand scale is in standardized units for both parameters ("standardized" is term used here when anomalies are expressed in terms of standard deviation of full time series). Right-hand scale represents actual temperature anomalies. Light lines represent actual monthly mean values. Heavy lines represent results of applying an 11-month Gaussian filter. Major ticks on horizontal axis correspond to January of indicated year. *B*, Tropical (lat. 20°S.–20°N.) tropospheric temperature based on microwave-sounding-unit data. Atmospheric transmission curves identical to those in *A*. *C*, Tropical (lat. 20°S.–20°N.) sea-surface temperature shown through December 1991. Atmospheric transmission curves identical to those in *A*.

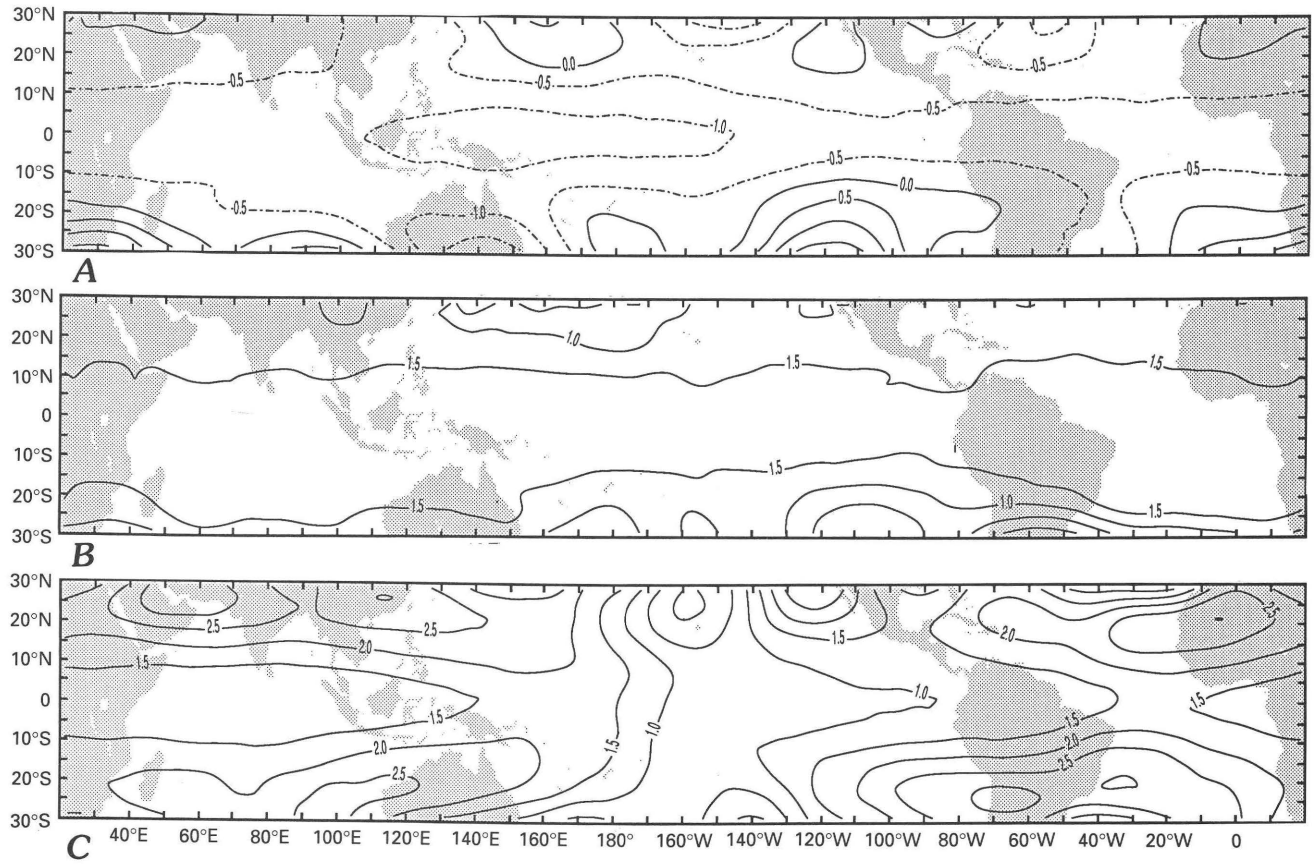


**Figure 6.** *A*, Temperature anomalies (with reference to means for 1982–92) for the lower tropical stratosphere based on September 1981 microwave-sounding-unit data. Data reflects conditions before El Chichón eruption. Contours of temperature anomalies are labeled in degrees Celsius. *B*, Temperature anomalies for September 1982 (after El Chichón eruption). *C*, Temperature anomalies for March 1992 (after Mt. Pinatubo eruption).

back scattering from the cloud measured by lidar (McCormick and others, 1984). A map for March 1992 is also included in figure 6 and shows similar anomalies to those that occurred after the eruption of El Chichón. Tropospheric temperature anomaly maps illustrate an evolution since the eruption of Pinatubo that is dominated by the 1991–92 El Niño. In the tropical Pacific, the period December 1991–April 1992 shows a bipolar structure centered on the equator that resembles the January 1983 pattern we reported earlier for the 1982–83 El Niño (Newell and Wu, 1992). Although not included in figure 5, the SST in the eastern tropical Pacific showed a maximum positive anomaly (of 2°–3°C) in May 1992, after which the anomalies decreased rapidly and became negative in the middle of July 1992. The maxima on either side of the equator may be associated with large-scale subsidence. This warming illustrates the great difficulty of estimating the influence of volcanic effects on the troposphere.

## PHYSICAL MECHANISMS FOR OBSERVED CHANGES

Meridional cross sections of atmospheric sulfate concentrations before and after Mount St. Helens and before and after El Chichón have been drawn up by Newell (1984) using data from Sedlacek and others (1983) and Mroz and others (1983). They show a strong source in the tropics for El Chichón with mixing-ratio isolines sloping downward with latitude; significant values are confined to the stratosphere. Because sulfate has a low absorptivity for solar radiation, it may not be the only item responsible for the climatic effect of volcanoes. Ogren and others (1981) found evidence for the absorption of visible radiation in the Mount St. Helens plume, and Clarke and others (1983) find significant absorption at visible wavelengths in aircraft samples from the El Chichón volcanic eruption cloud; samples were collected in the altitude range from 18 to 21 km. Woods and Chuan

(1983) found similar samples to contain carbon. There were no measurements of the infrared properties of this particular aerosol.

Normal background radiative heating-rate components in this region are shown in figure 7. The tropical lower stratosphere is normally heated by infrared absorption by ozone; by ultraviolet ozone absorption; and by solar near-infrared absorption by water vapor, carbon dioxide, and molecular oxygen. Cooling occurs mainly by infrared emission from carbon dioxide and water vapor. If the solar and infrared absorption by aerosol produce heating, the additional cooling necessary to produce near-equilibrium temperatures at an elevated temperature level, as was observed following these three recent eruptions, must come from net infrared divergence from the $CO_2$ in the layer. All three are associated with lower stratospheric temperatures that are about 4°–6°C higher than pre-eruption values. This value is likely to be that temperature rise that is required to bring about an increased $CO_2$ infrared flux divergence sufficient to offset heating by solar and infrared absorption by the aerosol.

We have selected temperature, specific humidity and ozone conditions appropriate to the tropical west Pacific (actually for Guam for August 1991) to compute the results used in figure 7. Stratospheric temperatures were then increased by about 6°C at 50 hPa and elsewhere using a vertical-profile modification based on a previous paper (on Mt. Agung—Newell, 1970b). This is justified by the fact that the three volcanoes produced about the same maximum temperature change. Modified cooling rates (in °C/day) are also shown in figure 7. Both $CO_2$ and $H_2O$ show larger infrared cooling rates, and $O_3$ shows a reduced infrared heating rate; the largest influence is from $CO_2$. Overall, cooling increases by approximately 0.34°C/day at 50 hPa. Hansen and others (1978) compared the results of a one-dimensional model of the Mt. Agung eruption cloud with the data on tropospheric and stratospheric temperature change included in Newell and Weare (1976b) and Newell (1970a) and found quite good agreement. Their model would presumably produce a similar balance in the lower stratosphere.

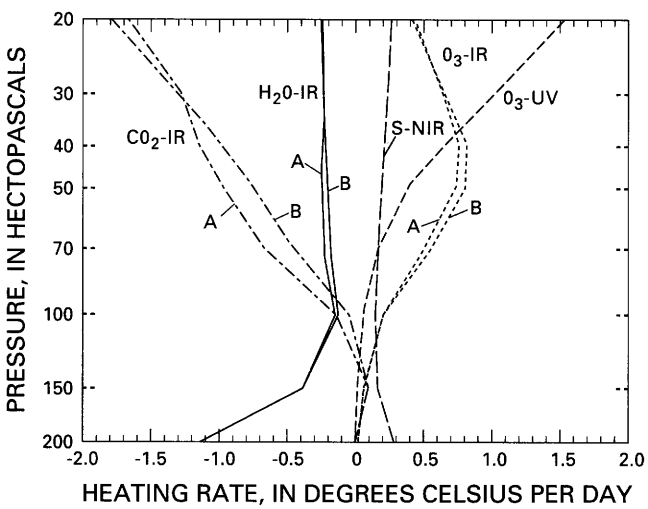


**Figure 7.** Radiative heating rate components for the lower stratosphere for conditions in the tropical west Pacific before and after an eruption. A sounding for Guam, August 1991, was used. The procedure followed for these calculations is that outlined in chapter 6 of Newell and others (1974) and in Hoffman (1981). Curves labeled "A" indicate data collected after eruption; curves labeled "B" indicate data collected before eruption (temperature at 50 hPa is 6°C higher—see text). $CO_2$-IR and $H_2O$-IR represent infrared cooling rates; S-NIR represents near-infrared solar heating by absorption by $O_2$, $CO_2$, and $H_2O$; $O_3$-UV is solar heating in the ultraviolet region by absorption by $O_3$; $O_3$-IR is infrared heating by $O_3$.

In cases where tropospheric cooling is definitely associated with a volcanic eruption, such as the 1963 Agung case, it is not yet known how much of the cooling is caused by a deficit of visible radiation at the surface, which would reduce evaporation and therefore subsequent latent heating in the troposphere, and how much is due to a deficit of solar near-infrared radiation reaching the troposphere, which normally produces heating through near-infrared absorption by $O_2$, $CO_2$ and $H_2O$, as illustrated in the lower part of figure 7. As stressed previously (Newell, 1981), it would be valuable to measure the wavelength dependence of incoming radiation in and below the volcanic cloud as well as the associated infrared fluxes. The problem of detecting a tropical troposphere temperature change after a volcanic eruption is clearly complicated by the strong influence of eastern equatorial Pacific sea temperature changes. The tropical air temperature changes associated with these SST changes are presumably produced through the intermediate mechanism of latent heat liberation. When attempting to account for the influence of volcanic eruptions on air temperature, oceanic storage of energy and transport by currents may also be involved.

Clearly, representation by a simple relationship like equation 1 is not adequate, and more studies with good air- and ocean-temperature data are necessary.

Another factor involved in the determination of stratosphere temperature is vertical motion: enhanced rising motion produces cooling, and subsidence produces heating. It is possible that the vertical motion in the tropical tropopause region may be responsible for the dips in the two maxima of the stratosphere temperature time series.

## INFLUENCE OF ATMOSPHERIC TEMPERATURE AND DENSITY CHANGES ON FLIGHT PERFORMANCE

As noted in the Introduction to this paper, air density is a critical parameter from the aviation point of view.

Temperature changes of 5°– 6°C in the tropical belt, perhaps on occasion extending up to 30 km or more from the tropical tropopause, will increase the scale height and density at all higher levels. For example, if the 5°C-anomaly extends only from 20 to 25 km, the density at 25 km increases by about 1.4 percent, whereas, if the anomaly extends to 30 km (a not unreasonable vertical extent for the aerosol cloud based on lidar observations by Adriani and others (1983)), there is a 3 percent increase at 30 km. These density effects increase aircraft drag, but they also increase engine thrust by about the same amount—the net effect on flight performance will be small. For vehicles flying at hypersonic speeds, aerodynamic heating is of major importance; this is proportional to air density and to the cube of velocity (Anderson, 1989) so that all vehicles flying at altitudes above the aerosol-warmed layer would be subject to enhanced heating.

## CONCLUDING REMARKS

The influence of volcanic eruptions on tropospheric temperature is difficult to determine because of the heating effect of El Niño phenomena every few years; in the case of the Mt. Agung and El Chichón eruptions, it was 0.5°C or less. In the case of Pinatubo, there was no cooling effect on the tropical troposphere for the first 6–8 months after the June 1991 eruption, due to El Niño, but this has now ended while a significant amount of aerosol remains.

Microwave-sounding-unit data for the lower stratosphere showed increased temperature by several degrees Celsius after the eruptions of El Chichón in 1982 and Pinatubo in 1991. It appears that some of the absorption that causes increases in temperature may be in the visible or near-infrared region. The increase in temperature appears to be about the same size for the eruptions of Mt. Agung in 1963, El Chichón in 1982, and Pinatubo in 1991. This may be due to the self-limiting effect of enhanced infrared flux divergence caused mostly by atmospheric carbon dioxide.

The temperature changes associated with volcanic aerosol are the largest that occur in the tropical lower stratosphere. For high-speed aircraft flying at and above about 20 km, these changes have a significant effect on atmospheric density and therefore on aerodynamic heating.

It is recommended that absorption measurements be made as a function of wavelength through significant aerosol clouds from future volcanic eruptions.

## ACKNOWLEDGMENTS

We are grateful to Roy W. Spencer and John R. Christy for their kindness in giving us access to the microwave-sounding-unit data. Support for this work was provided in part by MIT Lincoln Laboratory. Calculations based on recent data and revised figures have been supported by the National Science Foundation under Grant ATM 9106902. Thanks are due to Ellsworth Dutton of the NOAA climate monitoring and diagnostics laboratory and to the staff of the Mauna Loa Observatory for providing atmospheric transmission data.

## REFERENCES CITED

Adriani, A., Congeduti, F., Fiocco, G., and Gobbi, G.P., 1983, One-year lidar observation of the stratospheric aerosol at Frascati, March 1982–March 1983: Geophysical Research Letters, v. 10, p. 1005–1008.

Anderson, J.D., Jr., 1989, Hypersonic and High Temperature Gas Dynamics: New York, McGraw-Hill, 289 p.

Angell, J.K., 1988, Impact of El Niño on the delineation of tropospheric cooling due to volcanic eruptions: Journal of Geophysical Research, v. 93, p. 3697–3704.

Bluth, G.J.S., Doiron, S.D., Schnetzler, C.C., Krueger, A.J., and Walter, L.S., 1992, Global tracking of the $SO_2$ clouds from the June, 1991 Mount Pinatubo eruptions: Geophysical Research Letters, v. 19, p. 151–154.

Bottomley, M., Folland, C.K., Hsiung, J., Newell, R.E., and Parker, D.E., 1990, Global Ocean Surface Temperature Atlas (GOSTA): Bracknell, United Kingdom, U.K. Meteorological Office, 20 p., 313 plates.

Bradley, R.S., 1988, The explosive volcanic eruption signal in Northern Hemisphere continental temperature records: Climatic Change, v. 12, p. 221–243.

Clarke, A.D., Charlson, R.J., and Ogren, J.A., 1983, Stratospheric light absorption before and after El Chichón: Geophysical Research Letters, v. 10, p. 1017–1020.

Climate Analysis Center, 1992, Near real time analyses ocean/atmosphere: Camp Springs, Md., National Oceanic and Atmospheric Administration, Climate Diagnostics Bulletin, June, no. 6, p. 9, 42.

Dutton, E.G., 1992, A coherence between the QBO and the amplitude of the Mauna Loa atmospheric transmission annual cycle: International Journal of Climatology, v. 12, p. 383–396.

Hansen, J.E., Wang, W.C., and Lacis, A.A., 1978, Mt. Agung eruption provides test of a global climate perturbation: Science, v. 199, p. 1065–1068.

Helmes, L., 1987, Klimatologie der atmosphanischen Trüberg der letzten 100 Jahre basierend auf Langzeitreihen der Sonnenschein dauer und des Bedeckungsgrades [in German]: Mainz, Germany, Johannes Gutenberg Universität, unpub. Ph.D. thesis, 138 p.

Hoffman, R.N., 1981, A computer program which calculates radiative fluxes and heating rates in model atmospheres: Cambridge, Massachusetts, Massachusetts Institute of Technology Department of Meteorology and Physical Oceanography, Climatic Fluctuations, Volcanic Aerosol, and Carbon Dioxide Changes Scientific Report No. 4, 124 p.

Jaenicke, R., and Kasten, F., 1978, Estimation of atmospheric turbidity from the burned traces of the Campbell-Stokes sunshine recorder: Applied Optics, v. 17, p. 2617–2621.

Labitzke, K., Naujokat, B., and McCormick, M.P., 1983, Temperature effect on the stratosphere of the April 4, 1982 eruption of El Chichón, Mexico: Geophysical Research Letters, v. 10, p 24–26.

Labitzke, K., and McCormick, M.P., 1992, Stratospheric temperature increases due to Pinatubo aerosols: Geophysical Research Letters, v. 19, p. 207–210.

Lamb, H.H., 1970, Volcanic dust in the atmosphere; with a chronology and assessment of its meteorological significance: Royal Society of London Philosophical Transactions, Series A, v. 266, p. 425–533.

McCormick, M.P., Swissler, T.J., Fuller, W.H., Hunt, W.H., and Osborn, M.T., 1984, Airborne and ground-based lidar measurements of the El Chichón stratospheric aerosol from 90°N to 56°S: Geofisica Internacional, v. 23-2, p. 187–221.

McCormick, M.P., and Veiga, R.E., 1992, Sage II measurements of early Pinatubo aerosols: Geophysical Research Letters, v. 19, p. 155–158.

Meeks, M.L., and Lilley, A.E., 1963, The microwave spectrum of oxygen in the Earth's atmosphere: Journal of Geophysical Research., v. 68, p. 1683–1703.

Mroz, E.J., Mason, A.S., and Sedlacek, W.A., 1983, Stratospheric sulfate from El Chichón and the mystery volcano: Geophysical Research Letters, v. 10, p. 873–876.

Newell, R.E., 1963, Transfer through the tropopause and within the stratosphere: Royal Meteorological Society Quarterly Journal, v. 89, p. 167–204.

———1970a, Stratospheric temperature change from the Mt. Agung volcanic eruption of 1963: Journal of the Atmospheric Sciences, v. 27, p. 977–978.

———1970b, Modification of stratospheric properties by trace constituent changes; Direct evidence from the Bali volcanic eruption: Nature, v. 227, p. 697–698.

———1971, The global circulation of atmospheric pollutants: Scientific American, v. 224, p. 32–42.

———1981, Further studies of the atmospheric temperature change produced by the Mt. Agung volcanic eruption in 1963: Journal of Volcanology and Geothermal Research, v. 11, p. 61–66.

———1984, Volcanoes and climate, *in* Fiocco, G., ed., Proceedings of International Radiation Symposium, Perugia, Italy, 21–28 August 1984: Hampton, Va., A. Deepak Publishing, p. 93–101.

Newell, R.E. and Hsiung, J., 1984, Sea surface temperature, atmospheric $CO_2$ and the global energy budget; some comparisons between the past and present, *in* Morner, N.A., and Karlen, W., eds., Climatic Changes on a Yearly to Millennial Basis: Hingham, Mass., D. Reidel Publishing Company, p. 533–561.

Newell, R.E., Kidson, J.W., and Vincent, D.G., 1969, Annual and biennial modulations in the tropical Hadley-cell circulation: Nature, v. 222, p. 76–78.

Newell, R.E., Kidson, J.W., Vincent, D.G., and Boer, G.J., 1974, The General Circulation of the Tropical Atmosphere, Volume 2: Cambridge, Mass., MIT Press, p. 179–293.

Newell, R.E., and Weare, B.C., 1976a, Factors governing tropospheric mean temperature: Science, v. 194, p. 1413–1414.

———1976b, Ocean temperatures and large-scale atmospheric variations: Nature, v. 262, p. 40–41.

Newell, R.E., and Wu, Z-X., 1992, The interrelationship between temperature changes in the free atmosphere and sea surface temperature changes: Journal of Geophysical Research, v. 97, p. 3693–3709.

Newhall, G.G., and Self, S., 1982, The volcanic explosivity index (VEI): An estimate of explosive magnitude of historic eruptions: Journal of Geophysical Research, v. 87, p. 1231–1238.

Ogren, J.A., Charlson, R.A., Radke, L.F., and Domonkos, S.K., 1981, Absorption of visible radiation by aerosols in the volcanic plume of Mt. St. Helens: Science, v. 211, p. 836–838.

Parker, D.E., and Brownscombe, J.L., 1983, Stratospheric warming following the El Chichón volcanic eruption: Nature, v. 301, p. 406–408.

Philander, S.G., 1990, El Niño, La Niña, and the Southern Oscillation: San Diego, Academic Press, 293 p.

Quiroz, R.S., 1983, The isolation of stratospheric temperature change due to the El Chichón volcanic eruption from nonvolcanic signals: Journal of Geophysical Research, v. 88, p. 6773–6780.

Sedlacek, W.A., Mroz, E.J., Lazrus, A.L., and Gandrud, B.W., 1983, A decade of stratospheric sulfate measurements compared with observations of volcanic eruptions: Journal of Geophysical Research, v. 88, p. 3741–3776.

Selkirk, R., and Newell, R.E., 1984, Statistical modeling of the effect of El Chichón on stratospheric temperatures, *in* Proceedings, 8th Annual Climate Diagnostics Workshop, Downsview, Ontario, Oct. 17–21, 1983: U.S. Dept. of Commerce, National Oceanic and Atmospheric Administration, 401 p.

Spencer, R.W., and Christy, J.R., 1990, Precise monitoring of global temperature trends from satellites: Science, v. 247, p. 1558–1562.

Spencer, R.W., Christy, J.R., and Grody, N.C., 1990, Global atmospheric temperature monitoring with satellite microwave measurements, methods and results, 1979–84: Journal of Climate, v. 3, p. 1111–1128.

Stokes, G.G., 1880, Description of the card supporter for sunshine recorders adapted at the Meteorological Office: Royal Meteorological Society Quarterly Journal, v. 6, p. 83–94.

Woods, D.C., and Chuan, R.L., 1983, Size-specific composition of aerosols in the El Chichón volcanic cloud: Geophysical Research Letters, v. 10, p. 1041–1044.

Wright, P.B., 1975, An index of the southern oscillation: Norwich, United Kingdom, Climatic Research Unit, University of East Anglia, Report No. CRU RP4, 20 p.

Wu, Z-X., Newell, R.E., and Hsiung, J., 1990, Possible factors controlling global marine temperature variations over the past century: Journal of Geophysical Research, v. 95, p. 11799–11810.

VOLCANIC ASH AND AVIATION SAFETY:
Proceedings of the First International Symposium
on Volcanic Ash and Aviation Safety
U.S. GEOLOGICAL SURVEY BULLETIN 2047

# A MESOSCALE DATA ASSIMILATION SYSTEM ADAPTED FOR TRAJECTORY CALCULATIONS OVER ALASKA

*By* Thomas W. Schlatter *and* Stanley G. Benjamin

## ABSTRACT

Soon after a volcanic eruption, it is possible to locate the ash plume from satellite imagery, at least if the sky is clear. However, as the plume disperses and thins, remote detection becomes more difficult. A series of numerical analyses of atmospheric observations, which can supply wind data to a trajectory model at frequent intervals, is one way to accurately track the ash plume.

National Oceanic and Atmospheric Administration's (NOAA) Forecast Systems Laboratory has developed a mesoscale analysis and prediction system (MAPS) for assimilating surface and tropospheric weather observations over the contiguous United States every 3 hours. Designed to serve aviation and local nowcasting, MAPS was implemented at the National Meteorological Center in 1992. It relies heavily on automated aircraft reports supplied by Aeronautical Radio, Inc. (ARINC) through the aircraft communications addressing and reporting system (ACARS). These reports use isentropic coordinates (surfaces of constant potential temperature) in the free atmosphere and terrain-following coordinates near the ground.

MAPS is being adapted for use over Alaska where a special high-resolution topography field has been created to account for the rough terrain. However, more ACARS reports over all of Alaska must be collected in real time so that the tropospheric and lower stratospheric wind field can be adequately defined every few hours.

## INTRODUCTION

When a volcano spews ash high into the atmosphere, it is not difficult to identify the location of the eruption unless dense clouds hide the ash plume from satellites. If the eruption is sufficiently powerful, ash may enter the stratosphere, above the clouds. Aircraft in the immediate vicinity of the eruption are subject to the life-threatening hazard of engine shutdown. Other substantial hazards remain long after the eruption, sometimes far from its origin, and aircraft must avoid the drifting ash plume. It is important, therefore, to know where the plume is and where it is likely to drift. Satellites can track the ash plume as long as it can be detected. However, after the plume spreads and disperses, tracking becomes more difficult, and the levels where ash is concentrated are hard to discern. Trajectories calculated from a series of wind analyses or from a numerical forecast are solutions to the problems of tracking and predicting the plume location.

Trajectories are only as accurate as the analyses and forecasts on which they depend. At NOAA's Forecast Systems Laboratory, in Boulder, Colo., a team of meteorologists, a mathematician, and a systems programmer have been working for several years to develop a mesoscale analysis and prediction system (MAPS), which exploits several sources of atmospheric observations that are available almost continuously. Even now, analyses of upper-air conditions from the National Meteorological Center (NMC), in Washington, D.C., are available only twice a day, at 00:00 and 12:00 UTC. Over the contiguous 48 United States, sufficient observations are available to support upper-air analyses every 3 hours. MAPS assimilates these surface and tropospheric observations every 3 hours to better describe atmospheric conditions and make accurate short-term forecasts out to 12 hours.

A version of MAPS for the lower 48 States is already running experimentally at the National Meteorological Center, and another version is being developed for Alaska. The analyses and predictions from MAPS can be used as input for trajectory calculations whenever Alaskan volcanoes erupt. Simkin and others (1981) list 39 volcanoes on the Aleutian Islands, 27 on the Alaskan Peninsula, and 18 elsewhere in the State as being active at least once during the past 10,000 years. Beget and others (1991) estimate that Alaskan eruptions large enough to disrupt air traffic have an average recurrence interval of 5–10 years. The eruption of Redoubt Volcano on the west side of Cook Inlet during 1989 and 1990 is a recent example (Brantley, 1990).

In this paper, we describe how MAPS works, why it is useful for trajectory calculations, how it compares to the nested grid model (NGM) (the limited-area model currently in use at NMC), how MAPS is being adapted for use over Alaska, and some changes that must be made before the

Alaska version performs as well as the version for the lower 48 States.

## HOW MAPS WORKS

MAPS provides high-frequency analyses and short-range forecasts that incorporate "off-time" observations as well as synoptic observations (at 00:00 and 12:00 UTC). The current resolution of the MAPS grid is 60 km. The main users of MAPS are commercial aviation and operational forecasters who need short-term guidance for 6–12 hours into the future. The main components of MAPS are shown in figure 1.

### EXTERNAL DATA SOURCES

The upper-air assimilation system relies on two external sources of data: (1) a variety of meteorological observations from the surface, troposphere, and lower stratosphere (see following section), and (2) time-dependent boundary conditions supplied by NMC's nested grid model (NGM).

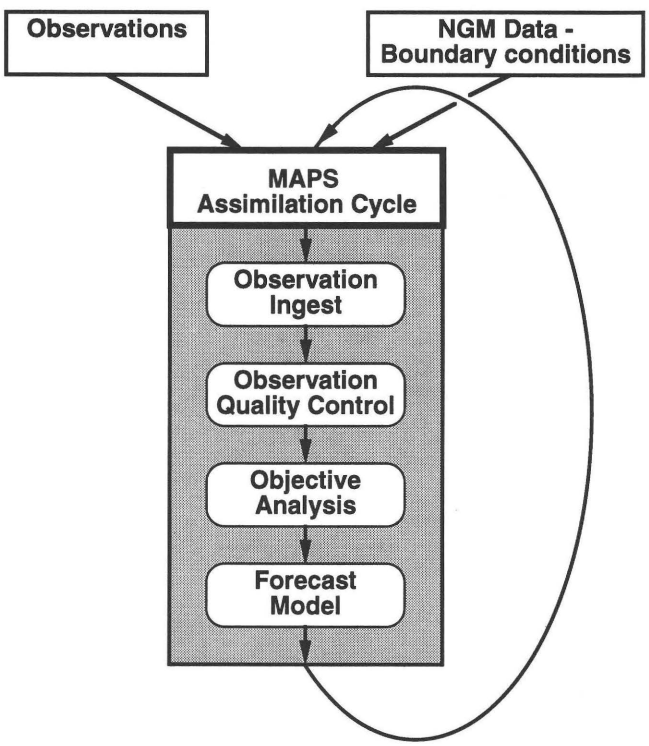


**Figure 1.** The major components of the mesoscale analysis and prediction system (MAPS). The upper-air assimilation cycle is self-contained except for the external inputs noted at the top. Observations of wind, temperature, pressure, and humidity by balloons, aircraft, radars, or observers are included. NGM, nested grid model at the National Meteorological Center, which supplies time-dependent lateral boundary conditions for the MAPS forecast model.

These boundary conditions are needed for the MAPS hybrid prediction model. They specify the evolution of the variables along the four edges of the forecast area, which pass through southern Canada, northern Mexico, and the coastal waters of the Atlantic and Pacific Oceans.

### OBSERVATIONS

The upper-air assimilation cycle begins with the incorporation of observations from four major sources in the contiguous United States and adjacent portions of Canada and Mexico:

- Rawinsondes—About 80 every 12 hours, providing observations of winds, altitudes, temperatures, and moisture.
- Wind profiler demonstration network in the Central United States—Twenty of the 30 expected profilers were operating by mid-December 1991. Wind profiling radars provide accurate hourly profiles of the horizontal wind in the troposphere and lower stratosphere.
- Surface observations—Six hundred to 900 surface observations per hour depending on the time of day plus about 25 moored buoys. These observations are used to analyze low-level altitudes, winds, temperatures, and moisture.
- ACARS aircraft reports—These are fully automated reports of wind and temperature collected from the airlines by ARINC (Aeronautical Radio, Inc.) and made available through ACARS, the ARINC aircraft communications addressing and reporting system. An average of 380 to 1,550 reports were available every 3 hours during December 1991 (fig. 2). For peak travel time, the density of reports can be quite remarkable (fig. 3).

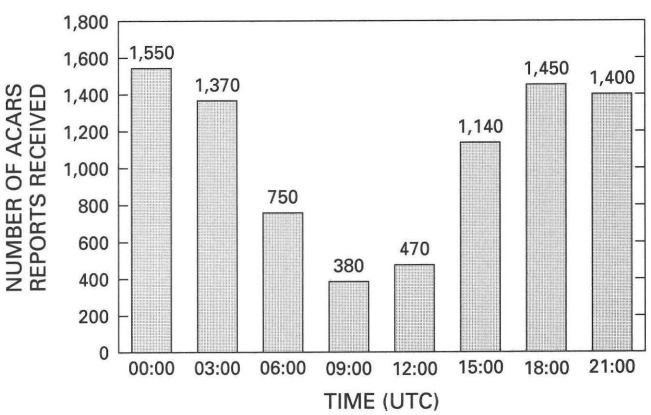


**Figure 2.** Average number of fully automated ACARS aircraft reports received in 3-hour windows during December 1991. There are peaks in air traffic at midday and during the late afternoon.

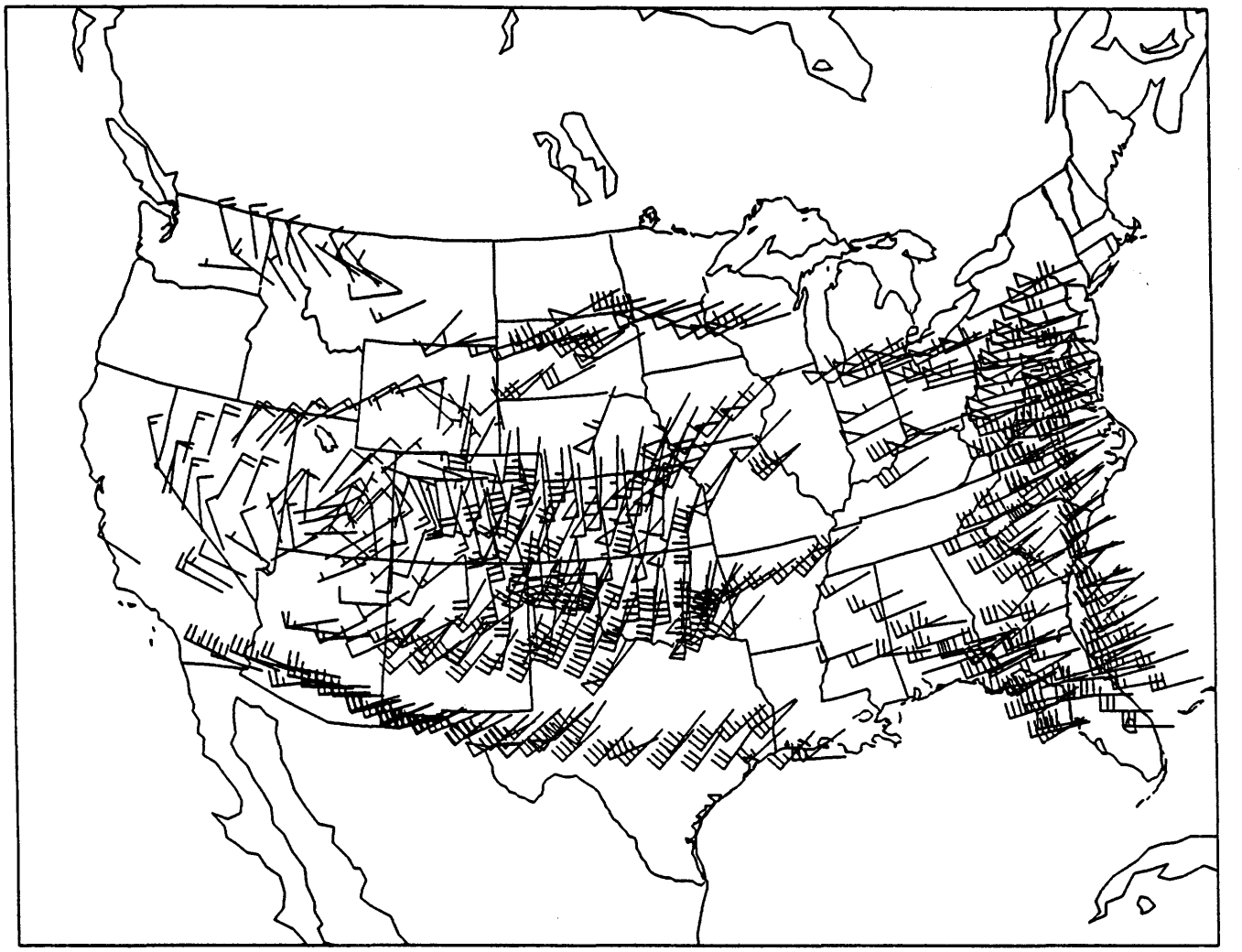

**Figure 3.** ACARS aircraft reports from between 175 and 225 mb (from 36,000 to 41,000 ft altitude) received between 16:30 and 19:30 UTC 19 January 1990. This represents 40 percent of the number received at all levels. The data plot is interpreted as follows: The staff extends into the wind; thus, winds along the East Coast are approximately from the west. Barbs on the staff give wind speed: small barbs represent 5 m/s; full barbs represent 10 m/s; and flags represent 50 m/s. The observations depict a jet stream from Kansas to the mid-Atlantic States.

ACARS observations are the single most important asynoptic data source for the MAPS 3-hour assimilation cycle (Benjamin, 1991). They are numerous, distributed fairly evenly over the lower 48 States, and are mostly from between 400 and 150 millibars (mb) (altitudes between 24,000 and 45,000 ft). Some ascent and descent data are also available. These will soon become much more common and will be triggered as aircraft pass through specified altitudes. Profilers provide excellent wind data in the lower troposphere, an area where ACARS reports are still sparse.

Satellite radiances (values of upwelling radiation measured in different wavelength intervals) offer the hope of estimating layer temperatures and vertically integrated moisture content. So far, we have been unable to demonstrate that this data source improves analyses or forecasts when the other sources of data are present. However, over Alaska, where observations are sparse in comparison to the lower 48 States, radiances from the polar-orbiting television and infrared observation satellites (TIROS) may prove more valuable. Satellite data are not assimilated in the present version of MAPS.

All incoming observations are subjected to several stages of quality control. The most rigorous of these is a "buddy" check. At each observation location, a value from neighboring observations is interpolated. If the interpolated value differs significantly from the observed value at that point, we run further tests to determine whether the central observation or one of its neighbors is at fault.

## OBJECTIVE ANALYSIS

For a meteorologist, the words "objective analysis" refer to a programmable method for estimating meteorological parameters on a regular set of points, usually a three-dimensional grid. The estimates depend upon the available observations, which are usually distributed irregularly in space and time. Numerical prediction models are often made part of the objective analysis for the reasons mentioned in the next section. In the case of MAPS, a 3-hour numerical forecast, valid at the analysis time, provides a first guess for the analysis.

The method of objective analysis employed in MAPS is known as optimum interpolation and is statistical in nature. The method, popularized by Gandin (1963) and still widely used, accounts for the errors in different observing systems. It also accounts for the geographical distribution of stations relative to each other and to the point being analyzed and allows observations of one variable to influence the analysis of another. For example, observations of the altitude of constant pressure surfaces influence the analysis of wind. Finally, the method mixes information from the forecast model and observations in a logical way.

## NUMERICAL PREDICTION MODEL

A numerical prediction model is an essential component of any system that assimilates meteorological data. First, the equations in these models summarize our understanding of atmospheric behavior. Second, our best a priori estimate of the current state of the atmosphere comes from a numerical prediction model, which provides the background for subsequent analysis. Moreover, the statistics of model performance tell us how to weight the model prediction (i.e., the background) relative to the observations. Third, the model imposes dynamic consistency on the system and retains the effects of all past observations.

The prediction model in MAPS is an outgrowth of the model introduced by Bleck (1984) and is based on the so-called primitive equations. These consist of three prognostic equations (for thermodynamic energy and the two components of horizontal momentum) and three diagnostic equations (the ideal gas law, the mass continuity equation, and the hydrostatic approximation). Calculations for both the analysis and the prediction are performed on a 60-km grid at each of 25 vertical levels. The model allows for stratiform and convective precipitation; turbulent transfer of heat, momentum and moisture in the vertical; and a diurnal heating cycle (Benjamin, Brewster, and others, 1991; Benjamin, Smith, and others, 1991).

Figure 4 summarizes the assimilation cycle. New observations are introduced every 3 hours, followed by a 3-hour forecast, which extrapolates atmospheric conditions forward to the next analysis time. Twice daily, at 00:00 and 12:00 UTC, the forecast runs out to 12 hours, mainly for comparison with NMC's nested grid model. As soon as NGM results are available, the time-dependent lateral boundary conditions for the MAPS domain are updated.

## USING MAPS FOR TRAJECTORY CALCULATIONS

MAPS itself does not compute trajectories; rather, it supplies a series of analyzed or predicted wind fields to NOAA's Air Resources Laboratory, in Washington, D.C., which has long experience in generating trajectories. See Stunder and Heffter (this volume) for details on trajectory calculations.

Why should wind fields from MAPS be particularly good for the generation of trajectories? The immediate answer is that frequent assimilation of "off-time" observations permits sharper definition of mesoscale flow features that are tens to hundreds of kilometers in size, thus leading to a more accurate wind field.

A less obvious answer is related to the choice of vertical coordinate. Analyses and predictions in MAPS are computed in hybrid vertical coordinates (Benjamin, Smith, and others, 1991), which are a combination of two kinds of coordinates. In the free atmosphere, we use isentropic coordinates (19 surfaces of constant potential temperature). In adiabatic flow when there are no heat sources or sinks, air on a particular isentropic surface will remain on that surface. Under this assumption, trajectory calculations become two-dimensional. The vertical spacing of isentropic coordinates is tied to the stability of the atmosphere; the surfaces are close together when the atmosphere is stably stratified and widely

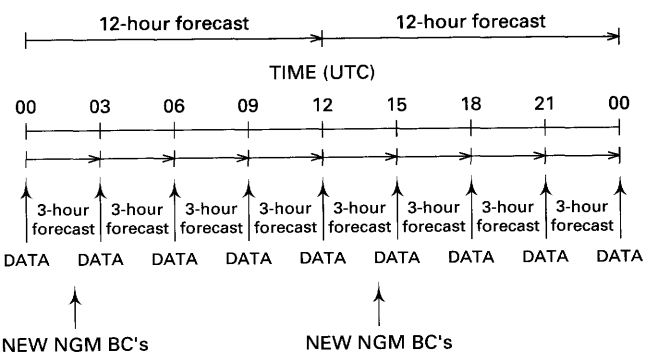


**Figure 4.** A 3-hour assimilation cycle. Every 3 hours, newly observed data are used to analyze atmospheric conditions. These analyses supply the initial conditions for a numerical prediction, which advances the atmospheric state forward to the next analysis time, when another batch of observations is assimilated. Twice a day, at 00:00 and 12:00 UTC, the forecast goes out to 12 hours. Each time the nested grid model (NGM) runs at NMC, a new set of time-dependent lateral boundary conditions (BC) replaces the old set.

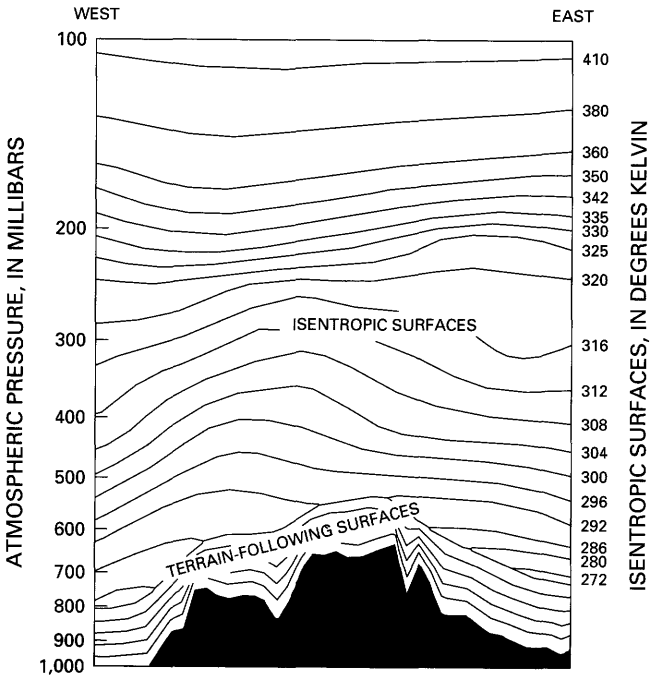


**Figure 5.** An illustration of the hybrid vertical coordinates used in MAPS. This vertical cross section was taken at 12:00 UTC 1 February 1990. It runs from the Pacific Ocean, off the Oregon coast on the left, to South Dakota, on the right. Terrain is silhouetted in black. Six terrain-following surfaces, each higher one smoother than the one below, occupy, on average, the first 150 mb above ground. In the free atmosphere, up to 19 isentropic surfaces with variable spacing (generally from 4 to 10 degrees Kelvin) are used for computation.

spaced when the lapse rate (decrease of temperature with altitude) is steep. This property gives enhanced spatial resolution where it is needed, such as in the vicinity of atmospheric fronts and jet streams.

One drawback of isentropic coordinates is that they become too widely spaced in deep, well-mixed boundary layers, which develop often on hot summer days and over elevated terrain. To overcome this drawback, terrain-following coordinates are used, spaced about 30 mb (or roughly 300 m) apart, on average, for the lowest six surfaces. This gives reasonable precision in the calculation of vertical fluxes of momentum, heat, and moisture close to the ground. The hybrid coordinate system is illustrated in figure 5. The surfaces move up or down depending upon atmospheric conditions; hence, this depiction is for a specific time and date.

## PERFORMANCE: MAPS VERSUS NGM

In a recent comparison between MAPS and NMC's nested grid model, we interpolated wind predictions by MAPS and the NGM to rawinsonde sites in the United States and southern Canada. We then computed the magnitude of the vector difference between predicted and observed winds. The root-mean-squares of these differences appear in figure 6 as a function of pressure level. The most striking result is that 3-hour and 6-hour MAPS wind forecasts are consistently better than the 12-hour NGM forecasts that are valid at the same time. This is true at all levels, but it is especially true at altitudes between 24,000 and 45,000 ft (or, equivalently, between 400 and 150 mb on fig. 6) where commercial jets provide most of the ACARS data This demonstrates clearly the advantage of frequent assimilation of off-time data. The choice of isentropic coordinates is also an advantage; these coordinates tend to crowd together and give good vertical resolution in the high troposphere and lower stratosphere in the vicinity of the jet stream.

During 1992, MAPS ran experimentally in real time on NMC's Cray Y-MP supercomputer on a domain covering the lower 48 States. Output stored on disks at NMC was carefully examined for evidence of mistakes in the computer code. By late 1992, the system was running reliably and performing well. Preliminary tests of an Alaskan version of MAPS are scheduled for 1993 at the Forecast Systems Laboratory in Boulder, Colo. If the available data show that a 3-hour assimilation cycle over Alaska is viable, more rigorous testing could begin at NMC.

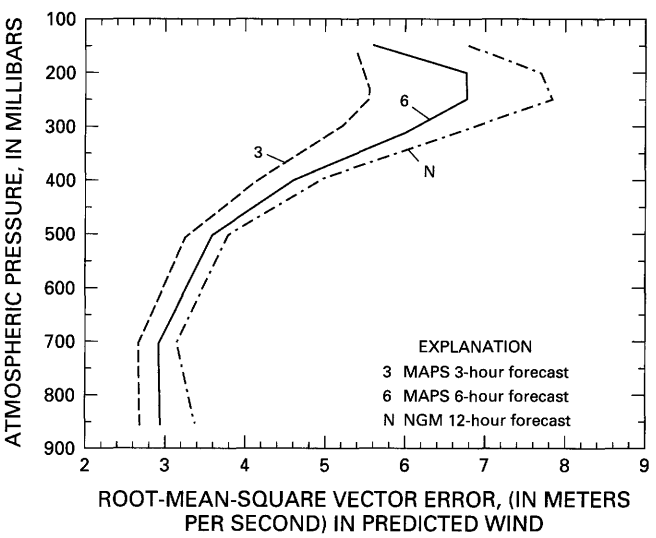


**Figure 6.** The root-mean-square vector error in wind forecasts produced by MAPS and the NGM. The error was estimated by comparing predicted winds with winds measured by rawinsonde in the United States and southern Canada from 26 November through 29 December 1991. All three forecasts shown are valid at the same time.

## ADAPTING MAPS FOR USE OVER ALASKA

Alaska has far greater topographical relief than any of the lower 48 States. It also has a longer, more convoluted shoreline. The terrain-following surfaces used in MAPS conform to the rough topography as closely as the horizontal resolution allows. Our first experiments over Alaska will employ "envelope" topography, obtained from a file of very high resolution topography in the following way. For each grid box of the prediction model, one adds the standard deviation of altitude to the mean altitude. Envelope topography accounts for the fact that mountain barriers to the wind are higher than the mean altitude. The MAPS domain for Alaska and envelope topography for a 60-km grid are shown in figure 7.

Roughly 50 percent of the domain in figure 7 is covered by ocean. The observation sources currently contributing to

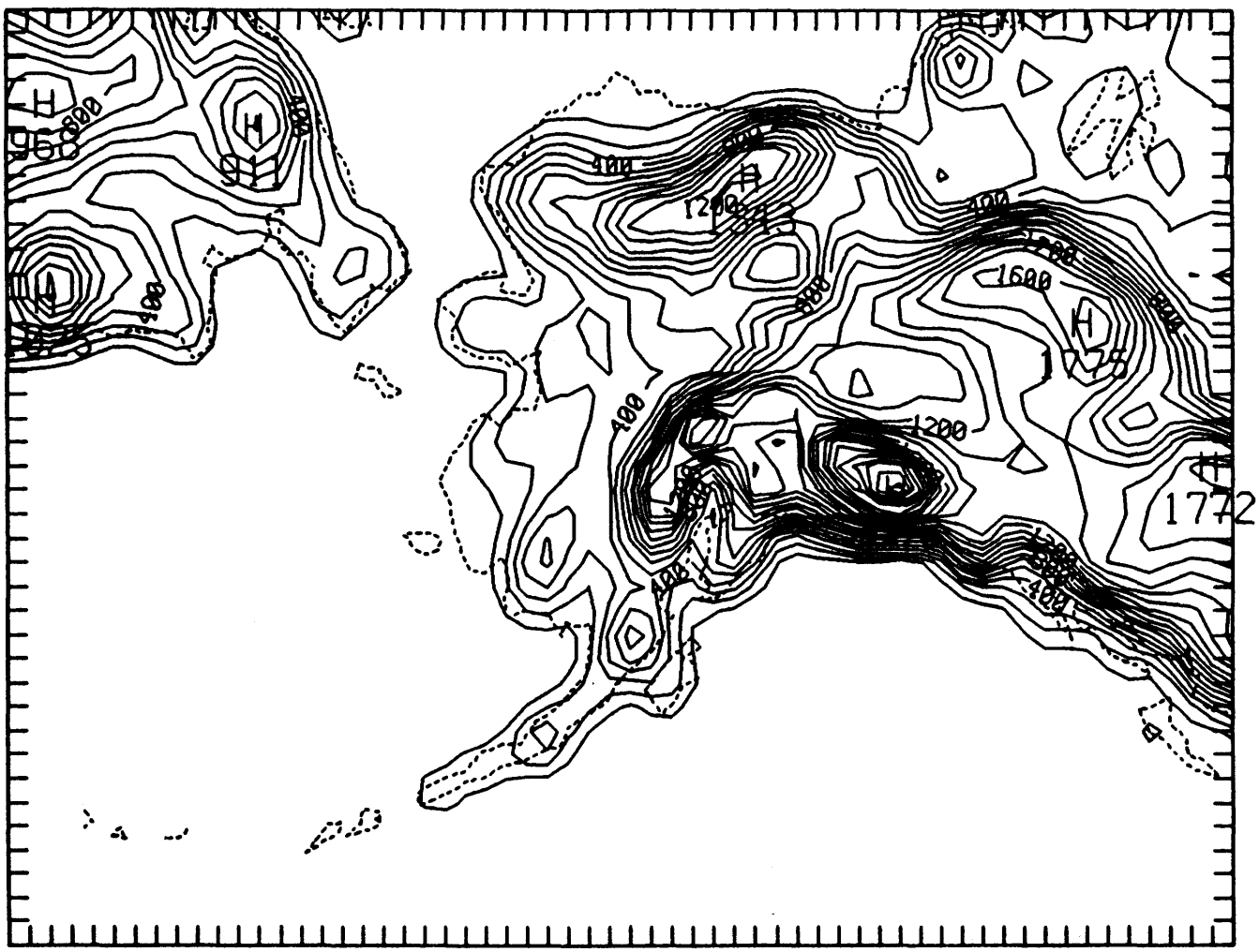


**Figure 7.** The geographical domain for the Alaska version of MAPS. Tick marks around perimeter are at 60-km spacing. Elevation contours for envelope topography (see text) are at 100-m intervals.

MAPS will supply scant information over the ocean because ACARS data are acquired only within a few hundred kilometers of a ground station. To improve analyses in oceanic regions, it will be necessary to adapt MAPS for assimilation of ship reports and TIROS radiance data. In addition, the western boundary of the NGM is so close to Alaska that the inflow conditions are likely to be poorly defined, thus quickly contaminating the forecast. To correct this problem, we also must replace the time-dependent lateral boundary conditions from the NMC's nested grid model with those from the aviation (global spectral) model.

## CONCLUDING REMARKS

MAPS is a system for the frequent assimilation of diverse surface, tropospheric, and lower stratospheric weather data. The system provides frequent updates on atmospheric conditions to aviation and local forecasters. A wealth of wind reports available from wind profilers and commercial jets permits detailed analyses every 3 hours and accurate short-term predictions of winds over the lower 48 States. These 3-hour "snapshots" and corresponding predictions can feed into trajectory calculations for tracking volcanic plumes and predicting their future movement (Stunder and Heffter, this volume).

One major obstacle prevents immediate application of MAPS over Alaska: the lack of data. Many aircraft fly over Alaska, and the Aleutian chain is a major international route. While many of these aircraft are equipped to provide automated reports, as of summer 1991, the only ground station for receipt of these reports was at Anchorage. In the same way that thousands of ACARS reports per day make MAPS a viable system for the lower 48 States, a similar density of reports is required for the Alaskan version.

The Federal Aviation Administration and Aeronautical Radio, Inc. are helping to alleviate this problem. As of January 1993, nine more ground receiving stations are operating in Alaska: at Shemya, Adak, Dutch Harbor, Cold Bay, St. Paul Island, Bethel, King Salmon, McGrath, and Fairbanks. By late 1993, eight more are expected in southeast Alaska and northwest Canada. This will greatly increase the number of reports. Efforts should also be made to obtain over-water reports relayed by satellite. Until about 100 reports can be collected every hour, reasonably distributed over the domain of figure 7, we should not expect that a rapid-update assimilation cycle will improve upon the operational 12-hour forecasts that are already available.

## ACKNOWLEDGMENTS

We thank our colleagues, Patty Miller, Tracy Smith, and Kevin Brundage and long-term visitors Jean-Marie Carriere and Pan Zaitao for their assistance in developing MAPS. We acknowledge the help of the Facilities Division of the Forecast Systems Laboratory in decoding ACARS reports. This project is funded by the National Weather Service.

## REFERENCES CITED

Beget, J.E., Swanson, S.E., and Stone, D., 1991, Frequency and regional extent of ash eruptions from Alaskan volcanoes [abs.], *in* Casadevall, T.J., ed., First International Symposium on Volcanic Ash and Aviation Safety, U.S. Geological Survey Circular 1065, p. 13.

Benjamin, S.G., 1991, Short-range forecasts from a 3h isentropic-sigma assimilation system using ACARS data: Boston, Mass., American Meteorological Society, Proceedings, Fourth International Conference on Aviation Weather Systems, 24–28 June, Paris, France, p. 329–334.

Benjamin, S.G., Brewster, K.A., Brummer, R., Jewett, B.F., Schlatter, T.W., Smith, T.L., and Stamus, P.A., 1991, An isentropic three-hourly data assimilation system using ACARS aircraft observations: Monthly Weather Review, v. 119, p. 888–906.

Benjamin, S.G., Smith, T.L., Miller, P.A., Kim, D., Schlatter, T.W., and Bleck, R., 1991, Recent improvements in the MAPS isentropic-sigma data assimilation system: Boston, Mass., American Meteorological Society, Proceedings, Ninth Conference on Numerical Weather Prediction, 14–18 October, Denver, Colo., p. 118–121.

Bleck, R., 1984, An isentropic coordinate model suitable for lee cyclogenesis simulation: Estratto dalla Rivista di Meteorologia Aeronautica, v. 44, p. 189–194.

Brantley, S.R., ed., 1990, The eruption of Redoubt Volcano, Alaska, December 14, 1989–August 31, 1990. U.S. Geological Survey Circular 1061, 33 p.

Gandin, L.S., 1963, Objective analyses of meteorological fields: Leningrad, Giderometeorologicheskae Izdatel'stvo, [original in Russian, translated in 1965 by Israel Program for Scientific Translators], 242 p.

Simkin, T., Siebert, L., McClelland, L., Bridge, D., Newhall, C., and Latter, J.H., 1981, Volcanoes of the World: Stroudsburg, Pa., Hutchinson Ross Publishing Co., Smithsonian Institution, 240 p.

VOLCANIC ASH AND AVIATION SAFETY:
Proceedings of the First International Symposium
on Volcanic Ash and Aviation Safety
U.S. GEOLOGICAL SURVEY BULLETIN 2047

# MODELING VOLCANIC ASH TRANSPORT AND DISPERSION

*By* Barbara J.B. Stunder *and* Jerome L. Heffter

## ABSTRACT

A real-time long-range volcanic ash forecast transport and dispersion model is described. Ash emitted into the atmosphere as high as 100 mb (≅ 53,000 ft) is modeled as a nearly steady eruption column. Falling ash is modeled as advecting downwind with the National Weather Service forecast wind fields. Maps of relative ash concentration for various layers in the atmosphere are produced. The presence of falling ash is clearly seen in the volcanic eruption example shown. Some of the ash shown in the lower layer output map must have fallen from above because it cannot be explained by transport and dispersion in the lower layer alone.

## INTRODUCTION

Airline pilots are clearly interested in avoiding volcanic ash clouds because of possible damage, ranging from abraded windscreens to engine failure. At least five commercial jet aircraft were damaged from encounters with airborne ash during the first 3 months of the eruption of Redoubt Volcano, near Anchorage, Alaska, beginning in December 1989 (Brantley, 1990).

A memorandum of understanding (MOU) concerning volcano hazards alert between the National Oceanic and Atmospheric Administration (NOAA) and the Federal Aviation Administration (FAA) was signed in 1988, prompted by the 1980 eruptions of Mount St. Helens, Washington, and the 1982 eruption of Galunggung, in Java, Indonesia. Under the terms of the MOU, the role of NOAA Air Resources Laboratory (ARL) is to provide volcanic-ash-trajectory forecasts. Upon notification of an eruption, ARL produces a forecast that gives the predicted location of volcanic ash at several levels in the atmosphere for times up to 48 hours after the eruption. Typically, an updated forecast is made 12 hours later when the meteorological analysis and new forecast data are available.

As of 1991, the NOAA-ARL volcano hazards alert message consisted of three parts: (1) a text message giving the regional extent of the ash cloud at several atmospheric levels in 6-hour periods after the release, (2) maps of the forecast isobaric trajectories for the ash cloud, and (3) latitude/longitude tabular listings of the trajectories. As an example, figure 1 shows the text message for a hypothetical 50,000-ft eruption of Mount St. Helens at 00 GMT (Greenwich Mean Time), September 11, 1991. Because the trajectories show the predicted path of air parcels rather than ash particles, a cautionary note regarding falling ash is added to the end of the descriptive paragraph in the text message. The 48-hour duration 200-mb, 300-mb, 500-mb, and 700-mb trajectory maps and tables are shown in figures 2*A*–2*D*. (See table 1 for an atmospheric pressure level to altitude reference.) The 200-mb and 300-mb trajectories both show the ash cloud moving south, across California, then northeastward, reaching Minnesota 48 hours after the eruption. The 500-mb trajectory is much shorter, with ash moving south across California, but reaching only Arizona at 48 hours. At 700 mb, ash is predicted to move south to the central California coastal region at 48 hours.

An evaluation of the forecast trajectories from similar model runs for a series of Redoubt Volcano eruptions shows that average trajectory forecast error at 300 mb is usually less than 25 percent of the downwind distance from the volcano (Heffter and others, 1990). Trajectory errors of this magnitude are typical (e.g., Rolph and Draxler, 1990).

Since December 1992, the ARL product is a graphic product. The model is now named the volcanic ash forecast transport and dispersion model (VAFTAD). VAFTAD was developed to provide a better three-dimensional depiction in time of the ash cloud than does the trajectory model. The ambiguity of the cautionary warning in the forecast trajectory text message (fig. 1) is addressed. The new model is designed for operation on a 386-class personal computer. National Weather Service (NWS) forecast wind data on nine isobaric levels, from 850 mb to 100 mb, are downloaded from an NWS mainframe computer as input to the model run. User inputs are volcano name, latitude and longitude, eruption date, time, and ash cloud height. Since the total amount of ash erupted is usually unknown at the time of the eruption, a unit mass is assumed. Also, since the eruption duration may not be known, a 3-hour eruption is assumed. The dynamics of the eruption column itself are not modeled;

**Table 1.** Selected atmospheric pressure levels.

| Pressure (millibars) | Approximate altitude (feet above sea level) |
|---|---|
| 100 | 53,000 |
| 150 | 44,000 |
| 200 | 39,000 |
| 250 | 34,000 |
| 300 | 30,000 |
| 400 | 24,000 |
| 500 | 18,000 |
| 700 | 10,000 |
| 850 | 5,000 |

```
******************************************************

              VOLCANO HAZARDS ALERT
                 MT ST HELENS

          NOAA-AIR RESOURCES LABORATORY
              SILVER SPRING, MD

                 09/11/91 1313Z

MT ST HELENS ERUPTED ON 09/11/91 AT 0000Z
WITH VOLCANIC ASH REPORTED AS HIGH AS 50000 FT.
LONG-RANGE FORECAST TRAJECTORIES INDICATE THAT ANY ASH
REMAINING IN THE ATMOSPHERE WILL MOVE OVER THE FOLLOWING
REGIONS AT THE HEIGHTS & DATE/TIMES GIVEN.
CAUTION: ASH MAY FALL FROM GIVEN REGIONS TO LOWER HEIGHTS.

   7000 TO 15000 FT
                  WEST OREGON       11/00Z TO 11/06Z
                  WEST OREGON       11/06Z TO 11/12Z
                  WEST OREGON       11/12Z TO 11/18Z
                  NORTH CALIFRNIA   11/18Z TO 12/00Z
                  NORTH CALIFRNIA   12/00Z TO 12/06Z
                  NORTH CALIFRNIA   12/06Z TO 12/12Z
                  NORTH CALIFRNIA   12/12Z TO 12/18Z
                  NORTH CALIFRNIA   12/18Z TO 13/00Z

   15000 TO 25000 FT
                  WEST OREGON       11/00Z TO 11/06Z
                  NORTH CALIFRNIA   11/06Z TO 11/12Z
                  NORTH CALIFRNIA   11/12Z TO 11/18Z
                  OFFSHOR-S CALIF   11/18Z TO 12/00Z
                  OFFSHOR-S CALIF   12/00Z TO 12/06Z
                  SOUTH CALIFRNIA   12/06Z TO 12/12Z
                  SOUTH CALIFRNIA   12/12Z TO 12/18Z
                  SOUTH CALIFRNIA   12/18Z TO 13/00Z

   25000 TO 35000 FT
                  WEST OREGON       11/00Z TO 11/06Z
                  NORTH CALIFRNIA   11/06Z TO 11/12Z
                  OFFSHOR-S CALIF   11/12Z TO 11/18Z
                  SOUTH CALIFRNIA   11/18Z TO 12/00Z
                  ARIZONA           12/00Z TO 12/06Z
                  UTAH              12/06Z TO 12/12Z
                  NORTHCENTRL US    12/12Z TO 12/18Z
                  NORTHCENTRL US    12/18Z TO 13/00Z

   35000 TO 45000 FT
                  WEST OREGON       11/00Z TO 11/06Z
                  NORTH CALIFRNIA   11/06Z TO 11/12Z
                  SOUTH CALIFRNIA   11/12Z TO 11/18Z
                  SOUTH CALIFRNIA   11/18Z TO 12/00Z
                  UTAH              12/00Z TO 12/06Z
                  NORTHCENTRL US    12/06Z TO 12/12Z
                  NORTHCENTRL US    12/12Z TO 12/18Z
                  NORTHCENTRL US    12/18Z TO 13/00Z
******************************************************
```

**Figure 1.** Volcano-hazards-alert text message for a hypothetical eruption to 50,000 ft of Mount St. Helens at 00 GMT (Greenwich Mean Time), September 11, 1991. "Z" indicates Zulu (equivalent to Greenwich Mean Time or Coordinated Universal Time).

instead, the eruption is assumed to be nearly steady, with ash particles of a given size distribution uniformly distributed throughout the column. The uniform vertical distribution is clearly an approximation; later versions of the model may incorporate more detail in the initial ash distribution. The ash falls, disperses, and is advected downwind following the forecast wind data. Maps of ash concentration relative to the unit source are output for three atmospheric layers of interest to the aviation community. Removal of ash by precipitation is not considered in order to produce a conservative estimate of the concentration and ash cloud location.

## ATMOSPHERIC TRANSPORT AND DISPERSION

The forecast wind data used in the transport and dispersion model are from one of the NWS National Meteorological Center's numerical weather prediction models: either the nested grid model (NGM) (Hoke and others, 1989) or the aviation run (AVN) of the medium range forecast model (Petersen and Stackpole, 1989). Both models are run twice daily and produce forecast data at 6-hour intervals. Wind fields on the following pressure levels are used by the volcano model: 850, 700, 500, 400, 300, 250, 200, 150, and 100 mb. The NGM is a regional model covering North America; the AVN is a global model. The spatial resolution of the NMC output for the NGM and AVN on a polar stereographic projection at 60° latitude are 190.5 km and 381 km, respectively. The meteorological model specifications are summarized in table 2. Model output should not be interpreted at sub-grid scales.

**Table 2.** Specifications of NMC data used in volcano model.

[NMC, National Meteorological Center; NGM, nested grid model (Hoke and others, 1989); AVN, aviation run of the medium range forecast model (Petersen and Stackpole, 1989)]

| | NGM model | AVN model |
|---|---|---|
| Coverage | North America | Global |
| Spatial resolution[1] | 190.5 km | 381 km |
| Forecast period | 48 h | 72 h |

[1] At 60° latitude on a polar stereographic projection.

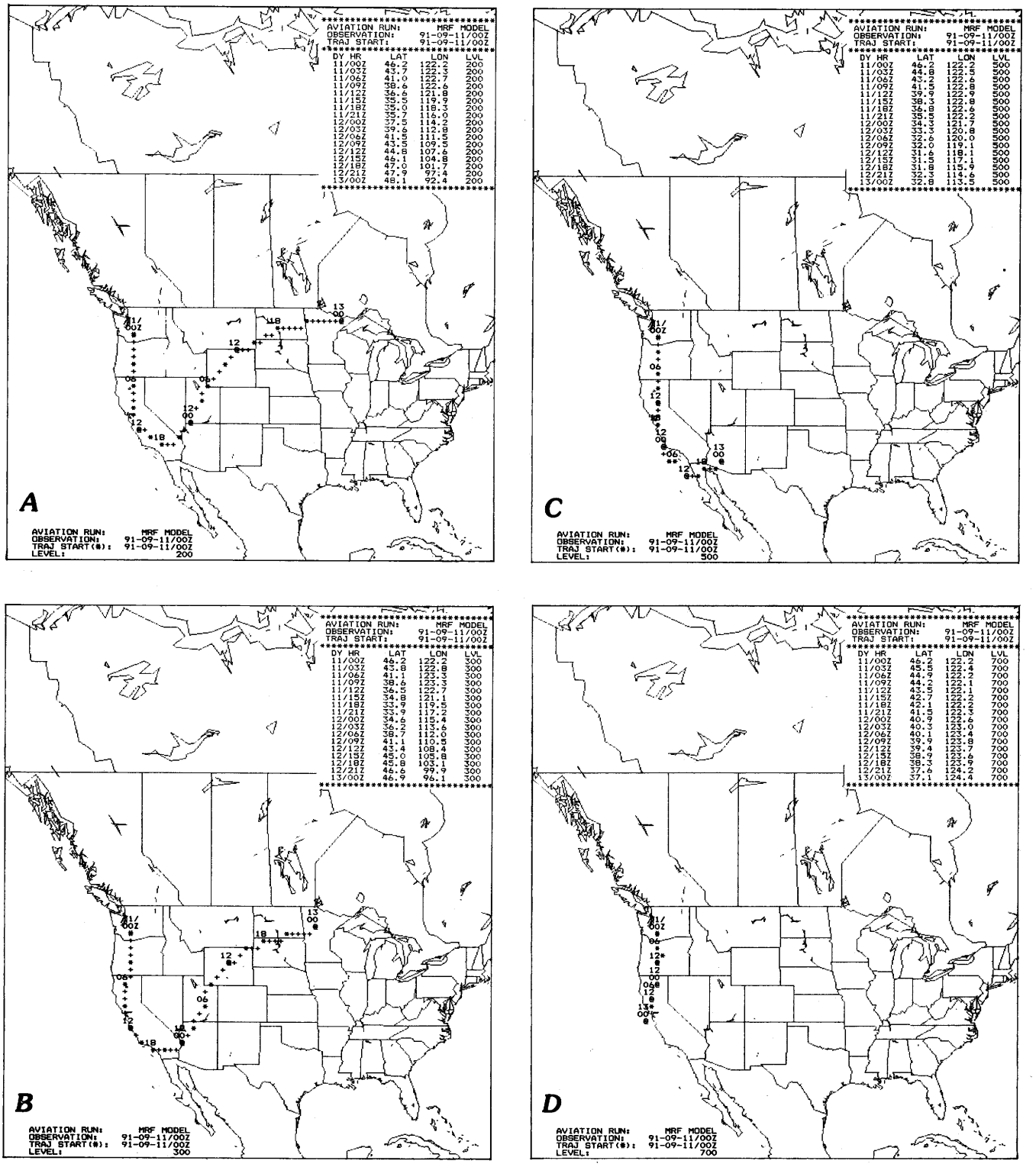


**Figure 2.** Forecast trajectory map and table corresponding to the text message in figure 1 for the following levels: *A*, 200 mb; *B*, 300 mb; *C*, 500 mb; and *D*, 700 mb. Mount St. Helens is identified by "#," and the eruption date and time (GMT, or Z) are given. Numbers along the trajectory give time; at 00 GMT the date is shown.

Transport trajectories are computed using a modified Euler advection technique to account for acceleration (Carnahan and others, 1969). This technique was also used by Heffter (1983). Horizontal dispersion causes puff size to grow linearly with time because:

$$\sigma = t/2 \quad (1)$$

where

$\sigma$ is the horizontal standard deviation, in meters, of the concentration, and

$t$ is time after the eruption, in seconds (Heffter, 1965).

This horizontal dispersion applies to long-range transport. A bivariate normal distribution gives the concentration at any radial distance from the center of a puff.

## ASH PARTICULATE

Given that different volcanoes and even multiple eruptions of one volcano may have different ash-particle size distributions, we assumed one typical distribution for our model. Measured ash-particle size distributions are obtained from either ground-level samples (e.g., Carey and Sigurdsson, 1982) or airborne samples (e.g., Hobbs and others, 1982). Because individual ground-level samples are not likely to be representative of the population of ash in the eruption column, Carey and Sigurdsson (1982) computed the "total" particle size distribution for the May 18, 1980, Mount St. Helens (MSH) eruption using many ground-level samples. The total particle size distribution is an estimate of the overall distribution in the eruption column. The resulting MSH total distribution (particles of diameter 2 μm to 16 mm) could be used in our model, but it does not include the smaller particles that remain airborne for extensive periods.

However, individual airborne samples also may not be representative, especially because research aircraft cannot safely fly through ash clouds near volcanoes. Airborne samples also do not contain larger particles that have already fallen out. Because our prime interest is with particles that remain airborne from 24 to 48 hours, we use a particle size distribution obtained from aircraft samples taken about 130 km downwind of a volcano (Hobbs and others, 1991), rather than a distribution obtained from ground-level samples. Aircraft samples closer to the volcano were not obtained because of safety considerations. The particles considered range in diameter from 0.1 μm to 100 μm.

Ash particles are assumed to fall as spheres according to Stokes' law modified by the Cunningham slip correction (Slade, 1968):

$$v=C[(gd^2\rho)/(18\mu)] \quad (2)$$

where

$v$ is the fall velocity (in m/s),

$g$ is the gravitational constant (in m/s$^2$),

$d$ is the particle diameter (in m),

$\rho$ is the ash particle density (in g/m$^3$),

$\mu$ is the kinematic viscosity of air (in g/ms),

$C=1+[\lambda/d][2.52+0.8(\exp(-0.55d/\lambda))]$ is the Cunningham slip correction (non-dimensional), and

$\lambda$ is the mean free path of air (in m).

The correction is important only for smaller particles (approximately less than 5 μm) whose fall velocities are greater than those according to Stokes' law because ash particles tend to slip past air molecules. Particle shape and rotation, such as addressed by Wilson and Huang (1979), are not considered. Our approximation is applicable given the spatial and temporal scales used here.

## MODEL OUTPUT

Output consists of maps of maximum 1-hour ash concentrations during a 24-hour period (0–24 h or 24–48 h). Maps for three layers are given. These layers will be referred to as layer 1 (15,000 to 25,000 ft), layer 2 (25,000 to 35,000 ft), and layer 3 (35,000 to 50,000 ft). Ground-level concentrations are not computed, and altitude is described in units of feet in deference to the aviation community. Symbols on the output maps indicate ranges of concentration (low, intermediate, and high) relative to the unit source. The exact computed concentration is not used for two reasons: (1) the amount of ash emitted is usually unknown, and (2) critical concentrations that affect the aircraft or its operation are unknown. The intermediate and low relative concentrations each span two orders of magnitude. These categories are somewhat arbitrary because even the low concentrations may still be hazardous to aircraft.

The forecast transport and dispersion model was run for the simulated eruption of Mount St. Helens on September 11, 1991 (as was the trajectory model—figs. 1 and 2*A*–2*D*). Figures 3*A*–3*C* and 4*A*–4*C* show the relative ash concentrations in the three layers for the two successive 24-hour periods after the eruption. For the first 24-hour period (figs. 3*A*–3*C*), the ash moved south across Oregon, continued generally along the California coast, then moved to the northeast across southern California toward the Nevada-Utah-Arizona region. The pattern in all three layers is fairly similar, with "high" concentrations generally found near the volcano. Ash concentrations lower than what are categorized as "low" are not shown on the maps. In the next 24-hour period (figs. 4*A*–4*C*), the ash was transported from the southern California region to the Lake Superior region, again with similar patterns at the three layers. In most areas, the concentrations are categorized as "intermediate", with no "high" concentrations and only some "low" concentrations.

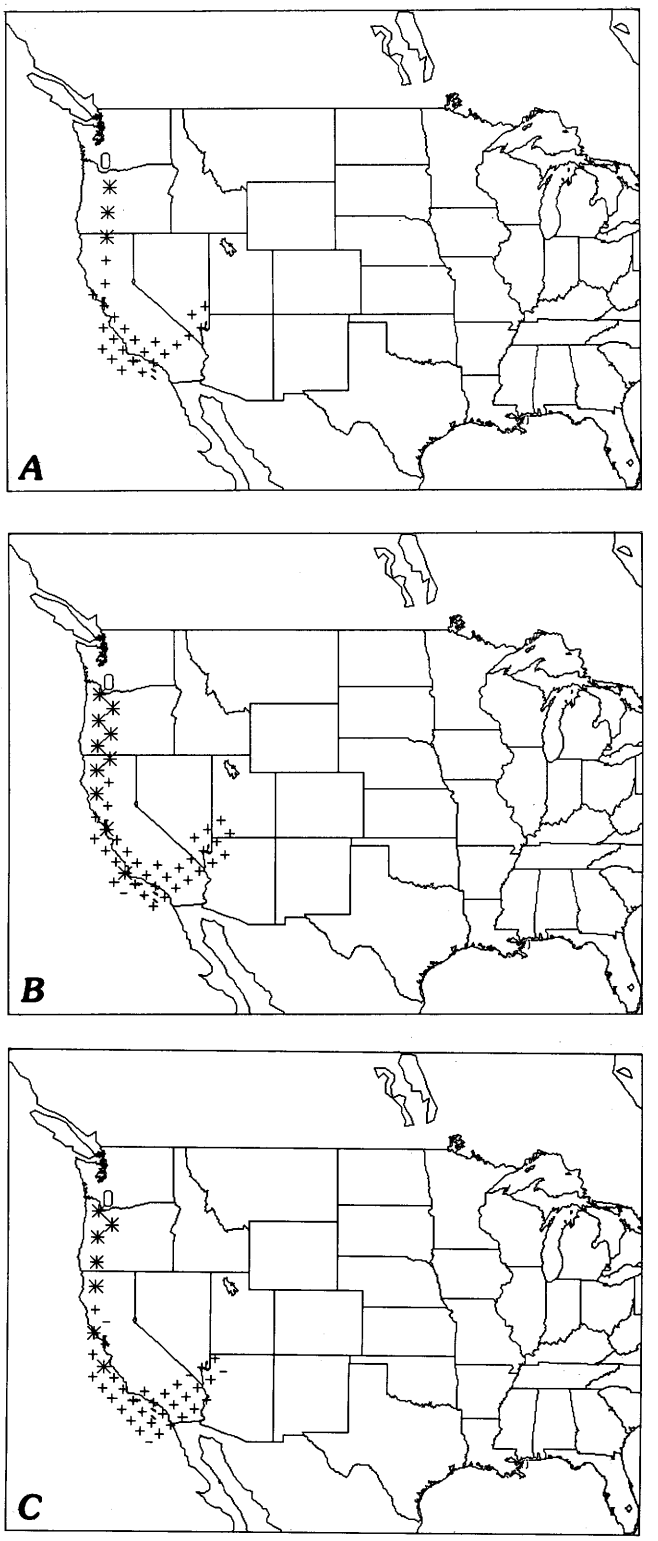


**Figure 3.** Relative concentration for hypothetical eruption given in figure 1 for the first 24-hour period after the eruption (00 GMT September 11 to 00 GMT September 12, 1991) for the following layers: *A*, 35,000 to 50,000 ft; *B*, 25,000 to 35,000 ft; and *C*, 15,000 to 25,000 ft. "O" shows volcano location; "*," "+," and "-" indicate high, intermediate, and low relative concentrations, respectively (see text for explanation of relative concentration).

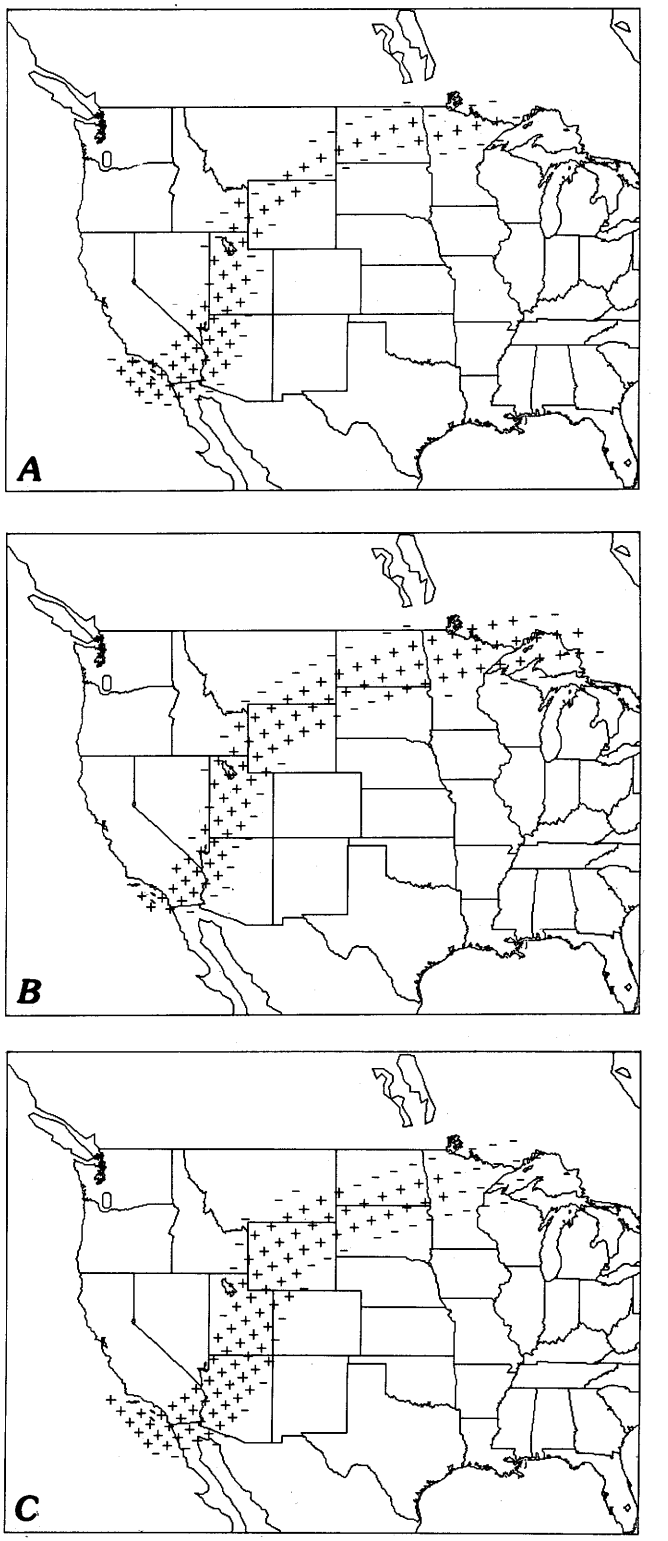


**Figure 4.** Relative concentration for hypothetical eruption given in figure 1 for the second 24-hour period after the eruption (00 GMT September 12 to 00 GMT September 13, 1991) for the following layers: *A*, 35,000 to 50,000 ft; *B*, 25,000 to 35,000 ft; and *C*, 15,000 to 25,000 ft. "O" shows volcano location; "*," "+," and "-" indicate high, intermediate, and low relative concentrations, respectively (see text for explanation of relative concentration).

A comparison of the transport and dispersion output (figs. 3*A*–3*C* and 4*A*–4*C*) with the trajectories (figs. 2*A*–2*D*) shows the presence of falling ash and dispersion. The concentration pattern in figure 3*A* agrees well with the first 24 hours of the 200-mb trajectory (fig. 2*A*). The ash off the California coast reflects the 150-mb trajectory (not shown). The concentration pattern in figure 3*B* agrees well with the 300-mb (fig. 2*B*) and 250-mb trajectories (not shown). Some ash has fallen from layer 3 to 2 during the first 24 hours. The "high" relative concentrations in central California in figure 3*B* may result from falling ash, but, otherwise, falling ash is not clearly evident for layer 2. In layer 1 (fig. 3*C*), the ash along the coast agrees with the 500-mb and 400-mb trajectories (figs. 2*C* and 2*D*), but the large region of ash over southern California and into Arizona is not reflected by the trajectories. The ash in that region must have fallen from layer 2 and possibly from layer 3.

For the second 24-hour period, again the layer 2 and layer 3 patterns correspond to the trajectories. The layer 1 pattern also corresponds to the trajectories but clearly contains ash falling from layers 2 and 3. The 500-mb and 400-mb trajectories corresponding to layer 1 terminate in central Arizona and northeastern Utah, respectively, but the ash across Wyoming, Montana, the Dakotas, and Minnesota must have fallen to this layer. For both 24-hour periods, layer 1 shows falling ash because the transport winds are much slower than those at higher altitudes. Falling ash at layer 2 is not apparent in the output maps because the transport winds are similar to those at layer 3.

## SUMMARY

A real-time long-range forecast volcanic ash transport and dispersion model has been developed for the aviation community. The model uses NWS forecast wind fields and Stokes' fall velocity with a slip correction for small particles. In the model, ash is emitted into the atmosphere to all layers by a nearly steady eruption column. The model produces maps of relative ash concentration in three layers in the atmosphere for times up to 48 hour after an eruption. Comparison of isobaric trajectories and the model output concentration maps show the presence of dispersion and falling ash.

In an example, the transport and dispersion model shows that a given region contains falling ash, but that same region may be free of ash according to the trajectory forecast. The trajectory model simply predicts an ash particle's position assuming it flows with the wind at a given atmospheric level. However, the transport and dispersion model produces a more realistic depiction of the three-dimensional ash plume because it accounts for falling and horizontally dispersing ash. The model generates relative ash concentrations because the critical concentrations that affect aircraft operations and the amounts of ash actually erupted are not known.

## ACKNOWLEDGMENT

This work was supported by the NOAA–National Weather Service Alaska volcano project.

## REFERENCES CITED

Brantley, S.R., ed., 1990, The eruption of Redoubt Volcano, Alaska, December 14, 1989–August 31, 1990: U.S. Geological Survey Circular 1061, 33 p.

Carey, S.N., and Sigurdsson, H., 1982, Influence of particle aggregation on deposition of distal tephra from the May 18, 1980, eruption of Mount St. Helens volcano: Journal of Geophysical Research, v. 87, p. 7061–7072.

Carnahan, B., Luther, H.A., and Wilkes, J.O., 1969, Applied Numerical Methods: New York, John Wiley and Sons, Inc., 362 p.

Heffter, J.L., 1965, The variation of horizontal diffusion parameters with time for travel periods of one hour or longer: Journal of Applied Meteorology, v. 4, p. 153–156.

———1983, Branching atmospheric trajectory (BAT) model: NOAA Technical Memorandum ERL ARL-121, Air Resources Laboratory, Rockville, Md., 16 p.

Heffter, J.L., Stunder, B.J.B., and Rolph, G.D., 1990, Long-range forecast trajectories of volcanic ash from Redoubt Volcano eruptions: American Meteorology Society Bulletin, no. 71, p. 1731–1738.

Hobbs, P.V., Radke, L.F., Lyons, J.H., Ferek, R.J., Coffman, D.J., and Casadevall, T.J., 1991, Airborne measurements of particles and gas emissions from the 1990 volcanic eruptions of Mount Redoubt: Journal of Geophysical Research, v. 96, p. 18735–18752.

Hobbs, P.V., Tuell, J.P., Hegg, D.A., Radke, L.F., and Eltgroth, M.W., 1982, Particles and gases in the emissions from the 1980–1981 volcanic eruptions of Mount St. Helens: Journal of Geophysical Research, v. 87, p. 11062–11086.

Hoke, J.E., Phillips, N.A., DiMego, G.J., Tuccillo, J.J., and Sela, J.G., 1989, The regional analysis and forecast system of the National Meteorological Center: Weather Forecasting, v. 4, p. 323–334.

Petersen, R.A., and Stackpole, J.D., 1989, Overview of the NMC production suite: Weather Forecasting, v. 4, p. 313–322.

Rolph, G.D., and Draxler, R.R., 1990, Sensitivity of three-dimensional trajectories to the spatial and temporal densities of the wind field: Journal of Applied Meteorology, v. 29, p. 1043–1054.

Slade, D., ed., 1968, Meteorology and atomic energy: U.S. Department of Energy, Division of Technical Information, 445 p.

Wilson, L., and Huang, T.C., 1979, The influence of shape on the atmospheric settling velocity of volcanic ash particles: Earth and Planetary Sciences Letters, v. 44, p. 311–324.

VOLCANIC ASH AND AVIATION SAFETY:
Proceedings of the First International Symposium
on Volcanic Ash and Aviation Safety
U.S. GEOLOGICAL SURVEY BULLETIN 2047

# DEVELOPMENT OF A PREDICTION SCHEME FOR VOLCANIC ASH FALL FROM REDOUBT VOLCANO, ALASKA

*By* Hiroshi L. Tanaka

## ABSTRACT

The purpose of this project is to develop a volcanic plume prediction model for volcanoes located in the Cook Inlet area, Alaska. Knowing where the ash plume is and predicting where it will go are important for public health and safety, as well as for flight operations and mitigating economic damage. For near-real-time plume prediction, acquisition of upper-air wind data is the essential part of the prediction scheme.

In this project, near-real-time meteorological data are provided by the National Meteorological Center, transmitted via Unidata. Reading the real-time and forecast wind data, the prediction model computes advection, diffusion, and gravitational fallout for the plume particles from the vertical column over the volcano. Three-dimensional dispersal of plume particles are displayed on the computerized graphic display as a function of time following the eruption. The model predictions appear on the screen about 15 minutes after the eruption report, showing the geographical distributions of plume dispersal for the following several hours. Although the model simulation inevitably has forecast errors owing largely to errors in the forecast wind input, the prediction product offers a useful guide for public safety, especially for the Cook Inlet area, Alaska.

## INTRODUCTION

Anchorage, Alaska is one of the focal points of international aviation activities. The city lies close to several active and potentially active volcanoes including Hayes, Spurr, Redoubt, Iliamna, Augustine, and Douglas along the west shore of Cook Inlet, and Wrangell Volcano to the east. In this century Spurr, Redoubt, and Augustine together have had eight significant eruptions that have spread ash over a broad area of south-central Alaska. It is necessary to establish a reliable scheme for predicting the distribution of volcanic ash fall after an eruption in order to avoid unnecessary disruptions of aircraft operations. For the plume prediction to be operational, an immediate eruption report and real-time upper-air data must be available. A quick response is one of the priorities of the plume-prediction system.

The Alaska Volcano Observatory (AVO) at the Geophysical Institute, University of Alaska, Fairbanks, has direct access to near-real-time satellite imagery and upper-air weather data (Dean and others, this volume). By combining this information with the established eruption-monitoring network provided by AVO, we have established a volcanic plume prediction model that predicts volcanic ash dispersal as a function of time immediately after the eruption. The upper-air wind data are the fundamental input to the plume-prediction model. The National Meteorological Center (NMC), in Washington, D.C., offers daily weather predictions as well as analyzed and initialized meteorological data on three-dimensional (3-D) gridded mesh. Recently, a national program in atmospheric sciences, referred to as Unidata, enables university researchers to use the real-time NMC data through a satellite downlink (Sherretz and Fulker, 1988; Tanaka, 1991a, 1991b). Therefore, the real-time upper-air wind data are available at AVO.

In response to the eruption of Redoubt Volcano at the end of 1989, a volcanic plume prediction model has been developed within the AVO (Tanaka, 1990). This project incorporates wind data from Unidata for predicting the distribution of volcanic ash plumes on a real-time basis after an eruption is reported. Using the real-time and predicted upper-air data, the model computes advection, diffusion, and gravitational fallout of the ash particles. Three-dimensional distributions of the ash plume are displayed on the computerized graphic display, predicting the direction and dispersion of ash clouds for the first several hours after eruption. This report describes the algorithm of the present particle-tracking model in a Lagrangian framework. The results of the demonstrations and the procedure of the information-transfer network are presented.

## UNIDATA

Unidata (University data) is a national program for providing near-real-time meteorological data to university

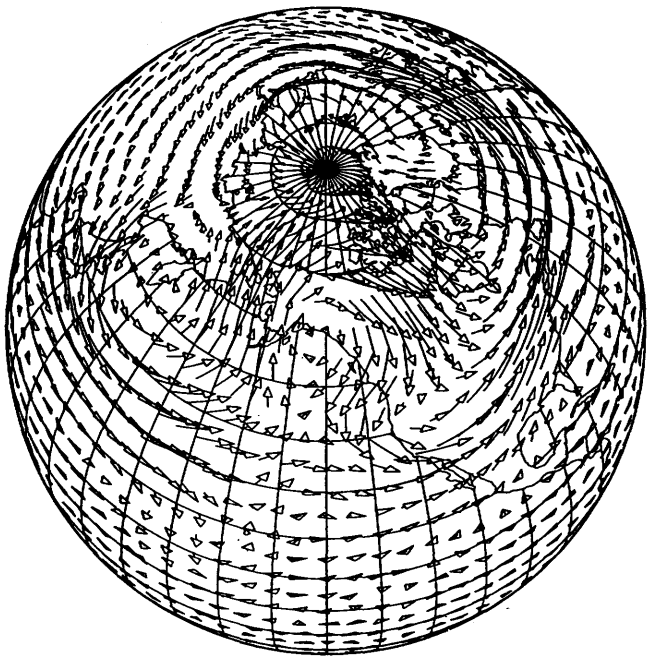

**Figure 1.** Example of NMC data received at the Alaska Climate Research Center via Unidata showing the global distribution of wind vectors at the 500-mb level, February 3–7, 1989. Length of staff indicates wind speed; pointer indicates wind direction. The horizontal grid interval available for Unidata is 5° for longitude and 2.5° for latitude.

users. The Unidata program center is located in Boulder, Colo., and it is managed by the University Corporation for Atmospheric Research (UCAR). The Unidata program established its own data feed from the National Weather Service operational circuit to distribute the near-real-time and forecast meteorological data for university users. Among the service programs, the NMC provides global analysis data and forecast gridded data. The meteorological data are transmitted by satellite downlink under a contract with Zephyr Weather Information Service.

The NMC meteorological variables of zonal and meridional wind speeds, $u$ and $v$ (m/s); temperature, $T$ (K); geopotential height, $\phi$ (m); and relative humidity, $R$ (percent) are given at 2.5° latitude and 5.0° longitude grids at 10 mandatory vertical levels of 1,000, 850, 700, 500, 400, 300, 250, 200, 150, and 100 mb over the whole global domain (fig. 1). Those basic meteorological variables are transmitted twice a day, for 00:00 and 12:00 UTC. In every data transmission, the global gridded data include not only the initial conditions for the weather-prediction model (plus 0-hour NMC initial data) but also the data for the forecasting time of 6, 12, 18, 24, 30, 36, 48, and 60 hours, provided by the NMC numerical weather-prediction model. The initialized global data at forecasting time 00:00 may be regarded as observed data.

Figure 2 illustrates a relation between NMC data transmission and the volcanic plume prediction. The twice daily NMC data, including the forecast data, are stored and continuously updated in the computerized database. The database always consists of past observed data and forecast data for 2 to 3 days ahead. Therefore, when an eruption is reported, the prediction model can use the present and future upper-air data for the computation of plume advection. The forecast upper-air wind data for a 1-day prediction are typically as good as the analyzed wind data (Kalnay and others, 1990), even though the analysis data often contain considerable discrepancy from the real upper-air wind.

As an example, figure 3 compares the analyzed wind field (solid arrows) at the 500-mb level with the corresponding wind field for the 24-hour forecast from 1 day before (dashed arrows). The differences appear to be minor for this example, suggesting that the forecast wind field is useful for real-time plume prediction. However, the accuracy of the predicted wind depends on the weather situation. For example, the prediction is generally good when a persistent, blocking, high-pressure system stays near Alaska, but the prediction is poor when a low-pressure system is passing the Cook Inlet. Moreover, the analyzed wind field, interpolated from the upper-air observations onto the longitude-latitude grids, often contains considerable errors due to the imperfect interpolation technique. Yet, knowing the degree of the analysis error, the NMC upper-air data is still useful for plume prediction when no alternative exists.

## DESCRIPTION OF THE MODEL

The volcanic plume prediction model is constructed by an application of pollutant dispersion models (e.g., Praham and Christensen, 1977; Suck and others, 1978; Kai and oth-

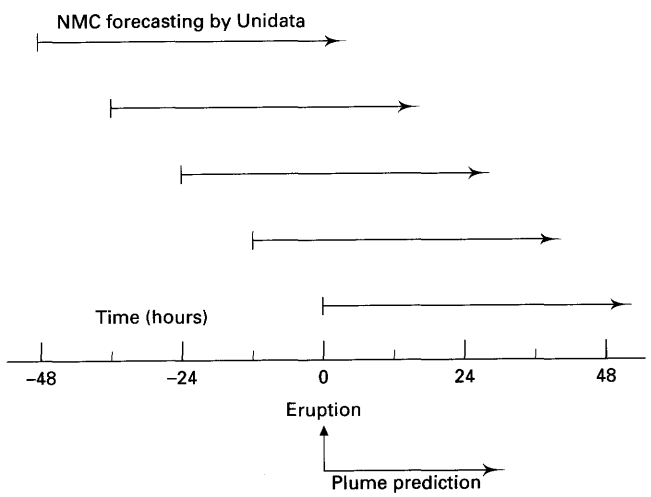


**Figure 2.** Schematic diagram showing the relation between the twice-daily NMC data transmitted by Unidata and the volcanic plume prediction. Arrow for NMC data describes a data span for the forecasting time from 0 to 48 hours. In response to an eruption report, the volcanic plume prediction model reads the archived NMC database to run the model using real-time wind data.

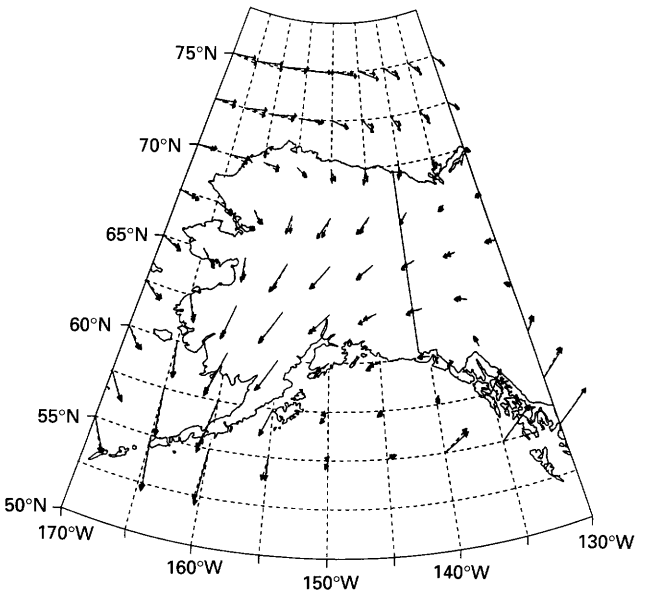


**Figure 3.** Comparison of analyzed wind vectors (solid arrows) at the 500-mb level and corresponding wind vector of the 24-hour forecast from 1 day before (dashed arrows), the State of Alaska, November 11, 1990. This example indicates the usefulness of the 1-day forecast data, although the wind error can be large depending on the weather situation (see text).

ers, 1988). The model is based on the three-dimensional (3-D) Lagrangian form of the diffusion equation. We assume a vertical column of pollutant source that diffuses along with the Gaussian distribution in the 3-D space. A diffusion approximation of the pollutant turbulent mixing is used with 3-D diffusion coefficients to evaluate the dispersion of pollutant concentration. In the Lagrangian framework, diffusion of plume particles may be described by a random walk process (Chatfield, 1984). Here, the diffusion is simulated by a sufficiently large number of random variables $r_i(t)$, ($i = 1 \cong M$), representing position vectors of $M$ particles from the origin (the volcanic crater). The diffusion is superimposed on advection and gravitational fallout.

With a discrete time increment, $\Delta t$, the Lagrangian form of the governing equation may be written as:

$$r_i(t+\Delta t) = r_i(t) + V\Delta t + Z\Delta t + G\Delta t, \quad i=1 \cong M \qquad (1)$$

where

$r_i(t)$ is a position vector of an $i$th particle at time $t$,

$V$ is the local wind velocity to advect the particle,

$Z = (z_h, z_h, z_v)$ is a vector containing three Gaussian random numbers with its standard deviation ($c_h$, $c_h$, $c_v$) for horizontal and vertical directions, and

$G$ is the gravitational fallout speed approximated by Stokes' law.

Note that the diffusion, $Z\Delta t$, is direction dependent, and the gravity settling, $G\Delta t$, depends on particle size.

For the computation of advection, the wind velocity, $V$, is obtained from NMC via Unidata. The gridded data are first interpolated in time onto the model's time step. The cubic spline method (Burden and others, 1981) is used up to the 3-hour interval, then a linear interpolation is applied for the 5-minute time steps. The wind velocity at an arbitrary spatial point is evaluated using the 3-D B-splines (Burden and others, 1981) from the nearby gridded data.

For the computation of diffusion, we consider the following diffusion equation in Eulerian form:

$$\frac{\partial q}{\partial t} = K\nabla^2 q \qquad (2)$$

where

$q$ is the plume mass density,

$\nabla^2$ denotes a Laplacian operator, and

$K$ denotes the diffusion coefficient.

For simplicity in derivation and for uncertainty in the magnitude of $K$, we consider a one-dimensional case in space along the $x$-axis. The solution of the diffusion equation for a point source at the origin is given by:

$$q(x, t) = \frac{1}{2\sqrt{\pi K t}} \exp\left(-\frac{x^2}{4Kt}\right) \qquad (3)$$

which may be regarded as a Gaussian distribution with its standard deviation

$$\sigma = \sqrt{2Kt} \qquad (4)$$

It is found that the plume dispersal, represented by $\sigma$, expands in proportion to $\sqrt{t}$.

On the other hand, a random walk process in Lagrangian form is defined as:

$$\begin{cases} r(0) = 0, \\ r(t+\Delta t) = r(t) + z(t)\Delta t \end{cases} \qquad (5)$$

where

$r(t)$ is the position of a particle along the $x$-axis,

$t = n\Delta t$, ($n = 0, 1, 2, \ldots N$), and

$z(t)$ is the zero-mean Gaussian random number with its standard deviation, $c$.

For this random walk process, the standard deviation of $r(t)$ is given by:

$$\sigma = c\sqrt{t\Delta t} \qquad (6)$$

Comparing these standard deviations in Eulerian form and in Lagrangian form, we obtain a relation between the diffusion coefficient, $K$, and the diffusion speed, $c$, as:

$$c = \sqrt{\frac{2k}{\Delta t}} \qquad (7)$$

The diffusion velocity depends on the time increment of the discrete time integration. We use $\Delta t$ = 5 minutes in this study. We have repeated diffusion tests with various values of $K$, and the resulting dispersals are compared with satellite images of actual dispersals from Redoubt Volcano. With these diffusion tests, we find that the appropriate diffusion coefficients are $K_h$=$10^4$ ($m^2$/s) and $K_v$=10 ($m^2$/s) for the horizontal and vertical directions, respectively. Note that values may be different for other volcanoes.

The diffusion speed may be sensitive to the scale in consideration. For example, the present value of the diffusion coefficient varies as the horizontal scale, which ranges from several hundreds of kilometers to 1,000 km in length. Figure 4 illustrates a result of the diffusion test. The steady plume at the origin spreads downstream of the source under the influence of constant wind. The theoretical standard deviation of the plume dispersal is indicated by the parabolic solid line in the figure.

The gravitational settling is based on Stokes' law as a function of the particle size, $d_i$. The fallout speed $|G|$ is approximated by the terminal velocity below:

$$|G| = \frac{2\rho g d_i^2}{9\eta} \tag{8}$$

where

$\rho$ is the density of plume particles,

$\eta$ is the dynamic viscosity coefficient, and

$g$ is the acceleration due to gravity.

We have assumed a constant for $\rho g/\eta = 1.08\times10^9$ $m^{-1}s^{-1}$ for simplicity. The actual eruption contains large fragments, up to few centimeters in diameter, as well as fine ash, which occupies a continuous particle-size range to less than 1 μm. Large particles typically settle out within a short time, and the particle-size spectrum in the air shifts toward smaller particles. Because we are interested in particles that can travel for several hours, we have assumed that the initial particle-size distribution is centered at 100 μm. It is assumed that the size distribution in logarithmic axis has a Gaussian distribution. Thus, about 95 percent of the particles are supposed to have diameters between 1 μm and 1 cm. Using Gaussian random numbers, every particle is assigned with its own diameter, between 1 μm and 1 cm, when it appears at the volcanic crater. In practice, particles larger than 100 μm drop quickly, within a few steps of time integration. Particles that are less than 100 μm in diameter can travel far from the source, providing important information on plume dispersion.

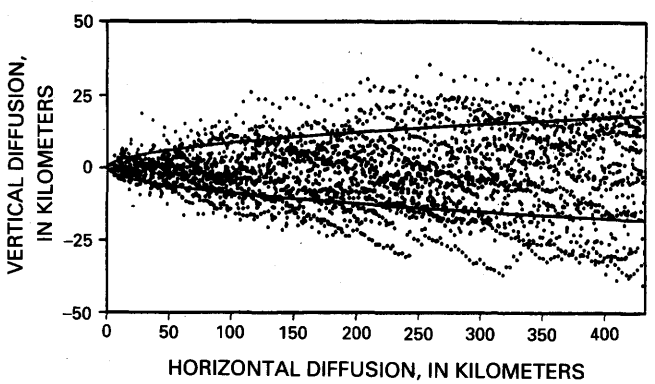


**Figure 4.** Plan view showing a 12-hour particle diffusion test for a steady plume at a constant zonal wind of 10 m/s. The parabolic line in the figure indicates a theoretical standard deviation of the plume distribution.

The initial particles are modeled to be uniformly distributed in the vertical column, between the top of the erupting volcano and the specified plume top, using a uniform random-number generator. The altitude of the plume top is assumed to have been reported to AVO by visual observers, which may include pilot reports and reports from ground-based observers. In a case of a short-lived explosive eruption, ash particles are generated only for the initial time of the time integration. When the eruption continues for a period of more than a few minutes, the model generates new particles over the same vertical column for every time step during the specified eruption period. For a steady eruption, the particle number tends to increase in the model atmosphere before the plume particles have dropped out. Therefore, the number of particles released at every time step is adjusted to draw optimal statistical information from the model products.

The total number of particles in the model atmosphere is kept at less than 1,000. Although it is possible to increase the number toward the limit of computer capability, the time integration will then be considerably slower, which is a disadvantage for the urgent prediction requirement. Likewise, excessive complication and sophistication are not recommended in the present application for urgent operational prediction. For comprehensive numerical predictions, refer to Sullivan and Ellis (this volume), Heffter and others (1990), Kai and others (1988), and Draxler (1988).

The plume-prediction model is tested first with a sheared flow in the vertical. Advective wind in the atmosphere has vertical shear with larger velocity, in general, at higher altitude. Figure 5 illustrates the result of the vertical cross sections of a plume-puff simulation for 1 through 6 hours after the eruption. Concentrated ash particles are released uniformly over the vertical column up to an altitude of 10 km at the origin. The plume clouds drift downstream by sheared flow. They diffuse and become thinner due to removal of larger particles. The result simulates reasonably well the transport of the ash plume.

The plume-prediction model is tuned by comparison with actual eruption records of Redoubt Volcano (Brantley, 1990). Model simulations are conducted for about 30 major and minor eruptions during December 1989 through April

1990, and the resulting plume-cloud distributions are compared with satellite images (K. Dean, University of Alaska, oral commun., 1991). Unfortunately, for this period, the Cook Inlet area is mostly covered by dense weather clouds, and there were not many satellite images that captured the ash plume immediately after the eruption.

Figure 6 illustrates a steady plume cloud for December 16, 1989, simulated by this model. Because Redoubt was in near-continuous ash emission on this date, we started the simulation assuming the eruption occurred at 10:00 UTC. A linear cloud extends from Redoubt Volcano toward the northern part of the Kenai Peninsula at 12:30 UTC. In the figure, open circles represent particles higher than 1,800 ft and solid circles represent particles lower than 1,800 ft. The simulation result is compared with satellite images from the NOAA-11 advanced very high resolution radiometer (AVHRR) at 12:18 UTC (see fig. 7). In figure 7, the black area over Cook Inlet describes a relatively dense ash cloud and the shaded area over the Kenai Peninsula represents a thin ash cloud. The satellite image describes the detailed structure of the cloud, which is beyond the model's resolution. Nevertheless, the overall agreement between the simulated and observed plume distributions is encouraging.

Figure 8 (*A–D*) illustrates a sequence of graphic products simulated for the eruption on January 8, 1990. The eruption started at 19:09 UTC and continued for 30 minutes. At 20:00, a cellular ash cloud is located near Redoubt Volcano (fig. 8*A*). The cloud crossed over the Cook Inlet and reached

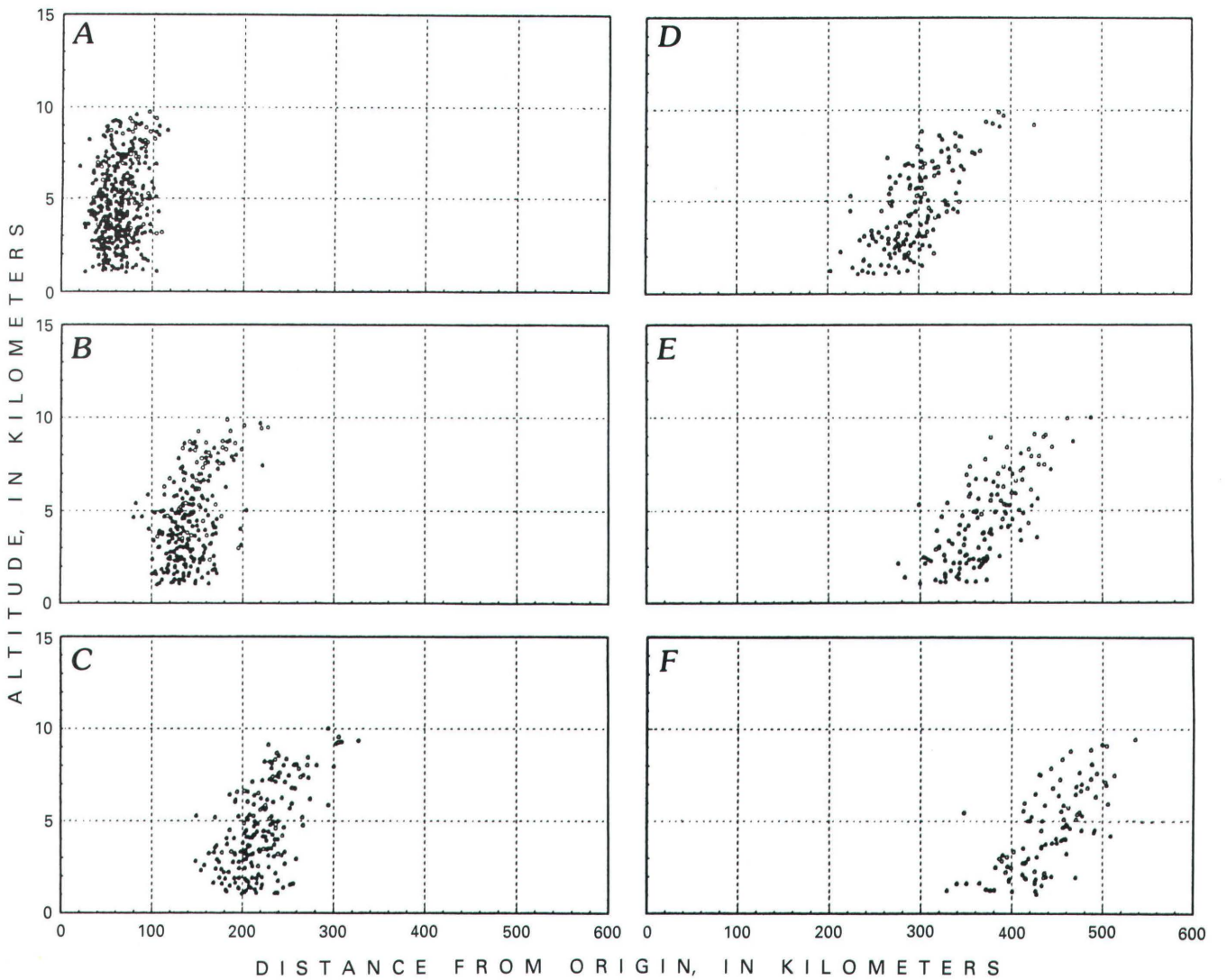


**Figure 5.** Vertical cross sections of a puff plume simulated for 1 through 6 hours after an eruption. In this test run, the initial ash particles are released uniformly over the vertical column up to an altitude of 10 km at the origin. *A*, plume simulation 1 hour after eruption; *B*, plume simulation 2 hours after eruption; *C*, plume simulation 3 hours after eruption; *D*, plume simulation 4 hours after eruption; *E*, plume simulation 5 hours after eruption; *F*, plume simulation 6 hours after eruption.

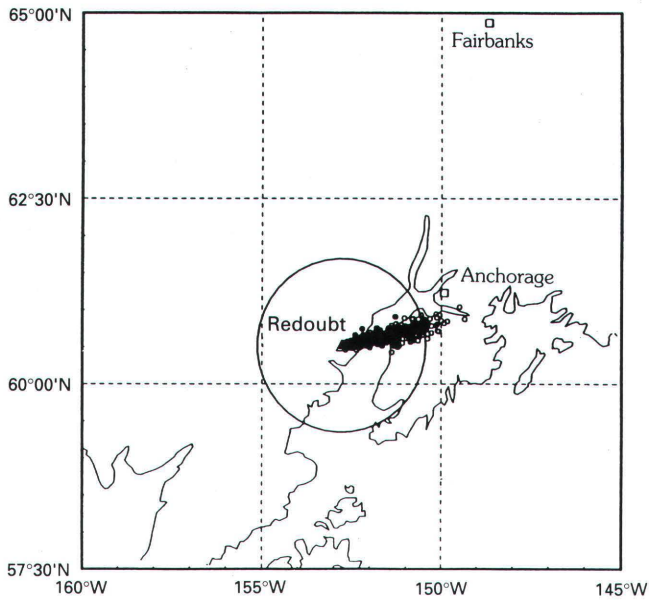


**Figure 6.** Simulated geographical distribution of particles from a steady plume for eruption of Redoubt Volcano, which started at 10:00 UTC, December 16, 1989. Illustration shows the model result at 12:30 UTC. Open circles, particles higher than 1,800 ft; solid circles, particles lower than 1,800 ft.

the Kenai Peninsula at 21:00 (fig. 8*B*). The cloud traveled over the Kenai Peninsula, indicating north-south elongation at 22:00 UTC (fig. 8*C*). A witness report describes that a dense volcanic ash cloud passed the western shore of the Kenai Peninsula at this time (Brantley, 1990), and, in downtown Soldotna, day time turned into darkness during the passage of the dense ash cloud. At 23:00, the northern edge of the elongated cloud reached just the south of Anchorage, and the southern edge of the cloud passed the Alaska coastline (fig. 8*D*). The simulation results are compared with a satellite image at 23:13 (fig. 9), which clearly shows a linear plume extending from the northern Kenai Peninsula to the Pacific coast near Seward. The satellite observation agrees well with the model simulation.

The graphic outputs (fig. 8) are stored in computer memory, which is connected with other systems through computer networks. The final stage of plume prediction is to distribute the graphic product to various users, including the Federal Aviation Administration (FAA), the National Weather Service (NWS), and the response center of the Alaska Volcano Observatory in Anchorage. In principle, any system connected with the ethernet electronic mail network can receive the graphic product through the network, and users in Anchorage can access the graphic product by telephone modem. For users without any computer facility, the graphic product is distributed by telephone facsimile.

This study demonstrates that the prediction model can provide useful information when it is applied for a real eruption. We have repeated similar demonstrations for each of the eruptions of Redoubt Volcano in 1989–90 and for Mt. Spurr in 1992. The results are compared with available satellite observations in order to increase the reliability of the prediction model. The model output will be especially useful when Cook Inlet is covered by dense cloud when neither satellite observations nor pilot's visual reports are available.

## SUMMARY AND REMARKS

A volcanic plume prediction model has been developed for Cook Inlet volcanoes in Alaska. Reading the real-time upper-air data provided by NMC via Unidata, the prediction model computes advection, diffusion, and gravitational settling for plume particles released from the vertical column over the volcano. Three-dimensional distributions of the simulated plume particles are displayed on computerized graphic display. Hence, we can have important information on the predicted location of the ash plume in a real-time basis.

The model predictions, showing the projected geographical location of the plume clouds for several hours after the eruption, can appear on the computer screen about 15 minutes after eruption reports are received. This prediction is immediately available for users through existing computer networks. The graphical model output is distributed to related organizations using ordinary telephone facsimile. The present model simulation will have forecast errors owing, in part, to the errors in the forecast wind input.

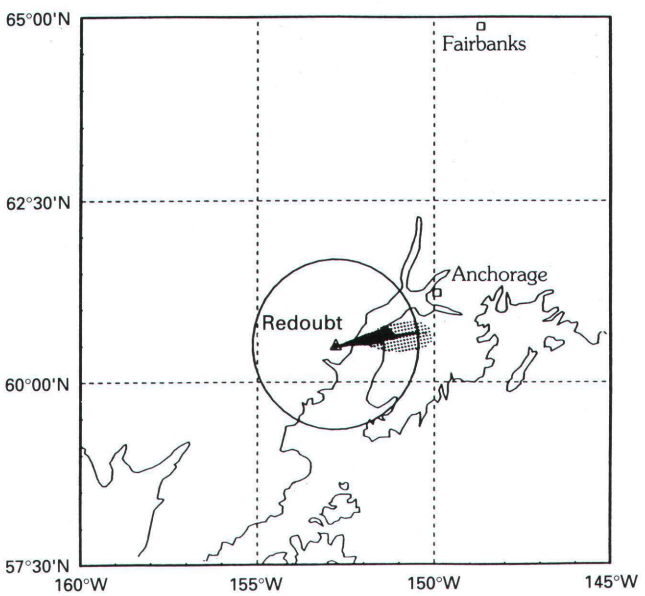


**Figure 7.** Sketch of satellite image of the steady plume at 12:18 UTC, December 16, 1989, derived by analysis of NOAA-11 data. Figure has been scaled to permit comparison with figure 6. Black area shows dense core of the ash cloud. Stippled area shows diffuse margin of the ash cloud (Kienle and others, 1990).

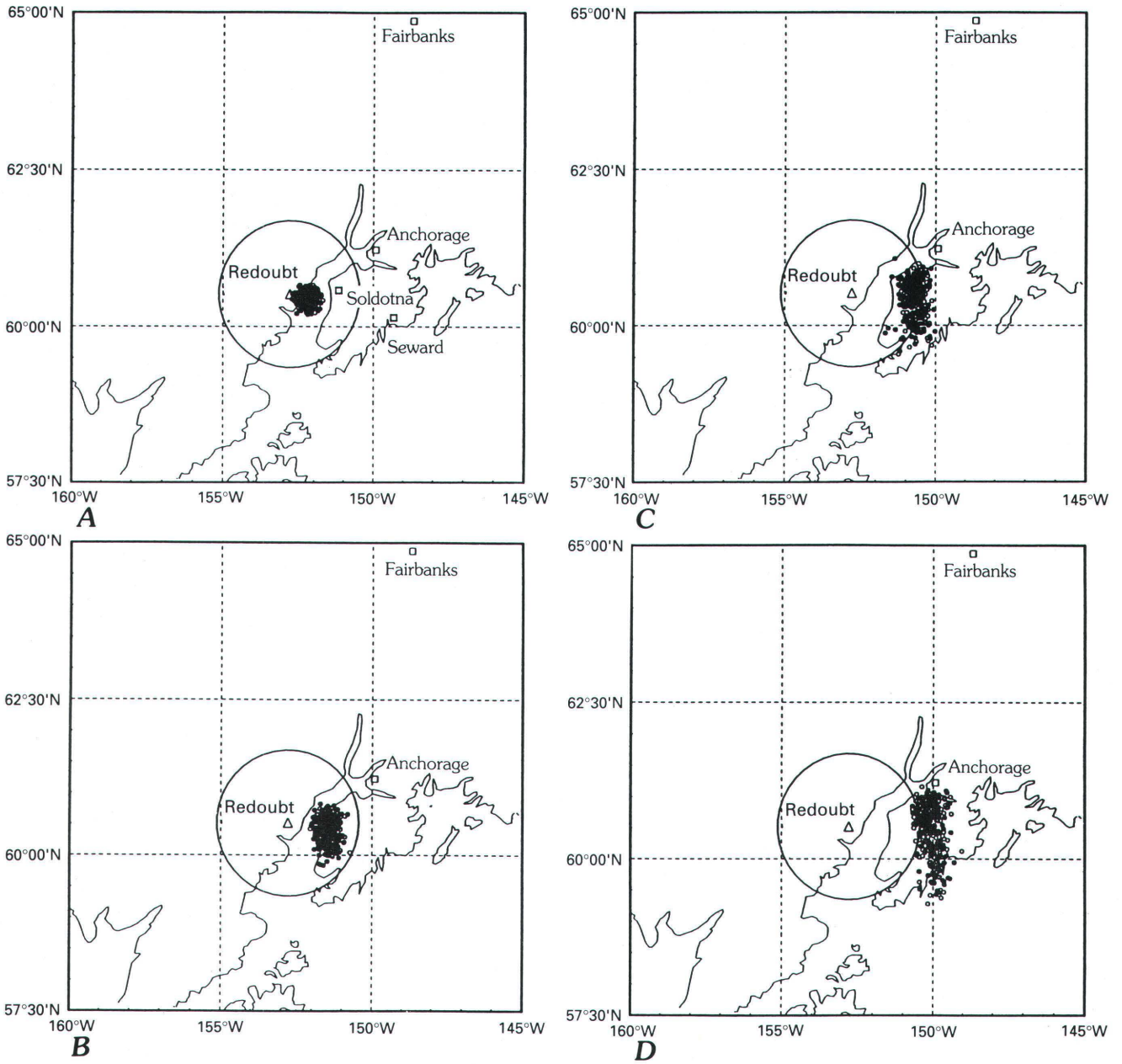


**Figure 8.** Simulated geographical distribution of a puff plume for the eruption of Redoubt Volcano on January 8, 1990, at 19:09 UTC. Model results are shown for *A*, 20:00 UTC; *B*, 21:00 UTC; *C*, 22:00 UTC; *D*, 23:00 UTC.

According to the latest statistics, upper-air wind has about 8 m/s root-mean-square (RMS) error on average for the Northern Hemisphere (Kalnay and others, 1990). Nevertheless, the prediction product, knowing the possible prediction errors, can offer a useful guide for public safety. The use of gridded data from a finer mesh weather prediction model would improve the advection computation. Because the NMC gridded data used in this project cover the whole globe, this prediction model can be applied for other volcanoes around the world.

## ACKNOWLEDGMENTS

This project was supported by ASTF grant agreement 90-2-058 with matching funds from National Science Foundation grant ATM-8923064, AVO/USGS, Anchorage International Airport, Municipality of Anchorage, Japan Airlines, Nippon Cargo Airlines, China Airway, Scandinavian Airways System, British Airways, Swissair, and Reeve Aleutian Airways. The author appreciates various suggestions from S-I. Akasofu and Thomas J. Casadevall.

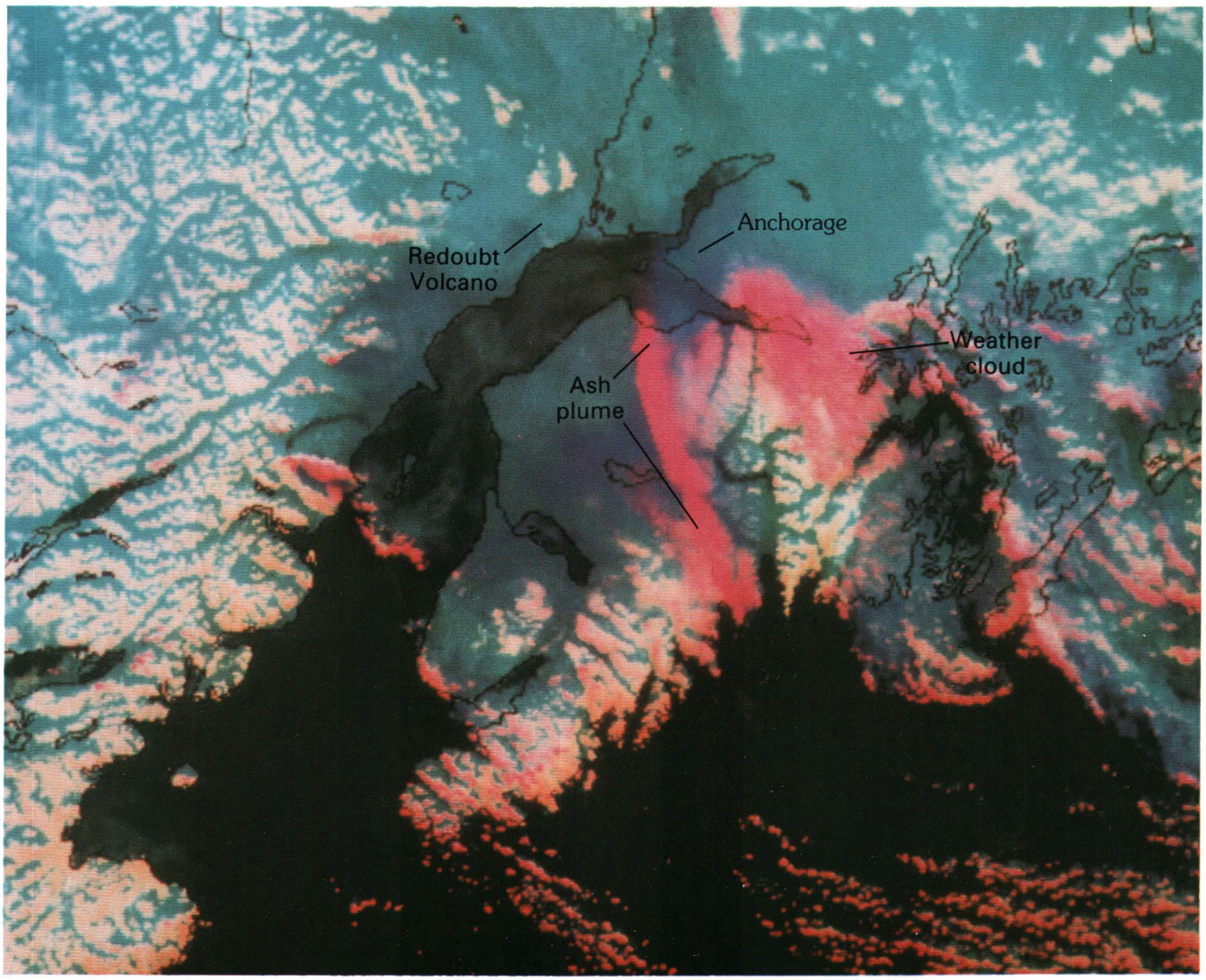


**Figure 9.** Satellite false-color image of the Cook Inlet area of Alaska showing ash plume produced by the eruption of Redoubt Volcano on January 8, 1990, at 19:09 UTC. The image shows the distribution of the ash plume at 23:13 UTC on January 8, 1990 (compare with figure 8*D*). The ash plume is elongated to the south-southeast and is shown in pink. The pink cloud east of the linear ash plume is a weather cloud and does not contain ash.

## REFERENCES CITED

Brantley, S.R., ed., 1990, The eruption of Redoubt Volcano, Alaska, December 14, 1989–August 31, 1990: U.S. Geological Survey Circular 1061, 33 p.

Burden, R.L., Faires, J.D., and Reynolds, A.C., 1981, Numerical Analysis: London, Prindle, Weber, and Schmidt, 598 p.

Chatfield, C., 1984, The analysis of time series, an introduction: New York, Chapman and Hall, 286 p.

Draxler, R.R., 1988, Hybrid single-particle Lagrangian integrated trajectories (Hy-Split): Model description: National Oceanic and Atmospheric Administration Technical Memorandum, ERL ARL-166, 23 p.

Heffter, J.L., Stunder, B.J.B., and Rolph, G.D., 1990, Long-range forecast trajectories of volcanic ash from Redoubt Volcano eruptions: Bulletin of the American Meteorological Society, v. 71, p. 1731–1738.

Kai, K., Okada, Y., Uchino, O., Tabata, I., Nakamura, H., Takasugi, T., and Nikaidou, Y., 1988, Lidar observation and numerical simulation of Kosa (Asian Dust) over Tsukuba, Japan, during the spring of 1986: Meteorological Society of Japan, v. 66, p. 457–472.

Kalnay, E., Kanamitsu, M., and Baker, W.E., 1990, Global numerical weather prediction at the National Meteorological Center: Bulletin of the American Meteorological Society, v. 71, p. 1410–1428.

Kienle, J., Dean, K., Rose, W., and Garbeil, H., 1990, The 1989 eruption of Redoubt Volcano, Alaska [abs.]: Eos, Transactions, American Geophysical Union, v., 71, p. 266.

Praham, L.P., and Christensen, O., 1977, Long-range transmission of pollutants simulated by a two-dimensional pseudospectral

dispersion model: Journal of Applied Meteorology, v. 16, p. 896–910.

Sherretz, L.A., and Fulker, D.W., 1988, Unidata: Enabling universities to acquire and analyze scientific data: Bulletin of the American Meteorological Society, v. 69, p. 373–376.

Suck, S.H., Upchurch, E.C., and Brock, J.R., 1978, Dust transport in Maricopa county, Arizona: Atmospheric Environment, v. 12, p. 2265–2271.

Tanaka, H.L., 1990, Model used to track volcanic plume: Geophysical Institute Quarterly, University of Alaska, Fairbanks, Fall 1990, p. 7–8.

———1991a, Unidata at Alaska.: Unidata Newsletter, Summer 1991, p. 10–11.

———1991b, Weather data access improved: Geophysical Institute Quarterly, University of Alaska, Fairbanks, Summer 1991, p. 1–3.

VOLCANIC ASH AND AVIATION SAFETY:
Proceedings of the First International Symposium
on Volcanic Ash and Aviation Safety
U.S. GEOLOGICAL SURVEY BULLETIN 2047

# THE AERONAUTICAL VOLCANIC ASH PROBLEM

*By* Jerald Uecker

## ABSTRACT

The International Civil Aviation Organization (ICAO) requires warnings and flight-planning information about one of the most potentially hazardous but non-meteorological aeronautical phenomena that exists, volcanic ash. This paper discusses the provision of required information based on the experiences gained from eruptions of Mount St. Helens and Redoubt Volcano in the United States. The frequency and duration of these eruptions, as well as the lack of guidelines about ash concentrations and their affect on aircraft, have made it difficult to meet the requirements for supporting safe and efficient aeronautical operations with available information messages. While progress has been achieved with warnings and flight-planning data, efficient dissemination has not been achieved for graphical representations of ash clouds. Meeting aeronautical information requirements for this non-meteorological phenomenon requires cooperation, research, and development among people in various disciplines to attain safe and efficient operations.

## INTRODUCTION

The experience gained in providing meteorological information on volcanic ash clouds to those in aeronautical operations has resulted in adjusting some procedures to accommodate requirements. This paper briefly discusses the requirements and challenges and how support will be improved, primarily through communications, in the near future.

During the past decade, a number of aircraft have encountered volcanic ash clouds while in flight. Three incidents involved loss of engine power and posed potential disaster for passengers and crew; these encounters caused extensive damage to the aircraft. Fortunately, such incidents have been rare, and disaster has been averted because of good crews and equipment. These incidents have, however, instilled a healthy awareness of and respect for the problem of volcanic ash.

The relative infrequency of large volcanic eruptions and the inability to predict the onset of eruptions in an aeronautically timely manner increases the potential danger faced by crews and operators. In spite of the non-meteorological nature of volcanic eruptions and ash, the responsibility rests with meteorologists for: (1) the issuance of alphanumeric significant meteorological (SIGMET) information to warn of the hazard, and (2) the inclusion of ash-cloud information in abbreviated, plain-language, area forecasts and on significant weather charts used for flight planning.

Satellite images, radar data, aircraft reports, and cooperation and information coordination with volcanologists are all essential for early detection of eruptions and for tracking ash clouds. However, there are considerable limitations inherent in the system that provides SIGMET information. Two limitations are: (1) forecasting the onset of eruption with the timeliness required for aeronautical operations—this goal will certainly elude meteorologists, and (2) determining the concentration of erupted ash particles and (or) gases that may or may not affect aircraft. Hopefully, studies that address these limitations will also provide guidance as to when ash concentrations are sufficiently low so that the ash no longer threatens aircraft.

Wind data in the form of particle-trajectory and dispersion-model forecasts for flight planning are essentially the only aspect of the volcanic eruption and ash problem that adheres to meteorological prediction principles (Murray and others, this volume; Stunder and Heffter, this volume). This means that meteorologists need help in providing the best ash-cloud-warning service for the aeronautical community.

The experience in the United States for issuing ash cloud warnings and SIGMET's began with the eruption of Mount St. Helens in 1980. The St. Helens experience differed considerably from the more than 25 eruptions at Redoubt Volcano, which is 177 km southwest of Anchorage, Alaska, and to which meteorologists responded beginning in December 1989. Mount St. Helens eruptions were longer in duration and less frequent that those of Redoubt Volcano. Initially, each Redoubt eruption lasted several hours, and subsequent eruptions, some consisting primarily of steam, lasted less than 30 minutes (Brantley, 1990).

## ALPHANUMERIC INFORMATION REQUIREMENTS

The international requirements for reports, warnings, and forecasts about volcanic ash are contained in the ICAO publication entitled "Meteorological Service for International Air Navigation, Annex 3," (ICAO, 1992)—this publication is hereinafter referred to as "ICAO Annex 3." United States domestic and international procedures and policies meeting these requirements are detailed in National Oceanic and Atmospheric Administration (NOAA) and National Weather Service (NWS) operations manuals. Within the United States, additional measures are taken both from a warning and flight-planning point of view. For warnings, NWS meteorologists assigned to air route traffic control centers (ARTCC) provide center weather advisories (CWA's) as a quick response to new or quickly changing conditions that may not be detailed in SIGMET's prepared by meteorological watch offices (MWO's). For flight planning, trajectory information (see Recent Developments section in this paper) is provided to aeronautical and meteorological facilities in accordance with existing agreements. Currently, this information is distributed on a limited basis, but extensive distribution of flight-planning information through meteorological graphics communications systems within the United States and internationally are planned and are nearing fruition. This will result in extensive distribution of this information to the aeronautical community and to information providers.

## REPORTS

Recommended practices concerning observations and reports of volcanic activity by meteorological stations are described in the ICAO Annex 3 (chap. 4, p. 20): "The occurrence of pre-eruption volcanic activity, volcanic eruptions, and volcanic ash clouds should be reported without delay to the associated air traffic services unit, aeronautical information services unit, and meteorological watch office. The report should be made in the form of a volcanic activity report [VAR—see Fox, this volume] comprising the following information in the order indicated:

a. Message type: volcanic activity report,
b. Station identifier: location indicator or name of station,
c. Date and time of message,
d. Location of volcano and name if known,
e. Concise description of event, including, as appropriate, level of intensity of volcanic activity, occurrence of an eruption and its date and time and the existence of a volcanic ash cloud in the area together with direction of ash cloud movement and height."

The standard concerning aircraft observations and reports that is cited in ICAO Annex 3 (chap. 5, p. 24) is that "special observations shall be made by all aircraft whenever...

c. Volcanic ash is observed or encountered,...
e. Pre-eruption volcanic activity or a volcanic eruption is observed."

Note—Pre-eruption volcanic activity, as used in both contexts cited above, means unusual and (or) increasing volcanic activity that could presage a volcanic eruption.

The ICAO standard for the contents of special air reports of pre-eruption volcanic activity, a volcanic eruption, or volcanic ash cloud and their order in the volcanic activity report (VAR) (Fox, this volume) is:

- Aircraft identification,
- Position,
- Time,
- Flight level or altitude,
- Volcanic activity observed,
- Air temperature,
- Wind, and
- Supplementary information.

## SIGMET INFORMATION

SIGMET's are aeronautical meteorological warnings, and they are issued in alphanumeric form. The ICAO Annex 3 (chap. 7, p. 34–36) standard on the issuance of SIGMET information includes the occurrence and (or) expected occurrence of volcanic ash cloud at subsonic, transonic, and supersonic cruising levels. The recommended issuance of "SIGMET messages concerning volcanic ash cloud... expected to affect a flight-information region (FIR) should be issued at least 12 hours before the commencement of the period of validity and should be updated at least every 6 hours."

This requirement combined the short-term requirement for hazardous SIGMET information and the longer term requirement for flight-planning data. However, at the ICAO communications-meteorology-operations divisions and the World Meteorological Organization (WMO) commission on aeronautical meteorology meeting (September 1990, held in Montreal, Canada), several states that have had experience with volcanic activity SIGMET's indicated that permitting the period of validity of SIGMET's for volcanic ash to be extended up to 12 hours, in their opinion, was quite impossible given current volcanic-activity-observing techniques, especially concerning ash particle size and density.

Even though the requirement does state "up to 12 hours," local user requirements during the Redoubt Volcano eruptions led to SIGMET updates as often as every 2 hours. This implied a dichotomy of purpose for the SIGMET (i.e., updates every 2 hours and the requirement for an outlook for up to 12 hours).

A few initial Redoubt Volcano eruptions in December 1989 and January 1990 lasted up to several hours; subsequent eruptions lasted usually less than 30 minutes (Brantley, 1990). With the frequency and duration of Redoubt Volcano eruptions, the MWO issuing SIGMET's would not have been able to comply with the spirit of the long-term requirement at the volcano or for flight-information regions (FIR's) affected downstream by the ash cloud.

Another significant aspect of SIGMET's being valid essentially from 12 to 24 hours is that the area encompassing volcanic ash could be very large. Situations did occur at Redoubt Volcano whereby ash was spread at high levels far to the southeast and at low levels to the north and northwest. In this case, the area was already quite large. However, consider the area that would be covered by ash with the wind directions indicated above and with a speed of 100 knots at high levels and 25 knots at low levels for a period of 12 to 24 hours. A SIGMET encompassing such as ash cloud would be meteorologically supportable but operationally difficult to implement. Even the 4-hour-valid-period SIGMET's issued for the initial Redoubt Volcano ash clouds resulted in large areas that unnecessarily restricted air traffic—this is a considerable impact at or near high-density routes and aerodromes, such as Anchorage International Airport.

Ash dispersion can quickly become complicated and can cover extensive areas with ash that is emanating only from the source. However, rapidly transported ash at high levels that falls into lower levels with different wind directions essentially results in multiple, albeit less concentrated, sources and an extremely complicated ash-cloud pattern.

### SIGMET DISSEMINATION

SIGMET's are disseminated over teletypewriter or computer networks in alphanumeric, abbreviated, plain language. ICAO Annex 3 (p. 36) recommends that "SIGMET messages should be disseminated to meteorological watch offices,... and to other meteorological offices, in accordance with regional air navigation agreement."

## GRAPHICS REQUIREMENTS

The requirements for graphical information (i.e., charts for flight documentation) reside in ICAO Annex 3, chapter 9, and is entitled "Service for Operators and Flight Crew Members." Flight documentation, usually in the form of charts, is provided "to operators and flight crew members for:

a. Pre-flight planning by operators,
b. Use by flight crew members before departure,
c. Aircraft in flight."

For pre-flight planning purposes by the operator, the ICAO recommendation for significant en-route weather information is that the information should normally be supplied as soon as available, but not later than 3 hours before departure.

Prior to the ICAO/WMO meeting in 1990, different ways to portray volcanic ash on significant weather charts were tried in the United States for the Redoubt Volcano eruptions. However, the inclusion of ash clouds on significant weather forecast charts caused concern among aeronautical operators. One of the early Redoubt eruptions occurred before the significant weather chart was disseminated, and the projected ash cloud area was determined by trajectory information. This area was enclosed by a scalloped line and identified with a plain-language note. Unfortunately, the area enclosed was larger than it might have been under those meteorological conditions, and it caused some anguish among users. It should be noted, however, that large areas can be expected under certain meteorological conditions.

Experience with these charts showed that:

1. Inclusion of ash clouds on significant weather forecast charts is consistently possible only if the volcano erupts shortly before or during the preparation of a chart and, of course, if the meteorologist is notified in time,
2. Providing long-term (up to 12 hours and beyond) volcanic ash information by outlining the ash cloud on significant weather charts, while possible, may be confusing and may be a disservice to the aeronautical user when the area delineated is significantly larger than it might be or if the chart is prepared for an eruption that turns out to be mostly steam (hence, posing little or no hazard), and
3. The lead time that must exist so that the charts are available to the operator, in addition to the time required to prepare the chart, makes it an extremely difficult task to include the information as precisely as desirable.

The Redoubt Volcano experience led the United States to suggest at the September 1990 ICAO/WMO meeting that the best way to inform flight planners about volcanic ash was to include a statement such as "see potential SIGMET's for volcanic ash" near the volcano on the significant weather chart—this statement would be included on all significant weather charts until the volcano becomes inactive again. Discussions pointed out that longer term, precise information on the occurrence and location of volcanic ash cannot be adequately depicted on significant weather charts. The reason for this is that these charts should be in the users' hands some 9 hours before the valid time—this time corresponds approximately to the midpoint of the flight. Also, these charts are prepared up to 6 hours before being disseminated. The net result is that a volcanic eruption and ash cloud may have occurred at any time during a period of 15 hours and may not be depicted on the significant weather chart that the air crew receives. It was agreed at the meeting that an ash

cloud could not be included reliably for short-term eruptions because of timing and dissemination requirements.

The participants at the ICAO/WMO meeting in 1990 felt that WMO should be requested to develop, in consultation with ICAO, appropriate symbology to represent the volcanic ash phenomenon on significant weather charts—this resulted in the recommendation that WMO, in consultation with ICAO, develop appropriate symbology to represent the occurrence of volcanic eruptions on world-area forecast system significant weather charts. Subsequently, it was agreed that symbology would be added to the significant weather chart at the location of the volcano and that adequate information would be added to the legend of the chart, including a statement advising concerned air crews to inquire about SIGMET's in an area where a volcanic eruption or ash contamination is suspected.

## RECENT DEVELOPMENTS

Since the First International Symposium on Volcanic Ash and Aviation Safety in 1991, graphic information has been developed. The volcanic ash forecast transport and dispersion (VAFTAD) model, developed by National Oceanic and Atmospheric Administration (NOAA) Air Resources Laboratory, is a three-dimensional, time-dependent depiction of the volcanic ash cloud (Stunder and Heffter, this volume). Eruption input includes volcano name and location, eruption time, and ash-cloud-top height. The model assumes a given particle-size distribution throughout the initial ash cloud. Ash is advected horizontally and vertically as it falls through the atmosphere, using either the Washington World Area Forecast Center global wind and temperature computer model data or a U.S. regional model.

This graphic information, produced automatically and shortly after notification of an eruption, will be disseminated internationally in addition to significant weather charts on ICAO world-area forecast system satellite broadcasts. Broadcasts operated by the United States are expected to begin in late 1993 or early 1994 over the Americas and in late 1994 over the Pacific Ocean–eastern Asia area. In the United States, the graphic will be disseminated on meteorological computer and graphic-dissemination systems.

## SUMMARY

Problems faced by meteorologists and operators concerning: (1) when and where an eruption may occur, (2) the timely notification of an eruption in the aeronautical sense, and (3) what concentrations of volcanic ash threaten life and property, contribute to the difficulty in providing useful volcanic ash information. However, improved dissemination of information will significantly assist in planning for efficient flight and will contribute to safe operations.

## REFERENCES CITED

Brantley, S.R., ed., 1990, The eruption of Redoubt Volcano, Alaska, December 14, 1989–August 31, 1990: U.S. Geological Survey Circular 1061, 33 p.

International Civil Aviation Organization (ICAO), 1992, Meteorological Service for International Air Navigation, Annex 3 (11th ed.): International Civil Aviation Organization.

VOLCANIC ASH AND AVIATION SAFETY:
Proceedings of the First International Symposium
on Volcanic Ash and Aviation Safety
U.S. GEOLOGICAL SURVEY BULLETIN 2047

# DEFINING A KEEP-OUT REGION FOR AIRCRAFT AFTER A VOLCANIC ERUPTION

*By* Peter L. Versteegen, Douglas D. D'Autrechy, Michael C. Monteith,
*and* Charles R. Gallaway

## ABSTRACT

This paper proposes a methodology for predicting the airspace that aircraft should avoid when the air contains volcanic ash. The proposed methodology consists of an ash-transport model and an avoidance-region-definition model. The ash model estimates the transport of ash particles from volcanic clouds by ambient winds. The avoidance-region-definition model uses predicted particle locations to determine a volume in airspace of minimal cross-sectional extent. The methodology is based on use of a personal computer and can estimate such avoidance regions in near real time. Individual elements of the models are operational but need to be configured with a user-friendly interface. Modules must be added to bring in wind data from all accessible sources and to generate a mass-consistent wind field. Furthermore, sensitivity studies need to be conducted to ensure that useful and not overly conservative results are generated. A model such as this could link a volcano observatory, a weather station, and an aircraft operation center.

The avoidance volume contains all possible ash-cloud particles at a user-specified time of interest. The avoidance region is defined as a rectangular prism extending from the ground to the top of the volcano cloud. The ash-transport model includes the following key elements: the specification of initial cloud conditions and a three-dimensional wind field, the transport and dispersion characteristics of the atmosphere, and the particle terminal fall velocities. The initial conditions of the cloud consist of a description of cloud geometry, mass distribution, and particle-size distribution. This initial cloud is represented by a number of horizontal wafers, each containing the mass and effective radius of each of the particle sizes of the distribution. The location of representative particles are computed with a modified Euler method, using a time-dependent wind field. Dispersion is modeled by an empirical correlation. The fall rate of a particle is determined from its local terminal velocity, which is a function of size and altitude.

## INTRODUCTION

The hazard to aircraft systems due to encounters with volcanic dust has been amply demonstrated over the past 20 years (Casadevall, 1992). Several aircraft have had life-threatening encounters with volcanic dust, and extensive damage has required expensive repairs of aircraft. Wind shields are crazed, leading edges become eroded, and excessive ingestion of dust by aircraft engines causes compressor erosion and deposition of melted ash in the turbine. Upon severe glassification, aircraft engines surge and shutdown and are difficult to restart. Two Boeing 747-200 aircraft encountered dust from Mt. Galunggung in June and July 1982 (Tootell, 1985) and experienced engine flameout. Fortunately, the crews were able to restart the engines and land the aircraft safely at Jakarta. In December 1989, a B-747-400, bound from Amsterdam to Anchorage, encountered the volcanic ash cloud from the Redoubt Volcano and had a four-engine flameout. Fortunately, the pilot was able to restart the engines. The aircraft suffered approximately $80 million of damage (Steenblik, 1990).

There are currently no safe procedures for operating aircraft when encountering ash clouds from erupting volcanoes. Pilots can report suspicious clouds through pilot reports (Fox, this volume), and they can follow recommended procedures developed by the Aerospace Industries Association volcanic ash committee (AIA Propulsion Committee 334-1, this volume). However, ash clouds are often difficult, if not impossible, to avoid because, even to the trained eye, a dust cloud at high altitude may look like an ordinary water/ice cloud. One approach to minimizing the chance of a fatal accident is to cancel all flights into a region defined by some radius around the erupting volcano. Such an estimate of affected area could be so large that such an action could severely impact local economies and be costly to the airlines due to reductions in passenger and freight load.

There is a need for a consistent procedure that can accurately define the airspace that could be a hazard to aircraft. Once such a region is defined, it can be broadcast via

the NOTAM (notice to airmen) process to aircraft that are approaching the hazardous airspace. This paper proposes a simple method, easily implemented, that could provide planning and real-time guidance about the location of the hazardous airspace. The approach defines a minimum volume of airspace inside of which all hazardous ash particles are expected to be present at the time of the forecast. Therefore, the region outside this minimum volume would be a zone in which aircraft can safely operate. Uncertainties in winds and methodology can be accounted for by suitably defining model parameters that enlarge the hazardous region.

## REQUIREMENTS

Any procedure that defines a restricted region as described above must be simple and easy to use, fast running, use local meteorology, make use of existing hardware and protocols, and be updateable. The underlying concepts of the procedure must be easy to understand and must be intuitive; the procedure should be operable by virtually anyone without comprehensive training or refresher sessions. The infrequent and widely distributed occurrences of volcanic events mean that the procedure would be used infrequently.

The procedure should be fast running so that near-instantaneous forecasts of airborne ash concentrations can be made. For this application a beginning-to-end forecast should take no longer than 5 minutes. The model should use local meteorology, including local measurements, whenever possible. Even though forecasts are generally available and would probably be used to generate the first estimates, the variability due to local or neighboring terrain should be accounted for either explicitly or statistically. The use of local measurements should be of high priority because they could be the only reliable source of accurate, high-resolution information. The model should make use of existing hardware and protocols. This facilitates implementations and allows a wider distribution of the results.

The procedure must be easy to update on a regular basis to provide a revised forecast of the hazardous region. Such revisions should be made frequently, but they are obviously dependent on the acquisition of better initial conditions and winds.

## METHODOLOGY

The proposed methodology is based on defining a keep-out or restricted region in airspace. Aircraft would stay outside of this region for a specified time period. The region is defined as a volume reaching from the ground up to the top of the volcanic cloud. Alternate, user-specified definitions could also be used. This geometry was chosen so that its specification is readily implemented in the existing NOTAM process by which only simple messages can be transmitted. More elaborate procedures can be devised.

The process involves the computation of particle displacements for different aerodynamic sizes from different altitudes, much along the lines of Hopkins and Bridgeman (1985). As particles settle, their trajectories are primarily affected by winds, atmospheric turbulence, and their own physical features. Other processes can be important, but they generally serve to reduce dust concentrations in the air and reduce direct hazards. Such processes include agglomeration of smaller particles into larger ones, the scavenging of particles by precipitation, and ash-induced downdrafts in the low-density, high-altitude air.

The mean wind field is typically the driving factor for particle transport and dispersion for the relatively short times considered here (several hours). Wind information can come from many sources, in different resolutions, and different accuracies, but current data are not always guaranteed to be available for the volcano region. Winds are available from forecasts with various meteorological models, from next-generation weather radar (NEXRAD) measurements, from TIROS operational vertical sounder (TOVS) measurements, and from rawinsonde measurements. When no data or information are available, persistence of the most recent winds can be used as a forecast, or analogous historical wind patterns anchored to the most recent data can be derived from a specialized clustering technique (Cockayne and Singer, 1991). All available wind information should be used in an objective analysis scheme to produce reasonably good wind fields for particle-transport and dispersion calculations.

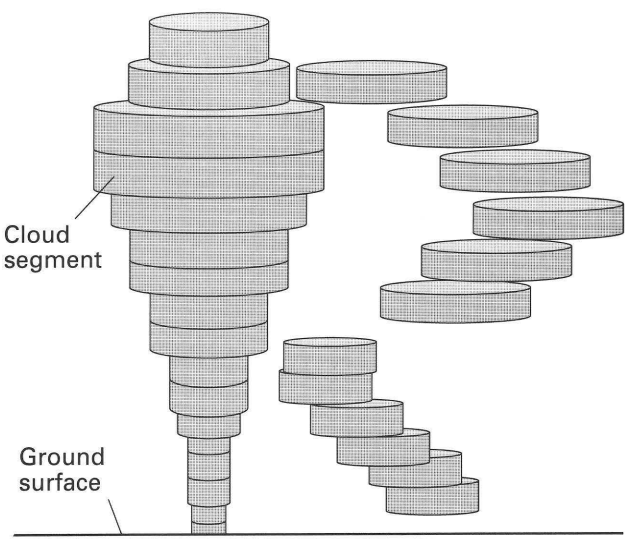


**Figure 1.** A volcano cloud is modeled by a stack of non-uniform wafers, each representing a characteristic particle size and a fraction of the total ash mass. Winds and gravity transport these wafers in multiple directions.

Particles can disperse over a large region, very much dependent on wind speed and vertical wind shear. This process is shown schematically in figure 1. The duration and mass eruption rate may also affect the size of the hazardous airspace. The columns of dust erupting from the volcano travel with the wind. The dust particles will fall out, and the speed of the fall depends on particle sizes. A schematic side view of the hazardous region for a single burst and a continuous eruption are shown in figure 2.

The restricted region is defined as the minimum volume inside of which all possible particles are located at the time specified. Computer hardware requirements for the proposed model are modest and depend on the complexity of the desired user interface and the number of particles that need to be tracked. The latter can be established through an appropriate set of sensitivity studies.

## THE TRAJECTORY MODEL

To compute particle locations, we use a trajectory model. The model used in this study is properly termed an isobaric model, based on a specification of winds on constant-pressure surfaces. Other trajectory models could have been used, such as isentropic or isosigma models. For isentropic models, trajectories are defined along surfaces of constant potential temperature in an attempt to conserve the energy of motion. Isosigma models use a terrain-following coordinate system that is a function of pressure. Evidence that any of the trajectory models can perform better than the other is a function of the meteorological situation. Kuo and others (1985) concluded that there was little difference between these models in terms of their horizontal transport

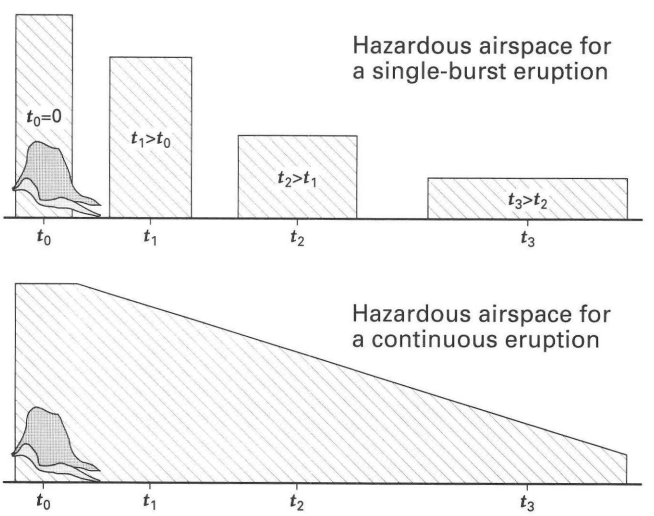


**Figure 2.** Side view of the restricted airspace. This is an exaggerated schematic perspective that illustrates the nature of the restricted region. Time of eruption is indicated by "$t_0$."

using the results of 14 experiments from a mesoscale (i.e., space scales of 2–2,000 km and a time scale of hours) model. They concluded that the limiting factor in these investigations was the resolution and quality of the available meteorological data. The isobaric model was thereby chosen to be consistent with typical methods for reporting wind information.

The trajectories of the particles are determined using the Lagrangian advection methodology. A Lagrangian description of a fluid flow is one that describes the path of a fluid parcel or particles with respect to space and time (i.e., the $x$, $y$, and $z$ spatial coordinates and time, $t$). This differs from a Eulerian description of the flow, which provides a description of the flow velocity at discrete points at an instant in time. An Eulerian description can be thought of as a snapshot of a flow field, while a Lagrangian description can be thought of as a step-by-step sequence of Eulerian flows of a parcel or particle. The trajectory model has been used with both a modified Euler advection integration scheme (Heffter, 1983), a two-step advection methodology that corrects for changing wind-field characteristics during the time step, and the Runge-Kutta-Merson variable time step, fourth-order method (Press and others, 1986).

## GRAVITATIONAL SETTLING

The capability to accurately simulate the transport of airborne particles is made complex due to the fact that particles settle to the ground at various rates as a function of particle size and shape and atmospheric conditions. Small particles tend to reside in the atmosphere for longer periods of time after injection, which can allow upper-level wind patterns to transport them great distances. Large particles can settle to the surface much quicker, and transport distances tend not to be as large. Not only are transport distances affected by particle-settling speeds, but so is the transport pattern. As particles of different sizes fall through the atmosphere at different rates, winds at a particular level will affect the transport of the particle as a function of the time spent in that layer.

We have developed a computer program that computes, for specified particle sizes, the fall time through the atmosphere. This program computes the time it takes for smooth, spherical particles to fall to the surface from various altitudes. Irregular particles are assumed to be represented by their equivalent aerodynamic size, meaning the spherical diameter that has the same terminal velocity.

The atmosphere is modeled with temperature, pressure, and density varying as a function of geometric altitude. Temperature is modeled as a combination of linear fits to data extracted from the U.S. standard atmosphere. Linear fits are used for the regions below 11.1 km and above 20 km, and the temperature is assumed to be a constant value of 216.65 K

between these altitudes. For altitudes below 11.1 km, the temperature is modeled as:

$$T=288.13-6.440z$$

Above 20.0 km, the temperature is computed as:

$$T=196.75+0.995z$$

where

$z$ is the altitude above mean sea level, in kilometers, and
$T$ is temperature in degrees Kelvin.

Air density, $\rho_a$, is modeled as a function of altitude by:

$$\rho_a=\rho_0 \exp(-z/H)$$

where

$\rho_0$ is the air density, in kg/m$^3$, at mean sea level, and
$H$ is the scale height of the atmosphere.

The value used for $\rho_0$ is 1.225 kg/m$^3$; the value used for $H$ is 8.23 km.

The dynamic viscosity of the atmosphere is modeled as a function of the temperature profile and is calculated as:

$$\mu=\beta T^{3/2}/(T+S)$$

where

$\mu$ is the dynamic viscosity in kg/sec-m,
$\beta$ is a constant ($1.458\times10^{-6}$ kg/sec m K$^{1/2}$), and
$S$ is Sutherland's constant (110.4 K).

The fall time, $\theta_k$, for particle type $k$, is computed by summing the fall time through user-specified atmospheric layers ($\Delta z_i$) as:

$$\theta_k=\Sigma V_{ki}(z)\Delta z_i$$

where

$V_{ki}$ is the terminal velocity of particle type $k$ in altitude slice $i$.

The terminal velocity is computed from the following equation:

$$V=(\mu)(Re_p)/(\rho_a)(d)$$

where

the particle Reynolds number ($Re_p$) is calculated using the method outlined in Norment (1979).

Davies (1945) defined a dimensionless number, $N_D$, as:

$$N_D=4g\rho_a(\rho_p-\rho_a)d^3/(3\mu^2)$$

where

$\rho_p$ is the density of the falling particle, in kg/m$^3$, and
$d$ is the particle diameter, in meters.

If $140 \le N_D \le 4.5\times10^7$, then:

$$\log_{10}(Re_p)=-1.29536+0.986X+(-0.4667)X^2 +1.1235\times10^{-3}X^3$$

where

$X=\log(N_D)$.

For $84.175 \le N_D \le 140$, then:

$$Re_p=4.16667\times10^{-2}+(-2.3363\times10^{-4})N_D +2.0154\times10^{-6}(N_D)^2-6.9105\times10^{-9}(N_D)^3$$

For $0.3261 \le N_D \le 84.175$, the correlation is due to Beard (1979):

$$Re_p=\exp[-3.18657+0.99269Y-0.153193\times10^{-2}Y^2 -0.987059\times10^{-3}Y^3-0.0578878\times10^{-3}Y^4 +0.855176\times10^{-4}Y^5-0.327815\times10^{-5}Y^6]$$

where

$Y=\ln(N_D)$.

Stokes' law is used for particles for which $N_D \le 0.3261$:

$$Re_p=N_D/24$$

When the size of the particles approach the mean free path of the molecules through which they are falling, particle mobility increases, and the terminal velocities must be modified by a slip correction factor known as the Cunningham factor ($C_c$). The correlation by Flanigan and Taylor (1966) was used:

$$C_c=1+A(2l/d)+Q(2l/d)\exp(-Bd/2l)$$

where

$d$ is in meters.

Using a mean free path, $l$, of $9.322\times10^{-8}$ meters, the value of the constants in the equation above are $A=1.234$, $Q=0.413$, and $B=0.904$. Using these values, multiplying by $\rho_0/\rho_a$, and substituting for $\rho_0$ gives:

$$C_c=1+2.8\times10^{-7}\rho_a/d$$

where

$d$ and $\rho_a$ are in meters and kg/m$^3$, respectively.

The terminal velocity, $V$, is multiplied by this factor.

We typically compute terminal velocities for particles residing at the midpoint of 500-m-thick layers of the atmosphere. The incremental fall times through each layer are determined using these terminal velocities for all particles in the layer. Total fall time is then calculated by summing the incremental fall times for each 500-m layer. Total fall times as a function of altitude for particles of six diameters, ranging from 30 to 300 μm, is shown in figure 3.

Analysis of material collected by sampling aircraft and on the ground indicates that shapes of dust particles from volcanic eruptions can be highly irregular (Leifer and others, 1981; Newell and Deepak, 1982). The terminal velocities of these irregularly shaped particles are defined in terms of an equivalent spherical radius as discussed earlier.

## DISPERSION

The volcanic cloud is modeled by a stack of circular wafers of non-uniform size, each representing a portion of the total cloud mass and also a portion of the particle-size spectrum existing in the cloud at the altitude of the wafer (fig. 1). The displacement of each wafer by local winds and its fall due to gravity represents the trajectory of the representative particle in that wafer. Turbulence in the atmo-

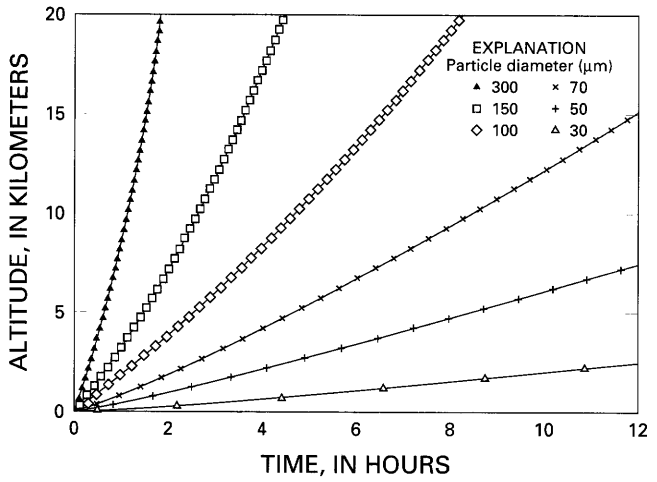


**Figure 3.** Duration of fall for particles of different size as a function of the altitude at which they are released.

sphere causes the wafer to grow in size both horizontally and vertically. The horizontal dispersion is modeled by one of two models: Heffter (1983) or Gifford and others (1988). The Heffter model has been used for the present application; however, the choice of model for this application is not very critical. Because the horizontal extent of the wafer is of most importance, vertical dispersion can be neglected. Conservative assumptions about dispersion due to atmospheric turbulence for the purpose of defining a restricted region are easily made. The location of the cloud elements is mainly affected by transport by wind.

## INITIAL AND BOUNDARY CONDITIONS

The calculation methodology does not need the exact evolution of the eruption column from the onset of eruption. We are interested in what happens when the wind takes over dispersion of the ash cloud. The initial estimate of ash in the air after cloud stabilization can be obtained from Wilson (this volume) for wet clouds or from Sparks and others (this volume) for dry clouds. To determine all potential particle locations, we position many particle sizes at regularly spaced altitudes up to the highest altitude of the volcano cloud. The initial height and shape of the cloud are estimated based on ground, satellite, or pilot observations. The diameter of the cloud could be taken as its maximum dimension because that would be more conservative than defining the actual shape of the cloud. For purposes of defining a conservative restricted region, an initial circular cylinder shape is adequate. The particles are specified as a uniform distribution that is the same throughout the cloud, and the particles are tracked through the wind field as they fall due to gravity.

## MINIMUM RESTRICTED AREA

Having defined the particle transport and settling methodology and the initial conditions, one can compute the locations of all the particles and the wafers that they represent at a given time. A vertical rectangular prism, extending from the ground to the top of the cloud, is then defined, enclosing the locations of all wafers regardless of their altitude. The restricted airspace, or air volume, is then defined as the rectangular prism with the minimum cross-sectional area that encloses all wafers. This cross-sectional area is determined by an iterative process.

## AN EXAMPLE

An example of how the procedures described in the previous sections could be implemented in an operational system is shown for a hypothetical eruption of Iliamna Volcano, Cook Inlet, Alaska. The winds in that region are shown in figure 4 in the form of zero-mass particle trajectories originating from different altitudes. The winds used in this case were from an archive of 2.5°×2.5° gridded wind fields obtained from the National Center for Atmospheric Research. In an operational scenario, actual winds should be used. In the example, the strong vertical shear is clearly evident by the fanning of the trajectories. Each trajectory is due to winds of a different altitude. The locations of all the

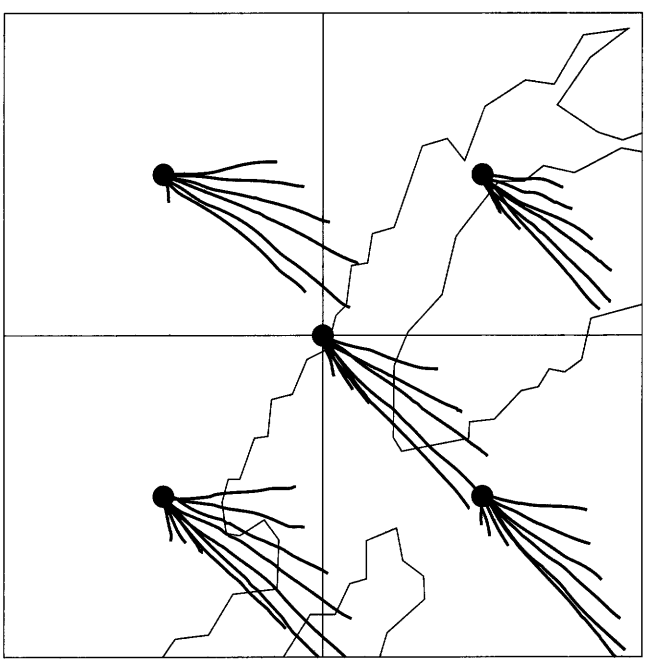

**Figure 4.** Map of Cook Inlet area, Alaska, showing the trajectories of particles with zero mass originating at different altitudes being transported over an undefined period. Fan-like patterns are the result of vertical wind shear.

wafers, represented by particles with mass, are calculated at different times, and a minimum volume is fitted around their locations. The results of the enclosed area computation as a function of angle are shown in figure 5. The inset in this figure defines the baseline angle. For the example, the minimum cross-sectional areas, and, hence, air volumes, are shown in figure 6 for two different forecast times.

As conceptualized, the software that would perform this calculation can be started at any time. When an eruption is about to take place, a user would provide some initial estimate of the eruption. The user selects the volcano of interest (fig. 7) and initiates the calculation process.

Next, screen 2, (fig. 8), is displayed instantaneously. A first estimate of the basic cloud parameters can be made here by entering appropriate values in the data blocks shown. The user is prompted throughout this process by the software, and help functions would be available to provide guidance. Pressing the "Go" button begins execution and results in a display of the restricted region shown in figure 9. If this region is found acceptable, the "Description" button is selected (fig. 10). Acceptability is subjective and is a function of the data that is available. The result is subsequently translated into a NOTAM-formatted description that can be transmitted by clicking the "Transmit" button. The whole process can be completed in a few minutes.

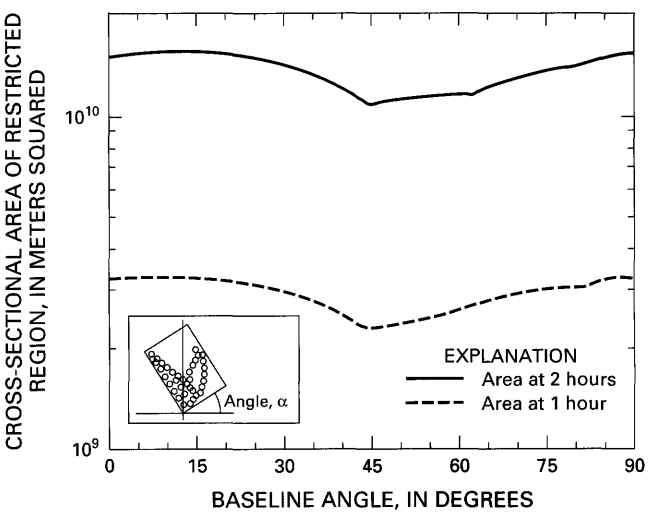


**Figure 5.** The cross-sectional area of the restricted region as a function of the baseline angle, α, for two elapsed times. This shows that a minimum region can be up to 50 percent smaller than some arbitrary region. Inset shows definition of baseline angle.

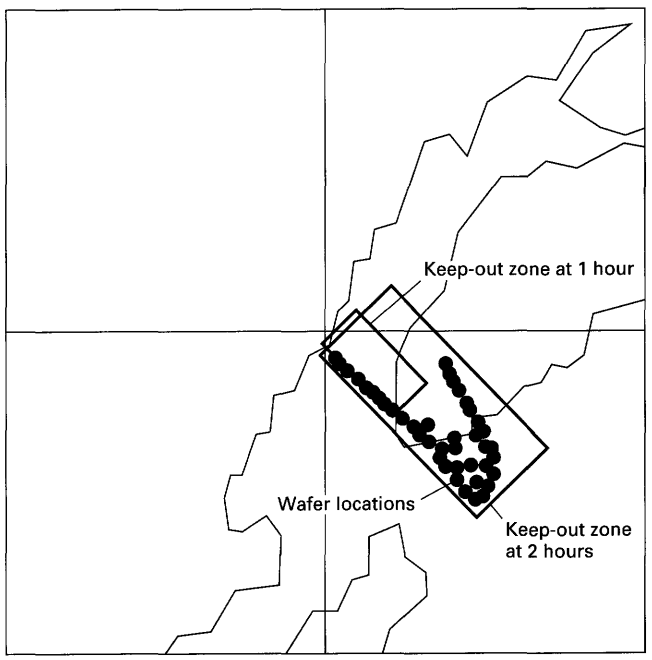


**Figure 6.** Map of Cook Inlet area, Alaska, showing the keep-out region at two times for a hypothetical eruption of Iliamna Volcano.

## CONCLUSIONS AND RECOMMENDATIONS

We have described an approach that could provide timely information to the air traffic industry to assist them in avoiding potentially hazardous areas contaminated with volcanic ash. Using existing methods, we have demonstrated computations for particle transport and settling and for defining the restricted airspace. While the whole process has been assembled by hand—the methodology can easily be implemented on low-end computer workstations, high-end personal computers, and using available graphical-user-interface building tools.

To transform the suggested approach into an operational tool will require additional development work. Specifically, workable interfaces adapted to potential users must be developed; interfaces with wind-data sources and the optimal interpolation of such data into a consistent wind field must be developed; the initial conditions must be relevant to the different types of volcanoes that are of interest; the hardware and software to generate and update the NOTAM must be designed and written. None of these are insurmountable problems. They require straightforward engineering work.

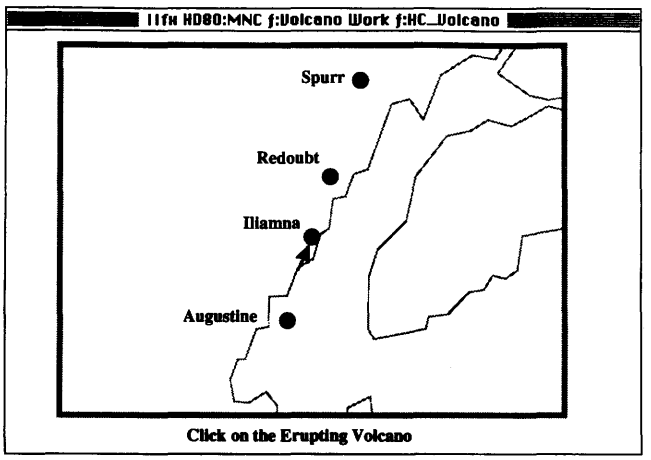


**Figure 7.** Startup screen for the Cook Inlet area, Alaska, example described in the text.

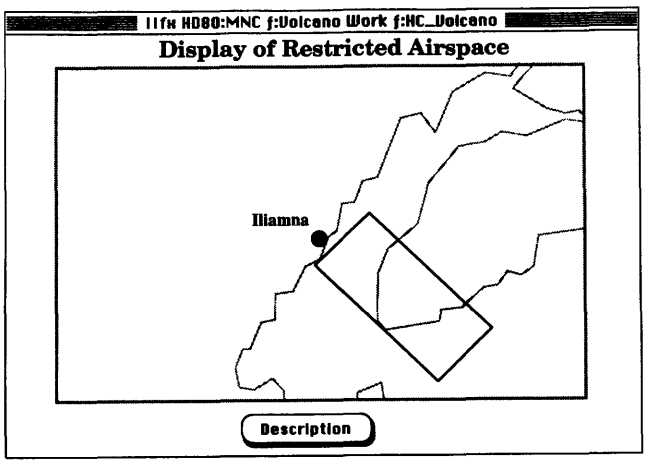


**Figure 9.** The restricted region for the Cook Inlet area, Alaska, as calculated by the software screen for the example.

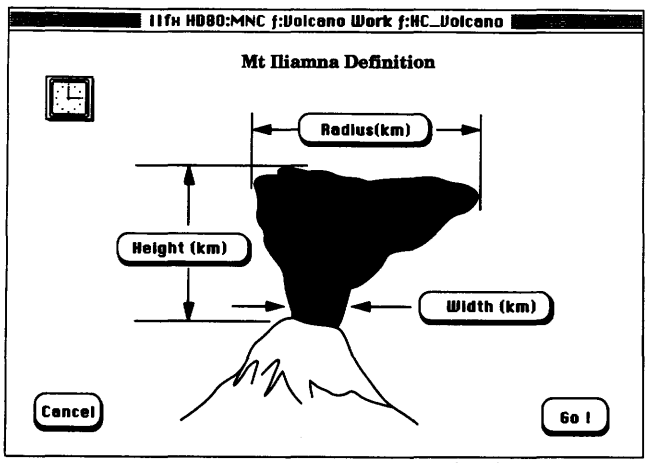


**Figure 8.** The screen that lets the user define cloud parameters that are needed for transport calculations.

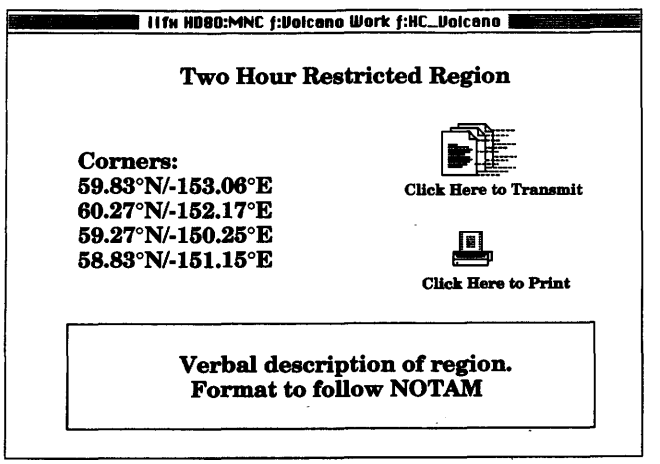


**Figure 10.** The NOTAM screen for the example.

## ACKNOWLEDGMENTS

Elements of the software used to generate the demonstration was developed under the Defense Nuclear Agency funding. John Cockayne of Science Applications International Corporation provided useful comments and insights into the problem of aircraft encounters with dust. We also appreciate comments from the reviewers.

## REFERENCES CITED

Beard, K.V., 1979, Terminal velocity and shape of cloud and precipitation drops aloft: Journal of Atmospheric Sciences, v. 33, p. 851–854.

Casadevall, T.J., 1992, Volcanic hazards and aviation safety, lessons of the past decade: Federal Aviation Administration, Aviation Safety Journal, v. 2, p. 3–11.

Cockayne, J.E., and Singer, H.A., 1991, Multiburst environments and fratricide effects. Volume 1—Cluster analysis of wind profiles for fratricide effects: Defense Nuclear Agency Report DNA-TR-90-122, v.1, 51 p.

Davies, C.N., 1945, Definitive equations for the fluid resistance of spheres: Proceedings of the Physical Society, pt. 4, v. 57, no. 322, p. 259.

Flanigan, V.P.R., and Taylor, P., 1966, Tables of aerosol physics functions: Central Electricity Generating Board, Berkeley Nuclear Laboratories, United Kingdom, tables 1–3.

Gifford, F.A., Barr, S., Malone, R.C., and Mroz, E.J., 1988, Tropospheric relative diffusion to hemispheric scales: Atmosphere Environment, v. 22, no. 8, p. 1871–1879.

Heffter, J.L., 1983, Branching atmospheric trajectory (BAT) model: Rockville, Md., NOAA Air Resources Laboratory Technical Memorandum ERL, ARL-121, 16 p.

Hopkins, T.H., and Bridgeman, C.J., 1985, A volcanic ash transport model and analysis of Mount St. Helens ashfall: Journal of Geophysical Research, v. 90, p. 10620–10630.

Kuo, Y.H., Skumanich, M., Haagenson, P.L., and Chang, J.S., 1985, The accuracy of trajectory models as revealed by the observing system simulation experiments: Monthly Weather Review, v. 113, p. 1852–1867.

Leifer, R., Hinchliffe, L., Fisenne, I., Knutson, E., Olden, M., Sedlacek, W., Mroz, E., and Cahill, T., 1981, Measurements of the stratospheric plume from the Mount St. Helens plume: Radioactivity and chemical composition: Science, v. 214, p. 904–907.

Newell, R.E., and Deepak, A., eds., 1982, Mount St. Helens eruptions of 1980; atmosphere effects and potential climate impact: A Workshop Report: National Aeronautics and Space Administration Report NASA SP-458, 119 p.

Norment, H.G., 1979, DELFIC: Department of Defense fallout prediction system, Volume I—Fundamentals: Defense Nuclear Agency Report DNA 5159F-1, 98 p.

Press, W.H., Flannery, B.P., Teukolsky, S.A., and Vetterling, 1986, Numerical Recipes in FORTRAN, the Art of Scientific Computing: New York, Cambridge University Press, 963 p.

Steenblik, J.W., 1990, Volcanic ash: A rain of terra: Air Line Pilot, June/July, p. 9–15, 56.

Tootell, B., 1985, All Four Engines Have Failed: The True and Triumphant Story of Flight BA 009 and the "Jakarta Incident:" Auckland, Hutchinson Group Ltd., 178 p.

VOLCANIC ASH AND AVIATION SAFETY:
Proceedings of the First International Symposium
on Volcanic Ash and Aviation Safety
U.S. GEOLOGICAL SURVEY BULLETIN 2047

# DETECTION AND DISCRIMINATION OF VOLCANIC ASH CLOUDS BY INFRARED RADIOMETRY—I: THEORY

*By* Alfred J. Prata *and* Ian J. Barton

## ABSTRACT

Volcanic ash clouds with a high concentration of silicate particles exhibit optical properties in the infrared (8–13 μm) that can be used to discriminate them from normal water/ice clouds. In principle, a simple radiometer equipped with at least two channels with appropriate passbands may be used to identify volcanic clouds. In this paper, we develop the theoretical basis for such a radiometer. We solve the radiative-transfer problem in a cloudy atmosphere by using a discrete-ordinates model and present results for a variety of viewing conditions. These include vertical viewing downward (from a satellite), horizontal viewing (from an aircraft), and vertical viewing upward (from the ground). We also present some LOWTRAN-7 calculations for representative atmospheres, which include height variation of temperature, cloudiness, water vapor, and other trace gases.

## INTRODUCTION

The thermal infrared window between 8 μm and 13 μm has frequently been exploited for remote sensing of clouds and the Earth's surface. It has been suggested by Prata (1989b) that this region may also be used for detection and discrimination of volcanic ash clouds. Theoretical calculations indicate that clouds containing silicate materials behave quite differently than ice and water clouds at wavelengths between 10 μm and 12 μm. There have been a number of ash-cloud studies using advanced very high resolution radiometer (AVHRR) satellite data that demonstrate this anomalous behavior (Prata and others, 1985; 1989a; Holasek and Rose, 1991). This behavior is due primarily to the much stronger dispersive nature of silicate-bearing materials compared to water and ice in the infrared window. Prata (1989b) used a radiative-transfer model to explain the difference in temperature obtained at wavelengths of 10.8 μm and 11.9 μm (appropriate to AVHRR channels 4 and 5) when viewing volcanic clouds from space. Here, we will also use the model to examine the effects when viewing horizontally (i.e., from an aircraft) or when viewing vertically from the ground. We are motivated in this work by the expectation that a multichannel radiometer when used from an aircraft or from the ground will also be able to discriminate ash clouds from normal water/ice clouds. Because viewing a cloud from the ground or from an aircraft involves paths that traverse a large part of the lower atmosphere, we also need to take account of absorption and emission by gases, such as water vapor.

In this paper we will present theoretical results, and, in part II (Barton and Prata, this volume), we will present some preliminary data from ground-based measurements of an actual volcanic cloud.

## RADIATIVE TRANSFER WITH SCATTERING

The radiative-transfer equation for a plane-parallel scattering atmosphere may be written (Chandrasekhar, 1960):

$$\mu \frac{\partial I}{\partial \tau}(\tau, \mu) = I(\tau, \mu) - (1 - \varpi_o) B(T) - \frac{\varpi_o}{2} \int_{-1}^{1} P(\mu; \mu') I(\tau, \mu') \, d\mu' \qquad (1)$$

where

$I$ is the radiance,
$\tau$ is the optical depth,
$\mu$ is the cosine of the zenith angle,
$T$ is temperature,
$B$ is the Planck function,
$\varpi_o$ is the single scattering albedo, and
$P$ is the axially symmetric phase function.

An illustration of the problem is shown in figure 1. The boundary conditions are that the radiances incident at the cloud top and base are isotropic, with Planck brightness temperatures of $T_s$ and $T_g$ respectively. That is:

$$I(0,-\mu)=B(T_s)$$

$$I(\tau_c,+\mu)=B(T_g)$$

The discrete-ordinates solution is given by:

$$I(\tau,\mu_i) = \sum_j L_j W_j(\mu_i)\, e^{-\kappa_j \tau} + B(T) \qquad (2)$$

where

$-n \le i, j \le n$, ($2n$ is the number of discrete radiation streams).

The eigenvalues, $\kappa_j$, and eigenvectors, $W_j$, are determined by using an algebraic eigenvalue equation solver as suggested by Stamnes and Swanson (1981).

## TWO-STREAM SOLUTION

To gain insight into what processes are important in the transport of thermal radiation through the cloud, a two-stream ($2n = 2$) solution is employed. This solution is analytic and can be easily derived (Liou, 1974). In this case, the general solution (given by equation 2) is:

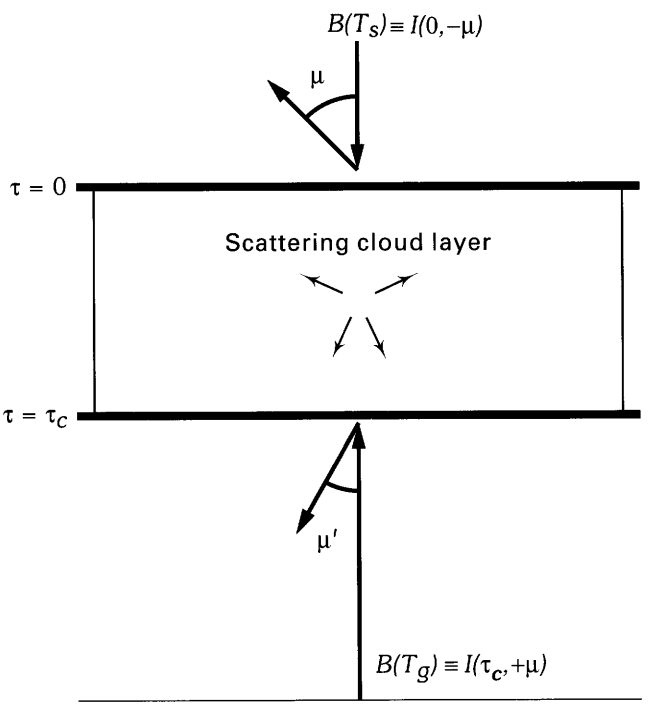


**Figure 1.** Schematic of the plane-parallel scattering cloud model.

$$I(\tau,\mu) = L_{-1}W_{-1}W_{-1}e^{+\kappa\tau} + L_{+1}W_{+1}e^{-\kappa\tau} + B(T_c) \qquad (3)$$

where

$T_c$ is the cloud temperature.

Applying the boundary conditions we have:

$$L_-W_- + L_+W_- = B(T_s) - B(T_c) \qquad (4)$$

$$L_-W_-e^{+\kappa\tau_c} + L_+W_+e^{-\kappa\tau_c} = B(T_g) - B(T_c) \qquad (5)$$

Where we have made use of the fact (Liou, 1974):

$$W_-(-\mu) = W_+(+\mu)$$

$$W_-(+\mu) = W_+(-\mu)$$

We have dropped explicit reference to $\mu$ and $n$ for notational convenience. Adding and subtracting these equations and solving for the $L$'s:

$$L_+ = \frac{1}{2}\left[\frac{B(T_s)+B(T_g)-2B(T_c)}{W_+e^{-\kappa\tau_c}+W_-} + \frac{B(T_g)+B(T_s)}{W_+e^{-\kappa\tau_c}-W_-}\right]$$

$$L_- = \frac{1}{2}\left[\frac{B(T_s)+B(T_g)-2B(T_c)}{W_+e^{-\kappa\tau_c}+W_-} + \frac{B(T_s)-B(T_g)}{W_+e^{-\kappa\tau_c}-W_-}\right]$$

The solution for the upward component at the cloud top is then:

$$I(0,+\mu) = W_-L_-e^{-\kappa\tau_c} + W_+L_+ + B(T_c) \qquad (6)$$

and the downward component at the cloud base is:

$$I(\tau_c,-\mu) = W_+L_- + W_-L_+e^{-\kappa\tau_c} + B(T_c) \qquad (7)$$

The eigenvalues ($\pm\kappa$) and eigenvectors ($W_-$, $W_+$) are:

$$\kappa = \pm\frac{1}{\mu}\left[(1-\varpi_o)\left(1-3\varpi_o g\mu^2\right)\right]^{1/2} \qquad (8)$$

$$W(\pm\mu) = \frac{1}{1\pm\mu\kappa}\left[\varpi_o \pm 3\varpi_o g(1-\varpi_o)\frac{\mu}{\kappa}\right] \qquad (9)$$

The cosine of the scattering angle has the value:

$$\mu = \frac{1}{\sqrt{3}}$$

We now consider two limiting cases that are of interest to the detection problem.

A. Optically thin limit ($\tau_c \to 0$).

In this case, it may be shown that:

$$I(0,+\mu) \to B(T_g)$$

and that:

$$I(\tau_c, -\mu) \rightarrow B(T_s)$$

B. Optically thick limit ($\tau_c \rightarrow \infty$).

From equation 5, we find that:

$$I(0, +\mu) \rightarrow B(T_c)\left[1 - \frac{W_{+1}}{W_{-1}}\right] + B(T_s)\frac{W_{+1}}{W_{-1}} \quad (10)$$

and, from equation 6:

$$I(\tau_c, -\mu) \rightarrow B(T_c)\left[1 - \frac{W_{+1}}{W_{-1}}\right] + B(T_g)\frac{W_{+1}}{W_{-1}} \quad (11)$$

Note that the factor

$$\left[1 - \frac{W_{+1}}{W_{-1}}\right]$$

may be interpreted as an effective emissivity of the cloud. It is seen that the radiance consists of two components: an emitted portion and a reflected portion. In the case of viewing from the ground, the reflected portion may be significant because $B(T_g) >> B(T_c)$.

## OPTICAL PROPERTIES

Mie calculations are performed to determine the scattering properties and phase function of a polydisperse ensemble of particles. These calculations require refractive indices, the particle-size distribution, and the particle shape. The results are given in terms of efficiency factors:

$$\hat{Q}_f = \frac{\int_0^\infty \pi r^2 Q_f\left(\frac{2\pi r}{\lambda}, m\right)\frac{dn(r)}{dr}dr}{\int_0^\infty \pi r^2 \frac{dn(r)}{dr}dr} \quad (12)$$

where

$Q_f$ is the Mie efficiency factor for extinction, scattering, or absorption, and

$n(r)$ is the size distribution of particles, with radius $r$, in units of number of particles per unit volume.

The extinction, absorption, and scattering efficiencies are related by:

$$\hat{Q}_{ext} = \hat{Q}_{abs} + \hat{Q}_{sca} \quad (13)$$

The single scattering albedo is:

$$\varpi_o = \frac{\hat{Q}_{sca}}{\hat{Q}_{ext}} \quad (14)$$

The asymmetry parameter, $g$, is:

$$g = \frac{1}{2}\int_{-1}^{1} P(\mu)\,\mu\,d\mu \quad (15)$$

## SIZE DISTRIBUTIONS

The modified-$\gamma$ size distribution has been used to include the effect of mean particle size on the scattering properties of the cloud. The distribution is given by:

$$\frac{dn(r)}{dr} = \frac{Nb^7}{6!}r^6 \exp(-br) \quad (16)$$

where

$r_o$ is the mean particle radius,

$N$ is the total number of particles per unit volume, and

$b=6/r_o$.

# OPTICAL THICKNESS

The optical thickness of the cloud depends on the size distribution, extinction efficiency, and the geometrical thickness of the cloud. These are related by:

$$\tau_c = \hat{Q}_{ext} L \int_0^\infty \pi r^2 \frac{dn(r)}{dr}dr \quad (17)$$

where

$L$ is the geometrical thickness.

For a 1-km-thick cloud of particles with a concentration of $10^2$ cm$^{-3}$, a mean particle radius of 3 μm, and $\hat{Q}_{ext} = 2$ (at 10 μm), $\tau_c \cong 5$.

## MIE CALCULATIONS

The scattering parameters required for the radiative-transfer calculations are obtained using Mie theory. A computer program developed by Evans (1988) was used. Refractive indices of quartz, volcanic dust, water, and ice are input to the program together with the appropriate size distribution and particle shape. The refractive indices of quartz are obtained from Petersen and Weinman (1969) and those of volcanic dust are from Volz (1973). The modified-$\gamma$ size distribution was used for these calculations with a mean particle radius of 3 μm—the particles were assumed to be spherical. Results of the calculations are given in table 1 and figures 2 and 3. These results show that volcanic substances (quartz and dust) have a larger extinction than water and ice and that the extinction decreases with wavelength between 10.8 μm and 12.0 μm. For water and ice, the extinction increases with wavelength in this region.

**Table 1.** Refractive indices, extinction efficiency factor, asymmetry parameter, and single scattering albedo for quartz, volcanic dust, ice, and water.

[Real part of refractive index is in column under $n_r$; imaginary part of refractive index is in column under $k$. $Q_{ext}$, extinction efficiency factor; $g$, asymmetry parameter; $\varpi_0$, single scattering albedo. The modified-$\gamma$ size distribution was used, with $r_o$ = 3 μm]

| Wavelength (μm) | $n_r$ | $k$ | $Q_{ext}$ | $g$ | $\varpi_o$ |
|---|---|---|---|---|---|
| **Quartz**[1] | | | | | |
| 8.6 | 0.658 | 1.448 | 3.171 | 0.622 | 0.603 |
| 10.1 | 2.607 | 0.048 | 2.198 | 0.427 | 0.976 |
| 10.9 | 2.140 | 0.027 | 3.377 | 0.405 | 0.860 |
| 11.8 | 1.627 | 0.050 | 2.832 | 0.632 | 0.825 |
| 12.0 | 1.515 | 0.063 | 2.247 | 0.650 | 0.766 |
| 12.5 | 1.526 | 2.240 | 3.224 | 0.491 | 0.595 |
| **Volcanic dust**[2] | | | | | |
| 8.6 | 1.221 | 0.650 | 2.330 | 0.758 | 0.411 |
| 10.1 | 2.078 | 0.101 | 3.248 | 0.561 | 0.659 |
| 10.9 | 1.780 | 0.100 | 3.259 | 0.639 | 0.713 |
| 11.8 | 1.776 | 0.218 | 2.960 | 0.661 | 0.577 |
| 12.0 | 1.756 | 0.230 | 2.890 | 0.660 | 0.566 |
| 12.5 | 1.713 | 0.270 | 2.718 | 0.653 | 0.530 |
| **Ice**[3] | | | | | |
| 8.6 | 1.288 | 0.039 | 1.658 | 0.776 | 0.758 |
| 10.1 | 1.185 | 0.058 | 0.837 | 0.731 | 0.495 |
| 10.9 | 1.087 | 0.204 | 1.126 | 0.704 | 0.233 |
| 11.8 | 1.224 | 0.395 | 1.799 | 0.675 | 0.322 |
| 12. 0 | 1.280 | 0.413 | 1.909 | 0.670 | 0.339 |
| 12.5 | 1.386 | 0.422 | 2.070 | 0.656 | 0.370 |
| **Water**[4] | | | | | |
| 8.6 | 1.275 | 0.037 | 1.557 | 0.777 | 0.758 |
| 10.1 | 1.215 | 0.052 | 0.925 | 0.723 | 0.596 |
| 10.9 | 1.172 | 0.078 | 0.805 | 0.702 | 0.386 |
| 11.8 | 1.122 | 0.159 | 0.955 | 0.669 | 0.232 |
| 12.0 | 1.111 | 0.199 | 1.072 | 0.662 | 0.228 |
| 12.5 | 1.123 | 0.259 | 1.254 | 0.643 | 0.244 |

[1] Refractive index data from Petersen & Weinman (1969).
[2] Refractive index data from Volz (1973).
[3] Refractive index data from Warren (1984).
[4] Refractive index data from Hale & Querry (1973).

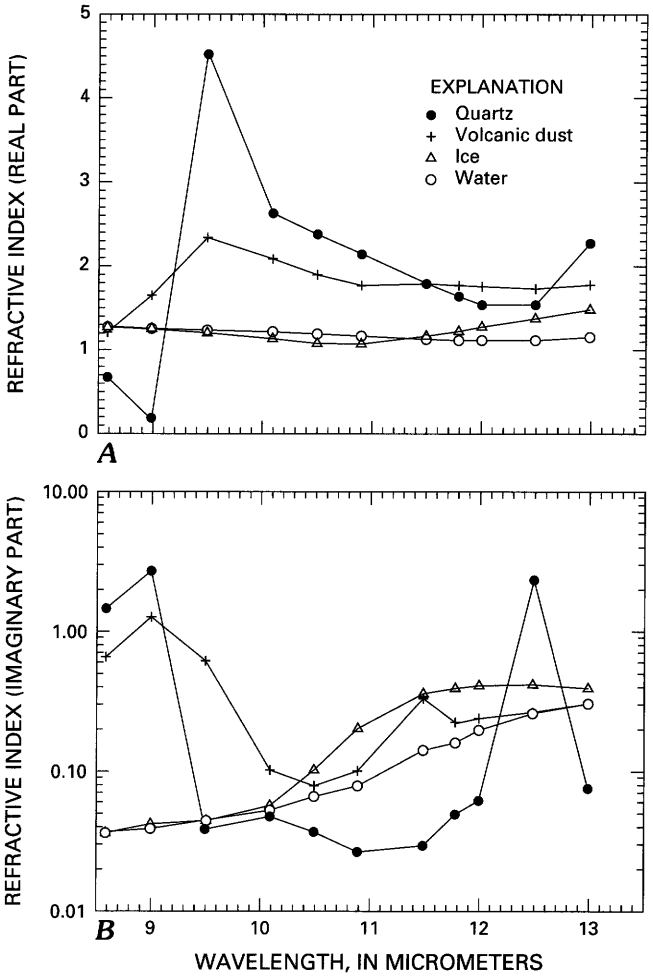


**Figure 2.** *A*, Real part of the refractive index of quartz, volcanic dust, ice, and water as a function of wavelength between 8.5 μm and 13.5 μm. *B*, Imaginary part of the refractive index.

## MODEL RESULTS

The discrete-ordinates model (with $2n = 32$) has been used to calculate the upward and downward radiation streams for the three cases of interest (satellite, ground-based sensing, and aircraft). The data given in table 1 were used in the calculations.

### SATELLITE SENSING

The cloud was assumed to have a temperature of –40°C, and the ground was assumed to have a temperature of 15°C. The optical thickness of the cloud was set to $\tau_c = 5$ at 10.1 μm. Figures 4*A* and 4*B* show the brightness temperatures as a function of zenith angle for quartz, volcanic dust, ice, and water. Note that, for all zenith angles, the temperatures at 10.9 μm are less than those at 11.8 μm for the volcanic substances, whereas the reverse is true for ice and water (except at large zenith angles when the limb-darkening effect appears to be more pronounced at 10.9 μm than at 11.8 μm). Note that at 60° the satellite scan angle is about 50° so this effect may be seen from the AVHRR, which scans to ±55.4°. For optically thick clouds, we have seen from the two-stream approximation that the satellite radiometer receives radiation at the cloud temperature multiplied by the effective emissivity (which is a function of the optical properties and, hence, wavelength) because, in this case, we may assume that the radiance of space is effectively negligible. It is not sufficient to simply insert the optical parameters from table 1 and take the limit $\tau_c \to \infty$ because, in reality, the cloud becomes optically thick due to large particles. This implies that, $Q_{ext}$, $\varpi_o$, and $g$ must be computed for a new size distribution. Clearly,

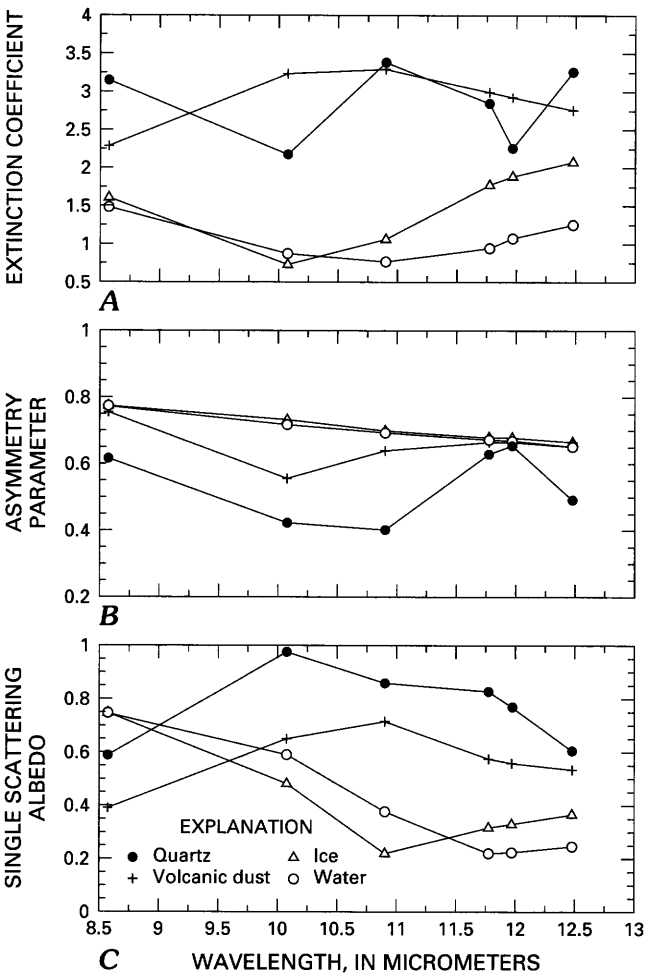


**Figure 3.** *A*, Extinction coefficient as a function of wavelength for quartz, volcanic dust, ice, and water. *B*, Asymmetry parameter as a function of wavelength. *C*, Single scattering albedo as a function of wavelength.

we cannot expect to model this situation accurately because the cloud structure would be extremely inhomogeneous and complex. To give an indication of what to expect, table 2 shows the results for the polydisperse cloud with $r_o = 3$ μm and $r_o = 30$ μm. Only the 10.9-μm and 11.8-μm brightness temperatures are shown along with the effective emissivities.

These results indicate that, for optically thick clouds, AVHRR channel-4 temperatures should be less than or equal to channel-5 temperatures. However, when ice and water are mixed in with volcanic debris, the temperature difference (channel 4 – channel 5) may lead to positive, negative, or zero differences. The optically thick case may be the most difficult to interpret.

## GROUND-BASED SENSING

In this case, the radiometer is assumed to be viewing the plume at an elevation angle of 26°. The plume temperature is set at 5°C, and the ground temperature is set at 15°C.

**Table 2.** Brightness temperatures and effective emissivities for two size distributions.

[Cloud-top temperature, $T_C$, is –40.0°C; $\tau_c = 100$ at 10.1 μm. Values are computed for the stream closest to vertical ($\cos^{-1}\mu = 4°$)]

| Wavelength (μm) | Temperature (°C) | Effective emissivity |
|---|---|---|
| | $r_o = 3$ μm; modified-γ | |
| 10.9 | -45.6 | 0.935 |
| 11.8 | -43.5 | 0.957 |
| | $r_o = 30$ μm; modified-γ | |
| 10.9 | -40.0 | 1.000 |
| 11.8 | -40.0 | 1.000 |

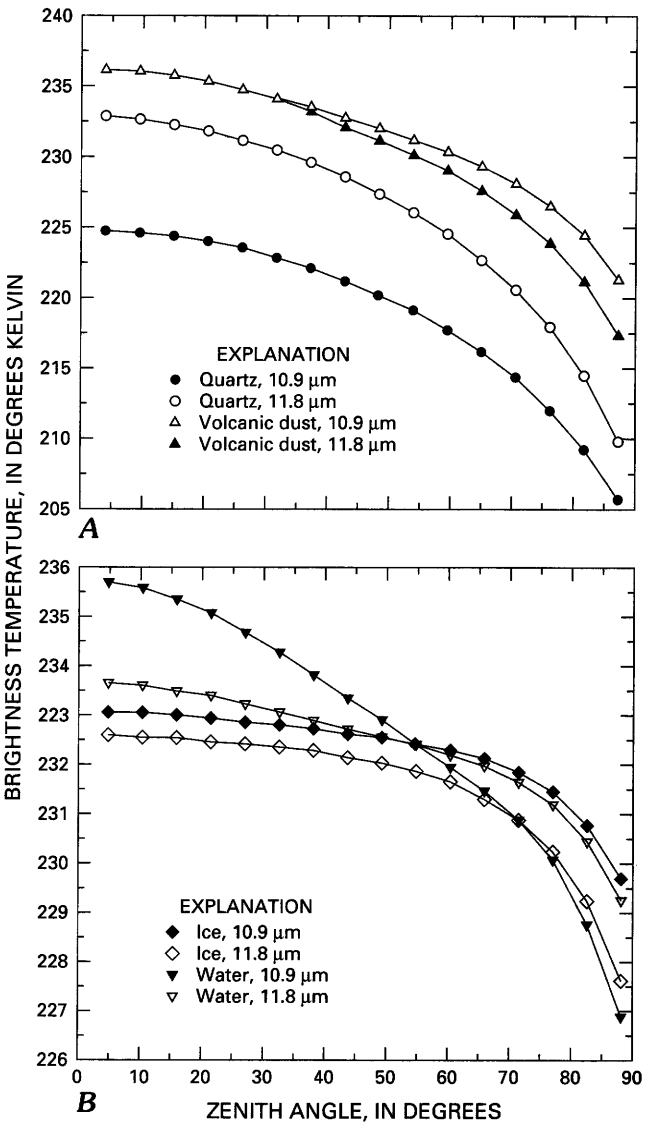


**Figure 4.** *A*, Satellite simulated brightness temperature as a function of zenith angle for quartz and volcanic dust clouds at 10.9 μm and 11.8 μm. *B*, As for *A*, but for water and ice clouds.

These temperatures are representative of the values measured at Sakurajima Volcano (see Barton and Prata, this volume). Results are given in figure 5 for quartz and water. Temperature differences between 10.9 μm and 11.8 μm are positive for the quartz cloud and negative for the water cloud.

These calculations do not include the influences of water vapor absorption and emission. These affects must be accounted for when viewing at low elevation angles in the troposphere. To take them into account, we have used the radiance/transmittance code developed by the U.S. Air Force known as LOWTRAN-7. We calculate the slant path radiance and transmittance for a radiometer viewing at an elevation angle of 26°. The total path length is governed by the location of the target. To simulate our measurements at Sakurajima, we assume that the target is at a height of between 1 and 2 km above the radiometer. By varying the model atmosphere and target height, a range of slant paths and water vapor amounts are obtained.

LOWTRAN-7 provides radiances and transmittances at a maximum resolution of 5 $cm^{-1}$; these are convolved with the filter functions of the airborne volcanic-ash-detection system (AVADS) instrument (Barton and Prata, this volume) to give the simulated radiances. Finally, the slant path radiance, $R_p$, and the slant path transmittance, $t_p$, are combined with the cloud radiance, $R_c$, that is computed by the scattering model to give the radiance at the radiometer, $R_i$. This is given by:

$$R_i = R_c t_p + R_p \qquad (18)$$

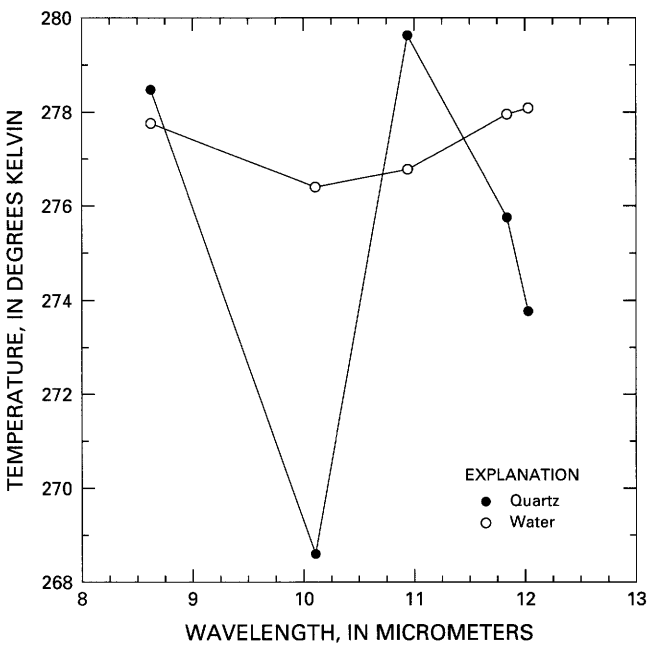


**Figure 5.** Simulated brightness temperatures as a function of wavelength for quartz and water.

The calculations described above have been done for a quartz cloud and a water cloud. Because it appears that only the 10.9-μm and 11.8-μm channels are a good pair for discriminating cloud types, the results are shown for these channels only. Figure 6 shows the variation in the brightness temperature difference, ΔT, between the 10.9-μm and 11.8-μm channels as a function of precipitable water. For the quartz cloud, the positive differences decrease with increasing precipitable water, and, for water clouds, the difference becomes more negative. Thus, water-vapor affects will tend to reduce the discrimination.

## AIRCRAFT SENSING

This situation is modeled by assuming that the plane parallel sides of the cloud are oriented in the vertical. The radiation entering the cloud is the same on both sides (i.e., $B(T_s) = B(T_g)$). For simplicity, we assume that the radiation is isotropic and composed of equal portions from the background sky and from the warm surface. A value of $T_s$ = –30°C is assumed, and the cloud temperature, $T_c$, equals –50°C. This temperature is equivalent to an aircraft cruising height of about 30,000 ft. Results are presented in table 3. We notice that, for optical thicknesses greater than $\tau_c = 5$,

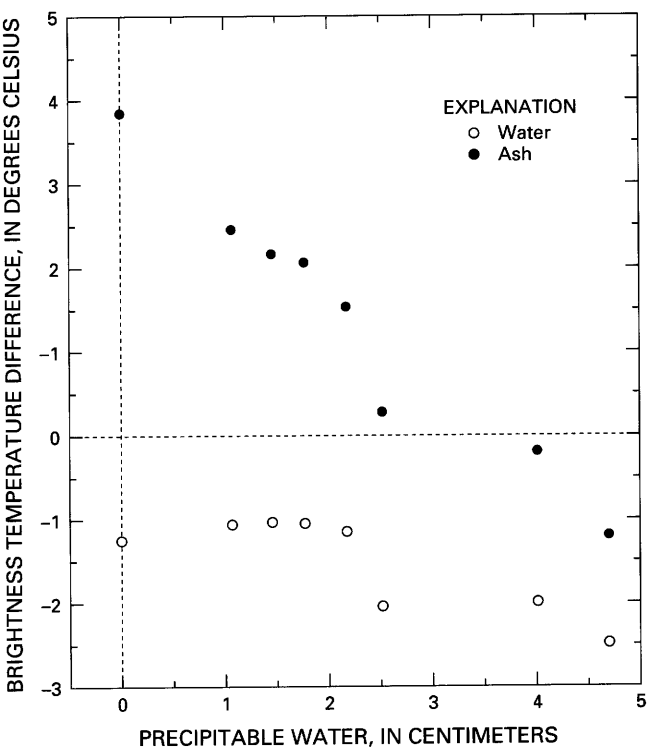


**Figure 6.** Simulated temperature differences (temperature at 10.9 μm minus that at 11.8 μm) as a function of water-vapor loading for a ground-based instrument viewing a cloud of ash (quartz) and a cloud of water.

pairs of channels can be selected that give very good discrimination between quartz and ice clouds. For example, the pairs 10.9 μm/11.8 μm and 10.1 μm/12.0 μm give positive temperature differences for the quartz cloud and negative differences for the ice cloud. It appears that the 10.1 μm/12.0 μm pair is a better discriminator. Calculations of the atmospheric path radiance have also been done using LOWTRAN-7 and assuming a view with an elevation of 4°, but these do not change the results noticeably.

## CONCLUSION

Radiative-transfer calculations for an idealized scattering cloud indicate that quartz and volcanic ash behave differently than water and ice between wavelengths of 10 μm and 12 μm. We have found that, for a ground-based radiometer viewing a volcanic cloud, the brightness temperature at 10.9 μm is greater than that at 11.8 μm. For water and ice clouds, the reverse is true. Absorption and emission by atmospheric gases, principally water vapor, causes the difference between the brightness temperature at 10.9 μm and 11.8 μm to decrease. Similar results are found for near-horizontal viewing of a cloud at 8 km. We also note that pairs of channels at 10.9 μm/11.8 μm and 10.1 μm/12.0 μm should give good ash-cloud discrimination from the ground and from aircraft. Further modeling studies are in progress to assess the affects of particle shape and cloud composition on radiative transfer.

**Table 3.** Cloud temperatures derived from the scattering model for quartz and ice particles at different optical thicknesses.

[$\tau_c$, optical thickness; temperatures shown are in °C]

| Wavelength (μm) | $\tau_c = 5$ | $\tau_c = 10$ | $\tau_c = 50$ | $\tau_c = 100$ |
|---|---|---|---|---|
| **Quartz** | | | | |
| 8.6 | –32.00 | –48.76 | –49.06 | –50.00 |
| 10.1 | –37.05 | –36.23 | –7.12 | –38.21 |
| 10.9 | –37.40 | –44.37 | –44.78 | –44.81 |
| 11.8 | –37.01 | –46.77 | –47.07 | –47.25 |
| 12.0 | –37.91 | –47.64 | –47.96 | –48.21 |
| 12.5 | –39.19 | –48.44 | –48.83 | –50.00 |
| **Ice** | | | | |
| 8.6 | –39.33 | –48.99 | –49.20 | –50.00 |
| 10.1 | –39.33 | –49.46 | –49.58 | –49.73 |
| 10.9 | –39.56 | –49.20 | –49.47 | –50.00 |
| 11.8 | –36.53 | –43.30 | –43.58 | –43.58 |
| 12.0 | –36.46 | –43.04 | –43.29 | –43.29 |
| 12.5 | –36.19 | –42.33 | –42.56 | –50.00 |

## REFERENCES CITED


Chandrasekhar, S., 1960, Radiative Transfer: New York, Dover Publications, Inc., 303 p.

Evans, B.T.N., 1988, An interactive program for estimating extinction and scattering properties of most particulate clouds: Australia Defense Science and Technology Organization, Materials Research Laboratory, Department of Defense Report MRL-R-1123.

Hale, G.M., and Querry, M.R, 1973, Optical constants of water in the 200 nm to 200 μm wavelength region: Applied Optics, v. 12, p. 555–563.

Holasek, R.E., and Rose, W.I., 1991, Anatomy of 1986 Augustine Volcano eruptions as recorded by multispectral image processing of digital AVHRR weather satellite data: Bulletin of Volcanology, v. 53, p. 420–435.

Liou, N-K., 1974, Analytic two-stream and four-stream solutions for radiative transfer: Journal of Atmospheric Sciences, v. 31, p. 1473–1475.

Peterson, J.T., and Weinman, J.A., 1969, Optical properties of quartz dust particles at infrared wavelengths: Journal of Geophysical Research, v. 74, no. 28, p. 6947–6952.

Prata, A.J., 1989a, Observations of volcanic ash clouds using AVHRR-2 radiances: International Journal of Remote Sensing, v. 4, p. 751–761.

———1989b, Radiative transfer calculations for volcanic ash clouds: Geophysical Research Letters., v. 16, p. 1293–1296.

Prata, A.J., Wells, J.B., and Ivanac, M., 1985, A "satellite's eye-view" of volcanoes on the Lesser Sunda Islands: Weather, v. 40, p. 245–250.

Stamnes, K., and Swanson, R. A., 1981, A new look at the discrete ordinates method for radiative transfer calculations in anisotropically scattering atmospheres: Journal of Atmospheric Sciences, v. 38, p. 387–399.

Volz, F.E., 1973, Infrared optical constants of ammonium sulfate, Sahara dust, volcanic pumice, and fly ash: Applied Optics, v. 12, p. 564–568.

Warren, S.G., 1984, Optical constants of ice from the ultraviolet to the microwave: Applied Optics, v. 23, p. 1206–1225.

VOLCANIC ASH AND AVIATION SAFETY:
Proceedings of the First International Symposium
on Volcanic Ash and Aviation Safety
U.S. GEOLOGICAL SURVEY BULLETIN 2047

# DETECTION AND DISCRIMINATION OF VOLCANIC ASH CLOUDS BY INFRARED RADIOMETRY—II: EXPERIMENTAL

*By* Ian J. Barton *and* Alfred J. Prata

## ABSTRACT

An airborne multichannel radiometer has been built to test the feasibility of using infrared radiation to detect and discriminate volcanic ash clouds. The radiometer has five selectable filters and two temperature-controlled precision black bodies for internal calibration. The instrument has been flight tested up to an altitude of 8,000 m and has performed well. During the flight tests, measurements were made in both clear and cloudy skies at varying heights and viewing angles. Results from these tests will be presented and compared to theoretical calculations. The radiometer has also been used to view the volcanic plume emanating from Mt. Sakurajima, on the Japanese island of Kyushu. For these tests, the radiometer was ground based and pointed upward, either toward the ash plume, water clouds, or the clear sky. The radiometer measurements support the concept of using an airborne radiometer to detect volcanic ash clouds ahead of an aircraft. The advantages of this detection technique over others are discussed.

## INTRODUCTION

In the first paper of this pair (Prata and Barton, this volume), theoretical calculations indicated that it should be possible to discriminate between water/ice clouds and volcanic ash clouds using infrared radiometry. This possibility is also evident when satellite instruments are used to investigate the infrared properties of volcanic ash clouds. It has been shown by Prata (1989) that the two thermal infrared channels of the advanced very high resolution radiometer (AVHRR) flying on the NOAA-7 operational meteorological satellite can be used to discriminate between normal clouds and volcanic ash clouds.

The major danger of volcanic ash clouds to commercial aircraft is the stalling of engines due to the ingestion of silicate rock particles. Because these particles have different optical properties to water droplets at 11 and 12 μm, a radiometer operating at these wavelengths should be able to discriminate between volcanic ash and water clouds.

To test this hypothesis, an infrared radiometer has been built and used to view both water/ice clouds and volcanic ash clouds in the thermal infrared band. The results of some airborne tests in Australia and some ground-based observations of volcanic ash clouds in Japan will be presented here.

## THE RADIOMETER

A diagram of the radiometer is shown in figure 1. The instrument has a single beam with a beam width of 3° and can sample incident thermal radiation in one of five wavelengths selected by choosing an appropriate interference filter (see fig. 2 and table 1). The filters included in the radiometer were varied depending on the location of the tests and the physical properties under investigation. The radiometer includes two internal black-body targets for accurate calibration. A mechanical chopper alternates the signal received by the detector between a known temperature and the incoming radiation; then a phase-locked loop ensures that background radiation is not detected. The incident radiation is focused onto the pyroelectric detector by a right-angle parabolic reflector. The radiometer has a typical noise temperature near 0.1°C, depending on the integration time used (normally 2 s) and the band width of the filter. For the airborne tests, the incoming radiation was first passed through a germanium window that has a transmission nearly equal to unity at the wavelengths of interest (see fig. 2).

The filter at 6.4 μm was included to investigate the possibility of detecting clear-air turbulence by observing water-vapor intrusions into the upper atmosphere (Kuhn and others, 1977). Unfortunately, the detector response at this lower wavelength was not sufficient to give a useful signal. The 8.6-μm filter was included for the detection of $SO_2$, which has a broad absorption band in this region of the spectrum.

**Table 1.** Details of filters used in the radiometer.

[CAT, clear-air turbulence]

| Central wavelength (μm) | Band width (μm) | Function |
|---|---|---|
| 6.4 | 0.3 | Water-vapor emission for CAT. |
| 8.6 | 0.5 | $SO_2$ emission. |
| 10.1 | 0.5 | Water cloud–ash cloud discrimination. |
| 10.8 | 0.6 | Water cloud–ash cloud discrimination. |
| 12.0 | 0.6 | Water cloud–ash cloud discrimination. |
| 10.91 | 1.0 | Water cloud–ash cloud discrimination. |
| 11.8 | 1.4 | Water cloud–ash cloud discrimination. |

Data from the radiometer were recorded on an IBM-compatible personal computer using a commercial analog-to-digital board.

## THE AIRBORNE EXPERIMENT AND RESULTS

Aircraft tests of the radiometer were carried out near Hobart, on the island of Tasmania. The radiometer was mounted in a pod that was fitted under the wing of a Navajo aircraft so that it looked directly ahead of the aircraft. A second pod, which included a forward-looking video camera, was fitted under the other wing. The video tape recording for each flight was later used to determine the target in the field of view of the radiometer. The radiometer electronics and data-logging system were included in the aircraft cabin. Flight data were also recorded on a second computer. Initially, the radiometer included the five narrow-band filters centered at wavelengths of 6.4, 8.6, 10.1, 10.8 and 12.0 μm. During the aircraft campaign, for the reason explained above, the 6.4 μm filter was replaced with a wider filter at 10.9 μm and, because no large concentrations of $SO_2$ were expected in the Tasmanian atmosphere, the filter at 8.6 μm was also replaced by a second broad filter at 11.8 μm.

The aircraft was flown at various altitudes up to 8,000 m, and measurements of the infrared radiation emitted by different water-and-ice clouds and the clear sky were taken. For each channel (filter), the signals measured by the radiometer were converted to temperatures using the inverse Planck function at a wavelength determined from a combination of the filter's spectral response, the germanium-window transmission, and the detector response. Figure 3 shows these "brightness" temperatures for the clear sky for level flight at 4,000 m. The measurements are as predicted from theoretical calculations. The temperatures at 10.8 μm are colder because there is less water-vapor absorption at this wavelength compared to that at 11.8 μm. The temperature at 10.1 μm is warmer due to the radiometer receiving radiation from the strong 9.6-μm absorption band of ozone in the warm stratosphere. For comparison, measurements taken from the ground looking at a clear sky are included in figure 3.

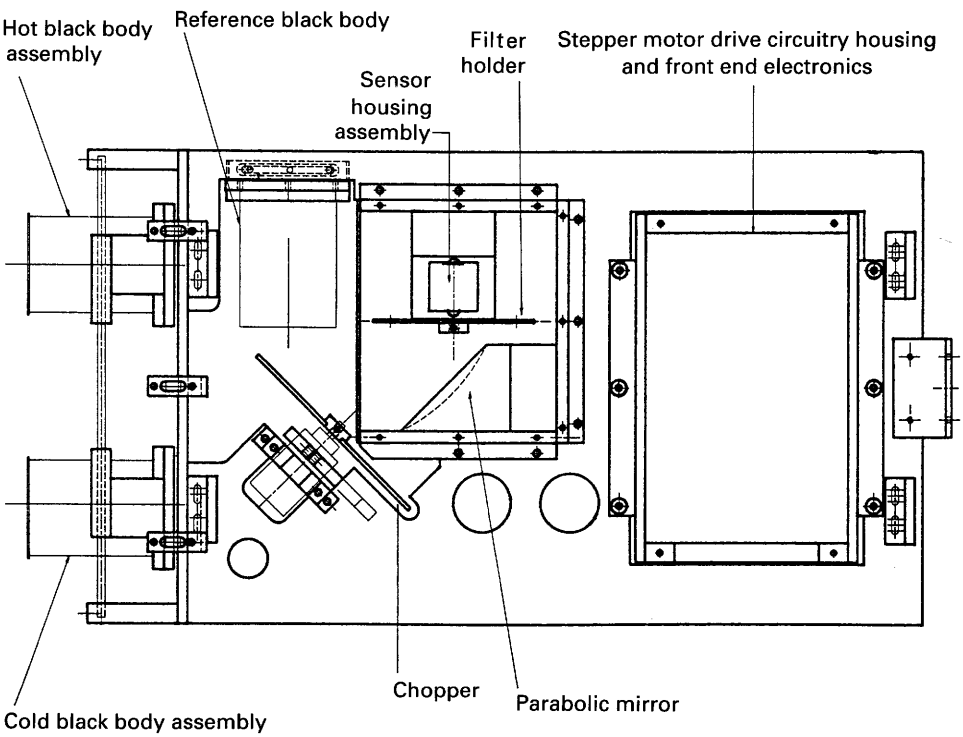


**Figure 1.** Diagram of the multichannel radiometer.

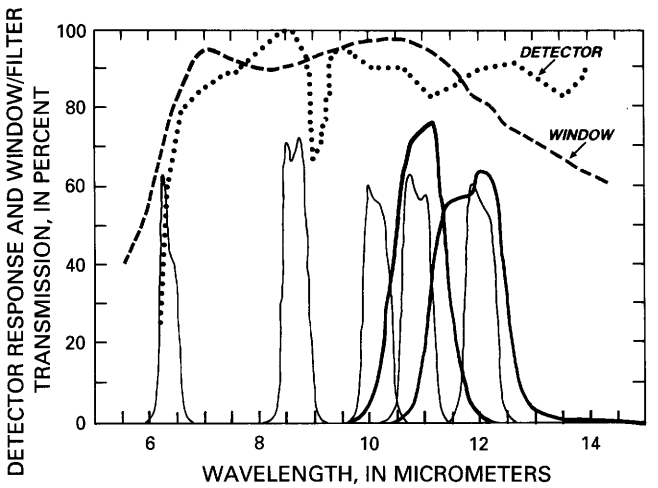


**Figure 2.** Relative spectral responses of the detector and transmittances of filters and the germanium window. Heavy lines indicate spectral response of broad filters; light lines indicate spectral response of narrow filters.

Figure 4 shows brightness temperatures measured when the aircraft was flying horizontally toward a cumulus cloud at 3,300 m. Again, the temperatures at 10.8 μm are less than those at 11.9 μm, as predicted by theory. In this case, the 10.1-μm channel shows a colder temperature due to the cloud obscuring warm stratospheric ozone.

The tests at Hobart showed that the radiometer could operate well in an aircraft flying at levels up to 8,000 m. All measurements with the radiometer agreed with theoretical calculations.

## VOLCANIC-ASH-CLOUD MEASUREMENTS

Having fully tested the radiometer on an airborne platform, it was then necessary to use the instrument to study the infrared characteristics of a real volcanic ash cloud. For this reason, the radiometer was taken to Mt. Sakurajima, on the southern Japanese island of Kyushu. Funds were not available to mount an aircraft campaign, but there were several advantages in operating the radiometer from the ground. Mt. Sakurajima has an altitude of 1,118 m and is an active volcano that erupts between 100 and 200 times annually. Between eruptions, there is almost continual ejection of volcanic ash into the atmosphere. During these passive ejections, the ash is usually carried to no more than 1,000 m above the crater. When the volcano erupts, however, ash can reach altitudes of several thousands of meters (Onodera and Kamo, this volume).

Observations of clear skies, water/ice clouds, and volcanic ash clouds were taken from different locations in the vicinity of Mt. Sakurajima. For the Japan measurements, the 8.6-μm $SO_2$ filter was used along with the narrow filters at

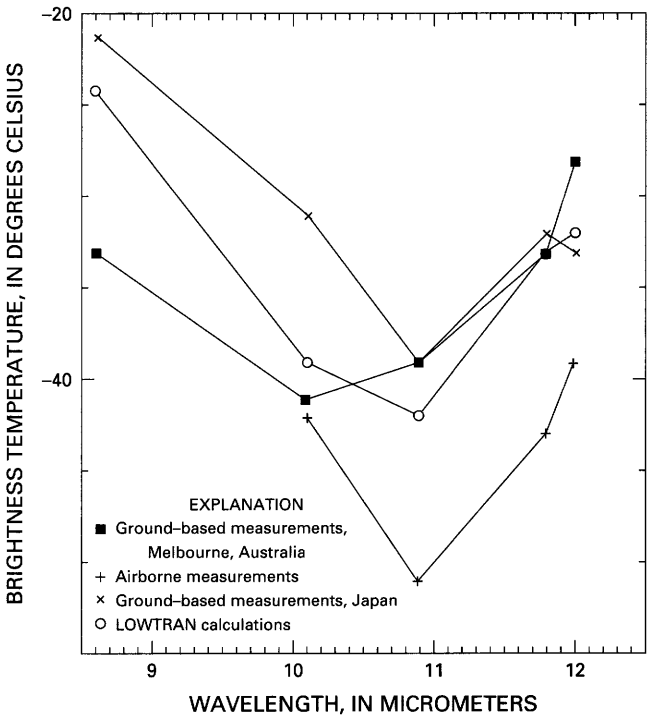


**Figure 3.** Clear-sky measurements using the infrared radiometer. LOWTRAN, a radiance/transmittance code developed by the U.S. Air Force. See Prata and Barton (this volume).

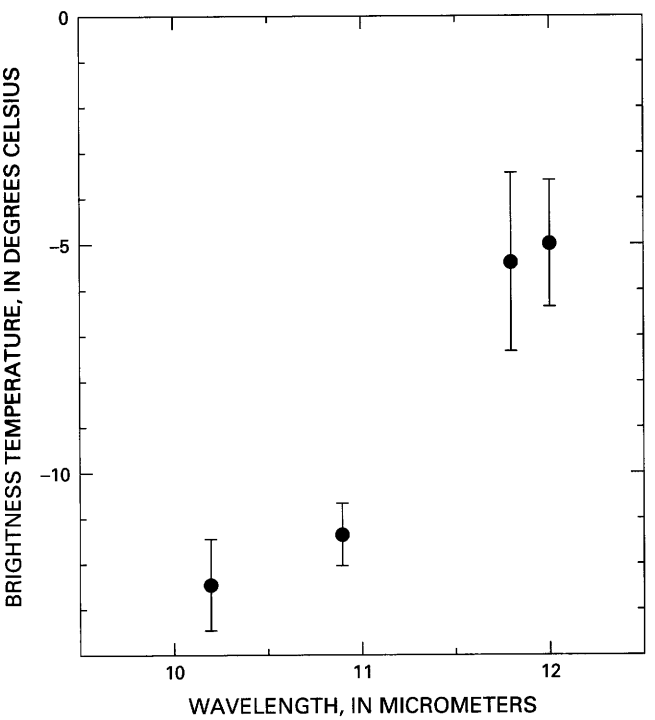


**Figure 4.** Airborne measurements of a cumulus cloud made near Mt. Sakurajima, Japan. Vertical bars indicate measurement uncertainty.

10.1 and 12.0 μm and the wider filters at 10.9 and 11.8 μm. The germanium window was not used in the measurements made in Japan.

The radiometer was operated under computer control with a calibration cycle for all channels used at the start and end of a measurement period. In between calibration cycles, the radiometer cycled between the selected filters. Typically the radiometer viewed at one wavelength for about 10 s before cycling to the next filter.

The results of clear-sky measurements have already been shown in figure 3. Of particular interest is the warmer signal in the 8.6- and 10.1-μm channels, presumably due to increased concentrations of $SO_2$ and $CO_2$ from the volcanic emissions. The other interesting feature is the difference between the 11.8- and 12.0-μm measurements. This is assumed to be due to excess sulfuric-acid particles in the hazy atmosphere near the volcano. Sulfuric acid has a much stronger absorption at 11.8 μm than at 12.0 μm.

On several days, the radiometer was used to view the volcanic ash cloud emanating from Mt. Sakurajima. On most occasions, there were sufficient water clouds in the vicinity to enable measurements of both volcanic ash clouds and water clouds from the same location under the same conditions. The results of measurements taken from the Sakurajima Volcanological Observatory on March 10, 1991, are shown in figures 5 and 6. In figure 5, the brightness temperatures of a cumulus cloud are shown as measured by the radiometer looking at an elevation of 21°. As with the airborne measurements, the temperature at 11.8 μm is warmer than that at 10.9 μm. Figure 6 shows the brightness temperatures in the five channels obtained at an elevation of 13.5° and looking toward the volcanic cloud. In contrast to the cloud observations and the clear-sky measurements, the temperature at 11.8 μm is cooler than that at 10.9 μm. Also, the figure shows that the same characteristic is true for the narrow-band channels: the temperature at 12.0 μm is cooler than that at 10.1 μm (fig. 4). In fact, these measurements show that the narrow-band channels give a better discrimination than the broader channels. However, this improved discrimination was not always observed in the radiometer data, perhaps due to changing concentrations of carbon dioxide and sulfuric-acid particles in the intervening atmosphere. Nevertheless, in all cases when viewing water and volcanic ash clouds, the radiometer was easily able to discriminate between the two cloud types.

## CONCLUSIONS

The multichannel infrared radiometer has been tested on both a high-flying aircraft in Australia and on the ground in the vicinity of a Japanese volcano. The results from these tests support the theoretical calculations of the spectral characteristics of the infrared radiance emitted by clear skies, water/ice clouds, and volcanic ash clouds. Radiometer measurements indicate that water clouds and volcanic ash clouds have markedly different optical properties at wavelengths

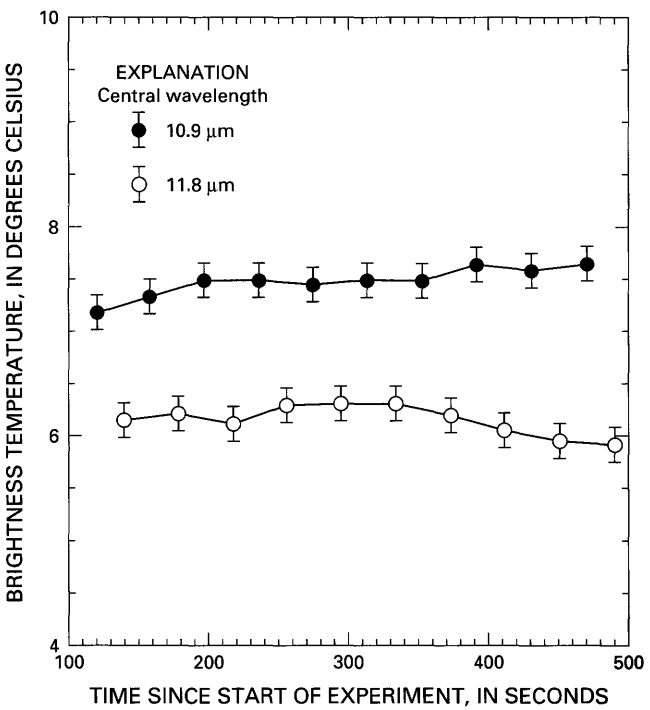


**Figure 5.** Ground-based measurements of a cumulus cloud near Mt. Sakurajima, Japan, March 10, 1991. Radiometer looking at an elevation of 21°. Vertical bars indicate measurement uncertainty.

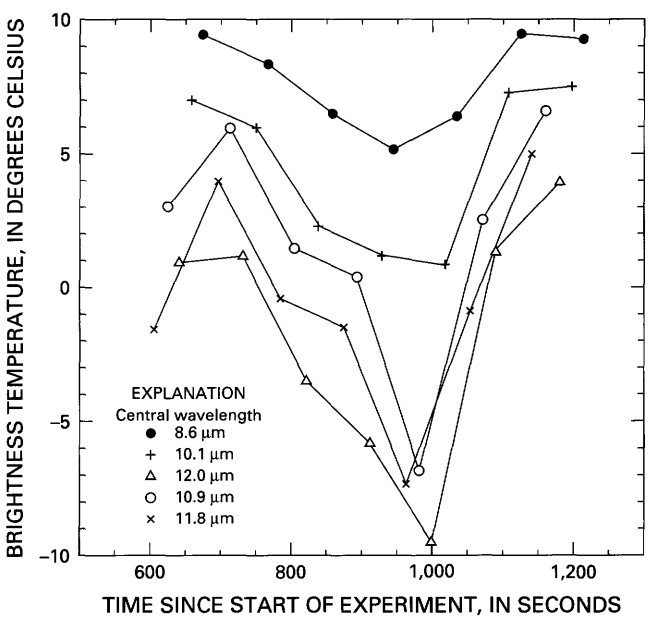


**Figure 6.** Ground-based measurements of volcanic ash cloud emanating from Mt. Sakurajima, Japan, March 10, 1991. Radiometer looking at an elevation of 13.5°.

near 11 and 12 μm. This contrast in the behavior of the two types of clouds clearly identifies a means whereby an airborne instrument can be used to successfully detect hazardous volcanic ash clouds in the flight path of commercial aircraft.

## CONSIDERATIONS FOR AN AIRBORNE DETECTION SYSTEM

The infrared technique for the airborne detection of volcanic ash clouds has several advantages over other systems.

1. An infrared instrument detects the presence of silicate particles, which are the actual constituents of volcanic ash clouds that cause aircraft engines to stall.
2. The instrument relies on passive remote sensing to detect the naturally emitted radiation from the ash cloud and does not rely on the reflection of energy transmitted from the aircraft itself.
3. The instrument would detect volcanic ash clouds well ahead of an aircraft (100–200 km), giving ample time for evasive action.
4. If infrared-detector arrays are used, the instrument could operate without any moving parts. This would be a great boon for reliability and maintenance.
5. The technique is ideally suited for incorporation into a multifunction instrument. Similar technology can be used to detect clear-air turbulence (Kuhn and others, 1977) as well as wind shear in the landing and take-off phases of flight (Sinclair and Kuhn, 1991).

## RECOMMENDATIONS

In view of the results presented in this paper it is recommended that:

1. Research work continues in order to identify the optimum wavelengths and bandwidths for an operational instrument,
2. Further tests are undertaken to investigate a volcanic ash cloud at aircraft-cruise altitudes,
3. Financial and other support be given to the development of a full airborne prototype instrument, and
4. Collaborative programs be developed to work toward a multifunction instrument using infrared radiometry.

## ACKNOWLEDGMENTS

Funding for the radiometer development and the airborne trials in Hobart was provided by the Commonwealth Scientific and Industrial Research Organization (CSIRO), Office of Space Science and Applications. The instrument was built in the CSIRO workshops by Mr. John Bennett and his staff. The field trip to Mt. Sakurajima was sponsored by the Australian Department of Industry, Technology, and Commerce under their bilateral science and technology program with Japan. The field program at Sakurajima would not have been possible without the enthusiastic support of Professor Kosuke Kamo and his staff at Sakurajima Volcanological Observatory. The authors would like to express their deep thanks to these colleagues who have made such a valuable contribution to this program.

## REFERENCES CITED

Kuhn, P., Carcena, F., and Gillespie, C.M., Jr., 1977, Clear air turbulence; detection by infrared observations of water vapor: Science, v. 196, p. 1099–1100.

Prata, A.J., 1989, Observations of volcanic ash clouds in the 10–12 μm window using AVHRR/2 data: International Journal of Remote Sensing, v. 10, p. 751–761.

Sinclair, P.C., and Kuhn, P.M., 1991, Aircraft low altitude wind shear detection and warning system: Journal of Applied Meteorology, v. 30, p. 3–16.

VOLCANIC ASH AND AVIATION SAFETY:
Proceedings of the First International Symposium
on Volcanic Ash and Aviation Safety
U.S. GEOLOGICAL SURVEY BULLETIN 2047

# SATELLITE MONITORING OF VOLCANOES USING ARGOS

*By* J.P. Cauzac, Christian Ortega, *and* Laurel Muehlhausen

## ABSTRACT

The Argos satellite system has been used for environmental data collection for more than 10 years. It was first used on a volcano in 1982, collecting data from field experiments on Mt. Etna. Since then, many more volcanoes have been monitored with portable data loggers transmitting through Argos. These provide year-long observations and give users regularly updated data sets for a better understanding of complex volcanic phenomena.

Argos stations provide permanent monitoring and help to detect increases in activity on remote volcanoes. Specialists can be brought in before the volcano erupts so that airline companies have information more quickly. For civil aviation, the most useful feature of Argos is its worldwide coverage. Orbiting satellites reach the world's most remote areas. Processing centers in Toulouse, France; Landover, Md.; Melbourne, Australia; and Tokyo, Japan, distribute all collected data to users. They also allow several users to share information simultaneously.

In collaboration with scientists from INSU (French Institute for Earth and Planetary Sciences), Collecte Localisation Satellites (CLS) Argos has recently developed two types of stations: one for monitoring seismic tremors and events (SISMO1), and one for monitoring physical-chemical parameters (MONOA). Along with the stations, users are provided with dedicated PC software that can automatically download data from one of the processing centers, put them in a database, and display the results graphically.

## INTRODUCTION

Most volcanologists agree that active volcanoes should be more widely monitored. But the significant eruptions in the 1980's were mostly at volcanoes with few previously observed eruptions. This is why volcanologists are now calling for permanent systems on more volcanoes (Tilling, 1990; Ward, 1990). Continuous monitoring of volcanoes would provide a way of recording early signs of activity and provide information on the physical-chemical processes that trigger and sustain eruptive activity. Monitoring more volcanoes would increase the probability of observing eruptions.

Owing to high investment and maintenance costs, it is not feasible to establish permanent, sophisticated observatories on each active volcano. It is even less feasible in remote, scarcely inhabited areas where the risk for local populations is low. The problem is that events at these unmonitored volcanoes can affect air traffic.

Remotely monitored data-collection platforms are a cost-effective alternative to large observatories. Data are relayed through the satellite to one or more institutes in charge of long-term monitoring and responsible for detecting early signs of increases in volcanic activity. If required, these institutes may decide to do more accurate observations using satellite images or by installing additional instruments. This continuous monitoring would help to protect civilian populations and would provide input data for scientific studies. For airline companies, this may help to save days in the decision process when air routes are to be modified.

Among other telemetered platforms, those reporting via the Argos satellites have many attractive features. They are easy to install and maintain and require little on-site equipment. Because they are reliable and use little power, they can be left unattended for a year or more while transmitting data several times per day. Finally, they benefit from the worldwide dissemination network operated by Argos, which has already been chosen to distribute data collected by thousands of environmental platforms (drifting buoys, fishing vessels, etc.).

This document outlines a global system for volcano observation using satellite transmission by Argos.

## ARGOS EXPERIENCE IN MONITORING VOLCANOES

The first application of Argos on a volcano was in 1982, when scientists from different earth-science agencies cooperated and developed common monitoring tools in the French PIRPSEV program (Interdisciplinary Research Program for the Forecasting of Volcanic Eruptions). Argos platforms are now installed on more than one dozen volcanoes worldwide (fig. 1).

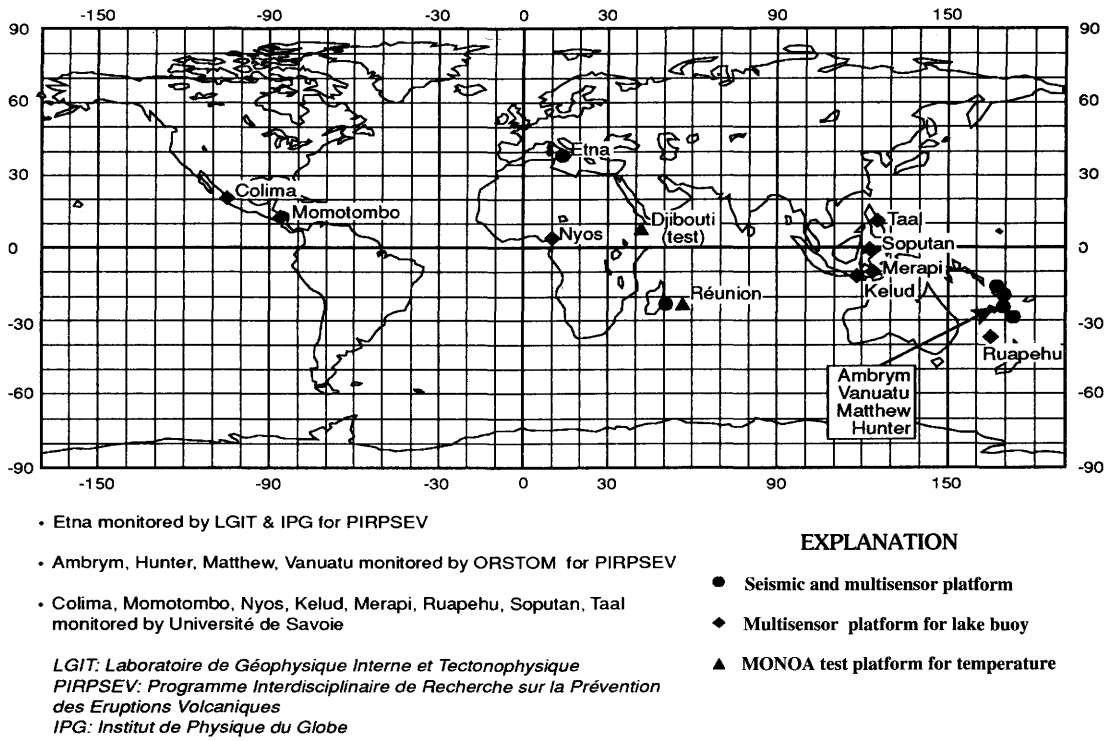


**Figure 1.** Volcanoes monitored using Argos platforms. MONOA, Argos station for monitoring physical-chemical parameters.

A 10-station seismic network was installed on Mt. Etna, Italy, in the early 1980's and operated continuously for several years with practically no maintenance, even though certain stations were at altitudes of over 3,000 m. Seismologists (Glot and others, 1984) developed on-site filtering of data to transmit significant seismic parameters in short Argos messages. The time-tag provided by the Argos satellites synchronized all stations down to 10 ms (milliseconds) and helped to locate seismic epicenters.

Further experiments led by ORSTOM (French Research Institute for Cooperative Development) at volcanic islands in the New Hebrides showed Argos to be a very adequate tool for monitoring remote and uninhabited sites on a long-term basis. Fumarole temperatures, heat-flux measurements, and local seismicity are among 15 parameters that are transmitted nine times per day. The first platforms were installed in 1986, and most are still reporting (Michel Lardy, unpub. data).

The February 1990 eruption of the Kelut Volcano, East Java, Indonesia, showed how permanent monitoring can help to mitigate the effects of an eruption. A single Argos buoy in the middle of the crater lake collected precursory signs months before the eruption. Some slowly varying effects would not have been easily monitored with discrete measurements. The buoy was designed by the University of Chambery, France, as part of a cooperative program with the Volcanological Survey of Indonesia (VSI). Sensors included

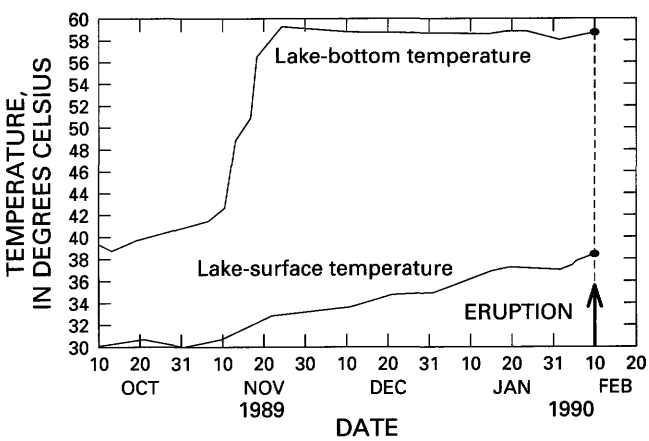


**Figure 2.** Kelut Volcano, Indonesia—Lake temperature before the eruption of February 1990 as transmitted via Argos and monitored by the Volcanological Survey of Indonesia. Temperature measurement ceased at the time of eruption.

thermistor strings and hydrophones to detect the bubbling noise; data were transmitted via Argos. Surface-temperature measurements increased constantly by about 1°C every 10 days from November 10, 1989, to February 10, 1990 (just before the eruption). The lake-bottom measurement showed a sharp increase, from 43°C to 58.5°C, within 10 days in November and remained the same until the first phreatic

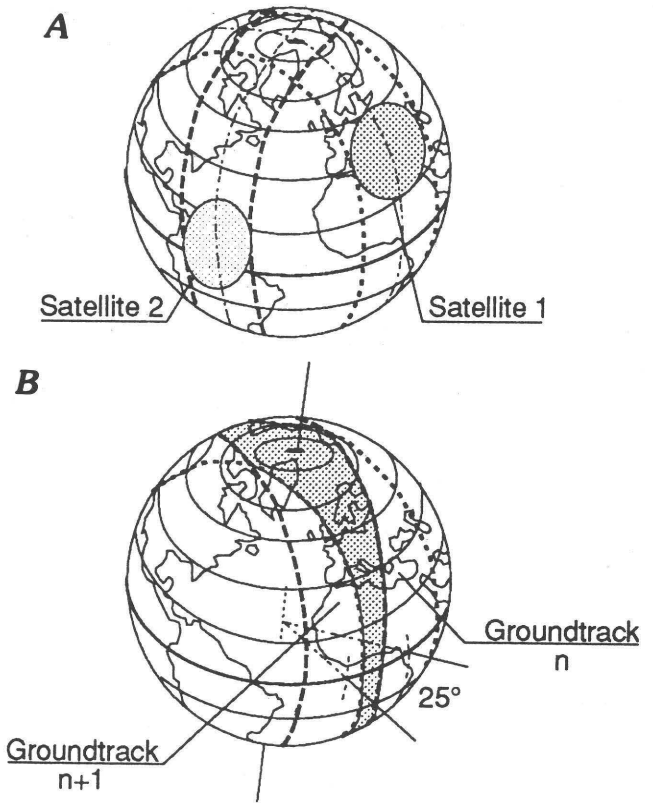


**Figure 3.** Satellite passes and ground coverage. Shaded area in *A* indicates the area of ground coverage. Shaded area in *B* indicates overlap between successive passes.

eruption (fig. 2). The low- and medium-frequency recordings of the hydrophone showed an increase of gas bubbles from January 15 to 20. Because of the ability to detect precursory signs, the alert was issued several months before the eruption, and large-scale engineering works were quickly carried out to prevent a major catastrophe. The combination of intensive volcano monitoring, warning systems, and volcanic-hazard assessment significantly reduced the number of victims (Sudradjat, 1991).

New joint studies with the Volcanological Survey of Indonesia are scheduled early in 1993 to monitor Merapi Volcano, Central Java, Indonesia. This program, funded by the French Délégation aux Risques Majeurs, includes installation of Argos platforms with extensometers (MONOA) and seismic recorders (SISMO1). The development of these platforms was funded by CLS, the operator of the Argos system.

## OVERVIEW OF THE ARGOS SYSTEM

Argos has been operational since 1978 and is the result of a cooperative program by National Aeronautics and Space Administration (NASA), National Oceanic Atmospheric Administration (NOAA), and the Centre National d'Etudes Spatiales (CNES, the French space agency). The Argos system offers two capabilities with worldwide coverage: (1) collecting environmental data from remote platforms, and (2) locating the platforms.

**Table 1.** Variation of Argos satellite "visibility" from the ground as a function of latitude.

[PTT, platform transmitter terminal (latitude shown in degrees); cum. visibility, cumulative visibility over a 24-hour period (in time units of minutes); min. passes, minimum number of passes per 24-hour period; mean passes, mean number of passes per 24-hour period; max. passes, maximum number of passes per 24-hour period. See text for additional explanation]

| PTT latitude | Cum. visibility | Min. passes | Mean passes | Max. passes |
|---|---|---|---|---|
| 0 | 80 | 6 | 7 | 8 |
| ±15 | 88 | 8 | 8 | 9 |
| ±30 | 100 | 8 | 9 | 12 |
| ±45 | 128 | 10 | 11 | 12 |
| ±55 | 170 | 16 | 16 | 18 |
| ±65 | 246 | 21 | 22 | 23 |
| ±75 | 322 | 28 | 28 | 28 |
| ±90 | 384 | 28 | 28 | 28 |

The first satellite was launched in 1978, and new satellites are launched every 1 or 2 years. The space segment is comprised of two NOAA satellites in a low Earth orbit (fig. 3). They receive all transmissions from platforms that are visible from the satellites during the entire orbital revolution. The signals are stored by tape recorders on board the satellites and are downloaded to three ground stations. The onboard equipment also retransmits the data in real time. Presently, two Argos satellites are in operation (NOAA-H and NOAA-D), and two others are backups.

The satellites provide worldwide coverage with polar orbits at 830 km and 870 km altitude. The orbital period is approximately 101 minutes; this gives 14 orbital revolutions per satellite per day.

Each satellite simultaneously sees all platforms within a 5,000-km-diameter circle. As the satellite orbits, the visibility zone sweeps a 5,000-km-wide swath around the Earth that passes over the North and South Poles. As a result of the Earth's rotation, the ground tracks and swath shift 25° west about the polar axis, with sidelap between successive swaths. Because sidelap increases with latitude, the number of daily passes over a given platform depends on latitude, from six messages per day at the equator, to more than twenty at the poles (table 1).

Argos platforms consist of data loggers with a 401.650-MHz platform transmitter terminal (PTT). Each PTT transmits a short message (up to 256 bits) that is repeated regularly (every 200 s, for example). Several messages can thus be received on a single pass, increasing transmission

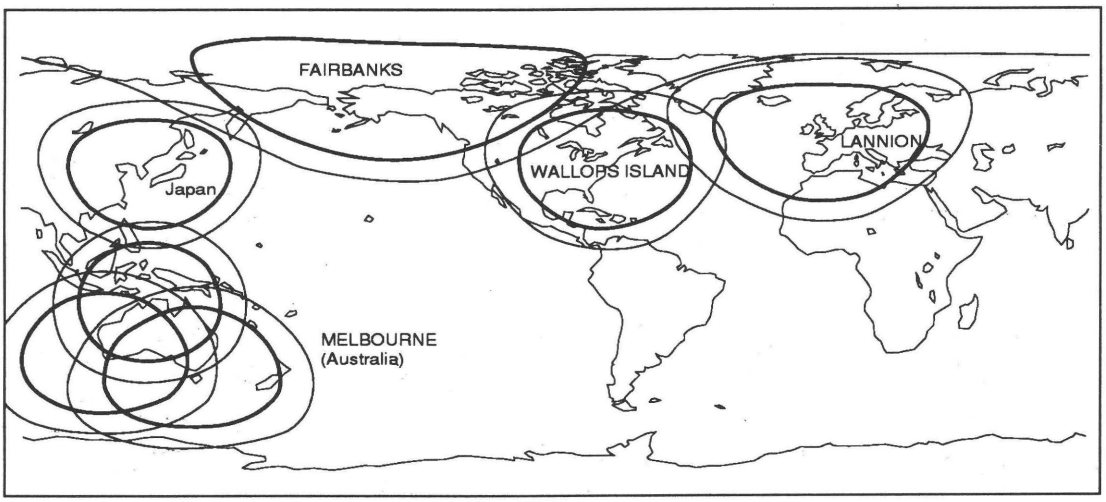


**Figure 4.** Argos worldwide coverage and areas processed in regional mode with shorter throughput times. Thick circles show area where 50 percent of all received messages are also processed in regional mode. Thin circles show area where 30 percent of all received messages are also processed in regional mode.

reliability. For mobile platforms, location can be calculated from the Doppler shift on the signal received by the satellite.

The Argos onboard equipment receives all messages transmitted by platforms within the satellite-visibility area. Messages are received, processed, and retransmitted back to Earth when the satellite is in view of one of the three ground stations (Lannion, France; Wallops Island, Va.; and Fairbanks, Alaska).

Data is processed in two manners: regional and global. Regional processing uses the real-time downlink and occurs when the satellite sees the platform and the receiving station simultaneously. Because the data from these platforms are received in real time, they are available to users more quickly (fig. 4). Global processing occurs for all platforms, even if they have been processed regionally, and uses the recorded data. Global and regional data flows are received by ground stations and are then sent to one of the Argos processing centers: either Toulouse, France, or Landover, Md. The two centers are linked by a dedicated line in order to back each other up and allow dual processing of data. Each center operates around the clock every day of the week and features full internal redundancy. A center has recently been opened in Melbourne, Australia, and provides regional coverage for platforms in that area. A similar center in Tokyo distributes data collected in the global mode.

The centers check and time-tag the messages and sort them by platform. On request, sensor data can be converted into physical values. Users access their results via an online dissemination system, supplying the last 4 days of data plus data for the current day. Data are also archived and can be recovered off line (tapes and floppy disks). Most users connect to the closest distribution center through public networks (Tymnet or Internet in the United States), using desktop computers with modems. They receive new messages upon interrogation or automatically at defined intervals.

Throughput time (the delay from when a message is received by satellite to when it is available to users) improves constantly due to frequent upgrades at the processing centers. In global mode, 60 percent of the messages are available in less than 3 hours. In regional mode, 60 percent of data are available in less than 45 minutes and 95 percent are available in less than 1 hour.

## AN ARGOS VOLCANOLOGICAL SYSTEM

CLS Argos has worked with seismologists and volcanologists to define a basic volcano-monitoring system. The system includes field stations with Argos transmitters and dedicated software to access the data (fig. 5). The main objective is to provide both local teams and cooperating scientists in other countries with continuously updated information on volcanoes where permanent laboratories cannot be installed.

The user has continual access to transmitted data in near real time (results available in less than 1 hour when the platform is served by regional processing mode). Several times per day, the user knows the status of scientific measurements and station-operating status (housekeeping parameters), which allow efficient scheduling of field work. Finally, many scientists worldwide can have access to the data through computer networks.

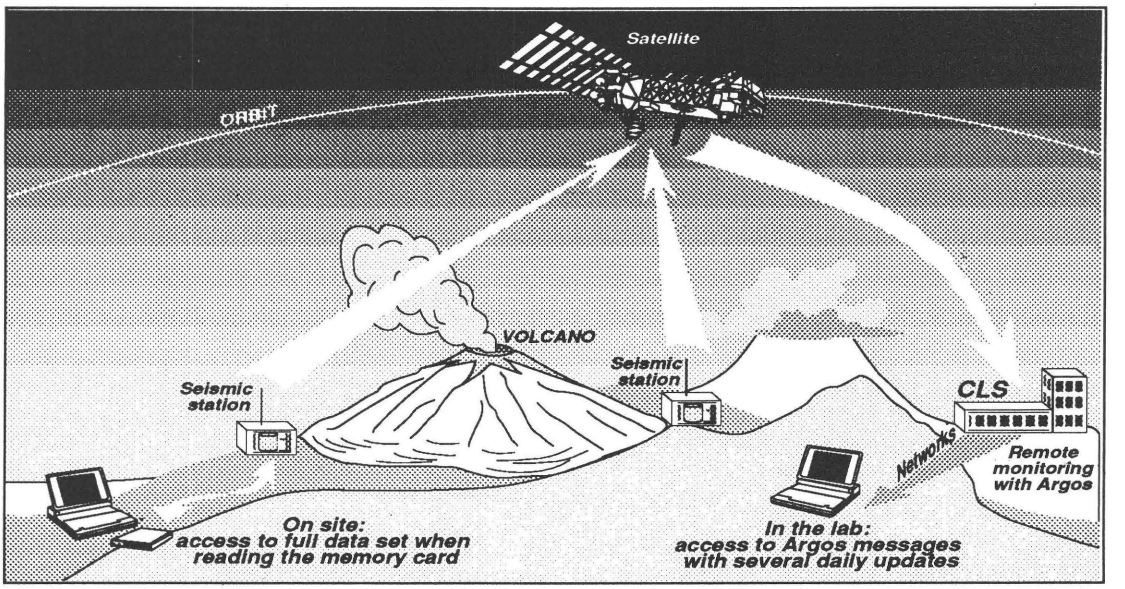


**Figure 5.** The Argos volcanological system provides two ways to access data: (1) locally, with full data set on removable memory card, and (2) by means of the Argos dissemination network.

In addition to remote monitoring via satellite, data can be accessed locally. The stations developed by CLS Argos have programs for configuring instruments and retrieving data. This can be done in the observatory or on site using a portable personal computer (PC)—this insures that local teams are fully involved in processing the data from their volcano. The software downloads all the data from global and regional Argos processing centers and displays graphics and tables on a PC. Data from several stations can be read with a single program.

The current Argos volcano-monitoring stations are SISMO1 and MONOA. The SISMO1 is dedicated to seismology. The MONOA records slowly varying parameters, such as fumarole temperature, extension of faults, etc. Both stations have high memory capacity, low power consumption, and include a miniature Argos transmitter. They are powered by solar panels and batteries.

The PC-based program to retrieve Argos data performs the following functions: interrogation via modem of the Argos processing center, access to the latest data, and storage on the PC hard disk. The program manages a database consisting of months of collected data for each platform; the program is built around the Novell XTrieve structure and is compatible with many scientific programs. Parameters can be displayed as curves or bar graphs; several parameters can be monitored on the same screen when correlation is useful.

The cost of the monitoring system is within reach of volcanological institutes. The basic MONOA station, ready to use with its Argos transmitter, starts at approximately $2,500; the SISMO1 starts at $5,000. With $25,000, one can set up a basic volcano observatory that has several stations and several years of transmission via satellite.

# TECHNICAL DESCRIPTION OF THE FIELD EQUIPMENT: SISMO1 AND MONOA

## TECHNICAL CHARACTERISTICS OF SISMO1

SISMO1 is a portable data logger that digitizes, processes, and stores the ground-velocity signal recorded by geophone. It also transmits significant data via Argos. It is for two types of applications: (1) long-term monitoring with a few stations per volcano, with transmission of mean energy, number of seismic events relative to given thresholds, and duration of tremors relative to given thresholds; (2) short-term, comprehensive, seismic studies, such as installation of large networks of stations for locating and tracking seismic events. The network can easily be synchronized by accurate time-coding done by the Argos satellite.

- The analog-input stage features adjustable gain (from 1 to 2,048) and sampling rates up to 200 Hz. A 12-bit analog-to-digital converter is used.
- The input signal is permanently processed. It triggers acquisition and storage according to one of three modes: (1) automatic seismic-event detection by short-term to long-term average ratio (STA/LTA); (2) time triggered, the signal being stored during up to 30 programmable time slots; (3) wired remote start up.
- Signal processing based on algorithms tested by Institute of Geophysics in Zürich (Baer and Kradolfer, 1987).
- Data are stored on a removable Flash memory card (credit-card size), with 4-megabyte capacity. A

64-megabyte version has been announced by card manufacturers. The Argos message warns when the card memory is 80 percent full. This helps to help to schedule card replacement. SISMO1 controls the card status and protects from overwriting data.

- The internal clock tags arrival of seismic events to 5 ms and can be synchronized with an external radio signal. Also, several stations can be externally synchronized by comparing their time with the accurate Argos satellite clock.
- The Argos message, transmitted at 401.650 MHz, includes a platform identifier plus 256 bits of data. The number of Argos messages received depends on station latitude (minimum of eight messages per day at equator; maximum of 28 at the poles).
- SISMO1 is powered by external 12-V dc supply, with an average current drain of less than 20 mA.

### TECHNICAL CHARACTERISTICS OF MONOA

MONOA is a single-input data logger with an Argos transmitter. Another version accommodates eight sensors. It is compatible with a broad range of sensors with voltage or current outputs (0–1 V, 0–15 V (±1 V), 4–20 mA). MONOA has a proven capability to immediately adapt to users' dedicated sensors, such as tiltmeters or extensometers.

- Data-acquisition rates are programmable for 5, 10, 15, 20, 30, or 60 seconds or minutes. Averaging periods are also user defined. A 10-bit analog-to-digital converter is used.
- Data is stored on a 128-Kbyte memory board. (One megabyte with 8-sensor version.)
- MONOA is powered by external 12-V dc supply, with an average current drain of less than 3 mA.
- The Argos message includes the last 12 measurements, time and date, and memory occupancy for the single-sensor version.

## A POTENTIAL APPLICATION: MONITORING VOLCANOES IN THE ALEUTIANS

Akutan Volcano is one of approximately 40 historically active volcanoes in the Aleutian Islands that lie close to busy northern Pacific air routes. Its most recent eruptions, in 1992, confirmed that volcano ash plumes may disrupt and endanger air traffic. However, at present, no Aleutian volcanoes are under surveillance by the Alaska Volcano Observatory.

Akutan is not yet fitted with Argos transmitters. However, the geographical position of volcanoes in the Aleutian Islands is favorable for the Argos system. At these high latitudes, there are an average of twenty Argos satellite passes every day, thereby providing frequently updated data. In addition, the proximity of these platforms to the ground station in Fairbanks means that data from these platforms would be processed in regional mode, and results would be available to users within 30 minutes to 1 hour of being generated. Collected data would be readily available, whatever the weather conditions.

## CONCLUSIONS

Many systems can now monitor volcanic activity remotely. Of these, Argos satellite-based data collection has unique strengths, including worldwide coverage and a proven dissemination network. Recently, CLS, the Argos system operator, has contributed to developing an end-to-end system that includes volcanological platforms and processing software. Volcanologists can now install platforms for years to sense, store, and transmit significant parameters. The data are available to: (1) cooperating organizations around the world via the Argos data network, and (2) to local volcanologists, straight from the data logger.

Argos data transmission is not hampered or degraded by cloud cover or darkness, as in some remote-sensing techniques. Argos provides advance information on volcanic-activity patterns and may be used to schedule further observation using remote sensing. Compared to permanently manned observatories, Argos volcano-monitoring stations and satellite telemetry are cost effective, and a budget of $25,000 would allow the monitoring of uninstrumented volcanoes.

The benefits of volcano monitoring for aviation are:

- Once long-term global databases are established, volcanoes will be better characterized and understood. Scientists may then be able to access the risk of eruptions from historical trends and current conditions.
- Argos can provide remote notification of increased volcanic activity, as it did on Kelut, Indonesia, in February 1990.
- Argos data can be accessed, via the operational Argos distribution network, anywhere in the world.

## REFERENCES CITED

Baer, M., and Kradolfer, U., 1987, An automatic phase picker for local and teleseismic events: Bulletin of the Seismological Society of America, v. 77, p. 1437–1445.

Glot, J.P., Gresta, S., Patane, G., and Poupinet, G., 1984, Earthquake activity during the 1983 Etna eruption: Bulletin of Volcanology, v. 47, p. 953–963.

Sudradjat, A., 1991, A preliminary account of the 1990 eruption of the Kelut Volcano: Geologische Jahrbuch, v. A127, p. 447–462.

Tilling, R.I., 1990, Coping with volcanic hazards: A global perspective: Earthquakes & Volcanoes, v. 22, p. 154–160.

Ward, P.L., 1990, Global data collection and the surveillance of active volcanoes: Palaeogeography, Palaeoclimatology, and Palaeoecology (Global and Planetary Change Section), v. 89, p. 263–267.

VOLCANIC ASH AND AVIATION SAFETY:
Proceedings of the First International Symposium
on Volcanic Ash and Aviation Safety
U.S. GEOLOGICAL SURVEY BULLETIN 2047

# CURRENT AND FUTURE CAPABILITIES IN FORECASTING THE TRAJECTORIES, TRANSPORT, AND DISPERSION OF VOLCANIC ASH CLOUDS AT THE CANADIAN METEOROLOGICAL CENTRE

*By* Real D'Amours

## ABSTRACT

The Canadian Meteorological Centre (CMC) Dorval, Quebec, is the main Canadian center for processing weather information. Because of its computer and communication facilities and because of its numerical weather-analysis and prediction models, CMC is the Canadian agency that can most rapidly respond to information requests about the large-scale evolution of pollution clouds. For that purpose, a 3-D trajectory model and a 3-D transport/diffusion model are in operation. These models are also used to estimate the motion of volcanic ash clouds. This paper briefly describes the CMC and the numerical models available for atmospheric transport. Application to volcanic ash clouds is illustrated by the simulation of a hypothetical eruption at Mt. Meager in British Columbia. Forthcoming improvements and direction of future developments for the models are presented.

## INTRODUCTION

The Canadian Meteorological Centre, in Dorval, Quebec, is part of Environment Canada and is the main Canadian center for processing weather information. It supports the nine regional weather centers of Atmospheric Environment Service (AES), plus the National Defense Weather Centres. CMC operates the AES supercomputer, a NEC SX-3/44, plus a variety of other mainframe computers, and the AES communication systems. CMC runs numerical weather-analysis and prediction models for AES. Weather observations from the world are continuously arriving at CMC through the global telecommunication system (GTS) as well as through the AES telecommunication network.

Weather analysis is performed automatically for the global atmosphere through a data-assimilation system. Analyses are done for four main synoptic times: 00:00 UTC, 06:00 UTC, 12:00 UTC, and 18:00 UTC. The data-assimilation system consists of an objective-analysis (OA) procedure based on a multivariate optimum interpolation method and on global and regional spectral numerical weather-prediction models. The prediction models produce 6-hour forecasts, which serve as initial guesses; those guess fields are then corrected with observational data by the OA. Analyses are done for temperature, geopotential height, wind, and humidity at 15 vertical levels, extending from the Earth's surface to about 100,000 ft. The analyzed fields are used as initial conditions for various forecast models.

Two numerical weather-prediction (NWP) models are currently in operation at CMC: a regional finite-element model and a global spectral model. The regional finite-element (RFE) model is a hemispheric model with variable resolution; the high-resolution (100 km) area covers North America. The model is executed twice a day, at 00:00 UTC and 12:00 UTC, and produces forecasts for up to 48 hours into the future. The global spectral model is also executed twice a day: into the future up to day 6 at 00:00 UTC and up to day 3 at 12:00 UTC. The accuracy of the forecasts produced by these models is comparable to forecasts produced by other national meteorological centers (table 1).

At all times, CMC has an accurate knowledge of the actual state of the synoptic-scale flow of the atmosphere and of its most probable evolution for the next few days. CMC is therefore the Canadian agency that can most rapidly respond to information requests about the large-scale evolution of pollution clouds during environmental emergencies. For that reason, a 3-D trajectory model and a 3-D transport/diffusion/deposition model have been implemented in CMC's operations. The primary purpose for implementing these models was to increase preparedness for nuclear emergencies. The models are also used to estimate the motion of volcanic ash plumes.

## THE TRAJECTORY MODEL

CMC's trajectory model is a simple 3-D Lagrangian model. Given a 3-D wind field, the model will calculate the motion of a neutrally buoyant air parcel, starting from a

**Table 1.** RMS (root-mean-square) error of wind vector, 24-hour forecast for North America, January 1, 1992, to April 30, 1992.

[Verifications were done by the issuing Canadian Meteorological Centre, Dorval, Quebec, following the World Meteorological Organization (WMO) recommendations for a standard set of radiosonde stations. UKMO, United Kingdom Meteorological Office]

| Models | 500 hPa (≅18,000 ft) | 200 hPa (≅35,000 ft) |
|---|---|---|
| Canadian global spectral model | 11.7 knots | 17.1 knots |
| U.S. global model (aviation run) | 11.5 knots | 16.8 knots |
| UKMO global model | 12.6 knots | 18.7 knots |

specified point of origin. The model considers no other process than advection by the wind. CMC's trajectory model operates on a polar stereographic grid in the horizontal plane, and in pressure coordinates in the vertical plane. It was designed mostly for use over North America (fig. 1).

The model can be executed in forecast or hindcast mode. It uses interpolated wind fields and vertical motions produced by the global data-assimilation and forecast systems. Trajectories are calculated for three air parcels originating from a single location but from three different vertical levels, all user specified.

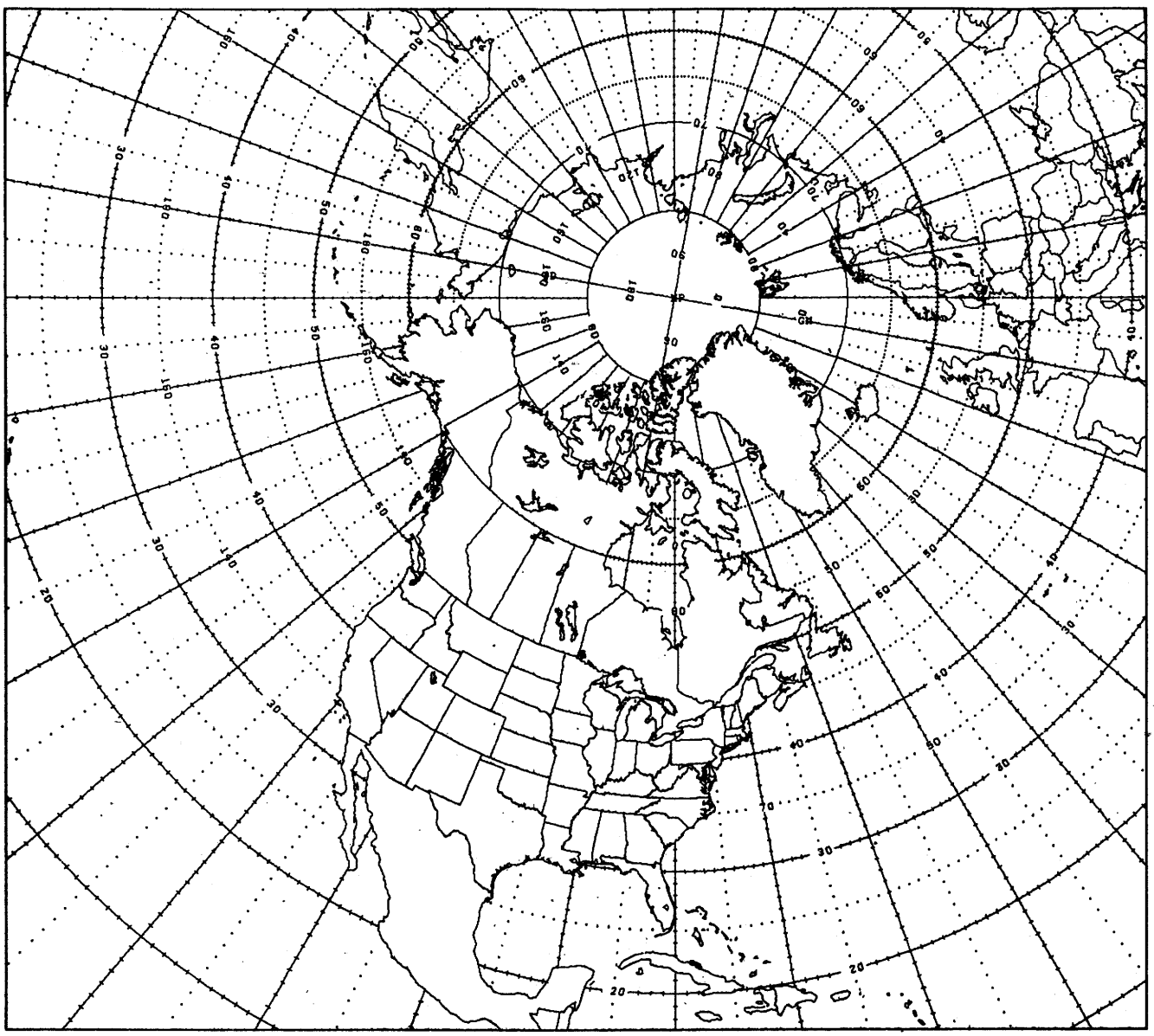

**Figure 1.** Window for the trajectory model. Trajectories for parcels exiting the window will terminate at the point of exit. CMC's trajectory model operates on a polar stereographic grid in the horizontal plane and on pressure coordinates in the vertical plane. It was designed for use over North America.

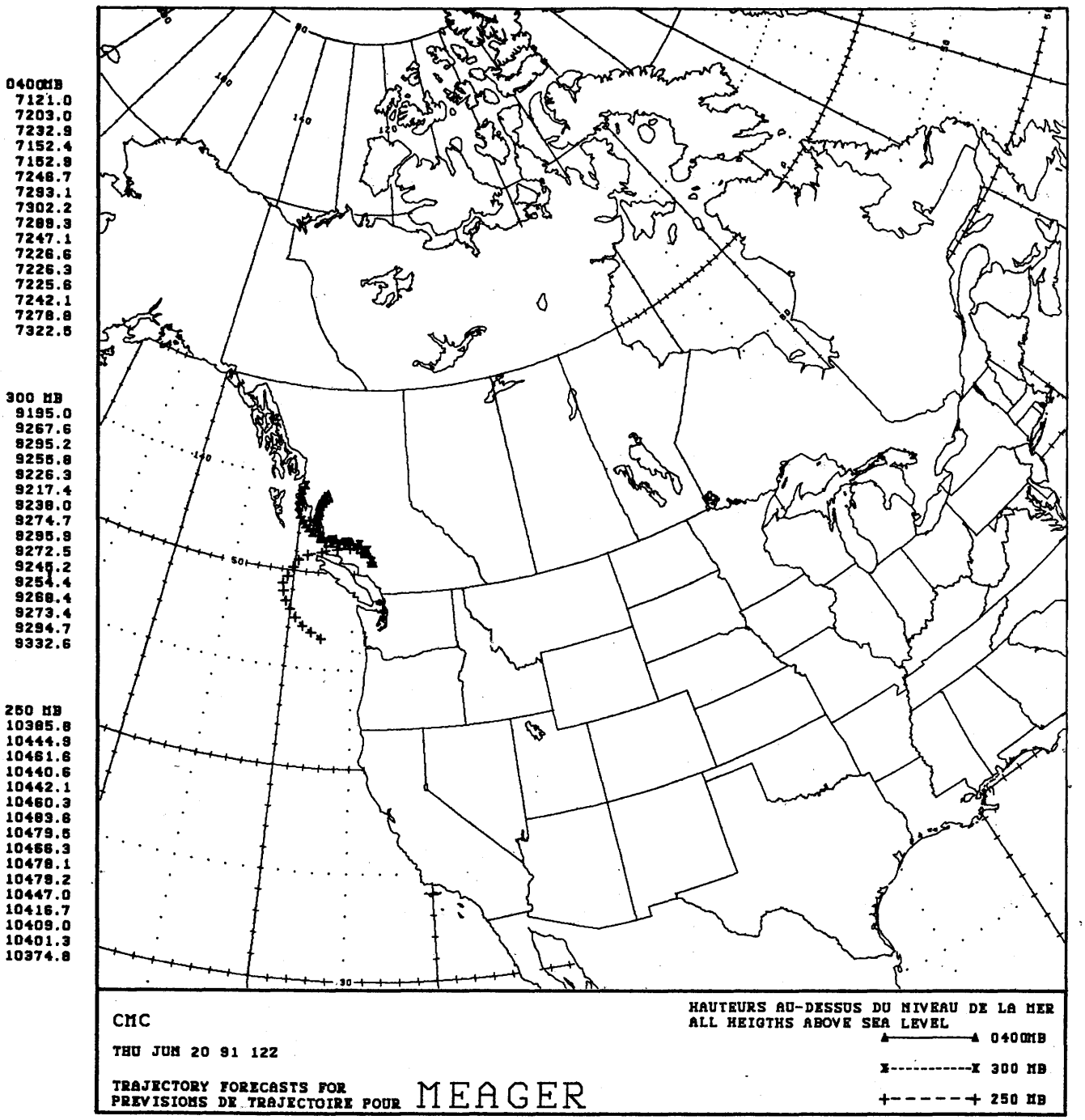


**Figure 2.** Sample output of trajectory model as it is made available to the user. Positions are plotted at 3-hour intervals. Heights along the trajectories are given on the left side of the map, in meters above mean sea level. The map is centered on the origin of the parcels for the north-south direction, but it is somewhat displaced to the west. As in most circumstances, parcels move rapidly eastward. Solid triangles, trajectory at 400 hPa; X's, trajectories at 300 hPa; crosses, trajectories at 250 hPa.

Results from the trajectory model can be made available to the users within 10 minutes of request. The results may be transmitted in chart form through the AES meteorological satellite information system (METSIS) or via telecopier. Positions calculated at 3-hour or 6-hour increments (latitude, longitude, and height) along the trajectories are also available in the form of alphanumeric messages on AES telecommunications networks.

The trajectory model can be useful for emissions of short duration. However, it does not provide any information on plume dimensions or size, on air concentrations, or on surface deposition.

## THE CANADIAN EMERGENCY RESPONSE MODEL (CANERM)

The Canadian emergency-response model (CANERM) was developed by J. Pudykiewicz of Environment Canada following the Chernobyl nuclear accident (Pudykiewicz, 1989). CANERM is a 3-D advection/diffusion model that simulates the effects of wet and dry scavenging, estimates wet and dry deposition, and models the mixing effects within the planetary boundary layer. Although the model was designed to assess the motion of radioactive clouds resulting from large nuclear accidents, it can be used to model volcanic ash clouds.

In the current operational setup, CANERM can execute on either the Northern or Southern Hemisphere. Three configurations are available: (1) a hemispheric domain at a horizontal resolution of 150 km, (2) a continental domain with a resolution of 50 km, and (3) a regional domain at a 25-km resolution. The continental domain covers a square area roughly $1.0\times10^8$ km$^2$ that is centered on the source of emission. The regional domain is also centered on the source and covers about $3.0\times10^7$ km$^2$. The vertical coordinate is the terrain-following $\sigma$-coordinate ($\sigma$ is the ratio of the atmospheric pressure at a given vertical level to the surface pressure at that location). The model has 11 vertical levels up to about 50,000 ft above sea level ($\sigma = 0.1$; this is approximately equal to 100 hPa). Winds, temperature, moisture, and geopotential must be provided to the model. These may come from an historical sequence of objective analyses (hindcast mode) or from the output of the global spectral model (forecast mode). The hindcast mode is used to obtain the best estimate of the actual state of the plume, and the forecast mode is used to obtain the expected state. The two modes can be used in sequence for events of extended duration.

The release to the model atmosphere near the source is modeled by a Gaussian function. The standard deviation is one grid length in the horizontal plane, and 0.1 $\sigma$ in the vertical plane. The height, intensity, and duration of the release are specified by the user. To simulate volcanic ash, an inert, neutrally buoyant gas tracer, not subject to washout, is used. CANERM produces estimates of the 3-D shape of the ash plume as it evolves in the atmospheric flow. Results can be made available to users in chart form via telecopier about 30 minutes after request.

## AN EXAMPLE: HYPOTHETICAL ERUPTION AT MT. MEAGER, BRITISH COLUMBIA

Mt. Meager volcano is part of the Garibaldi volcanic belt in British Columbia, where a volcanic eruption of consequence is possible (Hickson, this volume). A simulation was done for a hypothetical eruption at 12:00 UTC, June 20, 1991. Sample outputs of the trajectory and CANERM models are illustrated in figures 2 and 3 as they would be made available to users. An experimental run of CANERM was also done, at a resolution of 10 km, using interpolated fields produced by CMC's operational RFE model.

The meteorological situation for the simulation was characterized by a weak wind circulation over western North America at all levels. This is apparent in the unusual behavior of the trajectories (fig. 2), which indicate a northwestward motion immediately following the hypothetical eruption. The trajectories at 400 hPa and 300 hPa recurve northeastward after about 18 hours; the 250 hPa trajectory trends southeast after the same elapsed time. Figure 3 shows the ash plume produced by the CANERM run at 50-km resolution, after 48 hours, at 250 hPa. The modeled plume reaches far inland over Oregon and Idaho, but the end point of the trajectory at 250 hPa, which should indicate the position of an air parcel originating from above the volcano 48 hours later, is still over the ocean. The plume has also spread over northern British Columbia; this is not indicated from the trajectory at 250 hPa, but is hinted at by the trajectories at 300 and 400 hPa. The extent of the plume produced by CANERM is greater than what could be inferred from the trajectories. This can be explained by the fact that (1) the trajectory model has no diffusion in its formulation, and it tracks an air parcel that has, in fact, no dimensions, whereas CANERM has a well-developed ash column to begin with because of the Gaussian source model, and (2) the plume continues to spread throughout the simulation because of diffusion.

A test run of CANERM at a resolution of 10 km, based on interpolated wind fields produced by the RFE model was also performed for Mt. Meager for the same time. At that resolution, about 96 percent of the plume at 400 hPa is within a radius of 20 km at the first interval of 3 hours; this is comparable to the size of the umbrella cloud generated shortly after an eruption (Woods and Kienle, this volume). The winds provided to CANERM do not permit resolution of features

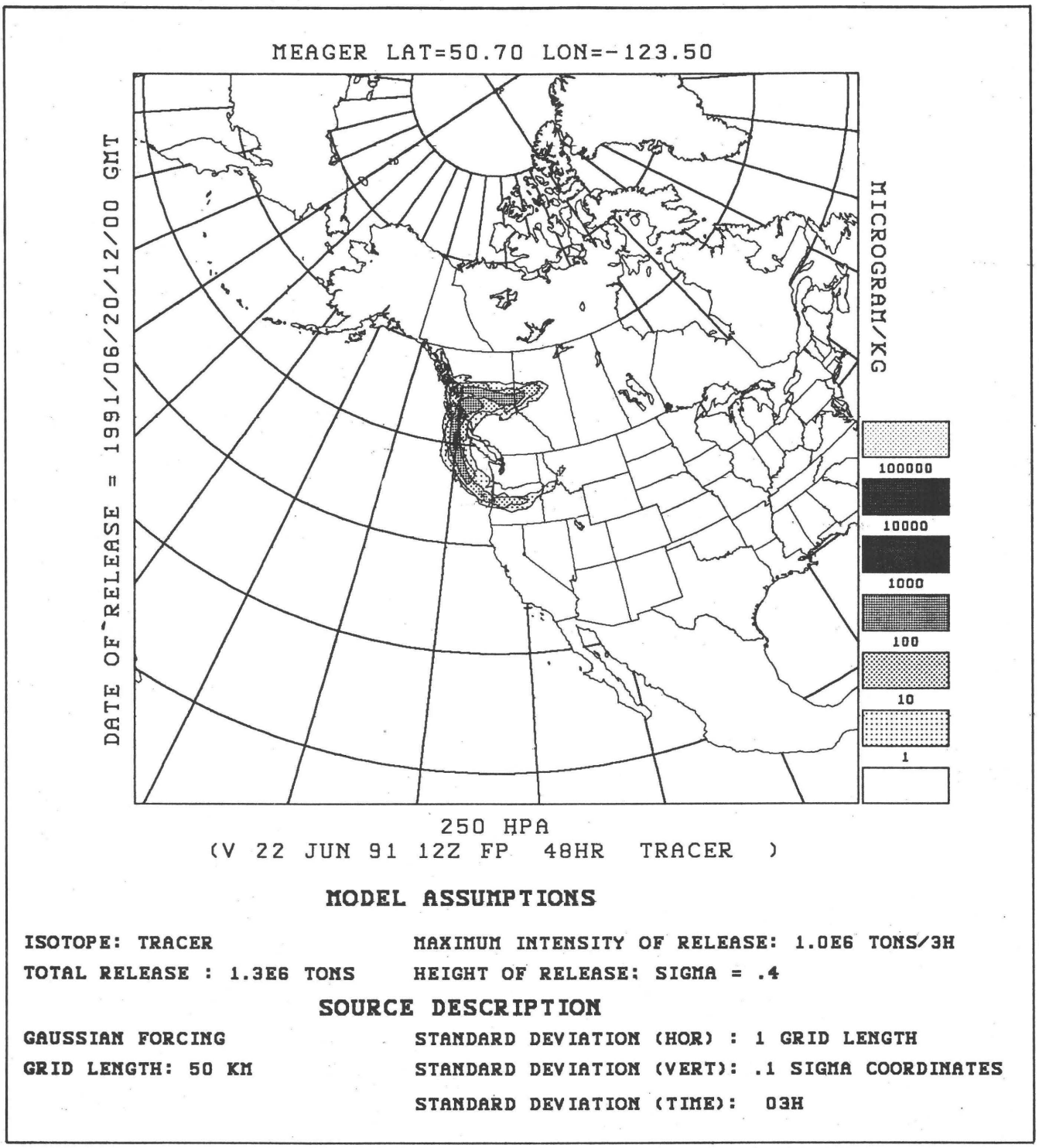


**Figure 3.** Sample output of CANERM as it would be transmitted to the user. This is a 48-hour forecast of the instantaneous plume, at 250 hPa (≅ 35,000 ft) from an execution with a resolution of 50 km. Ash concentration units are in μg/kg of air (ppbm—parts per billion by mass), given an emission of 1.3 megatons. In this simulation an inert gas tracer is used. Deposition and washout are not simulated. Release height is at 25,000 ft, and release duration is about 6 hours.

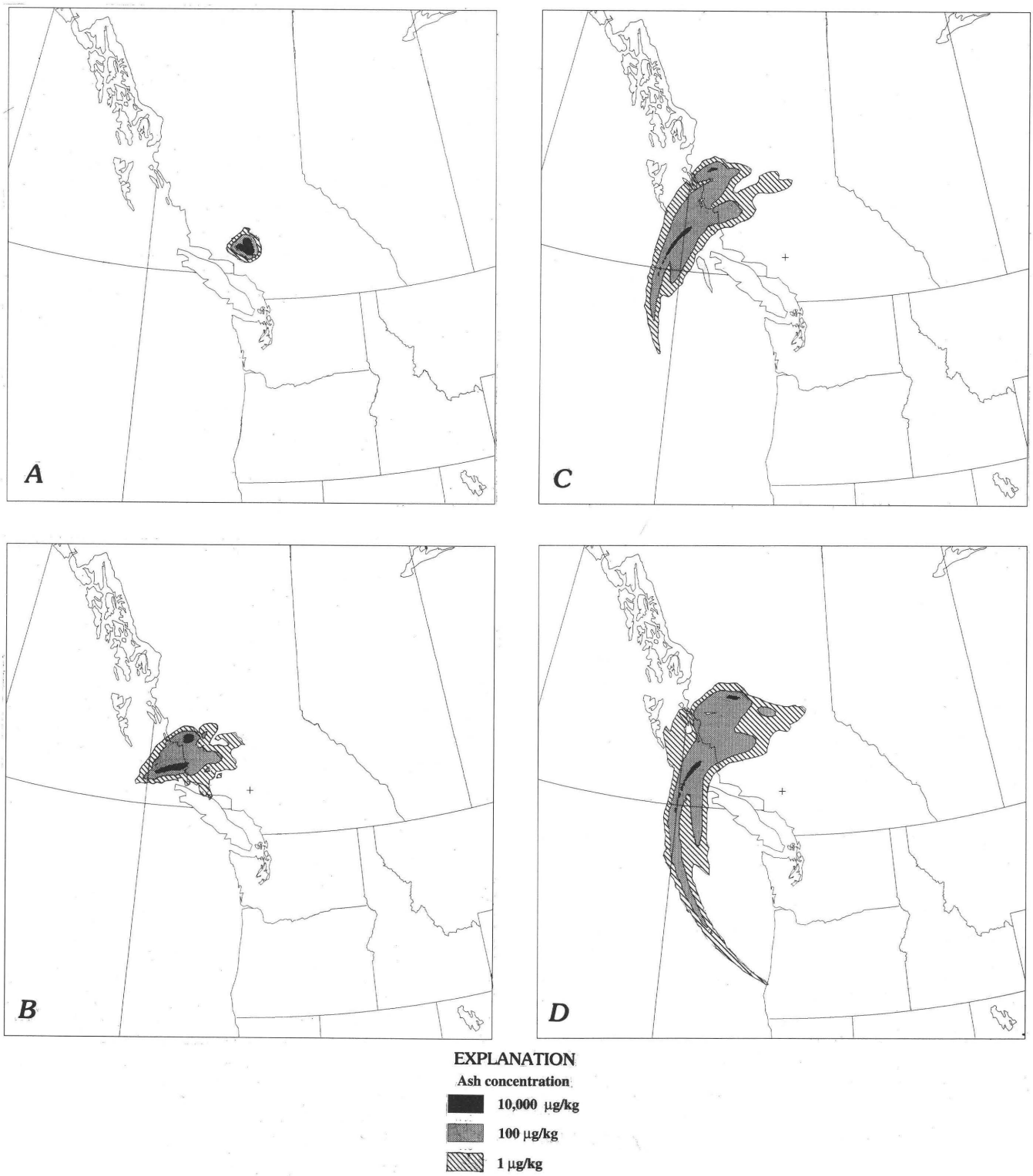


**Figure 4.** Forecasts of the instantaneous plume at 250 hPa (≅ 35,000 ft) from a test CANERM run at 10-km resolution using interpolated winds produced by the regional finite-element model for hypothetical eruption of Mt. Meager at 12:00 UTC, June 20, 1991. The geographical area shown on the map constitutes the total domain of the model for this run. Ash concentration units are µg/kg of air (ppbm), given an emission of 1.3 megatons. In this simulation, an inert gas tracer is used. Deposition and washout are not simulated. Release height is at 25,000 ft, and release duration is about 6 hours. Cross symbol, which is barely visible in *A*, indicates approximate location of Mt. Meager. *A*, 3-hour forecast; *B*, 18-hour forecast; *C*, 36-hour forecast; *D*, 48-hour forecast.

of less than 100 km in size. It can be argued, however, that, at upper levels (which are of interest for aviation), the flow is relatively smooth and most of the variability is in the synoptic scales, which are adequately resolved by the RFE. The evolution of the plume at 250 hPa is depicted in figure 4. At 3 hours (fig. 4*A*), a tendency for the plume to bifurcate is evident. At 18 hours (fig. 4*B*), the cloud has spread considerably and the maximum concentrations are well detached from the source. At 36 hours (fig. 4*C*), extensive stretching has occurred and a branch is moving rapidly southward. From 36 to 48 hours (fig. 4*D*), it can be seen that the whole cloud over the Pacific has started to translate eastward as the atmospheric flow aloft begins to reorganize. The final shape of the cloud at 250 hPa could not have been easily deduced from the trajectories alone.

## FUTURE CAPABILITIES

The NEC SX-3/44 supercomputer was installed at CMC in early October 1991, and the conversion of CMC's operational system was completed on December 15, 1992, resulting in a reduction of the response time by a factor of two for CANERM. A global mode for the trajectory model and CANERM will be implemented in early 1994.

Development work to account for particle-size distribution and settling velocities is in progress. CANERM's capacity to provide estimates of ash surface deposition will be activated in mid-1994. Improved wet scavenging will also be possible using available precipitation fluxes from NWP models.

Over the next few years, estimates of air concentrations and of surface deposition very near the source will improve with the introduction of more sophisticated sub-models to better estimate initial plume rise, vertical distribution of ejected materials, and other sub-grid-scale effects. Eventually a dedicated, high-resolution, non-hydrostatic meteorological model will be included to resolve the detailed structure of atmospheric motions in the vicinity of the source.

## REFERENCE CITED

Pudykiewicz, J., 1989, Simulation of the Chernobyl dispersion with a 3-D hemispheric tracer model: Tellus, v. 41B, p. 391–412.

VOLCANIC ASH AND AVIATION SAFETY:
Proceedings of the First International Symposium
on Volcanic Ash and Aviation Safety
U.S. GEOLOGICAL SURVEY BULLETIN 2047

# AN AIRCRAFT ENCOUNTER WITH A REDOUBT ASH CLOUD (A SATELLITE VIEW)

*By* Kenneson G. Dean, Lawrence Whiting, *and* Haitao Jiao

## ABSTRACT

Satellite images, wind measurements, and ground observations were used to track and map gas clouds and ash clouds emitted by Redoubt Volcano, Alaska, on 15 December 1989. This eruption resulted in a nearly catastrophic encounter between airborne ash and a Boeing 747 jet aircraft (most of southern Alaska was completely covered by clouds on that day). Four satellite images were analyzed using complex digital-processing techniques to locate geographic features and to distinguish eruption-related gas clouds from meteorological clouds. The technique of subtracting thermal infrared bands to detect ash clouds was applied to three images but was only successful on the 13:42 Alaska Standard Time (AST) image. The 13:42 image revealed the presence of two ash clouds near Fairbanks and Delta Junction that may have been involved in the encounter with the 747 aircraft earlier that morning. Ground samples from the two ash clouds help quantify the characteristics of ash clouds detected by satellite sensors. The eruption at 10:15 AST appears to be the origin of the ash involved in the aircraft encounter.

## INTRODUCTION

On 14 December 1989, Redoubt Volcano, located 177 km southwest of Anchorage, Alaska (fig. 1), erupted and expelled a huge eruption cloud composed of ash and gas to altitudes greater than 10 km (Brantley, 1990). For the next 4 months, 24 additional eruptions resulted in the deposition of ash throughout southern Alaska (Scott and McGimsey, 1991). Clouds of ash and gas from Redoubt Volcano drifted hundreds of kilometers to locations beyond Fairbanks, Delta Junction, and Glennallen.

The danger to airline traffic posed by airborne ash was exemplified on 15 December at 11:45 Alaska Standard Time, when a Boeing 747 jet flew into an ash cloud at an altitude of 7,600 m (25,000 ft) northeast of Talkeetna, Alaska. All four engines shutdown within minutes after the aircraft entered the cloud but were restarted about 8 minutes later, narrowly averting a catastrophe (Brantley, 1990; Casadevall, in press). The ability to detect, monitor, and predict the movement of volcanic plumes and ash clouds would help to minimize the possibility of aircraft encounters with ash. Satellite images are one potential source of this information. The 15 December 1989 chronology of events and National Oceanographic and Atmospheric Administration (NOAA) advanced very high resolution radiometer (AVHRR) satellite images used in our analysis are given in table 1.

NOAA AVHRR satellite images have been used to monitor and analyze eruption clouds from Redoubt (Dean and others, 1990; Kienle and others, 1990); from Augustine (Holasek and Rose, 1991); from Colo, Indonesia (Maligreau and Kaswanda, 1986); from Mt. Galunggung, Indonesia (Hanstrum and Watson, 1983); from El Chichón, Mexico (Matson, 1984); and from Mount St. Helens (Matson and Staggs, 1981). Techniques have been developed to distinguish ash clouds from meteorological clouds and other airborne volcanic constituents (Prata, 1989; Holasek and Rose, 1991). Images from the Earth observing system (EOS) spacecraft will become an additional source of data for analyzing volcanoes in the near future (Mouginis-Mark and others, 1991).

Images from the AVHRR sensor aboard the polar-orbiting NOAA-10 and NOAA-11 (N-10, N-11) satellites are recorded for the Cook Inlet region more than 10 times per 24-hour period. This high temporal resolution is unique to high latitudes due to extensive overlap on each image swath from adjacent orbits. The data have a spatial resolution of 1 km and a swath width greater than 2,000 km. The images are recorded in five wavelengths: visible band 1 (0.58–0.68 μm), near-infrared band 2 (0.72–1.1 μm), thermal-infrared band 3 (3.55–3.93 μm), thermal-infrared band 4 (10.3–11.3 μm), and thermal-infrared band 5 (11.5–12.5 μm). However, on even-numbered NOAA satellites up to but not including N-12, band 5 is a duplicate of band 4. The five-band coverage can detect both volcanic and non-volcanic cloud formations during both day and night.

In this paper, clouds composed of gas and ash emitted by a volcano are referred to as eruption clouds. Eruption clouds may have a conical shape with an apex ending at the

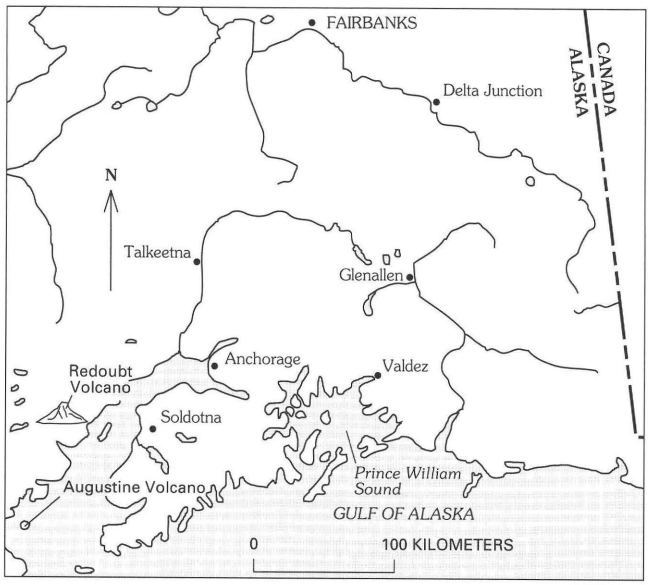


**Figure 1.** Location map of south-central Alaska.

volcano indicating that it is still being emitted, or the apex may be adrift and not connected to the volcano. An ash cloud is that portion of an eruption cloud containing volcanic ash that damages aircraft and other mechanical devices. Both ash and gas components of eruption clouds can be detected on satellite images, but they may not always be distinguishable from each other.

## OBJECTIVES

The objective of this analysis is to use satellite images to identify and monitor eruption clouds, including the ash clouds responsible for the near-downing of an aircraft on 15 December 1989. AVHRR images are used to distinguish eruption clouds from surrounding meteorological clouds, to map the trajectory and distribution of eruption clouds, and to detect and track the movement of the ash cloud that the aircraft encountered.

## METHODS

### SATELLITE ANALYSIS

Three eruptions occurred on the morning of 15 December: at 01:40, 03:48, and 10:15 AST. Four satellite images were recorded at 03:28, 05:09, 09:28, and 13:27 AST (table 1) and show that most of southern Alaska was completely covered by clouds. To relate cloud structures to ground locations, the images were registered to an Albers equal-area map projection, and geographic features were digitally superimposed. The values of individual pixels were

**Table 1.** Chronology of Events on 15 December 1989.

[AST, Alaska Standard Time]

| Time (AST) | Event |
|---|---|
| 01:40 | Eruption, 12 minutes duration |
| 03:28 | Image: NOAA-11; orbit no. 6305 |
| 03:48 | Eruption, 10 minutes duration |
| 05:09 | Image: NOAA-11; orbit no. 6306 |
| 09:28 | Image: NOAA-10; orbit no. 16851 |
| 10:15 | Eruption, 40 minutes duration |
| 11:45 | Aircraft–ash cloud encounter |
| 13:27 | Image: NOAA-11; orbit no. 6311 |

transformed to temperature and albedo using coefficients provided with the data as described in the NOAA polar orbiter data users guide (Kidwell, 1991). Contrast was enhanced to optimize the detection of eruption-related gas clouds and ash clouds. Individual bands of satellite data were combined to distinguish gas clouds, ash clouds, and other plume constituents from meteorological clouds using established experimental techniques. These included:

- Subtraction between bands 5 and 4 to distinguish ash clouds from meteorological clouds,
- Subtraction between bands 2 and 1 to help distinguish the water-vapor portion of eruption clouds from other plume constituents, and
- Principal-component analysis to distinguish eruption clouds from meteorological clouds.

Color composite images were generated using various combinations of raw images, band subtractions, and principal component images.

Images that result from the subtraction of two bands of data may detect distinct properties of eruption clouds. The image that results from subtracting the two thermal infrared bands on AVHRR data (bands 4 and 5 on NOAA-9, 11, and 12 satellites) detects ash clouds (Prata, 1989; Holasek and Rose, 1991). The image that results from subtracting visible and near-infrared bands may help to distinguish water vapor from other plume constituents (Dean and others, in press). These band-subtraction techniques were used in this analysis to help distinguish plume components.

The principal-component-analysis technique creates new images by performing coordinate transformations that recognize the maximum variance in multispectral data. This technique generates new images referred to as "principal-component images" (PC1, PC2, PC3, etc.). The first principal-component image is a weighted-average picture: the remaining principal-component images are similar to pairwise differences between bands (Sabins, 1987; Siegal and Gillespie, 1980). The principal-component images were used to help distinguish subtle eruption-cloud signatures from meteorological clouds.

Altitudes of the eruption clouds were estimated by comparing their temperatures with the temperature profile of the

atmosphere. The eruption cloud, which is hot when first emitted by the volcano, will rise due to buoyancy but is also mechanically lifted by the force of the eruption. These two factors often propel eruption clouds to altitudes higher than many cloud masses (Sparks and others, this volume; Woods and Kienle, this volume; Dean and others, in press) where they rapidly cool to the temperature of the surrounding air. The temperature of the upper surface of the eruption cloud is derived from the thermal-infrared (band 4) satellite images. The thermal profile of the atmosphere is derived by the National Weather Service (NWS) from radiosonde observations and compared to the eruption-cloud temperature to determine an estimate of eruption-cloud height. These estimates are subject to errors (Woods and Self, 1992). The perspective view of the upper cloud surface was generated based on these principles and is shown in figure 2.

Eruption clouds have some attributes that distinguish them from many meteorological clouds. They are often higher and, hence, colder; they often have a larger albedo and are thus brighter; and, eruption clouds often have an apex starting at a volcano. A perspective view to the northeast was generated to show some of these differences (fig. 2) based on the 13:27 AST satellite image using a combination of the visible (band 1) and thermal-infrared (band 4) bands. In this example, the volcanic plume seen emanating from Redoubt Volcano was not at a greater height than the surrounding clouds, even though it is shown that way on this image, but it was brighter due to its high albedo on the visible-band data.

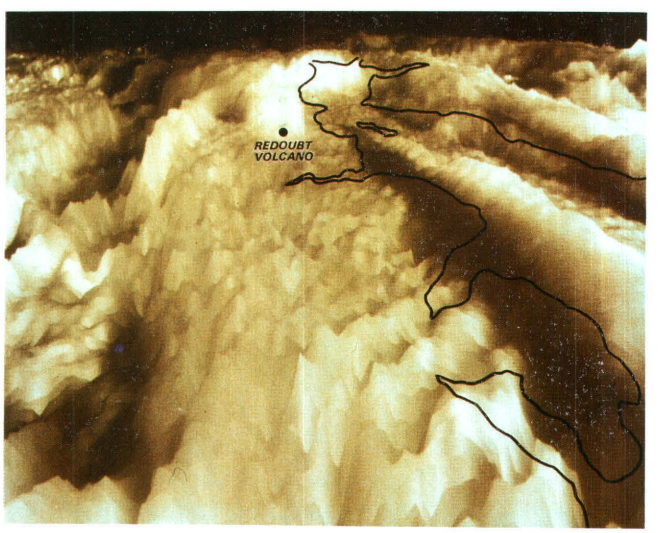


**Figure 2.** Perspective view, looking approximately northeast, of cloud tops generated from an AVHRR satellite image of south-central Alaska, 13:27 AST, 15 December 1989. The plume extends from Redoubt Volcano to the northeast and is brighter (high albedo) than most of the surrounding clouds. Cook Inlet is outlined on the right-hand side of the figure; refer to figure 1.

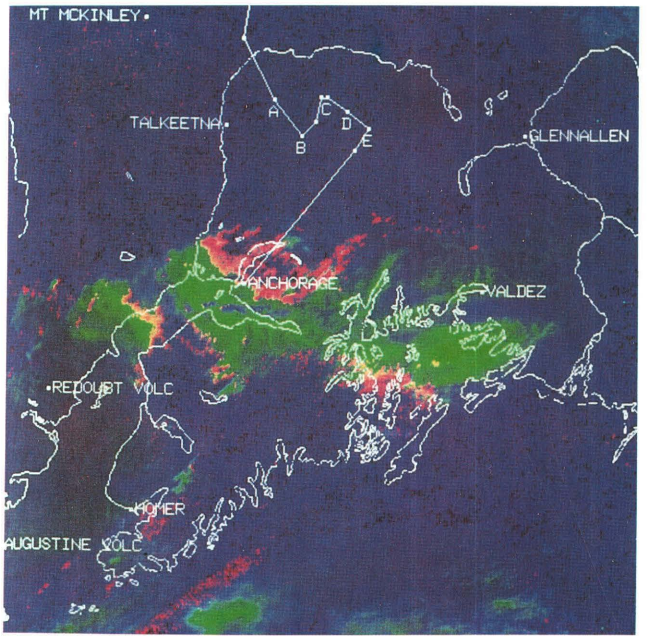


**Figure 3.** AVHRR satellite image of south-central Alaska, 03:28 AST, 15 December 1989. Suspected eruption clouds appear as green and red across the center of the image. The image is approximately 500 km on a side. The flight of the aircraft that encountered the ash cloud is shown as straight line segments in the upper and central parts of the figure. See text for explanation of A, B, C, D, and E.

The flight path of the aircraft that encountered the ash cloud is shown on figures 3 through 7. Labels along the flight path indicate the position of the aircraft at the time of critical events (Casadevall, in press):

- A—(11:46 AST)—Ash cloud encountered at 7,600 m (25,000 ft),
- B—(11:48 AST)—Engine shutdown at 7,600 m (25,000 ft),
- C—(11:50 AST)—Exit ash at 6,000 m (20,000 ft),
- D—(11:52 AST)—Restart two engines at 5,200 m (17,200 ft),
- E—(11:55 AST)—Restart two engines at 4,100 m (13,300 ft).

## RESULTS

The first AVHRR image (NOAA-11, orbit no. 6305), was recorded at 03:28 AST, 2 hours after the 01:40 AST eruption. A color composite image was generated to optimize differences in morphology and spectral response within the overlying cloud layer using PC3 as red, thermal-infrared band 3 as green, and PC1 as blue (fig. 3). This image shows a cloud structure (green and red) that may be an eruption

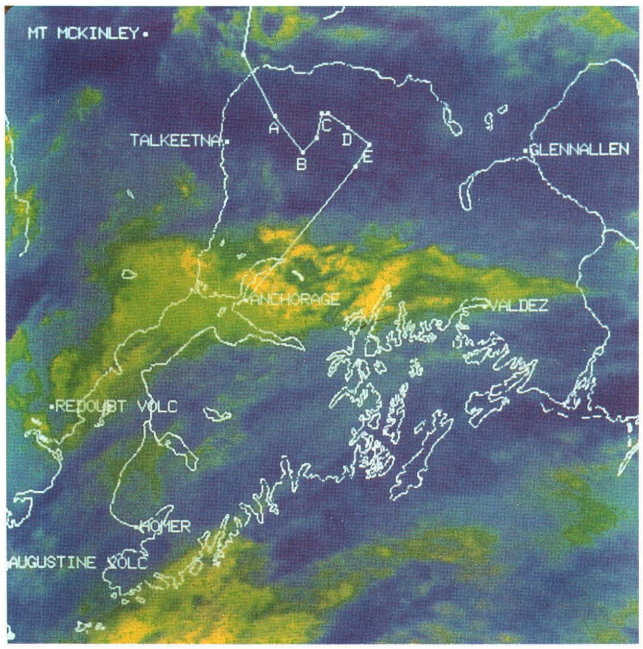


**Figure 4.** AVHRR satellite image of south-central Alaska, 05:09 AST, 15 December 1989. The suspected eruption cloud has an apex at Redoubt Volcano and appears as yellow across the center of the image. The image is approximately 500 km on a side. The flight path of the aircraft that encountered the ash cloud is shown as straight line segments in the upper and central parts of the figure. See text for explanation of A, B, C, D, and E.

cloud that starts northeast of Redoubt Volcano and extends to the east over Anchorage and beyond, to Prince William Sound, south of Valdez. The suspected eruption cloud was presumably emitted by the 01:40 AST eruption and appears to be in three segments, possibly indicating a discontinuous event comprised of three distinct eruptions. A subtraction of bands 5 and 4 was not successful in detecting the ash clouds.

The second AVHRR image (NOAA-11, orbit no. 6306) was recorded at 05:09 AST, 1.5 hours after the 03:48 AST eruption. A color composite image was generated to optimize differences in the morphology and spectral response within the overlying cloud layer. The optimal combinations used the thermal-infrared band 3 as red, thermal-infrared band 4 as green, and PC1 as blue (fig. 4). This band combination shows a suspected eruption cloud (yellow), with an apex near Redoubt Volcano, extending to the northeast and east, beyond Valdez. The eastern portion of this cloud is slightly detached and may be a remnant from the 01:40 AST eruption. A subtraction of bands 5 and 4 was not successful in detecting the ash clouds.

The third AVHRR image (NOAA-10, orbit no. 16851) was recorded at 09:28 AST, 6 hours after the 03:48 AST eruption and about 45 minutes before the 10:15 AST eruption. A color composite image was generated to optimize differences in the morphology and spectral response within the overlying cloud layer with PC1 as red, thermal-infrared band 4 as green, and thermal-infrared band 5 as blue (fig. 5). This image shows a suspected eruption-cloud (green and yellow) northeast of Redoubt Volcano that extends beyond Talkeetna and across the flight path of the aircraft that encountered an ash cloud. This cloud does not have an apex at Redoubt Volcano. Two possible volcanic-related clouds (yellow) can also be seen south of Glennallen and between Talkeetna and Fairbanks. Detection of ash clouds using the subtraction between bands 4 and 5 could not be applied because these bands are identical on the NOAA-10 satellite.

The fourth AVHRR image (NOAA-11, orbit no. 6311) was recorded at 13:27 AST, 3.25 hours after the start of the 10:15 AST eruption. A color composite image was generated to detect the plume and ash clouds using PC3 as red, subtraction of band 1 from 2 as green, and subtraction of band 4 from 5 as blue (fig. 6). This is the first 15 December image that unquestionably shows a volcanic plume despite the cloud layer and reveals an eruption cloud still emanating from Redoubt Volcano (yellow and green in the lower left portion of fig. 6) 2.5 hours after the end of the seismic event defining the 10:15 AST eruption. This plume trends northeast and east, ending just short of Anchorage, and is brightest

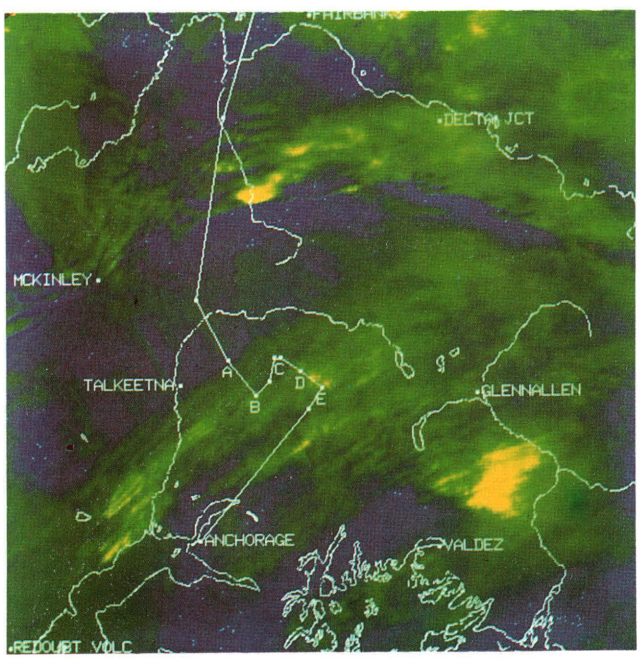


**Figure 5.** AVHRR satellite image of south-central Alaska, 09:28 AST, 15 December 1989. The suspected eruption clouds are green and yellow features that extend from Redoubt Volcano to Glennallen. The yellow features across the upper third of the figure may also be volcanic emissions. The image is approximately 500 km on a side. The flight path of the aircraft that encountered the ash cloud is shown as straight line segments in the central part of the figure. See text for explanation of A, B, C, D, and E.

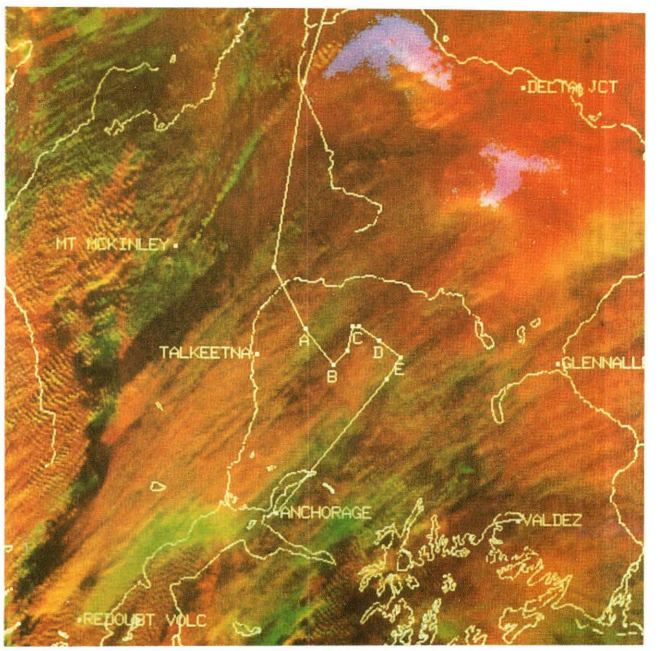


**Figure 6.** AVHRR satellite image of south-central Alaska, 13:27 AST, 15 December 1989. The eruption cloud (light green) has an apex at Redoubt Volcano and extends to Anchorage. The ash clouds (purple), which are south of Fairbanks and Delta Junction, may have been involved in the aircraft encounter. The image is approximately 500 km on a side. The flight path of the aircraft that encountered the ash cloud is shown as straight line segments in the central part of the figure. See text for explanation of A,B, C, D, and E.

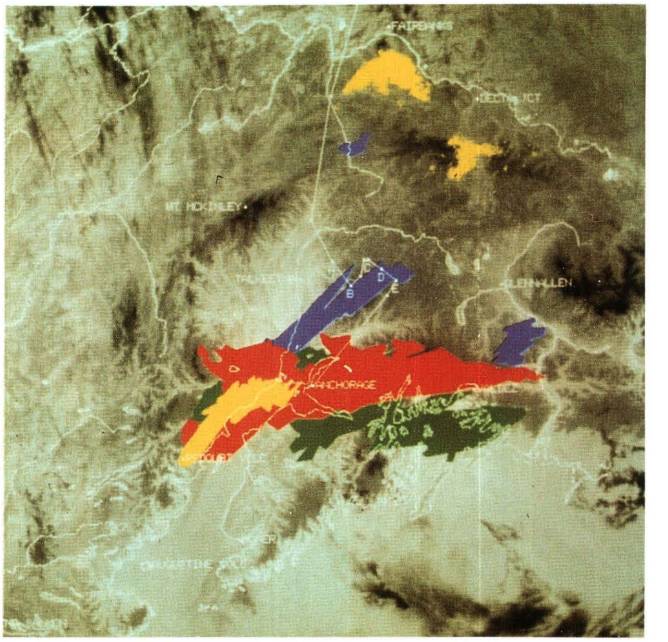


**Figure 7.** Artificially integrated satellite image that shows all of the possible eruption clouds on 15 December 1989. Colors designate the image from which the eruption clouds were extracted: green, 03:28 AST image; red, 05:09 AST image; blue, 09:28 AST image; yellow, 13:27 AST image. The flight path of the aircraft that encountered the ash cloud is shown as straight line segments in the upper and central parts of the figure. See text for explanation of A, B, C, D, and E.

on the band-2-minus-band-1 image, suggesting that its composition is something other than water vapor (Dean and others, in press). To the north, near Fairbanks and Delta Junction, two clouds (purple and pink) were observed in the band-5-minus-band-4 image, suggesting that they are composed of ash, as indicated by the signature generated by this band combination (Prata, 1989; Holasek and Rose, 1991).

# DISCUSSION

## GROUND ASH DISTRIBUTION AND ERUPTION-CLOUD TRAJECTORIES

To show more clearly the scenario of events on 15 December 1989, a summary image was compiled that integrated all of the "eruption clouds" observed on satellite data. The maximum extent of these clouds was extracted from individual images and transferred to a cloud-free reference image (fig. 7). Colors designate the image from which the suspected eruption clouds were extracted: green, 03:28 AST image; red, 05:09 AST image; blue, 09:28 AST image; yellow, 13:27 AST image. This integrated image shows that three of the four suspected eruption clouds have an eastward trajectory and that there is a northward progression in the trajectory of the early-morning eruption cloud, a northeast trend at 09:28 AST, and a northeast to eastward trend at 13:27 AST.

The predominantly eastward trajectory of the suspected eruption clouds does not agree with the distribution of surface ash collected by the U.S. Geological Survey (Scott and McGimsey, 1991). Surface ash deposited by the 15 December 1989 eruption is found northeast of Redoubt Volcano, not to the east, as the eruption cloud seen on the images would indicate. This suggests that either the suspicious clouds are not volcanic or that, as the ash falls from the plumes, it is swept northward by winds at a different altitude and that the clouds seen on the images do not contain ash. The elongated shape of the clouds with apexes at Redoubt Volcano (possibly two of four suspected plumes), geographic position, soft texture, and spectral signatures of these cloud structures indicate that they may be plumes, although absolute quantifying data is not available.

The second explanation is possible because winds below about 7-km altitude are to the north; at 7 to 12 km, the winds are to the northeast; and at 12 to 28 km, the winds are

to the northeast and east (03:00 AST, 15 December 1989, Anchorage radiosonde data). The wind directions indicate that the ash is in the lower air mass (below 7 km) and is being swept northward, whereas the eruption clouds seen on the images are in a higher air mass and are being transported northeast and east.

## AIRCRAFT–ASH CLOUD ENCOUNTER

Redoubt Volcano erupted three times during the morning of 15 December 1989: at 01:40, 03:48, and 10:15 AST. In order to identify which eruption cloud was involved in the encounter with the jumbo jet, we compare the velocity required to transport an ash cloud from Redoubt Volcano to the site where the encounter occurred to the wind velocity and direction obtained from radiosonde data from Anchorage International Airport. The required azimuth from Redoubt Volcano is approximately 40°, and the encounter occurred at an altitude of 7.6 km (25,000 ft).

The 10:15 AST eruption occurred 90 minutes prior to the aircraft-ash encounter at a point approximately 280 km northeast of Redoubt Volcano (Casadevall, in press). Based on these conditions, the ash cloud requires a velocity of 55 m/s to reach the site. The wind at 8 km altitude has a velocity of 55 m/s and a heading of 47° (15:00 AST sounding, 15 December 1989, Anchorage). Thus, measured wind parameters closely correlate with the transport of ash emitted by the 10:15 AST eruption.

## ASH CLOUD AT FAIRBANKS AND DELTA JUNCTION

The 13:27 AST AVHRR image (fig. 6) shows two ash clouds near Fairbanks and Delta Junction, approximately 3 hours after the 10:15 AST eruption. One or both of these ash clouds may be the one that the aircraft encountered near Talkeetna, 1.75 hours earlier. Back-tracking of cloud movement using wind data from Fairbanks atmospheric soundings were used to test this hypothesis.

The aircraft encountered ash at 7.6 km (25,000 ft) altitude (point A, figs. 3–7), 200 km from Fairbanks and Delta Junction. Temperature-height correlations of the cloud in the Fairbanks area range from 1.5 to 7 km (5,000 to 23,000 ft), and the height of the Delta cloud range from 2.5 to 13.5 km (8,000 to 44,500 ft) (15:00 AST sounding, 15 December 1989, Fairbanks). The range of heights of the cloud at Delta Junction spans the height of the encounter, and the upper height of the cloud near Fairbanks is slightly lower.

To transport the ash clouds from point of the encounter with the aircraft, to the Fairbanks and Delta Junction area, a velocity of 32 m/s and a northeast-blowing wind are required. Velocity calculations based on ground reports of ash fall are 31 m/s and show a northeast direction of movement (R. McGimsey, oral commun., 1992).

Meteorological measurements indicate that wind direction at approximately 7-km altitude would move the ash cloud that the aircraft encountered to either the Fairbanks or Delta Junction position. Wind at that altitude has a velocity of 31 m/s, with the wind blowing to the northeast. It does appear that either or both of these ash clouds were involved in the aircraft encounter, although the height of the cloud near Fairbanks is slightly lower than the altitude of the encounter.

Ground samples of ash from these ash clouds collected in the Fairbanks area had a mass of 0.1 g/m$^2$ (C. Nye, oral commun., 1991). Approximately 85 percent of the ash particles that fell from the Delta Junction cloud were in the 0.0039- to 0.0625-mm size range, based on two samples (R. Combellick, oral commun., 1991), and were composed predominantly of very angular glass and plagioclase (C. Nye, oral commun., 1991). The glass shards made up greater than 75 percent of the total ash weight.

# CONCLUSIONS

The 15 December 1989 eruption of Redoubt Volcano resulted in a near-fatal encounter of a jumbo jet passenger aircraft (Boeing 747) with the ash cloud from the 10:15 AST eruption. Despite the almost total cloud cover over south and

central Alaska, eruption clouds were observed on several satellite images. However, the position of the clouds seen on the images did not always agree with ground observations of fallen ash, probably due to height differences between the ash component and gas component of the eruption cloud (and the air masses that transported those parts). A technique of using multiple thermal bands to distinguish ash clouds from other clouds was successful on only one out of three possible images (fig. 6). This image, recorded at 13:27 AST, detected ash clouds near Fairbanks and Delta Junction. One or both of these ash clouds were very likely involved in the aircraft encounter at 11:45 AST.

Validation analyses of eruption clouds observed on satellite images have been minimal. It is not known how opacity, plume composition, particle size, and particle density affect the signatures observed on the satellite images. A thorough understanding of these factors would significantly improve the utility of satellite images for tracking and monitoring eruption clouds.

## REFERENCES CITED


Brantley, S.R., ed., 1990, The eruption of Redoubt Volcano, Alaska, December 14, 1989–August 31, 1990: U.S. Geological Survey Circular 1061, 33 p.

Casadevall, T. J., in press, The 1989–1990 eruption of Redoubt Volcano, Alaska: Impacts on aircraft operations: Journal of Volcanology and Geothermal Research.

Dean, K.G., Bowling, S.A., Shaw, G., and Tanaka, H., in press, Satellite analysis of movement and characteristics of the Redoubt Volcano plume: Journal of Volcanology and Geothermal Research.

Dean, K.G., Guritz, R., and Garbeil, H., 1990, Near-real time acquisition and analysis of satellite images of Redoubt Volcano [abs.]: Eos, Transactions, American Geophysical Union, v. 71, p. 1701.

Hanstrum, B.N., and Watson, A.S., 1983, A case study of two eruptions of Mount Galunggung and an investigation of volcanic cloud characteristics using remote sensing techniques: Australian Meteorological Magazine, v. 31, p. 171–177.

Holasek, R.E., and Rose, W.I., 1991, Anatomy of 1986 Augustine Volcano eruptions as recorded by multispectral image processing of digital AVHRR satellite data: Bulletin of Volcanology, v. 53, p. 420–425.

Kidwell, K.B., ed., 1991, NOAA polar orbiter data users guide (TIROS-N, NOAA-6, NOAA-7, NOAA-8, NOAA-9, NOAA-10, NOAA-11, and NOAA-12): Washington D.C., National Oceanic and Atmospheric Administration, National Environmental Satellite Data and Information Service, National Climatic Data Center, Satellite Data Services Division.

Kienle, J., Dean, K.G., Garbeil, H., and Rose, W.I., 1990, Satellite surveillance of volcanic ash plumes; application to aircraft safety: Eos, Transactions, American Geophysical Union, v. 71, p. 266.

Maligreau, J-P., and Kaswanda, O., 1986, Monitoring volcanic eruptions in Indonesia using weather satellite data: The Colo eruption of July 28, 1983: Journal of Volcanology and Geothermal Research, v. 27, p. 179–194.

Matson, M., 1984, The 1982 El Chichón eruptions—A satellite perspective: Journal of Volcanology and Geothermal Research, v. 23, p. 1–10.

Matson, M., and Staggs, S.J., 1981, The Mount St. Helens ash cloud: Bulletin of the American Meteorological Society, v. 62, p. 1486.

Mouginis-Mark, P., Rowland, S., Francis, P., Friedman, T., Garbeil, H., Gradie, J., Self, S., and Wilson, L., 1991, Analysis of active volcanoes from the Earth observation system: Remote Sensing of the Environment, v. 36: p. 1–12.

Prata, A.J., 1989, Observations of volcanic ash clouds in the 10–12 μm window using AVHRR/2 data: International Journal of Remote Sensing, v. 10, p. 751–761.

Sabins F.F., 1987, Remote Sensing: Principals and Interpretations (2nd ed.): New York, W.H. Freeman and Company, 449 p.

Scott, W.E., and McGimsey, R.G., 1991, Mass, distribution, grain size, and origin of 1989–1990 tephra-fall deposits of Redoubt Volcano, Alaska [abs.], *in* Casadevall, T.J., ed., First International Symposium on Volcanic Ash and Aviation Safety, U.S. Geological Survey Circular 1065, p. 39.

Siegal, B.S., and Gillespie, A.R., 1980, Remote Sensing in Geology: New York, John Wiley and Sons, 702 p.

Woods, A.W., and Self, S., 1992, Thermal disequilibrium at the top of volcanic clouds and its effect on estimates of the column heights: Nature, v. 355, p. 628–630.

VOLCANIC ASH AND AVIATION SAFETY:
Proceedings of the First International Symposium
on Volcanic Ash and Aviation Safety
U.S. GEOLOGICAL SURVEY BULLETIN 2047

# GEO-TOMS: TOTAL-OZONE MAPPING SPECTROMETER FOR OZONE AND SULFUR-DIOXIDE MONITORING FROM A GEOSTATIONARY SATELLITE

*By* Ulli G. Hartmann, Robert H. Hertel, Herbert A. Roeder, *and* J. Owen Maloy

## ABSTRACT

GEO-TOMS is a proposed ozone and sulfur-dioxide mapping spectrometer designed to fly on a geostationary satellite platform. It is an adaptation of the Nimbus-7 total ozone mapping spectrometer (TOMS), that is capable of imaging the whole Earth on a charge-coupled detector (CCD) array. The instrument will provide 12.2-km spatial resolution at nadir and will provide a complete multiband image every 10 minutes in 6 to 12 wavelength bands. Based on the performance of the Nimbus TOMS, GEO-TOMS will be capable of detecting volcanic eruptions and plumes and monitoring their progress in near real time, providing early warning of volcanic hazards to aviators and others.

## INTRODUCTION

Eruptions pose a hazard not only to people living nearby but also to aircraft and people in the path of ash fallout. Volcanic sulfur dioxide ($SO_2$) is an important component in volcanic plumes, and satellite-based instruments sensitive to sulfur dioxide can detect volcanic eruptions from space. Satellite weather instruments that respond primarily to temperature differences and cloud cover are not nearly as sensitive for detecting volcanic clouds as instruments that are sensitive to sulfur dioxide (Matson, 1984).

The total ozone mapping spectrometer (TOMS) was launched on the Nimbus-7 in 1978. The instrument monitors the state of the Earth's protective ozone layer by mapping the global ozone. TOMS measures sunlight reflected from the atmosphere at six wavelengths near the edge of the strong ozone absorption band in the ultraviolet. Stronger absorption at shorter wavelengths indicates a higher ozone concentration. TOMS has provided extensive and frequently cited data on the gradual deepening of the Antarctic ozone hole. In the years of operation of the first TOMS on the Nimbus polar-orbiter, users of TOMS data found that it had other unexpected capabilities and uses. TOMS not only maps ozone accurately, but it also can detect transients in total ozone and sulfur dioxide and track volcanic plumes over large distances (Bluth and others, 1992; Krueger, 1983, 1985; Krueger and others, 1990, this volume).

TOMS can detect $SO_2$ because this gas has an ultraviolet absorption band in the same wavelength region as ozone. The Nimbus-7 TOMS has detected 37 volcanic eruptions since 1978, including the $SO_2$ cloud from the May 18, 1980, eruption of Mount St. Helens as it drifted across the United States (Kerr and Evans, 1987; Krueger and others, this volume). An instrument that measures atmospheric ozone from space can also observe ozone discontinuities produced by severe storms and jet-stream winds and is potentially useful for warning aircraft of dangerous flight conditions (Shapiro and others, 1982).

## NEED FOR GEOSYNCHRONOUS OBSERVATIONS

At a conference for users of TOMS data held at Goddard Space Flight Center (GSFC) in 1986, the scientific contributors identified several uses for Nimbus-7 TOMS data beyond the daily ozone-mapping function. Some of these uses require observation of the Earth with higher time resolution, such as half-hourly or better. Table 1 lists the requirements for the principal time-critical applications (adapted from Schenk, 1987).

Measurements from a polar-orbiting satellite provide only one or two observations of the globe each day, not enough to provide a useful early-warning capability. Smaller eruptions may be missed by a single polar-orbiting satellite because the plume can be dispersed in less than 1 day. Many instruments would be needed in low-altitude polar orbits to provide sufficient time resolution. On the other hand, only a few instruments in geostationary orbit at an altitude of more than 35,800 km can provide a worldwide operational warning and monitoring network. For a geostationary TOMS to be fully useful, the ground resolution at nadir should be in the 10–30-km range (i.e., better than the 50-km resolution of the polar-orbiting TOMS). The time resolution should be at least 30 minutes.

**Table 1.** Applications requiring geostationary orbit.

[Achieving high temporal resolution and global coverage requires many instruments in low-altitude orbit but only a few in geostationary orbit. res., resolution. Adapted from Schenk (1987)]

| Phenomenon or feature | Temporal res. (minutes) | Spatial res. (kilometers) |
|---|---|---|
| Hurricanes | | |
| Eye | 5–10 | 5–10 |
| Environs | 30 | 10–30 |
| Convection-environment interaction | 5–10 | ≤10 |
| Jet streams | 10–30 | 10 |
| Volcanoes | | |
| First 12 hours | 5–10 | 5–10 |
| After first 12 hours | 30 | 30 |
| Full Earth-disk coverage | 30 | 10–30 |

A geostationary version of TOMS must either scan or image the entire Earth. Some ozone-detection capability can be obtained through use of a filter photometer following the main infrared and visible Earth scanner of a meteorological satellite. The stability and sensitivity of a filter system is unlikely to meet the quantitative specifications required for detecting volcanic plumes. In addition, the scan time is longer than 10 minutes. A resolution of 10 km implies an image with more than 1 million pixels. From a signal-to-noise standpoint, it is better to scan the few wavelength bands used than to scan so many pixels. This consideration led us to study an imaging spectrometer called GEO-TOMS.

We presented a preliminary version of the GEO-TOMS design in 1986 (Krueger and others, 1987), and, since then, we have further refined the design. No prototype has yet been built, however. The main goal in the GEO-TOMS

**Table 2.** Comparison of TOMS and GEO-TOMS spectral and radiometric requirements.

[TOMS, total ozone mapping spectrometer. The GEO-TOMS, in geostationary orbit, has similar spectral and radiometric requirements but has a smaller field of view and longer observing time per pixel. TOMS FM-1/2 is the original TOMS design; TOMS FM-3/4 is an improved design. deg., degrees; max. maximum; N/S, not specified]

| Design requirement | TOMS FM-1/2 | TOMS FM-3/4 | GEO-TOMS | Units |
|---|---|---|---|---|
| **General requirements** | | | | |
| Observing time per wavelength band | 0.014 | 0.010 | 50 | s |
| Pixel size at nadir | 50×50 | 50×50 | 12.2 | km |
| Pixels per field-of-view | 1 | 1 | 1,024×1,024 | |
| Pixel size (square) | 3×3 | 3×3 | 0.02×0.02 | deg. |
| Instrument overall field-of-view | 3×3 | 3×3 | 20×20 | deg. |
| **Spectral requirements** | | | | |
| Wavelength range | 312.5-380.0 | 308.6-360.0 | 308.6-360.0 | nm |
| Spectral bandpass (full-width at half-max.) | 1±0.1 | 1+0.3-0.0 | 1+0.3-0.0 | nm |
| Wavelength accuracy (λ<340 nm, 15°–35°C) | 0.05 | 0.1 | 0.1 | nm |
| Wavelength calibration accuracy | N/S | 0.005 | 0.005 | nm |
| Wavelength stability/repeatability | 0.02 | 0.005 | 0.005 | nm |
| Wavelength monitoring capability | 0.1 | 0.01 | 0.01 | nm |
| **Radiometric requirements** | | | | |
| Full-scale radiance | 500 | 500 | 500 | $W/cm^3$-sr |
| Maximum radiance | 320 | 400 | 400 | $W/cm^3$-sr |
| Minimum radiance | 0.32 | 0.4 | 0.4 | $W/cm^3$-sr |
| Radiometric resolution | 1.0 | 0.2 | 0.2 | % precision |
| Minimum-radiance signal-to-noise ratio | 30[1] | 30[1] | 30[1] | |
| Signal dynamic range | $1.56\times10^5$ | $6.25\times10^5$ | $6.25\times10^5$ | |
| Radiometric repeatability | N/S | 0.004 | 0.2 | %/hr |
| Detector stability | 5 | 5 | 5 | %/yr |
| Radiometric linearity | 2 | 1 | 2 | % signal |
| Spectral stray light | 1000:1 | 0.5 | 0.5 | % signal |
| Band-to-band crosstalk | N/S | 0.1 | 1 | % signal |
| Residual polarization sensitivity | 5 | 5 | 5 | % |
| Reflectance calibration capability | N/S | 0.1 | 5 | %/yr |

[1] Goal is 100.

design has been to develop a baseline for a future operational instruments by providing near-real-time global imaging capability while still meeting the stringent TOMS performance specifications. Table 2 lists the design requirements for the original TOMS (FM-1/2), the new improved TOMS (FM-3/4), and GEO-TOMS.

## PRELIMINARY DESIGN OF GEO-TOMS

GEO-TOMS is an ozone and sulfur-dioxide mapping instrument specifically designed to fly on a geostationary platform. GEO-TOMS will be a new member of a family of already-proven instruments that map atmospheric ozone distribution by measuring the solar ultraviolet radiation backscattered from the atmosphere. The first member of the family was the backscattered ultraviolet instrument (BUV), launched in 1970 on Nimbus-4. The solar/backscatter ultraviolet instrument (SBUV) and the total ozone mapping spectrometer (TOMS FM-1) were launched as a combined package on Nimbus 7 in 1978. These instruments demonstrated exceptional life: 8 years in orbit for BUV and SBUV—TOMS continues to operate after more than 15 years. Later versions of the spectrometer include the SBUV-2 series, flying on National Oceanic and Atmospheric Administration (NOAA) satellites, and TOMS FM-2, launched on a Soviet Meteor satellite in August, 1991. Perkin-Elmer is building a new version of the TOMS sensor to fly on the Japanese advanced Earth observing satellite (ADEOS).

The design of such instruments must provide solutions to several technical problems. Here is how the GEO-TOMS design solves the principal problems:

| Problems | Solutions |
|---|---|
| Light collection | Long observing time (10 minutes). Parallel observation of all pixels. |
| Wavelength stability and resolution | Diffraction-grating spectrometer. Cam-driven grating positioning mechanism. |
| Unwanted (stray) light rejection | Visible-light-absorbing coatings. High-quality grating. |
| Image readout and processing | On-board microprocessor, large memory. |

GEO-TOMS uses the technology of both SBUV and TOMS but images the whole Earth disk onto a silicon-array detector in one wavelength band at a time, without a spatial scanner. A diffraction grating rotates to select from six to 12 wavelength bands for imaging, as in the Nimbus-4 BUV, the Nimbus-7 SBUV, and SBUV-2. The wavelength bands will be selected to optimize both ozone and $SO_2$ detection. The proposed wavelength-scanning mechanism is essentially the same as the motor-driven mechanical cam proven on BUV and SBUV.

Figure 1 shows the optical layout of the GEO-TOMS. The field of view is 20°, so that the whole Earth is imaged at one time. The optical design is similar to the original TOMS except that there are two parabolic collimating mirrors instead of one spherical mirror. Optical ray traces show that a single mirror will not provide the needed image quality for the wide field. Light reflected from either the atmosphere or a calibration diffuser passes through a depolarizer and enters a diffraction-grating monochromator. Light from the grating passes through a single exit slit onto a 1,024×1,024 charge-coupled detector (CCD) through an optical system that corrects monochromator aberrations. A shutter provides optical zeroing. As in the previous instruments, in-flight wavelength calibration will use a mercury lamp.

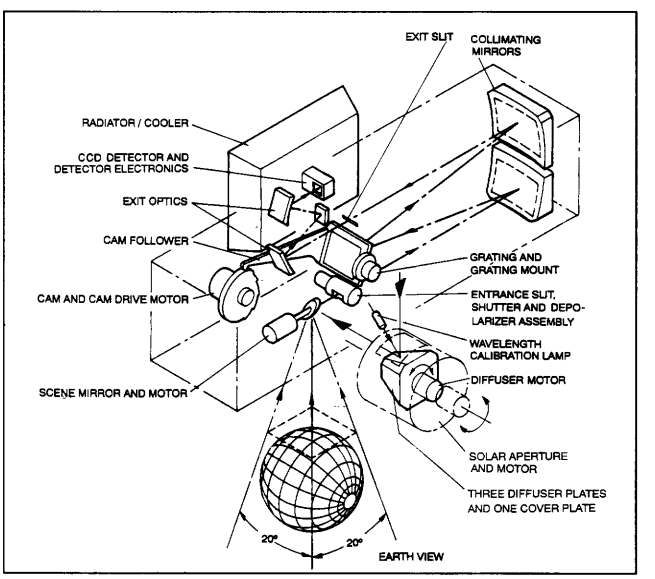


**Figure 1.** GEO-TOMS optical layout. The grating spectrometer collimates and diffracts light reflected from the Earth, forming an image of the entire Earth in one narrow-wavelength band at a time on the charge-coupled detector (CCD). The diffraction grating rotates, imaging the Earth at different wavelengths to determine the amounts of ozone and sulfur dioxide in the scene. A movable scene mirror permits the instrument to view the calibration diffuser.

With such faint signals and high spectral resolution, the rejection of radiation at unwanted wavelengths, or "stray light," must be excellent. GEO-TOMS needs a high-quality grating like that used for the newer TOMS models, because stray light increases when only a small part of the grating is used for each pixel. To reduce stray light, the GEO-TOMS will use mirrors coated to reflect the ultraviolet, but not the visible radiation.

## DETECTOR SELECTION

The ultraviolet sensitivity of CCD detectors has now advanced sufficiently so that such detectors can be planned on for GEO-TOMS. The use of a single, stable silicon CCD detector reduces drift problems. Reading out the image often enough to prevent saturation permits covering the wide dynamic range. Shielding will be used to prevent damage from charged particles. Even though the current design plans on an ultraviolet-sensitive CCD detector, the GEO-TOMS concept does not depend on the availability of such a detector. The Voyager ultraviolet spectrometer observed the atmospheres of the outer planets using a silicon-array detector with a microchannel plate for ultraviolet image intensification. Since then, many such detectors have been fabricated using higher resolution arrays. These are commercially available for space use with integrated detector arrays and fiber optics.

## DETECTOR COOLING

Because it is not necessary to cool the detector to cryogenic temperatures, a simple passive radiator cools the CCD detector to –40°C to reduce leakage current. There is evidently a weight and cost optimum, because a large instrument needs no cooler, whereas a small instrument must have a large cooler. As a baseline, we have made the monochromator the same size as in the present TOMS, but this choice does not necessarily provide the minimum weight or cost.

## LAYOUT

The baseline mechanical layout appears in figure 2. The mirrors will be mounted on lapped surfaces, as for TOMS. The rigid structure keeps the pixels in place on the detectors and assures the required wavelength stability. The monochromator and other optical components and mechanisms form an assembly that is mounted inside the housing. The stiff box structure of the mount incorporates the electronics as a structural element, providing part of the structural rigidity and reducing weight. One side of the instrument continually faces north, and the opposite side faces south. These sides provide locations for thermal radiators with a continuous space view. Separate radiators cool the detector (–40°C) and the electronics (+25°C). The detector temperature will be regulated by a small heater.

## ELECTRONICS

GEO-TOMS is mainly a digital instrument with few critical analog circuits and, therefore, does not need most of the sophisticated electronics components required for the polar-orbiting TOMS instruments. The instrument contains an image processor with a separate microprocessor for interfacing and control.

## DATA RATES

The noon data rate for the GEO-TOMS is about 409 kbits/s at maximum spatial resolution. This rate is comparable to other geostationary imaging instruments. On-board,

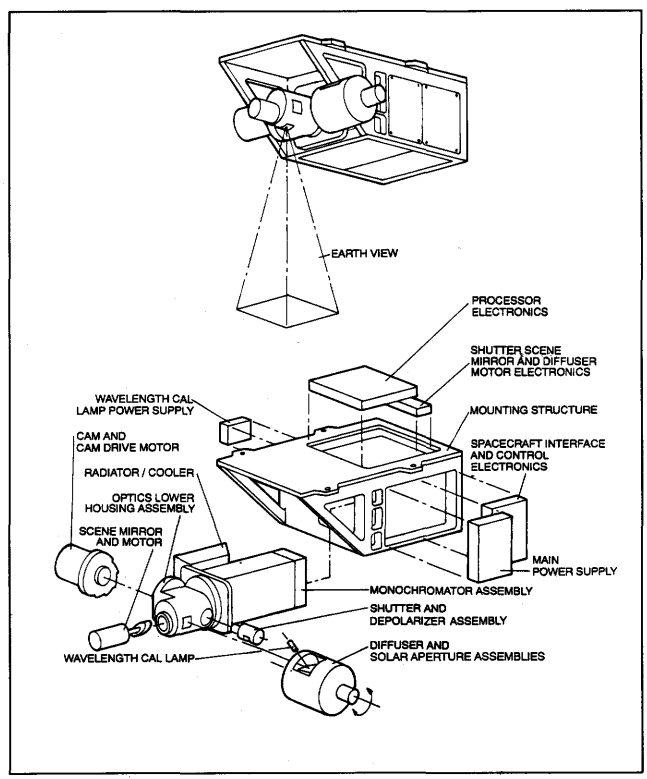


**Figure 2.** GEO-TOMS mechanical arrangement. The monochromator and scanner mounts into a frame that also supports the electronics assemblies. The instrument views the diffuser through a side port.

real-time event processing with detection of affected region with deletion of uninteresting data could reduce the real-time rate.

## DIFFUSER CALIBRATION

Calibration of the GEO-TOMS will use techniques borrowed from TOMS, SBUV, and SBUV-2, incorporating the benefit of the improved diffuser system used in later instruments. All backscattered-ultraviolet instruments, including TOMS and GEO-TOMS, measure the reflectance of the atmosphere. The absolute radiance is not of primary interest. The reflectance standard is a diffuse-reflecting plate, or diffuser, periodically exposed to sunshine and viewed by the instrument. So far, nothing surpasses the stability and uniformity of the simple, ground aluminum plate originally used on the first BUV instrument that was launched over 20 years ago, although the plate's reflectance declines with prolonged exposure to the sun. The diffuser calibration employs an ultraviolet light source to compare the reflectance of a protected reference diffuser and the active diffuser. The light source itself needs to be stable only during the comparison. By using more than one diffuser, the effects of sun exposure and vacuum exposure can be disentangled. Although less elaborate than the diffuser-calibration systems used in TOMS instruments designed for quantitative mapping, the GEO-TOMS system should be adequate for transient mapping.

# RESULTS

Our design study shows that the GEO-TOMS concept is feasible. Optical ray-trace results demonstrate that such a wide-field monochromator will work as an imager. The width of the nadir point-spread function is smaller than the desired resolution. Thus, the detectability for a point source is almost the same as for a cloud several pixels across. The inherent GEO-TOMS spectral resolution is somewhat better than 0.7 nm full-width at half-maximum and meets the TOMS specification. Because each pixel uses only a small part of the grating, the inherent resolution is comparable to the desired resolution and varies somewhat over the field of view. The longer integration time and larger entrance aperture compensate for the reduced solid angle of the field of view in the GEO-TOMS, as compared to the existing TOMS aboard Nimbus-7. The estimated signal-to-noise ratio of GEO-TOMS is 40:1 at minimum radiance, about the same as the Nimbus TOMS, including the effects of space radiation. This estimate assumes the use of 12 wavelength bands and the same 50-second integration time for each wavelength. In practice, exposure time will be optimized for each wavelength depending on current cloud and lighting conditions.

# CONCLUSIONS

Imaging of ozone and sulfur dioxide in the upper atmosphere from geostationary satellite orbit can provide early warning and monitoring of volcanic events and severe storms for the benefit of aviators and others. GEO-TOMS is a proposed geostationary instrument, based on the proven polar-orbiting TOMS, that can provide this imaging capability by detecting backscattered solar ultraviolet radiation. Analysis of the GEO-TOMS design has shown that the instrument concept can provide near-real-time maps of ozone and sulfur dioxide.

# REFERENCES CITED

Bluth, G.J.S., Doiron, S.D., Krueger, A.J., Walter, L.S., and Schnetzler, C.C., 1992, Global tracking of the $SO_2$ clouds from the June 1991 Mount Pinatubo eruptions: Geophysical Research Letters, v. 19, p. 151–154.

Kerr, J.B., and Evans, W.J., 1987, Comparison of ground-based and TOMS measurements of $SO_2$ from volcanic emissions: NASA Conference Publication 2497, p. 60–69.

Krueger, A.J., 1983, Sighting of El Chichón sulfur dioxide clouds with the Nimbus 7 total ozone mapping spectrometer: Science, v. 220, p. 1377–1378.

———1985, Detection of volcanic eruptions from space by their sulfur dioxide clouds: American Institute of Aeronautics and Astronautics, AIAA 23rd Aerospace Sciences Meeting, January 14–17, Reno, Nev., Report AIAA-85-0100, 4 p.

Krueger, A.J., Maloy, J.O., and Roeder, H.A., 1987, A geostationary imaging spectrometer TOMS instrument: NASA Conference Publication 2497, p. 88–89.

Krueger, A.J., Walter, L. S., Schnetzler, C.C., and Doiron, S.D., 1990, TOMS measurements of the sulfur dioxide emitted during the 1985 Nevado del Ruiz eruptions: Journal of Volcanology and Geothermal Research, v. 41, p. 7–15.

Matson, M., 1984, The 1982 El Chichón volcano eruptions—A satellite perspective: Journal of Volcanology and Geothermal Research, v. 23, p. 1–10.

Shapiro, M.A., Krueger, A.J., and Kennedy, P.J., 1982, Nowcasting the position and intensity of jet streams using a satellite-borne total ozone mapping spectrometer, *in* Browning, K.A., ed., Nowcasting: New York, Academic Press, p. 137–145.

Schenk, W.E., 1987, Observation guidelines for a total ozone mapping spectrometer (TOMS) in geostationary orbit: NASA Conference Publication 2497, p. 86–87.

VOLCANIC ASH AND AVIATION SAFETY:
Proceedings of the First International Symposium
on Volcanic Ash and Aviation Safety
U.S. GEOLOGICAL SURVEY BULLETIN 2047

# PASSIVE, TWO-CHANNEL, THERMAL-INFRARED IMAGING SYSTEMS FOR DISCRIMINATION OF VOLCANIC ASH CLOUDS

*By* Frank R. Honey

## ABSTRACT

The National Oceanic and Atmospheric Administration's advanced very high resolution radiometer image data, recorded and displayed in Perth, Australia, in June 1982, dramatically demonstrated a capability for satellite observation of the volcanic ash from the eruption of Galunggung Volcano, Indonesia. Analysis of the data, based on an understanding of the spectral-emissivity properties of silica-rich materials, and of water clouds, resulted in discrimination and display of the ash cloud over a period of several days.

Interest in the techniques that were used for this discrimination procedure led to the proposal in 1982 of a passive, two-channel, thermal imaging system that could be mounted in an aircraft. Display of the enhanced data from the proposed imaging system could be multiplexed into existing aircraft avionics and could alert the crew to the presence of silica-rich materials in the flight path over ranges up to or exceeding 100 km, assuming a clear line of sight. The initial instrument design is discussed, and several improvements on the original concept and limitations to the application of such an instrument are outlined.

## INTRODUCTION

Encounters of aircraft with ash plumes from volcanic eruptions have caused considerable damage and, in several cases, have had near-fatal consequences. The development of sensors for the detection of hazardous materials and other atmospheric phenomena in the flight paths of aircraft is assuming a high priority for agencies involved in enhancing aviation safety.

Opportunistic recording of data from the polar-orbiting satellites of the National Oceanic and Atmospheric Administration (NOAA) at the time of the eruption of Galunggung Volcano in Indonesia in June 1982, and the subsequent development of enhancement and display procedures, enabled a positive discrimination of volcanic ash and dust clouds from normal water and ice clouds. This research also provided an indication of the requirements for geosynchronous satellite sensors with appropriate thermal infrared channels and led to the proposal of a passive, two-channel, thermal-infrared imaging sensor that could be mounted in aircraft to alert the crew to potential hazard, with sufficient time to take nonviolent, evasive maneuvers.

The enhancement and discrimination procedures developed were based on an understanding of the spectral emissivity properties of silicate minerals expected to be present in the dust and ash plumes. Subsequent modeling by other workers using radiative-transfer theory provided an alternative mechanism to explaining the spectral discrimination (Prata, 1989; Prata and Barton, this volume).

## SATELLITE DATA COLLECTION AND ANALYSIS

The NOAA satellites are near-polar-orbiting environmental and meteorological satellites that are operated by the U.S. Department of Commerce, National Oceanic and Atmospheric Administration (Sabins, 1987). In general, two satellites are operational at any one time, giving a potential for coverage of an area four times per day (twice during daylight hours, twice during the night). In practice, however, there are gaps in coverage of any location due to the orbital characteristics of the spacecraft.

The advanced very high resolution radiometer (AVHRR) sensor on the NOAA satellite series has five spectral channels, with wavelength ranges of 0.55–0.68, 0.725–1.1, 3.55–3.95, 10.5–11.5, and 11.5–12.5 μm. The ground spatial resolution of the sensor is 1.1 km. Data are transmitted and recorded to 10-bit precision, providing sufficient dynamic range to accommodate targets ranging from sea surfaces to clouds and snow.

In late 1981, data from the NOAA-7 AVHRR sensor were being recorded on an irregular basis under a joint research effort between the Commonwealth Scientific and Industrial Research Organization (CSIRO) and the staff from the Western Australian Institute of Technology (WAIT) (now Curtin University of Technology). The CSIRO/WAIT team had developed a low-cost satellite

tracking and receiving facility (Carroll and others, 1981) to provide near-real-time access to the AVHRR data for application to research projects on oceanography, land use, geology, flooding, and fires.

The tracking and receiving facility in Perth had the capability to record data from the satellites down to elevations above the horizon of approximately 3°. Depending on the orbital position of the satellite, this enabled some data acquisition over the island of Java, Indonesia. Data from the NOAA-7 satellite were not recorded for the area around and to the southeast of Galunggung until 29 June 1982; however, ash plumes of sufficient concentrations and extent for satellite detection were likely emitted by the volcano for several weeks previous to that time. Data from earlier overpasses by the NOAA-7 spacecraft had either not been recorded or the satellite was too far to the east to provide coverage of the area.

Unfortunately NOAA-6, the only other operational NOAA satellite in orbit at that time, did not have channel 5 (11.5–12.5 μm) functioning. Thus, the two-thermal-channel technique could not be applied to the NOAA-6 data.

## DATA ANALYSIS, ENHANCEMENT, AND DISPLAY

The initial approach to data analysis was similar to the analysis applied to data from the Japanese geostationary meteorological satellite (GMS-2) by the Australian Bureau of Meteorology (Hanstrum and Watson, 1983). In that study, eruptions of Galunggung on 24 June and 13 July 1982 were observed using GMS-2 imagery. Enhanced infrared imagery revealed signatures for the volcanic ash clouds produced by these two eruptions that were similar to growing thunderstorms. The GMS-2 images were used to estimate cloud-top height, and cloud movement was monitored.

In the analysis by the CSIRO/WAIT team, individual thermal channels 3, 4, and 5 of the NOAA-AVHRR data were enhanced individually to accentuate radiometric variations due to areas of different temperature within clouds in the images. Although radiometric differences were observed, the area suspected of being the volcanic ash plume was not positively discriminated from the normal water clouds in the area. In an attempt to discriminate the clouds using possible albedo differences, the reflected bands on the daytime images were enhanced. However, this technique was also inconclusive, as were color combinations of contrast-enhanced single bands.

At the time of the Galunggung eruption, the author was designing an airborne multispectral scanner to be applied primarily for minerals exploration, based on the different reflectance and emittance spectra of various minerals (Honey and Daniels, 1985). The 13 spectral bands of this scanner included four thermal-infrared channels (8.5–8.9, 9.7–10.1, 10.8–11.2, 11.5–12.0 μm) that were specifically selected to discriminate rocks using differences in their silicate emission spectra (Lyon, 1964; Salisbury and others, 1987). The position of the emission minima, which is due to the asymmetric stretching modes of the O-Si-O units, is related to the structure of particular silicate minerals and ranges from approximately 8.5 μm for quartz to 10.7 μm for Fe-Mg minerals such as olivine.

Because ash from volcanic eruptions contains large proportions of silicate materials, particularly the ferromagnesian silicates whose emission minima overlap with the wavelength range of the NOAA-AVHRR band 4 (10.5–11.5 μm), differences and ratios between bands 4 and 5 of the AVHRR data were generated to provide a more definite discrimination between the plume of volcanic ash and normal water clouds in the area. These images display band 4 in blue, band 5 in green, and the difference between band 4 and band 5 in red—they show normal water clouds as black, the sea surface as blue-cyan, and volcanic ash plumes as orange to pink. The results of this method show positive discrimination of the volcanic ash plume from normal water clouds.

The procedures and displays developed by the CSIRO/WAIT team aroused the interest of the Australian aviation authorities and the media, and data collection and analysis activities continued for several weeks. The results of the analysis, enhancement, and display of the AVHRR data clearly demonstrated the potential for detecting and monitoring volcanic ash plumes using thermal channels similar to channels 4 and 5 of the NOAA-AVHRR sensors. However, following the period of intense data collection and analysis, it was considered that the low frequency of coverage by the NOAA-AVHRR satellites precluded their application to an operational monitoring and warning capability.

## ALTERNATIVE SENSOR SYSTEMS

During discussions in 1982 with Australian aviation authorities, the limitations of the polar-orbiting satellites as a means of monitoring eruptions of volcanoes, and for tracking ash and dust plumes, were reviewed. The possibility of applying geosynchronous meteorological sensors was considered, although the Japanese geostationary meteorological satellite (GMS-2) then operating only had one thermal channel, and the two-channel discrimination procedures could not be applied. Geosynchronous satellites, with their high frequency of coverage over large areas, could provide a capability for monitoring and tracking, assuming that future-generation systems have two thermal infrared channels: preferably one from approximately 10.0–11.0 μm and the second from 11.5–12.5 μm.

The second, more direct means of determining the presence of volcanic ash plumes in or near the path of aircraft would utilize a two-thermal-channel imaging system, with moderate spatial resolution, mounted on an aircraft.

## TWO-CHANNEL THERMAL-INFRARED IMAGING SENSOR

The infrared imaging sensor proposed to Australian aviation authorities in 1982 comprised an optical window transmitting in the 10–12.5-μm region; scanning optics; dispersion optics to split out the 10.0–11.0- and 11.5–12.5-μm regions; infrared camera optics; cooled infrared detectors; amplification, data storage, analysis, and display hardware; and an interface to aircraft avionics to enable the pilot and crew to view the imagery. The estimated maximum weight of the imaging sensor was 25 kg. The amplification, storage, analysis, and display electronics, together with the interfaces to aircraft avionics, would provide the crew with a real-time display of the region in front of the aircraft as well as providing an alarm capability upon detection of anomalous infrared signatures associated with silicate materials.

The scanning optics would acquire energy over a field of view of approximately ±10° in the horizontal direction (relative to the direction of flight) and would acquire energy from 2° above horizontal and 8° below horizontal in the vertical direction. At 100-km range, this system images an area 35 km wide, extending from 3.5 km above to 14 km below the aircraft's projected track. Assuming that each scan line comprises 64 picture elements and that 32 lines are scanned, the spatial resolution at 100 km would be 550 m. At 10-km range, the resolution would be 55 m.

Since the original design proposal in 1982, there have been a number of technical advances that would reduce both the weight and bulk of the original sensor. For example, the dispersion optics originally considered used a dichroic beam splitter to separate the two infrared regions, with cold infrared band-pass filters in front of the detectors limiting the energy to 10.0–11.0 and 11.5–12.5 μm. Other dispersion and multisensor systems developed in the past decade may now be more practical and compact.

When the initial concept was being developed, focal-plane-array technology for mercury-cadmium detectors was not readily available for commercial purposes. As this technology has developed, these arrays have become available so that the early imaging technique using two-axis scanning of mirrors is no longer necessary—this simplifies the mechanical construction of such imaging systems and increases their mechanical reliability.

The infrared camera optics, which focus energy onto detector elements or arrays, must pass through the entrance window of a liquid-nitrogen-filled Dewar cooling vessel within which the cold infrared band-pass/blocking filters are mounted in order to minimize the level of background energy. The requirement for the sensor's detector elements or arrays to be cooled to 78° Kelvin (liquid nitrogen) was a potentially limiting factor because either liquid-nitrogen-filled Dewar cooling vessels or in situ coolers, such as Joule-Thomson cryostats, were required. Commercially available cooling technology has matured considerably since 1982, with compact, reliable, closed-cycle Stirling coolers now capable of providing the necessary cooling.

Even though the concept of developing a forward-looking, imaging, two-channel volcanic ash discriminator is now a reality (Prata and others, 1991; Barton and Prata, this volume), considerable research is necessary to determine the limitations of such a system, particularly the sensitivity, range, and the influence of poor visibility due to other clouds in the area and field of view. Such instruments should never be assumed to provide a fail-safe means of detecting the presence of hazardous levels of volcanic dust and ash in the path of aircraft. They should only be considered as aids to the pilot and crew.

## RESEARCH SINCE 1982

Since 1982, the author has focused his research on the development of other advanced multispectral sensors (Honey and Daniels, 1985). However, activity to advance research and development of operational techniques for detecting and tracking volcanic ash clouds commenced again in CSIRO in 1984–85 with the work of A.J. Prata. Subsequent modeling of the volcanic ash phenomenon using scattering theory (Prata, 1989) reinforced the logic of the earlier analysis of AVHRR data. This earlier analysis was based on the assumption that the energy was being emitted by the dense volcanic ash cloud rather than considering the energy as being scattered and differentially absorbed, as in Prata's (1989) analysis. Prata (1989) also used the refractive indices of quartz in his modeling rather than the refractive indices for more basic mineral or rock types, such as the rhyolite, andesite, and basalt that are typical of volcanic materials. The complex refractive indices of volcanic ash (Volz, 1973) differ significantly from the values for quartz (Peterson and Weinman, 1969).

A third phenomenon may contribute to negative "temperature" differences, leading to the discrimination of a volcanic plume from normal water clouds. The temperature of the ash cloud from Galunggung was estimated at approximately –75°C, and the lowest temperature of water clouds in the area was calculated as –15°C (Scarone, 1987). For blackbody emission at 203° Kelvin, the emission maximum occurs at 14.28 μm, whereas for a black body at 263° Kelvin, the emission maximum occurs at 11.02 μm. Thus, for the warmer water-cloud masses in the area of the eruption, in the absence of any other factors and assuming an emissivity of 1.0, the difference of band 4 minus band 5 would be positive, whereas the difference would be negative for the volcanic plume. Further modeling and research will be necessary to determine the relative contributions of the phenomena outlined above. The most encouraging feature of all of the phenomena, however, is that the band differences, either expressed as radiance or as temperature, provide a means of discriminating cloud types.

The CSIRO group involved in research into the detection of hazardous material and phenomena has developed a two-thermal-channel radiometer to test the spectral and radiometric design criteria for an airborne imaging sensor (Prata and others, 1991; Barton and Prata, this volume; Prata and Barton, this volume).

## CONCLUSIONS

Image data from the AVHRR sensors on the operational NOAA satellite series have the appropriate spectral channels to enable discrimination of volcanic ash clouds from regular water and ice clouds. The limited frequency of overpass of these polar-orbiting satellites precludes their application for monitoring and tracking of the clouds to provide aircraft crews with warning of potential hazardous features in their flight path. The possibility of dual-channel thermal-infrared sensors being implemented on geosynchronous weather satellites offers some potential for developing procedures for locating and monitoring of volcanic eruptions and the tracking of their plumes.

More direct and immediate capability may be provided using dual-infrared-channel imaging instruments mounted in aircraft. The principles upon which such sensors will operate have been established from the analysis of the NOAA-AVHRR data and from modeling of the emission and radiative transfer processes. Further study is necessary to test models that lead to analysis and enhancement procedures and to the design of the appropriate instruments. It will be important to establish the limitations that apply to these sensors, in terms of the minimum detectable quantities of ash and dust, the range over which they will provide an effective early-warning adjunct, and the factors that will restrict or completely negate their capability.

## ACKNOWLEDGMENTS

The author gratefully acknowledges the effort, support, and enthusiasm of Professor Bill Carroll and the devoted team of CSIRO scientists and technicians who made this project both achievable and enjoyable. The author also acknowledges the effort of the team of WAIT engineering students who worked so diligently to collect much of the data upon which this work was based.

## REFERENCES CITED

Carroll, W., Honey, F.R., and Cargill, R.D., 1981, Real time multispectral imagery from the NOAA/TIROS AVHRR system, *in* Proceedings, 2nd Australasian Remote Sensing Conference—LANDSAT 81: Canberra, Australia, p. 721–726.

Hanstrum, B.N., and Watson, A.S., 1983, A case study of two eruptions of Mount Galunggung and an investigation of volcanic eruption cloud characteristics using remote sensing techniques: Australian Meteorological Magazine, v. 31, p. 171–177.

Honey, F.R., and Daniels, J.L., 1985, Application of Carr Boyd Minerals Limited airborne multispectral scanner to spectral discrimination of hydrothermally altered areas, *in* Proceedings of the International Symposium on Remote Sensing of the Environment, 4th Thematic Conference (Remote Sensing For Exploration Geology), San Francisco, v. 1, p. 227–231.

Lyon, R.J.P., 1964, Evaluation of infrared spectrophotometry for compositional analysis of lunar and planetary soils, part II, *in* Rough and Powdered Surfaces: Washington, D.C., National Aeronautics and Space Administration, NASA Contractor Report NASA CR-100.

Peterson, J.T., and Weinman, J.A., 1969, Optical properties of quartz dust particles at IR wavelengths: Journal of Geophysical Research, v. 74, p. 6947–6952.

Prata, A.J., 1989, Radiative transfer calculations for volcanic ash clouds: Geophysical Review Letters, v. 16, p. 1293–1296.

Prata, A.J., Barton, I.J., Johnson, R.W., Kamo, K., and Kingwell, J., 1991, Infrared radiometric detection of volcanic ash clouds: Nature, v. 354, p. 25.

Sabins, F.F., Jr., 1987, Remote Sensing: Principles and Interpretations: New York, W.H. Freeman and Company, 449 p.

Salisbury, J.W., Walter, L.S., and Vergo, N., 1987, Mid-infrared (2.1–25 μm) spectra of minerals: U.S. Geological Survey Open-File Report 87-263, 26 p.

Scarone, Hugo, 1987, Volcanic ash clouds—A continuing threat to international aviation: Earthquakes & Volcanoes, v. 19, p. 65–73.

Volz, F.E., 1973, Infrared optical constants of ammonium sulphate, Sahara dust, volcanic pumice and flyash: Applied Optics, v. 12, p. 564–568.

VOLCANIC ASH AND AVIATION SAFETY:
Proceedings of the First International Symposium
on Volcanic Ash and Aviation Safety
U.S. GEOLOGICAL SURVEY BULLETIN 2047

# SEISMIC IDENTIFICATION OF GAS-AND-ASH EXPLOSIONS AT MOUNT ST. HELENS—CAPABILITIES, LIMITATIONS, AND REGIONAL APPLICATION

*By* Chris Jonientz-Trisler, Bobbie Myers, *and* John A. Power

## ABSTRACT

Since 1980, analysis of seismic signals recorded by the University of Washington (UW) and U.S. Geological Survey (USGS) Mount St. Helens seismic network have been analyzed and correlated with observations made by field crews, pilots, radar operators, and the general public. These analyses have led to the development of criteria that enable identification of most kinds of seismic events that occur at Mount St. Helens. These events include gas-and-ash explosions, volcanic earthquakes, volcanic tremor, rockfalls, debris flows, dome-building eruptions, and many types of man-made seismic noise. Identification criteria are based on comparison of signal envelope, dominant frequencies, and relative amplitudes and timing among stations.

In general, gas-and-ash explosions (vigorous venting of steam and (or) other gases and volcanic ash) at Mount St. Helens are characterized by emergent, low-frequency signals of extended duration, often with pulsating amplitude changes. The signal amplitudes from stations in the crater are much higher than those from stations on the volcano's flanks. The amplitudes from different flank stations are approximately equal.

Several factors may complicate signal identification. These include: (1) evolution of the volcanic system with time, (2) overlap of signals that are recorded close together on seismograms, and (3) the temporary loss of data from key stations. Nevertheless, we have had considerable success identifying explosions within minutes of their occurrence. The criteria used to identify gas-and-ash explosion signals at Mount St. Helens and the techniques used to develop those criteria provide a foundation for signal identification at other active volcanoes.

## INTRODUCTION

Although Mount St. Helens is the only Cascade volcano to have erupted while the Washington-Oregon regional seismic network (fig. 1) has been in operation, there are about a dozen potentially hazardous volcanoes in the Cascade Range. This volcanic chain stretches from British Columbia (Hickson, this volume) southward through Washington and Oregon and into northern California. The proximity of these volcanoes to airports (fig. 1) means that any aircraft operating in the Pacific Northwest could be at risk from volcanic ash in the air or on an airport surface. This risk is regional because an ash cloud erupted from any of the Cascade volcanoes can drift in the direction of the wind for hundreds of kilometers.

On May 18, 1980, the eruption plume from Mount St. Helens climbed to approximately 60,000 ft (18,300 m) within 10 minutes of the start of the eruption (Rosenbaum and Waitt, 1981). The ash plume spread rapidly eastward, passing Yakima, Wash. (135 km downwind), 1 hour later and reaching midcontinent by the morning of May 19. Heaviest ash fall occurred in eastern Washington (Sarna-Wojcicki and others, 1981). The ash plume disrupted air traffic throughout the region, and hundreds of commercial operations in eastern Washington were canceled owing to accumulations of ash on airport surfaces (Schuster, 1981).

The May 18 eruption clearly demonstrated how major volcanic activity can affect air traffic. But even small, short-lived, gas-and-ash explosions can create a hazard for airports and air traffic within the approach and departure paths to major metropolitan areas such as Portland and Seattle. Hundreds of gas-and-ash explosions have occurred at Mount St. Helens since 1980. These varied in size and intensity from minor events, in which small amounts of steam and entrained ash rose less than 1,000 ft above the dome (to approximately 6,800 ft above sea level), to energetic events that generated large ash plumes, which rose as high as 20,000 ft above the dome. Minor ash fall from these events was reported as far as 100 miles (160 km) downwind.

The seismic and volcanic activity at Mount St. Helens since 1980 has provided an ideal opportunity to make real-time or near-real-time correlations between seismicity and field observations. From these correlations, criteria for

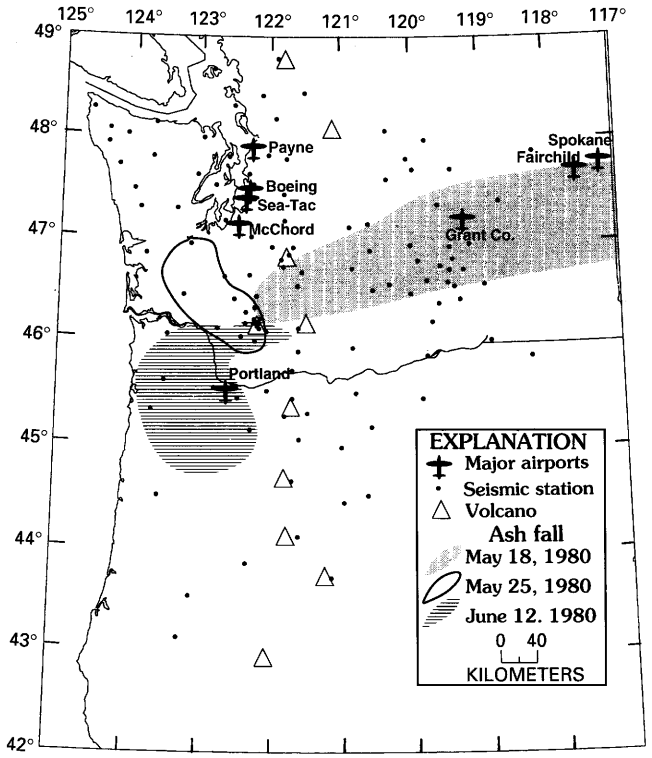


**Figure 1.** Map showing location of volcanoes, seismic stations, and major airports in Washington and Oregon. Many smaller airports (not shown) are also close to Cascade volcanoes. Areas of ash fall shown are from Mount St. Helens; dates of eruption are also shown.

identifying various types of events from their seismic signature were developed. The capability to recognize specific events when the mountain is not visible, such as during bad weather or at nighttime, greatly improves our ability to issue timely warnings about potential ash plumes.

## METHODS

In response to increased seismicity at Mount St. Helens in 1980, seismologists installed additional stations near the volcano to supplement data from the UW regional seismic network. The UW and USGS currently maintain a combined network of 18 seismic stations within 11 miles (18 km) of Mount St. Helens. At times, fewer or more stations have existed, depending on operational and research needs. Most of the stations are vertical-component seismometers with a 1-Hz response. A few stations are monitored only by the USGS Cascades Volcano Observatory (CVO) or by the UW, but most stations are monitored by both groups.

The data from all stations are recorded digitally on computer. Data from 20 to 40 percent of the stations are recorded in analog form on rotating drums called "helicorders." Although digital analysis is best for accurate location of earthquakes and some rockfalls, analog data permits rapid visual analysis of individual events and the overall pattern of seismicity.

Between 1981 and 1986, more than 3,070 seismic signals recorded on helicorders were correlated with field observations. These events included 1,376 rockfalls and avalanches (mostly in the crater), 1,277 earthquakes, and 394 gas-and-ash explosions (fig. 2). Most correlations were made by real-time radio communication with USGS-CVO field crews and pilots. Near-real-time communication with Federal Aviation Administration personnel, U.S. Forest Service observers, radar operators, the media, and the general public also provided valuable information.

By carefully observing and analyzing the seismic signals, identification criteria were developed for most event types. These criteria are based on comparisons of the shape of the signal envelope, dominant frequencies, and relative amplitudes and timing among stations located at various distances from the volcano (fig. 3).

## RESULTS AND DISCUSSION

Gas-and-ash explosion signals are usually characterized by emergent onset, whereby the amplitude of the signal builds over seconds to minutes; however, some events have more impulsive onsets or are preceded by small earthquakes. Signal frequency is relatively low and signal duration is long, lasting from a few minutes to about 30 minutes on flank stations. Occasionally, explosions are followed by hours of increased background noise and small earthquakes. Signal amplitude often increases and decreases in pulses during the event. Signal amplitudes recorded by stations located on the flanks of the volcano are roughly equal. In contrast, rockfalls from the lava dome and (or) the walls of the crater usually record at widely varying amplitudes on flank stations—the signal being largest at the station closest to the rockfall. During an explosion, signal amplitudes on stations in the crater, tens to hundreds of meters from the vent, are higher than those from stations on the flanks (fig. 4).

### CAPABILITIES

To identify a gas-and-ash explosion, the best results were obtained using four stations: one crater station, two flank stations, and one off-volcano station at least 11 miles (18 km) away. Using these stations and the above criteria, we became sufficiently skilled to recognize most gas-and-ash explosions from the seismic records during the first few minutes of the event.

During the fall and winter of 1983–84, an experienced seismic observer was stationed by the helicorders for several hours per day on most days that crews were working in the crater. The observer was responsible for rapidly evaluating all incoming signals and notifying crews of any

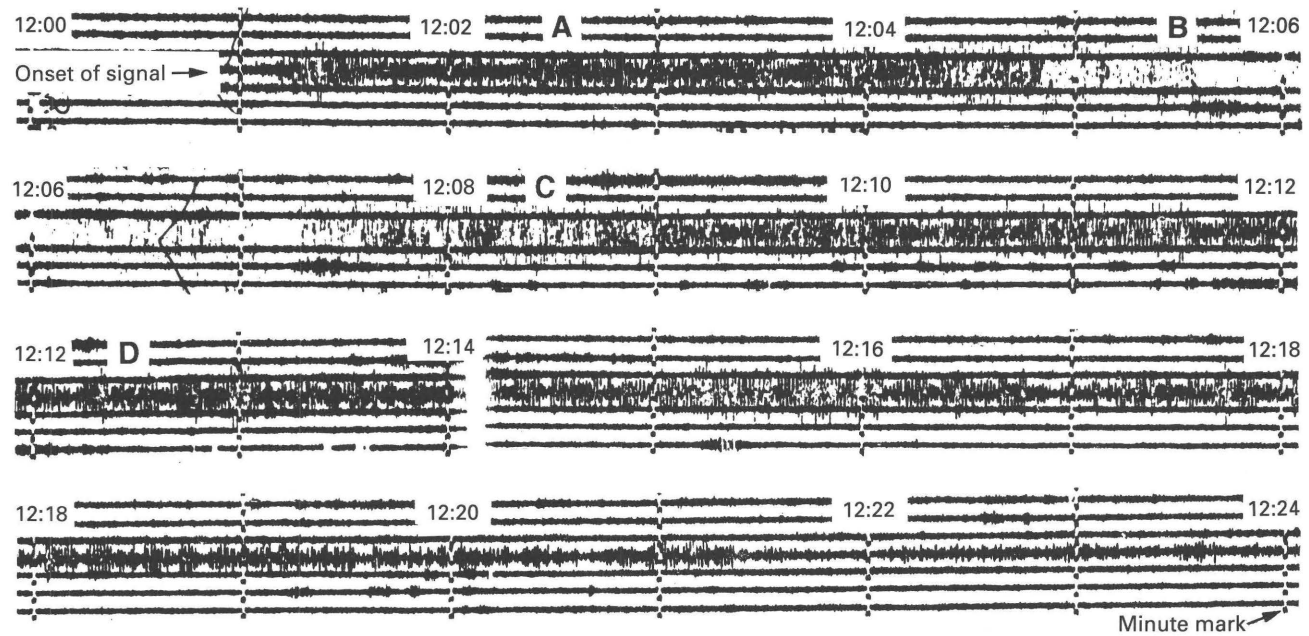


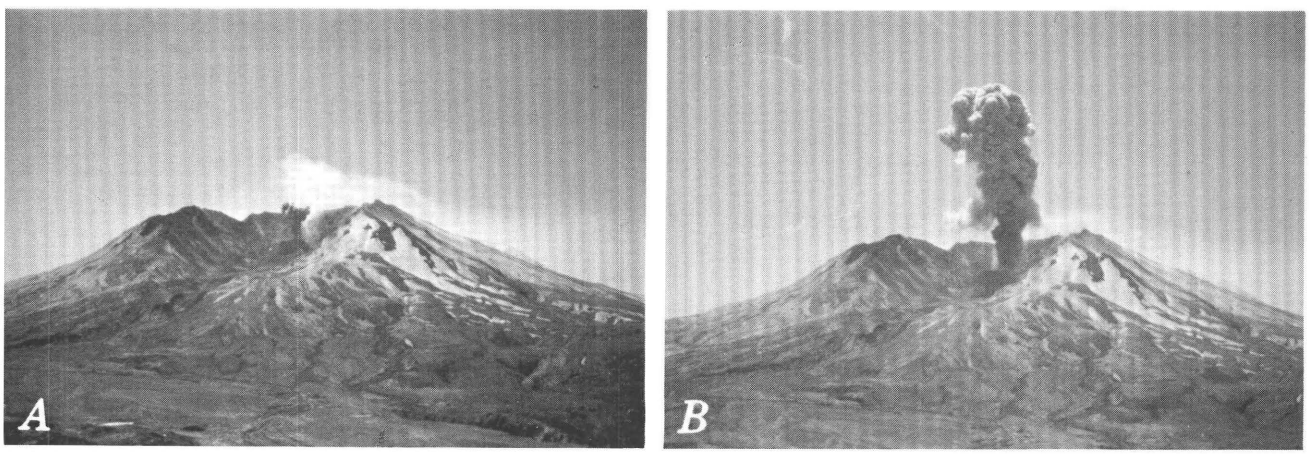


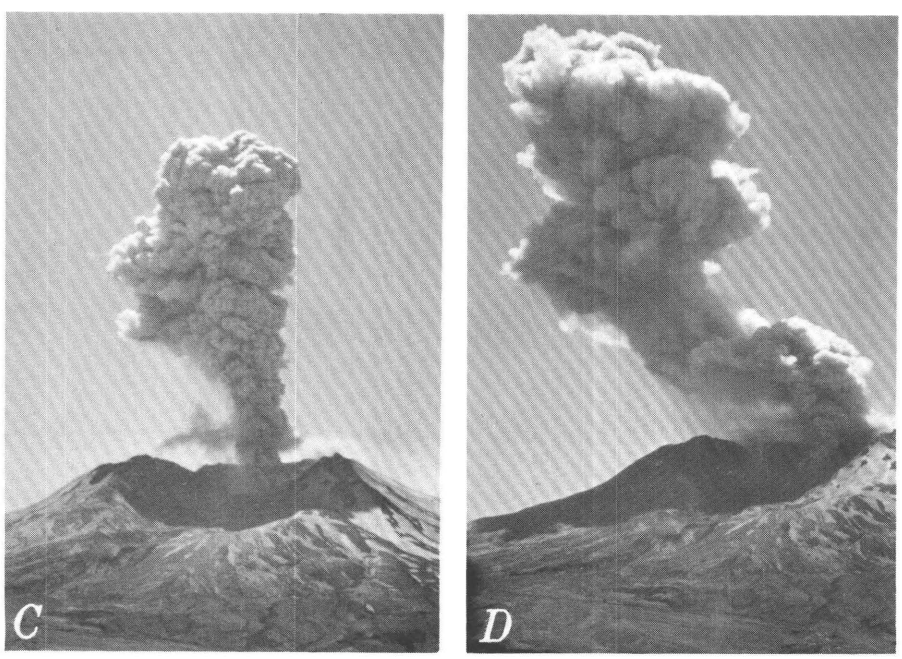


**Figure 2.** Seismic signal from gas-and-ash explosion on June 16, 1982. Tick marks on seismogram are at 1-minute intervals, beginning in the upper left part of the figure. Letters A, B, C, and D on seismogram mark the approximate time at which the corresponding photographs (*A*, *B*, *C*, and *D*) were taken. Times shown on seismogram are Pacific Daylight Time.

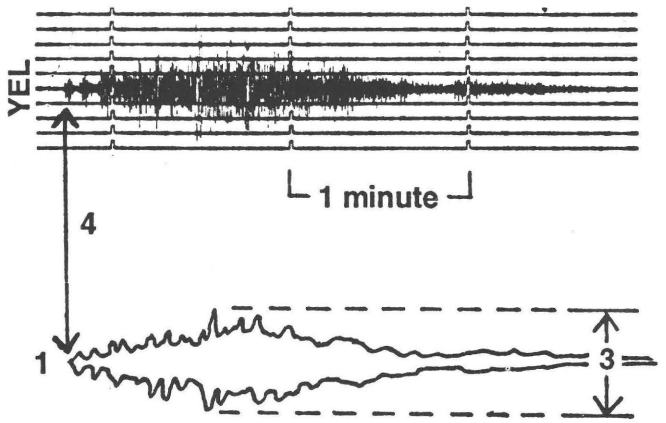


**Figure 3.** Seismic signal recorded at "yellow rock" (YEL) seismometer, which is located within the crater of Mount St. Helens (see fig. 4). Identification criteria for type of event are based on comparison of signal characteristics as follows (numbers keyed to figure): 1, shape of the signal envelope; 2, signal frequency (measured approximately by the number of times the pen crosses the "zero line"—the horizontal line traced by an undisturbed pen—during 1 minute (this is not labeled on the figure); 3, relative amplitudes among stations; and 4, relative timing of the first arrival among stations.

suspected gas-and-ash explosions. During this time, all gas-and-ash explosions that occurred were correctly identified from their seismic signals while they were occurring. In many cases, events were identified during the first 5–20 seconds, and warning was radioed to field crews before the gas-and-ash actually exited the top of the dome. Two less experienced observers who were taught to recognize these signals also had reasonable success: they did not miss any explosions, but they did radio several false alarms to field crews in the crater.

This type of continuous monitoring requires the constant surveillance by a trained observer and is too demanding to be practical on a regular basis. Normally, the helicorders are only monitored visually when USGS or UW crews are flying in or working in or near the crater or when overall levels of seismicity are elevated. A seismic alarm system (Myers and Theisen, this volume) is used to alert the scientist on duty to possible explosions at other times. Since 1984, we have continued to correctly identify most gas-and-ash explosions from seismic records, either in real time, when helicorders are visually monitored, or within minutes of checking the records, when the seismic-alarm system is used.

## LIMITATIONS AND COMPLICATIONS

Reliable signal recognition depends on experienced observers who are familiar with the character of a variety of signals from the network stations (Malone and others, 1981). During the past 10 years, a few gas-and-ash explosions have been missed or incorrectly identified, even by experienced observers. Several factors complicate rapid signal identification, including: (1) evolution of the volcanic system with time, (2) overlap of signals on the helicorder record, and (3) the temporary loss of data from key stations.

### EVOLUTION OF THE VOLCANIC SYSTEM WITH TIME

Signals generated by gas-and-ash explosions during 1982–85 tended to be more emergent and lower in amplitude than signals generated by gas-and-ash explosions of comparable height in 1986 and during 1989–91. Between October 1980 and October 1986, the lava dome grew in 16 distinct, dome-building eruptions (Swanson, 1990). The frequency of these eruptions probably helped keep the volcanic conduit relatively open. The March–April 1986 explosions, which generally had higher amplitudes and more impulsive (less emergent) signals than previous events, occurred near the end of a 1-year lull between dome-building eruptions. The 1989–91 gas-and-ash explosions (Myers, 1992), which were even higher in amplitude relative to plume height, occurred after nearly 3 years of quiescence. At least four explosion-like signals during the 1989–91 series did not generate a plume.

These changes in seismic characteristics may be associated with cooling of the dome and blocking of the conduit. Perhaps the higher amplitudes and more impulsive onsets reflect the higher energies and gas pressures required for magma to break through to the surface.

### OVERLAP OF SEISMIC EVENTS

Another factor that can complicate rapid signal identification is the overlapping of seismic signals on the helicorder. Overlap can obscure the onset, maximum signal amplitude, and shape of the seismic envelope. This overlap can be caused by (1) a single, long event that writes over portions of itself that were recorded 15 or 30 minutes earlier (one full revolution of the helicorder), (2) other events that were recorded 15 or 30 minutes before or after the event in question, or (3) several events that occur simultaneously.

Events that occur simultaneously can combine frequencies and amplitudes, producing signals that are atypical or that mimic other types of events. In the fall of 1990, the combined signal from a small distant earthquake (teleseism) and crater rockfall, which began a few seconds later, was misidentified as a gas-and-ash explosion. The distant earthquake gave the signal a low-frequency onset and similar amplitudes on the flank stations while the rockfall increased the amplitude on the crater stations. High-frequency, low-amplitude signals from an ongoing storm further complicated identification. The misidentification was recognized when the earthquake signal was identified on a regional seismic station more than 10 miles from the volcano.

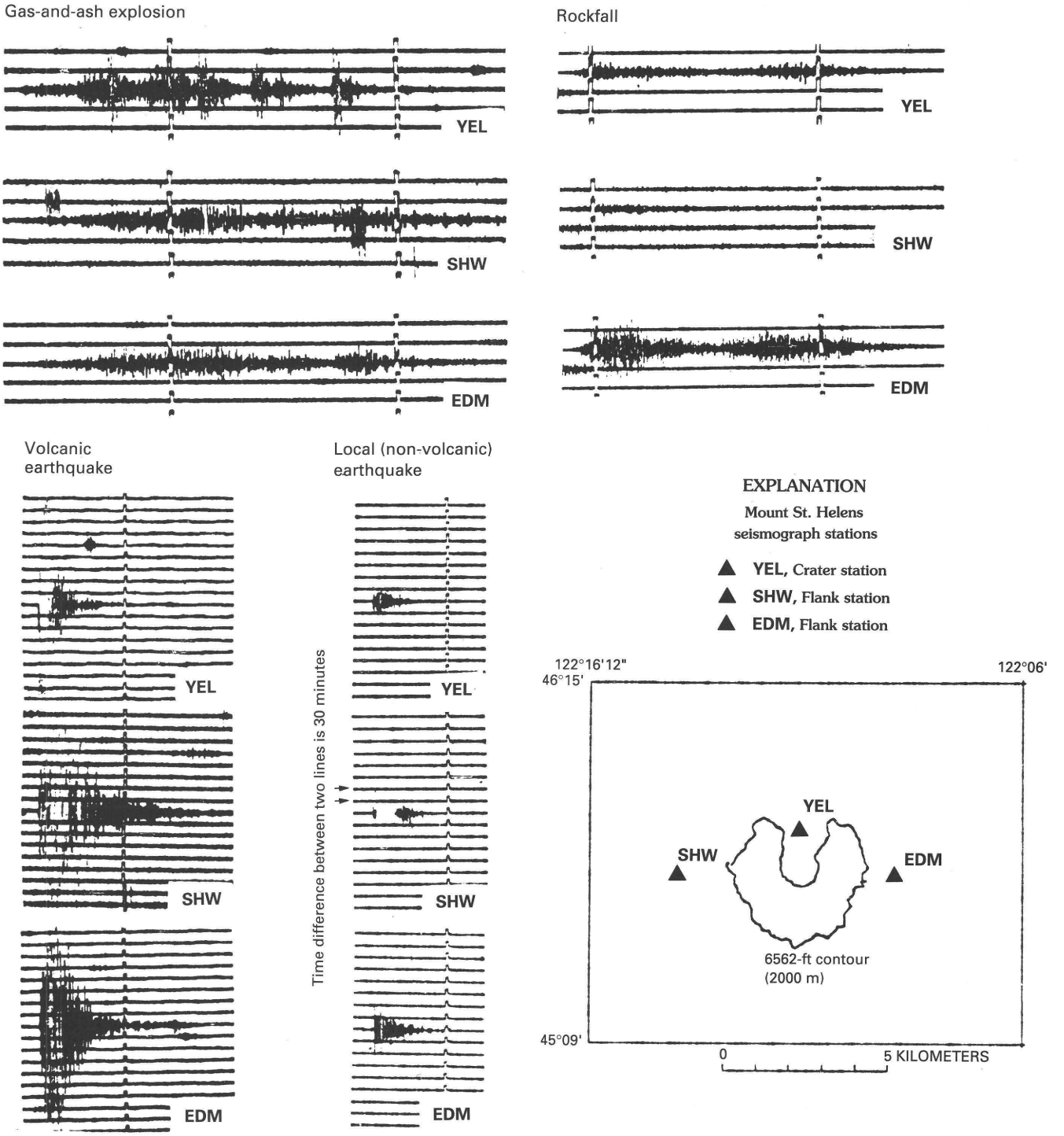


**Figure 4.** Examples of characteristic seismic signals for gas-and-ash explosions, rockfalls, and earthquakes at Mount St. Helens. Tick marks are at 1-minute intervals. Note the differences in signal amplitudes and relative timing at flank and crater stations during the explosion compared to the rockfall. Explosion signals have a higher amplitude at the crater station (YEL) than at flank stations; flank stations (EDM, SHW) show similar amplitudes. The amplitude of a rockfall signal is highest at the station closest to the rockfall. It is often possible to see differences in first-arrival times among stations during a rockfall—this is rarely possible with close stations during explosions. Explosion and rockfall signals are normally more emergent than earthquake signals.

**Table 1.** Approximate event counts, by event type, at five Cascade volcanoes, 1989–90.

| Volcano | Explosions | Earthquakes | Rockfalls | Ice quakes | Lahars |
|---|---|---|---|---|---|
| Mount St. Helens | $10^2$ | $10^4$ | $10^4$ | 0 | $10^1$ |
| Mt. Rainier | 0 | $10^2$ | $10^2$ | $10^3$ | $10^1$ |
| Mt. Hood | 0 | $10^1$ | 0 | $10^1$ | 0 |
| Mt. Baker | 0 | $10^1$ | $10^1$ | $10^3$ | 0 |
| Mt. Adams | 0 | $10^1$ | $10^1$ | $10^1$ | $10^1$ |

### LOSS OF DATA FROM KEY STATIONS

If data are lost from one or more stations normally used to identify differences among signal characteristics, identification can be difficult. For example, loss of data from either of the flank stations "east dome" (EDM) or "St. Helens west" (SHW) (see fig. 4) prevents comparison of their relative signal amplitudes, making it hard to distinguish explosions from rockfalls. Without data from a distant station, the misidentification of the small teleseism mentioned above would not have been corrected.

## REGIONAL APPLICATIONS

The UW also operates one or more seismic stations at or near nine other Cascade volcanoes, and, during the past few years, seismologists have established and compared "background" levels of seismicity at several of these volcanoes (table 1). At each volcano, signals that are larger than a pre-set threshold are categorized using the identification criteria discussed in this paper. Correlation of signals and field observations is done when practical; signals from debris flows and rockfalls exhibit similar characteristics at different volcanoes (Jonientz-Trisler and Qamar, 1989; R.D. Norris, oral commun., 1992). Even though the skill to interpret seismic signals at one volcano can be successfully applied to another volcano (Weaver and others, 1990), the cause may differ from volcano to volcano. If levels of seismicity increase above background at a volcano, more stations can be installed to improve the ability to interpret signals and locate events.

# CONCLUSIONS

By careful correlation of seismic events with field observations at Mount St. Helens, criteria have been developed for identifying gas-and-ash explosions and other volcanic or seismic events from the analog seismic record. Several seismic stations are needed to compare signal characteristics among stations. Use of the criteria allows rapid, accurate identification of events when the volcano is not visible owing to weather conditions or darkness.

The technique can be used by inexperienced observers if guidelines and samples of characteristic seismic signals from several stations are provided. But when signals are obscured by other events or data is missing from key stations, interpretation can be difficult, even for experienced observers.

Seismic signals at other Cascade volcanoes have been compared to visual observations when possible. These signals display similar characteristics to signals of similar events at Mount St. Helens. The criteria used to identify gas-and-ash explosion signals at Mount St. Helens and the techniques used to develop those criteria will help provide a foundation for signal identification at other active volcanoes.

# REFERENCES CITED

Jonientz-Trisler, Chris, and Qamar, A., 1989, Debris flow seismograms from Mount Rainier and Mount Adams [abs]: Eos, Transactions, American Geophysical Union, v. 70, p. 1190.

Malone, S.D., Endo, E.T., Weaver, C.S., and Ramey, J.W., 1981, Seismic monitoring for eruption prediction, *in* Lipman, P.W., and Mullineaux, D.R., eds., The 1980 Eruptions of Mount St. Helens, Washington: U.S. Geological Survey Professional Paper 1250, p. 803–813.

Myers, Bobbie, 1992, Small explosions interrupt 3-year quiescence at Mount St. Helens, Washington: Earthquakes & Volcanoes, v. 23, no. 2, p. 58–72.

Rosenbaum, J. G., and Waitt, R.B., 1981, Summary of eyewitness accounts of the May 18 eruption, *in* Lipman, P.W., and Mullineaux, D.R., eds., The 1980 Eruptions of Mount St. Helens, Washington: U.S. Geological Survey Professional Paper 1250, p. 53–67.

Sarna-Wojcicki, A.M., Shipley, S., Waitt, R.B., Dzurisin, D., and Wood, S.H., 1981, Areal distribution, thickness, mass, volume, and grain size of air-fall ash for the six major eruptions of 1980, *in* Lipman, P.W., and Mullineaux, D.R., eds., The 1980 Eruptions of Mount St. Helens, Washington: U.S. Geological Survey Professional Paper 1250, p. 577–600.

Schuster, R. L., 1981, Effects of the eruptions on civil works and operations in the Pacific Northwest, *in* Lipman, P.W., and Mullineaux, D.R., eds., The 1980 Eruptions of Mount St. Helens, Washington: U.S. Geological Survey Professional Paper 1250, p. 701–718.

Swanson, D.A., 1990, A decade of dome growth at Mount St. Helens, 1980–1990: Geoscience Canada, v. 17, no. 3, p. 154–157.

Weaver, C.S., Norris, R.D., and Jonientz-Trisler, C., 1990, Results of seismological monitoring in the Cascade Range, 1962–1989: Earthquakes, eruptions, avalanches and other curiosities: Geoscience Canada, v. 17, no. 3, p 158–162.

VOLCANIC ASH AND AVIATION SAFETY:
Proceedings of the First International Symposium
on Volcanic Ash and Aviation Safety
U.S. GEOLOGICAL SURVEY BULLETIN 2047

# INFRASONIC AND SEISMIC DETECTION OF EXPLOSIVE ERUPTIONS AT SAKURAJIMA VOLCANO, JAPAN, AND THE PEGASAS-VE EARLY-WARNING SYSTEM

*By* Kosuke Kamo, Kazuhiro Ishihara, *and* Makoto Tahira

## ABSTRACT

More than 6,000 explosive, summit eruptions have taken place at Sakurajima Volcano, Kyushu, Japan since 1955. The explosions can be predicted using tilt and strain data obtained near the summit area and from swarms of shallow seismic events generated beneath the active crater. The onset of explosions is detected by explosion earthquakes, by the air-shocks accompanying them, and by visual observation. The success rate of the automated warning system for strong eruptions is more than 80 percent.

Explosive eruptions at Sakurajima Volcano also have been detected frequently by infrasonic waves using an array of low-frequency microphones at Kariya, Aichi, 710 km from the volcano. The infrasonic system at Kariya is capable of detecting air waves generated by eruptions from volcanoes at distances of as much as 1,200 km. This capability forms the basis of a proposal for a worldwide network of air-wave sensors to monitor volcanic explosions. A scheme, PEGASAS-VE (pressure gage system for air-shocks by volcanic eruptions), is proposed for the acquisition of information on eruption locations and their estimated magnitudes. The scheme would be a very effective means of enhancing aviation safety and would be similar to the tsunami warning system, which is in worldwide operation.

## INTRODUCTION

Extensive studies have been undertaken at Sakurajima Volcano since 1960 to investigate the eruption mechanisms and to identify the precursors necessary for reliable prediction of the explosive eruptions (Kamo, 1978). Recent progress has made possible the prediction of explosive eruptions with high precision. The prediction techniques at Sakurajima, therefore, should provide useful information for aviation safety. Recent results from these studies of detection and prediction of summit eruptions at Sakurajima by the Sakurajima Volcanological Observatory of Kyoto University, are discussed in the first part of this paper.

One notable aspect of explosive eruptions is the release of air-shock waves. Detection of such waves is, therefore, an important way to record explosive, ash-producing eruptions. A combination of pressure sensors and seismographs at Sakurajima is used for identification of explosive eruptions. The air-shocks are also detectable at very large distances because they propagate in the atmosphere as infrasonic waves. Air-shocks generated by eruptions at Sakurajima have been observed frequently at Kariya, 710 km from the volcano (Tahira, 1981, 1988). The possibility of detecting volcanic eruptions using a system of infrasonic microphones within a large area has been discussed by Tahira and others (1988). Remarkable infrasonic signals associated with the eruptions of Mt. Pinatubo, in June 1991, were recorded by the infrasonic system at Kariya. A brief description of the recorded signals from Pinatubo is presented in this paper. The principles and results of observations at Kariya are described in the second part of this paper, and a system called PEGASAS-VE is proposed for simultaneous monitoring of many volcanoes and is suggested as a possible technique to reduce the threat that volcanic eruptions pose to aviation.

## DETECTION AND PREDICTION OF EXPLOSIVE ERUPTIONS AT SAKURAJIMA

An explosive eruption is accompanied not only by the ejection of volcanic bombs and ash but also by air-shocks and an explosion earthquake that originates beneath the active crater. The onset time and intensity of volcanic explosions at both Sakurajima and Suwanosejima Volcanoes have been monitored using a combination of seismometers and infrasonic microphones installed at distances of 2–5 km from the active craters (Iguchi and Ishihara, 1990). Data collected

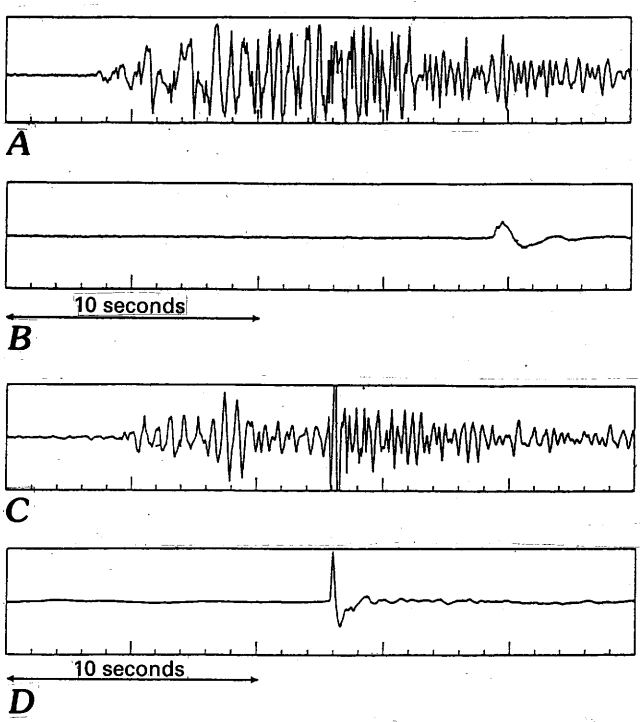


**Figure 1.** Examples of records of (1) the vertical component of explosion earthquakes, which originate beneath the summit crater, and (2) air-shocks. *A*, Explosion-earthquake record at Sakurajima Volcano (seismograph located 2.9 km from summit crater); *B*, Air-shock record at Sakurajima Volcano (infrasonic microphone located 5.5 km from summit crater); *C*, Explosion-earthquake record at Suwanosejima Volcano; *D*, Air-shock record at Suwanosejima Volcano. Both the seismograph and infrasonic microphone at Suwanosejima (*C* and *D*, respectively) are located 3.3 km from summit crater.

at Suwanosejima Volcano are transmitted through telephone networks to the Sakurajima Volcanological Observatory using a personal-computer communication system. Examples of seismic and infrasonic records at Sakurajima and Suwanosejima Volcanoes are shown in figure 1.

Kamo (1978) noticed from a series of observations at Sakurajima that successive explosive eruptions are preceded by a swarm of shallow, B-type earthquakes, and prediction of explosive eruptions has been attempted by monitoring these volcanic earthquakes. Ishihara and Iguchi (1989) classified B-type earthquakes into two types, BH and BL, by the dominant frequency of the seismic waves. BH earthquakes are related to the intrusion of magma into the conduit, and BL earthquakes are related to the movement of magma up to the summit crater. There is a good correlation between swarms of B-type earthquakes, in July to November 1987, with increases of explosion events at Sakurajima (fig. 2). Nineteen swarms and 87 explosions were observed during this period. Seventy explosions out of 87 occurred within a week after swarms of B-type earthquakes. Note that no swarms or explosions were observed from the end of September through October 1987. Uhira and Ueda (1988) examined the correlation between explosions at Sakurajima and swarms of B-type earthquakes for a longer period, from 1984 to 1988. They found that more than 80 percent of explosions originated within a week after swarms of B-type earthquakes.

To investigate eruption mechanisms and to establish a reliable prediction technique, Kamo and Ishihara (1989) have made detailed measurements of tilt and strain of the summit area of Sakurajima Volcano. An underground tunnel was constructed in a lava dome 2.8 km northwest of the summit crater, and a two-component water-tube tiltmeter and a three-component extensometer were installed inside the tunnel.

A characteristic inflation, which occurs shortly before summit eruptions, followed by deflation after eruption, has been noted. The duration of inflation ranges from several minutes to several hours. The inflation is interpreted to be caused by intrusion of magma into a shallow magma reservoir beneath the crater. The amount of ground deformation does not correspond necessarily to explosivity, but it is related to the total amount of volcanic ejecta (Ishihara, 1988).

An automated warning system has been developed, on the basis of the above-mentioned relationships, to assess eruptive activity at Sakurajima Volcano from the trend of deformation (fig. 3). The ground-deformation data are recorded continuously by a personal computer, and one of three levels of alarm (caution, critical, and warning) are issued when the amount of ground-tilt reaches 0.01, 0.05, and 0.1 microradians, respectively. The data and results of the assessment are displayed on a computer monitor screen in real time. The results of the automated warning system are shown in table 1 for the period from January 1987 through May 1991. Using this system, the prediction rate for the strong explosions with air-shocks that exceed 200 Pa (2 mb) is exceptional (87 percent). The exact onset time of eruption cannot be predicted at present because the amount of inflation that triggers an eruption changes from case to case.

## DETECTION OF DISTANT VOLCANIC EXPLOSIONS WITH INFRASONIC TECHNIQUE

Shock waves released into the air by explosive eruptions propagate without substantial loss of energy for long distances in the atmosphere as infrasonic waves. Infrasonic waves can be detected by using a set of sensitive infrasonic microphones at a station hundreds of kilometers away from the volcano (Goerke and others, 1965; Wilson and others, 1966; Wilson and Forbes, 1969). Infrasonic waves from summit eruptions at Sakurajima Volcano have been recorded frequently at Kariya (Tahira, 1982, 1988; Ishihara and others, 1986).

The infrasonic observation system operating at Kariya (fig. 4) consists of an array of three, low-frequency capacitor microphones installed on the ground at a spacing of

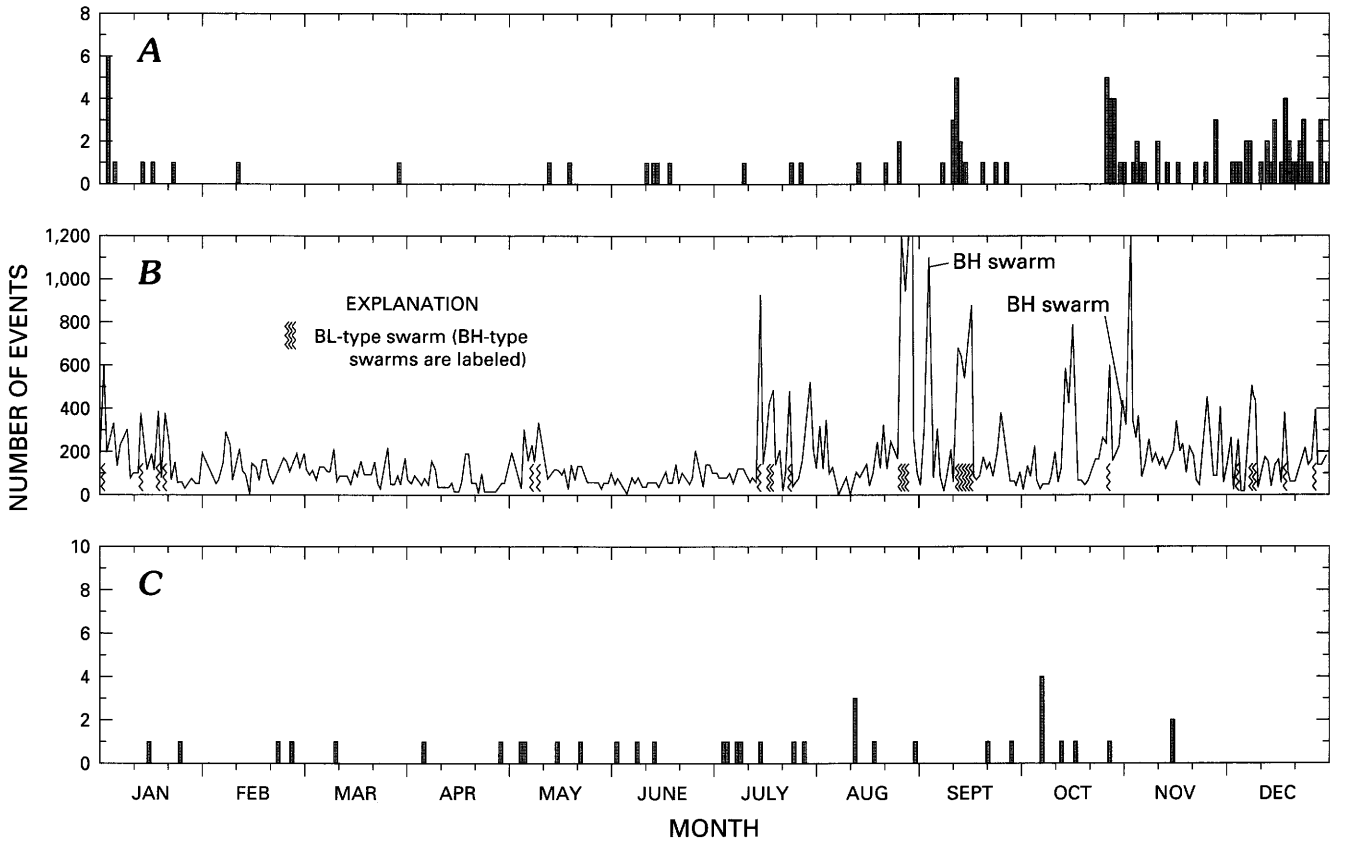


**Figure 2.** Number of events at Sakurajima Volcano during 1987. *A*, volcanic explosions; *B*, shallow, B-type volcanic earthquakes (depth < 3 km); *C*, deep, A-type earthquakes (depth between 1 km and 15 km).

**Table 1.** Results of automated warning system at Sakurajima Volcano, Japan, for the period from January 1987 through May 1991.

[Prediction rate refers to prediction rate for explosive eruptions. Comments in "remarks" column refer to level of alarms issued prior to explosive eruption. min., minimal]

| Explosive eruptions | | State of deformation at time of explosion | | | | |
|---|---|---|---|---|---|---|
| Intensity of air-shocks[1] (mb) | Number of explosions | Eruption (deflation) (%[2]) | Non-eruption (min. change) (%[2]) | Pre-eruption (inflation) (%[2]) | Prediction rate (%) | Remarks |
| ≤ 0.9 | 169 | 4 | 16 | 80 | 34 | "Caution" for 37 explosions. "Critical" for 11 explosions. "Warning" for 9 explosions. |
| 1.0–1.9 | 129 | 2 | 7 | 91 | 61 | "Caution" for 63 explosions. "Critical" for 12 explosions. "Warning" for 4 explosions. |
| 2.0–2.9 | 65 | 0 | 0 | 100 | 81 | "Caution" for 43 explosions. "Critical" for 8 explosions. "Warning" for 2 explosions. |
| 3.0–3.9 | 27 | 0 | 0 | 100 | 100 | "Caution" for 15 explosions. "Critical" for 11 explosions. "Warning" for 1 explosion. |
| ≥ 4.0 | 3 | 0 | 0 | 100 | 100 | "Critical" for 2 explosions. "Warning" for 1 explosion. |

[1] Approximate. Observed at 2.7 km from the summit crater.
[2] Percent of number of explosions.

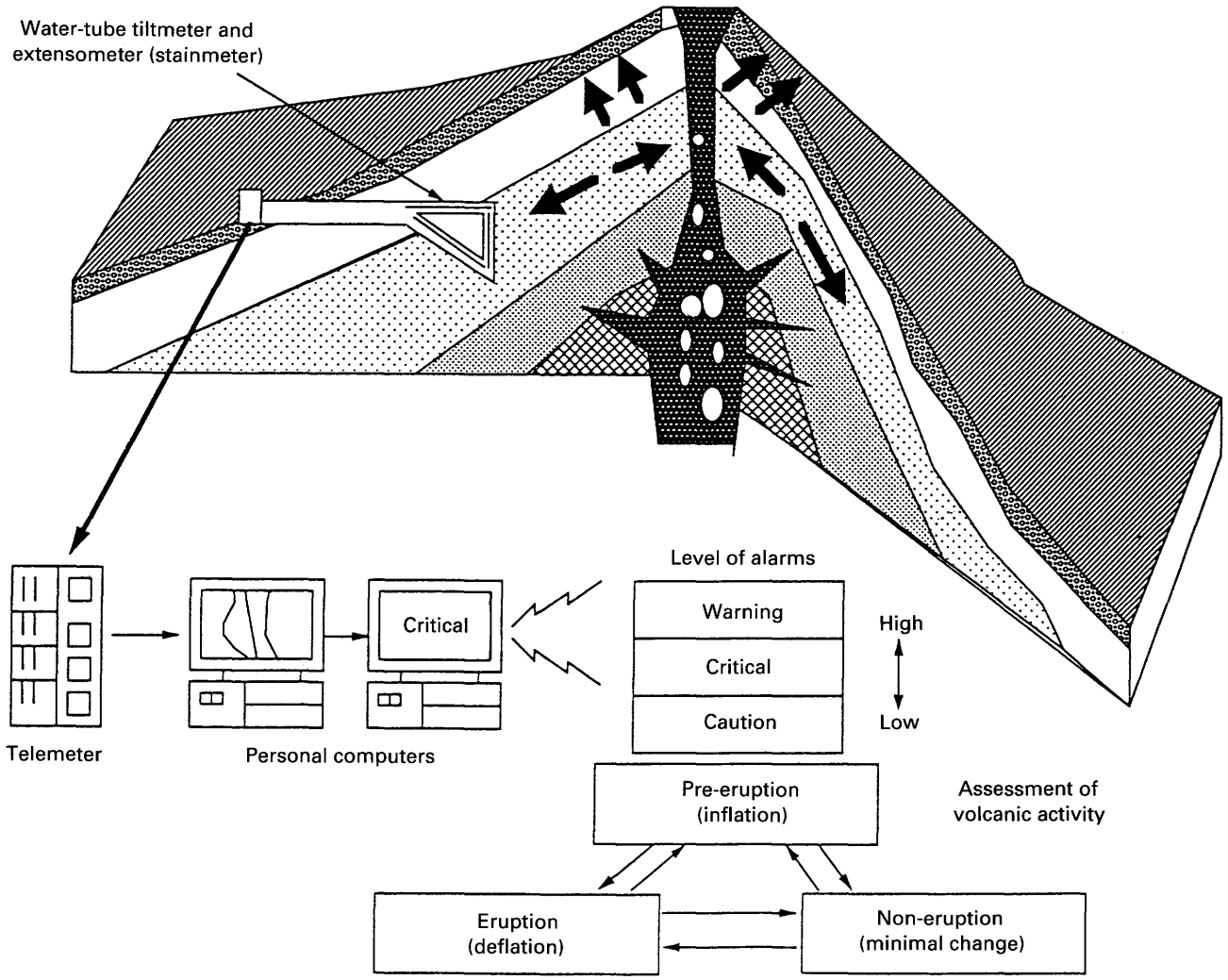


**Figure 3.** Schematic diagram of underground installation of tiltmeter and extensometer at Sakurajima Volcano. Alarm system is also shown.

470–580 m and a system for recording and analysis. The frequency range of the microphone is 0.04–1 Hz. Because the amplitude of the infrasound signals from distant volcanoes is commonly, but not always, well below the level of irregular noise caused by local atmospheric turbulence such as wind noise, a "line microphone" (Tahira, 1981) is attached to each microphone to reduce wind noise. The line microphone is made up of a number of vinyl-chloride pipes, 5 cm in diameter, arranged parallel to each other and connected to the central box containing the infrasonic microphone (fig. 5). The ends of each pipe are terminated by a capillary inlet opening, and the pressure fluctuations at the openings are propagated in the pipe and mixed in the central box, thus yielding spatially averaged pressure changes. Irregular wind noise is weakened considerably by this averaging process, but infrasonic waves of much longer wavelengths can survive the spatial averaging effect of the line microphone, thereby improving the signal-to-noise ratio.

The noise reducer used at Kariya takes a line average of the pressure field over a length of 100 m along the ground. Infrasonic signals transmitted to the recording room by wire transmission lines are recorded continuously on a magnetic, analog data recorder together with the time-code signal. The data also are recorded on a pen oscillograph for the purpose of visual monitoring. The corresponding portion of the magnetic tape is replayed and analyzed in detail by a personal computer when a similar waveform is found in the three channels. A computer program is provided to calculate the cross-correlation coefficient between every pair of channels from which optimum time lags of the signal traversing the microphone array are obtained. The speed and direction of arrival of the signals then are computed, taking into account the geometry of the tripartite array of the microphones. The association of the recorded infrasonic signals with an eruption is established easily from information on the direction of arrival once the source volcano and its eruption time are identified from other information. The association is also

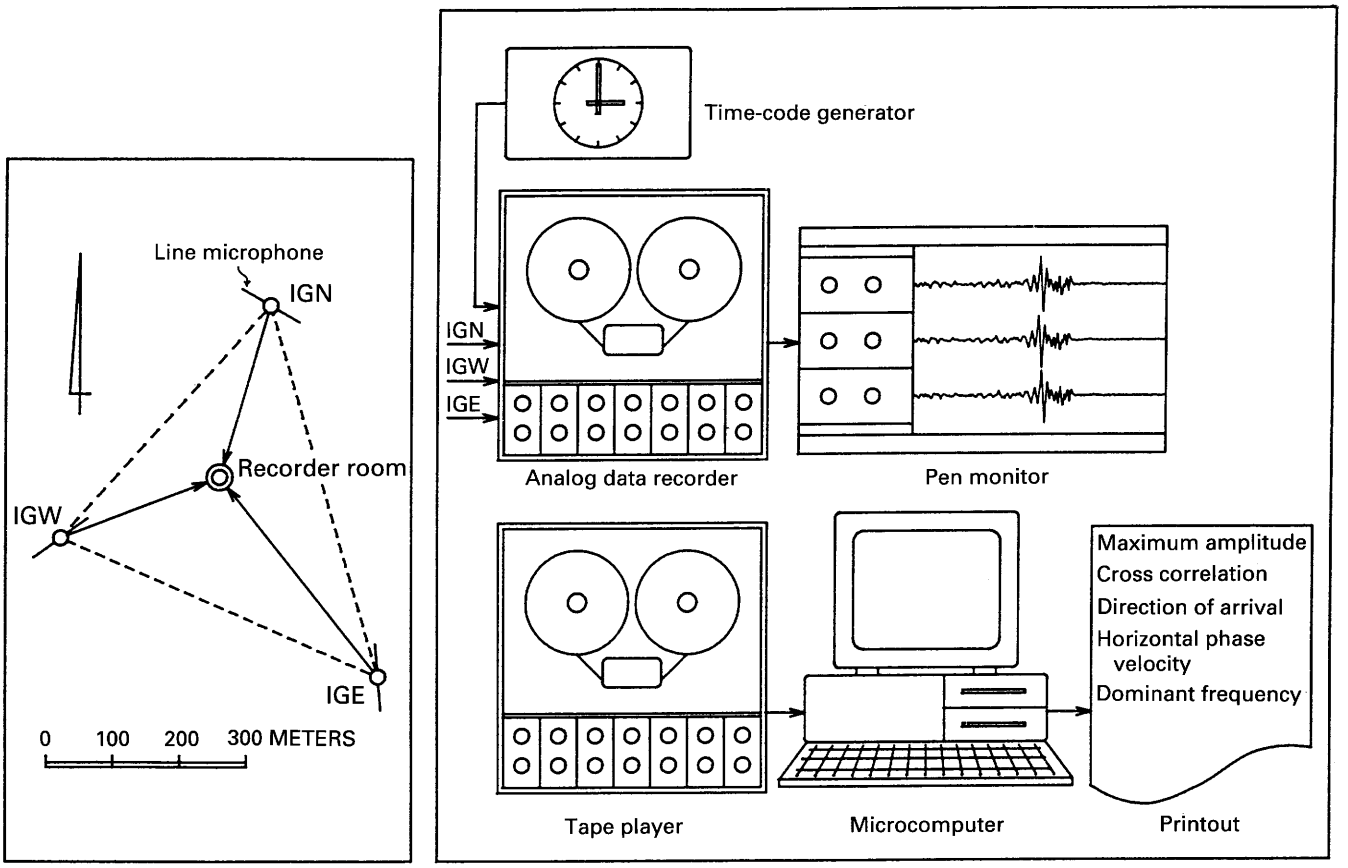


**Figure 4.** Infrasonic observation system currently operating at Kariya, Japan (lat 35.05°N., long 137.05°E.). A map of the microphone array is shown on the left, and a schematic diagram of the recording and analyzing system is on the right. IGN, IGW, and IGE are infrasonic microphone stations at Kariya.

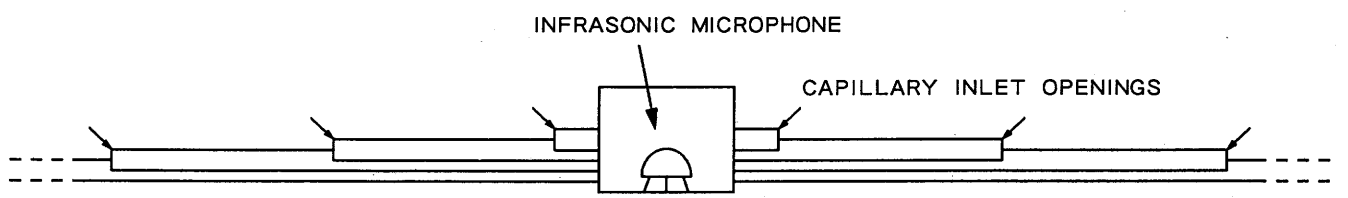


**Figure 5.** Schematic view of the multi-pipe line microphone used in the Kariya infrasonic system. Only a few pipes are illustrated here for simplicity, but the prototype has 13 pipes on each side and takes the spatial average of the pressure field over a length of 100 m.

checked from the arrival time of the infrasonic signals by seeing if this is reasonable for the source-receiver distance and speed of sound in the atmosphere. An example of the infrasonic wave generated by a summit explosion of Sakurajima Volcano is shown in figure 6.

The detection rate of the infrasonic system at Kariya for explosions at Sakurajima Volcano increases with the strength of explosion and reaches 81 percent for strong explosions that produce air-shocks greater than 400 Pa at the seismic station HAR, which is located about 2.7 km from the active crater (Tahira and others, 1988). One of the notable aspects of the infrasonic waves recorded at Kariya from explosive eruptions at Sakurajima is that two or more wave packets are frequently observed from a single eruption. Propagation paths for these infrasonic signals were studied by Tahira (1982) using a ray-tracing technique, and it has been shown that three different sound channels are possible from Sakurajima to Kariya, depending on the vertical profile of atmospheric temperature and winds. The lowest channel is formed between the ground and upper troposphere in which acoustic signals are propagated at a speed of 340–350 m/sec. Infrasonic waves take longer when propagated by downward refraction at higher altitudes, giving rise to apparent speeds of approximately 310 m/sec for stratospheric refraction and 260–280 m/sec for lower tropospheric refraction.

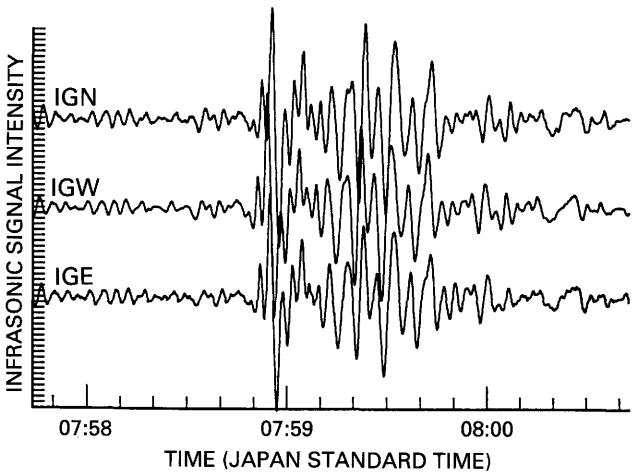


**Figure 6.** An example of the infrasonic signal at Kariya originating from a summit explosion of Sakurajima Volcano on November 21, 1986. Kariya is 710 km from Sakurajima. IGN, IGW, and IGE are infrasonic microphone stations at Kariya. Scale divisions on vertical axis are in 1-μb increments.

Infrasonic signals from eruptions of other volcanoes in Japan have been recorded by the microphone array at Kariya, including the 1983 eruption of Asamayama (200 km away), the 1986 eruption of the submarine volcano at Fukutoku-Okanoba (1,270 km away), the 1986 and 1987 eruptions of Izu-Oshima (215 km away) (Tahira and others, 1990), and the 1989 eruption of the submarine volcano near Ito (190 km away from Kariya).

## INFRASONIC SIGNALS FROM PINATUBO

Remarkable infrasonic signals were recorded at Kariya during the eruptions of Mt. Pinatubo in the Philippines on June 14–15, 1991. The direction of arrival of these infrasonic signals is SSW.–SW. and roughly coincides with the great-circle bearing of Pinatubo (i.e., 221° as measured clockwise from north). The time sequence (in Universal Time Code—UTC) of the infrasonic events at Kariya was examined by analyzing recorded data at successive 2-minute intervals. The results are shown in figure 7. The arrival of infrasonic waves is evident on figure 7 during the following intervals (in UTC): (A), June 14, 18:16–18:38; (B), June 14, 20:02–20:42; (C), June 14, 21:42–22:18; (D), June 15, 00:46–00:58; (E), June 15, 08:26–19:02. Additional infrasonic signals are observed also around 06:08, 06:52, 07:46, and 08:02 (UTC) on June 15. However, no further analyses for these signals were attempted because their exact onset times are not clear due to wind noise. The time sequence of infrasonic events (A)–(E) were compared with that of reported eruptions at Pinatubo (Smithsonian Institution, 1991). Eruption times are shown by the arrows in the left-hand column of figure 7. The onset of infrasonic

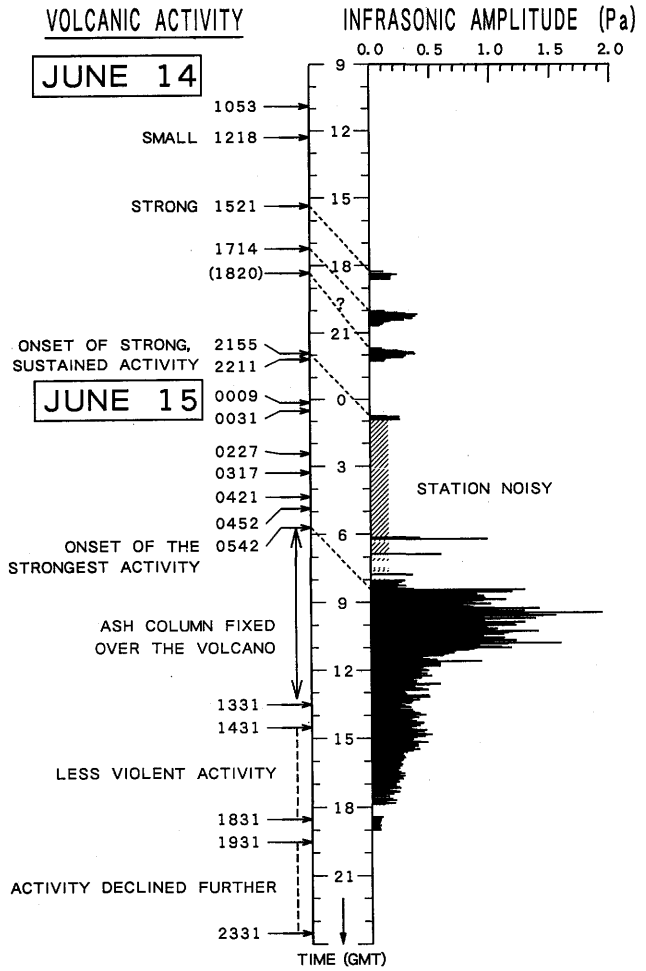


**Figure 7.** Association of the infrasonic events at Kariya with explosions of Mt. Pinatubo, Philippines, on June 14–15, 1991. Thick bars perpendicular to the time axis on right-hand part of figure indicate infrasonic arrivals; bar length shows amplitude. Hachured parts indicate the time during which reliable infrasonic observations were not possible due to severe wind noise. Actual eruption times are shown by arrows on the left-hand side of the figure. Onset times of infrasonic events are connected with corresponding eruptions by dotted lines.

events at Kariya are preceded by notable eruptions by between 2 hours 44 minutes and 2 hours 55 minutes, except for one case. The onset times of infrasonic events are connected with corresponding volcanic eruptions by dotted lines in figure 7.

The travel speed computed using these time lags and the distance between Kariya and Pinatubo (2,770 km) falls in the range from 264 to 282 m/sec. These speeds are commonly observed for infrasonic signals from the eruptions of Sakurajima Volcano in summer months when they are propagated by repeated reflections and refractions between the Earth's surface and lower thermosphere (Tahira, 1988).

The correspondence of infrasound with volcanic activity is questionable for signal (C). Its travel time would be 3 hours 22 minutes if the signal was generated by the eruption

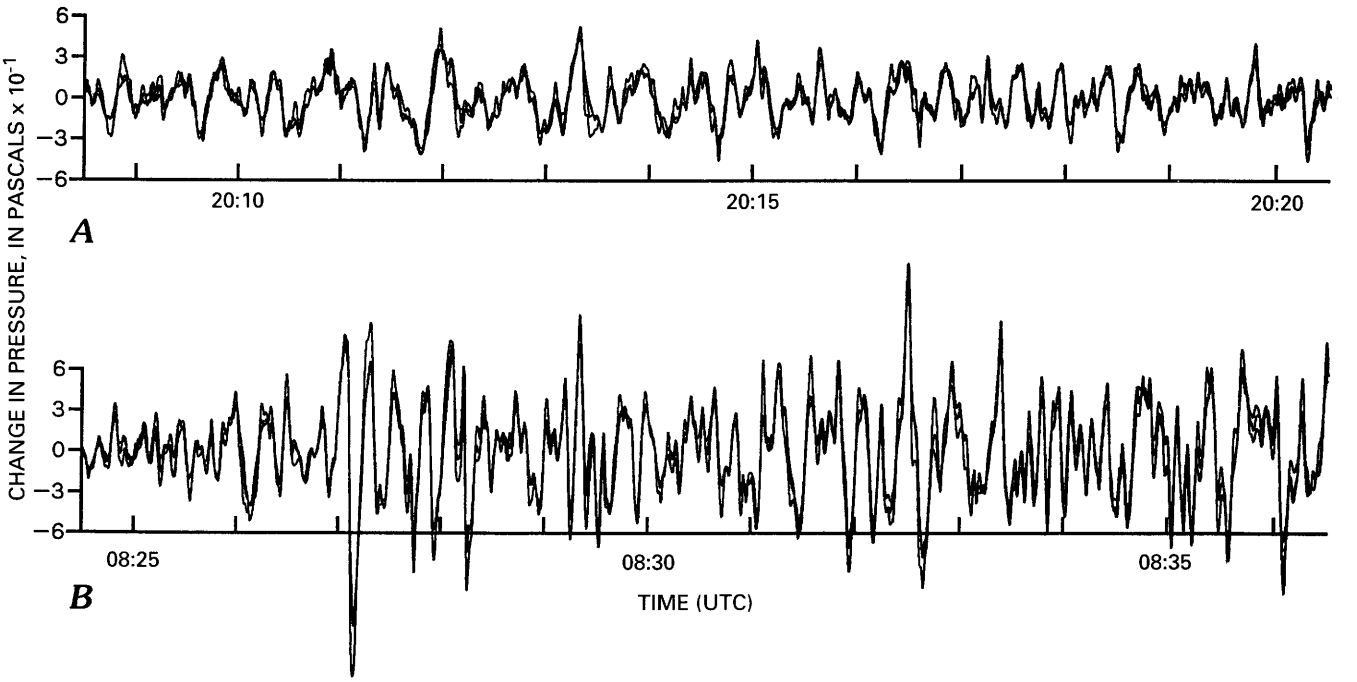


**Figure 8.** Examples of infrasonic signals recorded at Kariya, Japan, from the 1991 eruptions of Mt. Pinatubo, Philippines. Traces of the output data from three microphones are superposed after shifting the time axis to achieve the best phase match. See text for discussion. *A*, infrasonic signals for June 14, 1991; *B*, infrasonic signals for June 15, 1991.

reported to have occurred at 18:20 UTC. However, this is somewhat too long, and we believe that the explosion causing this infrasonic signal must have taken place between 18:47 UTC and 18:58 UTC on June 15. A major eruption was recorded at 18:57 UTC on June 15, according to eruption data based on the observations at a temporary station by PHIVOLCS (R. Punongbayan, oral commun., 1991). This occurrence time is well within the reasonable range to interpret our infrasonic signal (C).

The highest infrasonic activity was recorded from 08:26 UTC through 11:10 UTC on June 15, when amplitudes frequently exceeded 1 Pa. The activity then began to decrease, and the amplitude decreased to as low as 0.1 Pa by 19:00. The infrasonic signals, starting at 08:26 UTC is reproduced in figure 8*A* and may be compared with a less intense signal, at an early stage, at about 20:15 UTC on June 14 (fig. 8*B*). The onset time of the strongest eruptions of Pinatubo was 05:42 UTC on June 15. This time corresponds well with the onset of the largest infrasonic disturbances. The ash column was reported to have remained fixed over the volcano until 13:30 UTC, but our infrasonic data suggest that the climactic eruptions lasted only until around 08:00 UTC and that, thereafter, the eruption subsided gradually. Weak infrasonic signals were again recorded at Kariya about 36 hours after the onset of the strong eruption, at 05:42 UTC, and lasted about 8 hours. These later signals are inferred to be the ones propagated to Kariya via an antipodal path (A2 waves). More detailed analyses of the Pinatubo infrasonic waves will be published separately.

## PEGASAS-VE

Two or more infrasonic microphone arrays, operated 500–1,000 km apart, permit independent determination of the source location by extrapolation of the direction of arrival at different arrays. This leads to the proposal for a worldwide network of infrasonic microphone arrays to continuously monitor the volcanic eruptions in a wide area. The proposed system is called pressure gage system for airshocks by volcanic eruptions (PEGASAS-VE) and is shown diagramatically in figure 9.

Each array consists of three or more infrasonic microphones with wind-noise-reducing pipes, a time-code generator, and a personal computer. The personal computer continuously records small pressure changes picked up by the microphones. The incidence of the traveling signal is confirmed, and then the direction of arrival, horizontal phase velocity, occurrence time, and signal amplitude are computed. The results are transmitted automatically to a central station where the source location of the signal is estimated from data sent by other array stations.

Appropriate information would be given to the aviation system when a large eruption is detected. The information includes the time and place of the possible eruption and its explosivity. A satellite telemetry system such as Argos, making use of NOAA polar-orbiting satellites, can be useful to collect information from each infrasonic station and to transmit the result of analysis to the aviation system (Cauzac and others, this volume). The PEGASAS stations should be

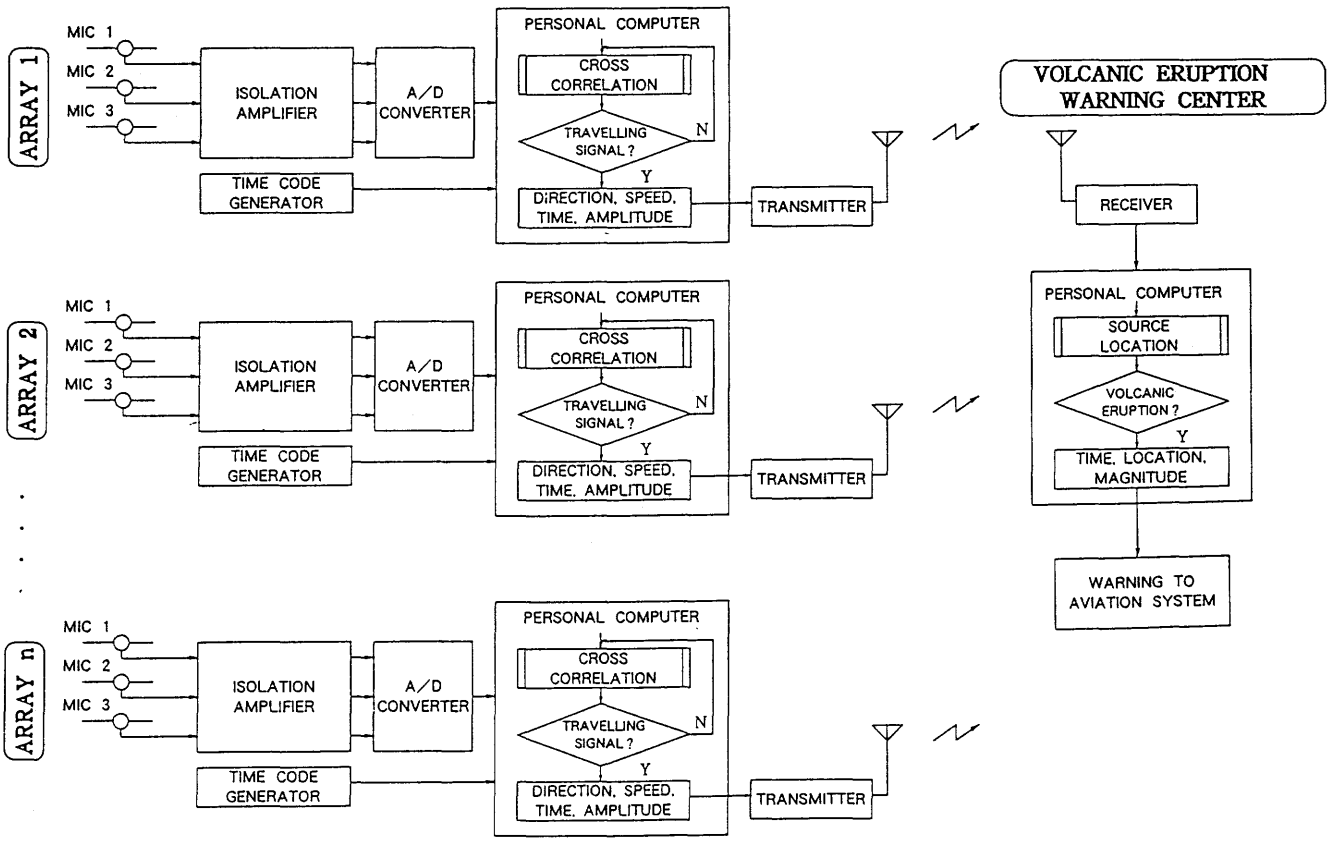


**Figure 9.** The PEGASAS-VE system consists of a number of infrasonic microphone arrays that are 500–1,000 km apart. Each array continuously monitors the incidence of traveling signals and computes the direction of arrival, horizontal phase velocity, signal amplitude, and dominant frequency. All of these data are transmitted to a data center where the source location, occurrence time, and source intensity are calculated. Appropriate information is given to the aviation system when the source of a significant eruption is identified.

located within a distance of about 500 km from the volcano to acquire the information of eruption within 30 minutes, taking into account the travel speed of infrasonic signals in the atmosphere.

## CONCLUSIONS

Many of the summit eruptions at Sakurajima Volcano are predicted by monitoring seismic activity at the volcano. The eruptions tend to occur within 1 week after swarms of B-type earthquakes. A prediction in the shorter term is also possible at Sakurajima by instrumental monitoring of inflation of the ground. These prediction techniques can provide a primary way to reduce the threat of volcanic eruptions to aviation safety.

Once an eruption has occurred, however, the most important thing is to detect the eruption as soon as possible. The combination of a seismograph with an infrasonic microphone has proved to be a useful technique to detect explosive eruptions, when installed at the volcano (Onodera and Kamo, this volume). In this paper, we have proposed an extension of this system, which we call PEGASAS-VE, that is essentially a set of infrasonic microphone arrays to detect infrasonic waves generated by volcanic eruptions. This system would be capable of detecting explosive volcanic eruptions within 30 minutes when the spacing of the station is on the order of 500 km from the volcano. It merits the attention of the world aviation community because of its ability to provide coverage, at relatively low expense, of a large number of unmonitored volcanoes, such as those of the Kurile-Kamchatka-Aleutian region.

## ACKNOWLEDGMENTS

The authors express their hearty thanks to Drs. Wally Johnson, Thomas Casadevall, and Steven McNutt for reviewing the manuscript and offering helpful suggestions.

## REFERENCES CITED

Goerke, V.H., Young, J.M., and Cook, R.K., 1965, Infrasonic observations of the May 16, 1963, volcanic eruption on the island of Bali: Journal of Geophysical Research, v. 70, p. 6017–6022.

Iguchi, M., and Ishihara, K., 1990, Comparison of earthquakes and air-shocks accompanied with explosive eruptions at Sakurajima and Suwanosejima Volcanoes: Kyoto University, Disaster Prevention Research Institute, Annual Report, v. 33B-1, p. 1–12.

Ishihara, K., 1988, Prediction of summit eruption by tilt and strain data at Sakurajima Volcano, Japan, *in* Proceedings, Kagoshima International Conference on Volcanoes, p. 207–210.

Ishihara, K., and Iguchi, M., 1989, The relationship between micro-earthquake swarms and volcanic activity at Sakurajima Volcano: Kyoto University, Disaster Prevention Research Institute, Annual Report, v. 32B-1, p. 1–11.

Ishihara, K., Iguchi, M., and Tahira, M., 1986, [Observations of air waves associated with volcanic explosions]: Report of the Sakurajima Volcano Observatory (October–December, 1982), p. 131–138. [In Japanese.]

Kamo, K., 1978, Some phenomena before the summit eruptions at Sakurajima Volcano: Bulletin of the Volcanological Society of Japan, v. 23, p. 53–64.

Kamo, K., and Ishihara, K., 1989, A preliminary experiment of automated judgment of the stages of eruptive activity using tiltmeter records: IAVCEI Proceedings in Volcanology, v.1, p. 585–598.

Smithsonian Institution, 1991, Pinatubo: Bulletin, Global Volcanism Network, v.16, no. 5, p. 2–8.

Tahira, M., 1981, A study of the infrasonic wave in the atmosphere, multi-pipe line microphone for infrasonic observation: Journal of the Meteorological Society of Japan., v. 59, p. 477–486.

———1982, A study of the infrasonic wave in the atmosphere. (II) Infrasonic waves generated by the explosions of the volcano Sakura-jima: Journal of the Meteorological Society of Japan, v. 60, p. 896–907.

———1988, A study of the long-range propagation of infrasonic waves in the atmosphere. (I) Observation of the volcanic infrasonic waves propagating through the thermospheric duct: Journal of the Meteorological Society of Japan, v. 66, p. 17–26.

Tahira, M., Ishihara, K., and Iguchi, M., 1988, Monitoring volcanic eruptions with infrasonic waves, *in* Proceedings, Kagoshima International Conference on Volcanoes, p. 530–533.

Tahira, M., Ishihara, K., and Ukai, E., 1990, [Infrasonic waves observed at Kariya in association with the 1986 and 1987 eruptions of Izu-Oshima Volcano]: Kazan, v. 35, p. 11–25. [In Japanese.]

Uhira, K., and Ueda, Y., 1988, Volcanic monitoring at Kagoshima local meteorological observatory of the Japan Meteorological Agency, *in* Proceedings, Kagoshima International Conference on Volcanoes, p. 227–229.

Wilson, C.R., Nichparenko, S., and Forbes, R.B., 1966, Evidence of two sound channels in the polar atmosphere from infrasonic observations of the eruption of an Alaskan volcano: Nature, v. 211, p. 163–165.

Wilson, C.R., and Forbes, R.B., 1969, Infrasonic waves from Alaskan volcanic eruptions: Journal of Geophysical Research, v. 74, p. 4511–4522.

VOLCANIC ASH AND AVIATION SAFETY:
Proceedings of the First International Symposium
on Volcanic Ash and Aviation Safety
U.S. GEOLOGICAL SURVEY BULLETIN 2047

# VOLCANIC HAZARD DETECTION WITH THE TOTAL OZONE MAPPING SPECTROMETER (TOMS)

*By* Arlin J. Krueger, Scott R. Doiron, Gregg S.J. Bluth, Louis S. Walter,
*and* Charles C. Schnetzler

## ABSTRACT

Volcanic clouds can be uniquely discriminated from weather clouds with the total ozone mapping spectrometer (TOMS) instrument on the Nimbus-7 and Meteor-3 satellites. Sulfur dioxide, which is carried along with water and ash in volcanic eruptions, is measured by TOMS as a by-product of ozone mapping. Eruptions are easily detected in sulfur dioxide maps because the background $SO_2$ amounts are relatively small and uniform, whereas visible and infrared satellite images must be searched manually for distinctive cloud shapes. The TOMS technique also produces a quantitative estimate of eruption size based on sulfur dioxide content. Sulfur dioxide data from polar-orbiting satellites, coupled with a short-term trajectory forecast, can be used to prepare volcanic aviation-hazard maps.

The detection and tracking capability of TOMS is illustrated with examples from the June 1991 Pinatubo and May 1980 Mount St. Helens eruptions. The 50 volcanic eruption clouds detected with TOMS since 1978 include: Pinatubo, Mount St. Helens, El Chichón, Cerro Hudson, Alaid, Nyamuragira, Galunggung, Una Una, Ruiz, Redoubt, Hekla, and several Galapagos volcanoes.

## INTRODUCTION

The detection of volcanic ash clouds for aviation safety currently depends on reports from the ground and air and manual screening of visible and infrared cloud images from satellites. Damage to aircraft from flying through ash clouds has cost the aviation industry hundreds of millions of dollars (Steenblik, 1990) since the first serious incidents during the 1982 eruptions of Galunggung. During the June 1991 eruptions of Mt. Pinatubo in the Philippine Islands, at least 16 aircraft were exposed to ash at distances up to 1,000 km from the volcano (Casadevall and De Los Reyes, 1991). Further aircraft damage results from the sulfuric acid haze that remains in the stratosphere long after the eruption. Thus, it is clear that the methods of detection of volcanic-hazard areas, as well as the communication of warnings, need improvement if future incidents are to be prevented. In this paper we discuss a satellite method for detection of explosive eruption clouds using sulfur dioxide gas as a tracer.

## DISCRIMINATION OF ERUPTION CLOUDS FROM METEOROLOGICAL CLOUDS

Earth-orbiting satellites provide an excellent platform for detection of volcanic eruptions because of the global coverage and the potential for rapid transmission of data. Presently, the National Oceanic and Atmospheric Administration (NOAA) operational polar and geostationary satellites carry visible and infrared imaging instruments, such as the advanced very high resolution radiometer (AVHRR), in which the primary products are cloud images and temperature-distribution maps. Eruptions can be detected by manual inspection of images for evidence of plumes (Matson, 1984; Sawada, 1987). This generally requires that the eruption column be sheared by winds into a plume, and, of course, the method fails if there is no contrast between the plume and underlying clouds. For example, Nevado del Ruiz Volcano, Columbia, produced no visible or infrared signature in its November 1985 eruption (M. Matson, NOAA, oral commun., 1986).

Manual searches of satellite images could be avoided if cloud-composition differences are exploited. Volcanic clouds are primarily water, with carbon dioxide, silicate rock particles, and sulfur dioxide, with trace gases, such as HCl, present in smaller amounts. A relatively weak silicate signal at infrared wavelengths has been detected in eruption clouds using multispectral data from the AVHRR (Prata, 1989; Holasek and Rose, 1991; Dean and others, this volume; Schneider and Rose, this volume). Sulfur dioxide also has a very strong absorption band in the near-ultraviolet portion of the spectrum. This has been successfully exploited in detection of eruption clouds with the TOMS instrument on the Nimbus-7 satellite (Krueger, 1983), as reported here.

## TOMS CAPABILITIES FOR DETECTION OF ERUPTIONS

TOMS measures the radiance of the atmosphere, as does AVHRR, but adds to this a measurement of the solar flux. From this measurement, the albedo (the ratio of reflected radiance to incident solar irradiance) of the atmosphere is computed. The albedo of the sunlit atmosphere is a result of scattering by air molecules; reflection from clouds or surface features, such as oceans, vegetation, soil, and snow or ice; and by absorption by specific atmospheric constituents. If narrow spectral bands are used, the quantity of absorbing gases (ozone and sulfur dioxide) below the spacecraft can be derived.

The TOMS instrument is an ultraviolet spectrometer with six narrow wavelength bands designed for measurement of total ozone. Four of the wavelengths are used in pairs (312.5–331.2 nm and 317.5–339.8 nm) in a differential-absorption mode. The two longest wavelengths (360 and 380 nm) are used to determine surface reflectivity.

Ozone strongly absorbs light at wavelengths less than 330 nm. To measure ozone from space, it is necessary to account for all the components of the system, including clouds and the reflectivity of the surface. If this were not done, clouds would produce artifacts in ozone maps. The success can be judged from the final ozone product, where the errors in total ozone from cloud effects are less than 1 percent.

Sulfur dioxide has larger absorption coefficients than ozone at wavelengths less than 320 nm, but the background concentrations of this gas are so low that it is virtually undetectable in the ultraviolet Earth albedo, except in volcanic eruptions. When sulfur dioxide is present, differences in the absorption spectra of ozone and sulfur dioxide allow separation of the two species (Krueger, 1985). Volcanic clouds have been detected by this method at all altitudes above the boundary layer, but the observations are limited to day time. In addition, volcanic clouds below the upper stratosphere may be masked by large ozone amounts and long slant paths for the sunlight during winter.

Horizontal structure in ozone and sulfur dioxide is resolved by scanning the field of view of the spectrometer perpendicular to the motion of the satellite. The width of the scan is designed for full global coverage on each day. The spatial resolution of 50×50 km on the ground directly below the satellite is crude by comparison with AVHRR. However, spatial resolution is not critical because the TOMS technique depends on identification of the sulfur dioxide rather than resolving the detailed shape of a volcanic cloud.

TOMS is on the National Aeronautical Space Administration (NASA) Nimbus-7 satellite that was launched into a polar, noon-midnight, sun-synchronous orbit in October 1978. A second TOMS instrument was launched on August 15, 1991, into polar orbit on a Russian Meteor-3 spacecraft. Data continuity is assured through new TOMS instruments, which are planned for launch on a U.S. Earth Probes satellite in 1994, on a Japanese advanced Earth observing satellite (ADEOS) in 1996, and on an undesignated satellite in 1998. NOAA plans to fly TOMS instruments on operational polar-orbiting satellites after the turn of the century.

The TOMS data-production system at NASA/Goddard Space Flight Center normally takes 3–5 weeks for release of archival data. These historical data are used in ozone research, for assessment of volcanic sulfur dioxide production, and for confirmation of reports of eruptions in remote areas. However, the capability for routine, near-real-time data production (release in hours after playback from the satellite) has now been developed, and the data can be provided to users on a best-effort basis. Some satellites carrying TOMS instruments can also transmit data in real time if ground-receiving stations are available.

The existing TOMS instrument design is optimized for ozone detection. Sulfur dioxide detection could be improved by changes in the field of view to improve ground resolution and by selecting the wavelengths for sulfur dioxide. Polar-orbiting satellites are limited to one or two overpasses of each volcano each day. This limitation can be averted by development of a modified TOMS for flight on geostationary satellites (Hartmann and others, this volume).

## EXAMPLES OF ERUPTION DETECTION WITH TOMS

Over the past 13 years, eruptions of 50 volcanoes have been measured with TOMS. The technique was devised following the eruption of El Chichón in 1982 (Krueger, 1983), then it was extended to all other known eruptions to make a comparison of cloud properties. The volcanoes include Alaid, Galunggung, Nyamuragira, Mauna Loa, Una Una, Nevado del Ruiz, Redoubt, Hekla, Cerro Hudson, and several Galapagos volcanoes. The 1985 Ruiz eruption (Krueger and others, 1990) is an example of a sulfur dioxide cloud without visible or infrared signatures. On the other hand, not all eruptions produce measurable amounts of sulfur dioxide. For example, phreatic (steam-driven) eruptions are not accompanied by large amounts of sulfur dioxide; however, they do not appear to present the same problem to aviation as magmatic eruptions because of their smaller size.

### PINATUBO

The 1991 eruptions of Mt. Pinatubo in the Philippines contain the largest masses of sulfur dioxide measured by TOMS (Bluth and others, 1992). They also produced the largest number of volcanic ash–aircraft incidents ever recorded (Casadevall and De Los Reyes, 1991). Twenty million tons of sulfur dioxide were injected into the atmosphere in a series of Plinian eruptions beginning on June 12, 1991,

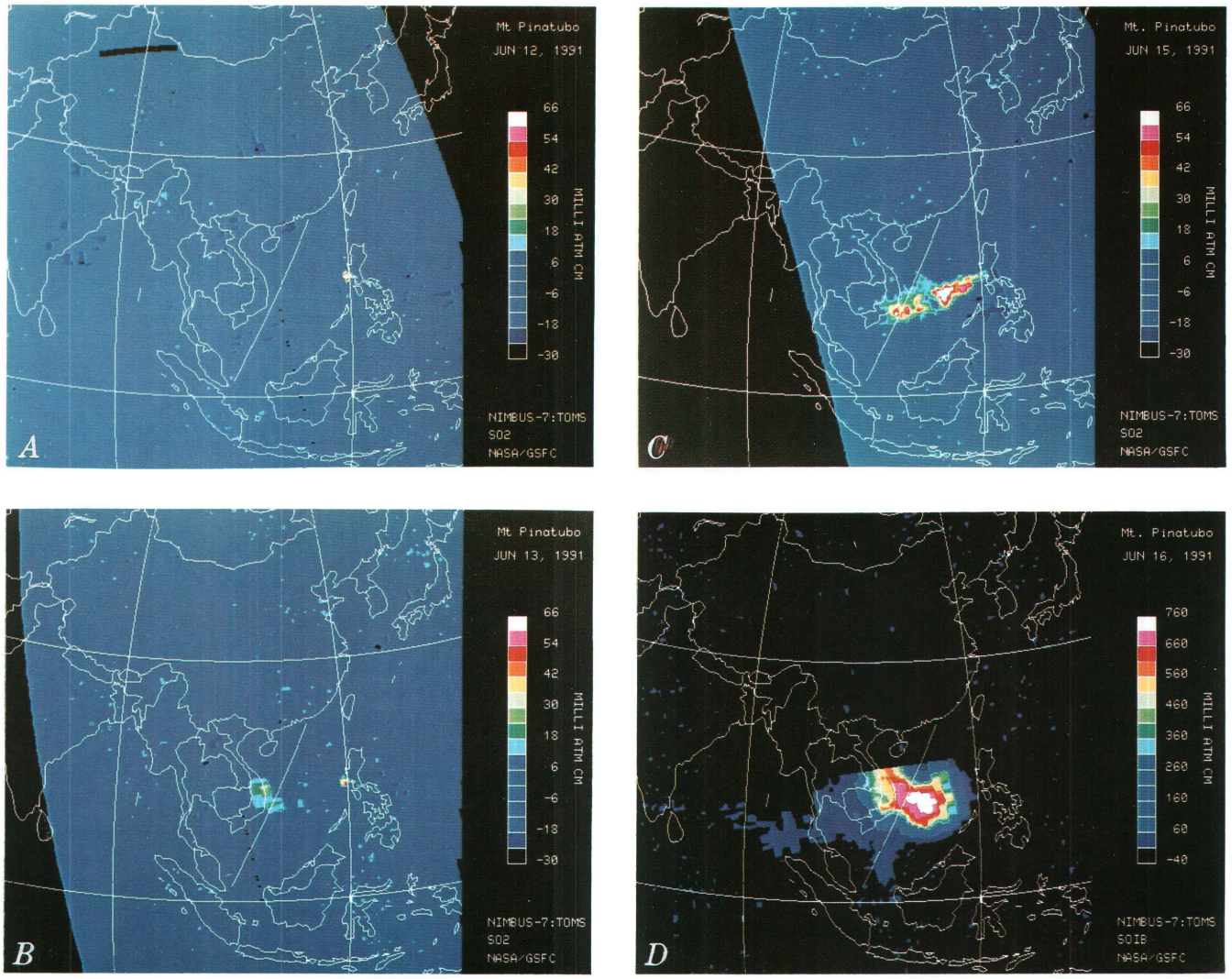


**Figure 1.** TOMS images of the Mount Pinatubo sulfur dioxide clouds on June 12–16, 1991. Sulfur dioxide amounts, in milli-atmosphere-centimeters (m-atm-cm), are represented by a false-color scale, as shown on the right of each image. The diagonal white line is a flight corridor from Singapore to Hong Kong, which was affected by ash from Pinatubo. *A*, Initial magmatic eruption on June 12, 1991, observed about 90 minutes after the eruption began at 08:51 Manila time (00:51 UTC). The cloud is the white-red spot near Luzon Island, Philippines. *B*, Pinatubo sulfur dioxide clouds on June 13, 1991. An eruption at 08:45 Manila time (00:45 UTC) has produced the yellow-red spot near the Philippines, and the cloud from the prior day's eruption is the green-yellow patch over Vietnam. *C*, Sulfur dioxide image from TOMS at 11:30 Manila time (03:30 UTC) on June 15, 1991. Increased activity has produced a plume extending across the South China Sea. *D*, The sulfur dioxide cloud produced by the paroxysmal eruption of Pinatubo on the afternoon of June 15, 1991. Note that the range of the color scale is an order of magnitude greater than in *A–C*. The cloud, observed at 11:45 Manila time (03:45 UTC) on June 16, covers much of the South China Sea. Numerous aircraft incidents took place along the Singapore–Hong Kong flight route.

and culminating in a paroxysmal explosion on June 15 (Pinatubo Volcano Observatory Team, 1991).

Figure 1*A* illustrates the initial June 12 eruption of Pinatubo as a bright white-red spot of sulfur dioxide just west of the volcano at lat 15°N., long 120°E. The Nimbus-7 satellite overpass of the Philippines was about 90 minutes after the eruption at 08:51–09:26 Manila time (00:51–01:26 UTC) (Pinatubo Volcano Observatory Team, 1991). The sulfur dioxide amounts at each geographic location are portrayed with a false-color scale, shown on the right-hand side of the figure. Sulfur dioxide amounts are given in units of milli-atmosphere-centimeters (m-atm-cm), a measure of the equivalent thickness of a layer of pure sulfur dioxide gas at standard temperature and pressure conditions. The peak $SO_2$ amounts in this cloud are about 60 m-atm-cm, and the total amount of $SO_2$ in the cloud is 100,000 metric tons, as determined on June 13 when the cloud was optically thin. The scattering of light and dark blue spots throughout the image are noise in the data. The black band over northwest China is an artifact due to two missing scan

lines. The diagonal white line over the South China Sea indicates the heavily traveled flight corridor from Singapore to Hong Kong which was the site of numerous aircraft incidents following the June 15 eruption.

The first reported aircraft incident was at 12:20 Manila time (04:20 UTC), about 2 hours after the Nimbus-7 overpass, at a location about 200 km southwest of the volcano (Casadevall and De Los Reyes, 1991). The NOAA-11 AVHRR image taken at 13:30 Manila time (05:30 UTC), 70 minutes after the incident, clearly shows an ash plume extending 330 km southwest of the volcano (Smithsonian Institute, 1991). This episode illustrates the importance of timing and communications in aviation safety.

Throughout the next 24 hours, this cloud was carried across the Singapore–Hong Kong flight corridor by tropical easterly winds. At the June 13 TOMS overpass, the $SO_2$ cloud from the June 12 eruption is already over Vietnam, some 1,300 km west of Manila (fig. 1*B*). Another eruption, which occurred at 8:41–8:46 Manila time (00:41–00:46 UTC) (Pinatubo Volcano Observatory Team, 1991), is visible as a yellow-red spot near Luzon. This eruption began two hours before the TOMS overpass. The first aircraft incident in the Singapore–Hong Kong corridor took place at 00:30 Manila time on June 14 (16:30 UTC, June 13) over the South China Sea.

Larger eruptions, which began on the morning of June 14, are observed on the 11:30 (03:30 UTC) June 15 overpass (fig. 1*C*) as a series of volcanic clouds extending 1,600 km WSW. from Pinatubo to Vietnam.

The paroxysmal eruption began in early morning on June 15 and continued for more than 12 hours. This eruption produced a massive cloud, which was observed with TOMS at 11:45 (03:45 UTC) on June 16 to be covering much of the South China Sea (fig. 1*D*). Note that the color scale has been expanded by more than a factor of ten from figures 1*A*–1*C* to display the approximately 20 million metric tons of sulfur dioxide produced in this eruption. This cloud was responsible for most of the aircraft encounters along the Singapore–Hong Kong flight corridor.

## MOUNT ST. HELENS

The eruption of Mount St. Helens on May 18, 1980, provides a second example of a volcanic cloud drifting across an area with a high volume of air traffic. Mount St. Helens produced only about 3 percent of the sulfur dioxide of Pinatubo, but the cloud drifted across the United States in less than 3 days. This eruption produced a diffuse, lower tropospheric dust cloud, which moved east and north, and an upper tropospheric ash and sulfur dioxide cloud, which drifted east and south (Newell and Deepak, 1982).

The sulfur dioxide cloud on May 19 is shown in figure 2*A* as an image produced during reanalysis of archived TOMS data. About 27 hours after the eruption, a trail extends from the volcano location in southwest Washington to central Wyoming. The bulk of the cloud is found in a plume extending to the southwest corner of South Dakota, then southeast across Nebraska and Kansas to the panhandle of Texas. On May 20, the trail of volcanic material extends from northern Oregon, across Idaho, Colorado, Kansas and Missouri, to the vicinity of Detroit (fig. 2*B*). At this time, the most dense part of the sulfur dioxide cloud was over Illinois, Indiana, Ohio, and Michigan. On succeeding days, the northern part of this cloud was sheared by jet stream winds into an elongated stream, whereas the remainder of the ash cloud stagnated in a ridge over the Central States. Based on radiosonde winds and other observations, the cloud was located primarily between the 100-mb (16-km) and 200-mb (12-km) surfaces.

Analyses of the ash-cloud trajectory, based on meteorological data, were prepared by the NOAA Air Resources Laboratory (see fig. 12-10 in McClelland and others, 1989) and by Ed Danielson of the Ames Research Center (Newell and Deepak, 1982). Figure 3 illustrates the Danielson trajectory for the 200- and 300-mb (9-km) levels. The general path is similar to the TOMS trajectories shown in figure 2; however, the actual cloud has a compact form with significant differences in timing and location. At the TOMS overpass time on May 19, the ash cloud is predicted to be over Arkansas at 9-km altitude (300 mb), over central Colorado at 12 km (200 mb), and (not shown here) over the Utah-Wyoming border at 16 km (100 mb). The actual cloud location from TOMS data is north and west of the forecast locations. On May 20, the trajectory forecast placed the ash south and east of the TOMS cloud. The differences illustrate the need for both a high degree of vertical and temporal resolution in meteorological data for trajectory forecasting.

# CONCLUSIONS

Avoidance of volcanic ash by aircraft requires use of all available sources of information. Once the plume is in the upper troposphere or lower stratosphere, the problem is detection and prediction of its motion. Meteorological data are needed to infer the height of a sulfur dioxide cloud based on measured wind speeds as a function of altitude. With only one satellite observation of cloud location per day, a forecast is required to estimate the location at intervening hours. Trajectory forecasts appear to need updating with volcanic-cloud information more than once per day due to weaknesses in the models and limitations in the meteorological database. However, good results have recently been obtained in forecasting the trajectory of Cerro Hudson under Southern Hemisphere polar-vortex conditions (Schoeberl and others, 1993).

The TOMS technique produces unequivocal information about sulfur dioxide clouds produced during magmatic eruptions. Data from the present class of TOMS instruments on polar-orbiting satellites will be collected for at least the next decade.

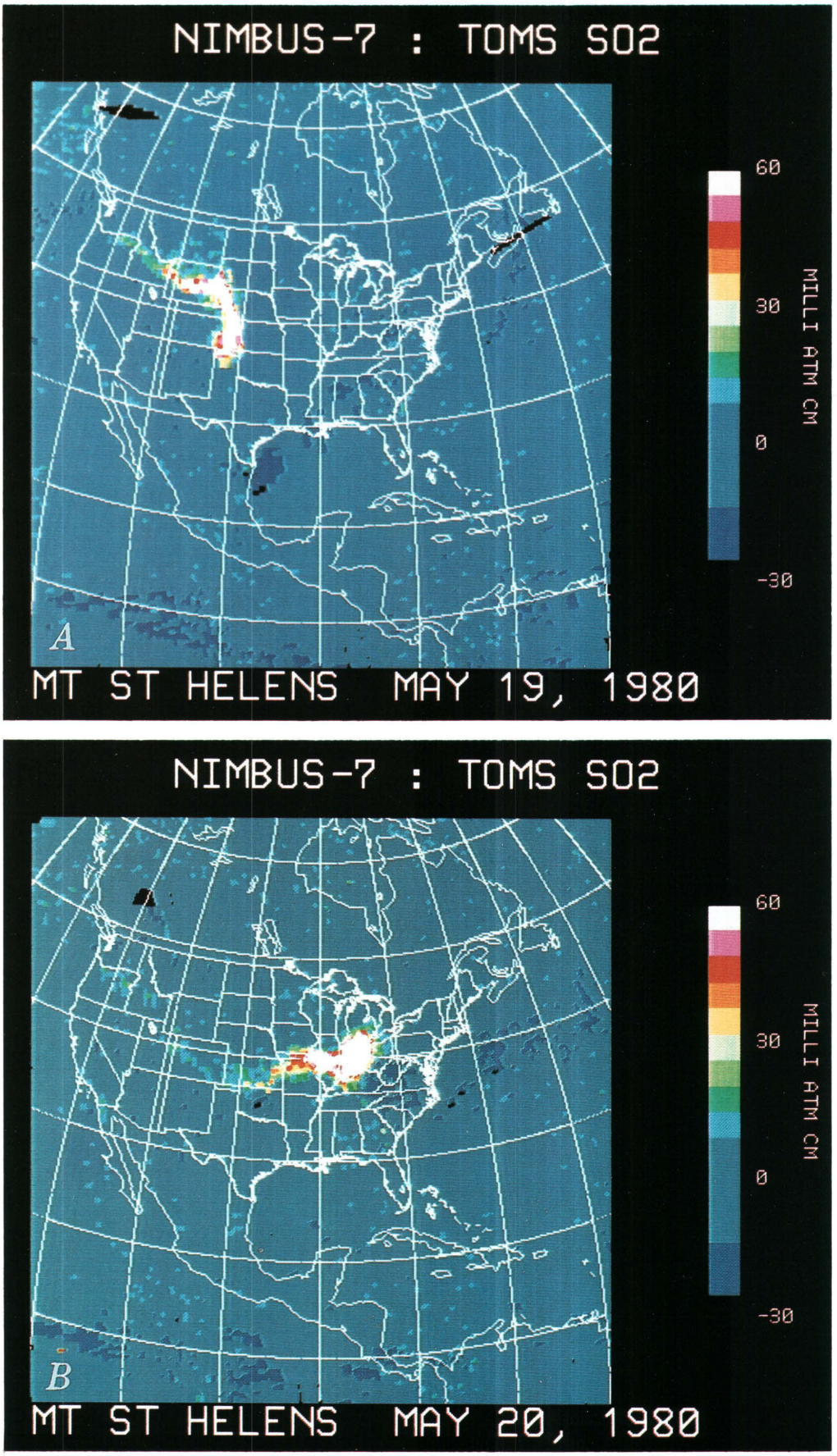


**Figure 2.** *A*, TOMS observations near local noon on May 19, 1980, of the sulfur dioxide cloud from the May 18, 1980, eruption of Mount St. Helens. The cloud appears as a red-white patch over the central Western States. A trail of smaller $SO_2$ amounts extends westward back toward the volcano, which is located in southern Washington State. *B*, The sulfur dioxide cloud from Mount St. Helens on May 20, 1980. The bulk of the cloud is now over Illinois, Indiana, Ohio, and Michigan.

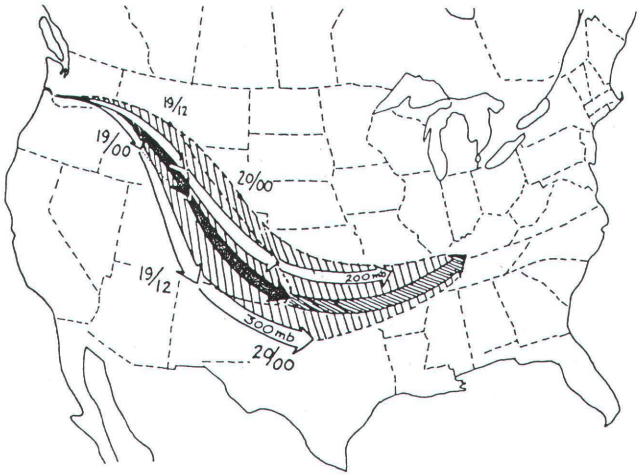


**Figure 3.** Trajectory analysis based on meteorological data indicating the predicted path of the Mount St. Helens cloud (May 18, 1980) at 200 and 300 mb. Note the general agreement with the actual locations shown in figure 2, but note also the differences in detail, such as a more northerly trajectory than predicted. Prepared by E. Danielson of the Ames Research Center (Newell and Deepak, 1982).

## REFERENCES CITED

Bluth, G.J.S., Doiron, S.D, Krueger, A.J., Walter, L.S., and Schnetzler, C.C, 1992, Global tracking of the $SO_2$ clouds from the June 1991 Mount Pinatubo eruptions: Geophysical Research Letters, v. 19, p. 151–154.

Casadevall, T.J., and De Los Reyes, P.J., 1991, Impact of June 1991 Pinatubo eruptions on aircraft operations in the western Pacific and southeast Asia [abs.]: Eos, Transactions, American Geophysical Union, v. 72, no. 44 [Supplement], p. 95.

Holasek, R.E., and Rose, W.I., 1991, Anatomy of the 1986 Augustine Volcano eruptions as revealed by digital AVHRR satellite imagery: Bulletin of Volcanology, v. 53, p. 529–544.

Krueger, A.J., 1983, Sighting of El Chichón sulfur dioxide clouds with the Nimbus 7 total ozone mapping spectrometer: Science, v. 220, p. 1377–1378.

———1985, Detection of volcanic eruptions from space by their sulfur dioxide clouds: American Institute of Aeronautics and Astronautics, 23rd Aerospace Sciences Meeting, January 14–17, Reno, Nev., Report AIAA-85-0100, 4 p.

Krueger, A.J., Walter, L.S., Schnetzler, C.C., and Doiron, S.D., 1990, TOMS measurements of the sulfur dioxide emitted during the 1985 Nevado del Ruiz eruptions: Journal of Volcanology and Geothermal Research, v. 41, p. 7–15.

Matson, M., 1984, The 1982 El Chichón volcano eruptions—A satellite perspective: Journal of Volcanology and Geothermal Research, v. 23, p. 1–10.

McClelland, L., Simkin, T., Summers, M., Nielsen, E., and Stein, T.C., 1989, Global Volcanism 1975–1985: Englewood Cliffs, N.J., Prentice-Hall, Inc., 655 p.

Newell, R.E., and Deepak, A., 1982, Mount St. Helens eruptions of 1980: Atmospheric effects and potential climatic impact: NASA Workshop Report SP-458, 119 p.

Pinatubo Volcano Observatory Team, 1991, Lessons from a major eruption: Mt. Pinatubo, Philippines [abs.]: Eos, Transactions, American Geophysical Union, v. 72, no. 44 [Supplement], p. 545–553.

Prata, A.J., 1989, Observations of volcanic clouds in the 10–12 μm window using AVHRR/2 data: International Journal of Remote Sensing, v. 10, p. 751–761.

Sawada, Y., 1987, Study on analyses of volcanic eruptions based on eruption cloud image data obtained by the geostationary meteorological satellite (GMS): Technical Report of the Meteorological Research Institute No. 22, Tsukuba, Japan, 335 p.

Smithsonian Institute, 1991, Pinatubo: Bulletin of Global Volcanism Network, v. 16, no. 5, p. 2–8.

Schoeberl, M.R., Doiron, S.D., Lait, L.R., Newman, P.A., and Krueger, A.J., 1993, A simulation of the Cerro Hudson $SO_2$ cloud: Journal of Geophysical Research, v. 98, p. 2949–2955.

Steenblik, J.W., 1990, Volcanic ash: A rain of terra: Air Line Pilot, June/July, p. 9–15 and p. 56.

VOLCANIC ASH AND AVIATION SAFETY:
Proceedings of the First International Symposium
on Volcanic Ash and Aviation Safety
U.S. GEOLOGICAL SURVEY BULLETIN 2047

# MONITORING VOLCANIC ERUPTIONS USING NOAA SATELLITES

*By* Michael Matson, James S. Lynch, *and* George Stephens

## ABSTRACT

National Oceanic and Atmospheric Administration (NOAA) meteorological satellite data have been used to detect volcanic eruptions and monitor the subsequent ash clouds since 1976. Imagery (analog or digital) can be used in conjunction with conventional radiosonde data to determine the altitude of a volcanic eruption column; the size, speed, and position of the eruption cloud; and the direction in which the cloud is moving. This information can be used to provide guidance to pilots flying in areas near active eruptions.

## INTRODUCTION

Many active volcanoes are located in remote areas of the globe, far from human habitation but near major flight routes (e.g., Aleutian and Kamchatkan volcanoes). Because of their remoteness, these volcanoes are often not monitored, and it is almost impossible to provide pilots with information about volcanic activity along the flight route. However, satellite systems, with their global coverage, can provide information on erupting volcanoes in virtually any part of the world (Sawada, 1987, this volume; Sudradjat, 1989).

## METHODS OF STUDY

### POLAR-ORBITING SATELLITES

The National Oceanic and Atmospheric Administration (NOAA) normally operates two weather satellites in polar orbits and two weather satellites in geostationary orbits (currently, four polar-orbiting satellites and one geostationary satellite are operational). The NOAA polar-orbiting satellites operate at 833 to 870 km above the Earth in near-circular sun-synchronous orbits with 98.89° inclination, which results in 14.25 revolutions per day and obtains complete global coverage every 24 hours.

The primary imaging system aboard the polar-orbiting satellites is the advanced very high resolution radiometer (AVHRR), a cross-track multispectral scanner with a nadir resolution of 1.1 by 1.1 km and an image swath width of 2,600 km. The AVHRR offers five spectral channels—two visible and three infrared (see table 1). Experimental multispectral techniques based on AVHRR imagery (channels 3, 4, and (or) 5) have been developed for monitoring volcanic plumes (Prata, 1989; Holasek and Rose, 1991; Potts and Whitby, this volume; Schneider and Rose, this volume).

The AVHRR imagery is available at full resolution to direct-readout stations acquiring automatic picture transmission data (frequencies of 137.50 or 137.62 MHz) or high-resolution picture transmission data (frequencies of 1,698.0 and 1,707.0 MHz). Data is also tape recorded on board the satellites and downloaded each orbit to the command and data-acquisition facilities in Fairbanks, Alaska, and Wallops Island, Va. The global data, resampled to 4-km resolution, are known as global area coverage or GAC data. Pre-specified, tape-recorded scenes, recorded at 1.1-km resolution, are known as local area coverage or LAC data. The two images in this paper (figs. 1 and 2) are from the AVHRR LAC coverage of the Philippines, which was established about June 1, 1991, 2 weeks prior to the paroxysmal eruption of Mt. Pinatubo.

Currently, imagery from two polar-orbiting satellites, NOAA-11 and NOAA-12, are operationally available. During any 24-hour period, the satellites will pass over any part of the world at least twice; once during the day, and 12 hours later at night. Coverage over the polar areas can be up to 9 times per day due to orbital overlaps at these latitudes. With two satellites, repetitive coverage of any area of the world is obtained at least 4 times daily at the equator and up to 18 times daily over the polar areas.

### GEOSTATIONARY OPERATIONAL ENVIRONMENTAL SATELLITE (GOES)

The geostationary operational environmental satellite (GOES-7) is in orbit 35,800 km above the Western Hemisphere equator and orbits around the Earth at the same rotation rate as the Earth. Thus, it is always viewing a constant portion of the Western Hemisphere between lat 60°N. and lat 60°S., providing repetitive coverage of the area as often as

**Table 1.** Spectral channels of the advanced very high resolution radiometer (AVHRR).

| Channel | Wavelength (μm) | Primary uses |
|---|---|---|
| 1 | 0.58–0.68 | Daytime cloud mapping. Snow/ice analysis. |
| 2 | 0.725–1.10 | Surface-water delineation. Vegetation analysis. |
| 3 | 3.55–3.93 | Forest fire monitoring. Nighttime cloud mapping. |
| 4 | 10.30–11.30 | Sea-surface temperature. Day/night cloud mapping. |
| 5 | 11.50–12.50 | Sea-surface temperature. Day/night cloud mapping. |

every 30 minutes. The scanner imaging system aboard GOES acquires one band of visible data (0.55–0.70 μm) with a 1-km resolution, and one band of thermal-infrared (IR) data (10.5–12.6 μm) is acquired at a resolution of 8 km (Sabin, 1987).

Because of the complete coverage between lat 60°N. and lat 60°S. provided by GOES-7, it is possible to monitor many volcanic eruptions in the Western Hemisphere. The imagery can be received as often as every 30 minutes, making near-real-time tracking of volcanic ash clouds possible. This tracking information can include plume altitude, position, size, speed, and directional movement. NOAA-11 and NOAA-12 can provide the same information for volcanic eruptions worldwide but only as often as every 6 hours near the equator and every 1 1/2 hours near the poles.

## PINATUBO ERUPTION

The Mt. Pinatubo eruption provides examples of the NOAA satellite capability to monitor such events. The largest and most violent of the eruptions began on the morning of 15 June 1991. The most violent eruptive phase is shown in figure 1. An extensive ash plume achieved heights of 25–30 km and, in the immediate vicinity of the volcano, attained altitudes of approximately 35–40 km. An overshooting top was fixed over the volcano for a 12-hour period. The ash from this phase of activity accounted for more than 95 percent of the resultant 2,700,000-km$^2$ plume.

The final phase of the eruption on June 16 was noted by a "wedge shaped" plume fixed on the volcano. During this phase (fig. 2), ash reached heights of 23–25 km. It is apparent from these satellite images that the areal extent and movement of the eruption cloud can be monitored. In addition, by comparing the satellite-derived black-body temperature of the eruption cloud to a nearby radiosonde station taking upper air temperature and wind profiles, it is possible to assign an altitude to the cloud.

## DRAWBACKS TO SATELLITE METHODS

There are two problems with utilizing satellite data for volcanic eruptions. First, it is often difficult, in early stages of an eruption, to distinguish a volcanic eruption from a meteorological cloud. Often, the spectral signature and shape of each are similar; however, multispectral image processing using AVHRR data can be useful in discriminating ash clouds from meteorological clouds (Prata, 1989; Holasek and Rose, 1991; Dean and others, this volume; Schneider and Rose, this volume). It is easier to look for a reported eruption on satellite imagery than it is to detect an eruption by using the imagery alone. Despite this difficulty, several volcanic eruptions have initially been detected by trained analysts using satellite data alone.

The second problem is assigning an altitude to the eruption cloud during the early stages of an eruption. Using satellite-derived temperature data alone and comparing it to nearby radiosonde temperature data may result in

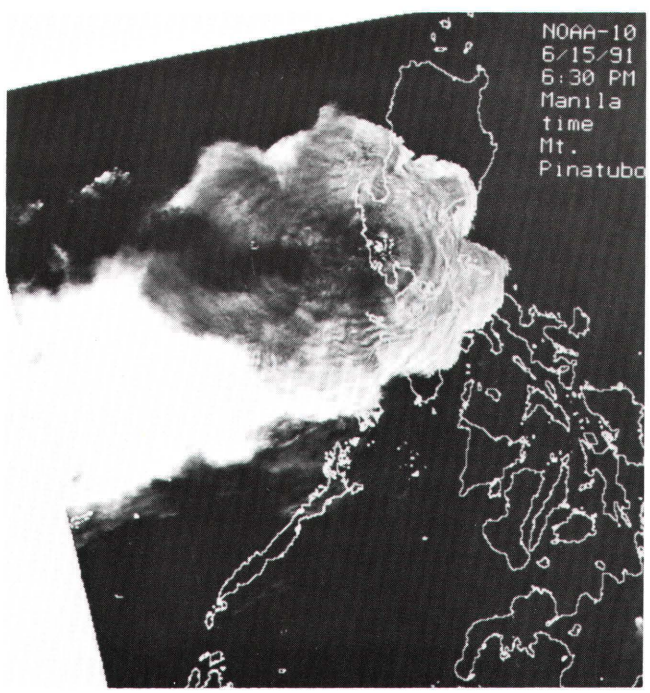


**Figure 1.** Mt. Pinatubo volcano, Philippines, NOAA-10 multispectral (infrared) image processed from 1.1-km data (reduced to 2.2 km) at 6:30 p.m. (local time) on 15 June 1991. The extensive canopy of ash over Luzon and the South China Sea was produced after nearly 8 hours of continuous eruption during the "paroxysmal" event, which lasted a total of 21 hours. The "overshooting top" can be seen over the volcano. Even though prevailing winds are from the northeast, the force of the eruption was great enough so that some ash was forced upwind. The concentric rings around the central core appear to be gravity waves propagating outward. Temperatures derived were as low as –80°C, and components of the ash cloud tracked west-southwestward at nearly 45 m/s at altitudes of 30 to 35 km.

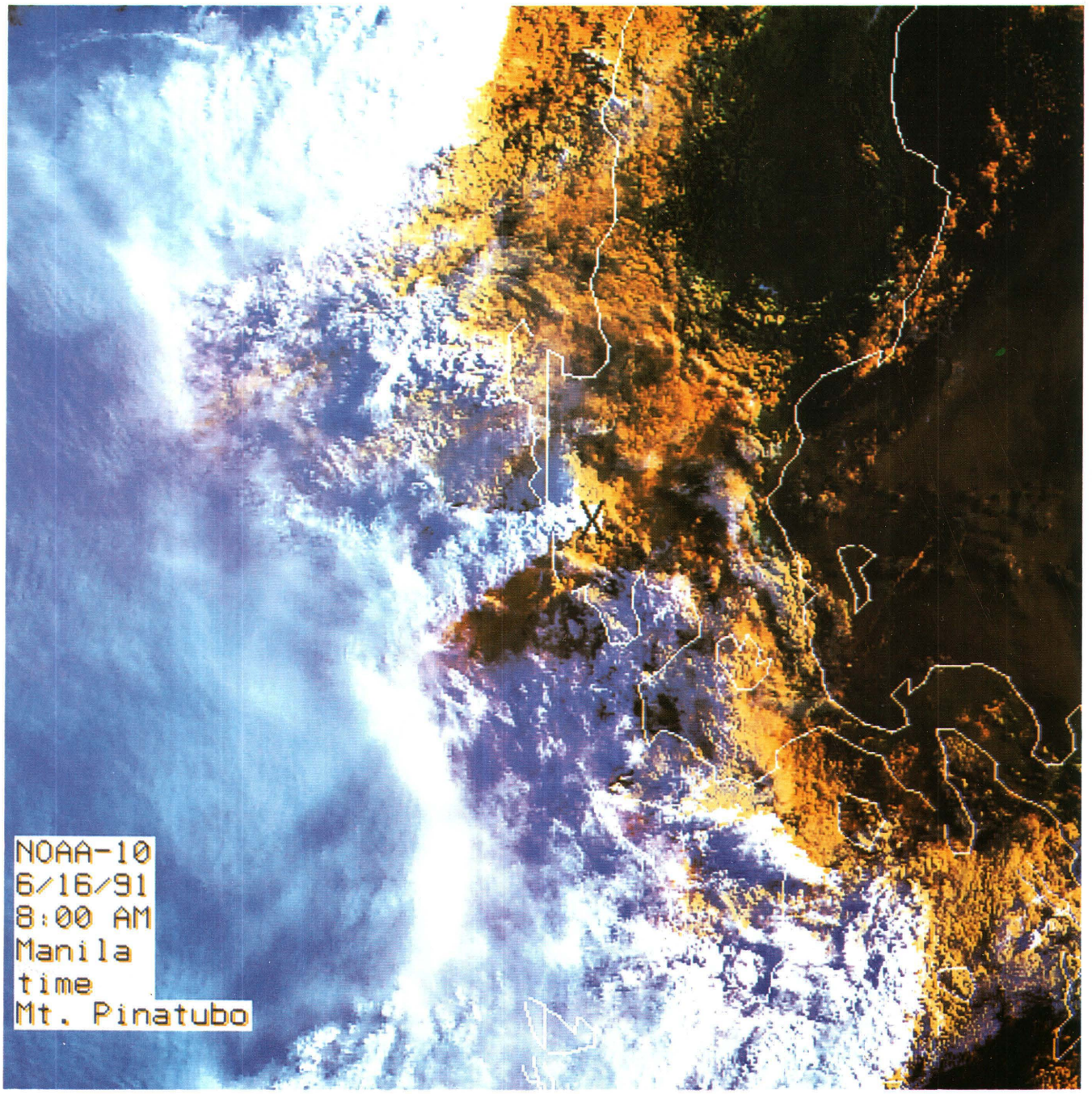


**Figure 2.** Mt. Pinatubo volcano, Philippines, NOAA-10 false-color, multispectral (visible and infrared) composite processed from 1.1-km data at 7:00 a.m. (local time) on 16 June 1991. A "wedge shaped" ash cloud, locked over the volcano (X), is depicted during the third phase of the "paroxysmal" eruption. Material can be seen rising from the volcano, spreading to form the blue-gray plume and ash cloud.

two altitude assignments due to atmospheric temperature inversions. The problem can be resolved after the ash cloud starts to spread by comparing the ash-cloud speed and direction to radiosonde wind speed and direction. An additional problem can arise if the cloud is not in thermal equilibrium with the atmosphere (Self and Walker, this volume; Woods and Kienle, this volume), which will cause incorrect altitude calculations.

## CONCLUSIONS

Although NOAA satellite data do have their limitations, used in conjunction with other sources of volcanic-eruption information, these data can provide near-real-time information on the altitude, size, speed, and direction of ash clouds. This information, along with trajectory forecasts, is now being operationally supplied by NOAA to the U.S. Federal Aviation Administration to provide volcanic-hazard alerts to aircraft in flight-information regions for which the United States is responsible. Operators of other national satellite systems could make similar information available to pilots flying near active volcanoes in areas covered by their meteorological satellites.

## REFERENCES CITED

Holasek, R.E., and Rose, W.I., 1991, Anatomy of 1986 Augustine Volcano eruptions as recorded by multispectral image processing of digital AVHRR satellite data: Bulletin of Volcanology, v. 53, p. 420–435.

Prata, A.J., 1989, Observations of volcanic ash clouds in the 10–12 μm window using AVHRR/2 data: International Journal of Remote Sensing, v. 10, p. 751–761.

Sabin, Jr., F.F., 1987, Remote Sensing: Principles and Interpretation: New York, W.H. Freeman and Co., 449 p.

Sawada, Y., 1987, Study on analyses of volcanic eruptions based on eruption cloud image data obtained by the geostationary meteorological satellite (GMS): Technical Reports of the Meteorological Research Institute, no. 22, 335 p.

Sudradjat, A., 1989, Volcanic eruption monitoring using space platforms: Journal of the Indonesian Association of Geologists, v. 12, p. 437–448.

VOLCANIC ASH AND AVIATION SAFETY:
Proceedings of the First International Symposium
on Volcanic Ash and Aviation Safety
U.S. GEOLOGICAL SURVEY BULLETIN 2047

# VOLCANIC TREMOR AMPLITUDE CORRELATED WITH ERUPTION EXPLOSIVITY AND ITS POTENTIAL USE IN DETERMINING ASH HAZARDS TO AVIATION

*By* Steven R. McNutt

## ABSTRACT

New data on volcanic tremor define an empirical relation between tremor amplitude or strength and eruption explosivity: as explosivity increases, tremor amplitude increases. Tremor data from 21 eruptions at 14 volcanoes were normalized to their reduced-displacement amplitudes, thereby permitting quantitative comparison. A linear regression of amplitudes plotted versus volcano explosivity index (VEI) yielded the formula:

$$\log_{10}(\text{reduced displacement}) = 0.46(\text{VEI}) + 0.08$$

Similarly, amplitudes plotted versus ash-column height yielded the formula:

$$\log_{10}(\text{reduced displacement}) = (1.80)\log_{10}(\text{ash-cloud height}) - 0.08$$

Both regressions are significant at the 95 percent level, although the VEI data fit slightly better.

A rapid assessment of a volcano's explosivity could help determine hazards from airborne ash. Thus, tremor amplitudes could form one component of a warning system. The tremor amplitudes are recorded in near real time as the volcanic materials exit the vent. It then takes at least several minutes for the ash to reach altitudes where it poses a hazard to aircraft. Therefore, in the best case, tremor amplitudes could help determine the size of an eruption and the amount of ash before the ash reached altitudes where it poses a hazard to aircraft. In terms of aviation hazards, the threshold or critical amplitude of tremor is 10 $cm^2$.

## INTRODUCTION

A fundamental problem with respect to volcanic ash and aviation safety is the prediction of the volume of tephra and the column height resulting from volcanic eruptions. Numerous jet aircraft have been adversely impacted by airborne volcanic ash over the past 10 years. For example, the recent eruptions of Mt. Pinatubo, Philippines, caused damage to more than 14 jet aircraft (Casadevall and De Los Reyes, 1991). Clearly, solutions to the problem of aircraft encounters with airborne ash need to be addressed before tragedy occurs. A main part of the problem has been the inability of monitoring teams to identify the presence and amount of ash resulting from a volcanic eruption at the time it occurs.

This paper describes new results based on analyses of volcanic tremor, a type of seismicity, and its relation to the explosivity of a volcanic eruption. It will be shown that the amplitude of volcanic tremor, as recorded on a seismogram and normalized to a common scale, is proportional to the explosivity of eruptions based on such parameters as ash-column height, volume of tephra, and eruption style. The paper describes the data and its limitations and recommends how seismological data on volcanic tremor may be used to help reduce aviation hazards caused by volcanic ash.

## METHOD OF STUDY

### VOLCANO EXPLOSIVITY

To compare the explosivity of eruptions to the amplitude of volcanic tremor accompanying them, the volcano explosivity index (VEI) of Newhall and Self (1982) is used (table 1). The VEI uses nine parameters to ascribe a numerical index, ranging from 0 to 8, to an eruption: general eruption description, volume of tephra, ash-column height, qualitative description, classification, duration, CAVW (Catalog of Active Volcanoes and Solfatara Areas of the World—see References Cited) maximum explosivity, tropospheric injection, and stratospheric injection. Of these parameters, ash-column height is the one of most concern to aviation safety.

VEI values are normally determined as whole units. In this respect, they are similar to earthquake intensities, such as Modified Mercalli intensities, rather than to earthquake magnitudes. In this study, both published values and values determined by the author were used. Selected component information is shown in table 2.

The VEI has several shortcomings; for example, ash-column height plotted versus the logarithm of total erupted mass shows some eruptions whose values fall outside

**Table 1.** Criteria for estimation of volcanic explosivity index.

[After Newhall and Self (1982). VEI, volcanic explosivity index. Criteria are listed in decreasing order of reliability. Mod, moderate; column height given in kilometers above vent for VEI 0–2 and in kilometers above sea level for VEI ≥ 3; CAVW, Catalog of Active Volcanoes and Solfatara Areas of the World]

| Criteria | VEI | | | | | | | | |
|---|---|---|---|---|---|---|---|---|---|
| | 0 | 1 | 2 | 3 | 4 | 5 | 6 | 7 | 8 |
| Description | Non-explosive | Small | Moderate | Mod-large | Large | Very large | | | |
| Volume of ejecta ($m^3$) | $<10^4$ | $10^4$–$10^6$ | $10^6$–$10^7$ | $10^7$–$10^8$ | $10^8$–$10^9$ | $10^9$–$10^{10}$ | $10^{10}$–$10^{11}$ | $10^{11}$–$10^{12}$ | $>10^{12}$ |
| Classification (Tsuya, 1955)[1] | I | II–III | IV | V | VI | VII | VIII | IX | |
| Column height (km) | <0.1 | 0.1–1 | 1–5 | 3–15 | 10–25 | >25 | | | |
| Qualitative description | "Gentle, effusive" | | "Explosive" | | "Cataclysmic, paroxysmal, colossal" | | | | |
| | | | | | | "Severe, violent, terrific" | | | |
| Classification | | "Strombolian" | | | "Plinian" | | | | |
| | "Hawaiian" | | "Vulcanian" | | "Ultra-Plinian" | | | | |
| Duration[2] | <1 | | | | >12 | | | | |
| | | | 1–6 | | | | | | |
| | | | | 6–12 | | | | | |
| CAVW maximum explosivity[3] | Lava flows | | Explosions or nuées ardentes | | | | | | |
| | | | Phreatic | | | | | | |
| | Dome or mudflow | | | | | | | | |
| Tropospheric injection | Negligible | Minor | Moderate | Substantial | | | | | |
| Stratospheric injection | None | None | None | Possible | Definite | Significant | | | |

[1] If all eruptive products were pyroclastic ejecta.
[2] In hours of continuous blast.
[3] The most explosive activity indicated for the eruption in CAVW.

**Table 2.** Eruption and tremor parameters.

[VEI, volcano explosivity index (see table 1); ash-cloud height given in kilometers above vent for VEI 0–2 and in kilometers above sea level for VEI ≥ 3; tephra volume refers to volume of uncompacted ash; leaders (--) indicate no data; Volc. Obs., Volcano Observatory]

| Volcano name | Elevation (m) | Eruption date | Tremor amplitude ($cm^2$) | VEI | Ash-cloud height (km) | Tephra volume ($\times 10^6 km^3$) | References |
|---|---|---|---|---|---|---|---|
| Augustine | 1,227 | 1976, January | 140 | 4 | 13 | -- | Reeder and Lahr, 1987 |
| | | | | | | | Simkin and others, 1981 |
| | | | | | | | McClelland and others, 1989 |
| Fuego | 3,763 | 1973, April 27 | 24 | 3 | >2 | | D. Harlow, unpub. data |
| Fuego | 3,763 | 1975, July–September | 8 | 2 | 1–2 | -- | Simkin and others, 1981 |
| | | | | | | -- | D. Harlow, unpub. data |
| Galeras | 4,482 | 1989, May 4–5 | 17 | 2 | 3 | -- | D. Harlow, unpub. data |
| Kilauea | 1,222 | 1983, January 5–12 | 18.3 | 2 | 1–2 | 14 | Koyanagi and others, 1988 |
| Masaya | 635 | 1977, February | 2.5 | 0 | <1 | -- | Simkin and others, 1981 |
| | | | | | | | D. Harlow, unpub. data |
| Mount St. Helens | 2,549 | 1980, May 18 | 260 | 5 | >24 | 1,100 | Fehler, 1983 |
| | | | | | | | Simkin and others, 1981 |
| | | | | | | | Sarna-Wojcicki and others, 1981 |
| Mount St. Helens | 2,549 | 1980, August 7 | 20 | 3 | 13.4 | 4.5 | Fehler, 1983 |
| | | | | | | | Harris and others, 1981 |
| | | | | | | | McClelland and others, 1989 |
| | | | | | | | Scandone and Malone, 1985 |
| Mount St. Helens | 2,549 | 1980, October 16–18 | 10 | 3 | 14.3 | 3.0 | Fehler, 1983 |
| | | | | | | | Harris and others, 1981 |
| | | | | | | | McClelland and others, 1989 |
| | | | | | | | Scandone and Malone, 1985 |
| Pacaya | 2,552 | 1973, May 7 | 5 | 1 | <1 | -- | McNutt and Harlow, 1983 |
| | | | | | | | Simkin and others, 1981 |
| Pacaya | 2,552 | 1979, October 6–7 | 9 | 2 | >1 | -- | D. Harlow, unpub. data |
| Pavlof | 2,518 | 1980, November 12–13 | 11 | 3 | 11 | 6 | McNutt, 1987 |
| | | | | | | | Simkin and others, 1981 |
| Pavlof | 2,518 | 1983, November 14–16 | 16 | 3 | 7.5 | 12 | McNutt, 1987 |
| | | | | | | | McClelland and others, 1989 |
| Pavlof | 2,518 | 1986, April 18–19 | 54 | 3 | 15 | 8 | McNutt, 1987 |
| | | | | | | | McClelland and others, 1989 |
| Pinatubo | 1,760 | 1991, June 15 | 1,070 | 6 | 30 | 3,000 | R. White, written commun., 1991 |
| | | | | | | | Pinatubo Volc. Obs. Team, 1991 |
| Plosty Tolbachik | 3,085 | 1975, July 9–26 | 146 | 4 | 13 | 1,000 | Fedotov and Markhinin, 1983 |
| | | | | | | | Gorel'chik and others, 1983 |
| | | | | | | | Simkin and others, 1981 |
| Redoubt | 3,108 | 1989, December 15 | 39 | 3 | >12 | 9–16 | Miller and Davies, 1990 |
| | | | | | | | Brantley, 1990 |
| | | | | | | | Scott and McGimsey, in press |
| Redoubt | 3,108 | 1990, April 21 | 15 | 3 | >8 | 0.6–1.3 | Miller and Davies, 1990 |
| | | | | | | | Brantley, 1991 |
| | | | | | | | Scott and McGimsey, in press |
| San Cristobal | 1,745 | 1976, March | 2.4 | 1 | >1 | -- | Simkin and others, 1981 |
| | | | | | | | D. Harlow, written commun.,1991 |
| Sheveluch | 3,395 | 1964, November 12 | 152 | 4 | 15 | 300 | Gorshkov and Dubik, 1970 |
| | | | | | | | Simkin and others, 1981 |
| Veniaminof | 2,507 | 1983, June 28 | 17 | 3 | 8 | 9 | McClelland and others, 1989 |
| | | | | | | | S. McNutt, unpub. data |

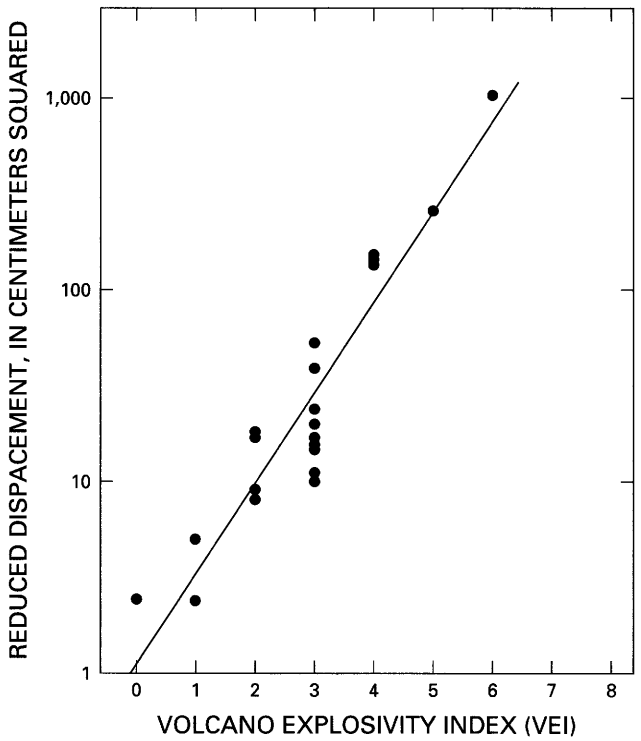


**Figure 1.** Volcanic tremor reduced displacement versus volcano explosivity index (VEI) of Newhall and Self (1982). The plotted line is a linear regression fit to the data. The correlation coefficient, $r$, is 0.93.

current VEI boundaries (Carey and Sigurdsson, 1989). Also, VEI = 3 is too broad a category in terms of aviation because it includes both eruptions that are hazardous to aviation as well as those that are not. VEI = 3 is also the unit that has the greatest scatter in figure 1. Despite these shortcomings, the VEI is well known and widely used in the volcanological community.

## VOLCANIC TREMOR

Volcanic tremor is a type of seismicity associated with active volcanoes. Its typical appearance on a seismic record, or seismogram, is that of an irregular sine curve or sine wave, and its key distinguishing feature is its long duration compared with earthquakes of the same amplitude or strength as recorded on a seismogram (McNutt, 1992). Terms such as "eruption signals" and "blast events" have also been used for some signals that are here referred to as volcanic tremor. Because terminology is not standardized and the purpose here is merely descriptive, the most general term has been used in this paper.

An example of a tremor seismogram is shown in figure 2, which shows data from Pacaya Volcano (Guatemala), recorded on a station 10 km from the vent. Tremor occurs for 1 hour, stops for 1 hour, then resumes for 2 hours. This is followed by an amplitude reduction for 1/2 hour, then strong tremor that nearly saturates the seismograms. This strong tremor was accompanied by an eruption of steam-and-ash clouds to a height of several kilometers. The seismogram shows several typical features of tremor: (1) long signal duration, (2) nearly monotonic low frequencies, and (3) amplitudes that vary over several time scales.

The Pacaya tremor was recorded at several seismic stations. In general, it is necessary to use a network of six to eight well-distributed stations, ranging in distance from 1 to 20 km from the volcanic vent. This permits the recording of both weak and strong volcanic tremor on-scale and the ability to discern tremor and other signals of volcanic origin from regional or distant earthquakes.

Volcanic tremor is nearly ubiquitous at active volcanoes. However, tremor occurs both during eruptions and during non-eruptive periods, so false alarms are possible. In general, eruption tremor is stronger and is of longer duration than non-eruption tremor. Otherwise, there are no known methods to distinguish eruption tremor from non-eruption tremor. Some data suggest that strong tremor has a longer period or lower frequency than weak tremor (Aki and Koyanagi, 1981), but the effect is slight.

The primary interest of this paper is to examine volcanic-tremor amplitudes or strengths during eruptions. For proper comparison between episodes of tremor at different volcanoes, the amplitudes are normalized to a common reference using a procedure called reduced displacement (R.D.). Two formulas are commonly used. For body waves (e.g., P-waves and S-waves) the formula of Aki and Koyanagi (1981) is:

$$\text{R.D.} = \frac{A(r)}{2\sqrt{2}\,M} \tag{1}$$

For surface waves (e.g., Rayleigh waves, Love waves, and PL-waves) the formula of Fehler (1983) is:

$$\text{R.D.} = \frac{A\sqrt{\lambda r}}{2\sqrt{2}M} \tag{2}$$

where

$A$ is the amplitude, in centimeters, peak-to-peak,
$r$ is the distance from source to seismic station, in centimeters,
$M$ is the seismograph magnification at the tremor frequency,
$\lambda$ is the tremor wavelength, in centimeters, and
$2\sqrt{2}$ is the root-mean-square (rms) amplitude correction.

Where possible, it is best to use values determined from several seismic stations located at a given volcano because these permit redundancy and error resolution. Such calculations have been performed for about 40 volcanoes; a subset of well-determined values from 21 eruptions at 14 well-studied volcanoes is shown in table 2 and figures 1 and 3. Note

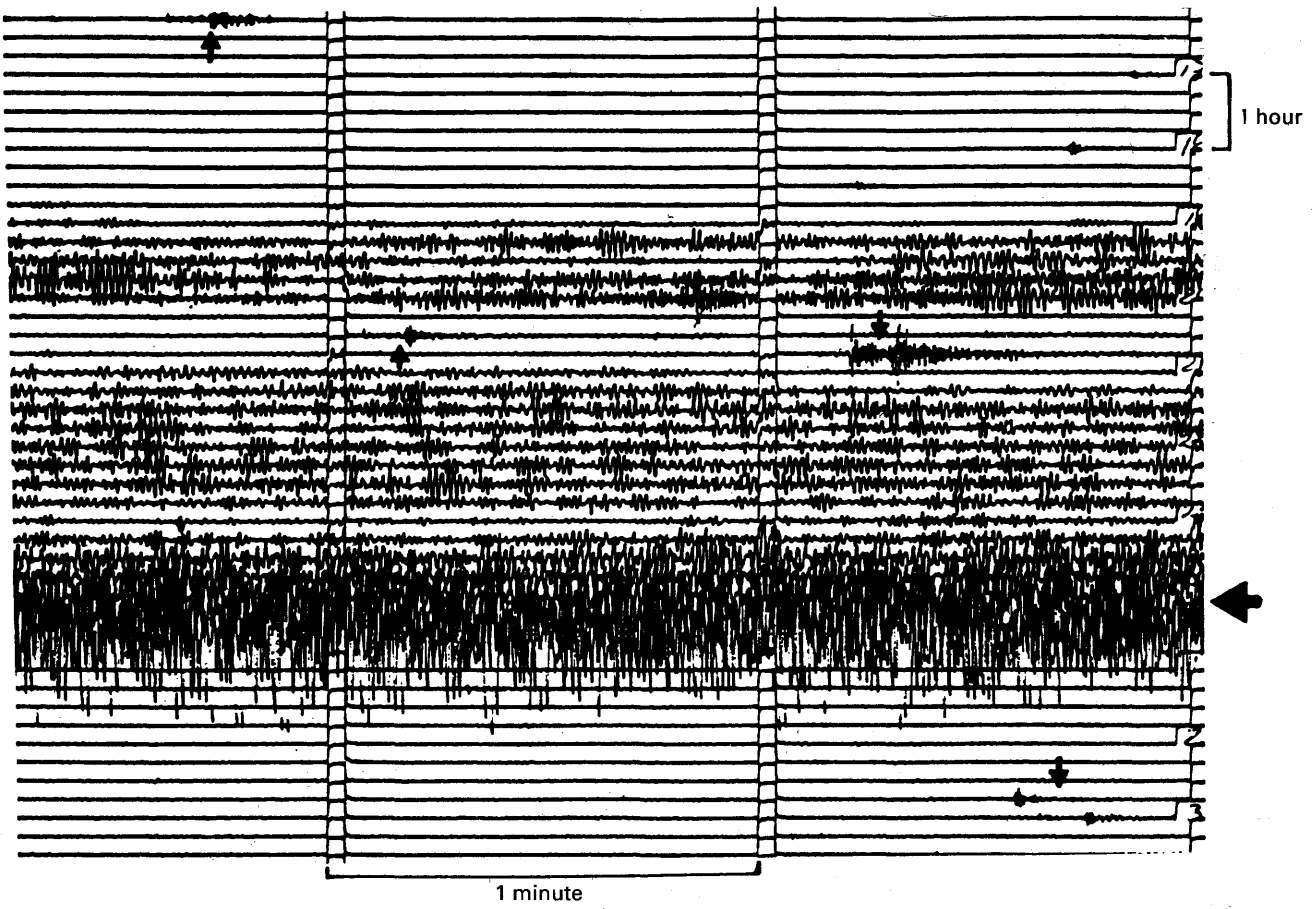


**Figure 2.** Portion of a seismogram from Pacaya Volcano, Guatemala, recorded on October 7, 1979. Time marks are at 1-minute intervals, and each line is 15 minutes apart from adjacent lines. Time increases from top to bottom and from left to right. Volcanic tremor of variable amplitude occurs for about 4.5 hours of the middle 6 hours of the record. A steam-and-ash eruption occurred during the strongest part of the signal (large arrow). The frequency of the tremor is about 1.5 Hz. Several nearby earthquakes are also recorded (small arrows).

that the tables and figures show one value per eruption. These are the tremor values that correspond to the peak VEI during each eruption.

## DATA SELECTION

Data used in this study are primarily published data from the last 20 years. A number of values were determined by the author from unpublished data that are part of an ongoing investigation (McNutt, 1992). For these cases, to assure quality control, it was necessary to examine the time series for both tremor and the eruption parameters so that details of the temporal relation between the two could be assessed.

Other studies have examined tremor amplitudes versus eruption parameters for many different times within single eruptions (Eaton and others, 1987; Koyanagi and others, 1988; McNutt and others, 1991). The present study, however, is concerned with establishing a general relationship between various volcanoes, assuming similarity of eruptions. Thus, plotting one value per eruption—the maximum tremor amplitude accompanying the maximum VEI—implies equal weighting of each eruption. VEI is the independent variable ($x$-axis). The accompanying tremor reduced displacement is plotted as the dependent variable ($y$-axis). The regression formula minimizes the $y$ errors. To use the data in the opposite sense—to forecast VEI from the tremor amplitude—the regression must be done with the variables reversed. For the data set of this paper, however, the difference is slight. An enlightening discussion of the issue of regression polarity is given by Bolt (1978).

A strength of the data set is that it spans six orders of magnitude in VEI. This is possible due to inclusion of data on Mt. Pinatubo (R. White, oral commun., 1991; White and others, 1992), which, at VEI = 6, is the largest eruption worldwide since the 1912 eruption of Katmai, Alaska. A limitation of the data set is that it consists of a relatively small number of eruptions. As more data are added, the derived parameters may change somewhat, although they will not change much because the six orders of magnitude of VEI provides stability. Roughly speaking, the VEI-5 and -6 data points "anchor" the upper end of the correlation; adding more data at the lower end will not significantly change the slope.

# RESULTS

## TREMOR AMPLITUDE VERSUS VEI

The primary result of this study is that tremor amplitudes increase as eruptions become more explosive. This is seen clearly in figure 1, which plots reduced displacement tremor amplitude versus VEI. A linear regression fit to the data yields the relation:

$$\log_{10}(\text{reduced displacement}) = 0.46(\text{VEI}) + 0.08$$

The correlation coefficient is $r = 0.93$, which is significant at greater than the 95 percent level. The derived relation spans six orders of magnitude of VEI and three orders of magnitude of tremor amplitude; hence, it is robust. There is scatter in the data of a factor of approximately 2 to 3, most of which is probably due to stochastic variation in parameters, similar to scatter shown in Carey and Sigurdsson (1989, their fig. 7).

## ASH-CLOUD HEIGHT VERSUS TREMOR AMPLITUDE

Tremor amplitudes increase as ash-cloud heights increase (fig. 3). A linear regression fit to the data for eruptions with ash-cloud heights of 3 km or more yields the relation:

$$\log_{10}(\text{reduced displacement}) = (1.80)\log_{10}(\text{ash-cloud height}) - 0.08$$

The correlation coefficient is $r = 0.75$, which is lower than for the VEI, but still significant at greater than the 95 percent level. For this plot, ash-cloud heights were measured above the vent, as opposed to above sea level (see tables 1 and 2). The derived relation spans two orders of magnitude in both tremor amplitude and cloud height. The scatter appears to be greater than in figure 1, and the correlation coefficient is lower, implying a worse fit. Further, there is a gap or offset in the data between about 1.5- and 3-km height. Four of the seven eruptions with cloud heights below 2 km are effusive eruptions of basaltic lava. Thus, the volumes are high, whereas the ash-column heights are low. The VEI is an aggregate index that averages these effects. This is probably the reason that no similar gaps are seen in figure 1.

## GENERAL FEATURES AND LIMITATIONS OF THE RELATIONSHIPS

Although volcanic tremor occurs during nearly all eruptions, specific features of tremor may be difficult to forecast in advance. Furthermore, physical conditions, such as vent geometry, may change as a function of time. Typically, the strongest tremor recorded at each volcano occurs during its largest or most explosive eruptions. Weaker tremor accompanies weaker or less explosive activity at the same volcano.

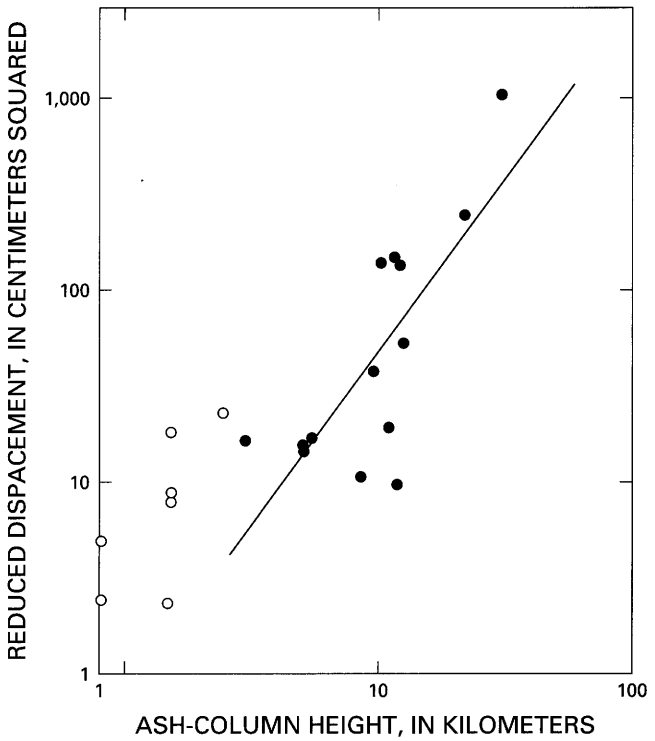


**Figure 3.** Volcanic tremor reduced displacement versus ash-cloud height above the vent. The plotted line is a linear regression fit of the data for eruptions in which the ash cloud reached a height of 3 km or more above the vent (solid symbols). Values below 3 km (open symbols) were not used in the regression. The correlation coefficient, $r$, is 0.75.

This assumes that the style of eruption remains similar. At some volcanoes, the first or "vent-clearing" phase of an eruption may be more explosive than later phases of activity. The vent-clearing phases are generally accompanied by strong tremor, whereas later phases are accompanied by weaker tremor. For example, many of the post-May 18, 1980, eruptions of Mount St. Helens, especially the dome-building eruptions, were very similar to each other; in fact the similarity of precursors permitted accurate forecasting of many of these events (Swanson and others, 1983). At Redoubt Volcano, Alaska, several of the later eruptions of the 1989–90 eruption sequence were forecast, whereas the earlier ones were not (Brantley, 1990; J.A. Power, written commun., 1992). At Mt. Spurr, Alaska, it took scientists 11 minutes to recognize the onset of the first eruption in June 1992, but only 3 minutes each for the second and third eruptions (Miller and others, 1992). Clearly, as volcanologists become more familiar with the characteristics of a specific volcano, a better job can be done in forecasting its eruptions and determining when an eruption is in progress.

Vent geometry and vent size can each affect tremor amplitudes for a given VEI. For example, at Kilauea Volcano (fig. 4) (Eaton and others, 1987), when the vents are

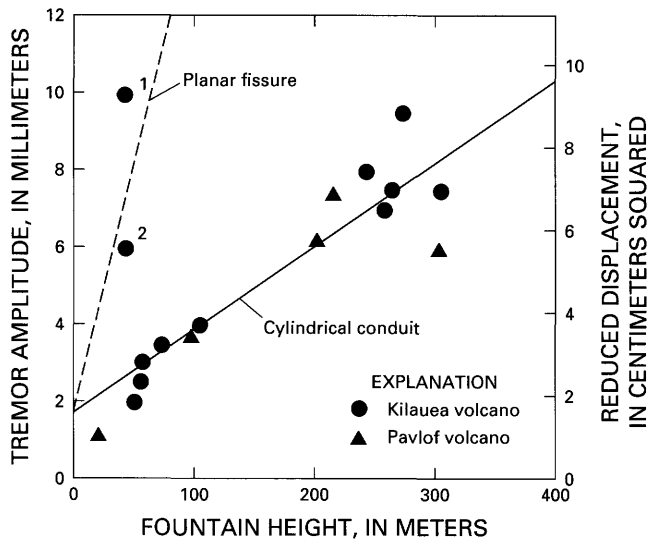


**Figure 4.** Volcanic tremor reduced displacement versus lava-fountain height. The solid line represents a linear regression fit to the Kilauea data. Points 1 and 2 are from fissures rather than cylindrical conduits. The dashed line fits these two points and is forced to intersect the $y$-axis at 1.7 $cm^2$. Figure modified from Eaton and others (1987).

more fissure-like, or less cylindrical, the tremor amplitudes are higher by about a factor of 7 for the same height of lava fountaining. Thus, knowledge of vent geometry prior to eruptions can be used to help estimate explosivity based on tremor amplitude, but the fact that many vents change size or shape during the course of eruptions may require frequent updating of such information. For many stratovolcanoes, vent geometry remains relatively unchanged for periods of years, such as Pavlof Volcano from 1973 to 1984 (McNutt, 1987). Other factors that may affect amplitudes are attenuation, coupling, and nonlinearity.

## NON-ERUPTION TREMOR

This study has focused on tremor that occurred during known eruptions. At a number of volcanoes, however, tremor occurs during times of no eruptions, although this tremor is generally weak. The strongest known non-eruption tremor is a deep (> 40 km) tremor at Kilauea (Aki and Koyanagi, 1981). Such non-eruption tremor could contribute substantially to the false-alarm rate of a warning system based on the detection of volcanic tremor. A threshold value, or critical amplitude of tremor, must be defined.

A recent study based on a worldwide sample of tremor from more than 80 volcanoes (McNutt, 1992) showed that about 60 percent of tremor episodes accompanied eruptions of gas, ash, or lava. About half of the remaining tremor episodes, or 20 percent, occurred within the 10 days immediately preceding or following eruptions. These data probably represent the upper range of the false-alarm rate: 20 to 40 percent of tremor episodes occur with no eruption. Combining information on amplitudes, frequencies of tremor, and durations of tremor episodes could reduce that rate significantly. It is not known whether the amplitude of precursory tremor can be used to forecast the size of an upcoming eruption.

# DISCUSSION AND CONCLUSIONS

The results of this paper can be thought of physically as an application of Newton's second law: for every action, there is an equal and opposite reaction. Ash, magma, and gas move up, and the ground deforms and vibrates in response. Thus, the observed relations translate the second law into volcano-seismology terms. The observed scatter is considerable, however, and is probably caused by stochastic variation as well as factors including vent size, vent geometry, attenuation, coupling, and possible nonlinearity. At volcanoes, we seldom know the size or shape of the vent at the time of eruption, and our knowledge of coupling of gas-charged magma to wallrock is very poor. A recent example is dome-collapse events at Unzen Volcano, some of which were nearly aseismic, although the events produced ash clouds (H. Okada, oral commun., 1991).

Despite these limitations, however, the derived relationships provide useful information, which must be applied with an appropriate level of conservatism. Two key factors are the threshold or critical amplitude of tremor and the false-alarm rate. Figures 1 and 3 show that ash typically does not reach altitudes hazardous to aircraft unless the tremor amplitude is $\geq 10$ $cm^2$. Therefore, this is the critical amplitude of tremor (the amplitude above which appropriate hazard-mitigation actions would be taken). Regarding false alarms, it was stated above that, in the worst case, the false-alarm rate is between 20 and 40 percent based on study of a worldwide sample (McNutt, 1992). Thus, if the critical amplitude of tremor is reached, results suggest that there is a 60 to 80 percent chance that a hazardous, ash-producing eruption is taking place, but there is a 20 to 40 percent chance that one is not.

Clearly, some sort of confirmation is needed. This might be visual confirmation, if weather conditions permit, or a signal observed on a microbarograph, lightning detector, slow-scan TV, hydrologic sensor, or other device. It is important to note that the onset of the tremor signal either precedes or occurs at the time the eruption begins, so it is the first geophysical signal to be recorded because seismic waves travel at speeds of several kilometers per second. Once confirmation is achieved, the tremor amplitude and duration together may be used to estimate the likely size of the eruption, including estimates of the tephra volume and height of ash clouds. Data published by Scandone and

Malone (1985) for Mount St. Helens illustrate one example of how this might work.

In practice, there would generally be a time delay of several minutes between the onset of tremor and the time that a warning could be issued. This is because tremor and some low-frequency or long-period discrete earthquakes share common onsets (Fehler, 1983). Because, by definition, discrete earthquakes will end whereas tremor is continuous, it may take several minutes to determine if the event ends. In general, discrete earthquakes have longer durations as their magnitudes increase, so the verification time increases with event size. For magnitude 2 events, typical durations are 50 seconds, increasing to 300 seconds for magnitude 4. However, since the rate of ascent of ash clouds is on the order of 20 to 100 m/sec (Voight, 1981), this would still give at least several minutes lead time before the ash reached altitudes hazardous to aircraft. Nevertheless, a procedure would need to be developed to turn off an alarm if an event thought to be tremor turned out to be a low-frequency earthquake instead.

Eruptions are not uniform processes, so tremor amplitudes and other parameters often vary by about an order of magnitude during a single eruption phase. In some cases, tremor amplitude is high at the beginning and end of an episode but low in the middle (e.g., Pinatubo—R. White, oral commun., 1991), whereas, in many others, amplitudes begin small, grow large, then decline (such as Puu Oo—Koyanagi and others, 1988; and Pavlof—McNutt, 1987). These observations suggest that estimates of tephra volume and ash-cloud height based on tremor amplitudes may need to be revised several times over the course of a single eruption.

These features suggest a practical approach consisting of warning, confirmation, and updates. The warning would be that an eruption producing tephra may be in progress based on the identification of volcanic tremor. Then the reduced displacement would be calculated, the duration measured, and the event detected using field observations and other monitoring techniques, such as microbarographs, lightning detectors, or slow-scan television. A confirmation would state that an eruption is taking place and would provide first estimates of ash-column height and tephra volume. Alternatively, this would be the time to cancel the warning if the suspected eruption was not confirmed or if a low-frequency seismic event occurred instead of tremor. Later updates would estimate ash-cloud height and tephra volume based on variations in tremor amplitude. Finally, a last notification would indicate that the eruption was over. As more experience is gained with a given volcano, it would be expected that the false-alarm rate would decline and the estimates of eruption parameters would improve.

## RECOMMENDATIONS

1. For volcanoes where we have no observational capability but where we have a seismic network, the method described in this paper offers an important chance to determine if an eruption has occurred and if that eruption produced ash that could threaten aircraft. Thus, it is necessary for seismologists to install a sufficient number of seismic stations, typically six to eight stations at each monitored volcano, to determine earthquake and tremor source locations and amplitudes with confidence and to permit error resolution.
2. Information on tremor could be important to giving early warnings and to developing a probabilistic format for information dissemination from volcano observatories to emergency management agencies. A warning only a few minutes after tremor is recorded could be based on seismic data alone, then confirmed and updated approximately every 20 to 30 minutes. Such a message might read, "Based on the recording of volcanic tremor of amplitude 10 $cm^2$, we believe that there is a 60 to 80 percent chance that an eruption began at 08:00 hours and may have produced ash clouds to heights of 10 km and a tephra volume of approximately $10^7$ $m^3$."
3. Volcano observatories need to standardize the reporting of volcanic tremor so that reduced displacements are routinely used. Reports of tremor should state the onset time, duration in minutes, frequency in hertz, and reduced tremor amplitude displacement in $cm^2$. Seismograph type and location should also be stated explicitly.
4. Volcanologists need to increase the observational database to make the results more robust and to better interpret scatter or trends depending on factors such as composition of the magma, vent geometry, and amplitude versus duration of individual tremor episodes. The VEI scale needs to be modified so that more eruptions fall within the parameter boundaries, such as ash-column height and volume. Further, a weighted VEI needs to be developed for use in aviation problems, with extra weight given to ash-column height and to suspended-ash volume.

## ACKNOWLEDGMENTS

I thank Thomas J. Casadevall, John A. Power, and Robert A. Page for reviewing the manuscript, William E. Scott for sending me a preprint of his Redoubt manuscript, and David H. Harlow for generously providing his unpublished data over the years.

## REFERENCES CITED

Aki, K., and Koyanagi, R.Y., 1981, Deep volcanic tremor and magma ascent mechanism under Kilauea, Hawaii: Journal of Geophysical Research, v. 86, p. 7095–7110.

Bolt, B.A., 1978, Incomplete formulations of the regression of earthquake magnitude with surface fault rupture length: Geology, v. 6, p. 233–235.

Brantley, S.R., ed., 1990, The eruption of Redoubt Volcano, Alaska, December 14, 1989–August 31, 1990: U.S. Geological Survey Circular 1061, 33 p.

Catalog of Active Volcanoes and Solfatara Areas of the World, 1950–1975: Rome, Italy, International Association of Volcanology and Chemistry of the Earth's Interior

Carey, S.N., and Sigurdsson, H., 1989, The intensity of Plinian eruption columns: Bulletin of Volcanology, v. 51, p. 28–40.

Casadevall, T.J., and De Los Reyes, P.J., 1991, Impact of June 1991 Pinatubo eruptions on aircraft operations in the western Pacific and southeast Asia [abs.]: Eos, Transactions, American Geophysical Union, v. 72, no. 44 [supplement], p. 95.

Eaton, J.P., Richter, D.H., and Krivoy, H.L., 1987, Cycling of magma between the summit reservoir and Kilauea Iki lava lake during the 1959 eruption of Kilauea Volcano, *in* Decker, R.W., Wright, T.L., and Stauffer, P.H., eds., Volcanism in Hawaii: U.S. Geological Survey Professional Paper 1350, p. 1307–1335.

Fedotov, S.A., and Markhinin, Ye. K., eds., 1983, The Great Tolbachik Fissure Eruption, Geological and Geophysical Data, 1975–1976: Cambridge, England, Cambridge University Press, 341 p.

Fehler, M., 1983, Observations of volcanic tremor at Mount St. Helens volcano: Journal of Geophysical Research, v. 88, p. 3476–3484.

Gorel'chik, V.I., Stepanov, V.V., and Khanzutin, V.P., 1983, Volcanic tremor during the great Tolbachik fissure eruption of 1975, *in* Fedotov, S.A., and Markhinin, Ye. K., eds., The Great Tolbachik Fissure Eruption: Cambridge, England, Cambridge University Press, p. 204–213.

Gorshkov, G.S., and Dubik, Y.M., 1970, Gigantic directed blast at Sheveluch Volcano (Kamchatka): Bulletin Volcanologique, v. 34, p. 261–288.

Harris, D.M., Rose, W.I., Jr., Roe, R., and Thompson, M.R., 1981, Radar observations of ash eruptions, *in* Lipman, P.W. and Mullineaux, D.R., eds., The 1980 Eruptions of Mount St. Helens, Washington: U.S. Geological Survey Professional Paper 1250, p. 323–333.

Koyanagi, R.Y., Tanigawa, W.R., and Nakata, J.S., 1988, Seismicity associated with the eruption, *in* Wolfe, E.W., ed., The Puu Oo eruption of Kilauea Volcano, Hawaii: Episodes 1 through 20, January 3, 1983, through June 8, 1984: U.S. Geological Survey Professional Paper 1463, p. 183–235.

McClelland, L., Simkin, T., Summers, M., Nielson, E., and Stein, T.C., 1989, Global Volcanism 1975–1985: Englewood Cliffs, N.J., Prentice-Hall, 655 p.

McNutt, S.R., 1987, Volcanic tremor at Pavlof Volcano, Alaska, October 1973–April 1986: Pure and Applied Geophysics, v. 125, p. 1051–1077.

———1992, Volcanic tremor, *in* Nierenberg, W.A., ed., Encyclopedia of Earth System Science, v. 4, p. 417–425.

McNutt, S.R., and Harlow, D.H., 1983, Seismicity at Fuego, Pacaya, Izalco, and San Cristobal Volcanoes, Central America, 1973–1974: Bulletin Volcanologique, v. 46, no. 3, p. 283–298.

McNutt, S.R., Miller, T.P., and Taber, J.J., 1991, Geological and seismological evidence of increased explosivity during the 1986 eruptions of Pavlof Volcano, Alaska: Bulletin of Volcanology, v.53, p. 86–98.

Miller, T.P., and Davies, J.N., 1990, The 1989–90 eruption of Redoubt Volcano: A chronological summary of events and effects [abs.]: Eos, Transactions, American Geophysical Union, v. 71, no. 43, p. 1700.

Miller, T.P., Power, J.A., Eichelberger, J.C., McNutt, S.R., and Davies, J.N., 1992, The 1989–90 Redoubt and 1992 Mt. Spurr volcanic eruptions: Response procedures of the Alaska Volcano Observatory [abs.]: Eos, Transactions, American Geophysical Union, v. 73, no. 43 [supplement], p. 68.

Newhall, C.G., and Self, S., 1982, The volcano explosivity index (VEI): An estimate of explosive magnitude for historical volcanism: Journal of Geophysical Research, v. 87, p.1231–1238.

Pinatubo Volcano Observatory Team, 1991, Lessons from a major eruption: Mt. Pinatubo, Philippines [abs.]: Eos, Transactions, American Geophysical Union, v. 72, p. 545, 552–553, 555.

Reeder, J.W., and Lahr, J.C., 1987, Seismological aspects of the 1976 eruptions of Augustine Volcano, Alaska: U.S. Geological Survey Bulletin 1768, 32 p.

Sarna-Wojcicki, A.M., Shipley, S., Waitt, R.B., Jr., Dzurisin, D., and Wood, S.H., 1981, Areal distribution, thickness, mass, volume, and grain size of air-fall ash from the six major eruptions of 1980, *in* Lipman, P.W., and Mullineaux, D.R., eds., The 1980 Eruptions of Mount St. Helens, Washington: U.S. Geological Survey Professional Paper 1250, p. 577–600.

Scandone, R., and Malone, S.D., 1985, Magma supply, magma discharge and readjustment of the feeding system of Mount St. Helens during 1980: Journal of Volcanology and Geothermal Research., v. 23, p. 239–262.

Scott, W.E., and McGimsey, R.G., in press, Character, mass, distribution, and origin of tephra-fall deposits of the 1989–1990 eruption of Redoubt Volcano, south-central Alaska: Journal of Volcanology and Geothermal Research.

Simkin, T., Siebert, L., McClelland, L., Bridge, D., Newhall, C., and Latter, J.H., 1981, Volcanoes of the World: Stroudsburg, Pa., Hutchinson Ross Co., 232 p.

Swanson, D.A., Casadevall, T.J., Dzurisin, D., Malone, S.D., Newhall, C.G., and Weaver, C.S., 1983, Predicting eruptions at Mount St. Helens, June 1980–December 1982: Science, v. 221, p. 1368–1376.

Tsuya, H., 1955, Geological and petrological studies of volcano Fuji 5: Tokyo Daigaku Jishin Kenkyusho Iho, v. 33, p. 341–382.

Voight, B., 1981, Time scale for the first moments of the May 18 eruption, *in* Lipman, P.W., and Mullineaux, D.R., eds., The 1980 Eruptions of Mount St. Helens, Washington: U.S. Geological Survey Professional Paper 1250, p. 69–86.

White, R.A., Harlow, D.H., and Chouet, B.A., 1992, Long period earthquakes preceding and accompanying the June 1991 Mount Pinatubo eruptions [abs.]: Eos, Transactions, American Geophysical Union, v. 73, no. 43 [supplement], p. 347.

VOLCANIC ASH AND AVIATION SAFETY:
Proceedings of the First International Symposium
on Volcanic Ash and Aviation Safety
U.S. GEOLOGICAL SURVEY BULLETIN 2047

# AIRBORNE RADAR DETECTION OF VOLCANIC ASH

*By* Mark E. Musolf

## ABSTRACT

Detection of volcanic ash clouds by both ground-based and airborne radar systems is highly desirable. Airborne radars would provide in-flight detection of ash clouds for regions where ground-based radar coverage is not available, allowing for real-time pilot reaction to a potentially dangerous situation. Present airborne weather radars are insufficient for detection of volcanic ash particles or clouds due to the power/aperture and sensitivity limitations of these systems. Three different airborne radar configurations, X-band (9.5 GHz), Ku-band (16 GHz), and millimeter (95 GHz), are analyzed to determine their effectiveness for detection of volcanic ash. Volcanic-ash-cloud detection and signal-to-noise ratio are evaluated as a function of operating frequency, radar cross section, and range. Along with performance evaluation, antenna parameters (gain, beam widths) and waveform parameters are addressed.

The results of the volcanic-ash-detection analysis revealed that a high-power Ku-band airborne radar could provide the necessary detection performance against light ash, given some prior knowledge of a volcanic eruption. The analysis also confirmed the inadequacy of existing X-band weather radars for detection of light volcanic ash.

## INTRODUCTION

For the past decade, volcanologists, meteorologists, and engineers have studied the effect of volcanic ash on air traffic safety. It has been well documented that aircraft flying into a volcanic ash cloud increase the risk of a major accident due to engine failure (Brantley, 1990). The airborne detection of a volcanic ash cloud would warn the pilot of potential danger ahead. During daylight hours, ash clouds can be visually distinguished from normal rain clouds; however, during night operations, pilots have no means of ash-cloud detection. Conventional X-band airborne weather radars (table 1) are specifically designed for detection of severe natural weather phenomena rather than clouds of very small dielectric particles.

This study addresses the limitation of existing radar systems and suggests an ideal, conceptual radar design based on the technology that exists today and will exist in the future. The radars selected for analysis contain parameters (power, antenna gain, beam widths) that are typical of many weather radars in existence today.

## APPROACH

A detailed radar analysis was performed for the detection of volcanic ash clouds. The study was subdivided into the following areas:

A. *Ash detection design considerations.*—Areas of study included (1) operating-frequency selection, based on reflectivity per unit volume and atmospheric attenuation, and (2) power/aperture limitations.

B. *Detection-range performance.*—Typical radar parameters from existing commercial and military weather radar systems were used in the analysis. Signal-to-noise ratio was calculated to determine detection-range performance based on the reflectivity of volcanic ash.

C. *Configuration summary matrix.*—Advantages and disadvantages of each of the radar operating frequencies that were analyzed for volcanic ash detection were summarized.

D. *Airborne radar technology advances.*—Applicability of the latest airborne radar technology advances to volcanic ash detection was addressed.

E. *Ideal conceptual-design requirements.*—Airborne radar conceptual-design requirements were developed based on existing technologies.

## ASH-DETECTION CONSIDERATIONS

The detection of volcanic ash clouds is very difficult for an airborne weather radar due to the very low reflectivity of ash-particle clouds. The reflectivity is orders of magnitude smaller than the reflectivity of light rain. Ash-cloud detection is also limited by the very low power/aperture products of existing airborne weather radars. This section will address each of these effects.

The detection of volcanic ash is highly dependent on the operating frequency of the radar because the reflectivity per

**Table 1.** Conventional airborne weather radars.

[From Business and Commercial Aviation, 1989; Blake, 1990]

| Radar type | Existing sensors | Frequency band |
|---|---|---|
| Commercial | Primus 500 | X-band |
| | Primus 708 | X-band |
| | WXR-700 | X-band |
| Military | AN/APS-133 | X-band |

**Table 2.** Atmospheric attenuation at 4-km altitude.

[From Nathanson, 1991; Norden Systems, Inc., unpub. data]

| Operating frequency | Two-way atmospheric attenuation (dB/km) |
|---|---|
| X-band | 0.02 |
| Ku-band | 0.03 |
| 95 GHz | 0.2 |

unit volume of ash is inversely proportional to wavelength. The reflectivity per unit volume ($\eta$, in units of $m^{-1}$) is computed using the following equation (Nathanson, 1991):

$$\eta = \frac{\pi^5}{\lambda^4}|K|^2 Z \qquad (1)$$

$$|K|^2 = \left|\frac{\varepsilon - 1}{\varepsilon + 1}\right|^2 = 0.36 = \text{(light ash fall)}; \quad Z = \Sigma D^6 \qquad (2)$$

where

$\lambda$ is the radar wavelength,

$\varepsilon$ is the dielectric constant of a spheroid, and

$D$ is the diameter of a droplet or particle.

The reflectivity for three rainfall rates (16 mm/hr, 4 mm/hr, and 1 mm/hr), dense ash cloud, and light ashfall were computed as a function of the radar operating frequency, based on parameters given in Harris and Rose (1983) for dense ash cloud, Harris and others (1981) for light volcanic ash, and Nathanson (1991) for rain. The results are given in figure 1. Note, for rain, $Z$ is expressed as $Z = ar^{1.6}$, where $r$ is the rainfall rate in mm/hr and $a$ is approximately 200. For frequencies above 35 GHz, the data were extrapolated from data of R. Crane and H. Burke, presented in Nathanson (1991, p. 216–218 and 232–234).

The reflectivity of light ash fall is approximately 40 dB ($10^4$ times) to 25 dB (320 times) smaller than the light rain (1 mm/hr) condition. Based on reflectivity alone, higher frequency radars will yield better detection due to stronger backscatter.

Atmospheric attenuation is also a function of operating frequency. Attenuation is inversely proportional to operating frequency. The round-trip atmospheric attenuation for X-band, Ku-band, and 95 GHz is given in table 2.

Both reflectivity and atmospheric-attenuation results for the selected operating frequencies were incorporated into the detection-range-performance analysis.

The airborne radar systems power/aperture product also contributes to detection performance. The power/aperture product is the product of the radiated average power and antenna gain of the radar. The larger the power/aperture product, the greater the detection performance. The power/aperture product of airborne weather radar systems are limited by the size, weight, and cost of the sensor. Conventional airborne weather radars utilize high-peak-power, low-duty-cycle transmitters producing very low average power. High-average-power transmitters, which are used on advanced military multi-mode radars, are heavy and too expensive for commercial application. As technology progresses, the weight and cost of high-average-power transmitters may be reduced to a level that is acceptable for future airborne weather radars.

Maximum antenna gain is determined by the largest physical area available for the antenna aperture. Conventional weather radars are located in the nose of the aircraft to provide for maximum forward-looking surveillance coverage. The physical dimensions available for the antenna aperture is 10 by 10 inches in small aircraft and 30 by 30 inches in larger aircraft. For a constant area, antenna gain is only a function of operating frequency. The gain is inversely proportional to wavelength. Therefore, higher operating frequencies will yield a higher antenna gain. Antenna gain as a function of operating frequency was considered in the detection analysis.

## DETECTION-RANGE PERFORMANCE

To determine the detection-range performance of volcanic ash clouds, the signal-to-noise ratio is computed. The generic signal-to-noise ratio (SNR) equation is given by (Barton, 1976, p. 110–114):

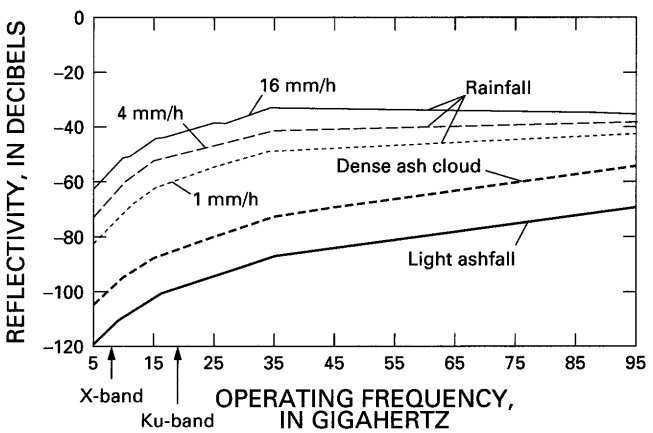


**Figure 1.** Reflectivity versus radar operating frequency for rain and volcanic ash.

$$\mathrm{SNR} = \frac{P_p \tau N G^2 \lambda^2 \sigma}{(4\pi)^3 K T F n L_{hp} L a R^4} \quad (3)$$

where

$P_p$ is peak power,
$\tau$ is the transmitted pulse width,
$N$ is the integration gain,
$G$ is the antenna gain,
$\lambda$ is the wavelength,
$\sigma$ is the radar cross section in resolution cell,
$KT$ is the thermal noise factor ($K$ is the Boltzmann constant; $T$ is the absolute temperature),
$Fn$ is the noise figure,
$L_{hp}$ is the hardware and processing loss,
$La$ is the atmospheric attenuation (two-way), and
$R$ is the range to target or clutter.

For a point target, such as an aircraft, truck, or building, $\sigma$ is the radar cross section of the specific target. Because volcanic-ash-cloud detection is based on a distributed target, $\sigma$ is a volumetric radar cross section. Therefore, the volumetric signal-to-noise ratio equation is required.

The volumetric radar cross section equation is given by (Eaves and Reedy, 1987):

$$\sigma = \eta V \quad (4)$$

where

$\sigma$ is the radar cross section in the resolution cell,
$\eta$ is the radar reflectivity per unit volume, and
$V$ is the volume of the resolution cell.

The volume of the resolution cell is computed by (Eaves and Reedy, 1987):

$$V = \frac{\pi}{4} R^2 \theta az \theta el Wr \quad (5)$$

where

$\theta az$ is the azimuth beam width,
$\theta el$ is the elevation beam width, and
$Wr$ is the range resolution.

The volumetric signal-to-noise ratio equation is given by:

$$\mathrm{SNR_V} = \frac{\pi^3 P_p \tau N G^2 \theta az \theta el Wr |K|^2 Z}{256 \lambda^2 R^2 K T F n L_{hp} La} \quad (6)$$

The conventional airborne radar configuration parameters that were utilized in the detection analysis are given in table 3.

The signal-to-noise ratio was calculated as a function of detection range for the four radar configurations based on the light-ash reflectivity previously computed. To achieve detection of the ash cloud, a signal-to-noise ratio (SNR) of at least 6 dB is required. The SNR detection plot is given in figure 2. The performance of the 95-GHz radar is very poor due to the low average power, large atmospheric attenuation, and small azimuth beam width. The commercial X-band radar has very low SNR due to very low reflectivity and low average power. The military X-band radar has better performance than the commercial radar due to 13 dB of greater average power. This radar would be able to detect ash clouds at approximately 10 km—this is too close to prevent penetration into the cloud. The best performance would be achieved with a scaled Ku-band weather radar, due to greater antenna gain and larger ash reflectivity. This radar would detect ash clouds out to approximately 25 km. For the desired detection range of 75 km, 10 dB in additional power/aperture and (or) integration gain would be required. To achieve 10 dB of integration gain, the radar scan rate would be reduced to approximately 1/18th of the normal scan rate. This new scan rate could be utilized in a special ash-detection radar mode. Based on detection-range-performance analysis, existing conventional airborne weather radar falls well short of achieving acceptable ash detection.

**Table 3.** Conventional airborne radar parameters.

[Radar parameters are based on various, existing airborne radar systems. Az, azimuth; elev., elevation; proc., processing; Atmos., Atmospheric]

| Parameter | X-band[1] | X-band[2] | Ku-band[3] | 95 GHz |
|---|---|---|---|---|
| Average power (W) | 3.4 | 65 | 65 | 4.5 |
| Antenna gain (dB) | 34 | 33 | 37 | 49 |
| Az. & elev. beam width (°) | 4 | 2.9 | 1.7 | 0.35 |
| Range resolution (m) | 525 | 750 | 750 | 60 |
| Reflectivity factor ($mm^6/m^3$) | 0.1 | 0.1 | 0.1 | 0.1 |
| Refractive index | 0.36 | 0.36 | 0.36 | 0.36 |
| Noise figure (dB) | 7 | 8 | 8 | 9.5 |
| Hardware & proc. loss (dB) | 4 | 4 | 4 | 4 |
| Atmos. loss (dB/km) | 0.02 | 0.02 | 0.03 | 0.2 |

[1] Commercial weather radar.
[2] APS-133.
[3] Scaled APS-133.

# CONCLUSIONS

The results of this detection analysis reveal that severe problems exist with the airborne detection of volcanic ash clouds. Each of the radar operating frequencies analyzed offers advantages and disadvantages for detection. A configuration summary is given in table 4.

Even though most conventional airborne weather radars are at X-band, this may not be the optimal frequency band for volcanic ash detection. Based on the results of this study, a high-average-power (at least 500 watts) Ku-band radar could provide the necessary detection performance. However, to insure detection, the airborne radar sensor would require a prior knowledge of a volcanic eruption. The radar would initiate a special radar mode of operation when volcanic ash is expected in the area. The antenna would be tilted

**Table 4.** Summary of radar operating frequencies.

| Configuration | Advantage | Disadvantage |
|---|---|---|
| X-band | •Existing commercial and military equipment.<br>•High power transmitters used on military multimode airborne radars.<br>•Light atmospheric and rain attenuation. | •Small reflectivity per unit volume. |
| Ku-band | •Existing military equipment.<br>•High-power transmitters used on military multimode airborne radars. | •No commercial weather radars at this band.<br>•Heavy atmospheric and rain attenuation. |
| 95 GHz | •Large reflectivity per unit volume.<br>•Light weight. | •Low average power transmitters.<br>•Very heavy rain attenuation.<br>•Narrow beam widths. |

up to eliminate ground-clutter effects, and an optimized waveform for close-in range surveillance (about 75 km) would be transmitted. The antenna scan rate would be reduced to allow for maximum integration gain. Advanced signal processing techniques could also be employed for volcanic-ash-cloud discrimination. Doppler processing, waveform pulse-code matching, and polarization diversity could be utilized for particle detection and identification. These areas will be a topic for further study.

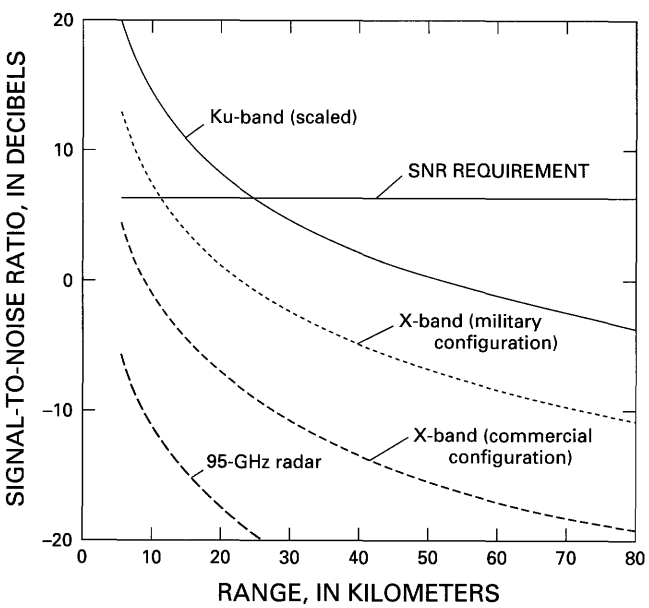


**Figure 2.** Signal-to-noise ratio (SNR) versus range for airborne detection of volcanic ash by radar.

## ACKNOWLEDGMENTS

The author would like to thank Dr. Lester Kosowsky, Dr. Dan Held, and Mr. Robert Guarino for their support and technical contributions in the area of volumetric detection.

## REFERENCES CITED

Barton, D.K., 1976, Radar System Analysis [Artech Radar Library]: Englewood Cliffs, N.J., Prentice-Hall, 608 p.

Blake, B., 1990, Radar and electronic warfare systems, *in* Jane's—Radar and Electronic Warfare Systems 1990–91: Alexandria, Va., Jane's Information Group, p. 213.

Brantley, S.R., 1990, The eruption of Redoubt Volcano, Alaska, December 14, 1989–August 31, 1990: U.S. Geological Survey Circular 1061, 33 p.

Business and Commercial Aviation, 1989, May, p. 208–213.

Eaves, J.L., and Reedy, E.K., 1987, Principles of Modern Radar: New York, Van Nostrand Reinhold Company, 712 p.

Harris, D.M., and Rose, W.I., 1983, A radar method for estimating particle sizes, concentrations and total ashfall mass in volcanic ash clouds: Applications and comparisons with ashfall data: Journal of Geophysical Research, v. 88, p. 10969–10983.

Harris, D.M., Rose, W.I., Roe, R., and Thompson, M.R., 1981, Radar observations of ash eruptions, *in* Lipman, P.W., and Mullineaux, D.R., eds., The 1980 Eruptions of Mount St. Helens, Washington: U.S. Geological Survey Professional Paper 1250, p. 323–333.

Nathanson, F.E., 1991, Radar Design Principles: Signal Processing and the Environment: New York, McGraw-Hill, 720 p.

VOLCANIC ASH AND AVIATION SAFETY:
Proceedings of the First International Symposium
on Volcanic Ash and Aviation Safety
U.S. GEOLOGICAL SURVEY BULLETIN 2047

# RADAR REMOTE SENSING OF VOLCANIC CLOUDS

*By* William I. Rose *and* Alexander B. Kostinski

## ABSTRACT

Ground-based meteorological radar systems have been very useful at tracking ash clouds for distances of several hundred kilometers from the radar station; however, aircraft-based radar with wavelengths of several centimeters does not detect volcanic ash clouds because ash particles are generally smaller than raindrops. Of even greater importance, ground-based radars represent the best known method for determining the height of ash clouds—these data are central to mitigating ash-cloud hazards. Although radar observations of ash clouds have been made only with radar systems designed for thunderstorms, it may be possible to design a volcanic-cloud radar system that would optimize parameters for volcanic clouds. An optimal system should have a wavelength range of 3 mm to 3 cm, a range of about 300 km, a Doppler capability, and it should be portable. A principal contribution of ground-based radar could be the real-time determination of volcanic-cloud locations in three dimensions. Such data could be overlain on air traffic control monitors and could serve as initial input to cloud-dispersal models to allow trajectory forecasts for the first few hours after detection.

## INTRODUCTION

Meteorological radar is a familiar tool for aviation. Ground-based meteorological radar systems exist at many airports to locate major storm clouds, and airborne radar systems help pilots avoid rain clouds. Recently, Doppler radar systems have been installed at airports to help identify windshear hazards. This paper is directed to the problem of how radar systems can help with the mapping of volcanic ash clouds. We review some uses of ground-based radar systems during ash eruptions and make recommendations about how radar systems can best contribute to a comprehensive plan for mitigating aviation hazards from ash clouds.

## METHODS OF STUDY

The use of radar to observe ash eruptions is not widespread. In the United States, radar was used during the 1976 eruptions of Augustine Volcano, Alaska (Johnston, 1976; Kienle and Shaw, 1979). During the Mount St. Helens activity of 1980–82, we had the opportunity to collect observations using National Weather Service (NWS) and Federal Aviation Administration (FAA) radar systems. These results were reported in detail by Harris and others (1981) and Harris and Rose (1983). A summary of those results is useful here to provide a basis for recommendations.

## SUMMARY OF RESULTS

The May 18, 1980, eruption of Mount St. Helens produced an extensive ash cloud that was detected and mapped by the geostationary operational environmental weather satellites (GOES) and FAA radar systems (fig. 1). As the data show, the radar detects a smaller, presumably denser, portion of the ash cloud than that detected in the GOES image. Subsequent eruptions of Mount St. Helens during 1980–82 produced ash clouds that were much smaller than the May 18 cloud. Some of these ash clouds were mapped by NWS radar at Portland, Oreg. The smallest eruption detected was the March 19, 1982, event, which was estimated to have produced about $4\times10^{11}$ g of ash and, more importantly, lasted only 30–40 seconds (Harris and Rose, 1983). This eruption duration is 1,000 times shorter and its ash volume is more than 1,000 times smaller than the $5\times10^{14}$–$6\times10^{14}$ g of ash produced on May 18, 1980. These data attest to the ability of meteorological radars to detect ash clouds that span a wide range of scales. Both of these eruptions probably had radar reflectivities that lie near the lower end of the wide dynamic range that is detectable by ground-based meteorological radar systems.

### ASH-CLOUD DETECTION

Ash clouds and thunderstorms cause backscatter of some of the radar energy that is incident upon them. The reflectivity of a radar target is a function of the abundance of particles and their scattering cross section within the target. The reflectivity, $\eta$, is the summation of the backscatter cross sections of the particles per unit volume averaged over the radar pulse volume (Atlas, 1964). For solid spherical

particles small enough to obey Rayleigh scattering, the back-scattered reflectivity is equal to:

$$\eta = \frac{2^6\pi^5}{\lambda^4} \times \left|\frac{\varepsilon - 1}{\varepsilon + 2}\right|^2 \Sigma r^6 \qquad (1)$$

where

$\lambda$ is the wavelength,

$\varepsilon$ is the dielectric constant of the reflecting particles, and

$r$ is the radius of spherical particles.

The expression for the received power ($P_r$) from a target composed of randomly distributed particles (Probert-Jones, 1962; Serafin, 1990) is:

$$P_r = \frac{\pi^3}{16\ln 2} \frac{P_o h G^2 \theta\phi}{\lambda^2 R^2} \times \left|\frac{\varepsilon - 1}{\varepsilon + 2}\right|^2 \Sigma r^6 \qquad (2)$$

where

$P_o$ is the peak transmitted power,

$h$ is the radar pulse length in space (distance),

$G$ is the actual gain of antenna,

$\theta$ is the horizontal beam width to the –3-dB level for one-way transmission,

$\phi$ is the vertical beam width to the –3-dB level for one-way transmission, and

$R$ is the range.

Some of the fundamental characteristics of ash clouds from the aviation perspective were reviewed by Rose (1987). Radar-target parameters calculated for a thin ash cloud that was sampled by a research aircraft (Rose and others, 1980) were compared by Harris and others (1981) with analogous parameters for warm orographic rain and thundershowers. The refractive index factor in equation 2 ($|\varepsilon-1/\varepsilon+2|^2$) for ash (0.36) is higher than for ice (0.197) and lower than for water droplets (0.93), and the sizes of particles in ash clouds are probably generally smaller than water droplets in rain clouds. Because of the $r^6$ term in both equations, ash clouds generally are not as pronounced a radar reflector as storm clouds (the reflectivity factor is equal to $\Sigma(2r)^6$, the summation of the sixth power of the particle radius for all the particles in a unit volume of target space). It is also for this reason that airborne radars, which have much lower transmitted power than ground-based systems, do not detect ash clouds well.

## CLOUD HEIGHT

In addition to being useful for mapping the dense interiors of ash clouds, ground-based radar systems have also produced data about the heights of ash clouds (fig. 2). This data is obtained by observation of the range-height indicator (RHI) on the radar system, which can detect a sharp top boundary of the eruption cloud, particularly above the vent. This data is very valuable because the eruption-column height is a measure of the rate of eruption of magma (Wilson and others, 1978). Thus, a series of column-height measurements allow the mass and dynamics of an eruption to be directly monitored.

When an ash cloud is dispersing in the atmosphere, the altitude of the cloud top above the vent represents information that is essential to aviation. Other methods of obtaining this data are flawed, particularly at stratospheric heights. Satellites are a proven way to track volcanic clouds (Krueger, 1983; Matson, 1984), and the satellite remote thermal sensing data of the temperature of cloud tops is very useful for determining the heights of clouds in the troposphere, where temperatures decrease regularly with height (Holasek and Rose, 1991). However, satellite remote-sensing methods do not always result in a unique solution for cloud-top heights at stratospheric levels, where temperatures do not decrease regularly with height (Schneider and Rose, this volume). Thus, radar systems appear to offer one of the best ways to obtain dependable column-height data. Because these data are vital inputs to dispersal models that forecast the movements of drifting clouds (Carey and Sigurdsson, 1982) and are needed for volcanologic reasons, a radar system appears to offer an important capability to address the ash cloud–aviation problem.

## CLOUD STRUCTURE

A potentially critical contribution of radar systems to volcanology is the possibility of doing detailed study of the proximal structure of volcanic clouds. It is likely that direct observations of the "umbrella" region of eruption clouds (Sparks and others, 1986; Self and Walker, this volume) can be made using radar and that variations in eruptive activity can be directly monitored. Radar can also detect high-reflectivity regions below the main volcanic clouds that represent early fallout of coarse particles. It can also be used to measure apparent wind speed by detecting ash-cloud drifting and using a Doppler capability.

Mapping and height determinations are the two simplest measurements that have been demonstrated by ground-based radar. It is also possible to recognize levels of reflection, as shown in the 16:40, 17:40, and 18:40 PDT (Pacific Daylight Time) images for the May 18, 1980, Mount St. Helens eruption (fig. 1). From these basic radar data, it is possible to determine or estimate a number of useful parameters such as: (1) the duration and rate of the eruption as a function of time, (2) the three-dimensional distribution of particle concentrations in the ash cloud, (3) the total mass of ash in the cloud, and (4) the locations and amounts of ashfall (Harris and Rose, 1983).

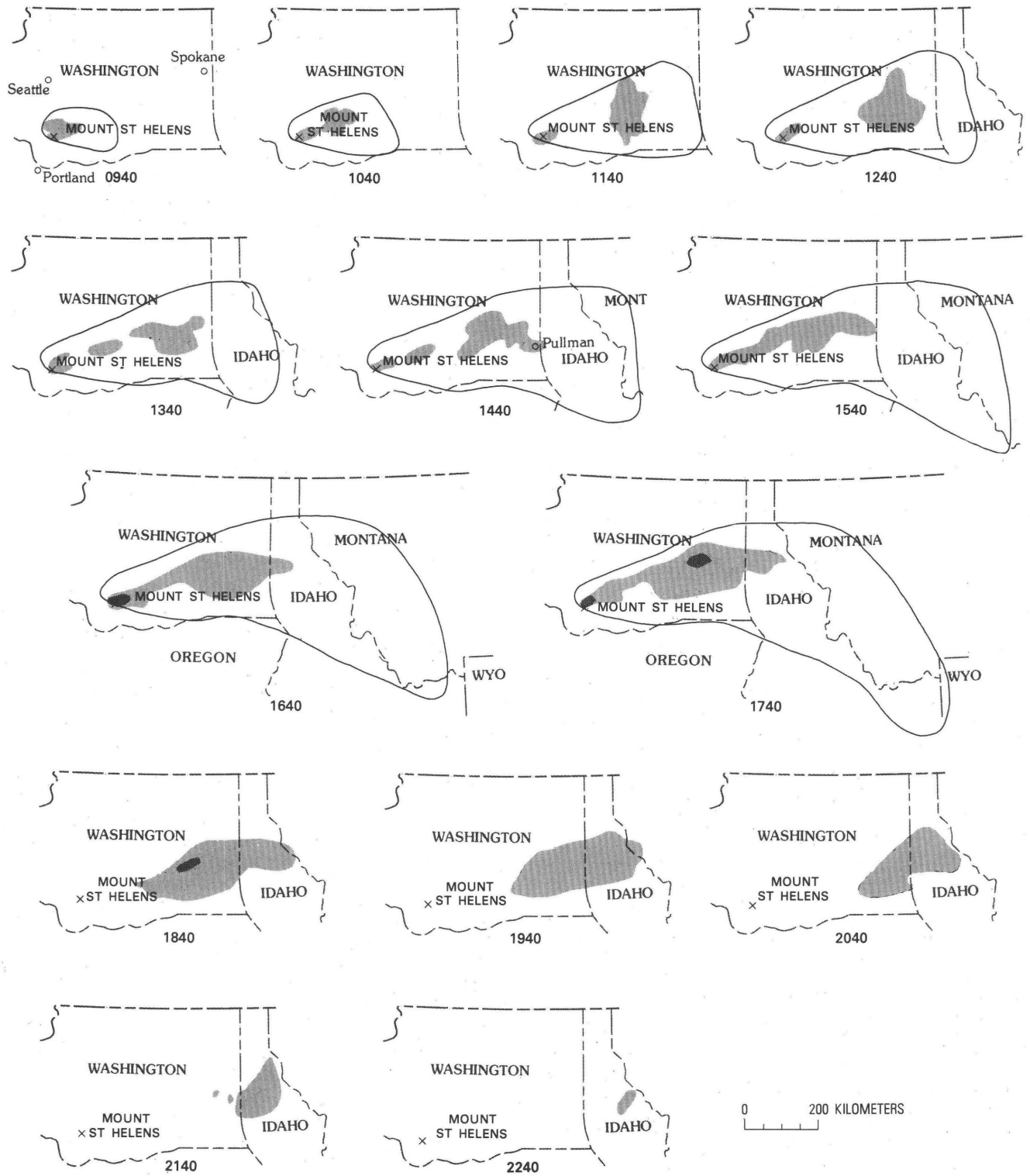


**Figure 1.** Shape and structure of May 18, 1980, eruption cloud from Mount St. Helens (X), as depicted by Seattle and Spokane radar systems and NOAA geostationary weather satellite. The solid line outlines the visible cloud as observed by the weather satellite. Hourly tracings of radar reflections at level 1 are shown as light patterned areas; level-2 reflections are shown as dark patterned areas. Times shown are Pacific Daylight Time (PDT). Figure from Harris and others (1981).

# A RADAR SYSTEM FOR VOLCANIC ASH CLOUDS

We now consider the feasibility of designing a radar system capable of detecting and monitoring volcanic ash clouds. In order to focus on the essential physics, we concentrate on the scattering process. The natural approach is to analyze the scaling allowed by the scattering equation (eq. 1). For a single particle, and in the Rayleigh regime appropriate for small particles, the backscattered reflectivity, $\eta$, is:

$$\eta \equiv \frac{\pi^5 \left|\frac{\varepsilon - 1}{\varepsilon + 2}\right|^2 D^6}{\lambda^4} \qquad (3)$$

where

$D$ is the diameter of the scattering particle.

There are three factors to consider here: $1/\lambda^4$ wavelength dependence, $D^6$ particle-size dependence, and the quadratic dependence on the dielectric constant ($\varepsilon$) of the reflecting particles.

Because we argue here that a shorter wavelength radar will be needed for volcanic applications, we need the $\varepsilon$ values for these wavelengths. A representative value at 35 GHz (about 8.6 mm) can be found in Ulaby and Elachi (1990). The permittivity (real part of $\varepsilon$) is given between 2.6 and 9.6 for volcanic materials (the imaginary part of $\varepsilon$, the loss tangent—Ulaby and Elachi (1990)—is generally between 0.01 and 0.05). Calculation of the $(\varepsilon-1)/(\varepsilon+2)$ factor shows that the volcanic-ash echo is about 1.7 to 4.4 times weaker than that of water, the rest of the conditions (size, distance, and wavelength) being the same. Let us therefore assume that the ash-detection system has a better sensitivity (e.g., a three-times-smaller minimal detectable signal) than a typical weather radar, and go on to consider the wavelength and size dependence.

In the dipole (small-particle or Rayleigh) approximation, the backscattered intensity is proportional to the sixth power of the diameter (eq. 3). Thus, the largest ash particles present in the cloud are the main scatterers. The size distribution usually contains many fewer large particles than small ones because they typically have a lognormal distribution. The number of small particles does not increase fast enough to counteract the dependence on $D^6$. Therefore, for this discussion, it is sufficient to assume that we deal with particles of a single size in the cases to be compared (e.g., rain and volcanic ash).

Even in the heaviest of rains (150 mm/hr) there are no more than a 1,000 large drops between 4 and 5 mm in diameter per cubic meter. However, a volcanic ash cloud with an ash concentration of 1 g/m$^3$ might have about 100,000 particles per cubic meter with sizes of 40 to 50 μm. The maximum size depends on the stage of cloud development, among other factors.

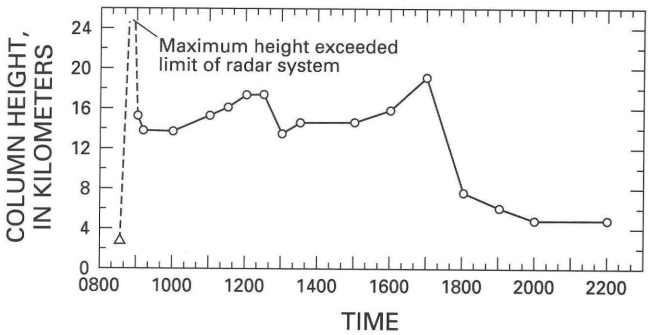


**Figure 2.** Heights of the May 18, 1980, eruption column at Mount St. Helens, as determined by Portland radar. Heights are relative to sea level. Base value (triangle) is plotted at time eruption began at approximate altitude of the vent; it is followed by a value that exceeded the limit of the radar system (dashed line). Times shown are Pacific Daylight Time (PDT). Figure adapted from Harris and others (1981).

In order to demonstrate the extreme sensitivity of radar observations to $D^6/\lambda^4$, consider the following two cases: (1) largest raindrops of 5 mm and ash particles of 0.05 mm (size ratio, SR, equals 100), and (2) largest rain drops of 2 mm along with 200-μm (0.2-mm) ash particles (SR = 10). We assume, for simplicity, that the number of ash particles per unit volume in both comparisons is 100,000.

In case 1 (SR = 100), the reflectivity per particle is lower by a factor of $10^{-12}$ for the ash than for rain because of the $D^6$ factor. There are 100 times more ash particles per unit volume, which leaves a factor of $10^{-10}$. In order to compensate for this lowered reflectivity with the $\lambda^4$ dependence, one must take a fourth root of $10^{-10}$, which yields a wavelength (0.6 mm) that is 178 times smaller than that of a typical weather radar (10 cm).

However, repeating the same calculations for case 2 (SR = 10) yields the decrease of $\lambda$ by a factor of only 10 (i.e., 5-mm radar). This is encouraging and probably explains the reasons for using millimeter radar in cloud-physics research (Atlas, 1990; Sauvegeot, 1992). Thus, at the number density of 100,000 particles per m$^3$ for ash, 200-μm ash particles can be detected 50–100 km away (in the clear troposphere) by a millimeter weather radar system, but 20-μm particles cannot be similarly detected. This explains previous observations that describe the visibility of an ash cloud on a radar monitor and its gradual disappearance as larger particles fall out of the plume. The major disadvantage of millimeter-wavelength radars as opposed to centimeter radars is the high atmospheric absorption by oxygen and water vapor (Sauvegeot, 1992, p. 103). However, the range can be improved considerably by operating in atmospheric "windows" of 35, 95, 140, and 220 GHz, especially for near-vertical-pointing radars.

Ideally, a ground-based radar should be placed at a site within range of the volcano and nearby airports where

aircraft would be landing and taking off. An operating range of 300 km would be very useful and would allow flexibility for installation at a site with power and road access. Portability would be desirable because permanent siting of a radar would experience the disadvantage of long reposes between periods of activity. For example, a mobile radar in Alaska could be placed at Kenai (between Redoubt Volcano and Anchorage) during Redoubt or Spurr activity and could be moved to Homer (between Augustine Volcano and Anchorage) in the event of activity at Augustine (Hufford, this volume).

Radar operators can be trained to identify ash clouds. Positions of potentially active volcanoes should be displayed as an overlay on radar monitor screens. Coordination with volcano observatories that monitor seismicity should be arranged so that radar operators are informed when eruptions are expected. Periodic, automated azimuthal and elevation scanning using an algorithm to eliminate ground clutter and to detect change could be performed as a useful routine procedure at radar systems with active volcanoes in range. Routine schemes should be designed to measure and track ash clouds automatically or semi-automatically once they are detected.

Other useful features of a volcanic-cloud radar system would be Doppler and polarimetric capabilities. If the system were equipped with Doppler features, signal processing could extract radial-velocity information in the form of a Doppler power spectrum, which is related directly to the particle-size distributions in the ash cloud. The lack of information about grain size of the particles in the cloud presents a serious uncertainty that has been ignored in previous discussions. Thus, a Doppler radar would clarify an important uncertainty about ash clouds. Polarimetric radars are useful in shape analysis of particles. Because we are uncertain about the shapes of particles as they move in the drifting cloud, polarimetry could be a potentially important capability for a volcanic-ash-cloud radar system.

## CONCLUSIONS AND RECOMMENDATIONS

Ground-based meteorological radar systems can provide valuable tracking information on drifting volcanic clouds at ranges of 50 to more than 500 km from the radar unit. Such ground-based radar systems currently offer the best known method of determining eruption-cloud heights, particularly if the ash cloud reaches the stratosphere. During eruptions this information is vitally needed in real time for accurate plume-dispersion forecasts and aviation routing.

A radar system designed for volcanic-cloud detection and tracking should probably have a wavelength in the range of 3 mm to 3 cm and a range of at least 300 km. Volcanic-cloud radar systems should be portable because long volcanic repose periods will likely occur during the life of the instrument, and relocation may be desirable to monitor other eruptions.

Doppler radar systems now available offer the possibility of sensing the particle-size distribution in a volcanic cloud, information that cannot be easily obtained in other ways and that is important in assessing ash-cloud hazards and dispersion forecasts.

## ACKNOWLEDGMENTS

The radar observations that formed much of the basis for this review came from papers by Harris and others (1981) and Harris and Rose (1983). The interest of Robert Roe of the National Weather Service at Portland, Oreg., and Martin Thompson at the NWS in Auburn, Wash., was essential to the observations. David M. Harris thoroughly reviewed the manuscript and made many helpful suggestions.

## REFERENCES CITED

Atlas, D., 1964, Advances in radar meteorology, *in* Landsberg, H.E., and Van Mieghem, J., eds., Advances in Geophysics, Volume 10: New York, Academic Press, p. 317–479.

———ed., 1990, Radar in Meteorology: Boston, American Meteorological Society, 806 p.

Carey, S.N., and Sigurdsson, H., 1982, Influence of particle aggregation on deposition of distal tephra from the May 18, 1980 eruption of Mount St. Helens volcano: Journal of Geophysical Research., v. 87, p. 7061–7072.

Harris, D.M., and Rose, W.I., 1983, Estimating particle sizes, concentrations, and total mass of ash in volcanic clouds using weather radar: Journal of Geophysical Research, v. 88, p. 10969–10983.

Harris, D.M., Rose, W.I., Roe, R., and Thompson, M., 1981, Radar observations of ash eruptions, *in* Lipman, P.W., and Mullineaux, D.R., eds., The 1980 Eruptions of Mount St. Helens, Washington: U.S. Geological Survey Professional Paper 1250, p. 323–333.

Holasek, R.E., and Rose, W.I., 1991, Anatomy of 1986 Augustine Volcano eruptions as recorded by multispectral image processing of digital AVHRR weather satellite data: Bulletin of Volcanology, v. 53, p. 420–435.

Johnston, D.A., 1976, Volatiles, magma mixing and the mechanism of eruption of Augustine Volcano, Alaska: Seattle, Wash., University of Washington, unpub. Ph.D. dissertation, 177 p.

Kienle, J., and Shaw, G.E., 1979, Plume dynamics, thermal energy and long-distance transport of Vulcanian eruption clouds from Augustine Volcano, Alaska: Journal of Volcanology and Geothermal Research, v. 6, p. 139–164.

Krueger, A.J., 1983, Sighting of the El Chichón sulfur dioxide clouds with the Nimbus 7 total ozone mapping spectrometer: Science, v. 220, p. 1377–1379.

Matson, M., 1984, The 1982 El Chichón volcano eruptions—A satellite perspective: Journal of Volcanology and Geothermal Research, v. 23, p. 1–10.

Probert-Jones, J.R., 1962, The radar equation in meteorology: Quarterly Journal of the Royal Meteorology Society, v. 88, p. 485–495.

Rose, W.I., 1987, Interaction of aircraft and explosive eruption clouds, a volcanologist's perspective: American Institute of Aeronautics and Astronautics Journal, v. 25, p. 52–58.

Rose, W.I., Chuan, R.L., Cadle R.D., and Woods, D.C., 1980, Small particles in volcanic eruption clouds: American Journal of Science, v. 280, p. 671–696.

Sauvegeot, H., 1992, Radar Meteorology: Boston, Artech House, 366 p.

Serafin, R.J., 1990, Meteorological radar, *in* Skolnik, M., ed., Radar Handbook (2d ed.): New York, McGraw-Hill, p. 23.1–23.33.

Sparks, R.S.J., Moore, J.G., and Rice, C., 1986, The initial giant umbrella cloud of the May 18, 1980 explosive eruption of Mount St. Helens: Journal of Volcanology and Geothermal Research, v. 28, p. 257–274.

Ulaby, F.T., and Elachi, C., eds., 1990, Radar Polarimetry for Geoscience Applications: Norwood, Mass., Artech House, 364 p.

Wilson, L., Sparks, R.S.J., Huang T.C., and Watkins, N.D., 1978, The control of volcanic column heights by eruption energetics and dynamics: Journal of Geophysical Research, v. 83, p. 1829–1836.

VOLCANIC ASH AND AVIATION SAFETY:
Proceedings of the First International Symposium
on Volcanic Ash and Aviation Safety
U.S. GEOLOGICAL SURVEY BULLETIN 2047

# TRACKING OF REGIONAL VOLCANIC ASH CLOUDS BY GEOSTATIONARY METEOROLOGICAL SATELLITE (GMS)

*By* Yosihiro Sawada

## ABSTRACT

Visible and infrared images from the Japanese geostationary meteorological satellite (GMS) have detected ash clouds generated by large volcanic eruptions in Kamchatka, Kurile Islands, Japan, Philippines, Indonesia, and Marianas since its launch in late 1977. Even though the GMS detection rate of ash clouds for eruptions that occurred within the GMS field of view was around 13 percent, ash clouds that are ejected to high altitudes, are widely dispersed, and may threaten aviation safety, have been tracked well in GMS images. Discrimination of ash clouds from atmospheric clouds and the tracking of small, thin ash clouds were not possible due to the limitations of the GMS's detector for spectrum analyses and ground resolution. Tentative estimations of altitudes of cloud tops and thermal energy releases of eruptions have been made from analyses of the imagery data.

## INTRODUCTION

Using visual observations from the ground or air, it is very difficult to observe and track the extent of volcanic ash clouds that are widely dispersed at high altitudes. Satellite imagery offers the opportunity for viewing large regions covered by ash clouds (Sudradjat, 1989). The GMS carries a detector known as the visible and infrared spin-scan radiometer (VISSR). The ground resolution of VISSR is 1.25 km and 5 km in the visible and infrared bands, respectively, and the wavelength is 0.5–0.75 μm for the visible band and 10.5–12.5 μm for the infrared band. Whereas the GMS detector's ground resolution is limited, it has a very wide field of view, and its short time interval between images compared to that of polar-orbiting satellites makes it very effective for tracking eruption clouds.

Through careful examination of GMS images, the rate of detection of ash clouds within the field of view of GMS has been evaluated. Estimates of the heights of tops of ash clouds were determined by analyses of GMS's digital data of infrared images. The results are applied to estimates of thermal energy release by ash clouds in order to evaluate the strengths of volcanic eruptions. Variations in eruption intensity are judged by evaluating intensified or weakened ash clouds over the volcano. Heights of cloud tops, estimated from image data, are compared to those observed from the ground, and discrimination of ash clouds from ambient atmospheric clouds is attempted using combinations of visible and infrared digital data from ash clouds and atmospheric clouds.

## METHODS OF STUDY

Detection and tracking of ash clouds for a number of eruptions between 1977 and 1991 were conducted by carefully examining successive GMS images near volcanoes, following notification of big volcanic eruptions (e.g., Sawada, 1987). At first, existence of volcanic-like clouds very near or over the volcano is sought in infrared images, then it is checked whether the volcanic-like cloud appears in the visible image during day time—in this case, the top surface of an eruption cloud containing ash particles may show a dark-toned surface compared to ambient atmospheric clouds. Drift direction of the ash cloud is determined by examining a sequence of images, and the width and length of the ash cloud are measured. Duration of the volcanic eruption can be judged by inspecting whether the ash cloud continues to originate at the site of the volcano or whether it has already detached and moved away from the volcano.

Estimation of the altitude of the ash cloud is made using the assumptions that the top of an ash cloud under the tropopause shows the coldest temperature and the surface temperature at high altitude coincides with ambient air temperature. Therefore, the height of the top of an ash cloud can be estimated using the air-temperature profile from radio-sounding observations near the volcano (Sawada, 1983a, 1983b, 1985a, 1985b, and 1987).

Evaluation of the strength of a volcanic eruption was made by estimating the thermal energy released by the ash cloud and by applying the following experimental equation proposed by Briggs (1969) for the case of a thermal plume:

$$Q = (0.0264)\,(\Delta h^3)\,(u^3)\,(x^2) \quad (1)$$

where

$Q$ is the thermal energy release rate in megawatts,

$\Delta h$ is the height of ash cloud in meters above the crater,

$u$ is the mean wind velocity in meters per second at the top altitude, and

$x$ is the horizontal distance from the crater in meters.

The horizontal distance is used under the condition of $x \leq 50h$, where $h$ is the altitude of the plume source, even though the limiting condition for applying Briggs's equation is $x \leq 10h$. The duration time of the volcanic explosion was estimated based on analyses of eruption-cloud data and from published information from the bulletins of the Global Volcanism Network (GVN) of the Smithsonian Institution (McClelland, this volume; McClelland and others, 1989) and from the Bulletin of Volcanic Eruptions (BVE) published by the Volcanological Society of Japan. The thermal energy release (Eth, in ergs) by ejected materials was calculated in the case of juvenile materials by the following equation, proposed by Yokoyama (1957), using abbreviated values for the parameters in the equation proposed by Nakamura (1965):

$$\mathrm{Eth} = (M)\,((TC) + H)\,(4.18\times10^7) \quad (2)$$

where

$M$ is the total mass of ejecta in grams,

$T$ is the difference in temperature (assumed to be 600°C) between ejected materials and ambient air temperature,

$C$ is the specific heat (0.25 cal/g°C), and

$H$ is the latent heat of melting (10 cal/g).

Discrimination of ash clouds from ambient atmospheric clouds was tried using numerical data for albedo and the temperature of surfaces for both ash clouds and atmospheric clouds because several examples of ash clouds showed dark-toned surfaces in visible-band GMS images.

## RESULTS AND OBSERVATIONS

Ash clouds produced by strong eruptions at 23 volcanoes have been detected in GMS images through 1985 (Sawada, 1987). Thereafter, ash clouds from large eruptions at nine volcanoes were detected through June 1991 (fig. 1). Table 1 is a list of eruption clouds detected in GMS images. Examples of ash clouds detected after 1986 are shown in figures 2–7.

**Table 1.** List of major ash clouds detected with GMS images, December 1977 through June 1991.

[GMS, geostationary meteorological satellite. a.s.l., above sea level]

| Date | Volcano | Data pertaining to highest ash cloud | | |
|---|---|---|---|---|
| | | Cloud top (km a.s.l.) | Length (km) | Width (km) |
| **1981** | | | | |
| Apr. 27–May 25 | Alaid, Kurile Is. | 12 | 2300 | 270 |
| May 14–15 | Pagan, Mariana Is. | 16 | 250 | 220 |
| Apr. 5–Oct. 14 | Galunggung, Java | 18 | 150 | 90 |
| Aug. 26–Nov. 10 | Soputan, Sulawesi | 15 | 170 | 70 |
| Oct. 24–25 | Lopevi, New Hebrides | 13 | 190 | 80 |
| July 23–Aug. 26 | Una Una, Sulawesi | 17 | 160 | 120 |
| May 25–26 | Soputan, Sulawesi | 16 | 260 | 170 |
| Aug. 31 | Soputan, Sulawesi | 15 | 410 | 310 |
| Sep. 10–Oct. 2 | Mayon, Luzon | 16 | 200 | 70 |
| July 30 | Sangeang Api (Sunda Is.) | 14 | 130 | 100 |
| **1986** | | | | |
| Nov. 19–20 | Chikurachiki, Kurile Is. | 8 | 380 | 90 |
| Nov. 21 | Izu-Oshima, Izu Is. | 8 | 150 | 40 |
| **1988** | | | | |
| May 8–9 | Banda Api, Banda Sea | 17 | 80 | 80 |
| July 29–31 | Makian, Halmahera (Kie Besi) | 16 | 120 | 50 |
| **1990** | | | | |
| Feb. 10 | Kelut, Java | 17 | 300 | 230 |
| **1991** | | | | |
| June 12 | Pinatubo, Luzon | 14 | 140 | 130 |
| June 14–15 | Pinatubo, Luzon | ≥ 28 | 2,800 | 1,700 |

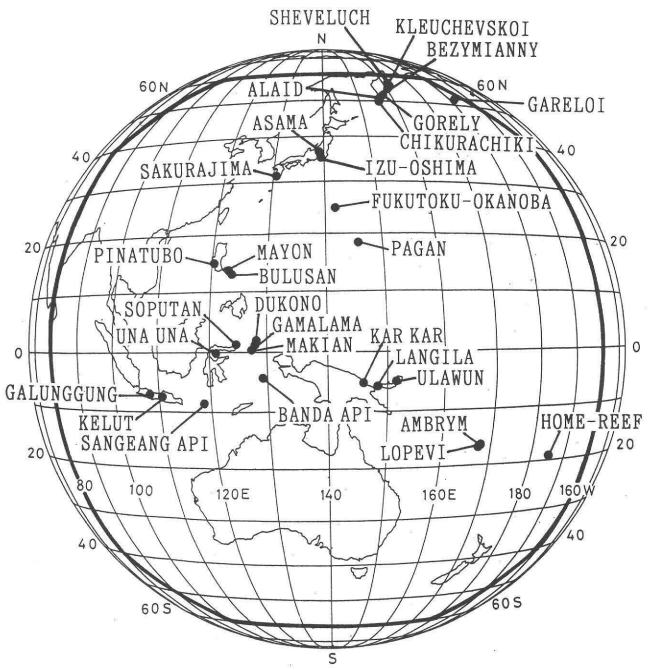


**Figure 1.** Distribution of volcanoes for which ash clouds have been detected in GMS images (December 1977–June 1991). Bold line denotes limits of GMS ground coverage.

Most ash clouds do not show clear differences in GMS images from atmospheric clouds. However, several examples do show the dark-toned surfaces of ash clouds in visible-band images, as in the cases of ash clouds of the 1988 eruption of Banda Api, the 1988 eruption of Makian, and the 1991 eruption of Pinatubo (figures 4, 5, and 7). The ash clouds of the 1981 Alaid eruption were well discriminated from ambient atmospheric clouds in visible-band images because of their dark-toned surfaces—this may be due to ash-rich contents (Sawada, 1983a, 1987).

The ash clouds show various shapes in GMS images under the influence of different prevailing winds at different altitudes. In general, the extent of an ash cloud influenced by slow wind velocities (< about 10 m/s) appears as a wide, fan-shaped region, but the cloud extent becomes narrow with strong winds (> about 20 m/s) (Sawada, 1987). In the case of the ash cloud from the 1990 Kelut eruption, very large scale ash clouds were seen over and around the volcano in GMS images (fig. 6). The eruption was a very large event (Sudradjat, 1991), but this large-scale cloud may have developed due to active convection by rising ash clouds over the volcano.

The ash cloud during the 1986 Izu-Oshima eruption was detected in GMS images (fig. 3). The height of the cloud top estimated from image data was 8–9 km, but the observations from the ground and photographic data showed the top altitude to be 12–14 km. The reason for the difference was due to the warm surface temperature of the cloud top compared to the ambient air temperature at that altitude, which

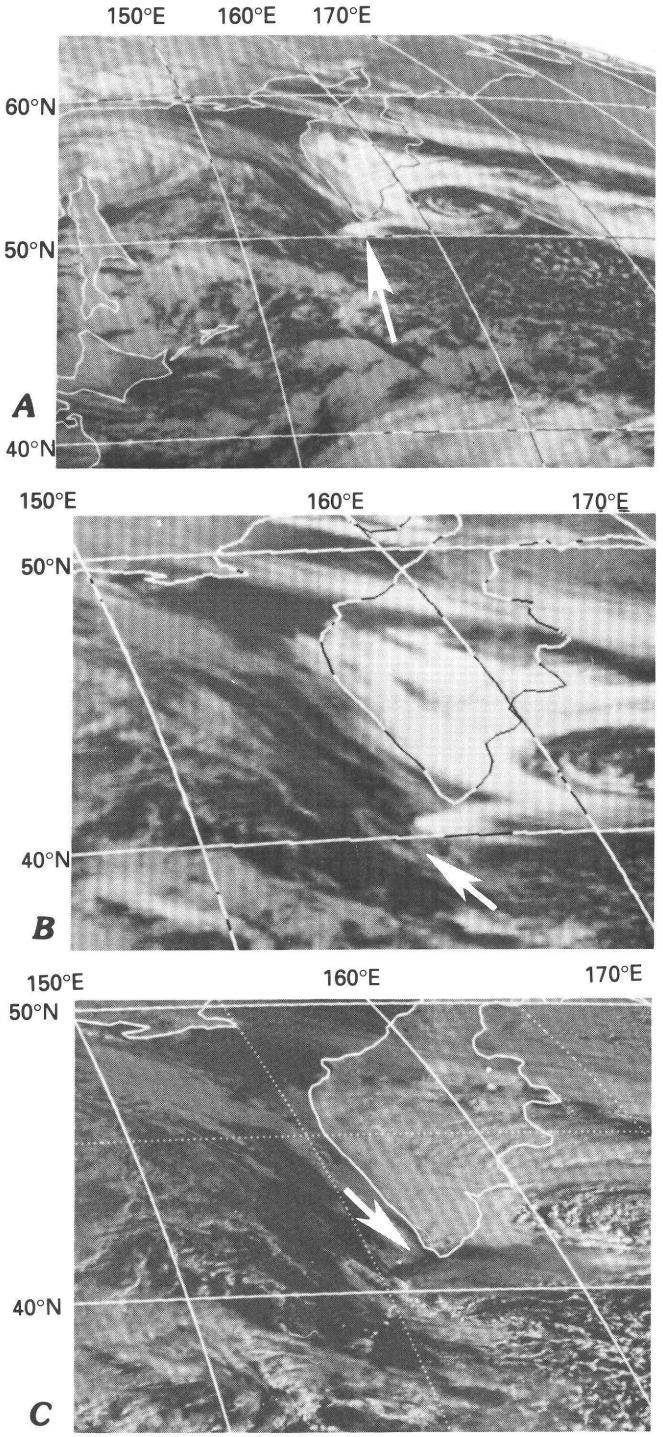


**Figure 2.** Eruption cloud from the November 1986 eruption of Chikurachiki Volcano, Russia. Cloud is drifting to the east from the volcano. *A*, Infrared-band image at 22:30 UTC, November 19, 1986. *B*, Infrared-band image at 00:00 UTC, November 20, 1986. *C*, Visible-band image taken at 00:00 UTC, November 20, 1986. Note dark-toned eruption cloud in *C*. Eruption clouds are indicated by white arrows.

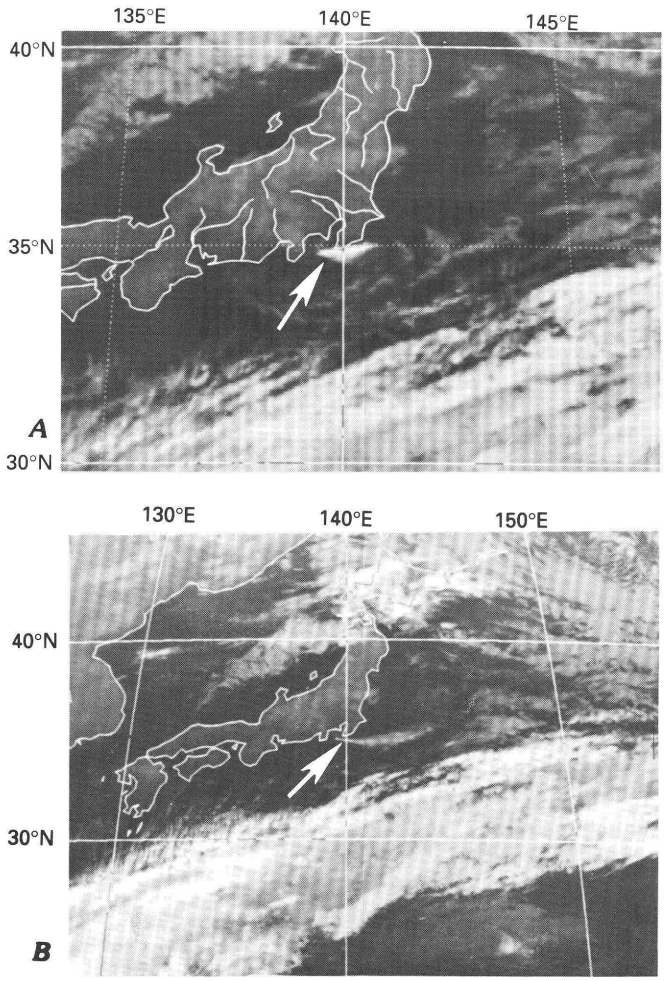


**Figure 3.** Eruption cloud from the November 1986 eruption of Izu-Oshima, Japan. Cloud is drifting to the east. *A*, Infrared-band image at 09:00 UTC, November 21, 1986. The north rim of the cloud appears over the tip of the Boso Peninsula due to GMS's parallax angle. *B*, Infrared-band image at 10:30 UTC, November 21, 1986. Eruption clouds are indicated by white arrows.

leads to an underestimation of the altitude of the cloud top. It may be possible that very active thermal emissions were occurring on the surface of the developing ash clouds. The northern edge of the ash cloud seen in the GMS image was located on the tip of the Boso Peninsula, but the same cloud was observed at almost the same time in imagery from the National Oceanic and Atmospheric Administration (NOAA) polar-orbiting satellite that was obtained over the volcano. In the NOAA imagery, the edge of the cloud was about 14 km off the tip of the peninsula. Therefore, the underestimated cloud top determined from the GMS imagery could be corrected by using the parallax of GMS.

The ash clouds of the 1986 Izu-Oshima eruption were also well detected by Japan Meteorological Agency's (JMA's) weather radars at Fuji, Haneda, Tokyo, and Nagoya. Fuji radar has a wavelength of 10 cm, whereas the

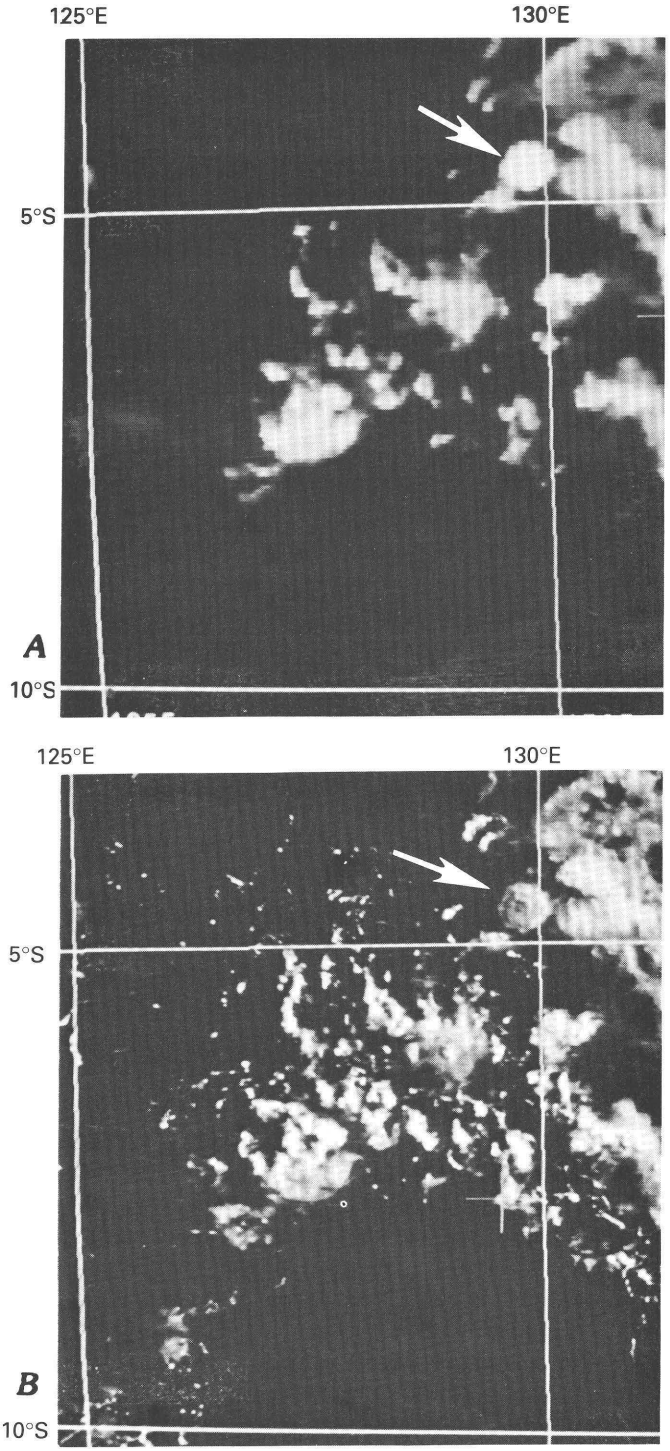


**Figure 4.** Eruption cloud from the May 1988 eruption of Banda Api, Indonesia. *A*, Infrared-band image at 23:00 UTC, May 8, 1988. *B*, Visible-band image at 23:00 UTC, May 8, 1988. Circular and dark-toned eruption cloud showing ring-shaped textures can be seen in *B*. Eruption clouds are indicated by white arrows.

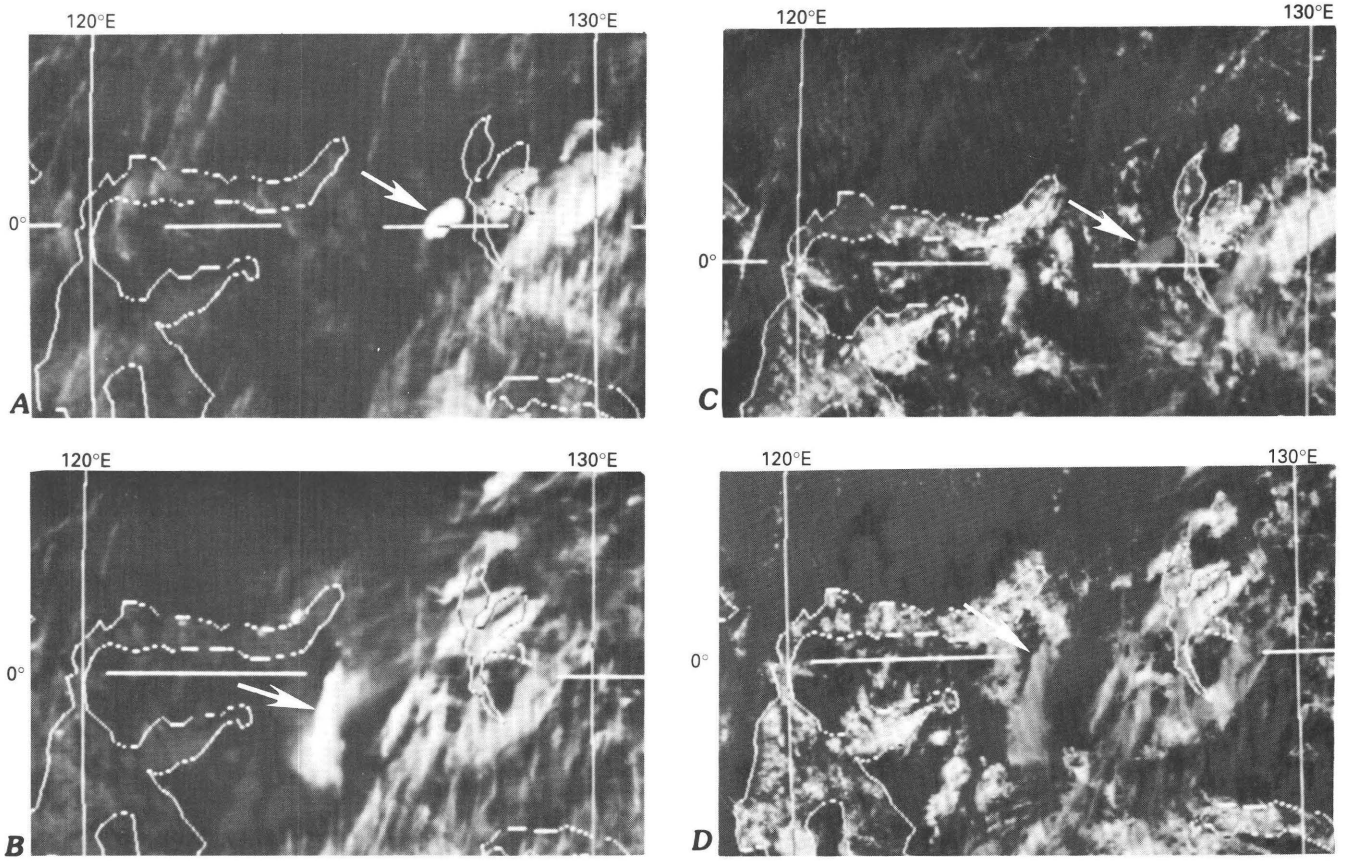


**Figure 5.** Eruption cloud from the July 1988 eruption of Makian, Indonesia. Infrared-band images taken on July 29, 1988 at *A*, 03:00 UTC and *B*, 06:00 UTC. Visible-band images taken on the same date at *C*, 03:00 UTC and *D*, 06:00 UTC. Cloud is drifting to the southwest from the volcano in the 03:00 UTC images (*A* and *C*). The detached cloud, southwest of the volcano, extended to the south, as shown in 06:00 UTC images (*B* and *D*). Dark-toned eruption cloud is seen in *C* and *D*. Eruption clouds are indicated by white arrows.

other stations have 5-cm radar (fig. 8). The ash clouds appear as dense rain clouds in these weather radars, and the top height of the clouds was determined to be at altitudes of 9–12 km (fig. 9). Although the number of examples is limited, dense ash clouds can be measured with weather radars; however, thin ash clouds are not observed. Detection of these dense ash clouds depends on ash content.

During day time, visible-band images can sometimes identify individual eruption clouds that are generated by intermittent eruptions: ash clouds appear as dark-toned surfaces owing to high ash content. For example, GMS visible-band images detected many large, discrete, dark-toned ash clouds from the June 15, 1991, Pinatubo eruption, showing strong individual eruptions (fig. 7). There were clear circular and linear textures on the surfaces of the giant eruption clouds (Tokuno, 1991).

Based on the number of volcanoes that erupted and the number of eruption clouds detected in GMS images during the period from December 1977 through June 1991, the detection rate of eruption clouds with GMS was 13.3 percent (table 2) (Sawada, 1989a, 1989b). For GMS, the detection limit of the extent of ash clouds was 20 by 30 km under very good weather conditions for visible-band imagery, and the detection limit of the altitude of ash clouds was 4–5 km (Sawada, 1989b). This low detection rate is due largely to the limitation of ground resolution and the difficulty in discriminating ash clouds from atmospheric clouds with VISSR data.

The thermal energy releases calculated from analyses of ash-cloud data and the mass of ejected materials show good agreement (fig. 10) and suggest the possibility that the strength of volcanic eruption may be estimated from ash-cloud data.

**Table 2.** Detection rate of ash clouds with GMS images within the GMS field of view, December 1977 through June 1991.

[GMS, geostationary meteorological satellite. Data from Bulletin of Volcanic Eruptions (Volcanological Society of Japan), Scientific Event Alert Network Bulletin (Smithsonian Institution), and Global Volcanism Network Bulletin (Smithsonian Institution)]

| | |
|---|---|
| Number of eruptions | 332 |
| Number of eruption clouds detected | 44 |
| Detection rate | 13.3 % |

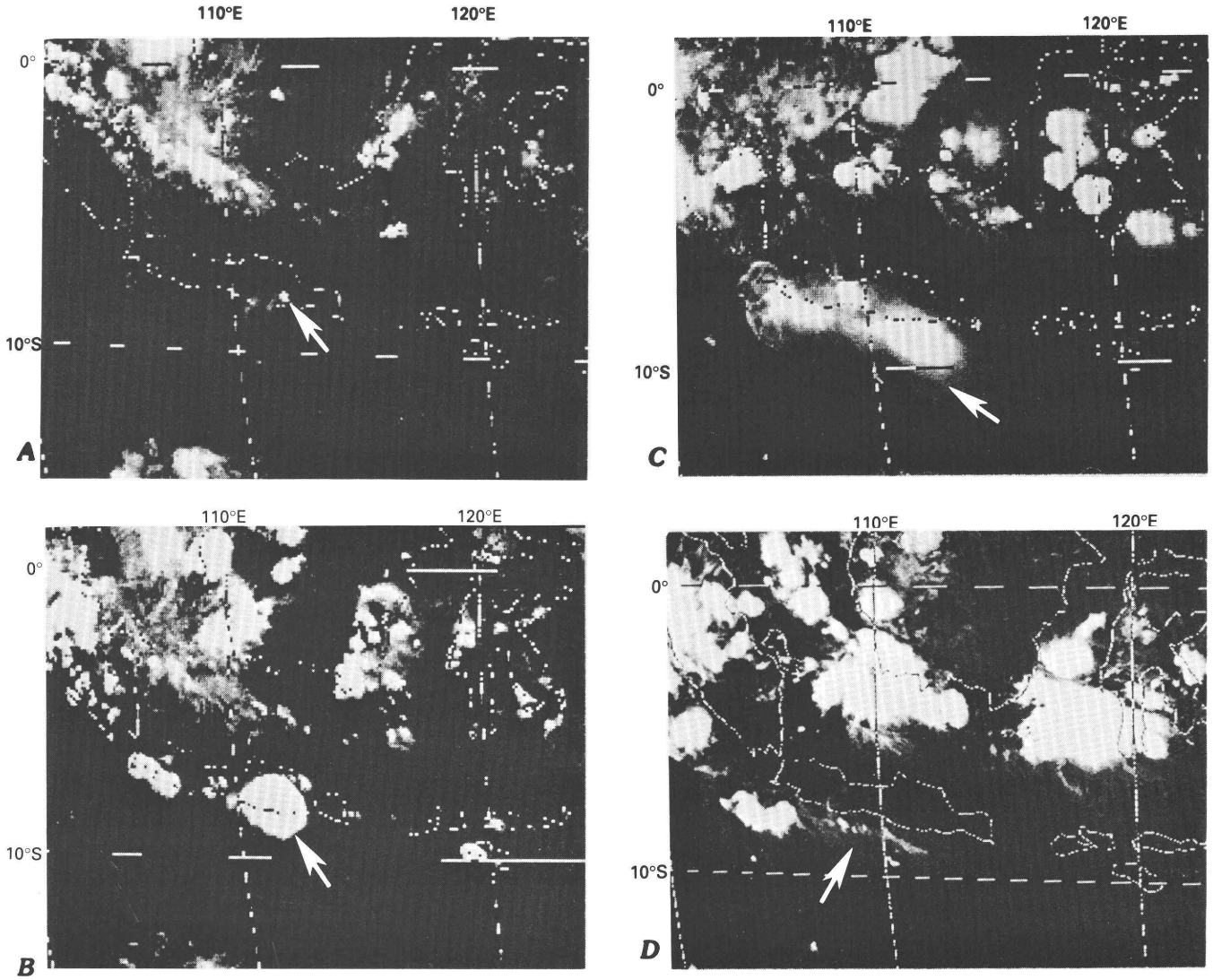


**Figure 6.** Eruption cloud from the February 1990 eruption of Kelut, Indonesia. Infrared-band images taken on February 10, 1990, at *A*, 06:00 UTC; *B*, 09:00 UTC; *C*, 15:00 UTC; and, *D*, on February 11, 1990, at 00:00 UTC. Initial, small eruption cloud rapidly expanded—this can be seen in *A*, *B*, and *C*. Eruption clouds are indicated by white arrows.

Discrimination of ash clouds from atmospheric clouds and the evaluation of ash content in ash clouds have been attempted, but good resolution has still not been achieved (Sawada 1987) because GMS's detection of single bands in infrared and visible wavelengths cannot separate the optical features of eruption clouds from those of atmospheric clouds.

## CONCLUSIONS AND RECOMMENDATIONS

GMS images can detect and track widely dispersed ash clouds from large volcanic eruptions. Due to the short time interval (30 minutes to 1 hour) between images, dynamic assessment of ash-cloud development is possible. The detection rate for low-altitude clouds (below about 10 km) is only about 13 percent, due largely to the limitation of the imaging system and the characteristics of the radiometer. However, widely dispersed ash clouds reaching altitudes higher than 10 km were almost always detectable and were well tracked in GMS images.

Under the influence of strong prevailing winds, ash clouds that had detached from the site of a volcano after major activity faded and became elongated in the wind direction. There are differences between maximum altitudes of ash clouds estimated based on the temperature of the top surface of the cloud and those altitudes as observed from the ground. Some of the differences may be due to active thermal emissions on the top surface of ash clouds—this will cause underestimation of cloud-top altitudes. The underestimated cloud top of the 1986 Izu-Oshima eruption could be corrected using the GMS's parallax.

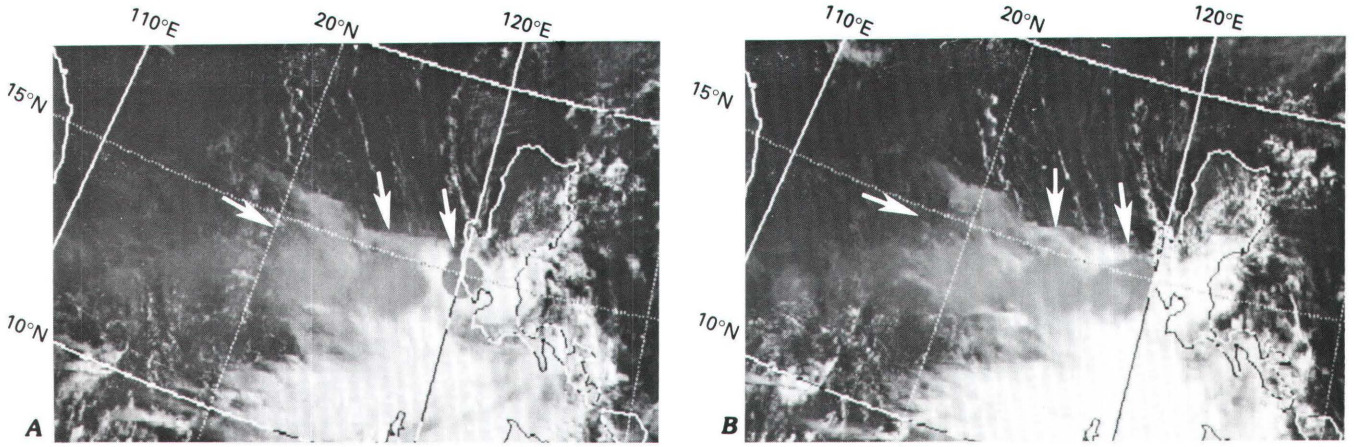


**Figure 7.** Eruption cloud from June 1991 eruption of Mt. Pinatubo, Philippines as seen on visible-band images taken at *A*, 01:00 UTC, June 15, 1991, and *B*, 02:00 UTC on the same date. Dark-toned ash clouds drifting to the west from the volcano were obtained at short time intervals during maximum activity—these images show the frequent occurrence of strong explosions. Eruption clouds are indicated by white arrows.

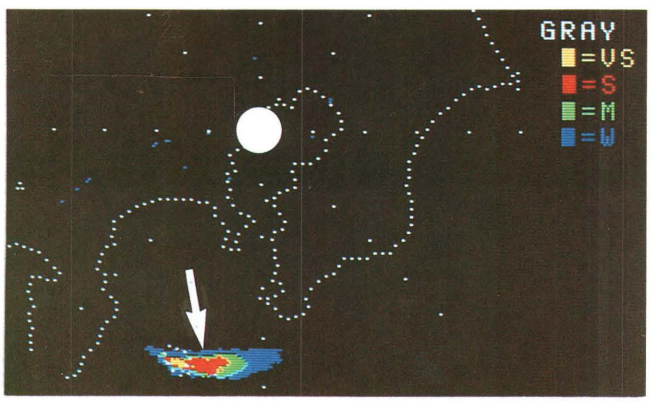


**Figure 8.** Ash cloud from the November 1986 eruption of Izu-Oshima, Japan (located at tip of white arrow), obtained at 08:30 UTC on November 21 with the weather radar at Haneda station (white circle), which is about 90 km NNE. of the crater. VS, S, M, and W in "gray" scale refer to the intensity of radar echo as very strong, strong, medium, and weak (this relative scale is applicable to rain clouds). The intensity of the radar echo from the eruption cloud grades from weak at the outer edge of the cloud to areas of medium and strong intensity near the center of the cloud.

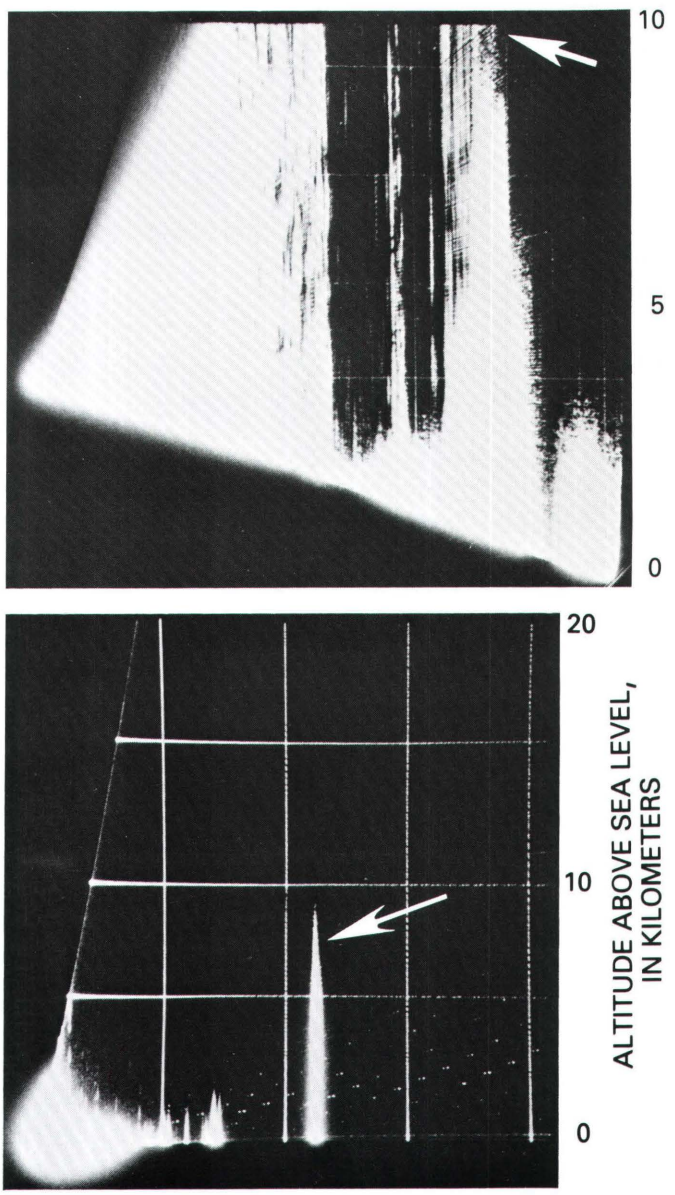


**Figure 9** (facing column). Observations of the altitude of ash-cloud tops for the November 21, 1986, eruption of Izu-Oshima, Japan. *A*, Data at 08:10 UTC, November 21, 1986, from weather radar at Fuji, which is about 96 km NW. of the crater. *B*, Data at 08:14 UTC on the same date from weather radar at Tokyo, which is about 105 km NNE. of the crater. Cloud tops are indicated by white arrows.

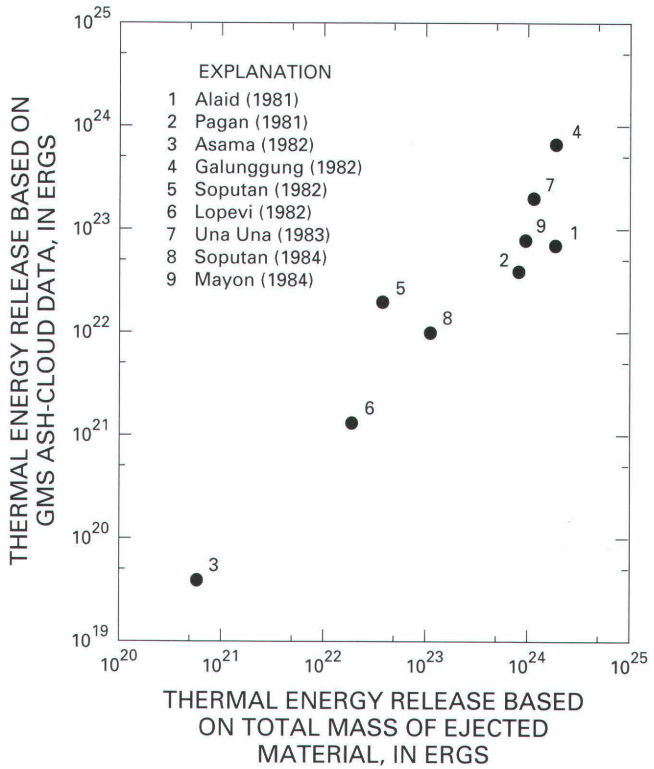


**Figure 10.** Relationship between thermal energy release based on ash-cloud data from GMS visible and infrared imagery (vertical axis) and thermal energy release based on total mass of ejected material reported in McClelland and others (1989) and by the annual Bulletin of the Volcanological Society of Japan (horizontal axis).

Weather radar can detect dense ash clouds and can determine their height; however, the detection rate is very low. Thermal energy release estimated from ash-cloud data was in good agreement with estimates based on the volume of erupted materials. This indicates the possibility of evaluating the strength of volcanic eruptions from eruption-cloud data obtained from satellite imagery.

Discrimination of ash clouds from ambient atmospheric clouds was usually not possible using GMS's visible and infrared data, except for dark-toned clouds in visible-band images in which ash content was high. Further acquisition of data on optical features of ash clouds are needed for discrimination of ash clouds from atmospheric clouds and for estimation of ash content in ash clouds. Further improvement of ground resolution and the establishment of a multispectral-detector capability for VISSR are needed to improve the detection rate of ash clouds.

## ACKNOWLEDGMENTS

The author expresses his cordial thanks to Dr. Christopher G. Newhall and Dr. Thomas J. Casadevall of the U.S. Geological Survey for providing the opportunity to attend the Seattle Symposium. He also expresses cordial thanks to the reviewers for their careful and scientific revisions of his manuscript.

## REFERENCES CITED

Briggs, G.A., 1969, Plume rise: Springfield, Va., U.S. Department of Commerce, National Technical Information Service, AEC Critical Review Series, TID-25075, 81 p.

McClelland, L., Simkin, T., Summers, M., Nielsen, E., and Stein, T.C., 1989, Global Volcanism 1975–1985: The First Decade of Reports from the Smithsonian Institution's Scientific Event Alert Network (SEAN): Englewood Cliffs, N.J., Prentice Hall, 655 p.

Nakamura, K., 1965, Energies dissipated with volcanic activities—Classification and evaluation: Bulletin of the Volcanological Society of Japan, 2nd ser., 10th Anniversary, p. 81–90 [in Japanese with English abstract].

Sawada, Y., 1983a, Analysis of eruption clouds by the 1981 eruptions of Alaid and Pagan Volcanoes with GMS images: Papers in Meteorology and Geophysics, v. 34, no. 4, p. 307–324 [in Japanese with English abstract].

———1983b, Attempt on surveillance of volcanic activity by eruption cloud image from artificial satellite: Bulletin of the Volcanological Society of Japan, 2nd ser, v. 28, no. 4, p. 357–373 [in Japanese with English abstract].

———1985a, Detection capability of eruption clouds and observations of eruption sequences by GMS images: Journal of the Remote Sensing Society of Japan, v. 5, no. 3, p. 207–224 [in Japanese with English abstract].

———1985b, GMS observation of eruption clouds of the 1984 September–October Mayon eruption: Philippine Journal of Volcanology, v. 2, p. 143–155.

———1987, Study on analyses of volcanic eruptions based on eruption cloud image data obtained by the geostationary meteorological satellite (GMS): Technical Reports of the Meteorological Research Institute, no. 22, 335 p.

———1989a, Regional monitoring of eruption clouds, and estimation of amount of air-borne ejecta, using satellite imagery: Proceedings of Kagoshima International Conference on Volcanoes, p. 539–542.

———1989b, The detection capability of explosive eruptions using GMS imagery, and the behavior of dispersing eruption clouds, *in* Latter, J.H., ed., IAVCEI Proceedings in Volcanology 1, Volcanic Hazards: International Association of Volcanology and Chemistry of the Earth's Interior, p. 233–245.

Sudradjat, A., 1989, Volcanic eruption monitoring using space platforms: Journal of the Indonesian Association of Geologists, v. 12, p. 437–448.

———1991, A preliminary account of the 1990 eruption of the Kelut Volcano: Geologische Jahrbuch, v. A127, p. 447–462.

Tokuno, M., 1991, GMS-4 observations of volcanic eruption clouds from Mt. Pinatubo, Philippines: Meteorological Satellite Center Technical Note, no. 23, p. 1–14.

Yokoyama, I., 1957, Energetics in active volcanoes: Bulletin of Earthquakes Research Institute, 2nd paper, no. 35, p. 75–97.

VOLCANIC ASH AND AVIATION SAFETY:
Proceedings of the First International Symposium
on Volcanic Ash and Aviation Safety
U.S. GEOLOGICAL SURVEY BULLETIN 2047

# OBSERVATIONS OF THE 1989–90 REDOUBT VOLCANO ERUPTION CLOUDS USING AVHRR SATELLITE IMAGERY

*By* David J. Schneider *and* William I. Rose

## ABSTRACT

The 1989–90 eruptions of Redoubt Volcano, Alaska, generated ash clouds that reached altitudes of as much as 12 km and provided an opportunity to test and refine the use of the advanced very high resolution radiometer (AVHRR) for satellite remote sensing of volcanic eruption clouds. Several aircraft encountered dispersed volcanic clouds, including a Boeing-747 that temporarily lost power from all four engines. Such near-tragic incidents highlighted the need for improved methods of discriminating and tracking volcanic clouds.

Thirty-one AVHRR images from various stages of the Redoubt eruption were examined. In the early, more energetic phases of the eruption, the Redoubt volcanic clouds could be discriminated by a technique that employs an apparent temperature difference between bands 4 and 5 of AVHRR. This method was particularly successful in clouds that were older than 1 hour, demonstrating that slight aging of the cloud during dispersal enhances its discrimination by this method. In the later stages of Redoubt activity, this method fails, probably because of environmental variables associated with the changing character of the eruption. The ash clouds associated with dome collapses that marked the later Redoubt clouds were of small volume and may not have contained as high a proportion of fine ash particles.

Laboratory biconical reflectance measurements were conducted to determine the spectral variability of ash that fell out of the Redoubt clouds. The results show that ash reflectance is controlled more by particle size than by particle composition, but these alone do not explain the variability we observed in the satellite data.

## INTRODUCTION

Satellite remote sensing of volcanic clouds is an important tool for scientists and those engaged in mitigating natural hazards. The total ozone mapping spectrometer (TOMS) has been used to measure the $SO_2$ released by eruptions (Krueger, 1983; Krueger and others, this volume), and multispectral image processing of advanced very high resolution radiometer (AVHRR) data has succeeded in discriminating volcanic clouds from weather clouds (Hanstrum and Watson, 1983; Prata, 1989a; Holasek and Rose, 1991). Perfection of image-processing algorithms and identification of primary physical parameters controlling success of the algorithms could lead to operational use of AVHRR data in reducing dangerous encounters between aircraft and volcanic clouds (Rose, 1987; Casadevall, 1990; Steenblik, 1990) and for monitoring the global dispersion of large atmospheric injections by volcanoes.

This paper attempts to advance satellite-based volcanic-cloud sensing through analysis of AVHRR data collected during the Redoubt eruptions of 1989–90. In particular, it tests a volcanic-cloud-discrimination algorithm developed by Holasek and Rose (1991) for the 1986 eruption of Augustine Volcano. Redoubt and Augustine Volcanoes, located in the Cook Inlet area of Alaska (Kienle, this volume), both erupted during the winter and early spring and have similar chemical compositions.

AVHRR satellite images collected during various stages of the Redoubt eruption were analyzed to test the utility of cloud-discrimination algorithms. In addition, the spectral variability of the Redoubt volcanic clouds were investigated through analysis of biconical reflectance measurements of samples of ash fallout and crushed pumice, glass, and minerals separated from Redoubt Volcano.

## AVHRR SENSOR

The AVHRR sensor, aboard the National Oceanic and Aeronautics Administration (NOAA) polar-orbiting weather satellites since 1978, has been used in the study of several eruptions (Kienle and Shaw, 1979; Hanstrum and Watson, 1983; Matson, 1984; Malingreau and Kaswanda, 1986; Glaze and others, 1989; Holasek and Rose, 1991). AVHRR data from NOAA-10 and NOAA-11 were used to study the Redoubt eruptions. This sensor images a 2,800-km-wide swath with a spatial resolution of 1.1 km at the nadir. The AVHRR sensor aboard NOAA-10 has four bands: band 1,

visible (0.58–0.68 μm); band 2, near-infrared (0.73–1.10 μm); band 3, mid-infrared (3.55–3.93 μm); and band 4, thermal-infrared (10.3–11.3 μm), whereas the AVHRR sensor aboard NOAA-11 contains the previous bands plus band 5, thermal-infrared (11.5–12.5 μm). Each satellite passes over a point on the ground twice per day, with more frequent coverage occurring at high latitudes where the orbits converge at the poles. The large swath width, frequent coverage, and multispectral capability make the AVHRR sensor a useful instrument for studying volcanic clouds.

## THE 1989–90 ERUPTION OF REDOUBT VOLCANO

Redoubt Volcano is an andesitic composite volcano located in the Cook Inlet region of Alaska, approximately 200 km southwest of Anchorage (fig. 1). In mid-December 1989, Redoubt erupted for the first time since 1966. During the next 5 months, there were more than 20 eruptive episodes, which produced ash clouds reaching greater than 12-km altitude (table 1) (Brantley, 1990). Scott and McGimsey (in press) estimate the total tephra-fall volume to be $2\times10^7$–$4\times10^7$ $m^3$, dense-rock equivalent, and note that two different tephra types were produced. Pumiceous tephra was generated by magmatically driven explosions on December 14 and 15, and fine-grained lithic-crystal tephra was erupted starting on December 16 and during all later events. The lithic-crystal tephra was generated by two processes: hydrovolcanic explosions dominated from December 16 to 19, and pyroclastic flows, resulting from dome collapse, became an increasingly important process from January 2, 1990, to the end of eruptive activity in April. Pyroclastic flows were the only mechanism generating tephra during the last five eruptive episodes (Scott and McGimsey, in press).

More than 60 percent of Alaska's population lives in the Cook Inlet region. Major oil facilities are also located in this region, and Anchorage is a major hub of air traffic between Asia and Europe. There were four incidents of commercial aircraft encountering volcanic clouds, including one incident in which a Boeing 747 carrying 246 people lost power from all four engines after flying through a cloud (Casadevall, 1990). The aircraft lost more than 4 km of altitude before two engines were restarted at 5.2 km—the remaining engines were restarted at about 4.1 km (Przedpelski and Casadevall, this volume). The aircraft was extensively damaged (Steenblik, 1990), and the incident highlighted the need for new techniques to detect and track volcanic clouds.

## MULTISPECTRAL IMAGE PROCESSING OF THE AVHRR IMAGES

More than 30 images of the Redoubt region were collected from the archive at the NOAA National Environmental Satellite Data and Information Service (NESDIS) and from the University of Alaska's Geophysical Institute following the eruption; 11 images are described in detail in this paper (table 2). In several cases, eruptive episodes are recorded in multiple images, providing an opportunity to track the ash clouds from the initial eruption through the dispersion of the volcanic clouds.

Image processing of the AVHRR scenes was conducted using Erdas and Terascan on a Sparc-1+ workstation. Images of the Redoubt region were extracted from the full scene; the thermal channels were calibrated using the procedure of Kidwell (1991); and the images were georeferenced to a common projection. Following the technique of Prata (1989a) and Holasek and Rose (1991), algebraic manipulations were

**Table 1.** Chronology of the 1989–90 eruption of Redoubt Volcano.

[Modified from Brantley (1990). X, volcanic activity occurred; na, not applicable; ?, volcanic activity uncertain; cont., continuous; fr., from]

| Day | Time[1] | Type of volcanic activity: Explosion[2] | Dome collapse | Plume height |
|---|---|---|---|---|
| **December 1989** | | | | |
| 14 | 9:47 | X(17) | na | >10 km |
| 15 | 1:40 | X(12) | na | ? |
| | 3:48 | X(10) | na | ? |
| | 10:15 | X(40) | na | >12 km |
| 16-18 | (Nearly cont. ejection of tephra fr. crater) | | | <7 km |
| 19 | 6:30 | X(9) | na | >9 km |
| **January 1990** | | | | |
| 2 | 17:48 | X(26) | X | >12 km |
| | 19:27 | X(61) | X | >12 km |
| 8 | 10:09 | X(15) | X | >12 km |
| 11 | 10:01 | X(5) | ? | >9 km |
| | 13:42 | X(12) | ? | ? |
| 16 | 22:48 | X(13) | ? | >11 km |
| **February 1990** | | | | |
| 15 | 4:10 | X(20) | X | >10 km |
| 21 | 12:32 | X(6) | X | 9 km |
| 24 | 5:05 | X(4) | X | 9 km |
| 28 | 9:47 | X(5) | X | 8 km |
| **March 1990** | | | | |
| 4 | 20:39 | X(8) | X | 12 km |
| 9 | 9:51 | X(10) | X | 10 km |
| 14 | 9:47 | X(14) | X | 12 km |
| 23 | 4:04 | X(8) | X | >10 km |
| 29 | 10:33 | X(7) | X | ? |
| **April 1990** | | | | |
| 6 | 17:23 | X(7) | X | 9 km |
| 15 | 14:49 | X(8) | X | >10 km |
| 21 | 18:11 | X(4) | X | >8 km |

[1] Alaska Standard Time.

[2] Numbers in parentheses indicate duration of explosive activity in minutes, based on seismicity.

**Table 2.** Satellite images of Redoubt volcanic clouds used in this study.

[LUT (look-up table) represents image channel color rendition in red (R), green (G), and blue (B)]

| Date and start time (GMT[1]) | Color, LUT | | | Satellite | Cloud type[2] |
|---|---|---|---|---|---|
| | R | G | B | | |
| 12/16/89 12:18 | 4m5 | 3 | 4 | NOAA-11 | 1 |
| 12/16/89 13:59 | 4m5 | 3 | 4 | NOAA-11 | 1 |
| 12/18/89 21:55 | 4m5 | 3 | 4 | NOAA-11 | 1 |
| 12/18/89 23:37 | 4m5 | 3 | 4 | NOAA-11 | 1 |
| 01/08/90 19:28 | 4 | 4 | 4 | NOAA-10 | 2 |
| 01/08/90 23:13 | 3m4 | 3 | 4 | NOAA-11 | 3 |
| 02/15/90 13:17 | 4 | 4 | 4 | NOAA-11 | 2 |
| 02/15/90 18:26 | 3m4 | 2 | 1 | NOAA-10 | 3 |
| 03/23/90 13:25 | 4 | 4 | 4 | NOAA-11 | 2 |
| 03/23/90 18:11 | 3m4 | 2 | 1 | NOAA-10 | 3 |
| 03/23/90 23:24 | 3m4 | 2 | 1 | NOAA-11 | 3 |

[1] Greenwich Mean Time. Local time is GMT minus 9 hours.
[2] See text for discussion of cloud types.

performed on AVHRR bands 4 and 5 to enhance the volcanic clouds and distinguish them from weather clouds. Ratios of band 4 to band 5 and differences between band 4 and band 5 were calculated and evaluated. The subtraction process results in an "apparent temperature difference," which we find particularly useful. The term "apparent temperature difference" is defined as the difference between temperature values derived from emitted energy measured at 10.5–11.3 μm (band 4) and 11.5–12.5 μm (band 5). The temperature difference is not real, but rather it is the result of differential emission of energy at these two wavelengths. When the emittance is converted to a temperature value, it produces an apparent temperature difference. An example of the band-4-minus-band-5 operation is shown in figure 2. In figure 2*A–B*, the single-band images are quite similar, and the volcanic plume is not very distinct. The plume is greatly enhanced by the band subtraction operation (fig. 2*C*), which generally produced better results, in terms of plume discrimination, than the ratio operation. When these operations were not successful, or when using data from NOAA-10 (which does not contain band 5), ratios and differences of band 3 and band 4 were calculated.

The results of these mathematical operations were visually evaluated to determine their ability to enhance volcanic clouds. False-color composites were generated on 24-bit graphic monitors by displaying algebraic enhancements along with several of the AVHRR bands in the red, green, and blue image planes of the monitor. False-color composites are helpful in interpreting the extent of the volcanic cloud because data from the individual bands interact to increase enhancement of the cloud. The various band combinations used to produce the false-color composites are shown in table 2.

# OBSERVATIONS OF THE AVHRR IMAGES

For the purpose of description and discussion, the Redoubt volcanic clouds shown in the satellite images are divided into three classes that are chosen on the basis of cloud spectral properties, morphology, and size. It is not implied that these cloud types will be produced by eruptions of other volcanoes or that they are the only type that will be produced. The classes include:

*Type-1 volcanic clouds.*—Clouds generated by magmatic explosions during the first week of activity (while there was a nearly continuous ejection of tephra from the crater). These clouds were low (< 7 km) and extended for hundreds of kilometers from the vent. Examples of this cloud type are shown in figure 3.

*Type-2 volcanic clouds.*—Clouds generated in part by dome collapse and subsequent pyroclastic flows (Scott and McGimsey, in press). These short-duration, discrete eruptive events were imaged within minutes of the onset of eruption. The type-2 clouds are higher (>10–12 km) than type-1 clouds and have a distinctive, circular morphology. Examples of these clouds are shown in figure 4.

*Type-3 volcanic clouds.*—Dispersed type-2 clouds. These clouds were imaged several hours after the initial eruptive event and show the dispersion of clouds produced by a single eruptive pulse. Examples of these clouds are shown in figure 5.

Although volcanic clouds were discriminated from weather clouds in many cases, no single algorithm was successful in enhancing all three cloud types. For the type-1 clouds, the band-4-minus-band-5 operation of Prata (1989a) and Holasek and Rose (1991) worked to discriminate portions of the volcanic cloud from the weather clouds (fig. 3*A–D*). This operation was successful for both daytime and nighttime images, but the discrimination is enhanced in the daytime images when band 3 data are included. All of the false-color composites in figure 3 were produced using identical band combinations (table 2), but a dramatic difference can be seen between the nighttime images from December 16 (fig. 3*A–B*) and the daytime images from December 18 (fig. 3*C–D*). Band 3 of the AVHRR sensor (3.53–3.93 μm) is a hybrid band, measuring thermal emittance at night and a combination of reflectance and emittance during the day. In the nighttime images, the enhanced portion of the volcanic cloud is red, indicating that the enhancement is solely caused by the band-4-minus-band-5 subtraction operation. By contrast, the volcanic cloud in the daytime images is yellow, indicating that the enhancement is a result of both the subtraction operation and high band 3 reflectance of the volcanic cloud with respect to the weather clouds.

The distal portions of two of the type-1 volcanic clouds were enhanced more than the proximal portions (fig. 3*A–B*). Near the vent, the volcanic cloud is spectrally similar to the weather clouds seen at the bottom of the image—the

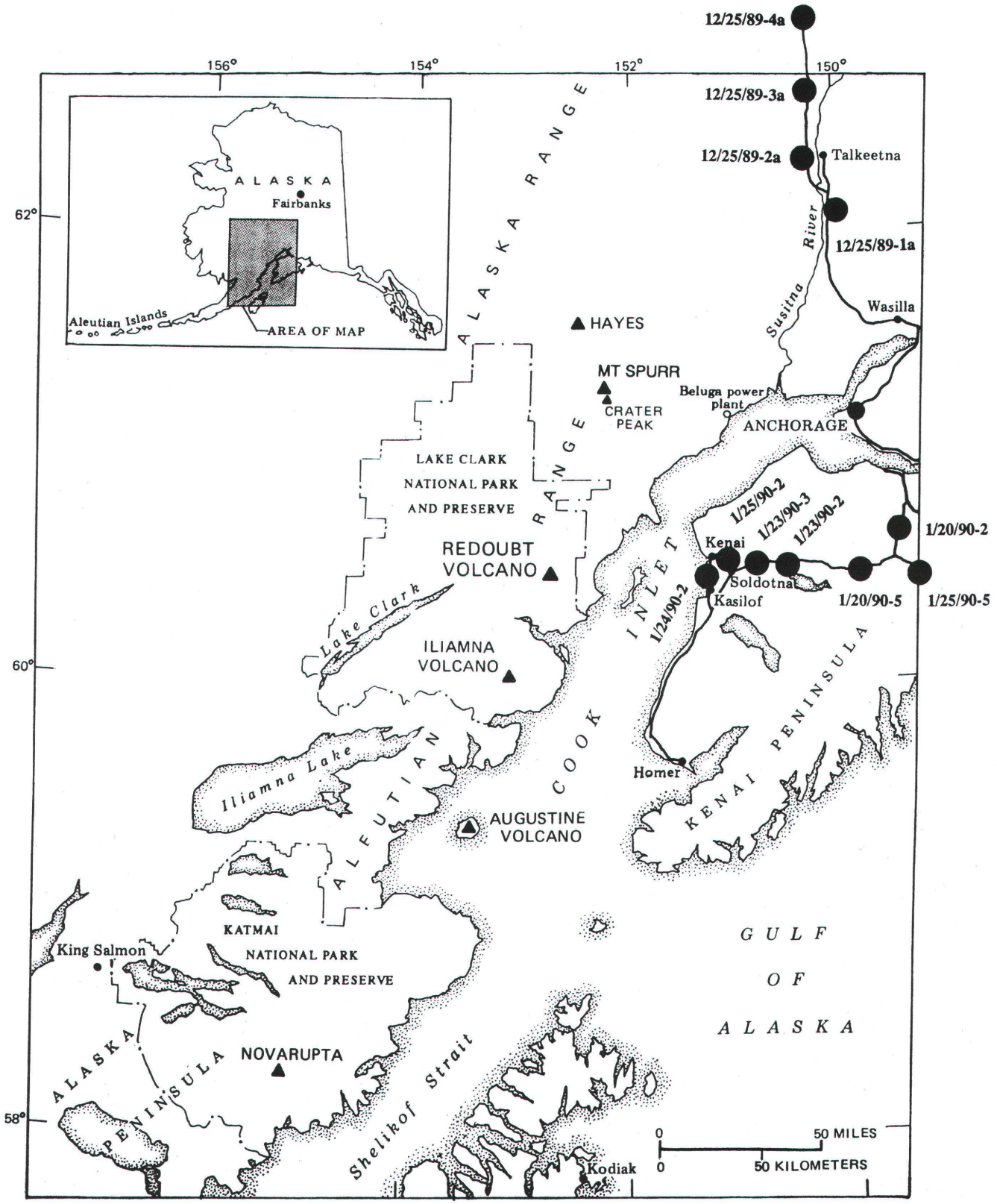


**Figure 1.** Index map of the Cook Inlet Region of Alaska. Sample locations of the ash spectra shown in figure 6 are indicated by solid circles. Figure modified from Brantley (1990).

subtraction operation is successful once the cloud disperses. Note that, in both cases, the subtraction operation is successful once the cloud has been transported approximately 100 km, or about 1 hour, from the vent. A z-shaped bend in the unenhanced portion of the volcanic cloud (east of Kenai) seen in figure 3*A* can be seen in figure 3*B* as an enhanced portion of the volcanic cloud. This image was collected about 1 hour after the previous image (fig. 3*A*) and shows that the discrimination becomes more distinctive as the volcanic cloud disperses.

In some cases, the effectiveness of the band-4-minus-band-5 operation in discriminating dispersed volcanic clouds is influenced by the underlying surface. Holasek and Rose (1991) found that their algorithm was more successful in discriminating volcanic clouds over water than over land, and effects of the underlying surface are observed in several images from Redoubt. In figure 3*A*, the discrimination of the volcanic cloud is distinct where the cloud passes over the western Kenai Peninsula and over the water of Prince William Sound, but the cloud is not apparent where it passes over the snow-covered mountains. In figure 3*C*, the discrimination of the cloud is reduced where it overlies low clouds over land.

Whereas the band-4-minus-band-5 difference was successful in discriminating type-1 volcanic clouds, this operation was not successful with type-2 clouds. These clouds are shown in figure 4 as band-4 thermal images, and they were identified by their anomalously low temperature (220°–230°K), their circular morphology, and their location relative to the vent. An inverted grayscale has been applied to the images in figure 4 so that details of the cold volcanic clouds are discernible.

These images were collected between 7 and 21 minutes after the onset of the eruption, as determined by seismicity (Brantley, 1990), and show that the cloud is detached from the vent, supporting the interpretation of Scott and McGimsey (in press) that these volcanic clouds were generated by

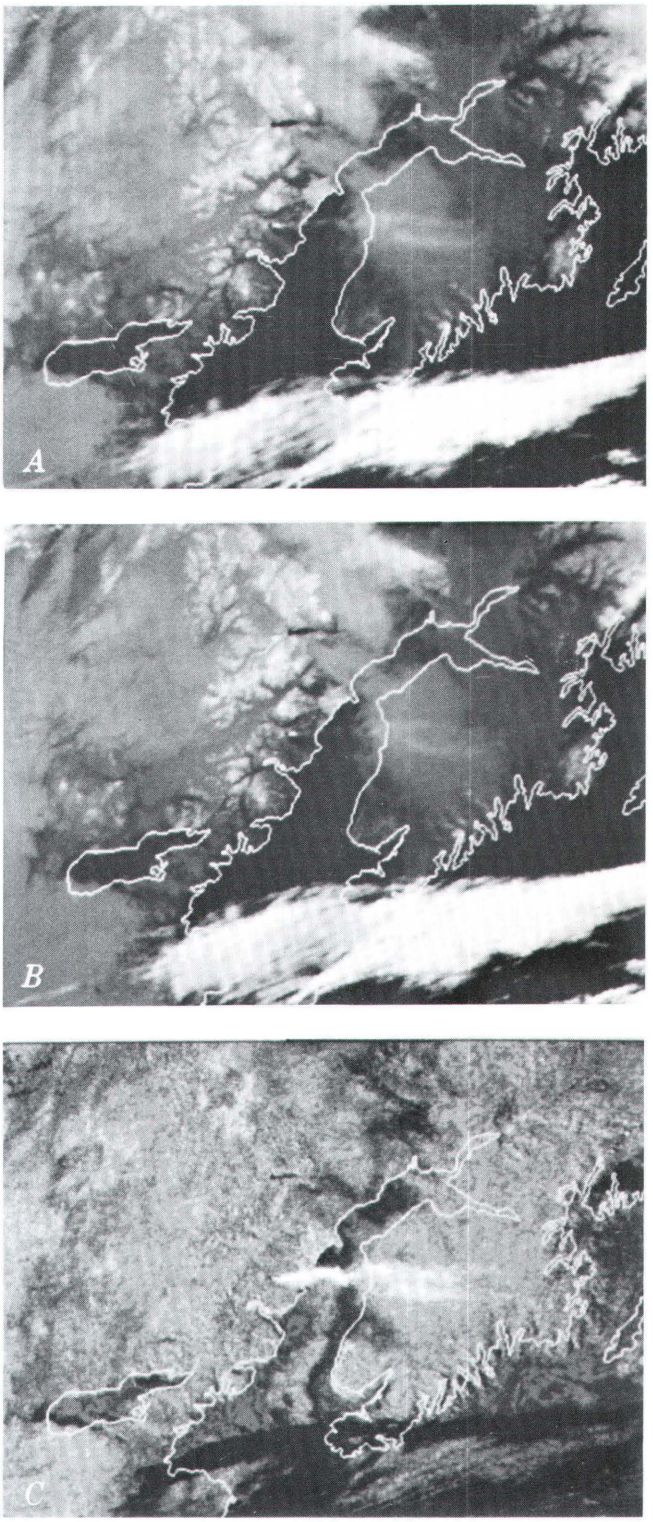


**Figure 2** (right). NOAA-11 AVHRR images demonstrating the discrimination of a volcanic eruption cloud from weather clouds. Image was collected on December 18, 1989, at 23:37 GMT. All images are shown with an inverted grayscale, so that cold objects are bright and warm objects are dark. *A*, AVHRR band-4 image showing an indistinct plume from Redoubt and weather clouds throughout the scene. *B*, AVHRR band-5 image. *C*, The result of a band-4-minus-band-5 operation. Note that the volcanic plume is a bright feature and that the weather clouds appear gray to black.

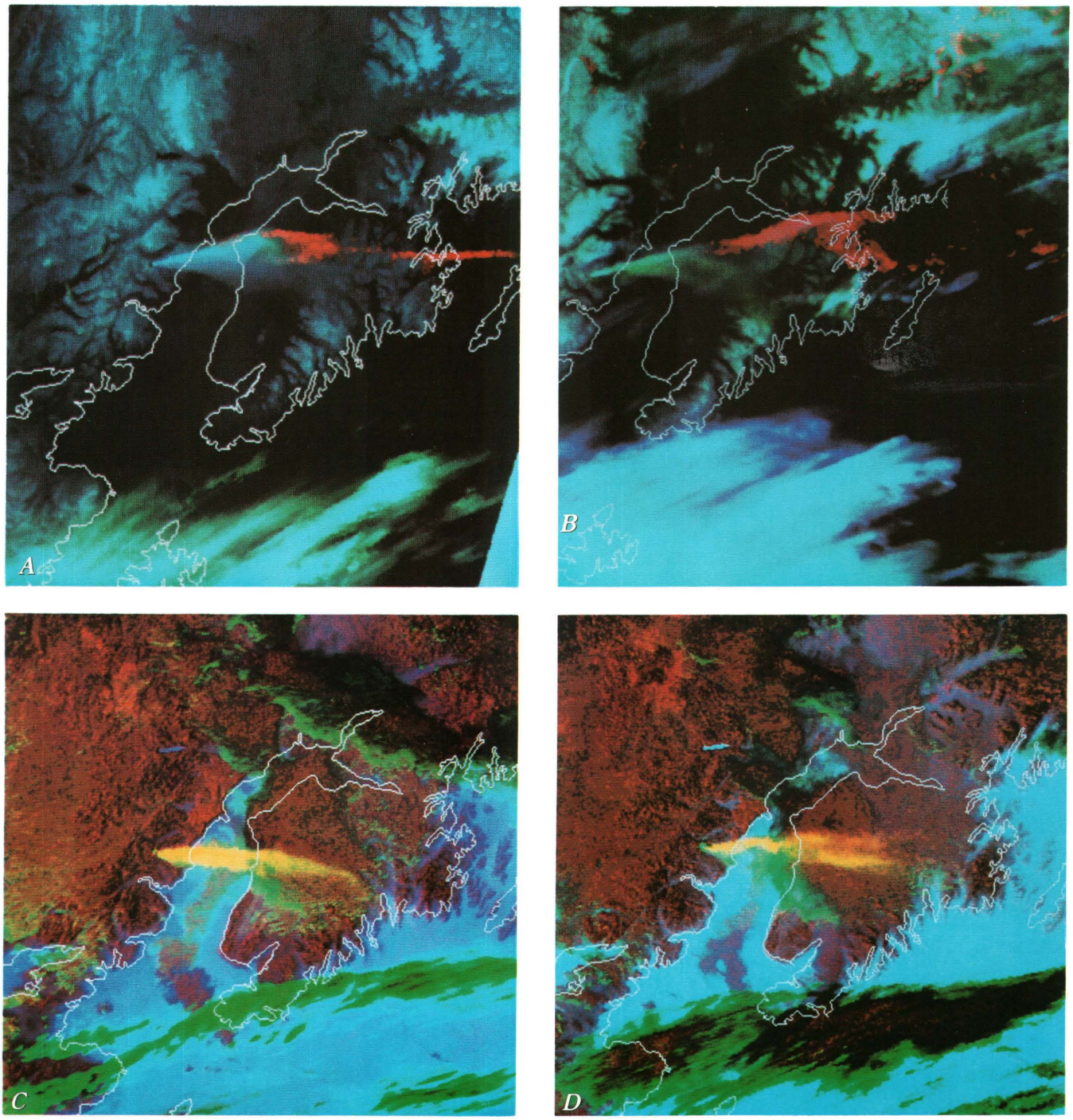


**Figure 3.** False-color composite AVHRR images of type-1 eruption clouds from Redoubt Volcano. All of the color composites were produced using band 4 minus band 5 in red, band 3 in green, and band 4 in blue. See text for description of cloud types. *A*, NOAA-11 image collected on December 16, 1989, at 12:18 GMT. *B*, NOAA-11 image collected on December 16, 1989, at 13:39 GMT. *C*, NOAA-11 image collected on December 18, 1989, at 21:55 GMT. *D*, NOAA-11 image collected on December 18, 1989, at 23:37 GMT.

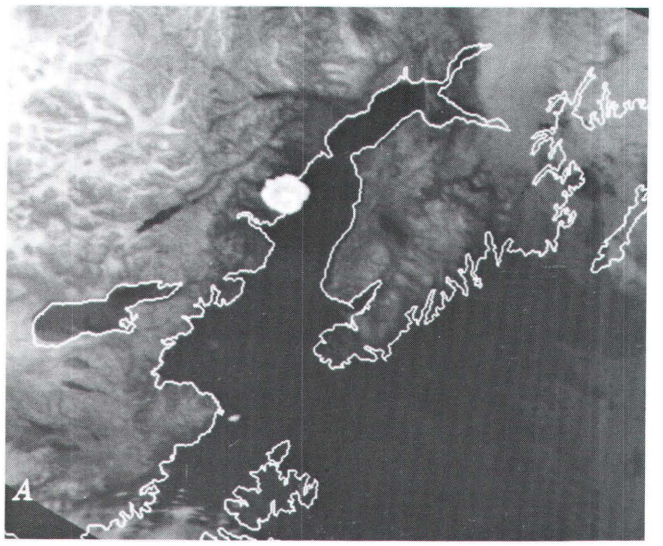


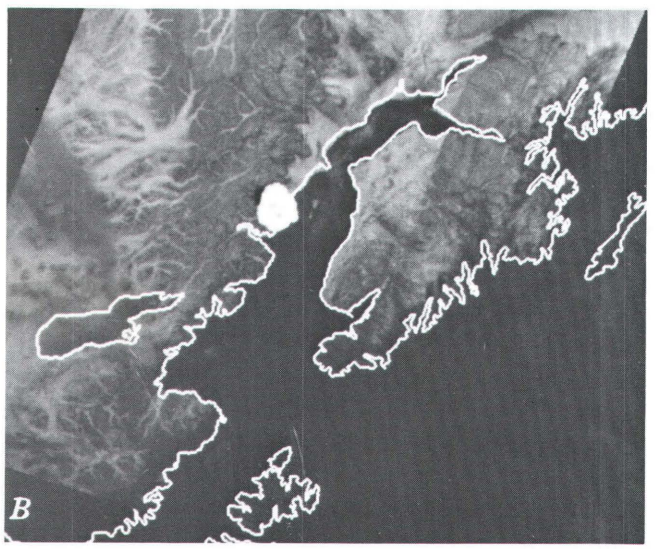


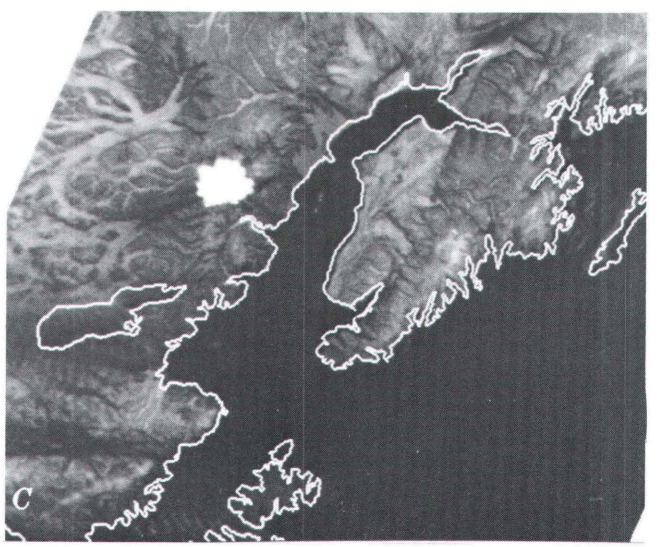


dome collapse and pyroclastic flows. Dispersal of these clouds and transformation into type-3 clouds are monitored in subsequent images, and the observations of these clouds are discussed below.

Even though it appears that the volcanic clouds show variation in cloud-top topography, this cannot be quantified. It is possible to determine cloud-top elevation and topography by relating the temperature of the cloud, as determined by one or more thermal bands of the satellite sensor, with a temperature profile of the atmosphere as determined by radiosonde or other methods. Altitude values for each cloud pixel can be determined in this manner. Whereas this method is useful for tropospheric clouds, it is unsuccessful at higher altitudes due to the temperature inversion that defines the tropopause. All of the type-2 volcanic clouds penetrated the stratosphere, which starts at about 10-km altitude during the Arctic winter, limiting height estimates of clouds to a minimum value and preventing the determination of cloud-top topography.

The frequent coverage of the NOAA satellites provided opportunities to observe the transport and dispersion of the Redoubt volcanic clouds. These dispersed, type-3, volcanic clouds were enhanced by a band-3-minus-band-4 operation. The dispersed volcanic cloud from the January 8, 1990, eruptive episode is seen in figure 5*A*. This image was collected about 5 hours after the start of the eruption seen in figure 4*A* and shows a yellow, comma-shaped cloud extending from north of Anchorage to the southern coast of the Kenai Peninsula and a more dilute, hazy cloud extending back toward the vent. The volcanic cloud is shown in yellow, indicating that the enhancement results from a combination of the band-3-minus-band-4 operation and high band-3 reflectance of the volcanic cloud with respect to weather clouds.

**Figure 4** (left). Inverted grayscale AVHRR band-4 thermal images of type-2 eruption clouds from Redoubt Volcano. See text for description of cloud types. *A*, NOAA-10 image collected on January 8, 1990, at 19:28 GMT. *B*, NOAA-11 image collected on February 15, 1990, at 18:26 GMT. *C*, NOAA-11 image collected on March 23, 1990, at 13:25 GMT.

**Figure 5** (following pages). False-color composite AVHRR images of type-3 eruption clouds from Redoubt Volcano. See text for description of cloud types. All of the color composites, except *A*, were produced using band 3 minus band 4 in red, band 2 in green, and band 1 in blue. *A*, NOAA-11 image collected on January 8, 1990, at 23:13 GMT. This color composite was produced using band 3 minus band 4 in red, band 3 in green, and band 4 in blue. *B*, NOAA-10 image collected on February 15, 1990, at 18:26 GMT. *C*, NOAA-10 image collected on March 23, 1990, at 18:11 GMT. *D*, NOAA-11 image collected on March 23, 1990, at 23:24 GMT.

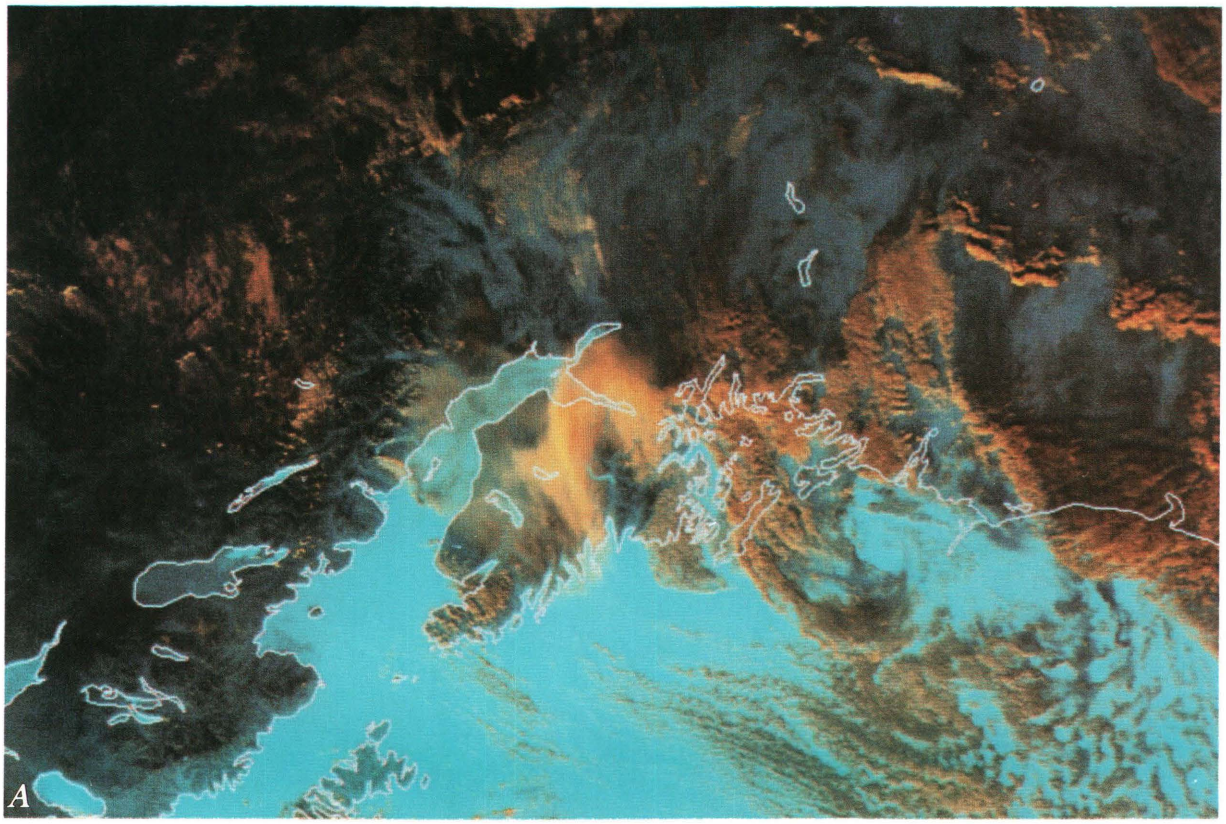
A

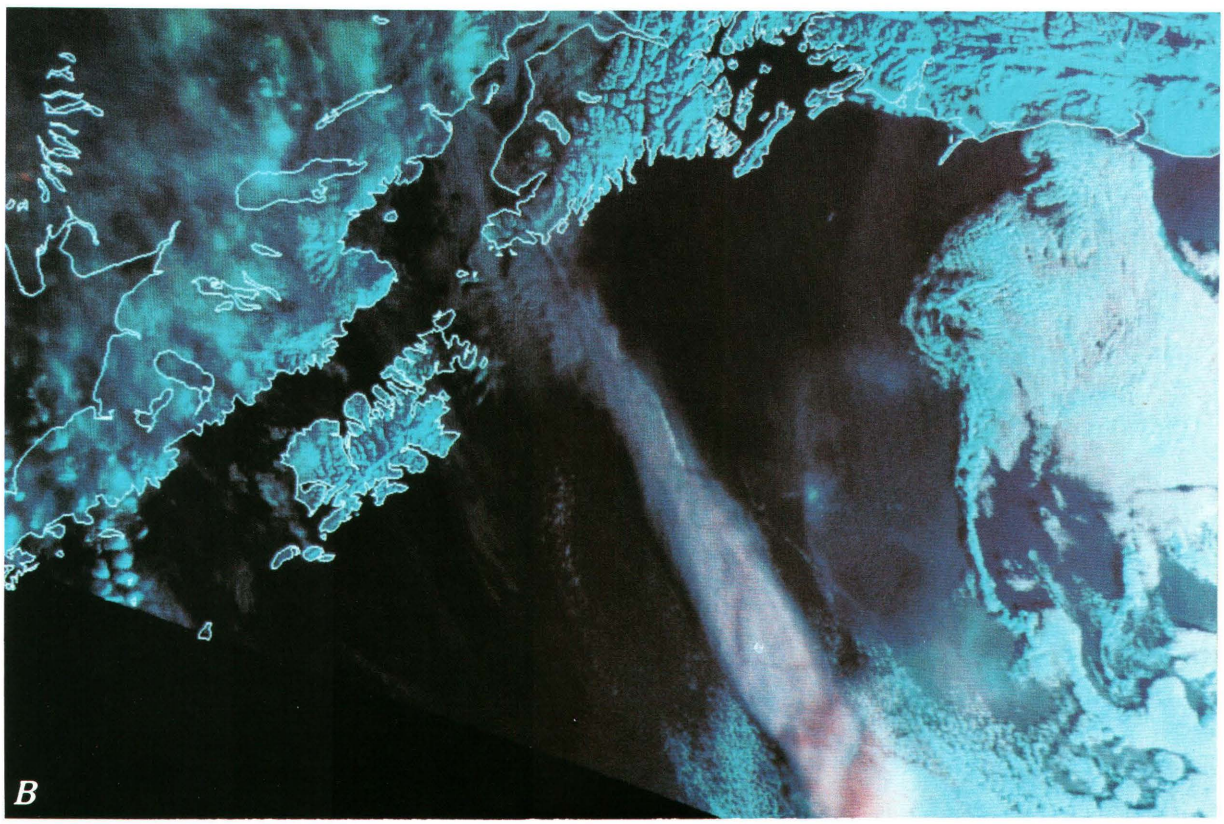
B

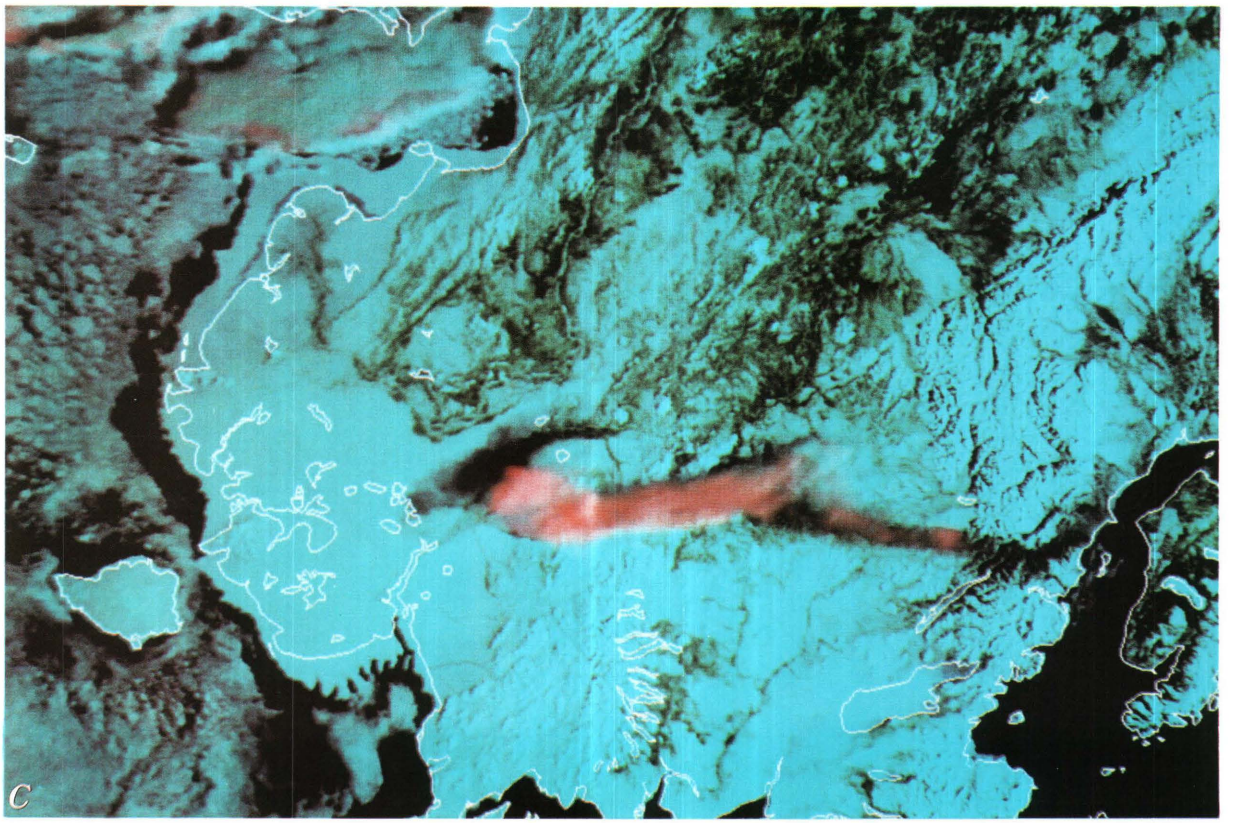
C

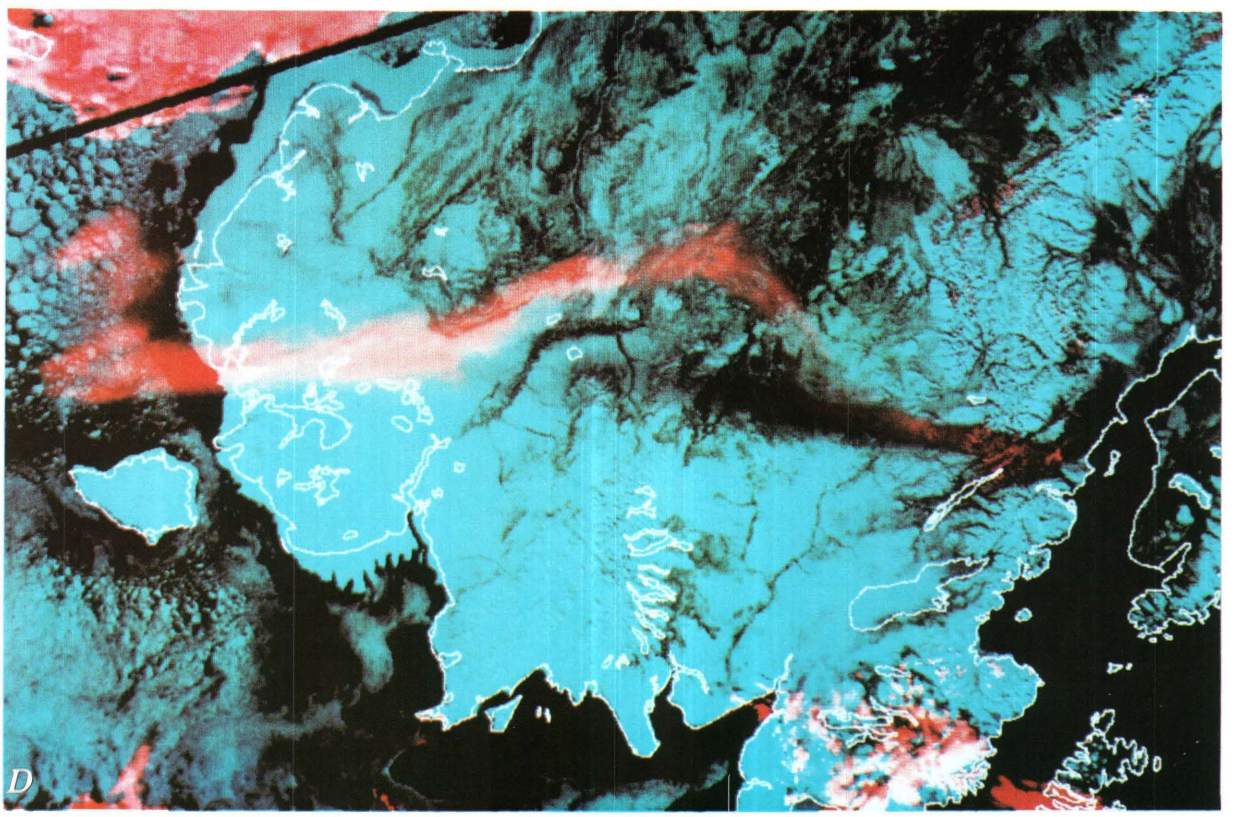
D

The band-4-minus-band-5 operation was not successful in discriminating this cloud, and theories regarding the failure of this operation are included in the discussion.

Another type-3 cloud, from the February 15, 1990, eruptive episode, is seen in figure 5*B*. The image was collected about 5 hours after the initial eruption seen in figure 4*B* and consists of a linear, light-red cloud extending from the bottom of the image back toward the volcano, in the upper left of the image. At this time, the cloud front had traveled more than 800 km to the southeast over the Gulf of Alaska. Even though the band-3-minus-band-4 operation was useful in enhancing the volcanic cloud, some of the weather clouds have a similar spectral signal. In this case, manual image interpretation is needed to define the limits of the volcanic cloud. This image was collected by NOAA-10, which contains one thermal band, so it was not possible to attempt the band-4-minus-band-5 operation.

A third type-3 volcanic cloud, from the March 23, 1990, eruption, is seen in two successive images, one NOAA-10 image collected 5 hours after the initial eruption (fig. 5*C*) and a NOAA-11 image collected 5 hours later (fig. 5*D*). In figure 5*C*, the circular volcanic cloud front has traveled about 450 km, and a tail trails back toward the vent. The band-3-minus-band-4 operation was used to enhance the volcanic cloud, but the clarity of the enhancement is diminished by multiple data line dropout along the northern boundary of the volcanic cloud.

In the NOAA-11 image acquired 5 hours later (fig. 5*D*), the continued dispersal of the volcanic cloud can be seen. The cloud front now extends for more than 825 km, from near the vent to the Bering Sea. Once again, the band-3-minus-band-4 operation helped to enhance the volcanic cloud, but it did not discriminate it from the weather clouds along the top of the scene. The northward bend in the cloud seen in this image is also apparent in the previous image (fig. 5*C*) and may be due to wind shear. Ash fallout from this eruption is visible as a dark band that trends west for about 300 km and is correlated to the distribution of ash on the ground as mapped by Scott and McGimsey (in press).

## REFLECTANCE SPECTRA OF VOLCANIC ASH

The reflectance properties of 19 volcanic ash samples from Redoubt were investigated to see how they varied with transport, and how they varied throughout the eruption. These samples were collected by personnel of the Alaska Volcano Observatory in the weeks to months following the eruption. All of the ash samples used in this study were collected from snowpits throughout Alaska (fig. 1) and were correlated by Scott and McGimsey (in press) to eruptive events by their stratigraphic position. The ash was separated from the snow by melting and filtration, eliminating any sulfuric-acid coatings that may have been present.

To aid in interpretation of the ash reflectance spectra, glass and mineral separates were also prepared. Pumice fragments from the December 15, 1989, eruptive event were crushed mechanically, and glass and crystals were separated using heavy-liquid-separation techniques. The pumice, crystal, and glass separates were sieved to produce a 0.25-mm to 0.088-mm sample, and subsets of these samples were crushed to produce a sample of less than 0.088 mm. This was done to reflect the reduction in grain size and the fractionation of the crystals with respect to glass that occurs as volcanic clouds age and are transported. The crystal separates were composed primarily of plagioclase, with lesser amounts of hornblende and pyroxene.

Laboratory biconical reflectance measurements were conducted on the ash samples and mineral separates by the Jet Propulsion Laboratory (JPL) (J. Crisp, JPL, oral commun., 1991). Although the AVHRR sensor measures emitted energy, reflectance measurements can be related to emittance, which is difficult to measure in the laboratory (Bartholomew and others, 1989). Kirkoff's law states that, for a given temperature and wavelength, emittance and reflectance are complementary. This law only applies to solid objects because scattering is ignored. Although this is a major simplification, we use it to correlate reflectance measurements to the emittance recorded by the satellite sensor.

Biconical reflectance spectra of ash fallout from eruptions on December 15, 1989, December 16, 1989, and from January 8, 1990, are shown in figure 6*A–C*. These reflectance spectra are typical of the 19 ash samples that were measured and show two reflectance peaks of interest to this study. The first peak extends from 3 μm to 5 μm and contains AVHRR band 3, whereas the second peak extends from 8 μm to 12 μm and contains AVHRR bands 4 and 5. In the region containing AVHRR band 3, the reflectance varies by 10–15 percent between eruptive episodes, and, for the December 15, 1989, event, the reflectance increases by 20 percent as the distance from the vent increases. In contrast, all of the samples show a broad similarity in reflectance in the region containing AVHRR bands 4 and 5, except for the sample suite from the December 15, 1989, event, where the reflectance increases by 1–2 percent with increasing distance from the vent.

The reflectance spectra of the pumice and the glass and crystal separates are shown in figure 7*A–B*. All of the coarse-grained samples (fig. 7*A*) show a reflectance peak at 9 μm. The reflectance at 9 μm is less prominent for the crystal separate and the pumice sample, and the glass separate has a smaller reflectance peak at 11.5 μm. The fine-grained samples (fig. 7*B*) show a much-diminished reflectance peak at 9 μm for the glass separate and none for the pumice sample and crystal separate. The peak at 11.5 μm is most prominent for the glass sample, but the pumice and crystal separates also have a broad peak in this region. These spectra show that reflectance is influenced more by particle size than by particle composition.

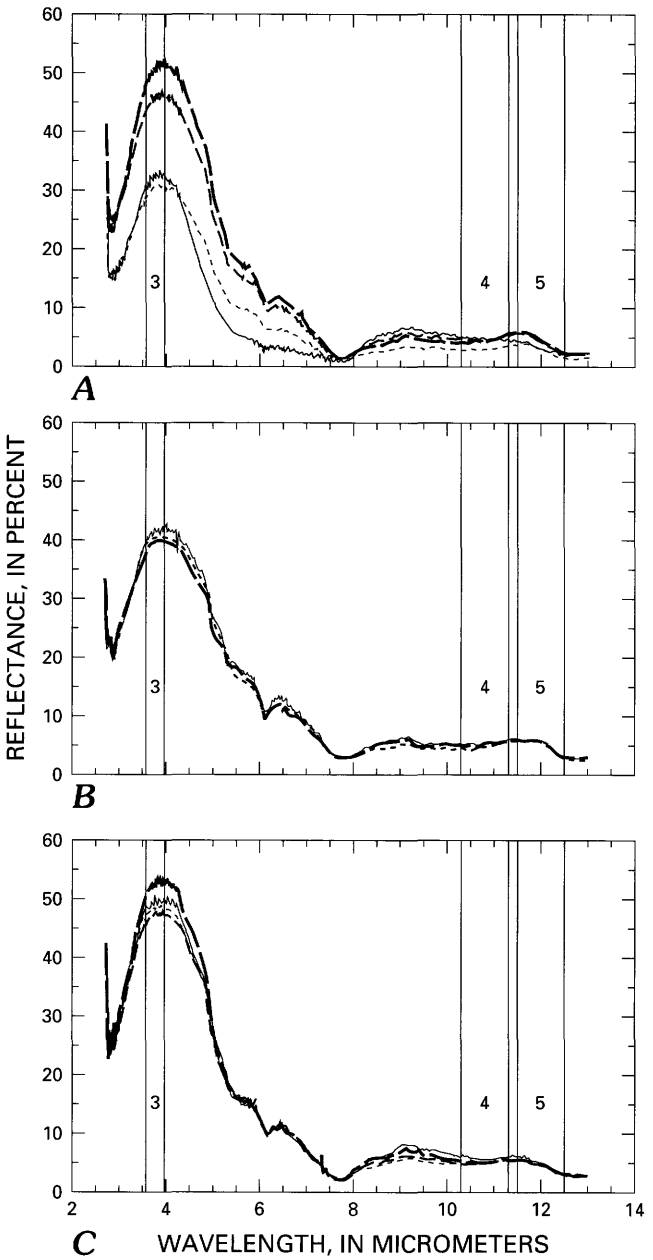


**Figure 6.** Biconical reflectance plot of ash samples from three eruptions of Redoubt Volcano. The band widths of AVHRR bands 3, 4, and 5 are indicated. Sample locations are shown in figure 1. *A*, Four ash samples from the December 15, 1989, eruption. *B*, Three ash samples from the December 16, 1989, eruption. *C*, Four ash samples from the January 8, 1990, eruption.

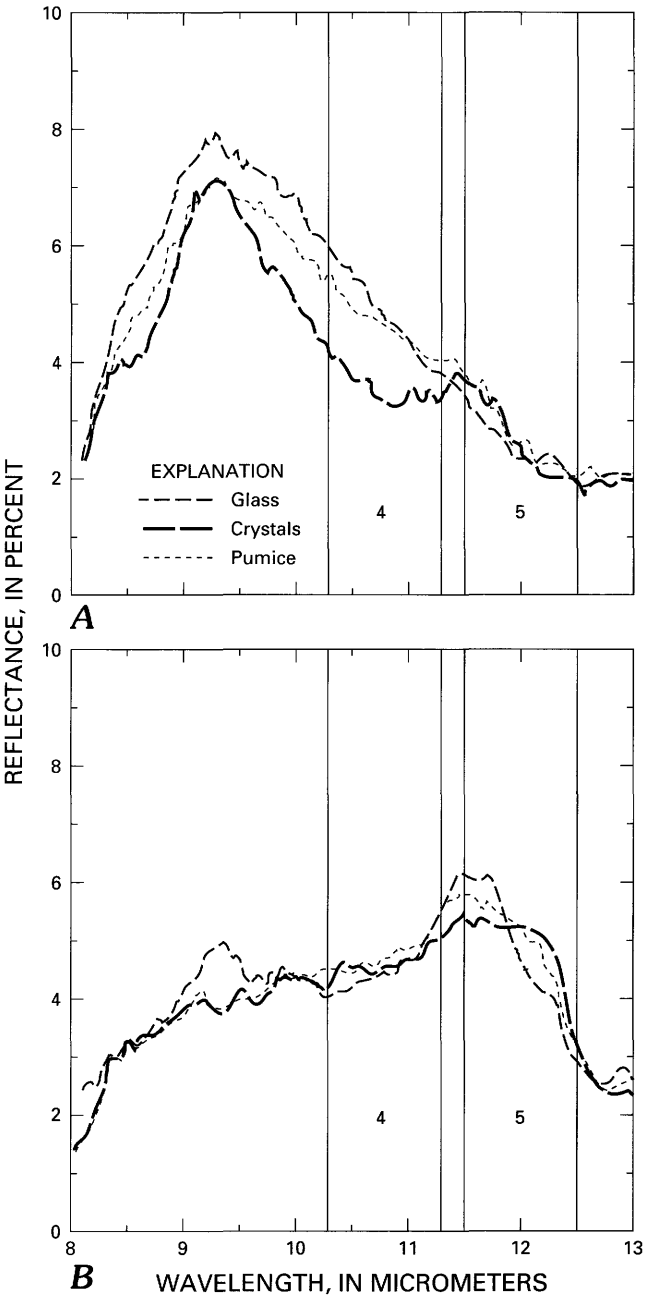


**Figure 7.** Biconical reflectance plots of pumice, glass, and crystal separates from Redoubt Volcano. *A*, Sieved 0.25–0.88-mm samples. *B*, Sieved > 0.088-mm samples. The band widths of AVHRR bands 4 and 5 are indicated.

## DISCUSSION

The spectral discrimination of volcanic clouds is complicated by dynamic processes that occur during the eruption, transport and dispersion of the cloud—these processes may prevent the use of a single image-processing algorithm for use on all volcanic clouds. Previous researchers (Prata, 1989a, 1989b; Holasek and Rose, 1991) have utilized differences and ratios of AVHRR bands 4 and 5 to discriminate volcanic clouds from weather clouds, but these operations were only partially successful at Redoubt. It has been shown that the band-4-minus-band-5 subtraction operation produces positive apparent temperature differences ($\Delta T$) for weather clouds and negative apparent temperature differences for volcanic clouds (Yamanouchi and others, 1987; Prata, 1989b). However, positive apparent $\Delta T$'s can occur for volcanic clouds if the cloud contains a large amount of water or if the particle size is large (Prata, 1989b).

The early eruptions of the Redoubt series (type-1 clouds) more closely resemble the kinds of ash clouds that are likely to be of most concern to aviation safety than do the later ones. Two important features of these early clouds are the success of the discrimination algorithm based on apparent $\Delta T$ determined from bands 4 and 5 and the indication that, for success of the algorithm, the cloud must have aged (dispersed freely in the atmosphere) for 1 hour or more. Several observations point to the role of fine silicate particles in explaining these phenomena. Biconical reflectance data suggest that fine particle size may enhance the 4-minus-5 effect, and magmatic explosions resulting from explosive vesiculation may be more likely to produce fine ash than dome collapse. Aging of a volcanic cloud will result in decreasing the grain size of suspended ash because fallout will remove larger particles, and it will also tend to reduce the water or ice in the cloud, thereby enhancing the relative importance of the fine ash particles. Because the largest and most broadly hazardous ash clouds are magmatic (and are likely to generate drifting ash clouds that contain significant concentrations of fine ash) these observations are likely to be of general applicability.

The band-4-minus-band-5 operation produced positive $\Delta T$'s for both volcanic and weather clouds in images of type-2 volcanic clouds from Redoubt, which were collected within 30 minutes of the start of the eruption. These volcanic clouds probably contained large amounts of water, due to the entrainment of moist air from the lower atmosphere, and were identified in band-4 thermal images by their proximity to Redoubt, their circular morphology, and cold temperature (fig. 4*A–C*). Volcanic clouds of this type could be confused with convective weather clouds, but this is unlikely in winter Arctic images. In two of the images (fig. 3*A–B*) of type-1 clouds, the band-4-minus-band-5 operation produced positive $\Delta T$'s for the proximal portion of the cloud and negative $\Delta T$'s for distal portions of the cloud. The region of negative $\Delta T$ is shown in red in figure 3*A–B*. We attribute the change in the spectral signature of this volcanic cloud to a decrease in particle size and water content during transport. Analysis of wind-speed data for this eruption indicates that the transition from positive to negative difference values in the volcanic cloud took about 1 hour.

Type-3 volcanic clouds were difficult to discriminate, perhaps due to their relatively small volume and the dispersion and sedimentation of ash that occurred before they were imaged. Whereas many volcanic clouds can be discriminated using the band-4-minus-band-5 operation, the concentration of ash required to produce a detectable signal is unknown. Another factor that affects the subtraction operation is particle size. The type-3 clouds may have contained fewer fine particles than the type-1 clouds because they were produced as part of a dome collapse, rather than from a purely explosive, volatile, effervescent mechanism, thus reducing the ash signal.

The band-3-minus-band-4 operation was useful in enhancing type-3 clouds, but it did not discriminate them from weather clouds. This operation was more successful during the daytime hours, when band-3 backscatter is important, than at night, when this band has a larger thermal component. Although this is a useful operation, it is difficult to make general observations regarding its success because the reflectance is dependent on a number of factors, including particle size, shape and abundance, sun azimuth and elevation, and the location of the cloud and the satellite relative to the sun. However, this operation, used in conjunction with observations of cloud morphology, can be used to interpret the extent of probable volcanic clouds.

The use of ash fallout reflectance measurements as "ground truth" for interpreting satellite imagery has several shortcomings. One fundamental problem is that the reflectance measurements were made on ash fallout, which by definition is not what is in the volcanic cloud. Very fine particles are probably the most important, yet their collection is difficult because their fallout may be too light to be distinguished on the ground, and the particles fall out long distances from the vent over very broad areas. Another problem lies in relating the reflectance measurements to the emittance recorded by the sensor. Volcanic clouds are heterogeneous assemblages of particles and gases; therefore, subtracting the reflectance measurements from a black body of the appropriate temperature is a poor approximation. Additional work needs to be done to determine the most effective way of using reflectance measurements of ash fallout as "ground truth" for image interpretation.

In spite of these difficulties, the mineral separate spectra show that reflectance is controlled more by particle size than by the particle composition. In a volcanic cloud, this would imply that the discrimination of distal clouds would be controlled more by the reduction in the size distribution of the particle with transport than by the increase in the proportions of volcanic glass in the cloud due to eolian fractionation. Although the exact relationship of reflectance to

emittance is unknown, the effects of particle size, particle shape, and particle composition would probably be enhanced for suspended particles. In this case, the complex shape of glass particles compared to crystals may have an important effect on the emittance of volcanic clouds.

This study has shown that the discrimination of volcanic clouds using AVHRR imagery is more complex than previously thought and has identified several parameters that contribute to this complexity. These include cloud water content and particle size, concentration, and composition. Additional factors not included in this study include the role of acid aerosols (Prata, 1989a) and sensor viewing geometry. The relative importance of each of these parameters can be investigated in laboratory experiments utilizing an imaging radiometer to observe simulated volcanic clouds. Images can be collected at the same wavelength intervals as the AVHRR sensor, and image-processing operations similar to the ones described in this paper can be conducted. Results of the laboratory studies can be used to guide future work on thermal imaging and particle and gas sampling of actual volcanic clouds.

## CONCLUSIONS

Volcanic clouds of a variety of types and scales were observed and mapped by AVHRR images during the Redoubt eruptions of 1989–90. These examples broaden the experience on volcanic cloud tracking and discrimination using multispectral image-processing techniques and provide insight on additional work that needs to be conducted.

A major conclusion of this paper is that volcanic clouds have natural variability that is reflected in satellite images and that affects the methods used to discriminate and map their dispersion. This variability is magnified for activity like that of Redoubt Volcano, which changed eruptive mechanism during its period of activity. Most ash-producing eruptions from other volcanoes, particularly the larger ones, are more likely to resemble the early (type-1) clouds of Redoubt. This is encouraging because the simple method of discrimination of volcanic clouds using apparent temperature differences between AVHRR bands 4 and 5 works well on type-1 clouds; therefore, the simplest methodology is likely to be useful in many of the most serious cases. Discrimination of volcanic clouds using the band-4-minus-band-5 operation is difficult or impossible for very young clouds with high water content and (or) a large particle size, but it is very useful for drifting volcanic clouds. A major uncertainty of this method is the particle concentration required to produce a measurable signal.

Ash reflectance is controlled more by particle size than by particle composition. The fractionation of glass and crystals in a volcanic cloud are not likely to produce reflectance and emittance differences on their own, but fractionation will operate in conjunction with the proportional increase of fine particles as the cloud disperses. Laboratory reflectance measurements are inadequate to explain the spectral variability observed in the imagery of the Redoubt volcanic clouds. Emittance measurements need to be made of simulated volcanic clouds in the laboratory and in situ measurements and particle sampling need to be conducted on actual volcanic clouds to provide "ground truth" for interpretation of satellite imagery.

## ACKNOWLEDGMENTS

We would like to thank the following people and organizations for their cooperation and support for this study. Mike Matson of NOAA/NESDIS provided most of the AVHRR data, and Ken Dean of the University of Alaska's Geophysical Institute provided several AVHRR scenes. Joy Crisp of the Jet Propulsion Lab made the ash reflectance measurements, and the Alaska Volcano Observatory furnished field support. This study was funded in part by NSF Grant 91-17726 and NASA Grant 1442-VC1P-011-91.

## REFERENCES CITED

Bartholomew, M.J., Kahle, A.B., and Hoover, G., 1989, Infrared spectroscopy (2.3–20 μm) for the geological interpretation of remotely sensed multispectral infrared data: International Journal of Remote Sensing, v. 10, p. 529–544.

Brantley, S.R., ed., 1990, The eruption of Redoubt Volcano, Alaska, December 14,1989–August 31, 1990: U.S. Geological Survey Circular 1061, 33 p.

Casadevall, T.J., 1990, The 1989–90 eruption of Redoubt Volcano, Alaska, impacts on aircraft operations in the vicinity of Anchorage [abs.]: Eos, Transactions, American Geophysical Union, v. 71, p. 1701.

Glaze, L.S., Francis, P.W., Self, S., and Rothery, D.A., 1989, The 16 September 1986 eruption of Lascar Volcano, north Chile, satellite investigations: Bulletin of Volcanology, v. 51, p. 911–923.

Hanstrum, B.N., and Watson, A.S., 1983, A case study of two eruptions of Mount Galunggung and an investigation of volcanic cloud characteristics using remote sensing techniques: Australian Meteorological Magazine, v. 31, p.171–177.

Holasek, R.E., and Rose, W.I., 1991, Anatomy of 1986 Augustine Volcano eruptions as revealed by digital AVHRR satellite imagery: Bulletin of Volcanology, v. 53, p. 420–435.

Kidwell, K.B., ed., 1991, National Oceanic and Atmospheric Administration Polar Orbiter Data Users Guide: Washington, D.C., National Oceanic and Atmospheric Administration/National Environmental Satellite Data and Information Service, 294 p.

Kienle, J., and Shaw, G.E., 1979, Plume dynamics, thermal energy and long-distance transport of Vulcanian eruption clouds from Augustine Volcano, Alaska: Journal of Volcanology and Geothermal Research, v. 6, p. 139–164.

Krueger, A.J., 1983, Sighting of the El Chichón sulfur dioxide clouds with the NIMBUS 7 total ozone mapping spectrometer: Science, v. 220, p. 1377–1379.

Malingreau, J.P., and Kaswanda, 1986, Monitoring volcanic eruptions in Indonesia using weather satellite data: The Colo eruption of July 28, 1983: Journal of Volcanology and Geothermal Research, v. 27, p. 179–194.

Matson, M., 1984, The 1982 El Chichón Volcano eruptions—A satellite perspective: Journal of Volcanology and Geothermal Research, v. 23, p. 1–10.

Prata, A.J., 1989a, Observations of volcanic ash clouds in the 10–12 μm window using AVHRR/2 data: International Journal of Remote Sensing, v. 10, p. 751–761.

———1989b, Infrared radiative transfer calculations for volcanic ash clouds: Geophysical Research Letters, v. 16, p. 1293–1296.

Rose, W.I., 1987, Interaction of aircraft and explosive eruption clouds: A volcanologist's perspective: American Institute of Aeronautics and Astronautics Journal, v. 25, p. 52–58.

Steenblik, J.W., 1990, Volcanic ash: A rain of terra: Air Line Pilot, v. 59, p. 9–15, p. 56.

Salisbury, J.W., and Walter, L.S., 1989, Thermal infrared (2.5–13.5 μm) spectroscopic remote sensing of igneous rock types on particulate planetary surfaces: Journal of Geophysical Research, v. 94, p. 9192–9202.

Scott, W.E., and McGimsey, R.G., in press, Character, mass, distribution, and origin of tephra-fall deposits of the 1989–90 eruption of Redoubt Volcano, south-central Alaska: Journal of Volcanology and Geothermal Research.

Yamanouchi, T., Suzuki, K., and Kawaguchi, S., 1987, Detection of clouds in Antarctica from infrared multispectral data of AVHRR: Journal of the Meteorological Society of Japan, v. 65, p. 949–961.

VOLCANIC ASH AND AVIATION SAFETY:
Proceedings of the First International Symposium
on Volcanic Ash and Aviation Safety
U.S. GEOLOGICAL SURVEY BULLETIN 2047

# APPLICATION OF CONTEMPORARY GROUND-BASED AND AIRBORNE RADAR FOR THE OBSERVATION OF VOLCANIC ASH

*By* Melvin L. Stone

## ABSTRACT

Radar detection and tracking of volcanic ash from Mount St. Helens demonstrated the usefulness of real-time surveillance of ash clouds. The radars used were operational National Weather Service (NWS) magnetron systems. The low radar reflectivity reported for volcanic ash clouds makes the detection and characterization of the potential threat to aviation a formidable task. The NWS is procuring pulsed Doppler radars with enhanced sensitivity that may find application in volcanic ash cloud surveillance. Contemporary airborne weather radars lack the capability to detect volcanic ash and provide warning information. An overview of radar principles and technical issues related to observing volcanic ash illustrates the capabilities and limitations of radar in this application. Azimuth and elevation scanning strategies are presented. A technique is discussed for measuring wind speed and particle fall velocity when an ash cloud passes over the radar. The functional elements of a digital radar processor are described to acquaint users with their potential. The WSR-88D (NEXRAD) is recognized as the most suitable candidate for volcanic ash cloud surveillance, both because of its sensitivity and its planned deployment in the vicinity of the Cascade Range and in Alaska. A candidate radar for research on volcanic ash is suggested.

## INTRODUCTION

Recent aircraft encounters with volcanic ash have renewed interest in the examination of the capability of radar to detect and characterize ash clouds. Successful use of National Weather Service (NWS) and Federal Aviation Administration (FAA) radars during the Mount St. Helens eruptions (fig. 1) demonstrated their ability to generate information of scientific value and their potential use in providing warnings to aviation (Harris and others, 1981; Harris and Rose, 1983; Rose, 1987). This report considers the capabilities and limitations of ground-based radars that will become operational during the 1990's as they apply to providing data useful in generating aviation warnings of volcanic ash. The inability of airborne weather radar to detect volcanic ash is noted.

The scientific and aviation interests in applying radar to the monitoring of volcanic activity include determining (1) whether an eruption is occurring, (2) the eruption height versus time (to use in estimating the rate of eruption), (3) cloud dimensions and altitude range as a function of time, (4) estimates of successive cloud positions and boundaries and initial trajectories (i.e., tracking and prediction), and (5) when the initial explosive pulse has ended (Harris, this volume; Rose, 1987).

Volcanic ash detection must be capable of providing wide area coverage to serve the needs of aviation. Owing to its small particle size, density, and dielectric constant, the low radar reflectivity of ash clouds may limit the range of ground-based radars to a few hundred kilometers. Noting that ash fall and aircraft damage have been reported more than 1,000 km from Mt. Pinatubo (Casadevall and De Los Reyes, 1991), it is clear that hazard-area coverage by direct detection of the ash cloud by a single, ground-based, 100–200-km-range radar is not possible.

Eruptions of Mt. Pinatubo (Pinatubo Volcano Observatory Team, 1991) and Mount St. Helens (Newell and Deepak, 1982) produced ash layers at several different altitudes that traveled in different directions. Because it is unlikely that distal ash clouds, which might be a threat to jet aircraft, will have sufficient particle size and density to be detectable by radar, it is necessary that proximal observations be made to determine the disposition of clouds for use in long-range forecasting. It should be noted that clouds that are several hours old still can have particle concentrations of 1 $g/m^3$ or higher in the cloud core along the plume axis, which will aid in radar detection (Harris, this volume).

If appropriately located with respect to the erupting volcano, the radar can detect and track the ash cloud and provide data to a warning network (Rose and Kostinski, this volume). Owing to the varied winds aloft, an important role for a radar operating near an erupting volcano is to report the altitude of ash cloud layers to the meteorological and aviation forecasting centers where the information can be combined with wind profiler (Leary, 1992) and satellite observations to develop an operationally useful two- or three-dimensional record of the disposition and motion of

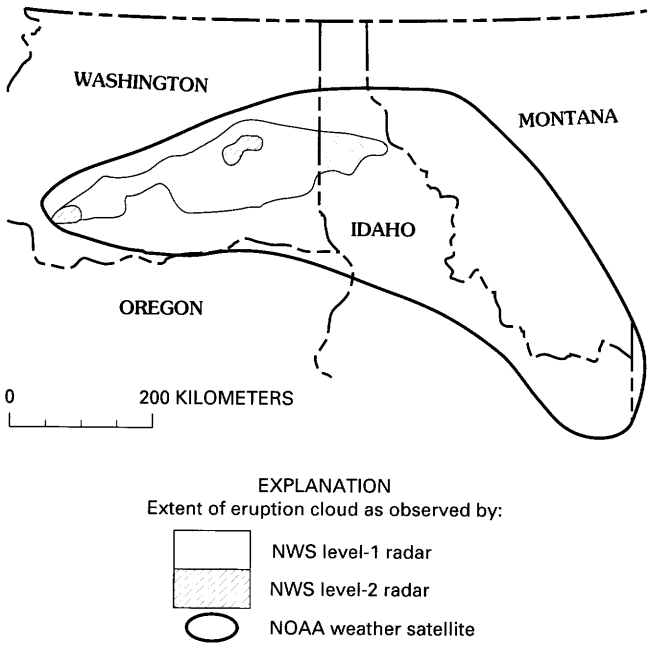


**Figure 1.** Radar and satellite depictions of Mount St. Helens eruption clouds on 18 May 1980 at 17:40 PDT as observed by Seattle and Spokane radar systems and NOAA weather satellite. The disparity in coverage between the two sensor systems indicates the need for multiple-radar and multi-sensor surveillance of volcanic ash. The radar reports may be understated due to omission of echoes whose signal strength was less than NWS (National Weather Service) level 1 and may be due to possible blockage by mountains east of Spokane. From Harris and others (1981).

the volcanic ash. Satellites such as NOAA-11 and NOAA-12, which carry the advanced very high resolution radiometer (AVHRR) (Holasek and Rose, 1991; Hastings and Emery, 1992; Matson and others, this volume) provide observations that can be useful in tracking and forecasting movement of volcanic ash. A recent example is the use of 5-cm radar to obtain timely vertical profiles of the erupting column from Mt. Spurr (Alaska Volcano Observatory, 1993).

Heffter and others (1990) have reported a forecast error of less than 25 percent of the downwind range (for distances often beyond 5,000 km) for 90 percent of the cases verified at 300 mb and less than 50 percent at 500 mb. Even though this is a significant accomplishment, better long-range forecasts are needed to support air traffic operations: damaging ash particles have been reported at 1,200 km from the erupting volcano (Casadevall and De Los Reyes, 1991). Forecasting will be enhanced by new radar facilities, which are planned or under evaluation (Hufford, this volume). The National Weather Service is installing a network of Doppler weather radars that will cover the conterminous United States, Alaska, and Hawaii. The locations of radars to be installed in the vicinity of the Cascade Range and in southern Alaska are shown in figure 2. If the current National Oceanic and Atmospheric Administration (NOAA) demonstration network of wind profilers is expanded to cover conterminous United States and Alaska, the winds from 1,600 to 53,000 ft will be measured 10 times per hour to provide data that will enhance the accuracy of prediction of cloud trajectories at different altitudes.

The remainder of the report will describe radar detection theory, the architecture and functions of a typical modern weather radar system, and the parameters and applicability to volcanic ash detection of both ground-based and airborne systems that are being deployed. Finally, a transportable radar will be recommended for emplacement near a volcano that is active or anticipated to erupt.

## DETECTION THEORY

Radar detection of volcanic ash is comparable to detection of precipitation and clouds—i.e., it involves a volumetric target of many, small, moving particles. One of the major challenges results from the difficulty in distinguishing ash cloud echoes from hydrometeor and clear-air reflections. Comparison of the position of the origin of clouds with the position of the volcano and correlation with current meteorological data provides information for identifying ash echoes.

Because the ash cloud is a volumetric target, the Probert-Jones (1962) equation (eq. 1), which is widely used by meteorologists, can be applied to calculate the effective reflectivity of the volcanic ash cloud.

$$P_r = \frac{P_t G^2 \lambda^2 \theta \phi c \tau}{512\,(2\ln)\,\pi^2 r^2} \sum_{i=1}^{N} \sigma_i \qquad (1)$$

where

$P_r$ is the received echo power (watts),

$P_t$ is the peak transmitter power (watts),

$G$ is the antenna gain ($[\pi^2 k^2]/[\theta\phi]$, where $k \cong 1$),

$\lambda$ is the wavelength (cm),

$\theta$ is the horizontal 3-dB beamwidth (radians),

$\phi$ is the vertical 3-dB beamwidth (radians),

$\tau$ is the pulse length (s),

$c$ is the velocity of light,

$r$ is the range (m), and

$\sum_{i=1}^{N} \sigma_i$ is the reflectivity per unit volume ($\equiv \eta$),

$$\eta = \frac{\pi^5}{\lambda^4} |K|^2 \sum_{i=1}^{N} D_i^6 = \frac{\pi^5}{\lambda^4} |K|^2 Z$$

where

$D_i$ is the diameter of the $i$th drop, and

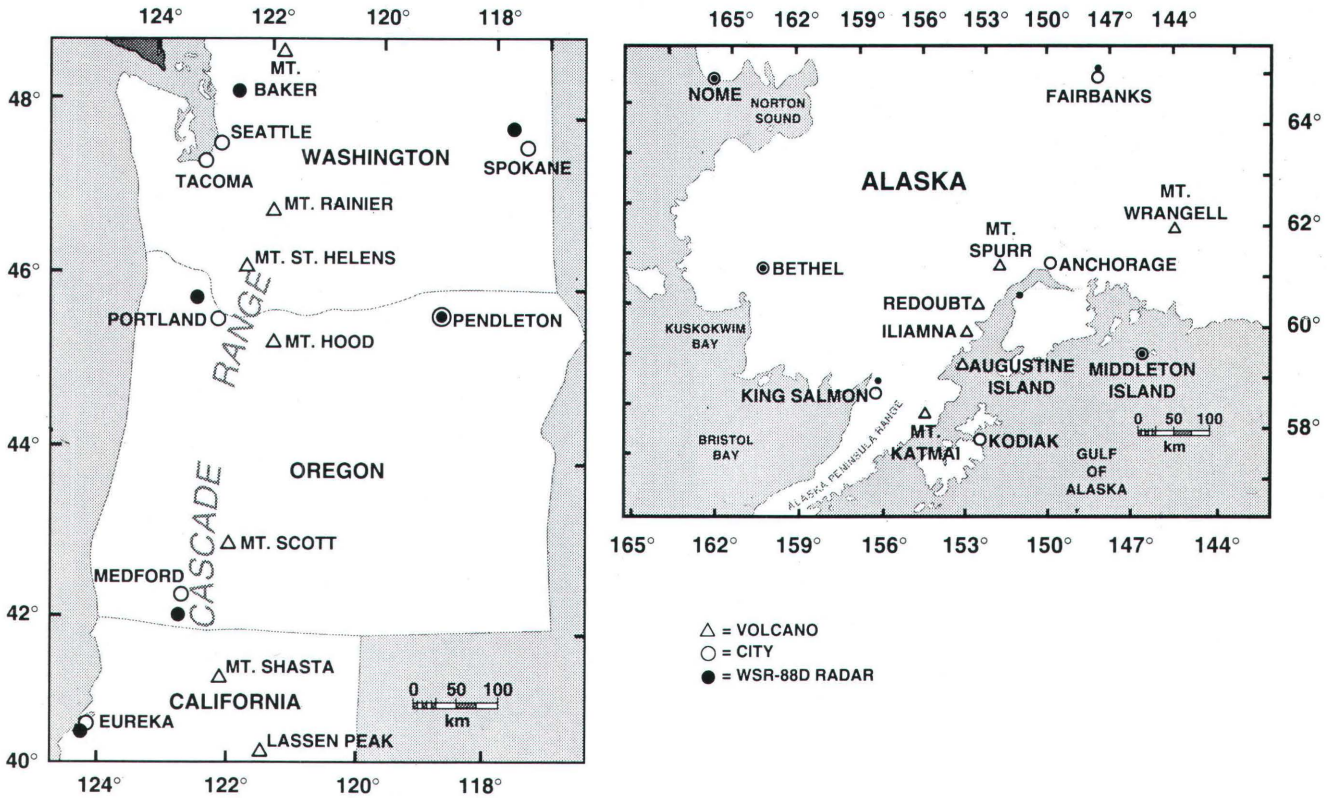


**Figure 2.** Location of planned National Weather Service radars (WSR-88D) in Alaska and in the vicinity of the Cascade Range.

$|K|^2 = \left|\frac{m^2 - 1}{m^2 + 2}\right|$ (where $m$ is the complex index of refraction).

The reflectivity factor, $Z = \sum_{i=1}^{N} D_i^6$. If metric units are used, $Z$ has the dimensions of $m^6/m^3$.

The Probert-Jones equation applies well to the beam-filled case. For spherical particles whose diameters are less than $0.07\lambda$ over a range of wavelengths from 0.9 to 10.0 cm, the Rayleigh backscattering approximation can be used in calculating $\sigma_i$. The reflectivity factor, $Z$, used by meteorologists is related to the summation of the sixth power of the diameter of spherical particles in a unit volume. When the scatterers are small with respect to the radar wavelength (i.e., when the Rayleigh approximation for backscatter is applicable), the index of refraction is known, and the beam is known to be filled, measurement of reflected power and range permit the calculation of $Z$, the reflectivity factor. In the case of volcanic ash, particle shape and concentration, and the extent of beam filling are generally unknown. Because all of the requirements of the formula for the reflectivity factor are not met, the effective reflectivity factor, $Z_e$, is used in place of $Z$.

The value of $|K|^2$ for water is 0.93, whereas for ash composed of silicate glass, $|K|^2$ is 0.36. Measurements of silicate glass made at frequencies of 0.450 and 35 GHz differ only slightly (Campbell and Ulrichs, 1969).

Estimates have been made of particle sizes based on falling velocities inferred from the decrease in ash cloud altitude with time (Harris and Rose, 1983). Owing to sixth power dependence of the reflectivity, the larger particles dominate in determining reflectivity. The shape of the airborne ash is complex due to agglomeration of the particles (Rose and Hoffman, 1980; Harris and Rose, 1983). However, the large particles tend to be equant and, because of their dominance in contributing to the total reflectivity, the asymmetry associated with the smaller particles is not of significance.

An example of cloud parameters that illustrate a taxing case for detecting light ash cloud from the Fuego Volcano is presented by Harris and others (1981). The ash cloud measurement compares with that of warm orographic rain (0.02 mm/h). Differences in particle size and number can significantly increase reflectivity. For example, Mount St. Helens had an equivalent reflectivity in the downwind ash cloud of 29–40 $dBZ_e$ (Harris and others, 1981). Harris (this volume) assumed that the lower reflectivity portion of the ash cloud was 10 dB weaker, corresponding to an effective reflectivity range of 20 to 30 $dBZ_e$.

Harris and Rose (1983) calculated reflectivity values for Mount St. Helens clouds based on particle size distributions and estimated accumulation rates of ash deposits. They provide an independent method of assessing ash cloud reflectivity that can be used in estimating radar detection performance.

## REFLECTIVITY AND DOPPLER VELOCITY MEASUREMENT

Weather radar techniques have been used effectively in the observation of volcanic ash, as noted above. Future observations will benefit from significant advances that have been made in microwave equipment, computers, Doppler and reflectivity signal processing, data-extraction algorithms, and automated operations in making quantitative weather measurements. Doppler radar facilitates direct measurement of the radial component of velocity, coherent signal integration, and removal of interfering ground-clutter echoes. The same techniques enhance the observation of volcanic ash whenever an eruption deposits measurable quantities of ash within the surveillance volume of the radar. This section describes the features of a generic Doppler weather radar. Doviak and Zrnic' (1984) present a comprehensive treatment of the measurement of reflectivity and Doppler velocity.

It is assumed that a weather radar operating at a 5- to 10-cm wavelength is used for volcanic ash surveillance. In the most commonly used volumetric observing mode, taking 3 to 5 minutes, its pencil-beam antenna is programmed to scan continuously in azimuth while stepping in elevation after each scan to cover the altitudes of interest. As an example, a 360° azimuth scan of a radar with a 1.5° beamwidth at an elevation angle close to the horizon, processing 64 samples per resolution cell (one beamwidth by one 150-m-range sample), takes approximately 40 seconds. Using the same radar parameters, observing in the range-height indicator mode with the antenna scanning over a range of elevation angles from the horizon to 30° takes about 3 seconds. The exact time to achieve the desired coverage is a function of the volume to be scanned, the radar parameters, and the signal integration employed. Variants of these scanning strategies are used to accommodate different meteorological situations. Others will be required for observation of volcanic ash and ejecta.

Figure 3 is a the generic block diagram of a radar system that employs a coherent transmitter and receiver to support Doppler processing of echoes. Transmission and reception use the same parabolic antenna. A transmit-receive (T/R) switch isolates and protects the receiver during the time that the transmitter is operating. Upon reception, the signal is translated to a lower frequency where filtering and detection take place. The detected signal is quantized using a sampling interval corresponding to a range of 0.15 to 1 km. Subsequent calculations of reflectivity, Doppler (radial) velocity, and spectral width are performed by a high-speed, digital processor. Ground clutter is substantially eliminated in the signal-processing operation. Spatial and temporal smoothing are applied to the reflectivity and radial velocity fields prior to transmitting the data to the display processor.

Owing to the height extent, the variability in the effective reflectivity of the desired signals as a function of the size distribution and composition, range to the scatterers, and the presence of intense ground-clutter echoes, the strength of the received signals can range over 90 dB. To accommodate a large range of signal intensity within the linear range of the receiver and analog-to-digital converter, appropriate gain-control circuits are employed.

A number of operational modes employing different scan strategies are used to accommodate different meteorological situations. Currently planned precipitation surveillance modes for the weather surveillance radar-88 Doppler (WSR-88D) take 5 to 6 minutes to provide range unambiguous coverage up to an altitude of 21 km. The dynamics of eruptions should be factored into the scan strategies designed for ash surveillance. For example, normal weather scans may be automatically interrupted in the interest of executing range-height scans around the plume. The volcanic observations could be cued by the detection of ejecta above a volcano or by an increase in seismic activity.

A radar located close enough to a volcano to observe the updraft of the plume would be both useful in identifying an event and in providing the volcanologist with important dynamic information on the ejecta. Doppler radar measures the radial component of velocity; hence, when situated close to a volcano, it may be capable of measuring the vertical velocity of the plume. As shown in figure 2, radars planned for installation in Alaska and in the vicinity of the Cascade Range are generally located beyond 100 km from volcanoes (Hufford, this volume) and may not provide reliable observation of the plume. A dedicated radar, located near the volcano, would characterize the plume and initiate generation of aviation hazard warnings.

With the advent of relatively inexpensive computers, automated weather radar algorithms have been implemented for identifying severe storms, measuring echo tops, calculating wind shear, tracking and predicting storm-cell and gust-front motion, and eliminating echoes due to anomalous propagation (Noyes and others, 1991; Weber and others, 1991). The results are automatically presented concisely to observers on a geographic situation display and can be readily transmitted over commercial telephone lines. Similar algorithms and facilities can be employed for volcanic ash observations.

Figure 4 is an example of a Doppler weather radar range-height display of a large sheared convective storm (S.G. Geotis and E. Williams, MIT Weather Radar Laboratory, written commun., 1991). This storm is morphologically similar to the volcanic plume distortion caused by wind shear shown in figure 5 (Newell and Deepak, 1982).

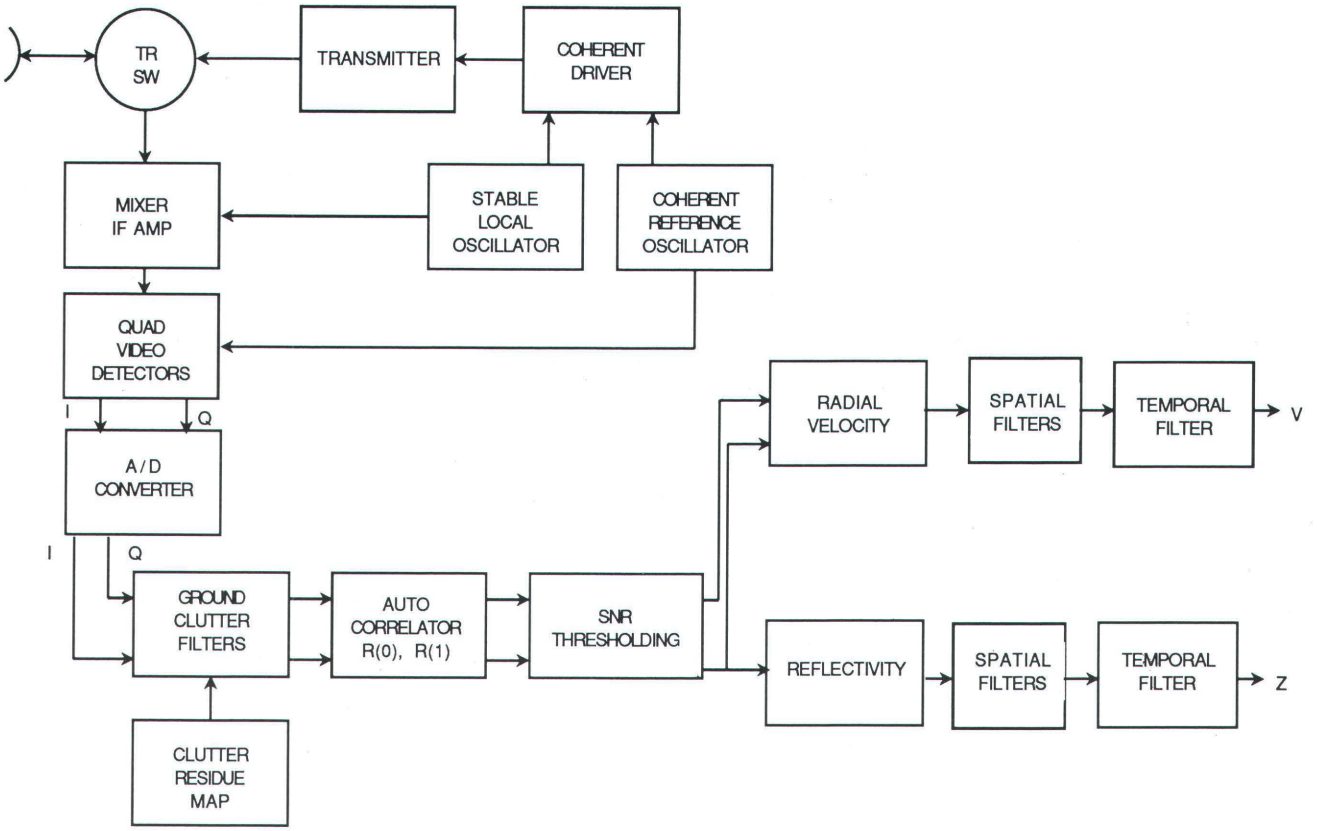


**Figure 3.** Generic block diagram of a modern Doppler weather radar system (modified from Weber and others, 1991).

## A TECHNIQUE FOR PROXIMAL OBSERVATION OF ASH CLOUDS

The wind velocity at the altitude of the ash clouds is essential to volcanologists and to forecasters in providing aviation hazard warnings. Doppler radar can determine only the radial component of the wind from a stand-off location. When the ash cloud passes over the radar, it is possible to determine the vertical profile of the horizontal wind within the cloud (L'hermitte and Atlas, 1961). The needed data are collected by holding the antenna at a constant elevation angle and by recording the radial velocity at several ranges while the antenna is scanned 360° in azimuth. The mean Doppler velocity varies sinusoidally as the antenna scans a volume of particles that have uniform wind velocity and particle fall speed. Maxima and minima are observed when the beam azimuth passes upwind ($\beta = 0$) and downwind ($\beta = \pi$). Using the following equations (from Atlas, 1964; L'hermitte and Atlas, 1961), the horizontal winds and terminal velocity of the precipitation particles are calculated.

When $\beta = 0$,

$$\bar{V}_1 = V_f \sin\alpha + V_h \cos\alpha \tag{2}$$

When $\beta = \pi$,

$$\bar{V}_1 = V_f \sin\alpha - V_h \cos\alpha \tag{3}$$

The wind speed at altitude, $h$, is:

$$V_h = \frac{\bar{V}_1 - \bar{V}_2}{2\cos\alpha} \tag{4}$$

and the particle fall speed is:

$$V_f = \frac{\bar{V}_1 + \bar{V}_2}{2\sin\alpha} \tag{5}$$

This processing, referred to as the velocity azimuth display (VAD), has been extended (Waldteufel and Corbin, 1979) to produce wind fields over a three-dimensional volume (volume velocity processing—VVP). Whenever the disposition of the radar and ash clouds are favorable for the performance of the 360° scan, the VAD or its later realization provides a capability to measure horizontal winds and the terminal velocity of ash particles.

## COMPARISON OF CANDIDATE RADAR SYSTEMS

The parameters of four radars (three ground-based and one airborne) are presented in table 1 for comparison. The

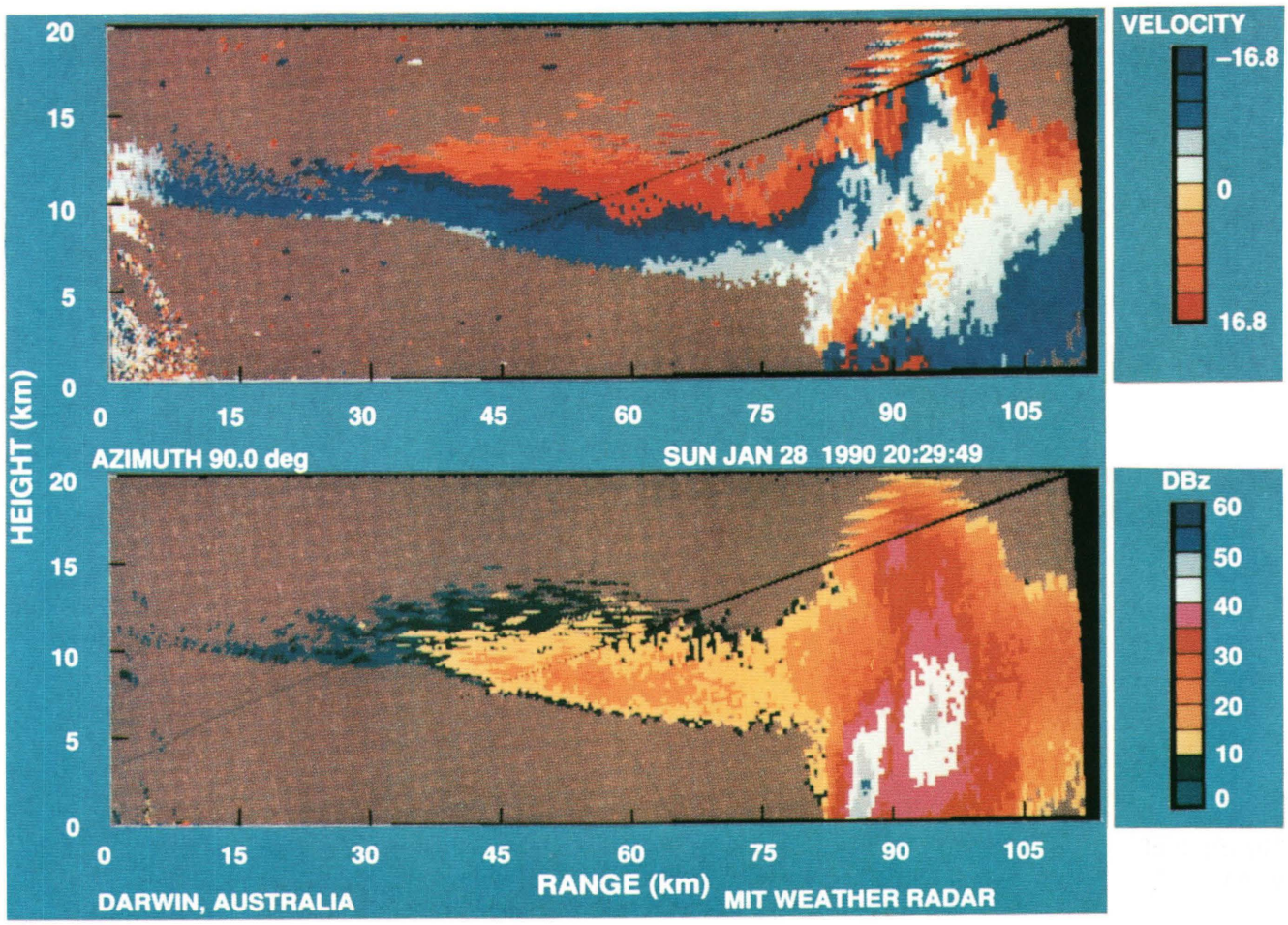


**Figure 4.** A two-dimensional representation of a sheared thunderstorm on a Doppler weather radar display, as viewed in real time. The upper panel shows the radial component of the velocity of the storm cloud. The velocity profile indicates Doppler folding as the wind exceeds 16 m/s in the range of 30 to 70 km from the radar. The lower panel shows the intensity of the sheared thunderstorm. Range label on horizontal scale indicates range from NEXRAD station. This type of large, sheared thunderstorm bears a strong resemblance to the schematic cross section of the volcanic ash cloud that is shown in figure 5. For additional information about Doppler radar, see Doviak and Zrnic' (1984).

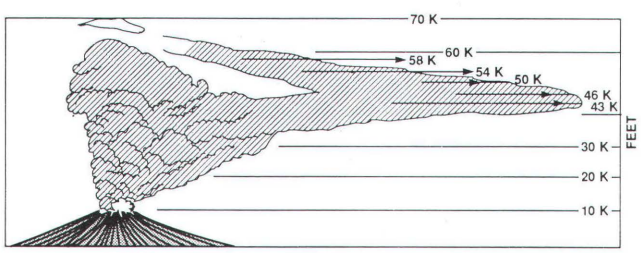


**Figure 5.** Schematic cross section of volcanic ash plume distortion caused by wind shears. Altitudes expressed in thousands of feet. From Newell and Deepak (1982).

three ground-based radars will be in widespread use for meteorological purposes in the 1990's. The WSR-88D is used by the NWS, the FAA, and the Department of Defense for long-range surveillance and severe storm detection. The terminal Doppler weather radar (TDWR) is used by the FAA for detecting thunderstorms and microbursts in the vicinity of an airport. The transportable C-band radar is used by a number of universities for research purposes and also finds widespread use in general weather radar service by governments and industry. The RDR-4A is typical of the small, lightweight units in use on commercial jet aircraft. Note that the performance of the RDR-4A radar is orders of magnitude lower than that of the ground-based radars, and this radar as well as other airborne radars in its size class should not be relied upon to detect the presence of hazardous volcanic ash.

**Table 1.** Parameters of various radar systems.

[NEXRAD, next-generation weather radar; TDWR, terminal Doppler weather radar. Sources of information: Heiss and others (1990), S.G. Geotis and E. Williams, MIT Weather Radar Laboratory, written commun. (1991)]

| Parameter | Transportable C-band | WSR-88D NEXRAD | TDWR | RDR-4A |
|---|---|---|---|---|
| Frequency (MHz) | 5,550 | 2,700–3,000 | 5,600–5,650 | 9,345 |
| Wavelength (cm) | 5.40 | 10.50 | 5.30 | 3.20 |
| Transmitter output power (Kw peak) | 250 | 750 | 250 | 0.13 |
| Antenna gain (dB) | 43.75 | 45.50 | 50.00 | 35.00 |
| Horizontal and vertical antenna beamwidth (°) | 1.6 | 0.95 | 0.50 | 3.40 |
| Noise figure (dB) | 1.8 | 4.07 | 1.80 | 5.00 |
| Pulse width (μs) | 1 | 1.57<br>4.50 | 1.10 | 6.00 |
| Pulse repetition frequency (Hz) | 250–1,200 | 318–1,304 | 300–2,100 | 363 |
| Minimum discernible signal (dBm) | –106 | –110 | –110 | –112 |
| Approximate reflectivity detectable[2] at 100 km ($dBZ_e$) | 12 | –2<br>–10 | –6.2 | 22 |

[1] WSR-74 modified for Doppler processing.
[2] Depends on scanning and processing.

To illustrate the relative performance of the four radars, signal-to-noise ratios as a function of range have been calculated for a reflectivity of 10 $dBZ_e$ and are shown in figure 6. The effects of propagation, target characteristics, signal integration, and specific radar system losses omitted from this simplified illustration must be included in estimating performance. The factors affecting detection are discussed in Doviak and Zrnic' (1984) and in Echard (1987).

It is clear from figure 6, which is drawn for a 10 $dBZ_e$ reflectivity value, that the WSR-88D and TDWR are capable of achieving reasonable detection performance. When it is located near the erupting volcano, the transportable C-band radar is useful in detecting volcanic ash clouds both for research and for generating hazard warning information.

The features of the WSR-88D radar are presented in table 2. This radar will be widely installed in the United States. Five systems will be located in the Washington-Oregon area near the Cascade Range; two will be installed at Anchorage and King Salmon, Alaska, within approximately 115 km or less of the volcanoes located to the west and southwest of Anchorage. The radar locations are listed in table 3. In order to serve many users, the system is partitioned so that the base data (comprising radar reflectivity, Doppler frequency, and spectrum width) are sent via telephone lines to the user's data-processing facility. The WSR-88D weather radar is the most powerful system being widely deployed and should give the best performance in detecting volcanic ash.

Even though the TDWR has a useful detection capability, the systems are programmed for installation in regions

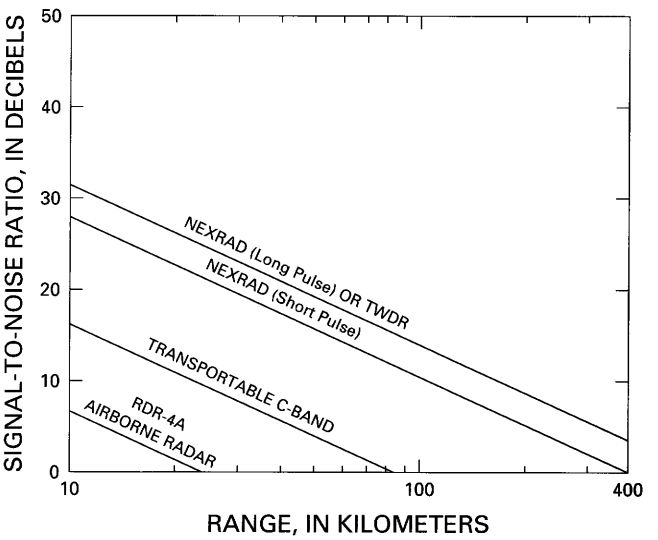


**Figure 6.** Comparison of the signal-to-noise performance of contemporary weather radars calculated for an equivalent reflectivity of 10 $dBZ_e$ (see text). Actual performance will depend on losses and processing gain. Note that the air-carrier radar (RDR-4A) is almost three orders of magnitude less capable than the WSR-88D (NEXRAD) system.

**Table 2.** Characteristics WSR-88D.

[After Heiss and others (1990). Reprinted with permission]

| | | |
|---|---|---|
| **Antenna subsystem** | | |
| **Radome** | Fiberglass skin foam sandwich. | |
| Diameter | 39 ft | |
| RF loss (two way) | 0.3 dB at 2,800 MHz. | |
| **Pedestal** | Elevation over azimuth. | |
| | Azimuth | Elevation |
| Steerability | 360° | −1° to 45° |
| Rotational rate (maximum) | 36° $s^{-1}$ | 36° $s^{-1}$ |
| Acceleration | 15° $s^{-2}$ | 15° $s^{-2}$ |
| Mechanical limits | | −1° to +60° |
| **Antenna** | Parabola of revolution. | |
| Polarization | Circular. | |
| Reflector diameter | 29 ft | |
| Gain (at 2,800 MHz) | 45.5 dB | |
| Beamwidth | 0.95° | |
| First sidelobe level | 29 dB | |
| **Transmitter and receiver subsystem (coherent-chain design)** | | |
| **Transmitter** | | |
| Frequency | 2,700 MHz to 3,000 MHz | |
| Peak power | 750 kW | |
| Pulse widths (nom.) | 1.57 μs and 4.5 μs | |
| RF duty cycle | 0.0021 (max.) | |
| PRF's | (Short pulse) 318 Hz to 1,304 Hz | |
| | (Long pulse) 318 Hz to 452 Hz | |
| **Receiver** | | |
| Dynamic range | 95 dB | |
| Noise temperature | 450° K | |
| Intermediate frequency | 57.6 MHz | |
| Bandwidth (3 dB) | 0.79 MHz | |
| **Signal Processor Subsystem** | | |
| **Clutter canceller** | Infinite impulse-response design. | |
| Suppression | 30 dB to 50 dB | |
| Notch half widths | 0.5 to 4 $ms^{-1}$ | |
| Reflectivity bias | 0 to 1 dB (on 4 $ms^{-1}$ width signal). | |
| Minimum usable velocity | 0 to 4 $ms^{-1}$ | |
| Range sampling | 0.25 km | |
| Azimuth sampling | 1° | |
| **Velocity calculation** | Complex covariance argument. | |
| Algorithm | Pulse-pair processing. | |
| Estimation accuracy (nom.) | 1 $ms^{-1}$ | |
| Number of pulses averaged | 40 to 200 | |
| Range increment | 0.25 km | |
| Azimuth increment | 1° | |
| **Spectrum width calculation** | Autocorrelation. | |
| Algorithm | Single lag correlation. | |
| Estimate accuracy (nom.) | 1 $ms^{-1}$ | |
| Number of pulses averaged | 40 to 200 | |
| Range increment | 0.25 km | |
| Azimuth increment | 1° | |
| **Reflectivity calculation** | Return power average. | |
| Algorithm | Linear power average. | |
| Estimate accuracy (nom.) | 1 dB | |
| Number of pulses averaged | 6 to 64 | |
| Range increment | 1 km | |
| Azimuth increment | 1° | |

**Table 3.** WSR-88D locations planned as of December 4, 1992.

[Est., Estimated; Sea/Tac, Seattle/Tacoma; TBD, to be determined]

| Area | Est. delivery date | Latitude (N.) | Longitude (W.) |
|---|---|---|---|
| **Cascades** | | | |
| Eureka, Calif. | Nov. 1994 | 40°29'55" | 124°17'27" |
| Medford, Oreg. | Aug. 1995 | 42°04'52" | 122°42'58" |
| Pendleton, Oreg. | Oct. 1995 | 45°41'26" | 118°51'09" |
| Portland, Oreg. | Nov. 1994 | 45°42'53" | 122°57'56" |
| Sea/Tac, Wash. | Feb. 1994 | 48°11'40" | 122°29' 45" |
| Spokane, Wash. | Nov. 1995 | 47°40'52" | 117°37'42" |
| **Alaska** | | | |
| Anchorage | June 1995 | 60°43'33" | 151°21'05" |
| Bethel | May 1996 | TBD | TBD |
| Fairbanks | Sep. 1995 | 65°02'05" | 147°30'04" |
| King Salmon | Apr. 1996 | 58°40'45" | 156°37'48" |
| Middleton Island | July 1995 | 59°26'02" | 146°19'57" |
| Nome | May 1996 | TBD | TBD |
| Sitka | Aug. 1995 | 56°51'11" | 133°31'38" |

having frequent thunderstorm activity and associated microbursts, which are hazardous to flight. No TDWR systems will be installed in the vicinity of the Cascade Range or in Alaska.

The transportable C-band radar, designated WSR-74, has proven to be a highly versatile research instrument as well as an operational system. The Massachusetts Institute of Technology weather radar group has installed their unit in sea containers for deployment in the South Pacific. Over the past 5 years, the radar has moved once or twice a year in support of operations in the United States and Australia. This radar, outfitted with a 10-m antenna, is the least expensive system for research. It can be rapidly deployed near a volcano when activity indicates an imminent eruption. Emplacement of a carefully packaged unit should take less than a week. Consideration should be given to acquiring such a system for use by volcanologists for basic research and for the further development of aviation-hazard-warning techniques.

## SUMMARY

Radar has proven to be useful in locating volcanic ash clouds and can be used in aviation hazard forecasting, particularly if the radar is located close to the erupting volcano and if hydrometeors can be identified independently during the eruption. Under these circumstances, any echo originating at the location of the volcano may be presumed to be an ash cloud and can be tracked in position and altitude. The altitude information, coupled with winds aloft data, can be used to infer trajectories for ash clouds at different altitudes—a valuable input to the aviation hazard warning system.

A brief overview of radar detection of volcanic ash, based on weather radar practice, highlights the potential of ground-based radar observations. The reduction of the effective reflectivity factor with time as a result of the precipitation of the larger ash particles, the location of the radar with respect to the ash cloud, and detection capability of a radar set a limit in the hazard warning area that may be served by a single radar.

Performance estimates show that the WSR-88D weather radar has a potential to perform volcanic ash surveillance. A program is underway to install a network of these radars covering all 50 States. Means to exploit the observational capability of the WSR-88D radars for volcanology and aviation-hazard-related applications should be investigated. It is anticipated that appropriate operating strategies, communications, processing data recording, and display equipment, as well as processing algorithms, will be specified (Evans, this volume).

A dedicated, transportable research radar is suggested for further study of volcanic ash clouds and for the perfection of automated algorithms for generating hazard warnings. Techniques for radar sensing that may be useful for enhancing radar surveillance of volcanic activity should be investigated. Spectral characteristics of echoes, dual-polarization observations, and multiple-frequency observations are among the candidates that may be considered.

## ACKNOWLEDGMENTS

The comprehensive review and valuable suggestions made by Dr. David M. Harris, Utah State University, are appreciated. This work was sponsored by the Federal Aviation Administration under contract no. DTFA01-89-Z-02033.

## REFERENCES CITED

Alaska Volcano Observatory, 1993, Mt. Spurr's 1992 eruption: Eos, Transactions, American Geophysical Union, v. 74, p. 217, 221–222.

Atlas, D., 1964, Advances in Radar Meteorology: Advances in Geophysics, Volume 10: New York, Academic Press, p. 317–478.

Campbell, M.J., and Ulrichs, J., 1969, Electrical properties of rocks and their significance for lunar radar observations: Journal of Geophysics, v. 74, no. 25, p. 5867–5881.

Casadevall, T.J., and De Los Reyes, P.J., 1991, Impact of June 1991 Pinatubo eruptions on aircraft operations in the western Pacific and southeast Asia [abs.]: Eos, Transactions, American Geophysical Union, v. 72, no. 44 [supplement], p. 95.

Doviak, R.J., and Zrnic', D.S., 1984, Doppler Radar and Weather Observations: Orlando, Fla., Academic Press, Inc., 458 p.

Echard, J.D., 1987, Target detection in noise and clutter, *in* Currie, N.C., and Brown, C.E., eds., Principles and Applications of Millimeter Wave Radar: Norwood, Mass., Artech House, p. 75–129.

Hastings, D.A., and Emery, W.J., 1992, The advanced very high resolution radiometer: A brief reference guide: Photogrammetric Engineering and Remote Sensing, v. 58, no. 8, p. 1183–1188.

Harris, D.M., and Rose, W.I., 1983, Estimating particle sizes, concentrations, and total mass of ash in volcanic clouds using weather radar: Journal of Geophysical Research, v. 88, no. C15, p 10969–10983.

Harris, D.M., Rose, W.I, Roe, R., and Thompson, M.R., 1981, Radar observations of ash eruptions, *in* Lipman, P.W., and Mullineaux, D.R., eds., The 1980 Eruptions of Mount St. Helens, Washington: U.S. Geological Survey Professional Paper 1250, p. 323–333.

Heffter, J.L., Stunder, B.J.B., and Rolph, G., 1990, Long-range forecast trajectories of volcanic ash from Redoubt Volcano eruptions: Bulletin of the American Meteorological Society, v. 71, p. 1731–1738.

Heiss, W.H., McGrew, D.L., and Sirmans, D., 1990, NEXRAD: Next generation weather radar (WSR-88D): Microwave Journal, v. 33, p. 79–80, 84–98.

Holasek, R.E., and Rose, W.I., 1991, Anatomy of 1986 Augustine Volcano eruptions as recorded by multi-image spectral processing of digital AVHRR weather satellite data: Bulletin of Volcanology, v. 53, p. 420–435.

Leary, W.E., 1992, Radar system gives forecasters more data on wind more often: New York Times—The Environment, July 21, 1992, section C, p. 4.

L'hermitte, R.M., and Atlas, D., 1961, Precipitation motion by pulse Doppler radar: Proceedings, Ninth Weather Radar Conference: Boston, Mass., American Meteorological Society, p. 218–223.

Newell, R.E., and Deepak, A., eds., 1982, Mount St. Helens eruptions of 1980: Atmospheric effects and potential climatic impact: NASA Special Publication SP-458, 119 p.

Noyes, T.A., Troxel, S.W., Weber, M.E., Newell, O.J., and Cullen, J., 1991, The 1990 airport surveillance radar wind shear processor (ASR-WSP) operational test at Orlando International Airport: Lexington, Mass., MIT Lincoln Laboratory, Project Report ATC-178, 68 p.

Pinatubo Volcano Observatory Team, 1991, Lessons from a major eruption: Mt. Pinatubo, Philippines: Eos, Transactions, American Geophysical Union, v. 72, no. 49, p. 545, 552–553, 555.

Probert-Jones, J.R., 1962, The radar equation in meteorology: Quarterly Journal of the Royal Meteorological Society, v. 88, p. 485–495.

Rose, W.I., 1987, Interaction of aircraft and explosive eruption clouds: A volcanologist's perspective: American Institute of Aeronautics and Astronautics Journal, v. 25, p. 52–58.

Rose, W.I., Jr., and Hoffman, M.F., 1980, Distal ashes of the May 18, 1980, eruption of Mount Saint Helens [abs]: Eos, Transactions, American Geophysical Union, v. 61, p. 1137.

Waldteufel, P., and Corbin, H., 1979, On the analysis of single Doppler data: Journal of Applied Meteorology, p. 18532–18542.

Weber, M., Stone, M., Primeggia, C., and Anderson, J., 1991, Airport surveillance radar based wind shear detection: Proceedings, Fourth International Conference on Aviation Weather Systems, Paris, p. J11–J20.

VOLCANIC ASH AND AVIATION SAFETY:
Proceedings of the First International Symposium
on Volcanic Ash and Aviation Safety
U.S. GEOLOGICAL SURVEY BULLETIN 2047

# THE POTENTIAL FOR USING GPS FOR VOLCANO MONITORING

*By* Frank H. Webb *and* Marcus I. Bursik

## ABSTRACT

Volcanic eruptions can adversely impact aircraft safety by ejecting vast quantities of ash into the atmosphere. The eruption of ash may go undetected by observers both on the ground and in the air, especially at remote volcanoes, at night, and in poor weather. It is therefore important to develop a system capable of monitoring the eruptive state of volcanoes that does not depend on visual ash-cloud sighting. Numerous geological techniques are being developed for this purpose, some of which depend on making careful measurements of ground movements at volcanoes. Ground deformation preceding volcanic eruptions occurs at relatively high strain rates, which can change on time scales of hours and perhaps minutes in the days directly before eruption. Geodesy using the global positioning system (GPS) is perhaps the most promising technique for autonomously monitoring volcanic ground deformation with daily and sub-daily time resolution. Recent launches of additional GPS satellites and increased tracking-station distribution have resulted in an increase in the number of short intervals during the day with strong satellite and ground-station geometry, making it possible to investigate high-strain-rate phenomena over sub-daily time scales that accompany volcanic eruptions. Once rapid volcanic ground movements are better understood, it may be possible to develop a relatively inexpensive GPS system that can be used in conjunction with other monitoring techniques to warn aircraft of an ash eruption.

## INTRODUCTION

Volcanoes present the most severe geological hazard to aviation because they can inject huge quantities of rock debris and fine particles and corrosive aerosols into the atmosphere. This debris can be directly ingested by aircraft engines and can cause flameout or serious malfunction, or the debris can remain for months in the atmosphere and contribute to the gradual deterioration and erosion of aircraft components.

Hazards to aircraft posed by volcanoes can be mitigated by a system for warning aviators of an impending or ongoing eruption, even when visual corroboration of eruptive activity is not available. Visual sightings are difficult during the night and poor weather or when a relatively remote active volcano lies along a flight path. In addition, very diffuse ash clouds can drift hundreds or even thousands of kilometers from their source and pose a hazard to aircraft. Therefore, an effective warning system must be based on the ability of earth scientists to gather and correctly interpret information regarding the status of a volcano's activity.

A variety of volcano-monitoring techniques have been devised in the hope that a clear indication of an impending eruption can be determined. The most commonly used techniques of volcano monitoring fall into three categories: (1) analysis of seismic patterns (McNutt, this volume), (2) analysis of the patterns of deformation of the Earth's surface, and (3) chemical analysis of the gas emissions from vent regions. As magma rises toward the surface, the Earth's crust is distorted or deformed to accommodate magma movements. The movements at the surface may be only as large as a few centimeters, but modern instrumentation is sufficiently precise to measure them.

The global positioning system (GPS) is one of several geodetic techniques that can be used to measure deformation at the Earth's surface associated with magma movement. Other techniques involve the use of: (1) leveling, in which vertical motions are measured with precise optical-level instruments, (2) laser geodimeters, or electronic distance meters (EDM's), which measure horizontal motions over distances up to approximately 10 km, (3) tilt meters, and (4) strainmeters, which record small changes in the dimensions of crustal rock that are induced by deformation.

Although most of the above monitoring methods are at least as precise as a GPS-based system, GPS has several important characteristics that are not shared by the others that suggest it could provide the most effective monitoring capability. GPS receivers are readily available and are becoming reasonably priced. In contrast, laser geodimeters and strainmeters are custom built and are expensive. GPS

data-collection and analysis costs are also becoming competitive and will decrease with time. Once a GPS receiver is in place, the only labor costs are those associated with data analysis and site maintenance. Most other monitoring methods, such as leveling, require many hours in the field by a crew of several people to collect data. In addition, as GPS monitoring is a remote technique—there is little risk to human life in a potentially hazardous geological environment. Probably the greatest advantage of GPS is that it can provide complete spatial positioning over a vast range of distances without a line-of-sight requirement among the stations. Although geodimeters measure distances with high precision, the lack of three-dimensional control means that interpretation of length changes becomes increasingly difficult as baseline slope increases (Savage and Lisowski, 1984). This contribution explores the use of GPS for a volcano-aviation warning system.

## RELATIONSHIP OF GROUND DEFORMATION TO ERUPTIONS

GPS techniques are commonly applied to the investigation of crustal deformation resulting from plate-tectonic motion. However, strain of the Earth's surface in volcanic environments differs markedly from tectonic strain associated with faults along and within plate boundaries. Spatially, volcanic signals are often characterized by large, local, vertical and dilatational (stretching) components (fig. 1). Temporally, the signals are transient, generally remaining nearly constant for long periods and sometimes increasing by the hour or minute in the days before an eruption. These unique characteristics are the direct result of the primary source of strain in volcanoes—pressurized magma migrating toward the Earth's surface. Dramatic examples of the peculiar features of volcanic deformation are provided by Iwo Jima and Mount St. Helens. At Iwo Jima, a volcanic island only 10 km across in its longest dimension, the shoreline on which Captain Cook landed in 1779 is now 40 m above sea level (Newhall and Dzurisin, 1988). In the month prior to the catastrophic sector collapse and eruption on May 18, 1980, the north flank of Mount St. Helens moved outward at a rate of 1.5–2.5 m/day (Lipman and others, 1981).

Not all ground deformation episodes in volcanic regions culminate with an eruption. Hill and others (1991) have summarized some of the most recent episodes of volcanic unrest that have been monitored with geodetic techniques. In the best known examples, volcanoes deform at rates ranging from centimeters per day to meters per day in the hours or days before eruption, whereas magma movement at depth can cause strain rates of centimeters per year for years or decades with no eruption. It is necessary for an aviation-warning capability to distinguish the rapid deformation that may culminate in the eruption of an ash column from the slower "background" deformation caused by noneruptive processes.

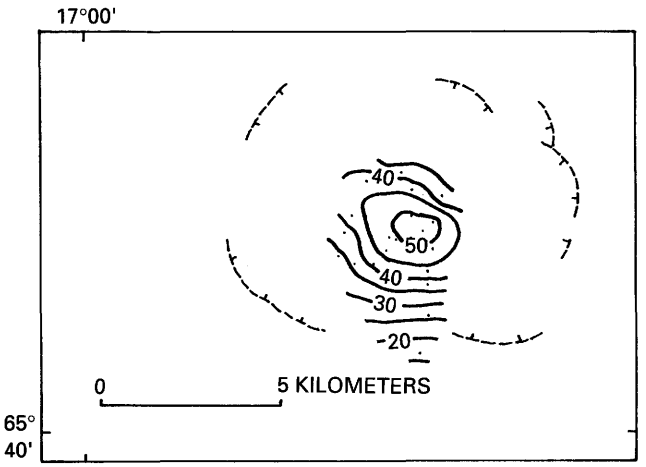


**Figure 1.** An example of a type of deformation found at volcanoes. This example is from Krafla caldera, Iceland, November 5, 1976, to January 8, 1977. Heavy lines indicate the amount of vertical uplift in centimeters. Note the distinct "bull's eye" pattern associated with magma at depth pushing the rock above it. Dashed lines indicate the rim of the caldera, a large crater formed previously by collapse of a partially emptied magma chamber. Modified from Ewart and others (1990).

To date, there is no known method for unambiguously distinguishing deformation leading to eruption. Swanson and others (1983) summarized the success of eruption prediction at Mount St. Helens in the period after the catastrophic May 18, 1980, event. A pattern of precursory seismic and geodetic events developed during a series of dome-building eruptions following May 18. Some of these eruptions also produced explosive emission of volcanic ash into the atmosphere. Because of the pattern of activity preceding eruptions, most of the events were successfully predicted in the days or weeks preceding the event. Swanson and others (1983) concluded that these smaller, quasi-periodic events that frequently occur after a paroxysmal blast are amenable to monitoring and prediction. These authors felt that the short-term prediction of a major ash-forming event that poses a serious aviation hazard, such as that of May 18 at Mount St. Helens, was a rather distant goal.

## THE GLOBAL POSITIONING SYSTEM

The global positioning system was developed and is being deployed by the United States Department of Defense (DOD) for worldwide, continuous, real-time point positioning. It is a satellite-based navigational system that is increasingly being used by the civilian and scientific communities

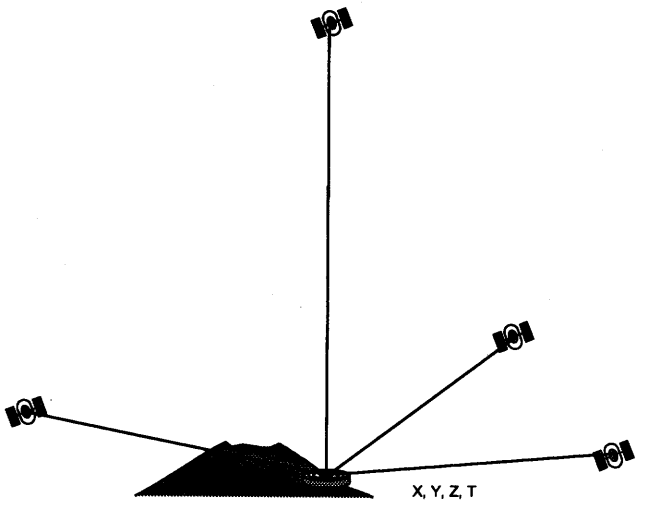


**Figure 2.** For three dimensional point positioning, the GPS receiver estimates four unknowns: its three-dimensional station coordinates and its clock offset from GPS time. This requires observations from four satellites. The geometry of the satellites determines the strength with which the receiver can estimate these parameters. The term PDOP (position dilution of precision) is a measure of the strength of the satellite geometry to estimate these unknown parameters (Wells and others, 1986). An example of good satellite geometry for 3-D positioning would be three receivers equally spaced on the horizon and one receiver directly overhead. Poor 3-D positioning geometry would have all the satellites directly above the receiver or all of the satellites clustered on the horizon. During 1 day, satellite geometry varies continuously at every station and so does the strength of point positioning.

for surveying and precise geodetic applications. GPS satellites orbiting the Earth passively broadcast timing codes and orbital information that receivers on the ground or in aircraft can use to determine their positions. The information is broadcast by the satellites on two L-band carrier frequencies, L1 and L2. These carriers, the timing codes, and the orbital information can be used in a number of ways to position one or more GPS receivers. The method implemented depends on the user's required precision, solution frequency, and the sophistication of the user's receiver. Processing algorithms can vary from independent point positioning of a single receiver in real time with 10-m accuracy to differential positioning using data from a global network of receivers for millimeter to centimeter accuracy and precision.

Real-time point positioning with GPS is the determination of the position of one receiver using signals broadcast by several GPS satellites. Each GPS satellite broadcasts ephemerides (orbital information) and timing information on the two L-band carrier frequencies. The receiver uses the timing information to determine its range to each of the satellites that are in view. These ranges and the ephemerides of the satellites are used to estimate the receiver's position vector in an Earth-centered reference frame and the offset of the receiver's clock from GPS time (fig. 2). To estimate these parameters, the receiver needs to collect data from at least four satellites simultaneously. The precision with which it can determine its position depends on the accuracy of the satellite ephemerides, the satellite geometry, and the accuracy of the ranges to the satellites.

There are three types of ranging information that can be extracted from the GPS signal: P-code on each of the L-band carriers (P1 and P2) and C/A code on the L1 carrier. C/A code provides a coarse estimate of the range to the satellite. Many receivers are commercially available that use the C/A code to provide 50–100-m positioning accuracy. More sophisticated receivers use the precise P-code for determining the range to the satellites to about 10 m. Receivers capable of using these codes have a greater real-time positioning capability; however, the P-code is subject to encryption by the DOD. This encryption, called anti-spoofing (AS), prevents unauthorized users from taking full advantage of the precise ranging information. The DOD can also degrade the real-time positioning capability with selective availability (SA), which consists in adding signal noise to the carriers and degrading the accuracy of the broadcast ephemeris message.

Even in the absence of SA and AS, P-code ranges are actually "pseudo ranges" to the satellites because they are contaminated by clock errors, atmospheric delay errors, and orbital errors—this limits the accuracy of point positioning to approximately 10 m. If real-time positioning is not required, the effects of these errors on the precision of the positioning can be reduced by processing the data after the fact (i.e., post-processing). Most post-processing algorithms exploit the information contained in tracking the L1 and L2 carriers. When the satellites are tracked over some time interval, satellite ranges to the receiver change. These changes can be coarsely determined by the pseudo range, but high-accuracy geodetic measurements require the more precise measurements of the receiver's accumulated phase observations. Ionospheric delays are removed by using an ionosphere-free linear combination of the dual-frequency observables. These phase observables, and the pseudo ranges if present, are used from a network of ground receivers to simultaneously estimate the positions, atmospheric corrections, and clock errors for the network and the clock errors and orbit errors of the GPS satellites. For the highest precision applications, 8 to 24 hours of data from a global network of receivers are used to estimate satellite and receiver parameters. In this global reference frame, relative station positions can be determined to a few millimeters in the horizontal and about 2 cm in the vertical over distances of approximately 1,000 km (Heflin and others, 1992; Blewitt and others, 1992).

Because near-real-time positioning is required for a volcano-monitoring and warning system, the attendant accuracy will be somewhat better than the current real-time accuracy but not necessarily as good as that obtained by

extensive post-processing. In addition, to clearly define rapid strain events preceding eruptions, it may be necessary to obtain solutions at sub-daily intervals. By combining post-processing estimation techniques with real-time data acquisition, relatively high precision positioning at sub-daily intervals can be obtained. It is possible to calculate nearly continuous relative positions of a receiver on a volcano at a precision level better than 1 cm, as we demonstrate in the next section.

## A DEMONSTRATION OF GPS CAPABILITY

A worldwide network of 31 continuously operating P-code receivers is currently being deployed for routine geodetic observations. A subset of 21 stations within the network was deployed in 1991 during a 3-week GPS experiment (Heflin and others, 1992) to test the ability of GPS to measure global geophysical parameters, such as polar motion and tectonic strain accumulation. Data from many of these receivers were remotely retrieved over commercial phone lines on a daily basis. Analysis of the data to determine station locations was performed after the entire data set had been accumulated.

There were 210 baselines within the network having lengths ranging from about 100 km to nearly the diameter of the Earth. All of the data were analyzed at the Jet Propulsion Laboratory (JPL) with an automated version of the GIPSY processing software (see Sovers and Border, 1987, for a mathematical description) on Micro-VAX computers. Central processing unit (CPU) speed limited the processing efficiency to more than 1 day of CPU per day of global network data. With currently available state-of-the-art workstations, processing time would be reduced to a few hours. Daily measurement precisions for baselines (of 4 parts in $10^9$ of the baseline length) were obtained from the global network (Heflin and others, 1992). This level of precision was the highest yet obtained with GPS over such a wide range of baseline lengths and has been attributed to the strength of the global receiver network and the satellite constellation.

Although the precise solutions discussed above were obtained daily, the temporal spacing of GPS baseline solutions can be adjusted according to the rate at which data are accumulated at the processing station and the precision that is required for a particular application. In the case of volcanoes, daily solutions collected over a period of 1 week would be sufficient to discern strain rates greater than a few millimeters per day. If such a week-long survey suggested that this several-millimeter-per-day threshold was being exceeded, as for example during increased activity preceding an eruption, solutions could be calculated more frequently than once per day. However, as the frequency at which solutions are calculated increases, the resolution of the position estimates decreases, but not dramatically.

There is another limit to the frequency at which solutions can be usefully calculated. Independent solutions at every data point (usually every 30–120 s) are currently not possible on a continuous basis because of the limitations of the present satellite constellation. At least four satellites are required for independent solutions to be derived at every data point because, at every observation, the data from one station are used to estimate its position in three dimensions and its time offset from GPS time. With the current GPS constellation, there are periods during the day when fewer than four satellites are visible. (Global 24-hour coverage with four-satellites is expected to be available in 1993 when GPS becomes fully operational.) Positions can be calculated during periods when fewer than four satellites are visible by assuming that a station's position is not completely independent from solution to solution. Because virtually all movements of the Earth's crust occur at rates that are less that centimeters per hour, even on volcanoes, it is generally reasonable to assume that a station's position is not excessively different from its position at earlier times or data points. That is, position estimates from one GPS observation to the next are not independent and can be modeled using process-noise-estimation techniques (Bierman, 1977).

Process-noise-estimation techniques have been applied to the estimation of static baselines of 22, 179, and 1,500 km with GPS field data to investigate strategies necessary to obtain relatively precise sub-daily solutions. Results show that solution strength, as measured by the formal error of the solution and the accuracy of the estimate, is dominated by satellite geometry. Because the satellite geometry (fig. 2) varies throughout the day, there are times during which baselines cannot be estimated independently at every observation epoch (figs. 3*A*, *B*). This results in noncontinuous estimates of the baseline throughout the day. If a process-noise model is used to apply a weak constraint between the estimates, baseline estimates can be obtained during periods of poor satellite geometry (fig. 3*C*). This model relies on the fact that the station does not move an excessive amount between observations. In the example, a random-walk process-noise constraint for a rate of change of the receiver coordinates of 40 cm/$\sqrt{\text{hr}}$ was used to estimate the station position of one of the stations. Solutions were estimated continuously using a 6-minute data interval. With this constraint and during the periods of the best satellite geometry, the formal errors indicate that motions < 1 cm/hr should be detectable in the length, transverse, and vertical components with two hours of observations. This rate is an order of magnitude less than that observed during the month preceding the May 18 eruption of Mount St. Helens (Lipman and others, 1981).

Based on the Mount St. Helens example, volcano monitoring for eruption prediction and aircraft warning may often require almost continuous calculation of receiver positions. In certain instances, it may even be useful to calculate

positions hourly, or even within fractions of an hour. The above results and those from the 1991 experiment suggest that precursory volcanic deformation at sub-daily and daily intervals could be monitored with high precision with a GPS volcano-monitoring network. On short baselines, an increase in the precision by a factor of about 2 could be obtained using ambiguity resolution (Blewitt, 1989). The outlook for less correlated solutions and increased sub-daily precision is good, given the continued filling of the GPS satellite constellation and increased ground-station distribution.

## A SYSTEM FOR IMPLEMENTATION OF REAL-TIME GPS MONITORING

GPS provides the most realistic possibility for eruption prediction based on monitoring surface deformation. The most important issues that need to be considered for real-time volcano monitoring with GPS are: (1) the hardware necessary for collecting, retrieving, and analyzing the data in real time, (2) the analysis strategy used to detect ground deformation, and (3) the scientific insight required to interpret the deformation signals in terms of volcanic processes.

The hardware necessary for the monitoring system is rather simple (fig. 4). A network of receivers is stationed on the volcano to be monitored. There are two types of receivers available: coded and codeless. The main drawback of codeless receivers is their lack of tracking the P-code (pseudo range), resulting in more frequent losses of lock by the receiver on the satellite signals. When losses of lock (cycle slips) occur, they must be repaired in the analysis of the data. For codeless receivers, this is a time-consuming process that usually involves bringing together data from several receivers in order to detect the cycle slip and properly correct for it (Blewitt, 1990). Communication links between the volcano receivers and a central processing station, and between the central processing station and other global receivers, must rely on telemetering of data, either via communications satellite or telephone lines. The link between the central processing station and the volcano receiver needs to be real time,

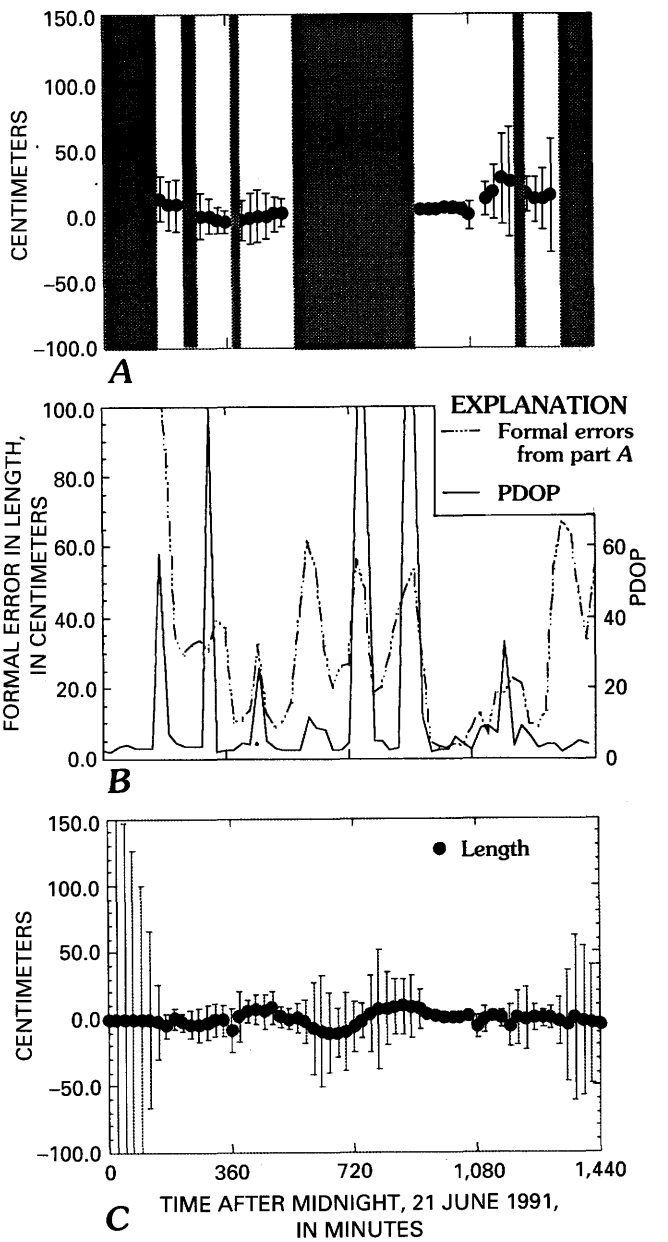


**Figure 3** (right). Sub-daily GPS baseline length obtained for a 22-km baseline in California between station M7115a and GOLD (at the Goldstone Deep Space Network facility). *A*, The plot shows the residual from a nominal value for baseline length. Solutions were estimated each time a GPS measurement was saved by the receiver. Each estimate for the position of M7115a is uncorrelated with the previous estimate. That is, the position of M7115a is modeled as a white-noise process. Shaded regions are regions when the satellite geometry was insufficient to estimate the station position and clock. Vertical bars indicate ± 1 sigma formal error in the baseline solution. *B*, Formal errors (dashed line) in the solutions from *A* track the position dilution of precision (PDOP, solid line) for these stations closely, suggesting that satellite geometry is the dominant error source for sub-daily solution strength. (The tail in the formal error at the beginning of the data arc is caused by no data being collected at M7115a for the first 100 minutes of the day.) *C*, Periods of bad satellite geometry can be spanned if the station position is modeled as being correlated from one GPS observation to the next. In this example, only baseline length is plotted for a random-walk model of the station position. Vertical bars indicate ± 1 sigma formal error in the baseline solution. This model is applied with process noise being added to the variance at a rate of 40 cm/$\sqrt{\text{hr}}$, resulting in solutions being obtained at every sample point, with a weak correlation from solution to solution. Periods when the station position could not be estimated with the white-noise model are now spanned. The usefulness of observations during these periods depends on the magnitude of the signal and the strength of the satellite constellation.

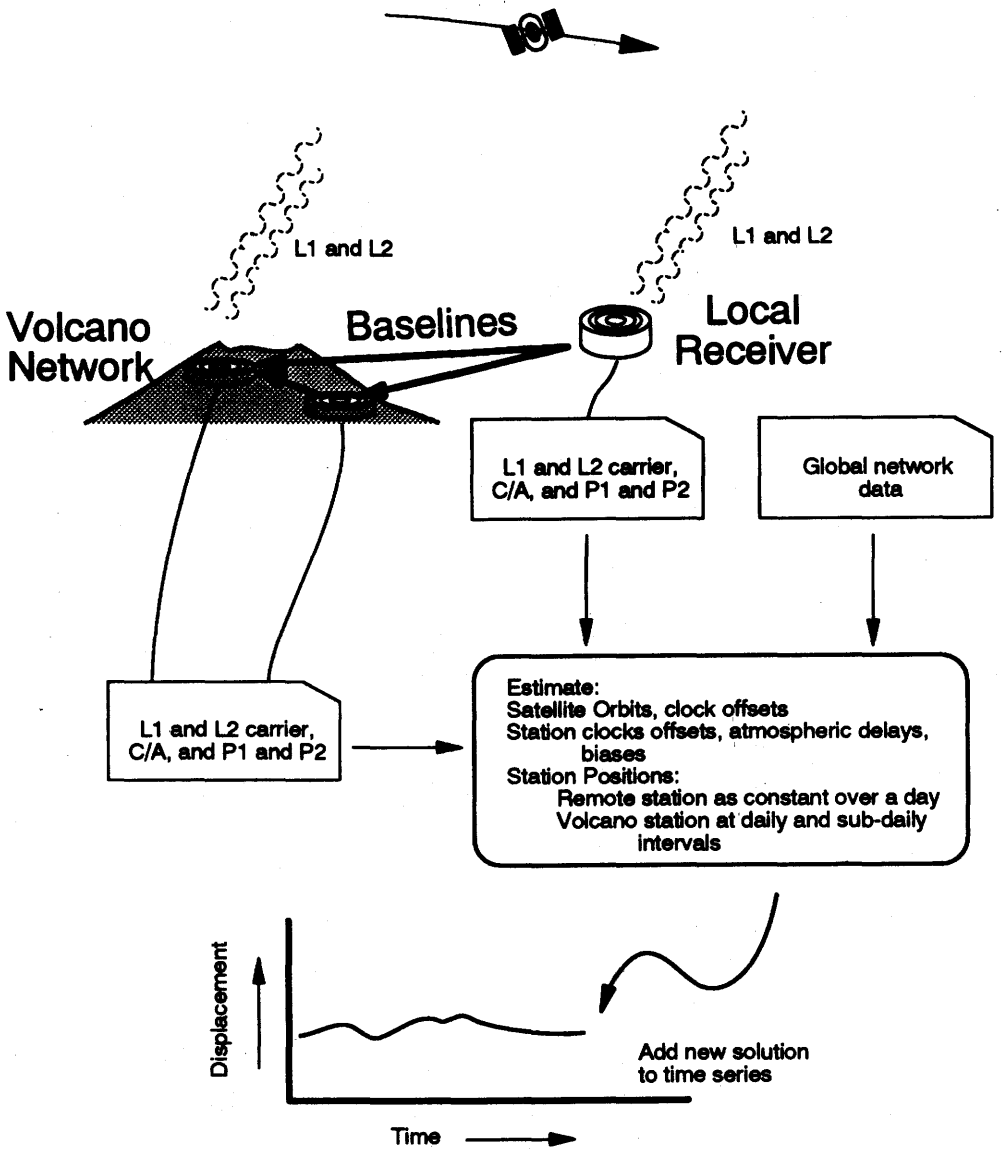


**Figure 4.** One possible design for a real-time, continuous, GPS volcano-monitoring system. Data collected at a volcano receiver are transmitted via modem to a central processing facility This facility also collects data from other global and (or) local receivers. Data from all receivers are "added" to the estimation of the baselines between the volcano monitoring stations and the local and (or) global receivers. The processing facility monitors the GPS baseline results for strain accelerations. This information is used to adjust the frequency with which data are obtained from the volcano station for estimating relative motion.

especially during high-strain-rate events. It is not necessary that data from the global stations, and from the volcano stations in times of quiescence, be retrieved in real time. This information can be added to the solution as it is acquired by the processing facility.

The particular analysis strategy pursued at any one time represents a trade-off between a desired precision and the frequency at which solutions are calculated. Fortunately, the trade-off between precision and solution spacing is mirrored in the physics relating ground deformation and eruptive events. In the time period leading up to an eruption, strain rates are expected to be relatively high and strain magnitudes to be relatively large. During these periods, more useful information will be derived by calculating more frequent, less precise positions than less frequent, more precise positions. When deformation is slow and an eruption is more likely to occur in the distant future, more precise solutions can be calculated less frequently. It is thus useful to exploit a flexible analysis strategy. Changes in the relatively infrequent, yet precise, positions together with other eruptive precursors could be used to trigger higher time resolution analysis strategies.

The GPS receivers must be judiciously stationed on a potentially active or hazardous volcano. Because of the impossibility of monitoring all volcanoes that might erupt explosively, the system must be based on portable receivers that can be deployed temporarily at potentially destructive volcanoes. At least two receivers should be deployed near the possible eruptive center, if this can be determined through seismic or geological methods, to exploit the magnitude of the deformation signal there. Data from these receivers are down-loaded daily to a central processing center. These data and data from other nearby stations and (or) global networks are then used to estimate baselines to the volcano stations, which are interpreted to discern accelerations in the movement of the positions of the volcano stations. This information is combined with other observations indicating increased activity and is used to alert the system to increase the frequency of solution calculation. Thus, the system must be sufficiently flexible to allow changes in the temporal spacing between baseline solutions. GPS analysis systems, currently in operation, facilitate and streamline the process of changing the frequency of solution calculation. Solutions can be rapidly calculated and included in a new solution time line at the expense of older, outdated solutions.

Efforts using GPS to monitor deformation at volcanoes have already been initiated. Many of these involve application of GPS techniques developed for measuring plate-boundary deformation to understanding regional crustal movements related to volcanism. Marshall and Stein (1991) and Meertens and Smith (1991) have reported somewhat ambiguous results of regional GPS geodetic surveys at Long Valley and Yellowstone calderas in the United States. There have also been important advances in developing systems useful for eruption prediction. Data from Unzen Volcano and Teshi Volcano (Shimada and others, 1990) were analyzed using standard post-processing techniques and showed that a geodetic signal was measured by GPS receivers that may have been useful for prediction purposes if real-time processing had been available. At Long Valley caldera and Augustine Volcano, Alaska, the U.S. Geological Survey and National Aeronautics and Space Administration are developing near-real-time GPS monitoring systems for eruption prediction. Any standardized GPS volcano-monitoring technique is still in the future, however. Receivers and telecommunications equipment are still too expensive for routine deployment. In addition, as described above, the analysis techniques necessary to obtain near-real-time, precise positions are still in the research-and-development stage. Rapid progress on these two fronts suggest that real-time GPS monitoring is not an unrealistic goal.

## CONCLUSIONS

Although volcanoes represent an inherently complex physical system, earth scientists have identified several types of phenomena, including ground deformation, that indicate an eruption may be imminent. Moreover, progress has been made in identifying how these features can be interpreted to obtain a near-real-time eruption-prediction capability. Our results suggest that the global positioning system will soon be able to provide precise, sub-daily, three-dimensional positioning information to monitor rapid ground deformation preceding an eruption. In addition, GPS hardware technology is sufficiently evolved that relatively inexpensive P-code receivers will be available in the near future to enable near-real-time data analysis. It is the combination of a flexible precision and solution-calculation interval with near-real-time analysis and communication that will define the optimum system for geodetic volcano monitoring, prediction, and aviation warning using GPS.

## ACKNOWLEDGMENTS

The research described in this publication was carried out by the Jet Propulsion Laboratory, California Institute of Technology, under contract with the National Aeronautics and Space Administration. M.B. acknowledges the receipt of a National Research Council/Jet Propulsion Laboratory Research Associateship. Dan Dzurisin, Geoff Blewitt, and Steve Lichten provided useful comments to improve the manuscript.

## REFERENCES CITED

Bierman, G.J., 1977, Factorization Methods for Discrete Sequential Estimation: New York, Academic Press, 241 p.

Blewitt, G., 1989, Carrier phase ambiguity resolution for the global positioning system applied to geodetic baselines up to 2,000 km: Journal of Geophysical Research, v. 94, p. 10187–10203.

———1990, An automatic editing algorithm for GPS data: Geophysical Research Letters, v. 17, p. 199–202.

Blewitt, G., Heflin, M.B., Webb, F.H., Lindqwister, U.J., and Malla, R.P., 1992, Global coordinates with centimeter accuracy in the International Terrestrial Reference Frame using GPS: Geophysical Research Letters, v. 19, p. 853–856.

Ewart, J.A., Voight, B., and Bjorneson, A., 1990, Dynamics of Krafla caldera, north Iceland: 1975–1985, *in* Ryan, M.P., ed., Magma Transport and Storage: New York, John Wiley and Sons, p. 225–276.

Heflin, M., Bertiger, W., Blewitt, G., Freedman, A., Hurst, K., Lichten, S., Lindqwister, U., Vigue, Y., Webb, F., Yunck, T., and J. Zumberge, 1992, Global geodesy using GPS without fiducials: Geophysical Research Letters, v. 19, p. 131–134.

Hill, D.P., Johnston, M.J.S., Langbein, J.O., McNutt, S. R., Miller, C.D., Mortensen, C.E., Pitt, A.M., and Rojstaczer, S., 1991, Response plans for volcanic hazards in the Long Valley caldera and Mono Craters area, California: U.S. Geological Survey Open-File Report 91-270, 65 p.

Lipman, P.W., Moore, J.G., and Swanson, D.A., 1981, Bulging of the north flank before the May 18th eruption—Geodetic data, *in* Lipman, P.W., and Mullineaux, D.R., eds., The 1980

Eruptions of Mount St. Helens, Washington: U.S. Geological Survey Professional Paper 1250, p. 143–156.

Marshall, G., and Stein, R., 1991, Monitoring ground deformation at Mono Craters, California, using a dense GPS network [abs.]: Eos, Transactions, American Geophysical Union, v. 72, p. 118.

Meertens, C.M., and Smith, R.B., 1991, Crustal deformation of the Yellowstone Caldera from first GPS measurements, 1987–1989: Geophysical Research Letters, v.18, p. 1763–1766.

Newhall, C.G., and Dzurisin, D., 1988, Historical unrest at large calderas of the world: U.S. Geological Survey Bulletin 1855, 1108 p.

Savage, J., and Lisowski, M., 1984, Deformation in the White Mountains seismic gap, California-Nevada, 1972–1982: Journal of Geophysical Research, v. 89, p. 7671–7687.

Shimada, S., Fujinawa, Y., Sekiguchi, S., Ohmi, S., Eguchi, T., and Okada, Y., 1990, Detection of a volcanic fracture opening in Japan using global positioning system measurements: Nature, v. 343, p. 631–633.

Sovers, O.J., and Border, J.S., 1987, Observation model and parameter partials for the JPL geodetic GPS modeling software "GPSOMC:" Jet Propulsion Laboratory Publication JPL 87-21.

Swanson, D.A., Casadevall, T.J., Dzurisin, D., Malone, S.D., Newhall, C.G., and Weaver, C.S. 1983, Predicting eruptions at Mount St. Helens, June 1980 through December 1982: Science, v. 221, p. 1369–1376.

Wells, D.E., Beck, N., Delikaraolou, D., Kleusberg, A., Krakiwsky, E. J., Lachapelle, G., Langley, R.B., Nakiboglu, M., Schwartz, K., Tranquilla, J.M., and Vanicek, P., 1986, Guide to GPS positioning: Fredricton, New Brunswick, Canada, Canadian GPS Associates.

# SELECTED GLOSSARY OF VOLCANOLOGY AND METEOROLOGY

**Active volcano.** A volcano that is erupting or has erupted in recorded history.

**Ash.** Finely fragmented particles of rocks and minerals less than 2 mm in diameter (less than 0.063-mm diameter for fine ash) produced by explosive volcanic eruption. See also *tephra, pyroclast, ejecta.*

**Ash cloud.** A cloud of volcanic ash and pyroclastic fragments, often containing gases and aerosols of volcanic origin, formed by volcanic explosion and carried by winds away from an eruption column. Ash clouds are often dark colored—brown to gray. Ash clouds may drift for hundreds to thousands of kilometers from their volcanic source. As ash clouds become more dilute, they may be difficult to distinguish from meteorological clouds. See also *eruption cloud.*

**Ash flow.** A mixture of hot gases and ash, which may move down the flanks of a volcano or along the ground surface at high speed. See also *pyroclastic flow.*

**Composite volcano.** A steep-sided volcano composed of many layers of volcanic rocks, usually lava flows and ash and pyroclastic deposits; also known as a *stratovolcano.*

**Dormant volcano.** A volcano that is not presently erupting but is considered capable of doing so in the future.

**Earthquake.** A sudden motion or trembling in the Earth caused by the sudden fracturing of a part of the Earth's crust. See also *tremor.*

**Ejecta.** General term for material thrown out by a volcano. See also *pyroclast* and *tephra.*

**Eruption cloud.** A cloud of volcanic ash and other pyroclastic fragments, and volcanic gases and aerosols, that forms by volcanic explosion. Eruption clouds are often dark colored—brown to gray. Often used interchangeably with *plume* or *ash cloud.*

**Eruption column.** The vertical pillar of ash and gas that forms above a volcano at the time of eruption. Eruption columns from energetic eruptions may rise to altitudes in excess of 100,000 ft (30 km).

**Fumarole.** A vent on a volcano from which gases and vapors are emitted.

**Hawaiian eruption.** An eruption characterized by the non-explosive eruption of fluid lava of basaltic composition. Hawaiian eruptions generally pose no threat to aviation safety.

**Isobars.** Lines on a weather map or chart connecting points of equal pressure.

**Lapilli.** Pyroclastic fragments with diameters between 2 and 64 mm.

**Lava.** Molten rock that erupts from a volcano.

**Magma.** Naturally occurring molten rock generated within the Earth that can be erupted as lava or pyroclasts.

**Mesoscale.** Term used to refer to weather phenomena with systems of length of about 100 km, of velocity of about 10 m/s, and with time scales of about 3 hours.

**Millibar.** A unit of atmospheric pressure equal to 1/1000 bar, or 1,000 dynes per square centimeter.

**Mudflow.** A general term for a flowing mass of predominantly fine-grained earth material mixed with water and possessing a high degree of fluidity during movement. The Indonesian term lahar is often used interchangeably with mudflow.

**Phreatic eruption.** A volcanic eruption or explosion of steam, mud, or other non-juvenile material, generally caused by the heating and expansion of ground water due to underlying magma.

**Plinian eruption.** A large explosive eruption that ejects a steady, turbulent stream of fragmented magma and magmatic gas to form an eruption column that may reach altitudes in excess of 100,000 ft (30 km).

**Plume.** Term often used to describe the elongated, downwind, dispersed portion of an eruption cloud and ash cloud.

**Pyroclast.** An individual volcanic particle ejected during an eruption. For example, ash, lapilli, and volcanic bombs are pyroclasts.

**Pyroclastic flow.** A turbulent flowing mass of fragmented volcanic materials mixed with hot gases that may move downhill at high speed. Pyroclastic flows may result from the collapse of tall eruption columns or from spillover of ejected materials from erupting vents. See also *ash flow.*

**Rawinsonde.** Observations of upper-air conditions, including wind direction and speed, temperature, pressure, and relative humidity using signals from a radiosonde that is tracked with radar or a radio-direction finder.

**Seismometer.** An instrument that detects earthquakes.

**Stratosphere.** The outer layer of the atmosphere that overlies the tropopause and is above an altitude of about 10 to 20 km.

**Stratovolcano.** A volcano that is constructed of alternating layers of lava and pyroclastic deposits; also known as a *composite volcano.*

**Strombolian eruption.** An eruption consisting of short, discrete, explosions which may eject pyroclasts for a few tens to a few hundreds of feet into the air. Each explosion may last for only a few seconds, and there may be pauses of tens of minutes between explosions.

**Tephra.** A collective term for all violently ejected materials from craters or vents during volcanic eruptions. These materials are either airborne momentarily or for a longer period of time depending primarily on the vigor of the eruption and the size of ejected fragments. Generally, coarser tephra are deposited closer to the erupting crater or vent and finer grained tephra are deposited farther away. Tephra includes volcanic dust, ash, cinder, lapilli, bombs, and blocks. See also *ejecta.*

**Tremor.** A type of seismicity characterized by continuous vibration of the ground related to the movement of magma and volcanic gas within or beneath a volcano.

**Tropopause.** An atmospheric transition zone located between the troposphere and the stratosphere at an altitude of about 10 to 20 km. In this region, temperatures and atmospheric stability begin to increase with increasing altitude.

**Troposphere.** That portion of the atmosphere next to the Earth's surface in which temperature generally decreases with altitude, clouds form, and weather systems and convection are active.

**Volcanic gas.** Volatile material, released during a volcanic eruption, that was previously dissolved in magma. The principal volcanic gases include water vapor, carbon dioxide, and sulfur dioxide.

**Volcano.** A vent or opening at the surface of the Earth through which magma erupts. Also the landform that is produced by the erupted material accumulated around the vent.

**Vulcanian eruption.** A type of volcanic eruption characterized by short-duration, violent, explosive ejection of fragments of lava. Vulcanian eruption columns may reach altitudes of 45,000 ft (15 km) or more.

# LIST OF SELECTED ACRONYMS

| | |
|---|---|
| A/C | air conditioning; also used as shorthand for "aircraft" |
| ACARS | aircraft communications addressing and reporting system |
| ACC | area control center |
| ACMS | aircraft condition monitoring systems |
| ADEOS | advanced Earth observing satellite (Japan) |
| ADPIC | atmospheric diffusion particle-in-cell model (Lange, 1978) |
| AEROS | ARAC emergency response operating system; see ARAC |
| AES | Atmospheric Environment Service (Canada) |
| AFGWC | see GWC |
| AFSS | aircraft flight service stations |
| AFTN | aeronautical fixed telecommunications network (Australia) |
| AGFS | aviation gridded forecast system |
| AGSO | Australian Geological Survey Organization |
| AGU | American Geophysical Union |
| AIA | Aerospace Industries Association of America |
| AIAA | American Institute of Aeronautics and Astronautics |
| AIP | aeronautical information publication |
| ALPA | Air Line Pilots Association |
| AMIC | area manager-in-charge |
| AOPA | Aircraft Owners and Pilots Association |
| APU | auxiliary power unit |
| ARAC | atmospheric release advisory capability (U.S. Department of Energy) |
| ARINC | Aeronautical Radio, Inc. |
| ARL | Air Resource Laboratory (NOAA) |
| ARO-NET | Alaska region operational (computer and) communications network |
| ARSI | Atmospheric Research Systems, Inc. |
| ARTCC | air route traffic control center |
| AS | anti-spoofing (DOD encryption of GPS P-code information) |
| ASD | aircraft situation displays |
| AST | Alaska Standard Time |
| ATA | Air Transport Association |
| ATC | air traffic control; air traffic center |
| ATCSCC | Air Traffic Control System Command Center (Washington, D.C.) |
| ATS | air traffic service; also air traffic system |
| AVADS | airborne volcanic-ash-detection system |
| AVHRR | advanced very high resolution radiometer |
| AVN | aviation run of the medium-range forecast model |
| AVO | Alaska Volcano Observatory |
| AWPG | aviation weather product generator |
| BOM | Bureau of Meteorology (Australia) |
| BUV | backscattered ultraviolet instrument |
| BVE | Bulletin of Volcanic Eruptions (Volcanological Society of Japan) |
| CAA | Civil Aviation Authority (Australia) |
| CANERM | Canadian emergency-response model |
| CAT | clear-air turbulence |
| CAVW | Catalog of Active Volcanoes and Solfatara Areas of the World |
| CCD | charge-coupled detector |
| CLS | Collecte Localisation Satellites (France) |
| CMC | Canadian Meteorological Centre |

| | |
|---|---|
| CNES | Centre National d'Etudes Spatiales (the French space agency) |
| COSSA | Office of Space Science and Application (Australia) |
| CSIRO | Commonwealth Scientific and Industrial Research Oraganization |
| CSLP | Center for Short-Lived Phenomena (Cambridge, Mass.) |
| CVO | Cascades Volcano Observatory (U.S. Geological Survey) |
| CWA | center weather advisory |
| CWSU | Central (Center) Weather Service Unit |
| DFDR | digital flight-data recorder |
| DIS | dust-injection system |
| DMSP | defense meteorological satellite program (United States) |
| DOD | Department of Defense (United States) |
| DOE | Department of Energy (United States) |
| DUAT | direct-user-access terminal |
| DVI | dust veil index |
| ECC | emergency coordination center |
| ECS | environmental control system |
| EDM | electronic distance meter |
| EFIS | electronic flight instrument system |
| EGT | exhaust-gas temperature |
| EOS | Earth observing system (spacecraft) |
| EPR | engine pressure ratio |
| ETA | estimated time of arrival |
| ETMS | enhanced traffic management system |
| FAA | Federal Aviation Administration (United States) |
| FADEC | full-authority digital electronic controls |
| FAR | Federal Aviation Regulation |
| FIR | flight-information region |
| FSF | Flight Safety Foundation |
| FTIT | turbine inlet temperature |
| GAC | global area coverage (data) |
| GMS | geostationary meteorological satellite |
| GMT | Greenwich Mean Time (equivalent to UTC) |
| GOES | geostationary orbiting (operational) environmental satellite |
| GOSTA | Global Ocean Surface Temperature Atlas |
| GPS | global positioning system |
| GRIB | gridded binary format |
| GSFC | Goddard Space Flight Center |
| GTS | global telecommunication system |
| GVN | Global Volcanism Network (Smithsonian Institution—formerly SEAN) |
| GWC | Global Weather Central (U.S. Air Force); also AFGWC |
| HARS | high-altitude routing system |
| HIPS | high-resolution image-processing system |
| HIRS | high-resolution infrared radiation sounder |
| HPC | high-pressure compressor |
| HPT | high-pressure turbine |
| IATA | International Air Transport Association |
| IAVCEI | International Association of Volcanology and Chemistry of the Earth's Interior |
| IAVW | International Airways Volcano Watch |
| ICAO | International Civil Aviation Organization |
| IFALPA | International Federation of Air Line Pilots' Associations |
| IFC | instrument flight conditions |
| IFR | instrument flight rules; see also VFR |
| IFSD | (engine) in-flight shut down |
| IMC | instrument meteorological conditions |

| | |
|---|---|
| INSU | Institute for Earth and Planetary Sciences (France) |
| IR | infrared |
| ITWS | integrated terminal weather system |
| JAL | Japan Air Lines |
| JMA | Japan Meteorological Agency |
| JPL | Jet Propulsion Laboratory (California Institute of Technology) |
| KLM | Royal Dutch Airlines |
| KLMO | Kagoshima Local Meteorological Observatory (part of JMA) |
| LAC | local area coverage (data) |
| LLNL | Lawrence Livermore National Laboratory (Livermore, Calif.) |
| LOWTRAN | radiance/transmittance code developed by the U.S. Air Force |
| LPT | low-pressure turbine |
| MAPS | mesoscale analysis and prediction system |
| McIDAS | man-computer interactive data access system |
| MEDIC | meteorological data interpolation code |
| METSIS | meteorological satellite information system (Canada) |
| MONOA | Argos station for monitoring physical-chemical parameters |
| MOU | memorandum of understanding |
| MSU | microwave sounding unit |
| MWO | meteorological watch office |
| MWP | meteorological weather processor |
| $N_1$ | fan speed |
| $N_2$, N2 | core (rotor) speed |
| NASA | National Aeronautics and Space Administration (United States) |
| NAWAU | national weather advisory unit |
| NESDIS | National Environmental Satellite Data and Information Service (NOAA) |
| NEXRAD | next-generation weather radar |
| NGM | nested grid model |
| NGV | nozzle guide vane |
| NMC | National Meteorological Center (Canada; Camp Springs., Md.; Melbourne, Australia) |
| NOAA | National Oceanic and Atmospheric Administration (United States) |
| NOTAM | notice to airmen |
| NVM | non-volatile memory (feature of FADEC) |
| NWP | numerical weather-prediction (model) |
| NWS | National Weather Service |
| OA | objective analysis |
| ORSTOM | Research Institute for Cooperative Development (France) |
| $P_B$ | burner pressure; burner static pressure |
| PDOP | position dilution of precision |
| PDT | Pacific Daylight Time; also abbreviation for Pendleton, Oreg. |
| PEGASAS-VE | pressure gage system for air-shocks by volcanic eruptions |
| PIREP | (also Pirep) pilot report |
| PIRPSEV | interdisciplinary research program for the forecasting of volcanic eruptions (France) |
| PLA | power lever angle |
| $P_{S3}$ | compressor discharge pressure; high-compressor static-discharge pressure |
| $P_{S3}$ | compressor-discharge pressure |
| $P_{T2}$ | inlet total pressure |
| $P_{T2.5}$ | fan-exit total pressure |
| RAWPG | regional aviation weather product generator |
| RFC | Regional Forecasting Center (part of BOM) |
| RFE | regional finite-element (model) |
| RHI | range-height indicator |
| RISC | reduced instruction set chip |
| RSAM | real-time seismic-amplitude monitoring system |

| | |
|---|---|
| SA | selective availability (GPS term) |
| SAB | Synoptic Analysis Branch (of the NWS) |
| SBUV | solar/backscattered ultraviolet instrument |
| SEAN | Scientific Event Alert Network (Smithsonian Institution—now called GVN) |
| SIGMET | significant meteorological advisory |
| SIGWX | significant weather chart |
| SISMO1 | Argos station for monitoring seismic tremors and events |
| SNR | signal-to-noise ratio |
| SOI | southern oscillation index |
| SVO | Sakurajima Volcanological Observatory (Kyoto University, Japan) |
| TDWR | terminal Doppler weather radar |
| TIROS | television and infrared observing (observation) satellite |
| TMU | traffic management unit |
| TOMS | total ozone mapping spectrometer |
| TOVS | TIROS observational vertical sounder |
| TRACON | terminal radar approach control |
| TSC | transportation system center |
| UAV | unmanned aircraft vehicle |
| UCAR | University Corporation for Atmospheric Research |
| USFS | U.S. Forest Service |
| USGS | U.S. Geological Survey |
| UTC | Coordinated Universal Time (also Universal Time Code; see also GMT, Zulu) |
| UW | University of Washington |
| VAD | velocity azimuth display (feature of NEXRAD) |
| VADAS | volcanic ash detection and aviation safety (study group) |
| VAFTAD | volcanic ash forecast transport and dispersion model |
| VAR | volcanic activity report (form); cf., Fox, this volume, fig. 1 |
| VARTAM | volcanic ash report to airmen |
| VAW | volcanic ash warning |
| VAWS | volcanic ash warning system |
| VEI | volcanic explosivity index |
| VFR | visual flight rules; see also IFR, IFC |
| VISSR | visible and infrared spin-scan radiometer |
| VOR | very high frequency omnidirectional radio range |
| VSI | Volcanological Survey of Indonesia |
| VULCAN | Volcanological/Airspace Liaison Committee–Australia/Indonesia |
| VULCAN-AUS | Australia-based working group of VULCAN |
| VULCAN-IND | Indonesia-based working group of VULCAN |
| VVP | volume velocity processing |
| VWS | volcano watching system |
| WAFS | world-area forecast system |
| WAIT | Western Australia Institute of Technology (now Curtin University of Technology) |
| WFO | weather forecast office |
| WMO | World Meteorological Organization |
| WOVO | World Organization of Volcano Observatories |
| WSFO | Weather Service Forecast Office |
| WSO | Weather Services Office (Australia) |
| WWW | World Weather Watch |
| Zulu | Coordinated Universal Time |

# AUTHORS' ADDRESS LIST


Mr. Jorge Barquero
Observatorio Vulcanologico y Sismologico de Costa Rica
Universidad Nacional
Apartado 86-3000, Heredia
Costa Rica
374570-377023-376363, ext. 2304, 2405
FAX: (506) 238-0086

Dr. Ian J. Barton
CSIRO Division of Atmospheric Research
Private Bag No. 1
Mordialloc, Victoria 3195
Australia
61-3-586-7668
FAX: 61-3-586-7600

Mr. Craig I. Bauer
National Weather Service
701 C Street, Box 23
Anchorage, AK 99513
(907) 271-5107
FAX: (907) 271-3711

Mr. Gregory K. Bayhurst
INC-7 MS J-514
Los Alamos National Laboratory
Los Alamos, NM 87545
(505) 667-4534
FAX: (505) 665-5688

Dr. James E. Beget
Department of Geology and Geophysics
University of Alaska
Fairbanks, AK 99775
(907) 474-7565
FAX: (907) 474-5163

Mr. Stanley G. Benjamin
NOAA Forecast Systems Laboratory
NOAA/ERL/FSL R/E/FS1
325 Broadway
Boulder, CO 80303
(303) 497-6938
FAX: (303) 497-6750

Dr. Gregg S.J. Bluth
Department of Geological Engineering
Michigan Technological University
1400 Townsend Dr.
Houghton, MI 49931
(906) 487-2531
FAX: (906) 487-2943

Dr. Marcus I. Bursik
Department of Geology
State University of New York at Buffalo
Buffalo, NY 14268
(716) 645-3992
FAX: (716) 645-3999

Captain Ernest E. Campbell
Boeing Commercial Airplane Group
P.O. Box 3707, M/S 2T-61
Seattle, WA 98124-2207
(206) 662-7886
FAX: (206) 662-7575

Dr. Thomas J. Casadevall
U.S. Geological Survey
Box 25046, MS 903
Denver Federal Center
Denver, CO 80225
(303) 236-1080
FAX: (303) 236-1414

Dr. Steven N. Carey
University of Rhode Island
School of Oceanography
Kingston, RI 02881
(401) 792-6222
FAX: (401) 792-6160

Mr. J.P. Cauzac
North American CLS, Inc.
9200 Basil Court, Suite 306
Landover, MD 20785
(301) 341-1814
FAX: (301) 341-2130

Dr. Real D'Amours
Canadian Meteorological Centre
2121 North Service Rroad, Suite 200
Trans Canada Highway
Dorval, Quebec H9P 1J3
Canada
(514) 421-4684
FAX: (514) 421-4639

Mr. Douglas D. D'Autrechy
Science Applications International Corporation
1710 Goodridge Dr.
McLean, VA 22102-1302
(703) 556-7142
FAX: (703) 356-8408

Mr. Kenneson G. Dean
Geophysical Institute
University of Alaska Fairbanks
Fairbanks, AK 99775-0800
(907) 474-4764
FAX: (907) 474-7290

Mr. Scott R. Doiron
ST Systems Corporation
4400 Forbes Boulevard
Lanham, MD 20706
(301) 286-8036
FAX: (301) 286-3460

Dr. Michael G. Dunn
Calspan Advanced Technology Center
4455 Genesee St.
Buffalo, NY 14225
(716) 631-6747
FAX: (716) 631-6815

Dr. James S. Ellis
Lawrence Livermore National Laboratory
Box 808 (L-262)
Livermore, CA 94551
(510) 422-1808
FAX: (510) 423-4527

Mr. Donald D. Engen
809 Duke St.
Alexandria, VA 22314
(703) 548-6750
FAX: (703) 548-6886

Dr. James E. Evans
Weather Sensing Group
Room HW29-119B
M.I.T. Lincoln Lab
P.O. Box 73
Lexington, MA 02139
(617) 981-7433
FAX: (617) 981-0632

Captain Peter M. Foreman
Air Traffic Services Committee
5351 Parker Avenue
Victoria, B.C., V8Y2N1
Canada
(604) 658-8045
FAX: (604) 276-8923

Mr. Tom Fox
International Civil Aviation Organization (ICAO)
1000 Sherbrooke St. West
Montreal, Quebec H3A 2R2
Canada
(514) 285-8194
FAX: (514) 285-6759

Dr. Charles R. Gallaway
Department of Defense
6801 Telegraph Road
Alexandria, VA 22310-3398
(703) 325-1282
FAX: (703) 325-2957

Dr. Jennie S. Gilbert
Department of Geology
University of Bristol
Wills Memorial Building
Queens Road, Bristol BS8 1RJ
United Kingdom
(0272) 303030, ext. 4795 or 0272
FAX: (0272) 253385

Mr. Robert F. Hamley
National Weather Service
FAA ARTCC
3101 Auburn Way South
Auburn, WA 98002
(206) 931-5401
FAX: (206) 931-5208

Dr. David M. Harris
Department of Forestry
Utah State University
Logan, UT 84321-5215
(801) 750-2585
FAX: (801) 750-3798

Dr. Ulli G. Hartmann
Perkin-Elmer Corporation
2771 N. Garey Ave.
Pomona, CA 91767
(714) 593-3581
FAX: (714) 596-2301

Dr. Jerome L. Heffter
NOAA Air Resources Laboratory
1325 East-West Highway, Room 9358
Silver Spring, MD 20910
(301) 713-0295
FAX: (301) 713-0119

Dr. Grant Heiken
ESS-1, Geology/Geochemistry
M/S D-462
Los Alamos National Laboratory
Los Alamos, NM 87545
(505) 667-8477
FAX: (505) 667-3494

Dr. Robert H. Hertel
Perkin-Elmer Corporation
2771 N. Garey Ave.
Pomona, CA 91767
(909) 593-3581
FAX: (909) 596-2301

Dr. Catherine J. Hickson
Geological Survey of Canada
100 West Pender Street
Vancouver, B.C. V6B 1R8
Canada
(604) 666-3955/0539
FAX: (604) 666-1124

Dr. Frank R. Honey
SpecTerra Systems Pty Ltd.
43 Hobbs Avenue
Dalkeith, Western Australia 6009
Australia
61 (9) 389-8050
FAX: 61 (9) 386-7935

Mr. Gary L. Hufford
National Weather Service
222 W. 7th Ave., #23
Anchorage, AK 99513
(907) 271-3886
FAX: (907) 271-3711

Dr. Lee Huskey
School of Public Affairs
University of Alaska Anchorage
3211 Providence Drive
Anchorage, AK 99508
(907) 786-1916
FAX: (907) 786-7739

Dr. Kazuhiro Ishihara
Sakurajima Volcano Observatory
Yokoyama, Sakurajima
Kagoshima 891-14
Japan
81-992-93-2058
FAX: 81-992-93-4024

Mr. Haitao Jiao
Geophysical Institute
University of Alaska Fairbanks
Fairbanks, AK 99775-0800
(907) 474-4764
FAX: (907) 474-7290

Dr. R. Wally Johnson
Australian Geological Survey Organization
GPO Box 378
Canberra ACT 2601
Australia
61-62-49-9377
FAX: 61-62-49-9983

Ms. Chris Jonientz-Trisler
Federal Emergency Management Agency
Federal Regional Center
130 - 228th SW
Bothell, WA 98021-9796
(206) 487-4645
FAX: (206) 487-4613

Dr. Kosuke Kamo
Sakurajima Volcanological Observatory
Koyto University
Yokoyama, Sakurajima
Kagoshima 891-14
Japan
81-992-93-2058
FAX: 81-992-93-4024

Dr. Juergen Kienle
Geophysical Institute
University of Alaska
Fairbanks, AK 99775-0800
(907) 474-5681
FAX: (907) 474-5618

Dr. Vladimir Yu. Kirianov
Institute of Volcanic Geology and Geochemistry
9 Piip Avenue
Petropavlovsk-Kamchatsky, 683006
Russia
415-00-59194

Dr. Alexander B. Kostinski
Department of Geological Engineering
Michigan Technological Univesity
Houghton, MI 49931
(906) 487-2531
FAX: (906) 487-2943

Dr. Arlin J. Krueger
Earth Sciences Directorate
NASA, Goddard Space Flight Center
Greenbelt, MD 20771
(301) 286-6358
FAX: (301) 286-3460

Dr. J.R. Labadie
JAYCOR
1212 N.E. 62nd St
Seattle, WA 98115
(206) 526-5125
FAX: (206) 526-5531

Dr. Stephen J. Lane
Department of Geology
University of Bristol
Wills Memorial Building
Queens Road, Bristol BS8 1RJ
United Kingdom
(0272) 303030, ext. 4795 or 0272
FAX: (0272) 253385

Mr. James S. Lynch
NOAA/NESDIS
World Weather Building, Room 410
Washington, DC 20230
(301) 763-8444
FAX: (301) 763-8142

Dr. Giovanni Macedonio
Centro di Studi per la Geologia e Dinamica
dell'Appennino—CNR
via Santa Maria 53
I-56100 Pisa
Italy
050-47383-6
FAX: 050-43163

Mr. J. Owen Maloy
Mountain Instruments Corporation
P.O. Box 2083
Mammoth Lakes, CA 93546
(619) 934-9511
FAX: (619) 934-4553

Dr. Allen S. Mason
INC-7 MS J-514
Los Alamos National Laboratory
Los Alamos, NM 87545
(505) 667-4534
FAX: (505) 665-5688

Mr. Michael Matson
NOAA/NESDIS
World Weather Building
5200 Auth Road
Washington, DC 20230
(301) 763-8142
FAX: (301) 763-8131

Mr. Lindsay McClelland
National Park Service
Wildlife and Vegetation Division
800 N. Capital St. N.W., Room 500
Washington, DC 20002
(202) 343-1004
FAX: (202) 343-8137

Dr. Stephen R. McNutt
Alaska Volcano Observatory
Geophysical Institute
University of Alaska
Fairbanks, AK 99775-800
(907) 474-7131
FAX: (907) 474-5618

Captain Edward Miller
Aviation Weather Committee
Air Line Pilots Association
535 Herndon Parkway
Herndon, VA 22070
(703) 689-4200
FAX: (703) 689-4370

Mr. Michael C. Monteith
Science Applications International Corporation
1710 Goodridge Dr.
McLean, VA 22102-1303
(703) 821-4517
FAX: (703) 356-8408

Ms. Laurel Muehlhausen
North American CLS, Inc.
9200 Basil Court, Suite 306
Landover, MD 20785
(301) 341-1814
FAX: (301) 341-2130

Mr. Thomas L. Murray
U.S. Geological Survey
5400 MacArthur Blvd.
Vancouver, WA 98661
(206) 696-7549
FAX: (206) 696-7866

Mr. Mark E. Musolf
United Technologies - Norden Systems
P.O. Box 5300
Norwalk, CT 06856
(203) 852-7533
FAX: (203) 852-7423

Ms. Bobbie Myers
U.S. Geological Survey
5400 MacArthur Blvd.
Vancouver, WA 98661
(206) 696-7908 or 7906
FAX: (206) 696-7866

Dr. Reginald E. Newell
Department of Earth, Atmospheric and Planetary Sciences
Massachusetts Institute of Technology
Cambridge, MA 02139
(617) 253-2940
FAX: (617) 253-6208

Mr. Saburo Onodera
Meteorology Section, Flight Operations Dept.
Japan Air Lines Co., Ltd.
JAL Operation Center Bldg.
1-1 Hanedakuko 2 Chome
Ota-Ku, Tokyo 144
Japan
81-3-3747-3357
FAX: 81-3-3747-4619

Mr. Christian Ortega
North American CLS, Inc.
9200 Basil Court, Suite 306
Landover, MD 20785
(301) 341-1814
FAX: (301) 341-2130

Mr. Donald H. Parkinson
National Weather Service
FAA ARTCC
3101 Auburn Way South
Auburn, WA 98002
(206) 390-5401
FAX: (206) 931-5208

Dr. P. Papale
Istituto Nazionale di Geofisics
via di Villa Ricotti 42,
I-00100 Roma
Italy

Dr. M. Teresa Pareschi
Centro Ricerca IBM,
via Santa Maria 67
I-56100 Pisa
Italy

Mr. John F. Paskievitch
U.S. Geological Survey
4200 University Dr.
Anchorage, AK 99508
(907) 786-7454
FAX: (907) 786-7450

Mr. John A. Power
U.S. Geological Survey
Geophysical Institute
University of Alaska Fairbanks
Fairbanks, AK 99775-0800
(907) 474-5333
FAX: (907) 474-5618

Mr. Rodney J. Potts
Bureau of Meteorology
GPO Box 1289K
Melbourne, Victoria 3001
Australia
61-3-6694584
FAX: 61-3-6694695

Dr. Alfred J. Prata
CSIRO, Division of Atmospheric Research
Private Bag No. 1
Mordialloc, Victoria 3195
Australia
61-3-586-7681
FAX: 61-3-586-7600

Mr. Zygmunt J. Przedpelski
24 Quartermaster Dr.
Salem, SC 29676
(803) 944-5622

Dr. Herbert A. Roeder
Perkin-Elmer Corporation
2771 N. Garey Ave.
Pomona, CA 91767
(909) 593-3581
FAX: (909) 596-2301

Dr. William I. Rose
Department of Geological Engineering
Michigan Technological University
1400 Townsend Dr.
Houghton, MI 49931
(906) 487-2531
FAX: (906) 487-2943

Dr. Mauro Rosi
Dipartimento di Scienze della Terra
via Santa Maria 53
I-56100 Pisa
Italy

Dr. Yosihiro Sawada
Sendai District Meteorological Observatory
1-3-15 Gorin, Miyagino-ku
Sendai 983
Japan
022-291-8171 (ext. 140)
FAX: 022-291-8110

Dr. Roberto Santacroce
Dipartimento di Scienze dalla Terra
via Santa Maria 53
I-56100 Pisa
Italy

Dr. Thomas W. Schlatter
NOAA Forecast Systems Laboratory
NOAA/ERL/FSL R/E/FS1
325 Broadway
Boulder, CO 80303
(303) 497-6938
FAX: (303) 497-6750

Mr. David J. Schneider
Department of Geological Engineering
Michigan Technological University
1400 Townsend Dr.
Houghton, MI 49931
(906) 487-2531
FAX: (906) 487-2943

Dr. Charles C. Schnetzler
Earth Sciences Directorate
NASA, Goddard Space Flight Center
Greenbelt, MD 20771
(301) 286-3532
FAX: (301) 286-4098

Dr. Stephen Self
Department Geology and Geophysics
University of Hawaii
2525 Correa Road
Honolulu, HI 96822
(808) 956-5996
FAX: (808) 956-2538

Dr. Tom Simkin
NHB MS 119
Smithsonian Institution
Washington, DC 20560
(202) 357-2786
FAX: (202) 357-2476

Dr. R.S.J. Sparks
Department of Geology
University of Bristol
Wills Memorial Building
Queens Road, Bristol BS8 1RJ
United Kingdom
(0272) 303030, ext. 4795 or 0272
FAX: (0272) 253385

Mr. George Stephens
NOAA/NESDIS
5200 Auth Road, Room 510
Camp Springs, MD 20746
(301) 763-8142
FAX: (301) 763-8131

Dr. Melvin L. Stone
ATC Surveillance Group
M.I.T. Lincoln Laboratory
Lexington, MA 02173-9108
(617) 981-7426
FAX: (617) 981-3495

Dr. Barbara J.B. Stunder
NOAA/Air Resources Laboratory
1325 East-West Highway, Room 9358
Silver Spring, MD 20910
(301) 713-0295
FAX: (301) 713-0119

Dr. Thomas J. Sullivan
Lawrence Livermore National Laboratory
Box 808 (L-262)
Livermore, CA 94551
(510) 422-1808
FAX: (510) 423-4527

Dr. Samuel E. Swanson
Department of Geology and Geophysics
University of Alaska
Fairbanks, AK 99775
(907) 474-7565
FAX: (907) 474-5163

Dr. Makoto Tahira
Koyto University
Yokoyama, Sakurajima
Kagoshima 891-14
Japan
81-992-93-2058
FAX: 81-992-93-4024

Dr. Hiroshi L. Tanaka
Institute of Geoscience
University of Tsukuba
Tsukuba, Ibaraki 305
Japan
0298 53 4502
FAX: 0298 51 9764

Mr. George J. Theisen
U.S. Forest Service
Gifford Pinchot National Forest
Vancouver, WA 98668
(206) 696-7856
FAX: (206) 696-7863

Dr. Bradford H. Tuck
School of Public Affairs
University of Alaska Anchorage
3211 Providence Drive
Anchorage, AK 99508
(907) 786-1915
FAX: (907) 786-7739

Mr. Jerald Uecker
NOAA-National Weather Service
Aviation Services Branch
1325 East-West Highway
Silver Spring, MD 20910
(301) 713-1726
FAX: (301) 713-1598

Dr. Peter L. Versteegen
Science Applications International Corporation
1710 Goodridge Dr.
McLean, VA 22102-1303
(703) 821-4517
FAX: (703) 356-8408

Major Douglas P. Wade
Headquarters, Defense Nuclear Agency
6801 Telegraph Road
Alexandria, VA 22310-3398
(703) 325-1054
FAX: (703) 325 2957

Dr. George P. L. Walker
University of Hawaii at Manoa
Dept. of Geology and Geophysics
2525 Correa Road
Honolulu, HI 96822
(808) 956-5996
FAX: (808) 956-2538

Dr. Louis S. Walter
Laboratory for Terrestrial Physics
NASA, Goddard Space Flight Center
Greenbelt, MD 20771
(301) 286-2538
FAX: (301) 286-9200

Dr. Frank H. Webb
Jet Propulsion Laboratory
4800 Oak Grove Laboratory
MS 238-625
Pasadena, CA 91109
(818) 354-4670

Mr. Frank Whitby
Bureau of Meteorology
GPO Box 1289K
Melbourne
Victoria 3001, Australia
61-3-6694584
FAX: 61-3-6694695

Mr. Lawrence Whiting
Geophysical Institute
University of Alaska Fairbanks
Fairbanks, AK 99775-0800
(907) 474-4764
FAX: (907) 474-7290

Dr. Colin J.N. Wilson
Institute of Geological and Nuclear
Sciences Ltd.
Wairakei Research Centre
Private Bag 2000, Taupo
New Zealand
64 7 374-8211
FAX: 64 7 374-8199

Dr. Andrew W. Woods
Institute of Theoretical Geophysics
Department of Applied Mathematics and Theoretical Physics
University of Cambridge
Cambridge CB3 9EW
United Kingdom
44-223-33-7095
FAX: 44-223-33-7918

Dr. Kenneth H. Wohletz
INC-7 MS J-514
Los Alamos National Laboratory
Los Alamos, NM 87545
(505) 667-4534
FAX: (505) 665-5688

Dr. Zhong Xiang Wu
Department of Earth, Atmospheric, and Planetary Sciences
Massachusetts Institute of Technology
Cambridge, MA 02139
(617) 253-2940
FAX: (617) 253-6208

Mr. Lester M. Zinser
351 W. North
Ajo, AZ 85321-2153
(602) 245-2936

Published in the Central Region, Denver, Colorado
Manuscript approved for publication May 4, 1994
Edited by Richard W. Scott, Jr.
Graphics prepared by Denny Welp, Roger Highland, Gayle Dumonceaux, Art Isom, and Springfield & Springfield. In places, extensive use has been made of author-drafted material.
Photocomposition by Joan Nadeau, Carol Quesenberry, and Mari L. Kauffmann
Additional proofing and review by Robert K. Wells
Printing contract administration by Debra Sokol

☆ U.S. GOVERNMENT PRINTING OFFICE: 1994-573-038/86047

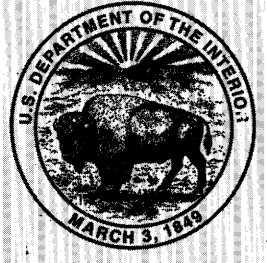
U.S. DEPARTMENT OF THE INTERIOR
MARCH 3, 1849